Part 1

DESIGN AND SYNTHESIS OF α6-GABA$_A$R SUBTYPE-SELECTIVE PYRAZOLOQUINOLINONES WITH IMPROVED METABOLIC STABILITY AND ENHANCED BIOAVAILABILITY

Part 2

PROCESS DEVELOPMENT OF α2/3-GABA$_A$R SUBTYPE-SELECTIVE IMIDAZODIAZEPINES: HZ-166 AND KRM-II-81

Part 3

PROCESS DEVELOPMENT OF α5-GABA$_A$R SUBTYPE-SELECTIVE IMIDAZODIAZEPINES: MIDD0301 AND GL-II-73

by

Daniel E. Knutson

A Dissertation Submitted in

Partial Fulfillment of the

Requirements for the Degree of

Doctor of Philosophy

in Chemistry

at

The University of Wisconsin-Milwaukee

May 2020

ABSTRACT

Part 1

DESIGN AND SYNTHESIS OF α6-GABA$_A$R SUBTYPE-SELECTIVE PYRAZOLOQUINOLINONES WITH IMPROVED METABOLIC STABILITY AND ENHANCED BIOAVAILABILITY

Part 2

PROCESS DEVELOPMENT OF α2/3-GABA$_A$R SUBTYPE-SELECTIVE IMIDAZODIAZEPINES: HZ-166 AND KRM-II-81

Part 3

PROCESS DEVELOPMENT OF α5-GABA$_A$R SUBTYPE-SELECTIVE IMIDAZODIAZEPINES: MIDD0301 AND GL-II-73

by

Daniel E. Knutson

The University of Wisconsin-Milwaukee, 2020
Under the Supervision of Professor James M. Cook

Abstract-Part 1

Examination of recent reports indicate that α6β2/3γ2 GABA$_A$R selective ligands may be important for the treatment of trigeminal orofacial pain and neuropsychiatric disorders with sensori-motor gating deficits. Based on 3 functionally α6β2/3γ2 GABA$_A$R selective pyrazoloquinolinones, 49 novel analogs were synthesized and their *in vitro* metabolic stability and cytotoxicity, as well as their *in vivo* pharmacokinetics, basic behavioral pharmacology, and

effects on locomotion were investigated. Incorporation of deuterium into the methoxy substituents of the ligands increased their duration of action via improved metabolic stability and bioavailability, while their selectivity for the $GABA_AR$ α6 subtype was retained. The deuterated pyrazoloquinolinone **DK-I-56-1** (**8b**) was identified as the lead compound with a substantially improved pharmacokinetic profile. The ligands allosterically modulated diazepam insensitive α6β2/3γ2 $GABA_ARs$ and were functionally silent at diazepam sensitive α1β2/3γ2 $GABA_ARs$, thus no sedation was detected. In addition, these analogs were not cytotoxic, which rendered them interesting candidates for treatment of CNS disorders mediated by $GABA_AR$ α6β2/3γ2 subtypes. Recently, the $GABA_AR$ α+β- binding site was discovered along with the first α6-$GABA_AR$ subtype-selective ligand, **PZ-II-029** (**8a**) and later, **LAU463** (**8n**). Subsequent research led to the development of the lead deuterated pyrazoloquinolinones, **DK-I-56-1** (**8b**), **DK-I-58-1** (**8o**) and **DK-II-58-1** (**13h**) which have been shown to exhibit functional selectivity for α6-$GABA_ARs$ with increased metabolic stability and enhanced bioavailability.

The pursuit of further improvements to the bioavailability of these α6-selective ligands led to the exploration of fluorinated substituents (trifluoromethoxy) as an alternative tactic to limit O-demethylation *in vivo* of the methoxy groups of these lead ligands **DK-I-56-1** (**8b**) and **DK-I-58-1** (**8o**).

Herein, the comparative *in vivo* and *in vitro* effects of deuteration versus fluorination of these pyrazoloquinolinones is reported. While the strategy of deuteration and fluorination both increased metabolic stability in HLM and MLM, the pharmacokinetic effect on plasma, brain, liver and kidney exposure was dramatically different. Additionally, the fluorinated analogs exhibited a slightly increased cytotoxic effect *in vitro* on liver and kidney cell lines. Efficacy

and functional selectivity for the α6+β3- interface (PQ Site) of α6-$GABA_A$Rs was reduced for the fluorinated analogs in comparison to the deuterated ligands, as was as the binding affinity at the Bz site (α+γ- interface). In summary, the deuteration strategy proved superior to fluorination of these pyrazoloquinolinones in terms of maintaining α6-selectivity while enhancing the bioavailability and drugability of these α6-$GABA_A$R ligands without detrimental effects. Finally, a more water-soluble phosphoric acid prodrug of **DK-I-58-1** (**8o**) was also synthesized.

Part 2

The need for improved medications for the treatment of epilepsy and chronic pain is essential. Epileptic patients typically take multiple antiepileptic drugs without complete seizure freedom. The (5-(8-ethynyl-6-(pyridin-2-yl)-4*H*-benzo[*f*]imidazole[1,5-α][1,4]diazepin-3-yl) oxazole (**KRM-II-81**) is a lead compound in a series of ligands designed as positive allosteric modulators (PAMs) of α2/3-containing $GABA_A$ receptors. Ligand **KRM-II-81** produced broad-based anticonvulsant efficacy in rodent models used to predict antiepileptic efficacy in patients and provides a wider margin over motoric side effects than that of other $GABA_A$ receptor PAMs. The present series of experiments was designed to fill key missing gaps in prior preclinical assessments to assess whether **KRM-II-81** could be further differentiated from non-selective $GABA_A$ receptor PAMs using the anticonvulsant diazepam (DZP) as a comparator. In multiple chemical seizure provocation models in mice, **KRM-II-81** was either equally or more efficacious than that of DZP. In addition, **KRM-II-81** but not DZP blocks the development of seizure sensitivity to the chemical convulsants cocaine and pentylenetetrazol. This antiepileptogenic effect is considered the holy grail of antiepileptic treatment. These and previous data have placed **KRM-II-81** into consideration for clinical development requiring the manufacture of kilogram amounts of GMP material. We describe here a novel synthetic route amenable to kilogram quantity production. The new biological and chemical data provide key steps forward in the development of **KRM-II-81** for patients who continue to suffer from pharmacoresistent epilepsy.

Part 3

MIDD0301 ((*R*)-8-bromo-6-(2-fluorophenyl)-4-methyl-4*H*-benzo[*f*]imidazo[1,5-*a*][1,4]diazepine-3-carboxylic acid) is a novel oral drug under development for the treatment of asthma, which targets peripheral α5-$GABA_A$Rs found in airway smooth muscle (ASM) and reduces lung inflammation. Because of the promising results of **MIDD0301** as an asthma therapy devoid of negative side effects, the need for clinical development was of interest. Consequently, the development of a synthetic procedure amenable to the GMP manufacture of kilograms quantities of **MIDD0301** was required to improve upon the discovery route. Described herein is an improved and novel synthetic route amenable to the production of kilogram quantities of **MIDD0301**.

Over the last 15 years worldwide life expectancy increased by 5 years jumping from 66 years to 71 years. With progress in science, medicine, and care one tends to live longer. Such extended life expectancy is still associated with age-related changes, including in the brain. The aging brain goes through various changes that can be called morphomolecular senescence. Overall, the brain volume changes, neuronal activity is modified, and plasticity of the cells diminishes, sometimes leading to neuronal atrophy and death. Altogether, these changes contribute to the emergence of cognitive decline where upon an efficient treatment is still not available. Many studies in the context of cognitive decline focused on pathological aging, targeting beta-amyloid in Alzheimer's disease, for example. However, beta-amyloid plaques are also present in healthy adults and treatments targeting plaques have failed to improve cognitive functions. In order to improve the quality of life of aging populations, it is crucial to focus on the development of novel therapies targeting different systems altered during aging, such as the

GABAergic system. In previous studies it has been shown that positive allosteric modulators (PAM) acting at α5-containing $GABA_A$ receptors improve cognitive performances, and that these α5-$GABA_A$ receptors are implicated in dendritic growth of pyramidal neurons. Here, we hypothesized that targeting the α5-$GABA_A$ receptors could contribute to the reduction of cognitive decline, directly through activity of the receptors, and indirectly by increasing neuronal morphology. Using primary neuronal culture and chronic treatment in mice, it was demonstrated that an α5-PAM (**GL-II-73**) increased dendritic length, spine count and spine density in brain regions involved in cognitive processes (prefrontal cortex and hippocampus). The pro-cognitive efficacy of the α5-PAM, **GL-II-73** was confirmed and the washout period diminished the precognitive effects without altering the effect on neuronal morphology. Future studies will be needed to investigate what downstream mechanisms are responsible for the neurotrophic effect of the α5-PAM (**GL-II-73**). These results and previous data have placed **GL-II-73** into consideration for clinical development requiring a route to manufacture of kilogram amounts of GMP material. Described herein is a novel synthetic route amenable to kilogram quantity production.

TO

my daughter Lauren Rose Knutson

To God be the Glory!

"I Can Do All Things Through Christ Who Strengthens Me"- Philippians 4:13

TABLE OF CONTENTS

LIST OF FIGURES xxvi

LIST OF TABLES xxxv

LIST OF SCHEMES xl

LIST OF ABBREVIATIONS xlii

ACKNOWLEDGEMENTS xlvi

General Introduction 1

Chapter 1: Design and Synthesis of α6-GABA$_A$R Subtype-Selective Pyrazoloquinolinones with Improved Metabolic Stability and Enhanced Bioavailability 5

1.1. Introduction to α6-GABA$_A$R Subtype-Selective Pyrazoloquinolinones[2] 5

1.2. *In vivo* Activity of α6-GABA$_A$R Subtype-Selective Pyrazoloquinolinones in Disease Models 12

1.2.1. Treatment of Migraine Using α6-GABA$_A$R Subtype-Selective PQ's (with Dr. LC Chiou: Taiwan) [46, 47] 12

1.2.2. Treatment of the Development of Trigeminal Neuropathic Pain Using α6-GABA$_A$R Subtype-Selective PQ's (with Dr. Miroslav M. Savić: Serbia) [48, 49] ... 16

1.2.3. Treatment of Sensorimotor Gating Deficits in Neuropsychiatric Disorders Using α6-GABA$_A$R Subtype-Selective PQ's (with Dr. LC Chiou: Taiwan) [50, 51] 20

1.2.4. Attempted Treatment of the Symptoms of Alcoholism in Baboons Using α6-GABA$_A$R Subtype-Selective PQ's (with Dr. Elise Weerts: Johns Hopkins University School of Medicine) 23

1.3. Dosage Form Strategies to Improve the Bioavailability of α6-GABA$_A$R Subtype-Selective Pyrazoloquinolinones 24

1.3.1. Prodrug Strategy 24

1.3.2. Nanoemulsion Strategy[68] 25

1.4. Synthesis of α6-GABA$_A$R Subtype-Selective Pyrazoloquinolinones 27

1.5. The Chemistry of Selected Reactions for the Synthesis of Pyrazoloquinolinones 38

1.5.1. Preparation of Aryl Hydrazines by the Reduction of Diazonium Intermediates .. 38

1.5.2. Preparation of 4-Oxo-1,4-dihydro-quinolines Using the Gould's Jacobs Cyclization 39

1.5.3. Preparation of 4-Chloro-quinolines Using a Catalytic Vilsmeier Chlorination 41

1.5.4. Preparation of Pyrazoloquinolinones Using 4-Chloro-quinolines and Phenyl-hydrazines 44

1.5.5. Preparation of the Prodrug Analogs 45

1.6. Metabolic Stability with Human Liver (HLM) and Mouse Liver (MLM) Microsomes with Revathi Kodali 48
1.7. Metabolite Study with Revathi Kodali 57
1.8. Study of $GABA_AR$ α6β3γ2 Subtype Efficacy and Selectivity with Dr. Margot Ernst and Dr. Janet Fisher[2, 79, 80] 60
1.9. PDSP Receptor Study with Dr. Bryan Roth 71
1.10. Study of Solubility and cLogP 73
1.11. Study of Potential Cytotoxicity in HEK293 (Kidney) cells and HEPG2 (Liver) cells with Dr. Michael Rajesh Stephen and Dr. Alexander Arnold 74
1.12. Study of the Lack of Motor Impairment on the Rotarod with Nicholas Zahn 75
1.13. Pharmacokinetic Study with Dr. Miroslav M. Savić 76
1.14. Pharmacokinetic Study of DK-I-56-1 (8b) via a Nanoemulsion with Dr. Miroslav M. Savic and Dr. Snežana D. Savić [68] 87
1.15. *In Vivo* behavioral studies on 8b versus the control compound 8m 91
1.16. *In Vivo* hyperlocomotor response studies on 8b versus the control compound 8m 92
1.17. Spontaneous Locomotor Activity α6-$GABA_AR$ Subtype-Selective Ligands 94
1.18. Discussion and Conclusions of α6-$GABA_AR$ Subtype-Selective Ligands 96
1.19. Experimental Section for α6-$GABA_AR$ Subtype-Selective Ligands 101
1.19.1. General Procedures for Chemistry 101
1.19.1.1. *N*-(4-Hydroxyphenyl)acetamide (2a) 102
1.19.1.2. *N*-(3-Hydroxyphenyl)acetamide (2b) 102
1.19.1.3. *N*-(2-Hydroxyphenyl)acetamide (2c) 103
1.19.1.4. *N*-(4-Methoxy-d_3-phenyl)acetamide (3a) 104
1.19.1.5. *N*-(3-Methoxy-d_3-phenyl)acetamide (3b) 104
1.19.1.6. *N*-(2-Methoxy-d_3-phenyl)acetamide (3c) 105
1.19.1.7. 4-Methoxy-d_3-phenylhydrazine (4a) 106
1.19.1.8. 3-Methoxy-d_3-phenylhydrazine (4b) 107
1.19.1.9. 2-Methoxy-d_3-phenylhydrazine (4c) 108
1.19.1.10. 4-Methoxy-d_3-aniline (5a) 109
1.19.1.11. 3-Methoxy-d_3-aniline (5b) 109
1.19.1.12. Ethyl 6-methoxy-d_3-4-oxo-1,4-dihydroquinoline-3-carboxylate (6a) 110
1.19.1.13. Ethyl 7-methoxy-d_3-4-oxo-1,4-dihydroquinoline-3-carboxylate (6b) 110
1.19.1.14. Ethyl 6-chloro-4-oxo-1,4-dihydroquinoline-3-carboxylate (6c) 111

1.19.1.15. Ethyl 7-bromo-4-oxo-1,4-dihydroquinoline-3-carboxylate (6d) 112
1.19.1.16. Ethyl 7-methoxy-4-oxo-1,4-dihydrquinoline-3-carboxylate (6e) 112
1.19.1.17. Ethyl 7-methoxy-4-oxo-1,4-dihydro-1,6-naphthyridine-3-carboxylate (6f)..... 113
1.19.1.18. Ethyl 7-methoxy-8-methyl-4-oxo-1,4-dihydroquinoline-3-carboxylate (6g)..... 114
1.19.1.19. Ethyl 6-bromo-8-fluoro-4-oxo-1,4-dihydroquinoline-3-carboxylate (6h)..... 114
1.19.1.20. Ethyl 4-oxo-7-(trifluoromethyl)-1,4-dihydroquinoline-3-carboxylate (6i) 115
1.19.1.21. Ethyl 4-chloro-6-methoxy-d_3-quinoline-3-carboxylate (7a)..... 116
1.19.1.22. Ethyl 4-chloro-7-methoxy-d_3-quinoline-3-carboxylate (7b)..... 116
1.19.1.23. Ethyl 4,6-dichloroquinoline-3-carboxylate (7c) 117
1.19.1.24. Ethyl 7-bromo-4-chloroquinoline-3-carboxylate (7d) 118
1.19.1.25. Ethyl 4-chloro-7-methoxyquinoline-3-carboxylate (7e)..... 119
1.19.1.26. Ethyl 4-chloro-7-methoxy-1,6-napththyridine-3-carboxylate (7f) 120
1.19.1.27. Ethyl 4-chloro-7-methoxy-8-methyl quinoline-3-carboxylate (7g)..... 121
1.19.1.28. Ethyl 6-bromo-4-chloro-8-fluoroquinoline-3-carboxylate (7h)..... 121
1.19.1.29. Ethyl 4-chloro-7-(trifluoromethyl)quinoline-3-carboxylate (7i) 122
1.19.1.30. 7-Methoxy-2-(4-methoxyphenyl)-2,5-dihydro-3*H*-pyrazolo[4,3-*c*]quinolin-3-one (PZ-II-029, 8a) 123
1.19.1.31. 7-Methoxy-2-(4-methoxy-d_3-phenyl)-2,5-dihydro-3*H*-pyrazolo[4,3-*c*]quinolin-3-one (DK-I-56-1, 8b) 124
1.19.1.32. 7-Methoxy-d_3-2-(4-methoxyphenyl)-2,5-dihydro-3*H*-pyrazolo[4,3-*c*]quinolin-3-one (RV-I-029, 8c)..... 125
1.19.1.33. 7-Methoxy-d_3-2-(4-methoxy-d_3-phenyl)-2,5-dihydro-3*H*-pyrazolo[4,3-*c*]quinolin-3-one (DK-I-60-3, 8d)..... 125
1.19.1.34. 7-Methoxy-d_3-2-(3-methoxy-d_3-phenyl)-2,5-dihydro-3*H*-pyrazolo[4,3-*c*]quinolin-3-one (DK-I-94-1, 8e)..... 126
1.19.1.35. 7-Methoxy-d_3-2-(2-methoxy-d_3-phenyl)-2,5-dihydro-3*H*-pyrazolo[4,3-*c*]quinolin-3-one (DK-I-90-1, 8f) 127
1.19.1.36. 7-Methoxy-2-(3-methoxy-d_3-phenyl)-2,5-dihydro-3*H*-pyrazolo[4,3-*c*]quinolin-3-one (DK-II-69-1, 8g)..... 127
1.19.1.37. 7-Methoxy-2-(2-methoxy-d_3-phenyl)-2,5-dihydro-3*H*-pyrazolo[4,3-*c*]quinolin-3-one (DK-I-88-1, 8h)..... 128
1.19.1.38. 8-Chloro-2-(3-methoxyphenyl)-2,5-dihydro-3*H*-pyrazolo[4,3-*c*]quinolin-3-one (LAU 159, 8i)..... 129
1.19.1.39. 8-Chloro-2-(3-methoxy-d_3-phenyl)-2,5-dihydro-3*H*-pyrazolo[4,3-*c*]quinolin-3-one (DK-I-59-1, 8j)..... 130

1.19.1.40. 8-Chloro-2-(4-methoxyphenyl)-2,5-dihydro-3*H*-pyrazolo[4,3-*c*]quinolin-3-one (PZ-II-028, 8k) 130
1.19.1.41. 8-Chloro-2-(4-methoxy-d_3-phenyl)-2,5-dihydro-3*H*-pyrazolo[4,3-*c*]quinolin-3-one (DK-I-93-1, 8l) 131
1.19.1.42. 8-Chloro-2-(2-methoxy-d_3-phenyl)-2,5-dihydro-3*H*-pyrazolo[4,3-*c*]quinolin-3-one (DK-I-87-1, 8m) 132
1.19.1.43. 7-Bromo-2-(4-methoxyphenyl)-2,5-dihydro-3*H*-pyrazolo[4,3-*c*]quinolin-3-one (LAU463, 8n) 132
1.19.1.44. 7-Bromo-2-(4-methoxy-d_3-phenyl)-2,5-dihydro-3*H*-pyrazolo[4,3-*c*]quinolin-3-one (DK-I-58-1, 8o) 133
1.19.1.45. 7-Bromo-2-(3-methoxy-d_3-phenyl)-2,5-dihydro-3*H*-pyrazolo[4,3-*c*]quinolin-3-one (DK-I-92-1, 8p) 134
1.19.1.46. 7-Bromo-2-(2-methoxy-d_3-phenyl)-2,5-dihydro-3*H*-pyrazolo[4,3-*c*]quinolin-3-one (DK-I-89-1, 8q) 134
1.19.1.47. 8-Methoxy-d_3-2-(4-methoxy-d_3-phenyl)-2,5-dihydro-3*H*-pyrazolo[4,3-*c*]quinolin-3-one (DK-I-95-3, 8r) 135
1.19.1.48. 8-Methoxy-d_3-2-(3-methoxy-d_3-phenyl)-2,5-dihydro-3*H*-pyrazolo[4,3-*c*]quinolin-3-one (DK-I-92-1, 8s) 136
1.19.1.49. 8-Methoxy-d_3-2-(2-methoxy-d_3-phenyl)-2,5-dihydro-3*H*-pyrazolo[4,3-*c*]quinolin-3-one (DK-I-98-1, 8t) 137
1.19.1.50. 2-Methoxy-d_3-5-nitropyridine (10) 137
1.19.1.51. 5-Amino-2-methoxy-d_3-pyridine (11a) 138
1.19.1.52. 5-Hydrazinyl-2-methoxy-d_3-pyridine (12a) 139
1.19.1.53. 5-Hydrazinyl-2-methoxypyridine (12b) 140
1.19.1.54. 7-Methoxy-2-(6-methoxypyridin-3-yl)-2,5-dihydro-3*H*-pyrazolo[4,3-*c*]quinolin-3-one (DK-II-13-1, 13a) 141
1.19.1.55. 7-Methoxy-2-(6-methoxy-d_3-pyridin-3-yl)-2,5-dihydro-3*H*-pyrazolo[4,3-*c*]quinolin-3-one (DK-II-60-1, 13b) 141
1.19.1.56. 7-Methoxy-d_3-2-(6-methoxypyridin-3-yl)-2,5-dihydro-3*H*-pyrazolo[4,3-*c*]quinolin-3-one (DK-I-86-1, 13c) 142
1.19.1.57. 7-Methoxy-d_3-2-(6-methoxy-d_3-pyridin-3-yl)-2,5-dihydro-3*H*-pyrazolo[4,3-*c*]quinolin-3-one (DK-III-6-1, 13d) 143
1.19.1.58. 8-Chloro-2-(6-methoxypyridin-3-yl)-2,5-dihydro-3*H*-pyrazolo[4,3-*c*]quinolin-3-one (DK-II-18-1, 13e) 144
1.19.1.59. 8-Chloro-2-(6-methoxy-d_3-pyridin-3-yl)-2,5-dihydro-3*H*-pyrazolo[4,3-*c*]quinolin-3-one (DK-II-59-1, 13f) 144

1.19.1.60. 7-Bromo-2-(6-methoxypyridin-3-yl)-2,5-dihydro-3*H*-pyrazolo[4,3-*c*]quinolin-3-one (DK-II-48-1, 13g) 145
1.19.1.61. 7-Bromo-2-(6-methoxy-d_3-pyridin-3-yl)-2,5-dihydro-3*H*-pyrazolo[4,3-*c*]quinolin-3-one (DK-II-58-1, 13h) 146
1.19.1.62. 7-Methoxy-2-(4-methoxyphenyl)-2,5-dihydro-3*H*-pyrazolo[4,3-*c*][1,6]naphthyridin-3-one (CW-03-030, 13i) 147
1.19.1.63. 7-Methoxy-d_3-2-phenyl-2,5-dihydro-3*H*-pyrazolo[4,3-*c*]quinolin-3-one (RV-I-037, 14a) 147
1.19.1.64. 7-Methoxy-2-(4-methoxyphenyl)-6-methyl-2,5-dihydro-3*H*-pyrazolo[4,3-*c*]quinolin-3-one (CW-02-073, 14b) 148
1.19.1.65. 7-Methoxy-6-methyl-2-phenyl-2,5-dihydro-3*H*-pyrazolo[4,3-*c*]quinolin-3-one (CW-02-078, 14c) 149
1.19.1.66. 7-Methoxy-6-methyl-2-(4-(trifluoromethoxy)phenyl)-2,5-dihydro-3*H*-pyrazolo[4,3-*c*]quinolin-3-one (CW-02-079, 14d) 150
1.19.1.67. 7-Methoxy-2-(4-(trifluoromethoxy)phenyl)-2,5-dihydro-3*H*-pyrazolo[4,3-*c*]quinolin-3-one (CW-02-082, 14e) 150
1.19.1.68. 8-Bromo-6-fluoro-2-(4-methoxyphenyl)-2,5-dihydro-3*H*-pyrazolo[4,3-*c*]quinolin-3-one (MM-I-03, 14f) 151
1.19.1.69. 8-Bromo-2-(4-chlorophenyl)-6-fluoro-2,5-dihydro-3*H*-pyrazolo[4,3-*c*]quinolin-3-one (MM-I-13, 14g) 152
1.19.1.70. 8-Bromo-6-fluoro-2-(4-fluorophenyl)-2,5-dihydro-3*H*-pyrazolo[4,3-*c*]quinolin-3-one (MM-I-18, 14h) 153
1.19.1.71. 2-(4-Methoxyphenyl)-7-(trifluoromethyl)-2,5-dihydro-3*H*-pyrazolo[4,3-c]quinolin-3-one (MM-I-06, 14i) 153
1.19.1.72. 2-(4-Chlorophenyl)-7-(trifluoromethyl)-2,5-dihydro-3*H*-pyrazolo[4,3-*c*]quinolin-3-one (MM-I-08, 14j) 154
1.19.1.73. 2-(4-Nitrophenyl)-7-(trifluoromethyl)-2,5-dihydro-3H-pyrazolo[4,3-c]quinolin-3-one (MM-I-09, 14k) 155
1.19.1.74. 2-(4-(Trifluoromethoxy)phenyl)-7-(trifluoromethyl)-2,5-dihydro-3H-pyrazolo[4,3-c]quinolin-3-one (MM-I-10, 14l) 155
1.19.1.75. 2-(4-Fluorophenyl)-7-(trifluoromethyl)-2,5-dihydro-3H-pyrazolo[4,3-c]quinolin-3-one (MM-I-11, 14m) 156
1.19.1.76. 2-(3-Methoxyphenyl)-7-(trifluoromethyl)-2,5-dihydro-3*H*-pyrazolo[4,3-*c*]quinolin-3-one (MM-I-12, 14n) 157
1.19.1.77. 7-(Methoxy-d_3)-2-(4-(trifluoromethoxy)phenyl)-2,5-dihydro-3*H*-pyrazolo[4,3-*c*]quinolin-3-one (DK-IV-20-1, 14o) 158

1.19.1.78. 7-Bromo-2-(4-(trifluoromethoxy)phenyl)-2,5-dihydro-3*H*-pyrazolo[4,3-*c*]quinolin-3-one (DK-IV-22-1, 14p) 158
1.19.1.79. 8-Chloro-2-(4-(trifluoromethoxy)phenyl)-2,5-dihydro-3*H*-pyrazolo[4,3-*c*]quinolin-3-one (DK-IV-23-1, 14q) 159
1.19.1.80. 2-(4-(Methoxy-d_3)phenyl)-7-(trifluoromethyl)-2,5-dihydro-3*H*-pyrazolo[4,3-*c*]quinolin-3-one (DK-IV-19-1, 14r) 160
1.19.1.81. 7-Bromo-2-(4-bromophenyl)-2,5-dihydro-3*H*-pyrazolo[4,3-*c*]quinolin-3-one (DK-V-67-1, 14s) 161
1.19.1.82. 2-(4-Bromophenyl)-7-methoxy-2,5-dihydro-3*H*-pyrazolo[4,3-*c*]quinolin-3-one (DK-V-68-1, 14t) 162
1.19.1.83. Chloromethyl chlorosulfate solution in DCM (15) 162
1.19.1.84. Di-*tert*-butyl (chloromethyl) phosphate (16) 163
1.19.1.85. (7-Bromo-2-(4-methoxyphenyl)-3-oxo-2,3-dihydro-5*H*-pyrazolo[4,3-*c*]quinolin-5-yl)methyl di-*tert*-butyl phosphate (DK-VI-9-3, 17a) 164
1.19.1.86. (7-Bromo-2-(4-methoxyphenyl)-3-oxo-2,3-dihydro-5*H*-pyrazolo[4,3-*c*]quinolin-5-yl)methyl dihydrogen phosphate (DK-VI-15-1, 18a) 165
1.19.2. General Procedures for the Biological Assays 166
1.19.2.1. Microsomal stability assay with Revathi Kodali 166
1.19.2.2. Metabolite Assay with Revathi Kodali 167
1.19.2.3. Electrophysiological Assay with *Xenopus oocytes* with Dr. Margot Ernst 167
1.19.2.4. Electrophysiological recordings from transfected HEK-293T cells with Dr. Janet Fisher 169
1.19.2.5. PDSP Compound-induced Radioligand Displacement Assays for 46 Receptors with Dr. Bryan Roth 170
1.19.2.6. Solubility Assay and cLogP 170
1.19.2.7. Cytotoxicity Assay with Dr. Michael Rajesh Stephen 171
1.19.2.8. Rotarod Motor Impairment Study with Nick Zahn and Coworkers 171
1.19.2.9. Pharmacokinetic Assay with Dr. Miroslav Savić and coworkers 172
1.19.2.10. Pharmacokinetic Cassette Study with Dr. Miroslav Savić and coworkers 173
1.19.2.11. Battery of Behavioral Tests in Rats with Miroslav M. Savić, Snežana D. Savić and coworkers 175
1.19.2.12. Spontaneous Locomotor Activity Assay in Rats and Mice with Miroslav M. Savić and coworkers 177
1.19.2.13. Statistical analysis with Miroslav M. Savić and coworkers 177

1.19.2.14. Spontaneous Locomotor Activity (Time Mobile and Distance Travelled) with Miroslav M. Savić and coworkers 178
1.20. Structural Analysis of α6-$GABA_AR$ Subtype-selective Pyrazoloquinolinones by NMR Spectroscopy 180
1.20.1. NMR Spectra of DK-I-56-1 (8b) 183
1.20.1.1. ^{1}H NMR of DK-I-56-1 (8b) 183
1.20.1.2. ^{13}C NMR of DK-I-56-1 (8b) 184
1.20.1.3. COSY Spectrum of DK-I-56-1 (8b) 185
1.20.1.4. ^{1}H-^{13}C-HSQC Spectrum of DK-I-56-1 (8b) 186
1.20.1.5. ^{1}H-^{13}C-HMBC Spectrum of DK-I-56-1 (8b) 187
1.20.2. NMR Spectra of DK-I-58-1 (8o) 188
1.20.2.1. ^{1}H NMR of DK-I-58-1 (8o) 188
1.20.2.2. ^{13}C NMR of DK-I-58-1 (8o) 189
1.20.2.3. COSY Spectrum of DK-I-58-1 (8o) 190
1.20.2.4. ^{1}H-^{13}C-HSQC Spectrum of DK-I-58-1 (8o) 191
1.20.2.5. ^{1}H-^{13}C-HMBC Spectrum of DK-I-58-1 (8o) 192
1.20.3. NMR Spectra of DK-I-59-1 (8j) 193
1.20.3.1. ^{1}H NMR of DK-I-59-1 (8j) 193
1.20.3.2. ^{13}C NMR of DK-I-59-1 (8j) 194
1.20.3.3. COSY Spectrum of DK-I-59-1 (8j) 195
1.20.3.4. ^{1}H-^{13}C-HSQC Spectrum of DK-I-59-1 (8j) 196
1.20.3.5. ^{1}H-^{13}C-HMBC Spectrum of DK-I-59-1 (8j) 197
1.20.4. NMR Spectra of DK-I-87-1 (8m) 198
1.20.4.1. ^{1}H NMR of DK-I-87-1 (8m) 198
1.20.4.2. ^{13}C NMR of DK-I-87-1 (8m) 199
1.20.4.3. COSY Spectrum of DK-I-87-1 (8m) 200
1.20.4.4. ^{1}H-^{13}C-HSQC Spectrum of DK-I-87-1 (8m) 201
1.20.4.5. ^{1}H-^{13}C-HMBC Spectrum of DK-I-87-1 (8m) 202
1.20.5. NMR Spectra of DK-I-86-1 (13c) 203
1.20.5.1. ^{1}H NMR of DK-I-86-1 (13c) 203
1.20.5.2. ^{13}C NMR of DK-I-86-1 (13c) 204
1.20.5.3. COSY Spectrum of DK-I-86-1 (13c) 205
1.20.5.4. ^{1}H-^{13}C-HSQC Spectrum of DK-I-86-1 (13c) 206

1.20.5.5. ^{1}H-^{13}C-HMBC Spectrum of DK-I-86-1 (13c) 207
1.20.6. NMR Spectra of DK-II-58-1 (13h) 208
1.20.6.1. ^{1}H NMR of DK-II-58-1 (13h) 208
1.20.6.2. ^{13}C NMR of DK-II-58-1 (13h) 209
1.20.6.3. COSY Spectrum of DK-II-58-1 (13h) 210
1.20.6.4. ^{1}H-^{13}C-HSQC Spectrum of DK-II-58-1 (13h) 211
1.20.6.5. ^{1}H-^{13}C-HMBC Spectrum of DK-II-58-1 (13h) 212
1.20.7. NMR Spectra of DK-VI-9-3 (17a) 213
1.20.7.1. ^{1}H NMR of DK-VI-9-3 (17a) 213
1.20.7.2. ^{13}C NMR of DK-VI-9-3 (17a) 214
1.20.7.3. ^{1}H-^{13}C-HSQC Spectrum of DK-VI-9-3 (17a) 215
1.20.7.4. ^{1}H-^{13}C-HMBC Spectrum of DK-VI-9-3 (17a) 216
1.20.8. NMR Spectra of DK-VI-15-1 (18a) 217
1.20.8.1. ^{1}H NMR of DK-VI-15-1 (18a) 217
1.20.8.2. ^{13}C NMR of DK-VI-15-1 (18a) 218
1.20.8.3. COSY Spectrum of DK-VI-15-1 (18a) 219
1.20.8.4. ^{1}H-^{13}C-HSQC Spectrum of DK-VI-15-1 (18a) 220
1.20.8.5. ^{1}H-^{13}C-HMBC Spectrum of DK-VI-15-1 (18a) 221
1.21. X-ray Structures of Lead Pyrazoloquinolinones 222
1.21.1. Ortep Representation of the X-Ray Structure of DK-I-56-1 (8b) 222
1.21.2. Ortep Representation of the X-Ray Structure of MM-I-10 (14l) 223
1.21.3. Ortep Representation of the X-Ray Structure of DK-IV-20-1 (14o) 223
1.21.4. Ortep Representation of the X-Ray Structure of DK-IV-22-1 (14p) 224
1.21.5. Ortep Representation of the X-Ray Structure of DK-IV-19-1 (14r) 224
1.22. Molecular Modeling of Lead Pyrazoloquinolinones at the Bz site / α1+γ2-Interface 225
1.22.1. Modeling of Diazepam 227
1.22.2. Modeling of Flumazenil 228
1.22.3. Modeling of DK-I-56-1 (8b) 229
1.22.4. Modeling of DK-I-86-1 (13c) 230
1.22.5. Modeling of DK-IV-20-1 (14o) 231
1.22.6. Modeling of DK-I-58-1 (8o) 232
1.22.7. Modeling of DK-II-58-1 (13h) 233

1.22.8. Modeling of DK-IV-22-1 (14p) 234
1.22.9. Modeling of DK-IV-19-1 (14r) 235
1.22.10. Modeling of MM-I-10 (14l) 236
1.22.11. Modeling of DK-I-59-1 (8j) 237
1.22.12. Modeling of DK-I-87-1 (8m) 238
Chapter 2: Process Development of α2/3-GABA$_A$R Subtype-selective Imidazodiazepines: HZ-166 and KRM-II-81 239
2.1. Introduction to α2/3-GABA$_A$R Subtype-selective Imidazodiazepines 239
2.2. Discussion and Conclusions of Anticonvulsant, KRM-II-81, which Produces Novel, Non-diazepam-like Antiepileptogentic Effects 244
2.3. Improved Synthesis of α2/3-GABA$_A$R Subtype-selective Imidazodiazepines .. 250
2.4. Experimental Section for α2/3-GABA$_A$R Subtype-selective Imidazodiazepines 266
2.4.1. General Procedures for the Synthesis of KRM-II-81 266
2.4.1.1. *N*-(4-Bromo-2-picolinoylphenyl)-2-chloroacetamide (2c) 266
2.4.1.2. 7-Bromo-5-(pyridin-2-yl)-1,3-dihydro-2*H*-benzo[*e*][1,4]diazepin-2-one (3) 267
2.4.1.3. Ethyl 8-bromo-6-(pyridin-2-yl)-4*H*-benzo[*f*]imidazo[1,5-*a*][1,4]diazepine-3-carboxylate (4) 268
2.4.1.4. Ethyl 6-(pyridin-2-yl)-8-((triisopropylsilyl)ethynyl)-4*H*-benzo[*f*]imidazo[1,5-*a*][1,4]diazepine-3-carboxylate (5b) 269
2.4.1.5. Ethyl 8-ethynyl-6-(pyridin-2-yl)-4*H*-benzo[*f*]imidazo[1,5-*a*][1,4]diazepine-3-carboxylate [HZ-166, 6] 271
2.4.1.6. 8-Ethynyl-6-(pyridin-2-yl)-4*H*-benzo[*f*]imidazo[1,5-*a*][1,4]diazepine-3-carbaldehyde (7) with Dr. Guanguan Li[136] 272
2.4.1.7. 5-(8-Ethynyl-6-(pyridin-2-yl)-4*H*-benzo[*f*]imidazo[1,5-*a*][1,4]diazepin-3-yl)oxazole [KRM-II-81, 8] with Dr. Guanguan Li[136] 273
2.4.2. General Procedures for the Biological Assays of KRM-II-81 (8) 274
2.4.2.1. Compounds 274
2.4.2.2. Rodent assays 275
2.4.2.3. Chemical Convulsant Studies. 275
2.4.2.4. Seizure Kindling 276
2.5. Structural Analysis of α2/3-GABA$_A$R Subtype-selective Imidazodiazepines by NMR Spectroscopy 277
2.5.1. NMR Spectra of HZ-166 278
2.4.1.1 ^{1}H NMR of HZ-166 278

2.4.1.2. ^{13}C NMR of HZ-166 279
2.4.1.3. COSY Spectrum of HZ-166 280
2.4.1.4. ^{1}H-^{13}C-HSQC Spectrum of HZ-166 281
2.4.1.5. ^{1}H-^{13}C-HMBC Spectrum HZ-166 282
2.4.1.6. ROESY Spectrum of HZ-166 283
Chapter 3: Process Development of α5-GABA$_A$R Subtype-selective Imidazodiazepines: MIDD0301 and GL-II-73 284
3.1. Introduction to α5-GABA$_A$R Subtype-selective Imidazodiazepines 284
3.1.1. MIDD0301 Introduction 286
3.1.2. GL-II-73 Introduction[191] 287
3.2. Application of α5-GABA$_A$R Subtype-Selective Imidazodiazepines in Disease Models 292
3.2.1. Treatment of Asthma Using the α5-GABA$_A$R Subtype-Selective Ligand MIDD0301 (with Dr. Alexander Arnold: UW-Milwaukee)[252] 292
3.2.2. Investigation of the Treatment of Diseases Using the α5-GABA$_A$R Subtype-Selective Ligand MP-III-022 292
3.2.3. Treatment of Memory Loss Using the α5-GABA$_A$R Subtype-Selective Ligand GL-II-73 (with Dr. Thomas Prevot and Dr. Etienne Sibille: CAMH)[191, 254] 293
3.2.3.1. Pharmacokinetic Profile of GL-II-73 in Rats and Mice 296
3.2.3.2. Pharmacokinetic Profile of GL-II-73 in Dogs 301
3.2.3.3. Receptor Subtype Selectivity Profile of GL-II-73: Electrophysiological Assay with Dr. Janet Fisher 305
3.2.3.4. Cytotoxicity with Dr. Michael Rajesh Stephen 307
3.2.3.4.1. CYP3A4 Inhibition Assay 309
3.2.3.5. Metabolic Stability Assays for GL-II-73 with Revathi Kodali 310
3.2.3.5.1. Metabolic Stability of GL-II-73 (Human and Mouse Liver Microsomal Assays) 310
3.2.3.5.2. Metabolic Stability of GL-II-73 (Dog and Monkey Liver Microsomal Assay) 311
3.2.3.6. Locomotion and Motor Coordination in Mice 311
3.2.3.6.1. Home Cage Locomotor Activity (with the Sibille/Banasr Group) – Distance Travelled 311
3.2.3.6.2. Spontaneous Locomotor Activity (with the Savić Group) 313
3.2.3.6.3. Locomotor Coordination - Rotarod Experiments using GL-II-73 315
3.2.3.6.4. Rotarod Experiments – Replicated by the Savić Group 316

3.2.3.6.5. Dose Escalation Study – Locomotor Assessment in Dogs 318
3.2.3.7. Cognition: The Influence of GL-II-73 on Working Memory in the Y Maze 321
3.2.3.8. Antidepressant Predictability (Forced Swim Test – FST) 327
3.2.3.9. Anxiolytic Predictability (Elevated Plus Maze – EPM) 328
3.2.3.10. Cognition / Chronic Administration Studies (Young Mice) with Drs. Thomas Prevot and Etienne Sibille..... 331
3.2.3.11. Cognition –Anxiety / Chronic Studies in Old Animals. 332
3.2.3.12. Blockade Experiments Using the Bz Antagonist, Flumazenil..... 337
3.2.3.13. The Acute and Chronic Treatment in Depression Models (Unpredictable Chronic Mild Stress)..... 340
3.2.3.14. The Effect of Chronic Administration in Old Mice: Behavior and Dendritic Morphology..... 349
3.2.3.15. Growth of Dendrites and Spines in Neuronal Cell Culture 361
3.2.3.16. Promoting the Generation of New Neurons in the Hippocampus 363
3.2.3.17. A Test of Abuse Liability 367
3.2.3.18. First in Human – Electrophysiology on Human Pyramidal Neurons from the Hippocampus (*ex vivo*) 368
3.3. Discussion and Conclusions of GL-II-73 369
3.4. Improved Synthesis of α5-$GABA_AR$ Subtype-selective Imidazodiazepines..... 373
3.4.1. Improvement of a Large-scale Process for MIDD0301..... 375
3.4.2. Experimental Section for MIDD0301..... 388
3.4.2.1. General Procedures for the Synthesis of MIDD0301 388
3.4.2.1.1. N-Carboxy-D-Alanine Anhydride [MIDD0101]..... 388
3.4.2.1.2. (*R*)-7-Bromo-5-(2-fluorophenyl)-3-methyl-1,3-dihydro-2*H*-benzo[*e*][1,4]diazepin-2-one [MIDD0002]..... 389
3.4.2.1.3. Ethyl (*R*)-8-bromo-6-(2-fluorophenyl)-4-methyl-4*H*-benzo[*f*]imidazo[1,5-*a*][1,4]diazepine-3-carboxylate [MIDD0003]..... 390
3.4.2.1.4. (*R*)-8-Bromo-6-(2-fluorophenyl)-4-methyl-4*H*-benzo[*f*]imidazo[1,5-*a*][1,4]diazepine-3-carboxylic acid [MIDD0301]..... 392
3.4.2.1.5. (9*H*-Fluoren-9-yl)methyl (*R*)-(1-chloro-1-oxopropan-2-yl)carbamate [MIDD0001] 393
3.4.2.1.6. (*R*)-7-Bromo-5-(2-fluorophenyl)-3-methyl-1,3-dihydro-2*H*-benzo[*e*][1,4]diazepin-2-one [MIDD0002]: FMOC route (Table 23, entry 5).. 394
3.4.2.1.7. *tert*-Butyl (*R*)-(1-((4-bromo-2-(2-fluorobenzoyl)phenyl)amino)-1-oxopropan-2-yl)carbamate [MIDD0002B]: DCC Route..... 397

3.4.2.1.8. *tert*-Butyl (*R*)-(1-((4-bromo-2-(2-fluorobenzoyl)phenyl)amino)-1-oxopropan-2-yl)carbamate [MIDD0002B]: EDC Route (Table 22, entry 10) 400
3.4.2.1.9. *tert*-Butyl (*R*)-(1-((4-bromo-2-(2-fluorobenzoyl)phenyl)amino)-1-oxopropan-2-yl)carbamate [MIDD0002B]: Mixed Anhydride Route (Table 22, entry 12) ... 401
3.4.2.1.10. (*R*)-7-Bromo-5-(2-fluorophenyl)-3-methyl-1,3-dihydro-2*H*-benzo[*e*][1,4]diazepin-2-one [MIDD0002]: BOC route (Table 23, entry 2) 402
3.4.2.2. General Analytical Procedures for the Synthesis of MIDD0301 406
3.4.2.2.1. Method 1: HPLC-PDA-MS Reverse Phase Method for Overall Purity Determination of MIDD0002 and MIDD0003 406
3.4.2.2.2. Method 2: HPLC-PDA-MS Reverse Phase Method for Overall Purity Determination of MIDD0301 407
3.4.2.2.3. Method 3: HPLC-DAD Normal Phase Method for the Determination of Optical Purity of *R*-MIDD0002 407
3.4.2.2.4. Method 4: HPLC-DAD Normal Phase Method for the Determination of Optical Purity of *R*-MIDD0003 408
3.4.2.2.5. Method 5: HPLC-DAD Normal Method for Determination of Optical Purity of R-MIDD0301 408
3.4.2.3. Chromatograms (HPLC Purity, Optical Purity and Mass Spectra) from the Synthesis of MIDD0301 410
3.4.2.3.1. HPLC Chromatogram (245 nm) for MIDD0002 (Method 1) 410
3.4.2.3.2. UV Spectrum of MIDD0002 and Impurities 410
3.4.2.3.3. Mass Spectrum of MIDD0002 (RT 8.07 min, Method 1) (97.28 % absolute area) 411
3.4.2.3.4. Mass Spectrum of Impurities (MIDD0002a) for Synthesis of MIDD0002: (RT 9.04, Method 1) (0.76 % absolute area) 411
3.4.2.3.5. Mass Spectrum of MIDD0002b Impurity (RT 9.37 min, Method 1) (1.96 % absolute area) 412
3.4.2.3.6. Optical Purity of MIDD0002 Determined by HPLC (Method 3) 412
3.4.2.3.7. HPLC Chromatogram (245 nm) for MIDD0003 (Method 1) 413
3.4.2.3.8. UV Spectrum of MIDD0003 and Impurities 413
3.4.2.3.9. Mass spectrum of MIDD0003 (RT 9.55 min, Method 1) (97.20 % absolute area) 414
3.4.2.3.10. Mass Spectrum of MIDD0003a (RT 11.24 min, Method 1) (1.36 % absolute area) 414
3.4.2.3.11. Mass spectrum of MIDD0003b (RT 11.54 min, method 1) (1.44 % absolute area) 415

3.4.2.3.12. Optical Purity of MIDD0003 Determined by HPLC (Method 4) 99.0 % EE..... 415
3.4.2.3.13. HPLC Chromatogram (245 nm) for MIDD0301 (Method 2)..... 416
3.4.2.3.14. UV Spectrum of MIDD0301 and Impurities..... 416
3.4.2.3.15. Mass Spectrum of MIDD0301 (RT 3.10 min, Method 2) (98.86 % absolute area) 417
3.4.2.3.16. Mass Spectrum MIDD0301a (RT 3.72 min, Method 2) (1.14 % absolute area) 417
3.4.2.3.17. Optical purity of MIDD0301 determined by HPLC (Method 5) >99.2 % EE ... 418
3.4.3. Large-scale Process Improvement of GL-II-73..... 419
3.4.4. Experimental Section for GL-II-73 and MP-III-022..... 422
3.4.4.1. General Procedures for the Synthesis of GL-II-73 and MP-III-022..... 422
3.4.4.1.1. N-Carboxy-D-Alanine Anhydride [MIDD0101]..... 422
3.4.4.1.2. (*R*)-7-Bromo-5-(2-fluorophenyl)-3-methyl-1,3-dihydro-2H-benzo[*e*][1,4]diazepin-2-one [MIDD0002]..... 423
3.4.4.1.3. Ethyl (*R*)-8-bromo-6-(2-fluorophenyl)-4-methyl-4*H*-benzo[f]imidazo[1,5-*a*][1,4]diazepine-3-carboxylate [MIDD0003]..... 425
3.4.4.1.4. Ethyl (*R*)-6-(2-fluorophenyl)-4-methyl-8-((triisopropylsilyl)ethynyl)-4*H*-benzo[*f*]imidazo [1,5-*a*][1,4]diazepine-3-carboxylate [SH-053-2'F-R-CH_3-TIPS] 426
3.4.4.1.5. Ethyl (*R*)-8-ethynyl-6-(2-fluorophenyl)-4-methyl-4*H*-benzo[*f*]imidazo[1,5-*a*][1,4]diazepine-3-carboxylate [SH-053-2'F-R-CH_3] 428
3.4.4.1.6. (*R*)-8-Bromo-6-(2-fluorophenyl)-4-methyl-4*H*-benzo[*f*]imidazo[1,5-*a*][1,4]diazepine-3-carboxylic acid [SH-053-2'F-R-CH_3-acid] 429
3.4.4.1.7. (*R*)-8-Ethynyl-6-(2-fluorophenyl)-*N,N*,4-trimethyl-4*H*-benzo[*f*]imidazo[1,5-*a*][1,4]diazepine-3-carboxamide [GL-II-73]..... 430
3.4.4.1.8. (*R*)-8-Ethynyl-6-(2-fluorophenyl)-*N*,4-dimethyl-4*H*-benzo[*f*]imidazo[1,5-*a*][1,4]diazepine-3-carboxamide [MP-III-022]..... 432
3.4.4.2. General Analytical Procedures for of GL-II-73 and MP-III-022..... 433
3.5. Structural Analysis of α5-$GABA_A$R Subtype-selective Imidazodiazepines by NMR Spectroscopy..... 434
3.5.1. NMR Spectra of MIDD0101..... 434
3.5.1.1. ^{1}H NMR Spectrum of MIDD0101..... 434
3.5.1.2. ^{13}C NMR Spectrum of MIDD0101..... 435
3.5.1.3. COSY Spectrum of MIDD0101..... 436
3.5.1.4. ^{1}H-^{13}C-HSQC Spectrum of MIDD0101..... 437
3.5.1.5. ^{1}H-^{13}C-HMBC Spectrum of MIDD0101..... 438

3.5.2. NMR Spectra of MIDD0002 439
3.5.2.1. ^{1}H NMR Spectrum of MIDD0002 439
3.5.2.2. ^{13}C NMR Spectrum of MIDD0002 440
3.5.2.3. COSY Spectrum of MIDD0002 441
3.5.2.4. ^{1}H-^{13}C-HSQC Spectrum of MIDD0002 442
3.5.2.5. ^{1}H-^{13}C-HMBC Spectrum of MIDD0002 443
3.5.2.6. ROESY Spectrum of MIDD0002 444
3.5.3. NMR Spectra of MIDD0003 445
3.5.3.1. ^{1}H NMR Spectrum of MIDD0003 445
3.5.3.2. ^{13}C NMR Spectrum of MIDD0003 446
3.5.3.3. COSY Spectrum of MIDD0003 447
3.5.3.4. ^{1}H-^{13}C-HSQC Spectrum of MIDD0003 448
3.5.3.5. ^{1}H-^{13}C-HMBC Spectrum of MIDD0003 449
3.5.3.6. ROESY Spectrum of MIDD0003 450
3.5.4. NMR Spectra of MIDD0301 451
3.5.4.1. ^{1}H NMR Spectrum of MIDD0301 451
3.5.4.2. ^{13}C NMR Spectrum of MIDD0301 452
3.5.4.3. COSY Spectrum of MIDD0301 453
3.5.4.4. ^{1}H-^{13}C-HSQC Spectrum of MIDD0301 454
3.5.4.5. ^{1}H-^{13}C-HMBC Spectrum of MIDD0301 455
3.5.4.6. ROESY Spectrum of MIDD0301 456
3.5.5. NMR Spectra of SH-053-2'F-R-CH3 457
3.5.5.1. ^{1}H NMR of SH-053-2'F-R-CH3 457
3.5.5.2. ^{13}C NMR of SH-053-2'F-R-CH3 458
3.5.5.3. COSY Spectrum of SH-053-2'F-R-CH3 459
3.5.5.4. ^{1}H-^{13}C-HSQC Spectrum of SH-053-2'F-R-CH3 460
3.5.5.5. ^{1}H-^{13}C-HMBC Spectrum of SH-053-2'F-R-CH3 461
3.5.5.6. ROESY Spectrum of SH-053-2'F-R-CH3 462
3.5.6. NMR Spectra of SH-053-2'F-R-CH3-acid 463
3.5.6.1. ^{1}H NMR of SH-053-2'F-R-CH3-acid 463
3.5.6.2. ^{13}C NMR of SH-053-2'F-R-CH3-acid 464
3.5.6.3. COSY Spectrum of SH-053-2'F-R-CH3-acid 465

3.5.6.4. ^{1}H-^{13}C-HSQC Spectrum of SH-053-2'F-R-CH3-acid 466
3.5.6.5. ^{1}H-^{13}C-HMBC Spectrum of SH-053-2'F-R-CH3-acid 467
3.5.6.6. ROESY Spectrum of SH-053-2'F-R-CH3-acid 468
3.5.7. NMR Spectra of GL-II-73 469
3.5.7.1. ^{1}H NMR of GL-II-73 469
3.5.7.2. ^{13}C NMR of GL-II-73 470
3.5.7.3. COSY Spectrum of GL-II-73 471
3.5.7.4. ^{1}H-^{13}C-HSQC Spectrum of GL-II-73 472
3.5.7.5. ^{1}H-^{13}C-HMBC Spectrum of GL-II-73 473
3.5.7.6. ROESY Spectrum of GL-II-73 474
3.5.8. NMR Spectra of MP-III-022 475
3.5.8.1. ^{1}H NMR of MP-III-022 475
3.5.8.2. ^{13}C NMR of MP-III-022 476
3.5.8.3. COSY Spectrum of MP-III-022 477
3.5.8.4. ^{1}H-^{13}C-HSQC Spectrum of MP-III-022 478
3.5.8.5. ^{1}H-^{13}C-HMBC Spectrum of MP-III-022 479
3.5.8.6. ROESY Spectrum of MP-III-022 480
3.6. Determination of Conformational Isomers by NMR Spectroscopy of MIDD0002, MIDD0003, GL-II-73 and MP-III-022 481
3.6.1. Analysis of Conformational Isomers of MIDD0002 Using NMR Spectroscopy 484
3.6.2. Analysis of Conformational Isomers of MIDD0003 Using NMR Spectroscopy 486
3.6.3. Analysis of Conformational Isomers of GL-II-73 Using NMR Spectroscopy ... 490
3.6.4. Analysis of Conformational Isomers of MP-III-022 Using NMR Spectroscopy 493
3.6.5. Coalescence Study of MIDD0003 Conformational Isomers Using NMR Spectroscopy 496
References 498
Appendix 542
4.1. X-ray Crystal Data for Selected Pyrazoloquinolinones (PQ's) 542
4.1.1. X-ray Crystal Data for DK-I-56-1 (8b) 542
4.1.2. X-ray Crystal Data for MM-I-10 (14l) 553
4.1.3. X-ray Crystal Data for DK-IV-20-1 (14o) 560
4.1.4. X-ray Crystal Data for DK-IV-22-1 (14p) 572
4.1.5. X-ray Crystal Data for DK-IV-19-1 (14r) 580

4.2. Primary Radioligand Binding Assays for Synthesized Pyrazoloquinolinones (PQ's) 587
4.3. Secondary Radioligand Binding Assays for Synthesized PQ's 595
4.4. Primary Radioligand Binding Assays for Additional PQ Analogs 597
4.5. Secondary Radioligand Binding Assays for Additional PQ Analogs 605
4.6. Cytotoxicity Studies for Selected Pyrazoloquinolinones 610
4.7. Motor Coordination Studies of Selected Pyrazoloquinolinones on the Rotorod 613
4.8. Human Liver (HLM) and Mouse Liver (MLM) Microsomal Assays for PQ's .. 615
4.9. Poster Presentations 813
4.9.1. Novel Deuterated GABAAR-α6 Subtype Selective Ligands with Improved Metabolic Stability. Targeting Trigeminal Orofacial Pain, Neuropsychiatric Disorders, & Depression[305] 813
4.9.2. Novel Deuterated GABAAR-α6 Subtype Selective Ligands with Improved Metabolic Stability and Enhanced Bioavailability Targeting Trigeminal Orofacial Pain, Neuropsychiatric Disorders, and Depression[306] 814
4.9.3. Design and Synthesis of Novel Deuterated GABAAR-a6 Subtype Selective Ligands with Improved Metabolic Stability and Enhanced Bioavailability[307] ... 815
4.9.4. Prevention of Trigeminal Neuropathic Pain Development in Rats Using Novel Deuterated GABAAR-α6 Subtype Selective Ligands[308] 816
4.9.5. Treatment of Sensorimotor Gating Deficits in Neuropsychiatric Disorders Using Deuterated α6-$GABA_AR$ Subtype Selective Ligands[51] 817
4.9.6. Combatting the Opioid and Benzodiazepine Epidemic by the Synthesis of Novel Safer Drugs Designed to be Functionally Selective for α5- or α6-containing $GABA_A$ Receptors[309] 818
4.9.7. A Comparative Study of Deuteration Versus Fluorination of α6-$GABA_AR$ Subtype- Selective Ligands as Strategies to Enhance Bioavailability, and their Impact on the Pharmacokinetic Profiles and α6-$GABA_AR$ Functional Selectivity[80] 819
4.10. Poster Presentations by Collaborators with Our Group 820
4.10.1. The Search for Water Soluble α6 Bz/$GABA_A$ Receptor Subtype Selective Ligands in Order to Determine Their *in vivo* Activity 820
4.10.2. Nanonization of New Patent Protected Substances—Carrier Selection of Preclinical Research: Physiochemical and *in vivo* Behavioral Characterization 821
4.10.3. Nanosuspensions of Novel Deuterated Pyrazoloquinolinones Ligand (DK-I-56-1): Lyophilization Procedure Development Through Cryoprotectant Selection and Stability Study 822

4.10.4. A Novel Drug Target for Migraine: the $GABA_A$ Receptor α6 Subtype in Trigeminal Ganglia 823
4.10.5. Studies Using von Frey Testing and Hot Plate Technique to Evaluate the Effects of Opioids, Novel Benzodiazepine-like Drugs, and Their Combinations 824
4.10.6. Role of GABA-A Receptor Subtypes in Respiratory Depression Induced by Benzodiazepines Alone and Combined With Fentanyl 825
4.10.7. Imbalanced Tonic Inhibition Between the Cortex and Thalamus Causes Epileptiform Activity in Mice Model of Angelman Syndrome 826
4.10.8. The Effect of a GABAA α5 Agonist on Mechanical Allodynia Following Nerve Injury 827
4.10.9. Pro-cognitive and Neurotrophic Effects of a Novel Molecule Enhancing α5-GABA-A Receptor Function in Adult or Aged Mice 828
CURRICULUM VITAE 829

LIST OF FIGURES

Figure 1: The Opioid and Benzodiazepine Epidemic on the Rise 1

Figure 2: The $GABA_A$ Receptor[a] 2

Figure 3: Associated Effects of the α1-6 $GABA_AR$ Subtypes[a] 3

Figure 4: Three Minute Thesis (3MT) Slide. Combatting the Opioid and Benzodiazepine Epidemic by the Design and Synthesis of Novel Safer Drugs 4

Figure 5: The $GABA_AR$ α6β3γ2 Subtype 6

Figure 6: Lead α6-Selective Ligands of this Work 8

Figure 7: General Strategy of this Work to Improve the Bioavailability of the Ligands 11

Figure 8: Schematic Diagrams Illustrating the Trigemino-vascular System (TGVS) and Proposed Changes in Trigeminal Ganglia after Migraine Induced by Repeated Nitroglycerin (NTG) Injections.[47] 13

Figure 9: Treatment with α6$GABA_AR$ PAMs Suppressed Migraine-like Response Induced by Repeated NTG Administration, and this Effect Can Be Reversed by Furosemide, an α6$GABA_AR$ Antagonist.[47] 14

Figure 10: Repeated Administration of DK-I-56-1, but not Compound 6, Exhibited Migraine Prophylaxis Effect without Drug Dependence Potential.[47] 15

Figure 11: Trigeminal Nerve System[a] 17

Figure 12: Prophylactic Antinociceptive Effect of DK-I-56-1 (**8b**).[48] 18

Figure 13: Comparative Effect of DK-I-56-1 (**8b**) vs. DK-I-87-1 (**8m**) in the Trigeminal Orofacial Pain Model.[48] 19

Figure 14: α6-$GABA_AR$ PAMs Rescue Meth-Induced PPI Disruptions.[51] 21

Figure 15: A Hypothesis for How α6-$GABA_AR$ PAMs Affect Canonical Cerebellar Circuits and Lead to the Restoration of PPI with Dr. LC Chiou.[50, 51] 22

Figure 16: The Effect on Alcoholism in Baboons Using the α6-$GABA_AR$ PAM (PZ-II-029, **8a**) with Dr. Elise Weerts[a] 23

Figure 17: Visual Exhibit of Formulations[68] 26

Figure 18: Aryl Hydrazines Synthesized in this Work[2] 38

Figure 19: Synthesized 4-Oxo-1,4-dihydro-quinolines in this Work[2] 41

Figure 20: Synthesized 4-Chloro-quinolines in this Work[2] 42

Figure 21: Impact of the Iodide Additive on the Stability of a Halomethyl Phosphate Reagent[66] 46

Figure 22: Metabolic Stability, Comparison of **PZ-II-029 (8a)** Related Ligands[2, 79] 54

Figure 23: Metabolic Stability, Comparison of **LAU 159 (8i)** Related Ligands[2, 79] 55

Figure 24: Metabolic Stability, Comparison of **LAU 463 (8n)** Related Ligands[2, 79] 56

Figure 25: Metabolic Stability, Comparison of **MM-I-06 (14i)** Related Ligands[2, 79] 56

Figure 26: $GABA_AR$ α6β3γ2 Subtype Selectivity of the Lead Ligands: **PZ-II-029 (8a)**, **LAU 463 (8n)** and **LAU 159 (8i)**[2] 63

Figure 27: The Effect of Substituting OCD_3 for OCH_3 Groups on the Lead Ligands on $GABA_AR$ α6β3γ2 Subtype Activity[2] 64

Figure 28: $GABA_AR$ α6β3γ2 Subtype Selectivity of the Ligands: **DK-I-56-1 (8b)** and **DK-I-87-1 (8m)**[48] 65

Figure 29: $GABA_AR$ α6β3γ2 Subtype Activity of the "D-ring" *ortho*-OCD_3 Isomer **DK-I-87-1 (8m)**[2] 66

Figure 30: $GABA_AR$ α6β3γ2 Subtype Selectivity of the Lead Ligands: **DK-I-58-1 (8n)** and **DK-II-58-1 (13h)**[79, 80] 67

Figure 31: The Effect of N-hetero Substitution onto the "A-ring" or "D-ring" of the Lead Ligands on $GABA_AR$ α6β3γ2 Subtype Activity[2] 68

Figure 32: $GABA_AR$ α6β3γ2 Subtype Selectivity of the N-hetero Ligand **DK-I-86-1 (13c)**[2] 69

Figure 33: The Effect of CF_3 Substitution onto the "A-ring" or OCF_3 Substitution onto the "D-ring" of the Lead Ligands on $GABA_AR$ α6β3γ2 Subtype Activity[79, 80] 70

Figure 34: Pharmacokinetic Profiles of Selected Ligands[2] 80

Figure 35: Pharmacokinetic Profiles in Plasma and Brain Following Oral Gavage (PO) or IV Administration of **8a** (**A**) and **8b** (**B**) with Dr. Miroslav M. Savić[2] 81

Figure 36: Pharmacokinetic Profiles (Plasma, Brain, Liver and Kidney) of **PZ-II-029 (8a)** Related Ligands: **DK-I-56-1 (8b)**, **RV-I-029 (8c)** and **DK-I-60-3 (8d)**.[79, 80] 82

Figure 37: Pharmacokinetic Profiles (Plasma, Brain, Liver and Kidney) of **PZ-II-029 (8a)** Related Ligands: **DK-I-56-1 (8b)**, **DK-I-86-1 (13c)** and **DK-IV-20-1 (14o)**.[79, 80] 83

Figure 38: Pharmacokinetic Profiles (Plasma, Brain, Liver and Kidney) of **LAU 463 (8n)** Related Ligands: **DK-I-58-1 (8o)**, **DK-II-58-1 (13h)** and **DK-IV-22-1 (14p)**.[79, 80] 84

Figure 39: Pharmacokinetic Profiles (Plasma, Brain, Liver and Kidney) of **LAU 159 (8i)** Related Ligands: **DK-I-59-1 (8j)** and **DK-I-87-1 (8m)**.[79, 80] 85

Figure 40: Pharmacokinetic Profiles (Plasma, Brain, Liver and Kidney) of **MM-I-06 (14i)** Related Ligands: **DK-IV-19-1 (14r)** and **MM-I-10 (14l)**.[79, 80] 86

Figure 41: Pharmacokinetic Profiles (Plasma, Brain, Liver and Kidney) of **DK-I-56-1 (8b)** Comparing Nanosuspension, Suspension and Solution Vehicles[68] 90

Figure 42: The Measurement of Influences on Locomotor Activity of Rats (Left Panels: A,C,E) or Mice (Right Panels: B,D,F)[2] 93

Figure 43: The Influence of 14 Pyrazoloquinolinones, Diazepam, GL-II-73 and Solvent on Total Distance Travelled and Time Mobile 95

Figure 44: ^{1}HNMR Spectrum Exhibiting Proton Position of **LAU 463 (8n)** in DMSO-*d*$_6$..... 180

Figure 45: COSY Spectrum Exhibiting Correlation of Protons of **LAU 463 (8n)** in DMSO-*d*$_6$ 181

Figure 46: HMBC Spectrum Exhibiting Exchangeable of Proton Position of **LAU 463 (8n)**. 182

Figure 47: The $GABA_AR$ α2/3β3γ2 Subtypes 240

Figure 48: The Lead α2/3-Selective Ligands of this Work 241

Figure 49: Effects of Vehicle, Diazepam (1.0 mg/kg), or KRM-II-81 (30 mg/kg) on Seizure Sensitization (kindling) Due to Every Other Day Dosing with PTZ (45 mg/kg). 247

Figure 50: Effects of Vehicle, Diazepam (1.0 mg/kg), or KRM-II-81 (30 mg/kg) on Seizure Sensitization (kindling) Due to Daily Dosing with COC (60 mg/kg). 249

Figure 51: NMR Evidence (^{1}H-^{15}N-HMBC) for Imidate Impurity **3c** (in DMSO-*d*$_6$) 255

Figure 52: HZ-166 3D Structure Exhibiting Pseudo Axial (H19) and Pseudo Equatorial (H29) Protons 277

Figure 53: The $GABA_AR$ α5β3γ2 Subtype..... 285

Figure 54: Lead α5-Selective Ligands of this Work..... 286

Figure 55: Concentration-time PK Profile of GL-II-73 with Dr. Miroslav M. Savić[254]..... 297

Figure 56: Plasma and Brain Concentration–Time Profiles of GL-II-73 Administered IV in Rats with Dr. Miroslav M. Savić 299

Figure 57: Plasma and Brain Concentration–Time Profiles of GL-II-73 Administered PO in Rats with Dr. Miroslav M. Savić 300

Figure 58: Plasma Concentration of GL-II-73 after PO Administration in Dogs 301

Figure 59: Plasma Concentration of GL-II-73 after IV Administration in Dogs 302

Figure 60: Plasma Concentration of GL-II-73 after PO Administration in Dogs 302

Figure 61: Average Plasma Concentration of GL-II-73 for Both Routes..... 303

Figure 62: Electrophysiological Response to GL-II-73 in Mammalian HEK Cells Transfected with α1, α2, α3, α4 α5, or α6 $GABA_A$ Receptors, and at α1β3γ2 and α1β3δ When Exposed to GABA 305

Figure 63: Approximated Electrophysiological Responses Elicited by the Estimated Free Brain Concentrations and Presented on the Concentration-Response Curves of GL-II-73 306

Figure 64: CYP3A4 Inhibition with 10 or 50 μM of GL-II-73 309

Figure 65: Effect of GL-II-73 on Locomotor Activity 312

Figure 66: Effect of Multiple Drugs on Locomotor Activity 313

Figure 67: Effect of Multiple Drugs on Locomotor Activity, per Bin of 5 Minutes..... 314

Figure 68: Effect of GL-II-73 on Locomotor Coordination 315

Figure 69: The Influence of the Increasing Doses of GL-II-73 on the Rotarod Performance.. 316

Figure 70: Influence of Increasing Doses of GL-II-73 and Diazepam on Locomotor Coordination 317

Figure 71: Heart Rate in Dogs after PO Administration of GL-II-73 318

Figure 72: Respiration Rate in Dogs after PO administration of GL-II-73 318

Figure 73: Body Temperature in Dogs after PO Administration..... 319

Figure 74: Average Activity in Dogs after PO Administration..... 319

Figure 75: Average Time at Each Activity Level per Dose 320

Figure 76: The Effect of GL-II-73 on Working Memory in Young Mice Exposed to Chronic Stress with Thomas Prevot and Etienne Sibille 322

Figure 77: The Effects of GL-II-73 on Working Memory at 50mg/kg with Drs.Thomas Prevot and Etienne Sibille 323

Figure 78: The Effect of the Racemic Mixture of GL-II-73 and GL-I-54 on Working Memory with Drs. Thomas Prevot and Etienne Sibille 324

Figure 79: The Effect of GL-II-73 on Working Memory in Old Mice with Drs. Thomas Prevot and Etienne Sibille 325

Figure 80: The Effect of GL-II-73 on Time Spent Immobile in the Forced Swim Test (FST) 327

Figure 81: The Effect of GL-II-73 on the Time Spent in the Open Arms of the Elevated Plus Maze 329

Figure 82: Time Spent in the Shelter, Overnight, Before, During and after a Light Challenge 330

Figure 83: The Effect of Chronic Administration of GL-II-73 on Working Memory 331

Figure 84: Distance Travelled after Chronic Administration of GL-II-73 in Old Mice. 332

Figure 85: Potential Anxiolytic Effect of GL-II-73 in Old Mice, When Given Chronically ... 333

Figure 86: Time Spent in the Shelter Before, During and After a Light Challenge 334

Figure 87: Residual Avoidance 335

Figure 88: The Effects of GLII-73 Administered Chronically, on Working Memory 336

Figure 89: Flumazenil Blocks the Effects of GL-II-73 in the Y-Maze 337

Figure 90: βCCt Blocks the Effects of GL-II-73 in the Y-Maze 338

Figure 91: XLI-093 Blocks the Effects of GL-II-73 in the Y-Maze 339

Figure 92: The Effect of GL-II-73 on Cognition in a UCMS Model 340

Figure 93: The Effect of GL-II-73 on Anxiety-like Behavior in a UCMS Model 341

Figure 94: The Effect of GL-II-73 on Immobility in the FST, in a UCMS Model 341

Figure 95: The Effect of Chronic GL-II-73 on Alternation in the YMaze, After UCMS Exposure 342

Figure 96: The Representative Images of CA1 Pyramidal Cells Between Groups (Control, UCMS, and UCMS+GL). 343

Figure 97: Comparison of Total Dendritic Lengths of Pyramidal Cells Between Groups. 345

Figure 98: Comparison of Overall Spine Density of Pyramidal Cells Between Groups 345

Figure 99: Representative Images of PFC Pyramidal Cells Between Groups (Control, UCMS, and UCMS+GL). 346

Figure 100: Comparison of Total Dendritic Lengths of Pyramidal Cells Between Groups. 347

Figure 101: Comparison of Total Spine Counts of Pyramidal Cells Between Groups..... 347

Figure 102: Comparison of Overall Spine Density of Pyramidal Cells Between Groups..... 348

Figure 103: The Chronic Administration of GL-II-73 in the Drinking Water Reverses Age-related Cognitive Deficits 349

Figure 104: Representative Images of PFC Pyramidal Cells Between Groups..... 352

Figure 105: Comparison of Total Dendritic Lengths of Pyramidal Cells Between Groups. 353

Figure 106: Comparison of Total Spine Counts of Pyramidal Cells Between Groups. 354

Figure 107: Comparison of Overall Spine Density of Pyramidal Cells Between Groups..... 355

Figure 108: Representative Images of HPC Principle Cells Between Groups 356

Figure 109: Comparison of Total Dendritic Lengths of Pyramidal Cells Between Groups. 357

Figure 110: Comparison of Total Spine Counts of Pyramidal Cells Between Groups 357

Figure 111: Comparison of Overall Spine Density of Pyramidal Cells Between Groups..... 358

Figure 112: Alternation Rate in Old Mice Receiving GL-II-73 Chronically, with or without a Washout Period 359

Figure 113: Comparison of Overall Spine Density of Pyramidal Cells Between Groups. 360

Figure 114: Images of Neuronal Culture with vehicle or GL-II-73, and Characterization of Spine Density (C) and Intersection in a Sholl Analysis (B) 361

Figure 115: Images of Neuronal Culture Incubated with Vehicle (Left Panels) or GL-II-73 (Right Panels) 362

Figure 116: Experimental Design of the Administration of GL-II-73, Fluoxetine and Bromodeoxyuridine 365

Figure 117: Proliferation and Survival of New Neurons in the Hippocampus 366

Figure 118: Maturation of New Neurons in the Hippocampus 366

Figure 119: Water Versus GL-II-73 Consumption 367

Figure 120: GL-II-73 Contributes to Tonic Inhibition in Human and Mouse PyCs 369

Figure 121: ^{1}HNMR and ^{19}FNMR of MIDD0002 484

Figure 122: ^{13}CNMR Exhibiting C-F Coupling of MIDD0002 485

Figure 123: ^{13}CNMR Exhibiting C-F Coupling of MIDD0003 486

Figure 124: Comparison of MIDD0003 Conformers Using ^{1}HNMR & ^{19}FNMR. 487

Figure 125: Comparison of MIDD0003 Conformers Using COSY 488

Figure 126: Comparison of MIDD0003 Conformers Using ROESY 489

Figure 127: Comparison of GL-II-73 Conformers Using ^{1}HNMR and ^{19}FNMR Evidence. 490

Figure 128: Comparison of GL-II-73 Conformers Using COSY 491

Figure 129: Comparison of GL-II-73 Conformers Using ROESY 492

Figure 130: Comparison of MP-III-022 Conformers Using ^{1}HNMR and ^{19}FNMR. 493

Figure 131: Comparison of MP-III-022 Conformers Using COSY 494

Figure 132: Comparison of MP-III-022 Conformers Using NOESY..... 495

Figure 133: ^{1}HNMR Coalescence Study of MIDD0003 Conformers..... 496

Figure 134: ^{19}FNMR Coalescence Study of MIDD0003 Conformers 497

Figure 135: Cytotoxicity of Deuterated and N-Hetero PQ's on HEK293 (Kidney) Cells (Left Panels: A,C,E) and HEPG2 (Liver) Cells (Right Panels: B,D,F)[a]..... 611

Figure 136: Cytotoxicity of Fluorinated PQ's on HEK293 (Kidney) Cells (Panel A) and HEPG2 (Liver) Cells (Panel B)[a] 612

Figure 137: Effect of Deuterated and N-Hetero PQ Ligands on Motor Coordination[a] 613

Figure 138: Effect of Fluorinated PQ Ligands on Motor Coordination[a]..... 614

LIST OF TABLES

Table 1: Structures of Ligands Synthesized via the Chemistry in **Scheme 3**[2] 30

Table 2: Ligands Synthesized via the Chemistry in **Scheme 3**[2] 31

Table 3: Structures of Ligands Synthesized via the Chemistry in **Scheme 4** and **Scheme 5**[2] 33

Table 4: Ligands Synthesized via the Chemistry in **Scheme 4** and **Scheme 5**[2] 34

Table 5: Structures of Additional Ligands Synthesized via the Chemistry in **Scheme 6** 36

Table 6: Additional Ligands Synthesized via the Chemistry in **Scheme 6** 37

Table 7: Prodrug Route Optimization 47

Table 8: Metabolic Stability in the Presence of HLM and MLM[2] 49

Table 9: Solubility and cLogP of Compounds Indicating the Effect of Adding the Nitrogen Atom to the A- or D-Ring of PQ Ligands[a,2] 74

Table 10: Binding Assays, Cytotoxicity and cLogP of Deuterated vs. N-Hetero vs. Fluorinated PQ Analogs[2, 79, 80] 75

Table 11: The Influence of IP 10 mg kg^{-1} Doses of **8b** and **8m** on the Selected Parameters of the Grip Strength, Elevated Plus Maze, and Cued Water Maze[2] 92

Table 12: Effects of KRM-II-81 in Models Predicting Antiepileptic Efficacy in Patients[130] ... 242

Table 13: Comparative Efficacy of Diazepam and KRM-II-81 as Anticonvulsants Against Some Chemoconvulant Agents.[a] 245

Table 14: Copper-Free Sonogashira Coupling Trials[130] 262

Table 15: Pharmacokinetic Parameters in Mice and Rats Calculated for GL-II-73.[254] 296

Table 16: PK of GL-II-73 after IV or PO Administration in Rats with Dr. Miroslav M. Savić 298

Table 17: Plasma PK Parameter Summary for IV Dosing of GL-II-73 304

Table 18: Plasma PK Parameter Summary for PO Dosing 304

Table 19: Metabolic Stability of GL-II-73 and GL-I-54 in Human or Mouse Liver Microsomes 310

Table 20: Metabolic Stability of GL-II-73 in Dog and Monkey Liver Microsomes 311

Table 21: Brain and Plasma Concentrations After Chronic Administration of GL-II-73 332

Table 22: Amide Coupling Trials 378

Table 23: Benzodiazepine Cyclization Trials 381

Table 24: Crystal data and structure refinement for **DK-I-56-1 (8b)**. 542

Table 25: Atomic coordinates (x 10^4) and equivalent isotropic displacement parameters ($Å^2$x 10^3) for **DK-I-56-1 (8b)**. U(eq) is defined as one third of the trace of the orthogonalized U^{ij} tensor. 543

Table 26: Bond lengths [Å] and angles [°] for **DK-I-56-1 (8b)**. 545

Table 27: Anisotropic displacement parameters ($Å^2$x 10^3) for **DK-I-56-1 (8b)**. The anisotropic 548

Table 28: Hydrogen coordinates (x 10^4) and isotropic displacement parameters ($Å^2$x 10^3) for **DK-I-56-1 (8b)**. 550

Table 29: Torsion angles [°] for **DK-I-56-1 (8b)**. 551

Table 30: Hydrogen bonds for **DK-I-56-1 (8b)** [Å and °]. 552

Table 31: Crystal data and structure refinement for **MM-I-10 (14l)**. 553

Table 32: Atomic coordinates (x 10^4) and equivalent isotropic displacement parameters ($Å^2$x 10^3) for **MM-I-10 (14l)**. U(eq) is defined as one third of the trace of the orthogonalized U^{ij} tensor. 554

Table 33: Bond lengths [Å] and angles [°] for **MM-I-10 (14l)**. 555

Table 34: Anisotropic displacement parameters ($Å^2 x\ 10^3$) for **MM-I-10 (14l)**. The anisotropic 557

Table 35: Hydrogen coordinates (x 10^4) and isotropic displacement parameters ($Å^2 x\ 10^3$) for **MM-I-10 (14l)**. 558

Table 36: Torsion angles [°] for **MM-I-10 (14l)**. 559

Table 37: Hydrogen bonds for **MM-I-10 (14l)** [Å and °]. 559

Table 38: Crystal data and structure refinement for **DK-IV-20-1 (14o)**. 560

Table 39: Atomic coordinates (x 10^4) and equivalent isotropic displacement parameters ($Å^2 x\ 10^3$) for **DK-IV-20-1 (14o)**. U(eq) is defined as one third of the trace of the orthogonalized U^{ij} tensor. 561

Table 40: Bond lengths [Å] and angles [°] for **DK-IV-20-1 (14o)**. 563

Table 41: Anisotropic displacement parameters ($Å^2 x\ 10^3$)for **DK-IV-20-1 (14o)**. The anisotropic displacement factor exponent takes the form: $-2\pi^2[h^2 a^{*2} U^{11} + ... + 2\ h\ k\ a^*\ b^*\ U^{12}]$ 567

Table 42: Hydrogen coordinates (x 10^4) and isotropic displacement parameters ($Å^2 x\ 10^3$) for **DK-IV-20-1 (14o)**. 569

Table 43: Torsion angles [°] for **DK-IV-20-1 (14o)**. 570

Table 44: Hydrogen bonds for **DK-IV-20-1 (14o)** [Å and °]. 571

Table 45: Crystal data and structure refinement for **DK-IV-22-1 (14p)**. 572

Table 46: Atomic coordinates (x 10^4) and equivalent isotropic displacement parameters ($Å^2 x\ 10^3$) for **DK-IV-22-1 (14p)**. U(eq) is defined as one third of the trace of the orthogonalized U^{ij} tensor. 573

Table 47: Bond lengths [Å] and angles [°] for **DK-IV-22-1 (14p)**. 574

Table 48: Anisotropic displacement parameters ($Å^2 x\ 10^3$) for **DK-IV-22-1 (14p)**. The anisotropic displacement factor exponent takes the form: $-2\pi^2[h^2 a^{*2} U^{11} + ... + 2\ h\ k\ a^*\ b^*\ U^{12}]$ 576

Table 49: Hydrogen coordinates ($x\ 10^4$) and isotropic displacement parameters ($Å^2 x\ 10^3$) for **DK-IV-22-1 (14p)**. 577

Table 50: Torsion angles [°] for **DK-IV-22-1 (14p)**. 578

Table 51: Hydrogen bonds for **DK-IV-22-1 (14p)** [Å and °]. 579

Table 52: Crystal data and structure refinement for **DK-IV-19-1 (14r)**..... 580

Table 53: Atomic coordinates ($x\ 10^4$) and equivalent isotropic displacement parameters ($Å^2 x\ 10^3$) for **DK-IV-19-1 (14r)**. U(eq) is defined as one third of the trace of the orthogonalized U^{ij} tensor. 581

Table 54: Bond lengths [Å] and angles [°] for **DK-IV-19-1 (14r)**. 582

Table 55: Anisotropic displacement parameters ($Å^2 x\ 10^3$) for **DK-IV-19-1 (14r)**. The anisotropic displacement factor exponent takes the form: $-2\pi^2[h^2 a^{*2} U^{11} + ... + 2\ h\ k\ a^*\ b^*\ U^{12}]$ 584

Table 56: Hydrogen coordinates ($x\ 10^4$) and isotropic displacement parameters ($Å^2 x\ 10^3$) for **DK-IV-19-1 (14r)**. 585

Table 57: Torsion angles [°] for **DK-IV-19-1 (14r)**. 586

Table 58: Hydrogen bonds for **DK-IV-19-1 (14r)** [Å and °]. 586

Table 59: Primary Radioligand Binding Assays. Compound-induced radioligand displacement assays for 46 receptors, transporters and channels conducted by the National Institute of Medical

Health Psychoactive Drugs Screening Program (B. Roth et al., UNC, available at http://pdsp.med.unc.edu).[a] 587

Table 60: Secondary Radioligand Binding Assays. Binding affinity (Ki, nM) values obtained from non-linear regression of radioligand competition binding isotherms. Testing conducted by the National Institute of Medical Health Psychoactive Drugs Screening Program (B. Roth et al., UNC, available at http://pdsp.med.unc.edu).[a] 595

Table 61: Primary Radioligand Binding Assays for additional PQ ligands. Compound-induced radioligand displacement assays for 46 receptors, transporters and channels conducted by the National Institute of Medical Health Psychoactive Drugs Screening Program (B. Roth et al., UNC, available at http://pdsp.med.unc.edu).[a] 597

Table 62: Secondary Radioligand Binding Assays for Additional PQ Ligands. Binding affinity (Ki, nM) values obtained from non-linear regression of radioligand competition binding isotherms. Testing conducted by the National Institute of Medical Health Psychoactive Drugs Screening Program (B. Roth et al., UNC, available at http://pdsp.med.unc.edu).[a] 605

Table 63: Results of Cytotoxicity Studies on HEPG2 and HEK293 Cell Lines[a] 610

LIST OF SCHEMES

Scheme 1: Development of α6-Selective Ligands 8

Scheme 2: Prodrug Release Mechanism[52] 25

Scheme 3: Synthesis of Deuterated Analogs[2] 28

Scheme 4: Synthesis of "D-Ring" N-Hetero Analogs[2] 32

Scheme 5: Synthesis of "A-Ring" N-Hetero Analogs[2] 33

Scheme 6: Synthesis of Additional Analogs 35

Scheme 7: Proposed Aryl Hydrazine Formation by the Reduction of Diazonium Salts[a] 39

Scheme 8: Proposed Gould's Jacobs Cyclization Mechanism[77] 40

Scheme 9: Proposed Catalytic Vilsmeier Mechanism of Chlorination 43

Scheme 10: Proposed Mechanism of the Pyrazoloquinolinone Cyclization 44

Scheme 11: Prodrug Model Alkylation Reaction 45

Scheme 12: Prodrug Synthesis 47

Scheme 13: Metabolite Study. O-Demethylation of OCH_3 Versus OCD_3 by CYP_{450} Enzymes in HLM and MLM[2] 59

Scheme 14: Discovery Synthesis of KRM-II-81 251

Scheme 15: Proposed Route to Chloroacetamide (**2c**) Via Pyridium Salt (**2b**) 252

Scheme 16: Discovery Route to Benzodiazepine (**3**) with Imidate Impurity (**3c**) 253

Scheme 17: Proposed Imidate (**3c**) Formation Mechanism 254

Scheme 18: Hexamethylenetetramine-(HMTM)-based Cyclization Reaction 256

Scheme 19: Proposed Delépine Reaction Mechanism 257

Scheme 20: Synthetic Route to Imidazodiazepine **4** 258

Scheme 21: Proposed Mechanism for the Formation of the Imidazole Top 260

Scheme 22: Proposed Mechanism of the Copper-Free Sonogashira Cross Coupling 263

Scheme 23: Proposed Mechanism of the Cleavage of the TIPS Group 264

Scheme 24: Improved Large-Scale Synthesis of **HZ-166** 265

Scheme 25: Development of α5-Selective Ligand **MIDD0301** 287

Scheme 26: Development of α5-Selective Ligand **GL-II-73** 291

Scheme 27: Discovery Synthesis of **MIDD0301** 375

Scheme 28: Proposed Amide Coupling Mechanism 377

Scheme 29: FMOC Route to **MIDD0002** 379

Scheme 30: Proposed Racemization Mechanism of **MIDD0002** 380

Scheme 31: NCA Route to **MIDD0002** 382

Scheme 32: Synthesis of Imidazodiazepine **MIDD0003** 383

Scheme 33: Proposed Racemization Mechanism of **MIDD0003** 386

Scheme 34: Improved Large-Scale Synthesis of **MIDD0301** 387

Scheme 35: Discovery Synthesis of **GL-II-73** 419

Scheme 36: Improved **GL-II-73** Synthetic Scheme with 99%EE 421

Scheme 37: Synthesis of Optically Pure **MP-III-022** 421

LIST OF ABBREVIATIONS

ACh	acetylcholine
AHR	airway hyperresponsiveness
AP-4	4-Aminopyridine
ASM	airway smooth muscle
ASP	Anticonvulsant Screening Program
AUC	area under the curve
BBB	blood-brain barrier
BQL	below quantification limit
Bz	benzodiazepine
BZD	benzodiazepine
Bz/$GABA_AR$	benzodiazepine γ-aminobutyric acid type A receptor
cLogP	octanol-water partition coefficient
CCI	chronic constriction injury
CDAP	chlordiazepoxide
CFA	complete Freund's adjuvant
CINP	Chemotherapy-induced neuropathic pain
CMC	carboxymethyl cellulose
CNS	central nervous system
COPD	chronic obstructive pulmonary disease
CRO	contracted research organization
CRS	chronic restraint stress
CYP_{450}	cytochrome P450
DIE	deuterium isotope effect

DI	diazepam insensitive
DLM	dog liver microsomes
DS	diazepam sensitive
EC_3	effective concentration eliciting 3% of maximal GABA current
EC_{3-5}	effective concentration eliciting 3-5% of maximal GABA current
ETSP	Epilepsy Therapy Screening Program
FDA	Food and Drug Administration
FLIPR	fluorescence imaging plate reader
FST	forced swim test
GABA	γ-aminobutyric acid
$GABA_AR$	γ-aminobutyric acid type A receptor
GINA	Global Initiative for Asthma
GPCRs	G-protein-coupled receptors
hERG	human ether-à-go-go-related gene
HEK	human embryonic kidney cells
HLM	human liver microsomes
HRMS	high-resolution mass spectrometry
HPLC	high-performance liquid chromatography
IBZD	imidazobenzodiazepine
IC_{50}	half maximal inhibitory concentration
IP	intraperitoneal
IV	intravenous
KOR	kappa opioid receptors
Kp	brain-to-plasma partition coefficient

LABA long-acting β_2 agonist

LC liquid chromatography

LCMS liquid chromatography-mass spectrometry

LCMS-IT-TOF liquid chromatography-mass spectrometry ion trap time-of flight

LR Lawesson's reagent

LTG lamotrigine

MAM methylazoxymethanol acetate

MCh methacholine

MDD major depressive disorder

MES maximal electroshock

MLM mouse liver microsomes

MPE maximum possible effect

MRM multiple reaction monitoring

MTD minimal toxic dose

mTLE mesial temporal lobe epilepsy

MW molecular weight

NAM negative allosteric modulator

NMDA *N*-methyl-D-aspartate

NMR nuclear magnetic resonance

NIMH National Institute of Mental Health

NINDS National Institute for Neurological Disorders and Stroke

Ova s/c ovalbumin sensitized challenged

PAM positive allosteric modulator

PBR peripheral benzodiazepine receptor

PCP	phencyclidine
PDA	photodiode array
PDSP	Psychoactive Drug Screening Program
PEG	polyethylene glycol
PFC	mouse prefrontal cortex
PI	protective indices
PK	pharmacokinetics
PO	per os
PPI	prepulse inhibition
PQ	pyrazoloquinolinone
PTZ	pentylenetetrazole
PWT	paw withdrawal threshold
RLM	rat liver microsomes
SABA	short-acting β_2 agonist
SAR	structure-activity relationship
scMET	subcutaneous pentylenetetrazole
SE	severe epilepsy
SEM	standard error of the mean
SLA	spontaneous locomotor activity
SNL	sciatic nerve ligation
SSRI	selective serotonin reuptake inhibitors
TLC	thin-layer chromatography

ACKNOWLEDGEMENTS

I would like to first thank my advisor Dr. James M. Cook for the opportunity and support to complete my doctorate in organic and synthetic medicinal chemistry. I would also like to thank the Cook research group for their helpful discussions and the members of my doctoral committee, Professor's Alexander E. Arnold, Arsenio A. Pacheco, M. Mahmum Hossain, and Allan W. Schwabacher, for their insightful suggestions, constructive criticism and instructive discussions.

It was a pleasure working with our numerous and outstanding collaborators. I have personally benefitted and gained unmeasurable knowledge in the various fields of medicinal chemistry through intriguing and professional interactions with each individual, especially Drs. Miroslav Savić (University of Belgrade), Margot Ernst (Medical University of Vienna), Lih-Chu Chiou (National Taiwan University), Werner Sieghart (Medical University of Vienna), Thomas Prevot (Campbell Family Mental Health Research Institute of CAMH, Toronto), Etienne Sibille (Campbell Family Mental Health Research Institute of CAMH, Toronto), Janet Fisher (University of South Carolina School of Medicine, Columbia, SC), and Jeffrey M. Witkin (Ascension St. Vincent Hospital, Indianapolis, IN).

Thank you to my family for their prayers, support, encouragement and love throughout my life and especially during this doctoral adventure. Special recognition and thanks to my mom Janice, my dad in heaven Delmer, my sister Jill, my daughter Lauren and my wonderful wife Lisa.

Finally, all the glory and honor of this work goes to my Lord and Savior Jesus Christ with whom all things are possible!

General Introduction

The opioid and benzodiazepine epidemic is clearly on the rise (**Figure 1**) as the total number of overdose deaths in the U.S., which involves, both types of drugs rose from 1,500 in 2002 to over 11,000 deaths in 2017, according to the CDC. Alternative treatments are needed and the search for new ligands (potential new drugs) that selectively interact with specific subtypes of $GABA_A$ receptors ($GABA_ARs$) is one of those avenues.

Figure 1: The Opioid and Benzodiazepine Epidemic on the Rise

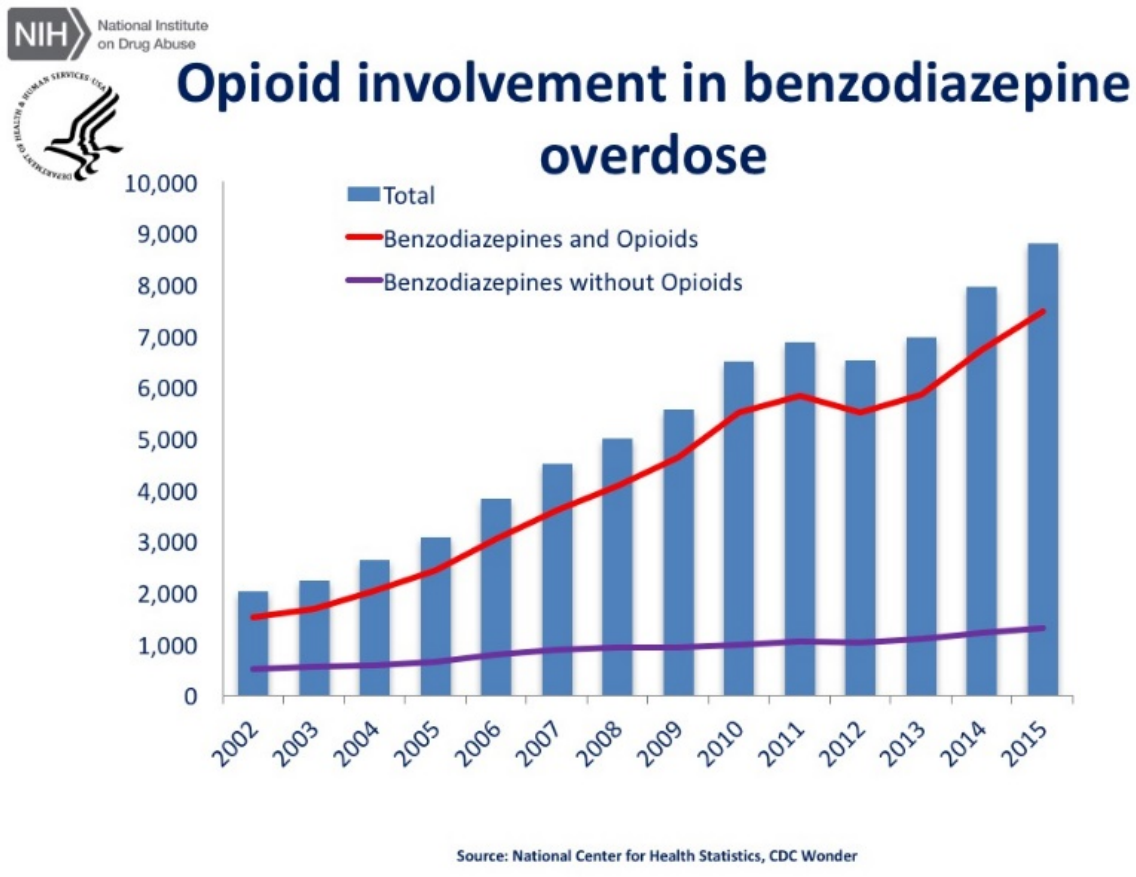

Figure 2: The $GABA_A$ Receptor[a]

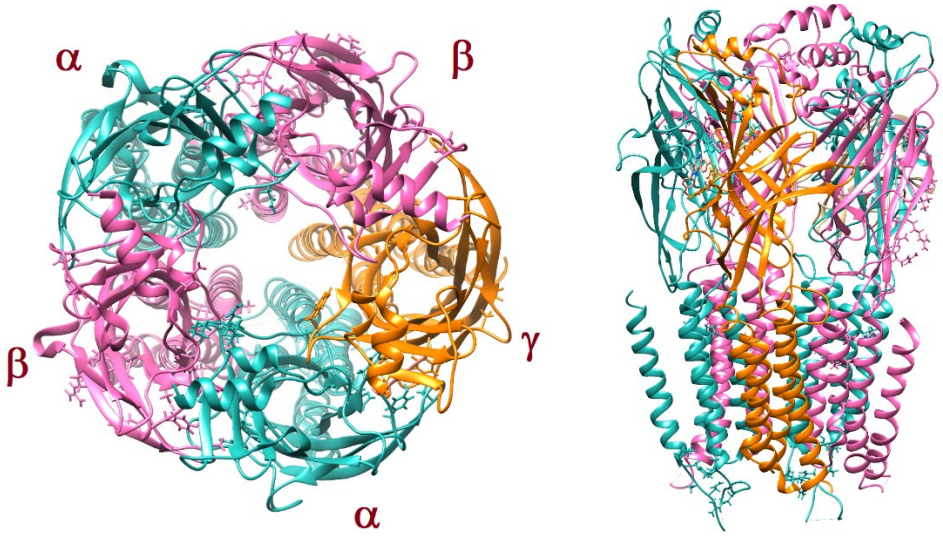

[a] Images derived from the high-resolution cryo-electron microscopy structures of the α1β3γ2 $GABA_AR$ using Chimera X.[1]

The problem with current neurological and psychiatric drugs on the market is that they lack selectivity, meaning that in addition to modulating the desired receptor or receptor subtype of interest, these drugs also modulate activity of undesired receptors, which causes serious side effects. For example, the commonly prescribed benzodiazepine, alprazolam (Xanax) is used to treat anxiety and panic disorders but also causes side effects such as sedation, ataxia, and amnesia, as well as dependence. Alprazolam interacts with four of the major $GABA_AR$ subtypes (α1, α2, α3 and α5) and, therefore, is not considered selective. Each of the $GABA_AR$ subtypes (α1-6) exhibits a unique associated physiological effect (**Figure 3**). Since α2-, α3- α5-, and α6-containing $GABA_ARs$ are not associated with the typical benzodiazepine-type side effects, utilization of novel ligands that are functionally selective for α2-, α3-, α5- or α6-containing $GABA_ARs$ could provide a key to combat this epidemic (**Figure 4**).

Figure 3: Associated Effects of the α1-6 $GABA_AR$ Subtypes[a]

Subtype	Associated Effect
α1	DS Site: Sedation, ataxia, anterograde amnesia, anticonvulsant action, and addition
α2	DS Site: Anxiolytic, antihyperalgesic effects, anticonvulsant action
α3	DS Site: Some anxiolytic, some antinociceptive effects, anticonvulsant action, muscle relaxation
α4	DI Site: Lung disorders in the periphery
α5	DS Site: Cognition, learning, temporal and spatial memory (maybe memory component of anxiety); schizophrenia, depression and in the periphery, asthma
α6	DI Site: Tic disorders, Tourette's syndrome, schizophrenia, migraine, trigeminal orofacial pain

[a]Mohler, et al., ACNP, December 2004; Paul, et al., *Neuropsychopharm.*, **39**, 477 (2014); van Rijinsoever, et al., *J. Neurosci.*, **24**, 6785 (2004).

The α6-$GABA_AR$ subtype selective pyrazoloquinolinone, PZ-II-029 has shown promise in preclinical models of migraine and tic disorders (such as Tourette's syndrome). Deuteration of certain pyrazoloquinolinones such as PZ-II-029, originally synthesized in 1995 in Milwaukee, revived these ligands as drug candidates by increasing their metabolic stability via utilization of the kinetic isotope effect (KIE). It doubled the concentration that reached the brain. The deuterated PZ-II-029, DK-I-56-1, recently has been shown to be effective in pain reduction in a preclinical models of trigeminal neuropathic pain and migraine.

In a different area, the lead imidazodiazepine, GL-II-73 was designed as an α5-$GABA_AR$ subtype selective ligand and exhibits promise in preclinical models of cognition and depression.

By design, these α2/3- or α5-targeting imidazodiazepines, as well as α6-targeting pyrazoloquinolinones are functionally selective positive allosteric modulators (PAMS) for the $GABA_AR$ subtype of interest. Thus, these ligands are predominantly devoid of the sedative,

amnesic, euphoric, and ataxic side effects associated with current GABAergic drugs on the market today. Therefore, these novel and safer drugs provide a potential alternative treatment for $GABA_AR$-related neurological and psychiatric disorders and a solution for ending the opioid and benzodiazepine epidemic.

Figure 4: Three Minute Thesis (3MT) Slide. Combatting the Opioid and Benzodiazepine Epidemic by the Design and Synthesis of Novel Safer Drugs

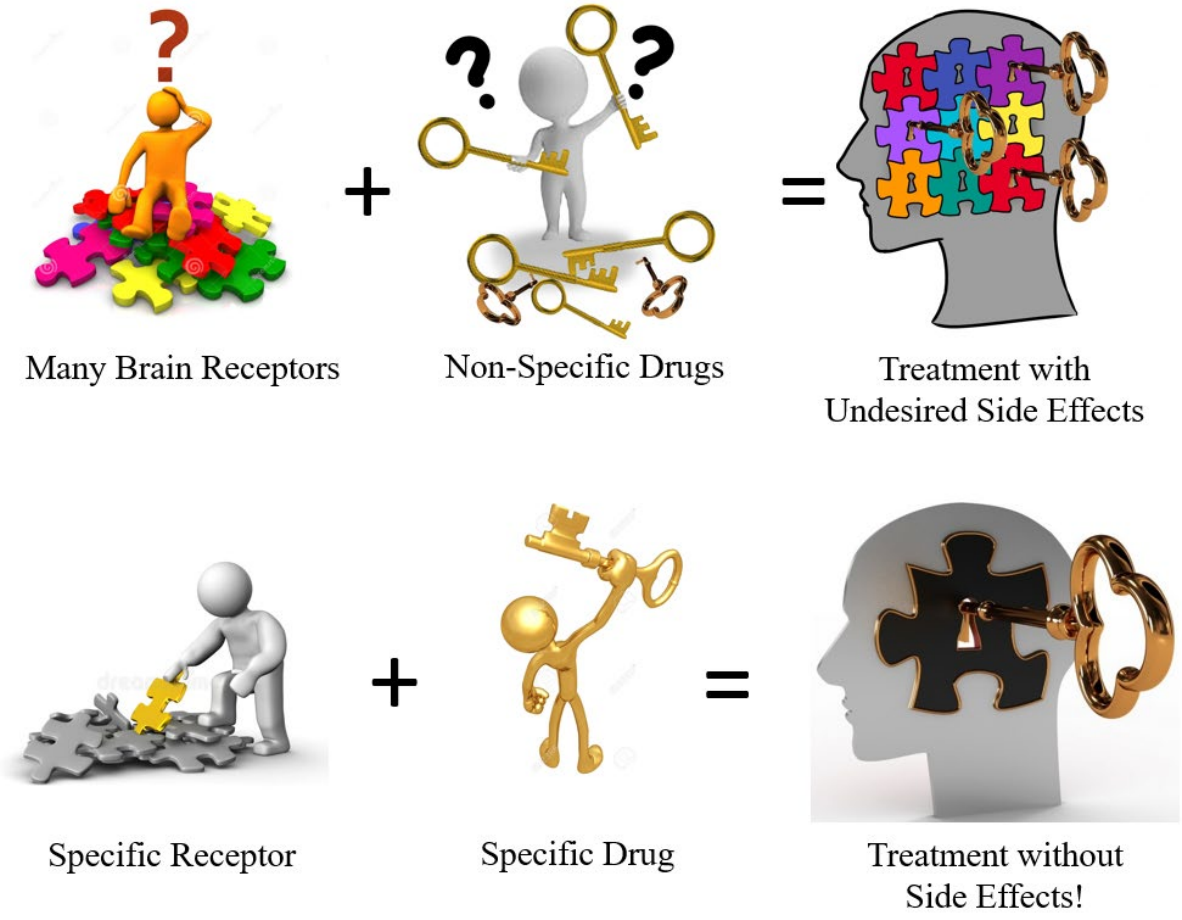

From Three Minute Thesis (3MT) competition (April 2018 and April 2019). Graphic designed by Lauren R. Knutson

Chapter 1: Design and Synthesis of α6-GABA$_A$R Subtype-Selective Pyrazoloquinolinones with Improved Metabolic Stability and Enhanced Bioavailability

1.1. Introduction to α6-GABA$_A$R Subtype-Selective Pyrazoloquinolinones[2]

GABA$_A$ receptors (GABA$_A$Rs) are the major inhibitory neurotransmitter receptors in the mammalian brain and the target of many clinically important drugs, which act at GABA$_A$R binding sites. GABA$_A$Rs are ligand-gated pentameric chloride channels mainly comprised of combinations of 19 different subunits (α_{1-6}, β_{1-3}, γ_{1-3}, δ, ε, π, θ, ρ_{1-3}).[3, 4] Classical GABA$_A$Rs consist of two α, two β and one "tertiary" subunit (γ, δ, ε, θ, or π).[3, 5] Due to the vast array of subunit combinations and their diverse regional, cellular and subcellular distribution, a wide-range of pharmacological properties are potentially mediated by these ion channels.[4, 6, 7] GABAergic drugs including benzodiazepines (Bzs) and barbiturates modulate GABA$_A$Rs via allosteric binding sites.[8] Many GABAergic drugs on the market today offer little alpha subtype selectivity and thus exhibit undesired side effects (sedation, ataxia, amnesia, tolerance, and dependence), in addition to their therapeutic benefits. Recently, a renewed search for GABA$_A$R subtype selective ligands began[9] with the discovery of a new GABA$_A$R $\alpha_x+\beta_y$- ligand binding site.[10] The identification of new ligands which specifically interact with this interface might lead to novel therapeutic entities and provided the initial interest in this area of research.[11-13]

GABA$_A$Rs containing the α6 subunit (α6βγ2, **Figure 5,** or α6βδ) are found primarily expressed in the granule cells of the cerebellum,[7] where they are located synaptically or extrasynaptically, respectively,[14] as well as in the olfactory bulb and the cochlear nucleus.[15] Lower expression of α6-GABA$_A$Rs has recently been reported for the hippocampus where they

Figure 5: The $GABA_AR$ α6β3γ2 Subtype

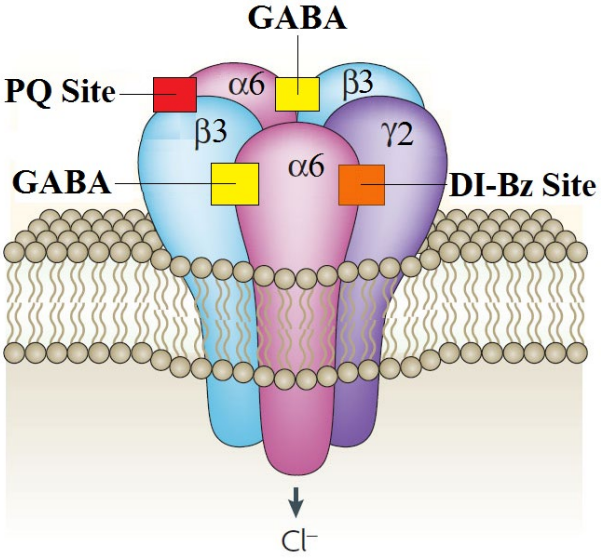

"The $GABA_AR$ α6β3γ2 subtype is a pentameric ligand-gated chloride channel comprised of two α6, two β3 and one γ2 subunits. PQs, like **8b**, mediate their effects at the α6+β3- interface (PQ Site) as positive allosteric modulators and act at the DI-Bz site (α6+γ2- interface) as null modulators. The PQ site, the DI-Bz binding site and the endogenous ligand (GABA) binding sites at the β3+α6- interfaces are displayed. Image modified from Jacob et al., Nature Reviews Neuroscience, 2008.

might play a role in depressive behaviors.[16] Recent reports also suggest that α6-containing receptors may play a role in neuropsychiatric disorders with sensori-motor gating deficits (such as tic disorders, certain symptoms of schizophrenia, obsessive compulsive disorder and attention deficit disorders),[17, 18] as well as in migraine,[19] and trigeminal orofacial pain.[20] However, our understanding of the function of α6-containing receptors in the CNS is still in its infancy, and currently it is not possible to indicate with certainty whether α6βγ2, or α6βδ, or both of these receptors, play a major role in the above mentioned disorders. In any case, the synthesis of ligands selective for α6 subunit-containing $GABA_ARs$ is important to help determine which

physiological processes might be mediated by these particular ion channels and if they are a valid target for drug development.

The Ciba-Geigy Corporation reported pyrazoloquinolinones (PQs), CGS 8216, CGS-9895 and CGS 9896, as the first nonbenzodiazepine ligands to interact with the Bz site of $GABA_ARs$.[21, 22] These compounds exhibited Bz site agonist (positive allosteric modulatory) and antagonist (null modulatory) properties at $GABA_ARs$, but their receptor binding selectivity between diazepam sensitive (DS, αβγ $GABA_ARs$ containing α1, α2, α3, or α5 subunits) and diazepam insensitive (DI, αβγ $GABA_ARs$ containing α4 or α6 subunits) $GABA_AR$ subtypes was rather poor.[23] Incorporation of a 7-methoxy substituent on the "A-ring" (see **Figure 6**) of PQs by the Skolnick group resulted in improved DI affinity.[24] Deconstruction of the CGS-related compounds via application of the pharmacophore/receptor model for $GABA_AR$ subtypes was used to incorporate structural modifications (**Scheme 1**) of the "A-ring" and "D-ring" (**Figure 6**) of PQs. [25, 26] These modifications resulted in the synthesis of PZ-II-029 (**8a**) and several other ligands which bound tightly to the Bz/$GABA_AR$ α6 subtype with a similar affinity as imidazodiazepines.[27] The size and position of substituents on the "D-ring" affected the affinity towards the Bz/$GABA_AR$ α6 subtype.[28, 29] More recently, structural analogues including **8a** were found not only to bind to α6β2/3γ2 $GABA_ARs$, but also to potentiate these receptors, representing the first functionally selective α6β3γ2 subtype ligands reported to date.[12] Prototypes of these ligands mediated their physiological effects at the recently discovered α6+β3- interface[10] of $GABA_ARs$ as positive allosteric modulators, while in addition acting as antagonists (null modulators) at the Bz site (α+γ2- interface) of α1-6βγ2 receptors.[12, 13] In a parallel study, the Ernst, Treven group synthesized very similar analogs LAU 159 (**8i**)[30] and

LAU 463 (**8n**).[31] These compounds exhibited a functional selectivity at α6β2/3γ2 $GABA_A$Rs comparable to **8a**, within the series of α1-6β2/3γ2 receptors. Compounds **8a**, **8i** and **8n** thus represent the three lead compounds described in this study (see **Figure 6**).[31] Since all these PQs exert their positive allosteric modulation via the α6+β3- interface[10] of $GABA_A$Rs, they also are able to modulate α1-6β2/3δ receptors or any receptors containing an α1-6β2/3 interface.[32] But the modulation of α1β3δ, α4β3δ, or α6β3δ receptors by all three lead compounds (**8a**, **8i**, **8n**) is much weaker than that of α6β3γ2 receptors,[31] and was thus not investigated in the present study.

Scheme 1: Development of α6-Selective Ligands

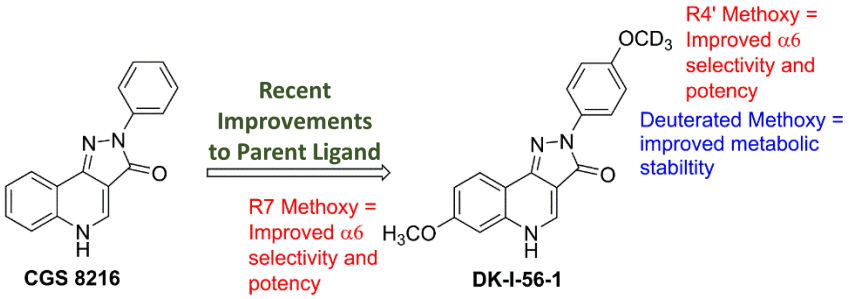

Figure 6: Lead α6-Selective Ligands of this Work[a]

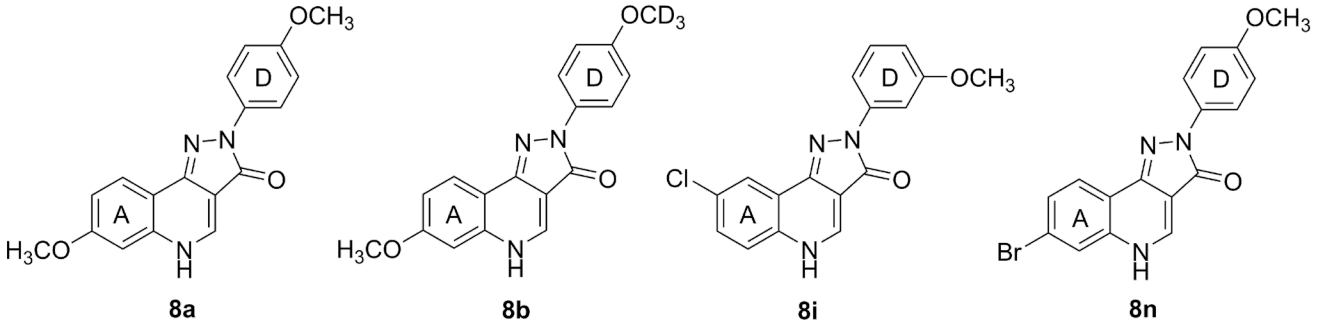

[a]The lead ligands with the "A-ring" and "D-ring" displayed.

Due to the possibility of O-demethylation *in vivo* in this series, as well as their limited solubility in water,[33] the bioavailability and half-life of these α6β3γ2 $GABA_A$R selective ligands were of concern. One way to enhance the bioavailability of compounds is via selective

replacement of hydrogen atoms with deuterium atoms at key metabolic positions on the ligand (see **Figure 7**). Deuteration has been shown to positively affect the metabolic stability, while retaining the pharmacologic profile of active compounds.[34] Consequently, the primary deuterium kinetic isotope (D vs H) effect (DIE) was employed here to enhance metabolic stability.[35] The kinetic DIE results from a difference in the zero-point energy of C-D and C-H bonds due to the lower vibrational frequency of C-D bonds. Consequently, C-D bond cleavage requires a higher activation energy, accompanied by a concomitant slower metabolic rate than a C-H bond. Since the lead compounds contained methoxy groups, it was assumed that those would be primary metabolic sites for O-demethylation by cytochrome P450 enzymes.[36] Thus, one could take advantage of the stability of the C-D bond to reduce O-demethylation of the deuterated analogs.[37] Herein, the first synthesis of novel deuterated $GABA_AR$ α6 subtype selective ligands is reported, as well as the concomitant improved metabolic profile with respect to their parent OCH_3 containing counterparts. Moreover, it was found that their improved metabolic stability resulted in improved bioavailability *in vivo* and ultimately the achievement of higher brain concentrations via both oral and intraperitoneal (ip) administration, a circumstance that is very important in regard to drug development.

Another approach to improve ligand bioavailability of CNS-acting drugs is to improve the solubility and lipophilicity since these modifications can impact membrane permeability and enhance their bioavailability, as well as the ability to reach the desired biological target.[38, 39] Therefore, nitrogen atoms were incorporated into the "A-ring" or "D-ring" of the lead ligands (**8a**, **8n** and **8i**) to improve the water solubility (see **Figure 7**), while still maintaining a

reasonable cLogP. In addition to their metabolic stability, $GABA_AR$-α6 subtype selective efficacy and the pharmacokinetic profile of these N-hetero-modified ligands were also studied.

An additional tactic in the pursuit of further improvements to the bioavailability of these α6-selective ligands led to the exploration of fluorinated substituents (trifluoromethoxy) as an alternative tactic to limit O-demethylation *in vivo* of the methoxy groups of these lead ligands. Fluorination has been shown to improve the metabolic stability and influence the pharmacokinetic properties of the molecule, while also affecting its membrane permeability and intrinsic potency for the desired receptor.[40] Fluorine exhibits the highest electronegativity of any element on the periodic table and when bound to carbon it forms an extremely strong bond.[41] By comparison, the carbon-fluorine bond (98-115 kcal/mol)[42] is much stronger than C—H bonds (89-110 kcal/mol).[41] Thus, fluorination is an attractive tactic to favorably affect the metabolic stability and bioavailability of drug candidates.[40, 41, 43-45]

The final tactic explored in this work was to improvement the oral bioavailability of the α6 subtype selective ligands by either a prodrug or a formulation (nanoemulsion) strategy. These strategies are discussed in more detail in later chapters.

Figure 7: General Strategy of this Work to Improve the Bioavailability of the Ligands

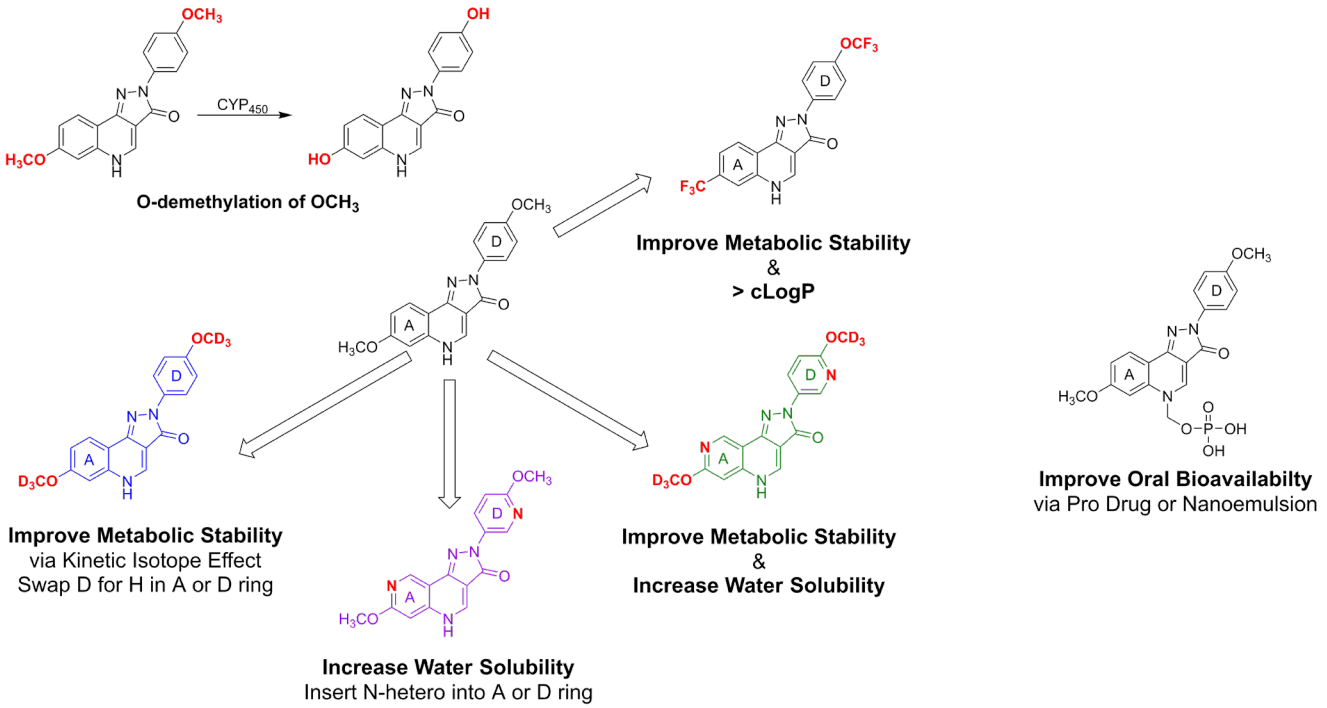

To expand the structure-activity relationship (SAR) library of the $GABA_AR$-α6 subtype selective ligands, a series of 42 structural analogs related to **8a**, **8n** and **8i** were synthesized. $GABA_AR$-α6 subtype efficacy of some of these novel ligands was measured to analyze the effect of deuteration and structural modifications. Furthermore, a binding affinity screen over a panel of 46 receptors (including the hERG) was conducted to determine the possibility of off-target interactions of these novel compounds. In addition, the effects of these compounds on the rotarod test and on HEPG2 (liver) and HEK293 (kidney) cell lines were examined to screen motor activity and hepato and renal toxicities, respectively. Finally, basic *in vivo* behavioral tests on the elevated plus maze, grip strength and cued water-maze training were run on these ligands to assess the occurrence of anxiolysis, muscle strength and basic sensorimotor activity, respectively.

1.2. *In vivo* Activity of α6-GABA$_A$R Subtype-Selective Pyrazoloquinolinones in Disease Models

1.2.1. Treatment of Migraine Using α6-GABA$_A$R Subtype-Selective PQ's (with Dr. LC Chiou: Taiwan) [46, 47]

Background and Purpose: Migraine is caused by a hyperactivity of the trigeminovascular system (TGVS), where the trigeminal ganglia (TG) play an important role (**Figure 8**). This hyperactivity might originate from an underfunctional GABAergic inhibitory system in the TG.

Experimental Approach: To investigate this possibility, a mouse model of migraine was established by inducing migraine-like grimaces in male ICR mice via intraperitoneal (*i.p.*) injections of nitroglycerin (NTG, 10 mg/kg) once every 2 days, in up to 5 sessions to mimic clinical manifestations of migraine. Migraine-like facial pain scores were measured using the mouse grimace scale. The repeated NTG-treatment caused significant increases in migraine-like grimaces that were aborted by sumatriptan and prevented by topiramate.

Key Results: After 5 sessions of NTG injections, the GABA synthesizing enzyme (65kDa) glutamate decarboxylase (GAD65), but not the GABA transporter 1 (GAT1) or the α6 subunit-containing GABA$_A$ receptors (α6GABA$_A$Rs), was down-regulated in mouse TG tissues. The α6GABA$_A$R-selective positive allosteric modulator (PAM), DK-I-56-1, exhibited both migraine abortive (**Figure 9**) and prophylactic (**Figure 10**) effects in repeated NTG-treated mice, comparable with clinically used anti-migraine agents, sumatriptan and topiramate, respectively. The brain impermeable furosemide significantly reversed the anti-migraine effect of DK-I-56-1,

which suggests, it has a peripheral site-of-action, likely via enhancing the α6GABA$_A$R activity in TG.

Conclusion and Implications: These findings suggest that decreased GABA synthesis caused by the reduced GAD65 expression contributes to the TGVS activation and migraine attacks in this repeated NTG-induced migraine model, and that the unaltered α6GABA$_A$Rs in TG are potential targets for treatment of migraine. Thus, α6GABA$_A$R-selective PAMs are potential anti-migraine agents for both abortive (**Figure 9**) and preventive therapies (**Figure 10**).

Figure 8: Schematic Diagrams Illustrating the Trigemino-vascular System (TGVS) and Proposed Changes in Trigeminal Ganglia after Migraine Induced by Repeated Nitroglycerin (NTG) Injections.[47]

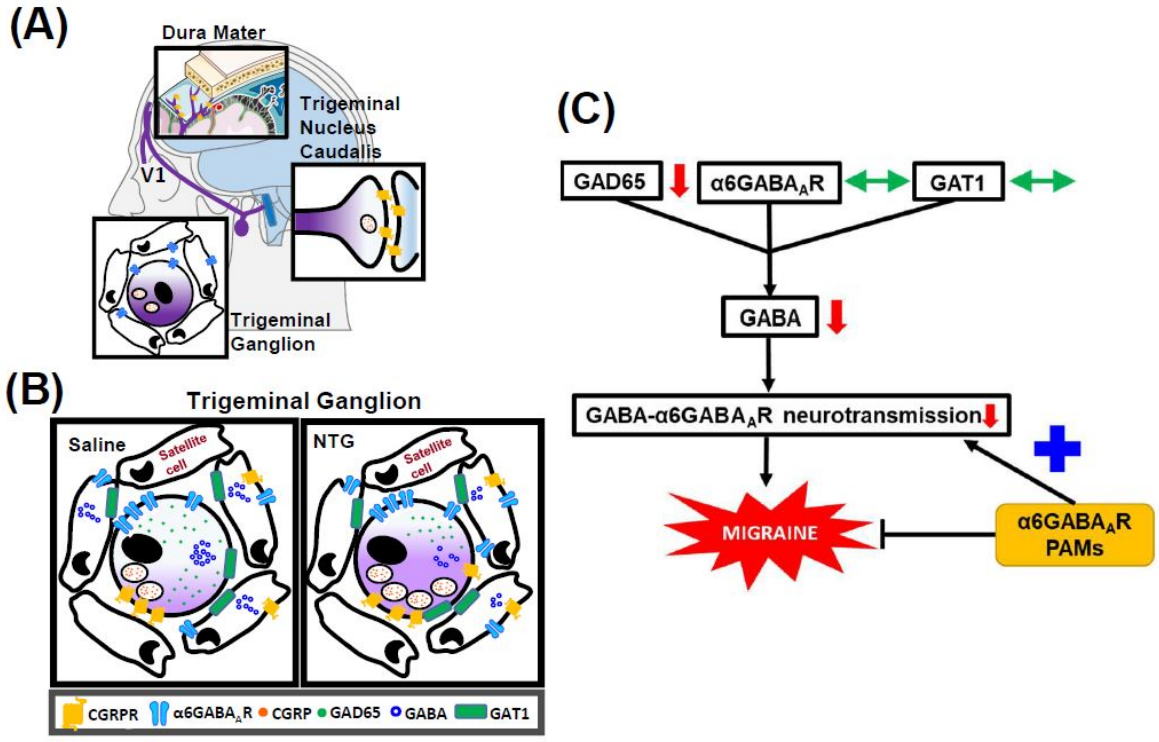

(A) The TGVS consisting of peripheral dura matter, TG and central trigeminal nucleus caudalis, is involved in migraine. (**B)** Repeated NTG injections may lead to impaired GABA-α6GABA$_A$R neurotransmission, resulted from lower GABA in TG due downregulation of GAD65, the synthesizing enzyme of GABA, in TG neurons. However, the expressions of α6GABA$_A$R and GAT1 are not affected by repeated NTG injections. **(C)** Possible anti-migraine mechanisms of α6GABA$_A$R PAMs. As impaired GABA-α6GABA$_A$R neurotransmission in TG is hypothesized to contribute to the pathogenesis of migraine**,** the fact that unaffected TG α6GABA$_A$R level during migraine may be exploited as the therapeutic target. The presence of α6GABA$_A$R PAMs may activate TG α6GABA$_A$Rs, thus restored the TG GABA-α6GABA$_A$R neurotransmission which was impaired due to decreased GABA synthesis.
CGRPR: Calcitonin-gene related peptide receptor CGRP: Calcitonin-gene related peptide ; GAT-1: GABA transporter 1 ; GAD65:65kDa glutamate decarboxylase[47]

Figure 9: Treatment with α6GABA$_A$R PAMs Suppressed Migraine-like Response Induced by Repeated NTG Administration, and this Effect Can Be Reversed by Furosemide, an α6GABA$_A$R Antagonist.[47]

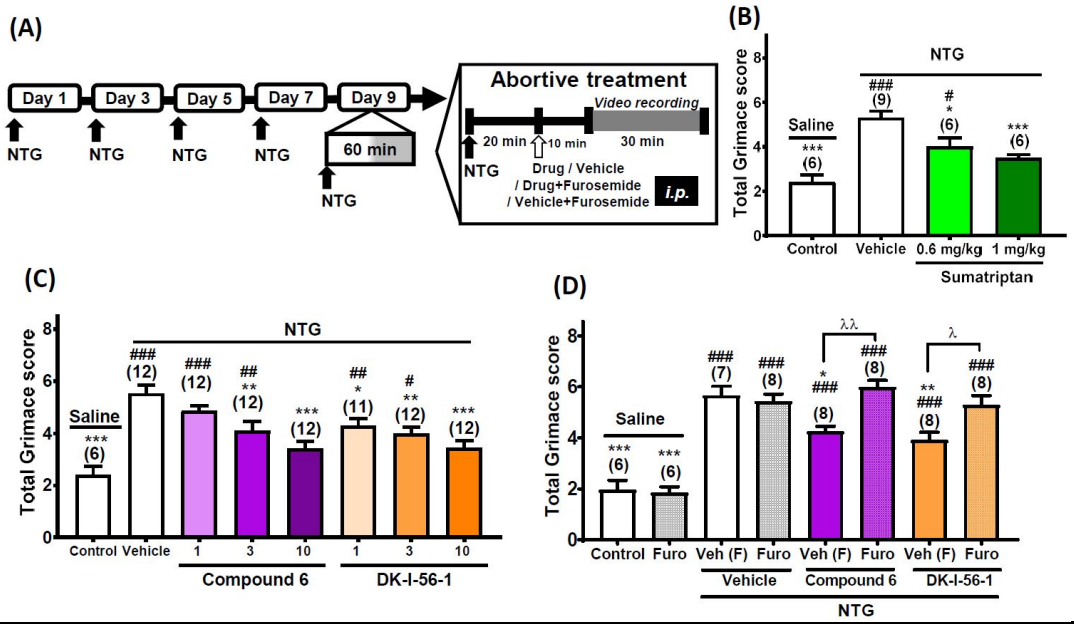

(A) Mice received injections of NTG (10 mg/kg, *i.p.*) or saline on Days 1, 3, 5, 7 and 9. Twenty min after the final NTG injection on Day 9, mice were treated with the tested drugs including sumatriptan (0.6 or 1.0 mg/kg, *i.p.*), the α6GABA$_A$R-selective PAMs, *e.g.* Compound 6 (1, 3 or 10 mg.kg, *i.p.*) or DK-I-56-1 (1, 3 or 10 mg.kg, *i.p.*). After 10 mins, the facial expressions of each mouse were videotaped for 30 mins and the AUs of MGS were subsequently measured. The criteria of MGS are detailed in Supplementary Fig. S2. In separate groups, furosemide (an α6GABA$_A$R antagonist, 20 mg/kg, *i.p.*) was co-administered with Compound 6 (3 mg.kg, *i.p.*) or DK-I-56-1 (3 mg.kg, *i.p.*) to discern the involvement of α6GABA$_A$Rs in migraine abortive effect of these drugs. **(B)** The total grimace score in the control group that received repeated saline injections and in the repeated NTG-injected groups that received vehicle, 0.6 mg/kg or 1 mg/kg of sumatriptan on Day 9. Note that sumatriptan significantly reduced total grimace score in this model. *p< 0.05, ***p< 0.001 *vs.* vehicle, $^{\#}p$< 0.05, $^{\#\#\#}p$< 0.001 *vs.* control, one-way ANOVA followed by Sidak's *post hoc* test. **(C)** Comparison of total grimace score in the control group that received repeated saline injections with the repeated NTG-treated groups that received vehicle, Compound 6 (1, 3 or 10 mg/kg, *i.p.*) or DK-I-56-1 (1, 3 or 10 mg.kg, *i.p.*) on Day 9. Note that 10 mg/kg of Compound 6 and DK-I-56-1, similar to 1 mg/kg or sumatriptan, significantly suppressed the total MGS comparable to control group. *p< 0.05, **p< 0.01, ***p< 0.001 *vs.* vehicle, $^{\#}p$< 0.05, $^{\#\#}p$< 0.01, $^{\#\#\#}p$< 0.001 *vs.* control, one-way ANOVA followed by Sidak's *post hoc* test. (D) The total grimace score in the control group that received repeated saline injections with the repeated NTG-treated groups that then received Compound 6 (3 mg/kg, *i.p.*) or DK-I-56-1 (10 mg/kg, *i.p.*) alone or in combination with furosemide (20 mg/kg, *i.p.*) on Day 9. Note that the migraine abortive effect of Compound 6 or DK-I-56-1 was significantly reversed by furosemide co-administration. *p< 0.05, **p< 0.01, ***p< 0.001 *vs.* vehicle, $^{\#\#\#}p$< 0.001 *vs.* control, $^{\lambda}p$< 0.05, $^{\lambda\lambda}p$< 0.01 vs. furosemide co-administered group, one-way ANOVA followed by Sidak's *post hoc* test.[47]

Figure 10: Repeated Administration of DK-I-56-1, but not Compound 6, Exhibited Migraine Prophylaxis Effect without Drug Dependence Potential.[47]

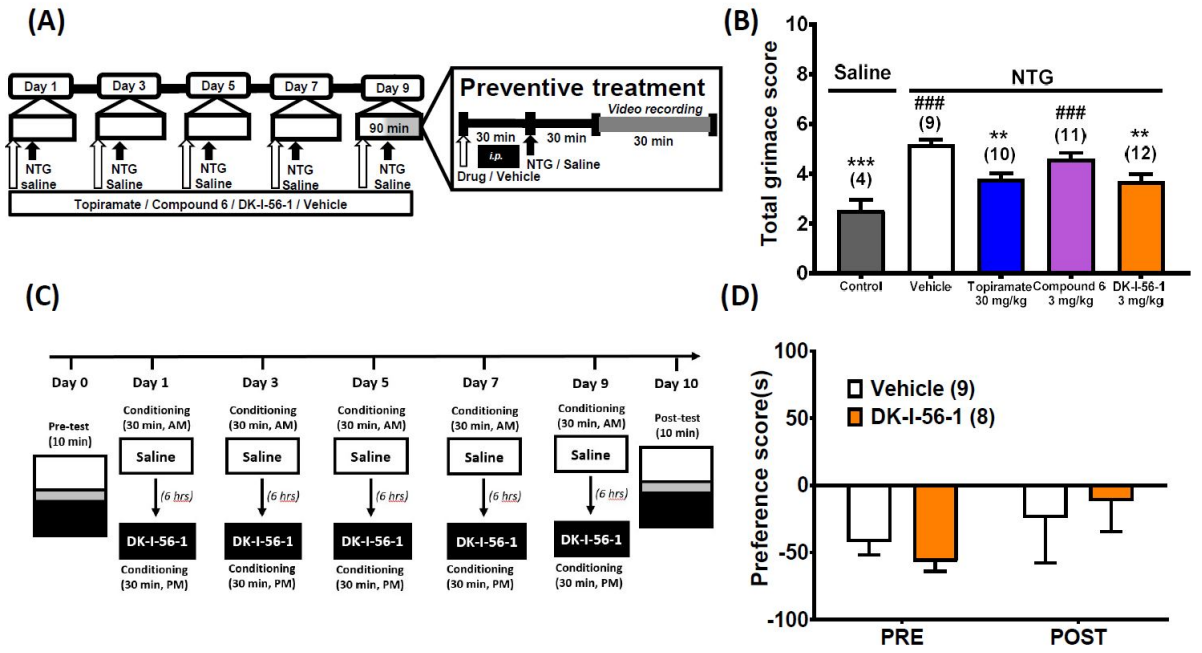

(A) To evaluate the migraine prophylaxis effect of the tested drugs, DK-I-56-1 (3 mg/kg, *i.p.*), Compound 6 (3 mg/kg, *i.p.*), topiramate (30 mg/kg, *i.p.*) or vehicle (*i.p.*) were administered to the mice 30 mins before NTG administration on Days 1, 3, 5, 7 and 9. In the final session, the video was recorded 30 mins after NTG or saline administration for 30 mins, and the total MGS was measured for each mouse. **(B)** Comparison of total grimace score of control group that received repeated saline injections with the repeated NTG-treated groups that received vehicle, Compound 6 (3 mg/kg, *i.p.*), DK-I-56-1 (3 mg.kg, *i.p.*) or topiramate (30 mg/kg, *i.p.*) for 5 sessions. Note that pretreatment with DK-I-56-1 and topiramate, but not Compound 6, significantly suppressed migraine-like responses in NTG-treated mice, comparable to control group. $^{**}p< 0.01$, $^{***}p< 0.001$ *vs.* vehicle, $^{###}p< 0.001$ *vs.* control, one-way ANOVA followed by Sidak's *post hoc* test. (C) CPP test was conducted to examine if pharmacological activation of α6GABA$_A$Rs would cause potential drug dependence in mice, protocol is described in detail in MATERIAL AND METHODS. (D) Preference score of mice received total 5 injections of vehicle or DK-I-56-1 (10 mg/kg, *i.p.*) in 9 days. Note that both groups did not develop significant preference towards DK-I-56-1 conditioned chamber. [47]

1.2.2. Treatment of the Development of Trigeminal Neuropathic Pain Using α6-GABA$_A$R Subtype-Selective PQ's (with Dr. Miroslav M. Savić: Serbia) [48, 49]

γ-Aminobutyric acid type A ($GABA_A$) receptors containing the α6 subunit are principally located in the trigeminal ganglia (**Figure 11**), and their reduction by small interfering RNA increases inflammatory temporomandibular and myofascial pain in rats. It was then hypothesized that enhancement of that activity may help alleviate neuropathic syndromes originating from the trigeminal system. Here, a detailed electrophysiological and pharmacokinetic analysis of two recently developed deuterated structurally similar pyrazoloquinolinone compounds was performed. The ligand, DK-I-56-1 at concentrations below 1 μM enhanced γ-aminobutyric acid (GABA) currents at recombinant rat α6β3γ2, α6β3δ and α6β3 receptors, whereas it was inactive at most $GABA_A$ receptor subtypes which contained other α subunits. The ligand, DK-I-87-1 at concentrations below 1 μM was inactive at α6-containing receptors and only weakly modulated other $GABA_A$ receptors investigated. Both plasma and brain tissue kinetics of DK-I-56-1 were relatively slow, with half-lives of 6 and 13 hr, respectively, enabling the persistence of estimated free brain concentrations in the range 10–300 nM throughout a 24-hr period. The results obtained in two protocols of chronic constriction injury of the infraorbital nerve in rats dosed intraperitoneally with DK-I-56-1 during 14 days after surgery (**Figure 12**) or with DK-I-56-1 or DK-I-87-1 during 14 days after trigeminal neuropathy (**Figure 13**) were readily established, and examination of the data demonstrated that DK-I-56-1 but not DK-I-87-1 significantly reduced the hypersensitivity response to von Frey filaments.

Significance: Neuropathic pain induced by trigeminal nerve damage is poorly controlled by current treatments. The ligand, DK-I-56-1 which positively modulates α6 $GABA_A$ receptors is appropriate for repeated administration and thus may represent a novel treatment option against the development and maintenance of trigeminal neuropathic pain.

Figure 11: Trigeminal Nerve System[a]

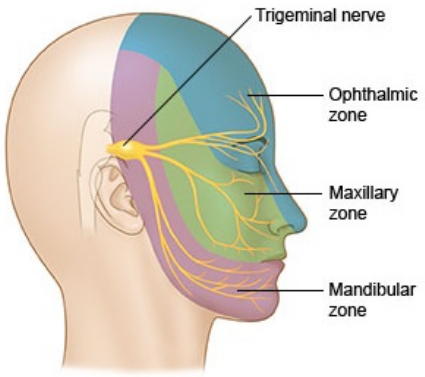

[a] Image modified from: https://www.drugs.com/cg/trigeminal-neuralgia-discharge-care.html

Figure 12: Prophylactic Antinociceptive Effect of DK-I-56-1 (**8b**).[48]

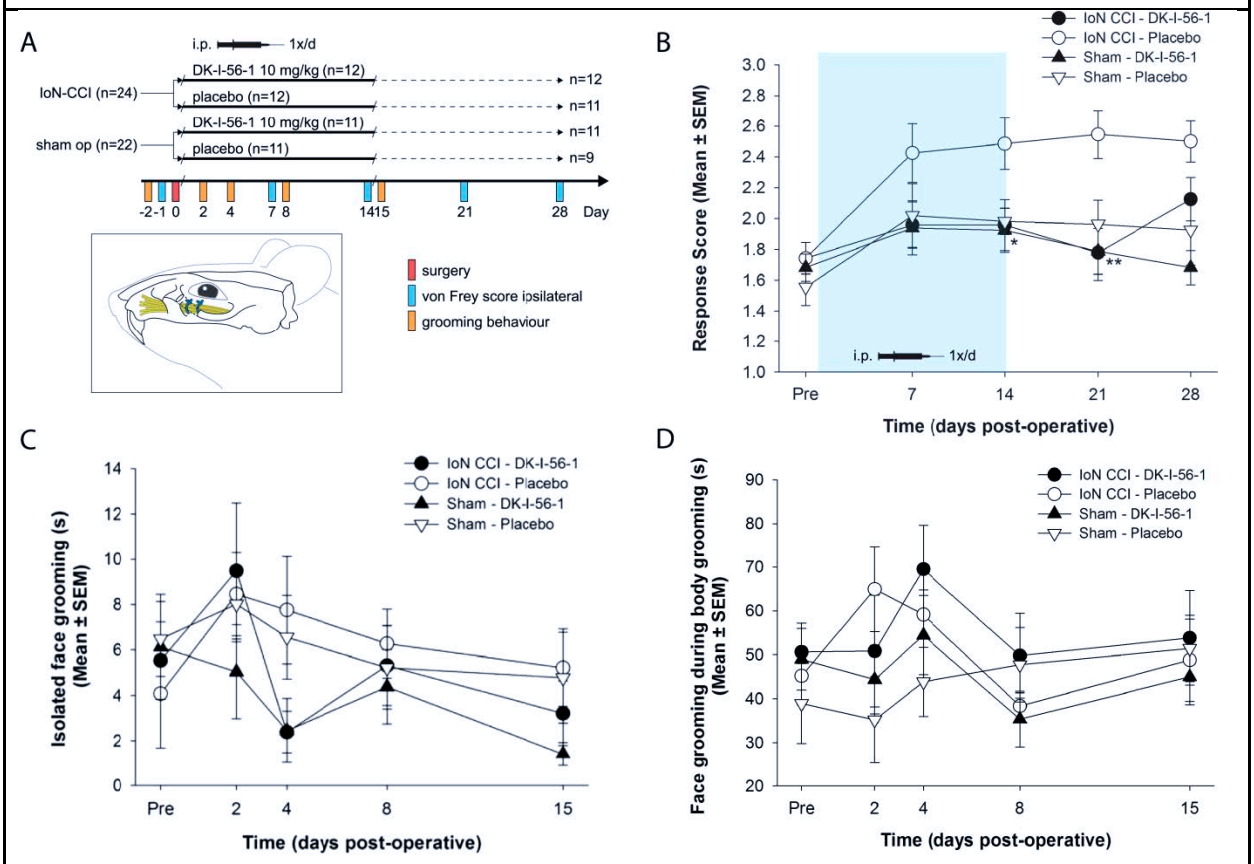

(**A**) Treatment group timeline.
(**B**) Response score to von Frey filament stimulation. Response to the application of a graded series of three von Frey filaments onto ipsilateral (left) vibrissal pad of IoN-CCl and Sham operated animals was measured one day before surgery (pre) and on post-operative days 7, 14, 21 and 28. Treatment (10 mg/kg DK-I-56-1 or placebo) was administered during 14 days, started one day after operation. Experimental groups: IoN-CCI–DK-I-56-1, IoN-CCI–placebo, sham–DK-I-56-1 and sham–placebo consisted of 12, 11, 11 and 9 animals, respectively. Values are presented as mean ± *SEM*. Data were analysed using one-way ANOVA and SNK post hoc test. Significant differences versus placebo are indicated by * = $p < 0.05$.
(**C**) Isolated face grooming recordings were taken two day before surgery (pre) and 2, 4, 8 and 15 days after surgery. See B for treatment groups. Values are presented as mean ± SEM.
(**D**) Face grooming during body grooming recordings were taken two days before surgery (pre) and 2, 4, 8 and 15 days after surgery. See **B** for treatment groups. Values are presented as mean ± *SEM*.[48]

Figure 13: Comparative Effect of DK-I-56-1 (**8b**) vs. DK-I-87-1 (**8m**) in the Trigeminal Orofacial Pain Model.[48]

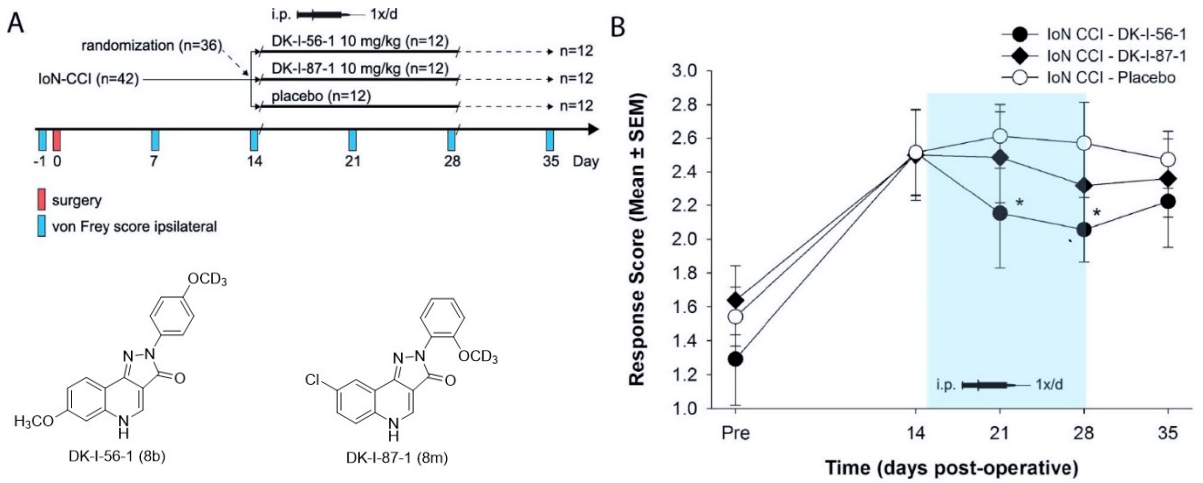

(**A**) Treatment group timeline. (B) Response score to von Frey filament stimulation for three groups. Response to the application of a graded series of three von Frey filaments onto ipsilateral (left) vibrissal pad of IoN-CCI animals was measured one day before surgery (pre) and on post-operative days 14, 21, 28 and 35. Treatment (DK-I-56-1, DK-I-87-1 or placebo) was administered after assessment of mechanical hypersensitivity on day 15. Animals were treated during 14 consecutive days. Twelve animals were in each treatment group (DK-I-56-1, DK-I-87-1 and placebo). Values are presented as mean ± *SEM*. Data were analysed using one-way ANOVA and SNK post hoc test. Significant differences versus placebo are indicated by * = $p < 0.05$.[48]

1.2.3. Treatment of Sensorimotor Gating Deficits in Neuropsychiatric Disorders Using α6-GABA$_A$R Subtype-Selective PQ's (with Dr. LC Chiou: Taiwan) [50, 51]

GABA$_A$ receptors (GABA$_A$Rs) which contain the α6 subunit are primarily found in the granule cells of the cerebellum as indicated above. Attenuation of granule cell activity by positive allosteric modulation of cerebellar α6-GABA$_A$Rs has recently been shown to rescue disrupted prepulse inhibition of the startle response (PPI). Consequently, it was hypothesized that enhancement of the activity of α6-GABA$_A$Rs in the cerebellum may be effective in the treatment of neuropsychiatric disorders with sensorimotor gating deficits, such as, but not limited to schizophrenia, Tourette's syndrome, obsessive compulsive disorder, and attention deficit disorders (**Figure 15**). Herein, the results of electrophysiological, pharmacokinetic and PPI (prepulse inhibition) studies of three deuterated, structurally similar pyrazoloquinolinones (**DK-I-56-1**, **DK-I-58-1** and **DK-I-59-1**) are reported. All three are functionally selective ligands and act at the α6+β3- interface (PQ Site) of α6-GABA$_A$Rs as positive allosteric modulators (PAMs). Deuteration of the methoxy groups of these ligands improved their metabolic stability and enhanced their bioavailability. A study of the results obtained indicated that PAM action at cerebellar α6-GABA$_A$Rs significantly rescued the effect of methamphetamine induced PPI disruption in mice (**Figure 14**).[50] Additionally, α6-selective ligands have been shown to be non-toxic to liver or kidney cells and devoid of the classical benzodiazepine-type side effects such as sedation, motor-impairment and ataxia. Therefore, these ligands which selectively modulate α6-GABA$_A$Rs are novel candidates to treat neuropsychiatric disorders with sensorimotor gating deficits.

Figure 14: α6-GABA$_A$R PAMs Rescue Meth-Induced PPI Disruptions.[51]

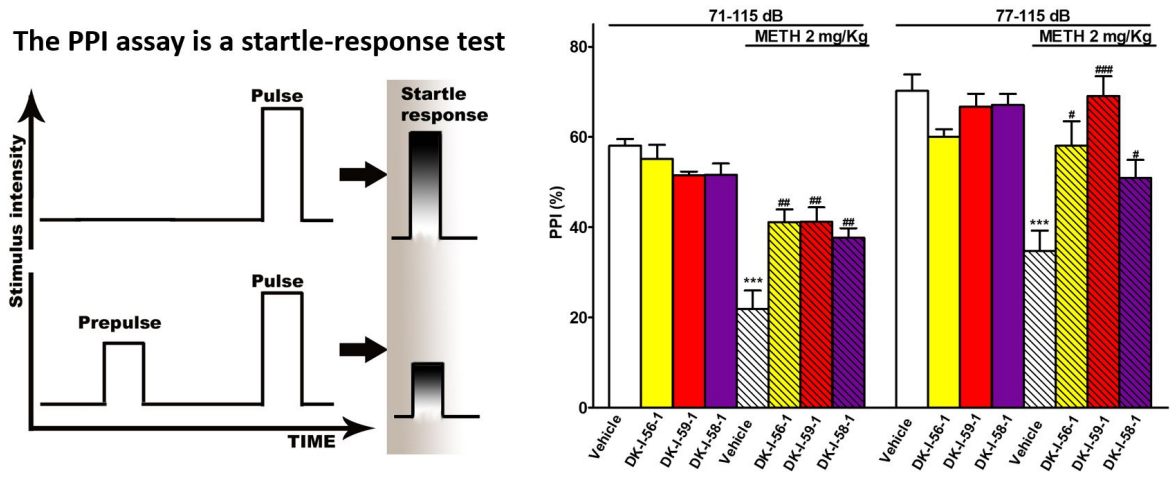

Methamphetamine (METH, 2mg/kg) disrupted PPI in mice.
α6-GABA$_A$R PAMs (3 and 10 mg/kg) reversed METH-PPI.
This activity was completely abolished by use of the α6-GABA$_A$R antagonist, furosemide.[51]

Figure 15: A Hypothesis for How α6-GABA$_A$R PAMs Affect Canonical Cerebellar Circuits and Lead to the Restoration of PPI with Dr. LC Chiou.[50, 51]

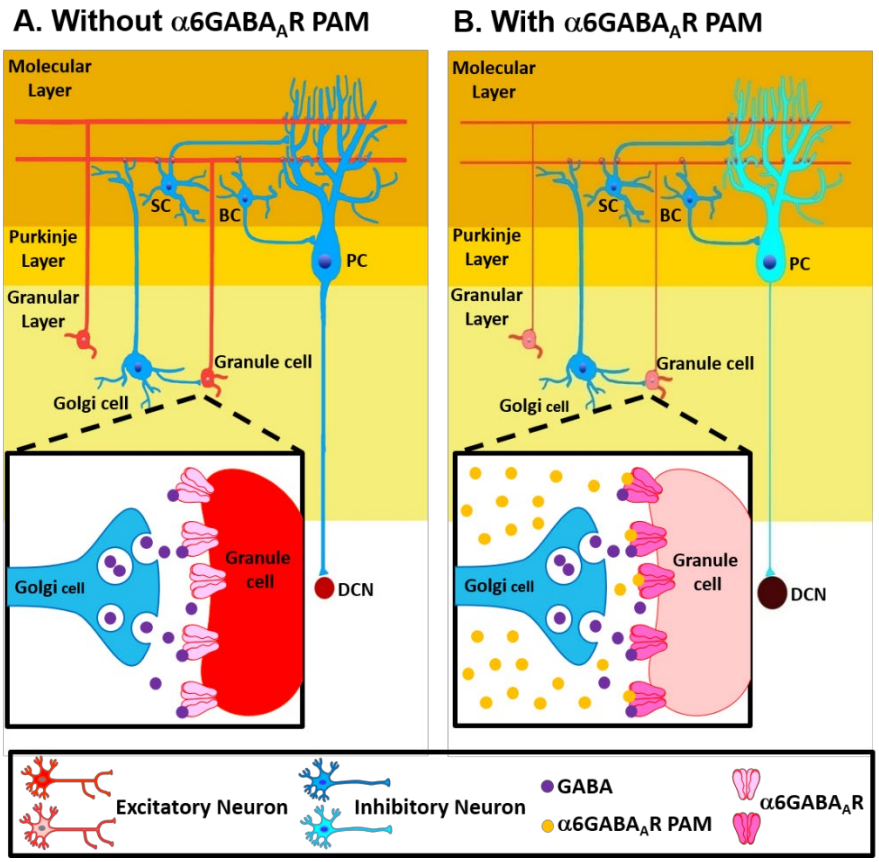

- Basic circuit of the cerebellar cortex before (**A**) and after (**B**) treatment with an α6-GABA$_A$R PAM.
- The excitatory (**red**) and inhibitory (**blue**) neurons in the cerebellar cortex that may be involved in the action of α6-GABA$_A$R PAMs, including Golgi cells that form GABAergic synapses onto granule cells, where the α6-GABA$_A$Rs are located synaptically and extrasynaptically.
- Granule cells form excitatory synapses on dendrites of Purkinje cells (PCs) and send feedforward inhibition onto PCs indirectly through GABAergic interneurons such as basket cells (BCs) and stellate cells (SCs).
- PCs are GABAergic output neurons in the cerebellar cortex, providing an inhibitory control onto the downstream deep cerebellar nuclei (DCN).
- Thinner lines and lighter colors represent reduced neurotransmission and neuronal activity, respectively, after α6-GABA$_A$R PAM treatment.
- α6-GABA$_A$R PAMs act by enhancing Golgi-GABAergic transmission to granule cells, which then decreases PC activity as a result of the attenuated excitatory inputs from granule cells and this sequence of events ultimately decreases the inhibitory output from the cerebellar cortex.
- This will activate the DCN, to increase dopamine levels in the prefrontal cortex (PFC), leading to the restoration of PPI.[50, 51]

1.2.4. Attempted Treatment of the Symptoms of Alcoholism in Baboons Using α6-GABA$_A$R Subtype-Selective PQ's (with Dr. Elise Weerts: Johns Hopkins University School of Medicine)

The α6-GABA$_A$R subtype-selective ligand, PZ-II-029 (**8a**) was also evaluated as a potential treatment for alcoholism in baboons by Dr. Elise Weerts at John Hopkins University School of Medicine. Baboons who had been addicted to alochol were used in the study and the effect of the α6-PAM was assessed by measuring the number of drinks and the quantity (mg/kg) of alcohol consumed. The drug (PZ-II-029) was administered orally with an increasing dose. Examination of both assays (**Figure 16**) indicated that the α6-PAM (PZ-II-029) did not have the desired effect which would typically be displayed by a downward trend in the drinks taken with an increasing dose. Therefore, one could conclude that the α6-GABA$_A$R subtype may not play a role in the addictive behavior of alcoholism in baboons.

Figure 16: The Effect on Alcoholism in Baboons Using the α6-GABA$_A$R PAM (PZ-II-029, **8a**) with Dr. Elise Weerts[a]

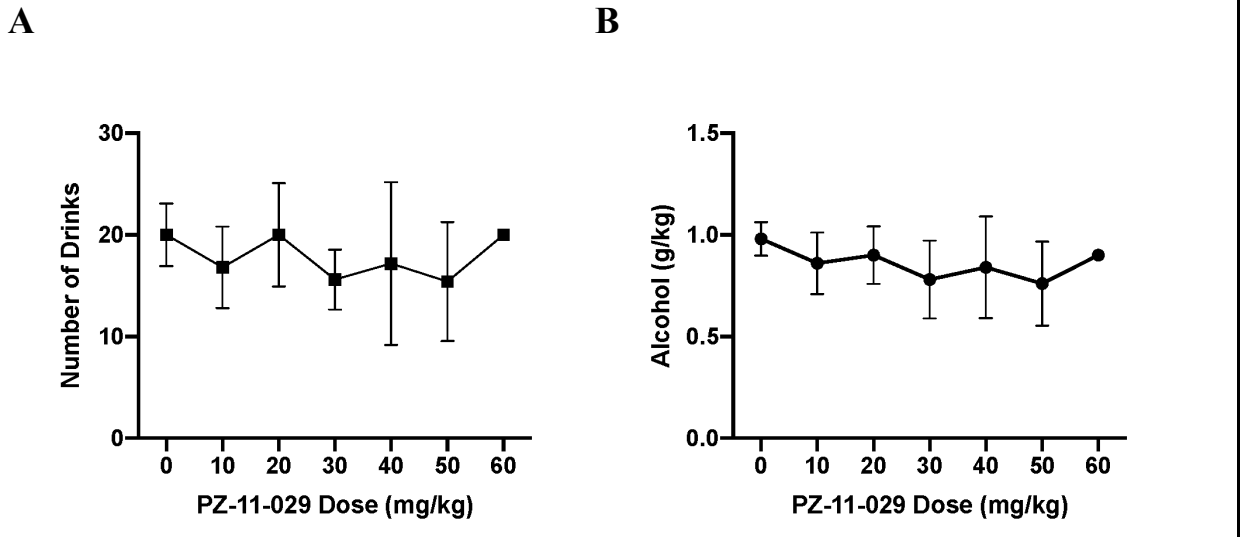

A: The effect on number of drinks taken with an increasing dose of the ligand.
B: The effect on the quantity of alcohol consumed (g/kg) with an increasing dose of the ligand.
[a]Elise Weerts, D. E. Knutson, J. M. Cook, et al., unpublished results.

1.3. Dosage Form Strategies to Improve the Bioavailability of α6-GABA$_A$R Subtype-Selective Pyrazoloquinolinones

1.3.1. Prodrug Strategy

The synthesis and evaluation of a prodrug approach for improving the water solubility of the α6-GABA$_A$R subtype-selective PQ's was explored. The prodrug approach was inspired by the work of many others to seek improvement in water solubility and oral bioavailability. Early prodrug models included using quinuclidine, cinnarizine, loxapine, and amiodarone, 1999[52]; an antifungal azole, Ravuconazole, 2003;[53] Nocathiacin anitibioties, 2004;[54] a Buparvoquone prodrug for cutaneous and visceral leishmaniasis, 2004;[55] a Pochoxime prodrug as HSP90 inhibitors, 2009;[56] *N*1-Alkyl pyrimidinediones for HIV-1, 2010;[57] a prodrug for Parkinson's disease, 2011;[58] the Bristol-Meyers Squibb's HIV-1 drug, 2012[59] and 2014.[60] Other prodrugs include benzimidazole derivatives for the treatment of fasciolosis, 2014;[61] substituted aminothiazoles as anti-hepatocellular carcinoma agents, 2016;[62] anilinopyrazinones by BMS, 2017;[63] in a cystic fibrosis treatment, 2018;[64] the Mebendazole prodrug for cancer therapy, 2018;[65] development of the HIV-1 drug, Fostemsavir in 2018[66]; and the Doravirine prodrug for HIV-1 in 2019.[67] The prodrug synthesis employed herein involved a nucleophilic substitution reaction between the parent quinoline nitrogen and the derivatizing reagent, di-*tert*-butyl chloromethyl phosphate. The tertiary butyl groups are easily removed under acidic conditions with trifluoroacetic acid to give the N-phosphonooxymethyl prodrug in the free phosphoric acid form (**Scheme 12**). These prodrugs were designed to undergo a two-step bioreversion process.[52] The first step involves an enzyme-catalyzed rate-determining dephosphorylation followed by

spontaneous chemical breakdown of the *N*-hydroxymethyl intermediate to afford the parent drug and formaldehyde (**Scheme 2**).

Scheme 2: Prodrug Release Mechanism[52]

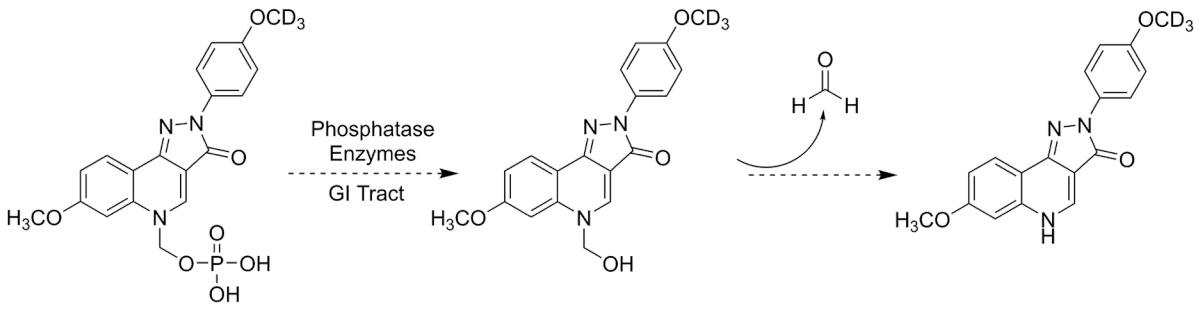

1.3.2. Nanoemulsion Strategy[68]

The ligand, DK-I-56-1 (7-methoxy-2-(4-methoxy-d_3-phenyl)-2,5-dihydro-3*H*-pyrazolo[4,3-*c*]quinolin-3-one), a recently developed deuterated pyrazoloquinolinone, has been recognized as a lead candidate for the treatment of various neuropsychiatric disorders. During preclinical investigation of poorly water-soluble compounds such as DK-I-56-1, the application of nanotechnology as a delivery agent (formulation) could be advantageous due to a good safety profile and the possibility for increased bioavailability of nanosized formulations. Nanosuspensions of DK-I-56-1, which were stabilized by polysorbate 80, alone or in combination with poloxamer 188, poloxamer 407 or d-α-tocopheryl polyethylene glycol 1000 succinate, were prepared by a small-scale media milling approach. With particle size 208.7–250.6 nm and polydispersity index <0.250, selected formulations were stable for three weeks, and the crystallinity of DK-I-56-1 was retained during the preparation step (**Figure 17**).

Pharmacokinetic and biodistribution studies (**Figure 41**), which followed intraperitoneal administration of three types of formulation in mice indicated high plasma DK-I-56-1 levels after nanosuspension but not suspension administration (area under the curve values: 6770.4 ± 770.7; 966.0 ± 58.1; 10228.6 ± 1037.2 ngh/mL, for nanosuspension, suspension and solution, respectively). On the other hand, distribution of DK-I-56-1 after solution was heavily influenced by its composition, and brain availability of the nanosuspension was superior to that of solution formulation. In spontaneous locomotor activity test, the expected hyperlocomotor effect was observed after nanosuspension administration, with no contribution of the vehicle used. Therefore, the simplified qualitative content and low surfactant concentration, together with small particle size in nanosuspensions, could be appropriate for further thorough testing of the preclinical efficacy of DK-I-56-1. The comparison of the pharmacokinetic profiles in plasma, brain, liver and kidney is discussed below in the PK chapter.

Figure 17: Visual Exhibit of Formulations[68]

Nanosuspension (NS2-G, left), solution (SOL, middle) and suspension (SUSP, right) formulations used for *in vivo* pharmacokinetic and biodistribution studies.[68]

1.4. Synthesis of α6-GABA$_A$R Subtype-Selective Pyrazoloquinolinones

The synthesis of **8a**[27] and **8i**,[30] but not that of **8n** has been reported before. Since the route of their synthesis as well as their purification, has been improved herein, those syntheses are also reported here.[2] The synthesis of analogs of the α6β2/3γ2-subtype selective ligand **8a**,[13] which contained deuterium on the methoxy groups of the "A-ring" and/or "D-ring" of the quinolinone nucleus was undertaken. Analogs of **8i** and **8n**, which also contained deuterium on the methoxy groups of the "D-ring" of the PQ nucleus, were also prepared. To permit an extension of the SARs of possible α6β2/3γ2-selective PQ compounds to be performed, additional deuterated compounds were synthesized, in which the OCD_3 group in the "D-ring" was moved to alternative positions, or in which the 8-Cl of **8i** or **8k** in the "A-ring" was replaced by 8-OCD_3 (**Table 2**). The compounds (**8a-t**) in **Table 1** and **Table 2** were generated in a convergent fashion following the steps outlined in **Scheme 3** First, the deuterated methoxy phenyl hydrazines (**4a-c**) were synthesized starting from the appropriate hydroxyanilines (**1a-c**). The amide protection of the amine functionality was achieved using acetic anhydride. The *N*-acetylation was accomplished over *O*-acetylation via strict stoichiometric (1.05 eq.) control of the amount of acetic anhydride employed. This was followed by installation of the OCD_3 groups via alkylation of the hydroxyphenylacetamides (**2a-c**) using iodomethane-d_3 and base to yield the deuterated methoxy phenyl acetamides (**3a-c**) in high yield. Aryl hydrazines (**4a-c**) were obtained via a one-pot procedure, which involved the deprotection of the amine with hydrochloric acid, diazonium salt formation with sodium nitrite and finally reduction of the diazonium salts with tin (II) chloride to yield the desired hydrazines.[69] As reported by Frahn and Illman,[70] control of the temperature (-20^{o}C) of the diazotization and reduction steps was key to avoid elimination of

nitrogen from the decomposition of the diazonium salt, especially in the cases of the activated *para*- and *ortho*-methoxy substituted hydrazines.[70]

Scheme 3: Synthesis of Deuterated Analogs[2]

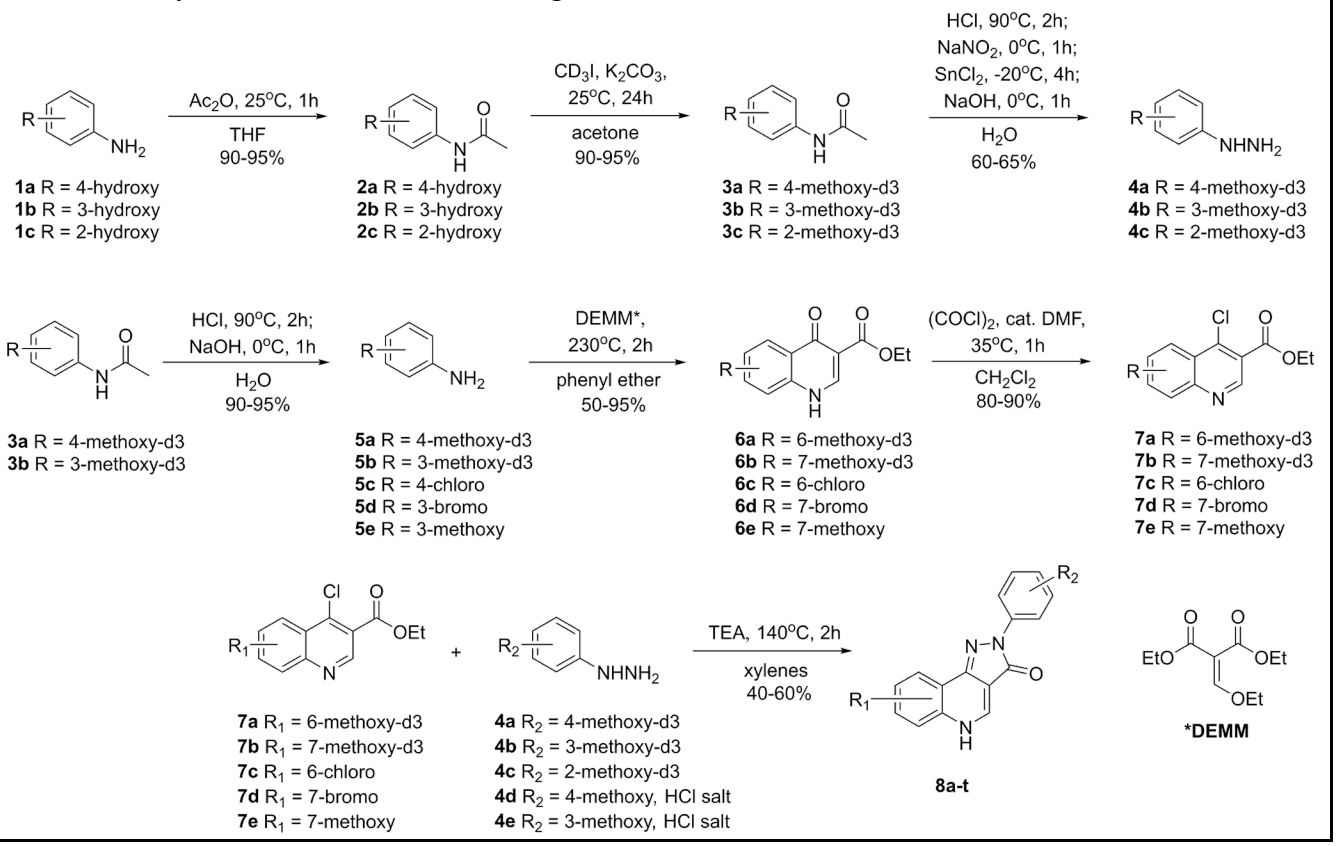

The hydrolysis of methoxyphenylacetamides (**3a** and **3b**) yielded deuterated anisidines (**5a** and **5b**) in excellent yields. The 4-oxo-1,4-dihydroquinoline derivatives (**6a-e**) were then prepared in a modified "one pot" procedure following previous reports (**6c**[71] and **6e**[72]) which involved condensation of the substituted anilines (**5a-e**) with diethyl ethoxymethylenemalonate and this was followed by cyclo-acylation to the quinolone core using the Gould-Jacobs reaction.[73] The application of *para*-substituted anilines typically resulted in higher yields than *meta*-substituted anilines since the cyclo-acylation with *para*-anilines resulted in only one 4-oxo-1,4-dihydroquinoline regioisomer with the substituent in the 6-position of the final target

compound. The cyclo-acylation with *meta*-anilines resulted in the formation of the 5-substituted 4-oxo-1,4-dihydroquinolines, in addition to the desired 7-substituted 4-oxo-1,4-dihydroquinolines in a 1:5 ratio. The undesired 5-substituted 4-oxo-1,4-dihydroquinolines were easily removed during the isolation process by using ethanol to selectively dissolve the undesired isomer. The 4-chloroquinolines (**7a-i**) were obtained by chlorination of the respective 4-oxo-1,4-dihydroquinolines (**6a-i**) by generation of the catalytic Vilsmeier reagent *in situ* using oxalyl chloride and a catalytic amount of N,N-dimethylformamide[74] in high yields (80-90%). Typically, the hydrochloride salts of the 4-chloroquinolines were formed in the chlorination reactions and the free bases were generated by quenching the reaction mixtures into aqueous potassium carbonate solution during the isolation of 4-chloroquinolines (**7a-i**). Utilization of the catalytic Vilsmeier reagent simplified the purification and improved the yield and safety of this chlorination reaction over the reported methods using phosphorus oxychloride (**7c**)[72] and thionyl chloride (**7e**).[71]

Finally, PQs (**8a-t**) in **Table 1** and **Table 2** were obtained by the convergent coupling of phenylhydrazines (**4a-e**) with appropriate chloroquinolines (**7a-e**) by simple modification of the previous work of Ciba-Geigy[21, 22] in mixed xylenes at 135-140ºC. A similar procedure was reported in the deconstruction approach to PQs by He et al.[28] In all cases, excess triethylamine (1.2 eq.) was used to scavenge the hydrogen chloride formed from the nucleophilic aromatic substitution (S_NAr) of chlorine by the primary amino group of the respective phenylhydrazines. Following the S_NAr reaction, thermal cyclization via the secondary amine of the phenylhydrazine occurred with subsequent elimination of ethanol to form the PQ core. Upon completion of the cyclization, the reaction mixtures were quenched into ethanol and filtered to yield the pure PQs

(**8a-t**) in 40 - 60% yields. This improved procedure required no further purification in contrast to the previously reported methods.[71, 75] In cases where phenylhydrazine hydrochloride salts were employed, the amount of triethylamine was adjusted to accommodate for the additional mole of hydrogen chloride.

Table 1: Structures of Ligands Synthesized via the Chemistry in **Scheme 3**[2]

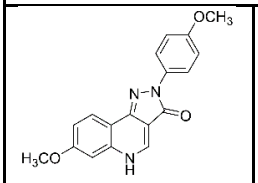 PZ-II-029 (8a)	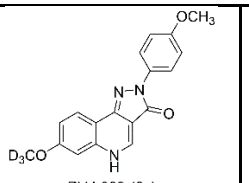 RV-I-029 (8c)	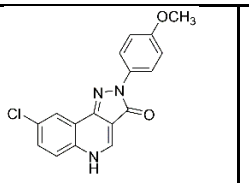 PZ-II-028 (8k)	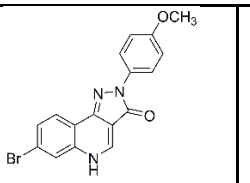 LAU 463 (8n)	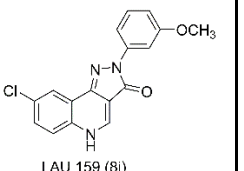 LAU 159 (8i)
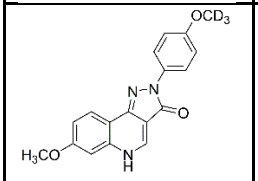 DK-I-56-1 (8b)	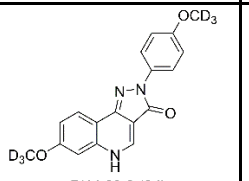 DK-I-60-3 (8d)	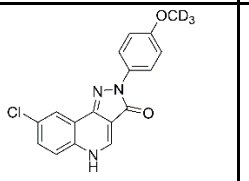 DK-I-93-1 (8l)	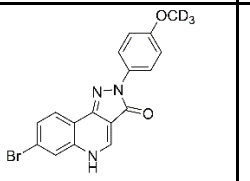 DK-I-58-1 (8o)	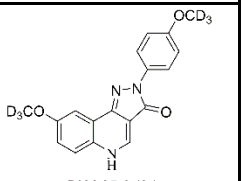 DK-I-95-3 (8r)
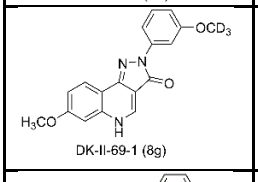 DK-II-69-1 (8g)	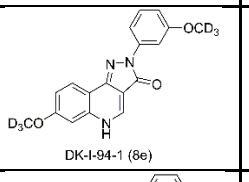 DK-I-94-1 (8e)	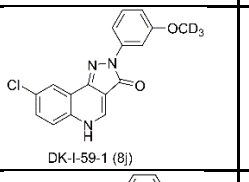 DK-I-59-1 (8j)	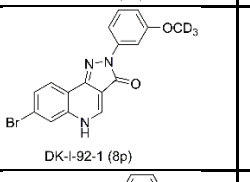 DK-I-92-1 (8p)	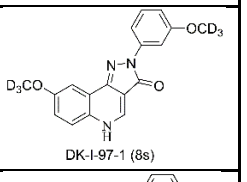 DK-I-97-1 (8s)
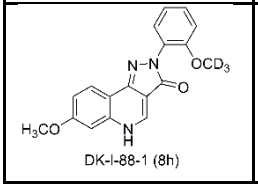 DK-I-88-1 (8h)	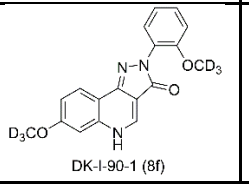 DK-I-90-1 (8f)	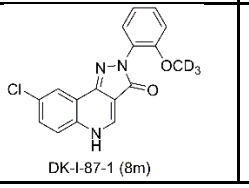 DK-I-87-1 (8m)	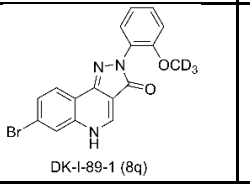 DK-I-89-1 (8q)	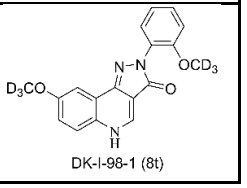 DK-I-98-1 (8t)

Table 2: Ligands Synthesized via the Chemistry in **Scheme 3**[2]

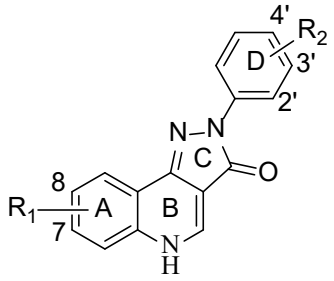

8a-t

Compound	Code	R_1	R_2
8a	PZ-II-029	7-OCH_3	4'-OCH_3
8b[a]	DK-I-56-1	7-OCH_3	4'-OCD_3
8c[a]	RV-I-029	7-OCD_3	4'-OCH_3
8d[a]	DK-I-60-3	7-OCD_3	4'-OCD_3
8e[a]	DK-I-94-1	7-OCD_3	3'-OCD_3
8f[a]	DK-I-90-1	7-OCD_3	2'-OCD_3
8g[a]	DK-II-69-1	7-OCH_3	3'-OCD_3
8h[a]	DK-I-88-1	7-OCH_3	2'-OCD_3
8i	LAU159	8-Cl	3'-OCH_3
8j[b]	DK-I-59-1	8-Cl	3'-OCD_3
8k[b]	PZ-II-028	8-Cl	4'-OCH_3
8l[b]	DK-I-93-1	8-Cl	4'-OCD_3
8m[b]	DK-I-87-1	8-Cl	2'-OCD_3
8n	LAU463	7-Br	4'-OCH_3
8o[c]	DK-I-58-1	7-Br	4'-OCD_3
8p[c]	DK-I-92-1	7-Br	3'-OCD_3
8q[c]	DK-I-89-1	7-Br	2'-OCD_3
8r	DK-I-95-3	8-OCD_3	4'-OCD_3
8s	DK-I-97-1	8-OCD_3	3'-OCD_3
8t	DK-I-98-1	8-OCD_3	2'-OCD_3

[a]**8a** related analogs in **red**. [b]**8i** related analogs in **blue**. [c]**8n** related analogs in **green**.[31]

To increase the solubility and lipophilicity of the lead compounds, the "A-ring" and "D-ring" N-hetero PQs (**13a-i**) in **Table 3** and **Table 4** were synthesized in a convergent fashion following the steps depicted in **Scheme 4** and **Scheme 5**. Initially, to install the "N-hetero"

methoxypyridyl groups into the "D-ring" of PQs (**13a-h**), pyridylhydrazines (**12a-b**) were synthesized. The 2-methoxy-d_3-5-nitropyridine (**10**) was generated in 87% yield by reaction of 2-chloro-5-nitropyridine (**9**) in deuterated methanol (CD_3OD) as the solvent in the presence of potassium *t*-butoxide. The reduction of the nitro group with iron metal in aqueous hydrogen chloride yielded 5-amino-2-methoxy-d_3-pyridine (**11a**) in 95% yield. The aminopyridines (**11a-b**) were converted into their respective pyridylhydrazines (**12a-b**) using the same procedure via diazonium salt formation and tin reduction, as described above for aryl hydrazines (**4a-c**). A similar procedure for the synthesis of **12b** has been reported.[76] Finally, reaction of the pyridylhydrazines (**12a-b**) with chloroquinolines (**7a-e**) yielded PQs (**13a-h**) in moderate yields (40-75%) using the same condensation process as described above.

Scheme 4: Synthesis of "D-Ring" N-Hetero Analogs[2]

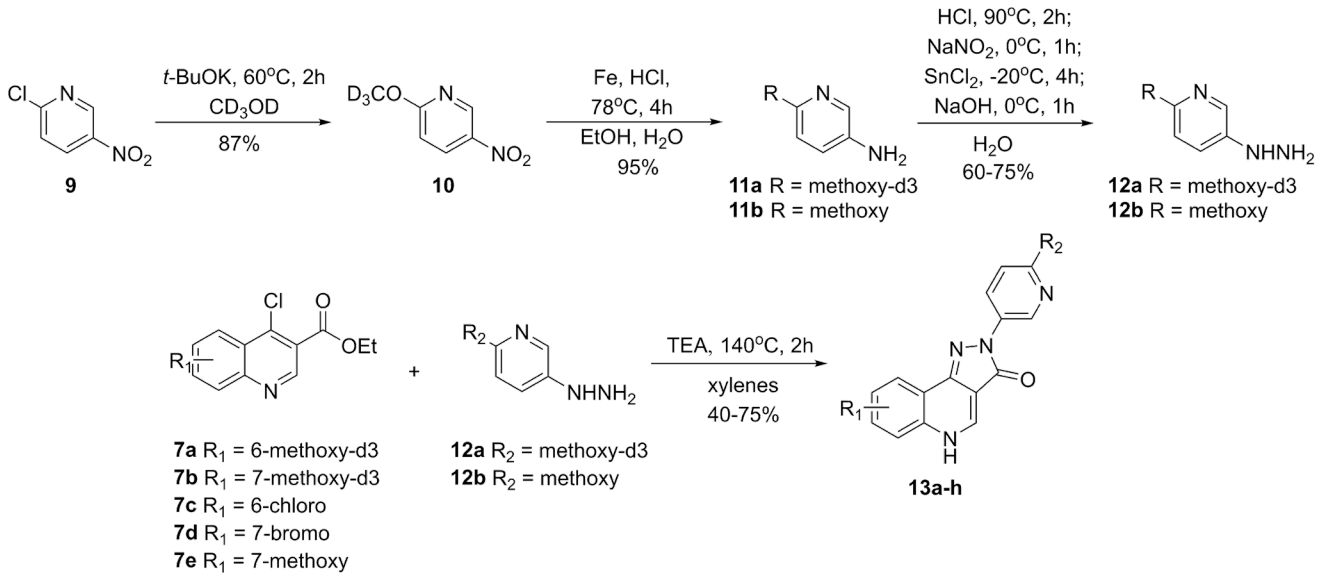

Scheme 5: Synthesis of "A-Ring" N-Hetero Analogs[2]

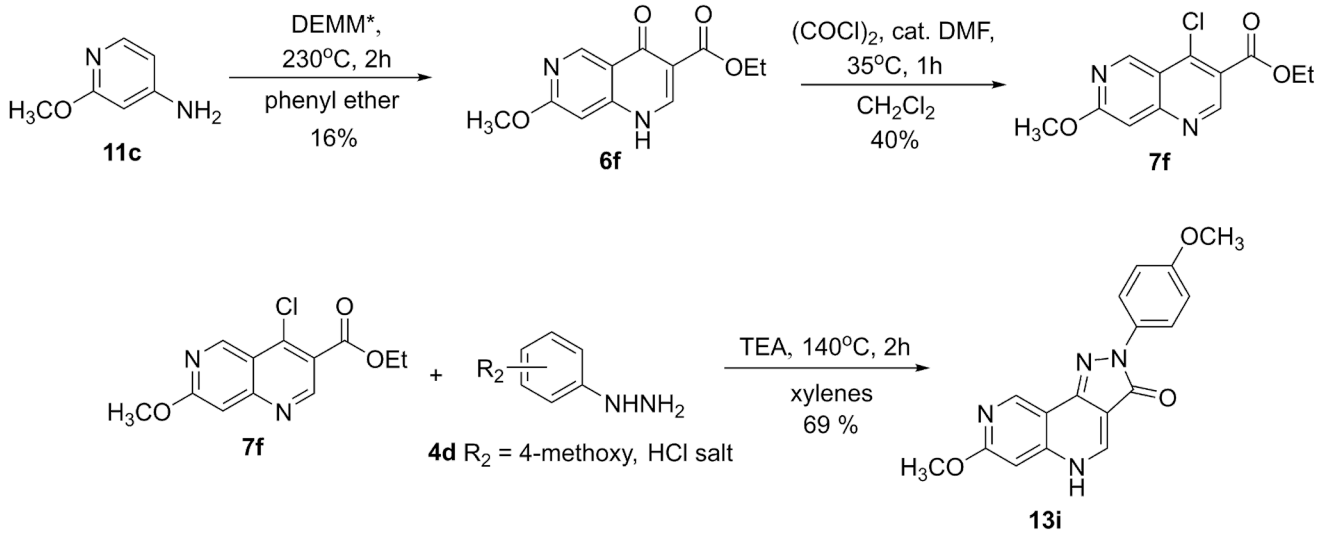

Table 3: Structures of Ligands Synthesized via the Chemistry in **Scheme 4** and **Scheme 5**[2]

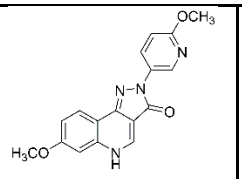 DK-II-13-1 (13a)	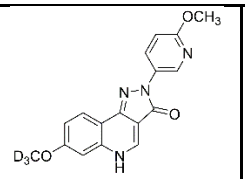 DK-I-86-1 (13c)	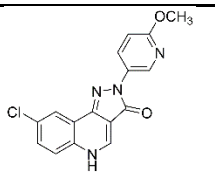 DK-II-18-1 (13e)	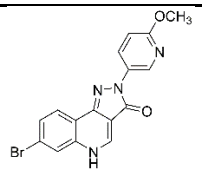 DK-II-48-1 (13g)	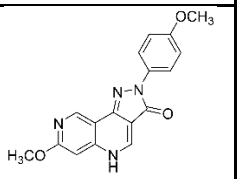 CW-03-030 (13i)
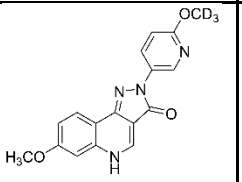 DK-II-60-1 (13b)	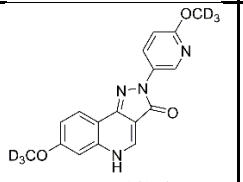 DK-III-6-1 (13d)	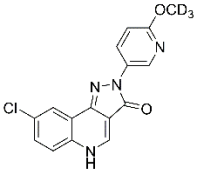 DK-II-59-1 (13f)	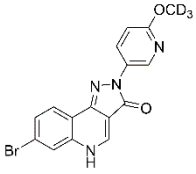 DK-II-58-1 (13h)	

Table 4: Ligands Synthesized via the Chemistry in **Scheme 4** and **Scheme 5**[2]

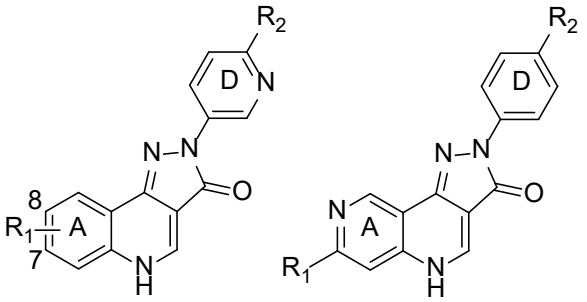

Compound	Code	R_1	R_2
13a[a]	DK-II-13-1	7-OCH_3	4'-OCH_3
13b[a]	DK-II-60-1	7-OCH_3	4'-OCD_3
13c[a]	DK-I-86-1	7-OCD_3	4'-OCH_3
13d[a]	DK-III-6-1	7-OCD_3	4'-OCD_3
13e[b]	DK-II-18-1	8-Cl	4'-OCH_3
13f[b]	DK-II-59-1	8-Cl	4'-OCD_3
13g[c]	DK-II-48-1	7-Br	4'-OCH_3
13h[c]	DK-II-58-1	7-Br	4'-OCD_3
13i[a]	CW-03-030	7-OCH_3	4'-OCH_3

[a]**8a** related analogs in **red**. [b]**8i** related analogs in **blue**. [c]**8n** related analogs in **green**.[31]

The "A-ring" substituted N-hetero PQ (**13i**) provided a unique challenge (**Scheme 5**). The poor electron density of the amino pyridine ring (**11c**) disfavored the Gould-Jacobs cyclization as compared to the previous syntheses that were described. The lower yields (15%) to form 4-hydroxynaphthyridine (**6f**) was not desirable. In addition, chlorination of 4-hydroxynaphthyridine (**6f**) using the catalytic Vilsmeier reagent was also not as selective as in the 4-oxo-1,4-dihydroquinoline series. The cleavage of the pyridyl methoxy group under the acidic reaction conditions to a pyridone appeared to be the problem, which resulted in degradation. Despite, degradation of the product which resulted in a low overall yield (40%) of 4-chloronapthridine (**7f**), as mentioned, the pure product was isolated. Lastly, the reaction of 4-

methoxyphenylhydrazine hydrochloride (**4d**) with 4-chloronapthyridine (**7f**) to form PQ (**13i**) proceeded in 69% yield.

The synthesis of 20 additional structural analogs (**14a-t**) of the parent compounds were also pursued to explore fluorinated analogs as alternatives to deuteration to improve metabolic stability and to further expand the SAR library of $GABA_AR$-α6 subtype selective ligands (see **Table 5** and **Table 6** and **Scheme 6**). These analogs incorporated substituent modifications in the "A-ring" and "D-ring" of the PQ core which included: bromo-, chloro-, fluoro-, methoxy-, methyl-, nitro-, trifluoromethyl-, and trifluoromethoxy- groups (see **Experimental**).

Scheme 6: Synthesis of Additional Analogs

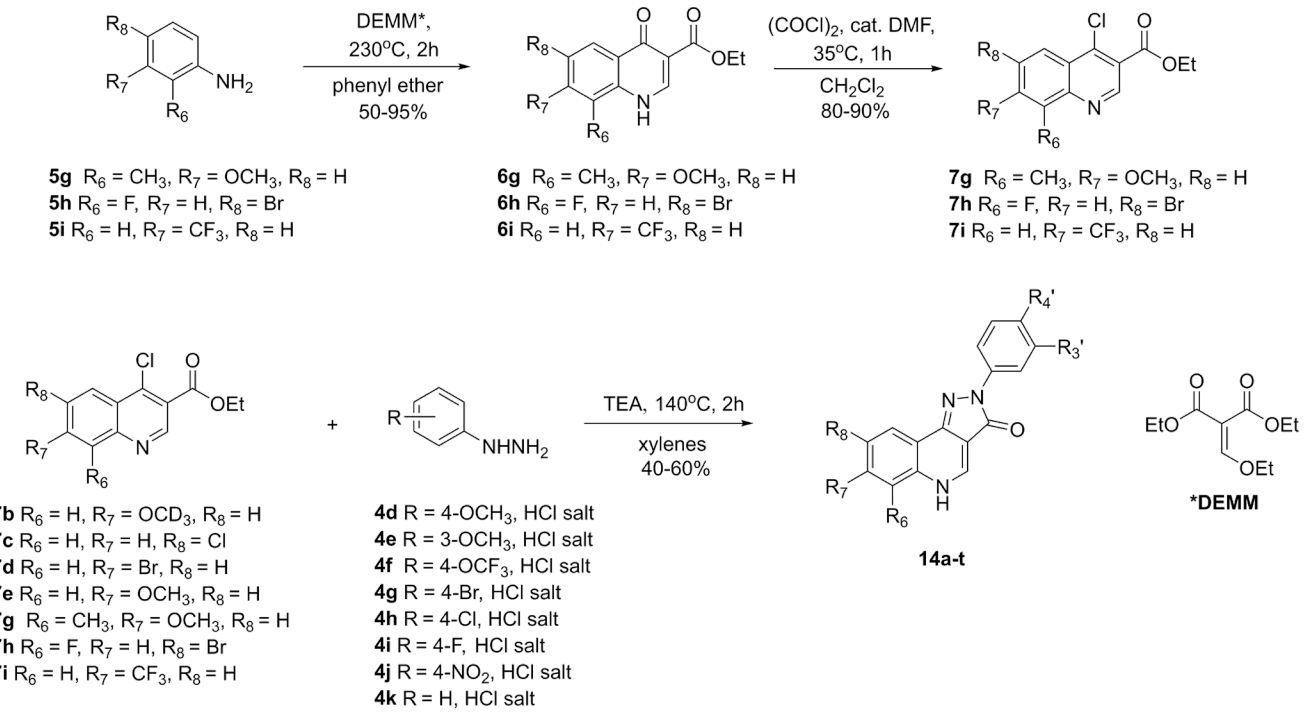

5g R_6 = CH_3, R_7 = OCH_3, R_8 = H
5h R_6 = F, R_7 = H, R_8 = Br
5i R_6 = H, R_7 = CF_3, R_8 = H

6g R_6 = CH_3, R_7 = OCH_3, R_8 = H
6h R_6 = F, R_7 = H, R_8 = Br
6i R_6 = H, R_7 = CF_3, R_8 = H

7g R_6 = CH_3, R_7 = OCH_3, R_8 = H
7h R_6 = F, R_7 = H, R_8 = Br
7i R_6 = H, R_7 = CF_3, R_8 = H

7b R_6 = H, R_7 = OCD_3, R_8 = H
7c R_6 = H, R_7 = H, R_8 = Cl
7d R_6 = H, R_7 = Br, R_8 = H
7e R_6 = H, R_7 = OCH_3, R_8 = H
7g R_6 = CH_3, R_7 = OCH_3, R_8 = H
7h R_6 = F, R_7 = H, R_8 = Br
7i R_6 = H, R_7 = CF_3, R_8 = H

4d R = 4-OCH_3, HCl salt
4e R = 3-OCH_3, HCl salt
4f R = 4-OCF_3, HCl salt
4g R = 4-Br, HCl salt
4h R = 4-Cl, HCl salt
4i R = 4-F, HCl salt
4j R = 4-NO_2, HCl salt
4k R = H, HCl salt

Table 5: Structures of Additional Ligands Synthesized via the Chemistry in **Scheme 6**

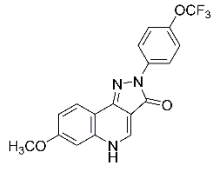 CW-02-082 (14e)	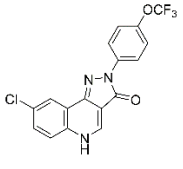 DK-IV-23-1	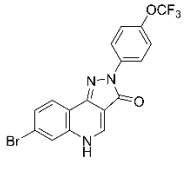 DK-IV-22-1	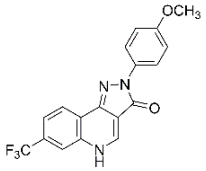 MM-I-06 (14i)	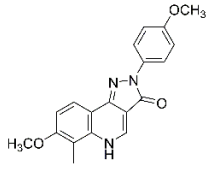 CW-02-073 (14b)
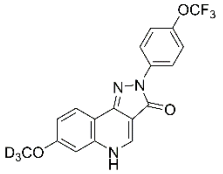 DK-IV-20-1	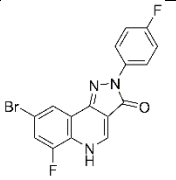 MM-I-18 (14h)	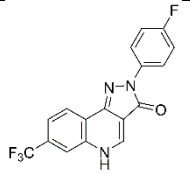 MM-I-11 (14m)	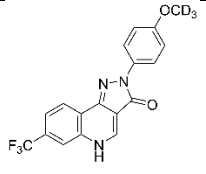 DK-IV-19-1	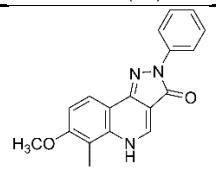 CW-02-078 (14c)
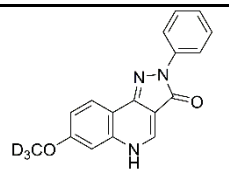 RV-I-037 (14a)	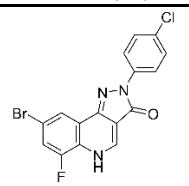 MM-I-13 (14g)	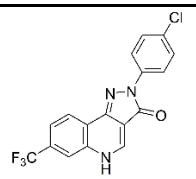 MM-I-08 (14j)	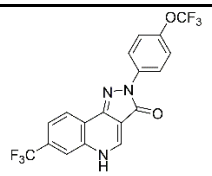 MM-I-10 (14l)	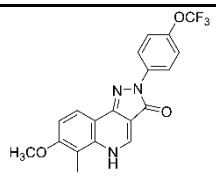 CW-02-079 (14d)
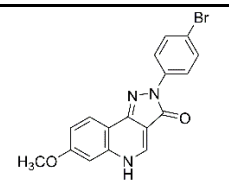 DK-V-68-1 (14t)	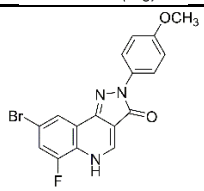 MM-I-03 (14f)	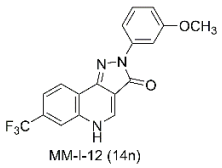 MM-I-12 (14n)	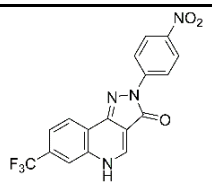 MM-I-09 (14k)	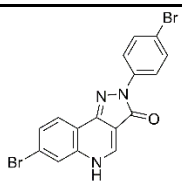 DK-V-67-1 (14s)

Table 6: Additional Ligands Synthesized via the Chemistry in **Scheme 6**

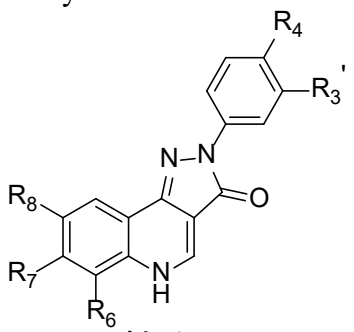

14a-t

Compound	Code	R_8	R_7	R_6	R_4'	R_3'
14a	RV-I-037	H	OCD_3	H	H	H
14b	CW-02-073	H	OCH_3	CH_3	OCH_3	H
14c	CW-02-078	H	OCH_3	CH_3	H	H
14d	CW-02-079	H	OCH_3	CH_3	OCF_3	H
14e	CW-02-082	H	OCH_3	H	OCF_3	H
14f	MM-I-03	Br	H	F	OCH_3	H
14g	MM-I-13	Br	H	F	Cl	H
14h	MM-I-18	Br	H	F	F	H
14i	MM-I-06	H	CF_3	H	OCH_3	H
14j	MM-I-08	H	CF_3	H	Cl	H
14k	MM-I-09	H	CF_3	H	NO_2	H
14l	MM-I-10	H	CF_3	H	OCF_3	H
14m	MM-I-11	H	CF_3	H	F	H
14n	MM-I-12	H	CF_3	H	H	OCH_3
14o	DK-IV-20-1	H	OCD_3	H	OCF_3	H
14p	DK-IV-22-1	H	Br	H	OCF_3	H
14q	DK-IV-23-1	Cl	H	H	OCF_3	H
14r	DK-IV-19-1	H	CF_3	H	OCD_3	H
14s	DK-V-67-1	H	Br	H	Br	H
14t	DK-V-68-1	H	OCH_3	H	Br	H

1.5. The Chemistry of Selected Reactions for the Synthesis of Pyrazoloquinolinones

1.5.1. Preparation of Aryl Hydrazines by the Reduction of Diazonium Intermediates

Aryl hydrazines (**4a-c**, **12a-b**, **Figure 18**) were synthesized by deprotection of the amine (in the cases of **4a-c**) with hydrochloric acid, and this was followed by diazonium salt formation with sodium nitrite. Subsequently the reduction (see the proposed mechanism in (**Scheme 7**)) of the diazonium salts to yield the desired hydrazines using tin (II) chloride in a one pot procedure was carried out.[69] As reported by Frahn and Illman,[70] control of the temperature (-20°C) of the diazotization and reduction steps was key to avoid elimination of nitrogen from the decomposition of the diazonium salt, especially in the cases of the *para*- and *ortho*-methoxy substituted series.[70] Since one wished to prepare the aryl hydrazines in an anhydrous manner for the final pyrazoloquinolinone cyclization step, the aryl hydrazines were isolated as the free base rather than an as HCl salt.[2]

Figure 18: Aryl Hydrazines Synthesized in this Work[2]

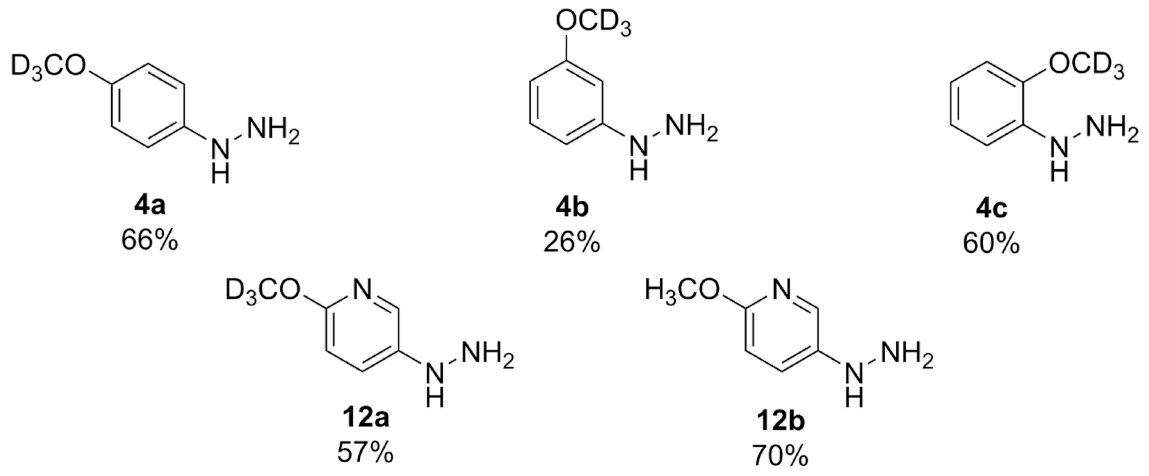

Scheme 7: Proposed Aryl Hydrazine Formation by the Reduction of Diazonium Salts[a]

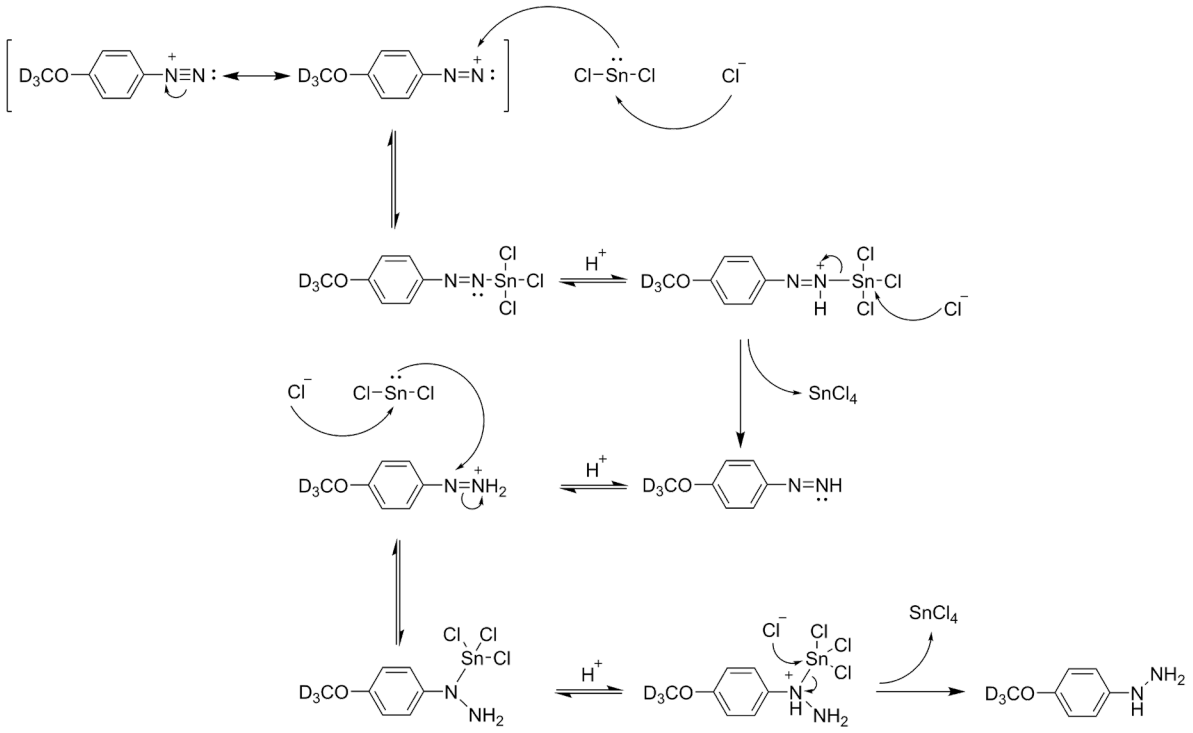

[a]Proposed mechanism modified from: https://chemistry.stackexchange.com/questions/53522/does-this-reduction-mechanism-of-an-diazonium-via-stannic-chloride-sense

1.5.2. Preparation of 4-Oxo-1,4-dihydro-quinolines Using the Gould's Jacobs Cyclization

The Gould-Jacobs cyclization[73] involves the condensation of substituted anilines with diethyl ethoxymethylene malonate and this is followed by thermal cyclization of the anilinomethylenemalonic ester to afford the quinoline product. Flash vacuum pyrolysis (FVP) was used to explore the proposed reaction mechanism (**Scheme 8**).[77] The FVP experiment revealed that the anilinomethylenemalonic ester intermediate proceeded through either a ketene

or enol pathway prior to the electrocyclization (6π) and tautomerization steps to afford the quinoline core. A third, destructive pathway was also possible by loss of CO_2 and ethene.

Scheme 8: Proposed Gould's Jacobs Cyclization Mechanism[77]

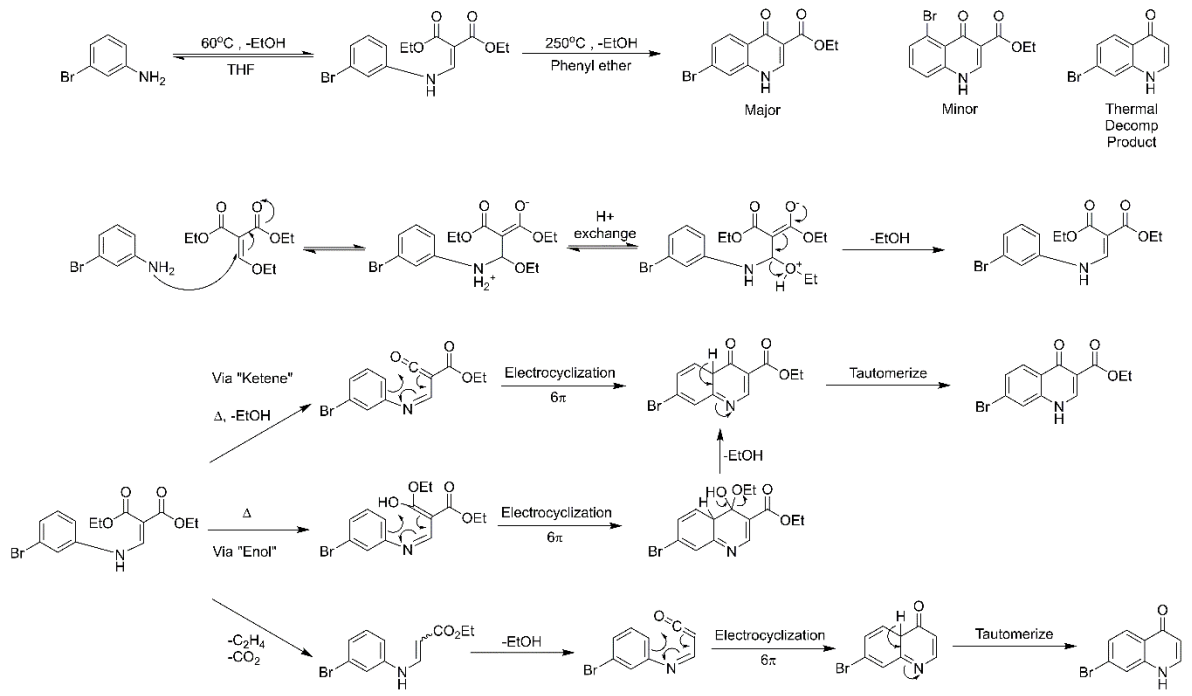

The observations in this work support the mechanism proposed by Malvacio, et al.[77] since in the lower yielding cases off-gassing during the cyclization step was observed. If the reaction temperature was kept below 250°C this seemed to mitigate the propensity of the destructive pathway from occurring. Nine different 4-oxo-1,4-dihydroquinoline derivatives (**6a-i**) were prepared in this work with varying yields (**Figure 19**). The *para*-substituted anilines typically resulted in higher yields than *meta*-substituted anilines since the cyclo-acylation with *para*-anilines resulted in only one 4-oxo-1,4-dihydroquinoline regioisomer with the substituent in the 6-position of the final compound. The cyclo-acylation with *meta*-anilines resulted in the

formation of the 5-substituted 4-oxo-1,4-dihydroquinolines in addition to the desired 7-substituted 4-oxo-1,4-dihydroquinolines in a 1:5 ratio. The aniline starting materials which contained halogens afforded higher yields than anilines containing electron donating methoxy substituents. The *meta*-anilines, which contained an *ortho*-substituent, afforded higher yields than *meta*-anilines devoid of an *ortho*-substituent (compare **6g** to **6e**, **Figure 19**). The undesired 5-substituted 4-oxo-1,4-dihydroquinolines and quinoline byproducts (from the destructive pathway) were easily removed during the isolation process by using ethanol to selectively dissolve the undesired isomer and byproduct.

Figure 19: Synthesized 4-Oxo-1,4-dihydro-quinolines in this Work[2]

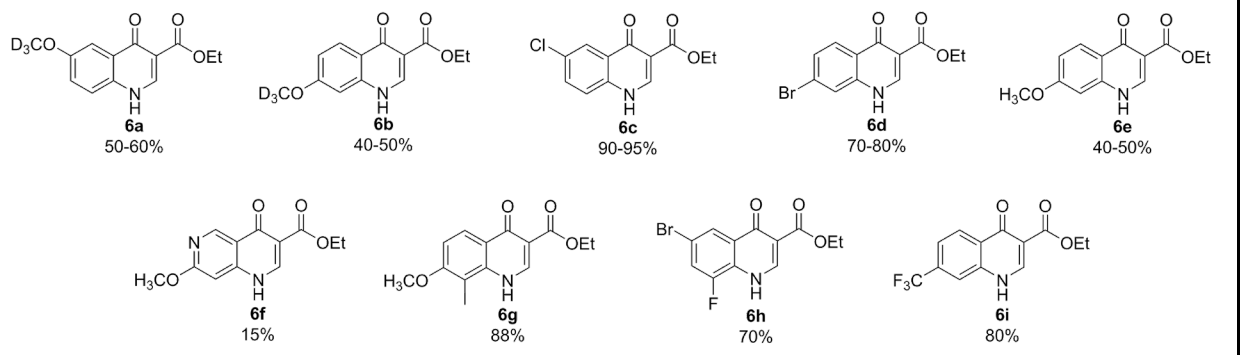

1.5.3. Preparation of 4-Chloro-quinolines Using a Catalytic Vilsmeier Chlorination

The Vilsmeier reagent was used in a catalytic fashion for the chlorination of 4-oxo-1,4-dihydroquinolines (**6a-i**) to produce the desired 4-chloroquinolines (**7a-i**, **Figure 20**), analogous to the literature procedure.[2]

Figure 20: Synthesized 4-Chloro-quinolines in this Work[2]

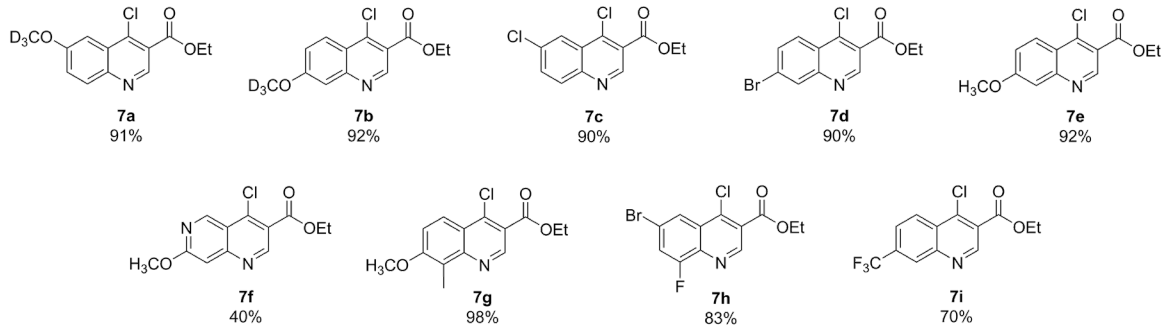

The Vilsmeier reagent was generated *in situ* using oxalyl chloride and catalytic *N*,*N*-dimethylformamide.[74] The advantage of the catalytic Vilsmeier reagent over the reported phosphorus oxychloride[72] and thionyl chloride[71] methods is it allows one to conduct the reaction at a lower temperature (35-40ºC) and also control the reaction rate by the addition rate of the oxalyl chloride reagent. The proposed reaction mechanism exhibiting the regeneration of the DMF catalyst is shown in **Scheme 9**.

Scheme 9: Proposed Catalytic Vilsmeier Mechanism of Chlorination

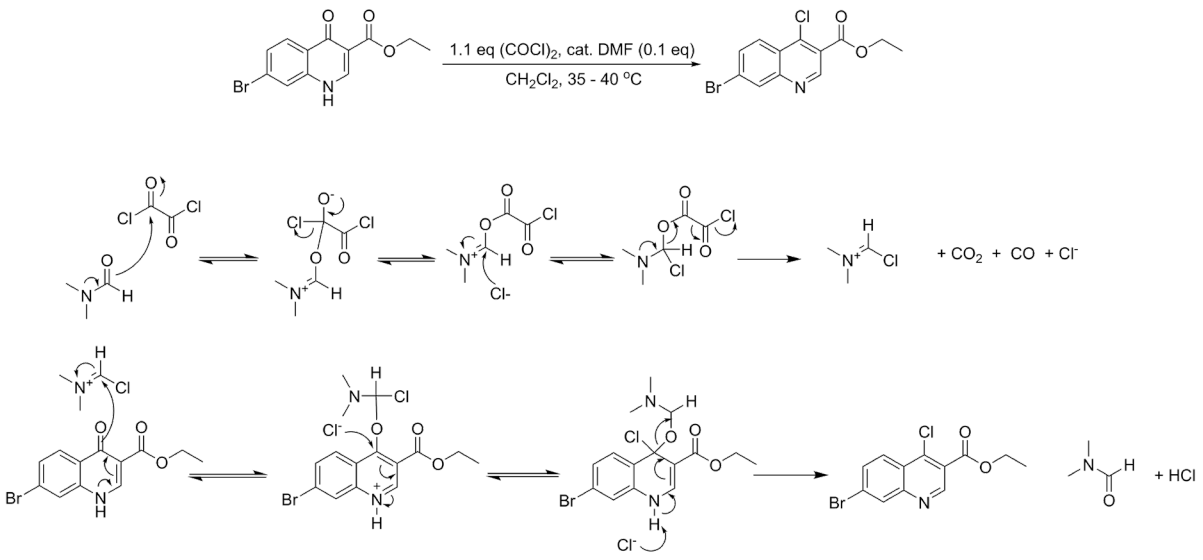

1.5.4. Preparation of Pyrazoloquinolinones Using 4-Chloro-quinolines and Phenyl-hydrazines

The proposed mechanism for the pyrazoloquinolinone cyclization is shown in **Scheme 10**. First, a nucleophilic aromatic substitution (S_NAr) of a chlorine atom by the primary amino group of the respective phenylhydrazines is proposed to occur. Following the S_NAr reaction, thermal cyclization via the secondary amine of the phenylhydrazine occurred with subsequent elimination of ethanol to form the PQ core.

Scheme 10: Proposed Mechanism of the Pyrazoloquinolinone Cyclization

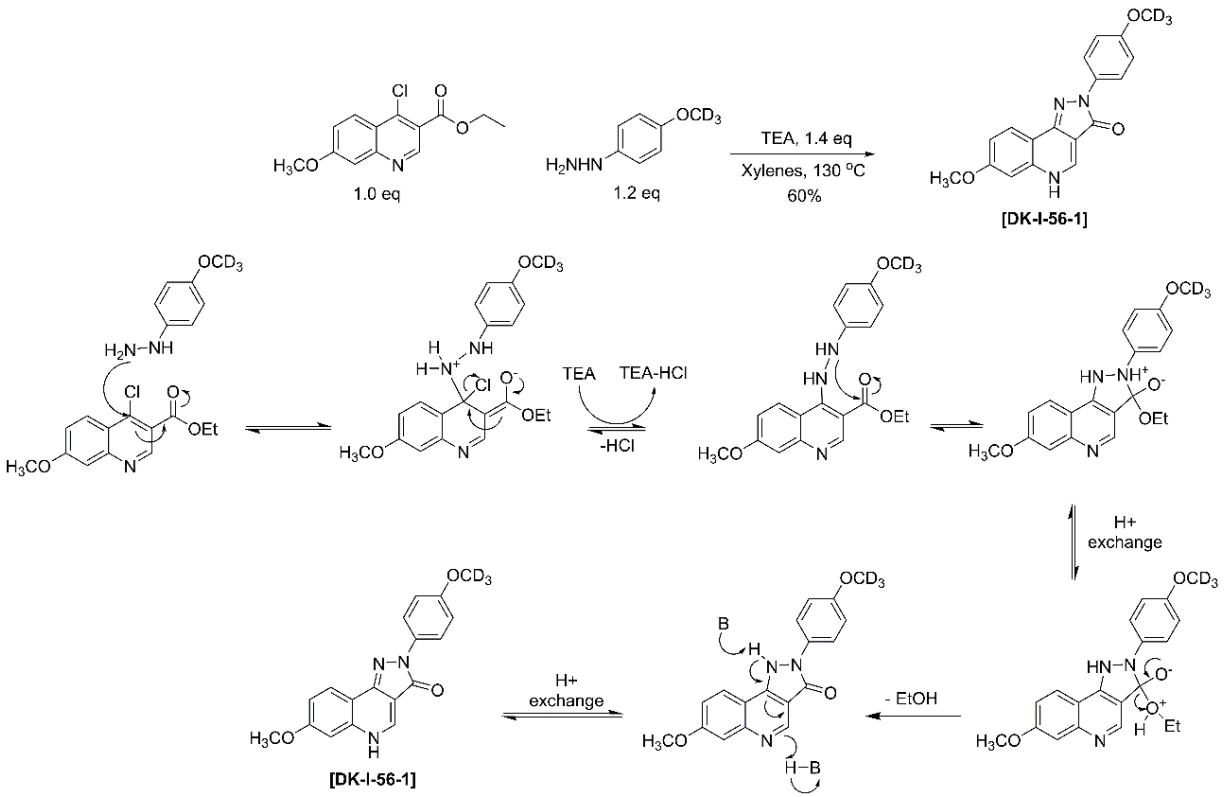

1.5.5. Preparation of the Prodrug Analogs

Installation of the prodrug attachment (di-*tert*-butyl chloromethyl phosphate) was proposed to occur by a nucleophilic substitution reaction with the B-ring nitrogen of the pyrazoloquinolinone parent (LAU 463) as depicted in **Table 7**. The initial reaction conditions utilized those reported by Meanwell et al. at Bristol-Myers Squibb in the development of the HIV-1 drug, Fostemsavir.[66] These conditions (**Table 7**, trial 1) failed to undergo the nucleophilic substitution reaction in the present case, presumably, due to the difference in acidity of the PQ N-H (**LAU 463**, **8n**) proton as compared to the azaindole N-H proton in their case. Adequate deprotonation was deemed important, consequently, a series of bases (*t*-BuOK, K_2CO_3, and NaH), temperatures, and various solvents were employed (**Table 7**, trials 2-5). The solubility of the PQ's in various solvents was limited except for the case of DMF where complete solubility was observed. The use of sodium hydride was able to effect complete deprotonation of the PQ N-H proton in DMF as exhibited in an alkylation model reaction using methyl iodide with 99% yield (**Scheme 11**). Interestingly, two alkylation isomers were confirmed by integration of the NMR spectrum of the crude material (80% B-ring / 20% C-ring).

Scheme 11: Prodrug Model Alkylation Reaction

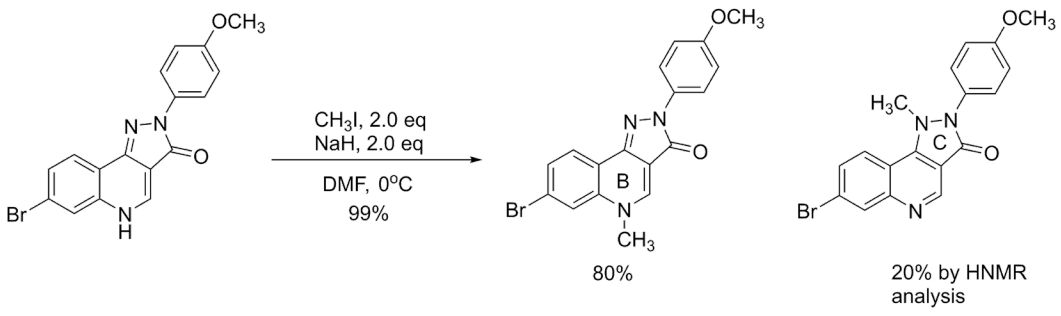

These conditions were then applied using the di-*tert*-butyl chloromethyl phosphate derivatizing agent (**Table 7**, trials 6 and 7), but this process exhibited poor yields even with elevated temperatures (45-50°C). Sodium iodide was then utilized as an additive to induce an *in situ* Finkelstein reaction to affect a halogen exchange of the chloromethyl phosphate to an iodomethyl phosphate, which resulted in a low, but useable yield (25%) of the *tert*-butyl protected N-phosphonooxymethyl prodrug **17a** (**Table 7**, trial 8). The low yield was most likely due to the instability of the halomethyl phosphate reagent under the reaction conditions (**Figure 21**).[66] Future trials should explore tetrabutylammonium iodide (TBAI) as a replacement for NaI. Only a minimal amount of the C-ring alkylated product was observed. The free phosphoric acid form of the prodrug (**18a**) was then obtained by removal of the tertiary butyl groups with trifluoroacetic acid in moderate yield (60%).

Figure 21: Impact of the Iodide Additive on the Stability of a Halomethyl Phosphate Reagent[66]

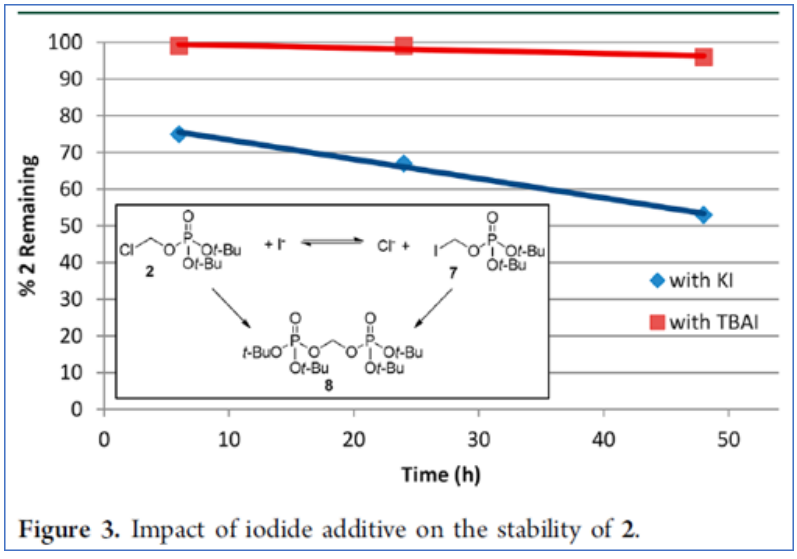

Figure 3. Impact of iodide additive on the stability of 2.

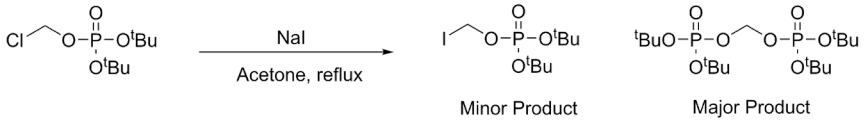

Table 7: Prodrug Route Optimization

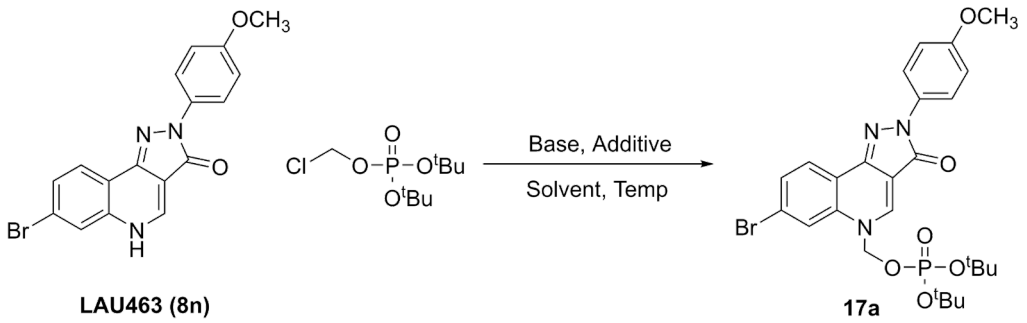

LAU463 (8n) 17a

Trial #	Phosphate	Base	Additive	Solvent	Temp	Result
1	1.5 eq	K_2CO_3, 1.2 eq	Et_4NI, 0.6 eq	ACN, H_2O	45-50 ºC	all SM[a]
2	1.5 eq	*t*-BuOK, 1.5 eq	Et_4NI, 0.6 eq	THF	20-25 ºC	all SM[a]
3	1.5 eq	K_2CO_3 ,1.5 eq	None	DMF	45-50 ºC	<5% Product
4	1.5 eq	NaH, 1.1 eq	None	THF	20-25 ºC	<5% Product
5	1.5 eq	NaH, 1.1 eq	None	THF	45-50 ºC	<5% Product
6	2.0 eq	NaH, 2.0 eq	None	DMF	20-25 ºC	<5% Product
7	2.0 eq	NaH, 2.0 eq	None	DMF	45-50 ºC	< 10% Product
8	2.0 eq	NaH, 2.0 eq	NaI, 2.0 eq	DMF	45-50 ºC	**25% Yield**

[a] SM equals starting material

Scheme 12: Prodrug Synthesis

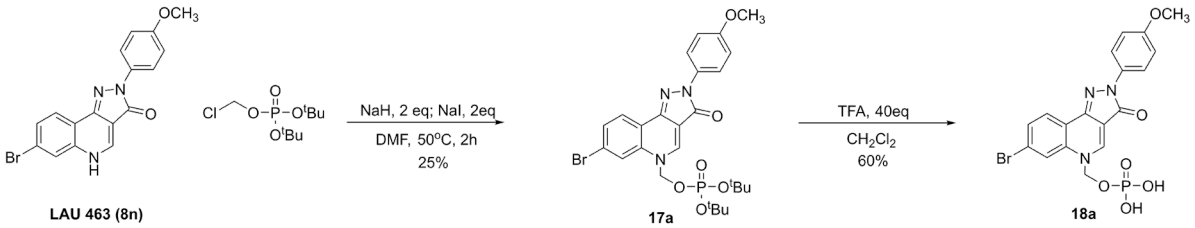

LAU 463 (8n) 17a 18a

1.6. Metabolic Stability with Human Liver (HLM) and Mouse Liver (MLM) Microsomes with Revathi Kodali

Since it was assumed that the α6β3γ2 selectivity of deuterated ligands would not be significantly different from that of the non-deuterated ligands, and since the generation of compounds with increased metabolic stability was the main aim of this study, the compounds synthesized were first investigated for their metabolic stability. The deuterated analogs displayed improved metabolic stability in both HLM and MLM, as compared to their respective nondeuterated parent compounds in all cases (**Table 8**). The non-deuterated parent ligands **8a** and **8i** both exhibited similar HLM-mediated metabolic half-lives of 3.6 and 3.4 hours, respectively, while **8n** displayed the most rapid metabolic rate of 1.7 hours in the presence of HLM. In MLM, **8a** exhibited a half-life of 3.2 hours and **8n** displayed a half-life of 1.9 hours, while **8i** displayed the most rapid metabolic rate in MLM with a half-life of 1.5 hours. Among the **8a** series, deuteration of the "A-ring" methoxy group (**8c**) exhibited a three-fold increase in stability in the presence of HLM and a four-fold increase of stability in MLM with respect to the parent ligand. Deuteration of the "D-ring" methoxy group (**8b**) exhibited a 2.5-fold increased half-life in HLM and a three-fold increase in MLM, as compared to **8a**. These results indicated a slightly faster metabolism of the "A-ring" methoxy group over the "D-ring" methoxy group in the **8a** parent series within experimental error. The comparison of metabolic stability in the presence of HLM of the "D-ring" *meta*-OCD_3 isomers between "A-ring" OCD_3 ligand **8e** and "A-ring" OCH_3 ligand **8g** further supports the evidence of faster metabolism of the "A-ring" versus the "D-ring" methoxy group. Additionally, a similar trend was observed for the "D-ring" *ortho*-OCD_3 isomers between "A-ring" OCD_3 ligand **8f** and "A-ring" OCH_3 ligand **8h**. The %

Table 8: Metabolic Stability in the Presence of HLM and MLM[2]

Compound	Half-life (HLM) (hr)	% left after 1 hr. (HLM)	Half-life (MLM) (hr)	% left after 1 hr. (MLM)
8a[p]	3.6 ± 0.6	86.10 ± 0.71	3.2 ± 0.1	80.35 ± 0.10
8b[b,p]	8.7 ± 0.6	91.69 ± 0.09	10.5 ± 0.9	92.80 ± 0.07
8c[b,p]	11.1 ± 3.6	92.00 ± 0.21	14.3 ± 2.8	93.17 ± 0.11
8d[b,p]	13.0 ± 3.0	91.51 ± 0.13	14.1 ± 3.2	93.08 ± 0.14
8e[b,m]	7.7 ± 1.1	89.50 ± 0.14	9.9 ± 1.9	90.50 ± 0.15
8f[b,o]	9.9 ± 1.5	90.50 ± 0.14	13.9 ± 4.2	92.00 ± 0.18
8g[b,m]	3.9 ± 0.3	81.28 ± 0.15	14.5 ± 4.2	91.56 ± 0.23
8h[b,o]	3.5 ± 0.2	79.92 ± 0.14	10.9 ± 1.5	93.04 ± 0.09
13a[b,e]	13.2 ± 2.2	92.85 ± 0.10	2.3 ± 0.1	74.77 ± 0.09
13b[b,e]	9.9 ± 1.1	92.58 ± 0.09	10.7 ± 1.2	92.39 ± 0.09
13c[b,e]	12.5 ± 3.1	92.30 ± 0.10	9.2 ± 0.9	91.38 ± 0.09
13d[b,e]	9.8 ± 2.8	90.00 ± 0.32	14.5 ± 4.8	92.50 ± 0.23
13i[b,f]	10.6 ± 2.7	91.00 ± 0.20	12.0 ± 4.0	93.00 ± 0.30
8i[m]	3.4 ± 0.2	81.44 ± 0.16	1.5 ± 0.1	59.83 ± 0.17
8j[c,m]	10.8 ± 1.0	93.00 ± 0.09	2.8 ± 0.1	76.59 ± 0.08
8k[c,p]	2.3 ± 0.1	72.50 ± 0.11	1.9 ± 0.1	69.20 ± 0.11
8l[c,p]	10.7 ± 1.5	92.20 ± 0.15	4.4 ± 0.3	85.54 ± 0.05
8m[c,o]	16.5 ± 1.8	94.80 ± 0.07	16.6 ± 2.0	94.91 ± 0.07
13e[c,e]	8.5 ± 0.5	91.60 ± 0.10	4.4 ± 0.2	85.62 ± 0.08
13f[c,e]	12.1 ± 1.9	93.00 ± 0.12	4.2 ± 0.2	85.11 ± 0.07
8n[p]	1.7 ± 0.1	66.86 ± 0.13	1.9 ± 0.1	68.96 ± 0.12
8o[d,p]	3.4 ± 0.1	81.50 ± 0.11	2.3 ± 0.1	73.85 ± 0.11
8p[d,m]	1.8 ± 0.1	63.50 ± 0.32	3.6 ± 0.3	79.50 ± 0.20
8q[d,o]	14.2 ± 3.0	92.85 ± 0.11	1.5 ± 0.3	61.31 ± 0.15
13g[d,e]	12.1 ± 1.4	93.40 ± 0.11	11.4 ± 1.4	93.13 ± 0.09
13h[d,e]	38.6 ± 7.7	97.80 ± 0.06	70.8 ± 25.8	98.39 ± 0.04

[a]Compounds were incubated with HLM or MLM for 60 minutes and quantified by LC-MS/MS. [b]**8a** related analogs in **red**. [c]**8i** related analogs in **blue**. [d]**8n** related analogs in **green**. [e]D-ring N-hetero analogs. [f]A-ring N-hetero analogs. [o]D-ring "*ortho*". [m]D-ring "*meta*". [p]D-ring "*para*".

percent remaining after 1 hour in the presence of HLM and MLM for each of the three deuterated ligands (**8b**, **8c**, and **8d**) was virtually identical between 91.5 and 93.1%, within experimental error. In the case of **8d**, deuteration of both methoxy groups did not have an additive effect on the metabolic stability in comparison with the mono-OCD_3 analogs **8b** and **8c**. Thus, from a cost and ease of synthesis point of view the mono-OCD_3 substituted analogs were pursued versus the di-OCD_3 substituted analog **8d** for further studies. In the **8i** series, the deuterated analog **8j** exhibited a three-fold increase in HLM-mediated half-life and a two-fold increase in MLM-mediated half-life. Similarly, the deuterated analog **8o** of the parent **8n** exhibited a two-fold increase in HLM-mediated half-life and a 20 % increase in MLM-mediated half-life. In summary, deuteration of the methoxy substituent(s) resulted in the desired improvement in metabolic stability in the presence of both HLM and MLM for the compounds.

Interestingly, the position of the methoxy substituent on the "D-ring" also seemed to have an impact on the metabolic stability of the PQs, and the effects observed differed in HLM and MLM, as indicated by a comparison of *ortho*-OCD_3 ligands with their *para*-OCD_3 analogs (**8e** vs **8d**; **8h** vs **8b**; **8m** vs **8l**; **8q** vs **8o**). A similar mixed half-life improvement in the presence of HLM and MLM was observed when *meta*-OCD_3-isomers were compared with the *para*-OCD_3 series (**8c** vs **8d**; **8g** vs **8b**; **8j** vs **8l**; **8p** vs **8o**). The introduction of *ortho*-OCD_3 substituents appeared to have the largest effect on metabolic stability in the **8i** and **8n** series (**8m** and **8q**, respectively), but notably this effect was not the case in the **8a** series (**8f** and **8h**). The *meta*-OCD_3 substituted ligands generally had the least improvement on metabolic stability in all three series (**8e**, **8g**, **8j**, and **8p**). Clearly, the observed mixed effect on metabolic stability governed by the position of the OCD_3 group on the "D-ring" was in line with the activity of CYP_{450} enzymes

in HLM versus MLM. Therefore, it is not possible, at present, to predict trends in the metabolic stability between the *para*- versus *ortho*- versus *meta*-methoxy substituted analogs as the HLM and MLM enzymes appeared non-discriminate in regards to the position of the methoxy group on the "D-ring" during the microsomal studies.

The N-heterocyclic ligands also exhibited better metabolic stability than the parent compounds. The N-hetero ligands are more polar (see cLogP data in **Table 8**) than their respective parent ligands and therefore should not undergo metabolism as quickly as the more lipophilic parent ligands, since the CYP_{450} enzymes primarily consist of lipophilic membrane-associated proteins.[78] Here, the N-hetero ligand **13a** when compared to the parent ligand **8a** exhibited a four-fold increase in half-life in the presence of HLM, yet a slightly decreased half-life was observed in the presence of MLM. Interestingly, the "A-ring" N-hetero ligand **13i** displayed a four-fold increase in the presence of both HLM and MLM. Similar improvement was seen when **13e** was compared to its parent compound **8k** where a nearly four-fold increase in half-life (HLM) and a two-fold increase in half-life (MLM) was observed. In the case of **8n**, the N-hetero ligand **13g** exhibited a seven-fold increase in half-life in both HLM and MLM which is significant.

Notably, the effect of incorporation of both the "D-ring" N-hetero (pyridine-like) substituents and the deuterated methoxy groups onto the lead ligands, exhibited even an further improvement in the metabolic stability over either case individually. Herein, the OCD_3 substituted N-hetero ligand **13f** when compared to the OCH_3 substituted N-hetero ligand **13e** exhibited a 40% increased half-life (HLM) and no change with respect to the half-life in the

presence of MLM. Additionally, the OCD_3 substituted N-hetero ligand **13h** exhibited a three-fold increased stability (HLM) and six-fold increased stability (MLM) with respect to their half-lives when compared to the OCH_3 substituted N-hetero ligand **13g**. Of special note, the 7-bromo-4'-OCD_3 substituted N-heterocyclic compound **13h** displayed the best metabolic stability of all the analogs in the series with half-lives of 38.6 hours (HLM) and 70.8 hours (MLM), respectively.

The effect of deuteration of the "A-ring" and / or the "D-ring" methoxy groups was also examined in the case of the **13a** related analogs (**13b**, **13c** and **13d**). A definitive metabolic rate difference between the "A-ring" methoxy group and the "D-ring" methoxy group (see **13c**, "A-ring" OCD_3 group and **13b**, "D-ring" OCD_3 group) as compared to **13a** was not evident; the effect was much more subtle than the metabolic stability observed in the α6 selective **8a** series above and again was different in the presence of HLM or MLM. In the case of di-OCD_3 analog **13d**, deuteration of both methoxy groups did not have an additive effect on the metabolic stability in comparison to the mono-OCD_3 analogs **13c** and **13b**. Obviously, the concurrent effect on the metabolic stability between the N-hetero and OCD_3 substitution is too complex to draw clear conclusions based on the impact of deuteration of the "A-ring" versus "D-ring" methoxy groups in the case of **13a** related analogs. It is very possible that retardation of the rate of the O-demethylation reaction in both the "A-ring" and "D-ring" has directed the metabolism rapidly towards another metabolic pathway.

The effect of fluorination (-OCF_3) of the methoxy groups is exhibited in **Figure 22**, **Figure 23**, **Figure 24** and **Figure 25** with the -OCF_3 substituted ligands shown on the far right of

each graph. In general, the fluorination tactic improved the observed metabolic stability observed in HLM and MLM versus the parent -OCH_3 substituted ligands (far left of each graph). In comparison with the deuterated and *N*-hetero ligands, fluorination proved to be a less effective method of improving metabolic stability except in the case of the LAU463 related -OCF_3 ligand, DK-IV-22-1. Here, the -OCD_3 ligand, DK-I-58-1 exhibited slightly less stability in the presence of the human liver and mouse liver microsomes than its fluorinated counterpart, DK-IV-22-1.

Figure 22: Metabolic Stability, Comparison of **PZ-II-029 (8a)** Related Ligands[2, 79]

A

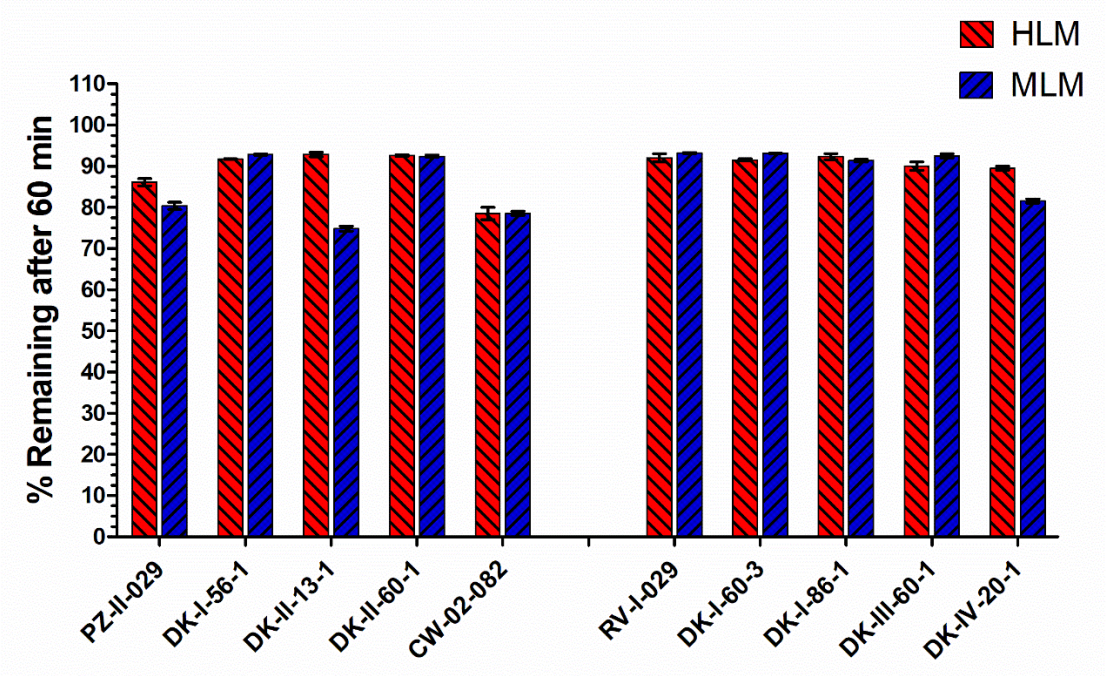

B

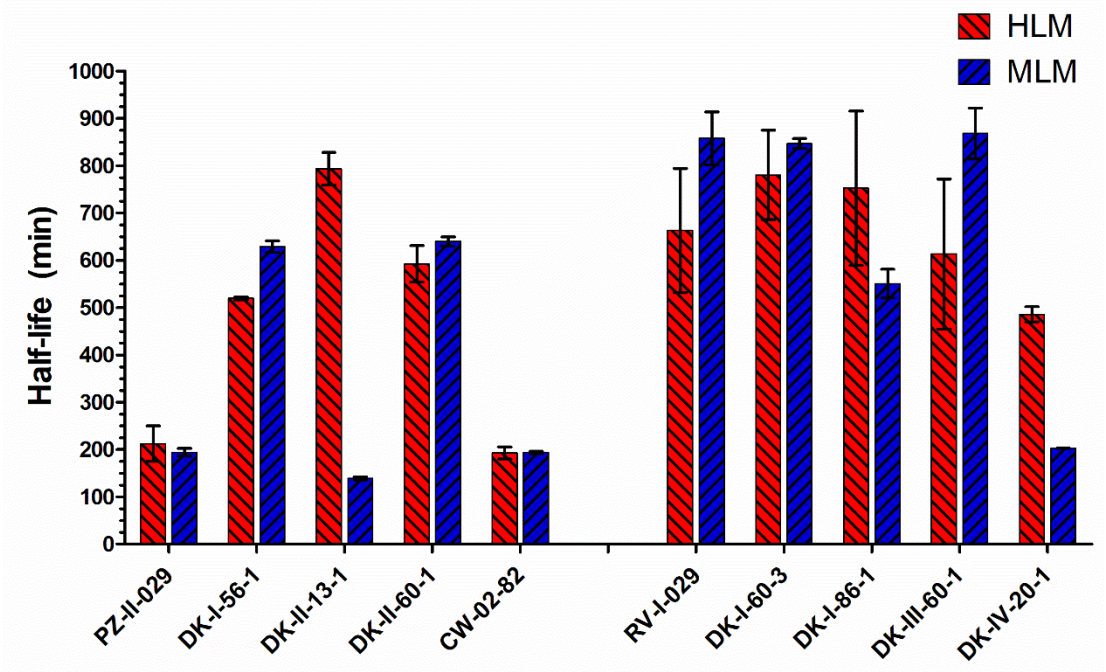

Compounds were incubated with HLM or MLM for 60 minutes and quantified by LC-MS/MS. PZ-II-029 / RV-I-029 = 4'-OCH_3. DK-I-56-1 / DK-I-60-3 = 4'-OCD_3. DK-II-13-1 / DK-I-86-1 = *N*-Hetero with 4'-OCH_3. DK-II-60-1 / DK-III-60-1 = *N*-Hetero with 4'-OCD_3. CW-02-82 / DK-IV-20-1 = 4'-OCF_3. (A) = % Remaining after 60 min. (B) = Half-life (min).

Figure 23: Metabolic Stability, Comparison of **LAU 159 (8i)** Related Ligands[2, 79]

A

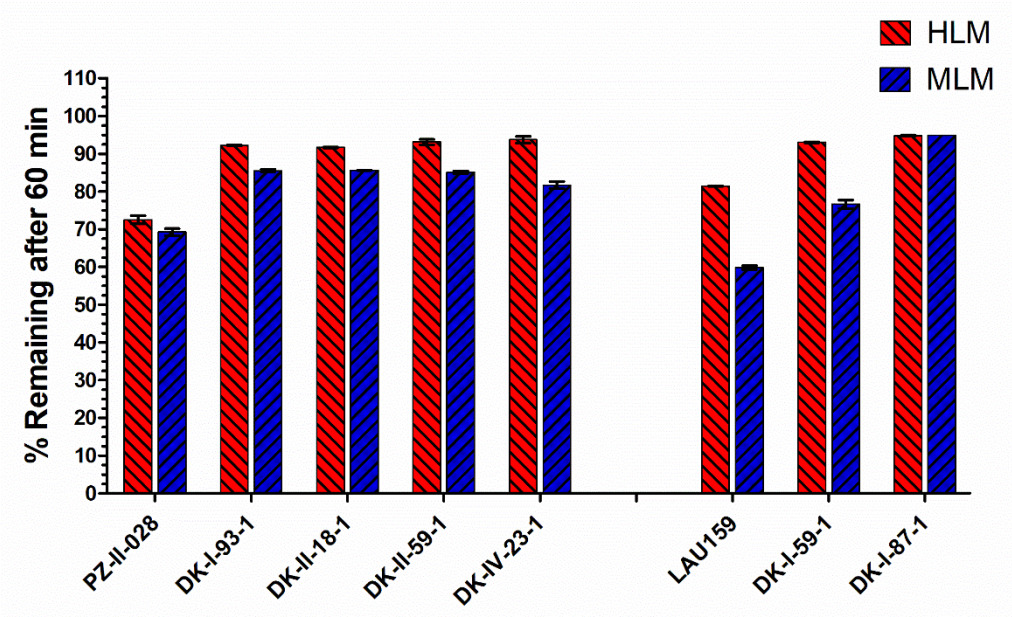

B

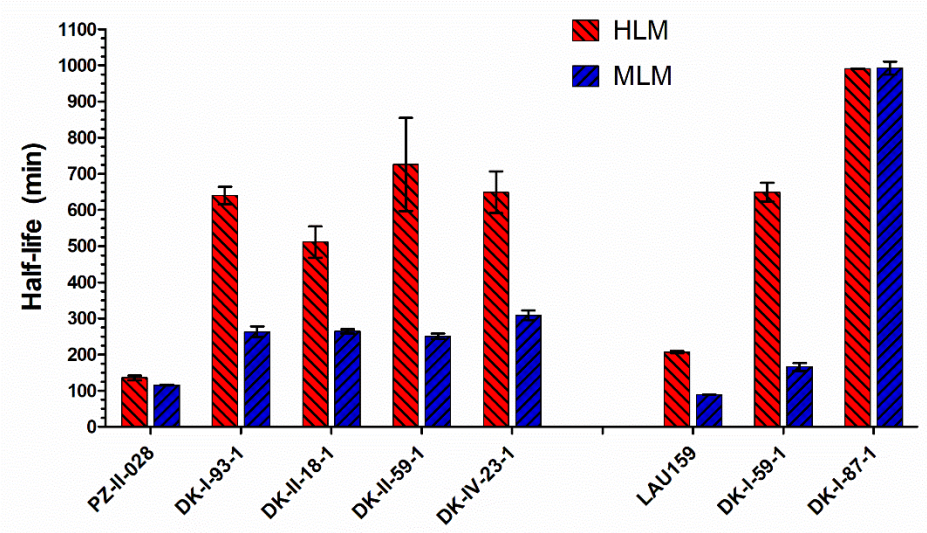

Compounds were incubated with HLM or MLM for 60 minutes and quantified by LC-MS/MS. PZ-II-028 = 4'-OCH_3. DK-I-93-1 = 4'-OCD_3. DK-II-18-1 = *N*-Hetero with 4'-OCH_3. DK-II-59-1 = *N*-Hetero with 4'-OCD_3. DK-IV-23-1 = 4'-OCF_3. LAU159 = 3'-OCH_3. DK-I-59-1 = 3'-OCD_3. DK-I-87-1 = 2'-OCH_3. (A) = % Remaining after 60 min. (B) = Half-life (min).

Figure 24: Metabolic Stability, Comparison of **LAU 463 (8n)** Related Ligands[2, 79]

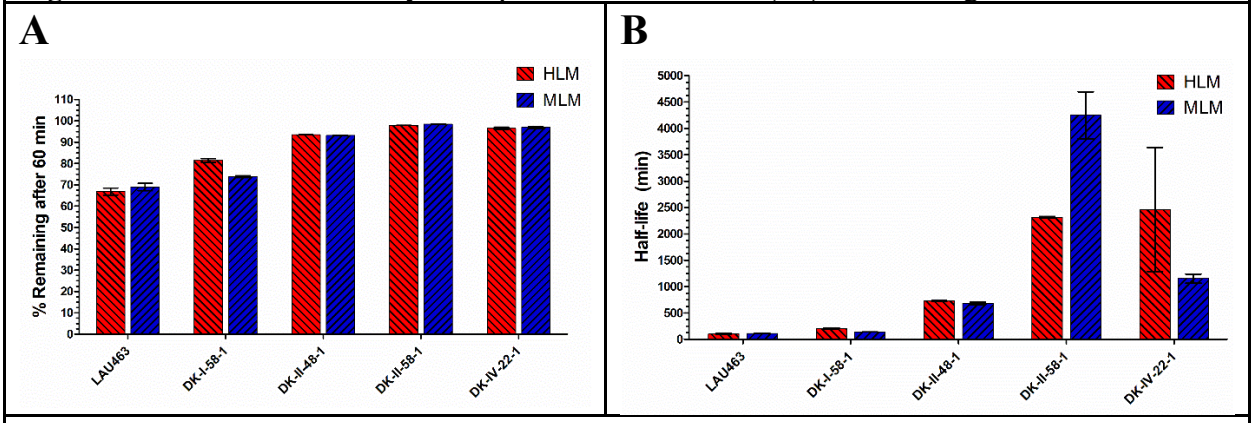

Compounds were incubated with HLM or MLM for 60 minutes and quantified by LC-MS/MS. LAU463 = 4'-OCH_3. DK-I-58-1 = 4'-OCD_3. DK-II-48-1 = *N*-Hetero with 4'-OCH_3. DK-II-58-1 = *N*-Hetero with 4'-OCD_3. DK-IV-22-1 = 4'-OCF_3. (A) = % Remaining after 60 min. (B) = Half-life (min).

Figure 25: Metabolic Stability, Comparison of **MM-I-06 (14i)** Related Ligands[2, 79]

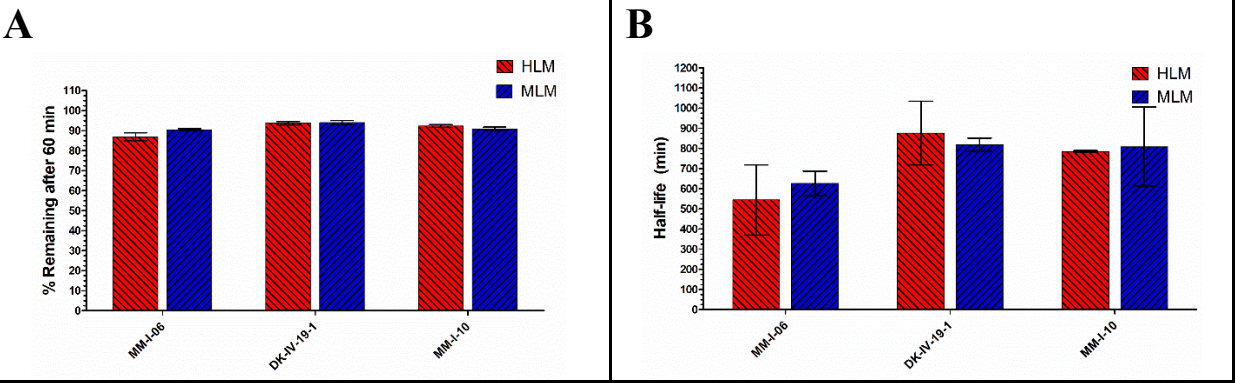

Compounds were incubated with HLM or MLM for 60 minutes and quantified by LC-MS/MS. MM-I-06 = 4'-OCH_3. DK-IV-19-1 = 4'-OCD_3. MM-I-10 = 4'-OCF_3. (A) = % Remaining after 60 min. (B) = Half-life (min).

1.7. Metabolite Study with Revathi Kodali

Analysis of the metabolites from the HLM and MLM studies confirmed that the primary metabolic function of CYP_{450} enzymes[36] with respect to methoxyarylpyrazoloquinolinones proceeded by O-demethylation of the methoxy groups (OCH_3) in either the "A-ring" or "D-ring" to form hydroxyarylpyrazoloquinolinones. This is in agreement with Nelson et al.[37] Furthermore, this study confirmed the kinetic DIE[35] and illustrated that $k_H > k_D$ for compounds with both a OCD_3 and a OCH_3 group in either the "A-ring" or "D-ring" (**Scheme 13**) was in operation. Qualitative assessment by mass spectroscopy confirmed for the "D-ring" OCD_3 substituted ligand **8b** (**Scheme 13A**), the primary metabolite **I** (in **bold**) existed at a much higher concentration than metabolite **II** and the di-desmethoxy metabolite **III** in both (HLM and MLM) metabolism studies after sixty minutes. Similarly, for "A-ring" OCD_3 substituted ligand **8c** (**Scheme 13B**), the primary metabolite **IV** (in **bold**) was present at a higher concentration than either metabolite **V** or **VI**. Examples **A** and **B** in **Scheme 13**, clearly indicated that the kinetic DIE predominated in the metabolic pathway ($k_H > k_D$) of the O-demethylation (OCD_3 versus OCH_3) of these ligands over which ring ("A-ring" or "D-ring") the deuterated versus non-deuterated methoxy groups was placed upon.

For the case of N-hetero substituted ligand **13b** (**Scheme 13A**), primary metabolite **VII** (in **bold**) existed at a much higher concentration than metabolite **VIII** and the di-desmethoxy metabolite **IX** in both the HLM and MLM metabolism study after 60 minutes. Similarly, for "A-ring" OCD_3 substituted ligand **13c** (**Scheme 13B**), primary metabolite **X** (in **bold**) was present at a higher concentration than either metabolite **XI** or **XII**. Examination of examples **A** and **B** in **Scheme 13** not only indicated that substitution of OCD_3 for OCH_3 predominated during

metabolism over the effect of which ring ("A-ring" versus "D-ring)" the deuterated methoxy group was placed upon, but also showed that the kinetic DIE prevailed over the effect of N-hetero substitution onto the "D-ring" of the ligands on the rate of metabolism.

In the cases of **8o** and **8j**, it was also confirmed (see **Scheme 13C** and **Scheme 13D**) that the primary metabolic pathway occurred via O-demethylation of the methoxy groups since the primary metabolite **XIII** was found for **8o** and the primary metabolite **XIV** was found for **8j**. In summary, this metabolite study confirmed the importance of deuteration of the methoxy groups to positively impact the metabolic stability of this series of $GABA_AR$ α6 subtype selective ligands. In addition, the metabolic rate of these ligands was governed predominately by the kinetic DIE over the position of the deuterated versus non-deuterated methoxy group on the "A-ring" versus "D-ring" or the impact of a "D-ring" N-hetero substituent, as mentioned above.

Scheme 13: Metabolite Study. O-Demethylation of OCH_3 Versus OCD_3 by CYP_{450} Enzymes in HLM and MLM[2]

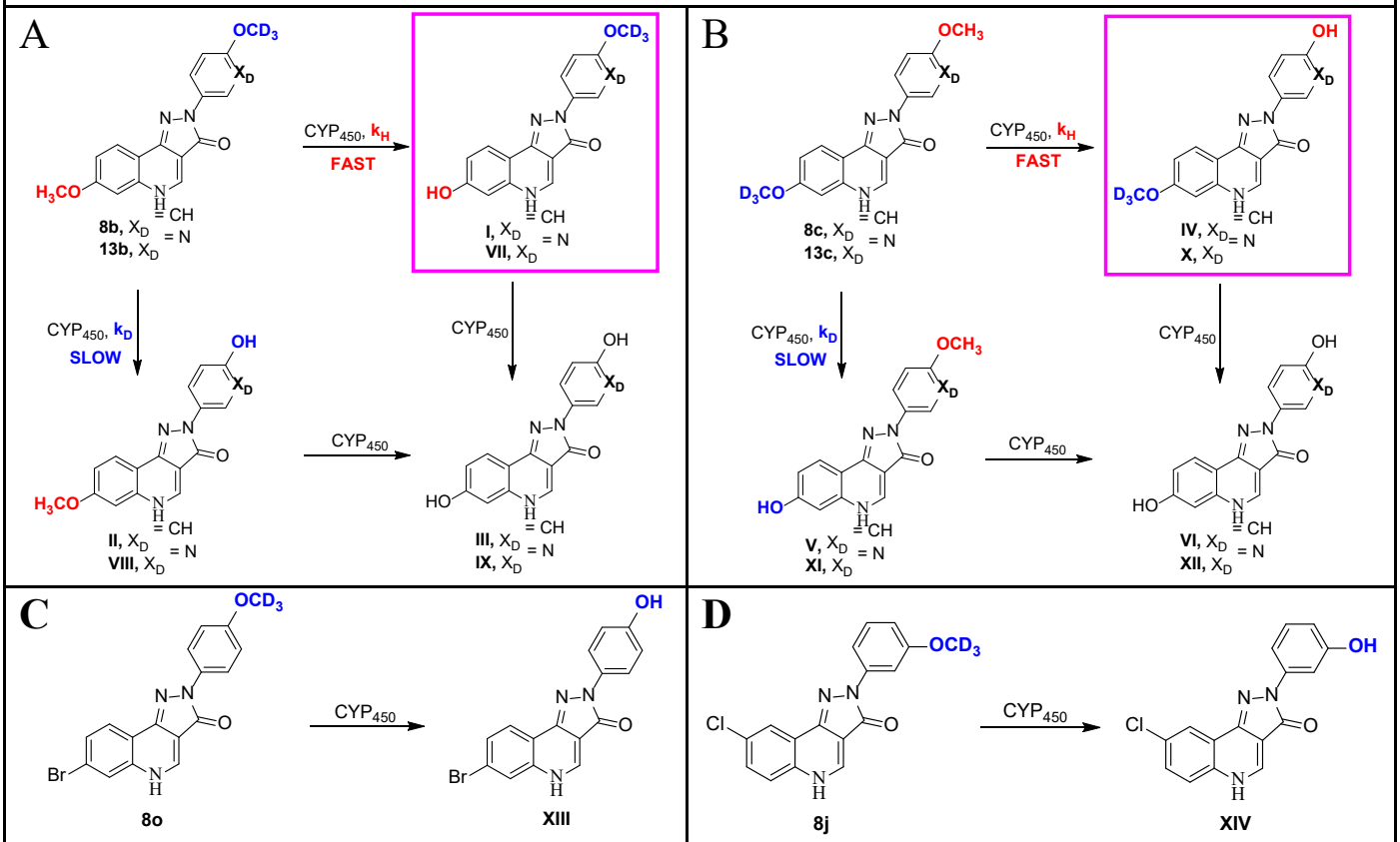

[a]Metabolites found confirmed $k_H > k_D$ in both HLM and MLM using an LCMS. k_H = O-demethylation of OCH_3, k_D = O-demethylation of OCD_3, CYP_{450} = metabolism by Cytochrome P450 enzymes. Primary metabolites (**I**, **IV**, **VII** and **X**) are highlighted in examples **A** and **B** respectively.

1.8. Study of $GABA_AR$ α6β3γ2 Subtype Efficacy and Selectivity with Dr. Margot Ernst and Dr. Janet Fisher[2, 79, 80]

The three lead ligands (**8a**, **8n** and **8i**) all displayed a pronounced functional selectivity for the $GABA_AR$ α6β3γ2 subtype,[12, 31] and modulated the EC_3-GABA induced currents strongly with efficacies at 30 μM ranging from ~400% (**8i**) to ~ 900% (**8a** and **8n**) potentiation (**Figure 26**). Electrophysiological experiments confirmed that within experimental error, replacement of OCH_3 by OCD_3 groups did not significantly change the efficacy of five different deuterated ligands for modulation of GABA-induced currents at the α6β3γ2 $GABA_AR$ subtype (**Figure 27**), as compared to the three lead compounds. It thus could be assumed that this also would hold true for the efficacy of these ligands for modulating GABA-induced currents at the other receptor subtypes that was zero or close to zero for the three lead compounds up to a concentration of 1 μM (**Figure 26**), and that these compounds would exhibit a comparable α6β3γ2 $GABA_AR$ selectivity. Specifically, the deuterated analogs of **8a** (**8b**, **8c**, **8d**) and **8n** (**8o**) exhibited the best efficacy and selectivity. The full dose response curves for DK-I-56-1 (**8b**) are exhibited in **Figure 28**A and DK-I-58-1 (**8o**) in **Figure 30**A which display the α6β3γ2 subtype selectivity for these novel deuterated ligands.

In a different series of compounds based on PZ-II-028 (**8k**)[27] which exhibited higher efficacy but poor α6 selectivity, as compared with **8a**,[12] the methoxy group on the "D-ring" was moved from *para* to the *meta* (**8i**) and to the *ortho* (**8m**) positions. These modifications dramatically changed the properties of the compounds. As a result the *meta*-OCH_3 substituted compound, LAU 159 (**8i**), in contrast to its non-selective parent compound **8k** was a selective modulator of the α6β3γ2 subtype,[30] while the *ortho*-OCD_3 analogue **8m** was completely inactive

(**Figure 28D** and **Figure 29**). The same turned out to be true for the non-deuterated analogue of **8m** (LAU 165).[30] Since LAU 165 was not able to inhibit the effects of **8i**,[30] it might not be able to bind to the α6+β3- interface. Since deuteration does not change the activity of compounds at the receptor, this conclusion also holds true for **8m**. Consequently, **8m** can be further investigated in *in vivo* studies as a negative control compound from the same chemotype to establish that an observed biological effect was connected with the modulation of the α6β3γ2 subtype.

In an additional study, ligands with heteroatoms in the core scaffold with substituents at positions analogous to the parent ligands (**8a**, **8n** and **8k**) were also investigated. Incorporation of the N-hetero atoms into the "A-ring" or "D-ring" of the PQ core was accompanied by a drop in efficacy at the α6β3γ2 subtype relative to parent compounds **8a** and **8k**, but not relative to the parent compound **8n**, as revealed by the data **Figure 31**. Four compounds retained some efficacy (**13b**, **13c**, **13h**, and **13i**), while one N-hetero ligand **13f** displayed much poorer efficacy. The deuterated *N*-hetero analog **13c** was then characterized in the whole panel of six receptors (**Figure 32**). While the maximum efficacy of **13c** was weaker than that for the lead ligands, the α6 subtype selectivity was very good and if its bioavailability is as good or better, this compound may be a good alternative to **8a** for use in *in vivo* studies. The full dose-response curve for DK-II-58-1 (**13h**) displayed in **Figure 30**B revealed this *N*-hetero ligand exhibited similar α6β3γ2 subtype selectivity as the deuterated lead ligands DK-I-56-1 (**8b**) and DK-I-58-1 (**8o**).

In a later study, ligands with a 4'-OCF_3 and/or 7-CF_3 groups were assessed for α6β3γ2 subtype selectivity. Unfortunately, these ligands (**Figure 33**) were neither selective nor as potent when compared to the lead ligands of this study. Only DK-IV-20-1 (**14p**, **Figure 33**D) with a 4'-OCF_3 and 7-OCD_3 substituents retained α6-selectivity, yet its potency was much less than the parent ligands.

Figure 26: $GABA_AR$ α6β3γ2 Subtype Selectivity of the Lead Ligands: **PZ-II-029 (8a)**, **LAU 463 (8n)** and **LAU 159 (8i)**[2]

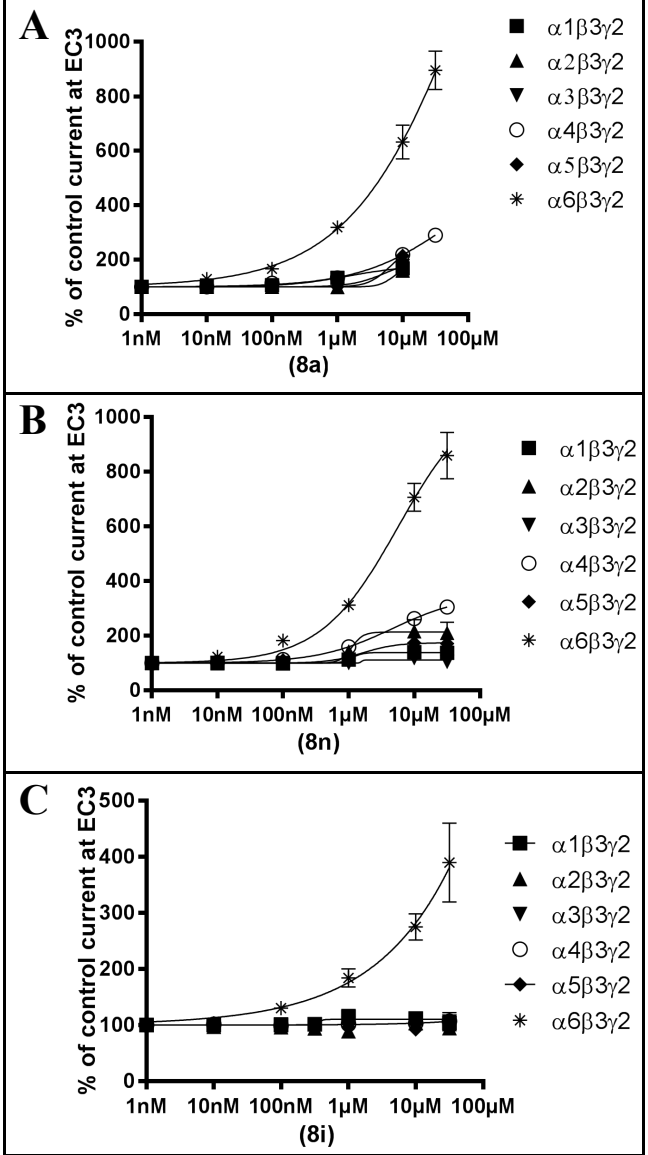

[a]Concentration response curves of the change of GABA EC_3 currents (modulation, referenced to 100% for the EC_3 current) by increasing compound concentrations. **8a** (**A**), **8n** (**B**) and **8i** (**C**) preferentially modulate GABA currents of α6β3γ2 receptors.

Figure 27: The Effect of Substituting OCD_3 for OCH_3 Groups on the Lead Ligands on $GABA_AR$ α6β3γ2 Subtype Activity[2]

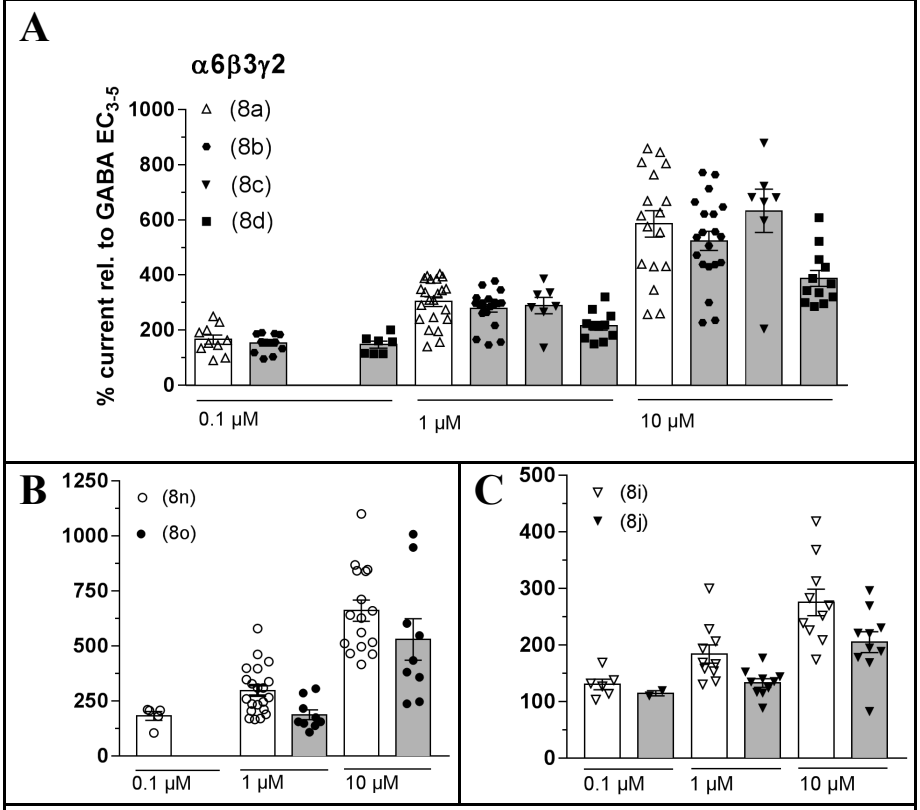

[a]Electrophysiological experiments confirmed that OCD_3 groups do not change the activity (within experimental error) of the ligands for the α6β3γ2 subtype. **8a** related ligands (**A**). **8n** related ligands (**B**). **8i** related ligands (**C**).

Figure 28: $GABA_AR$ α6β3γ2 Subtype Selectivity of the Ligands: **DK-I-56-1 (8b)** and **DK-I-87-1 (8m)**[48]

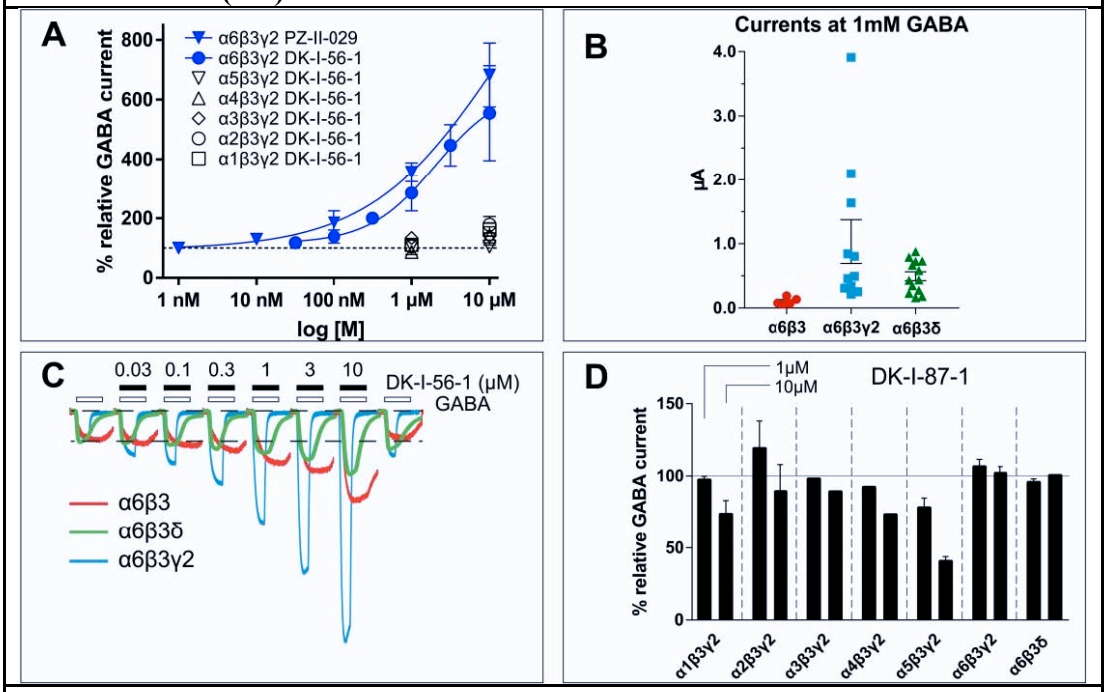

(A) Concentration-response curves of the modulation of GABA EC3-6 (100%) currents by increasing concentrations of PZ-II-029 and DK-I-56-1 in the α6β3γ2 receptor. Concentration-response curves for PZ-II-029 were taken from Varagic et al (2013). Other receptor subtypes were investigated only at 1 and 10 μM DK-I-56-1, because this compound did not significantly modulate GABA EC3-6 at these receptors below 1 μM concentration. (B) Currents elicited by 1 mM GABA in cells expressing α6β3γ2, α6β3δ and α6β3 receptors. (C) Representative traces of the cells expressing α6β3γ2, α6β3δ and α6β3 receptors, while applying GABA at a fixed concentration and an increasing concentration of DK-I-56-1. The traces are scaled to reflect EC3-6 for α6β3γ2 receptor and ~ EC90 for α6β3δ and α6β3 receptors. (D) Screening receptor subtypes for modulatory effects of DK-I-87-1. Bars per subunit combination represent compound concentrations of 1 and 10 μM, respectively. Data is presented relative to reference currents elicited by GABA alone (~ GABA EC3-6 for all αβ3γ2 receptors, ~ EC90 for α6β3δ receptors).

Figure 29: $GABA_AR$ α6β3γ2 Subtype Activity of the "D-ring" *ortho*-OCD_3 Isomer **DK-I-87-1 (8m)[2]**

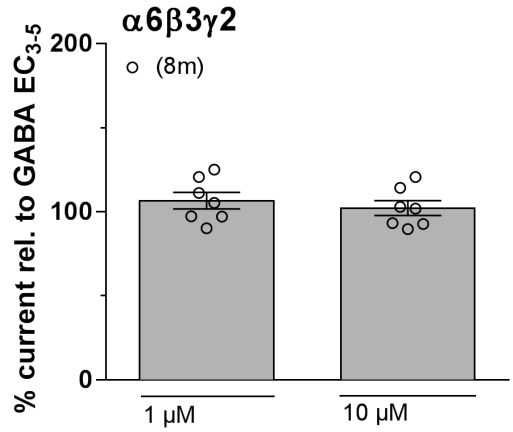

[a]Two-point electrophysiological experiments displayed that ligand **8m** with a "D-ring" *ortho*-OCD_3 substituent and "A-ring" 8-chloro substituent had no activity at the $GABA_AR$ α6β3γ2 subtype.

Figure 30: $GABA_AR$ α6β3γ2 Subtype Selectivity of the Lead Ligands: **DK-I-58-1 (8n)** and **DK-II-58-1 (13h)**[79, 80]

A

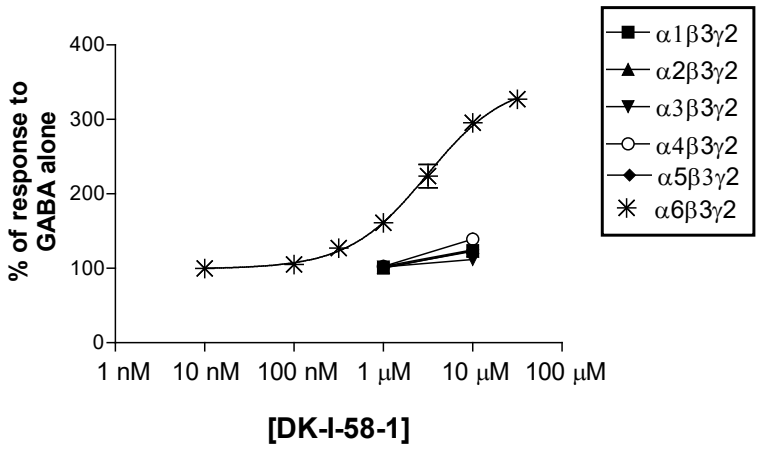

B

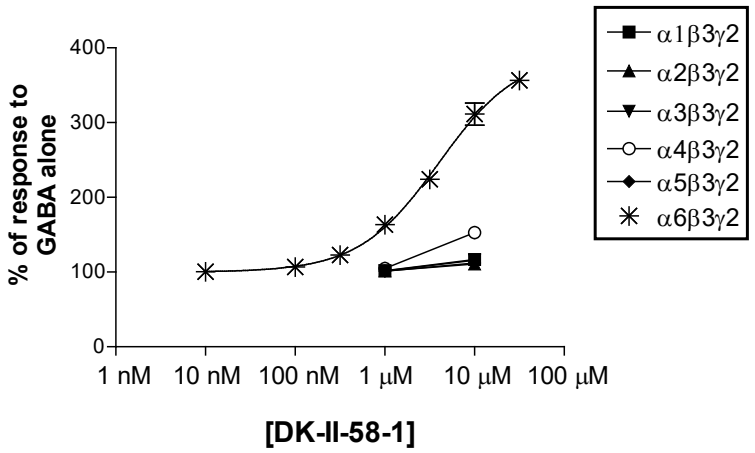

[a]Concentration response curves of the change of GABA EC_3 currents (modulation, referenced to 100% for the EC_3 current) by increasing compound concentrations. **8n** (**A**), and **13h** (**B**) preferentially modulate GABA currents of α6β3γ2 receptors.

Figure 31: The Effect of N-hetero Substitution onto the "A-ring" or "D-ring" of the Lead Ligands on $GABA_AR$ α6β3γ2 Subtype Activity[2]

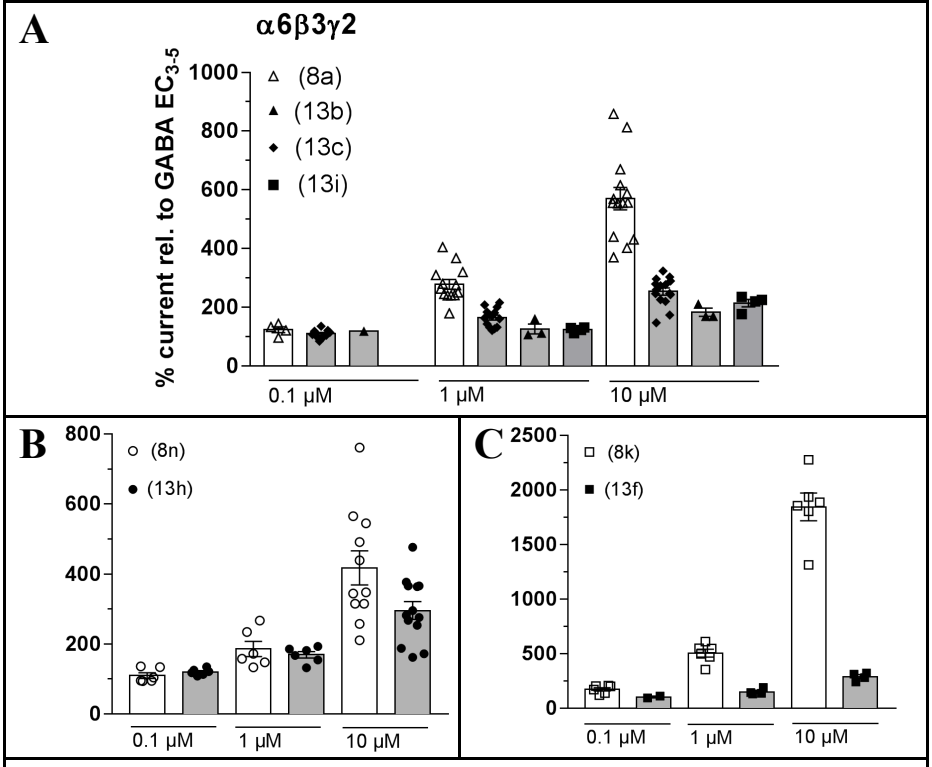

[a]Electrophysiological experiments exhibited that N-hetero substitution onto the "A-ring" or "D-ring" of the parent ligands decreased the activity of the ligands for the α6β3γ2 subtype. **8a** related ligands (**A**). **8n** related ligands (**B**). **8k** related ligands (**C**).

Figure 32: $GABA_AR$ α6β3γ2 Subtype Selectivity of the N-hetero Ligand **DK-I-86-1 (13c)**[2]

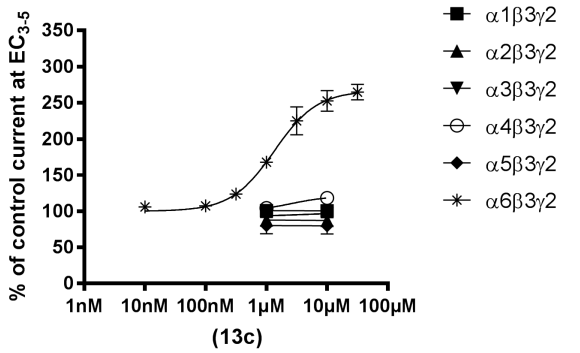

[a]Concentration response curves of the change of GABA EC_3 currents (modulation, referenced to 100% for the EC_3 current) by increasing compound concentrations. Ligand **13c** preferentially modulated GABA currents of α6β3γ2 receptors. In the α1-5β3γ2 receptors, lack of activity was confirmed in two-point experiments.

Figure 33: The Effect of CF_3 Substitution onto the "A-ring" or OCF_3 Substitution onto the "D-ring" of the Lead Ligands on $GABA_AR$ α6β3γ2 Subtype Activity[79, 80]

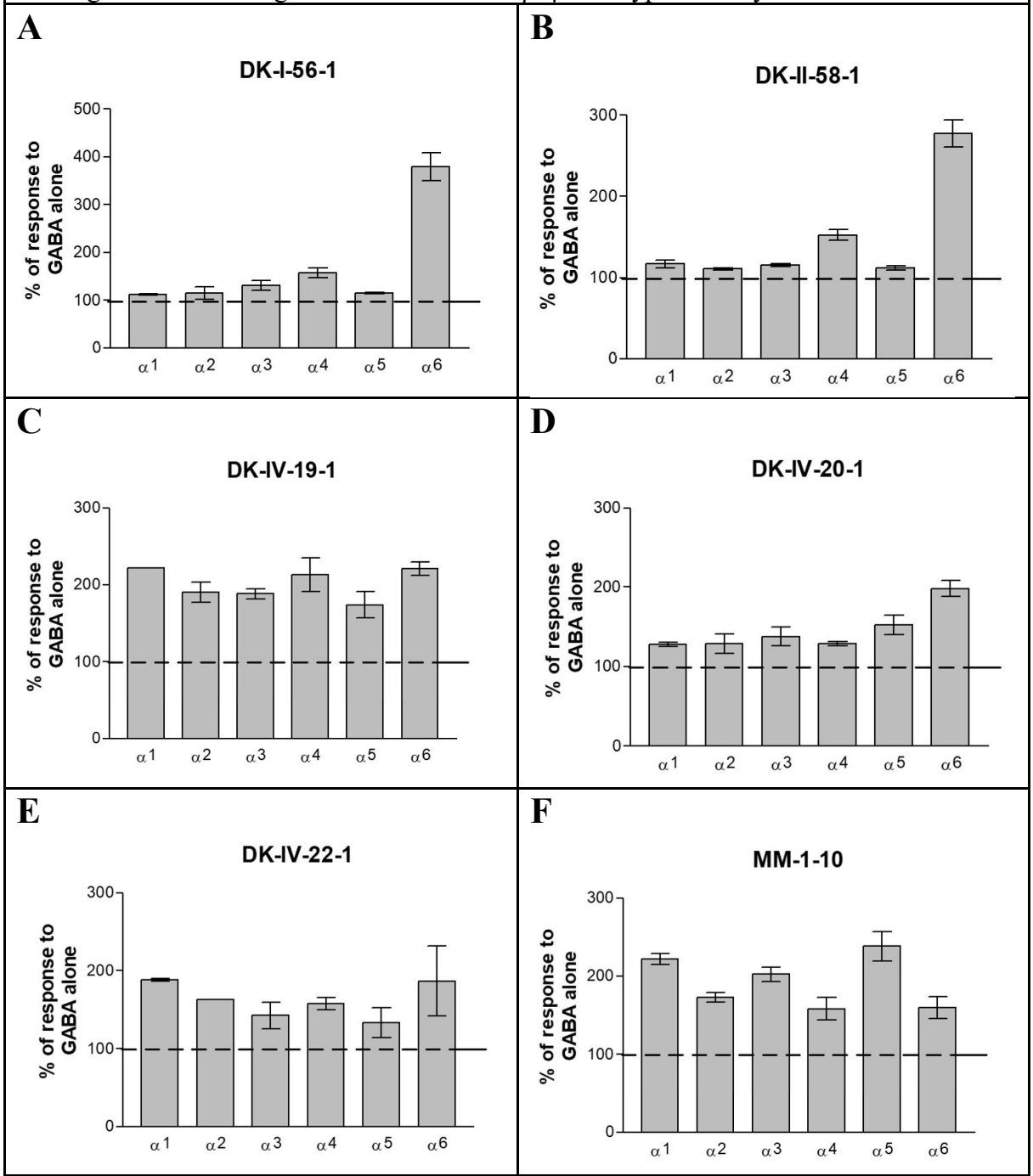

[a]Electrophysiological experiments at 10μM exhibited that 7-CF_3 substitution onto the "A-ring" or 4'-OCF_3 substitution onto "D-ring" of the parent ligands decreased the activity and selectivity of the ligands for the α6β3γ2 subtype.

1.9. PDSP Receptor Study with Dr. Bryan Roth

In addition to this $GABA_AR$ α6β3γ2 subtype selectivity, a screening of the ligands were screened against a panel of 46 receptors, transporters and ion channels including the hERG channel which confirmed selective binding of these ligands towards the Bz/$GABA_A$ receptors (**Table 59**). The analogs related to **8i** only displaced the radiolabeled probe [^{3}H]flunitrazepam from the benzodiazepine (BZP) rat brain site of $GABA_ARs$, except for **8l**, that also weakly interacted with DOR ([^{3}H]DADLE). No affinity of these analogs was observed for the other 45 receptors (**Table 59**). The BZP rat brain site is a homogenized mixture of rat brain cells and membranes consisting of all $GABA_AR$ subtypes (α1-α6) where the binding affinity reflects affinity at the α+γ- site. The ligands related to **8a** showed no activity in all assays except the BZP rat brain site of $GABA_ARs$. There was weak activity observed at serotonin (5-HT_7, [^{3}H]LSD), and μ-opioid (MOR, [^{3}H]DAMGO) receptors. However, individual ligands such as **8a**, also showed weak activity at dopamine D_5 receptors ([^{3}H]SCH233930), or **13a** at muscarinic M_4 ([^{3}H]QNB) receptors. The **8n** related structures again only showed activity at the BZP rat brain site of $GABA_ARs$, but individual compounds weakly interacted also with serotonin 5-HT_{2B} ([^{3}H]LSD), 5-HT_{2C} ([^{3}H]Mesulergine) and 5-HT_7 ([^{3}H]LSD) receptors, or μ-opioid (MOR, [^{3}H]DAMGO) receptors. Most of these individual additional interactions resulted in about 50% inhibition of binding of the respective ligand at a 10 μM drug concentration, suggesting an IC_{50} of about 10 μM. **Secondary binding studies (Table 60) were then conducted to determine the binding affinities for any ligand that displaced >50% radioligand in the primary (PDSP) assay, which demonstrated that off-target binding for most ligands was 1,000 times less potent compared to the primary target.** The *ortho* isomers of **8b** and **8o** (**8h** and **8q**, respectively) exhibited significantly less binding to the BZP rat brain site, while the *ortho*-OCD_3

isomer of **8i (8m**) still displayed a reasonable binding affinity to the BZP rat brain site, but less as compared to its *para*-OCD_3 isomer **8l**. Thus, the *ortho* isomer **8m** was identified as a control compound because of its lack of efficacy exhibited at the $GABA_AR$ α6β3γ2 subtype, as described above. Overall, the library of potential α6 ligands do have high specificity for binding at the BZP rat brain site and importantly do not bind at the hERG channel nor any of the other 44 receptors, transporters and channels examined in a significant fashion. However, it cannot be ruled out from the PDSP assays that these compounds do not interact with binding sites at these receptors for which no radiolabeled ligands are available or at other receptors, transporters and channels that were not investigated in this study. Thus, although it is proposed that these α6 subtype selective ligands bind at both the α6+β3- (PQ) site as positive allosteric modulators and at the α6+γ2- (DI-Bz) site as null modulators of $GABA_ARs$,[10, 12, 13] there is no way to assess their binding affinity at the α6+β3- (PQ) site at present. Deuterated and N-hetero analogs of the parent compounds did not display a meaningful change in binding behavior in the panel of radioligand binding assays explored (B. Roth et al., NIMH Psychoactive Drug Screening Program, UNC, available at http://pdsp.med.unc.edu) when compared to the parent OCH_3 lead compounds. The fluorinated analogs exhibited similar selective binding for the BZP rat brain site and importantly did not bind at the hERG channel nor any of the other 44 receptors, transporters and channels examined in a significant fashion (**Table 61** and **Table 62**). Interestingly, the fluorinated ligands exhibited much less binding affinity for the BZP rat brain site (**Table 10**) than the parent ligands or the newly discovered α6-selective deuterated or *N*-Hetero ligands. Presumably, the binding affinity at the α+γ- site was negatively impacted by the size of the 4'-OCF_3 groups and the inability to form hydrogen bonds in the binding pocket. This observation is discussed in more detail in the molecular modeling chapter below.

1.10. Study of Solubility and cLogP

The introduction of *N*-hetero atoms into either the "A-ring" (**13i)** or "D-ring" (**13a)** of α6 ligands such as **8a** increased the water solubility, as compared to the parent ligands in both neutral and acidic media only significantly in the case of the lead ligand **8a** (see **Table 9**). In the case of **8k**, introduction of a pyridine-like nitrogen atom into the "D-ring" (**13e**) actually decreased the water solubility by almost 10-fold in both neutral and acidic aqueous media. Additionally, N-hetero introduction into the "D-ring" of **8n** resulted in only a minimal impact on the neutral and acidic solubility in the case of **13g**. Finally, **8i** had similar solubility as **8k** and **8n**. Ultimately, the aqueous solubility for **8a** was the best over the other non-N-hetero substituted ligands; however, N-hetero ligands **13i** and **13a** displayed significant improvement in water solubility. The water solubility in 0.01 M HCl (pH = 2) of the ligands did not improve over the water solubility (pH = 7) substantially in any of the cases explored, presumably because the nitrogen of the N-hetero substituent lacks sufficient basicity to positively impact hydrogen chloride salt formation. Because the "A-ring" analog **13i** was difficult to synthesize, only the deuterated analogs of **8a** and **13a** were carried forward for pharmacokinetic studies. Of note, the calculated cLogP (octanol-water partition coefficient[39]) values (**Table 9**) also dropped in all cases for the N-hetero analogs as expected; however, this did have an important positive effect on metabolic stability, as indicated by a comparison of **8a** and **13a**, **8k** and **13e**, or **8n** and **13g**. The fluorinated analogs exhibited increased cLogP values (**Table 10**), as expected, given the propensity of fluorination to increase ligand lipophilicity and membrane permeability.[40, 45] Interestingly, however, *N*-hetero substitution together with deuteration resulted in an 11-fold increase in metabolic stability in HLM, and a 30-fold increase in stability in MLM in the **8n** series (compare **8o** and **13h** in **Table 9**).

Table 9: Solubility and cLogP of Compounds Indicating the Effect of Adding the Nitrogen Atom to the A- or D-Ring of PQ Ligands[a,2]

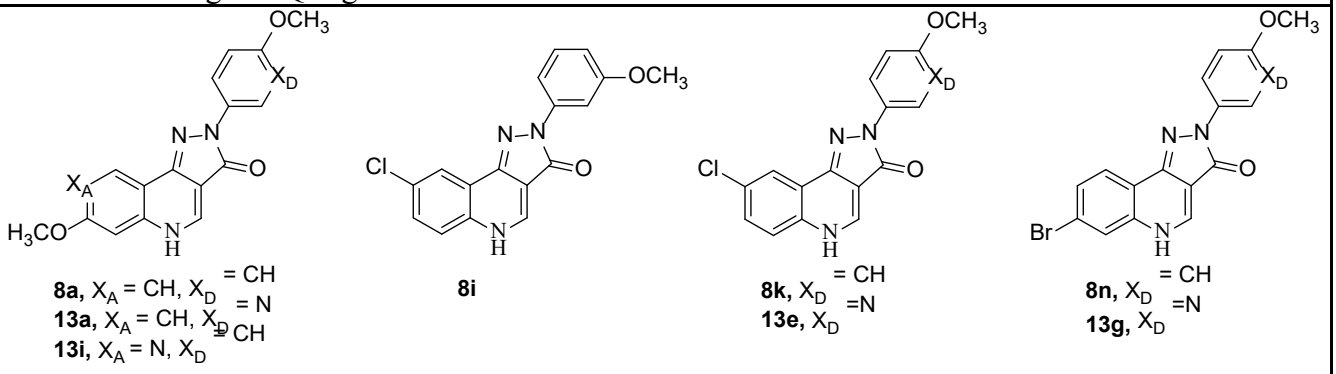

Compound	cLogP[e]	Solubility (µM) in DI Water, pH = 7[f]	Solubility (µM) in 0.01M HCl, pH = 2[f]
8a	2.76	24.3 ± 3.8	27.8 ± 0.9
13a[b]	2.17	67.2 ± 7.9	115.4 ± 14.9
13i[b]	2.28	103.7 ± 28.5	135.9 ± 2.9
8i	3.56	6.8 ± 0.3	2.6 ± 0.2
8k[c]	3.56	6.4 ± 0.5	8.5 ± 1.9
13e[c]	2.93	0.8 ± 0.1	0.9 ± 0.2
8n	3.71	8.3 ± 0.2	3.3 ± 0.1
13g[d]	3.08	7.3 ± 0.2	7.2 ± 0.4

[a]Solubility experiments performed in water at pH = 7 and pH =2 to mimic physiological and gastrointestinal conditions and to examine the impact of N-hetero substitution on hydrogen chloride salt formation. [b]**8a** related analogs in **red**. [c]**8i** related analogs in **blue**. [d]**8n** related analogs in **green**. [e]cLogP values calculated using ChemBioDraw® Ultra (ver.13.0.0.3015). [f]Calculated using an LCMS. n = 3

1.11. Study of Potential Cytotoxicity in HEK293 (Kidney) cells and HEPG2 (Liver) cells with Dr. Michael Rajesh Stephen and Dr. Alexander Arnold

An examination of the cell viability, indicated that these ligands are non-toxic even at a concentration of 400 µM in the presence of HEK293, as well as HEPG2 cell lines (see **Table 63** and **Figure 135** for details). In both cell lines, substitution of OCD_3 for OCH_3 in either the "A-ring" or "D-ring" of the parent ligands did not have a negative impact on cell viability. Additionally, variation of the substitution pattern of the methoxy groups on the "D-ring" to the *meta* position (**8e** and **8j**) or *ortho* position (**8f** and **8m)** had no impact on cytotoxicity. The *N*-

hetero atom insertion into the "D-ring" to provide **13c**, **13e** and **13g** also had no impact of cell viability. All of the potential α6β3γ2 subtype selective ligands tested here were nontoxic. Finally, the fluorinated analogs exhibited some cytotoxicity. The ligands with 3 fluorine atoms (DK-IV-20-1, DK-IV-22-1 and DK-IV-19-1) were toxic to HEK293 (kidney) cells while the ligand with 6 fluorine atoms (MM-I-10) exhibited cytotoxicity to both HEK293 (kidney) and HEPG2 (liver) cells (**Table 10**). Details of the assays for the fluorinated analogs are exhibited in the Appendix (see **Figure 136**).

Table 10: Binding Assays, Cytotoxicity and cLogP of Deuterated vs. N-Hetero vs. Fluorinated PQ Analogs[2, 79, 80]

Ligand	BZP Rat Brain Site Binding Affinity (nM)	Radioligand % Inhibition		Cytotoxicity		cLogP
		BZP Rat Brain Site	hERG Channel	HEK293 (Kidney) LD_{50} (μM)	HEPG2 (Liver) LD_{50} (μM)	
PZ-II-029	2.7	92.4	7.4	>400	>400	2.76
DK-I-56-1	2.1	96.2	-0.1	>400	>400	2.76
DK-I-86-1	8.2	98.2	8.6	>400	>400	2.28
DK-IV-20-1	444	90.1	0.8	**51.7**	>200	3.87
LAU 463	12.2	93.2	-2.7	>400	>400	3.71
DK-I-58-1	5.5	97.4	8.8	>400	>400	3.71
DK-II-58-1	6.2	93.3	-10.3	>400	>400	3.08
DK-IV-22-1	686	83.5	5.7	**82.2**	>200	4.82
DK-IV-19-1	32	96.0	-4.5	**69.0**	>200	3.75
MM-I-10	964	91.0	0.9	**22.6**	**26.5**	4.85

1.12. Study of the Lack of Motor Impairment on the Rotarod with Nicholas Zahn

Analysis of the data from the rotarod studies indicated that none of the $GABA_AR$-α6 subtype selective PQ analogs were incapacitating in mice on the rotarod when dosed by oral gavage at 40mg/kg. The deuteration of the methoxy groups of the parent ligands (**Figure 137**), and introduction of *N*-hetero substituents into the "D-ring", as well as deuteration of the N-hetero analogs (**Figure 137**) resulted in no further change of the physiological response, in contrast to

the effect on motor impairment observed for diazepam at 5mg/kg. The fluorinated analogs were also not incapacitating in mice on the rotarod (**Figure 138**).

1.13. Pharmacokinetic Study with Dr. Miroslav M. Savić

In vivo plasma and brain kinetic profiles of six ligands (**8a**, **8b**, **8c**, **8d**, **13c**, and **8m)** suspended in a standard vehicle[81] and dosed by IP injection at 10 mg/kg in male Wistar rats, are illustrated in **Figure 34**. The time-concentration curves of all ligands tested indicated they were rapidly absorbed and distributed in the brain. The non-deuterated molecule **8a** demonstrated a low brain-to-plasma partition coefficient (Kp = $AUC_{0\text{-}t}$, brain/$AUC_{0\text{-}t}$, plasma) of 0.08 ± 0.01. The three deuterated analogs **8b**, **8c** and **8d** had increased Kp values, equal to 0.13 ± 0.01, 0.16 ± 0.02, and 0.17 ± 0.02, respectively, together with longer half-lives, both in plasma and brain. The brain $AUC_{0\text{-}12}$ value of the N-hetero ligand **13c** was only 45%, 36% and 55% of that obtained with **8b**, **8c** and **8d**, respectively. The *ortho*-OCD_3 substituted ligand **8m** exhibited a reasonable Kp value of 0.15 ± 0.01 which additionally illustrated its usefulness in further *in vivo* studies as a control compound with a favorable pharmacokinetic profile.

Because the three deuterated analogs of **8a** generally had similar values of pharmacokinetic parameters, it was decided to pursue the study of **8b** and **8d**. The key ligands **8b** and **8d** were employed for calculation of the estimated free concentrations available for binding to receptors in brain tissue and free fractions were found to be 0.194 and 0.105, respectively. These values gave rise to more than two-fold higher AUC values of estimated free brain concentrations of **8b** as compared to **8d** (651.72 ± 217.70 ng h g^{-1} and 288.78 ± 61.07 ng h g^{-1}, respectively). Having in mind the electrophysiological activity presented in **Figure 27A**, the free

(unbound) brain concentrations of **8b** in the range close to 100 nM were sufficiently high to mediate α6β3γ2 modulation in vivo. Hence, the "D-ring" substituted OCD_3 ligand **8b** was chosen to be tested in a battery of basic behavioral paradigms. The "A-ring" OCD_3 ligand **8c** was not pursued further because it requires more steps to synthesize than ligand **8b**.

The concentration–time profiles of **8a** and **8b** in rat plasma and brain after oral (gavage) as well as after intravenous (IV) administration, with the calculated pharmacokinetic parameters, are presented in **Figure 35**. The values of absolute oral bioavailability of **8a** and **8b** from nanoemulsion formulations, calculated on the basis of the plasma AUC values obtained following two routes of administration, were 66.9% and 100.0%, respectively. These data reveal that deuteration of **8a** resulted in optimization of pharmacokinetic behavior after oral administration, which was further supported by respective values of brain bioavailability of **8a** and **8b** (82.6% vs. 89.5%).

The pharmacokinetic parameters of $-OCH_3$, $-OCD_3$, *N*-hetero and $-OCF_3$ ligands in mouse plasma, brain, liver and kidney after IP administration, with the calculated pharmacokinetic parameters, obtained through five cassettes are presented in **Figure 36**, **Figure 37**, **Figure 38**, **Figure 39** and **Figure 40**. The pharmacokinetic study was performed in order to evaluate and compare the *in vivo* destiny of 14 pyrazoloquinolinones with similar structures, after intraperitoneal administration, and assess their potential to become lead compounds for preclinical studies. The systemic exposure to ligands studied, as evidenced by AUC and C_{max} values in plasma, was generally high. The $AUC_{0\text{-}36}$ values in plasma were in the range from 1500 to 3900 ng*h/mL, except for the three fluorinated derivatives (MM-I-10, DK-IV-22-1, DK-IV-

19-1) with conspicuously higher AUC_{0-36} values (19935.27 ± 1847.19, 10816.44 ± 146.06, 6609.31 ± 447.63 ng*h/mL, respectively). The C_{max} values in plasma were mainly in the range from 1000 to 4000 ng/mL, while six ligands had values below 1000 ng/mL (LAU463, DK-I-58-1, DK-IV-20-1, DK-I-86-1, DK-IV-22-1 and MM-I-10). Crucially important for any in vivo studies, all 14 ligands were clearly penetrated the blood brain barrier (BBB). The range of AUC_{0-36} values in brain was between 1000 and 3500 ng*h/g, except for two fluorinated derivatives (DK-IV-22-1 and MM-I-10) with the highest AUC_{0-36} values in brain (8147.74 ± 1044.88, and 6374.56 ± 619.90, respectively). The calculated Kp values were the highest for DK-I-56-1, DK-I-58-1, DK-IV-20-1, DK-II-58-1 and DK-I-86-1 (1.12 ± 0.52, 1.10 ± 0.43, 0.99 ± 0.17, 0.94 ± 0.35, and 0.92 ± 0.37, respectively) and the lowest for MM-I-10, LAU 463 and DK-IV-19-1 (0.34 ± 0.03, 0.25 ± 0.04, 0.22 ± 0.04). In general terms, the values of this parameter close to or greater than unity indicated excellent brain targeting of the ligand. The part of the total AUC that reached the brain was above 5% for DK-I-56-1, DK-I-60-3, DK-I-58-1, DK-II-58-1, RV-I-029 and DK-I-59-1 (6.16 ± 2.15, 6.13 ± 2.47, 6.08 ± 2.56, 5.65 ± 1.89, 5.05 ± 2.49, 5.03 ± 2.45 respectively) and lower than 2% for DK-I-87-1, MM-I-10, DK-IV-19-1 and LAU 463 (1.79 ± 0.84, 1.72 ± 0.12, 1.54 ± 0.17, 1.39 ± 0.37, respectively). The total exposure of excretory organs was the lowest for DK-I-60-3, DK-I-59-1, PZ-II-029 and DK-I-56-1, while the highest was for DK-IV-22-1 and MM-I-10. Consequently, while the relative contribution of target brain tissue in total exposure was high for DK-I-58-1 and DK-II-58-1, the introduction of fluorine into the respective molecules has resulted in an increase of five times higher exposure in excretory organs, with corresponding substantial decreases in alpha values for DK-IV-22-1 and MM-I-10.

Observing in parallel the results for PZ-II-029 and its analogues (DK-I-56-1, RV-I-029 and DK-I-60-3) on one hand, and LAU 463 and its analogues (DK-I-58-1 and DK-II-58-1) on the other, it can be concluded that introduction of deuterium into the parent ligand substantially increased the Kp, alpha and C_{max} values in all cases, while the excretory organ exposure remained approximately the same as compared to the parent structures (PZ-II-029 and LAU 463).

It can be concluded that all ligands reached substantial micromolar maximum concentrations in plasma, while their penetration into the central nervous system was slightly restricted. Nevertheless, kinetic studies in rodents have shown that these ligands, and especially DK-I-56-1, possess pharmacokinetic properties beneficial for the proposed neuropsychopharmacological application.

Figure 34: Pharmacokinetic Profiles of Selected Ligands[2]

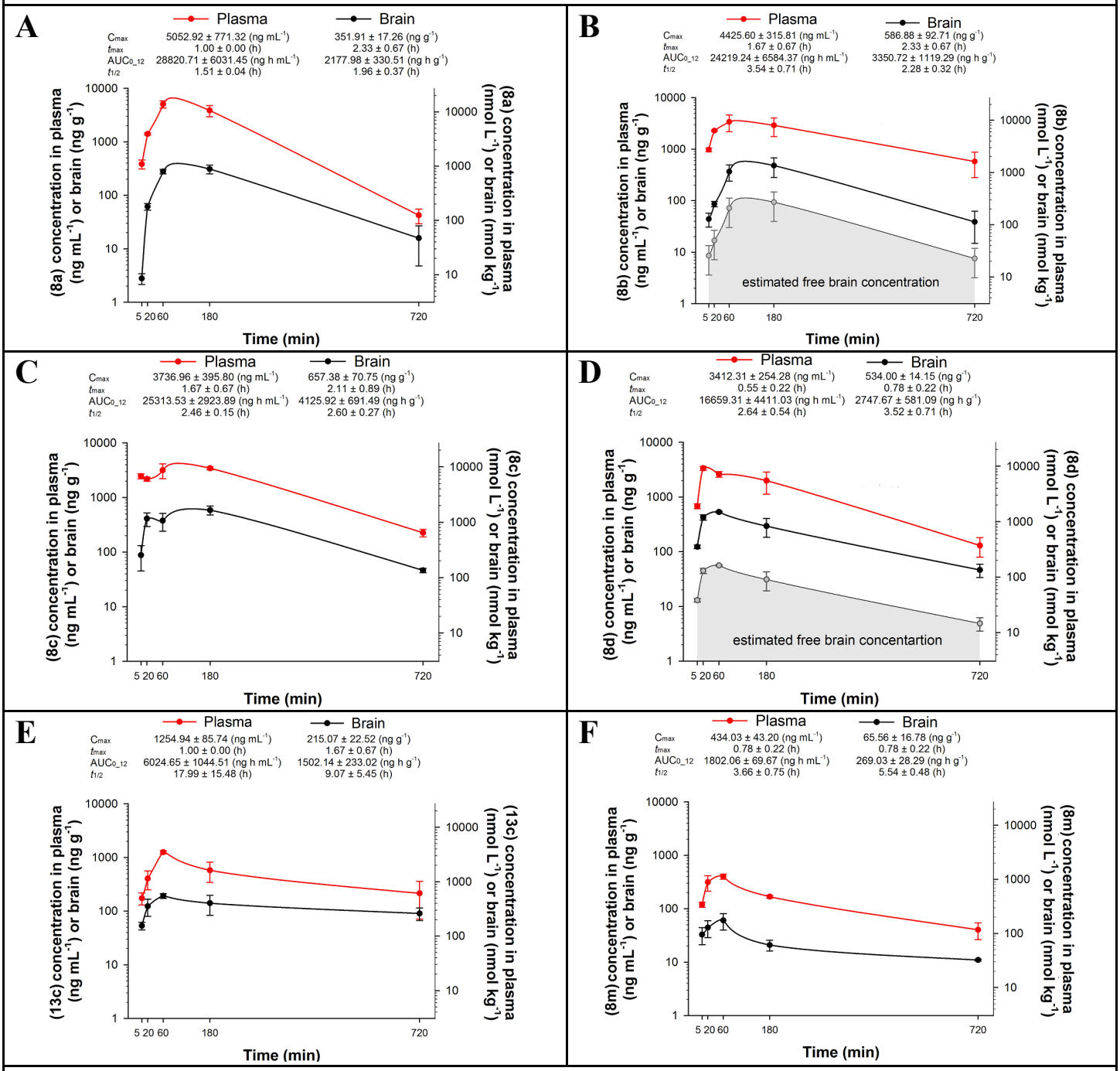

[a]Plasma and brain concentration–time profiles of **8a** (**A**), **8b** (**B**), **8c** (**C**), **8d** (**D**), **13c** (**E**), and **8m** (**F**) after IP administration of a 10 mg kg^{-1} dose (n = 3 per time point). C_{max} = maximum concentration in brain or plasma; t_{max} = time of maximum concentration in brain or plasma; $t_{1/2}$ = terminal elimination half-life; $AUC_{0–12}$ = area under the concentration versus time curve from zero to last measurable time point.[2]

Figure 35: Pharmacokinetic Profiles in Plasma and Brain Following Oral Gavage (PO) or IV Administration of **8a** (**A**) and **8b** (**B**) with Dr. Miroslav M. Savić[2]

A

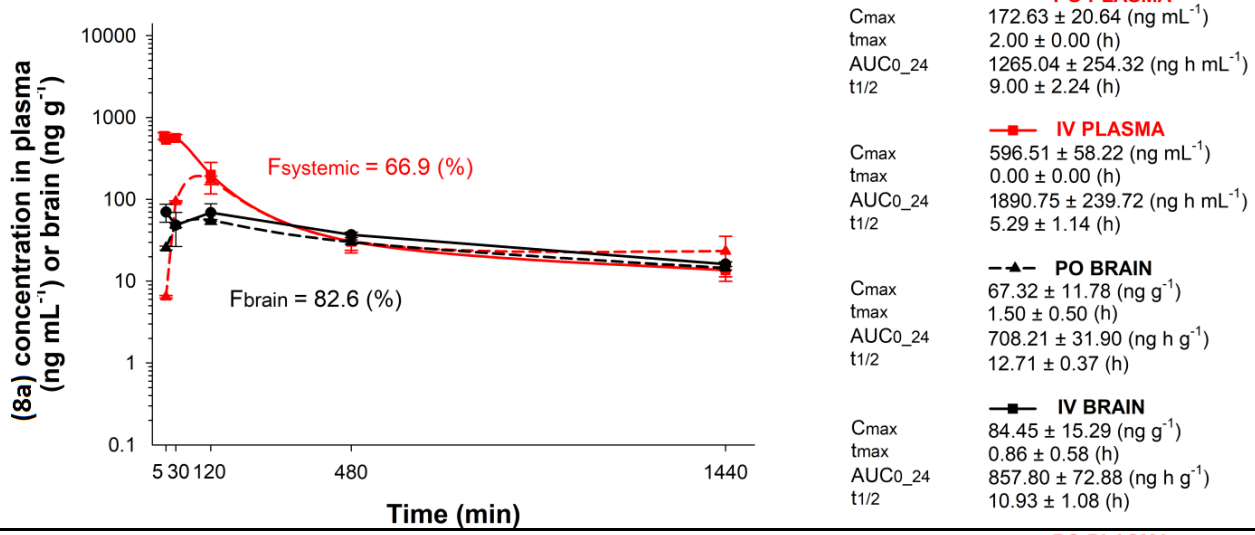

B

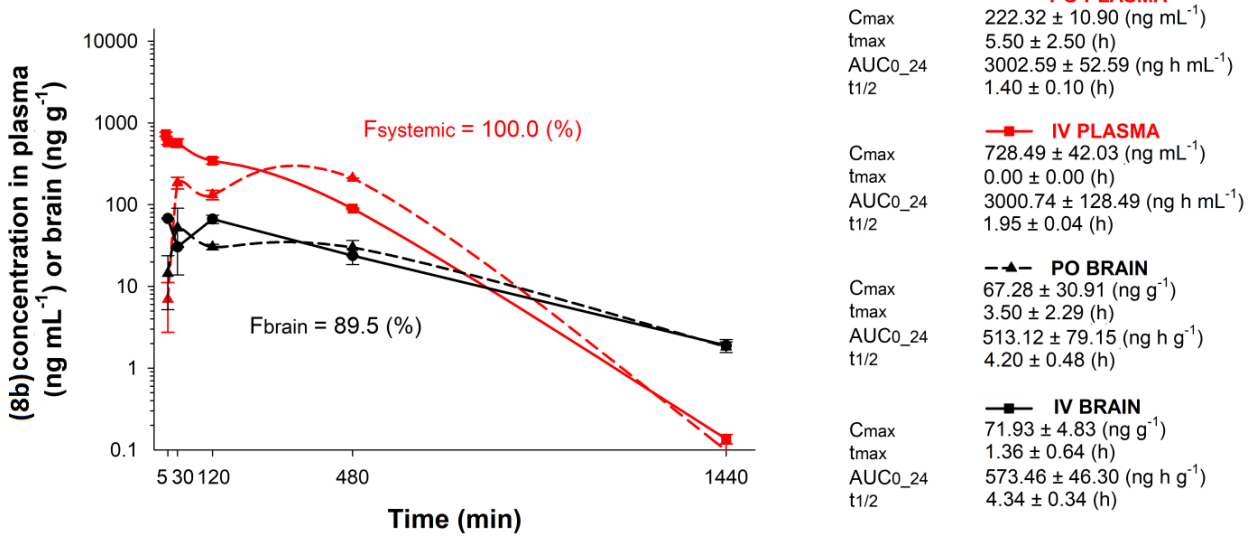

[a]Plasma and brain absolute bioavailability profiles of **8a** (**A**), and **8b** (**B**) presented in respective graphs as $F_{systemic}$ and F_{brain} is calculated as a ratio of respective AUC_{0-24} values obtained after IV and oral gavage (PO) administration of a 2 mg kg^{-1} dose (n = 3 per time point). C_{max} = maximum concentration in brain or plasma; t_{max} = time of maximum concentration in brain or plasma; $t_{1/2}$ = terminal elimination half-life; AUC_{0-24} = area under the concentration versus time curve from zero to last measurable time point.[2]

Figure 36: Pharmacokinetic Profiles (Plasma, Brain, Liver and Kidney) of **PZ-II-029 (8a)** Related Ligands: **DK-I-56-1 (8b)**, **RV-I-029 (8c)** and **DK-I-60-3 (8d)**.[79, 80]

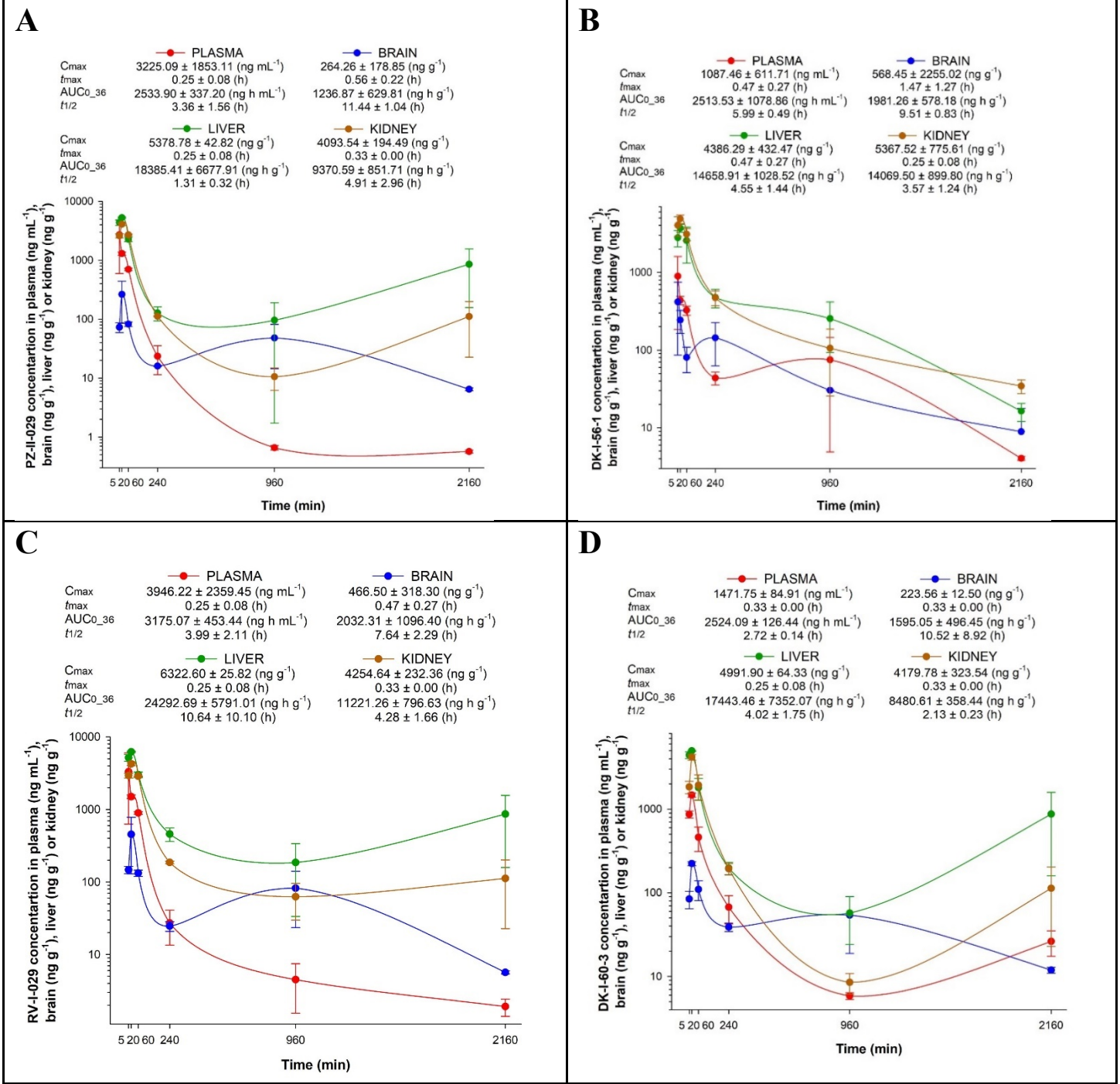

[a]Plasma (**red**), brain (**blue**), liver (**green**) and kidney (**brown**) concentration–time profiles of **PZ-II-029** (**A**), **DK-I-56-1** (**B**), **RV-I-029** (**C**), and **DK-I-60-3** (**D**) after IP administration of a 3 mg kg^{-1} dose (n = 3 per time point) in adult male C57/BL/6J mice. C_{max} = maximum concentration; t_{max} = time of maximum concentration; $t_{1/2}$ = terminal elimination half-life; $AUC_{0–36}$ = area under the concentration versus time curve from zero to last measurable time point.[79, 80]

Figure 37: Pharmacokinetic Profiles (Plasma, Brain, Liver and Kidney) of **PZ-II-029 (8a)** Related Ligands: **DK-I-56-1 (8b)**, **DK-I-86-1 (13c)** and **DK-IV-20-1 (14o)**.[79, 80]

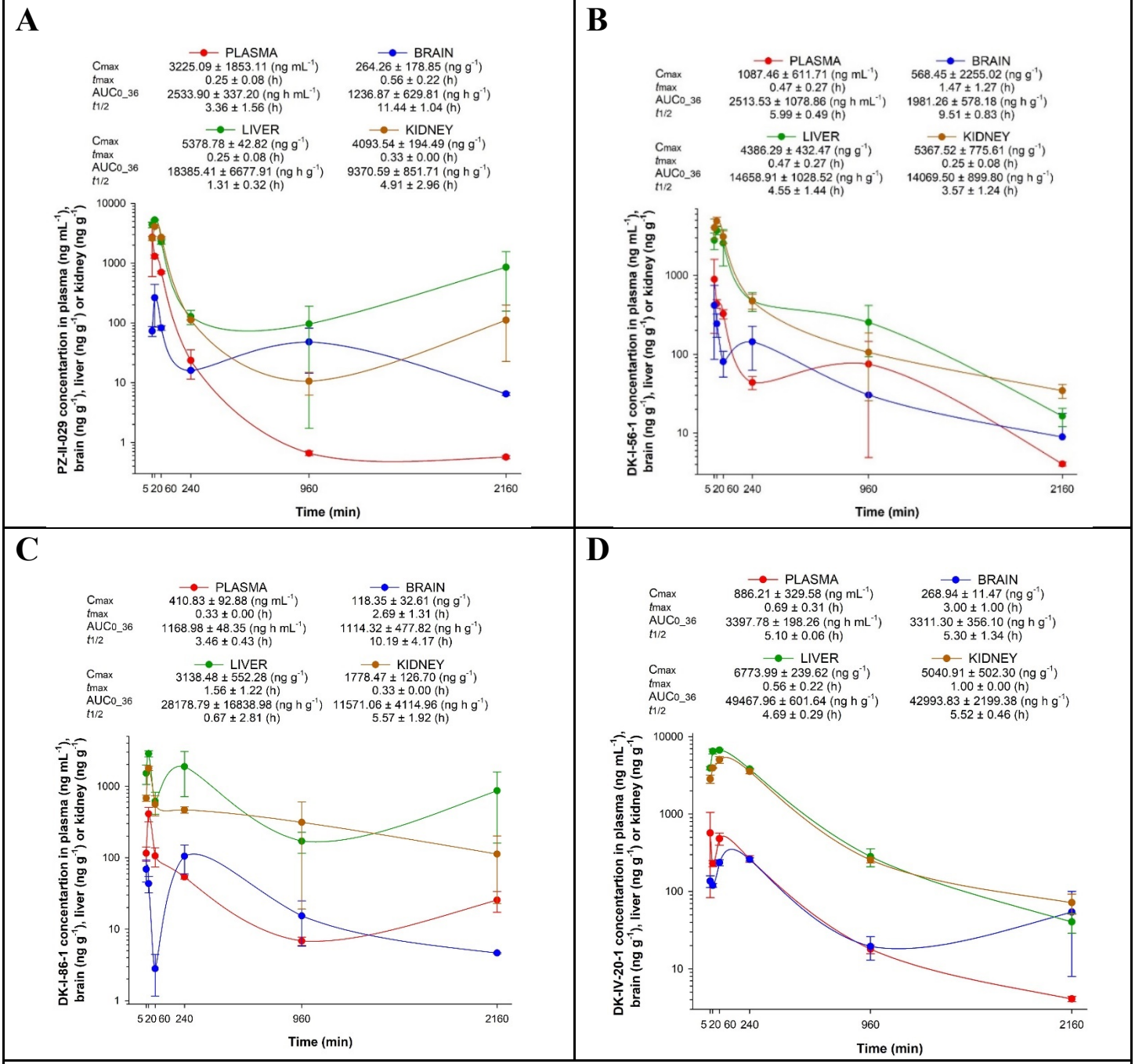

[a]Plasma (**red**), brain (**blue**), liver (**green**) and kidney (**brown**) concentration–time profiles of **PZ-II-029** (**A**), **DK-I-56-1** (**B**), **DK-I-86-1** (**C**), and **DK-IV-20-1** (**D**) after IP administration of a 3 mg kg^{-1} dose (n = 3 per time point) in adult male C57/BL/6J mice. C_{max} = maximum concentration; t_{max} = time of maximum concentration; $t_{1/2}$ = terminal elimination half-life; $AUC_{0–36}$ = area under the concentration versus time curve from zero to last measurable time point.[79, 80]

Figure 38: Pharmacokinetic Profiles (Plasma, Brain, Liver and Kidney) of **LAU 463 (8n)** Related Ligands: **DK-I-58-1 (8o)**, **DK-II-58-1 (13h)** and **DK-IV-22-1 (14p)**.[79, 80]

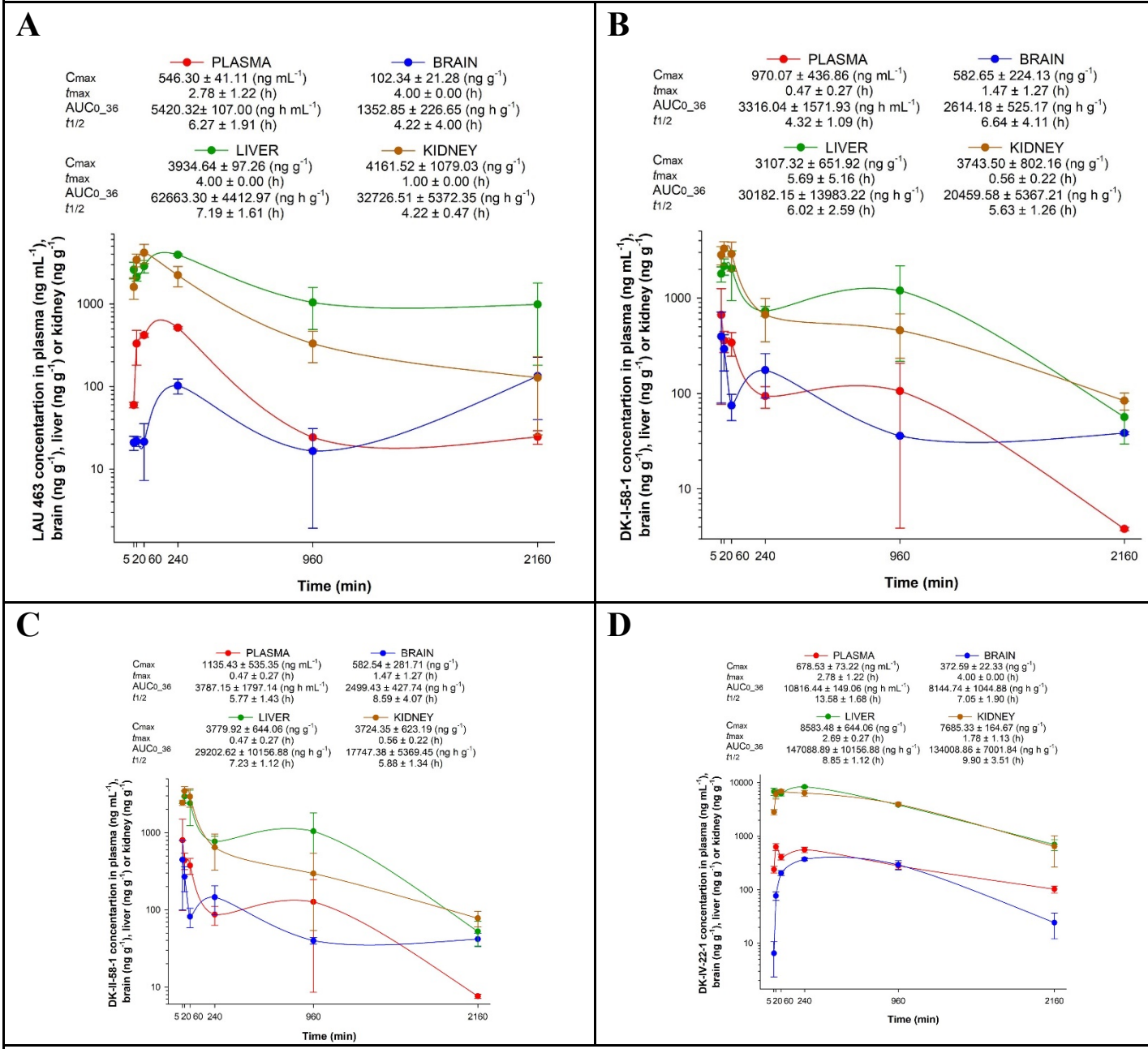

[a]Plasma (**red**), brain (**blue**), liver (**green**) and kidney (**brown**) concentration–time profiles of **LAU463** (**A**), **DK-I-58-1** (**B**), **DK-II-58-1** (**C**), and **DK-IV-22-1** (**D**) after IP administration of a 3 mg kg^{-1} dose (n = 3 per time point) in adult male C57/BL/6J mice. C_{max} = maximum concentration; t_{max} = time of maximum concentration; $t_{1/2}$ = terminal elimination half-life; $AUC_{0–36}$ = area under the concentration versus time curve from zero to last measurable time point.[79, 80]

Figure 39: Pharmacokinetic Profiles (Plasma, Brain, Liver and Kidney) of **LAU 159 (8i)** Related Ligands: **DK-I-59-1 (8j)** and **DK-I-87-1 (8m)**.[79, 80]

A

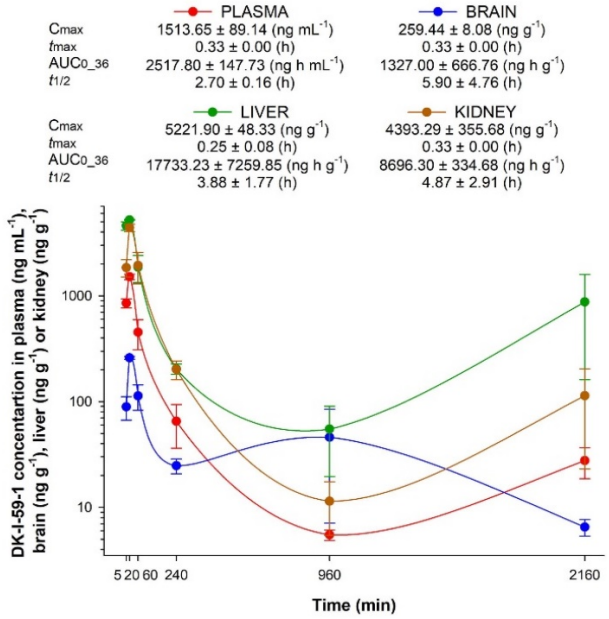

B

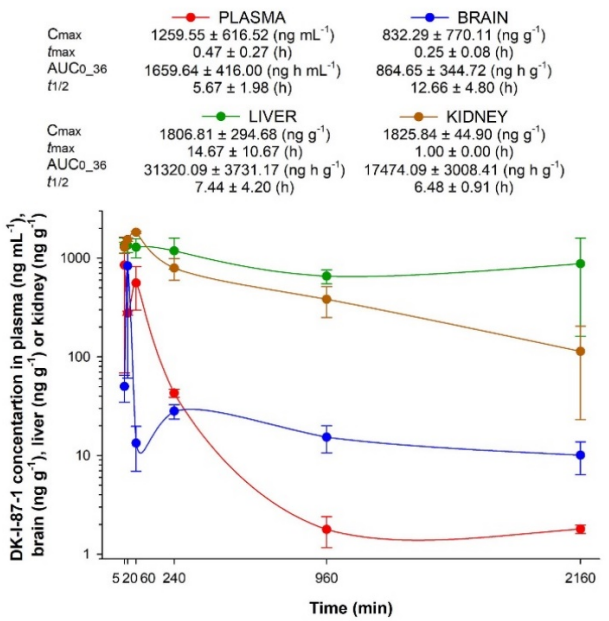

[a]Plasma (**red**), brain (**blue**), liver (**green**) and kidney (**brown**) concentration–time profiles of **DK-I-59-1** (**A**), and **DK-I-87-1** (**B**) after IP administration of a 3 mg kg^{-1} dose (n = 3 per time point) in adult male C57/BL/6J mice. C_{max} = maximum concentration; t_{max} = time of maximum concentration; $t_{1/2}$ = terminal elimination half-life; $AUC_{0–36}$ = area under the concentration versus time curve from zero to last measurable time point.[79, 80]

Figure 40: Pharmacokinetic Profiles (Plasma, Brain, Liver and Kidney) of **MM-I-06 (14i)** Related Ligands: **DK-IV-19-1 (14r)** and **MM-I-10 (14l)**.[79, 80]

A

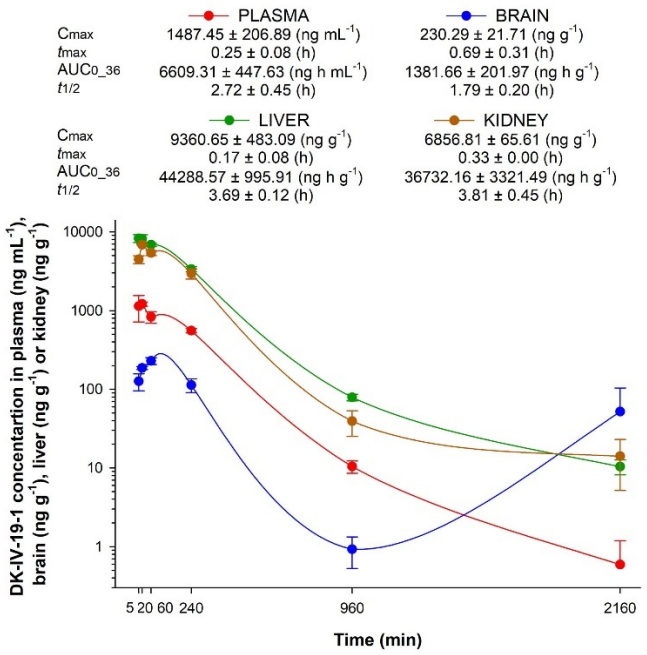

B

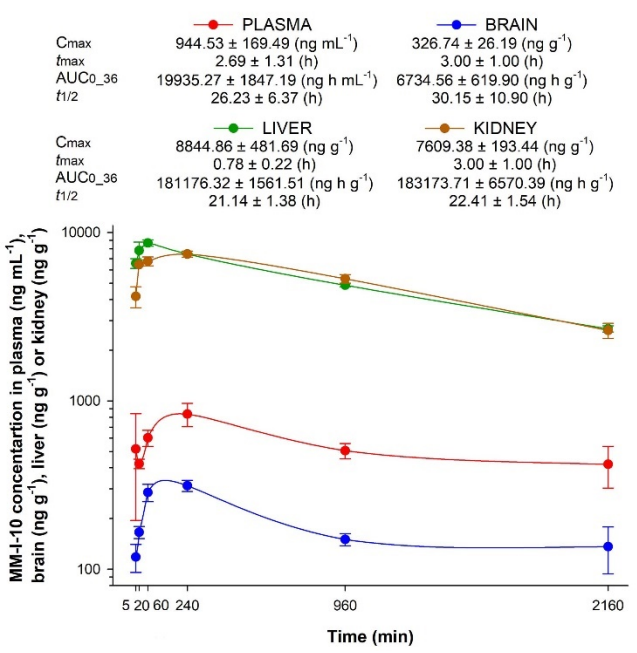

[a]Plasma (**red**), brain (**blue**), liver (**green**) and kidney (**brown**) concentration–time profiles of **DK-IV-19-1** (**A**), and **MM-I-10** (**B**) after IP administration of a 3 mg kg^{-1} dose (n = 3 per time point) in adult male C57/BL/6J mice. C_{max} = maximum concentration; t_{max} = time of maximum concentration; $t_{1/2}$ = terminal elimination half-life; $AUC_{0–36}$ = area under the concentration versus time curve from zero to last measurable time point.[79, 80]

1.14. Pharmacokinetic Study of DK-I-56-1 (8b) via a Nanoemulsion with Dr. Miroslav M. Savic and Dr. Snežana D. Savić [68]

A pharmacokinetic study was performed in order to evaluate the *in vivo* fate of **8b** in a nanosuspension after i.p. administration in mice to investigate its suitability for preclinical pharmacokinetic studies. In line with general recommendations for parenteral preparations to keep qualitative and quantitative composition as simple as possible, a nanosuspension stabilized by polysorbate 80 alone was chosen for *in vivo* experiments, with the addition of glycerol as a tonicity adjuster. After preparation, the nanosuspension formulation (NS2-G) was with z-ave of 273.3 ± 2.2 nm and PDI of 0.263 ± 0.017. The formulation was suitable for parenteral administration with osmolality 289 mOsm/kg. SOL formulation was yellow, with no separation of phases, while SUSP formulation was easily re-dispersed into homogenous suspension by manual shaking and applying ultrasound before administration (**Figure 17**). However, particle size distribution of the suspension was broad, with D(v, 0.1) 1.40 ± 0.01 μm, D(v, 0.5) 12.97 ± 0.58 μm and D(v, 0.9) 87.33 ± 2.63 μm.

The area under the curve values (AUC_{0-36}), reflected availability calculated from plasma concentration-time curves, and were significantly different for the three formulations ($F(2,6) = 39.280$, $p < 0.001$). After administration, the highest plasma concentrations of DK-I-56-1 were achieved after SOL, which was followed by NS2-G and SUSP, respectively, and the same trend was observed for plasma AUC_{0-36} values (**Figure 41**A). Probably, Cremophor EL and DMSO increased the absorption rate, thus enabling higher plasma levels after SOL administration. In consideration of the high quantities of excipients used in SOL formulation (molar ratio of DK-I-

56-1/DMSO/Cremophor EL was 1/413/236), it could be assumed that they can have an impact on DK-I-56-1 distribution as well. Cremophor EL is a widely used solubilizer in parenteral formulations for numerous poorly soluble drugs, but it may exert a range of biological effects, including changes in drug disposition.[82] It was stated that Cremophor EL, by changing drug-protein interactions, influences paclitaxel and doxorubicin distribution.[83, 84] This could be an important factor in DK-I-56-1 pharmacokinetics as well, because its free fraction was reported to be low (0.194).[2] Brain availability after SOL administration was not higher than after NS2-G and SUSP ($H(2) = 0.622$, $p = 0.733$), despite superior plasma levels (**Figure 41**B). In high concentrations, DMSO can act as an opener of the blood brain barrier, which allows higher drug passage into the brain.[85] However, in this research only 3.12 ± 0.38% of total AUC_{0-36} (sum of AUC_{0-36} in four investigated compartments) reached the brain after SOL, and this brain portion of DK-I-56-1 was similar as in the case of other two formulations (3.79 ± 1.48% and 3.48 ± 2.21%, for NS2-G and SUSP, respectively). This indicates the absence of the suggested effect of DMSO. The AUC_{0-36} values in liver and kidney were not significantly different ($F(2,6) = 0.332$, $p = 0.730$ and $H(2) = 0.356$, $p = 0.837$, respectively) between the three formulations, and concentration profiles after NS2-G and SOL were similar (**Figure 41**C and **Figure 41**D). Actually, a higher percentage of total AUC_{0-36} remained in blood after SOL (19.52 ± 1.11%, compared to 11.83 ± 4.75% and 1.43 ± 0.48% after NS2-G and SUSP, respectively), while the calculated tissue percentages were similar for all three formulations (around 3% in brain, 40% in liver and 50% in kidney). This confirms a suggestion that influence of Cremophor EL on distribution may be profound only in the central blood compartment.[82] Interestingly, total AUC_{0-36} values in plasma and organs after SOL was substantially lower than after NS2-G and SUSP (52368.97 ± 4502.09; 75459.86 ± 26699.73 and 86880.56 ± 29533.80 ng·h/mL, respectively), indicating that SOL

formulation gave rise to an enhanced elimination from the body. **Stated in some reports the presence of nephrotoxicity of DMSO and Cremophor EL, with tubular cell necrosis and oliguria,[86, 87] which could contribute to non-physiological handling of DK-I-56-1 from SOL.** Therefore, a simplistic formulation of NS2-G, without any organic solvent and with low surfactant concentration, may be thought of as a major advantage over SOL formulation, by eliminating erratic pharmacokinetic behavior and toxicity caused by excipients.

A smaller particle size of the nanosuspension, and therefore, an increased surface area available for dissolution, was the most probable reason for faster absorption and higher systemic exposure of DK-I-56-1 after nanosuspension when compared to suspension administration.[88, 89] This was supported by results from *in vitro* dissolution studies.[68] On the other hand, brain AUC_{0-36} values after NS2-G and SUSP were similar ($p = 0.733$). However, concentration profiles in brain after SUSP administration showed bimodal distribution (**Figure 41**B), and the same behavior of this formulation could be noticed in liver and kidney as well (**Figure 41**C and **Figure 41**D). The explanation of this phenomenon could be found in formation of a DK-I-56-1 depot at the site of administration due to small quantities of liquid available for dissolution. This results in erratic absorption and distribution, as observed in the case of intramuscular and subcutaneous injections.[90] The main advantage of NS2-G over SUSP would, therefore, be a smaller drug particle size and narrower particle size distribution, which leads to a reliable bioavailability and more regular pharmacokinetics. This is very important in preclinical studies of drug candidates with poor solubility.

Figure 41: Pharmacokinetic Profiles (Plasma, Brain, Liver and Kidney) of **DK-I-56-1 (8b)** Comparing Nanosuspension, Suspension and Solution Vehicles[68]

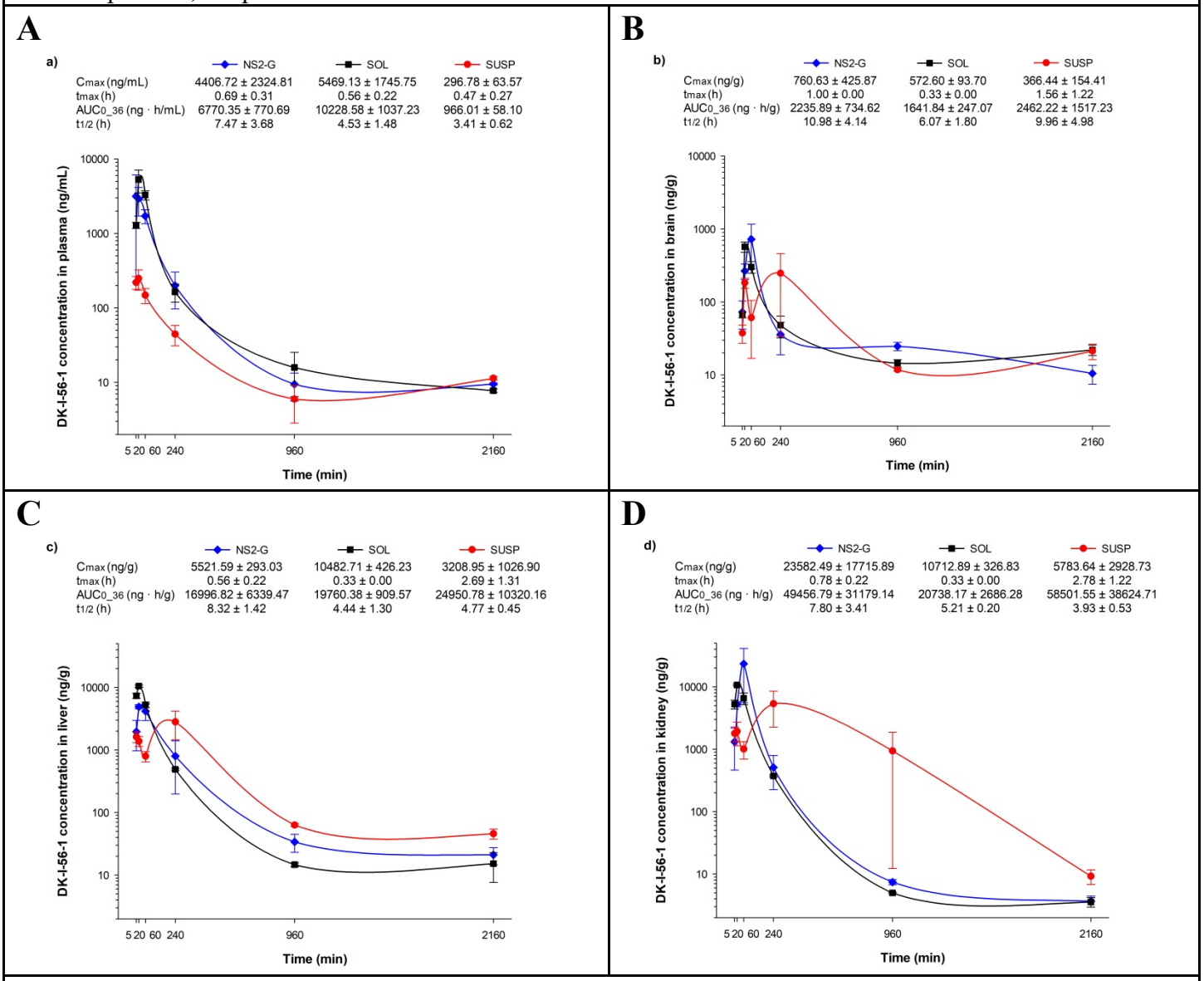

Pharmacokinetic profiles and calculated parameters of nanosuspension (NS2-G), suspension (SUSP) and solution (SOL) in (a) plasma, (b) brain, (c) liver and (d) kidney after intraperitoneal administration in mice (n = 3 per time point) at dose of 10 mg/kg. C_{max} – maximum concentration; t_{max} – time of maximum concentration; $AUC_{0\text{-}36}$ – area under the concentration versus time curve from zero to last measurable time point; $t_{1/2}$ - terminal elimination half-life.[68]

1.15. *In Vivo* behavioral studies on 8b versus the control compound 8m

Since the ligand **8b** exhibited a longer duration of action, it was subjected to *in vivo* studies after IP administration at a 10 mg/kg dose. In addition, the control ligand **8m** of the same chemotype, was also studied in parallel. The behavioral assays were run on these ligands to determine the occurrence of anxiolysis, assess muscle strength and basic sensorimotor activity on the elevated plus maze, grip strength and cued water-maze training, respectively **(Table 11)**. The nanoemulsion formulation[91] employed for the behavioral studies, which permits a more reliable dosing, did not grossly affect the pharmacokinetic profile of **8b** obtained with the suspension formulation (data not shown). Moreover, the corresponding placebo (nanoemulsion alone) was not behaviorally active when compared to saline (data not shown). The changes in behavioral parameters analyzed above, which are generally observed with typical Bzs or Bz site ligands,[81] were not elicited by either of the two ligands. In addition, motor coordination and balance on the rotarod were retained after IP doses as high as 55 mg/kg **8b** and 60 mg/kg **8m**. Taken together, these results indicate that selective *in vivo* potentiation of $GABA_A$Rs containing the α6 subtype did not mimic any of the behavioral effects of classical Bzs supporting the role of the $GABA_A$R α6 (DI) receptor in the following *in vivo* data.

Table 11: The Influence of IP 10 mg kg^{-1} Doses of **8b** and **8m** on the Selected Parameters of the Grip Strength, Elevated Plus Maze, and Cued Water Maze[2]

Compound	Grip Strength (kg kg^{-1})[b]	Elevated Plus Maze			Cued Water Maze		
		Total Distance (m)	Closed Arm Entries	% Open Arm Entries	Total Distance (m)	Average Swim Speed (m s^{-1})	% Peripheral Ring Distance
Placebo	2.79 ± 0.16	6.71 ± 0.56	3.63 ± 0.42	23.07 ± 5.47	8.04 ± 1.16	0.21 ± 0.01	67.44 ± 4.60
8b	2.67 ± 0.18	5.84 ± 0.50	2.63 ±0.42	22.36 ± 8.76	11.01 ± 1.41	0.20 ± 0.01	67.2 ± 3.83
8m	2.66 ± 0.19	6.14 ± 0.73	3.50 ± 0.39	20.60 ± 6.51	9.93 ± 1.50	0.22 ± 0.01	69.34 ± 4.37

[a]Three behavioral *in* vivo studies exhibited that selective $GABA_AR$ α6 potentiation had no classical DS effects. [b]The peak force of experimenter's pull necessary to overcome the strength of the animal's grip.[2]

1.16. *In Vivo* hyperlocomotor response studies on 8b versus the control compound 8m

In rats, DK-I-56-1 (**8b**), but not DK-I-87-1 (**8m**) at an IP dose of 10 mg/kg induced a hyperlocomotor response (**Figure 42A**); in the repeated experiment, the effect of 10 mg/kg **8b** did not reach statistical significance (**Figure 42C**), while in the third experiment it was present at both the dose of 3 and 10 mg/kg (**Figure 42E**). In mice, both **8b** and **8a** induced a hyperlocomotor action at a wide range of IP doses (3, 10 and 30 mg/kg, **Figure 42B** and **Figure 42D**, respectively). The hyperlocomotor effect of 10 mg/kg **8b** was present even in mice that received a sedative IP dose of diazepam (3 mg/kg) in combination (**Figure 42F**). This suggested that **8b** was able to antagonize the effects of diazepam at Bz binding sites and additionally elicit locomotor stimulation presumably exerted through $GABA_ARs$ containing the α6 subunit.

Figure 42: The Measurement of Influences on Locomotor Activity of Rats (Left Panels: A,C,E) or Mice (Right Panels: B,D,F)[2]

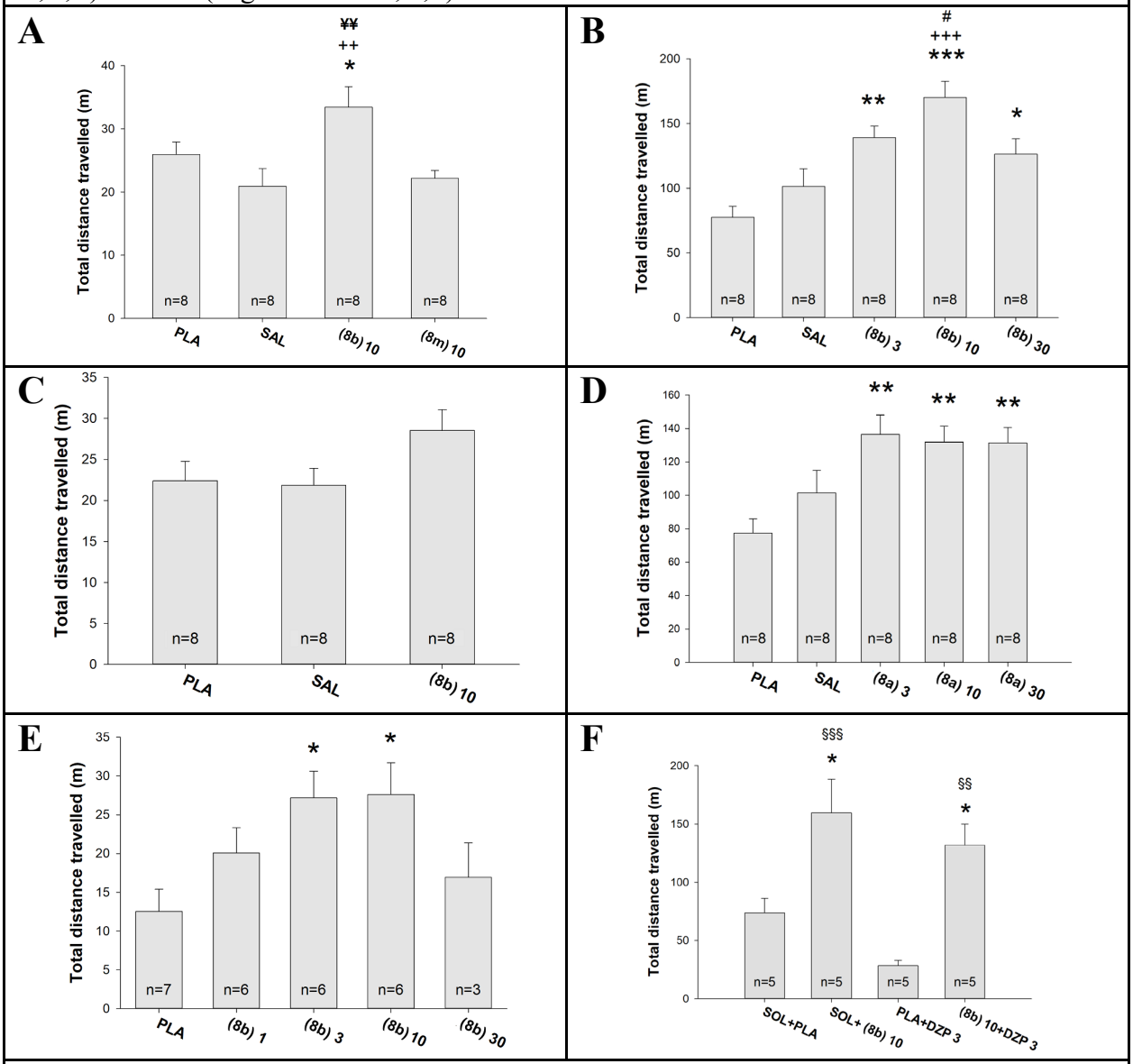

[a]The locomotor activity tests were performed in rats (A,C,E) and mice (B,D,F) in six experiments in total. The ligands used were **8a**, **8b**, **8m** and diazepam (DZP), while control groups were placebo nanoemulsion (PLA) and saline (SAL) via IP administration. The number of animals per group is given within columns. The results of ANOVA are as follow: (A) $F(3,28)=5.335$, $p=0.005$; (B) $F(2,21)=2.542$, $p=0.103$; (C) $F(4,23)=3.685$, $p=0.018$; (D) $F(4,35)=9.932$, $p<0.001$; (E) $F(4,35)=5.745$, $p<0.001$; (F) $F(3,16)=10.345$, $p<0.001$. Post hoc significant differences are as follows: *,** and ***, $p<0.05$, $p<0.01$, and $p<0.001$ vs. PLA; ++ and +++, $p<0.01$ and $p<0.001$ vs. SAL; #, $p<0.05$ vs. **8b**, 30 mg/kg; ¥¥, $p<0.01$ vs. **8m**, 10 mg/kg; §§ and §§§, $p<0.01$ and $p<0.001$ vs. PLA + DZP 3 mg/mg.[2]

1.17. Spontaneous Locomotor Activity α6-GABA$_A$R Subtype-Selective Ligands

The influence of 14 pyrazoloquinolinones, diazepam, GL-II-73 and solvent on total distance travelled and time mobile is presented in **Figure 43**. Two-tailed t-tests showed a significant decrease, or at least a trend, in distance travelled (**Figure 43**A) in groups treated with DZP, DK-I-86-1, DK-II-58-1, LAU 463, DK-I-58-1 and DK-IV-20-1 when compared with control [$p<0.001$, $p<0.001$, $p=0.005$, $p=0.008$, $p=0.023$, $p=0.094$, respectively]; and a significant increase only in group treated with GL-II-73 [$p<0.018$]. Total time mobile (**Figure 43**B) appeared to be an exceptionally robust parameter of behavioral hyperactivity in groups treated with DZP, DK-I-86-1, LAU 463, DK-II-58-1, DK-I-58-1 and DK-IV-20-1 in comparison to solvent control [$p<0.001$, $p<0.001$, $p=0.005$, $p=0.007$, $p=0.020$, $p=0.056$ respectively], but also of behavioral hyperactivity in the DK-I-56-1 and RV-I-029 treated groups [$p=0.010$, $p=0.013$, respectively].

Figure 43: The Influence of 14 Pyrazoloquinolinones, Diazepam, GL-II-73 and Solvent on Total Distance Travelled and Time Mobile

A

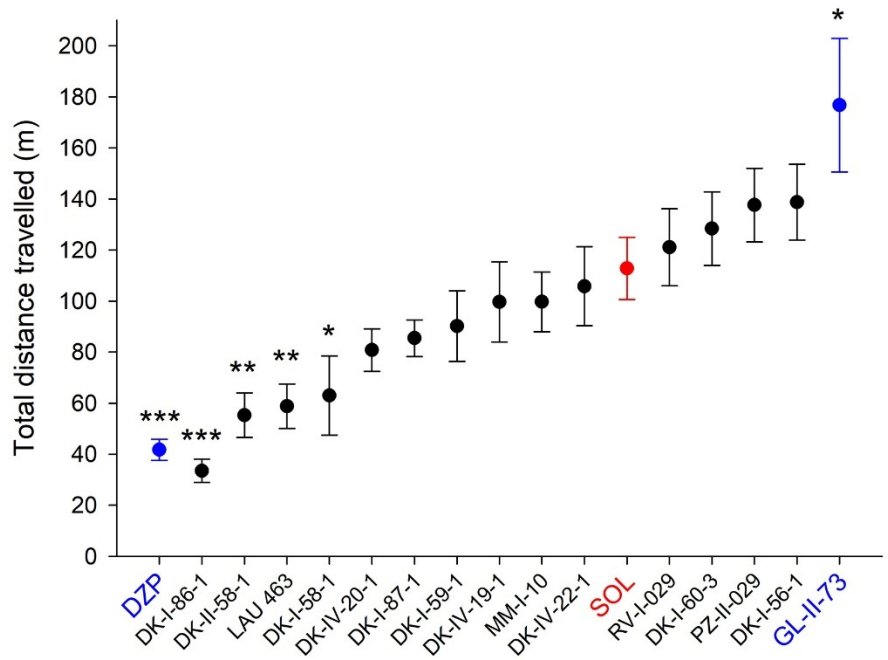

B

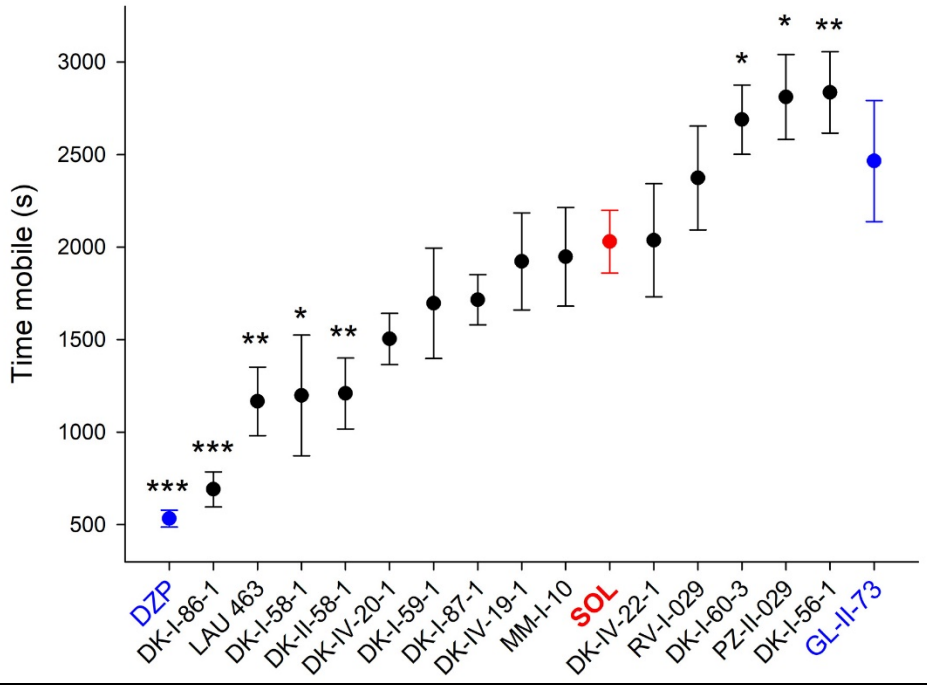

1.18. Discussion and Conclusions of α6-GABA$_A$R Subtype-Selective Ligands

GABA$_A$Rs containing the α6 subunit are primarily located in the granule cells of cerebellum,[5, 12] but are also expressed in other brain regions.[13, 14] To date, not much is known about the function of these receptors in the brain, but recent evidence indicates that they play a role in a variety of diseases. These include disorders of the trigeminal system,[20] neuropsychiatric disorders with sensori-motor gating deficits (such as tic disorders, certain symptoms of schizophrenia, obsessive compulsive disorder and attention deficit disorders),[17, 18] and depression,[16] as well as migraine.[19] Recently, some α6 PQ binding site ligands were identified as the very first compounds that were able to modulate α6-GABA$_A$Rs with high selectivity.[10, 11, 28, 29] Based on three highly α6-GABA$_A$R-subtype-selective PQ lead compounds (**8a**, **8n** and **8i**), a total of 49 PQ compounds were synthesized in the present study with the aim to increase their limited water solubility,[31] as well as their metabolic stability. The replacement of deuterium for hydrogen atoms has been shown previously to positively affect the metabolic stability of drugs while retaining the pharmacologic profile of active compounds.[34] Despite these successes, deuteration sometimes has also been observed to have no effect on metabolic stability.[92,93] In the present study, the substitution of OCD_3 groups for OCH_3 groups in the lead ligands (**8a**, **8n** and **8i**) resulted in the deuterated α6β3γ2 GABA$_A$R subtype selective ligands (**8b**, **8c**, **8d**, **8j** and **8o**) with an improved metabolic stability profile in both HLM and MLM assays (**Table 8**) and an improved pharmacokinetic profile (**Figure 34**). However, the half-life of some compounds increased but that of others also decreased on deuteration depending on the structure of the compound investigated and the position of the incorporated deuterium. This effect was different in HLM and MLM, as expected (**Table 8**). The changes in half-life observed on deuteration

were thus not predictable. The same was true for the N-heterocyclic compounds (**13a**, **13e**, **13g** and **13i)** and their deuterated derivatives (**13b**, **13c**, **13d**, **13f** and **13h**) (**Table 4)**. The N-heterocyclic compounds were synthesized to increase the water solubility of the lead compounds. Although the water solubility was increased in some of the N-heterocyclic compounds as compared to the lead compounds (compare **8a** with **13a** and **13i**), in other cases the water solubility was unchanged (compare **8n** with **13g**), or even decreased (compare **8k** with **13e**) in the N-heterocyclic substituted compounds (**Table 8**).

As expected, the deuterated derivatives exhibited an efficacy comparable to the respective lead compound for α6β3γ2 receptors, presumably via the PQ binding site (**Figure 27**). In contrast, incorporation of N-atoms into the "A-ring" or “D-ring” of the PQ core was accompanied by a drop in efficacy at the α6β3γ2 subtype relative to parent compounds **8a** and **8k**, but not relative to the parent compound **8n**, as revealed in **Figure 31**.

The synthesis of 49 novel ligands also expanded the SAR library of potential α6β3γ2 subtype selective ligands (**Table 2**, **Table 4**, and **Table 6**). Ligand **8k** had previously been identified as a compound with three times higher α6β3γ2 efficacy at 10 μM than **8a** and **8n**, but the selectivity between α1-6β3γ2 $GABA_A$Rs was much poorer for **8k**.[12] Hence, the 8-chloro substituent in “Ring A” of **8k** appeared to play a role in the increased potentiation of GABA-currents at several $GABA_A$R subtypes (α1-6β3γ2), whereas a 7-methoxy substituent in “Ring A” of **8a** appeared to be the key for α6β3γ2 subtype selectivity. The example of **8n** (**Figure 26B**) provided evidence that the 7-position can also be substituted with an electron withdrawing group such as bromine, and still retain a similar α6β3γ2 efficacy and selectivity as **8a**.

The "D-ring" substituent seems to play a role in the binding affinity at the Bz site[25-27] as well as in the α6β3γ2 positive efficacy mediated via the PQ site.[12, 30, 31] Therefore, substitution of *ortho*-methoxy groups onto the "D-ring" of 7-methoxy (**8h**) and 7-bromo (**8q**) compounds resulted in a significantly reduced affinity at the BZP rat brain site as shown in **Table 59**and **Table 60**. The affinity at the BZP rat brain site was measured by a compound-induced displacement of [^{3}H]flunitrazepam binding to brain membranes. It thus represents the affinity at the DS-Bz binding site of all $GABA_A$ receptors present in brain membranes and no conclusions can be made on a possible interaction of these compounds with the DI-Bz site at α6β3γ2 receptors. Interestingly, for the 8-chloro ligand **8m**, that also contains an *ortho*-methoxy group in the "D-ring", the binding affinity at the BZP rat brain site was retained, although it was about 50-100-fold reduced compared to that of other compounds investigated (**Table 60**). However, **8m** displayed almost no efficacy via the PQ site of the α6β3γ2 subtype (**Figure 29**) rendering this ligand an ideal "control compound" for future *in vivo* experiments.

N-Heterocyclic fragments have often been used in drug design to enhance bioavailability via manipulation of the aqueous solubility, lipophilicity and polarity of molecules.[94]
As detailed in this study, introduction of an N-atom into the "D-ring" of the parent ligand **8a** resulted in **13a** with about 3-fold increased water solubility (**Table 8**) and a 3.6-fold increased half-life in HLM (**Table 8**). The 7-OCD_3 derivative of **13a**, compound **13c**, exhibited a similarly increased half-life as **13a** in HLM (**Table 8**) while retaining α6β3γ2 subtype selective efficacy (**Figure 32**). The "D-ring" N-hetero substituted analogs of **8i** and **8n** (**13e** and **13g**, respectively) did not exhibit improved aqueous solubility and were not pursued further in this study.

The analogs **8b**, **8c**, **8d** and **13c**, the deuterated derivatives of **8a**, all exhibited a similarly enhanced metabolic stability (within experimental error) over the parent **8a** with half-lives of 8.3 – 12.5 hours (HLM) and 9.2 – 14.2 hours (MLM) (**Table 8**). Examination of the pharmacokinetic studies, however, indicated an almost two-fold increase in the brain concentrations (Cmax) for the deuterated analogs (**8b**, **8c** and **8d**), whereas the Cmax for the deuterated *N*-hetero analog **13c** was considerably less than that of the parent **8a** (**Figure 34**). The metabolic stability alone thus does not necessarily result in higher brain concentrations. Many other factors mediate brain exposure such as: lipid solubility, charge, tertiary structure and degree of protein binding.[95] Despite the increased solubility of **13c** (see OCH_3 analog, **13a** in **Table 8)**, the decreased lipophilicity (cLogP = 2.17) may have retarded the ability to cross the BBB by the introduction of the "D-ring" N-hetero atom substituent.[96]

In summary, the deuterated *para* analogs (**8b**, **8c**, **8d** and **8o**) of **8a** and **8n** displayed the ideal combination of α6β3γ2 $GABA_AR$ subtype selectivity and efficacy (**Figure 26**, **Figure 27**). The deuterated *meta* analog **8j** was not pursued further in this study due to its poorer efficacy as compared to **8b**, **8c**, **8d** and **8o**. The **8n** related ligands (**8o** and **13h**) exhibited efficacies comparable to **8n** (**Figure 27** and **Figure 31**, respectively), but increased metabolic stability (**Table 8**) and will be explored in the future with pharmacokinetic studies. The deuterated, "D-ring" N-hetero substituted **13h** was the metabolically most stable ligand of the series developed, to date (**Table 8**). In the future, a number of other ligands including the additional compounds reported in this work (**Table 6**) with a variety of substituents in the "A-ring" and "D-ring" of the

PQ scaffold will have to be investigated for their α6β3γ2 $GABA_AR$-selectivity to obtain a more accurate SAR profile.

Due to the ease of synthesis, the functionally α6β3γ2 $GABA_AR$-selective ligand **8b** was ultimately chosen as the lead ligand from this work for future *in vivo* studies, although analogs **8c** and **8d**, exhibited a similarly increased brain concentration (C_{max}) as **8b** over the parent ligand **8a** (**Figure 34**). The deuteration of the methoxy group in the "D-ring" (**8b**) was achieved in four synthetic steps (**Scheme 3**), whereas, deuteration of the "A-ring" methoxy group in **8c** required six synthetic steps. The di-OCD_3 substituted ligand **8d** required nine convergent steps but did not result in a beneficial increase in bioavailability over the mono-OCD_3 substituted ligand **8b** to warrant the extra synthetic steps required to obtain it.

As indicated in the rotarod experiments **(Figure 137**), as well as in the elevated plus maze, grip strength and cued water maze experiments (**Table 11**), **8b** was devoid of many of the effects characteristic of classical Bzs (sedation, motor incoordination, amnesia, anxiolytic action). While the predominant lack of significant influence on behavioral parameters are expected to improve the safety and tolerability profile of this ligand **8b**, the unexpected mild hyperlocomotor activity (**Figure 42**), induced in rodents by **8b**, but not **8m**, requires further examination in order to identify the underlying biological mechanism. Such activity may reflect a subtle increase in motivational drive and might be useful in depressive conditions;[97] this speculative interpretation needs to be evaluated in future studies.

Cellular viability assays on HEK293 cells and HEP2G cells indicated that the ligands described herein are non-toxic even at 400 μM (**Table 63**). In addition, a screen of these compounds with a panel (PDSP) of a wide range of 46 membrane receptors, channels and transporters including the hERG channel indicated that there were no off-target effects (no hERG inhibition at > 10 μM) (**Table 59** and **Table 60**). This result coupled with the lack of adverse Bz-like effects in basic behavioral tests, suggest that **8b** is a potential agonist-like clinical agent targeted for α6β2/3γ2 GABAergic receptors, presumably through PAM action at the α6+β3- (PQ) binding site. **This is a new binding site and leads credence to further studies**. Further work in this area will define its application in those diseases that are of practical relevance.

1.19. Experimental Section for α6-GABA$_A$R Subtype-Selective Ligands

1.19.1. General Procedures for Chemistry

All reactions were performed in oven-dried round-bottom flasks with magnetic stir bars or overhead mechanical stirrers under an argon atmosphere. Organic solvents were purified when necessary by standard methods[98] or purchased from Sigma-Aldrich.™ The chemicals were purchased from either Sigma Aldrich™, Oakwood Chemical, Alfa Aesar, Matrix Scientific, or Acros Organic. The progress of the reactions was monitored by TLC on a silica gel plate (25% EtOAc in hexanes or 10% MeOH in DCM). The ^{1}H, ^{13}C, ^{19}F, and ^{31}P NMR spectral data were obtained on Bruker Spectrospin 300 MHz and 500 MHz instruments with the chemical shifts in δ (ppm) reported. The HRMS spectral data was obtained on a LCMS-IT-TOF by Shimadzu Scientific. The purity of all final compounds was 98% or higher and was determined by HPLC on a LC-MS with Shimadzu LCMS 2020, (Shimadzu Scientific Instruments,

Columbia, MD) using a PDA detector at 254 nm. The column was a Shimadzu C18 3 µm 50 x 4.6mm reversed phase LC column. LC mobile phase: 90% acetonitrile (w. 0.1% TFA) and 10% H_2O (w/ 0.1% TFA) with a flow rate of 1 mL min^{-1}, column temperature: 25 °C, injection size: 1.0µL.

1.19.1.1. *N*-(4-Hydroxyphenyl)acetamide (2a)

To a mixture of 4-aminophenol **1a** (50.0 g, 458.2 mmol) and THF (200 mL), acetic anhydride (49.1 g, 481.1 mmol) was added dropwise over 30 min while keeping the temperature below 50 °C. The reaction mixture was then allowed to stir for 30 min at 50 °C and then allowed to cool to rt. The reaction mixture was then diluted with hexanes (200 mL) to precipitate **2a**. After stirring for 1 h, the solid was filtered and washed with hexanes (50 mL x 2). The solid was dried under vacuum at 40 °C to afford **2a** as a white crystalline solid (62.7 g, 90.0%)**:** mp 170-171 °C; ^{1}H NMR (300 MHz, DMSO-d_6) δ 9.64 (s, 1H), 9.13 (s, 1H), 7.34 (d, J = 8.8 Hz, 2H), 6.67 (d, J = 8.8 Hz, 2H), 1.98 (s, 3H); ^{13}C NMR (75 MHz, DMSO-d_6) δ 167.95, 153.57, 131.49, 121.26, 115.44, 24.19; HRMS (ESI) m/z calculated for $C_8H_{10}NO_2$ $(M + H)^+$ 152.0706; found 152.0715. The spectroscopic properties of **2a** were identical to those reported in the literature.[99]

1.19.1.2. *N*-(3-Hydroxyphenyl)acetamide (2b)

To a mixture of 3-aminophenol **1b** (25.0 g, 229.1 mmol) and THF (100 mL), acetic anhydride (24.5 g, 240.5 mmol) was added dropwise over 30 min while keeping the temperature below 50 °C. The reaction mixture was then allowed to stir for 30 min at 50 °C and then allowed to cool to rt. The reaction mixture was then diluted with hexanes (100 mL) to precipitate **2b**. After stirring

for 1 h, the solid was filtered and washed with hexanes (25 mL x 2). The solid was dried under vacuum at 40 °C to afford **2b** as a white crystalline solid (33.2 g, 96.0%)**:** mp 145-148 °C; ^{1}H NMR (300 MHz, DMSO-d_6) δ 9.77 (s, 1H), 9.32 (s, 1H), 7.18 (s, 1H), 7.04 (t, J = 8.0 Hz, 1H), 6.92 (d, J = 8.1 Hz, 1H), 6.42 (dd, J = 7.9, 2.1 Hz, 1H), 2.01 (s, 3H); ^{13}C NMR (75 MHz, DMSO-d_6) δ 168.60, 158.01, 140.81, 129.72, 110.55, 110.18, 106.60, 24.50; HRMS (ESI) m/z calculated for $C_8H_{10}NO_2$ $(M + H)^+$ 152.0706; found 152.0715. The spectroscopic properties of **2b** were identical to those reported in the literature.[99]

1.19.1.3. *N*-(2-Hydroxyphenyl)acetamide (2c)

To a mixture of 2-aminophenol **1c** (25.0 g, 229.1 mmol) and THF (100 mL), acetic anhydride (24.5 g, 240.5, mmol) was added dropwise over 30 min while keeping the temperature below 50 °C. The reaction mixture was then allowed to stir for 30 min at 50 °C and then allowed to cool to rt. The reaction mixture was then diluted with hexanes (100 mL) to precipitate **2c**. After stirring for 1 h, the solid was filtered and washed with hexanes (25 mL x 2). The solid was dried under vacuum at 40 °C to afford **2c** as a light brown solid (33.1 g, 95.7%)**:** mp 211-213 °C; ^{1}H NMR (300 MHz, DMSO-d_6) δ 9.75 (s, 1H), 9.31 (s, 1H), 7.67 (d, J = 7.7 Hz, 1H), 6.85 (ddd, J = 33.6, 14.6, 7.2 Hz, 3H), 2.10 (s, 3H); ^{13}C NMR (75 MHz, DMSO-d_6) δ 169.44, 148.34, 126.88, 125.08, 122.80, 119.40, 116.38, 24.05; HRMS (ESI) m/z calculated for $C_8H_{10}NO_2$ $(M + H)^+$ 152.0706; found 152.0716. The spectroscopic properties of **2c** were identical to those reported in the literature.[99]

1.19.1.4. *N*-(4-Methoxy-d_3-phenyl)acetamide (3a)

To a mixture of *N*-(4-hydroxyphenyl)acetamide **2a** (62.0 g, 410.1 mmol), potassium carbonate (113.4 g, 615.2 mmol), and acetone (230 mL), iodomethane-d_3 (100 g, 689.8 mmol) was added dropwise over 30 min. The reaction mixture was then allowed to stir for 24 h at 20-25 °C in a RB flask equipped with a dry ice condenser. The reaction mixture was diluted with EtOAc (300 mL) and H_2O (300 mL). The biphasic mixture, which resulted, was allowed to stand for 15 min and the layers were separated. The aq layer was extracted with EtOAc (200 mL) and the combined organic layers were washed with 10% aq potassium carbonate solution (200 mL). The organic layer was dried ($MgSO_4$). The solvents were removed under reduced pressure and the residue was slurried with hexanes (200 mL). The solid was filtered and washed with hexanes (50 mL x 2). The solid was dried under vacuum at 40 °C to afford **3a** as an off-white solid (71.7 g, 99%)**:** mp 125-126 °C; ^{1}H NMR (300 MHz, DMSO-d_6) δ 9.77 (s, 1H), 7.48 (d, J = 9.0 Hz, 2H), 6.85 (d, J = 9.0 Hz, 2H), 3.38 (s, 3H), 2.00 (s, 3H); ^{13}C NMR (75 MHz, DMSO-d_6) δ 168.20, 155.48, 132.94, 121.01, 114.21, 24.23; HRMS (ESI) m/z calculated for $C_9H_9D_3NO_2$ $(M + H)^+$ 169.1051; found 169.1071.

1.19.1.5. *N*-(3-Methoxy-d_3-phenyl)acetamide (3b)

To a mixture of *N*-(3-hydroxyphenyl)acetamide **2b** (35.0 g, 231.5 mmol), potassium carbonate (64.0 g, 463.1 mmol), and acetone (140 mL), iodomethane-d_3 (50.3 g, 347.3 mmol) was added dropwise over 30 min. The reaction mixture was then allowed to stir for 24 h at 20-25 °C in a RB flask equipped with a dry ice condenser. The reaction mixture was diluted with EtOAc (150 mL) and H_2O (150 mL). The biphasic mixture, which resulted, was allowed to stand for 15 min and the layers were separated. The aq layer was extracted with EtOAc (100 mL) and then the

combined organic layers were washed with 10% aq potassium carbonate solution (100 mL). The organic layer was dried ($MgSO_4$). The solvents were then removed under reduced pressure and the residue was slurried with hexanes (100 mL). The solid was then filtered and washed with hexanes (50 mL x 2). The solid was dried under vacuum at 40 °C to afford **3b** as an off-white solid (38.9 g, 99%)**:** mp 89-91 °C; ^{1}H NMR (300 MHz, DMSO-d_6) δ 9.89 (s, 1H), 7.27 (s, 1H), 7.18 (t, J = 8.1 Hz, 1H), 7.10 (d, J = 8.2 Hz, 1H), 6.60 (dd, J = 7.8, 2.0 Hz, 1H), 2.03 (s, 3H); ^{13}C NMR (75 MHz, DMSO-d_6) δ 168.76, 159.93, 140.96, 129.89, 111.71, 108.76, 105.30, 24.53; HRMS (ESI) m/z calculated for $C_9H_9D_3NO_2$ $(M + H)^+$ 169.1051; found 169.1062.

1.19.1.6. *N*-(2-Methoxy-*d*$_3$-phenyl)acetamide (3c)

To a mixture of *N*-(2-hydroxyphenyl)acetamide **2c** (30.0 g, 198.5 mmol), potassium carbonate (54.9 g, 396.9 mmol) and acetone (140 mL), iodomethane-d_3 (50.3 g, 347.3 mmol) was added dropwise over 30 min. The reaction mixture was then allowed to stir for 24 h at 20-25 °C in a RB flask equipped with a dry ice condenser. The reaction mixture was diluted with EtOAc (150 mL) and H_2O (150 mL). The biphasic mixture, which resulted, was allowed to stand for 15 min and the layers were separated. The aq layer was extracted with EtOAc (100 mL) and the combined organic layers were washed with 10% aq potassium carbonate solution (100 mL). The organic layer was then dried ($MgSO_4$). The solvents were removed under reduced pressure and the residue was slurried with hexanes (100 mL). The solid was then filtered and washed with hexanes (50 mL x 2). The solid was dried under vacuum at 40 °C to afford **3c** as an off-white solid (31.9 g, 99%)**:** mp 82-83 °C; ^{1}H NMR (300 MHz, DMSO-d_6) δ 9.10 (s, 1H), 7.93 (d, J = 7.8 Hz, 1H), 7.22 – 6.97 (m, 2H), 6.97 – 6.79 (m, 1H), 2.08 (s, 3H); ^{13}C NMR (75 MHz, DMSO-

d$_6$) δ 168.87, 149.98, 127.87, 124.63, 122.45, 120.57, 111.50, 24.30; HRMS (ESI) m/z calculated for $C_9H_9D_3NO_2$ $(M + H)^+$ 169.1051; found 169.1060.

1.19.1.7. 4-Methoxy-*d*$_3$-phenylhydrazine (4a)

A mixture of *N*-(4-methoxy-*d*$_3$-phenyl)acetamide **3a** (30 g, 178.4 mmol), concentrated hydrochloric acid (72 mL), and H_2O (72 mL) was heated to 90 ºC and held at 90 ºC for 2 h to hydrolyze the amide functionality. The reaction mixture was then cooled to 0 to 5ºC and a solution of sodium nitrite (12.9 g, 187.7 mmol) in H_2O (25 mL) was slowly added drop-wise to the reaction mixture. Upon completion of the addition, the reaction mixture was allowed to stir for an additional 15 min at 0 to 5 ºC. The reaction mixture was then cooled to -25 to -20ºC and a solution of tin (II) chloride (74.4 g, 392.4 mmol) and concentrated hydrochloric acid (150 mL) was added drop-wise to the reaction mixture over 30 min. Upon completion of the addition, the reaction mixture was allowed to stir for an additional 4 h at -25 to -20 ºC. The reaction mixture was then diluted with diethyl ether (300 mL) and the solids were filtered off and washed with diethyl ether (100 mL x 3). The tin adduct of the product was then dissolved in a mixture of sodium hydroxide (60 g), H_2O (250 mL) and DCM (250 mL). After stirring for 2 h at 0 to 5 ºC, the solids completely dissolved. The layers were separated and the aq layer was extracted with DCM (100mL x 3). The combined organic layers were dried ($MgSO_4$). The solvents were removed under reduced pressure and the residue was slurried with hexanes (50 mL). The solid was then filtered and washed with hexanes (50 mL x 2). The solid was dried under vacuum at rt to afford **4a** as a pale orange crystalline solid (16.6 g, 66%)**:** ^{1}H NMR (300 MHz, MeOD) δ 6.91 – 6.85 (m, 2H), 6.85 – 6.78 (m, 2H), 4.88 (s, 3H); ^{13}C NMR (75 MHz, DMSO-*d*$_6$) δ 152.05,

147.27, 114.60, 113.38; HRMS (ESI) m/z calculated for $C_7H_8D_3N_2O$ $(M+H)^+$ 142.1054; found 142.1063.

1.19.1.8. 3-Methoxy-*d*$_3$-phenylhydrazine (4b)

A mixture of *N*-(3-methoxy-*d*$_3$-phenyl)acetamide **3b** (25 g, 148.6 mmol), concentrated hydrochloric acid (60 mL), and H_2O (60 mL) was heated to 90 ºC and held at 90 ºC for 2 h to hydrolyze the amide functionality. The reaction mixture was then cooled to 0 to 5 ºC and a solution of sodium nitrite (10.8 g, 156.1 mmol) in H_2O (21 mL) was slowly added drop-wise to the reaction mixture. Upon completion of the addition, the reaction mixture was allowed to stir for an additional 15 min at 0 to 5 ºC. The reaction mixture was then cooled to -25 to -20 ºC and a solution of tin (II) chloride (62.0 g, 327.0 mmol) and concentrated hydrochloric acid (125 mL) was added drop-wise to the reaction mixture over 30 min. Upon completion of the addition, the reaction mixture was allowed to stir for an additional 2 h at -25 to -20 ºC. The reaction mixture was then diluted with diethyl ether (250 mL) and the solids were filtered off and washed with diethyl ether (100 mL x 3). The tin adduct of the product was then dissolved in a mixture of sodium hydroxide (20 g), H_2O (100 mL) and DCM (100 mL). After stirring for 1 h at 0 to 5 ºC, the solids completely dissolved. The layers were separated and the aq layer was extracted with DCM (50mL x 3). The combined organic layers were dried ($MgSO_4$). The solvents were then removed under reduced pressure to afford **4b** as an orange-red oil (5.4 g, 26%)**:** ^{1}H NMR (300 MHz, DMSO-*d*$_6$) δ 6.98 (t, *J* = 8.0 Hz, 1H), 6.65 (s, 1H), 6.51 – 6.27 (m, 2H), 6.16 (d, *J* = 7.9 Hz, 1H), 3.91 (s, 2H); ^{13}C NMR (75 MHz, DMSO-*d*$_6$) δ 160.68, 154.54, 129.69, 104.96, 102.72, 97.52; HRMS (ESI) m/z calculated for $C_7H_8D_3N_2O$ $(M+H)^+$ 142.1054; found 142.1060. This material was employed in a later experiment with no further purification.

1.19.1.9. 2-Methoxy-d_3-phenylhydrazine (4c)

A mixture of *N*-(2-methoxy-d_3-phenyl)acetamide **3c** (25 g, 148.6 mmol), concentrated hydrochloric acid (60 mL), and H_2O (60 mL) was heated to 90 ºC and held at 90 ºC for 2 h to hydrolyze the amide functionality. The reaction mixture was then cooled to 0 to 5 ºC and a solution of sodium nitrite (10.7 g, 156.1 mmol) in H_2O (21 mL) was slowly added drop-wise to the reaction mixture. Upon completion of the addition, the reaction mixture was allowed to stir for an additional 15 min at 0 to 5 ºC. The reaction mixture was then cooled to -25 to -20 ºC and a solution of tin (II) chloride (62.0 g, 327.0 mmol) and concentrated hydrochloric acid (125 mL) was added drop-wise to the reaction mixture over 30 min. Upon completion of the addition, the reaction mixture was allowed to stir for an additional 2 h at -25 to -20 ºC. The reaction mixture was then diluted with diethyl ether (300 mL) and the solids were filtered off and washed with diethyl ether (100 mL x 3). The tin adduct of the product was then dissolved in a mixture of sodium hydroxide (20 g), H_2O (100 mL) and DCM (100 mL). After stirring for 1 h at 0 to 5 ºC, the solids completely dissolved. The layers were separated and the aq layer was extracted with DCM (100mL x 3). The combined organic layers were dried ($MgSO_4$). The solvents were then removed under reduced pressure and the residue was slurried with hexanes (50 mL). The solid was then filtered and washed with hexanes (25 mL x 2). The solid was dried under vacuum at rt to afford **4c** as a pale pink solid (12.5 g, 60%)**:** ^{1}H NMR (300 MHz, DMSO-d_6) δ 7.01 (dd, J = 7.8, 1.3 Hz, 1H), 6.92 – 6.71 (m, 2H), 6.61 (td, J = 7.7, 1.4 Hz, 1H), 5.92 (s, 1H), 3.92 (s, 2H); ^{13}C NMR (75 MHz, DMSO-d_6) δ 146.33, 141.94, 121.26, 117.23, 111.20, 110.07; HRMS (ESI) m/z calculated for $C_7H_8D_3N_2O$ $(M+H)^+$ 142.1054; found 142.1050.

1.19.1.10. 4-Methoxy-*d*$_3$-aniline (5a)

A mixture of *N*-(4-methoxy-*d*$_3$-phenyl)acetamide **3a** (20.0 g, 118.9 mmol), 12 M hydrochloric acid (20 mL, 240 mmol), and H_2O (60 mL) was heated at 90-95 ºC for 2 h. The reaction mixture was then allowed to cool to 20-25 ºC and the pH was adjusted to 14 with a solution of sodium hydroxide (20g, 500 mmol) and H_2O (20 mL). The product was then extracted from the aq layer with DCM (50 mL x 4). The combined organic layers were dried ($MgSO_4$). Removal of the solvents under reduced pressure afforded **5a** as a dark orange oil (14.4 g, 96%)**:** ^{1}H NMR (300 MHz, DMSO-*d*$_6$) δ 5.75 – 5.62 (m, 2H), 5.62 – 5.47 (m, 2H), 3.50 (s, 2H); ^{13}C NMR (75 MHz, DMSO-*d*$_6$) δ 150.34, 141.51, 114.62, 113.89; HRMS (ESI) m/z calculated for $C_7H_7D_3NO$ $(M + H)^+$ 127.0945; found 127.0948. This material was employed in a later experiment with no further purification.

1.19.1.11. 3-Methoxy-*d*$_3$-aniline (5b)

A mixture of *N*-(3-methoxy-*d*$_3$-phenyl)acetamide **3b** (20.0 g, 118.9 mmol), 12 M hydrochloric acid (20 mL, 240 mmol), and H_2O (60 mL) was heated at 90-95 ºC for 2 h. The reaction mixture was then allowed to cool to 20-25 ºC and the pH was adjusted to 14 with a solution of sodium hydroxide (20g, 500 mmol) and H_2O (20 mL). The product was then extracted from the aq layer with DCM (50 mL x 4). The combined organic layers were dried ($MgSO_4$). Removal of the solvents under reduced pressure afforded **5b** as a golden yellow oil (13.5 g, 90%)**:** ^{1}H NMR (300 MHz, $CDCl_3$) δ 7.10 (t, *J* = 8.0 Hz, 1H), 6.35 (dddd, *J* = 11.9, 11.2, 3.4, 2.0 Hz, 3H), 4.00 (s, 2H); ^{13}C NMR (75 MHz, $CDCl_3$) δ 160.78, 147.54, 130.16, 108.14, 104.22, 101.28; HRMS

(ESI) m/z calculated for $C_7H_7D_3NO$ $(M + H)^+$ 127.0945; found 127.0947. This material was employed in a later experiment with no further purification.

1.19.1.12. Ethyl 6-methoxy-*d*$_3$-4-oxo-1,4-dihydroquinoline-3-carboxylate (6a)

A mixture of 4-methoxy-*d*$_3$-aniline **5a** (10 g, 81.2 mmol), diethyl ethoxymethylenemalonate (21.1 g, 97.4 mmol) and diphenyl ether (100 mL) was slowly heated to 230 ºC. The EtOH, which evolved, was collected in a Dean-Stark trap. Once the EtOH formation had ceased, the reaction mixture was heated for an additional 30 min at 230 ºC. The reaction mixture was then cooled to 80 ºC and diluted with hexanes (100 mL). Upon cooling to 20-25 ºC the solid, which formed, was collected by filtration and washed with hexanes (50 mL x 2). The solid was dried under vacuum at 40 ºC to afford **6a** as a light brown solid (9.9 g, 49%). ^{1}H NMR (300 MHz, TFA) δ 11.66 (s, 1H), 9.15 (s, 1H), 8.05 (d, *J* = 9.2 Hz, 1H), 7.97 – 7.74 (m, 2H), 4.67 (q, *J* = 7.1 Hz, 2H), 1.67 – 1.39 (m, 3H); ^{13}C NMR (75 MHz, TFA) δ 171.68, 167.54, 160.89, 141.86, 134.62, 129.91, 121.73, 121.28, 104.58, 102.17, 64.41, 11.97; HRMS (ESI) m/z calculated for $C_{13}H_{11}D_3NO_4$ $(M+H)^+$ 251.1106; found 251.1115.

1.19.1.13. Ethyl 7-methoxy-*d*$_3$-4-oxo-1,4-dihydroquinoline-3-carboxylate (6b)

A mixture of 3-methoxy-*d*$_3$-aniline **5b** (10 g, 81.2 mmol), diethyl ethoxymethylenemalonate (21.1 g, 97.4 mmol) and diphenyl ether (100 mL) was slowly heated to 230 ºC. The EtOH, which evolved, was collected in a Dean-Stark trap. Once the EtOH formation had ceased, the reaction mixture was heated for an additional 30 min at 230 ºC. The reaction mixture was then cooled to 80 ºC and diluted with hexanes (100 mL). Upon cooling to 20-25 ºC the solid, which

formed, was collected by filtration and washed with hexanes (50 mL x 2). The solid was dried under vacuum at 40 ºC to afford **6b** as a brown solid (13.0 g, 64%)**:** ^{1}H NMR (300 MHz, TFA) δ 11.64 (s, 1H), 9.23 (s, 1H), 8.57 (d, *J* = 9.3 Hz, 1H), 7.59 (dd, *J* = 9.4, 2.3 Hz, 1H), 7.48 (d, *J* = 2.2 Hz, 1H), 4.71 (q, *J* = 7.2 Hz, 2H), 1.58 (t, *J* = 7.2 Hz, 3H); ^{13}C NMR (75 MHz, TFA) δ 171.89, 167.92, 167.64, 144.50, 142.44, 126.28, 121.93, 114.05, 103.81, 99.25, 64.29, 12.01; HRMS (ESI) m/z calculated for $C_{13}H_{11}D_3NO_4$ $(M+H)^+$ 251.1106; found 251.1081.

1.19.1.14. Ethyl 6-chloro-4-oxo-1,4-dihydroquinoline-3-carboxylate (6c)

A mixture of 4-chloroaniline **5c** (45.5 g, 356.7 mmol), diethyl ethoxymethylenemalonate (80.9 g, 374.1 mmol) and diphenyl ether (200 mL) was slowly heated to 230 ºC. The EtOH, which evolved, was collected in a Dean-Stark trap. Once the EtOH formation had ceased, the reaction mixture was heated for an additional 30 min at 230 ºC. The reaction mixture was then cooled to 80 ºC and diluted with EtOH (200 mL). Upon cooling to 20-25ºC the solid, which formed, was collected by filtration and washed with EtOH (50 mL x 2) and with hexanes (50 mL x 2). The solid was dried under vacuum at 40 ºC to afford **6c** as an off-white crystalline solid (85.1 g, 95%)**:** ^{1}H NMR (300 MHz, TFA) δ 11.66 (s, 1H), 9.32 (d, *J* = 4.5 Hz, 1H), 8.62 (d, *J* = 2.5 Hz, 1H), 8.12 (d, *J* = 13.0 Hz, 2H), 4.82 – 4.55 (m, 2H), 1.53 (dd, *J* = 11.8, 7.0 Hz, 3H); ^{13}C NMR (75 MHz, TFA) δ 172.51, 167.19, 144.95, 138.35, 137.62, 137.58, 123.58, 121.35, 120.82, 105.30, 64.70, 11.96; HRMS (ESI) m/z calculated for $C_{12}H_{11}ClNO_3$ $(M+H)^+$ 252.0422; found 252.0411. The spectroscopic properties of **6c** were identical to those reported in the literature.[100]

1.19.1.15. Ethyl 7-bromo-4-oxo-1,4-dihydroquinoline-3-carboxylate (6d)

A mixture of 3-bromoaniline **5d** (8.7 g, 58.1 mmol), diethyl ethoxymethylenemalonate (10.9 g, 58.1 mmol) and diphenyl ether (40 mL) was slowly heated to 230 ºC. The EtOH, which evolved, was collected in a Dean-Stark trap. Once the EtOH formation had ceased, the reaction mixture was heated for an additional 30 min at 230 ºC. The reaction mixture was then cooled to 80 ºC and diluted with EtOH (40 mL). Upon cooling to 20-25 ºC the solid, which formed, was collected by filtration and washed with EtOH (10 mL x 2) and with hexanes (10 mL x 2). The solid was dried under vacuum at 40 ºC to afford **6d** as a light brown solid (11.5 g, 77%)**:** ^{1}H NMR (300 MHz, TFA) δ 11.64 (s, 1H), 9.38 (s, 1H), 8.57 (d, *J* = 8.9 Hz, 1H), 8.43 (s, 1H), 8.15 (d, *J* = 8.9 Hz, 1H), 4.75 (q, *J* = 7.1 Hz, 2H), 1.60 (t, *J* = 7.2 Hz, 3H); ^{13}C NMR (75 MHz, TFA) δ 173.48, 167.33, 145.75, 139.71, 134.19, 134.06, 125.60, 122.70, 118.57, 105.08, 64.74, 12.01; HRMS (ESI) m/z calculated for $C_{12}H_{10}BrNO_3$ $(M+H)^+$ 295.9917; found 295.9894. The spectroscopic properties of **6d** were identical to those reported in the literature.[100]

1.19.1.16. Ethyl 7-methoxy-4-oxo-1,4-dihydrquinoline-3-carboxylate (6e)

A mixture of 3-methoxyaniline **5e** (50.0 g, 406.0 mmol), diethyl ethoxymethylenemalonate (87.8 g, 406.0 mmol) and diphenyl ether (200 mL) was slowly heated to 230 ºC. The EtOH, which evolved, was collected in a Dean-Stark trap. Once the EtOH formation had ceased, the reaction mixture was heated for an additional 30 min at 230ºC. The reaction mixture was then cooled to 80 ºC and diluted with EtOH (200 mL). Upon cooling to 20-25 ºC the solid, which formed, was collected by filtration and washed with EtOH (50 mL x 2) and with hexanes (50 mL x 2). The solid was dried under vacuum at 40 ºC to afford **6e** as a light brown solid (37.1 g, 37%)**:** ^{1}H NMR (300 MHz, TFA) δ 11.63 (s, 1H), 9.22 (d, *J* = 6.3 Hz, 1H), 8.56 (dd, *J* = 9.1, 6.7 Hz, 1H),

7.66 – 7.54 (m, 1H), 7.47 (d, J = 4.2 Hz, 1H), 4.69 (dd, J = 13.8, 6.9 Hz, 2H), 4.13 (d, J = 6.4 Hz, 3H), 1.57 (q, J = 6.8 Hz, 3H); ^{13}C NMR (75 MHz, TFA) δ 171.88, 167.91, 167.62, 144.49, 142.43, 126.28, 121.92, 114.05, 103.81, 99.24, 64.28, 55.45, 12.00; HRMS (ESI) m/z calculated for $C_{13}H_{14}NO_4$ $(M+H)^+$ 248.0917; found 248.0908. The spectroscopic properties of **6e** were identical to those reported in the literature.[100]

1.19.1.17. Ethyl 7-methoxy-4-oxo-1,4-dihydro-1,6-naphthyridine-3-carboxylate (6f)

A mixture of 4-amino-2-methoxypyridine **11c** (10.0 g, 80.6 mmol), diethyl ethoxymethylenemalonate (17.4 g, 80.6 mmol) and diphenyl ether (40 mL) was slowly heated to 230 ºC. The EtOH, which evolved, was collected in a Dean-Stark trap. Once the EtOH formation had ceased, the reaction mixture was heated for an additional 30 min at 230ºC. The reaction mixture was then cooled to 80 ºC and diluted with EtOH (200 mL). Upon cooling to 20-25 ºC the solid, which formed, was collected by filtration and washed with EtOH (10 mL x 2) and with hexanes (10 mL x 2). The impure solid was then allowed to stir with EtOH (40 mL) at reflux for 30 min. Upon cooling to 20-25 ºC, the solid was collected by filtration and washed with EtOH (10 mL x 2) and with hexanes (10 mL x 2). The solid was dried under vacuum at 40 ºC to afford **6f** as a light brown solid (3.1 g, 15%)**:** ^{1}H NMR (500 MHz, TFA) δ 11.63 (s, 1H), 9.40 (s, 1H), 8.18 (d, J = 7.7 Hz, 1H), 7.26 (d, J = 7.6 Hz, 1H), 4.74 (q, J = 7.0 Hz, 2H), 3.99 (s, 3H), 1.63 (t, J = 7.1 Hz, 3H); ^{13}C NMR (126 MHz, TFA) δ 175.82, 164.29, 162.82, 149.50, 148.69, 145.32, 111.96, 108.86, 100.58, 64.48, 36.92, 12.07; HRMS (ESI) m/z calculated for $C_{12}H_{13}N_2O_4$ $(M+H)^+$ 249.0870; found 249.0880.

1.19.1.18. Ethyl 7-methoxy-8-methyl-4-oxo-1,4-dihydroquinoline-3-carboxylate (6g)

A mixture of 3-methoxy-2-methylaniline **5g** (25 g, 182.2 mmol), diethyl ethoxymethylenemalonate (39.4 g, 182.2 mmol) and diphenyl ether (100 mL) was slowly heated to 230 ºC. The EtOH, which evolved, was collected in a Dean-Stark trap. Once the EtOH formation had ceased, the reaction mixture was heated for an additional 30 min at 230 ºC. The reaction mixture was then cooled to 80 ºC and diluted with ethanol (100 mL). Upon cooling to 20-25 ºC the solid, which formed, was collected by filtration and washed with ethanol (50 mL x 2) and then hexanes (50 mL x 2). The solid was dried under vacuum at 40 ºC to afford **6g** as a light brown solid (41.9 g, 88%); ^{1}H NMR (300 MHz, TFA) δ 11.66 (s, 1H), 9.13 (s, 1H), 8.53 (d, J = 9.3 Hz, 1H), 7.60 (d, J = 9.4 Hz, 1H), 4.60 (q, J = 7.1 Hz, 2H), 4.11 (s, 3H), 2.52 (s, 3H), 1.46 (t, J = 7.1 Hz, 3H); ^{13}C NMR (75 MHz, TFA) δ 172.57, 167.57, 164.66, 144.78, 139.23, 124.90, 114.60, 114.12, 113.61, 102.73, 64.14, 55.62, 11.94, 6.58; HRMS (ESI) m/z calculated for $C_{14}H_{16}NO_4$ $(M+H)^+$ 262.1074; found 262.1097.

1.19.1.19. Ethyl 6-bromo-8-fluoro-4-oxo-1,4-dihydroquinoline-3-carboxylate (6h)

A mixture of 4-bromo-2-fluoroaniline **5h** (10 g, 52.6 mmol), diethyl ethoxymethylenemalonate (11.4 g, 52.6 mmol) and diphenyl ether (40 mL) was slowly heated to 230 ºC. The EtOH, which evolved, was collected in a Dean-Stark trap. Once the EtOH formation had ceased, the reaction mixture was heated for an additional 30 min at 230 ºC. The reaction mixture was then cooled to 80 ºC and diluted with ethanol (40 mL). Upon cooling to 20-25 ºC the solid, which formed, was collected by filtration and washed with ethanol (10 mL x 2) and then hexanes (10 mL x 2). The solid was dried under vacuum at 40 ºC to afford **6h** as a light brown solid (41.9 g, 88%); ^{1}H

NMR (300 MHz, TFA) δ 11.65 (s, 1H), 9.37 (s, 1H), 8.61 (s, 1H), 8.07 (d, J = 9.3 Hz, 1H), 4.68 (q, J = 7.0 Hz, 2H), 1.52 (t, J = 7.1 Hz, 3H); ^{13}C NMR (75 MHz, TFA) δ 172.48 (s), 166.96 (s), 151.48 (d, $^{1}J_{CF}$ = 261.7 Hz), 145.48 (s), 128.08 (d, $^{2}J_{CF}$= 14.9 Hz), 125.44 (d, $^{2}J_{CF}$ = 19.3 Hz), 124.22 (d, $^{3}J_{CF}$ = 8.1 Hz), 123.00 (d, $^{3}J_{CF}$ = 4.7 Hz), 121.87 (s), 106.18 (s), 65.01 (s), 11.92 (s); HRMS (ESI) m/z calculated for $C_{12}H_{10}BrFNO_3$ $(M+H)^+$ 313.9823; found 313.9822.

1.19.1.20. Ethyl 4-oxo-7-(trifluoromethyl)-1,4-dihydroquinoline-3-carboxylate (6i)

A mixture of 3-(trifluoromethyl)aniline **5i** (25 g, 155.1 mmol), diethyl ethoxymethylenemalonate (33.6 g, 155.1 mmol) and diphenyl ether (100 mL) was slowly heated to 230 ºC. The EtOH, which evolved, was collected in a Dean-Stark trap. Once the EtOH formation had ceased, the reaction mixture was heated for an additional 30 min at 230 ºC. The reaction mixture was then cooled to 80 ºC and diluted with ethanol (100 mL). Upon cooling to 20-25 ºC the solid, which formed, was collected by filtration and washed with ethanol (25 mL x 2) and then hexanes (25 mL x 2). The solid was dried under vacuum at 40 ºC to afford **6i** as an off-white solid (35.6 g, 80%); ^{1}H NMR (300 MHz, TFA) δ 11.65 (s, 1H), 9.44 (s, 1H), 8.81 (d, J = 8.7 Hz, 1H), 8.50 (s, 1H), 8.16 (d, J = 8.7 Hz, 1H), 4.68 (q, J = 7.1 Hz, 2H), 1.52 (t, J = 7.1 Hz, 3H); ^{13}C NMR (75 MHz, TFA) δ 173.51 (s), 167.08 (s), 146.62 (s), 139.51 (q, $^{2}J_{CF}$ = 35.7 Hz), 138.80 (s), 126.21 (s), 125.92 (q, $^{3}J_{CF}$ = 2.9 Hz), 121.94 (q, $^{1}J_{CF}$ = 263.7 Hz), 121.61 (s), 117.70 (q, $^{3}J_{CF}$ = 4.0 Hz), 105.92 (s), 64.87 (s), 11.91 (s); HRMS (ESI) m/z calculated for $C_{13}H_{11}F_3NO_3$ $(M+H)^+$ 286.0686; found 286.0688.

1.19.1.21. Ethyl 4-chloro-6-methoxy-*d*$_3$-quinoline-3-carboxylate (7a)

A mixture of ethyl 6-methoxy-*d*$_3$-4-oxo-1,4-dihydroquinoline-3-carboxylate **6a** (10.0 g, 40.0 mmol), phosphorus oxychloride (6.7 g, 44.0 mmol) and toluene (40 mL) was heated to 80-90 ºC. The reaction mixture was then held for 1 h at 80-90 ºC. The brown solution, which resulted, was then allowed to cool to 20-25 ºC. The reaction mixture was diluted with hexanes (40 mL). The solids, which remained, were collected by filtration and washed with hexanes (20 mL x 2). The solids were then dissolved in DCM (100 mL) and brought to pH = 10 (pH paper) by slowly adding a 25% solution of aq potassium carbonate (10 g) in H_2O (40 mL). The layers were then separated and the aq layer was extracted with DCM (50 mL). The combined organic layers were then washed with a 25% solution of aq potassium carbonate (10 g) in H_2O (40 mL). The combined organic layers were dried ($MgSO_4$). The solvents were removed under reduced pressure and the residue was slurried with hexanes (50 mL). The solid, which formed, was then filtered and washed with hexanes (25 mL x 2). The solid was dried under vacuum at 40 ºC to afford **7a** as an off-white solid (8.5 g, 79%)**:** ^{1}H NMR (300 MHz, DMSO-*d*$_6$) δ 8.95 (s, 1H), 8.03 (d, *J* = 9.1 Hz, 1H), 7.67 – 7.45 (m, 2H), 4.42 (q, *J* = 7.1 Hz, 2H), 1.38 (t, *J* = 7.1 Hz, 3H); ^{13}C NMR (75 MHz, DMSO-*d*$_6$) δ 164.49, 159.57, 147.25, 145.36, 139.99, 131.67, 126.91, 125.20, 123.87, 102.96, 62.36, 14.47; HRMS (ESI) m/z calculated for $C_{13}H_{10}D_3ClNO_3$ $(M+H)^+$ 269.0767; found 269.0762.

1.19.1.22. Ethyl 4-chloro-7-methoxy-*d*$_3$-quinoline-3-carboxylate (7b)

A mixture of ethyl 7-methoxy-*d*$_3$-4-oxo-1,4-dihydroquinoline-3-carboxylate **6b** (13.0 g, 51.9 mmol), phosphorus oxychloride (8.8 g, 57.1 mmol) and toluene (52 mL) was heated to 80-90 ºC. The reaction mixture was then held for 1 h at 80-90 ºC). The brown solution, which resulted,

was then allowed to cool to 20-25 ºC. The reaction mixture was diluted with hexanes (50 mL). The solids, which remained, were collected by filtration and washed with hexanes (50 mL x 2). The solids were then dissolved in DCM (100 mL) and brought to pH = 10 (pH paper) by slowly adding a 25% solution of aq potassium carbonate (12.5 g) in H_2O (50 mL). The layers were then separated and the aq layer was extracted with DCM (50 mL). The combined organic layers were then washed with a 25% solution of aq potassium carbonate (12.5 g) in H_2O (50 mL). The combined organic layers were dried ($MgSO_4$). The solvents were removed under reduced pressure and the residue was slurried with hexanes (50 mL). The solid, which formed, was then filtered and washed with hexanes (25 mL x 2). The solid was dried under vacuum at 40 ºC to afford **7b** as an off-white solid (11.5 g, 82%)**:** ^{1}H NMR (300 MHz, DMSO-d_6) δ 9.07 (s, 1H), 8.23 (d, J = 9.2 Hz, 1H), 7.54 – 7.38 (m, 2H), 4.40 (q, J = 7.1 Hz, 2H), 1.37 (t, J = 7.1 Hz, 3H); ^{13}C NMR (75 MHz, DMSO-d_6) δ 164.29, 162.85, 151.53, 150.75, 142.41, 126.84, 122.11, 121.07, 120.56, 108.27, 62.15, 14.49; HRMS (ESI) m/z calculated for $C_{13}H_{10}D_3ClNO_3$ $(M+H)^+$ 269.0767; found 269.0774.

1.19.1.23. Ethyl 4,6-dichloroquinoline-3-carboxylate (7c)

A mixture of ethyl 6-chloro-4-oxo-1,4-dihydroquinoline-3-carboxylate **6c** (85.1 g, 338.1 mmol), *N,N*-dimethylformamide (1.0 mL, 12.9 mmol), and DCM (640 mL) was heated to 35-40ºC. Oxalyl chloride (47.2 g, 371.9 mmol) was added dropwise to the reaction mixture over 30 min. The reaction mixture was heated for 6 h at reflux (38-40 ºC). The pale yellow solution, which resulted, was then allowed to cool to 20-25 ºC. The reaction mixture was brought to pH = 10 (pH paper) by slowly adding a 25% solution of aq potassium carbonate (75 g) in H_2O (300 mL). The layers were then separated and the aq layer was extracted with DCM (200 mL). The

combined organic layers were then washed with a 25% solution of aq potassium carbonate (50 g) in H_2O (200 mL). The combined organic layers were dried ($MgSO_4$). The solvents were then removed under reduced pressure and the residue was slurried with hexanes (200 mL). The solid, which formed, was filtered and washed with hexanes (50 mL x 2). The solid was dried under vacuum at 40 ºC to afford **7c** as an off-white solid (81.9 g, 90%)**:** ^{1}H NMR (300 MHz, DMSO-*d*$_6$) δ 9.13 (s, 1H), 8.30 (d, *J* = 2.2 Hz, 1H), 8.14 (d, *J* = 9.0 Hz, 1H), 7.97 (dd, *J* = 9.0, 2.3 Hz, 1H), 4.44 (q, *J* = 7.1 Hz, 2H), 1.39 (t, *J* = 7.1 Hz, 3H); ^{13}C NMR (75 MHz, DMSO-*d*$_6$) δ 164.01, 150.53, 147.73, 141.04, 134.30, 133.34, 132.20, 126.53, 124.37, 124.08, 62.59; HRMS (ESI) m/z calculated for $C_{12}H_{10}Cl_2NO_2$ $(M+H)^+$ 270.0083; found 270.0089. The spectroscopic properties of **7c** were identical to those reported in the literature.[72]

1.19.1.24. Ethyl 7-bromo-4-chloroquinoline-3-carboxylate (7d)

A mixture of ethyl 7-bromo-4-oxo-1,4-dihydroquinoline-3-carboxylate **6d** (11.0 g, 37.1 mmol), *N,N*-dimethylformamide (0.1 mL, 1.3 mmol), and DCM (50 mL) was heated to 35-40 ºC. Oxalyl chloride (5.2 g, 40.9 mmol) was added dropwise to the reaction mixture over 30 min. The reaction mixture was heated for 1 h at reflux (38-40ºC). The brown solution, which resulted, was then allowed to cool to 20-25 ºC. The reaction mixture was diluted with DCM (150 mL) and then brought to pH = 10 (pH paper) by slowly adding a 25% solution of aq potassium carbonate (12.5 g) in H_2O (50 mL). The layers were then separated and the aq layer was extracted with DCM (50 mL). The combined organic layers were washed with a 25% solution of aq potassium carbonate (12.5 g) in H_2O (50 mL). The combined organic layers were dried ($MgSO_4$). The solvents were then removed under reduced pressure and the residue was slurried with hexanes (50 mL). The solid, which formed, was filtered and washed with hexanes

(25 mL x 2). The solid was dried under vacuum at 40 °C to afford **7d** as an off-white solid (7.2 g, 61%)**:** ^{1}H NMR (300 MHz, DMSO-d_6) δ 9.15 (s, 1H), 8.36 (d, J = 1.9 Hz, 1H), 8.28 (d, J = 9.0 Hz, 1H), 7.98 (dd, J = 9.0, 1.9 Hz, 1H), 4.44 (q, J = 7.1 Hz, 2H), 1.39 (t, J = 7.1 Hz, 3H); ^{13}C NMR (75 MHz, DMSO-d_6) δ 164.04, 151.40, 149.74, 142.34, 132.67, 131.88, 127.50, 126.64, 124.70, 123.96, 62.55, 14.46; HRMS (ESI) m/z calculated for $C_{12}H_{10}BrClNO_2(M+H)^+$ 313.9578; found 313.9568.

1.19.1.25. Ethyl 4-chloro-7-methoxyquinoline-3-carboxylate (7e)

A mixture of ethyl 7-methoxy-4-oxo-1,4-dihydroquinoline-3-carboxylate **6e** (37.1 g, 150.0 mmol), *N,N*-dimethylformamide (0.5 mL, 6.5 mmol), and DCM (150 mL) was heated to 35-40 °C. Oxalyl chloride (20.9 g, 165.0 mmol) was added dropwise to the reaction mixture over 30 min. The reaction mixture was heated for 2 h at reflux (38-40 °C). The brown solution, which resulted, was allowed to cool to 20-25 °C. The reaction mixture was diluted with DCM (150 mL) and then brought to pH = 10 (pH paper) by slowly adding a 25% solution of aq potassium carbonate (75 g) in H_2O (300 mL). The layers were separated and the aq layer was extracted with DCM (100 mL). The combined organic layers were then washed with a 25% solution of aq potassium carbonate (75 g) in H_2O (300 mL). The combined organic layers were dried ($MgSO_4$). The solvents were removed under reduced pressure and the residue was slurried with hexanes (200 mL). The solid, which formed, was then filtered and washed with hexanes (50 mL x 2). The solid was dried under vacuum at 40 °C to afford **7e** as an off-white solid (36.3 g, 91%)**:** ^{1}H NMR (300 MHz, DMSO-d_6) δ 9.08 (s, 1H), 8.25 (d, J = 9.2 Hz, 1H), 7.57 – 7.37 (m, 2H), 4.41 (q, J = 7.1 Hz, 2H), 3.98 (s, 3H), 1.38 (t, J = 7.1 Hz, 3H); ^{13}C NMR (75 MHz, DMSO-

d$_6$) δ 164.32, 162.83, 151.62, 150.81, 142.02, 126.85, 122.12, 121.11, 120.56, 108.36, 62.15, 56.45, 14.49; HRMS (ESI) m/z calculated for $C_{13}H_{13}ClNO_3$ $(M+H)^+$ 266.0578; found 266.0578.

1.19.1.26. Ethyl 4-chloro-7-methoxy-1,6-napththyridine-3-carboxylate (7f)

A mixture of ethyl 7-methoxy-4-oxo-1,4-dihydro-1,6-naphthyridine-3-carboxylate **6f** (3.0 g, 120.9 mmol), *N,N*-dimethylformamide (0.1 mL, 1.3 mmol), and DCM (40 mL) was heated to 35-40 ºC. Oxalyl chloride (1.7 g, 13.3 mmol) was added dropwise to the reaction mixture over 30 min. The reaction mixture was heated for 2 h at reflux (38-40 ºC). The brown solution, which resulted, was then allowed to cool to 20-25 ºC. The reaction mixture was diluted with DCM (40 mL) and then brought to pH = 10 (pH paper) by slowly adding a 25% solution of aq potassium carbonate (12.5 g) in H_2O (50 mL). The layers were then separated and the aq layer was extracted with DCM (50 mL). The combined organic layers were then washed with a 25% solution of aq potassium carbonate (12.5 g) in H_2O (50 mL). The combined organic layers were dried ($MgSO_4$). The solvents were then removed under reduced pressure and the residue was slurried with hexanes (25 mL). The solid, which formed, was then filtered and washed with hexanes (10 mL x 2). The solid was dried under vacuum at 40 ºC to afford **7f** as an off-white solid (1.3 g, 40.4%)**:** ^{1}H NMR (500 MHz, $CDCl_3$) δ 8.99 (s, 1H), 7.44 (d, *J* = 7.4 Hz, 1H), 6.71 (d, *J* = 7.5 Hz, 1H), 4.47 (q, *J* = 7.0 Hz, 2H), 3.60 (s, 3H), 1.44 (t, *J* = 7.1 Hz, 3H); ^{13}C NMR (126 MHz, $CDCl_3$) δ 164.43, 160.49, 157.34, 153.76, 145.84, 138.50, 126.66, 118.46, 106.93, 62.27, 37.76, 14.18; HRMS (ESI) m/z calculated for $C_{12}H_{12}ClN_2O_3$ $(M+H)^+$ 267.0531; found 267.0531.

1.19.1.27. Ethyl 4-chloro-7-methoxy-8-methyl quinoline-3-carboxylate (7g)

A mixture of ethyl 7-methoxy-8-methyl-4-oxo-1,4-dihydroquinoline-3-carboxylate **6g** (41.0 g, 156.9 mmol), *N,N*-dimethylformamide (0.5 mL, 6.5 mmol), and DCM (500 mL) was heated to 35-40°C. Oxalyl chloride (21.9 g, 172.6 mmol) was added dropwise to the reaction mixture over 30 min. The reaction mixture was heated for 6 h at reflux (38-40 °C). The pale yellow solution, which resulted, was then allowed to cool to 20-25 °C. The reaction mixture was brought to pH = 10 (pH paper) by slowly adding a 25% solution of aq potassium carbonate (62.5 g) in H_2O (250 mL). The layers were then separated and the aq layer was extracted with DCM (250 mL). The combined organic layers were then washed with a 25% solution of aq potassium carbonate (62.5 g) in H_2O (250 mL). The combined organic layers were dried ($MgSO_4$). The solvents were then removed under reduced pressure and the residue was slurried with cold hexanes (200 mL). The solid, which formed, was filtered and washed with cold hexanes (50 mL x 2). The solid was dried under vacuum at 40 °C to afford **7g** as an off-white solid (42.9 g, 97%); ^{1}H NMR (300 MHz, $CDCl_3$) δ 9.21 (s, 1H), 8.27 (d, J = 9.4 Hz, 1H), 7.41 (d, J = 9.4 Hz, 1H), 4.49 (q, J = 7.1 Hz, 2H), 4.02 (s, 3H), 2.66 (s, 3H), 1.46 (t, J = 7.1 Hz, 3H); ^{13}C NMR (75 MHz, $CDCl_3$) δ 164.78, 159.33, 149.82, 149.23, 143.84, 124.25, 122.51, 120.88, 119.92, 114.35, 61.74, 56.20, 14.25, 10.00; HRMS (ESI) m/z calculated for $C_{14}H_{15}ClNO_3$ $(M+H)^+$ 280.0735; found 280.0746.

1.19.1.28. Ethyl 6-bromo-4-chloro-8-fluoroquinoline-3-carboxylate (7h)

A mixture of ethyl 6-bromo-8-fluoro-4-oxo-1,4-dihydroquinoline-3-carboxylate **6h** (11.0 g, 35.0 mmol), *N,N*-dimethylformamide (0.1 mL, 1.3 mmol), and DCM (200 mL) was heated to 35-40°C. Oxalyl chloride (4.9 g, 38.5 mmol) was added dropwise to the reaction mixture over 30 min. The reaction mixture was heated for 6 h at reflux (38-40°C). The pale yellow solution,

which resulted, was then allowed to cool to 20-25°C. The reaction mixture was brought to pH = 10 (pH paper) by slowly adding a 25% solution of aq potassium carbonate (25 g) in H_2O (100 mL). The layers were then separated and the aq layer was extracted with DCM (100 mL). The combined organic layers were then washed with a 25% solution of aq potassium carbonate (25 g) in H_2O (100 mL). The combined organic layers were dried ($MgSO_4$). The solvents were then removed under reduced pressure and the residue was slurried with cold hexanes (50 mL). The solid, which formed, was filtered and washed with cold hexanes (10 mL x 2). The solid was dried under vacuum at 40°C to afford **7h** as a pale yellow solid (9.7 g, 83%); ^{1}H NMR (300 MHz, $CDCl_3$) δ 9.21 (s, 1H), 8.36 (d, J = 1.3 Hz, 1H), 7.68 (dd, J = 9.1, 1.6 Hz, 1H), 4.52 (q, J = 7.1 Hz, 2H), 1.48 (t, J = 7.1 Hz, 3H); ^{13}C NMR (75 MHz, $CDCl_3$) δ 163.79 (s), 157.55 (d, $^1J_{CF}$ = 263.7 Hz), 150.38 (s), 142.17 (s), 138.63 (d, $^2J_{CF}$ = 12.4 Hz), 128.50 (s), 124.90 (s), 123.64 (d, $^3J_{CF}$ = 5.0 Hz), 121.59 (d, $^3J_{CF}$ = 9.4 Hz), 120.15 (d, $^2J_{CF}$ = 22.0 Hz), 62.54 (s), 14.21 (s); HRMS (ESI) m/z calculated for $C_{12}H_9BrClFNO_2$ $(M+H)^+$ 331.9484; found 331.9485.

1.19.1.29. Ethyl 4-chloro-7-(trifluoromethyl)quinoline-3-carboxylate (7i)

A mixture of ethyl 4-oxo-7-(trifluoromethyl)-1,4-dihydroquinoline-3-carboxylate **6i** (35.0 g, 122.7 mmol), *N,N*-dimethylformamide (0.5 mL, 6.5 mmol), and DCM (500 mL) was heated to 35-40°C. Oxalyl chloride (17.1 g, 135.0 mmol) was added dropwise to the reaction mixture over 30 min. The reaction mixture was heated for 6 h at reflux (38-40°C). The pale yellow solution, which resulted, was then allowed to cool to 20-25°C. The reaction mixture was brought to pH = 10 (pH paper) by slowly adding a 25% solution of aq potassium carbonate (62.5 g) in H_2O (250 mL). The layers were then separated and the aq layer was extracted with DCM (250 mL). The combined organic layers were then washed with a 25% solution of aq potassium carbonate (62.5

g) in H_2O (250 mL). The combined organic layers were dried ($MgSO_4$). The solvents were then removed under reduced pressure and the residue was slurried with cold hexanes (50 mL). The solid, which formed, was filtered and washed with cold hexanes (10 mL x 2). The solid was dried under vacuum at 40 ºC to afford **7i** as an off-white solid (26.1 g, 70%); ^{1}H NMR (300 MHz, $CDCl_3$) δ 9.28 (s, 1H), 8.54 (d, J = 8.8 Hz, 1H), 8.45 (s, 1H), 7.87 (dd, J = 8.8, 1.6 Hz, 1H), 4.53 (q, J = 7.1 Hz, 2H), 1.49 (t, J = 7.1 Hz, 3H); ^{13}C NMR (75 MHz, $CDCl_3$) δ 163.98 (s), 151.40 (s), 148.60 (s), 143.38 (s), 133.46 (q, $^2J_{CF}$ = 33.1 Hz), 127.80 (s), 127.64 (q, $^3J_{CF}$ = 4.4 Hz), 126.90 (s), 124.65 (s), 123.97 (q, $^3J_{CF}$ = 3.0 Hz), 123.41 (q, $^1J_{CF}$ = 272.9 Hz), 62.44 (s), 14.20 (s); HRMS (ESI) m/z calculated for $C_{13}H_{10}ClF_3NO_2$ $(M+H)^+$ 304.0347; found 304.0344.

1.19.1.30. 7-Methoxy-2-(4-methoxyphenyl)-2,5-dihydro-3*H*-pyrazolo[4,3-*c*]quinolin-3-one (PZ-II-029, 8a)

A mixture of ethyl-4-chloro-7-methoxyquinoline-3-carboxylate **7e** (4 g, 15.1 mmol), 4-methoxyphenylhydrazine hydrochloride **4d** (3.15 g, 18.1 mmol), triethylamine (3.66g, 36.1 mmol) and xylenes (32 mL) was heated to reflux (138 ºC) and held at reflux for 2 h. The yellow-orange slurry, which resulted, was cooled to 100 ºC and diluted with EtOH (32 mL). The reaction mixture was heated at reflux at 80ºC for 30 min and then allowed to cool to 20-25 ºC. The solids, which remained, were collected by filtration and washed with a 1:1 mixture of EtOH (2.5 mL x 2) and hexanes (2.5 mL x 2) and then washed with hexanes (5 mL x 2). The solid was dried under vacuum at 40 ºC to afford **8a** as a yellow powder (2.0 g, 41%)**:** ^{1}H NMR (300 MHz, DMSO-d_6) δ 12.59 (s, 1H), 8.65 (s, 1H), 8.10 (t, J = 8.7 Hz, 3H), 7.34 – 7.12 (m, 2H), 7.01 (d, J = 9.1 Hz, 2H), 3.87 (s, 3H), 3.78 (s, 3H); ^{13}C NMR (75 MHz, DMSO-d_6) δ 161.45, 160.85,

156.22, 143.11, 139.33, 137.42, 134.10, 124.05, 120.68, 115.77, 114.25, 112.68, 106.87, 102.26, 55.98, 55.68; HRMS (ESI) m/z calculated for $C_{18}H_{16}N_3O_3$ $(M+H)^+$ 322.1186; found 322.1178; HPLC purity, 99.9%.

1.19.1.31. 7-Methoxy-2-(4-methoxy-*d*$_3$-phenyl)-2,5-dihydro-3*H*-pyrazolo[4,3-*c*]quinolin-3-one (DK-I-56-1, 8b)

A mixture of ethyl-4-chloro-7-methoxyquinoline-3-carboxylate **7e** (2 g, 7.4 mmol), 4-methoxy-*d*$_3$-phenylhydrazine **4a** (1.25 g, 8.9 mmol), triethylamine (0.90g, 8.9 mmol) and xylenes (16 mL) was heated to reflux (138 ^{o}C) and held at reflux for 2 h. The yellow-orange slurry, which resulted, was cooled to 100 ^{o}C and diluted with EtOH (16 mL). The reaction mixture was heated at reflux at 80^{o}C for 30 min and then allowed to cool to 20-25 ^{o}C. The solids, which remained, were collected by filtration and washed with a 1:1 mixture of EtOH (2.5 mL x 2) and hexanes (2.5 mL x 2) and then washed with hexanes (5 mL x 2). The solid was dried under vacuum at 40 ^{o}C to afford **8b** as a yellow powder (1.5 g, 62.5%)**:** ^{1}H NMR (300 MHz, DMSO-*d*$_6$) δ 12.60 (s, 1H), 8.66 (s, 1H), 8.10 (t, J = 9.7 Hz, 3H), 7.18 (s, 2H), 7.01 (d, J = 8.4 Hz, 2H), 3.88 (s, 3H); ^{13}C NMR (75 MHz, DMSO-*d*$_6$) δ 160.73, 160.43, 156.39, 143.09, 139.34, 137.43, 134.08, 124.08, 120.68, 115.80, 114.24, 112.69, 106.87, 102.28, 56.00; HRMS (ESI) m/z calculated for $C_{18}H_{13}D_3N_3O_3$ $(M+H)^+$ 325.1374; found 325.1372; HPLC purity, 99.2%.

1.19.1.32. 7-Methoxy-*d*$_3$-2-(4-methoxyphenyl)-2,5-dihydro-3*H*-pyrazolo[4,3-*c*]quinolin-3-one (RV-I-029, 8c)

A mixture of ethyl-4-chloro-7-methoxy-*d*$_3$-quinoline-3-carboxylate **7b** (2 g, 7.4 mmol), 4-methoxyphenylhydrazine hydrochloride **4d** (1.56 g, 8.9 mmol), triethylamine (1.81g, 17.6 mmol) and xylenes (16 mL) was heated to reflux (138 ºC) and held at reflux for 2 h. The yellow-orange slurry, which resulted, was cooled to 100 ºC and diluted with EtOH (16 mL). The reaction mixture was heated at reflux at 80 ºC for 30 min and then allowed to cool to 20-25 ºC. The solids, which remained, were collected by filtration and washed with a 1:1 mixture of EtOH (2.5 mL x 2) and hexanes (2.5 mL x 2) and then washed with hexanes (5 mL x 2). The solid was dried under vacuum at 40 ºC to afford **8c** as a yellow powder (1.0 g, 41%)**:** ^{1}H NMR (300 MHz, DMSO-*d*$_6$) δ 12.59 (s, 1H), 8.65 (s, 1H), 8.10 (t, J = 8.7 Hz, 3H), 7.17 (d, J = 2.0 Hz, 2H), 7.01 (d, J = 8.9 Hz, 2H), 3.78 (s, 3H); ^{13}C NMR (75 MHz, DMSO-*d*$_6$) δ 161.45, 160.86, 156.22, 143.11, 139.32, 137.42, 134.11, 124.05, 120.68, 115.76, 114.25, 112.66, 106.87, 102.25, 55.68; HRMS (ESI) m/z calculated for $C_{18}H_{13}D_3N_3O_3$ $(M+H)^+$ 325.1374; found 325.1371; HPLC purity, 99.9%.

1.19.1.33. 7-Methoxy-*d*$_3$-2-(4-methoxy-*d*$_3$-phenyl)-2,5-dihydro-3*H*-pyrazolo[4,3-*c*]quinolin-3-one (DK-I-60-3, 8d)

A mixture of ethyl-4-chloro-7-methoxy-*d*$_3$-quinoline-3-carboxylate **7b** (2 g, 7.4 mmol), 4-methoxy-*d*$_3$-phenylhydrazine **4a** (1.26 g, 8.9 mmol), triethylamine (0.90g, 8.9 mmol) and xylenes (16 mL) was heated to reflux (138ºC) and held at reflux for 2 h. The yellow-orange slurry, which resulted, was cooled to 100 ºC and diluted with EtOH (16 mL). The reaction mixture was heated at reflux (80 ºC) for 30 min and then allowed to cool to 20-25 ºC. The solids, which

remained, were collected by filtration and washed with a 1:1 mixture of EtOH (2.5 mL x 2) and hexanes (2.5 mL x 2) and then washed with hexanes (5 mL x 2). The solid was dried under vacuum at 40 ºC to afford **8d** as a yellow powder (1.2 g, 50.0%)**:** ^{1}H NMR (300 MHz, DMSO-*d*$_6$) δ 12.57 (s, 1H), 8.65 (s, 1H), 8.10 (t, J = 9.0 Hz, 3H), 7.17 (d, J = 5.7 Hz, 2H), 7.01 (d, J = 9.0 Hz, 2H); ^{13}C NMR (75 MHz, DMSO-*d*$_6$) δ 161.45, 160.85, 156.21, 143.12, 139.37, 137.48, 134.10, 124.05, 120.69, 115.76, 114.24, 112.68, 106.86, 102.30; HRMS (ESI) m/z calculated for $C_{18}H_{10}D_6N_3O_3$ $(M+H)^+$ 328.1563; found 328.1549; HPLC purity, 98.5%.

1.19.1.34. 7-Methoxy-*d*$_3$-2-(3-methoxy-*d*$_3$-phenyl)-2,5-dihydro-3*H*-pyrazolo[4,3-*c*]quinolin-3-one (DK-I-94-1, 8e)

A mixture of ethyl-4-chloro-7-methoxy-*d*$_3$-quinoline-3-carboxylate **7b** (2 g, 7.4 mmol), 3-methoxy-*d*$_3$-phenylhydrazine **4b** (1.26 g, 8.9 mmol), triethylamine (0.90g, 8.9 mmol) and xylenes (16 mL) was heated to reflux (138 ºC) and held at reflux for 2 h. The yellow-orange slurry, which resulted, was cooled to 100 ºC and diluted with EtOH (16 mL). The reaction mixture was heated at reflux at 80 ºC for 30 min and then allowed to cool to 20-25 ºC. The solids, which remained, were collected by filtration and washed with a 1:1 mixture of EtOH (2.5 mL x 2) and hexanes (2.5 mL x 2) and then washed with hexanes (5 mL x 2). The solid was dried under vacuum at 40 ºC to afford **8e** as a yellow powder (1.5 g, 62.0%)**:** ^{1}H NMR (300 MHz, DMSO-*d*$_6$) δ 12.62 (s, 1H), 8.66 (s, 1H), 8.13 (d, J = 9.4 Hz, 1H), 7.93 – 7.73 (m, 2H), 7.34 (t, J = 8.2 Hz, 1H), 7.18 (d, J = 6.7 Hz, 2H), 6.74 (d, J = 8.2 Hz, 1H); ^{13}C NMR (75 MHz, DMSO-*d*$_6$) δ 162.13, 161.02, 159.97, 143.50, 141.73, 139.59, 137.58, 129.94, 124.18, 115.84, 112.56, 111.30, 109.60, 106.83, 104.81, 102.32; HRMS (ESI) m/z calculated for $C_{18}H_{10}D_6N_3O_3$ $(M+H)^+$ 328.1563; found 328.1545; HPLC purity, 99.9%.

1.19.1.35. 7-Methoxy-*d*$_3$-2-(2-methoxy-*d*$_3$-phenyl)-2,5-dihydro-3*H*-pyrazolo[4,3-*c*]quinolin-3-one (DK-I-90-1, 8f)

A mixture of ethyl-4-chloro-7-methoxy-*d*$_3$-quinoline-3-carboxylate **7b** (2 g, 7.4 mmol), 2-methoxy-*d*$_3$-phenylhydrazine **4c** (1.26 g, 8.9 mmol), triethylamine (0.90g, 8.9 mmol) and xylenes (16 mL) was heated to reflux (138 ºC) and held at reflux for 2 h. The yellow-orange slurry, which resulted, was cooled to 100 ºC and diluted with EtOH (16 mL). The reaction mixture was heated at reflux at 80ºC for 30 min and then allowed to cool to 20-25 ºC. The solids, which remained, were collected by filtration and washed with a 1:1 mixture of EtOH (2.5 mL x 2) and hexanes (2.5 mL x 2) and then washed with hexanes (5 mL x 2). The solid was dried under vacuum at 40 ºC to afford **(8f)** as a yellow powder (1.8 g, 75.0%)**:** ^{1}H NMR (300 MHz, DMSO-*d*$_6$) δ 12.47 (s, 1H), 8.57 (s, 1H), 7.99 (d, J = 8.7 Hz, 1H), 7.51 – 7.24 (m, 2H), 7.22 – 6.93 (m, 4H); ^{13}C NMR (75 MHz, DMSO-*d*$_6$) δ 162.19, 160.63, 155.66, 142.97, 139.04, 137.26, 129.88, 129.67, 128.51, 123.87, 120.65, 115.49, 112.96, 112.91, 105.83, 102.15; HRMS (ESI) m/z calculated for $C_{18}H_{10}D_6N_3O_3$ $(M+H)^+$ 328.1563; found 328.1552; HPLC purity, 99.9%.

1.19.1.36. 7-Methoxy-2-(3-methoxy-*d*$_3$-phenyl)-2,5-dihydro-3*H*-pyrazolo[4,3-*c*]quinolin-3-one (DK-II-69-1, 8g)

A mixture of ethyl-4-chloro-7-methoxy-quinoline-3-carboxylate **7e** (2 g, 7.5 mmol), 3-methoxy-*d*$_3$-phenylhydrazine **4b** (1.28 g, 9.0 mmol), triethylamine (0.91g, 9.0 mmol) and xylenes (16 mL) was heated to reflux (138 ºC) and held at reflux for 2 h. The yellow-orange slurry, which resulted, was cooled to 100 ºC and diluted with EtOH (16 mL). The reaction mixture was heated

at reflux at 80 ºC for 30 min and then allowed to cool to 20-25 ºC. The solids, which remained, were collected by filtration and washed with a 1:1 mixture of EtOH (2.5 mL x 2) and hexanes (2.5 mL x 2) and then washed with hexanes (5 mL x 2). The solid was dried under vacuum at 40 ºC to afford **(8g)** as a yellow powder (0.9 g, 37.0%)**:** ^{1}H NMR (300 MHz, DMSO-d_6) δ 12.61 (s, 1H), 8.66 (d, J = 2.9 Hz, 1H), 8.14 (dd, J = 9.4, 3.0 Hz, 1H), 7.97 – 7.69 (m, 2H), 7.34 (td, J = 8.2, 2.9 Hz, 1H), 7.18 (d, J = 1.3 Hz, 2H), 6.74 (d, J = 8.0 Hz, 1H), 3.89 (s, 3H); ^{13}C NMR (75 MHz, DMSO-d_6) δ 162.13, 161.03, 159.99, 143.51, 141.74, 139.58, 137.59, 129.94, 124.19, 115.84, 112.60, 111.31, 109.61, 106.84, 104.83, 102.36, 56.02; HRMS (ESI) m/z calculated for $C_{18}H_{13}D_3N_3O_3$ $(M+H)^+$ 325.1374; found 325.1365; HPLC purity, 98.8%.

1.19.1.37. 7-Methoxy-2-(2-methoxy-d_3-phenyl)-2,5-dihydro-3*H*-pyrazolo[4,3-*c*]quinolin-3-one (DK-I-88-1, 8h)

A mixture of ethyl-4-chloro-7-methoxy-quinoline-3-carboxylate **7e** (2 g, 7.5 mmol), 2-methoxy-d_3-phenylhydrazine **4c** (1.28 g, 9.0 mmol), triethylamine (0.91g, 9.0 mmol) and xylenes (16 mL) was heated to reflux (138 ºC) and held at reflux for 2 h. The yellow-orange slurry, which resulted, was cooled to 100 ºC and diluted with EtOH (16 mL). The reaction mixture was heated at reflux at 80 ºC for 30 min and then allowed to cool to 20-25 ºC. The solids, which remained, were collected by filtration and washed with a 1:1 mixture of EtOH (2.5 mL x 2) and hexanes (2.5 mL x 2) and then washed with hexanes (5 mL x 2). The solid was dried under vacuum at 40 ºC to afford **8h** as a yellow powder (1.6 g, 65.6%)**:** ^{1}H NMR (300 MHz, DMSO-d_6) δ 12.46 (d, J = 4.9 Hz, 1H), 8.57 (d, J = 5.8 Hz, 1H), 7.99 (d, J = 8.7 Hz, 1H), 7.40 (t, J = 7.8 Hz, 1H), 7.31 (d, J = 7.6 Hz, 1H), 7.15 (dd, J = 9.7, 6.0 Hz, 3H), 7.03 (t, J = 7.5 Hz, 1H), 3.87 (s, 3H); ^{13}C NMR (75 MHz, DMSO-d_6) δ 184.22, 162.19, 160.62, 155.66, 142.95, 139.04, 137.26, 129.88, 129.66,

128.51, 123.88, 120.65, 115.49, 112.97, 112.94, 105.83, 102.15, 55.94; HRMS (ESI) m/z calculated for $C_{18}H_{13}D_3N_3O_3$ $(M+H)^+$ 325.1374; found 325.1367; HPLC purity, 99.9%.

1.19.1.38. 8-Chloro-2-(3-methoxyphenyl)-2,5-dihydro-3*H*-pyrazolo[4,3-*c*]quinolin-3-one (LAU 159, 8i)

A mixture of ethyl-4,6-dichloro-quinoline-3-carboxylate **7c** (2 g, 7.4 mmol), 3-methoxyphenylhydrazine hydrochloride **4e** (1.55 g, 8.9 mmol), triethylamine (1.80g, 17.8 mmol) and xylenes (16 mL) was heated to reflux (138 ºC) and held at reflux for 2 h. The yellow-orange slurry, which resulted, was cooled to 100 ºC and diluted with EtOH (16 mL). The reaction mixture was heated at reflux at 80 ºC for 30 min and then allowed to cool to 20-25 ºC. The solids, which remained, were collected by filtration and washed with a 1:1 mixture of EtOH (2.5 mL x 2) and hexanes (2.5 mL x 2) and then washed with hexanes (5 mL x 2). The solid was dried under vacuum at 40 ºC to afford **8i** as a yellow powder (0.7 g, 30.0%)**:** ^{1}H NMR (300 MHz, DMSO-d_6) δ 12.85 (s, 1H), 8.69 (s, 1H), 8.15 (d, J = 1.9 Hz, 1H), 7.83 (d, J = 8.7 Hz, 2H), 7.70 (dt, J = 9.0, 5.4 Hz, 2H), 7.34 (t, J = 8.1 Hz, 1H), 6.83 – 6.65 (m, 1H), 3.81 (s, 3H); ^{13}C NMR (75 MHz, DMSO-d_6) δ 161.99, 159.98, 142.44, 141.52, 140.02, 134.81, 131.11, 130.62, 129.97, 122.17, 121.62, 120.42, 111.47, 110.04, 106.80, 104.96, 55.59; HRMS (ESI) m/z calculated for $C_{17}H_{13}ClN_3O_2$ $(M+H)^+$ 326.0691; found 326.0693; HPLC purity, 99.5%.

1.19.1.39. 8-Chloro-2-(3-methoxy-d_3-phenyl)-2,5-dihydro-3*H*-pyrazolo[4,3-*c*]quinolin-3-one (DK-I-59-1, 8j)

A mixture of ethyl-4,6-dichloro-quinoline-3-carboxylate **7c** (2 g, 7.4 mmol), 3-methoxy-d_3-phenylhydrazine hydrochloride **4b** (1.45 g, 8.1 mmol), triethylamine (1.87g, 18.5 mmol) and xylenes (16 mL) was heated to reflux (138 ºC) and held at reflux for 2 h. The yellow-orange slurry, which resulted, was cooled to 100 ºC and diluted with EtOH (16 mL). The reaction mixture was heated at reflux at 80 ºC for 30 min and then allowed to cool to 20-25 ºC. The solids, which remained, were collected by filtration and washed with a 1:1 mixture of EtOH (2.5 mL x 2) and hexanes (2.5 mL x 2) and then washed with hexanes (5 mL x 2). The solid was dried under vacuum at 40 ºC to afford **8j** as a yellow powder (2.0 g, 87.0%)**:** ^{1}H NMR (300 MHz, DMSO-d_6) δ 12.85 (s, 1H), 8.71 (s, 1H), 8.17 (s, 1H), 8.00 – 7.49 (m, 4H), 7.35 (t, J = 7.7 Hz, 1H), 6.77 (d, J = 7.4 Hz, 1H); ^{13}C NMR (75 MHz, DMSO-d_6) δ 162.01, 160.01, 142.48, 141.54, 140.10, 134.76, 131.15, 130.72, 130.01, 122.14, 121.68, 120.45, 111.42, 110.04, 106.87, 104.95; HRMS (ESI) m/z calculated for $C_{17}H_{10}D_3ClN_3O_2$ $(M+H)^+$ 329.0879; found 329.0854; HPLC purity, 98.9%.

1.19.1.40. 8-Chloro-2-(4-methoxyphenyl)-2,5-dihydro-3*H*-pyrazolo[4,3-*c*]quinolin-3-one (PZ-II-028, 8k)

A mixture of ethyl-4,6-dichloro-quinoline-3-carboxylate **7c** (2 g, 7.4 mmol), 4-methoxyphenylhydrazine hydrochloride **4d** (1.55 g, 8.9 mmol), triethylamine (1.80g, 17.8 mmol) and xylenes (16 mL) was heated to reflux (138 ºC) and held at reflux for 2 h. The yellow-orange slurry, which resulted, was cooled to 100 ºC and diluted with EtOH (16 mL). The reaction mixture was heated at reflux at 80ºC for 30 min and then allowed to cool to 20-25 ºC.

The solids, which remained, were collected by filtration and washed with a 1:1 mixture of EtOH (2.5 mL x 2) and hexanes (2.5 mL x 2) and then washed with hexanes (5 mL x 2). The solid was dried under vacuum at 40 ºC to afford **8k** as a yellow powder (1.7 g, 71.0%)**:** ^{1}H NMR (300 MHz, DMSO-d_6) δ 12.95 (d, J = 5.6 Hz, 1H), 8.72 (d, J = 6.2 Hz, 1H), 8.14 (d, J = 2.1 Hz, 1H), 8.08 (d, J = 9.0 Hz, 2H), 7.70 (dt, J = 8.9, 5.5 Hz, 2H), 7.02 (d, J = 9.1 Hz, 2H), 3.79 (s, 3H); ^{13}C NMR (75 MHz, DMSO-d_6) δ 161.37, 156.48, 141.97, 139.79, 134.59, 133.87, 131.04, 130.46, 122.08, 121.50, 120.89, 120.48, 114.29, 106.86, 55.71; HRMS (ESI) m/z calculated for $C_{17}H_{13}ClN_3O_2$ $(M+H)^+$ 326.0691; found 326.0682; HPLC purity, 98.6%.

1.19.1.41. 8-Chloro-2-(4-methoxy-*d*$_3$-phenyl)-2,5-dihydro-3*H*-pyrazolo[4,3-*c*]quinolin-3-one (DK-I-93-1, 8l)

A mixture of ethyl-4,6-dichloro-quinoline-3-carboxylate **7c** (2 g, 7.4 mmol), 4-methoxy-d_3-phenylhydrazine **4a** (1.25 g, 8.9 mmol), triethylamine (0.90g, 8.9 mmol) and xylenes (16 mL) was heated to reflux (138 ºC) and held at reflux for 2 h. The yellow-orange slurry, which resulted, was cooled to 100 ºC and diluted with EtOH (16 mL). The reaction mixture was heated at reflux at 80 ºC for 30 min and then allowed to cool to 20-25 ºC. The solids, which remained, were collected by filtration and washed with a 1:1 mixture of EtOH (2.5 mL x 2) and hexanes (2.5 mL x 2) and then washed with hexanes (5 mL x 2). The solids were dried under vacuum at 40 ºC to afford **8i** as a yellow powder (1.3 g, 53.6%)**:** ^{1}H NMR (300 MHz, DMSO-d_6) δ 12.89 (s, 1H), 8.74 (s, 1H), 8.24 – 7.89 (m, 3H), 7.86 – 7.56 (m, 2H), 7.02 (d, J = 8.9 Hz, 2H); ^{13}C NMR (75 MHz, DMSO-d_6) δ 161.38, 156.49, 141.98, 139.86, 134.59, 133.84, 131.05, 130.49, 122.09, 121.52, 120.91, 120.49, 114.29, 106.88; HRMS (ESI) m/z calculated for $C_{17}H_{10}D_3ClN_3O_2$ $(M+H)^+$ 329.0879; found 329.0855; HPLC purity, 99.5%.

1.19.1.42. 8-Chloro-2-(2-methoxy-d_3-phenyl)-2,5-dihydro-3*H*-pyrazolo[4,3-*c*]quinolin-3-one (DK-I-87-1, 8m)

A mixture of ethyl-4,6-dichloro-quinoline-3-carboxylate **7c** (2 g, 7.4 mmol), 2-methoxy-d_3-phenylhydrazine **4c** (1.25 g, 8.9 mmol), triethylamine (0.9g, 8.9 mmol) and xylenes (16 mL) was heated to reflux (138 ºC) and held at reflux for 2 h. The yellow-orange slurry, which resulted, was cooled to 100 ºC and diluted with EtOH (16 mL). The reaction mixture was heated at reflux at 80 ºC for 30 min and then allowed to cool to 20-25 ºC. The solids, which remained, were collected by filtration and washed with a 1:1 mixture of EtOH (2.5 mL x 2) and hexanes (2.5 mL x 2) and then washed with hexanes (5 mL x 2). The solid was dried under vacuum at 40 ºC to afford **8m** as a yellow powder (1.0 g, 41.0%)**:** ^{1}H NMR (300 MHz, DMSO-d_6) δ 12.74 (s, 1H), 8.66 (s, 1H), 8.03 (s, 1H), 7.69 (p, J = 9.0 Hz, 2H), 7.42 (t, J = 7.8 Hz, 1H), 7.32 (d, J = 7.6 Hz, 1H), 7.17 (d, J = 8.3 Hz, 1H), 7.05 (t, J = 7.5 Hz, 1H); ^{13}C NMR (75 MHz, DMSO-d_6) δ 162.15, 155.64, 141.87, 139.59, 134.48, 130.83, 130.23, 129.91, 129.85, 128.22, 121.91, 121.40, 120.76, 120.68, 113.00, 105.81; HRMS (ESI) m/z calculated for $C_{17}H_{10}D_3ClN_3O_2$ $(M+H)^+$ 329.0879; found 329.0858; HPLC purity, 99.9%.

1.19.1.43. 7-Bromo-2-(4-methoxyphenyl)-2,5-dihydro-3*H*-pyrazolo[4,3-*c*]quinolin-3-one (LAU463, 8n)

A mixture of ethyl-7-bromo-4-chloro-quinoline-3-carboxylate **7d** (2 g, 6.3 mmol), 4-methoxyphenylhydrazine hydrochloride **4d** (1.33 g, 7.6 mmol), triethylamine (1.54g, 15.3 mmol) and xylenes (16 mL) was heated to reflux (138 ºC) and held at reflux for 2 h. The yellow-orange

slurry, which resulted, was cooled to 100 ºC and diluted with EtOH (16 mL). The reaction mixture was heated at reflux at 80 ºC for 30 min and then allowed to cool to 20-25 ºC. The solids, which remained, were collected by filtration and washed with a 1:1 mixture of EtOH (2.5 mL x 2) and hexanes (2.5 mL x 2) and then washed with hexanes (5 mL x 2). The solid was dried under vacuum at 40 ºC to afford **8n** as a yellow powder (1.4 g, 60.0%)**:** ^{1}H NMR (300 MHz, DMSO-d_6) δ 12.75 (s, 1H), 8.74 (s, 1H), 8.09 (dd, J = 17.7, 8.8 Hz, 3H), 7.89 (d, J = 1.6 Hz, 1H), 7.68 (dd, J = 8.6, 1.6 Hz, 1H), 7.02 (d, J = 9.1 Hz, 2H), 3.79 (s, 3H); ^{13}C NMR (75 MHz, DMSO-d_6) δ 161.37, 156.47, 142.38, 140.08, 136.98, 133.85, 129.65, 124.51, 122.95, 122.22, 120.87, 118.22, 114.31, 107.21, 55.71; HRMS (ESI) m/z calculated for $C_{17}H_{13}BrN_3O_2$ $(M+H)^+$ 370.0186; found 370.0176; HPLC purity, 99.0%.

1.19.1.44. 7-Bromo-2-(4-methoxy-d_3-phenyl)-2,5-dihydro-3*H*-pyrazolo[4,3-*c*]quinolin-3-one (DK-I-58-1, 8o)

A mixture of ethyl-7-bromo-4-chloro-quinoline-3-carboxylate **7d** (2 g, 6.3 mmol), 4-methoxy-d_3-phenylhydrazine **4a** (1.08 g, 7.6 mmol), triethylamine (0.77g, 7.6 mmol) and xylenes (16 mL) was heated to reflux (138 ºC) and held at reflux for 2 h. The yellow-orange slurry, which resulted, was cooled to 100 ºC and diluted with EtOH (16 mL). The reaction mixture was heated at reflux at 80 ºC for 30 min and then allowed to cool to 20-25 ºC. The solids, which remained, were collected by filtration and washed with a 1:1 mixture of EtOH (2.5 mL x 2) and hexanes (2.5 mL x 2) and then washed with hexanes (5 mL x 2). The solid was dried under vacuum at 40 ºC to afford **8o** as a yellow powder (1.0 g, 42.0%)**:** ^{1}H NMR (300 MHz, DMSO-d_6) δ 12.75 (s, 1H), 8.74 (d, J = 4.9 Hz, 1H), 8.09 (dd, J = 17.8, 8.7 Hz, 3H), 7.88 (s, 1H), 7.69 (d, J = 8.4 Hz, 1H), 7.01 (d, J = 8.8 Hz, 2H); ^{13}C NMR (75 MHz, DMSO-d_6) δ 161.35, 156.49, 141.88, 140.06,

136.95, 133.83, 129.65, 124.51, 122.93, 122.18, 120.86, 118.22, 114.24, 107.22; HRMS (ESI) m/z calculated for $C_{17}H_{10}D_3BrN_3O_2$ $(M+H)^+$ 373.0374; found 373.0359; HPLC purity, 99.8%.

1.19.1.45. 7-Bromo-2-(3-methoxy-*d*$_3$-phenyl)-2,5-dihydro-3*H*-pyrazolo[4,3-*c*]quinolin-3-one (DK-I-92-1, 8p)

A mixture of ethyl-7-bromo-4-chloro-quinoline-3-carboxylate **7d** (1.5 g, 4.8 mmol), 3-methoxy-*d*$_3$-phenylhydrazine **4b** (0.81 g, 5.7 mmol), triethylamine (0.58g, 5.7 mmol) and xylenes (12 mL) was heated to reflux (138 ^oC) and held at reflux for 2 h. The yellow-orange slurry, which resulted, was cooled to 100 ^oC and diluted with EtOH (12 mL). The reaction mixture was heated at reflux at 80 ^oC for 30 min and then allowed to cool to 20-25 ^oC. The solids, which remained, were collected by filtration and washed with a 1:1 mixture of EtOH (2.5 mL x 2) and hexanes (2.5 mL x 2) and then washed with hexanes (5 mL x 2). The solid was dried under vacuum at 40 ^oC to afford **8p** as a yellow powder (0.7 g, 40.0%)**:** ^1H NMR (300 MHz, DMSO-*d*$_6$) δ 12.78 (s, 1H), 8.76 (s, 1H), 8.15 (d, J = 8.5 Hz, 1H), 7.95 – 7.76 (m, 3H), 7.71 (d, J = 8.6 Hz, 1H), 7.35 (t, J = 8.2 Hz, 1H), 6.76 (d, J = 8.3 Hz, 1H); ^{13}C NMR (75 MHz, DMSO-*d*$_6$) δ 162.00, 160.00, 142.81, 141.51, 140.33, 137.11, 130.03, 129.75, 124.65, 123.22, 122.26, 118.16, 111.39, 109.98, 107.20, 104.92; HRMS (ESI) m/z calculated for $C_{17}H_{10}D_3BrN_3O_2$ $(M+H)^+$ 373.0374; found 373.0366; HPLC purity, 99.7%.

1.19.1.46. 7-Bromo-2-(2-methoxy-*d*$_3$-phenyl)-2,5-dihydro-3*H*-pyrazolo[4,3-*c*]quinolin-3-one (DK-I-89-1, 8q)

A mixture of ethyl-7-bromo-4-chloro-quinoline-3-carboxylate **7d** (2 g, 6.3 mmol), 2-methoxy-*d*$_3$-phenylhydrazine **4c** (1.08 g, 7.6 mmol), triethylamine (0.77g, 7.6 mmol) and xylenes (16 mL)

was heated to reflux (138 ºC) and held at reflux for 2 h. The yellow-orange slurry, which resulted, was cooled to 100 ºC and diluted with EtOH (16 mL). The reaction mixture was heated at reflux at 80 ºC for 30 min and then allowed to cool to 20-25 ºC. The solids, which remained, were collected by filtration and washed with a 1:1 mixture of EtOH (2.5 mL x 2) and hexanes (2.5 mL x 2) and then washed with hexanes (5 mL x 2). The solid was dried under vacuum at 40 ºC to afford **8q** as a yellow powder (1.2 g, 50.6%)**:** ^{1}H NMR (300 MHz, DMSO-*d*$_6$) δ 12.60 (s, 1H), 8.64 (d, J = 16.3 Hz, 1H), 8.00 (d, J = 8.5 Hz, 1H), 7.86 (s, 1H), 7.64 (d, J = 8.5 Hz, 1H), 7.41 (t, J = 7.8 Hz, 1H), 7.32 (d, J = 7.7 Hz, 1H), 7.17 (d, J = 8.3 Hz, 1H), 7.04 (t, J = 7.5 Hz, 1H); ^{13}C NMR (75 MHz, DMSO-*d*$_6$) δ 162.14, 158.75, 155.64, 142.23, 139.79, 136.89, 129.84, 129.45, 128.23, 124.36, 122.64, 122.04, 120.69, 118.50, 112.99, 106.18; HRMS (ESI) m/z calculated for $C_{17}H_{10}D_3BrN_3O_2$ $(M+H)^+$ 373.0374; found 373.0386; HPLC purity, 99.9%.

1.19.1.47. 8-Methoxy-*d*$_3$-2-(4-methoxy-*d*$_3$-phenyl)-2,5-dihydro-3*H*-pyrazolo[4,3-*c*]quinolin-3-one (DK-I-95-3, 8r)

A mixture of ethyl-4-chloro-6-methoxy-*d*$_3$-quinoline-3-carboxylate **7a** (2 g, 7.4 mmol), 4-methoxy-*d*$_3$-phenylhydrazine **4a** (1.26 g, 8.9 mmol), triethylamine (0.90g, 8.9 mmol) and xylenes (16 mL) was heated to reflux (138 ºC) and held at reflux for 2 h. The yellow-orange slurry, which resulted, was cooled to 100 ºC and diluted with EtOH (16 mL). The reaction mixture was heated at reflux at 80 ºC for 30 min and then allowed to cool to 20-25 ºC. The solids, which remained, were collected by filtration and washed with a 1:1 mixture of EtOH (2.5 mL x 2) and hexanes (2.5 mL x 2) and then washed with hexanes (5 mL x 2). The solid was dried under vacuum at 40 ºC to afford **8r** as a yellow powder (0.9 g, 37.0%)**:** ^{1}H NMR (300 MHz, DMSO-*d*$_6$) δ 12.77 (s, 1H), 8.64 (s, 1H), 8.11 (d, J = 8.8 Hz, 2H), 7.68 (d, J = 9.1 Hz, 1H), 7.57 (s, 1H),

7.28 (d, J = 9.1 Hz, 1H), 7.02 (d, J = 8.8 Hz, 2H); ^{13}C NMR (75 MHz, DMSO-*d*$_6$) δ 161.59, 157.98, 156.34, 143.00, 138.11, 134.10, 130.13, 121.70, 120.92, 120.50, 119.95, 114.23, 105.70, 102.96; HRMS (ESI) m/z calculated for $C_{18}H_{10}D_6N_3O_3$ $(M+H)^+$ 328.1563; found 328.1562; HPLC purity, 99.9%.

1.19.1.48. 8-Methoxy-*d*$_3$-2-(3-methoxy-*d*$_3$-phenyl)-2,5-dihydro-3*H*-pyrazolo[4,3-*c*]quinolin-3-one (DK-I-92-1, 8s)

A mixture of ethyl-4-chloro-6-methoxy-*d*$_3$-quinoline-3-carboxylate **7a** (2 g, 7.4 mmol), 3-methoxy-*d*$_3$-phenylhydrazine **4b** (1.26 g, 8.9 mmol), triethylamine (0.90g, 8.9 mmol) and xylenes (16 mL) was heated to reflux (138 ºC) and held at reflux for 2 h. The yellow-orange slurry, which resulted, was cooled to 100 ºC and diluted with EtOH (16 mL). The reaction mixture was heated at reflux at 80 ºC for 30 min and then allowed to cool to 20-25 ºC. The solids, which remained, were collected by filtration and washed with a 1:1 mixture of EtOH (2.5 mL x 2) and hexanes (2.5 mL x 2) and then washed with hexanes (5 mL x 2). The solid was dried under vacuum at 40 ºC to afford **8s** as a yellow powder (1.8 g, 74.0%)**:** ^{1}H NMR (300 MHz, DMSO-*d*$_6$) δ 12.80 (s, 1H), 8.65 (s, 1H), 7.99 – 7.80 (m, 2H), 7.67 (d, J = 9.1 Hz, 1H), 7.59 (s, 1H), 7.41 – 7.21 (m, 2H), 6.76 (d, J = 8.2 Hz, 1H); ^{13}C NMR (75 MHz, DMSO-*d*$_6$) δ 162.25, 159.98, 158.04, 143.42, 141.76, 138.36, 130.26, 129.94, 121.73, 120.45, 120.10, 111.53, 109.64, 105.70, 105.11, 103.16; HRMS (ESI) m/z calculated for $C_{18}H_{10}D_6N_3O_3$ $(M+H)^+$ 328.1563; found 328.1550; HPLC purity, 99.9%.

1.19.1.49. 8-Methoxy-*d*$_3$-2-(2-methoxy-*d*$_3$-phenyl)-2,5-dihydro-3*H*-pyrazolo[4,3-*c*]quinolin-3-one (DK-I-98-1, 8t)

A mixture of ethyl-4-chloro-6-methoxy-*d*$_3$-quinoline-3-carboxylate **7a** (2 g, 7.4 mmol), 2-methoxy-*d*$_3$-phenylhydrazine **4c** (1.26 g, 8.9 mmol), triethylamine (0.90g, 8.9 mmol) and xylenes (16 mL) was heated to reflux (138 ºC) and held at reflux for 2 h. The yellow-orange slurry, which resulted, was cooled to 100 ºC and diluted with EtOH (16 mL). The reaction mixture was heated at reflux at 80 ºC for 30 min and then allowed to cool to 20-25 ºC. The solids, which remained, were collected by filtration and washed with a 1:1 mixture of EtOH (2.5 mL x 2) and hexanes (2.5 mL x 2) and then washed with hexanes (5 mL x 2). The solid was dried under vacuum at 40 ºC to afford **8t** as a yellow powder (0.5 g, 20.0%)**:** ^{1}H NMR (300 MHz, DMSO-*d*$_6$) δ 12.65 (s, 1H), 8.57 (s, 1H), 7.65 (d, J = 9.1 Hz, 1H), 7.54 – 7.28 (m, 3H), 7.28 – 7.21 (m, 1H), 7.16 (d, J = 8.3 Hz, 1H), 7.05 (t, J = 7.5 Hz, 1H); ^{13}C NMR (75 MHz, DMSO-*d*$_6$) δ 162.38, 157.83, 155.76, 142.92, 137.98, 130.05, 129.94, 129.83, 128.54, 121.50, 120.75, 120.65, 119.64, 112.91, 104.61, 102.88; HRMS (ESI) m/z calculated for $C_{18}H_{10}D_6N_3O_3$ $(M+H)^+$ 328.1563; found 328.1546; HPLC purity, 99.9%.

1.19.1.50. 2-Methoxy-*d*$_3$-5-nitropyridine (10)

To a mixture of potassium t-butoxide (13.3 g, 111.8 mmol) and methanol-*d*$_4$ (50 mL) was slowly added 2-chloro-5-nitropyridine **9** (15.0 g, 94.6 mmol). The exothermic reaction warmed up to 50 ºC and then was heated at reflux at 65ºC for 2 h to complete the reaction. The reaction mixture was then cooled to 20-25 ºC and poured into H_2O (750 mL). After stirring the mixture for 1 h the solid, which formed, was filtered and washed with H_2O (25 mL x 2). The solid was dried under vacuum at 40 ºC to afford **10** as a light yellow powder (13.0g, 87%). ^{1}H NMR (300 MHz,

DMSO-d_6) δ 9.08 (s, 1H), 8.47 (d, J = 9.1 Hz, 1H), 7.03 (d, J = 9.1 Hz, 1H); ^{13}C NMR (75 MHz, DMSO-d_6) δ 167.45, 145.02, 139.99, 135.01, 111.67; HRMS (ESI) m/z calculated for $C_6H_4D_3N_2O_3$ $(M+H)^+$ 158.0639; found 158.0634.

1.19.1.51. 5-Amino-2-methoxy-d_3-pyridine (11a)

A mixture of 2-methoxy-d_3-5-nitropyridine **10** (13.0 g, 82.7 mmol), iron powder (15.9 g, 284.7 mmol), H_2O (5 mL) and EtOH (50 mL) was heated to reflux (78 °C). Once at reflux, concentrated aqueous hydrochloric acid (1 mL, 83.3 mmol) was added dropwise. The reaction mixture was heated at reflux for 4 h to complete the reaction. Upon cooling to 20-25 °C, the mixture was filtered to remove the iron and the solids were washed 3 times with EtOH (25 mL x 3). Sodium bicarbonate (5.0 g) was added to the filtrate and the EtOH was removed under reduced pressure. Then, H_2O (50 mL) and DCM (50 mL) were added to dissolve the residue. The layers were separated and the aq layer was extracted with DCM (50 mL x 2). The combined organic layers were dried ($MgSO_4$). The solvents were then removed under reduced pressure to afford **11a** as a clear orange-red oil (10.0 g, 95.1%)**:** ^{1}H NMR (300 MHz, DMSO-d_6) δ 7.57 (d, J = 2.7 Hz, 1H), 7.05 (dd, J = 8.6, 2.9 Hz, 1H), 6.56 (d, J = 8.7 Hz, 1H), 4.74 (s, 2H); ^{13}C NMR (75 MHz, DMSO-d_6) δ 156.29, 139.77, 131.63, 126.85, 110.42; HRMS (ESI) m/z calculated for $C_6H_6D_3N_2O$ $(M+H)^+$ 128.0898; found 128.0910. This material was employed in the next experiment with no further purification.

1.19.1.52. 5-Hydrazinyl-2-methoxy-d_3-pyridine (12a)

A mixture of 5-amino-2-methoxy-d_3-pyridine **11a** (10 g, 78.6 mmol), concentrated hydrochloric acid (24 mL), and H_2O (24 mL) was cooled to 0 to 5ºC and an aqueous solution of sodium nitrite (5.7 g, 82.5 mmol) in H_2O (12 mL) was slowly added drop-wise to the reaction mixture. Upon completion of the addition, the reaction mixture was allowed to stir for an additional 15 min at 0 to 5 ºC. The reaction mixture was then cooled to -25 to -20 ºC and a solution of tin (II) chloride (32.8 g, 173.0 mmol) in concentrated hydrochloric acid (70 mL) was added dropwise to the reaction mixture over 30 min. Upon completion of the addition, the reaction mixture was allowed to stir for an additional 2 h at -25 to -20 ºC. The reaction mixture was then diluted with DCM (100 mL). A solution of potassium hydroxide (100 g) in H_2O (200 mL) was added dropwise to the reaction mixture at 0 to 5 ºC over 30 min. After stirring for 1 h at 0 to 5 ºC, the solids completely dissolved. The layers were separated and the aq layer was extracted with DCM (50mL x 4). The combined organic layers were dried ($MgSO_4$). The solvents were then removed under reduced pressure and the residue was slurried with hexanes (20 mL). The slurry was placed in a freezer at -20 ºC for 24 h to fully precipitate the product. The solid was then filtered off and washed with hexanes (10 mL x 2). The solid was dried under vacuum at rt to afford **12a** as a pale yellow-brown solid (6.4 g, 57%)**:** ^{1}H NMR (300 MHz, DMSO-d_6) δ 7.70 (d, J = 2.8 Hz, 1H), 7.31 – 7.19 (m, 1H), 6.61 (d, J = 8.8 Hz, 1H), 6.42 (s, 1H), 4.00 (s, 2H); ^{13}C NMR (75 MHz, DMSO-d_6) δ 157.01, 144.07, 129.87, 125.27, 110.22; HRMS (ESI) m/z calculated for $C_6H_7D_3N_3O$ $(M+H)^+$ 143.1007; found 143.1005.

1.19.1.53. 5-Hydrazinyl-2-methoxypyridine (12b)

A mixture of 5-amino-2-methoxypyridine **11b** (10 g, 80.6 mmol), concentrated hydrochloric acid (24 mL), and H_2O (24 mL) was cooled to 0 to 5 ºC and an aqueous solution of sodium nitrite (5.8 g, 84.6 mmol) in H_2O (12 mL) was slowly added drop-wise to the reaction mixture. Upon completion of the addition, the reaction mixture was allowed to stir for an additional 15 min at 0 to 5 ºC. The reaction mixture was then cooled to -25 to -20 ºC and a solution of tin (II) chloride (33.6 g, 177.2 mmol) in concentrated hydrochloric acid (70 mL) was added dropwise to the reaction mixture over 30 min. Upon completion of the addition, the reaction mixture was allowed to stir for an additional 2 h at -25 to -20 ºC. The reaction mixture was then diluted with DCM (100 mL). A solution of potassium hydroxide (100 g) in H_2O (200 mL) was added dropwise to the reaction mixture at 0 to 5 ºC over 30 min. After stirring for 1 h at 0 to 5 ºC, the solids completely dissolved. The layers were separated and the aq layer was extracted with DCM (50mL x 4). The combined organic layers were dried ($MgSO_4$). The solvents were then removed under reduced pressure and the residue was slurried with hexanes (20 mL). The slurry was placed in a freezer at -20 ºC for 24 h to fully precipitate the product. The solid was then filtered off and washed with hexanes (10 mL x 2). The solid was dried under vacuum at rt to afford **12b** as a pale yellow-brown solid (7.8 g, 70%)**:** ^{1}H NMR (300 MHz, DMSO-*d*$_6$) δ 7.70 (s, 1H), 7.20 (d, *J* = 8.7 Hz, 1H), 6.61 (d, *J* = 8.8 Hz, 1H), 6.41 (s, 1H), 3.97 (s, 2H), 3.73 (s, 3H); ^{13}C NMR (75 MHz, DMSO-*d*$_6$) δ 156.98, 144.09, 129.85, 125.25, 110.22, 53.19; HRMS (ESI) m/z calculated for $C_6H_{10}N_3O$ $(M+H)^+$ 140.0818; found 140.0814.

1.19.1.54. 7-Methoxy-2-(6-methoxypyridin-3-yl)-2,5-dihydro-3*H*-pyrazolo[4,3-*c*]quinolin-3-one (DK-II-13-1, 13a)

A mixture of ethyl-4-chloro-7-methoxy-quinoline-3-carboxylate **7e** (2 g, 7.5 mmol), 5-hydrazinyl-2-methoxypyridine **12b** (1.26 g, 9.0 mmol), triethylamine (0.91g, 9.0 mmol) and xylenes (16 mL) was heated to reflux (138 ºC) and held at reflux for 2 h. The yellow-orange slurry, which resulted, was cooled to 100 ºC and diluted with EtOH (16 mL). The reaction mixture was heated at reflux at 80 ºC for 30 min and then allowed to cool to 20-25 ºC. The solids, which remained, were collected by filtration and washed with a 1:1 mixture of EtOH (2.5 mL x 2) and hexanes (2.5 mL x 2) and then washed with hexanes (5 mL x 2). The solid was dried under vacuum at 40 ºC to afford **13a** as a yellow powder (1.2 g, 49.0%)**:** ^{1}H NMR (300 MHz, DMSO-d_6) δ 12.65 (s, 1H), 8.92 (d, J = 2.4 Hz, 1H), 8.68 (s, 1H), 8.43 (dd, J = 9.0, 2.6 Hz, 1H), 8.24 – 7.91 (m, 1H), 7.29 – 7.02 (m, 2H), 6.92 (d, J = 9.0 Hz, 1H), 3.88 (s, 6H); ^{13}C NMR (75 MHz, DMSO-d_6) δ 161.74, 160.98, 160.43, 143.86, 139.71, 137.45, 137.37, 131.88, 130.77, 124.13, 115.94, 112.59, 110.56, 106.22, 102.30, 56.00, 53.71; HRMS (ESI) m/z calculated for $C_{17}H_{15}N_4O_3$ $(M+H)^+$ 323.1139; found 323.1133; HPLC purity, 99.8%.

1.19.1.55. 7-Methoxy-2-(6-methoxy-d_3-pyridin-3-yl)-2,5-dihydro-3*H*-pyrazolo[4,3-*c*]quinolin-3-one (DK-II-60-1, 13b)

A mixture of ethyl-4-chloro-7-methoxy-quinoline-3-carboxylate **7e** (2 g, 7.5 mmol), 5-hydrazinyl-2-methoxy-d_3-pyridine **12a** (1.28 g, 9.0 mmol), triethylamine (0.91 g, 9.0 mmol) and xylenes (16 mL) was heated to reflux (138 ºC) and held at reflux for 2 h. The yellow-orange slurry, which resulted, was cooled to 100 ºC and diluted with EtOH (16 mL). The reaction mixture was heated at reflux at 80 ºC for 30 min and then allowed to cool to 20-25 ºC. The

solids, which remained, were collected by filtration and washed with a 1:1 mixture of EtOH (2.5 mL x 2) and hexanes (2.5 mL x 2) and then washed with hexanes (5 mL x 2). The solid was dried under vacuum at 40 ºC to afford **13b** as a yellow powder (1.2 g, 49.0%)**:** ^{1}H NMR (300 MHz, DMSO-*d*$_6$) δ 12.68 (s, 1H), 8.91 (d, J = 2.1 Hz, 1H), 8.68 (s, 1H), 8.42 (dd, J = 9.0, 2.4 Hz, 1H), 8.16 – 8.03 (m, 1H), 7.18 (d, J = 5.9 Hz, 2H), 6.92 (d, J = 9.0 Hz, 1H), 3.87 (s, 3H); ^{13}C NMR (75 MHz, DMSO-*d*$_6$) δ 161.74, 160.98, 160.44, 143.85, 139.69, 137.44, 137.39, 131.86, 130.77, 124.13, 115.94, 112.58, 110.54, 106.22, 102.29, 56.00; HRMS (ESI) m/z calculated for $C_{17}H_{12}D_3N_4O_3$ $(M+H)^+$ 326.1327; found 326.1316; HPLC purity, 99.9%.

1.19.1.56. 7-Methoxy-*d*$_3$-2-(6-methoxypyridin-3-yl)-2,5-dihydro-3*H*-pyrazolo[4,3-*c*]quinolin-3-one (DK-I-86-1, 13c)

A mixture of ethyl-4-chloro-7-methoxy-*d*$_3$-quinoline-3-carboxylate **7b** (2 g, 7.4 mmol), 5-hydrazinyl-2-methoxypyridine **12b** (1.24 g, 8.9 mmol), triethylamine (0.90 g, 8.9 mmol) and xylenes (16 mL) was heated to reflux (138 ºC) and held at reflux for 2 h. The yellow-orange slurry, which resulted, was cooled to 100 ºC and diluted with EtOH (16 mL). The reaction mixture was heated at reflux at 80 ºC for 30 min and then allowed to cool to 20-25 ºC. The solids, which remained, were collected by filtration and washed with a 1:1 mixture of EtOH (2.5 mL x 2) and hexanes (2.5 mL x 2) and then washed with hexanes (5 mL x 2). The solid was dried under vacuum at 40 ºC to afford **13c** as a yellow powder (1.0 g, 41.0%)**:** ^{1}H NMR (300 MHz, DMSO-*d*$_6$) δ 12.69 (s, 1H), 8.92 (s, 1H), 8.69 (s, 1H), 8.43 (d, J = 9.0 Hz, 1H), 8.12 (d, J = 9.4 Hz, 1H), 7.18 (s, 2H), 6.92 (d, J = 9.0 Hz, 1H), 3.88 (s, 3H); ^{13}C NMR (75 MHz, DMSO-*d*$_6$) δ 161.75, 161.01, 160.44, 143.88, 139.73, 137.46, 137.39, 131.88, 130.79, 124.15, 115.96,

112.57, 110.58, 106.22, 102.31, 53.72; HRMS (ESI) m/z calculated for $C_{17}H_{12}D_3N_4O_3$ $(M+H)^+$ 326.1327; found 326.1324; HPLC purity, 99.9%.

1.19.1.57. 7-Methoxy-*d*$_3$-2-(6-methoxy-*d*$_3$-pyridin-3-yl)-2,5-dihydro-3*H*-pyrazolo[4,3-*c*]quinolin-3-one (DK-III-6-1, 13d)

A mixture of ethyl-4-chloro-7-methoxy-*d*$_3$-quinoline-3-carboxylate **7b** (2 g, 7.4 mmol), 5-hydrazinyl-2-methoxy-*d*$_3$-pyridine **12a** (1.27 g, 8.9 mmol), triethylamine (0.90 g, 8.9 mmol) and xylenes (16 mL) was heated to reflux (138 ºC) and held at reflux for 2 h. The yellow-orange slurry, which resulted, was cooled to 100 ºC and diluted with EtOH (16 mL). The reaction mixture was heated at reflux at 80 ºC for 30 min and then allowed to cool to 20-25 ºC. The solids, which remained, were collected by filtration and washed with a 1:1 mixture of EtOH (2.5 mL x 2) and hexanes (2.5 mL x 2) and then washed with hexanes (5 mL x 2). The solid was dried under vacuum at 40 ºC to afford **13d** as a yellow powder (1.7 g, 69.7%)**:** ^{1}H NMR (500 MHz, DMSO-*d*$_6$) δ 12.70 (s, 1H), 8.92 (d, *J* = 2.3 Hz, 1H), 8.69 (s, 1H), 8.43 (dd, *J* = 8.9, 2.4 Hz, 1H), 8.12 (d, *J* = 9.4 Hz, 1H), 7.19 (d, *J* = 7.4 Hz, 2H), 6.93 (d, *J* = 8.9 Hz, 1H).; ^{13}C NMR (126 MHz, DMSO-*d*$_6$) δ 161.75, 160.99, 160.45, 143.87, 139.71, 137.45, 137.39, 131.87, 130.79, 124.15, 115.96, 112.57, 110.57, 106.23, 102.28.; HRMS (ESI) m/z calculated for $C_{17}H_9D_6N_4O_3$ $(M+H)^+$ 329.1515; found 329.1507; HPLC purity, 99.9%.

1.19.1.58. 8-Chloro-2-(6-methoxypyridin-3-yl)-2,5-dihydro-3*H*-pyrazolo[4,3-*c*]quinolin-3-one (DK-II-18-1, 13e)

A mixture of ethyl-4,6-dichloroquinoline-3-carboxylate **7c** (2 g, 7.4 mmol), 5-hydrazinyl-2-methoxypyridine **12b** (1.24 g, 8.9 mmol), triethylamine (0.90 g, 8.9 mmol) and xylenes (16 mL) was heated to reflux (138 ºC) and held at reflux for 2 h. The yellow-orange slurry, which resulted, was cooled to 100 ºC and diluted with EtOH (16 mL). The reaction mixture was heated at reflux at 80 ºC for 30 min and then allowed to cool to 20-25 ºC. The solids, which remained, were collected by filtration and washed with a 1:1 mixture of EtOH (2.5 mL x 2) and hexanes (2.5 mL x 2) and then washed with hexanes (5 mL x 2). The solid was dried under vacuum at 40 ºC to afford **13e** as a yellow powder (1.0 g, 41.0%)**:** ^{1}H NMR (300 MHz, DMSO-d_6) δ 12.96 (s, 1H), 8.92 (d, J = 2.6 Hz, 1H), 8.77 (s, 1H), 8.42 (dd, J = 8.9, 2.6 Hz, 1H), 8.14 (s, 1H), 7.89 – 7.60 (m, 2H), 6.93 (d, J = 9.0 Hz, 1H), 3.89 (s, 3H); ^{13}C NMR (75 MHz, DMSO-d_6) δ 161.62, 160.64, 142.70, 140.12, 137.57, 134.58, 131.66, 131.15, 130.92, 130.64, 122.11, 121.58, 120.38, 110.59, 106.25, 53.74; HRMS (ESI) m/z calculated for $C_{16}H_{12}ClN_4O_2$ $(M+H)^+$ 327.0643; found 327.0623; HPLC purity, 99.8%.

1.19.1.59. 8-Chloro-2-(6-methoxy-d_3-pyridin-3-yl)-2,5-dihydro-3*H*-pyrazolo[4,3-*c*]quinolin-3-one (DK-II-59-1, 13f)

A mixture of ethyl-4,6-dichloroquinoline-3-carboxylate **7c** (2 g, 7.4 mmol), 5-hydrazinyl-2-methoxy-d_3-pyridine **12a** (1.26 g, 8.9 mmol), triethylamine (0.90 g, 8.9 mmol) and xylenes (16 mL) was heated to reflux (138 ºC) and held at reflux for 2 h. The yellow-orange slurry, which resulted, was cooled to 100 ºC and diluted with EtOH (16 mL). The reaction mixture was heated at reflux at 80 ºC for 30 min and then allowed to cool to 20-25 ºC. The solids, which remained,

were collected by filtration and washed with a 1:1 mixture of EtOH (2.5 mL x 2) and hexanes (2.5 mL x 2) and then washed with hexanes (5 mL x 2). The solid was dried under vacuum at 40 °C to afford **13f** as a yellow powder (1.4 g, 57.0%)**:** ^{1}H NMR (300 MHz, DMSO-*d*$_6$) δ 12.92 (s, 1H), 8.90 (d, J = 1.7 Hz, 1H), 8.74 (d, J = 9.1 Hz, 1H), 8.40 (dd, J = 8.9, 2.4 Hz, 1H), 8.09 (s, 1H), 7.78 – 7.61 (m, 2H), 6.90 (d, J = 8.9 Hz, 1H); ^{13}C NMR (75 MHz, DMSO-*d*$_6$) δ 161.60, 160.63, 142.67, 140.06, 137.55, 134.55, 131.64, 131.13, 130.87, 130.60, 122.07, 121.56, 120.37, 110.55, 106.26; HRMS (ESI) m/z calculated for $C_{16}H_9D_3ClN_4O_2$ $(M+H)^+$ 330.0832; found 330.0811; HPLC purity, 99.7%.

1.19.1.60. 7-Bromo-2-(6-methoxypyridin-3-yl)-2,5-dihydro-3*H*-pyrazolo[4,3-*c*]quinolin-3-one (DK-II-48-1, 13g)

A mixture of ethyl-7-bromo-4-chloroquinoline-3-carboxylate **7d** (2 g, 6.3 mmol), 5-hydrazinyl-2-methoxypyridine **12b** (1.06 g, 7.6 mmol), triethylamine (0.77 g, 7.6 mmol) and xylenes (16 mL) was heated to reflux (138 °C) and held at reflux for 2 h. The yellow-orange slurry, which resulted, was cooled to 100 °C and diluted with EtOH (16 mL). The reaction mixture was heated at reflux at 80 °C for 30 min and then allowed to cool to 20-25 °C. The solids, which remained, were collected by filtration and washed with a 1:1 mixture of EtOH (2.5 mL x 2) and hexanes (2.5 mL x 2) and then washed with hexanes (5 mL x 2). The solid was dried under vacuum at 40 °C to afford **13g** as a yellow powder (1.6 g, 67.0%)**:** ^{1}H NMR (300 MHz, DMSO-*d*$_6$) δ 12.81 (s, 1H), 10.29 – 10.27 (m, 1H), 8.89 (s, 1H), 8.75 (s, 1H), 8.40 (dd, J = 8.9, 2.2 Hz, 1H), 8.09 (d, J = 8.5 Hz, 1H), 7.86 (s, 1H), 7.68 (d, J = 8.1 Hz, 1H), 6.91 (d, J = 8.9 Hz, 1H), 3.88 (s, 3H); ^{13}C NMR (75 MHz, DMSO-*d*$_6$) δ 161.63, 160.61, 143.11, 140.38, 137.53, 136.95, 131.65, 130.88,

129.74, 124.54, 123.15, 122.26, 118.12, 110.61, 106.58, 53.74; HRMS (ESI) m/z calculated for $C_{16}H_{12}BrN_4O_2$ $(M+H)^+$ 371.0138; found 371.0119; HPLC purity, 99.7%.

1.19.1.61. 7-Bromo-2-(6-methoxy-*d*$_3$-pyridin-3-yl)-2,5-dihydro-3*H*-pyrazolo[4,3-*c*]quinolin-3-one (DK-II-58-1, 13h)

A mixture of ethyl-7-bromo-4-chloroquinoline-3-carboxylate **7d** (3.00 g, 9.5 mmol), 5-hydrazinyl-2-methoxy-*d*$_3$-pyridine **12a** (1.63 g, 11.4 mmol), triethylamine (1.16 g, 11.4 mmol) and xylenes (30 mL) was heated to reflux (138 ºC) and held at reflux for 2 h. The yellow-orange slurry, which resulted, was cooled to 100 ºC and diluted with EtOH (30 mL). The reaction mixture was heated at reflux at 80 ºC for 30 min and then allowed to cool to 20-25 ºC. The solids, which remained, were collected by filtration and washed with a 1:1 mixture of EtOH (2.5 mL x 2) and hexanes (2.5 mL x 2) and then washed with hexanes (5 mL x 2). The solid was dried under vacuum at 40 ºC to afford **13h** as a yellow powder (1.7 g, 48.0%)**:** ^{1}H NMR (300 MHz, DMSO-*d*$_6$) δ 12.77 (s, 1H), 8.88 (d, J = 2.3 Hz, 1H), 8.75 (d, J = 8.4 Hz, 1H), 8.39 (dd, J = 8.9, 2.5 Hz, 1H), 8.07 (d, J = 8.5 Hz, 1H), 7.83 (s, 1H), 7.65 (d, J = 8.6 Hz, 1H), 6.90 (d, J = 8.9 Hz, 1H); ^{13}C NMR (75 MHz, DMSO-*d*$_6$) δ 161.60, 160.60, 143.08, 140.33, 137.51, 136.93, 131.63, 130.83, 129.70, 124.50, 123.11, 122.24, 118.10, 110.56, 106.58; HRMS (ESI) m/z calculated for $C_{16}H_9D_3BrN_4O_2$ $(M+H)^+$ 374.0326; found 374.0306; HPLC purity, 99.8%.

1.19.1.62. 7-Methoxy-2-(4-methoxyphenyl)-2,5-dihydro-3*H*-pyrazolo[4,3-*c*][1,6]naphthyridin-3-one (CW-03-030, 13i)

A mixture of ethyl-4-chloro-7-methoxy-1,6-naphthyridine-3-carboxylate **7f** (1.2 g, 4.5 mmol), 4-methoxyphenylhydrazine hydrochloride **4d** (0.94 g, 5.4 mmol), triethylamine (1.09 g, 10.8 mmol) and xylenes (15 mL) was heated to reflux (138 ºC) and held at reflux for 2 h. The yellow-orange slurry, which resulted, was cooled to 100 ºC and diluted with EtOH (16 mL). The reaction mixture was heated at reflux at 80 ºC for 30 min and then allowed to cool to 20-25 ºC. The solids, which remained, were collected by filtration and washed with a 1:1 mixture of EtOH (2.5 mL x 2) and hexanes (2.5 mL x 2) and then washed with hexanes (5 mL x 2). The solid was dried under vacuum at 40 ºC to afford **13i** as a yellow powder (1.0 g, 69.0%)**:** ^{1}H NMR (500 MHz, DMSO-d_6) δ 12.61 (s, 1H), 8.60 (s, 1H), 8.08 (d, J = 7.9 Hz, 2H), 7.83 (d, J = 7.3 Hz, 1H), 7.02 (d, J = 8.3 Hz, 2H), 6.45 (d, J = 7.1 Hz, 1H), 3.79 (s, 3H), 3.51 (s, 3H); ^{13}C NMR (126 MHz, DMSO-d_6) δ 161.75, 160.99, 160.45, 143.87, 139.71, 137.45, 137.39, 131.87, 130.79, 124.15, 115.96, 112.57, 110.57, 106.23, 102.28.; HRMS (ESI) m/z calculated for $C_{17}H_{15}N_4O_3$ $(M+H)^+$ 323.1139; found 323.1139; HPLC purity, 98.6%.

1.19.1.63. 7-Methoxy-d_3-2-phenyl-2,5-dihydro-3*H*-pyrazolo[4,3-*c*]quinolin-3-one (RV-I-037, 14a)

A mixture of ethyl-4-chloro-7-methoxy-d_3-quinoline-3-carboxylate **7b** (2.0 g, 7.4 mmol), phenylhydrazine hydrochloride **4k** (1.29g, 89.3 mmol), and triethylamine (1.8 g, 17.8 mmol) in xylenes (16mL) was heated to reflux (138ºC) for 2 hr. The yellow-orange slurry, which resulted, was cooled to 100 ºC and diluted with EtOH (16 mL). The reaction mixture was heated

at reflux at 80ºC for 30 min and then allowed to cool to 20-25ºC. The solids, which remained, were collected by filtration and washed with a 1:1 mixture of EtOH (2.5 mL x 2) and hexanes (2.5 mL x 2) and then washed with hexanes (5 mL x 2). The solid was dried under vacuum at 40 ºC to afford **14a** as a yellow powder (1.7g, 78%): ^{1}H NMR (300 MHz, DMSO-d_6) δ 12.63 (s, 1H), 8.68 (s, 1H), 8.21 (d, J = 8.0 Hz, 2H), 8.12 (d, J = 9.1 Hz, 1H), 7.43 (t, J = 7.6 Hz, 2H), 7.16 (t, J = 7.4 Hz, 3H); ^{13}C NMR (75 MHz, DMSO-d_6) δ 162.05, 160.97, 143.55, 140.62, 139.61, 137.56, 129.11, 124.24, 124.12, 118.98, 115.82, 112.62, 106.79, 102.31; HRMS (ESI) m/z calculated for $C_{17}H_{11}D_3N_3O_2$ $(M+H)^+$ 295.1274; found 295.1272; HPLC purity, 99.9%.

1.19.1.64. 7-Methoxy-2-(4-methoxyphenyl)-6-methyl-2,5-dihydro-3*H*-pyrazolo[4,3-*c*]quinolin-3-one (CW-02-073, 14b)

A mixture of ethyl 4-chloro-7-methoxy-8-methylquinoline-3-carboxylate **7g** (2 g, 7.1 mmol), 4-methoxyphenylhydrazine hydrochloride **4d** (1.5 g, 8.6 mmol), triethylamine (1.7 g, 17.2 mmol) and xylenes (16 mL) was heated to reflux (138 ºC) and held at reflux for 2 h. The yellow-orange slurry, which resulted, was cooled to 100 ºC and diluted with EtOH (16 mL). The reaction mixture was heated at reflux at 80ºC for 30 min and then allowed to cool to 20-25 ºC. The solids, which remained, were collected by filtration and washed with a 1:1 mixture of EtOH (2.5 mL x 2) and hexanes (2.5 mL x 2) and then washed with hexanes (5 mL x 2). The solid was dried under vacuum at 40 ºC to afford **14b** as a yellow powder (1.7 g, 70%): ^{1}H NMR (300 MHz, DMSO-d_6) δ 11.80 (s, 1H), 8.37 (s, 1H), 8.08 (dd, J = 8.9, 5.1 Hz, 3H), 7.29 (d, J = 9.0 Hz, 1H), 7.01 (d, J = 9.1 Hz, 2H), 3.92 (s, 3H), 3.78 (s, 3H), 2.36 (s, 3H); ^{13}C NMR (75 MHz, DMSO-d_6) δ 161.39, 158.24, 156.22, 143.58, 139.11, 135.37, 134.09, 121.18, 120.66, 114.33, 114.25,

112.80, 111.11, 106.53, 56.65, 55.68, 10.03; HRMS (ESI) m/z calculated for $C_{19}H_{18}N_3O_3$ $(M+H)^+$ 336.1343; found 336.1342; HPLC purity, 97.8%.

1.19.1.65. 7-Methoxy-6-methyl-2-phenyl-2,5-dihydro-3*H*-pyrazolo[4,3-*c*]quinolin-3-one (CW-02-078, 14c)

A mixture of ethyl 4-chloro-7-methoxy-8-methylquinoline-3-carboxylate **7g** (2 g, 7.1 mmol), phenylhydrazine hydrochloride **4k** (1.2 g, 8.6 mmol), triethylamine (1.7 g, 17.2 mmol) and xylenes (16 mL) was heated to reflux (138 ºC) and held at reflux for 2 h. The yellow-orange slurry, which resulted, was cooled to 100 ºC and diluted with EtOH (16 mL). The reaction mixture was heated at reflux at 80ºC for 30 min and then allowed to cool to 20-25 ºC. The solids, which remained, were collected by filtration and washed with a 1:1 mixture of EtOH (2.5 mL x 2) and hexanes (2.5 mL x 2) and then washed with hexanes (5 mL x 2). The solid was dried under vacuum at 40 ºC to afford **14c** as a yellow powder (2.0 g, 92%): ^{1}H NMR (500 MHz, DMSO-d_6) δ 11.86 (s, 1H), 8.42 (s, 1H), 8.22 (d, J = 8.2 Hz, 2H), 8.11 (d, J = 8.8 Hz, 1H), 7.45 (t, J = 7.9 Hz, 2H), 7.33 (d, J = 8.9 Hz, 1H), 7.17 (t, J = 7.3 Hz, 1H), 3.95 (s, 3H), 2.39 (s, 3H); ^{13}C NMR (126 MHz, DMSO-d_6) δ 162.00, 158.41, 144.04, 140.60, 139.43, 135.49, 129.15, 124.29, 121.32, 118.98, 114.42, 112.77, 111.22, 106.48, 56.71, 10.08; HRMS (ESI) m/z calculated for $C_{18}H_{16}N_3O_2$ $(M+H)^+$ 306.1243; found 306.1237; HPLC purity, 99.8%.

1.19.1.66. 7-Methoxy-6-methyl-2-(4-(trifluoromethoxy)phenyl)-2,5-dihydro-3*H*-pyrazolo[4,3-*c*]quinolin-3-one (CW-02-079, 14d)

A mixture of ethyl 4-chloro-7-methoxy-8-methylquinoline-3-carboxylate **7g** (2 g, 7.1 mmol), 4-(trifluoromethoxy)phenylhydrazine hydrochloride **4f** (2.0 g, 8.6 mmol), triethylamine (1.7 g, 17.2 mmol) and xylenes (16 mL) was heated to reflux (138 ºC) and held at reflux for 2 h. The yellow-orange slurry, which resulted, was cooled to 100 ºC and diluted with EtOH (16 mL). The reaction mixture was heated at reflux at 80ºC for 30 min and then allowed to cool to 20-25 ºC. The solids, which remained, were collected by filtration and washed with a 1:1 mixture of EtOH (2.5 mL x 2) and hexanes (2.5 mL x 2) and then washed with hexanes (5 mL x 2). The solid was dried under vacuum at 40 ºC to afford **14d** as a yellow powder (1.9 g, 97%): ^{1}H NMR (300 MHz, DMSO-d_6) δ 11.87 (s, 1H), 8.34 (dd, J = 16.0, 11.7 Hz, 3H), 8.07 (d, J = 8.7 Hz, 1H), 7.44 (d, J = 8.0 Hz, 2H), 7.29 (d, J = 8.8 Hz, 1H), 3.92 (s, 3H), 2.35 (s, 3H); ^{13}C NMR (75 MHz, DMSO-d_6) δ 162.09 (s), 158.47 (s), 144.48 (s), 144.41 (s), 139.63 (s), 139.57 (s), 135.45 (s), 121.97 (s), 121.29 (s), 120.66 (q, $^{1}J_{CF}$ = 256.6 Hz), 120.09 (s), 114.44 (s), 112.60 (s), 111.22 (s), 106.09 (s), 56.64 (s), 10.01 (s); HRMS (ESI) m/z calculated for $C_{19}H_{15}F_3N_3O_3$ $(M+H)^+$ 390.1066; found 390.1068; HPLC purity, 99.9%.

1.19.1.67. 7-Methoxy-2-(4-(trifluoromethoxy)phenyl)-2,5-dihydro-3*H*-pyrazolo[4,3-*c*]quinolin-3-one (CW-02-082, 14e)

A mixture of ethyl-4-chloro-7-methoxyquinoline-3-carboxylate **7e** (2 g, 7.5 mmol), 4-(trifluoromethoxy)phenylhydrazine hydrochloride **4f** (2.1 g, 9.0 mmol), triethylamine (1.8, 18.1 mmol) and xylenes (16 mL) was heated to reflux (138 ºC) and held at reflux for 2 h. The

yellow-orange slurry, which resulted, was cooled to 100 ºC and diluted with EtOH (16 mL). The reaction mixture was heated at reflux at 80ºC for 30 min and then allowed to cool to 20-25 ºC. The solids, which remained, were collected by filtration and washed with a 1:1 mixture of EtOH (2.5 mL x 2) and hexanes (2.5 mL x 2) and then washed with hexanes (5 mL x 2). The solid was dried under vacuum at 40 ºC to afford **14e** as a yellow powder (1.9 g, 67%)**:** ^{1}H NMR (300 MHz, DMSO-*d*$_6$) δ 12.71 (s, 1H), 8.71 (s, 1H), 8.33 (s, 2H), 8.12 (s, 1H), 7.45 (s, 2H), 7.18 (s, 2H), 3.88 (s, 3H); ^{13}C NMR (75 MHz, DMSO-*d*$_6$) δ 162.18, 161.10, 144.50, 144.48, 143.97, 139.93, 139.60, 137.61, 124.15, 121.98, 120.12, 115.95, 112.52, 106.45, 102.37, 56.00; HRMS (ESI) m/z calculated for $C_{18}H_{13}F_3N_3O_3$ $(M+H)^+$ 376.0909; found 376.0914; HPLC purity, 99.9%.

1.19.1.68. 8-Bromo-6-fluoro-2-(4-methoxyphenyl)-2,5-dihydro-3*H*-pyrazolo[4,3-*c*]quinolin-3-one (MM-I-03, 14f)

A mixture of ethyl 6-bromo-4-chloro-8-fluoroquinoline-3-carboxylate **7h** (0.5 g, 1.5 mmol), (4-methoxyphenyl)hydrazine hydrochloride **4d** (0.31 g,1.8 mmol)**,** and triethylamine (2 mL) in xylenes (8 mL) was heated to reflux (138ºC) for 4 hr. The reaction was cooled to rt and filtered. The solid, which formed, was washed several times with hexane and water. Then, the solid was dissolved in a basic aqueous solution of 3 N NaOH and stirred for 15 min. The basic solution was brought to pH = 7 (pH paper) with 3 N aqueous HCl and filtered. The solid was recrystallized using hot ethanol and dried in vacuo to afford a yellow solid **14f**, (0.28 g, 48%)**:** mp 333-334°C; ^{1}H NMR (300 MHz, DMSO-*d*$_6$) δ 13.05 (s, 1H), 8.51 (s, 1H), 8.09 (s, 1H), 8.03 (d, *J* = 8.9 Hz, 2H), 7.89 (d, *J* = 10.5 Hz, 1H), 7.01 (d, *J* = 9.0 Hz, 2H), 3.78 (s, 3H); ^{13}C NMR (75 MHz, DMSO-*d*$_6$) δ 161.11 (s), 156.65 (s), 152.72 (d, $^{1}J_{CF}$ = 254.3 Hz), 140.93 (s), 139.49 (s), 133.57 (s), 124.28 (d, $^{2}J_{CF}$ = 13.7 Hz), 122.02 (s), 121.00 (s), 120.62 (d, $^{3}J_{CF}$ = 2.4 Hz), 118.96

(d, $^{2}J_{CF}$ = 20.5 Hz), 118.28 (d, $^{3}J_{CF}$ = 9.0 Hz), 114.32 (s), 107.83 (s), 55.73 (s); HRMS (ESI) m/z calculated for $C_{17}H_{12}BrFN_3O_2$ $(M+H)^+$ 388.0097; found 388.0094; HPLC purity, 98.4%.

1.19.1.69. 8-Bromo-2-(4-chlorophenyl)-6-fluoro-2,5-dihydro-3*H*-pyrazolo[4,3-*c*]quinolin-3-one (MM-I-13, 14g)

A mixture of ethyl 6-bromo-4-chloro-8-fluoroquinoline-3-carboxylate **7h** (0.2 g, 0.64 mmol), (4-chlorophenyl)hydrazine hydrochloride **4h** (0.18 g, 1.2 mmol), and triethylamine (2 mL) in xylenes (8 mL) was heated to reflux (138ºC) for 4 hr. The reaction was cooled to rt and filtered. The solid, which formed, was collected by filtration and washed with hexane and water. The solid was dissolved in DMSO-d_6 (10mL). The solution was then poured into H_2O (30mL), and filtered in order to remove the triethylamine hydrochloride salt. After this, a recrystallization using EtOH (15mL) and H_2O (2mL) was employed to afford yellow crystals **14g**, (0.17 g, 70%)**:** ^{1}H NMR (300 MHz, DMSO-d_6) δ 12.96 (s, 1H), 8.49 (s, 1H), 8.18 (d, J = 8.4 Hz, 2H), 8.04 (s, 1H), 7.86 (d, J = 10.5 Hz, 1H), 7.46 (d, J = 8.5 Hz, 2H); ^{13}C NMR (75 MHz, DMSO-d_6) δ 161.66 (s), 152.70 (d, $^{1}J_{CF}$ = 254.4 Hz), 141.68 (s), 139.92 (s), 138.99 (s), 129.07 (s), 128.48 (s), 124.50 (d, $^{2}J_{CF}$ = 13.3 Hz), 121.86 (d, $^{4}J_{CF}$ = 3.3 Hz), 120.70 (d, $^{3}J_{CF}$ = 3.6 Hz), 120.35 (s), 119.19 (d, $^{2}J_{CF}$ = 20.3 Hz), 118.40 (d, $^{3}J_{CF}$ = 9.3 Hz), 107.55 (s); HRMS (ESI) m/z calculated for $C_{16}H_9BrClFN_3O$ $(M+H)^+$ 391.9596; found 391.9599; HPLC purity, 99.9%.

1.19.1.70. 8-Bromo-6-fluoro-2-(4-fluorophenyl)-2,5-dihydro-3*H*-pyrazolo[4,3-*c*]quinolin-3-one (MM-I-18, 14h)

A mixture of ethyl 6-bromo-4-chloro-8-fluoroquinoline-3-carboxylate **7h** (0.2 g, 0.64 mmol), (4-fluorophenyl)hydrazine hydrochloride **4i** (0.22 g, 1.3 mmol) and triethylamine (2 mL) in xylenes (8mL) was heated to reflux (138ºC) for 4 hr. The reaction was cooled to rt and filtered. The solid, which formed, was collected by filtration and washed with hexane and water. After this, a recrystallization using EtOH (15mL) and H_2O (2mL) was employed to afford yellow crystals **14h**, (0.120 g, 50 %)**:** ^{1}H NMR (300 MHz, DMSO-d_6) δ 12.99 (s, 1H), 8.50 (s, 1H), 8.28 – 8.10 (m, 2H), 8.05 (s, 1H), 7.88 (d, J = 10.4 Hz, 1H), 7.27 (t, J = 8.7 Hz, 2H); ^{13}C NMR (75 MHz, DMSO-d_6) δ 161.45 (s), 159.29 (d, $^{1}J_{CF}$ = 241.3 Hz), 152.72 (d, $^{1}J_{CF}$ = 255.0 Hz), 141.38 (d, $^{4}J_{CF}$ = 2.5 Hz), 139.88 (d, $^{4}J_{CF}$ = 2.8 Hz), 136.64 (d, $^{4}J_{CF}$ = 2.3 Hz), 124.42 (d, $^{2}J_{CF}$ = 12.4 Hz), 121.95 (d, $^{4}J_{CF}$ = 3.0 Hz), 120.96 (d, $^{3}J_{CF}$ = 8.0 Hz), 120.69 (d, $^{3}J_{CF}$ = 3.1 Hz), 119.17 (d, $^{2}J_{CF}$ = 22.2 Hz), 118.40 (d, $^{3}J_{CF}$ = 8.9 Hz), 115.84 (d, $^{2}J_{CF}$ = 22.3 Hz), 107.65 (s); HRMS (ESI) m/z calculated for $C_{16}H_9BrF_2N_3O$ $(M+H)^+$ 375.9892; found 375.9891; HPLC purity, 99.9%.

1.19.1.71. 2-(4-Methoxyphenyl)-7-(trifluoromethyl)-2,5-dihydro-3*H*-pyrazolo[4,3-c]quinolin-3-one (MM-I-06, 14i)

A mixture of ethyl 4-chloro-7-(trifluoromethyl)-quinoline-3-carboxylate **7i** (0.5 g, 1.5 mmol), (4-methoxyphenyl)hydrazine hydrochloride **4d** (0.57 g, 1.8 mmol), and triethylamine (2 mL) in xylenes (8mL) was heated to reflux (138ºC) for 4 hr. The reaction was cooled to rt and filtered. The solid, which formed, was collected by filtration and washed with hexane and water. After this, a recrystallization using EtOH (15mL) and H_2O (2mL) was employed to afford yellow

crystals **14i**, (0.51 g, 82 %)**:** mp 315 – 316°C; ^{1}H NMR (300 MHz, DMSO-*d*$_6$) δ 12.93 (s, 1H), 8.84 (s, 1H), 8.40 (d, J = 8.4 Hz, 1H), 8.08 (d, J = 9.1 Hz, 2H), 8.03 (s, 1H), 7.83 (d, J = 8.1 Hz, 1H), 7.03 (d, J = 9.1 Hz, 2H), 3.79 (s, 3H); ^{13}C NMR (75 MHz, DMSO-*d*$_6$) δ 161.38 (s), 156.60 (s), 141.99 (s), 140.79 (s), 135.83 (s), 133.75 (s), 130.02 (q, $^{2}J_{CF}$ = 32.5 Hz), 124.15 (q, $^{1}J_{CF}$ = 272.7 Hz), 124.05 (s), 122.66 (q, $^{3}J_{CF}$ = 3.3 Hz), 122.12 (s), 121.00 (s), 117.21 (q, $^{3}J_{CF}$ = 4.2 Hz), 114.34 (s), 107.42 (s), 55.71 (s); HRMS (ESI) m/z calculated for $C_{18}H_{13}F_3N_3O_2$ $(M+H)^+$ 360.0954; found 360.0956; HPLC purity, 99.9%.

1.19.1.72. 2-(4-Chlorophenyl)-7-(trifluoromethyl)-2,5-dihydro-3*H*-pyrazolo[4,3-*c*]quinolin-3-one (MM-I-08, 14j)

A mixture of ethyl 4-chloro-7-(trifluoromethyl)-quinoline-3-carboxylate **7i** (0.5 g, 1.6 mmol), (4-chlorophenyl)hydrazine hydrochloride **4h** (0.47 g, 3.2 mmol), and triethylamine (2 mL) in xylenes (8mL) was heated to reflux (138ºC) for 4 hr. The reaction was cooled to rt and filtered. The solid, which formed, was collected by filtration and washed with hexane and water. After this, a recrystallization using EtOH (15mL) and H_2O (2mL) was employed to afford yellow crystals **14j**, (0.44 g, 75%)**:** mp 346 – 347°C; ^{1}H NMR (300 MHz, DMSO-*d*$_6$) δ 12.98 (s, 1H), 8.84 (s, 1H), 8.34 (d, J = 8.3 Hz, 1H), 8.21 (d, J = 8.9 Hz, 2H), 7.98 (s, 1H), 7.80 (d, J = 8.3 Hz, 1H), 7.47 (d, J = 8.9 Hz, 2H); ^{13}C NMR (75 MHz, DMSO-*d*$_6$) δ 161.92 (s), 142.71 (s), 141.03 (s), 139.11 (s), 135.84 (s), 130.29 (q, $^{2}J_{CF}$ = 32.5 Hz), 129.08 (s), 128.45 (s), 124.11 (s), 124.08 (q, $^{1}J_{CF}$ = 272.8 Hz), 122.73 (q, $^{3}J_{CF}$ = 3.8 Hz), 121.92 (s), 120.40 (s), 117.15 (q, $^{3}J_{CF}$ = 4.2 Hz), 107.15 (s); HRMS (ESI) m/z calculated for $C_{17}H_{10}ClF_3N_3O$ $(M+H)^+$ 364.0459; found 364.0453; HPLC purity, 99.8%.

1.19.1.73. 2-(4-Nitrophenyl)-7-(trifluoromethyl)-2,5-dihydro-3H-pyrazolo[4,3-c]quinolin-3-one (MM-I-09, 14k)

A mixture of ethyl 4-chloro-7-(trifluoromethyl)-quinoline-3-carboxylate **7i** (1.0 g, 3.3 mmol), (4-nitrophenyl)hydrazine hydrochloride **4j** (0.75 g, 3.9 mmol), and triethylamine (0.80g, 7.9 mmol) in xylenes (8 mL) was heated to reflux (138 ºC) and held at reflux for 2 h. The yellow-orange slurry, which resulted, was cooled to 100 ºC and diluted with EtOH (8 mL). The reaction mixture was heated at reflux at 80ºC for 30 min and then allowed to cool to 20-25 ºC. The solids, which remained, were collected by filtration and washed with a 1:1 mixture of EtOH (2.5 mL x 2) and hexanes (2.5 mL x 2) and then washed with hexanes (5 mL x 2). The solid was dried under vacuum at 40 ºC to afford **14k** as a yellow powder (0.7 g, 57%)**:** mp > 350 °C; ^{1}H NMR (300 MHz, DMSO-d_6) δ 13.73 (s, 1H), 8.74 (s, 1H), 8.35 (d, J = 9.0 Hz, 2H), 8.24 (dd, J = 17.0, 8.7 Hz, 3H), 8.11 (s, 1H), 7.75 (d, J = 8.3 Hz, 1H); ^{13}C NMR (75 MHz, DMSO-d_6) δ 162.70 (s), 145.21 (s), 144.09 (s), 142.95 (s), 141.13 (s), 136.15 (s), 130.50 (q, $^{2}J_{CF}$ = 33.2 Hz), 125.16 (s), 124.14 (s), 123.99 (q, $^{1}J_{CF}$ = 272.3 Hz), 122.78 (q, $^{3}J_{CF}$ = 3.7 Hz), 121.66 (s), 118.06 (s), 117.31 (q, $^{3}J_{CF}$ = 3.7 Hz), 106.46 (s); HRMS (ESI) m/z calculated for $C_{17}H_{10}F_3N_4O_3$ $(M+H)^+$ 375.0700; found 375.0706; HPLC purity, 99.9%.

1.19.1.74. 2-(4-(Trifluoromethoxy)phenyl)-7-(trifluoromethyl)-2,5-dihydro-3H-pyrazolo[4,3-c]quinolin-3-one (MM-I-10, 14l)

A mixture of ethyl-4-chloro-7-(trifluoromethyl)-quinoline-3-carboxylate **7i** (2.00 g, 6.6 mmol), 4-(trifluoromethoxy)-phenylhydrazine hydrochloride **4f** (1.81g, 7.9 mmol), and triethylamine

(1.67 g, 16.5 mmol) in xylenes (20mL) was heated to reflux (138ºC) for 2 hr. The yellow-orange slurry, which resulted, was cooled to 100 ºC and diluted with EtOH (20 mL). The reaction mixture was heated at reflux at 80ºC for 30 min and then allowed to cool to 20-25ºC. The solids, which remained, were collected by filtration and washed with *t*-BME (5 mL x 2), then a 1:1 mixture of MeOH / water (5 mL x 2) and finally washed with hexanes (5 mL x 2). The solid was dried under vacuum at 40 ºC to afford **14l** as a yellow powder (2.5g, 92%): mp 286 – 287°C; ^{1}H NMR (300 MHz, DMSO-d_6) δ 12.94 (s, 1H), 8.86 (s, 1H), 8.36 (d, J = 8.4 Hz, 1H), 8.29 (d, J = 9.0 Hz, 2H), 7.99 (s, 1H), 7.81 (d, J = 8.3 Hz, 1H), 7.43 (d, J = 8.8 Hz, 2H); ^{13}C NMR (75 MHz, DMSO-d_6) δ 161.98 (s), 144.85 (s), 142.85 (s), 141.22 (s), 139.27 (s), 135.96 (s), 130.33 (q, $^{2}J_{CF}$ = 33.0 Hz), 124.12 (s), 124.09 (q, $^{1}J_{CF}$ = 272.4 Hz), 122.78 (s), 122.29 (q, $^{3}J_{CF}$ = 3.2 Hz), 121.98 (s), 120.64 (q, $^{1}J_{CF}$ = 255.2 Hz), 120.37 (s), 117.26 (q, $^{3}J_{CF}$ = 5.3 Hz), 107.07 (s); HRMS (ESI) m/z calculated for $C_{18}H_{10}F_6N_3O_2$ $(M+H)^+$ 414.0672; found 414.0674; HPLC purity, 99.7%.

1.19.1.75. 2-(4-Fluorophenyl)-7-(trifluoromethyl)-2,5-dihydro-3H-pyrazolo[4,3-c]quinolin-3-one (MM-I-11, 14m)

A mixture of ethyl 4-chloro-7-(trifluoromethyl)quinoline-3-carboxylate **7i** (0.2 g, 0.66 mmol), (4-fluorophenyl)hydrazine hydrochloride **4i** (0.22 g, 1.3 mmol), and triethylamine (2 mL) in xylenes (8 mL) of xylene was heated to reflux (138ºC) for 4 hr. The reaction was cooled to rt and filtered. The solid, which formed, was collected by filtration and washed with hexane and water. After this, a recrystallization using EtOH (15mL) and H_2O (2mL) was employed to afford yellow crystals **14m** (0.15 g, 65%), the pure **14m**, which was finally obtained by recrystallization from hot EtOH**:** mp 296 – 297 °C; ^{1}H NMR (300 MHz, DMSO-d_6) δ 12.98 (s, 1H), 8.84 (s, 1H),

8.36 (d, J = 8.3 Hz, 1H), 8.19 (dd, J = 9.0, 5.1 Hz, 2H), 8.00 (s, 1H), 7.81 (d, J = 8.4 Hz, 1H), 7.27 (t, J = 8.9 Hz, 2H); ^{13}C NMR (75 MHz, DMSO-d_6) δ 161.69 (s), 159.26 (d, $^{1}J_{CF}$ = 241.2 Hz), 142.41 (s), 140.94 (s), 136.76 (d, $^{3}J_{CF}$ = 2.5 Hz), 135.78 (s), 130.21 (q, $^{2}J_{CF}$ = 32.4 Hz), 124.09 (q, $^{1}J_{CF}$ = 272.3 Hz), 124.07 (s), 122.73 (q, $^{3}J_{CF}$ = 3.0 Hz), 121.98 (d, $^{4}J_{CF}$ = 0.6 Hz), 120.97 (d, $^{3}J_{CF}$ = 7.9 Hz), 117.14 (q, $^{3}J_{CF}$ = 3.9 Hz), 115.80 (d, $^{2}J_{CF}$ = 22.4 Hz), 107.21 (s); HRMS (ESI) m/z calculated for $C_{17}H_{10}F_4N_3O$ $(M+H)^+$ 348.0755; found 348.0766; HPLC purity, 99.8%.

1.19.1.76. 2-(3-Methoxyphenyl)-7-(trifluoromethyl)-2,5-dihydro-3*H*-pyrazolo[4,3-*c*]quinolin-3-one (MM-I-12, 14n)

A mixture of ethyl 4-chloro-7-(trifluoromethyl)quinoline-3-carboxylate **7i** (0.5 g, 1.6 mmol), (3-methoxyphenyl)hydrazine hydrochloride **4e** (0.575 g, 4.1 mmol), and triethylamine (2 mL) in xylenes (15mL) was heated to reflux (138ºC) for 4 hr. The reaction mixture was cooled to rt and filtered. The solid, which formed, was collected by filtration and washed with hexane and water. After this, a recrystallization using EtOH (15mL) and H_2O (2mL) was employed to afford yellow crystals **14n**, (0.762 g, 46 %)**:** mp > 350 °C; ^{1}H NMR (300 MHz, DMSO-d_6) δ 12.94 (s, 1H), 8.84 (s, 1H), 8.40 (d, J = 8.3 Hz, 1H), 8.02 (s, 1H), 7.89 – 7.71 (m, 3H), 7.35 (t, J = 8.2 Hz, 1H), 6.78 (dd, J = 8.2, 1.9 Hz, 1H), 3.81 (s, 3H); ^{13}C NMR (75 MHz, DMSO-d_6) δ 161.97 (s), 159.98 (s), 142.41 (s), 141.40 (s), 140.97 (s), 135.93 (s), 130.23 (q, $^{2}J_{CF}$ = 31.5 Hz), 130.06 (s), 124.18 (s), 124.11 (q, $^{1}J_{CF}$ = 270.8 Hz), 122.75 (q, $^{3}J_{CF}$ = 3.8 Hz), 122.04 (s), 117.21 (q, $^{3}J_{CF}$ = 4.4 Hz), 111.50 (s), 110.14 (s), 107.40 (s), 105.01 (s), 55.58 (s); HRMS (ESI) m/z calculated for $C_{18}H_{13}F_3N_3O_2$ $(M+H)^+$ 360.0954; found 360.0958; HPLC purity, 99.6%.

1.19.1.77. 7-(Methoxy-d_3)-2-(4-(trifluoromethoxy)phenyl)-2,5-dihydro-3*H*-pyrazolo[4,3-*c*]quinolin-3-one (DK-IV-20-1, 14o)

A mixture of ethyl-4-chloro-7-methoxy-d_3-quinoline-3-carboxylate **7b** (2.0 g, 7.4 mmol), 4-(trifluoromethoxy)phenylhydrazine hydrochloride **4f** (1.29g, 8.9 mmol), and triethylamine (1.8 g, 18.6 mmol) in xylenes (20mL) was heated to reflux (138ºC) for 2 hr. The yellow-orange slurry, which resulted, was cooled to 100 ºC and diluted with EtOH (20 mL). The reaction mixture was heated at reflux at 80ºC for 30 min and then allowed to cool to 20-25ºC. The solids, which remained, were collected by filtration and washed with *t*-BME (5 mL x 2), then a 1:1 mixture of MeOH / water (5 mL x 2) and finally washed with hexanes (5 mL x 2). The solid was dried under vacuum at 40 ºC to afford **14o** as a yellow powder (1.8g, 64%): ^{1}H NMR (500 MHz, DMSO-d_6) δ 12.69 (s, 1H), 8.71 (s, 1H), 8.33 (d, J = 9.2 Hz, 2H), 8.12 (d, J = 9.0 Hz, 1H), 7.44 (d, J = 8.8 Hz, 2H), 7.19 (d, J = 2.4 Hz, 1H), 7.17 (s, 1H); ^{13}C NMR (126 MHz, DMSO-d_6) δ 162.19, 161.11, 144.49, 143.98, 139.94, 139.62, 137.62, 124.16, 121.99, 120.66 (q, $^1J_{CF}$ = 255.7 Hz), 120.12, 115.94, 112.51, 106.46, 102.37; ^{19}F NMR (471 MHz, DMSO-d_6) δ -56.95; HRMS (ESI) m/z calculated for $C_{18}H_9D_3F_3N_3O_3$ $(M+H)^+$ 379.1092; found 379.1044; HPLC purity, 99.9%.

1.19.1.78. 7-Bromo-2-(4-(trifluoromethoxy)phenyl)-2,5-dihydro-3*H*-pyrazolo[4,3-*c*]quinolin-3-one (DK-IV-22-1, 14p)

A mixture of ethyl-7-bromo-4-chloro-quinoline-3-carboxylate **7d** (2.0 g, 6.4 mmol), 4-(trifluoromethoxy)phenylhydrazine hydrochloride **4f** (1.74 g, 7.6 mmol), and triethylamine (1.6

g, 15.9 mmol) in xylenes (20mL) was heated to reflux (138ºC) for 2 hr. The yellow-orange slurry, which resulted, was cooled to 100 ºC and diluted with EtOH (20 mL). The reaction mixture was heated at reflux at 80ºC for 30 min and then allowed to cool to 20-25ºC. The solids, which remained, were collected by filtration and washed with *t*-BME (5 mL x 2), then a 1:1 mixture of MeOH / water (5 mL x 2) and finally washed with hexanes (5 mL x 2). The solid was dried under vacuum at 40 ºC to afford **14p** as a yellow powder (1.8g, 67%): ^{1}H NMR (500 MHz, DMSO-d_6) δ 12.88 (s, 1H), 8.82 (s, 1H), 8.32 (d, J = 9.2 Hz, 2H), 8.15 (d, J = 8.5 Hz, 1H), 7.90 (d, J = 1.9 Hz, 1H), 7.72 (dd, J = 8.5, 1.9 Hz, 1H), 7.46 (d, J = 8.4 Hz, 2H); ^{13}C NMR (126 MHz, DMSO-d_6) δ 162.07, 144.77, 143.32, 140.75, 139.40, 137.16, 129.91, 124.65, 123.40, 122.36, 122.09, 121.17 (q, $^{1}J_{CF}$ = 252.3 Hz), 120.33, 118.13, 106.84; ^{19}F NMR (471 MHz, DMSO-d_6) δ -56.93; HRMS (ESI) m/z calculated for $C_{17}H_{10}BrF_3N_3O_2$ $(M+H)^+$ 423.9903; found 423.9871; HPLC purity, 99.9%.

1.19.1.79. 8-Chloro-2-(4-(trifluoromethoxy)phenyl)-2,5-dihydro-3*H*-pyrazolo[4,3-*c*]quinolin-3-one (DK-IV-23-1, 14q)

A mixture of ethyl-4,6-dichloro-quinoline-3-carboxylate **7c** (2.00 g, 7.4 mmol), 4-(trifluoromethoxy)phenylhydrazine hydrochloride **4f** (2.03 g, 8.9 mmol), and triethylamine (1.87 g, 18.5 mmol) in xylenes (20mL) was heated to reflux (138ºC) for 2 hr. The yellow-orange slurry, which resulted, was cooled to 100 ºC and diluted with EtOH (20 mL). The reaction mixture was heated at reflux at 80ºC for 30 min and then allowed to cool to 20-25ºC. The solids, which remained, were collected by filtration and washed with *t*-BME (5 mL x 2), then a 1:1 mixture of MeOH / water (5 mL x 2) and finally washed with hexanes (5 mL x 2). The solid was dried under vacuum at 40 ºC to afford **14q** as a yellow powder (2.6g, 93%): ^{1}H NMR (500 MHz,

DMSO-d_6) δ 12.94 (d, J = 3.1 Hz, 1H), 8.75 (d, J = 5.3 Hz, 1H), 8.31 (d, J = 9.2 Hz, 2H), 8.11 (dd, J = 2.1, 0.6 Hz, 1H), 7.69 (d, J = 0.6 Hz, 1H), 7.69 (d, J = 2.1 Hz, 1H), 7.44 (d, J = 9.1 Hz, 2H); ^{13}C NMR (126 MHz, DMSO-d_6) δ 162.02 (s), 144.77 (d, J = 1.7 Hz), 142.84 (s), 140.29 (s), 139.39 (s), 134.72 (s), 131.21 (s), 130.78 (s), 122.12 (s), 121.97 (s), 121.61 (s), 120.65 (q, $^1J_{CF}$ = 255.8 Hz), 120.34 (s), 120.32 (s), 106.52 (s); ^{19}F NMR (471 MHz, DMSO-d_6) δ -56.93; HRMS (ESI) m/z calculated for $C_{17}H_{10}ClF_3N_3O_2$ $(M+H)^+$ 380.0408; found 380.0366; HPLC purity, 99.9%.

1.19.1.80. 2-(4-(Methoxy-d_3)phenyl)-7-(trifluoromethyl)-2,5-dihydro-3*H*-pyrazolo[4,3-*c*]quinolin-3-one (DK-IV-19-1, 14r)

A mixture of ethyl-4-chloro-7-trifluoromethyl-quinoline-3-carboxylate **7i** (2.00 g, 6.6 mmol), 4-methoxy-d_3-phenylhydrazine **4a** (1.12g, 7.9 mmol), and triethylamine (0.83 g, 8.2 mmol) in xylenes (20mL) was heated to reflux (138ºC) for 2 hr. The yellow-orange slurry, which resulted, was cooled to 100 ºC and diluted with EtOH (20 mL). The reaction mixture was heated at reflux at 80ºC for 30 min and then allowed to cool to 20-25ºC. The solids, which remained, were collected by filtration and washed with *t*-BME (5 mL x 2), then a 1:1 mixture of MeOH / water (5 mL x 2) and finally washed with hexanes (5 mL x 2). The solid was dried under vacuum at 40 ºC to afford **14r** as a yellow powder (1.4g, 59%): ^{1}H NMR (500 MHz, DMSO-d_6) δ 12.88 (s, 1H), 8.80 (s, 1H), 8.34 (d, J = 8.3 Hz, 1H), 8.06 (d, J = 9.1 Hz, 2H), 8.01 – 7.94 (m, 1H), 7.78 (dd, J = 8.5, 1.8 Hz, 1H), 7.00 (d, J = 9.2 Hz, 2H); ^{13}C NMR (126 MHz, DMSO-d_6) δ 161.35, 156.57, 141.90, 140.54, 135.67, 133.72, 129.99 (q, $^2J_{CF}$ = 32.2 Hz), 124.13 (q, $^1J_{CF}$ = 272.5 Hz), 123.97, 122.56 (q, $^3J_{CF}$ = 3.4 Hz), 122.06, 120.95, 117.05 (q, $^3J_{CF}$ = 4.1 Hz), 114.24,

107.46; ^{19}F NMR (471 MHz, DMSO-d_6) δ -61.40; HRMS (ESI) m/z calculated for $C_{18}H_{10}D_3F_3N_3O_2$ $(M+H)^+$ 363.1143; found 363.1106; HPLC purity, 99.9%.

1.19.1.81. 7-Bromo-2-(4-bromophenyl)-2,5-dihydro-3*H*-pyrazolo[4,3-*c*]quinolin-3-one (DK-V-67-1, 14s)

A mixture of ethyl-7-bromo-4-chloro-quinoline-3-carboxylate **7d** (2.00 g, 6.4 mmol), 4-bromophenylhydrazine hydrochloride **4g** (1.71 g, 7.6 mmol), and triethylamine (1.54 g, 15.2 mmol) in xylenes (20mL) was heated to reflux (138ºC) for 2 hr. The yellow-orange slurry, which resulted, was cooled to 100 ºC and diluted with EtOH (20 mL). The reaction mixture was heated at reflux at 80ºC for 30 min and then allowed to cool to 20-25ºC. The solids, which remained, were collected by filtration and washed with *t*-BME (5 mL x 2), then a 1:1 mixture of MeOH / water (5 mL x 2) and finally washed with hexanes (5 mL x 2). The solid was dried under vacuum at 40 ºC to afford **14s** as a yellow powder (0.7g, 26%): ^{1}H NMR (500 MHz, DMSO-d_6) δ 12.80 (s, 1H), 8.77 (s, 1H), 8.18 (d, J = 7.9 Hz, 2H), 8.11 (d, J = 8.2 Hz, 1H), 7.86 (s, 1H), 7.68 (d, J = 8.0 Hz, 1H), 7.62 (d, J = 8.0 Hz, 2H); ^{13}C NMR (126 MHz, DMSO-d_6) δ 162.03, 143.29, 140.81, 139.69, 137.43, 132.01, 129.74, 124.58, 123.27, 122.54, 120.71, 118.15, 116.41, 106.86.; HRMS (ESI) m/z calculated for $C_{16}H_{10}Br_2N_3O$ $(M+H)^+$ 417.9191; found 417.9194; HPLC purity, 99.9%.

1.19.1.82. 2-(4-Bromophenyl)-7-methoxy-2,5-dihydro-3*H*-pyrazolo[4,3-*c*]quinolin-3-one (DK-V-68-1, 14t)

A mixture of ethyl-4-chloro-7-methoxy-quinoline-3-carboxylate **7e** (2.00 g, 7.5 mmol), 4-bromophenylhydrazine hydrochloride **4g** (2.02 g, 9.0 mmol), and triethylamine (1.85 g, 18.0 mmol) in xylenes (20mL) was heated to reflux (138ºC) for 2 hr. The yellow-orange slurry, which resulted, was cooled to 100 ºC and diluted with EtOH (20 mL). The reaction mixture was heated at reflux at 80ºC for 30 min and then allowed to cool to 20-25ºC. The solids, which remained, were collected by filtration and washed with *t*-BME (5 mL x 2), then a 1:1 mixture of MeOH / water (5 mL x 2) and finally washed with hexanes (5 mL x 2). The solid was dried under vacuum at 40 ºC to afford **14t** as a yellow powder (0.8g, 29%): ^{1}H NMR (500 MHz, DMSO-d_6) δ 12.34 (s, 1H), 8.70 (s, 1H), 8.21 (d, J = 8.8 Hz, 2H), 8.12 (d, J = 9.5 Hz, 1H), 7.61 (d, J = 8.8 Hz, 2H), 7.18 (d, J = 6.5 Hz, 2H), 3.88 (s, 3H); ^{13}C NMR (126 MHz, DMSO-d_6) δ 162.18, 161.09, 143.95, 139.97, 139.87, 137.72, 131.97, 124.17, 120.60, 116.05, 115.93, 112.55, 106.51, 102.46, 56.03; HRMS (ESI) m/z calculated for $C_{17}H_{13}BrN_3O_2$ $(M+H)^+$ 370.0192; found 370.0194; HPLC purity, 99.9%.

1.19.1.83. Chloromethyl chlorosulfate solution in DCM (15)

To a mixture of chlorosulfonic acid (54.5 g, 467.7 mmol) and thionyl chloride (27.0 g, 226.7 mmol) in dichloromethane (500 mL) was added chloroiodomethane (50.0g, 283.4 mmol) dropwise over 5 – 10 min while keeping the temperature between 20-25ºC. The purple solution, which resulted, was heated to reflux (38-40ºC) for 6 hr at which point the reaction was deemed complete on analysis by ^{1}H NMR ($CDCl_3$: the disappearance of chloroiodomethane CH_2

protons, 4.9 ppm). The reaction mixture was then cooled to 0-5°C, at which point 6.0% aq bleach (850 mL) was added dropwise to the reaction mixture over 30 min while keeping the temperature at 0-5°C. The biphasic mixture, which resulted, was then stirred for 30 min 0-5°C, at which point the layers were allowed to stand and the layers were separated. The organic layer was then washed with a 0.6% aq bleach solution (250 mL) to afford the product (**15**) as a pale yellow solution in DCM (~500 mL): ^{1}H NMR (500 MHz, $CDCl_3$) δ 5.99 (s, 2H); ^{13}C NMR (126 MHz, $CDCl_3$) δ 53.47.

1.19.1.84. Di-*tert*-butyl (chloromethyl) phosphate (16)

To a mixture of potassium-di-*tert*-butylphosphate (50 g, 201.4 mmol), potassium phosphate dibasic (157.8 g, 906.2 mmol) and tetrapropylammonium chloride (4.5 g, 20.1 mmol) in water (350 mL) was added the chloromethyl chlorosulfate (500 mL, 302.0 mmol, solution in DCM) dropwise over a 30 min period while keeping the temperature between 25-30°C. The biphasic, colorless mixture, with minimal white solids, which resulted, was then allowed to stir for 12 hr at 20-25°C. The reaction mixture was diluted with water (750 mL) and then allowed to stir for 30 min to obtain a biphasic solution. The biphasic mixture was allowed to stand for 30 min at which point the layers were separated. The organic layer was then washed with a 5% aq potassium carbonate solution (200 mL) and then dried (K_2CO_3). The solvents were then removed under reduced pressure to afford the product (**16**) as a pale yellow liquid (28.6g, 54.9% through 2 steps): ^{1}H NMR (500 MHz, $CDCl_3$) δ 5.60 (d, J = 14.9 Hz, 2H), 1.47 (s, 18H); ^{13}C NMR (126 MHz, $CDCl_3$) δ 84.05 (d, J = 7.4 Hz), 73.23 (d, J = 6.9 Hz), 29.76 (d, J = 4.2 Hz); ^{31}P NMR (202 MHz, $CDCl_3$) δ -11.92. The phosphate product (**16**) was dissolved in

dichloromethane (28.6 g), stabilized with anhydrous potassium carbonate (1g) and stored in a freezer (-20ºC).

1.19.1.85. (7-Bromo-2-(4-methoxyphenyl)-3-oxo-2,3-dihydro-5*H*-pyrazolo[4,3-*c*]quinolin-5-yl)methyl di-*tert*-butyl phosphate (DK-VI-9-3, 17a)

To a mixture of 7-Bromo-2-(4-methoxyphenyl)-2,5-dihydro-3*H*-pyrazolo[4,3-*c*]quinolin-3-one (LAU463 (**8n**), 1 g, 2.7 mmol) and sodium iodide (0.8 g, 5.4 mmol) in *N*,*N*-dimethylformamide (20 mL) was added sodium hydride (0.22 g, 5.4 mmol, 60 wt% dispersion in mineral oil). The brown solution, which resulted, was allowed to stir at 20-25ºC for 1 hr to ensure complete deprotonation of the starting material. Di-*tert*-butyl (chloromethyl) phosphate (2.8 g, 5.4 mmol, 50 wt% solution in DCM) was then added to the reaction mixture in one portion. The mixture, which resulted, was heated to 50-55ºC for 2 hr, and then allowed to cool to 20-25ºC. The reaction mixture was diluted with water (100 mL) and then extracted three times with dichloromethane (50 mL x 3). The combined organic layers were then washed twice with water (50 mL x 2) and then dried (Na_2SO_4). The solvents were then removed under reduced pressure. The residue, which remained, was triturated with a mixture of *t*-butyl methyl ether (50 mL) and hexanes (50 mL). The yellow solid, LAU463 (**8n**), which remained, was removed by filtration (0.3 g). The filtrate was concentrated under reduced pressure and the residue, which remained, was triturated with a mixture of ethyl acetate (50 mL) and hexanes (50 mL) and then placed in a freezer at -20ºC to maximize product precipitation. The solids, which resulted, were collected by filtration and washed with hexanes (5 mL x 2). The solid was dried under vacuum at 40ºC to afford **17a** as a yellow powder (0.4g, 25%): ^{1}H NMR (500 MHz, DMSO-d_6) δ 8.86 (s, 1H), 8.20 (d, J = 8.5 Hz, 1H), 8.11 (d, J = 1.8 Hz, 1H), 8.03 (d, J = 9.1 Hz, 2H), 7.81 (dd, J = 8.5, 1.8 Hz,

1H), 7.03 (d, *J* = 9.2 Hz, 2H), 6.23 (d, *J* = 12.4 Hz, 2H), 3.79 (s, 3H), 1.35 (s, 18H); ^{13}C NMR (126 MHz, DMSO-*d*$_6$) δ 161.20, 156.69, 144.59, 141.76, 136.46, 133.40, 130.39, 124.82, 123.93, 121.36, 120.86, 118.73, 114.41, 107.82, 83.86 (d, *J* = 7.4 Hz), 78.28 (d, *J* = 5.6 Hz), 55.74, 29.72 (d, *J* = 4.1 Hz); ^{31}P NMR (202 MHz, DMSO-*d*$_6$) δ -11.37; HRMS (ESI) m/z calculated for $C_{26}H_{32}BrN_3O_6P$ $(M+H)^+$ 592.1213; found 592.1217.

1.19.1.86. (7-Bromo-2-(4-methoxyphenyl)-3-oxo-2,3-dihydro-5*H*-pyrazolo[4,3-*c*]quinolin-5-yl)methyl dihydrogen phosphate (DK-VI-15-1, 18a)

To a mixture of 7-bromo-2-(4-methoxyphenyl)-3-oxo-2,3-dihydro-5*H*-pyrazolo[4,3-*c*]quinolin-5-yl)methyl di-*tert*-butyl phosphate (**17a**, 0.4 g, 0.68 mmol) and dichloromethane (10 mL) was added trifluoroacetic acid (2.0 mL, 27.0 mmol). The yellow solution, which resulted, was then allowed to stir at rt for 30 min, at which point the reaction was deemed complete by TLC analysis (silica gel and 100% ethyl acetate with 1% MeOH and 1% TEA; ***Rf*** starting material: 0.6, ***Rf*** product: 0.1). The solvents were then removed under reduced pressure. The residue, which remained, was triturated with ethyl acetate (20 mL). The solids, which resulted, were collected by filtration and washed with ethyl acetate (5mL x 2) and then hexanes (5 mL x 2). The yellow-orange solid was dried under vacuum at 40^{o}C to afford **18a** as a yellow powder (0.19 g, 60%): ^{1}H NMR (500 MHz, DMSO-*d*$_6$) δ 8.77 (s, 1H), 8.18 (d, *J* = 8.5 Hz, 1H), 8.13 (d, *J* = 1.8 Hz, 1H), 8.02 (d, *J* = 9.1 Hz, 2H), 7.78 (dd, *J* = 8.4, 1.7 Hz, 1H), 7.03 (d, *J* = 9.1 Hz, 2H), 6.16 (d, *J* = 12.4 Hz, 2H), 3.79 (s, 3H); ^{13}C NMR (126 MHz, DMSO-*d*$_6$) δ 161.26, 156.67, 144.51, 141.93, 136.60, 133.45, 130.25, 124.74, 123.90, 121.35, 120.93, 118.84, 114.39, 107.62, 77.99 (d, *J* = 4.6 Hz), 55.74; ^{31}P NMR (202 MHz, DMSO-*d*$_6$) δ -2.16; HRMS (ESI) m/z calculated for $C_{18}H_{16}BrN_3O_6P$ $(M+H)^+$ 479.9961; found 479.9965.

1.19.2. General Procedures for the Biological Assays

1.19.2.1. Microsomal stability assay with Revathi Kodali

The 4 µL of 1 mM test compound at a final concentration of 10µM dissolved in either DMSO, ACN, MeOH, or EtOH (depending on compound solubility) was preincubated at 37°C for 5 minutes on a digital heating shaking dry bath (Fischer Scientific, Pittsburgh, PA) in a mixture containing 282 µL of H_2O, 80 µL of phosphate buffer (0.5 M, pH 7.4), 20 µL of NADPH Regenerating System Solution A (BD Bioscience, San Jose, CA) and 4 µL of NADPH Regenerating System Solution B (BD Bioscience, San Jose, CA) in a total volume of 391.2 µL. Following preincubation, the reaction was initiated by addition of 8.8 µL of either HLM (BD Gentest, San Jose, CA), or MLM (Life technologies, Rockford, IL), at a protein concentration of 0.5 mg/mL. Aliquots of 50 µL were taken at time intervals of 0 (without microsomes), 10, 20, 30, 40, 50 and 60 minutes. Each aliquot was added to 100 µL of cold acetonitrile solution containing 1 µM/2 µM internal standard. This was followed by sonication for 10 seconds and centrifugation at 10,000 rpm for 5 minutes. The 100 µL of the supernatant was transferred into Spin-X HPLC filter tubes (Corning Incorporated, NY) and centrifuged at 13,000 rpm for 5 minutes. The filtrate was diluted 100 fold and subsequently analyzed by LC-MS/MS with a Shimadzu LCMS 8040 (Shimadzu Scientific Instruments, Columbia, MD). The ratio of the peak areas of the internal standard and test compound was calculated for every time point and the natural log of the ratio was plotted against time to determine the linear slope (k). The metabolic rate ($k*C_0/C$), half-life (0.693/k), and internal clearance (V*k) were calculated, where k is the slope, C_0 is the initial concentration of test compound, C is the concentration of microsomes, and V is the volume of incubation in µL per microsomal protein in mg. All experiments (**Table 8**)

were repeated three times in duplicate and followed the experimental procedures reported in Forkuo et al.[101,102] and Jahan et al.[103]

1.19.2.2. Metabolite Assay with Revathi Kodali

Metabolite analysis by LCMS confirmed the OCH_3 rate > OCD_3 rate of metabolism and that the primary metabolites for the PQs was generated via O-demethylation of the methoxy groups to form hydroxypyrazoloquinolinones. The 60 min samples from the metabolism study above were injected on a LC-MS with Shimadzu LCMS 2020, (Shimadzu Scientific Instruments, Columbia, MD) using a SIM mode (Dual Ion Source (DUIS) ionization, simultaneous ESI and APCI) method calibrated to the respective retention times and mass units of each component and the respective peak intensities were measured. Compound peaks were resolved using a Shimadzu C18 3 µm 50 x 4.6mm reversed phase LC column. LC mobile phase: 90% acetonitrile (w. 0.1% TFA) and 10% H_2O (w/ 0.1% TFA). The results are shown in **Scheme 13**.

1.19.2.3. Electrophysiological Assay with *Xenopus oocytes* with Dr. Margot Ernst

The details of electrophysiological experiments with *Xenopus oocytes* have been reported.[23, 104] Mature female *Xenopus laevis* (Nasco, Fort Atkinson, WI, USA) were anaesthetized in a bath of ice-cold 0.17% Tricain (Ethyl-m-aminobenzoat, Sigma-Aldrich, St. Louis, MO, USA) before decapitation and transfer of the frog's ovary to ND96 medium (96 mM NaCl, 2 mM KCl, 1 mM $MgCl_2$, 5 mM HEPES; pH 7.5). Following incubation in 1mg/ml collagenase (Sigma-Aldrich, St. Louis, MO, USA) for 30 min, stage 5 to 6 oocytes were singled out of the ovary and defolliculated using a platinum wire loop. The oocytes were stored and incubated at 18°C in

NDE medium (96 mM NaCl, 2 mM KCl, 1 mM $MgCl_2$, 5 mM HEPES, 1.8 mM $CaCl_2$; pH 7.5) that was supplemented with 100 $U \cdot mL^{-1}$ penicillin, 100 $\mu g \cdot mL^{-1}$ streptomycin and 2.5 mM pyruvate. The oocytes were injected with an aq solution of mRNA. A total of 2.5 ng of mRNA per oocyte was injected. The subunit ratio was 1:1:5 for $\alpha x \beta \gamma 2$ (x = 1,2,3,5) and 3:1:5 for $\alpha 4/6 \beta 3 \gamma 2$ and $\alpha \beta \delta$ receptors. Injected oocytes were incubated for at least 36 h before electrophysiological recordings. The oocytes were placed on a nylon-grid in a bath of NDE medium. For current measurements, the oocytes were impaled with two microelectrodes (2–3MΩ), which were filled with 2M KCl. The oocytes were constantly washed by a flow of 6 $mL \cdot min^{-1}$ NDE that could be switched to NDE containing GABA and/or drugs. The drugs were diluted into NDE from DMSO solutions, which resulted, in a final concentration of 0.1% DMSO. The maximum currents measured in mRNA injected oocytes were in the microampere range for all receptor subtypes. To test for modulation of GABA induced currents by compounds, a GABA concentration that was titrated to trigger 3-5% of the respective maximum GABA-elicited current of the individual oocyte (EC3-5) was applied to the cell together with various concentrations of test compounds. All recordings were performed at room temperature at a holding potential of -60 mV using a Warner OC-725C TEV (Warner Instrument, Hamden, CT, USA) or a Dagan CA-1B Oocyte Clamp or a Dagan TEV-200A TEV (Dagan Corporation, Mineapolis, MN, USA). The data were digitized using a Digidata 1322A or 1550 data acquisition system (Axon Instruments, Union City, CA, USA), recorded using Clampex 10.5 software (Molecular Devices, Sunnyvale, CA, USA), and analyzed using Clampfit 10.5 and GraphPad Prism 6.0 (La Jolla, CA, USA) software. Concentration-response data were fitted using the Hill equation. The data are given as mean±SEM from at least three oocytes of two batches.

1.19.2.4. Electrophysiological recordings from transfected HEK-293T cells with Dr. Janet Fisher

The human fibroblast cells (HEK-293T) were transiently transfected with full-length cDNAs encoding human (α2), or rat (α1, α3, α4, α5, α6, γ2L, β3) $GABA_A$ receptor subunits using calcium phosphate precipitation. The positively transfected cells were isolated by utilizing co-transfection of a plasmid encoding a surface antibody (pHook^{TM}-1,Invitrogen). 20-52 hours following transfection, cells were mixed with magnetic beads coated with antigen specific for the pHook antibody, isolated with a magnetic stand, and then plated onto coverslips and used for patch-clamp recordings 18-28 hours later.

Current responses to GABA were recording in the whole-cell configuration, with cells voltage-clamped at -50 mV. The bath solution contained (in mM): 142 NaCl, 8.1 KCl, 6 $MgCl_2$, 1 $CaCl_2$, and 10 HEPES (4-(2-hydroxyethyl)-1-piperazineethanesulfonic acid) with pH = 7.4 and osmolarity adjusted to 295-305 mOsm. The electrode (internal) solution consisted of (in mM); 153 KCl, 1 $MgCl_2$, 5 K-EGTA (ethylene glycol-bis (β-aminoethyl ether N,N,N′N′-tetraacetate), and 10 HEPES with pH = 7.4 and osmolarity adjusted to 295-305 mOsm. The drug-containing solutions were applied to cells for 5 sec. using a computer-driven applicator (open tip exchange <50 msec, SF-77B, Warner Instruments). Currents were recorded with an Axon 200B (Foster City, CA) patch clamp amplifier. GABA concentrations were EC_{3-5} for each receptor isoform, based on previously published data (Picton and Fisher, 2007).[105]

1.19.2.5. PDSP Compound-induced Radioligand Displacement Assays for 46 Receptors with Dr. Bryan Roth

Binding affinity (Ki) determinations, receptor binding profiles, agonist and/or antagonist functional data, HERG data, MDR1 data, etc. as appropriate was generously provided by the National Institute of Mental Health's Psychoactive Drug Screening Program, Contract # HHSN-271-2013-00017-C(NIMH PDSP). The NIMH PDSP is directed by Bryan L. Roth MD, PhD at the University of North Carolina at Chapel Hill and Project Officer Jamie Driscol at NIMH, Bethesda MD, USA. See **Table 59** for the respective primary inhibition studies and **Table 60** for secondary binding affinity studies.

1.19.2.6. Solubility Assay and cLogP

Solubility method: 10mg of each respective compound was dissolved in 2mL of DMAC. The water solubility (pH = 7) samples were prepared by adding 10 µL of the resulting DMAC solution to 2mL of DI H_2O and sonicated at 37°C for 2 h. The acidic solubility (pH = 2) samples were prepared by adding 10 µL of the resulting DMAC solution to 2mL of 0.01 M aq HCl and held at 37°C for 2 hours. The mixtures were then filtered using a 0.45 micron syringe filter. The resultant solutions were injected onto a LC-MS with Shimadzu LCMS 2020, (Shimadzu Scientific Instruments, Columbia, MD) using a SIM mode (Dual Ion Source (DUIS) ionization, simultaneous ESI and APCI) method calibrated to the respective retention times and mass units of each compound. The compound peaks were resolved using a Shimadzu C18 3 µm 50 x 4.6mm reversed phase LC column. LC mobile phase: 90% acetonitrile (w. 0.1% TFA) and 10% H_2O (w/ 0.1% TFA). The calibration curves using standard solutions (n = 5) of each compound dissolved in DMAC were used to calculate the unknown aq concentrations of each compound,

n=3. The cLogP data was calculated using ChemBioDraw® Ultra (ver. 13.0.0.3015).[39, 106] The data are shown in **Table 9**.

1.19.2.7. Cytotoxicity Assay with Dr. Michael Rajesh Stephen

Human liver hepatocellular carcinoma (HEPG2) and human embryonic kidney 293T (HEK293T) cell lines were purchased (ATCC) and cultured in 75 cm^2 flasks (CellStar). The cells were grown in DMEM/High Glucose (Hyclone, #SH3024301) media to which non-essential amino acids (Hyclone, #SH30238.01), 10 mM HEPES (Hyclone, #SH302237.01), 5 x 106 units of penicillin and streptomycin (Hyclone, #SV30010), and 10% of heat inactivated fetal bovine serum (Gibco, #10082147) were added. The cells were harvested using 0.05% trypsin (Hyclone, #SH3023601), washed with PBS, and dispensed into sterile white, optical bottom 384-well plates (NUNC, #142762). After three hours, small molecule solutions were transferred with a Tecan Freedom EVO liquid handling system equipped with a 100 nL pin tool (V&P Scientific). The controls were 3-dibutylamino-1-(4-hexyl-phenyl)-propan-1-one (25 mM in DMSO, positive control) and DMSO (negative control). The cells were incubated for 48 h followed by the addition of CellTiter-Glo™, a luminescence-based cell viability assay (Promega, Madison, WI). All luminescence readings were performed on a Tecan Infinite M1000 plate reader. The assay was carried out in quadruplet with three independent runs. The data was normalized to the controls and analyzed by nonlinear regression (GraphPad Prism), see **Table 63** and **Figure 135**.

1.19.2.8. Rotarod Motor Impairment Study with Nick Zahn and Coworkers

The possible adverse CNS sensorimotor effects were evaluated using a rotarod apparatus (**Figure 137**). Female Swiss Webster mice were dosed via oral gavage with 40 mg/kg of the indicated

compound. The sensorimotor rotarod test was carried out after 10, 30 and 60 minutes. The diazepam positive control (5mg/kg), showed the greatest impairment of sensorimotor steadiness at 10 minutes, followed by 30 and 60 minutes. Several of the compounds were not soluble in the standard vehicle (50% PBS, 40% propylene glycol, 10% DMSO) and were subsequently administered via oral gavage at 40mg/kg in a vehicle of 2% polyethylene glycol and 2.5% hydroxymethyl cellulose solution. None of the compounds displayed motor impairment.

1.19.2.9. Pharmacokinetic Assay with Dr. Miroslav Savić and coworkers

The pharmacokinetic study of **8a**, **8b**, **8c**, **8d** and **13c** in male Wistar rats weighing 250-350 g was performed after an acute treatment with the 5 mg/ml suspension formulated in the vehicle consisting of 85% distilled H_2O, 14% propylene glycol and 1% Tween 80. Single 10 mg/kg doses of each of the ligands were administered i.p. to three rats per time point (5, 20, 60, 180 and 720 min after dosing), at which time, blood and brain samples of the rats were collected after sacrificing. In addition, the absolute oral bioavailability of **8a** and **8b** was measured after respective single 2 mg/kg oral gavage (PO) or IV administration to three rats per post-dosing time 5, 30, 120, 480 and 1440 min (24 h). The ligands were extracted from the respective samples by solid phase extraction and their concentrations were determined by high performance liquid chromatography-tandem mass spectrometry (HPLC-MS/MS). In a separate *in vitro* experiment, the rapid equilibrium dialysis assay was used to determine the free fractions of **8b** and **8d** in rat plasma and brain tissue. See **Figure 34** and **Figure 35**.

1.19.2.10. Pharmacokinetic Cassette Study with Dr. Miroslav Savić and coworkers

MATERIALS AND METHODS

Animals

In order to assess the influence of the pyrazoloquinolinone compounds on motor behavior and to determine pharmacokinetic parameters and concentration-time profiles of the ligands, the tests of spontaneous locomotor activity (SLA) as well as pharmacokinetic studies were performed in adult male C57BL/6 mice. The mice supplied by Military Medical Academy, Belgrade, Serbia, were housed in groups of five and maintained under standard laboratory conditions (21 ± 2 °C, relative humidity 40–45% and the illumination 120 lx) with free access to pellet food and tap water. The animals were kept on 12:12 h light/dark cycle with lights on at 06.00 h. All handling and testing took place during the light phase of the diurnal cycle. All procedures were conducted in accordance with the National Institutes of Health Animal Care and Use Committee guidelines and were approved by the Ethical Committee on Animal Experimentation of the Faculty of Pharmacy in Belgrade, Serbia.

Pharmacokinetic study

Ninety mice weighing 21-35 g were divided into five cohorts and subjected to cassette dosing of different sets of compounds. Each cohort consisted of six groups of animals, with three animals per group in each of the predetermined time intervals (5, 20, 60, 240, 960 and 2160 min). The five cohorts of animals received the following respective sets of compounds: DK-I-56-1, DK-I-58-1 and DK-II-58-1; DK-VI-19-1, DK-IV-20-1 and MM-I-10; DK-IV-22-1, DK-I-86-1 and LAU 463; RV-I-029, PZ-II-029, and DK-I-87-1; as well as DK-I-60-3, DK-I-86-1, and DK-I-59-1, respectively. They were suspended with the aid of sonication in the vehicle (SOL), which consisted

of 85% distilled water, 14% propylene glycol, and 1% Tween 80. The mice were treated i.p. in a volume of 10 ml/kg to obtain a 3 mg/kg dose of each compound tested.

The animals were anesthetized with ketamine hydrochloride (10% Ketamidor, Richter Pharma Ag, Wels, Austria, dosed i.p. at 100 mg/kg) and samples of blood (collected via cardiac puncture in heparinized syringes), liver, kidney and brain were taken. Plasma was obtained after centrifugation for 10 min. at 1.0 rcf (MiniSpin® plus centrifuge, Eppendorf, Germany). The tissue samples were weighted and homogenized in 1.25 mL (liver and brain) or 1.00 mL (kidney) of methanol via ultrasonic probe (70% amplitude 2 x 20 s for brain, 80% amplitude 3 x 20 s for liver and kidney). Supernatants were separated after centrifugation for 20 min. at 3.4 rcf (MiniSpin® plus centrifuge, Eppendorf, Germany). The plasma and supernatant samples were further processed with solid phase extraction (Oasis HLB cartridges, Waters Corporation, Milford, Massachusetts).

The compounds were extracted from plasma and tissue supernatants by solid phase extraction, using Oasis HLB cartridges (Waters Corporation, Milford, Massachusetts). Cartridges were preconditioned with methanol and water, loaded with samples and the internal standard solution and DK-I-56-1 was eluated by 1 ml of methanol for 1 min. The procedure of sample preparation and determination of concentration by ultraperformance liquid chromatography–tandem mass spectrometry (UPLC–MS/MS) with Thermo Scientific Accela 600 UPLC system connected to a Thermo Scientific TSQ Quantum Access MAX triple quadrupole mass spectrometer (Thermo Fisher Scientific, San Jose, California), equipped with electrospray ionization (ESI) source, has been already described in detail (Obradović et al., 2014). The non-compartmental pharmacokinetic analysis was performed using PK functions for Microsoft Excel software (by Joel Usansky, Atul Desai, and Diane Tang-Liuwere; https://www.pharmpk.com/soft.html), while graphs were constructed in Sigma Plot 12 (Systat Software Inc., USA). The brain-to-plasma partition

coefficient was calculated as follows: Kp = $AUC_{0–36}$, brain/$AUC_{0–36}$, plasma, where AUC_{0-36} stands for area under the curve concentration versus time curve from zero to 36 hours. The percentage of the substance in brain related to all four compartments where it was measured (α) was calculated using the equation: $\alpha = AUC_{0\text{-}36,\ brain} / (AUC_{0\text{-}36,\ plasma} + AUC_{0\text{-}36,\ brain} + AUC_{0\text{-}36,\ liver} + AUC_{0\text{-}36,\ kidney})$, and the exposure of excretory organs as follows: AUC (0-36) liver + AUC (0-36) kidney.

1.19.2.11. Battery of Behavioral Tests in Rats with Miroslav M. Savić, Snežana D. Savić and coworkers

The behavioral studies (**Table 11**) in male Wistar rats weighing 200-300 g was performed with the biocompatible nanoemulsions of **8b** and **8m** formulated at 2 mg /mL^{-1}. The nanoemulsions, with and without a ligand, were prepared by a procedure slightly modified from Djordjevic et al.,[91] and injected IP in a 5 mL kg^{-1} volume (10 mg kg^{-1}). They were composed of medium chain triglycerides, castor oil, soybean lecithin, sodium oleate, polyoxyethylensorbitan monooleate, butylhydroxytoluene, DMSO and ultra-pure H_2O. Forty-five minutes after treatment, the rats (eight animals per group) were consecutively subjected to a battery of behavioral tests, consisting of the elevated plus maze, grip strength and cued water maze.

Elevated Plus Maze

The elevated plus maze apparatus was constructed of black Plexiglas, and was elevated to a height of 50 cm and consisted of two open (50×10 cm^2) and two enclosed arms (50×10×40 cm^3) connected by a junction area measured 10×10 cm^2. Single rats were placed in the center of the maze, facing one of the enclosed arms, and their behavior was recorded for 5 min. An entry into

an arm was scored when 90% of the animal crossed the virtual line separating the central square of the maze from an arm, whereas an exit occurred when more than 90% of the animal left the respective arm. Dependent variables chosen for analysis were total distance traveled, closed arm entries and percent of open arm entries.

Grip Strength

The rat pulled by the tail grasps the trapeze connected to a force transducer of the grip strength meter (Ugo Basile, Milan, Italy, model 47105), and the apparatus measured the peak force of the experimenter's pull (in grams) necessary to overcome the strength of the animal's forelimb grip. Each animal was given three consecutive trials, and the median value of the three measurements, normalized against body weight, was used for further statistics.

Cued Water-Maze

The cued water-maze experiment was performed in a 2 m diameter circular pool filled to a height of 30 cm with water at 22 ± 1 °C. The fixed escape platform (15 cm × 10 cm) submerged 2 cm below the water surface was flagged with an object protruding 15 cm above water level. Rats were given one swimming block, consisting of four trials. For each trial the rat was placed in the water at the same starting position, most distant to the platform. Once the rat has found and mounted the escape platform it was permitted to remain on the platform for 15 s. The rat was guided to the platform by the experimenter if it failed to locate it within 120 s. Dependent variables chosen for tracking were: total distance traveled, mean speed and % of distance swam in the peripheral annulus.

Rotarod Protocol

As a separate pilot experiment, the influence of **8b** and **8m** on motor performance of rats was assessed using an automated rotarod (Ugo Basile, Italy). Before testing, rats were trained for three days until they could remain for 180 s on the rod revolving at 15 rpm. On the fourth day, selection was made and rats fulfilling the given criteria were treated with the suspension formulations of **8b** and **8m** in the range 10-55 or 60 mg/kg (2-3 animals per group). The latency to fall from the rotarod was recorded 45 min later.

1.19.2.12. Spontaneous Locomotor Activity Assay in Rats and Mice with Miroslav M. Savić and coworkers

The spontaneous locomotor activity (SLA) assay was performed in adult male Wistar rats or C57BL/6 mice in the apparatus consisting of four white and opaque Plexiglas chambers (40 × 25 × 35 cm) under dim red light (20 lux). A digital camera mounted above the apparatus recorded animal activity, which was tracked and analyzed using ANY-maze Video Tracking System software (Stoelting Co, Wood Dale, IL, US). Three experiments in both, rats and mice were performed; the treatments were administered IP and immediately afterwards, a single rat or mouse was placed in the center of the chamber with its activity being followed for a total of 60 min. The chambers were cleaned with 70% ethanol after every trial. See **Figure 42**.

1.19.2.13. Statistical analysis with Miroslav M. Savić and coworkers

All *in vivo* data are expressed as mean ± SEM. The pharmacokinetic parameters were calculated using PK Functions for Microsoft Excel software (by Joel Usansky, Atul Desai, and Diane Tang-Liuwere). The animals were tracked by Any Maze software (Stoelting, Wood Dale, US) and

behavioral parameters analyzed using one-way analysis of variance (ANOVA), with treatment as between-subject factor, with exception of the water-maze data, which were subjected to two-way repeated measures ANOVA (SigmaPlot 12.0, SPSS, Chicago, US).

1.19.2.14. Spontaneous Locomotor Activity (Time Mobile and Distance Travelled) with Miroslav M. Savić and coworkers

The spontaneous locomotor activity (SLA) assay was carried out on nine to eleven week old male C57BL/6 mice weighing 24-33 g (N=72). The behavior was recorded by a ceiling – mounted camera and analyzed by ANY–maze Video Tracking System software (Stoelting Co, Wood Dale, IL, USA).

Seventeen ligands were tested in the SLA test (14 pyrazoloquinolinone compounds - DK-I-56-1, DK-II-58-1, DK-IV-20-1, DK-IV-22-1, RV-I-029, DK-I-87-1, DK-I-60-3, DK-I-58-1, DK-IV-19-1, MM-I-10, LAU 463, DK-I-86-1, PZ-II-029, DK-I-59-1 all at dose of 3 mg/kg, and diazepam at 1.5 mg/kg as a putative negative control. The GL-II-73 at a dose of 10 mg/kg was included as a putative positive control and SOL). All ligands were suspended with the aid of sonication in the SOL. The treatments were applied intraperitoneally (i.p.) in the 10 ml/kg volume. Immediately after the treatment, a single mouse was placed in the center of the tracking chamber and its activity was recorded for a total of 90 min, without any acclimatization period, under dim red light (20 lx). The apparatus consisted of four white and opaque Plexiglas chambers (40 × 25 × 35 cm). After every trial, the chambers were cleaned with 70% ethanol.

SLA was performed in two sequences, widely separated by the wash-out and dishabituation period of 16 days. Each sequence of the experiment lasted for five days. All 72 animals were tested in a

sequence, giving rise to n=4 for all groups, except for the solvent with N=8. The order of treatments per animal was reversed between two sequences. In total, after both parts of experiment, an n=8 was obtained per group, except for solvent with n=16.

The behavioral parameters analyzed were total distance travelled (m) and time mobile (s). The statistical analysis (one-way ANOVA and post hoc SNK tests where applicable) was performed with SigmaPlot 12 software (Systat, USA).

1.20. Structural Analysis of α6-GABA$_A$R Subtype-selective Pyrazoloquinolinones by NMR Spectroscopy

The NMR experiments below provided evidence that the B-ring nitrogen atom carried the proton rather than the C-ring nitrogen atom. The ^{1}HNMR spectrum in **Figure 44** exhibited the splitting as a doublet between the N-H (12.81ppm) group and the neighboring proton (8.72 ppm) on carbon 8 with an observed coupling of J = 5.4 Hz. This doublet would not be observed if the C-ring nitrogen atom carried the proton.

Figure 44: ^{1}HNMR Spectrum Exhibiting Proton Position of **LAU 463 (8n)** in DMSO-d_6

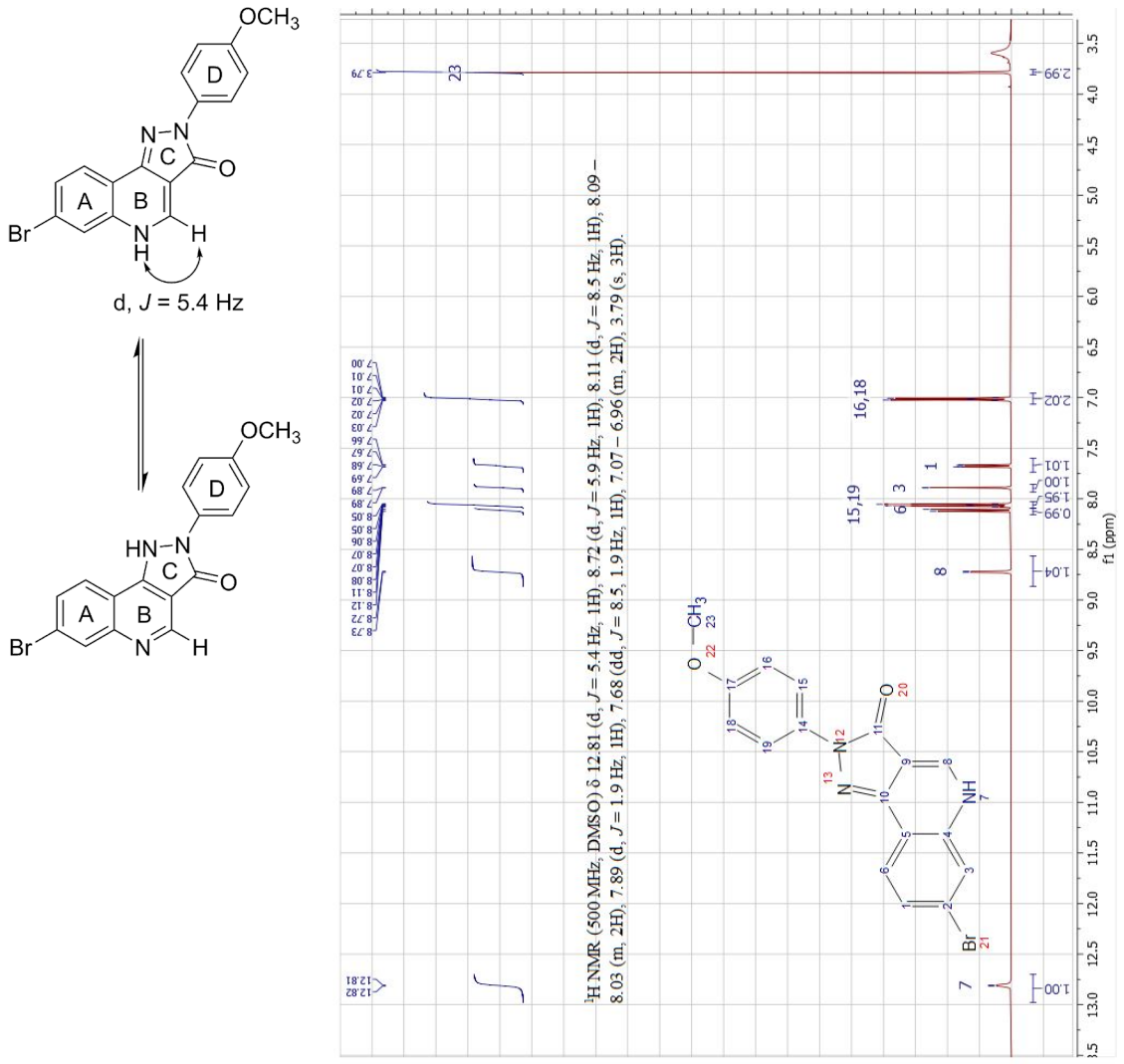

Examination of the COSY spectrum in **Figure 45** exhibited the correlation between the N-H (12.81ppm) and the neighboring proton (8.72 ppm) on carbon 8. This correlation would not be observed if the C-ring nitrogen atom carried the proton instead. Additionally, the correlations between H1 and H6 in A-ring and H18 and H19 in D-ring were observed, as expected.

Figure 45: COSY Spectrum Exhibiting Correlation of Protons of **LAU 463 (8n)** in DMSO-d_6

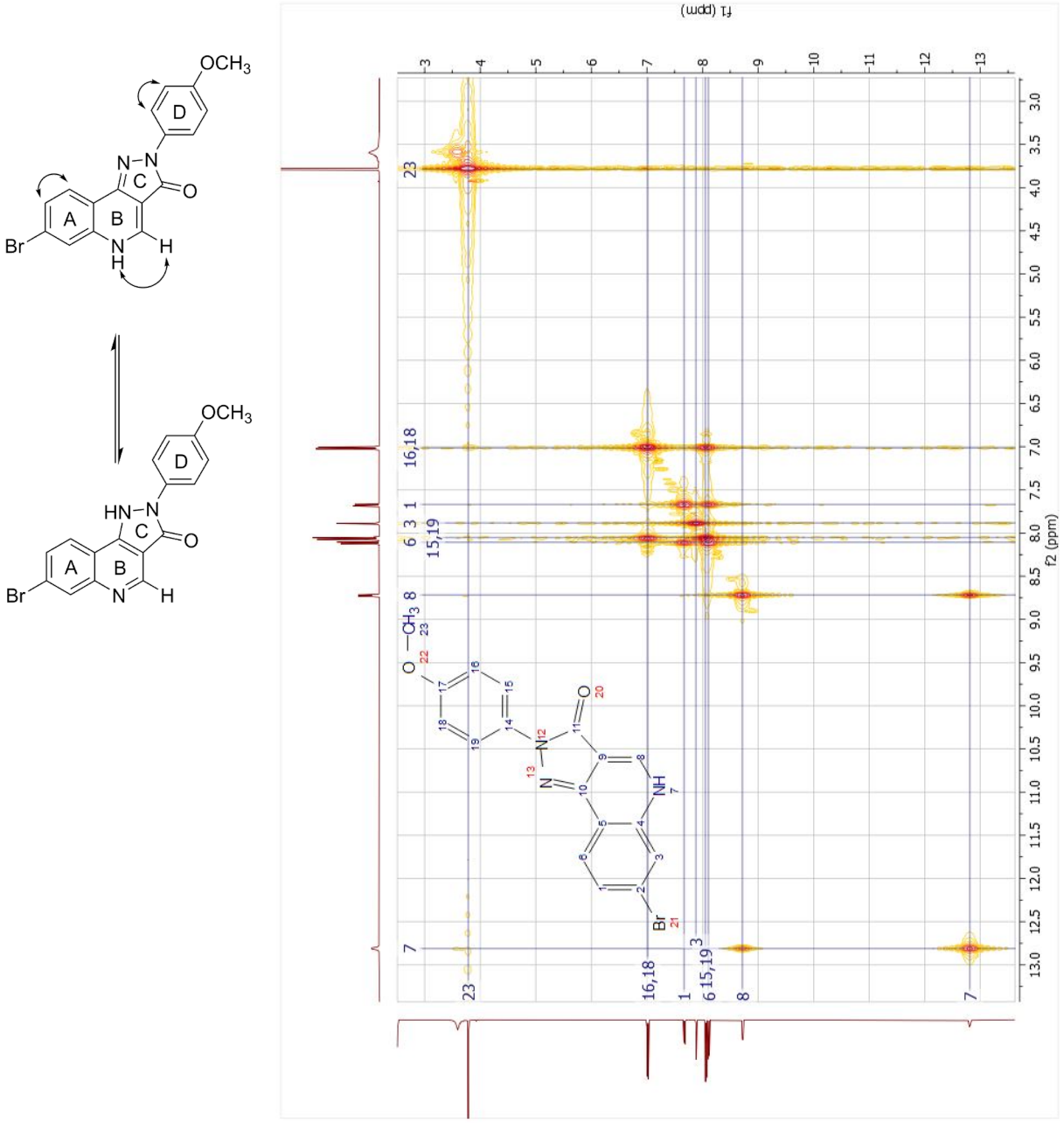

Analysis of the HMBC spectrum in **Figure 46** exhibited the correlations between the N-H proton (H7, 12.81ppm) and its neighboring carbon atoms (C9, C5, C3 and C4). These correlations would not be observed if the C-ring nitrogen atom was carrying the proton instead.

Figure 46: HMBC Spectrum Exhibiting Exchangeable of Proton Position of **LAU 463 (8n)**

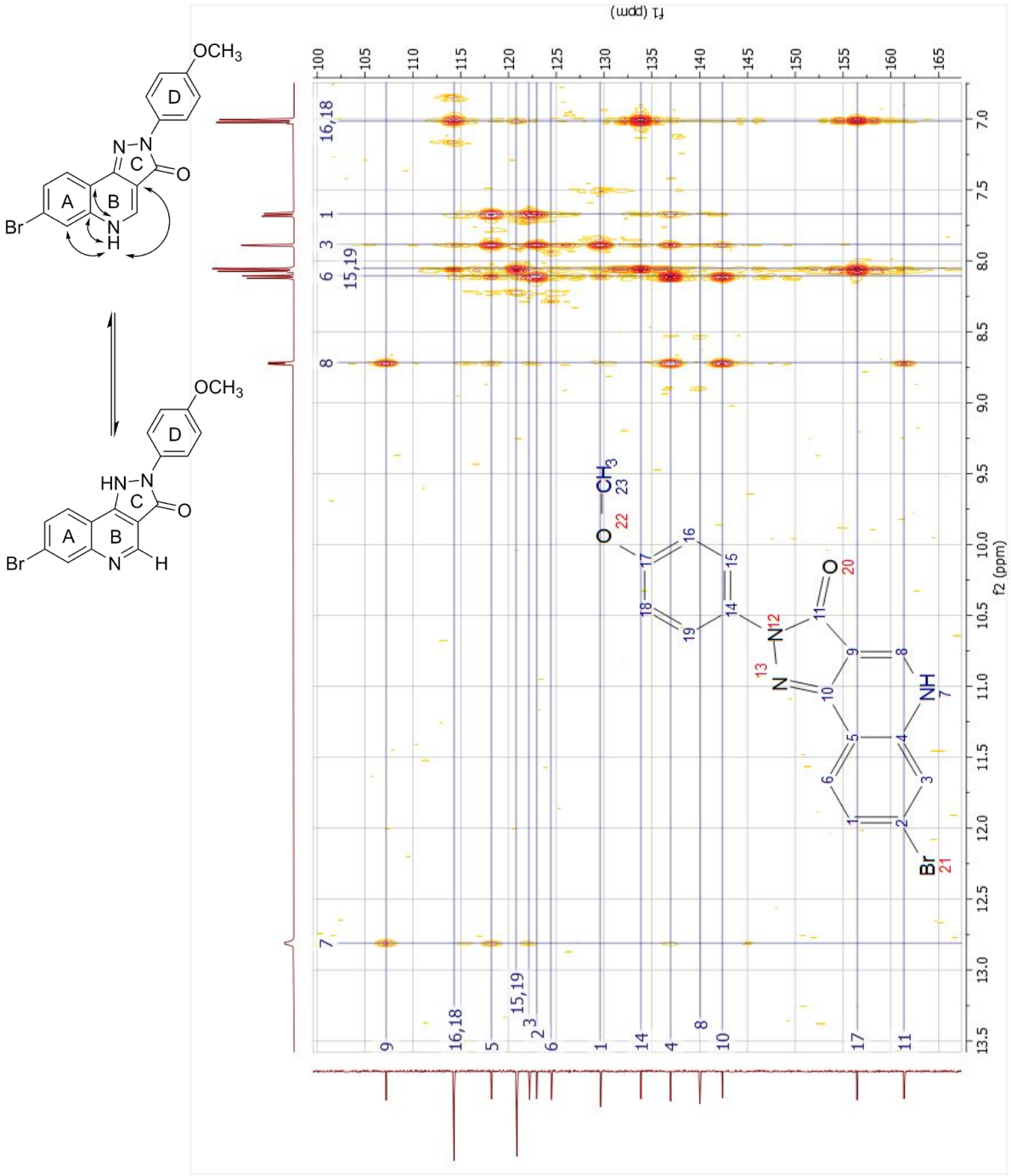

1.20.1. NMR Spectra of DK-I-56-1 (8b)

1.20.1.1. ^{1}H NMR of DK-I-56-1 (8b)

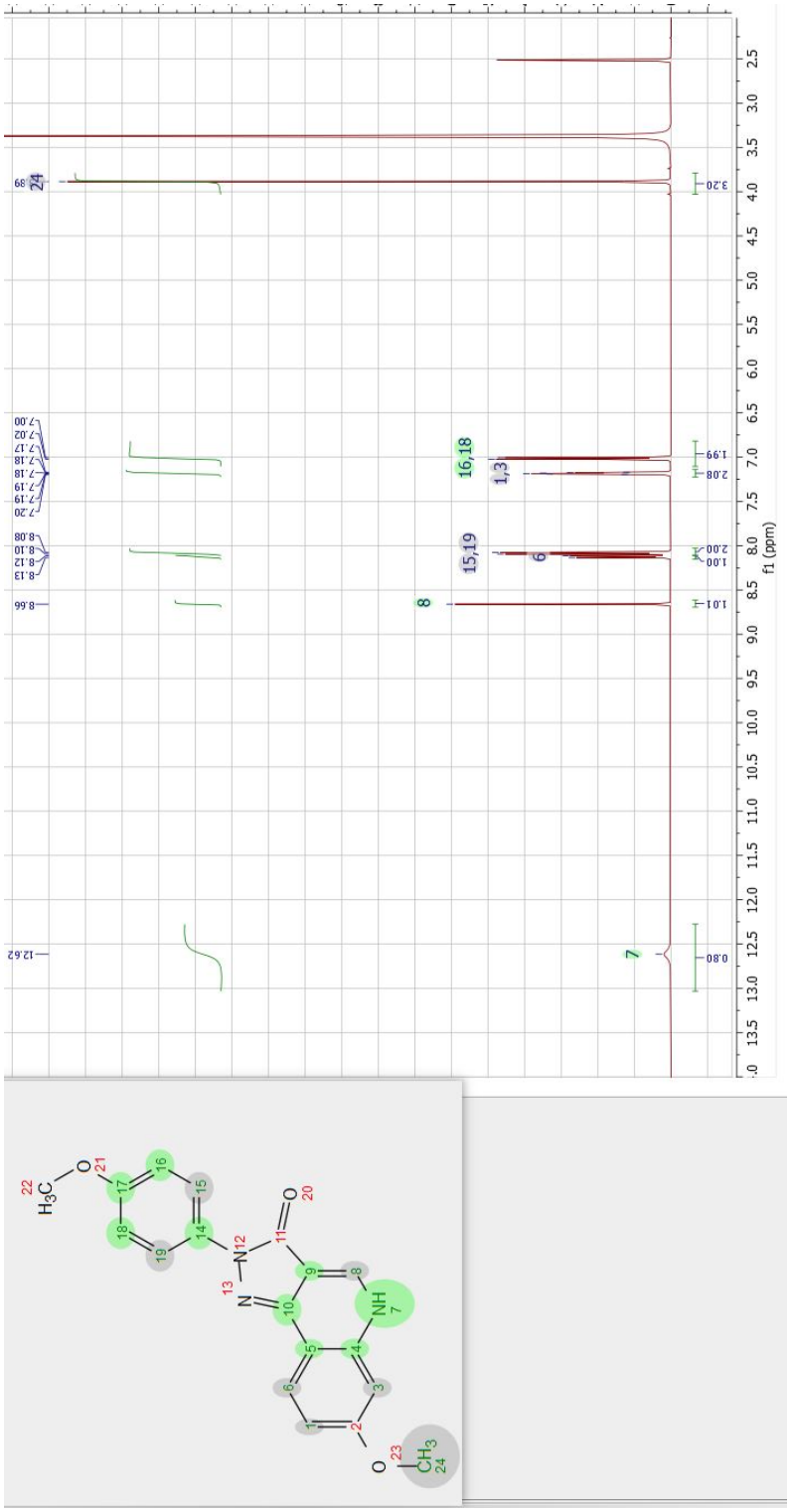

1.20.1.2. ^{13}C NMR of DK-I-56-1 (8b)

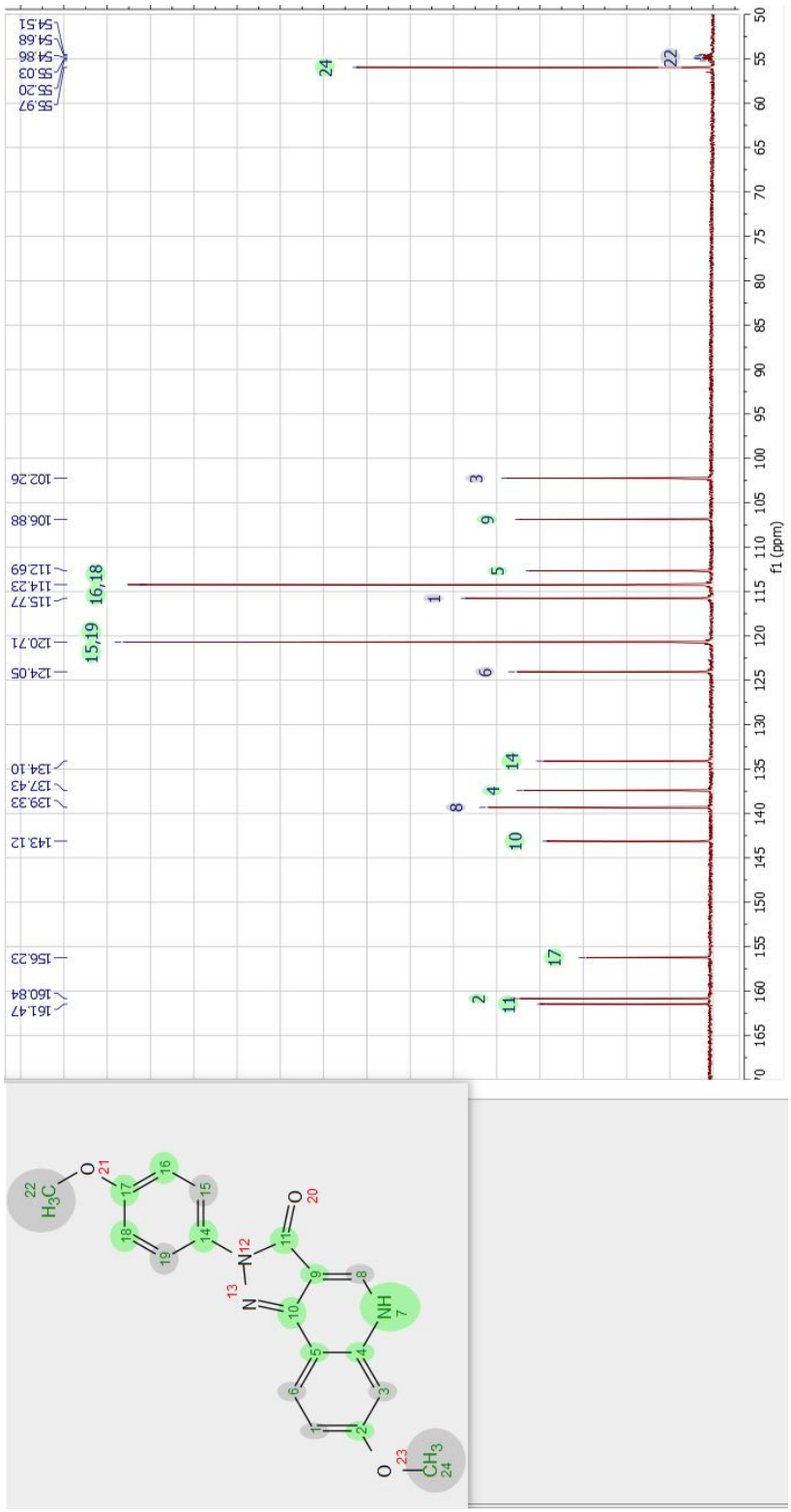

1.20.1.3. COSY Spectrum of DK-I-56-1 (8b)

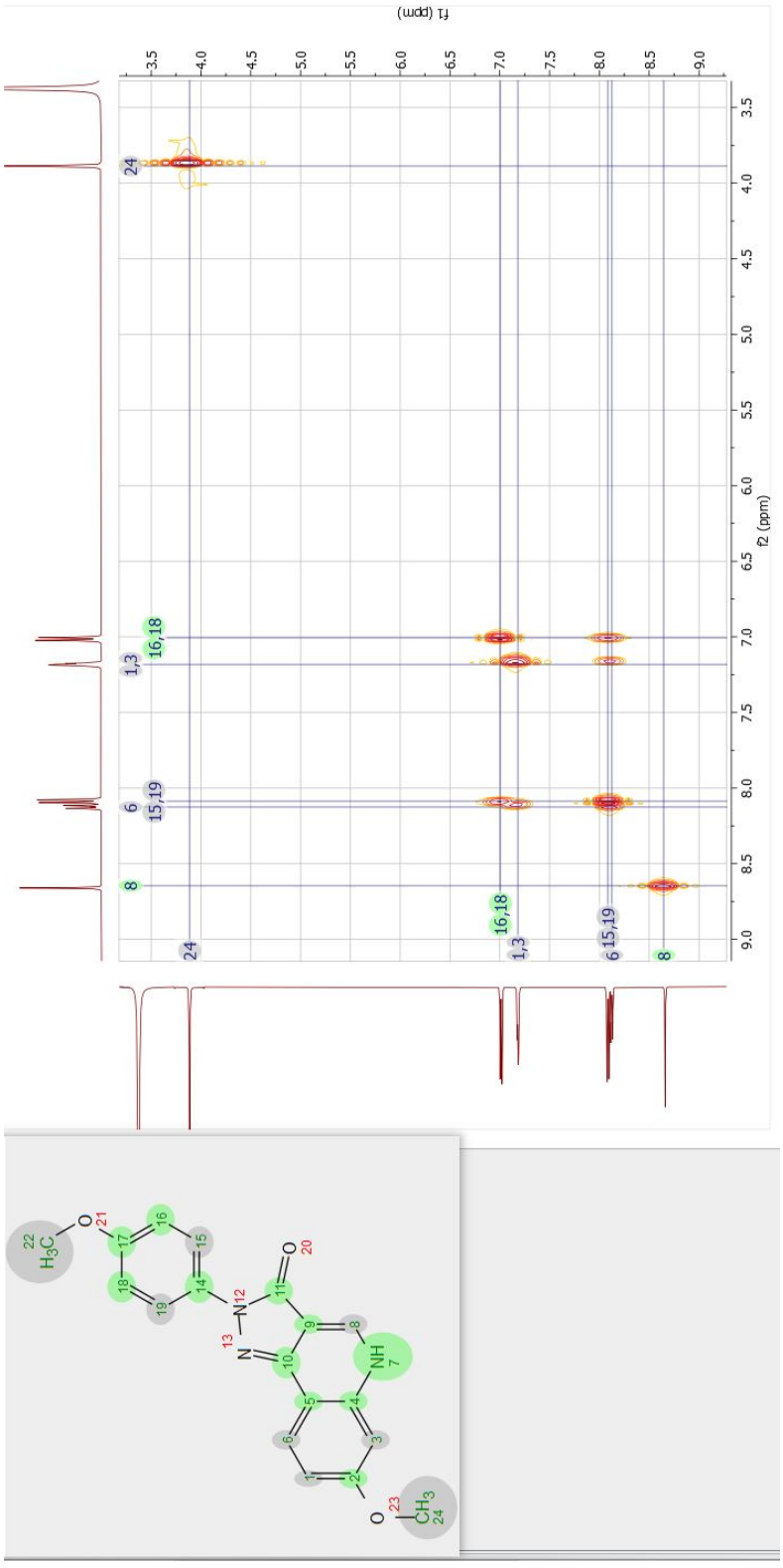

1.20.1.4. ^{1}H-^{13}C-HSQC Spectrum of DK-I-56-1 (8b)

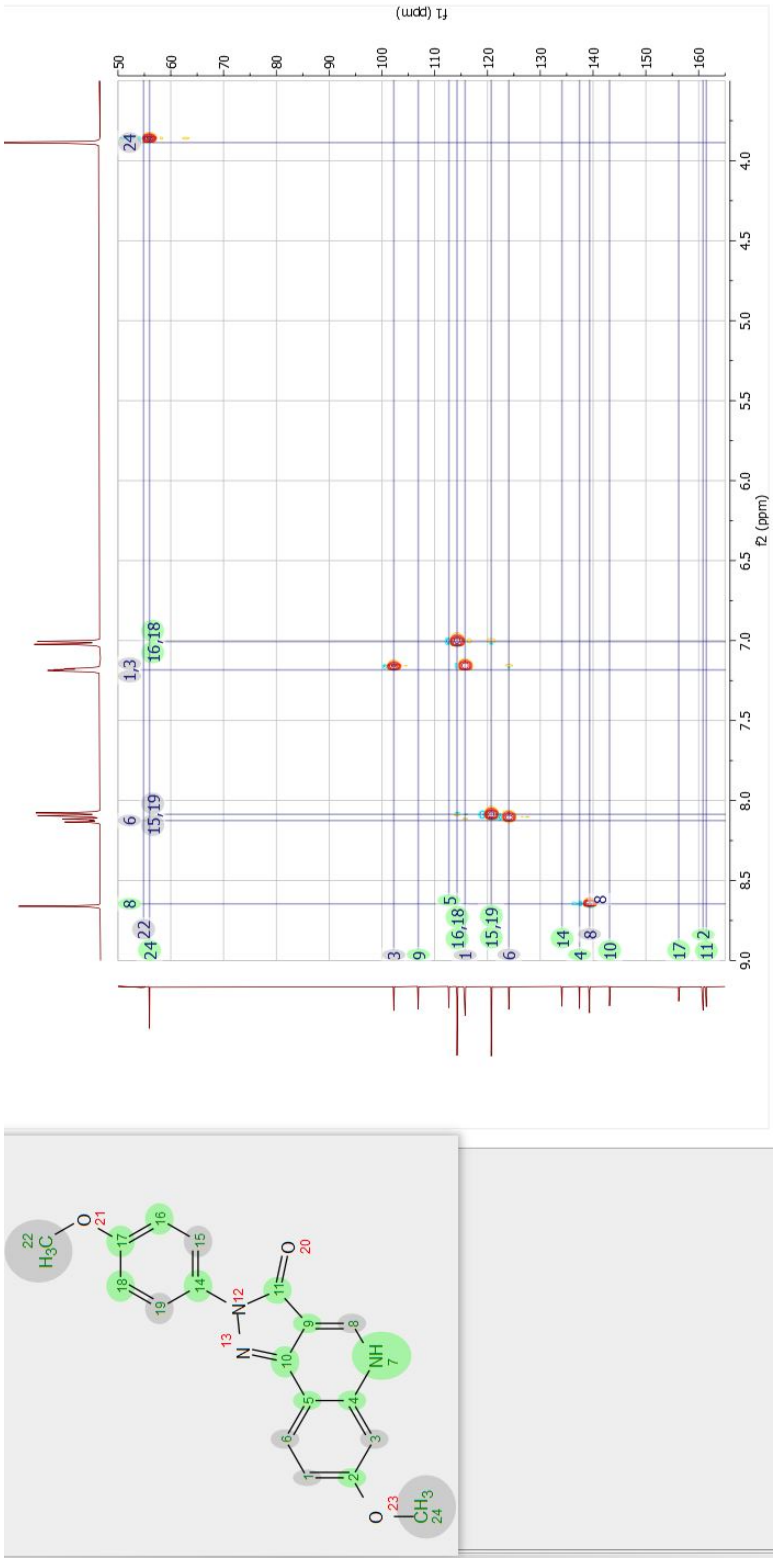

1.20.1.5. ^{1}H-^{13}C-HMBC Spectrum of DK-I-56-1 (8b)

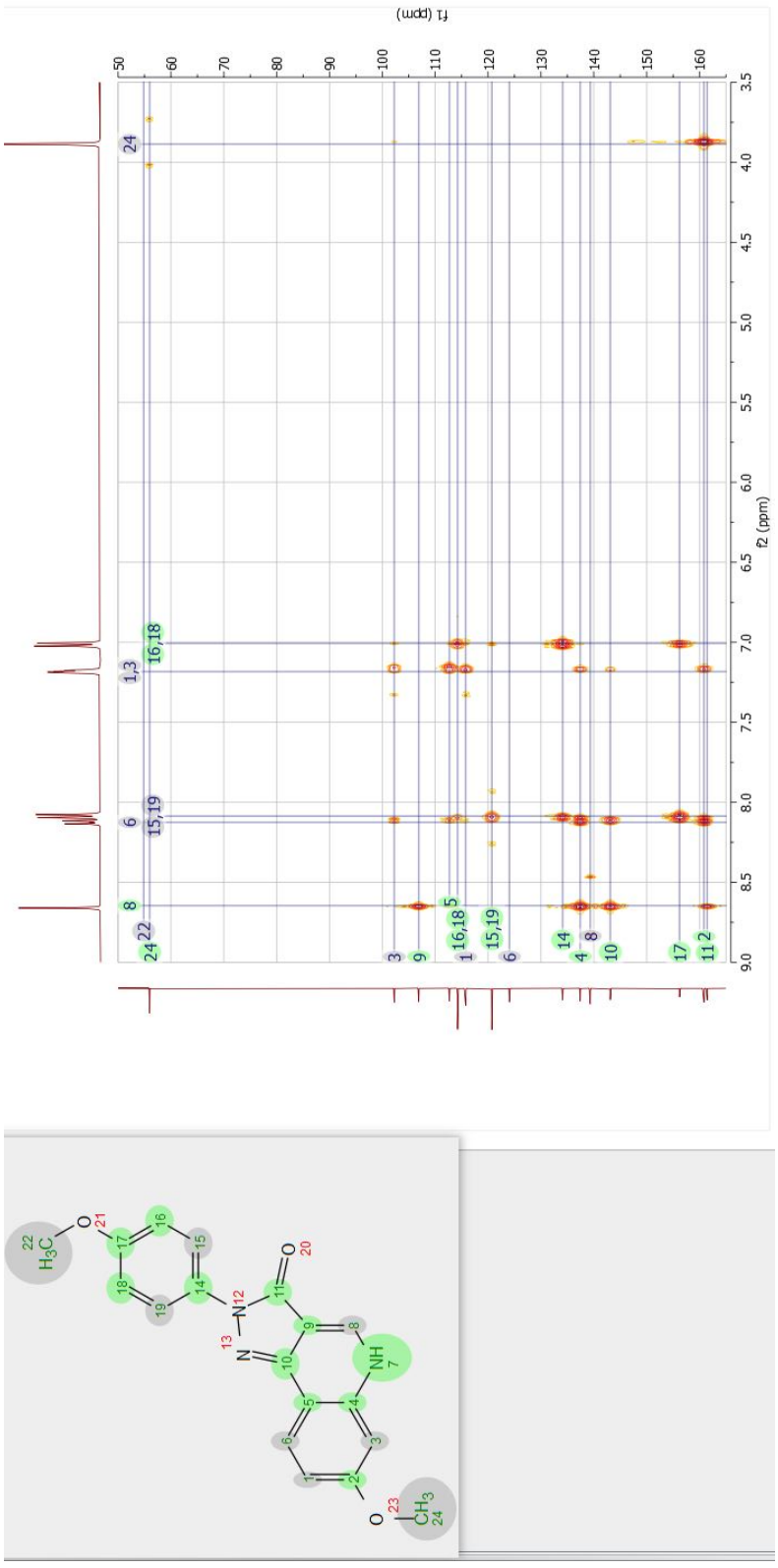

1.20.2. NMR Spectra of DK-I-58-1 (8o)

1.20.2.1. ^{1}H NMR of DK-I-58-1 (8o)

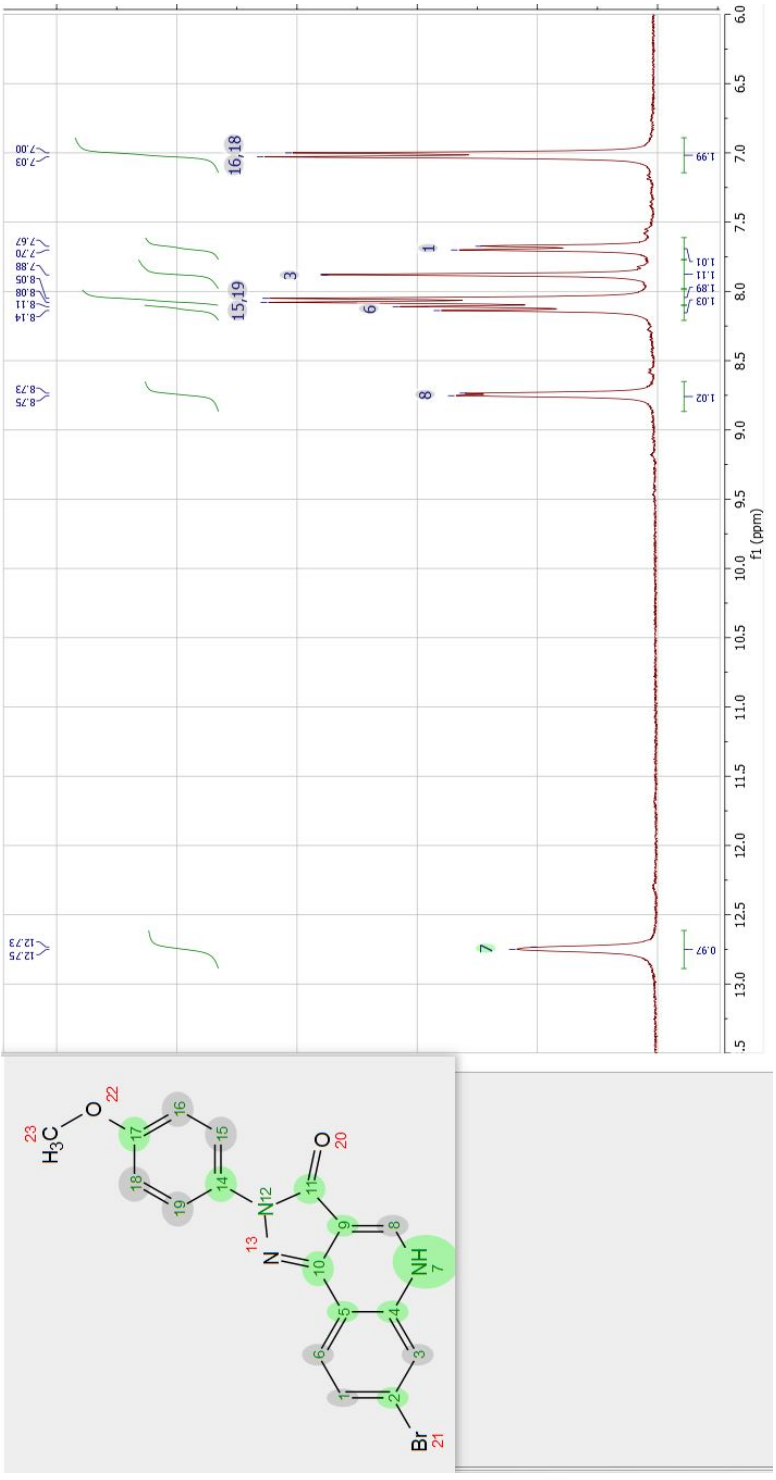

1.20.2.2. ^{13}C NMR of DK-I-58-1 (8o)

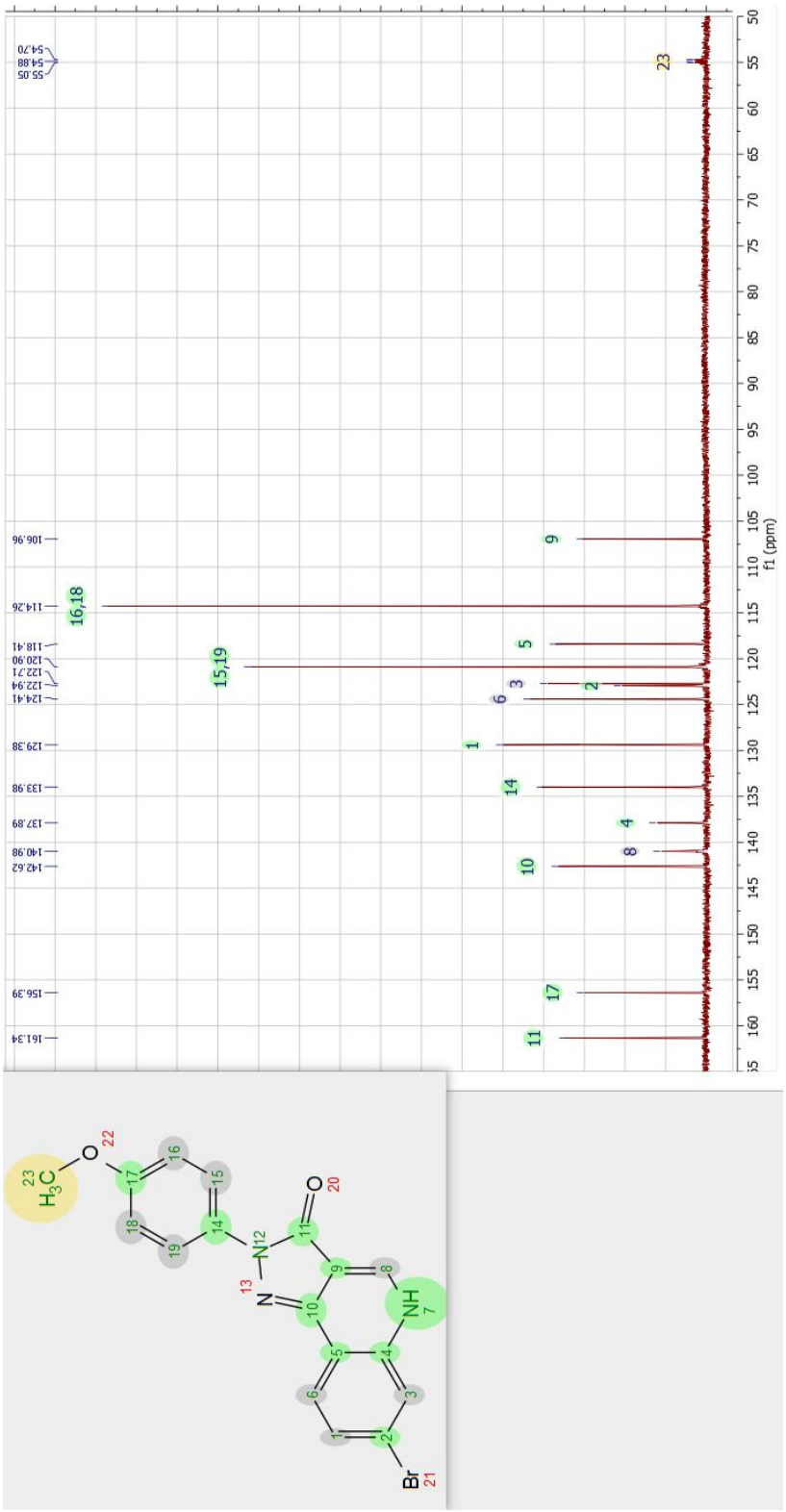

1.20.2.3. COSY Spectrum of DK-I-58-1 (8o)

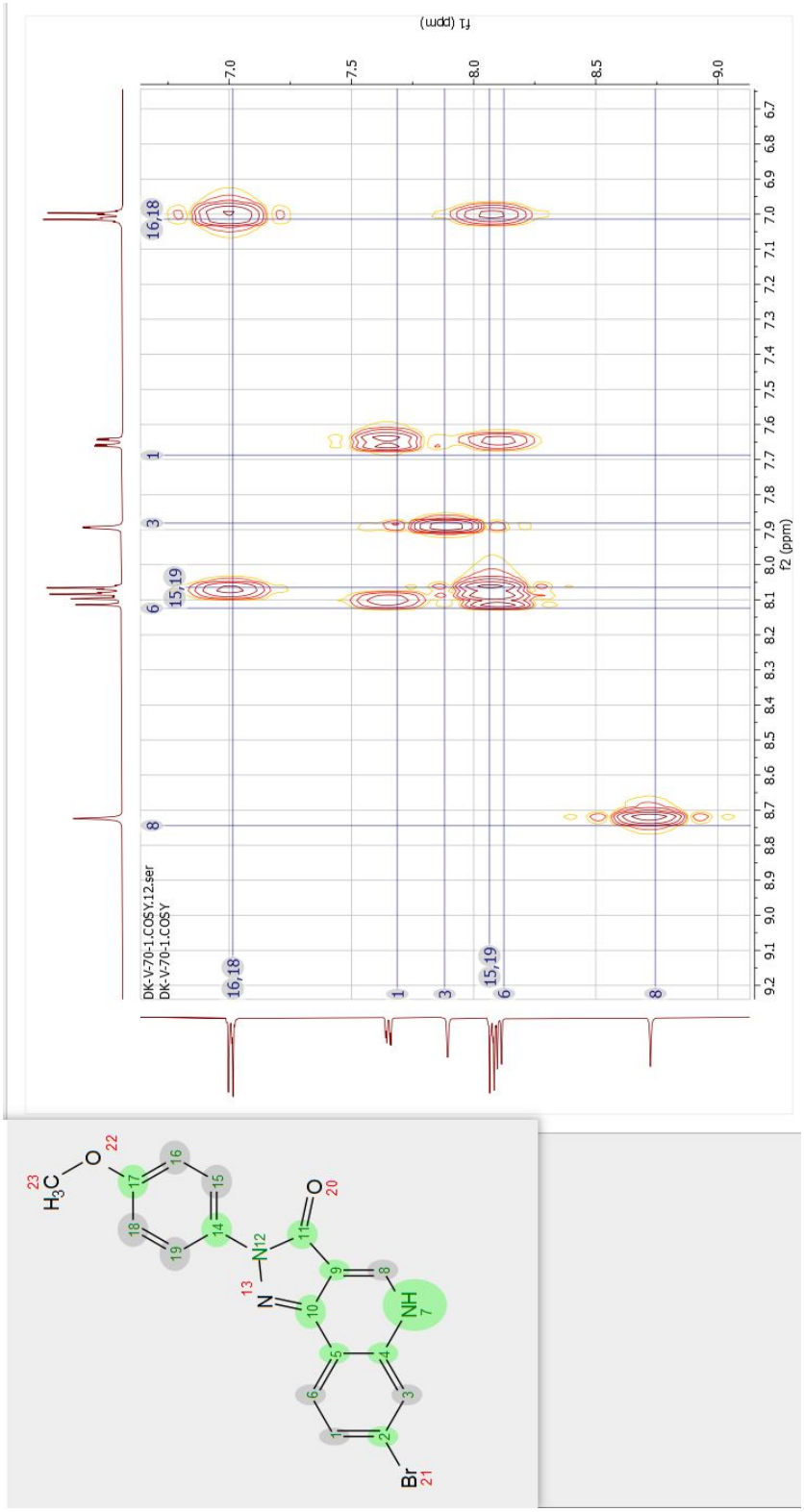

1.20.2.4. ^{1}H-^{13}C-HSQC Spectrum of DK-I-58-1 (8o)

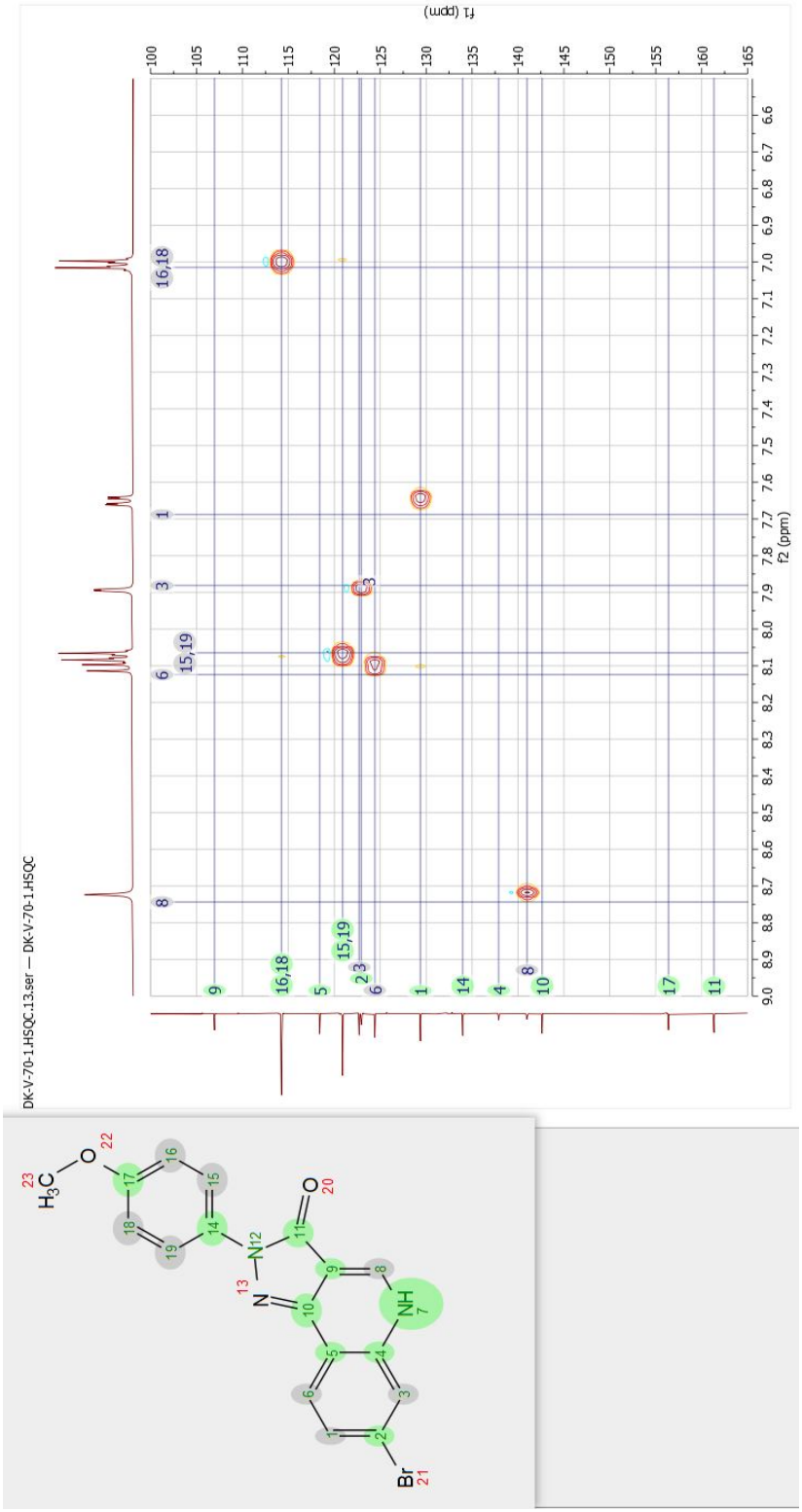

1.20.2.5. ^{1}H-^{13}C-HMBC Spectrum of DK-I-58-1 (8o)

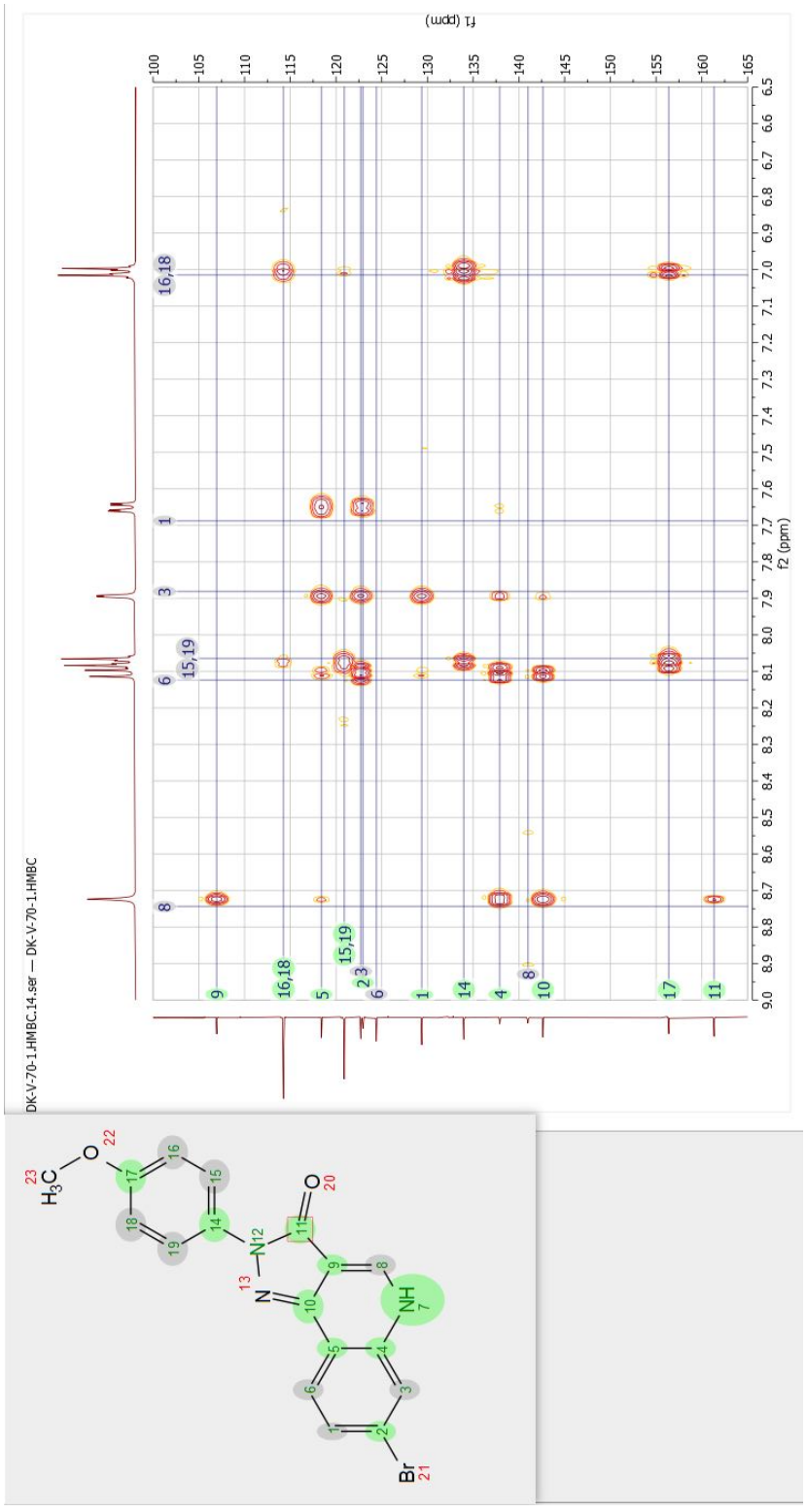

1.20.3. NMR Spectra of DK-I-59-1 (8j)

1.20.3.1. ^{1}H NMR of DK-I-59-1 (8j)

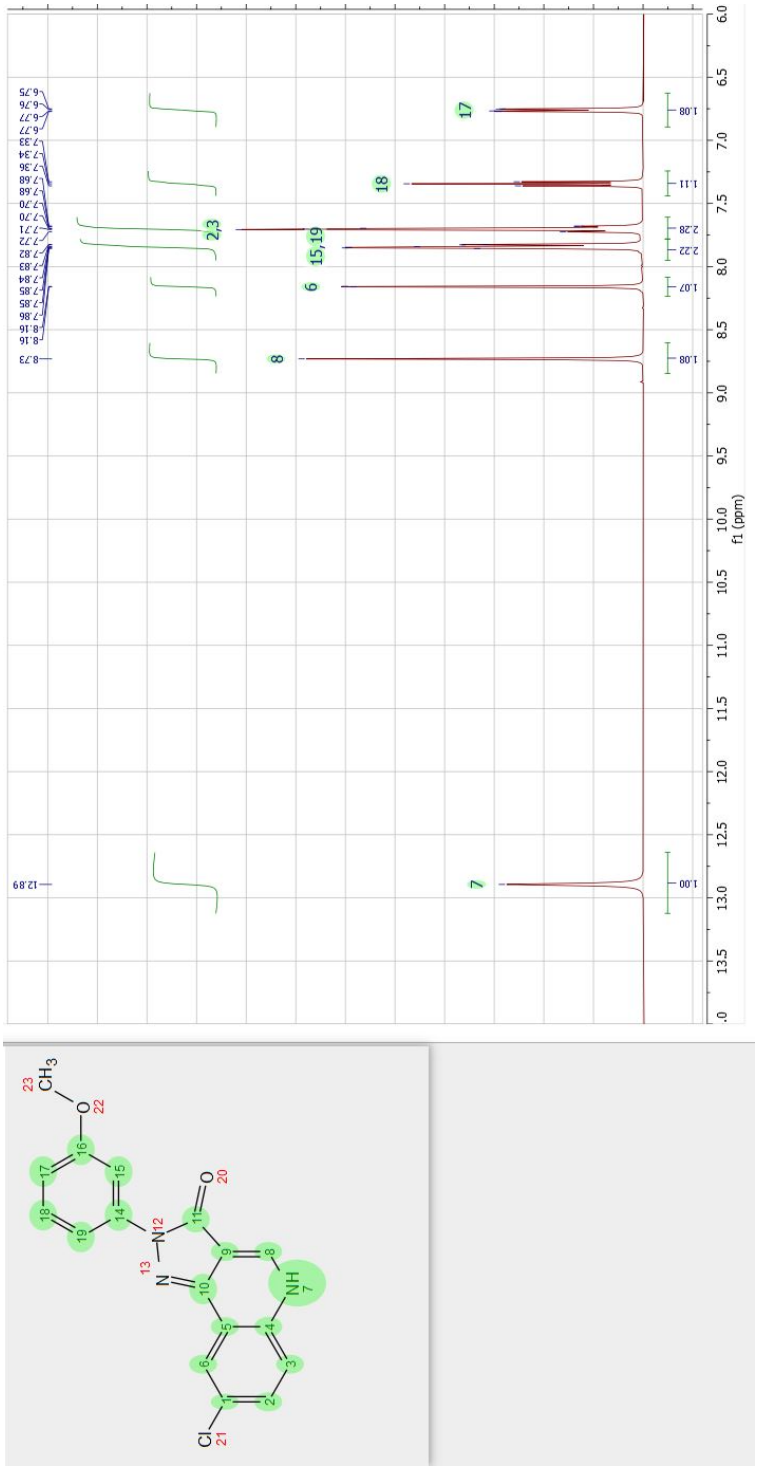

1.20.3.2. ^{13}C NMR of DK-I-59-1 (8j)

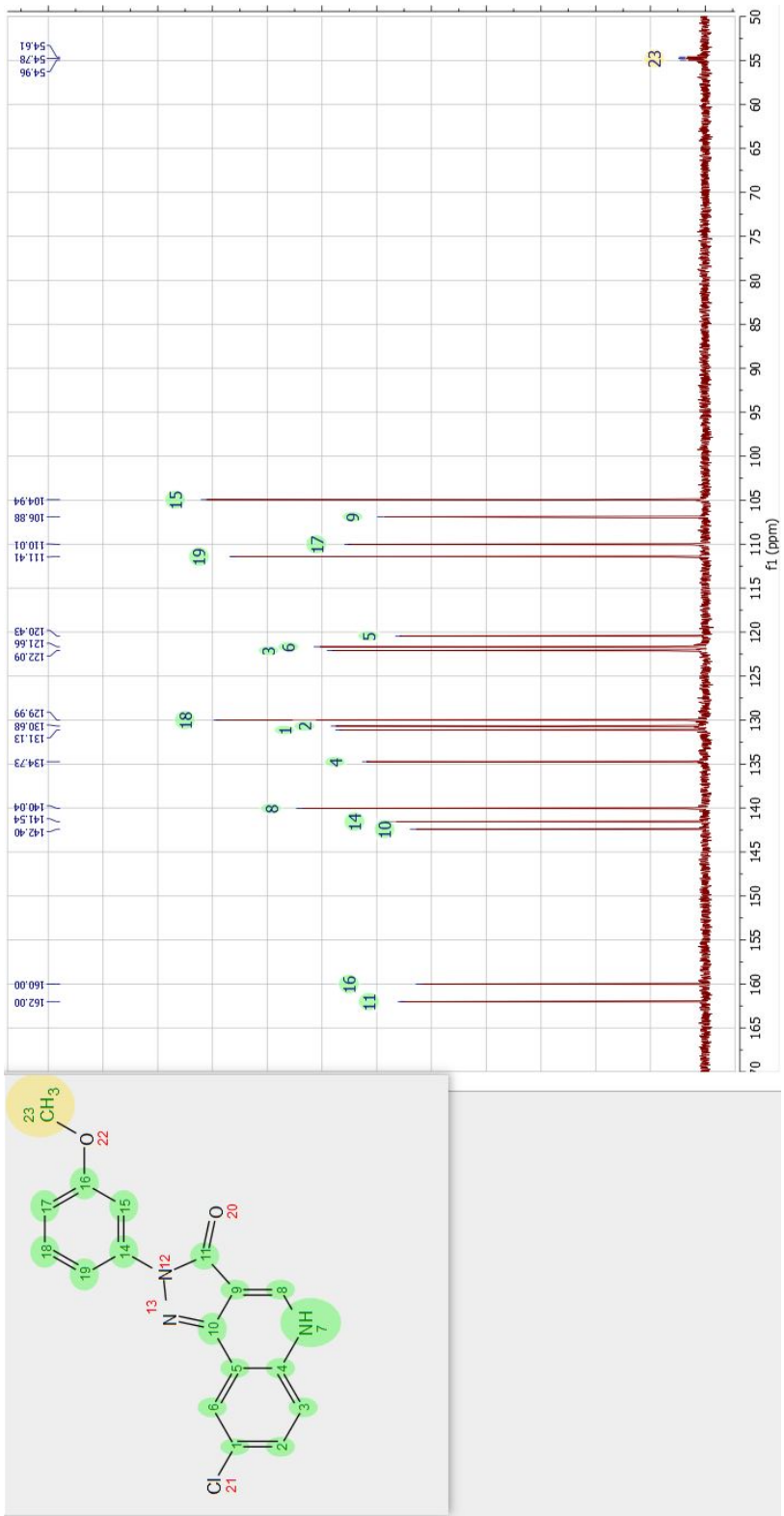

1.20.3.3. COSY Spectrum of DK-I-59-1 (8j)

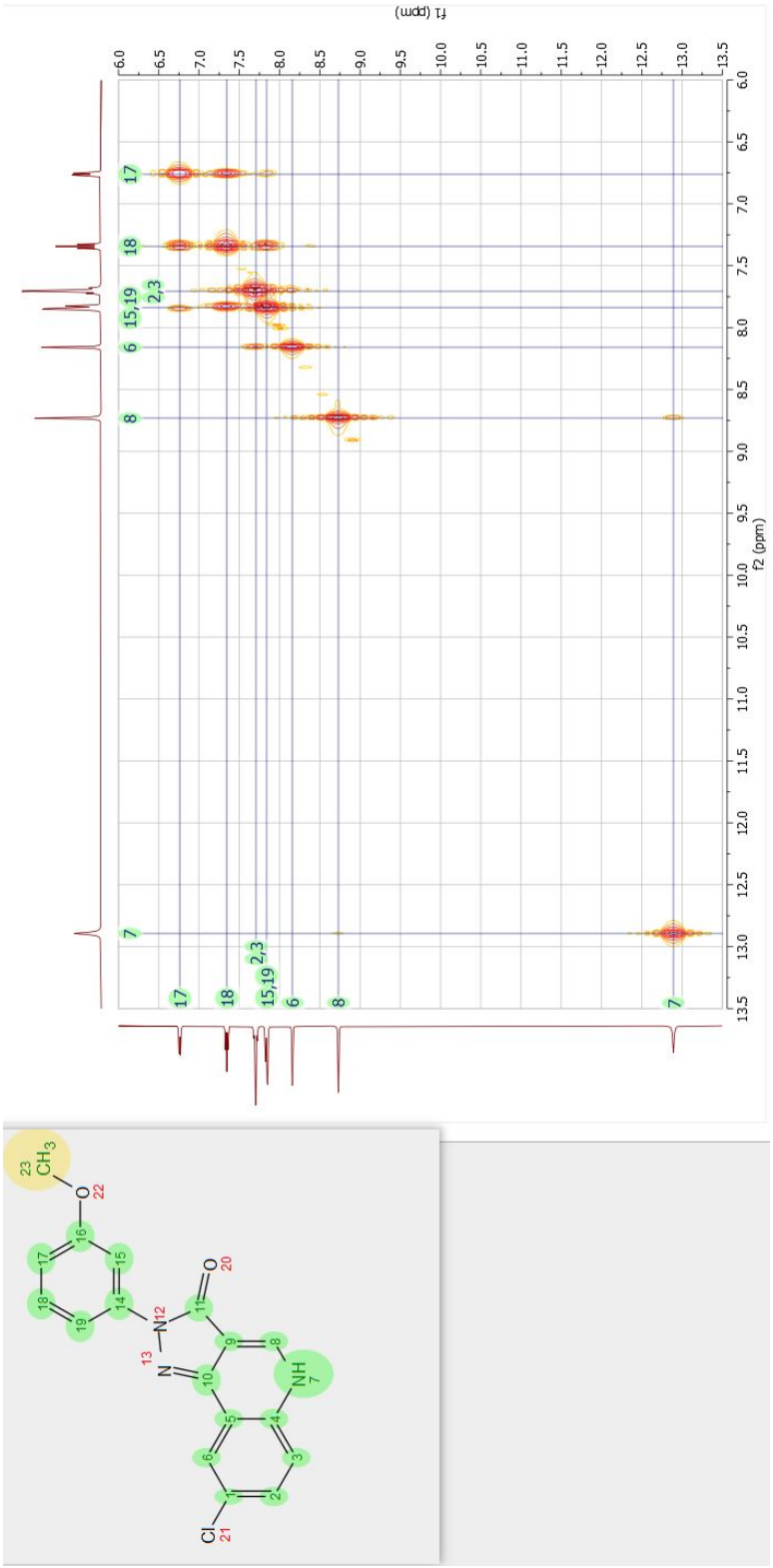

1.20.3.4. ^{1}H-^{13}C-HSQC Spectrum of DK-I-59-1 (8j)

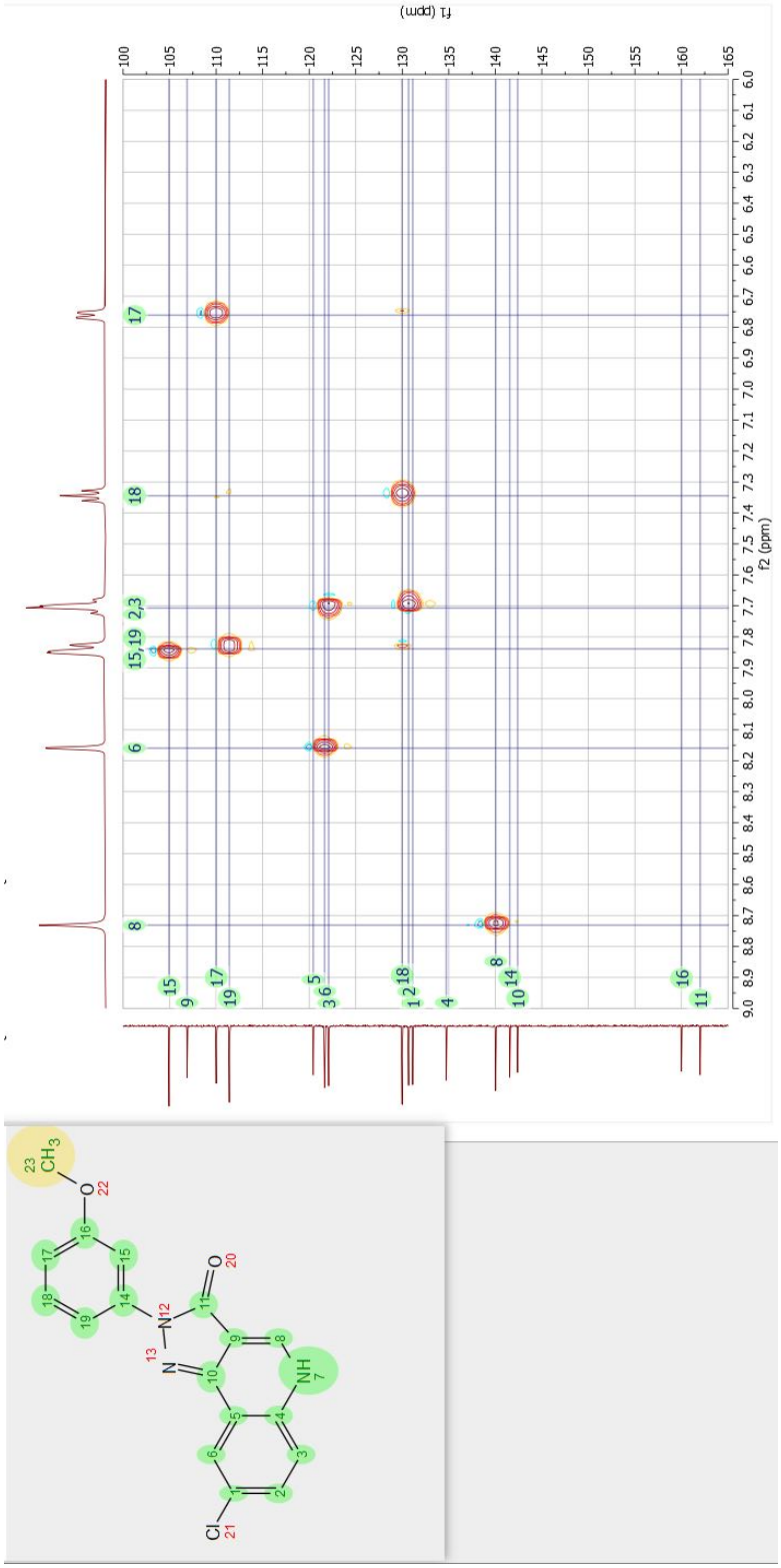

1.20.3.5. ^{1}H-^{13}C-HMBC Spectrum of DK-I-59-1 (8j)

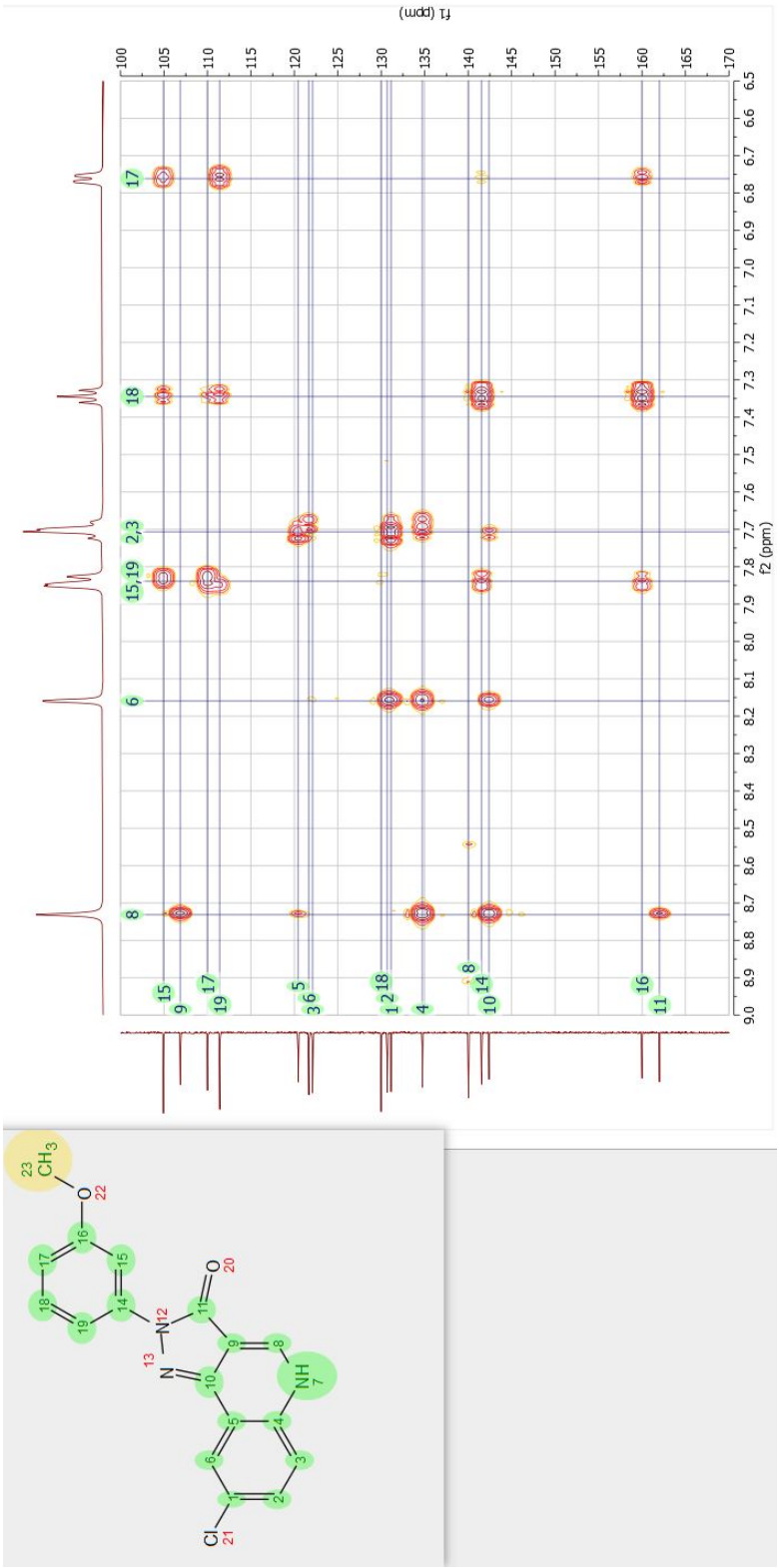

1.20.4. NMR Spectra of DK-I-87-1 (8m)

1.20.4.1. ^{1}H NMR of DK-I-87-1 (8m)

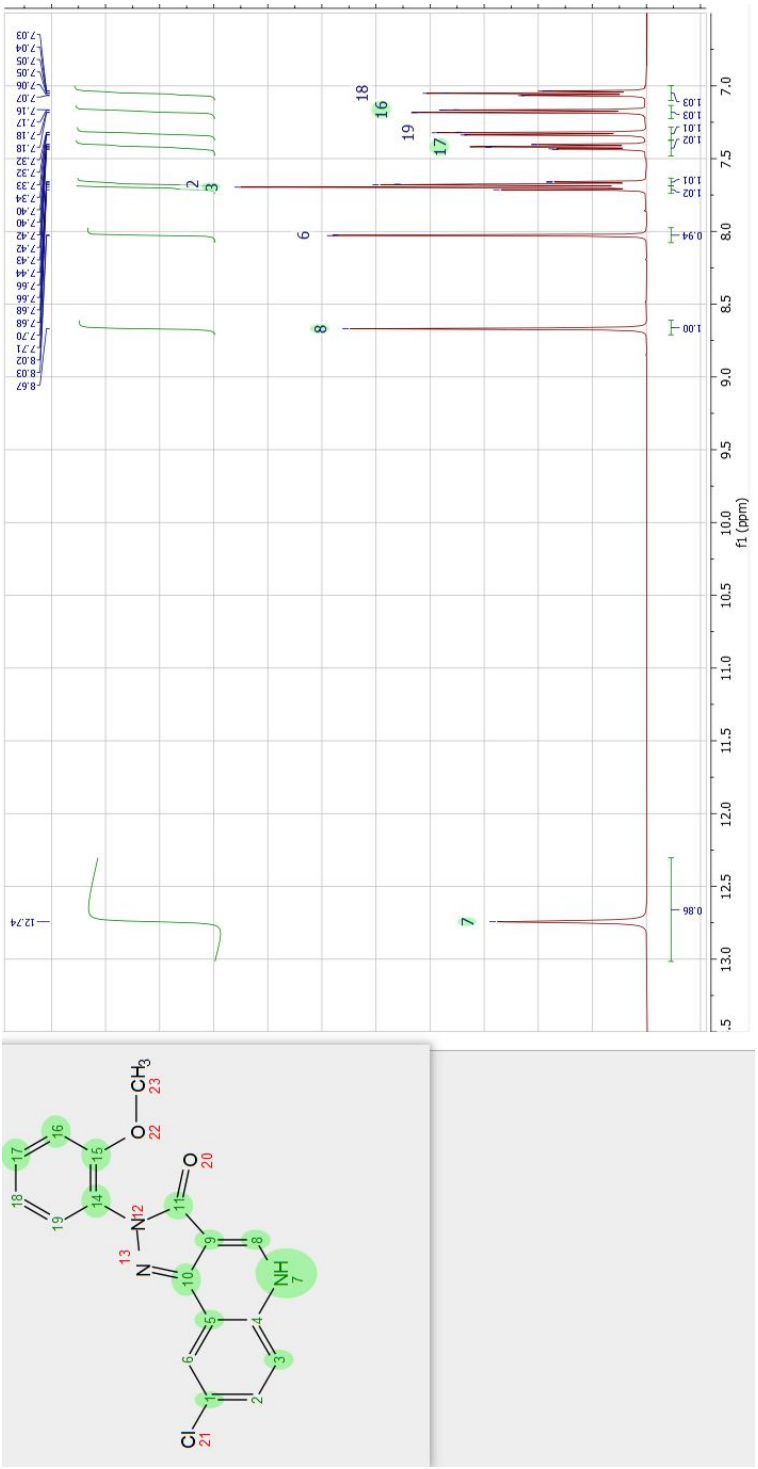

1.20.4.2. ^{13}C NMR of DK-I-87-1 (8m)

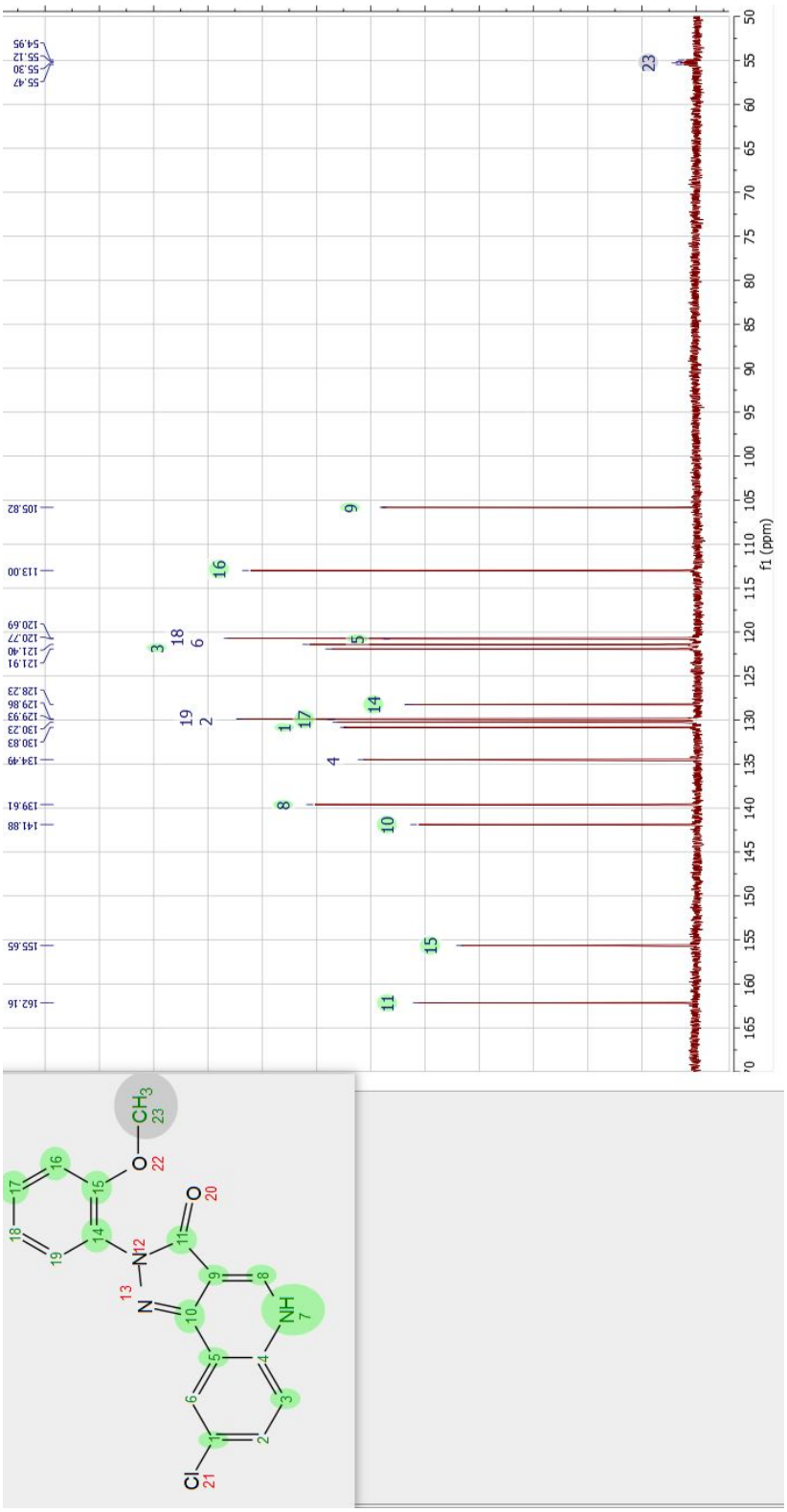

1.20.4.3. COSY Spectrum of DK-I-87-1 (8m)

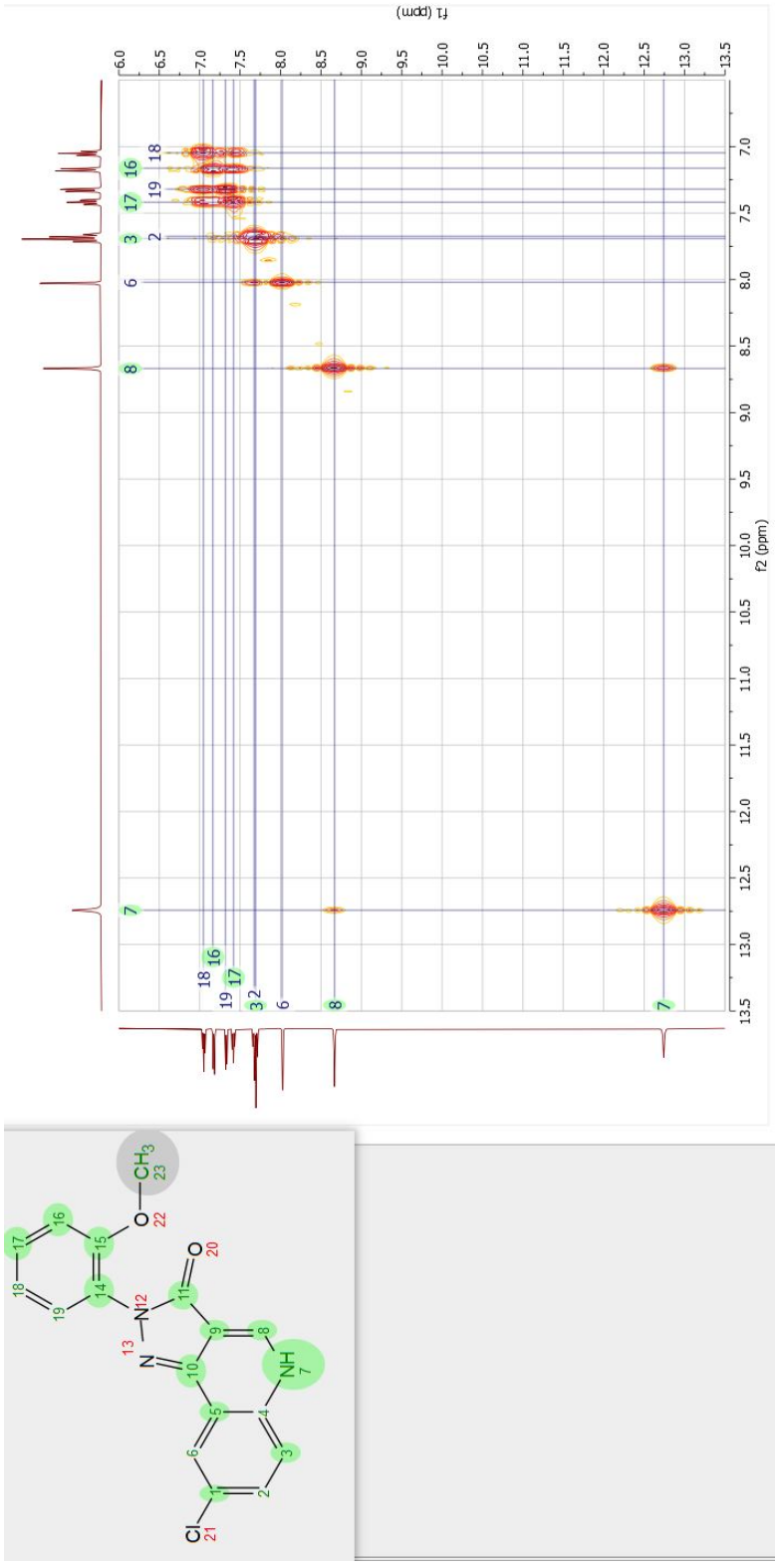

1.20.4.4. ^{1}H-^{13}C-HSQC Spectrum of DK-I-87-1 (8m)

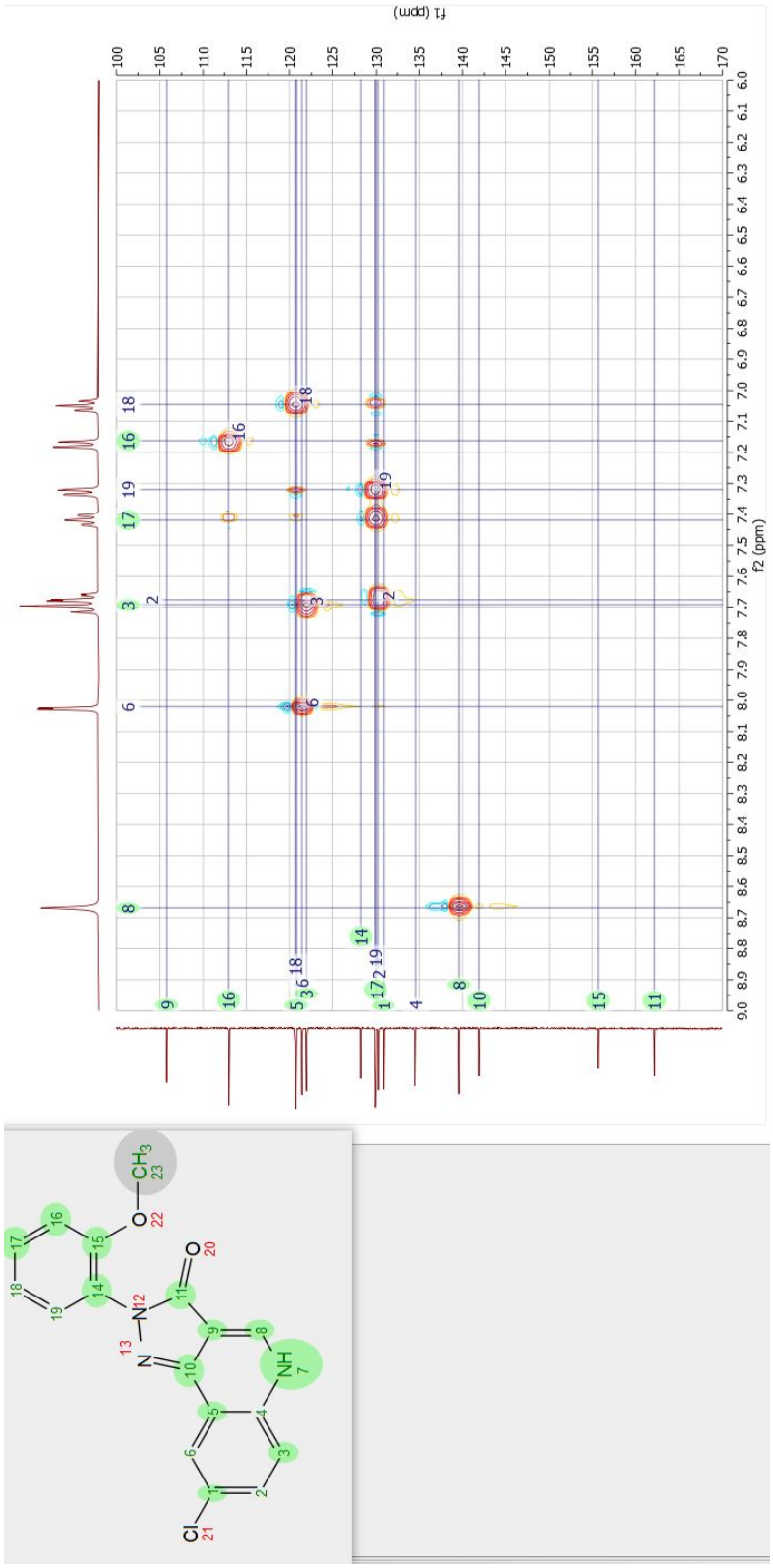

1.20.4.5. ^{1}H-^{13}C-HMBC Spectrum of DK-I-87-1 (8m)

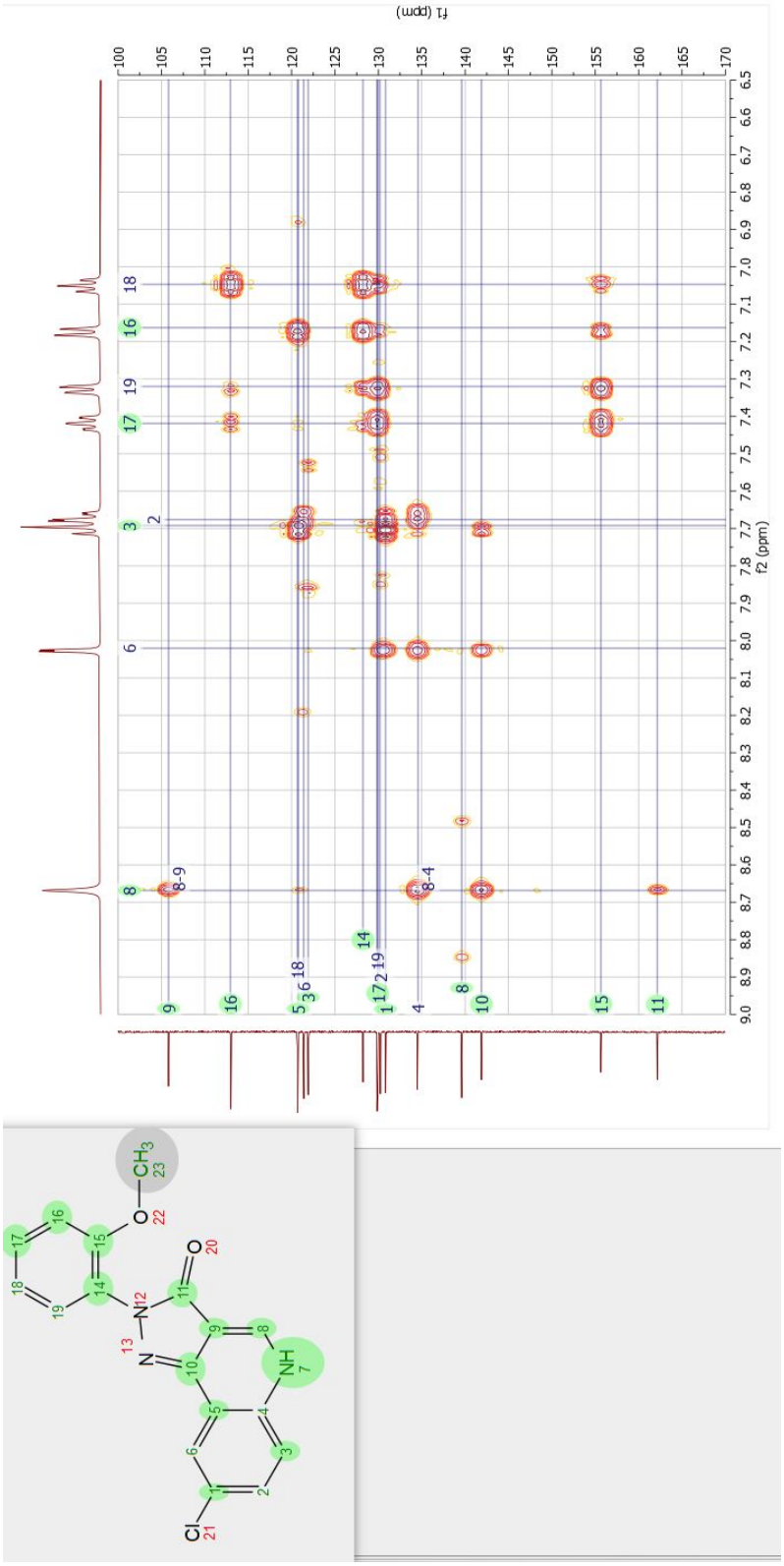

1.20.5. NMR Spectra of DK-I-86-1 (13c)

1.20.5.1. ^{1}H NMR of DK-I-86-1 (13c)

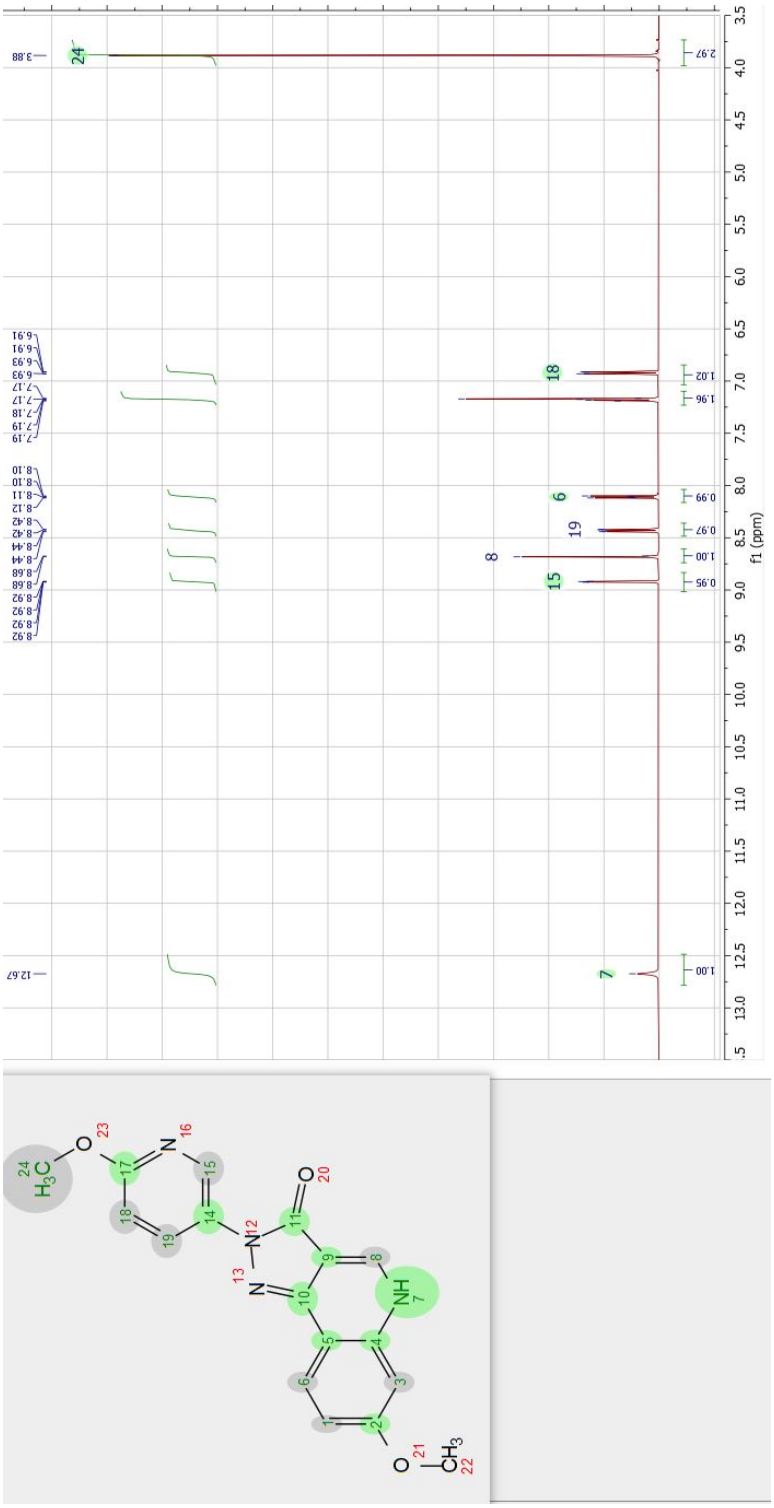

1.20.5.2. ^{13}C NMR of DK-I-86-1 (13c)

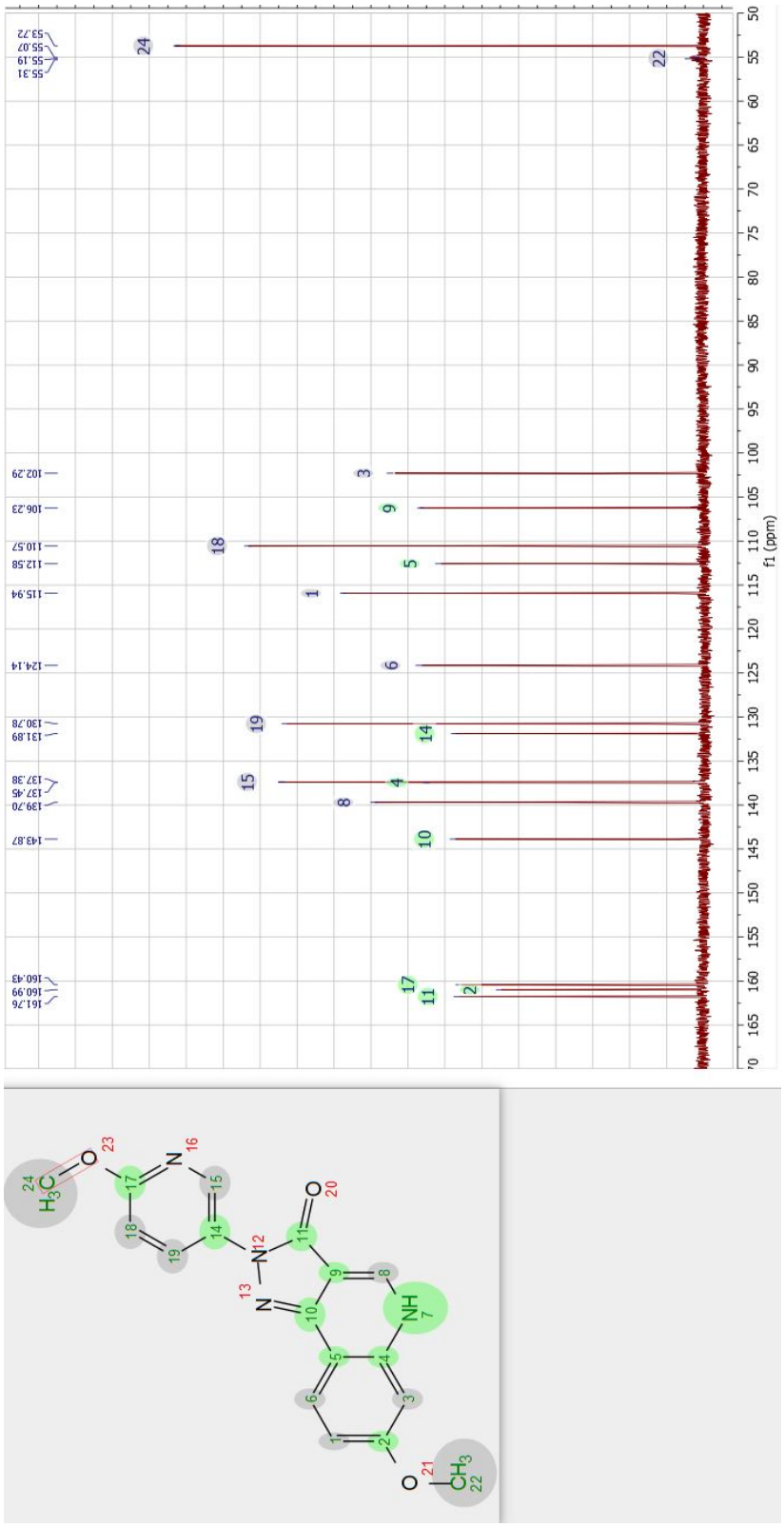

1.20.5.3. COSY Spectrum of DK-I-86-1 (13c)

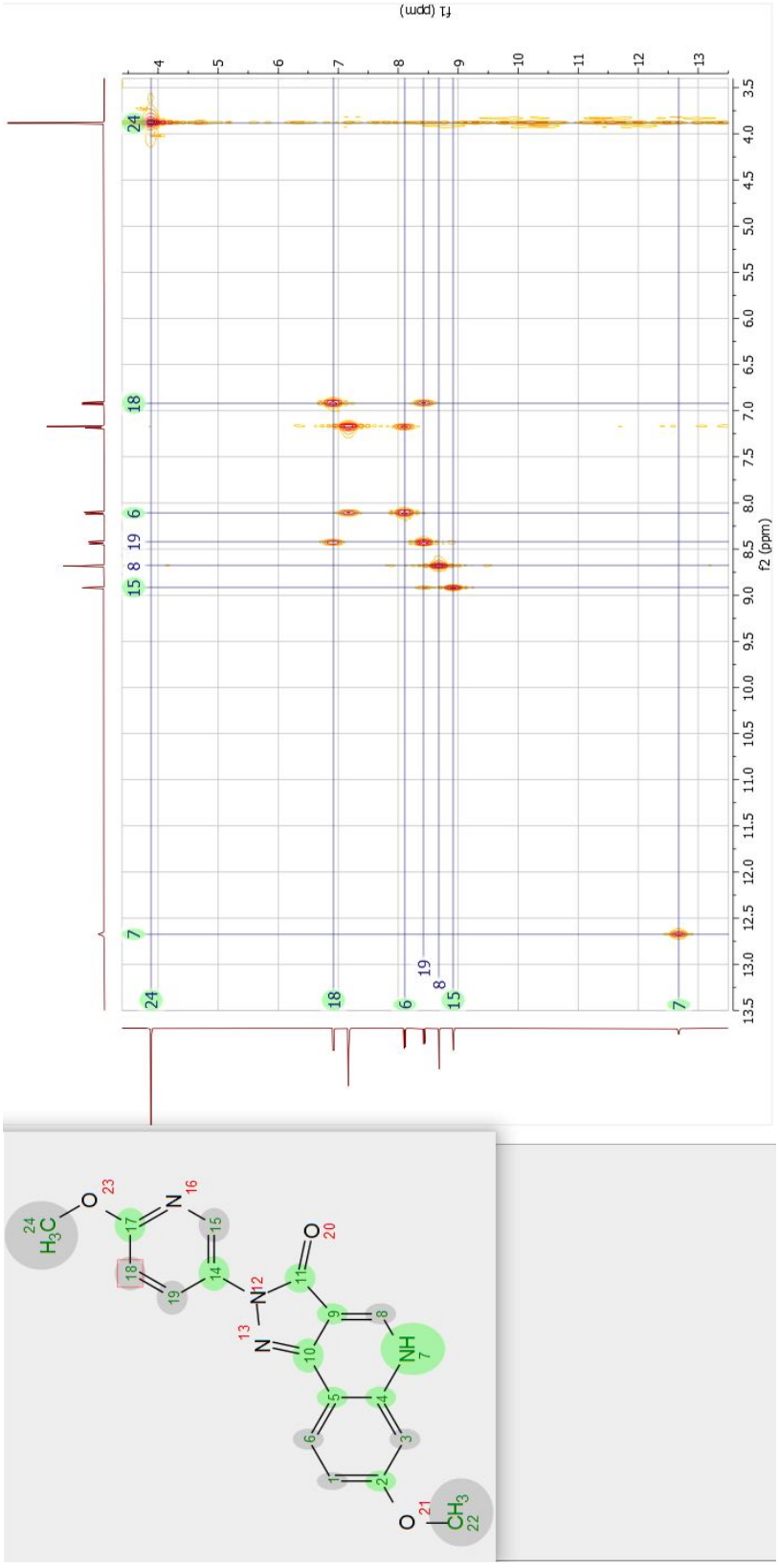

1.20.5.4. ^{1}H-^{13}C-HSQC Spectrum of DK-I-86-1 (13c)

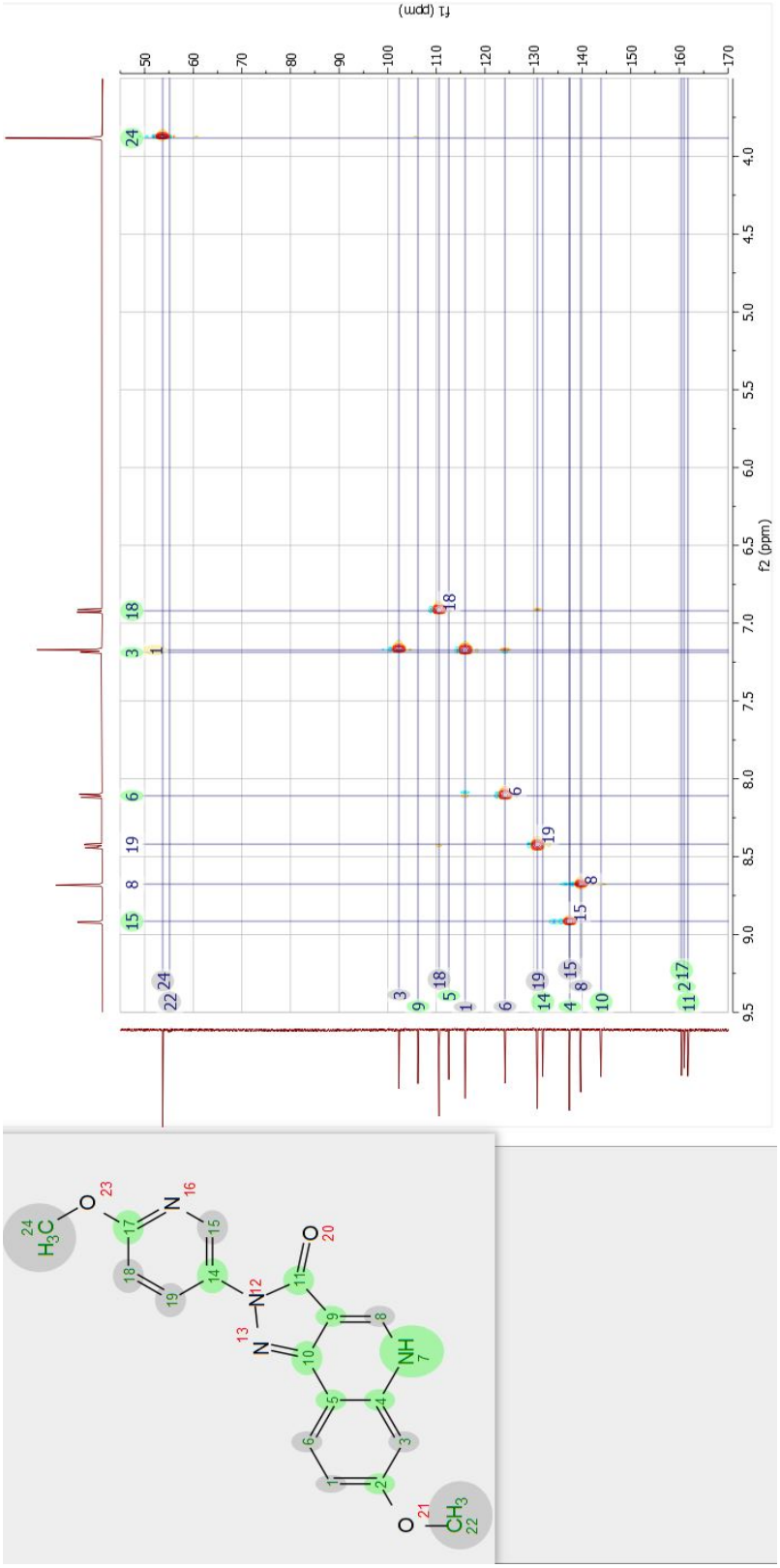

1.20.5.5. ^{1}H-^{13}C-HMBC Spectrum of DK-I-86-1 (13c)

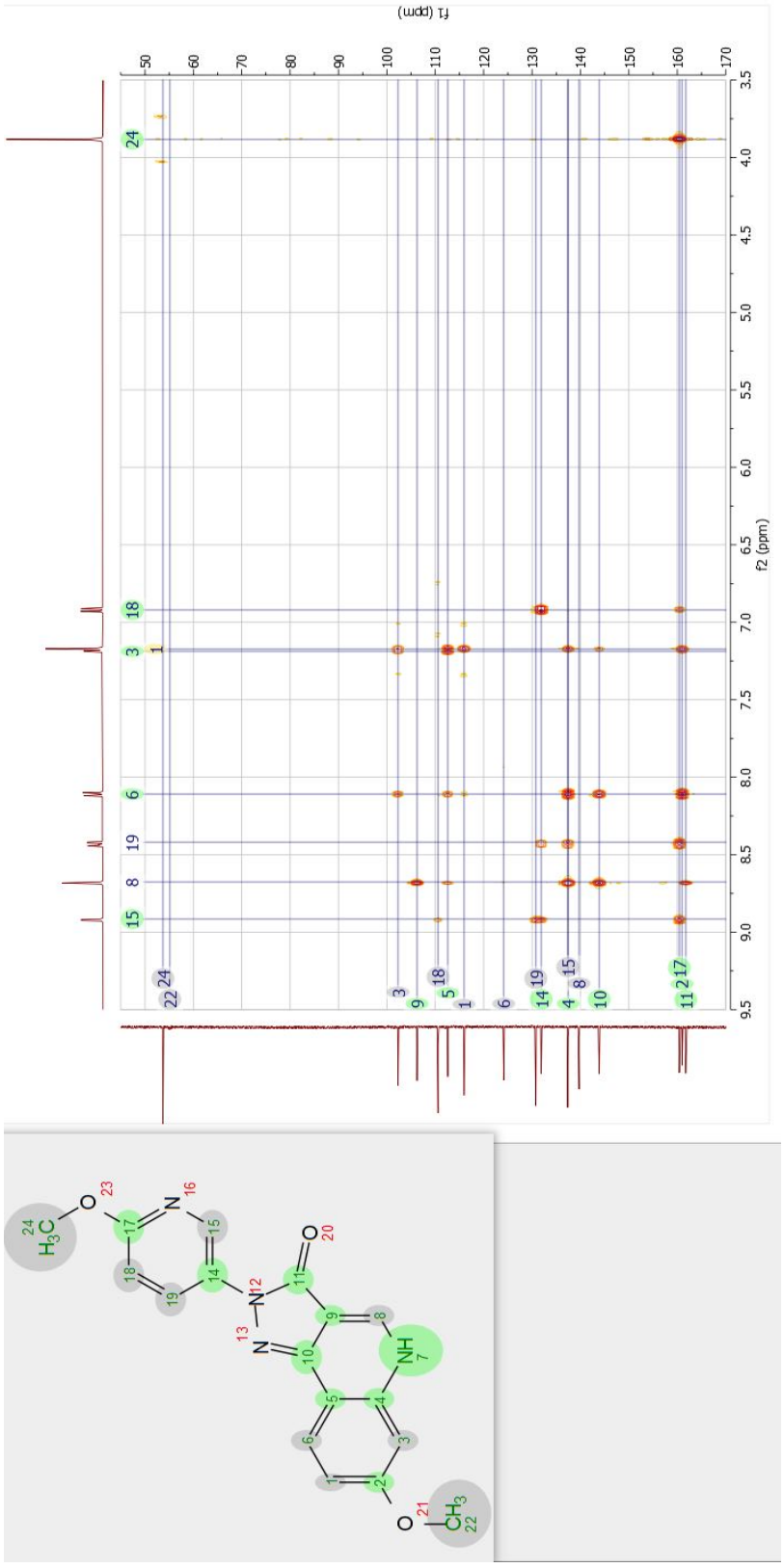

1.20.6. NMR Spectra of DK-II-58-1 (13h)

1.20.6.1. ^{1}H NMR of DK-II-58-1 (13h)

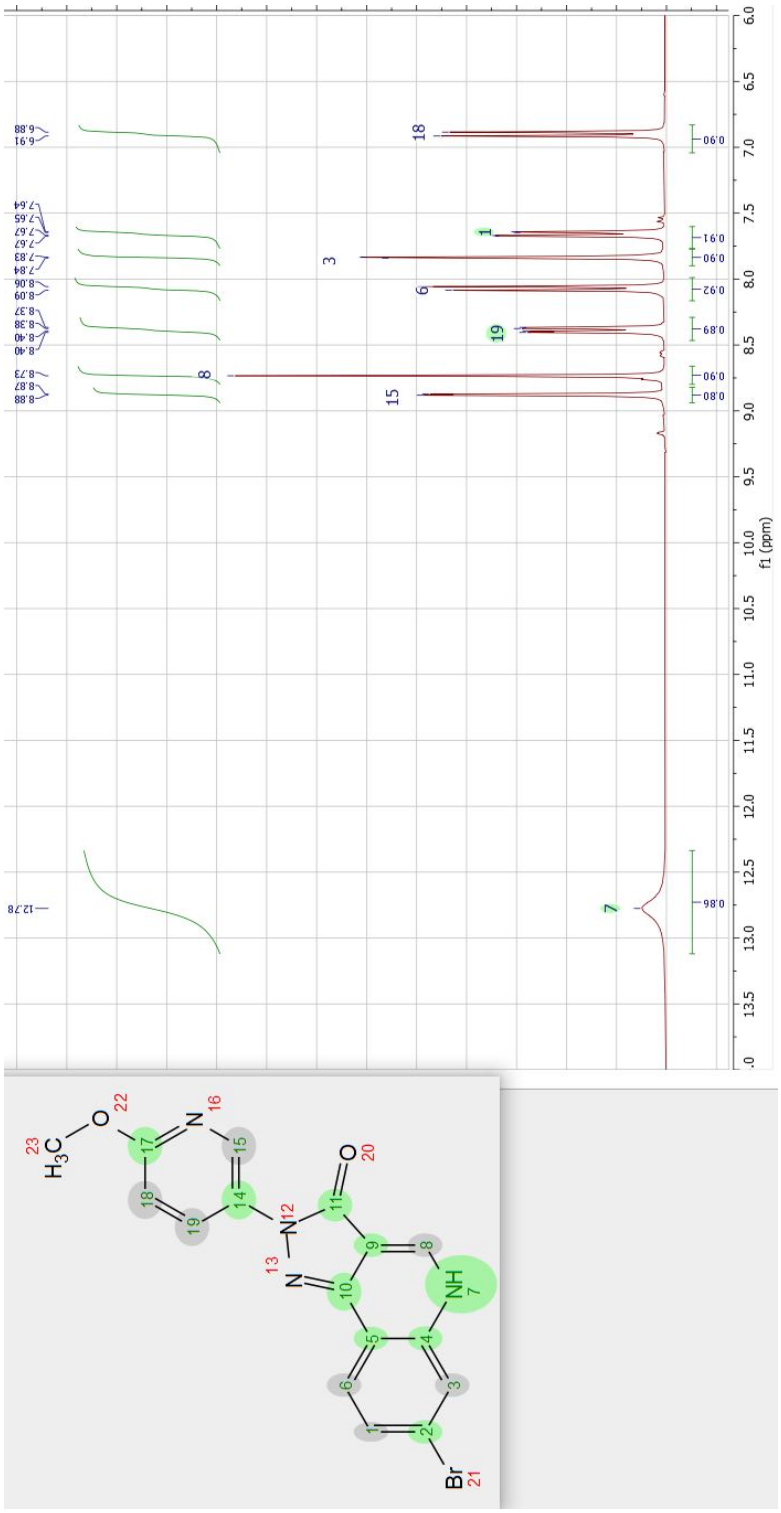

1.20.6.2. ^{13}C NMR of DK-II-58-1 (13h)

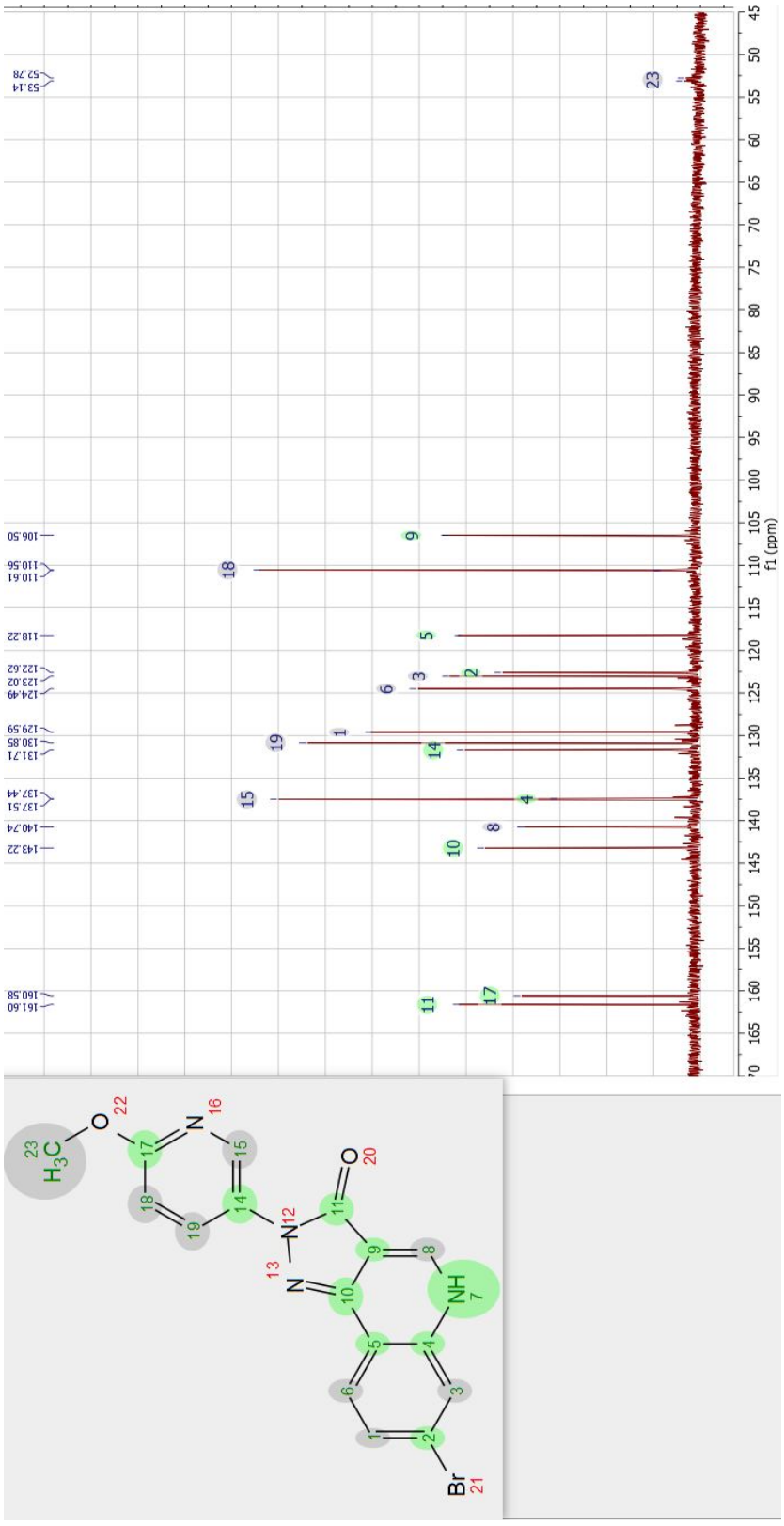

1.20.6.3. COSY Spectrum of DK-II-58-1 (13h)

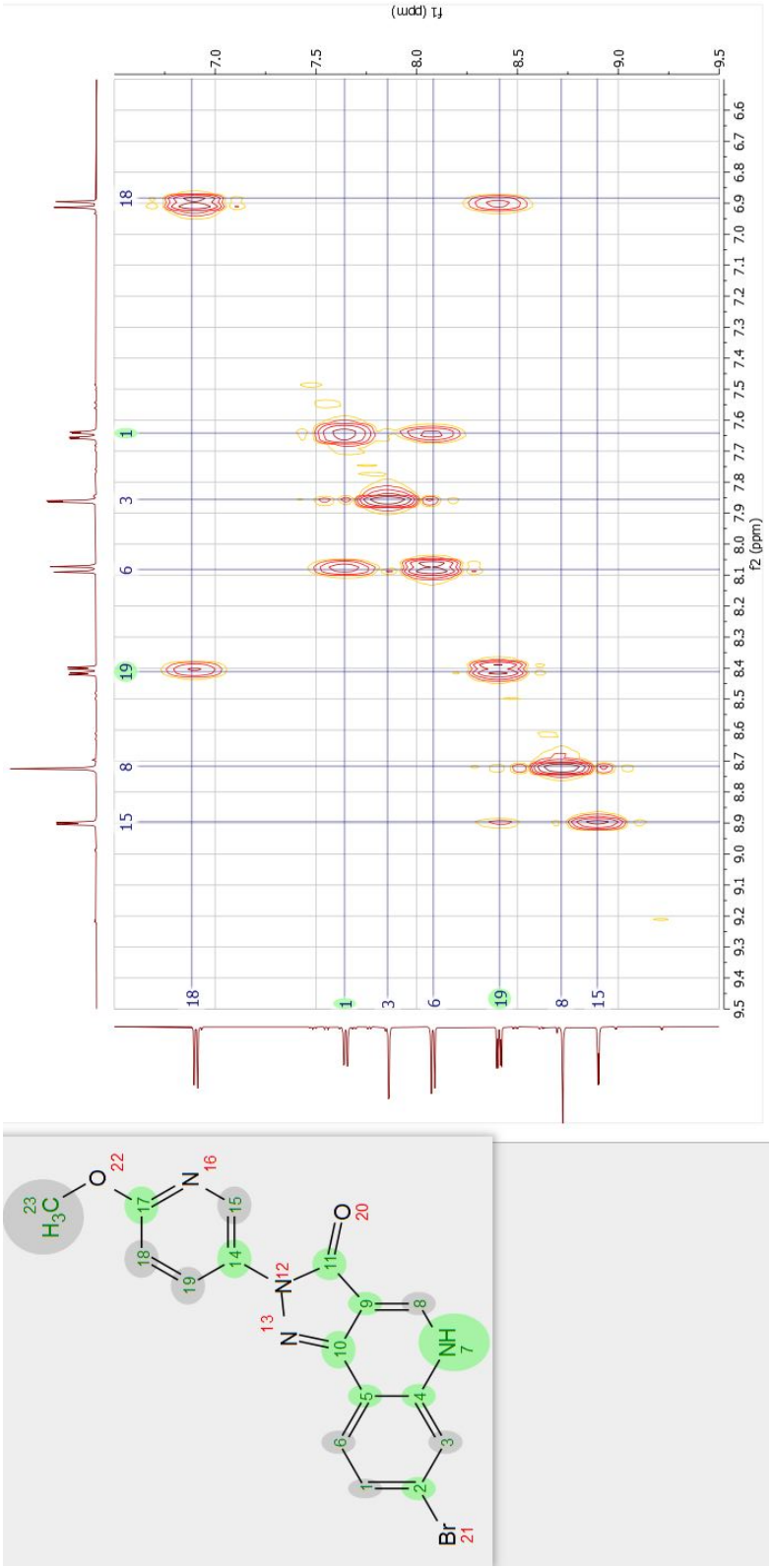

1.20.6.4. ^{1}H-^{13}C-HSQC Spectrum of DK-II-58-1 (13h)

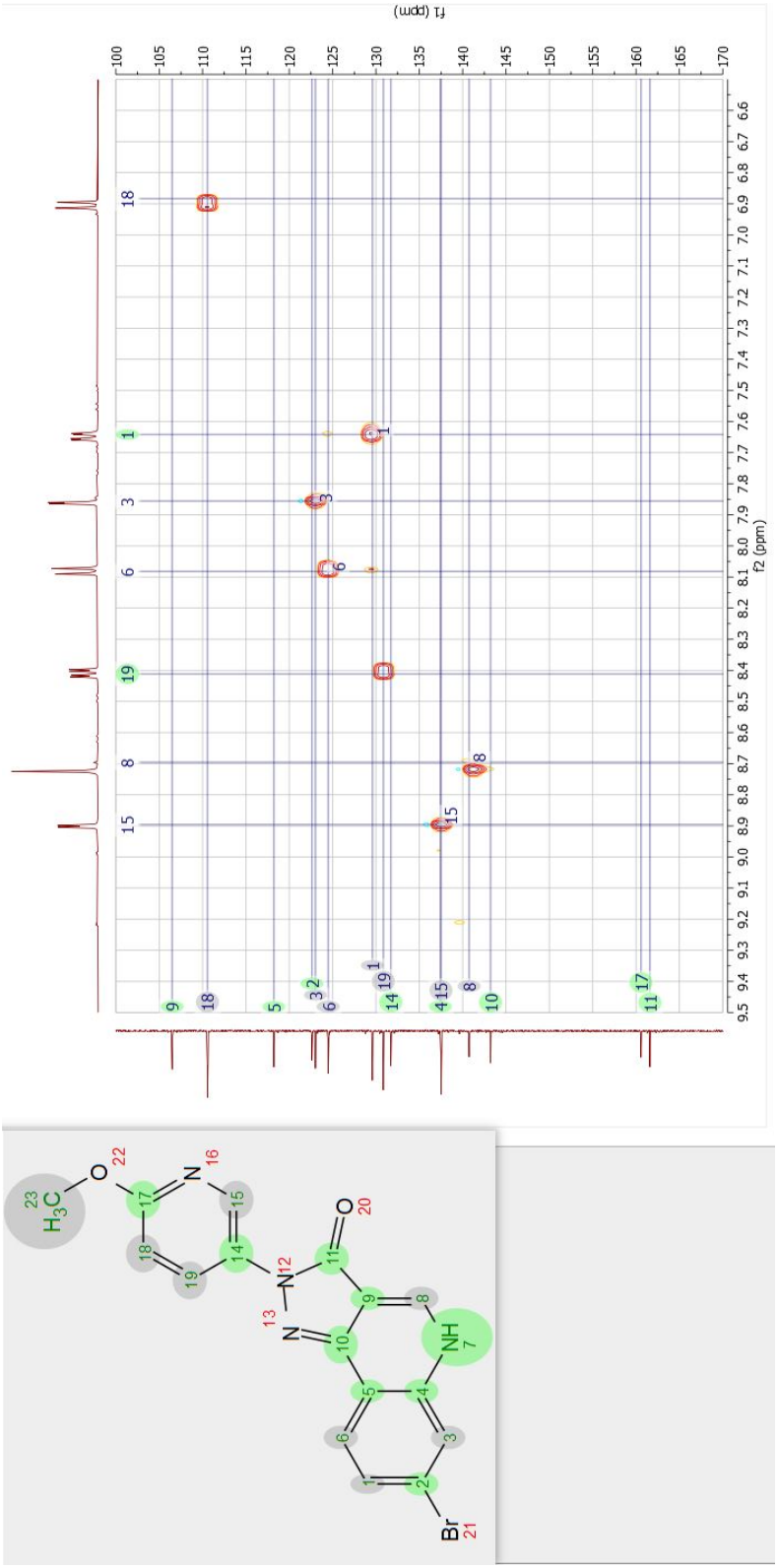

1.20.6.5. ^{1}H-^{13}C-HMBC Spectrum of DK-II-58-1 (13h)

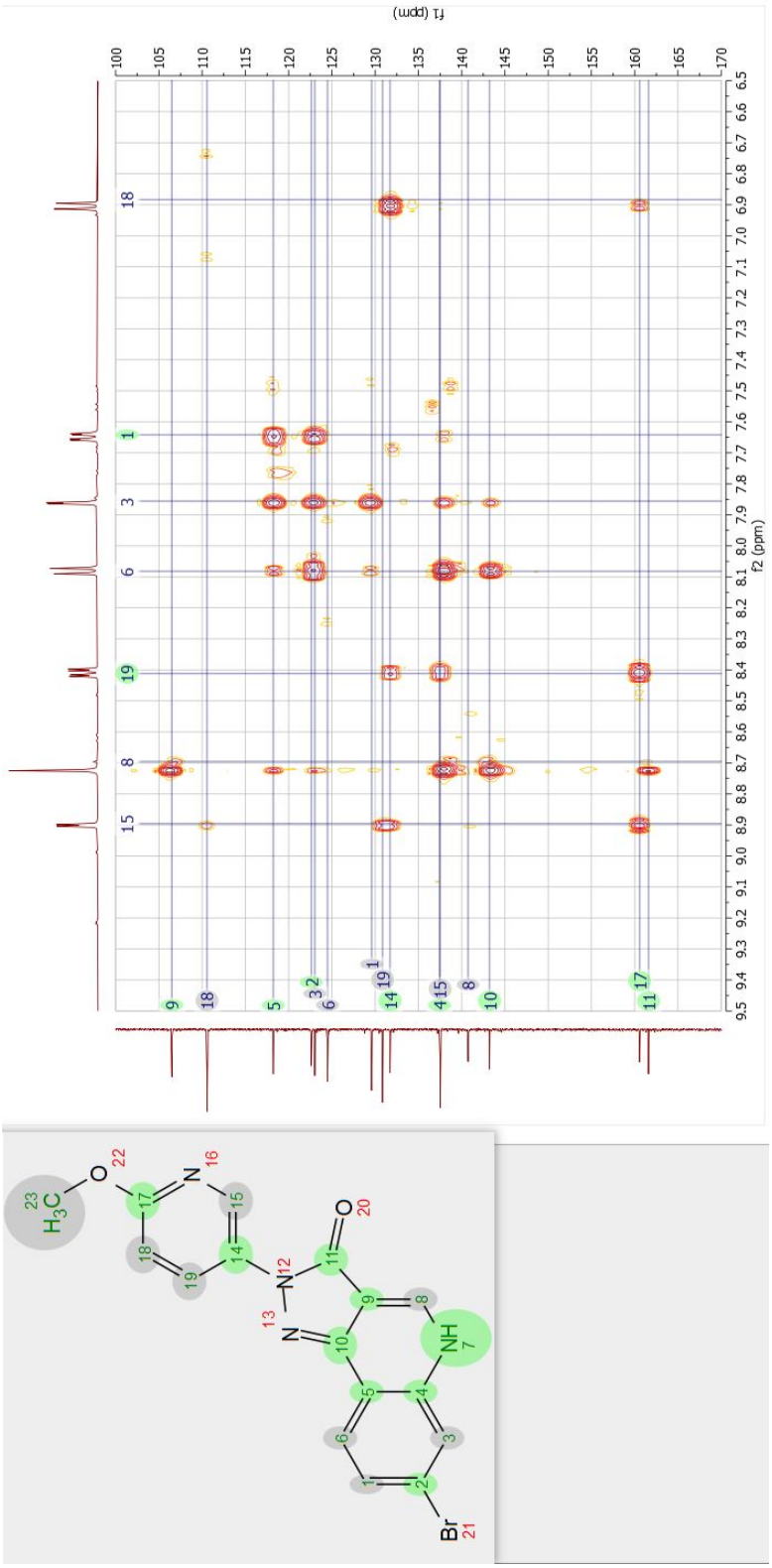

1.20.7. NMR Spectra of DK-VI-9-3 (17a)

1.20.7.1. ^{1}H NMR of DK-VI-9-3 (17a)

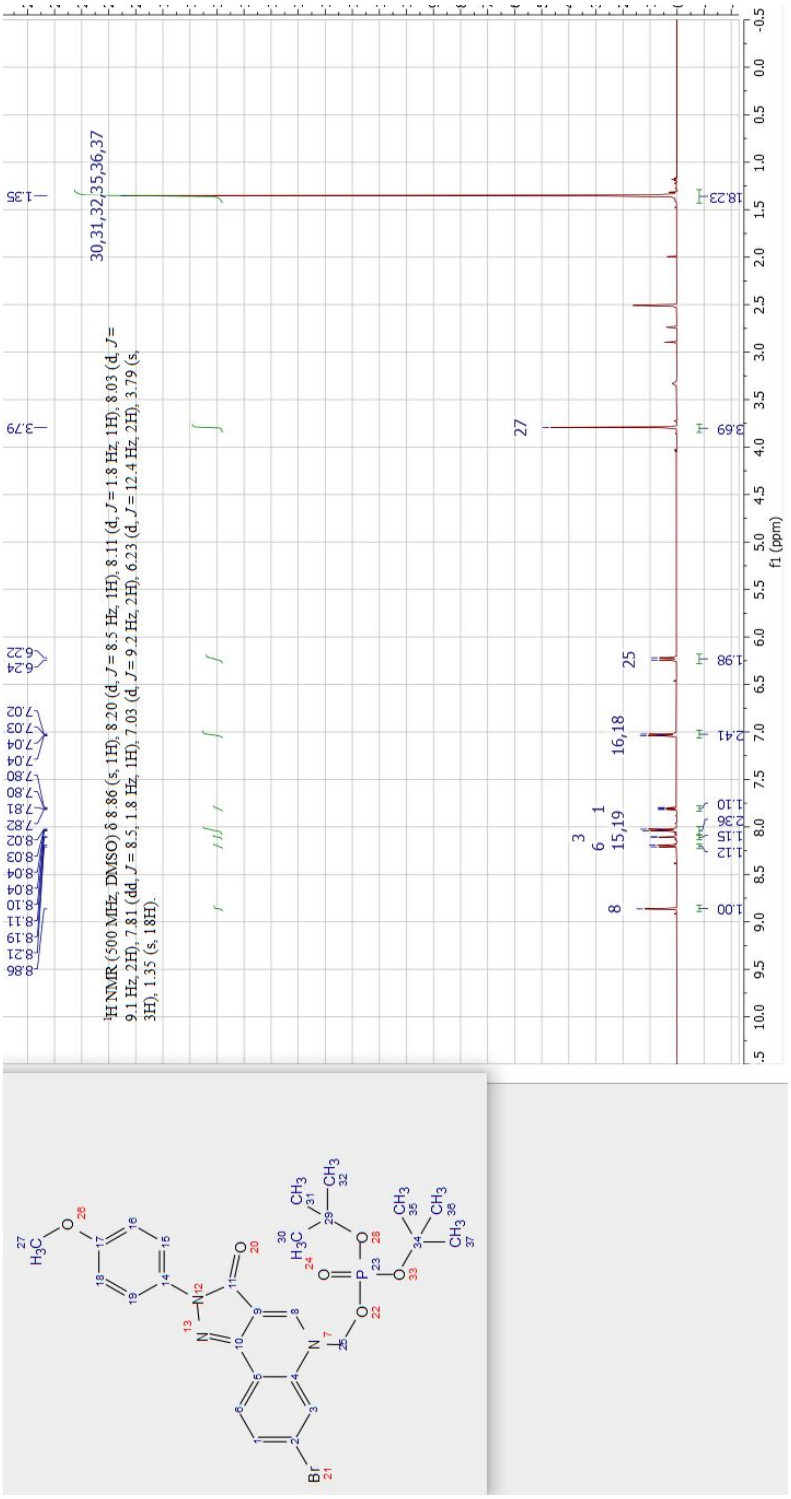

1.20.7.2. ^{13}C NMR of DK-VI-9-3 (17a)

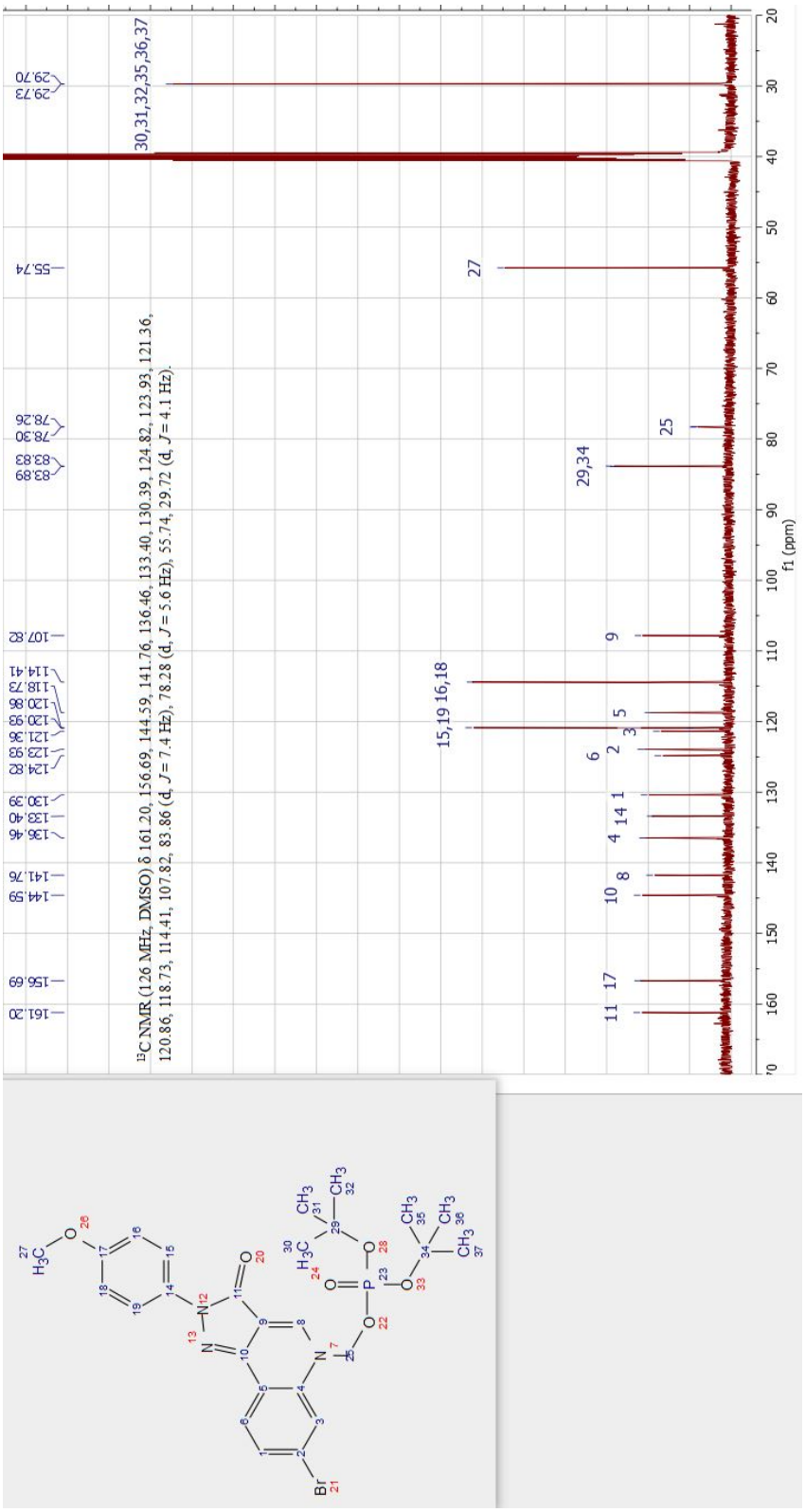

1.20.7.3. ^{1}H-^{13}C-HSQC Spectrum of DK-VI-9-3 (17a)

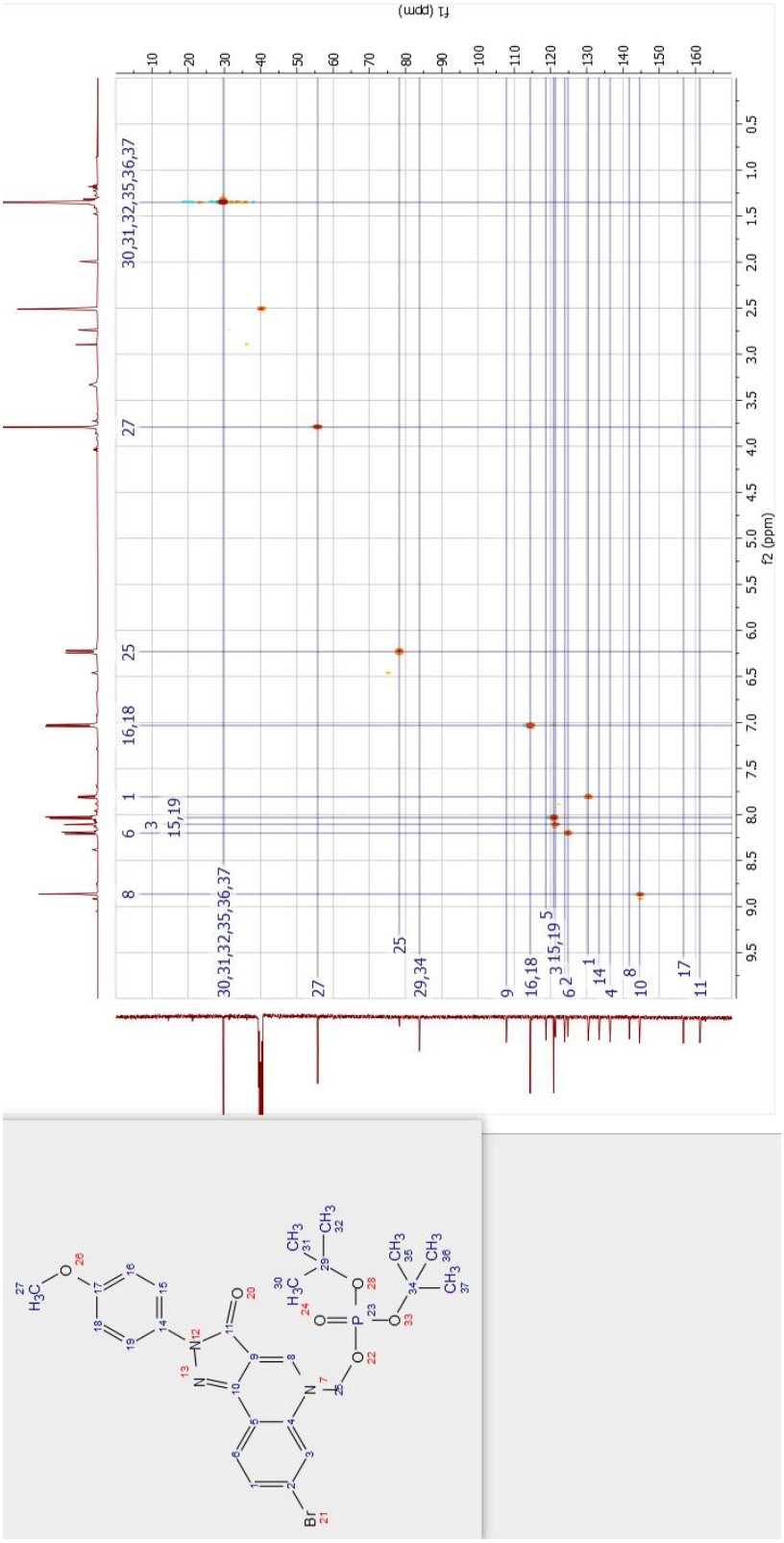

1.20.7.4. ^{1}H-^{13}C-HMBC Spectrum of DK-VI-9-3 (17a)

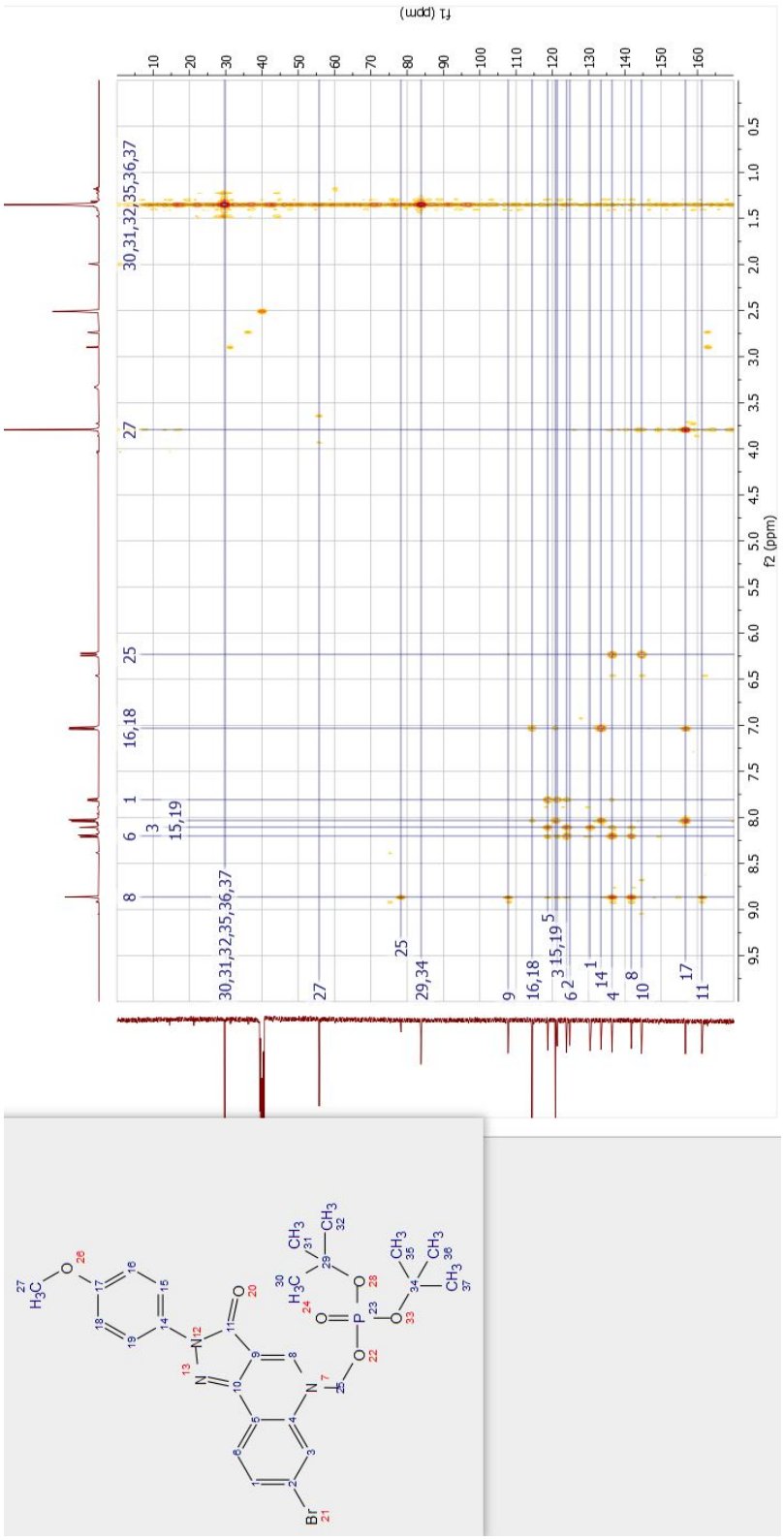

1.20.8. NMR Spectra of DK-VI-15-1 (18a)

1.20.8.1. ^{1}H NMR of DK-VI-15-1 (18a)

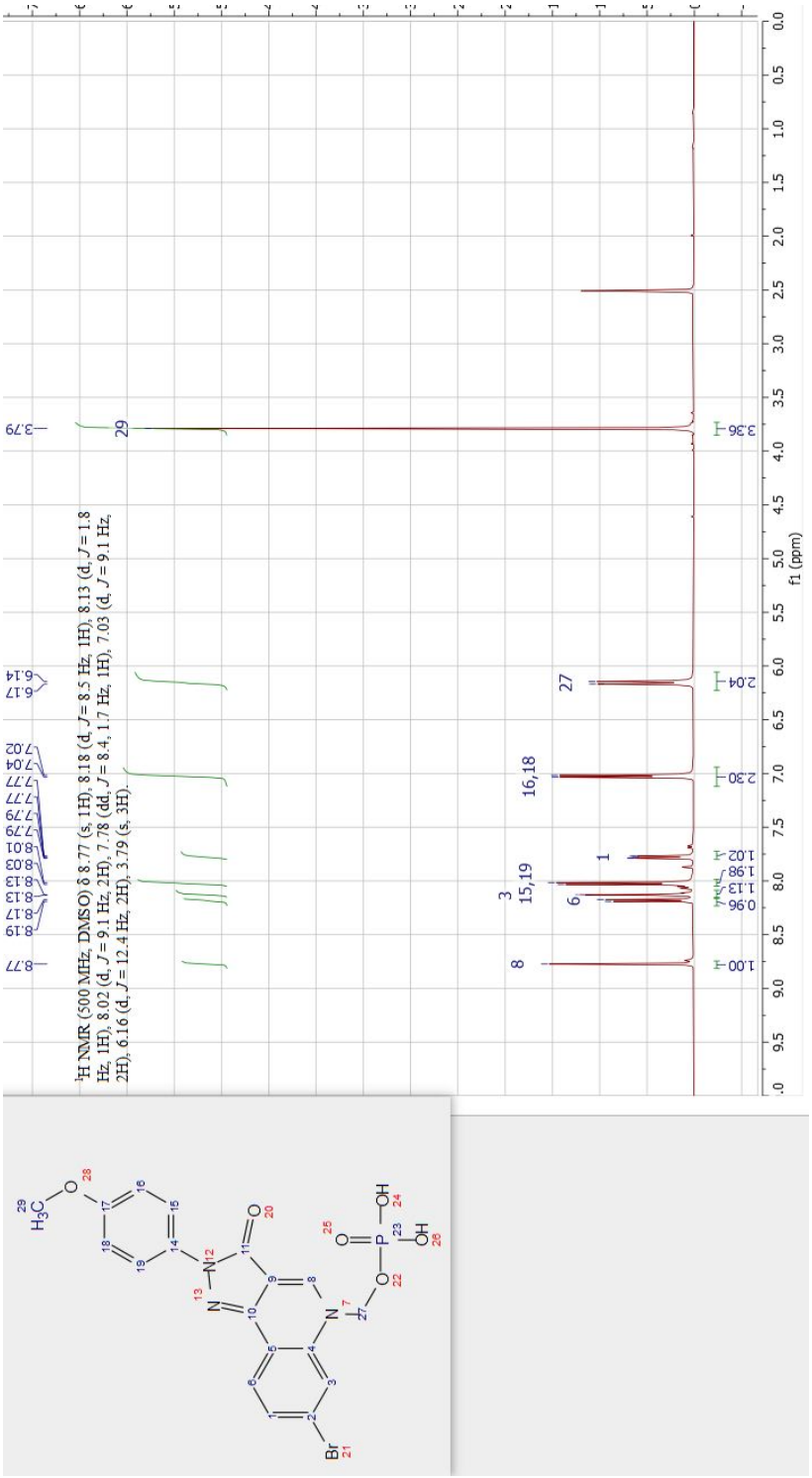

1.20.8.2. ^{13}C NMR of DK-VI-15-1 (18a)

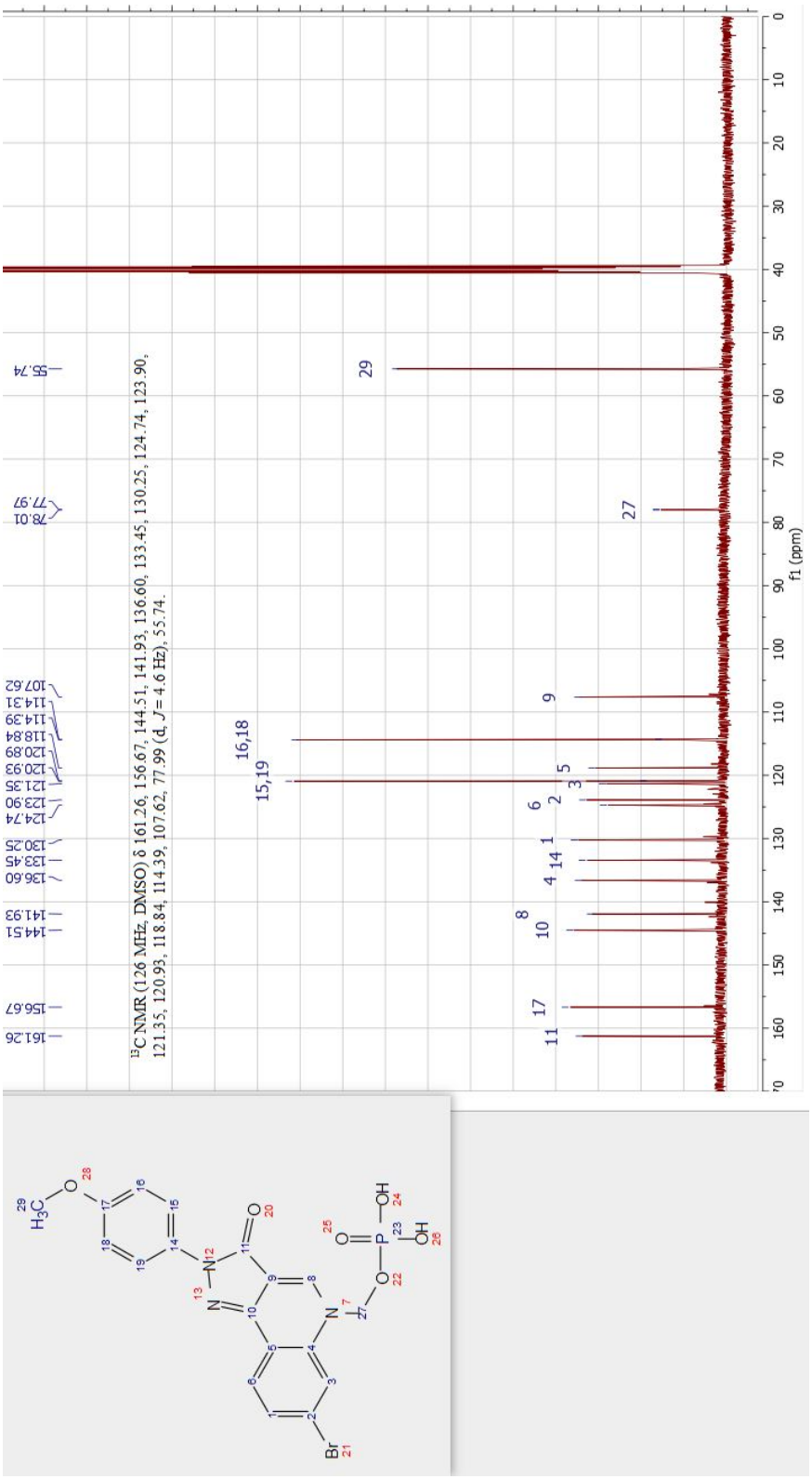

1.20.8.3. COSY Spectrum of DK-VI-15-1 (18a)

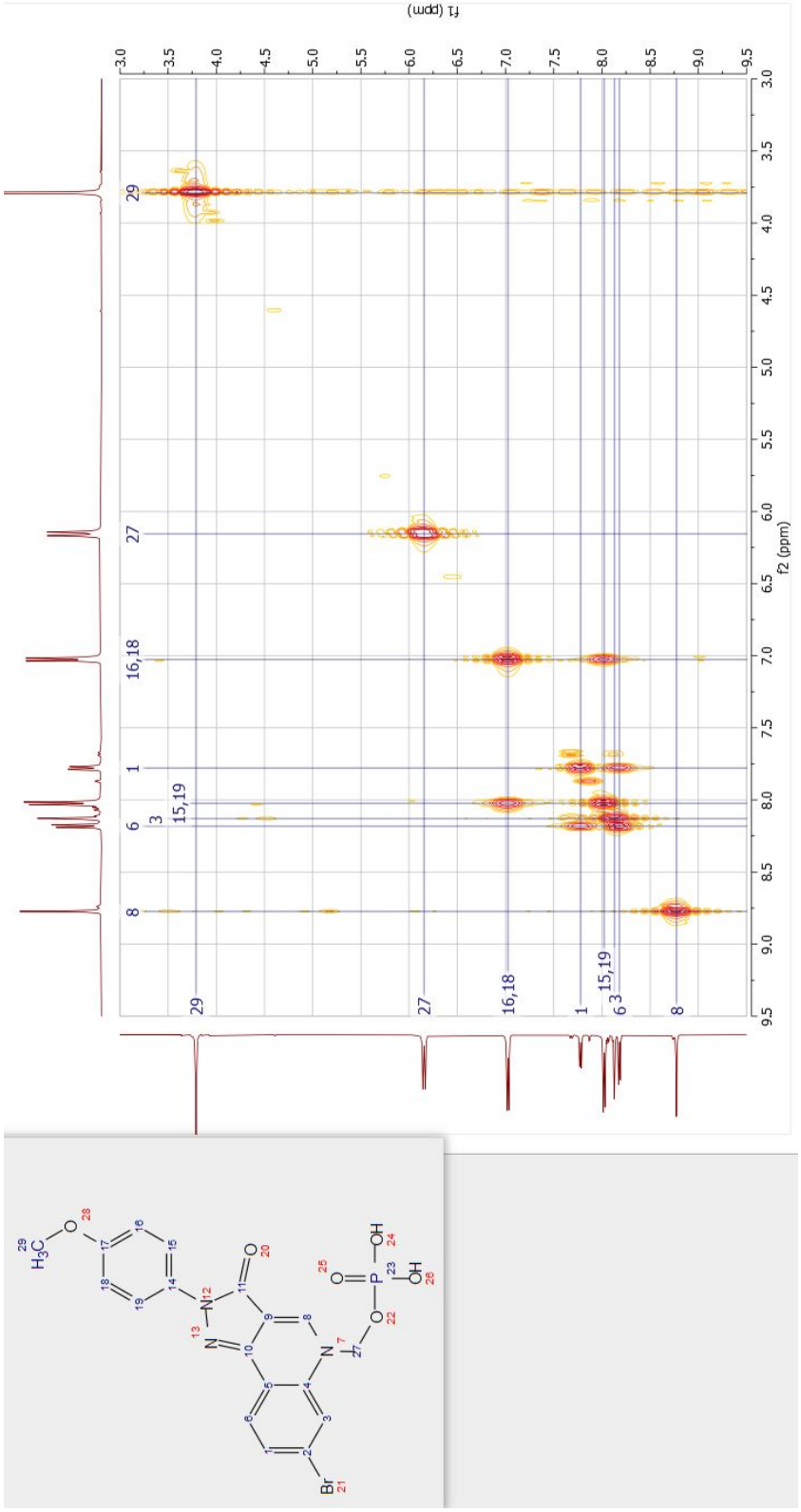

1.20.8.4. ^{1}H-^{13}C-HSQC Spectrum of DK-VI-15-1 (18a)

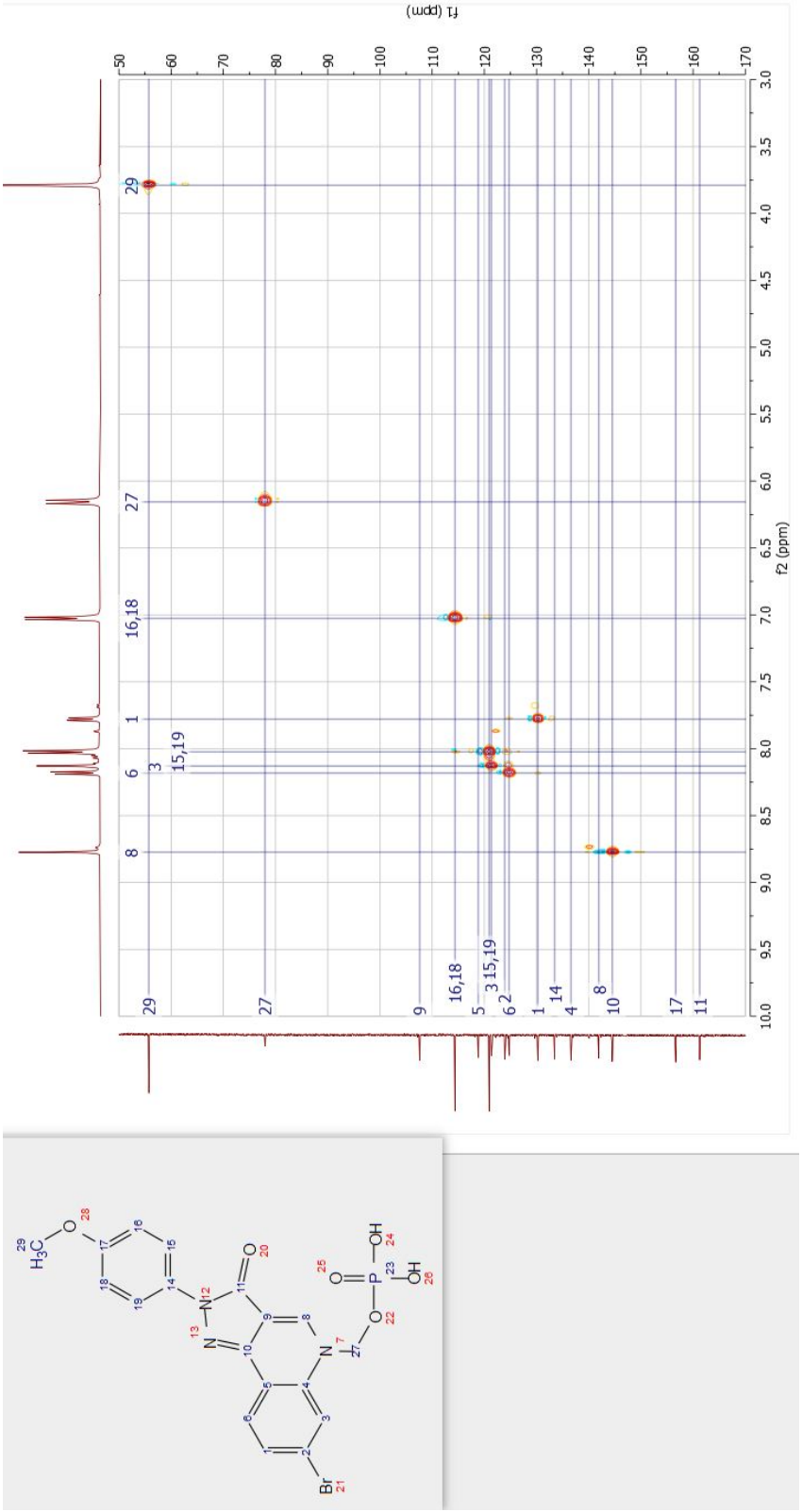

1.20.8.5. ^{1}H-^{13}C-HMBC Spectrum of DK-VI-15-1 (18a)

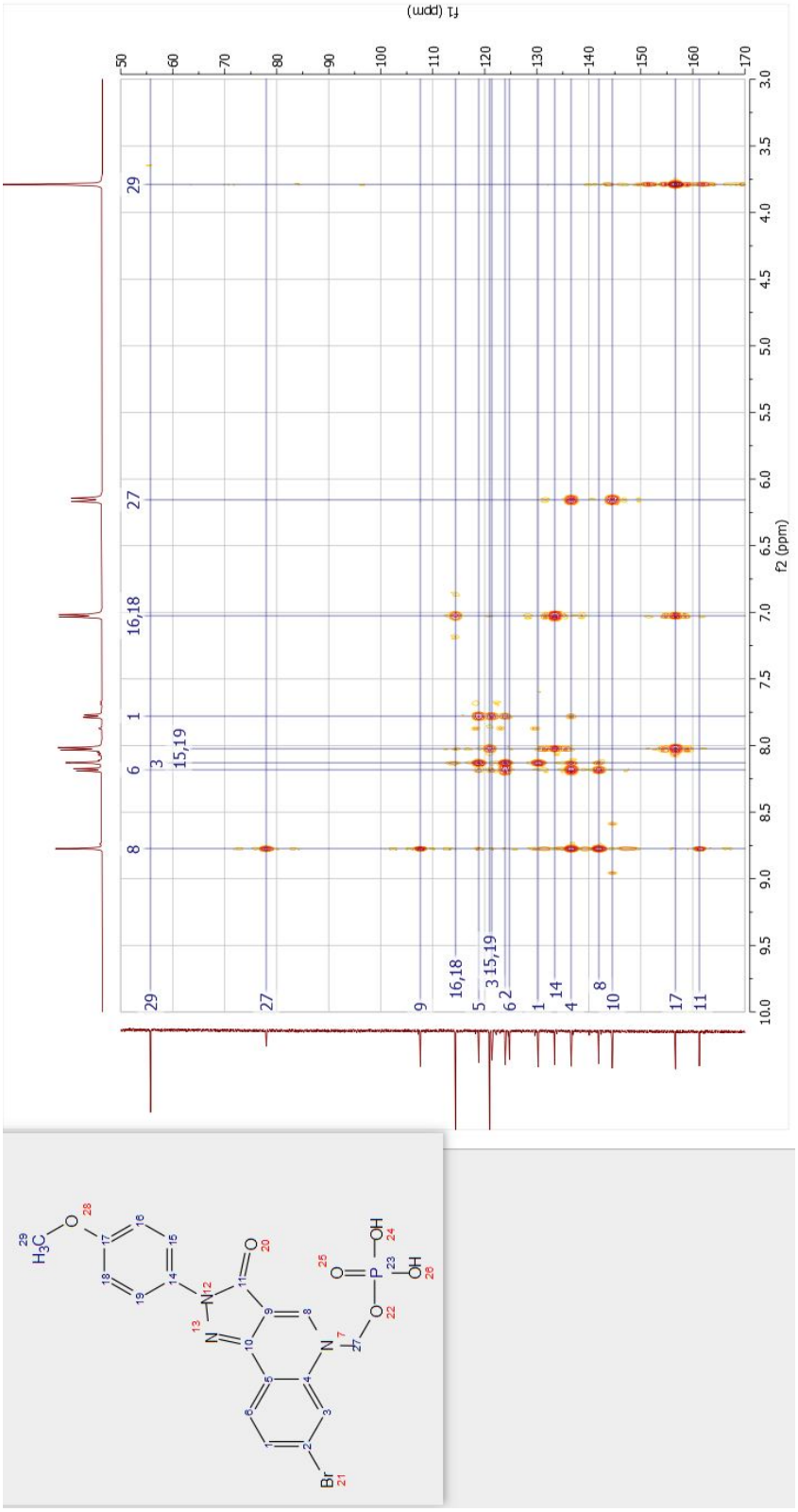

1.21. X-ray Structures of Lead Pyrazoloquinolinones

X-ray structures were determined for select PQ's by Jeffery Deschamps and Greg Imler at the Naval Research Laboratory in Washington D.C. These results confirm the flat, planar nature of the pyrazoloquinolinones synthesized in this work as well as the electron densities for specific atoms (see Appendix).

1.21.1. Ortep Representation of the X-Ray Structure of DK-I-56-1 (8b)

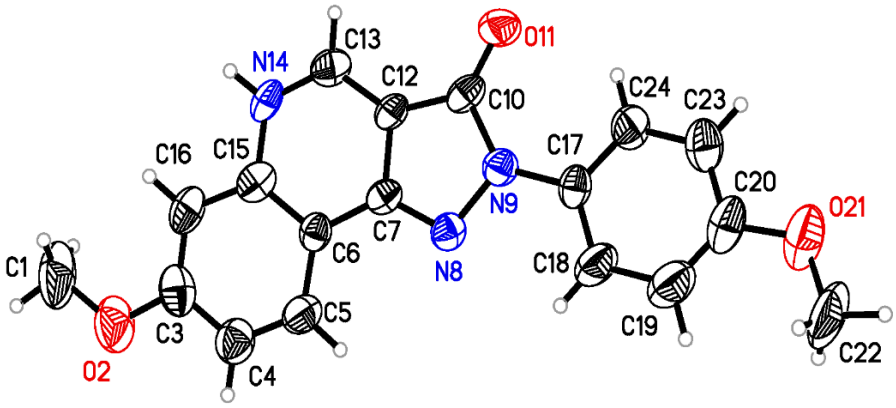

1.21.2. Ortep Representation of the X-Ray Structure of MM-I-10 (14l)

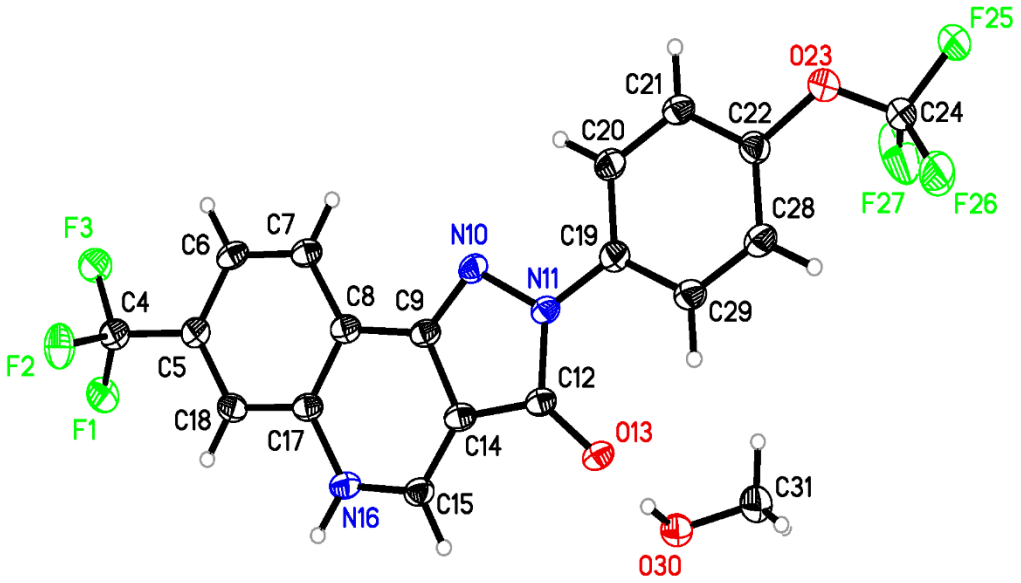

1.21.3. Ortep Representation of the X-Ray Structure of DK-IV-20-1 (14o)

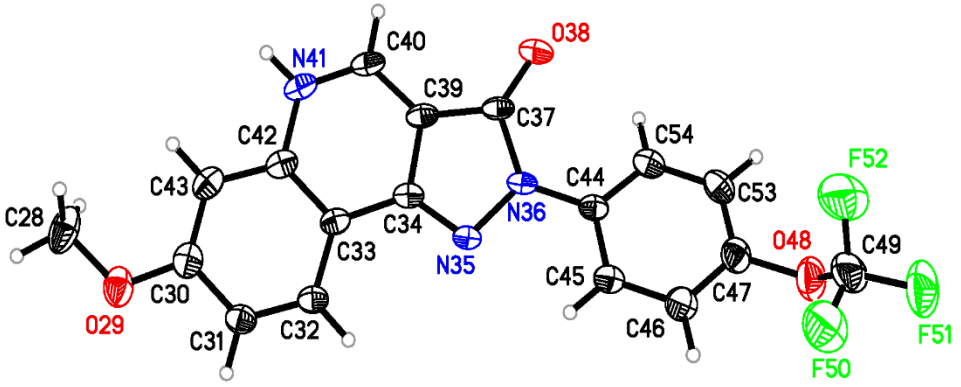

1.21.4. Ortep Representation of the X-Ray Structure of DK-IV-22-1 (14p)

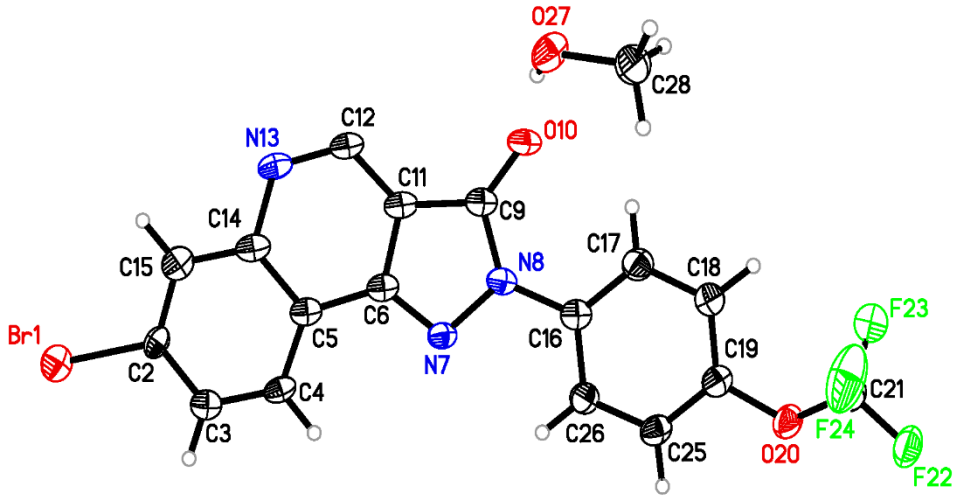

1.21.5. Ortep Representation of the X-Ray Structure of DK-IV-19-1 (14r)

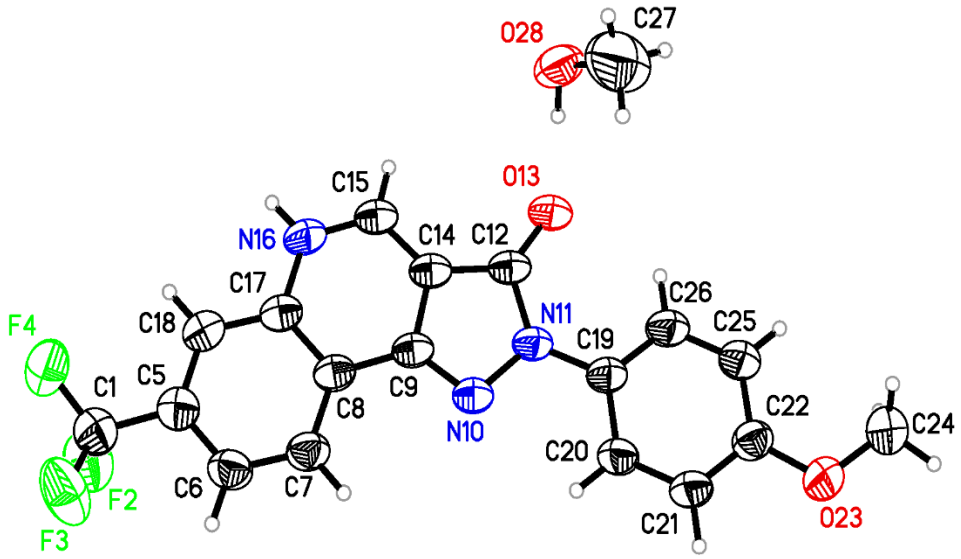

1.22. Molecular Modeling of Lead Pyrazoloquinolinones at the Bz site / α1+γ2- Interface

Many groups have worked to understand the structure of the $GABA_AR$ binding sites using pharmacophore models[25, 26] or homology models[107] and specifically the mode of action of pyrazoloquinolinones at the α1β2γ2 diazepam sensitive (DS) binding site.[108] Very recently, a high-resolution cryo-electron microscopy structure of the α1β2γ2 $GABA_AR$ was determined as a complex with flumazenil by Zhu et al. in 2018[109] and then with alprazolam, as well as diazepam by Masiulis et al. in 2019.[1] With these new cryo-structures in hand it became possible to perform docking studies using the pyrazoloquinolinone library generated here to possibly rationalize the differences in binding affinity data at the BZP rat brain site (the α1+γ2- interface) that had been observed (**Table 60** and **Table 62**). Additionally, a SAR-guided pose-related scoring function was developed by the Siebert and Ernst groups to identify the likely binding modes of the PQ, CGS-8216 at the benzodiazepine binding site (the α1+γ2- interface).[110] Using the proposed binding mode of PQ's (Binding mode I, BM I) developed by Siebert et al.[110] with the flumazenil based cryo-structure[109] and the Chimera X software to perform the docking study, the $-OCD_3$, *N*-hetero and $-OCF_3$ pyrazoloquinolinone ligands were docked. We then selected the pose in which the orientation best matched Binding Mode I,[110] which is displayed below. The A and B rings lie flat under the C-loop, while the carbonyl oxygen and the D-ring orients towards the γ2 subunit. The quinoline nitrogen engages in a possible hydrogen-bond with the backbone of α1Y160. Some possible hydrophobic and/or π-π interactions are displayed between the quinoline ring and γ2F77 and α1Y210. The ligands, which exhibited the best binding affinity (DK-I-56-1 (2.1 nM), DK-I-58-1 (5.5 nM) and DK-I-59-1 (1.2 nM) engaged in a possible hydrogen bond between D-ring methoxy groups and γD56, while the A-ring substituent

(methoxy, bromo or chloro) engaged in a possible hydrogen bond with αH102. The *N*-hetero ligands (DK-I-86-1 (8.2 nM) and DK-II-58-1 (6.2 nM)) exhibited similar interactions. The observed binding affinities for the D-ring trifluoromethoxy analogs (-OCF_3) were much poorer (DK-IV-20-1 (444 nM), DK-IV-22-1 (686 nM) and MM-I-10 (964 nM). The inability of these -OCF_3 ligands to fully insert parallel under the C-loop are, presumably, due to the steric restrictions and/or the lack of hydrogen bonding interactions with the γ2 subunit (γD56). These facts appear to be the most logical explanation for the poorer binding affinity which was observed. The less potent binding affinity (32 nM) observed for the A-ring substituted trifluoromethyl ligand, DK-IV-19-1 was best explained by the lack of a hydrogen bonding interaction with αH102. In a similar fashion, the D-ring ortho-methoxy ligand, DK-I-87-1 (98 nM) was devoid of the key hydrogen bond with residue γD56.

1.22.1. Modeling of Diazepam

Blue: α1 subunit **Pink**: γ2 subunit

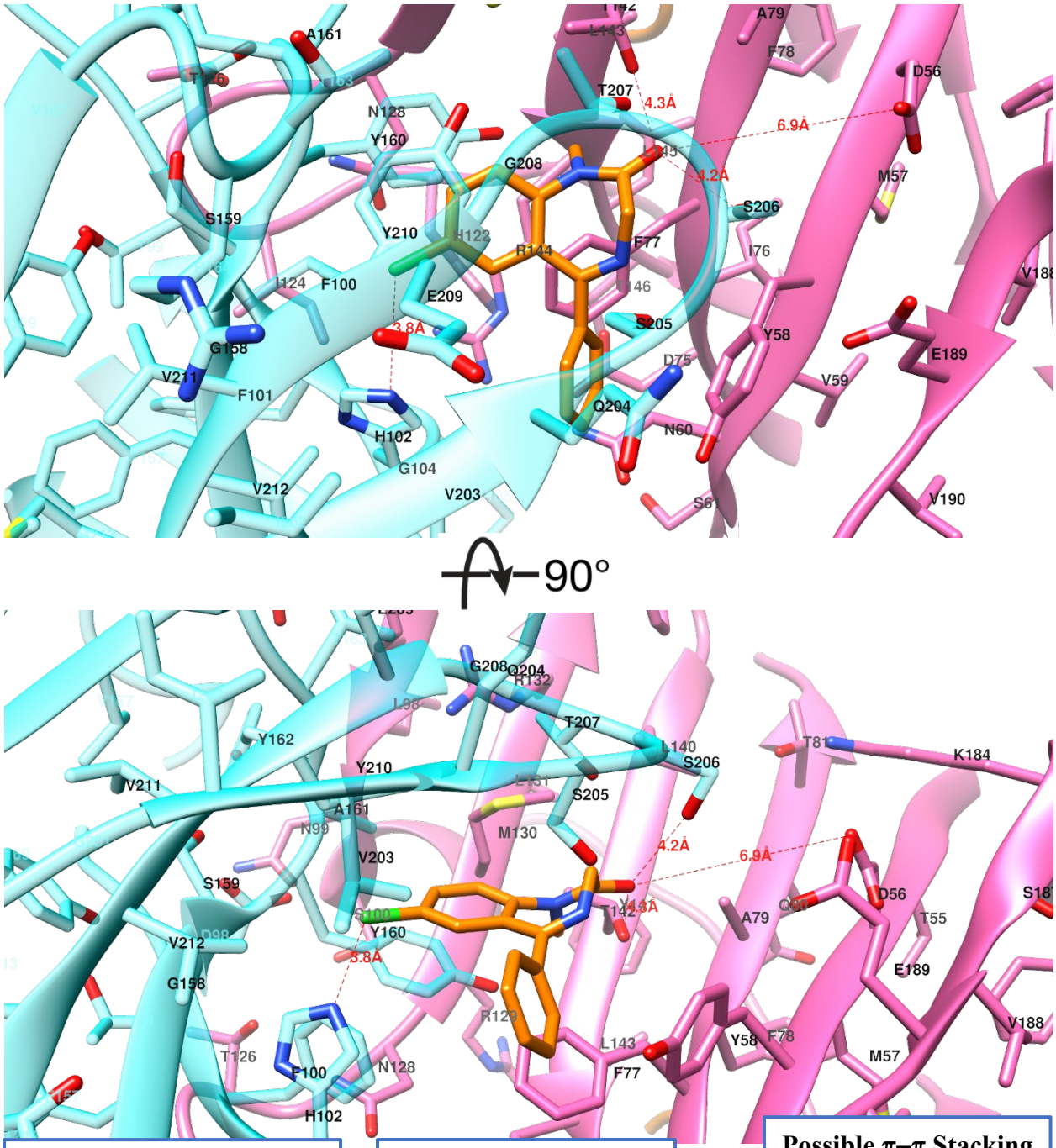

Possible Hydrogen Bonds	Possible Electrostatic Interactions	Possible π–π Stacking
αH102	αS205	αF100
γT142	αS206	αY160
	αT207	αY210
		γF77
		γY58

1.22.2. Modeling of Flumazenil

Blue: α1 subunit **Pink**: γ2 subunit

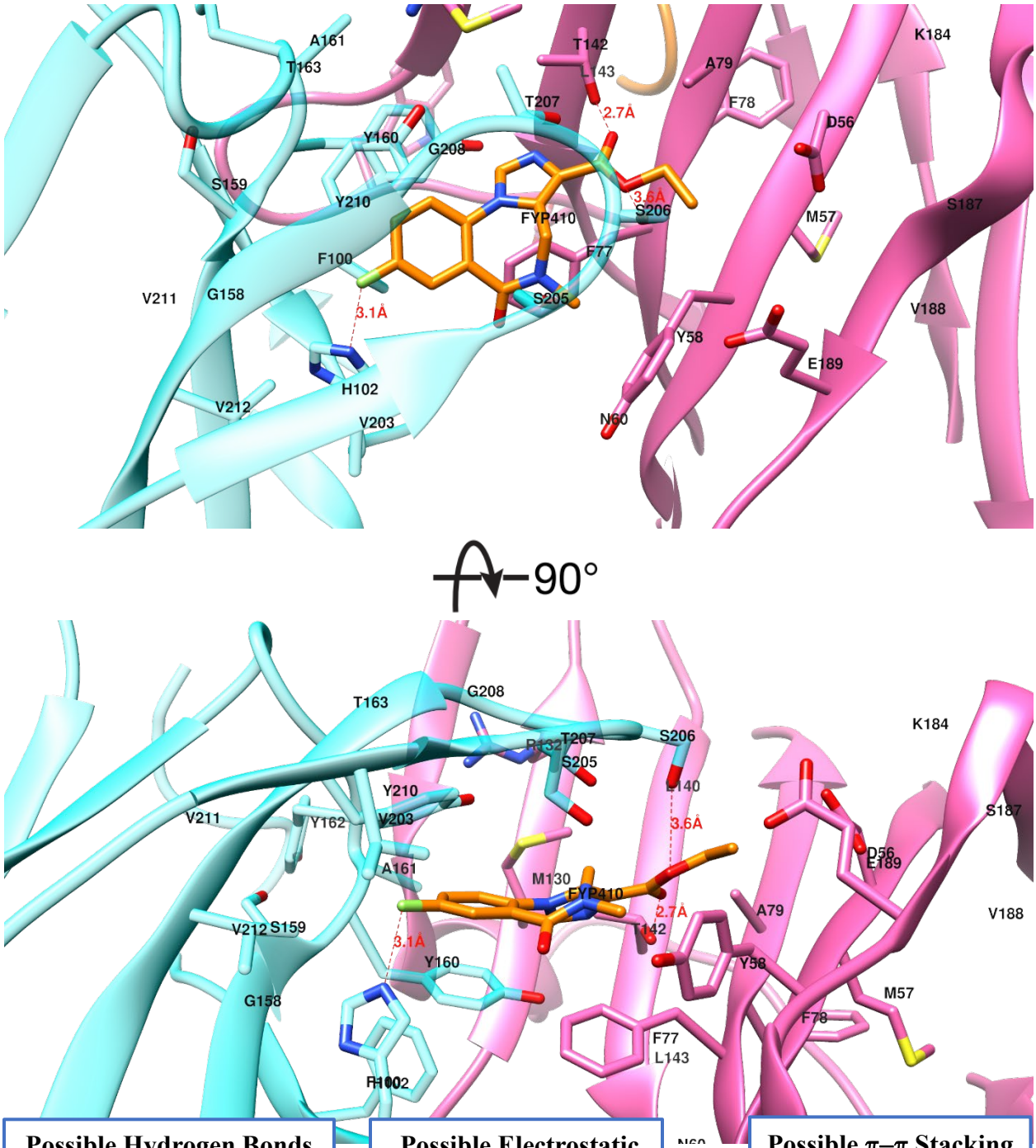

Possible Hydrogen Bonds	Possible Electrostatic Interactions	Possible π–π Stacking
αH102	αS205	αF100
γT142	αS206	αY160
	αT207	αY210
		γF77

1.22.3. Modeling of DK-I-56-1 (8b)

BZP Binding Affinity: 2.1 nM: **Blue:** α1 subunit **Pink:** γ2 subunit

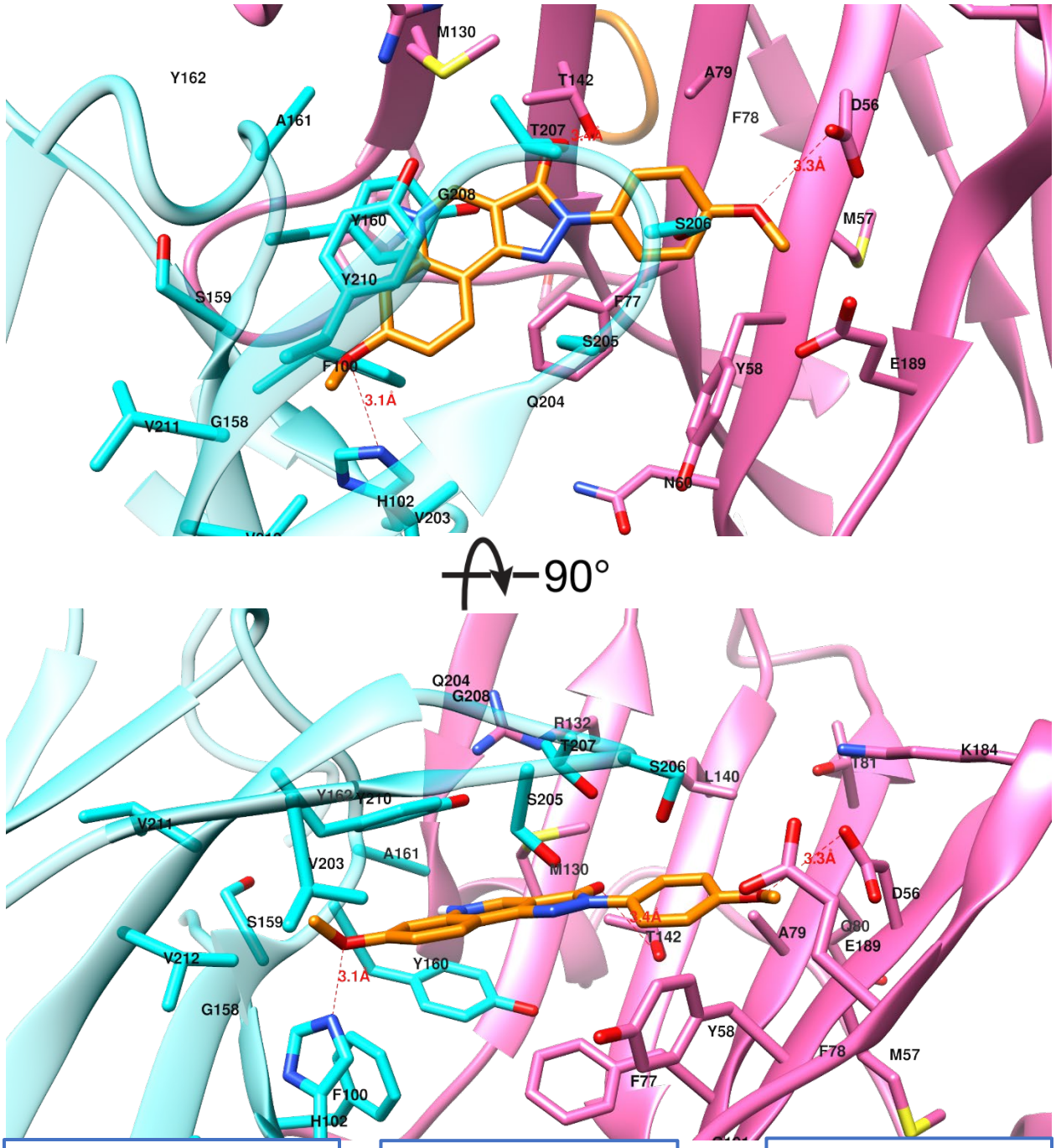

Possible Hydrogen Bonds	Possible Electrostatic Interactions	Possible π–π Stacking
αH102	αS205	αF100
γD56	αS206	αY160
γT142	αT207	αY210
		γF77

1.22.4. Modeling of DK-I-86-1 (13c)

BZP Binding Affinity: 8.2 nM: **Blue:** α1 subunit **Pink:** γ2 subunit

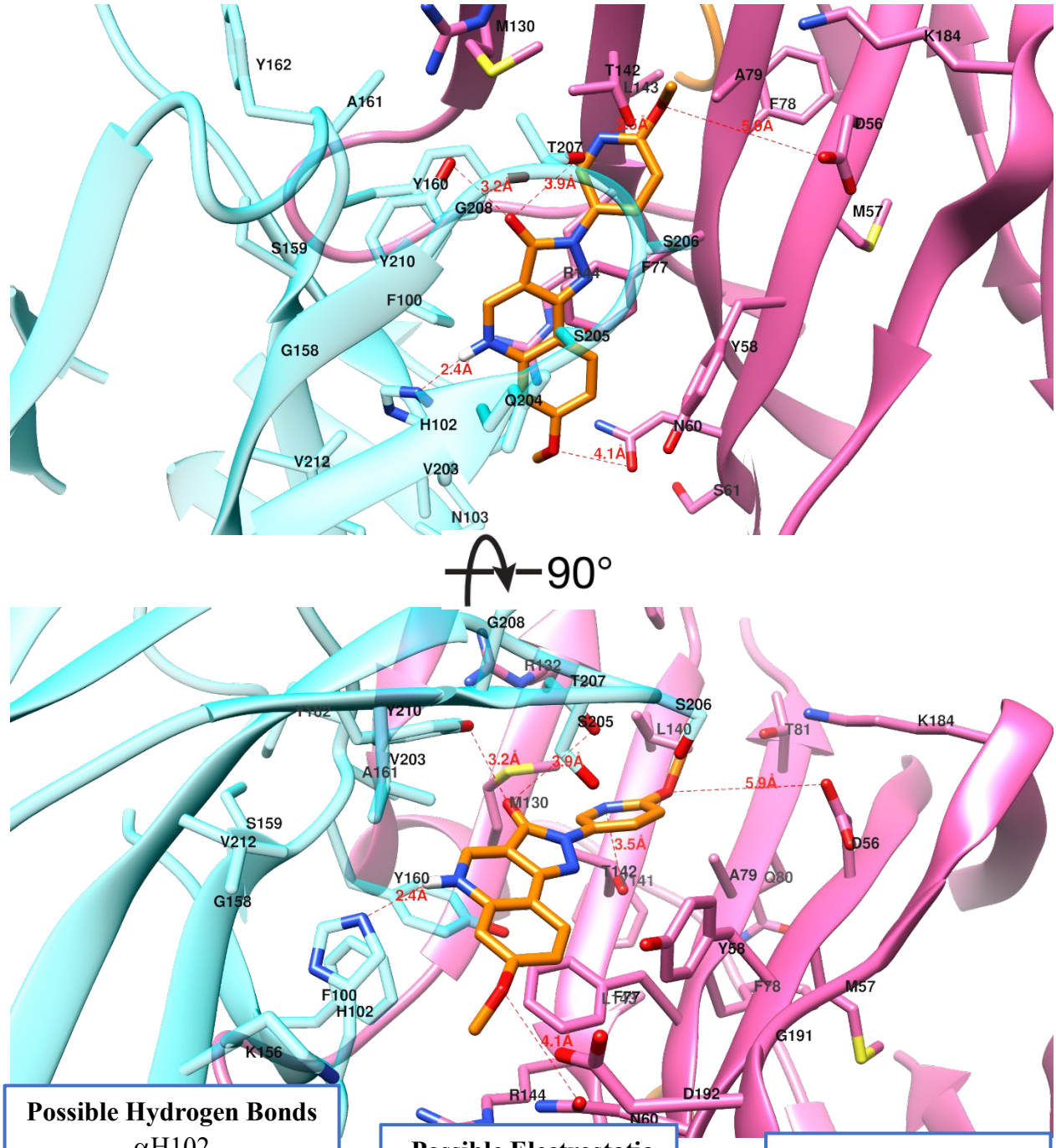

Possible Hydrogen Bonds	Possible Electrostatic Interactions	Possible π–π Stacking
αH102	αS205	αF100
αY210	αS206	αY160
γD56	αT207	αY210
γN60		γF77
γT142		

1.22.5. Modeling of DK-IV-20-1 (14o)

BZP Binding Affinity: 444 nM: **Blue:** α1 subunit **Pink:** γ2 subunit

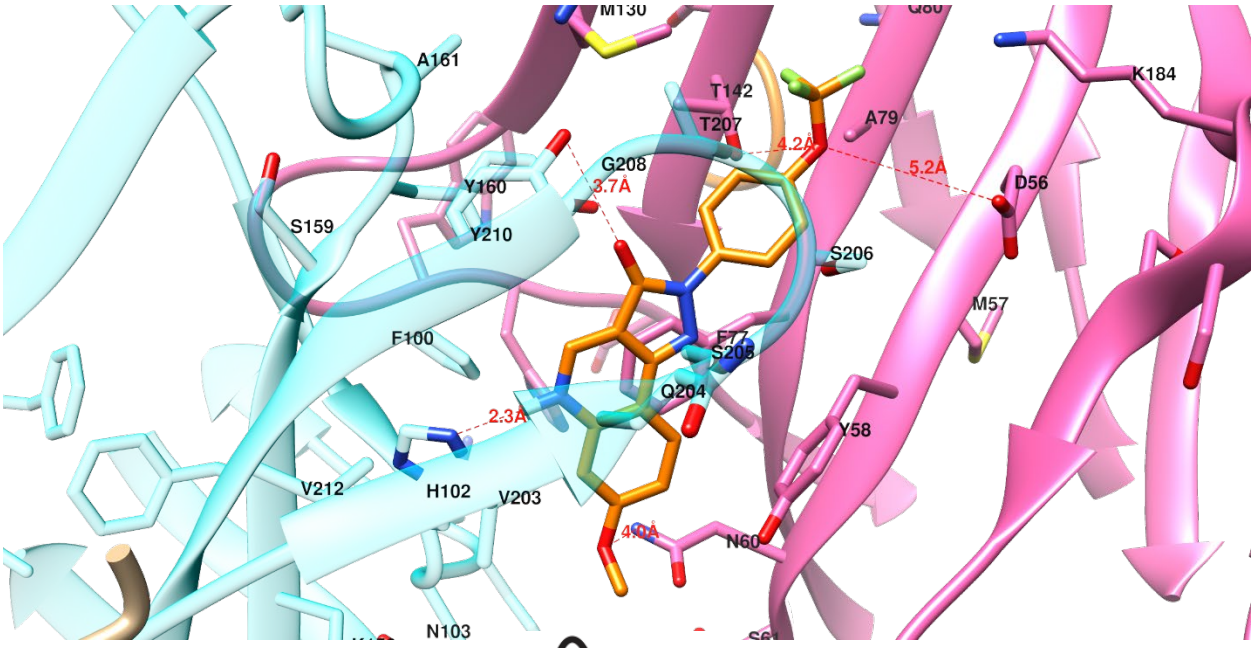

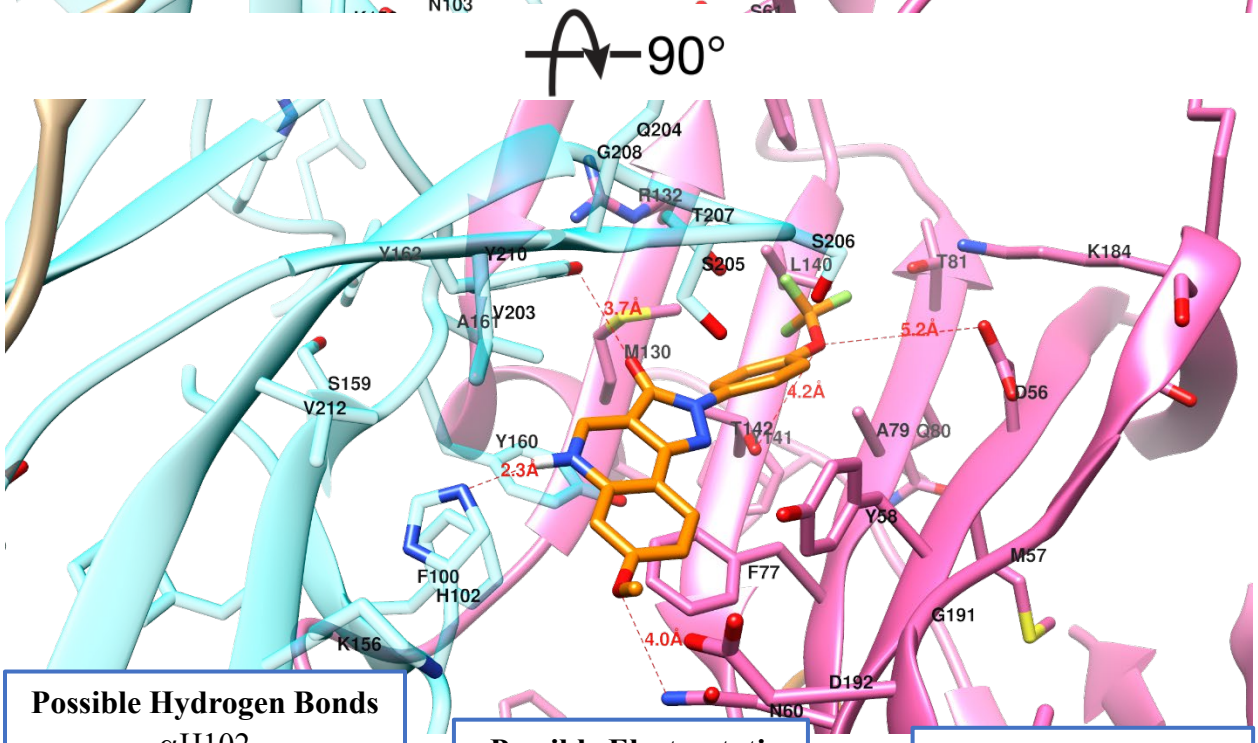

Possible Hydrogen Bonds	Possible Electrostatic Interactions	Possible π–π Stacking
αH102	αS205	αF100
αY210	αS206	αY160
γN60	αT207	αY210
γD56		γF77
γT142		

1.22.6. Modeling of DK-I-58-1 (8o)

BZP Binding Affinity: 5.5 nM: **Blue:** α1 subunit **Pink:** γ2 subunit

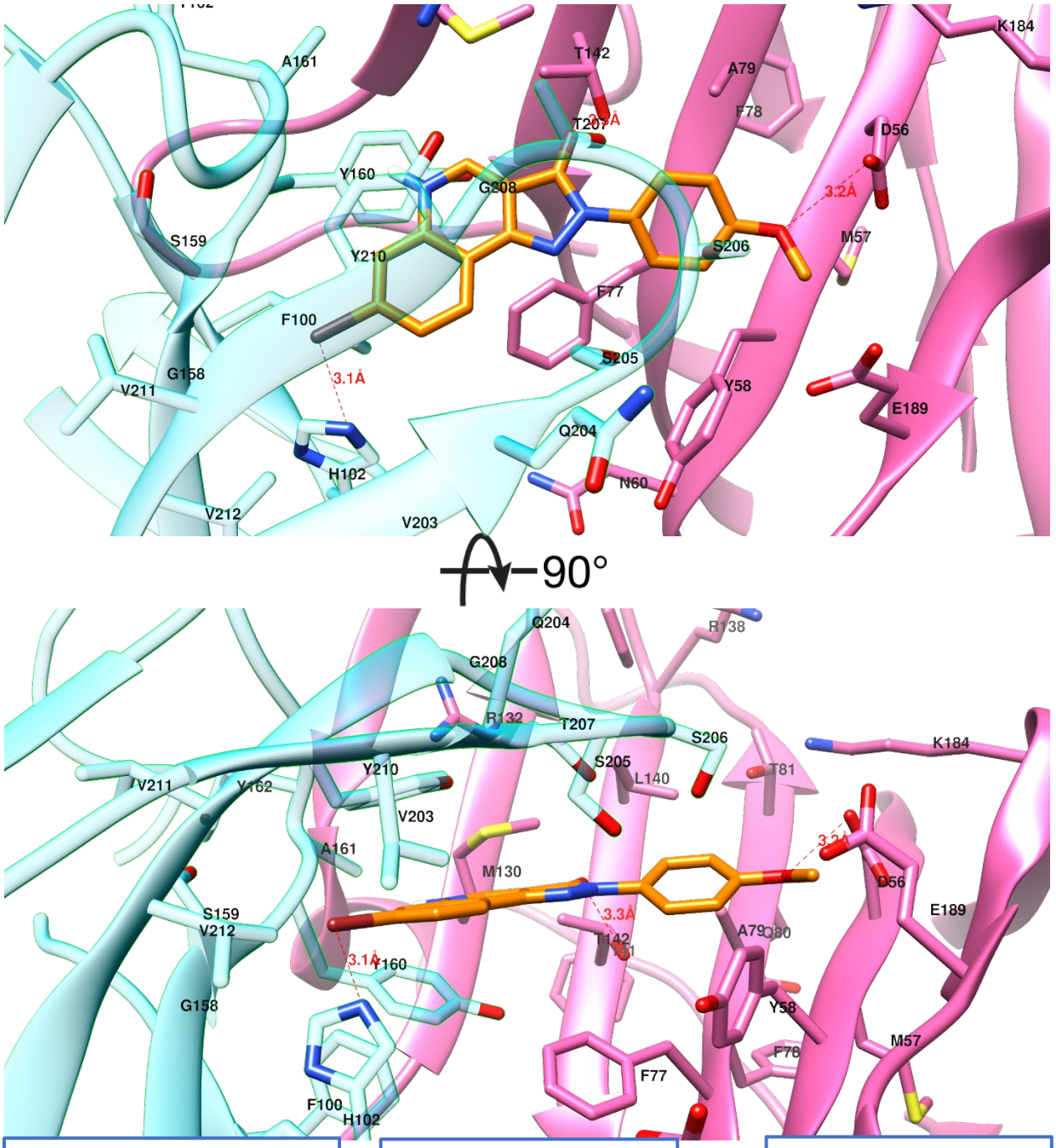

Possible Hydrogen Bonds	Possible Electrostatic Interactions	Possible π–π Stacking
αH102	αS205	αF100
γD56	αS206	αY160
γT142	αT207	αY210
		γF77

1.22.7. Modeling of DK-II-58-1 (13h)

BZP Binding Affinity: 6.2 nM: **Blue:** α1 subunit **Pink:** γ2 subunit

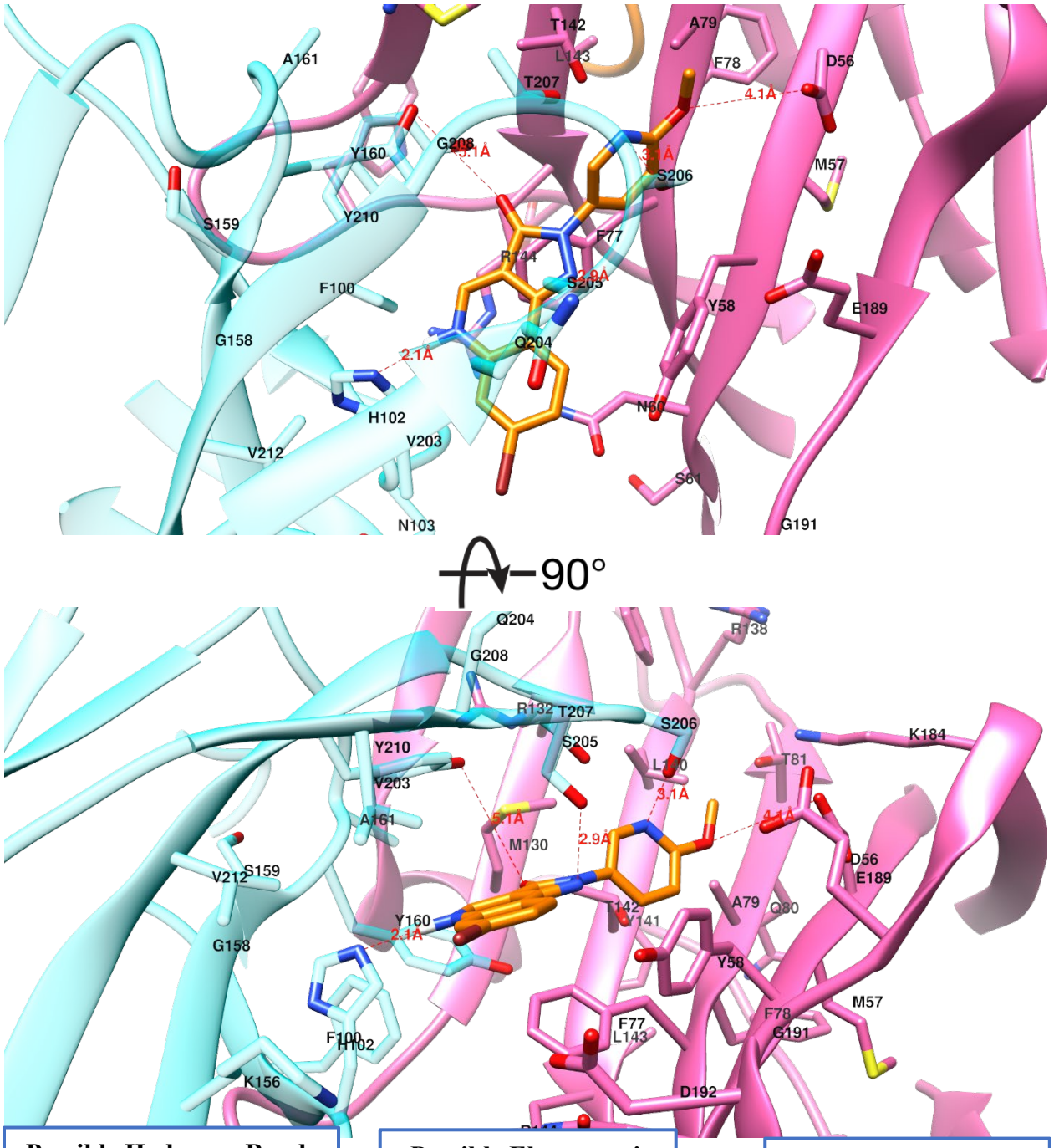

Possible Hydrogen Bonds	Possible Electrostatic Interactions	Possible π–π Stacking
αH102	αS205	αF100
αY210	αS206	αY160
γD56	αT207	αY210
γT142		γF77

1.22.8. Modeling of DK-IV-22-1 (14p)

BZP Binding Affinity: 686 nM: **Blue:** α1 subunit **Pink:** γ2 subunit

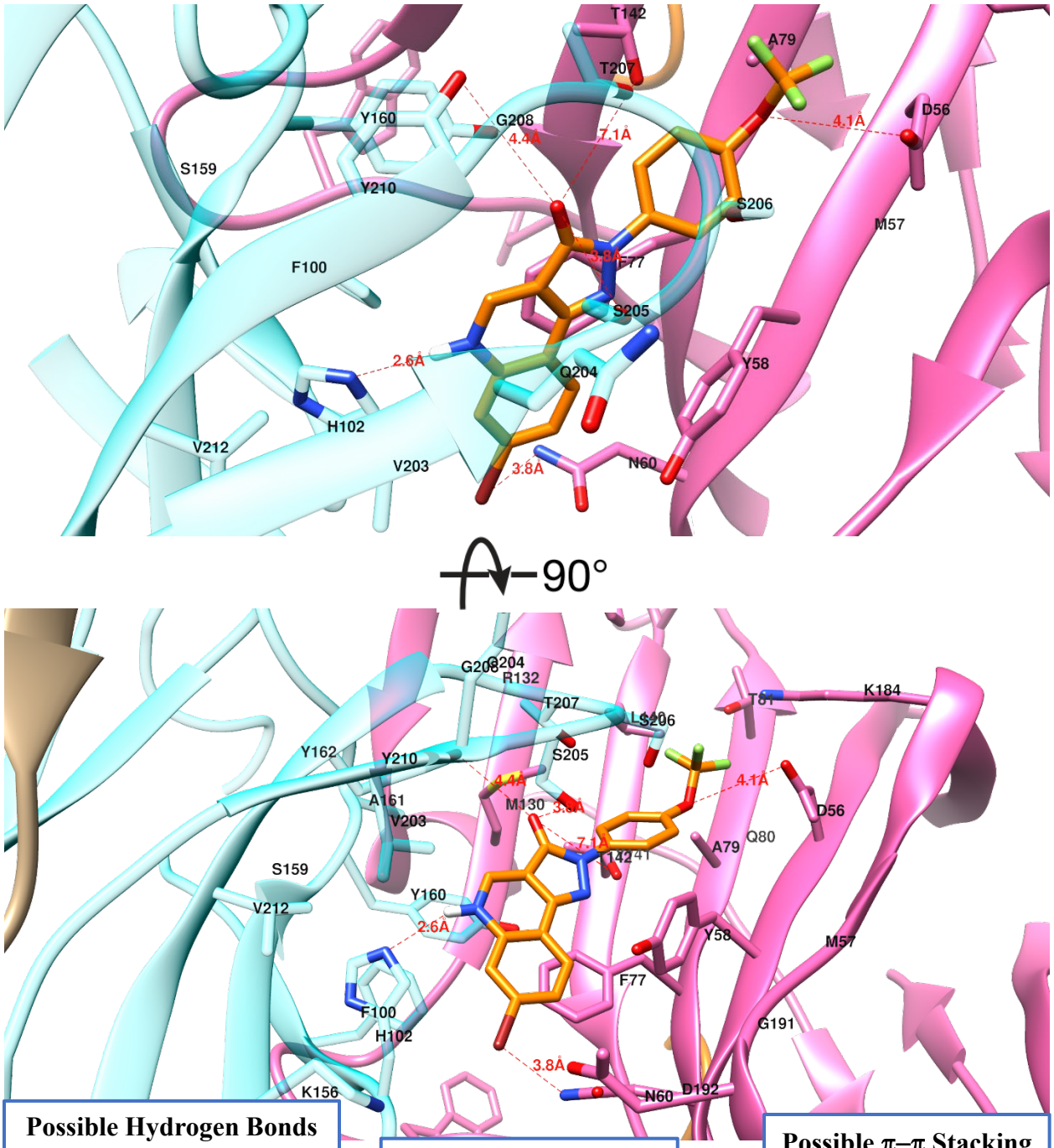

Possible Hydrogen Bonds	Possible Electrostatic Interactions	Possible π–π Stacking
αH102	αS205	αF100
αY210	αS206	αY160
γD56	αT207	αY210
γN60		γY58
γT142		γF77

1.22.9. Modeling of DK-IV-19-1 (14r)

BZP Binding Affinity: 32 nM: **Blue:** α1 subunit **Pink:** γ2 subunit

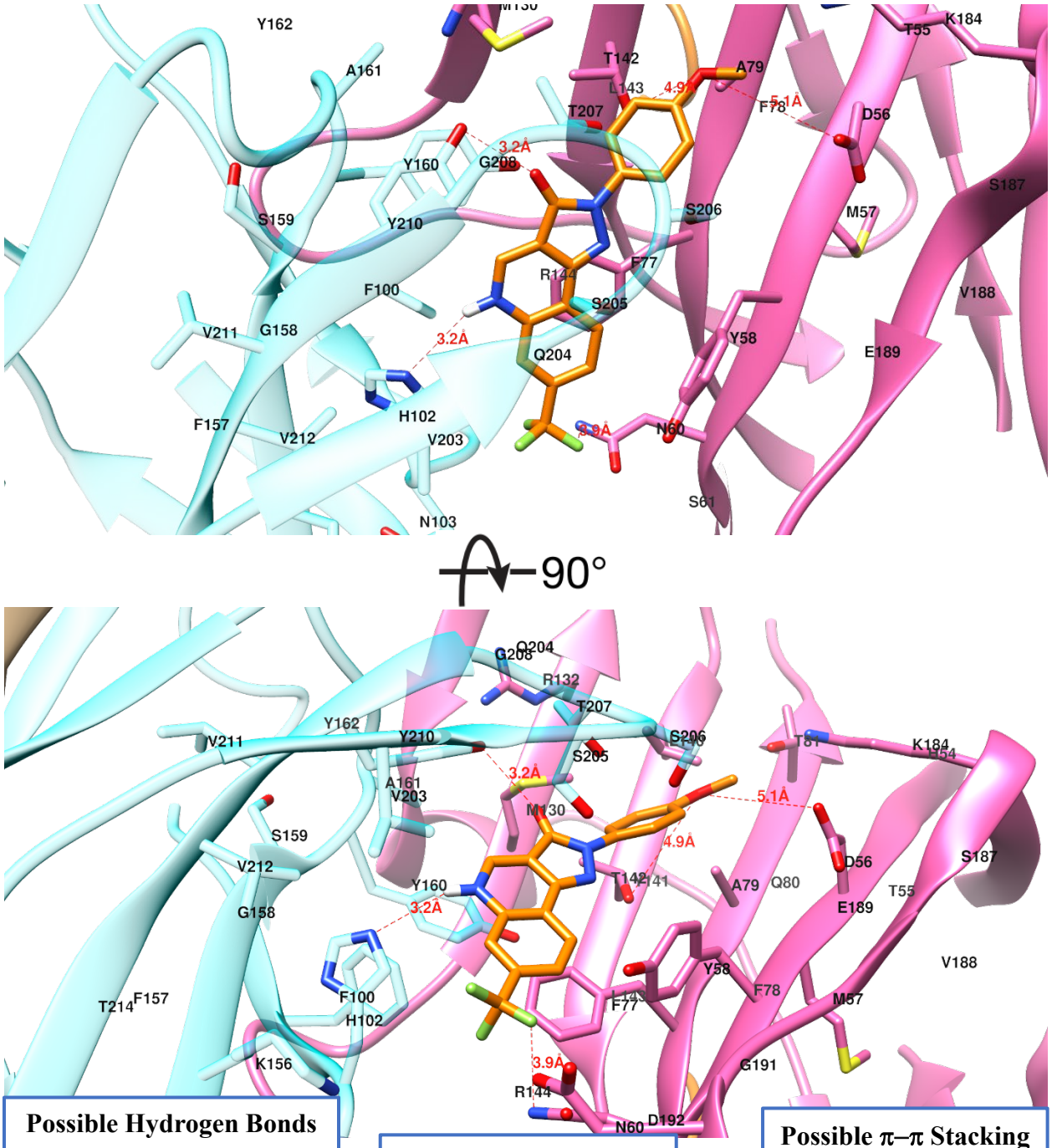

Possible Hydrogen Bonds	Possible Electrostatic Interactions	Possible π–π Stacking
αH102	αS205	αF100
αY210	αS206	αY160
γD56	αT207	αY210
γN60		γY58
γT142		γF77

1.22.10. Modeling of MM-I-10 (14l)

BZP Binding Affinity: 964 nM: **Blue:** α1 subunit **Pink:** γ2 subunit

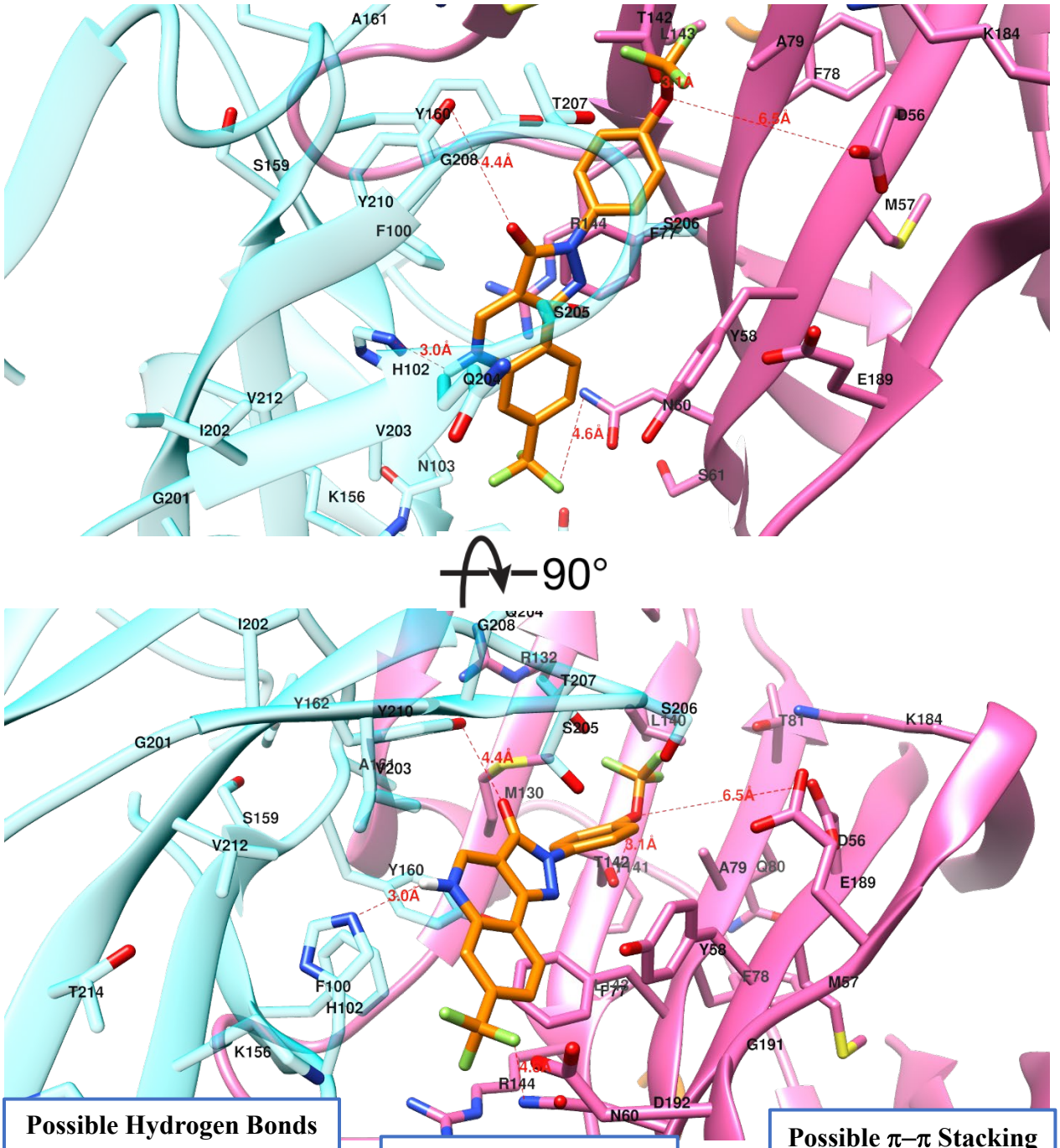

Possible Hydrogen Bonds	Possible Electrostatic Interactions	Possible π–π Stacking
αH102	αS205	αF100
αY210	αS206	αY160
γD56	αT207	αY210
γN60		γY58
γT142		γF77

1.22.11. Modeling of DK-I-59-1 (8j)

BZP Binding Affinity: 1.2 nM: **Blue:** α1 subunit **Pink:** γ2 subunit

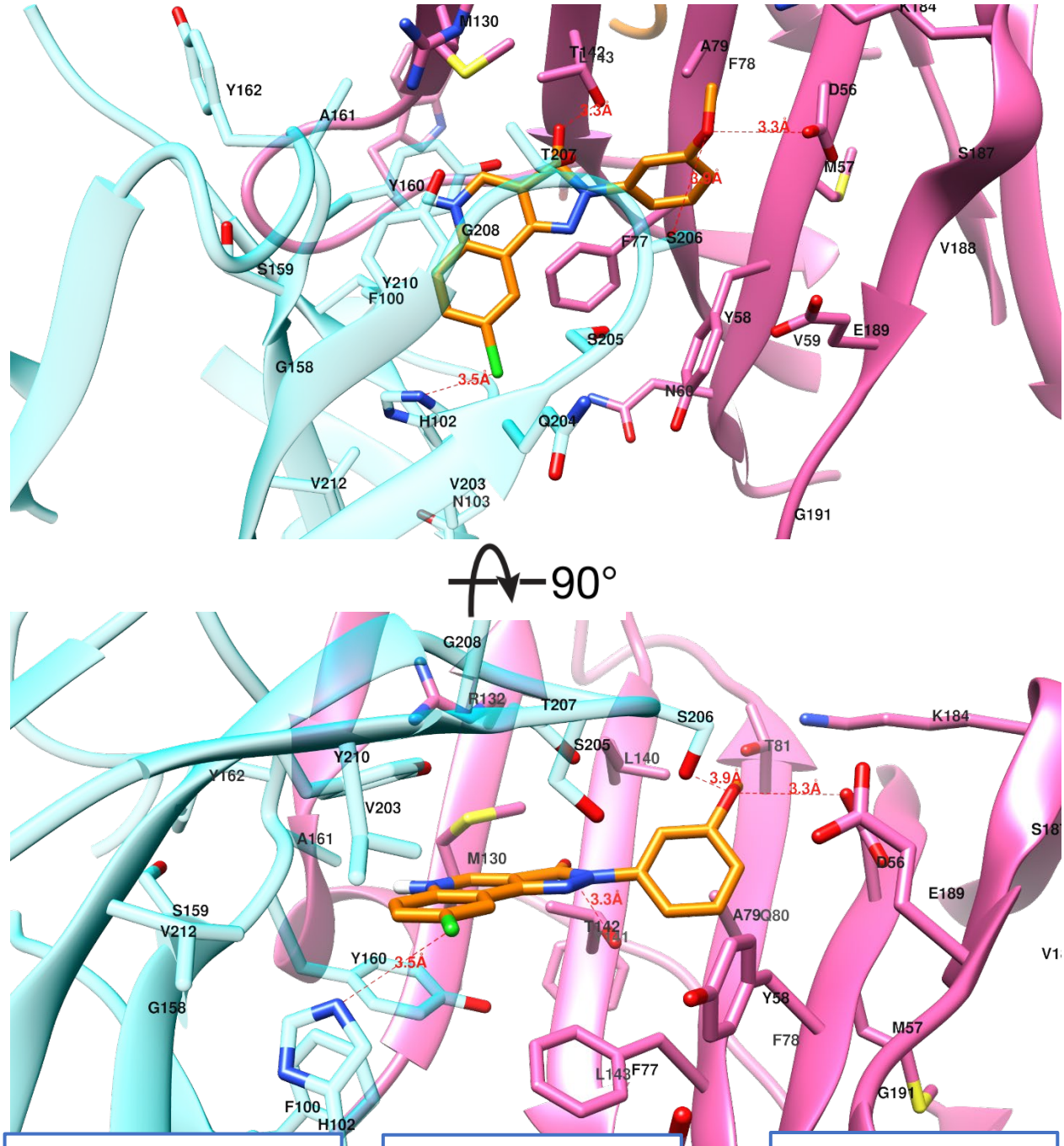

Possible Hydrogen Bonds	Possible Electrostatic Interactions	Possible π–π Stacking
αH102	αS205	αF100
γD56	αS206	αY160
γT142	αT207	αY210
		γF77

1.22.12. Modeling of DK-I-87-1 (8m)

BZP Binding Affinity: 98 nM: **Blue:** α1 subunit **Pink:** γ2 subunit

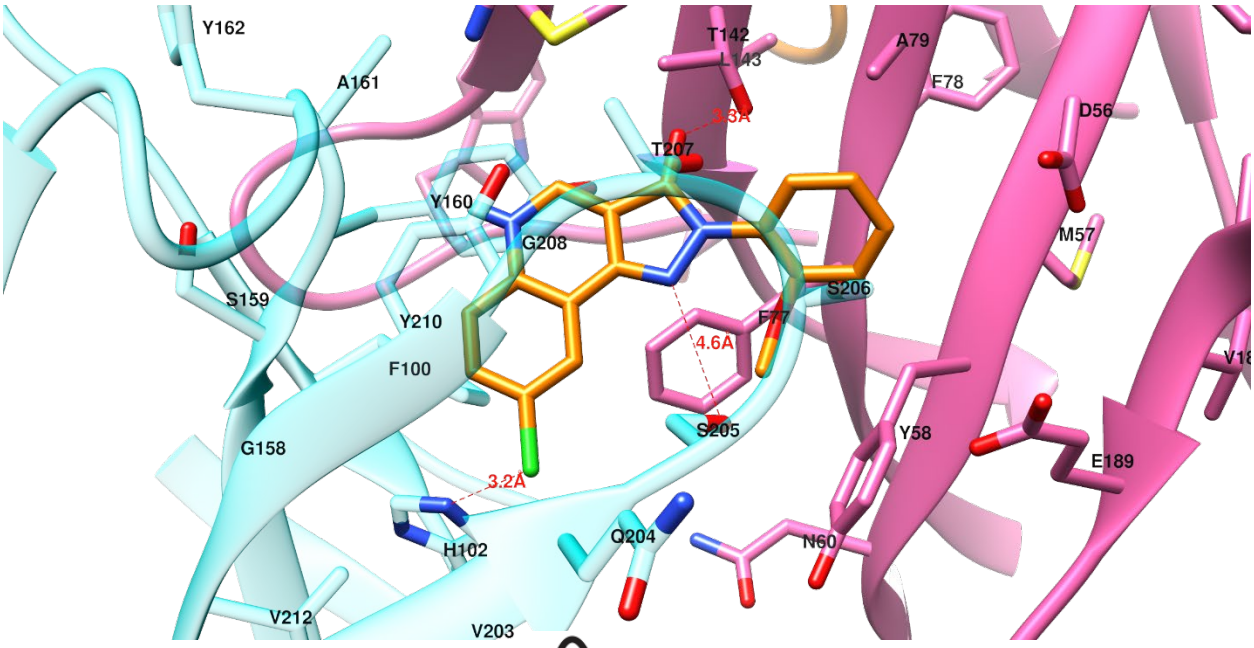

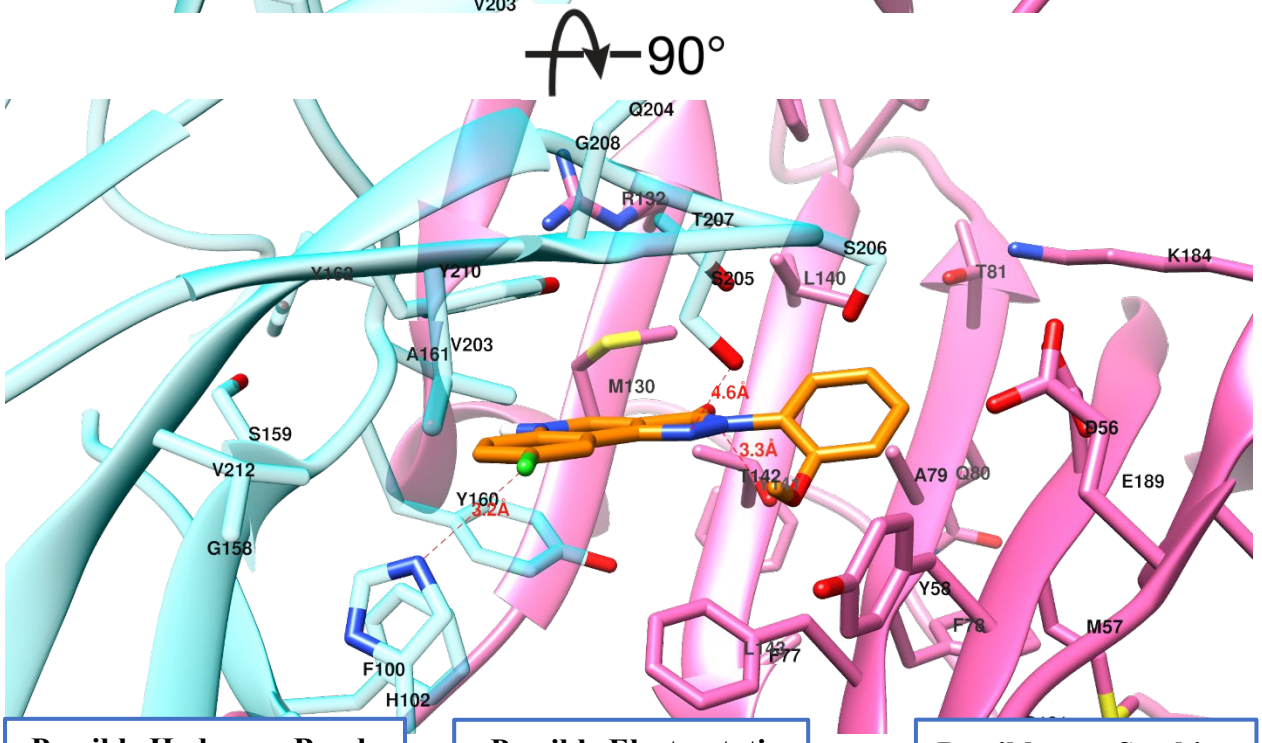

Possible Hydrogen Bonds	Possible Electrostatic Interactions	Possible π–π Stacking
αH102	αS205	αF100
γT142	αS206	αY160
	αT207	αY210
		γF77

Chapter 2: Process Development of α2/3-GABA$_A$R Subtype-selective Imidazodiazepines: HZ-166 and KRM-II-81

2.1. Introduction to α2/3-GABA$_A$R Subtype-selective Imidazodiazepines

Epilepsy is a chronic neurological disorder suffered by millions of people world-wide with large negative health outcomes and life disruption.[111] Many antiepileptic drugs of different structural and pharmacological classes have been approved for medical use.[112] Nonetheless, seizures are often not fully controlled despite the daily administration of more than one antiepileptic. In up to 70% of epileptic patients, standard of care medicines are not efficacious.[113-115] The uncontrolled seizures can also increase the probability of subsequent epileptic events through sensitization mechanisms termed seizure kindling.[116-119] Chronic, uncontrolled seizures and the side effects arising from seizure medications have a negative impact on the developing and adult brain and can lead to severe impairment of neurocognitive function.[120, 121] Uncontrolled seizures can also increase the liklihood of neuronal cell death and patient lethality.[122] Therefore, there continues to be an urgent need for improved antiepileptic drugs (http://advocacy.epilepsy.com).[123]

The ligand, 5-(8-ethynyl-6-(pyridin-2-yl)-4*H*-benzo[*f*]imidazo[1,5-*a*][1,4]diazepin-3-yl)oxazole or KRM-II-81 (**Figure 48**) is a positive allosteric modulator (PAM) of α2/3-containing GABA$_A$ receptors (**Figure 47**) with potential for medicinal use in epilepsy based upon preclinical data acquired over the past several years (**Table 12**). Excitement over this molecule arises from the fact that although GABA is a long-known modulator of epilepsy, GABA$_A$ receptor PAMs like DZP cannot be used as antiepileptic agents due to the sedation and motoric side effects occurring at anticonvulsant doses.[112] DZP

does not discriminate among $GABA_A$ receptors composed of different alpha subunits, whereas KRM-II-81 is selective for α2/3-containing $GABA_A$ receptors.[124, 125] Genetic mutation experiments combined with pharmacological studies with alpha subtype-selective molecules have long suggested eliminating potentiation of α1-containing $GABA_A$ receptors as one means of reducing sedation and motor impairment.[126]

Figure 47: The $GABA_AR$ α2/3β3γ2 Subtypes

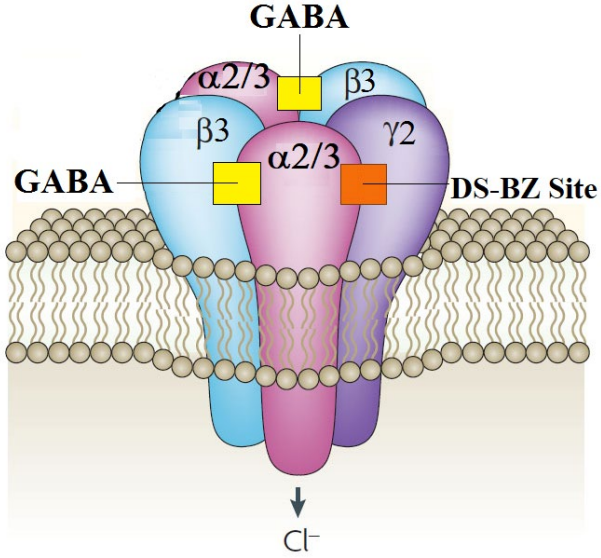

[a]The GABAAR α2/3β3γ2 subtypes are a pentameric ligand-gated chloride channels comprised of two α2(or two α3), two β3 and one γ2 subunits. IBDZs (like HZ-166 and KRM-II-81) mediate their effects at the DS-Bz site (α2+γ2- interface or α3+γ2-) as positive allosteric modulators (PAMs). The IBDZ site (DS-Bz binding site) and the endogenous ligand (GABA) binding sites at the β3+α2- and β3+α3- interfaces are displayed. Image modified from Jacob et al., Nature Reviews Neuroscience, 2008.

Figure 48: The Lead α2/3-Selective Ligands of this Work

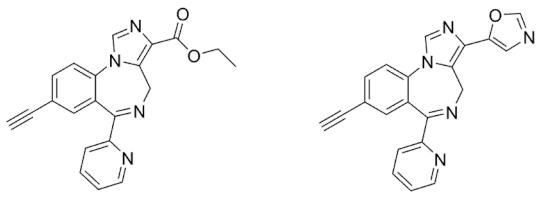

KRM-II-81 exhibits reduced sedation and motoric burden compared to DZP.[127, 128] As such there is the opportunity for achieving higher drug exposures with KRM-II-81 to modulate $GABA_A$ receptors for improved therapeutic advantage. This gain in efficacy has been demonstrated with KRM-II-81 in models of pain where DZP could not be dosed sufficiently high enough to achieve efficacy, whereas KRM-II-81 was at least as efficacious and more potent than the clinical agent tramadol.[129] In rodent epilepsy models, KRM-II-81 has also shown greater efficacy than DZP under most assay conditions (**Table 12**).

A recent licensing option agreement from RespireRx to acquire this molecule from the University of Wisconsin-Milwaukee established increased prioritization toward the development of KRM-II-81 for epileptic patients. Although the case for development of KRM-II-81 as an antiepileptic agent is gaining traction (**Table 12**), there are some gaps in the biology. As an anticonvulsant against chemically induced seizures, KRM-II-81 has only been studied against pentylenetetrazol (PTZ). However, since PTZ is a $GABA_A$ receptor antagonist, the blockade of seizures with a $GABA_A$ receptor PAM like KRM-II-81 or DZP is expected on pharmacological grounds; blockade of seizures might be due to receptor pharmacology rather than to suppression

of the seizurogenic effects of PTZ per se. The present study addresses this deficiency by studying a broader array of chemical convulsants with diverse non-$GABA_A$ receptor mechanisms, thus enabling a pure test of the antiepileptic hypothesis.

Table 12: Effects of KRM-II-81 in Models Predicting Antiepileptic Efficacy in Patients[130]

Model System	Species	Activity	Efficacy	Reference
NEURONAL CULTURE				
Dissociated cortical neurons	Rat	Yes	ND	Witkin et al., 2018
CHEMICAL SEIZURE PROVOCATION MODELS				
Pentylenetetrazol – clonic seizures	Rat	Yes	= Diazepam	Witkin et al., 2018
ELECTRICAL SEIZURE PROVOCATION MODELS				
6Hz stimulation – 44mA	Mouse	Yes	ND	Witkin et al., 2018
Electroconvulsive Shock	Mouse	Yes	= Diazepam	Witkin et al., 2018
SEIZURE SENSITIZATION				
Corneal kindling	Mouse	Yes	>Tpm	Witkin et al., 2020
Amygdala kindling-ADT	Rat	Yes	> Diazepam	Witkin et al., 2018
Amygdala kindling-ADD	Rat	Yes	= Diazepam	Witkin et al., 2018
Amygdala kindling-Seizure Severity	Rat	Yes	= Diazepam	Witkin et al., 2018
PHARMACORESISTANT MODELS				
Mesial temporal lobe epilepsy	Mouse	Yes	>Ltg, Val	Witkin et al., 2020
Ltg-insensitive kindling	Rat	Yes	>Ltg, Tpm	Witkin et al., 2020
Kainate-induced chronic epilepsy	Rat	Yes	>Ltg, Lev	Witkin et al., 2020
HUMAN EPILEPTIC TISSUE				
Picrotoxin stimulation	Human	Yes	ND	Witkin et al., 2018
4-Aminopyridine stimulation	Human	Yes	ND	Witkin et al., 2018

ADT – After-discharge threshold, ADD- After-discharge duration, Tpm – topiramate, Ltg – lamotrigine,Val – valproate, Lev – levetiracetam, ND – no comparative data

KRM-II-81 (**8**) has also shown an ability to block seizures in rodent models where seizures have been developed over time by sensitizing seizure networks by daily brain stimulation, a process known as seizure kindling. Seizure kindling can be modeled in rodents and is often used to model the pathogenesis of pharmacoresistant or refractory epilepsy.[131, 132] The data in **Table 12** summarize the ability of KRM-II-81 to suppress the expression of seizures that have already been developed (blockade of seizure expression). What remains unknown is whether KRM-II-81 can block the development of the seizure sensitization process. Suppression or reduction in the development of seizure sensitization is the holy grail of antiepileptic drug development, a result suggesting that disease progression can be halted or slowed.[131, 133] In contrast to other $GABA_A$ receptor PAMs like some neuroactive steroids, DZP has limited impact on this process.[134, 135] In order to determine the relative efficacy of KRM-II-81 on seizure sensitization, the effects of DZP and KRM-II-81 were compared in two seizure kindling models in the present study.

Another obstacle to the development of KRM-II-81 (**8**) for epileptic patients is the synthesis of GMP material on large scale for IND-enabling toxicology and for first in human dosing. Previous work has created synthetic routes from the precursor molecule HZ-166 (**6**) (**Figure 48**). The first route employed a three step approach which involved a low yielding LAH reduction of the ester (HZ-166) to an alcohol which was then subsequently oxidized by manganese dioxide to the aldehyde **7**.[125] A modification of this synthesis by Li et al.[136] improved these final steps of the synthesis by converting HZ-166 to its respective ester bioisostere KRM-II-81 in two steps by switching the reduction reagent to PDBBA to afford the key aldehyde **7** directly. However, a process conducive to larger scale chemistry was still required to synthesize

the ester precursor (HZ-166) to KRM-II-81. One sought to replace the chromatographic purification steps employed in all five steps of the earlier discovery process for the synthesis of HZ-166 (**6**) with crystallizations. In addition, to address scale up issues including poor stirring, side product formation, long process times and yield losses on large scale. Provided herein is a method for production of kg quantities of HZ-166 and KRM-II-81.

2.2. Discussion and Conclusions of Anticonvulsant, KRM-II-81, which Produces Novel, Non-diazepam-like Antiepileptogentic Effects

KRM-II-81 (8) has Broader Efficacy Against Chemical Convulsant Agents than DZP with Dr. Jeffrey M. Witkin and coworkers. In order to extend the observations on the anticonvulsant activity of KRM-II-81 to other, non-GABA convulsants, the convulsant chemicals that act upon monoamine transporters (cocaine), sodium channels (4-aminopyridine or 4-AP), N-methyl-D-aspartate (NMDA) receptors (NMDA), glycine receptors (strychnine), and muscarinic cholinergic receptors (pilocarpine) were studied. In addition, PTZ and another antagonist of $GABA_A$ receptors, picrotoxin, were also studied. The comparative efficacy of DZP (1 mg/kg, i.p.) and KRM-II-81 (30 mg/kg, i.p.) are summarized in **Table 13**. The dose of DZP and KRM-II-81 were based upon maximal, but not supramaximal, efficacious doses for blocking PTZ-induced clonus.[128, 134] In these experiments, KRM-II-81 was effective against some or all measures of toxicity driven by each of the convulsant agents whereas diazepam was not universally effective. For PTZ, both DZP and KRM-II-81 significantly attenuated clonic convulsions, as previously reported in rats.[128]

Table 13: Comparative Efficacy of Diazepam and KRM-II-81 as Anticonvulsants Against Some Chemoconvulant Agents.[a]

Drug	Event	Vehicle	Diazepam	KRM-II-81	Efficacy Bias
Cocaine	Clonus	8/8	6/10	4/10*	
75 mg/kg, i.p.	Tonus	0/8	0/10	0/10	
	Lethality	0/8	0/10	0/10	
PTZ	Clonus	8/8	2/8*	1/8*	
75 mg/kg, s.c.	Tonus	6/8	2/8*	1/8*	
	Lethality	7/8	0/8*	0/8*	
4-AP	Clonus	8/8	5/8	2/8*	
14 mg/kg, i.p.	Tonus	7/8	4/8	1/8*	
	Lethality	7/8	1/8*	0/8*	
NMDA	Clonus	7/8	4/8	2/8*	
200 mg/kg, i.p.	Tonus	0/8	0/8	0/8	
	Lethality	7/8	4/8	2/8*	
Pictrotoxin	Clonus	8/8	2/8*	1/8*	
6 mg/kg, i.p.	Tonus	4/8	2/8	0/8*	
	Lethality	5/8	2/8	0/8*	
Strychnine	Clonus	8/8	6/8	3/8*	
2 mg/kg, i.p.	Tonus	8/8	6/8	3/8*	
	Lethality	8/8	7/8	4/8*	
Pilocarpine	Clonus	8/8	2/8*	1/8*	
300 mg/kg, i.p.	Tonus	3/8	1/8	0/8	
	Lethality	7/8	2/8*	0/8*	

Bias: KRM-II-81 > Diazepam
Bias: Diazepam > KRM-II-81
Bias: Diazepam = KRM-II-81
Bias: No Difference from Vehicle
Diazepam: 1 mg/kg, s.c., 30 min prior
KRM-II-81: 30 mg/kg, i.p., 30 min prior

[a]Blue and red data indicate animals that convulst.

Prior studies with PTZ[128] did not study doses inducing tonic seizures and lethality. Here we show that both DZP and KRM-II-81 also significantly reduce these toxic endpoints induced by PTZ. Although a similar profile of comparative protection occurred when studying $GABA_A$

receptor antagonist picrotoxin, the statistical preference for KRM-II-81 might be due to the relatively small percentage of tonic convulsions and lethality that were produced by the dose of picrotoxin studied. As with the $GABA_A$ receptor antagonists PTZ and picrotoxin, both DZP and KRM-II-81 were also equally effective against the muscarinic cholinergic receptor agonist pilocarpine.

In contrast, for cocaine (COC), 4-AP, NMDA, and strychnine, KRM-II-81 was efficacious when DZP was not. Clonic convulsions were blocked by KRM-II-81 for all of these convulsant compounds. But the differential efficacy of KRM-II-81 over DZP extended also to tonic seizures and lethality in the case of 4-AP, strychnine, and NMDA (lethality). The findings reported here are consistent with the literature on the anticonvulsant effects of DZP.[119, 137-141] Overall, the data support the conclusion that KRM-II-81 has broad ranging anticonvulsant efficacy against chemical convulsants (**Table 13**). Further, the data in **Table 13** support the conclusion that KRM-II-81 has a superior efficacy profile to that of DZP as shown earlier with other seizure provoking stimuli (**Table 12**).

KRM-II-81 but Not DZP Blocks the Development of PTZ Kindling. When PTZ, in a subconvulsant dose (45 mg/kg), is given every other day for 4 days, the percentage of mice exhibiting clonic seizures increases (**Figure 49A**) as previously reported[134]. On the 5th experimental session, either vehicle, DZP (1 mg/kg, i.p.), or KRM-II-81 (30 mg/kg, i.p.) was given prior to PTZ. Both DZP and KRM-II-81 prevented clonic seizures in these PTZ-sensitized mice (**Figure 49A**) thus demonstrating their abilities to block seizures in fully sensitized animals.

In order to test whether these compounds also prevent the expression of seizure kindling, either vehicle, DZP or KRM-II-81 was administered prior to each dose of PTZ. Under these conditions, both drugs fully protected mice from the occurrence of seizures and the increased sensitivity that develops to PTZ in the absence of treatment (**Figure 49B**). Another experiment was conducted in order to assess whether these compounds can prevent or attenuate the development of seizure sensitization. In this study, vehicle, DZP, or KRM-II-81 was given on each of the first 4 experimental sessions prior to PTZ. Then, on day 10 (experimental session 5), mice were given PTZ alone (with vehicle pretreatments). While prior exposure to KRM-II-81 + PTZ inoculated mice from the seizure sensitizing effects of PTZ dosing, DZP did not (**Figure 49C**). Thus, despite the ability of DZP to block both acute and sensitized effects of PTZ, DZP was not able to dampen the sensitization process.

Figure 49: Effects of Vehicle, Diazepam (1.0 mg/kg), or KRM-II-81 (30 mg/kg) on Seizure Sensitization (kindling) Due to Every Other Day Dosing with PTZ (45 mg/kg).

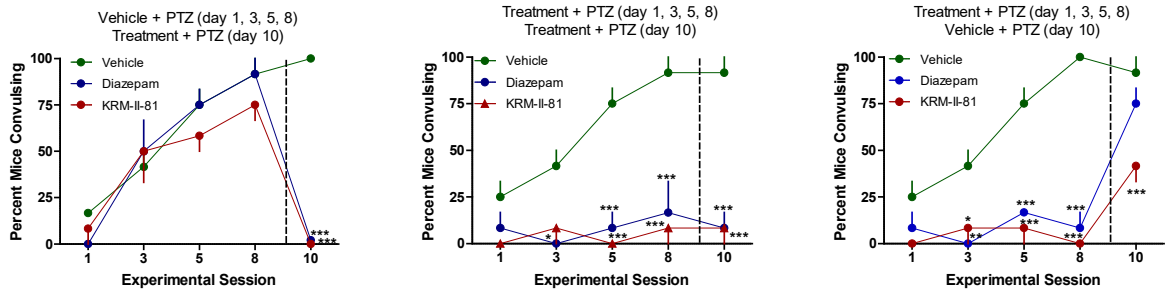

A. Effects of compounds on fully developed PTZ kindled seizures. **B**. Effects of compounds on the expression of PTZ kindling. **C.** Effects of compounds on the development of PTZ kindling. Each point represents the mean ± S.E.M. of 6 mice each. Statistical evaluation of the data with two-way ANOVA with repeated measures followed by Bonferroni post-hoc tests comparing vehicle to diazepam or KRM-II-81 – **A.** Effects of compound treatment: $F_{2,12}$=8.25, p=0.06; Experimental session: $F_{4,12}$=49, p<0.001; Interaction: $F_{8,12}$=10.2, p<0.001; Subjects: $F_{3,12}$=1.92, p=0.18. **B.** Effects of compound treatment: $F_{2,12}$=409, p< 0.001; Experimental session: $F_{4,12}$=5.22, p<0.05; Interaction: $F_{8,12}$=3.22, p<0.05; Subjects: $F_{3,12}$=0.16, p=0.92. **C.** Effects of compound treatment: $F_{2,12}$=154, p< 0.001; Experimental session: $F_{4,12}$=30.7, p<0.0001; Interaction: $F_{8,12}$=6.89, p<0.05; Subjects: $F_{3,12}$=0.55, p=0.66.

Another study was conducted in order to extend these observations to another seizure kindling agent. Cocaine (COC) was chosen since the DZP and KRM showed differential efficacy against PTZ and COC convulsant challenge. Whereas in the case of PTZ, DZP and KRM-II-81 were equieffective in preventing seizures induced by acutely-administered PTZ, only KRM-II-81 was efficacious against acutely-administered COC (**Table 13**). Seizure kindling with COC was studied as with PTZ kindling with the exception that COC kindling was conducted every day[142, 143] vs. the every other day dosing method that is established for PTZ kindling[134]. In this study, COC given daily for 5 days produced significant and large changes in the percentage of mice exhibiting clonic convulsions on day 5 vs. day 1 (**Figure 50A**) demonstrating the occurrence of seizure kindling. On day 6, either vehicle, DZP (1 mg/kg, i.p.) or KRM-II-81 (30 mg/kg, i.p.) was given prior to COC challenge. The KRM-II-81 but not DZP significantly attenuated clonic seizure incidence in mice (**Figure 50A**) as was observed after acute COC challenge (**Table 13**). Thus, both in non-sensitized mice and fully kindled mice, KRM-II-81 but not DZP is an effective seizure protectant. The expression of kindled seizures over the 6-day period of COC dosing was assessed next. KRM-II-81 significantly attenuated the expression of COC seizures across 6 days of COC dosing; DZP was not active (**Figure 50B**).

Figure 50: Effects of Vehicle, Diazepam (1.0 mg/kg), or KRM-II-81 (30 mg/kg) on Seizure Sensitization (kindling) Due to Daily Dosing with COC (60 mg/kg).

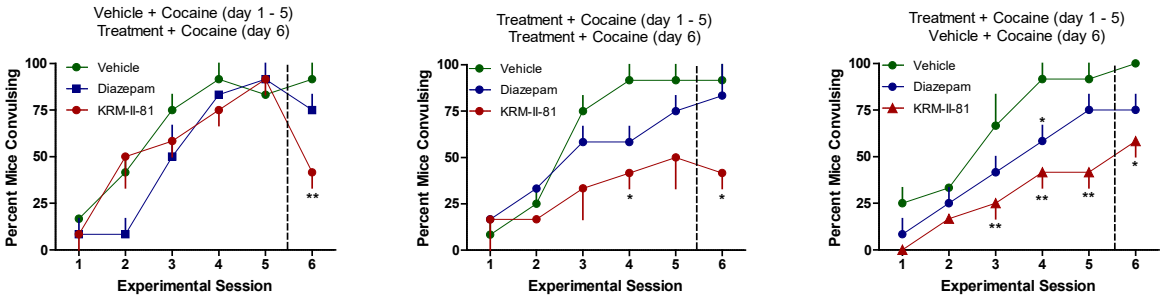

A. Effects of compounds on fully developed COC kindled seizures. **B**. Effects of compounds on the expression of COC kindling. **C.** Effects of compounds on the development of COC kindling. Each point represents the mean ± S.E.M. of 6 mice each. Statistical evaluation of the data with two-way ANOVA with repeated measures followed by Bonferroni post-hoc tests comparing vehicle to diazepam or KRM-II-81 – **A.** Effects of compound treatment: $F_{2,15}$=2.75, p=0.21; Experimental session: $F_{5,15}$=37.8, p<0.0001; Interaction: $F_{10,15}$=2.95, p<0.05; Subjects: $F_{3,15}$=1.77, p=0.20. **B.** Effects of compound treatment: $F_{2,15}$=18.0, p<0.05; Experimental session: $F_{5,15}$=17.3, p<0.0001; Interaction: $F_{10,15}$=1.61, p=0.20; Subjects: $F_{3,15}$=0.74, p=0.54. **C.** Effects of compound treatment: $F_{2,15}$=109, p<0.05; Experimental session: $F_{5,15}$=28.1, p<0.0001; Interaction: $F_{10,15}$=0.78, p=0.65; Subjects: $F_{3,15}$=0.26, p=0.85.

A final seizure kindling study was initiated to determine whether DZP or KRM-II-81 could prevent the development of COC seizure kindling. In this study, vehicle, DZP, or KRM-II-81 was given prior to each COC kindling session on days 1-5. On day 6, COC alone was given (+ vehicle) to ascertain whether seizure sensitization was suppressed by the prior drug treatments. On the day 6 test, KRM-II-81 (**8**) but not DZP significantly attenuated the development of seizure sensitization (**Figure 50C**). The blockade of seizure sensitization by KRM-II-81 appeared to be greater for PTZ kindling (**Figure 49C**) than that observed with COC kindling (**Figure 50C**) perhaps as a result of the more prominent effects of KRM-II-81 on acute PTZ vs. COC seizures (**Table 13**) and the greater ability to block expression of PTZ vs. COC kindling (**Figure 49B** vs. **Figure 50B**). However, it is critical to emphasize that even though

DZP is an effective anticonvulsant against acute seizures induced by PTZ (**Table 13**) and is efficacious as a suppressor of the expression of PTZ sensitization, DZP is still not effective as a blocker of the epileptogenic phenomenon of seizure sensitization while KRM-II-81 is. The data for DZP reported here are consistent with prior findings.[134, 135, 142, 143] Overall, the kindling experiments document the differential ability of KRM-II-81 to significantly suppress the development of the seizure sensitization process and that this antiepileptogenic effect is not confined to the $GABA_A$ receptor antagonist convulsant PTZ. It also must be remembered that DZP in humans develops tolerance to the anticonvulsant effects in 2 to 3 days. Consequently, it can only be employed for status epilepticus for 1-3 days.

2.3. Improved Synthesis of α2/3-$GABA_A$R Subtype-selective Imidazodiazepines

Given the potential therapeutic value of KRM-II-81 for patients as discussed above and elsewhere,[127, 128, 144] a novel method for the synthesis of KRM-II-81 with efficiency on a large scale was developed. The synthesis of **KRM-II-81** (**Scheme 14**) has been reported previously,[125, 136] but the discovery chemistry was not well-suited for scale up in a potential GMP manufacturing setting. All five steps of the synthesis to the key intermediate **HZ-166**[145, 146] required purification by column chromatography, while several steps exhibited typical scaleup issues such as inefficient stirring, side product formation, prolonged process times and yield loss upon scale up.

Scheme 14: Discovery Synthesis of KRM-II-81

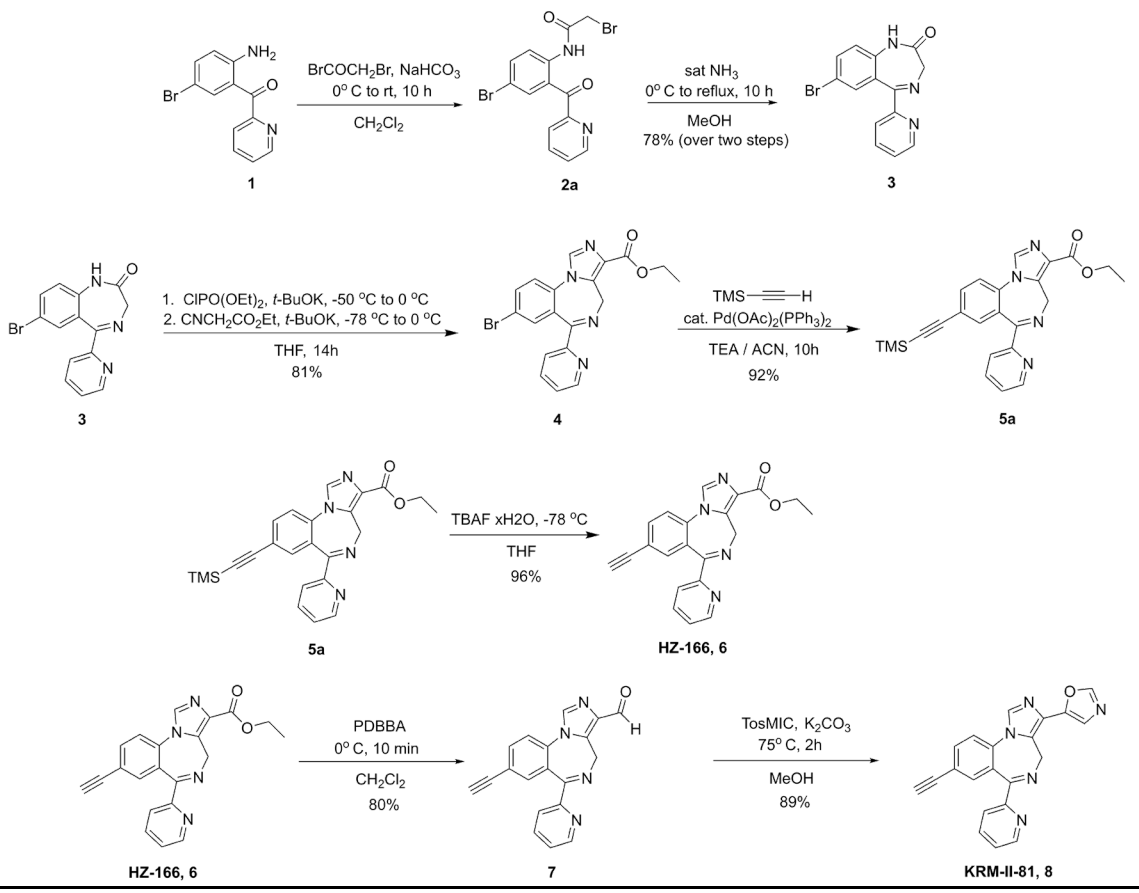

The challenge in the first step of the synthesis was to improve upon the stirring difficulties of the reaction media and the lack of an adequate purification procedure for multigram quantities. The discovery route developed by Li et al.[147] based on the work of Selnick et al.[148] called for cooling the mixture of 2'-pyridyl ketone **1**, sodium bicarbonate and dichloromethane to 0°C prior to the addition of bromoacetyl bromide. Early into the addition process an extremely thick red gelatinous-like solid developed that made efficient stirring of the reaction mixture near impossible. Upon warming to room temperature, the gelatinous solid would slowly dissipate, which resulted in a more readily stirred reaction mixture. Obviously, any procedure that is being developed for

large-scale synthesis cannot involve agitation issues. Similar research in the group utilized the same reaction protocol,[145, 149] but those analogs lacked the 2'-pyridine function and therefore lacked the stirring difficulties encountered herein. Upon consideration of a possible reaction mechanism (**Scheme 15**), it was proposed that formation of the desired 2-halooacetamide product **2c** must proceed through the insoluble acetyl pyridinium intermediate **2b** for which the red, gelatinous-like solid can be attributed.

Scheme 15: Proposed Route to Chloroacetamide (**2c**) Via Pyridium Salt (**2b**)

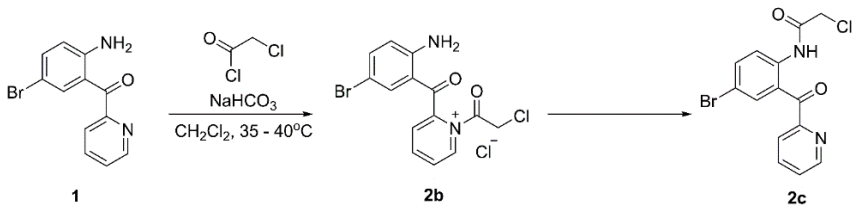

As a remedy, the initial reaction temperature was raised to 25 - 30°C prior to the addition of bromoacetyl bromide, while the bromo acetyl reagent was added over a 60 min time period. Utilization of this new approach completely avoided the agitation issue while the red, insoluble pyridinium intermediate **2b** was not observed to a significant amount. Presumably, the elevated process temperature increased the reaction rate enough, so the reaction did not stall at the pyridinium salt stage. Analysis of this reaction progress immediately after the addition of the bromide by TLC confirmed this observation for there was no evidence of the 2'-pyridyl ketone **1** nor pyridinium intermediate **2b**. Upon completion of the reaction, the inorganic salts were partitioned into the aqueous layer, after which the solvent was exchanged to ethanol to precipitate the pure halooacetamide product **2a** or **2c** (individually). No further purification was required. The employment of 2-chloroacetyl chloride as an economical substitute for 2-bromoacetyl bromide proved to perform equally as well in the reaction protocol with no detrimental effects to

the chemistry in the following steps. In summary, the modifications employed to the synthesis provided 125.6g of **2c** in 98.5% yield (2L reaction flask).

Scheme 16: Discovery Route to Benzodiazepine (**3**) with Imidate Impurity (**3c**)

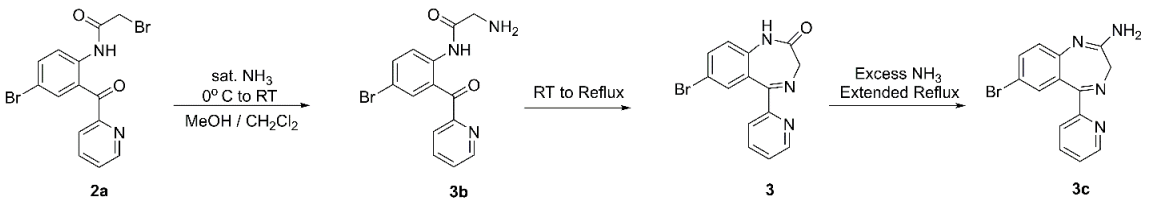

The second step of the synthesis furnished the benzodiazepine core **3** via the conversion of the chloroacetamide material **2c** into a β-amino amide intermediate **3b** prior to condensation of the amine with the carbonyl function. The process problems presented in this reaction sequence included the lack of a reliable and efficient method for purification of the amide **3** and the formation of detrimental side products observed on scale up. The discovery route (**Scheme 16**) utilized saturated methanolic ammonia to furnish the β-amino amide intermediate **3b** *in situ* by nucleophilic aliphatic substitution of the alkyl halide **2a** which then should cyclize via a carbinolamine condensation to yield the 2'-pyridyldiazepine **3**. As is typical with scale-up chemistry, process times (heating and cooling) and reaction times are prolonged, as compared to smaller scales and a subsequent drop in yield of the amide **3** was observed. An investigation of the causes revealed the formation of a significant side product that was observed to a small extent by TLC on small scale, but increased substantially as the scale was increased. The isolation of the impurity (m/z = 314.0167) indicated a mass unit one less than that of the desired product **3** (m/z = 315.0007). A thorough analysis of the structure of the impurity using ^{1}H NMR, ^{13}C NMR, HSQC, ^{1}H-^{13}C-HMBC, ^{1}H-^{15}N-HMBC spectroscopy experiments provided evidence which supported the proposed imidate **3c** as the structure of the impurity. The ^{1}H-^{15}N-HMBC experiments were

especially revealing because examination of them indicated the identity of the impurity **3c** contained 4 nitrogen atoms in the structure (**Figure 51**). The pyridine nitrogen atom (N13) correlated to pyridine ring protons (H11 and H12), while the remaining nitrogen atoms (N15, N18 and N19) correlated to the aliphatic CH_2 protons (H16). Finally, the iminium nitrogen atom (N18) correlated to the A-ring proton, H6. The logical explanation for the formation of the imidate (**3c**) would be through a dehydration mechanism first involving addition of ammonia into the benzodiazepine amide carbonyl via nucleophilic acyl substitution, which was followed by the elimination of water (**Scheme 17**). The mechanism seems reasonable because of the extended reaction times under high concentrations of ammonia. The considerations to mitigate the formation of the imidate **3c** included shorter reaction times and lower ammonia concentrations, but the application of these solutions were ruled out due to concern for low yields attributed to incomplete consumption of the starting material, which would then have to be removed.

Scheme 17: Proposed Imidate (**3c**) Formation Mechanism

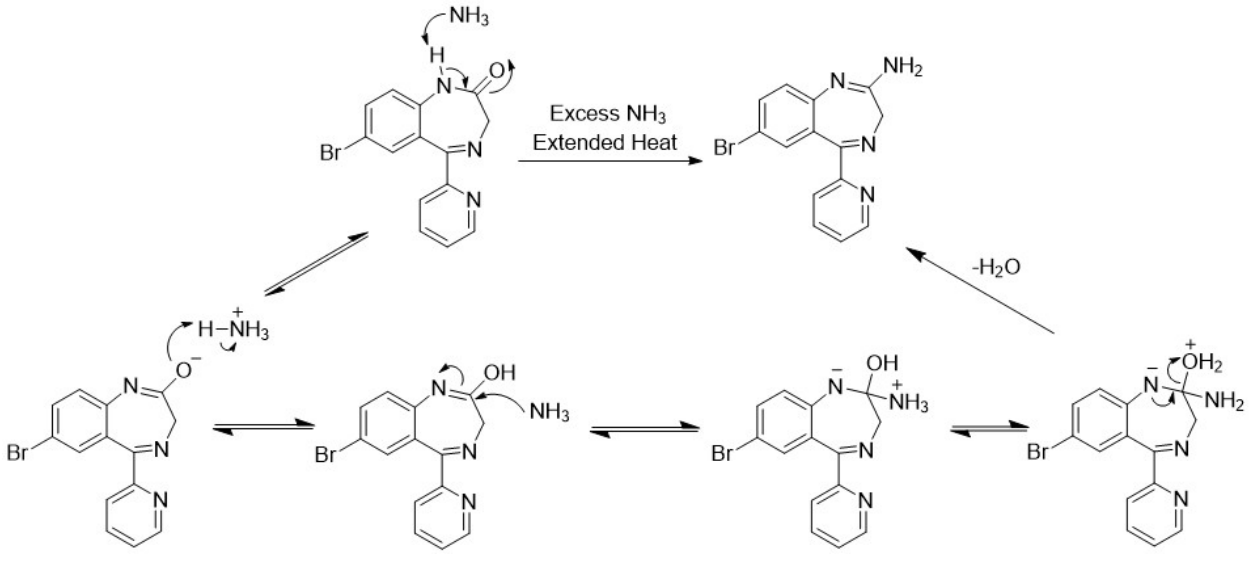

Figure 51: NMR Evidence (^{1}H-^{15}N-HMBC) for Imidate Impurity **3c** (in DMSO-d_6)

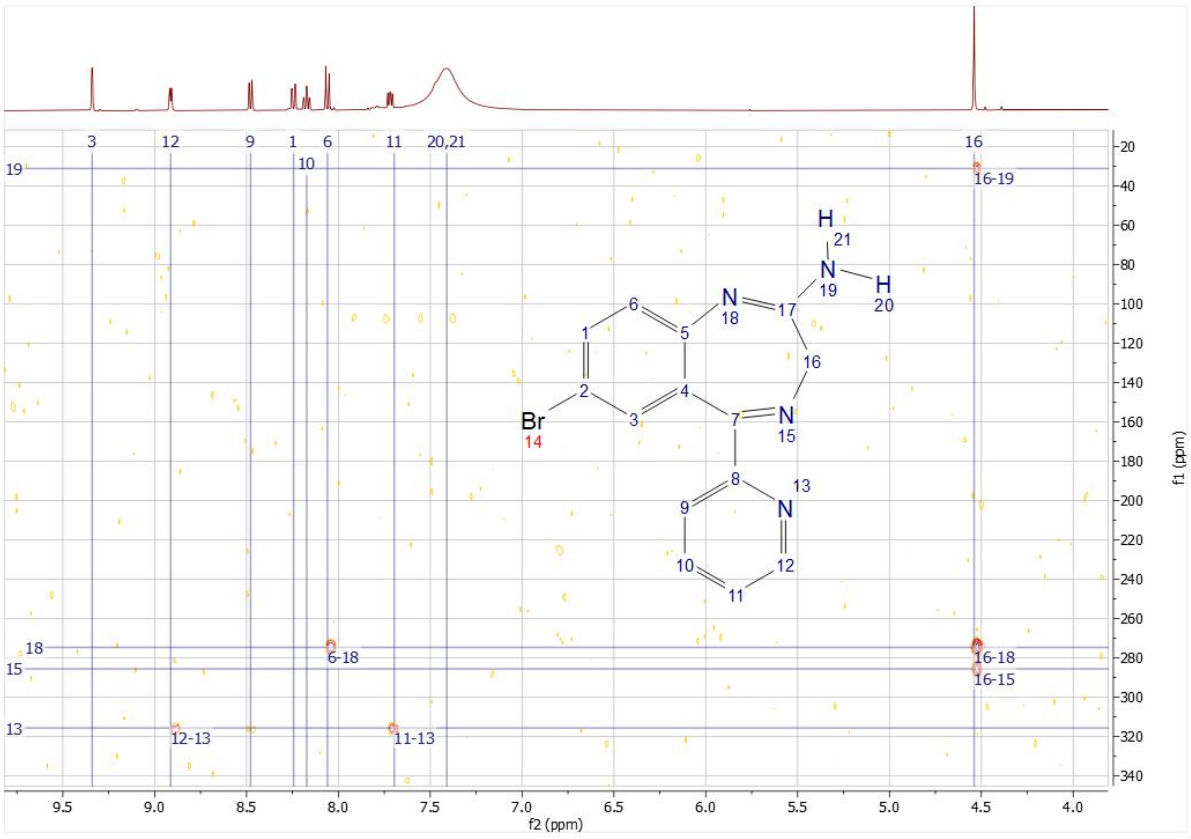

Scheme 18: Hexamethylenetetramine-(HMTM)-based Cyclization Reaction

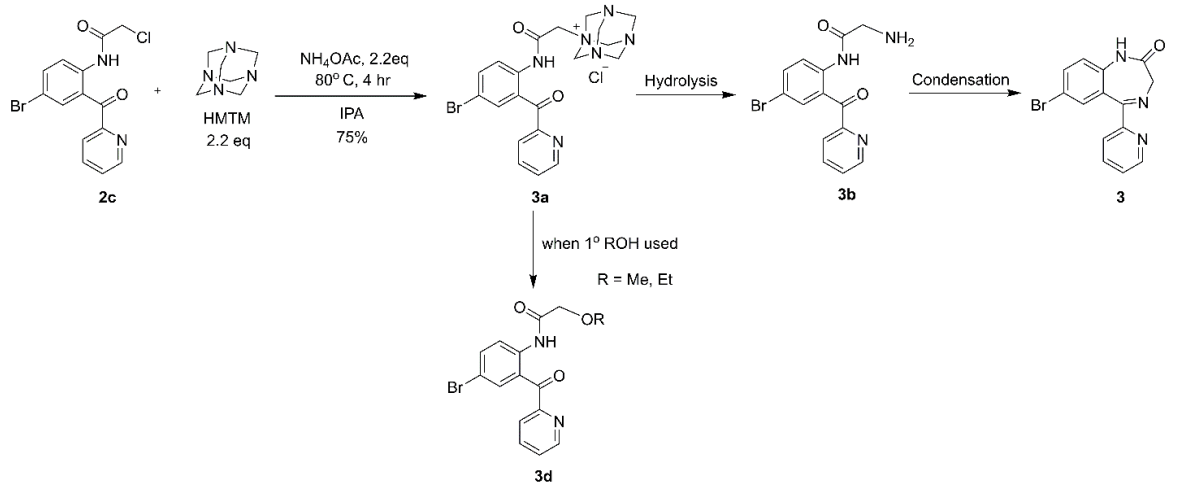

Clearly, a new approach to synthesis the key 2'-pyridyl-benzodiazepine core (**3**) was warranted. Here, one turned to the Delépine reaction developed by French chemist Stéphane Marcel Delépine.[150] It entailed incorporation of the hexamethylenetetramine-(HMTM)-based cyclization reaction first developed by Blažević and Kajfež[151] and further refined by Cepanec, et al.[152] The HMTM-based cyclization (**Scheme 18**) involved first, the formation of quaternary ammonium salt **3a** by nucleophilic aliphatic substitution of the alkyl halide **2** and this was followed by *in situ* hydrolysis to the β-amino amide intermediate **3b**, which was then condensed with the carbonyl function to provide the 2'-pyridyl-benzodiazepine **3**. This new approach performed well albeit slightly lower than expected yields (60-65%) than the literature report.[152] An investigation into the side products revealed a 5-10 % impurity identified as β-alkoxy amide **3d**. Presumably, when a primary alcohol (methanol or ethanol) was used as the solvent this undesired Sn2 addition of the alcohol to displace the tetramine to provide to **3d** was possible. Modification of the reaction

solvent to the secondary alcohol, 2-propanol (IPA) eliminated this side reaction since the corresponding β-alkoxy amide impurity **3d** was not detected, while the corresponding yield increase was realized. Gratifyingly, on large-scale (2L flask) the utilization of the Delépine reaction delivered 75g (75% yield) of 2'-pyridyl-benzodiazepine **3**. The proposed Delépine reaction mechanism is exhibited in **Scheme 19**.

Scheme 19: Proposed Delépine Reaction Mechanism

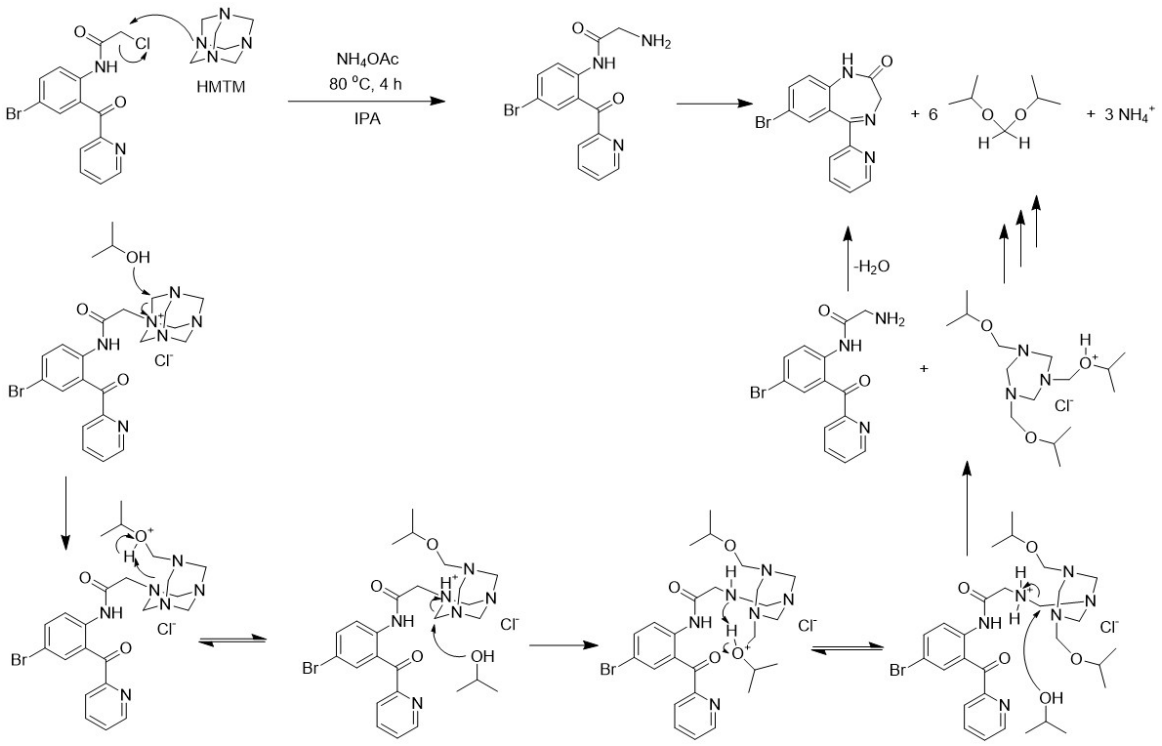

Scheme 20: Synthetic Route to Imidazodiazepine **4**

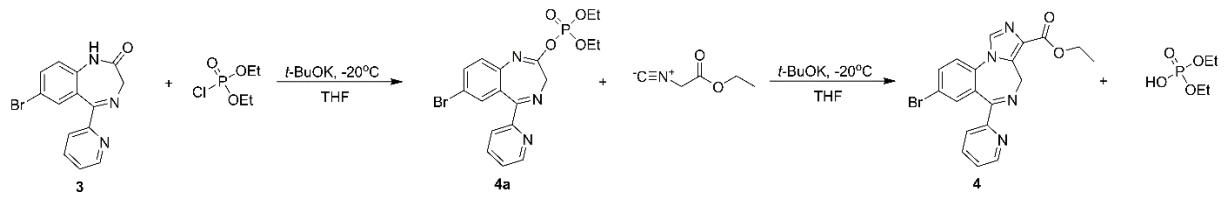

The third step of the synthesis of **HZ-166** was to install the imidazole ring C to produce imidazodiazepine **4**. The previous procedure[153] involved formation of the iminophosphate **4a** (**Scheme 20**) by deprotonation of the starting amide using potassium *t*-butoxide and this was followed by the addition of diethylchlorophosphate. Then, iminophosphate **4a** subsequently underwent a nucleophilic addition with the enolate of ethyl isocyanoacetate to furnish the desired imidazodiazepine **4**. Several improvements to the original chemistry were required in order to provide a reliable and scalable procedure. Initially, the purification was conducted using column chromatography. Secondly, the reagents were added in an "all in one" fashion and specifically as a solid in the case of the portions of potassium *t*-butoxide. Thirdly, each subsequent addition of a reagent involved cooling of the reaction mixture to below -35°C. Then, the next reagent was added and finally the mixture was allowed to warm to 0°C for each constituent of the process to react. With those challenges in mind one sought to develop a purification method by crystallization and to determine a reaction temperature in which the reagents could be added in a controlled fashion at a temperature at which they would react. By careful monitoring of the reaction progress by TLC it was determined that the iminophosphate **4a** did not form until the reaction temperature reached -20°C. Similarly, it was determined that the required reaction temperature of the condensation of the enolate of ethyl isocyanoacetate with the iminophosphate **4a** was -35 to -30°C. Consequently, it was felt that addition of the reagents in a controlled, dropwise fashion would allow one to simply

hold the reaction mixture at -20 to -15ºC throughout the sequence of additions. This procedure first involved dissolving benzodiazepine **3** in tetrahydrofuran and cooling that solution to -20ºC. Then, a solution of potassium *t*-butoxide (1.3 eq) in THF was added dropwise over 30 minutes to the reaction mixture. The reaction mixture was then stirred for 30 minutes at -20 to -15ºC to ensure complete deprotonation of the amide starting material. Next, diethylchlorophosphate (1.4 eq) was added over a 15 minute time span. Within 2 hours after the addition of the phosphate reagent, consumption of the amide starting material **3** was observed to generate the iminophosphate intermediate **4a**. Then, ethyl isocyanoacetate (1.3 eq) was added over 15 minutes, and this was followed by a dropwise addition of a solution of potassium *t*-butoxide (1.3 eq) in THF at -20 to -15ºC. The isocyanoacetate / butoxide addition sequence was designed in this manner so that the enolate would react with the iminophosphate as readily as it formed. As predicted, the formation of imidazodiazepine **4** was complete immediately after the *t*-butoxide addition with no detectable iminophosphate intermediate **4a** observed. Upon completion of the reaction procedure, the imidazodiazepine product **4** was partitioned into the organic layer using dichloromethane. An aqueous bicarbonate work-up removed the potassium salts and unreacted butoxide. The purification of the product was achieved by crystallization from *t*-butyl methyl ether (*t*BME), which adequately removed any traces of side products related to the phosphate related byproducts. The trituration of the crystals with hot ethanol was then employed to remove any residual benzodiazepine starting material **3**, if necessary. With the goal of eliminating the column chromatography and a more robust and scalable procedure in hand, successful execution of the large-scale synthesis provided 61.0 g (52 % yield) of imidazodiazepine **4** (5 L flask). The proposed imidazole top reaction mechanism is exhibited in **Scheme 21**.

Scheme 21: Proposed Mechanism for the Formation of the Imidazole Top

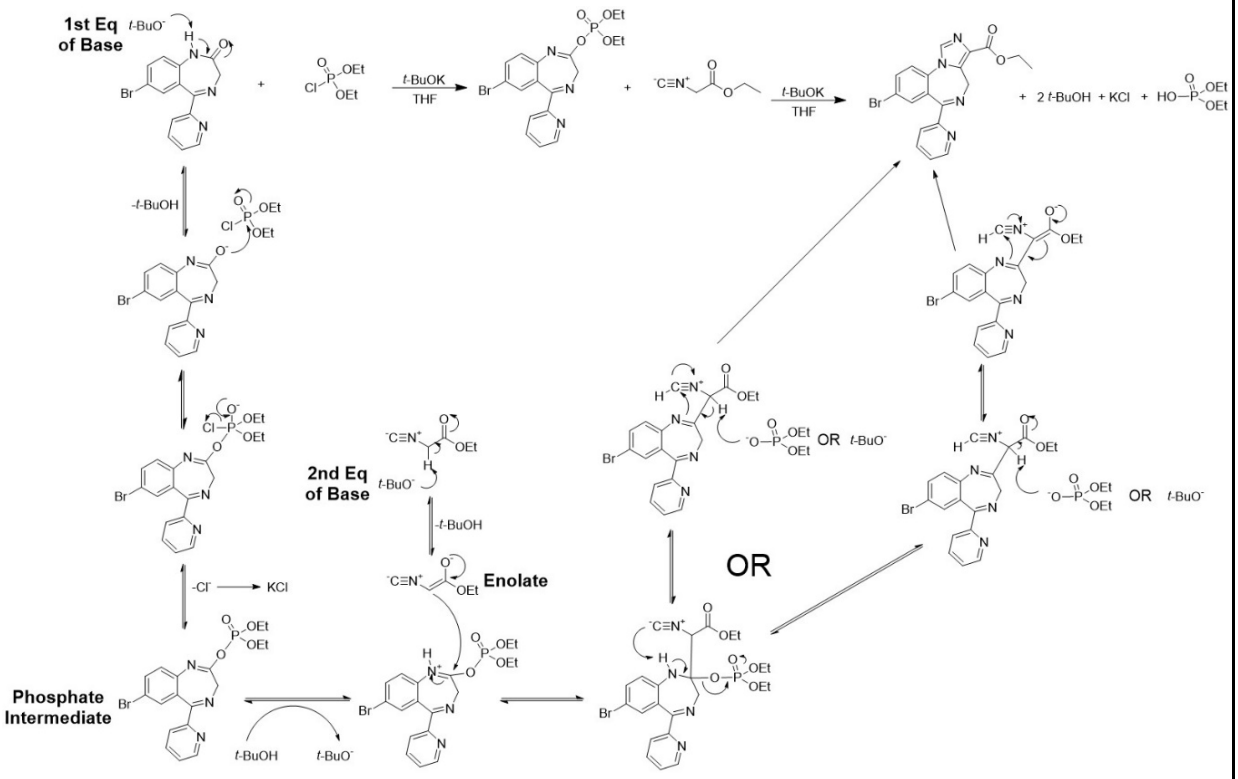

The next step in the reaction sequence employed the copper-free Sonogashira coupling[154, 155] to covert aryl bromide **4** into the silyl-protected acetylene **5**. The earlier discovery chemistry used TMS-acetylene (1.5 eq) and bis(triphenylphosphine)palladium(II) diacetate ($Pd(OAc)_2(PPh_3)_2$) as the catalyst, as well as a large excess of triethylamine. Under these conditions the reaction time was typically 15 hours at reflux (75ºC) to achieve the desired consumption of the aryl bromide **4** (**Table 14**, **entry 1**). These reaction conditions presented an opportunity for improvement. First, the catalyst was prone to poisoning and the procedure required an extensive de-gassing protocol prior to initiating the reaction. The degree of proper degassing (to remove dissolved oxygen in the solvents) played a direct role on the success or failure of the coupling reaction. Secondly, the reaction conditions employed an excess of TMS-acetylene (1.5

eq) to drive the reaction to completion, while most often catalytic poisoning and perhaps degradation of the TMS-reagent stalled the reaction with 5-10% of aryl-bromide **4** which remained. Typically, additional TMS-acetylene and fresh catalyst were added to complete the reaction. Thirdly, solvent quantities of triethylamine (coupled with acetonitrile in 1:1 mixture) were used to dissolve the imidazobenzodiazepine **4** starting material in the reaction medium. Finally, difficult column chromatography was required to purify the product to remove the closely eluting aryl bromide **4** starting material from the crude mixture. This process was also further complicated by the triethylammonium bromide side product, which remained in the crude residue by the previous processing protocol. Therefore, in order to develop a reliable large-scale procedure for the copper-free Sonogashira coupling, the catalyst poisoning, the acetylene reagent, the isolation process and the purification of the silyl target **5** must be improved.

To remedy the problem of the poisoning of the catalyst, which was caused by the oxidation of triphenylphosphine to the corresponding phosphine oxide, a ligand less prone to oxidation was required. A trial with tri-ortho-tolylphosphine (P-*o*-tol_3) developed by Greg Fu was first attempted because it has a larger cone angle (194°) than that of triphenylphosphine (PPh_3, 145°)[156, 157] and should exhibit improved resistance to oxide formation and subsequent catalyst poisoning. As mentioned, the ligand in the process was altered to P-*o*-tol_3, which significantly shortened the reaction time to 6h (from 15h) and no cumbersome degassing was required (**Table 14**, **entry 2**). The starting TMS-acetylene (1.5 eq) was replaced with the inherently more stable TIPS-acetylene reagent (1.2 eq), which shortened the reaction time further to 4 hours, even with reduced equivalents of the protected-acetylene reagent. (**Table 14**, **entry 3**). Finally, reduction of triethylamine from the solvent quantities to stoichiometric quantities (2.0 eq) exhibited no

detrimental impact on the reaction time (**Table 14**, **entry 4**). With the optimal reaction conditions in hand the product isolation and purification procedure were then refined. The spent and undissolved catalyst was filtered from the reaction media through a small pad of silica gel. The filtrate, which resulted, was concentrated and then partitioned between dichloromethane and aqueous sodium bicarbonate to remove triethylammonium bromide. Finally, the concentrated residue was run through a short flash column to remove the baseline impurities. No other purification was needed in order to carry the product **5b** forward into the next step since the aryl bromide starting material **4** was completely consumed using the refined reaction conditions. In a 3L flask, the improved copper-free Sonogashira coupling process produced 65.0g of the TIPS-protected acetylene **5b** in 85% yield. The proposed copper-free Sonogashira mechanism is displayed in **Scheme 22**.[158]

Table 14: Copper-Free Sonogashira Coupling Trials[130]

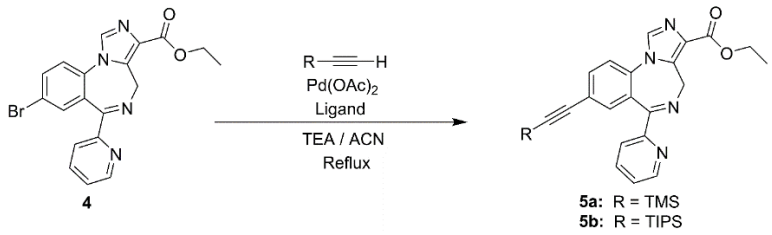

4 → **5a:** R = TMS; **5b:** R = TIPS

Entry	Acetylene	Ligand	TEA Qty	Degassing?	Reaction Time
1	TMS (1.5 eq)	PPh_3	Solvent	yes	15 h
2	TMS (1.5 eq)	P-o-tol_3	Solvent	no	6 h
3	TIPS (1.2 eq)	P-o-tol_3	Solvent	no	4 h
4	TIPS (1.2 eq)	P-o-tol_3	2.0 eq	no	4 h

Reactions were monitored for completion using TLC analysis. Samples were pulled every 60 minutes and spotted on silica gel plates. Mobile phase = ethyl acetate with 1% TEA. Respective *Rf's*: **4** = 0.3, **5a** = 0.5, **5b** = 0.7. Disappearance of starter **4** indicated reaction completion.[130]

Scheme 22: Proposed Mechanism of the Copper-Free Sonogashira Cross Coupling

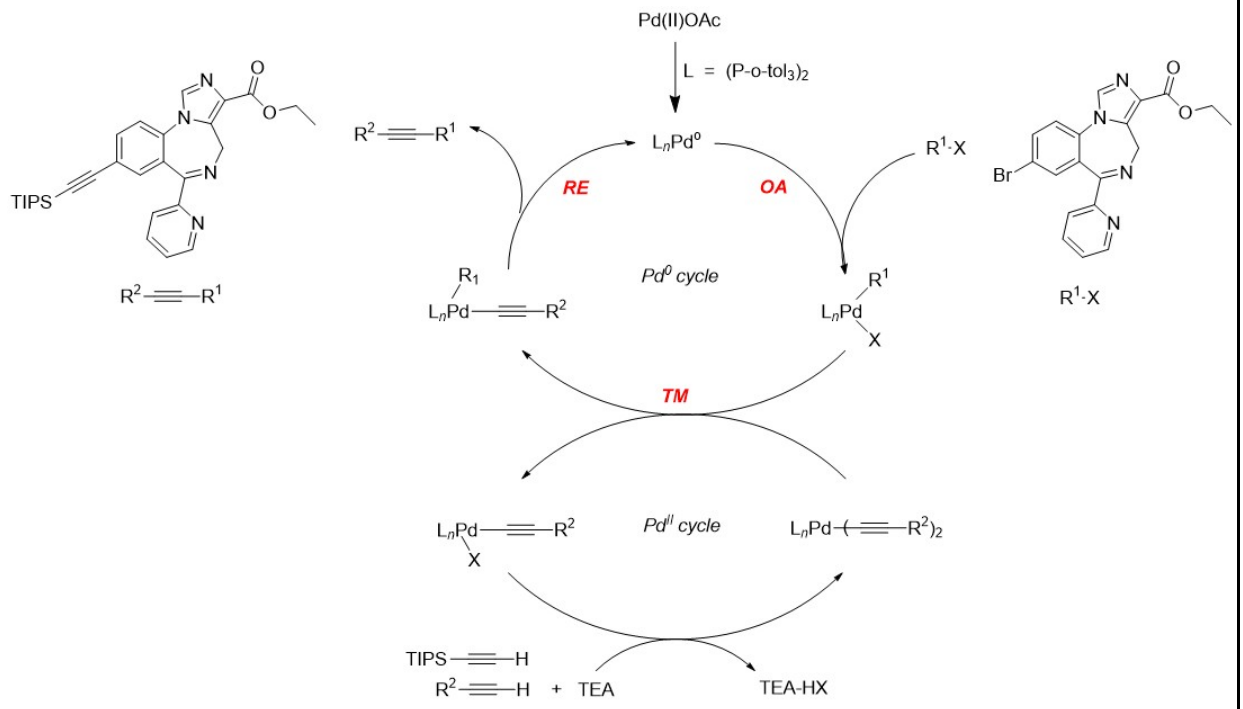

The final step of this development process provided the key intermediate **HZ-166** via deprotection of the TIPS-acetylene function using fluoride anion. The improvements to this process included optimization of the reaction temperature and replacement of the chromatographic purification with crystallization. The discovery process utilized tetrabutylammonium fluoride (TBAF) as the fluoride source. This reagent performed, as required, but the isolation and purification of **HZ-166** target (**6**) required removal of the tetrabutylammonium hydroxide byproduct, adequately. Additionally, the purification protocol would also need to efficiently remove the TIPS-fluoride side product. The discovery route cooled the reaction media to -78ºC prior to the addition of TBAF. Careful monitoring of the reaction by TLC indicated that deprotection did not initiate, however, until the temperature reached -20ºC. Consequently, the process temperature was modified to – 20 to -15ºC, at which point the TBAF·xH_2O (1.0M in THF)

was added over a 30 minute time period. The process was monitored by TLC, which indicated complete deprotection had occurred upon completion of the TBAF addition. The proposed TIPS Cleavage Mechanism is displayed in **Scheme 23**.

Evaluation of variety of solvents led to the selection of 2-propanol (IPA) as the ideal crystallization solvent, which exhibited minimal product solubility with efficient side-product (TBA-OH and TIPS-F) solubility. The improved final step of the **HZ-166** synthesis employed the optimum temperature, while eliminating the chromatographic purification providing the 38.4g (85.0%) of **HZ-166** (3L flask).

In summary, the five-step synthesis of **HZ-166** was refined to provide a more reliable and robust procedure (**Scheme 24**) with a 27.6% overall yield. As noted, the chromatographic purifications were replaced with large-scale crystallizations, while importantly, the overall reaction times were reduced.

Scheme 23: Proposed Mechanism of the Cleavage of the TIPS Group

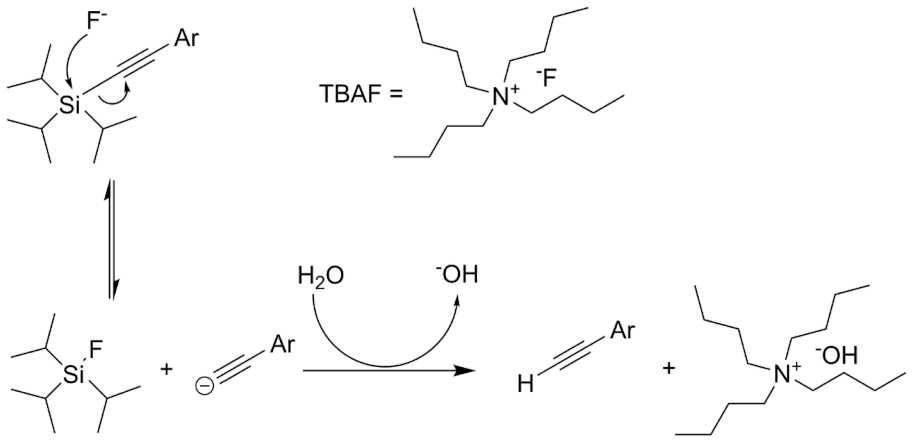

Scheme 24: Improved Large-Scale Synthesis of **HZ-166**

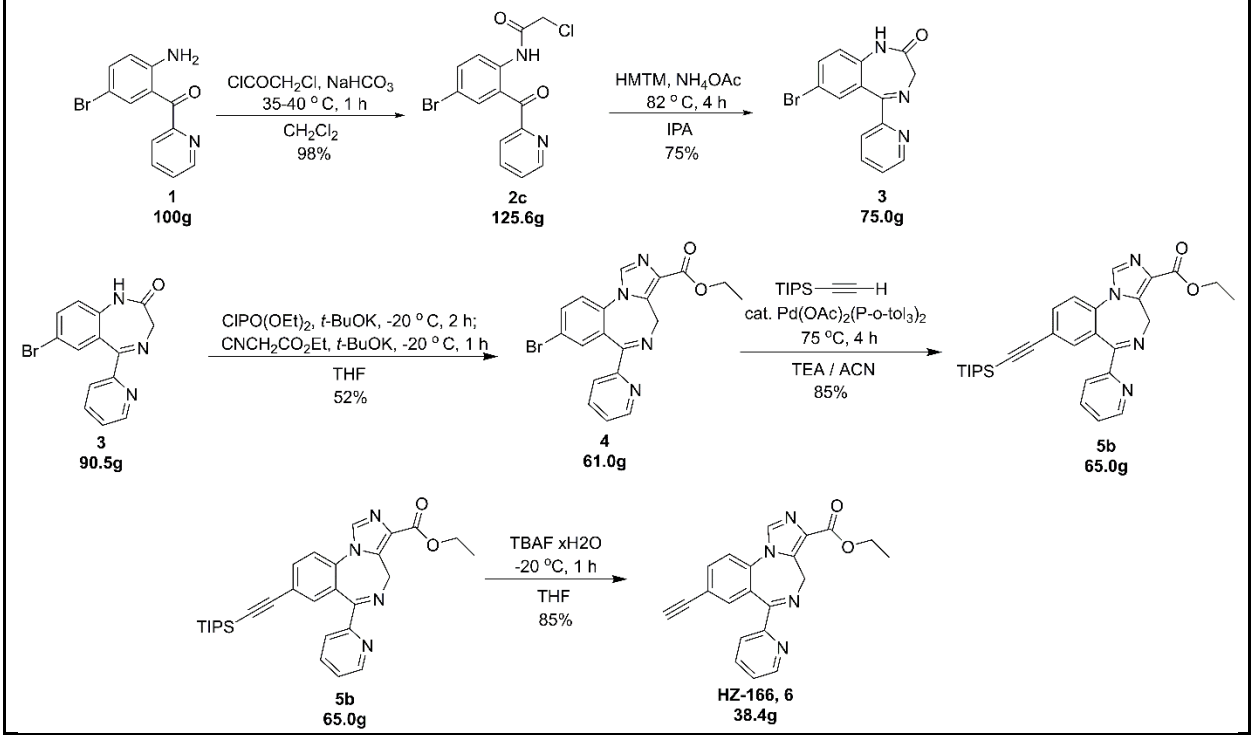

2.4. Experimental Section for α2/3-GABA$_A$R Subtype-selective Imidazodiazepines

2.4.1. General Procedures for the Synthesis of KRM-II-81

All reactions were performed in oven-dried round-bottom flasks with magnetic stir bars or overhead mechanical stirrers under an argon atmosphere. Organic solvents were purified when necessary by standard methods or purchased from Sigma-Aldrich.™ Chemicals were purchased from either Sigma Aldrich™, Oakwood Chemical, Alfa Aesar, Matrix Scientific, Admiral Chemical or Acros Organic. The ^{1}H and ^{13}C NMR data were obtained on Bruker Spectrospin 300 MHz and 500 MHz instruments with the chemical shifts in δ (ppm) reported. The HRMS spectral data was obtained on a LCMS-IT-TOF by Shimadzu Scientific.

2.4.1.1. *N*-(4-Bromo-2-picolinoylphenyl)-2-chloroacetamide (2c)

To a mixture of (2-amino-5-bromophenyl)(pyridine-2yl)methanone (**1**, 100 g, 360.9 mmol), sodium bicarbonate (60.6 g, 721.7 mmol), and dichloromethane (1000 mL), chloroacetyl chloride (43.0 mL, 541.3 mmol) was added dropwise over 60 min, while keeping the temperature between 25 – 30°C. The bright red reaction mixture, which resulted, was then allowed to stir for greater than 1 h at rt. The completion of the reaction process was verified by analysis by TLC using silica gel and 50% ethyl acetate / hexanes. The reaction mixture was then slowly diluted over 30 min with water (500 mL) as carbon dioxide gassing evolved. The biphasic mixture, which resulted, was allowed to stand for 15 min and the layers were separated. The aq layer was extracted with dichloromethane (500 mL) and the combined organic layers were washed with 5% aq sodium bicarbonate solution (500 mL) and then 10% aq sodium chloride solution (500

mL). The organic layer was dried (Na_2SO_4). The solvents were removed under reduced pressure and the residue was slurried with ethanol (500 mL) at 50 – 55°C for 30 min. Upon cooling to rt and after holding the temperature for 1 h, the solid was filtered and washed with ethanol (100 mL x 3). The solid was dried under vacuum at 40°C to afford **2c** as an off-white solid (115.2 g, 90.3%). Additional **2c** was obtained as a 2nd crop by concentrating the filtrate (10.4 g, 8.2%). Total yield: 125.6g, 98.5%: ***Rf*** = 0.6 (EtOAc-hexanes, 1:1 and 1% of TEA); **^{1}H NMR** (500 MHz, $CDCl_3$) δ 11.66 (s, 1H), 8.76 (ddd, *J* = 4.8, 1.7, 0.9 Hz, 1H), 8.58 (d, *J* = 9.0 Hz, 1H), 8.03 (dt, *J* = 7.8, 1.1 Hz, 1H), 8.01 (d, *J* = 2.4 Hz, 1H), 7.96 (td, *J* = 7.7, 1.7 Hz, 1H), 7.72 (dd, *J* = 9.0, 2.4 Hz, 1H), 4.21 (s, 2H); ^{13}C NMR (126 MHz, $CDCl_3$) δ 195.29, 165.34, 154.76, 148.83, 138.80, 137.43, 137.19, 136.88, 126.70, 124.99, 124.62, 122.99, 115.81, 43.15; **HRMS** (ESI/IT-TOF): m/z [M + H]+ calcd for $C_{14}H_{11}BrClN_2O_2$: 352.9693; found: 352.9690.

2.4.1.2. 7-Bromo-5-(pyridin-2-yl)-1,3-dihydro-2*H*-benzo[*e*][1,4]diazepin-2-one (3)

A mixture of *N*-(4-bromo-2-picolinoylphenyl)-2-chloroacetamide (**2c**, 115 g, 325.2 mmol), hexamethylenetetramine (HMTM, 100.3 g, 715.5 mmol), ammonium acetate (55.2 g, 715.5 mmol), and isopropanol (2000 mL) was heated to reflux (82°C). The reaction mixture was held at reflux for 4 h at which point the reaction was deemed complete by TLC analysis (silica gel and 50% ethyl acetate / hexanes). The reaction mixture was then cooled to 0 – 5°C using an ice bath. The solid, which resulted, was filtered and washed with cold isopropanol (100 mL x 2) and then water (100mL x 4). The solid was dried under vacuum at 40°C to afford **3** as an off-white solid (75.1 g, 75%): **Mp** 228-229 °C; ***Rf*** = 0.4 (EtOAc-hexanes, 1:1 and 1% of TEA); **^{1}H NMR** (500 MHz, DMSO-d_6) δ 10.64 (s, 1H), 8.57 (dd, *J* = 4.7, 0.7 Hz, 1H), 8.05 (d, *J* = 7.9 Hz, 1H), 7.95 (td, *J* = 7.7, 1.7 Hz, 1H), 7.71 (dd, *J* = 8.7, 2.3 Hz, 1H), 7.51 (ddd, *J* = 7.5, 4.8, 1.1 Hz, 1H), 7.43

(d, J = 2.3 Hz, 1H), 7.18 (d, J = 8.7 Hz, 1H), 4.23 (s, 2H); **^{13}C NMR** (126 MHz, DMSO-d_6) δ 170.36, 168.13, 156.32, 148.88, 139.31, 137.60, 134.43, 134.17, 127.93, 125.41, 123.93, 123.57, 114.50, 57.58; **HRMS** (ESI/IT-TOF): m/z [M + H]+ calcd for $C_{14}H_{11}BrN_3O$: 316.0080; found: 316.0076.

2.4.1.3. Ethyl 8-bromo-6-(pyridin-2-yl)-4*H*-benzo[*f*]imidazo[1,5-*a*][1,4]diazepine-3-carboxylate (4)

A mixture of 7-bromo-5-(pyridin-2-yl)-1,3-dihydro-2*H*-benzo[*e*][1,4]diazepin-2-one (**3**, 90.5 g, 286.2 mmol) and tetrahydrofuran (1200 mL) was cooled to -20ºC using a dry ice / IPA bath. A solution of potassium *t*-butoxide (41.8 g, 372.1 mmol) and tetrahydrofuran (300 mL) was added dropwise to the reaction mixture over a 30 min period, while maintaining the temperature at -20 to -15ºC. Upon completion of the addition, the reaction mixture was allowed to stir for an additional 60 min at -20ºC. The diethyl chlorophosphate (57.9 mL, 400.7 mmol) was then added dropwise to the reaction mixture over 15 min while maintaining the temperature at -20 to -15ºC. Upon completion of the addition, the reaction mixture was allowed to stir for an additional 2 h at -20 ºC at which point the reaction was deemed complete on analysis by TLC (silica gel and 1% triethylamine / ethyl acetate). The ethyl isocyanoacetate (40.7 mL, 372.1 mmol) was then added dropwise to the reaction mixture over 15 min while maintaining the temperature at -20 to -15ºC. Immediately, a solution of potassium t-butoxide (41.8 g, 372.1 mmol) and tetrahydrofuran (300 mL) was added dropwise to the reaction mixture over 30 min while maintaining the temperature at -20 to -15ºC. Upon completion of the addition, the reaction mixture was allowed to warm to rt and stirred for an additional 12 h at which point the reaction was deemed complete by analysis by TLC (silica gel and 1% triethylamine / ethyl acetate). The reaction mixture was then diluted

with 5% aq sodium bicarbonate (1000 mL). The biphasic mixture, which resulted, was allowed to stand for 15 min and the layers were separated. The aq layer was then extracted twice with dichloromethane (1000 mL x 2) and the combined organic layers were washed with 5% aq sodium bicarbonate solution (1000 mL) and then 10% aq sodium chloride solution (1000 mL). The organic layer was dried (Na_2SO_4). The solvents were removed under reduced pressure and the residue was slurried with *t*-butyl methyl ether (1000 mL) at 50 – 55°C for 30 min. Upon cooling to rt and after holding for 12 h, the solid was filtered and washed with *t*-butyl methyl ether (100 mL x 3). The solid was then purified by stirring with ethanol (300 mL) at reflux for 1h. Upon cooling to -20°C and after holding for 12 h, the solid was filtered and washed with cold ethanol (50 mL x 2). The solid was dried under vacuum at 40°C to afford **4** as a light brown powder (61.0 g, 51.8%): **MP** 212-213 °C; ***Rf*** = 0.4 (EtOAc with 1% TEA); **^{1}H NMR** (500 MHz, $CDCl_3$) δ 8.57 (dd, *J* = 4.9, 0.9 Hz, 1H), 8.09 (d, *J* = 8.0 Hz, 1H), 7.89 (s, 1H), 7.81 (td, *J* = 7.8, 1.8 Hz, 1H), 7.78 (dd, *J* = 8.6, 2.2 Hz, 1H), 7.59 (d, *J* = 2.2 Hz, 1H), 7.47 (d, *J* = 8.6 Hz, 1H), 7.37 (ddd, *J* = 7.6, 4.8, 1.2 Hz, 1H), 6.12 (d, *J* = 12.6 Hz, 1H), 4.51 – 4.36 (m, 2H), 4.15 (d, *J* = 12.6 Hz, 1H), 1.43 (t, *J* = 7.1 Hz, 3H); **^{13}C NMR** (126 MHz, $CDCl_3$) δ 167.08, 162.93, 156.20, 148.73, 138.43, 136.94, 135.32, 134.99, 134.57, 134.44, 129.37, 128.54, 124.90, 124.29, 123.99, 120.57, 60.81, 45.02, 14.45; **HRMS** (ESI/IT-TOF): m/z [M + H]+ calcd for $C_{19}H_{16}BrN_4O_2$: 411.0451; found: 411.0454.

2.4.1.4. Ethyl 6-(pyridin-2-yl)-8-((triisopropylsilyl)ethynyl)-4*H*-benzo[*f*]imidazo[1,5-*a*][1,4]diazepine-3-carboxylate (5b)

A mixture of palladium acetate (1.67 g, 7.4 mmol), tri-*o*-tolylphosphine (4.51g, 14.8 mmol) and acetonitrile (400 mL) was stirred for 30 min at rt. To the reaction mixture was then added in

sequence ethyl 8-bromo-6-(pyridin-2-yl)-4*H*-benzo[*f*]imidazo[1,5-*a*][1,4]diazepine-3-carboxylate (**4**, 61.0 g, 148 mmol), triethylamine (41.3 mL, 297 mmol), (triisopropylsilyl)acetylene (39.9 mL, 178 mmol) and additional acetonitrile (500 mL). The reaction mixture was then heated to reflux (75°C) and held for 4 h at which point the reaction was deemed complete on analysis by TLC (silica gel and 1% triethylamine / ethyl acetate). Upon completion of the reaction, the mixture was cooled to rt and silica gel (25 g) was added. After stirring for 30 min, the spent silica gel was removed by filtration and washed with acetonitrile (100 mL x 2). The solvents were removed under reduced pressure and the residue was dissolved in dichloromethane (900 mL) and 5% aq sodium bicarbonate (900 mL). The biphasic mixture, which resulted, was allowed to stand for 15 min and the layers were separated. The aq layer was then extracted with dichloromethane (900 mL) and the combined organic layers were washed with 5% aq sodium bicarbonate solution (900 mL) and then 10% aq sodium chloride solution (900 mL). The organic layer was dried (Na_2SO_4). The solvents were removed under reduced pressure and the residue was purified by flash chromatography using silica gel (750 g) and 50% ethyl acetate / hexanes with 5% triethylamine. The pure fractions were pooled and the solvents were removed under reduced pressure. The oil, which resulted, was dried under reduced pressure at 40°C for 2 h to afford the **5b** as a clear, light brown oil (65.0 g, 85%): ***Rf*** = 0.6 (EtOAc with 1% TEA) **^{1}H NMR** (500 MHz, $CDCl_3$) δ 8.55 (dt, *J* = 4.7, 1.4 Hz, 1H), 8.04 (d, *J* = 7.9 Hz, 1H), 7.89 (s, 1H), 7.78 (td, *J* = 7.8, 1.8 Hz, 1H), 7.70 (dd, *J* = 8.4, 1.8 Hz, 1H), 7.51 (d, *J* = 8.4 Hz, 1H), 7.49 (d, *J* = 1.8 Hz, 1H), 7.33 (ddd, *J* = 7.5, 4.8, 1.2 Hz, 1H), 6.07 (d, *J* = 12.5 Hz, 1H), 4.42 (ddt, *J* = 30.1, 14.8, 7.4 Hz, 2H), 4.15 – 4.10 (m, 1H), 1.40 (t, *J* = 7.1 Hz, 3H), 1.08 (d, *J* = 3.6 Hz, 21H); **^{13}C NMR** (126 MHz, $CDCl_3$) δ 167.74, 162.94, 156.47, 148.67,

138.48, 136.80, 135.70, 135.30, 134.93, 134.50, 129.24, 126.97, 124.74, 123.99, 122.71, 122.59, 104.89, 93.78, 60.71, 45.02, 18.58, 14.42, 11.20.

2.4.1.5. Ethyl 8-ethynyl-6-(pyridin-2-yl)-4*H*-benzo[*f*]imidazo[1,5-*a*][1,4]diazepine-3-carboxylate [HZ-166, 6]

A mixture of ethyl 6-(pyridin-2-yl)-8-((triisopropylsilyl)ethynyl)-4*H*-benzo[*f*]imidazo[1,5-*a*][1,4]diazepine-3-carboxylate (**5b**, 65.0 g, 126.8 mmol), water (6.5 mL) and tetrahydrofuran (650 mL) was cooled to -20ºC using a dry ice / IPA bath. Tetrabutylammonium fluoride hydrate, 1M in THF (145.4 mL, 145.4 mmoL) was added dropwise to the reaction mixture over a 30 min period, while maintaining the temperature at -20 to -15ºC. Upon completion of the addition, the reaction mixture was allowed to warm to rt and stir for an additional 60 min at which point the reaction was deemed complete on analysis by TLC (silica gel and 1% triethylamine / ethyl acetate). The reaction mixture was then diluted with ethyl acetate (650 mL) and 10% aq sodium chloride (650 mL). The biphasic mixture, which resulted, was allowed to stand for 15 min and the layers were separated. The aq layer was then extracted with ethyl acetate (650 mL) and the combined organic layers were washed with 10% aq sodium chloride solution (650 mL). The organic layer was dried (Na_2SO_4). The solvents were removed under reduced pressure and the residue was slurried with 2-propanol (IPA, 250 mL) at 70 – 75ºC for 30 min. Upon cooling to -20ºC and after holding for 2 h, the solid was filtered and washed with cold IPA (50 mL x 3) and then hexanes (50 mL x 3). The solid was dried under vacuum at 40ºC to afford the product as an off-white crystalline solid (38.4 g, 85%): **Mp** 204-205 °C; ***Rf*** = 0.4 (EtOAc with 1% TEA); **^{1}H NMR** (500 MHz, CDCl3) δ = 8.58 (d, *J* = 4.3 Hz, 1H), 8.07 (d, *J* = 8.0 Hz, 1H), 8.05 (s, 1H), 7.83 (dd, *J* = 11.8, 4.4 Hz, 1H), 7.78 (dd, *J* = 8.4, 1.3 Hz, 1H), 7.61 (d, *J* = 8.3 Hz, 1H), 7.57 (d, *J*

= 1.0 Hz, 1H), 7.38 (dd, *J* = 6.7, 5.3 Hz, 1H), 6.16 (d, *J* = 11.4 Hz, 1H), 4.29 (d, *J* = 11.2 Hz, 1H), 3.19 (s, 1H), 2.85 (q, *J* = 7.6 Hz, 2H), 1.44 (t, *J* = 7.6 Hz, 3H); **^{13}C NMR** (126 MHz, CDCl3) δ 171.92, 170.75, 167.87, 156.29, 148.73, 137.08, 136.33, 136.15, 135.92, 135.46, 135.25, 127.08, 124.97, 124.78, 124.08, 122.87, 121.45, 81.60, 79.75, 44.93, 19.79, 11.56; **HRMS** (ESI/IT-TOF): m/z [M + H]+ calcd for $C_{21}H_{17}N_4O_2$: 357.1346; found: 357.1344.

2.4.1.6. 8-Ethynyl-6-(pyridin-2-yl)-4*H*-benzo[*f*]imidazo[1,5-*a*][1,4]diazepine-3-carbaldehyde (7) with Dr. Guanguan Li[136]

The preparation of PDBBA. Potassium tert-butoxide (29.3 g, 261 mmol) was suspended in dry THF (261 mL). DIBALH (261 mL, 1.0 M in hexane, 261 mmol) was added dropwise to the solution of potassium *t*-butoxide at 0 °C using an ice-water bath. The mixture was allowed to stir at rt for 2 h to achieve a colorless homogeneous solution. The concentration of PDBBA solution in THF-hexanes was measured by GC analysis by hydrolysis of the solution with a mixture of t-butyl alcohol-THF (1:1) at 0 °C.

The reduction of the ethyl ester to the aldehyde. The ethyl ester (20 g, 56.1mmol) was dissolved in dry DCM (500 mL) at 0 °C. The ice-water bath was removed, and PDBBA solution (0.42 M in THF-hexanes, 200 mL) was added in one portion with vigorous stirring. The reaction was monitored by TLC (silica gel) after each 3 minutes and was completed in 20 min, and this was followed by hydrolysis of the mixture in 1N aq HCl at 0 °C. Water (200 mL) was added to the mixture, and it was stirred for 0.5 h. The aluminum salt was formed and filtered off on a celite pad. The filtrate was extracted with DCM (3 x 150 mL). The organic layers were combined and concentrated with reduced pressure, and this was followed by washing with brine and dried

(Na_2SO_4). The solid residue was dissolved in a mixture of DCM (100 mL) and EtOAc (100 mL) at 50 °C. A seed crystal was added to the mixture and solvent was reduced to 1/4th of its original volume. The aldehyde was recrystallized from the mixture at rt and washed with cold Et_2O. The filtrate was combined and further purified by flash chromatography (silica gel, EtOAc and 1% each of TEA and MeOH) to afford additional aldehyde 4 as a white solid (14 g, 80% yield): **Mp** 242-243 °C; ***Rf*** = 0.6 (EtOAc and 1% of TEA): **^{1}H NMR** (300 MHz, CDCl3) δ 10.04 (s, 1H), 8.54 (d, *J* = 4.1 Hz, 1H), 8.06 (d, *J* = 7.9 Hz, 1H), 7.96 (s, 1H), 7.78 (dd, *J* = 17.3, 8.8 Hz, 2H), 7.56 (dd, *J* =4.6, 3.3 Hz, 2H), 7.35 (dd, *J* = 6.6, 5.1 Hz, 1H), 5.99 (s, 1H), 4.18 (s, 1H), 3.18 (s, 1H); **^{13}C NMR** (75 MHz, CDCl3) δ 186.82, 167.82, 156.33, 148.72, 137.85, 136.92, 136.71, 136.32, 135.49, 135.32, 134.97, 127.19, 124.87, 123.97, 122.83, 121.45, 81.58, 79.76, 44.40; **HRMS** (ESI/IT-TOF): m/z [M + H]+ calcd for $C_{19}H_{13}N_4O$: 313.1084; found: 313.1087.

2.4.1.7. 5-(8-Ethynyl-6-(pyridin-2-yl)-4*H*-benzo[*f*]imidazo[1,5-*a*][1,4]diazepin-3-yl)oxazole [KRM-II-81, 8] with Dr. Guanguan Li[136]

The toluenesulfonylmethyl isocyanide (TosMIC, 10.6 g, 54.6 mmol), K_2CO_3 (18.9 g, 136.5 mmol) and the aldehyde 4 (14.2 g, 45.5 mmol) were placed in a dry two neck round bottom flask. Dry MeOH (600 mL) was added to the mixture under an argon atmosphere at rt. The reaction mixture was allowed to warm to reflux for 2 h. After completion of the reaction on analysis by TLC (silica gel, EtOAc and 1% each of TEA and MeOH), the reaction mixture was quenched with cold water (300 mL) and extracted with EtOAc (3 x 100 mL). The organic layers were combined and this was followed by washing with brine. The solution was then dried (Na_2SO_4) and concentrated under reduced pressure to dryness. The solid residue, which formed, was dissolved in EtOAc (200mL) at 60 °C, and the solvent was reduced to 1/4th of its original

volume. A seed crystal was then added to the solution. The majority of oxazole was crystallized at rt and filtered. This was followed by washing with cold Et_2O. The filtrate was combined and further purified by flash chromatography (silica gel, EtOAc and 1% each of TEA and MeOH) to afford additional oxazole as a white solid (14.2 g, 89% yield): **Mp** 241-242 °C; ***Rf*** = 0.3 (EtOAc with 1% TEA): **^{1}H NMR** (500 MHz, CDCl3) δ 8.55 (d, *J* = 4.5 Hz, 1H), 8.00 (d, *J* = 7.9 Hz, 1H), 7.95 (s, 1H), 7.92 (s, 1H), 7.78 (t, *J* = 7.4 Hz, 1H), 7.72 (d, *J* = 8.2, 0.8 Hz, 1H), 7.58-7.49 (m, 2H), 7.42 (s, 1H), 7.33 (dd, *J* = 6.9, 5.3 Hz, 1H), 5.72 (d, *J* = 11.9 Hz, 1H), 4.27 (d, *J* = 12.0 Hz, 1H), 3.16 (s, 1H); **^{13}C NMR** (126 MHz, CDCl3) δ 167.81, 156.63, 149.82, 148.84, 146.60, 136.88, 136.31, 135.72, 135.36, 135.23, 129.76, 127.39, 126.91, 124.79,123.93, 122.72, 122.53, 120.89, 81.75, 79.51, 45.16; **HRMS** (ESI/IT-TOF): m/z [M + H]+ calcd for $C_{21}H_{14}N_5O$: 352.1193; found: 352.1195.

2.4.2. General Procedures for the Biological Assays of KRM-II-81 (8)

2.4.2.1. Compounds

KRM-II-81 was synthesized by here and as previously described.[125, 136] The other compounds were obtained from Sigma-Aldrich (St. Louis, MO, USA). The KRM-II-81was suspended in 1% carboxymethylcellulose and dosed at 1 mL/kg in rats below doses of 30 mg/kg; 30 mg/kg (dosed at 3 ml/kg), 60 mg/kg (dosed at 6 ml/kg). Mice were dosed in a volume of 10 mL/kg. The other compounds were dissolved in sterile water with sonication as needed. Compounds were dosed i.p. with the exception of pentylenetetrazol (PTZ) that was given by s.c. injection in the acute convulsant tests.

2.4.2.2. Rodent assays

All studies were performed in accordance with guidelines of the National Institutes of Health and by local animal care and use committees. The local animal care and use committee and veterinary staff provided direct oversight of the animals by inspections, protocol reviews, laboratory site visits, and animal health monitoring. Male, CD1 mice were used for the testing. The mice were allowed to acclimate to the vivariam for at least 4 days prior to testing and for at least 45 min in the testing room prior to experimentation. Animals were housed in temperature- and humidity-controlled rooms with a 12 h light/dark cycle (on at 0600). Mice were group housed in large plastic containers with sawdust bedding. Standard mouse food pellets and water were continuously available except during experimental sessions. The mice used in the acute convulsant studies were used only once and then euthanized. Mice in the kindling studies were used only for their respective test group and then euthanized after the last test session.

2.4.2.3. Chemical Convulsant Studies.

Experiments were conducted with doses and routes of administration per the general protocol of Witkin et al. (2003)[143] with the exception that PTZ was given at 75 mg/kg by the s.c. route and the mice were a different outbred strain than previously used. Mice were given either vehicle, diazepam (DZP) (1 mg/kg, i.p.) or KRM-II-81 (30 mg/kg, i.p.) and placed into a holding cage for 30 min. Doses of DZP and KRM-II-81 were close to maximal protectant doses against PTZ-induced clonic convulsions but not supramaximal (Gasior et al., 1998, 2000a; Witkin et al., 2018).[128, 134, 135] After 30 min, the mice were given the convulsant agent and placed into individual observation chambers where they were observed for 60 min for clonic convulsions, tonic convulsions and lethality by trained observers. The percentage of mice exhibiting clonus,

tonus, and lethality were recorded. Statistical significant differences from vehicle treatments were assessed by Fisher's Exact Probability test with $p<0.05$ as an a priori level of significance.

2.4.2.4. Seizure Kindling

The seizure kindling was established in separate groups of mice by giving close to subconvulsant doses of cocaine (COC) (60 mg/kg, i.p.) or PTZ (45 mg/kg), as previously described for COC[142, 143] where cocaine was given every day and for PTZ,[134, 135] where PTZ was given every other day. Each experiment was independently conducted twice with groups of 6 mice each. For PTZ seizure kindling, PTZ was given on days 1,3,5, and 8 and then the mice were tested with PTZ again on day 10. For COC, COC was given on days 1,2,3,4, and 5 and then tested with COC on day 6. Three separate groups of mice were studied in each of three separate experiments to study drug effects on fully kindled seizures, the expression of kindled seizures, and on the development of kindling where either vehicle, DZP (1 mg/kg, i.p.), or KRM-II-81 (30 mg/kg, i.p.) was studied. Fully-Kindled Seizures: Vehicle + PTZ or COC were given on kindling days/vehicle, DZP, or KRM-II-81with PTZ or COC given on test day; Expression of Kindling: Vehicle + PTZ or COC, DZP + PTZ or COC, or KRM-II-81 + PTZ or COC was given for each kindling day and for the test day; Development of Kindling: Vehicle, DZP, or KRM-II-81 + PTZ or COC was given on each kindling day/Vehicle + PTZ or COC was given on the test day. The data were analyzed by two-way ANOVA analyzing treatment and treatment day with repeated measures on subjects. Bonferonni post-hoc tests compared each treatment day to its vehicle control ($p<0.05$ considered to be statistically significant a priori).

2.5. Structural Analysis of α2/3-GABA$_A$R Subtype-selective Imidazodiazepines by NMR Spectroscopy

The 3D Structure of HZ-166 is displayed below in **Figure 52**. The CH_2 protons (H19 and H29) were shown to exist very different environments as indicated by analysis of NMR experiments. The proton H19 resided in the pseudo axial position and was observed at 4.17 ppm in the ^{1}H NMR experiment. In comparison the pseudo equatorial proton (H29) was observed downfield at 6.13 ppm, clearly deshielded by the carbonyl oxygen predicted at a distance of 2.39Å using an energy minimized structure generated by molecular modeling software, Chimera X. A ROESY experiment below was employed to illustrate the correlation between H6 and H22 at a predicted distance of 2.48Å.

Figure 52: HZ-166 3D Structure Exhibiting Pseudo Axial (H19) and Pseudo Equatorial (H29) Protons

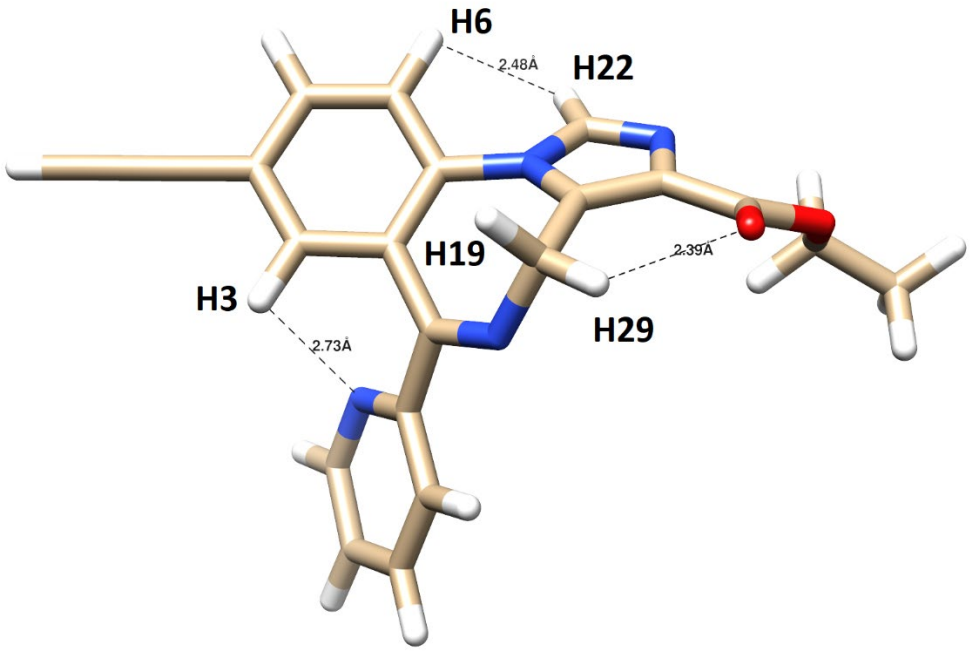

2.5.1. NMR Spectra of HZ-166

2.4.1.1 ^{1}H NMR of HZ-166

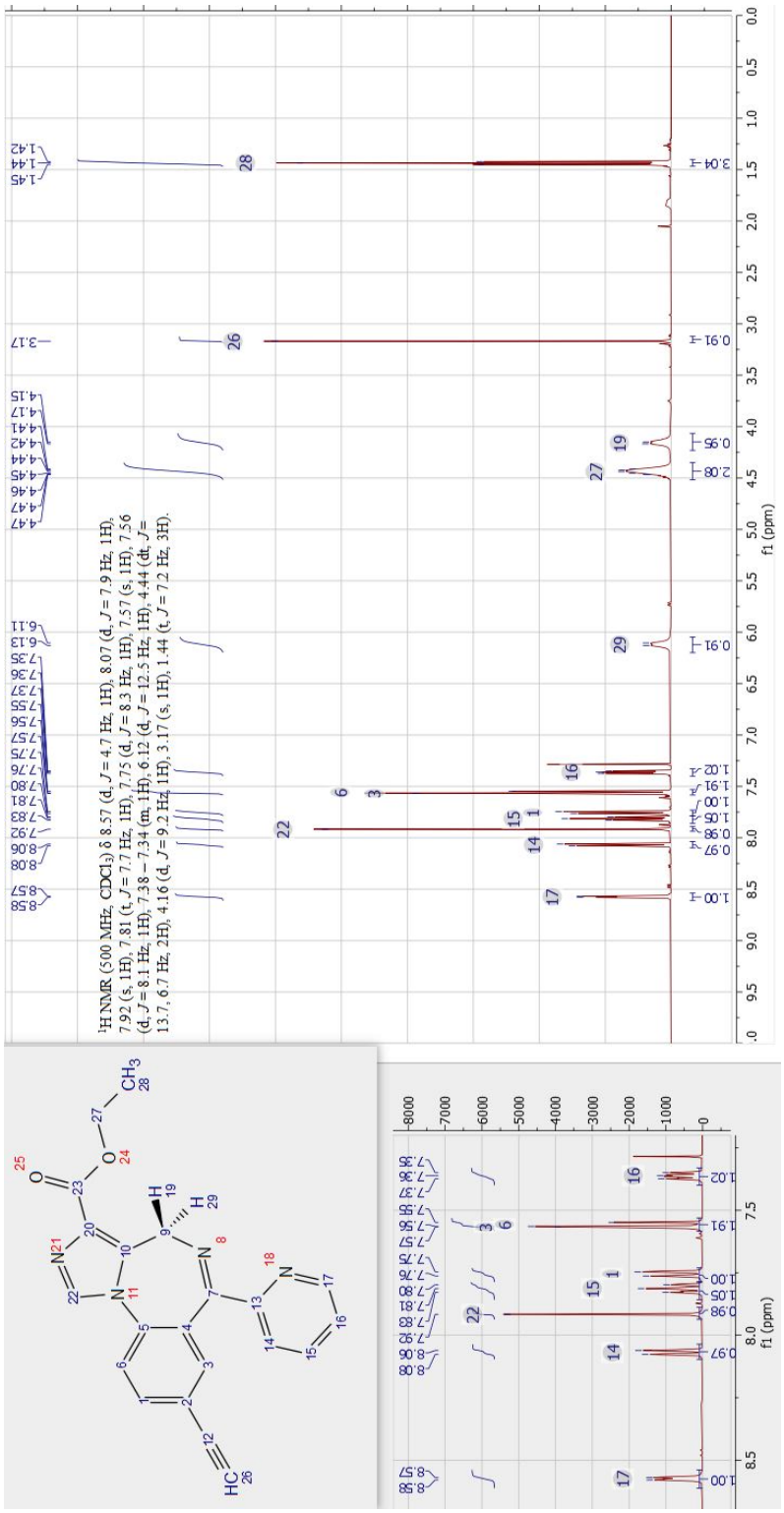

2.4.1.2. ^{13}C NMR of HZ-166

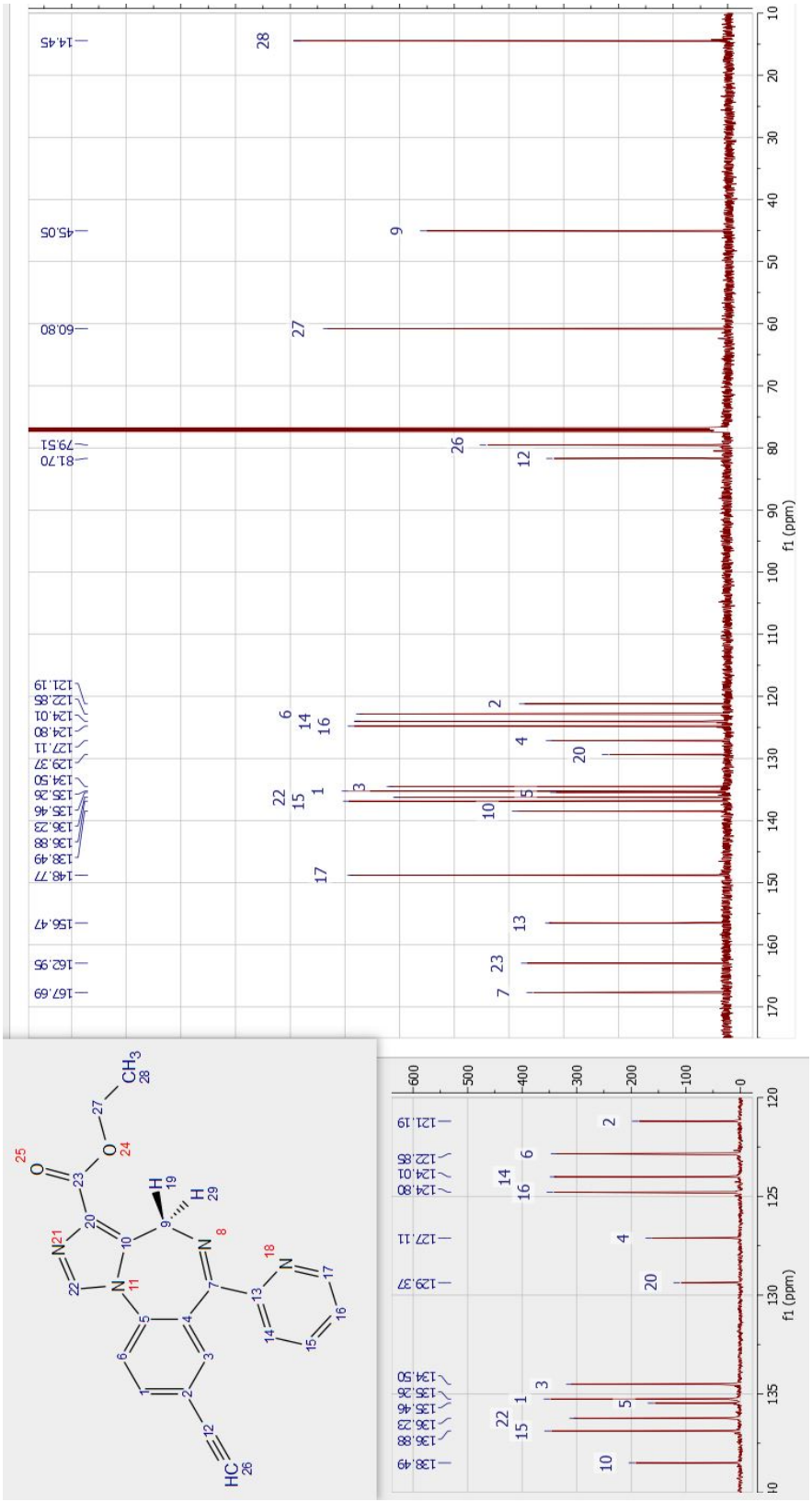

2.4.1.3. COSY Spectrum of HZ-166

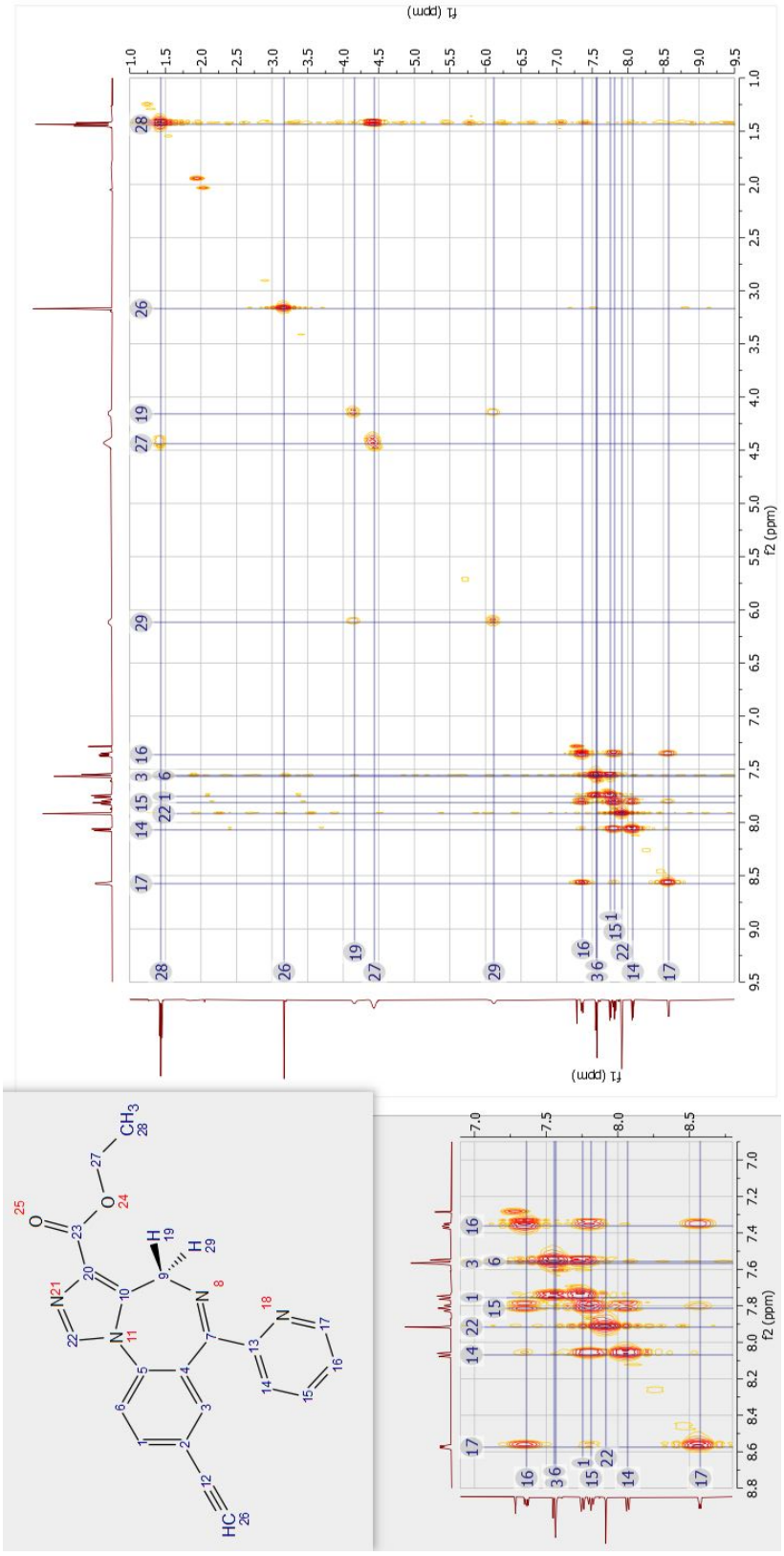

2.4.1.4. ^{1}H-^{13}C-HSQC Spectrum of HZ-166

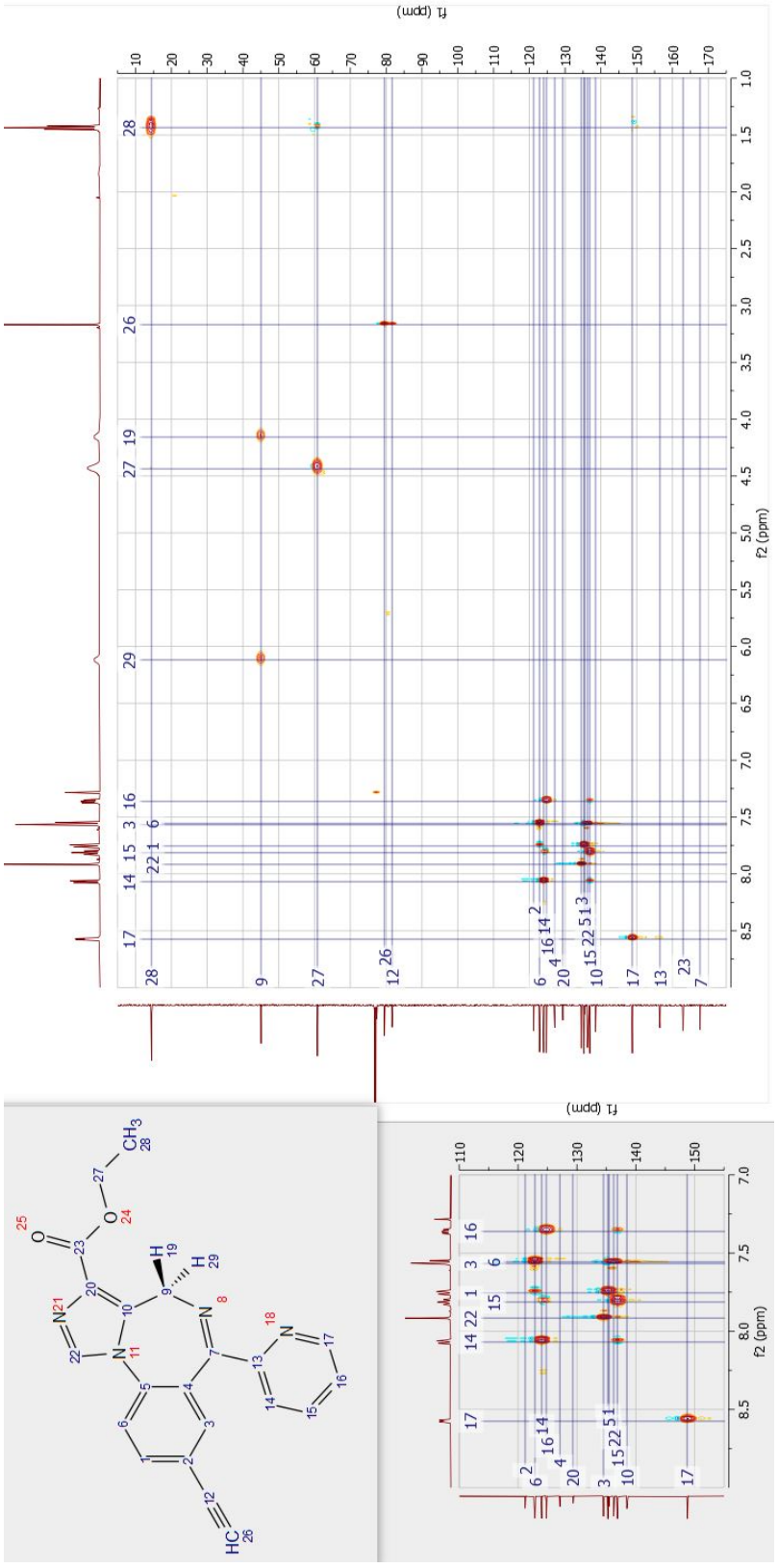

2.4.1.5. ^{1}H-^{13}C-HMBC Spectrum HZ-166

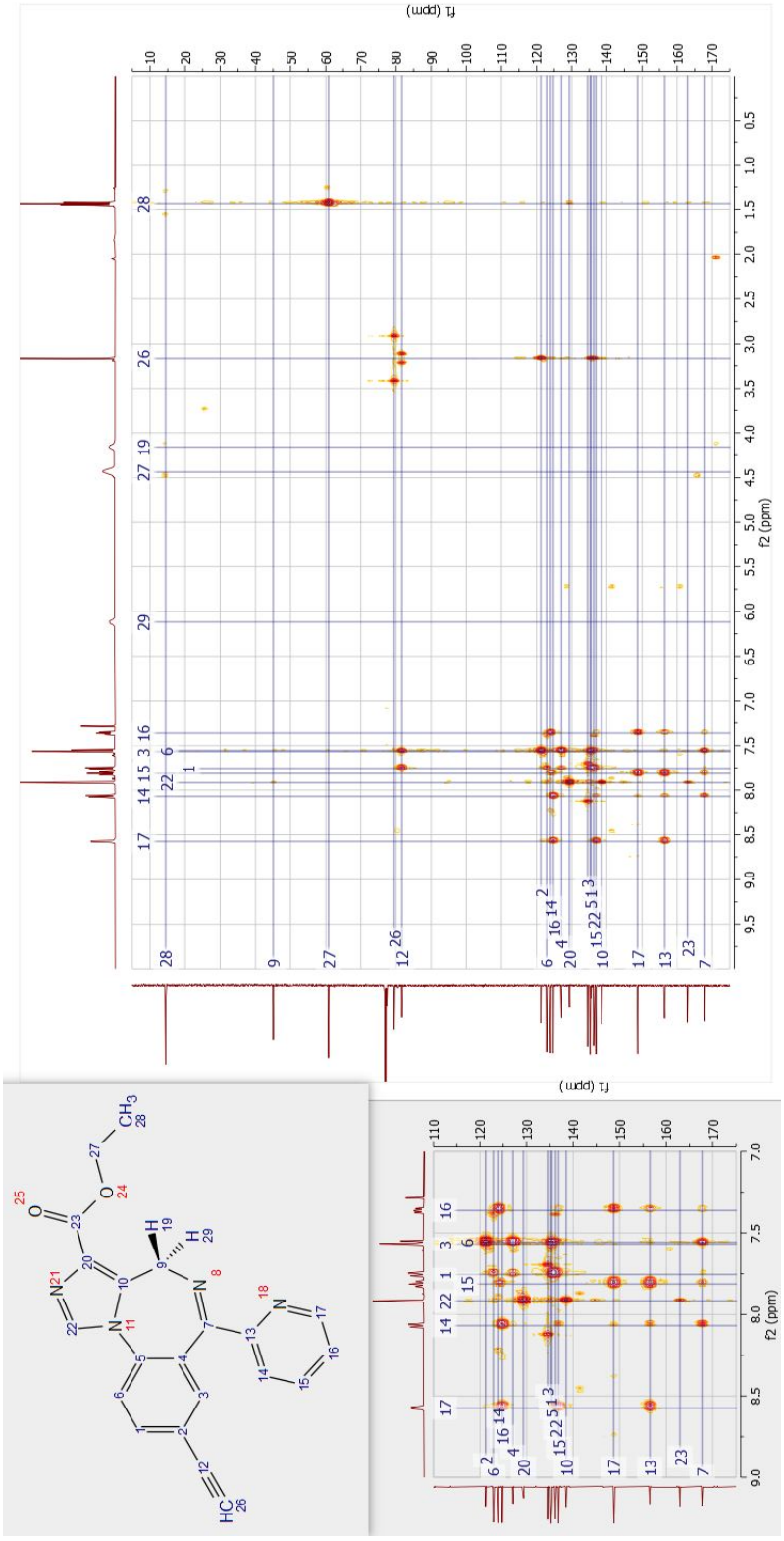

2.4.1.6. ROESY Spectrum of HZ-166

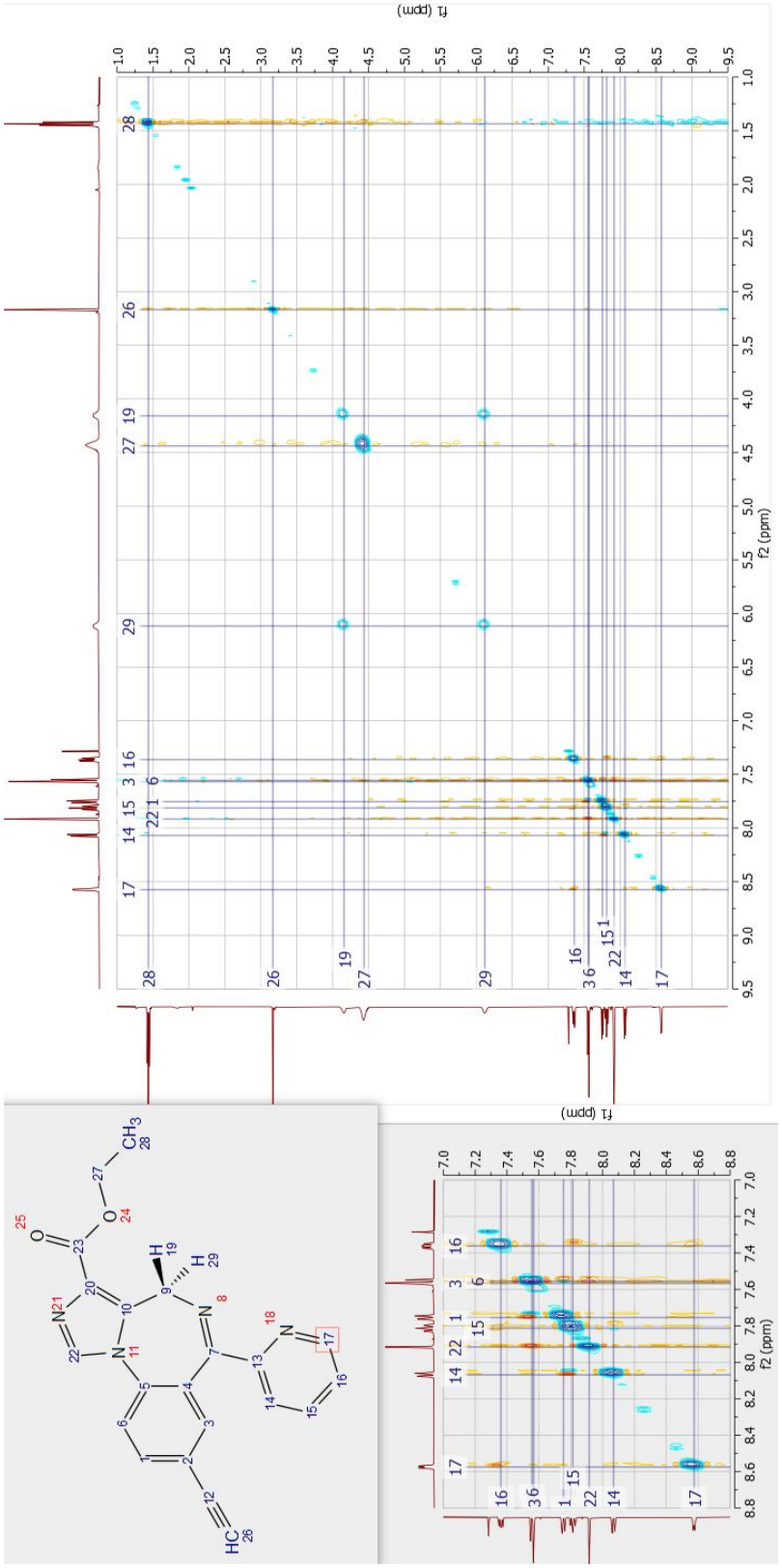

Chapter 3: Process Development of α5-GABA$_A$R Subtype-selective Imidazodiazepines: MIDD0301 and GL-II-73

3.1. Introduction to α5-GABA$_A$R Subtype-selective Imidazodiazepines

The α5-GABA$_A$R subtype (**Figure 53**) is primarily located in the hippocampus and accounts for approximately 5% of all GABA$_A$R α-subtypes in the brain.[159, 160] The drugs targeting the α5-GABA$_A$R subtype, have shown encouraging results in pro cognitive assays, including memory and spatial learning.[161] Included in these cognitive disorders are Alzheimer's disease,[162] Huntington's disease,[163] Down syndrome,[164] schizophrenia[165-169] and also depression.[170]

The α5-GABA$_A$R subtype is also found in the airway smooth muscle (ASM)[171], airway epithelia,[172, 173] and airway leucocytes such as $CD4^+$ T cells[174] and alveolar macrophages.[175] The Emala group first demonstrated the treatment of asthma by that targeting α4 or α5GABA$_A$Rs in the lungs of asthmatic mice.[171, 176-180] A collaboration between the Cook and Emala groups studied a variety of α4 or α5-subtype selective PAMs as potential treatments for asthma prior to identifying MIDD0301 as the lead ligand.[180-184] Thus, the α5-subtype selective PAM, MIDD0301 that only interacts with the subtypes in ASM to achieve ASM relaxation and decrease inflammation and doesn't cross the BBB is promising drug target for asthma.[179, 180]

A number of novel α5-selective ligands (**Figure 54**) have been developed in recent years in Milwaukee which culminated with the discovery of MIDD0301 (for asthma), GL-II-73 (for memory loss and cognition) and MP-III-022 (for respiratory depression, Angelman's Syndrome,

and neuropathic pain). Given the promising results of these α5-$GABA_AR$ subtype selective ligands in animal models, development of reliable and scalable syntheses would be a key component in pushing this technology into clinical trials.

Figure 53: The $GABA_AR$ α5β3γ2 Subtype

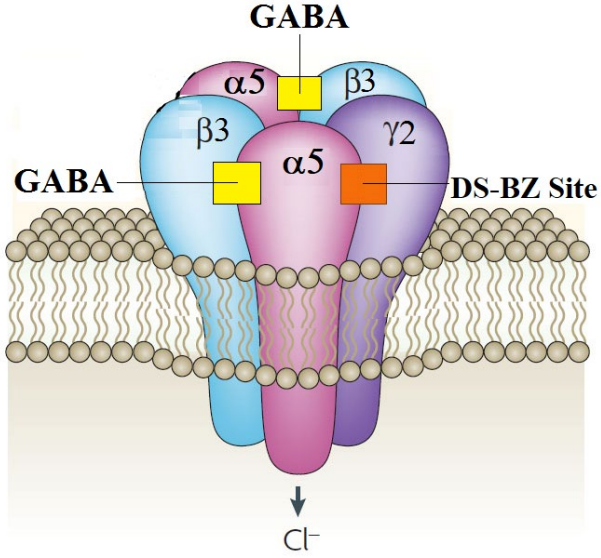

[a]The GABAAR α5β3γ2 subtype is a pentameric ligand-gated chloride channel comprised of two α5, two β3 and one γ2 subunits. IBDZs (like GL-II-73, MP-III-022 and MIDD0301) mediate their effects at the DS-Bz site (α5+γ2- interface) as positive allosteric modulators (PAMs). The IBDZ site (DS-Bz binding site) and the endogenous ligand (GABA) binding sites at the β3+α5- interfaces are displayed. Image modified from Jacob et al., Nature Reviews Neuroscience, 2008.

Figure 54: Lead α5-Selective Ligands of this Work

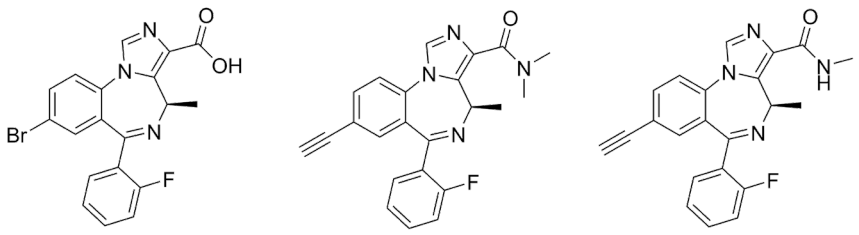

3.1.1. MIDD0301 Introduction

Asthma effects an estimated 39.5 million people in the United States, including 8.7 million children.[185] Inhalers have long been the mainstay of asthma treatment which involved a low-dose corticosteroid.[186] However, in refractory asthma, the patients respond poorly to corticosteroids, requiring oral dose escalation with the unfortunate result of side effects.[187] The high cost of injectable biologics which can effectively treat inflammation in a small sampling of patients precludes these as a practical treatment option.[188] As an alternative to these treatments, MIDD0301 was developed as a novel asthma drug which targets α5-$GABA_A$Rs in airway smooth muscle (ASM) and inflammatory cells.[180] Based on the parent ligand synthesized in Milwaukee,[149, 153, 189, 190] MIDD0301 was developed with three key structural modifications to improve the *in vivo* profile as a lead candidate for the treatment of asthma.[179] The MIDD0301 is an allosteric $GABA_A$R agonist that has exhibited the ability to treat the asthmatic symptoms in animal models after oral dosing.[179, 180] A chiral R-CH_3 function at C4 improved α5-subtype selectivity and the 2'F substituent increased potency, while the carboxylic acid function substantially reduced BBB penetration. However, these changes still preserved its ability to

reach lung cells as on PO administration (**Scheme 25**). However, the discovery chemistry was not well-suited for scale up in a potential GMP manufacturing setting. All 4 steps of the synthesis to the MIDD0301 required purification by column chromatography, while several steps exhibited typical scaleup issues such as efficient stirring, side product formation, prolonged process times and yield loss upon scale up.

Scheme 25: Development of α5-Selective Ligand **MIDD0301**

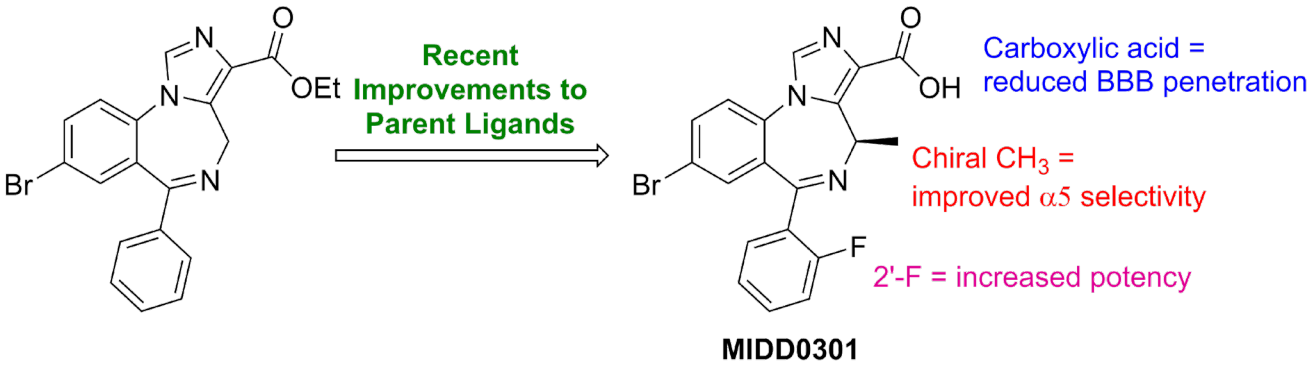

3.1.2. GL-II-73 Introduction[191]

In thinking about cognitive decline in aging, the first things that come to mind are Alzheimer's disease and related dementias, but humans and animals suffer from cognitive decline during normal aging without necessarily developing neurodegenerative diseases. With progress in medicine and health care, human populations tends to live longer. Since 2018, persons aged 65 or above have outnumbered children under 5 years of age globally.[192, 193] By 2050, it is estimated that 16% of the global population will be over 65 years of age, while in 2019 only 9% of the population is over 65 years of age.[193, 194] Overall, such extended lifespan is accompanied by normal cognitive decline and changes in brain architecture.

Normal aging has been studied for decades and it is now acknowledged that neurocognitive, structural, functional and cellular changes are hallmarks of aging.[195] Cognitive changes with aging are not necessarily associated with poorer functions. For example, vocabulary use or general knowledge and expert skills remain intact or can even improve with aging.[196, 197] On the other hand, other functions such as problem solving,[198] memory,[199, 200] processing speed[201] and psychomotor abilities[202] (also known as executive functions) suffer gradual impairment with increasing age. More specifically, episodic memory[203] (memory of personal experienced events) and working memory[204] (temporary maintenance, storage and update of information while performing a task) are altered during aging.[199]

Cognitive decline has been linked with brain changes at multiple levels that can be defined as "morphomolecuclar senescence".[205] Aging causes a grey matter volume decline, particularly in the frontal areas of the cortex (anterior cingulate cortex).[206] Subcortical regions including the hippocampus, a brain region critically involved in cognitive processes, also suffer from volume atrophy.[207] Such decrease in grey matter in frontal areas and in the hippocampus has been suggested to be caused by neuronal shrinkage and cell death,[208, 209] altogether contributing to cognitive decline. Pyramidal neurons, excitatory neurons in cortical layers, are particularly vulnerable during aging,[210-212] and exhibit reduced spine density and dendritic shrinkage during normal aging. This neuronal atrophy has been showed across species, from human post mortem studies[213] to rodents,[214] including monkeys.[215] Multiple factors contribute to neuronal shrinkage during normal aging, including, neuroinflammation[216] accumulation of β-amyloid[217-220] or dysregulation of neuronal excitation-inhibition.[212]

Neuroinflammation and β-amyloid load have been extensively studied, especially in the context of Alzheimer's disease.[221-223] However, more and more studies are showing that amyloid load is a normal process during aging,[220] and the relationship between amyloid load and cognitive decline remains uncertain in healthy elderly.[224, 225] Multiple pharmaceutical companies have tried to develop treatments by targeting β-amyloid plaques,[226] with very limited success to date.[227] To increase the chances of success at countering cognitive decline, scientists have had to explore other paths than β-amyloid.

Neuronal activity and the excitation/inhibition balance is also impaired during normal and pathological aging. Some studies have shown conflicting results sometimes suggesting a decreased excitability of neurons toward a hyper-inhibition,[228, 229] and sometimes showing an overall decrease in both excitation and inhibition.[230-232] GABAergic neurons represent the major inhibitory players to control excitability of excitatory cells. Using magnetic resonance spectroscopy, GABAergic activity has been shown to be downregulated during normal and pathological aging, and such deficits in GABA levels was associated with cognitive decline.[233] GABA signals through two main types of receptor, known as GABA- A and GABA-B receptors. The GABA-A receptors are ion-channel receptors that hyperpolarize the post- synaptic cell by chloride influx.[234] The GABA-A receptors are pentameric, composed of a combination of 5 subunits between α, β, γ, δ, ε, θ, π and ρ.[235] The different subunits of the GABA-A receptors show variable dysregulation with aging, depending on the brain regions.[236] Analysis of studies showed downregulation of α1, β1, β2, γ1 and γ2 subunits in the rat auditory cortex[237] and others showed that α3 and α5 subunits were downregulated in the rat motor cortex.[238] Examination of other studies also indicated an upregulation of the α1-subunit in the hippocampus of old rats,[239]

while a decrease of the same subunit was observed in monkeys.[240] Despite variability in the changes of the $GABA_A$ receptors associated with age, all studies agree that a decrease in the number of $GABA_A$ receptors can result in behavioral changes,[241] including cognitive deficits.[242] The α5-subunit has a particularly important distribution in the brain, since it is located exclusively in brain regions highly involved in cognitive processes, such as the hippocampus and the prefrontal cortex.[243] Analysis of preclinical and clinical data showed that the α5-subunit is downregulated in aging,[244-246] and a recent study showed that synaptic localization of α5-containing $GABA_A$ receptors contributes to dendritic outgrowth and spine maturation.[247] Altogether, this data suggests a critical role of this particular subunit in the regulation of cognitive function mediated by the GABAergic system, directly through reversal of decreased activity of the receptor during aging, or indirectly through dendritic growth.

Benzodiazepines, such as diazepam, bind at the interface between the α1,2,3,5-subunit and the γ-subunit,[248] and act as a positive allosteric modulator (PAM). They are the most commonly prescribed medication for the treatment of anxiety, widely prescribed to elderly despite apparent issues and complications linked with age.[249] The wide range of activity at different subunits is responsible for a considerable number of side effects that can be potentiated by GABAergic dysregulation occurring during normal or pathological aging.[239] Novel developments have tried to reduce the side effects of novel benzodiazepines, or derivatives, by increasing subtype selectivity to the α5-subunit and reducing selectivity to the α1-subunit.[250] Examination of previous data from Milwaukee showed that the α5- positive allosteric modulator (α5-PAM) GL-II-73 (**Scheme 26**), developed here, improved working memory in a mouse model of chronic stress and aging.[250] This ligand (with Etienne Sibille and Thomas Prevot)

demonstrated improved cognitive functions in old rats using different α5-PAMs, namely Compound **44** and Compound **6**.[251] Knowing the distribution of the α5-subunit in the brain, its downregulation during aging, its potential role in dendritic growth, and the known procognitive effect of GL-II-73 in old mice, it was hypothesized that facilitating the action of GABA at the α5-GABA receptors with GL-II-73 will improve cognitive functions in old mice. Either directly through activity at the receptor, or indirectly through reversal of dendritic shrinkage due to normal aging. To validate this hypothesis, primary neuronal cultures from mouse hippocampus were used to test the effect of GL-II-73 in vitro, at promoting dendritic growth. The effect of GL-II-73 i*n vivo*, was then tested in old mice, to demonstrate if chronic treatment can improve cognitive deficits and reverse dendritic shrinkage, and if such effects are maintained when the treatment stops.[191]

Scheme 26: Development of α5-Selective Ligand **GL-II-73**

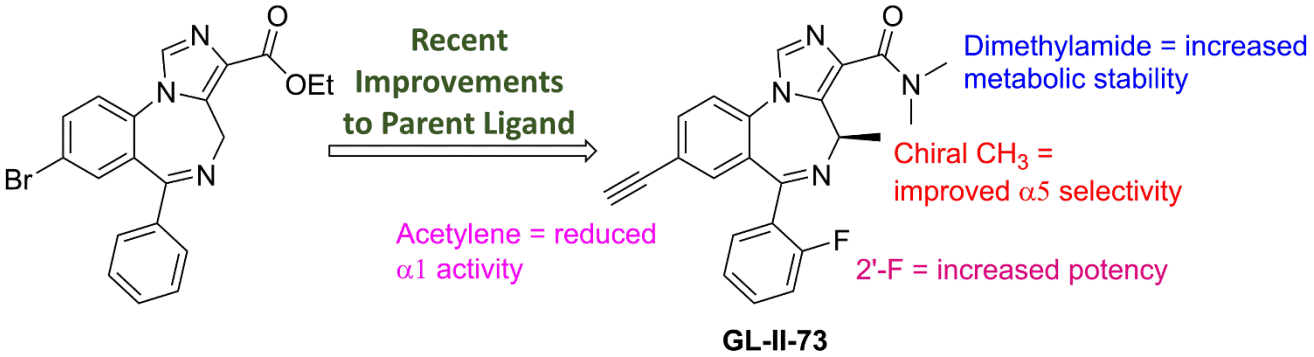

3.2. Application of α5-GABA$_A$R Subtype-Selective Imidazodiazepines in Disease Models

3.2.1. Treatment of Asthma Using the α5-GABA$_A$R Subtype-Selective Ligand MIDD0301 (with Dr. Alexander Arnold: UW-Milwaukee)[252]

MIDD0301 has been extensively studied as a treatment for asthma by the Arnold and Cook groups in recent years. Initially, the α4-subtype selective analogs of XHE-III-74 were developed.[181, 182] However, the lead asthma drug, MIDD0301 (α5-subtype selective PAM) was discovered with favorable pharmacokinetic properties in which good exposure to the desired and readily permeable lung tissues was observed, yet brain exposure was restricted.[180] This was accomplished by a modification to the initial α5-ligand with the Arnold group.[179, 180] Further work on MIDD0301 has unearthed its anti-inflammatory properties in lung tissue[179] and ability to relax airway smooth muscle (ASM).[183] Finally, the unique pH dependent structural and bioavailability properties of MIDD0301 were discovered with the Arnold group.[253]

3.2.2. Investigation of the Treatment of Diseases Using the α5-GABA$_A$R Subtype-Selective Ligand MP-III-022

The α5-subtype selective ligand MP-III-022 was synthesized and supplied to three different collaborators who used the ligand in disease models of respiratory depression,

Angelman's Syndrome, and neuropathic pain. The poster presentations for each are attached in the Appendix.

3.2.3. Treatment of Memory Loss Using the α5-GABA$_A$R Subtype-Selective Ligand GL-II-73 (with Dr. Thomas Prevot and Dr. Etienne Sibille: CAMH)[191, 254]

This study was based on the observation that normal aging induces neuronal loss which contributed to cognitive decline. Here, it was first confirmed that normal aging in mice induces cognitive deficits, with old mice exhibiting impaired working memory in the alternation task, consistent with previous findings.[250, 255, 256] Many compounds,[257] drugs,[258] natural extracts[256] or physical exercises[259] demonstrated potential at reversing cognitive decline in animal models, but with little-to-no success in human populations.[260, 261] This lack of efficacy can partially be explained by the focus of such approaches directed toward reversing the symptoms more than the underlying pathology. Indeed, it is unclear at the moment if treatment avenues that show pro-cognitive efficacy actually alleviate the underlying pathology, such as neuronal dysfunction or neuronal shrinkage. Companion tools, such as radio-ligands for PET imaging can be developed to demonstrate such efficacy, but priority is still given at alleviating the symptoms.

In the context of aging, the "morphomolecular" senescence has a broad impact on different systems, including the GABAergic system. Reduced GABAergic functions are a hallmark of aging, and previous studies from Milwaukee demonstrated that targeting α5-GABA$_A$ receptors to bypass such deficits could reverse age-related cognitive decline.[250] In the present study, the potential combined efficacy of GL-II-73 on symptoms and underlying

pathology, i.e. neuronal shrinkage was investigated. It was demonstrated that chronic treatment with GL-II-73 not only reversed cognitive decline, but also reversed dendritic shrinkage and spine atrophy in the PFC and the CA1. Indeed, chronic treatment with GL-II-73 increased dendritic length, spine count and spine density in the both important brain regions, in old mice. To our knowledge, it is the first time that a drug acting on the GABAergic system demonstrated neurotrophic effects, while commonly used benzodiazepines seem to decrease spine density in cortical pyramidal neurons.[262] Other drugs have shown neurotrophic effects,[263] such as ketamine for the treatment of depressive episodes.[264] Recent studies have shown that the antidepressant action of ketamine is mediated by its activity on the NMDA receptor of GABA neurons.[265, 266] Further studies will be needed to identify what could be the mechanism of action of GL-II-73 permitting this neurotrophic effect, and if it is a shared pathway with ketamine.

Interestingly, the neurotrophic effect of GL-II-73 was more pronounced in the apical segment of the pyramidal neuron dendrites as compared to the basal segment. It is known that the α5-GABA-A receptors are located on the apical segment of the pyramidal neurons,[243] so these results suggest that the α5-$GABA_A$ receptors directly mediate this neurotrophic effect. However, a significant increase of spine counts and spine density in the basal segment of pyramidal neurons of the CA1 from the treatment group was also observed. This effect can either suggest the potential presence of the α5-$GABA_A$ receptors in the basal segment of pyramidal neurons of the CA1, or a generalized effect happening downstream of the apical effect. Such hypotheses will need to be validated but it is consistent with previous findings, which showed, that the α5-$GABA_A$ receptors are involved in the dendritic outgrowth and spine maturation of pyramidal neurons.[247]

When GL-II-73 is no longer given to the animals, the neurotrophic effect remains but the pro-cognitive effect diminishes. One could argue that the drug needs to be on board to improve cognitive performance continuously, even in the event of a strong neurotrophic effect. This would suggest that the neurotrophic effect alone is not sufficient to recover normal cognitive processes and suggests that the "rejuvenated" neurons are not as functional as neurons of younger animals. Here, one did not investigate if the "rejuvenated" neurons were similarly functional compared to neurons from younger animals, or if their functions were more similar to neurons from old animals. Using slice electrophysiology one could answer this question and investigate if these neurons were truly rejuvenated or if the neurotrophic effect was limited to morphological features. In addition, the present study only tested one treatment duration (4 weeks) and one washout period (1 week). Investigation if longer treatment with GL-II-73 improves the stability of the cognitive functions when the treatment is spotted could be a solution to improve the functions of the rejuvenated neurons. This must be studied.[191]

Despite promising results in mice which suggests a relief of the cognitive symptoms and a rejuvenation of neurons in brain regions involved in cognitive processes, it would be naïve to think that a single drug could reverse all the changes induced by normal aging. However, GL-II-73 is the first drug targeting an inhibitory system that shows neurotrophic effects, associated with symptom relief. With its potential anxiolytic and antidepressant effects,[250] GL-II-73 could become a game changer for patients suffering from cognitive decline due to GABAergic downregulation. In the context of aging, and early stages of Alzheimer's disease, GL-II-73 could possibly be paired with Aducanumab,[226] a potent monoclonal antibody directed against β-amyloid oligomers, to further slow down the progression of the disease and strengthen neuronal

"health" and cognitive functions. Further testing in other cognitive domains, and other models (Alzheimer's disease, neurodegenerative disease etc.) will demonstrate the validity of this new drug (GL-II-73) for future therapeutic uses.[191]

3.2.3.1. Pharmacokinetic Profile of GL-II-73 in Rats and Mice

Table 15: Pharmacokinetic Parameters in Mice and Rats Calculated for GL-II-73.[254]

Compound	Animal species and dosing	Tissue	Route of admini-stration	C_{max} (Mean ± SEM, ng/ml – plasma, ng/g - brain)	T_{max} (Mean ± SEM, h)	AUC_{0-12} (Mean ± SEM, ng*h/ml – plasma, ng*h/g – brain)	$AUC_{0-\infty}$ (Mean ± SEM, ng*h/ml – plasma, ng*h/g – brain)	$T_{1/2}$ (Mean ± SEM, h)	β (Mean ± SEM, 1/h)
GL-II-73	Mouse 10 mg/kg	Plasma	IP	5384.54 ± 838.04	0.08 ± 0.00	4620.09 ± 323.21	4626.35 ± 322.80	1.20 ± 0.02	0.58 ± 0.01
		Brain	IP	1195.94 ± 51.75	0.17 ± 0.08	1311.86 ± 85.86	1397.47 ± 119.30	2.44 ± 0.20	0.29 ± 0.02
	Rat 3 mg/kg	Plasma	IV	777.76 ± 31.34	0.00 ± 0.00	434.48 ± 63.02	435.03 ± 62.92	1.21 ± 0.07	0.58 ± 0.03
			PO	79.43 ± 50.72	0.25 ± 0.08	68.54 ± 19.28	144.52 ± 65.73	7.16 ± 1.82	2.70 ± 2.58
		Brain	IV	239.70 ± 11.83	0.08 ± 0.00	103.79 ± 7.18	110.44 ± 7.05	2.35 ± 0.26	0.30 ± 0.03
			PO	20.50 ± 13.49	1.22 ± 0.89	54.09 ± 8.58	68.79 ± 13.69	7.20 ± 3.94	0.16 ± 0.06

Figure 55: Concentration-time PK Profile of GL-II-73 with Dr. Miroslav M. Savić[254]

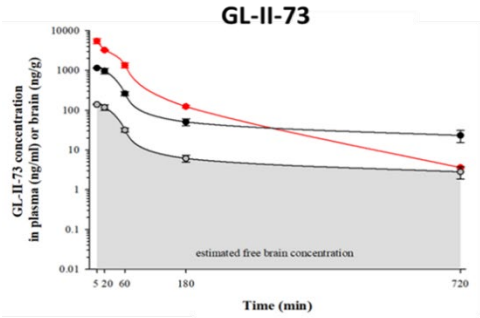

GL-II-73

	Plasma	Brain	
C_{max}	5384.54 ± 838.04	1195.94 ± 51.75	(ng/ml)
T_{max}	5.00 ± 0	10.00 ± 5.00	(min)
AUC_{0-12}	4620.09 ± 323.21	1311.86 ± 85.86	(ng*h/ml)
$AUC_{0-\infty}$	4626.35 ± 322.80	1397 ± 119.3	(ng*h/ml)
T½	72.06 ± 1.44	146.58 ± 12.30	(min)
ß	0.0096 ± 0.0002	0.0048 ± 0.0004	(1/min)
K_p	0.30 ± 0.04		
$K_{p,uu}$	0.18 ± 0.02		

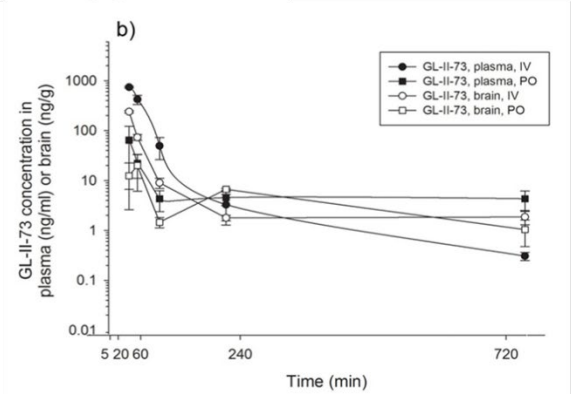

The concentration–time profile of GL-II-73 after intraperitoneal (IP) administration of the 10 mg/kg dose in male C57BL/6 mice plasma and brain (a) and after intravenous (IV) and peroral (PO) administration of the 3 mg/kg dose in rat plasma and brain (b). n=3 per time point.

Summary of PK Data

The pharmacokinetic parameters in mice and rats obtained for GL-II-73 are presented in **Table 15**. Considering in parallel the respective concentration–time profiles (**Figure 55**), it can be concluded that the potential of GL-II-73 for systemic exposure, as evidenced by AUC and C_{max} values in plasma, is generally quite high, irrespective of the route of administration. Moreover, and of crucial importance for any in vivo studies, GL-II-73 is also brain-penetrant. The calculated Kp values after i.p. administration in mice, rounded to the second decimal place was 0.30 for GL-II-73. In general terms, the values of this parameter close to or greater than unity indicate excellent brain targeting of the ligand. To ease comparison between the concentrations obtained in vivo and

those used in vitro, it is illustrative to express the kinetic results in molar in addition to the weight concentrations. After i.p. dosing at 10 mg/kg dose, GL-II-73, GL-II-74 and GL-II-75 were in the micromolar range of brain concentrations. Similarly, moderate to high submicromolar or micromolar values were measured in rat brain tissue as well.

GL-II-73 is orally available, which is usually an optimal delivery route to be developed for CNS-active drugs. The calculated F values (oral bioavailability) after i.v. or p.o. administration of 3 mg/kg in rats, rounded to the first decimal place for GL-II-73 was 0.33.

The terminal elimination half-time ($t_{1/2}$) after i.p. administration of GL-II-73 in mice was 1.20 h and 2.44 h, as measured in plasma and brain, respectively. With a $t_{1/2}$ higher than 1 h, GL-II-73 could be appropriate for a repeated-dose regimen. Nonetheless, the analogous parameter of the elimination from mouse brain tissue after i.p. administration was above 1 h, confirming that GL-II-73 meets the requirements for a potential CNS-active drug.

Table 16: PK of GL-II-73 after IV or PO Administration in Rats with Dr. Miroslav M. Savić

Type of tissue	Time point (minutes)	Concentration of GLII-73 after IV administration (nmol/l – plasma, nmol/kg – brain)	Concentration of GLII-73 after PO administration (nmol/l – plasma, nmol/kg - brain)
Plasma	5	1918.05 ± 72.70	166.43 ± 149.04
	20	1091.62 ± 229.06	57.37 ± 28.54
	60	127.85 ± 60.28	11.19 ± 5.02
	180	8.53 ± 5.20	11.79 ± 3.66
	720	0.79 ± 0.15	11.22 ± 4.45
Brain	5	620.31 ± 30.60	32.33 ± 25.56
	20	190.18 ± 25.56	51.52 ± 35.69
	60	23.34 ± 5.37	3.79 ± 0.87
	180	4.61 ± 0.59	17.30 ± 0.82
	720	4.81 ± 1.44	2.69 ± 1.47

Figure 56: Plasma and Brain Concentration–Time Profiles of GL-II-73 Administered IV in Rats with Dr. Miroslav M. Savić

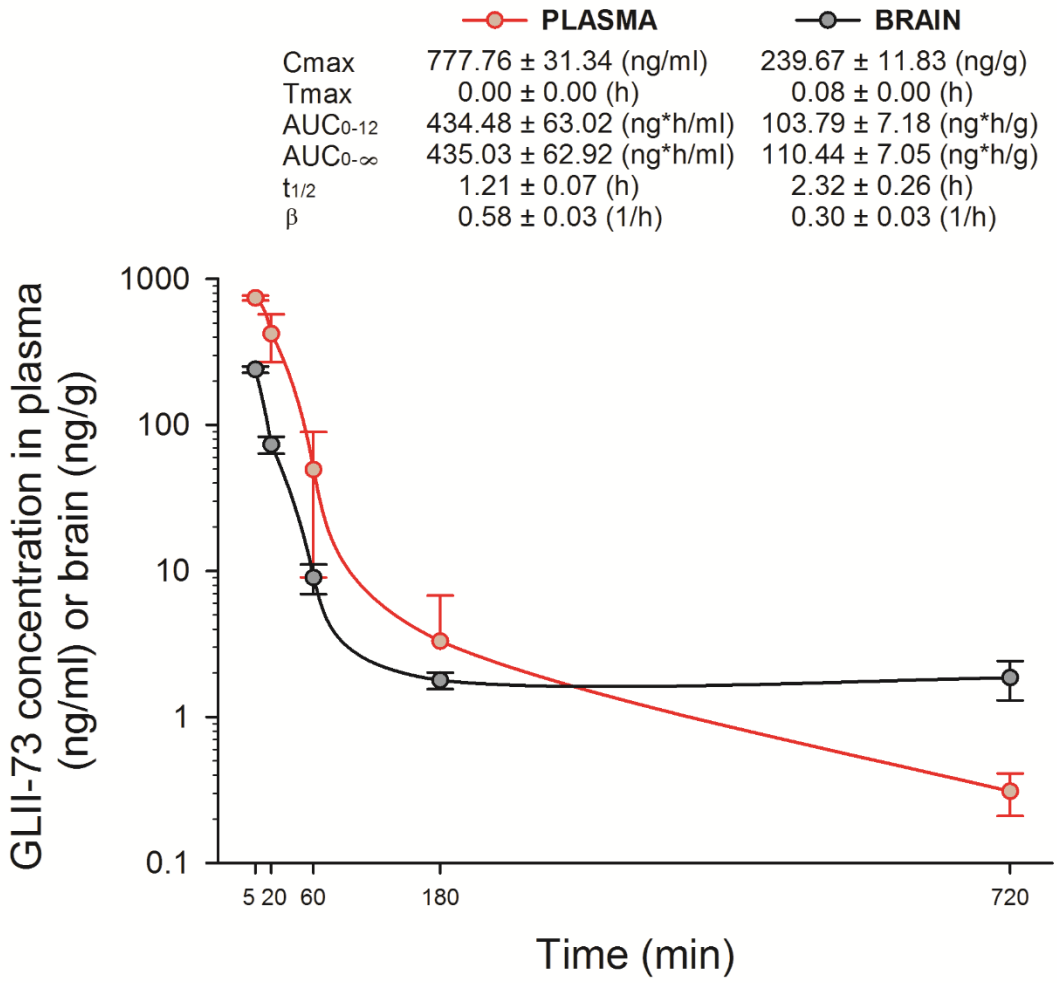

Plasma and brain concentration–time profiles of GLII-73 administered intravenously in rats in a dose of 3 mg/kg (n = 3 per time point) with the calculated pharmacokinetic parameters. C_{max} = maximum concentration in brain or plasma; T_{max} = time of maximum concentration in brain or plasma; $t_{1/2}$ = elimination half-life from brain or plasma; β = elimination rate constant; AUC_{0-12} = area under the brain or plasma concentration–time curve from 0 to 12 h; $AUC_{0-\infty}$ = area under the brain or plasma concentration–time curve from 0 to extrapolated infinite time.

Figure 57: Plasma and Brain Concentration–Time Profiles of GL-II-73 Administered PO in Rats with Dr. Miroslav M. Savić

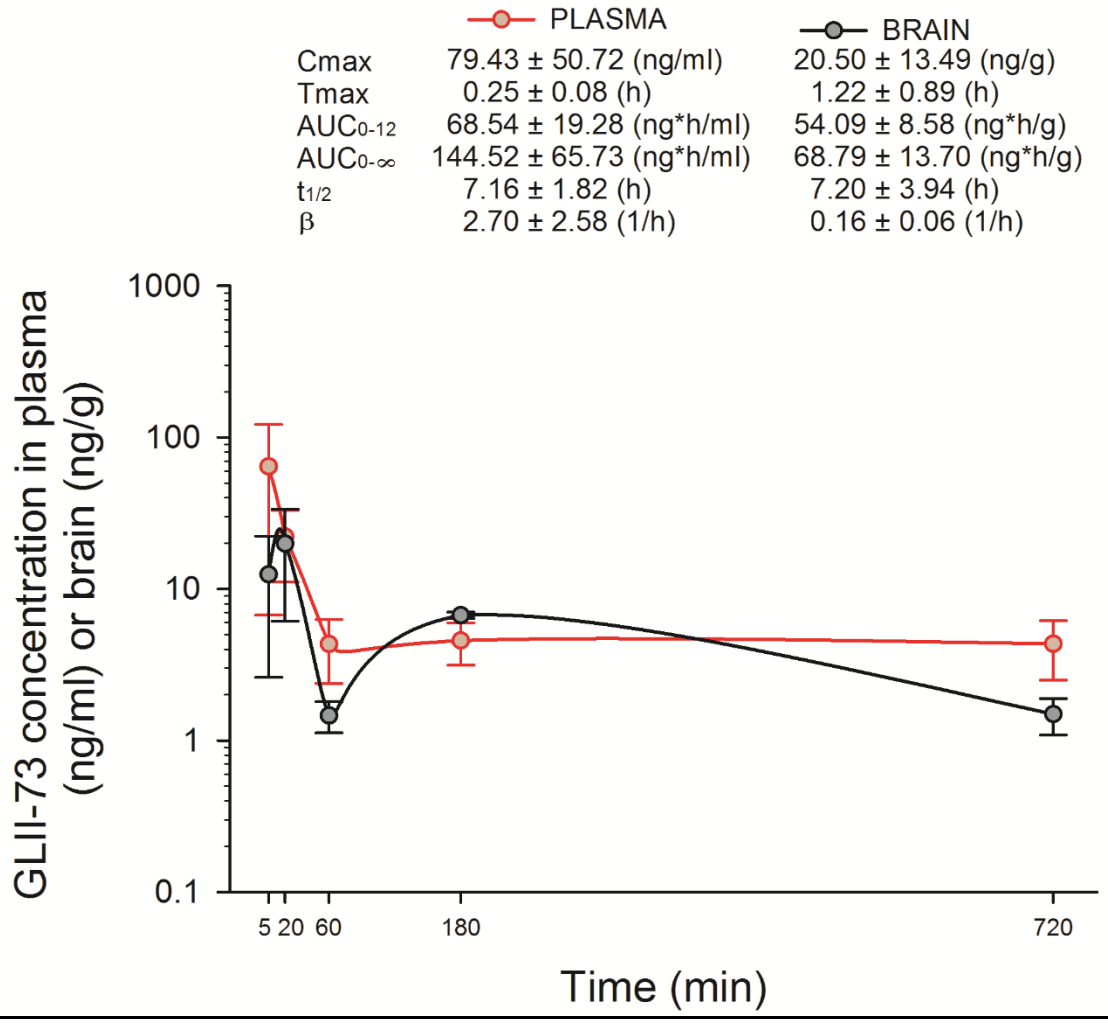

Plasma and brain concentration–time profiles of GL-II-73 administered perorally in rats in a dose of 3 mg/kg (n = 3 per time point) with the calculated pharmacokinetic parameters. C_{max} = maximum concentration in brain or plasma; T_{max} = time of maximum concentration in brain or plasma; $t_{1/2}$ = elimination half-life from brain or plasma; β = elimination rate constant; AUC_{0-12} = area under the brain or plasma concentration–time curve from 0 to 12 h; $AUC_{0-\infty}$ = area under the brain or plasma concentration–time curve from 0 to extrapolated infinite time.

Summary of Data

The pharmacokinetic study of compound GL-II-73 administered PO in rats at a dose of 3 mg/kg by Savić et al. provided the following data: AUC_{0-12} = 68.54 ± 19.28 ng*h/ml, $AUC_{0-\infty}$ = 144.52 ± 65.73 ng*h/ml, T_{max} = 0.25 ± 0.08 h, $t_{1/2}$ = 7.16 ± 1.82 h (in plasma) and AUC_{0-12} = 54.09 ± 8.58

ng*h/ml, $AUC_{0-\infty}$ = 68.79 ± 13.70 ng*h/ml, Tmax = 1.22 ± 0.89 h and $t_{1/2}$ = 7.20 ± 3.94 h (in brain). The oral bioavailability (F) of GLII-73 was 33.22% in plasma and 62.29% in brain. The results met the requirements for a potential drug candidate ($t_{1/2}$ > 2 h in plasma and brain and F in plasma > 30%).

3.2.3.2. Pharmacokinetic Profile of GL-II-73 in Dogs

PK after IV or PO administration in dogs

The PK studies were performed by a CRO – CanCog, Fergus ON (Canada) – in female dogs. The studies began with IV and PO administration of the compound at 10mg/kg, but an adverse event made us reduce the dose to 0.5mg/kg for both routes of administration.

Figure 58: Plasma Concentration of GL-II-73 after PO Administration in Dogs

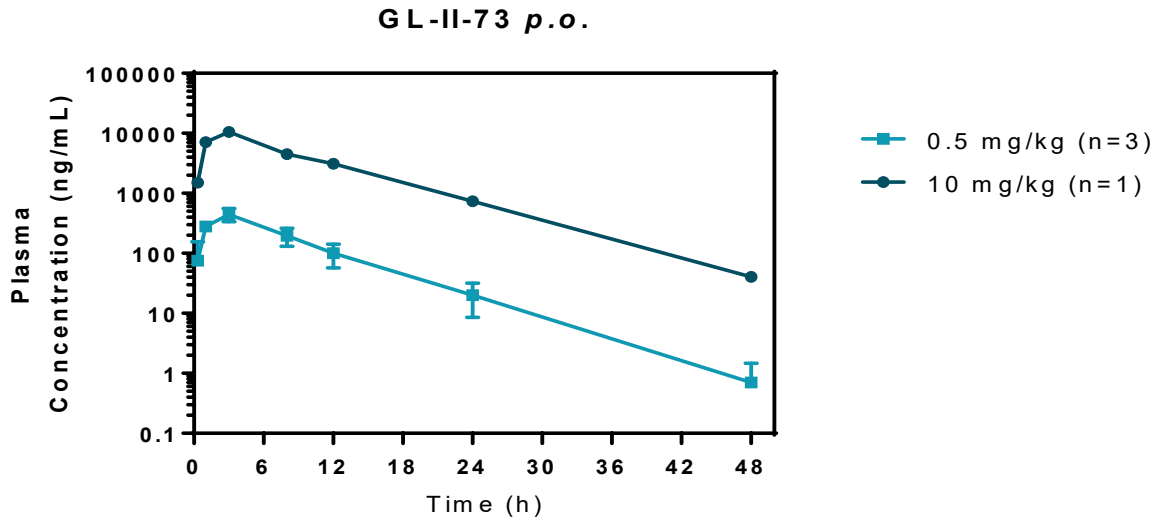

Figure 59: Plasma Concentration of GL-II-73 after IV Administration in Dogs

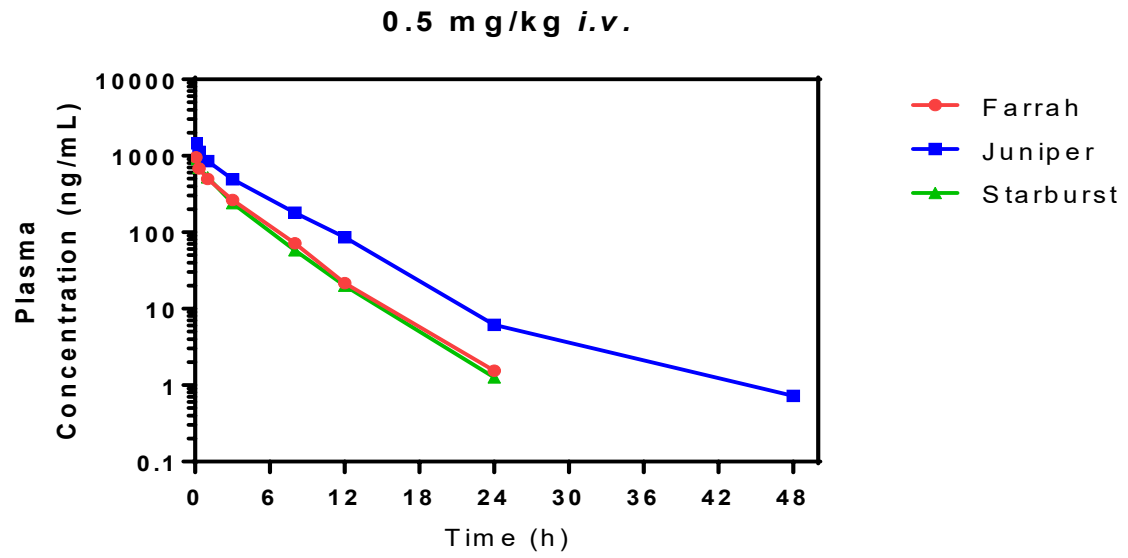

Figure 60: Plasma Concentration of GL-II-73 after PO Administration in Dogs

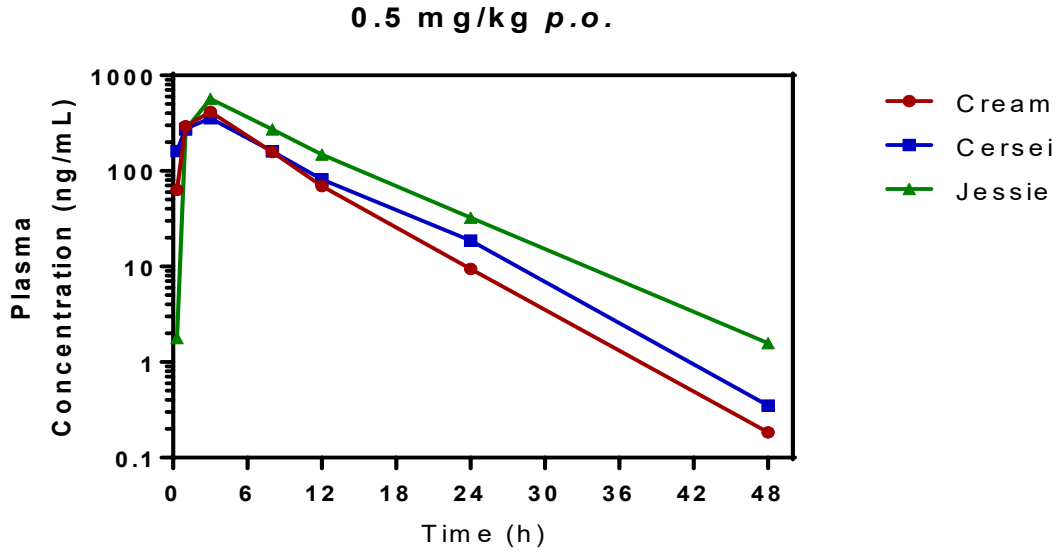

Figure 61: Average Plasma Concentration of GL-II-73 for Both Routes

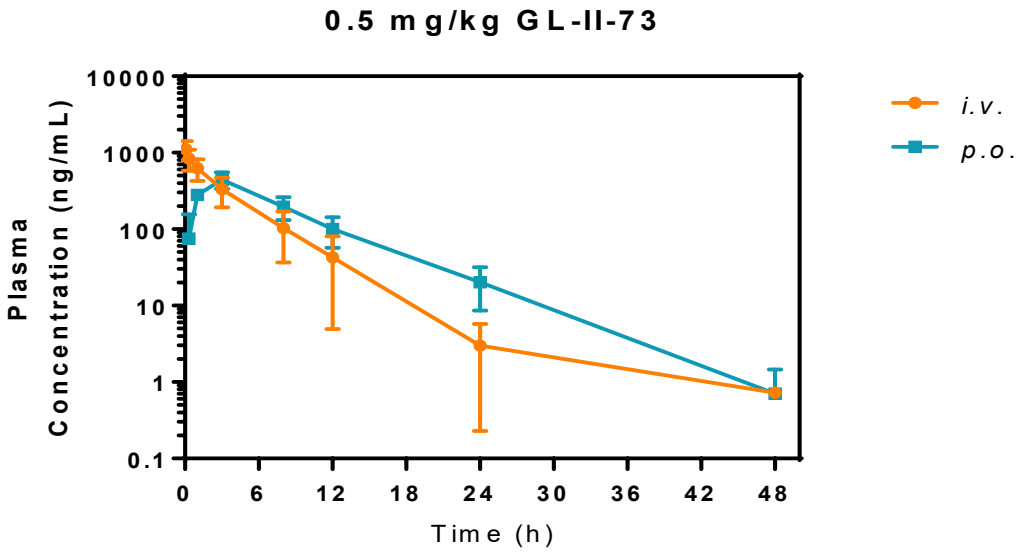

Table 17: Plasma PK Parameter Summary for IV Dosing of GL-II-73

Parameter	Parameter estimate for each animal				
	Farrah	Juniper	Starburst	Mean	SD
C_0 (ng/mL)	1070	1590	979	1213	330
Apparent $t_{1/2}$ (h)	2.94	5.06	2.92	3.64	1.23
$AUC_{0\text{-}tlast}$ (h*ng/mL)	2420	4900	2270	3197	1477
$AUC_{0\text{-}inf}$ (h*ng/mL)	2420	4910	2280	3203	1480
CL_s (mL/h/kg)	206	102	219	176	64.1
$MRT_{0\text{-}inf}$ (h)	3.55	4.85	3.34	3.91	0.818
V_{ss} (mL/kg)	732	494	734	653	138

Table 18: Plasma PK Parameter Summary for PO Dosing

Parameter	Parameter estimate for each animal				
	Cersei	Cream	Jessie	Mean	SD
t_{max} (h)	3.00	3.00	3.00	3.00	0.000
C_{max} (ng/mL)	355	416	569	447	110
Apparent $t_{1/2}$ (h)	4.52	4.21	5.49	4.74	0.668
$AUC_{0\text{-}tlast}$ (h*ng/mL)	3120	3020	4920	3687	1069
$AUC_{0\text{-}inf}$ (h*ng/mL)	3120	3020	4940	3693	1081
$MRT_{0\text{-}inf}$ (h)	7.77	6.69	8.90	7.79	1.11
F (%)	97.4	94.3	154	115	33.7

Other parameters measured during the dosing include heart rate, body temperature, respiration rate and blood pressure. No change was noticed after dosing for all parameters (data not shown, but available).

3.2.3.3. Receptor Subtype Selectivity Profile of GL-II-73: Electrophysiological Assay with Dr. Janet Fisher

Figure 62: Electrophysiological Response to GL-II-73 in Mammalian HEK Cells Transfected with α1, α2, α3, α4 α5, or α6 $GABA_A$ Receptors, and at α1β3γ2 and α1β3δ When Exposed to GABA

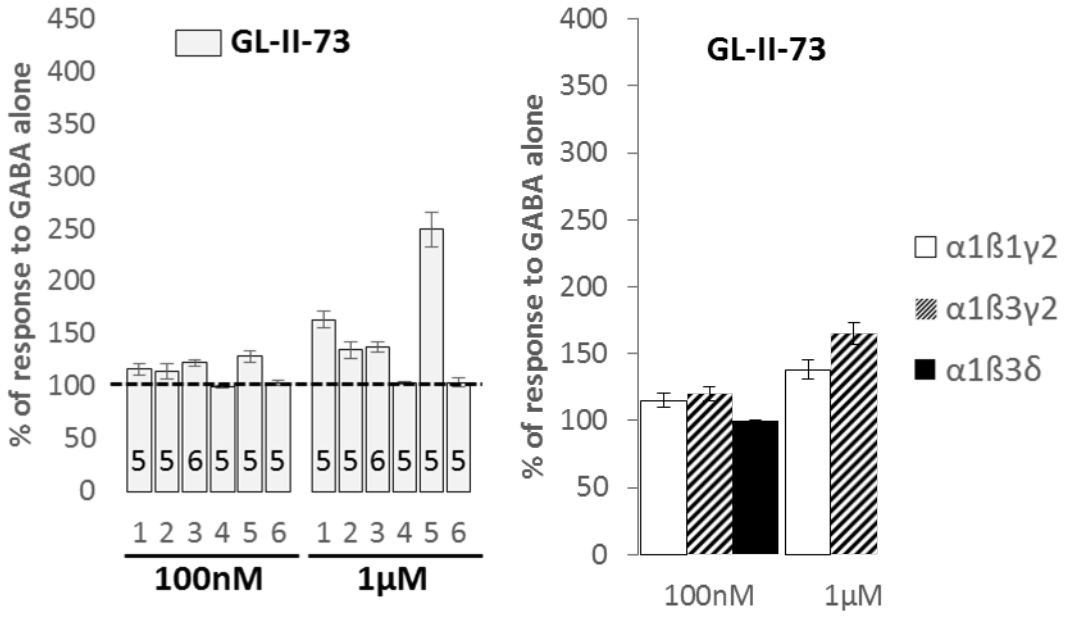

The percent response to GABA in the presence of 100 nM or 1 µM concentrations of GL-II-73 in human embryonic kidney cell line HEK-293T transfected with plasmids expressing α1, 2, 3, 4, 5, or 6 $GABA_A$ receptor subtypes, or α1β3γ2 or α1β3δ, show a preferential effect of GL-II-73 on α5-$GABA_A$ receptors. The presence of β1 or β3 subunit does not seem to modify the effect of the drug, while absence of γ subunit abolishes the effect.

Figure 63: Approximated Electrophysiological Responses Elicited by the Estimated Free Brain Concentrations and Presented on the Concentration-Response Curves of GL-II-73

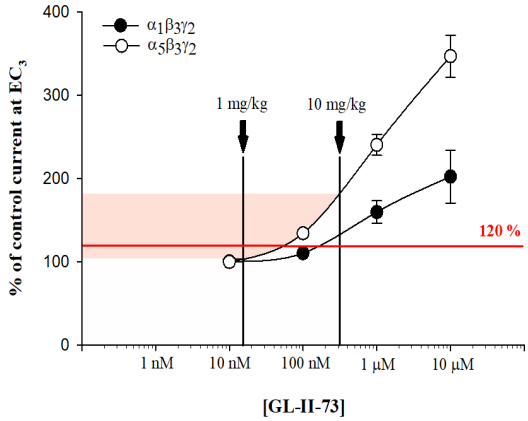

The approximated electrophysiological responses elicited by the estimated free brain concentrations and presented on the concentration-response curves of GL-II-73 at rat recombinant $\alpha_1\beta_3\gamma_2$ and $\alpha_5\beta_3\gamma_2$ $GABA_A$ receptors measured at GABA EC_3 (eliciting 3% of the maximal GABA current in the respective subtype). Brain tissue density of 1.04 g/ml (Weaver et al., 2001[267]) was used to convert brain concentrations from ng/g into ng/ml. The shaded range delineates the interpolated lower and upper limit of potentiation at α_5GABA_ARs in the dose range used; the vertical lines mark the approximated free brain concentration of the given dose of each of three ligands. The level of potentiation of 120% was arbitrarily set as borderline for eliciting in vivo behavioral effects (cf. data for diazepam in Alhambra et al., 2011[268] and in Savić et al., 2010[81]).

Summary of the Data

Exposure at 1 micromolar, but not 100 nM concentration induced an increased % of response to GABA in cells transfected with the α5 subunit. GL-II-73 had the greatest response at 1 µM, but not at 100 nM. GL-II-73 does not exhibit potent affinity for the receptor expressing the δ subunit, and the expression of β1 instead of β3 does not significantly change the affinity of the compound for the two receptors.

Binding Affinity of GL-II-73

	α1β3γ2	α2β3γ2	α3β3γ2	α5β3γ2
GL-II-73	55±4μM (n=3)	30±5 μM (n=3)	63±7μM (n=4)	5±2 μM*** (n=5)
Reported in Prevot et al. (2019)[254], GL-II-73 binds preferentially at α5-containing $GABA_A$ receptors, as compared to α2 (6 fold), α1 (11 fold) and α3 (12.5 fold) GABAergic/Bz subtypes.				

3.2.3.4. Cytotoxicity with Dr. Michael Rajesh Stephen

Cytotoxicity Assay

Cell line culture and procedure: Human liver hepatocellular carcinoma (HEPG2) and human embryonic kidney 293 (HEK293) cell lines were purchased (ATCC) and cultured in 75 cm2 flasks (CellStar). The cells were grown in DMEM/High Glucose (Hyclone, #SH3024301) media to which non-essential amino acids (Hyclone, #SH30238.01), 10 mM HEPES (Hyclone, #SH302237.01), 5 x 106 units of penicillin and streptomycin (Hyclone, #SV30010), and 10% of heat inactivated fetal bovine serum (Gibco, #10082147) were added. Cells were harvested using 0.05% trypsin (Hyclone, #SH3023601), washed with PBS, and dispensed into sterile white, optical bottom 384-well plates (NUNC, #142762). After three hours small molecule solutions were transferred with a Tecan Freedom EVO liquid handling system equipped with a 100 nL pin tool (V&P Scientific). The controls were (E)-10-(bromotriphenylphosphoranyl)decyl 4-(4-(tert-butyl)phenyl)-4-oxobut-2-enoate (400 μM in DMSO, positive control) and DMSO (negative control). The cells were incubated for 48 hours and this was followed by the addition of CellTiter-

Glo™, a luminescence-based cell viability assay (Promega, Madison, WI). All luminescence readings were performed on a Tecan Infinite M1000 plate reader. The assay was carried out in quadruplet with three independent runs. The data was normalized to the controls and analyzed by nonlinear regression (GraphPad Prism).

Compound Name	HEK293 LD_{50} (µM)	HEPG2 LD_{50} (µM)
GL-II-73	>200	>400

Summary of Data

Examination of the cytotoxicity assays demonstrated that GL-II-73 was not toxic to the respective cell lines in varying high concentrations.

3.2.3.4.1. CYP3A4 Inhibition Assay

Figure 64: CYP3A4 Inhibition with 10 or 50 µM of GL-II-73

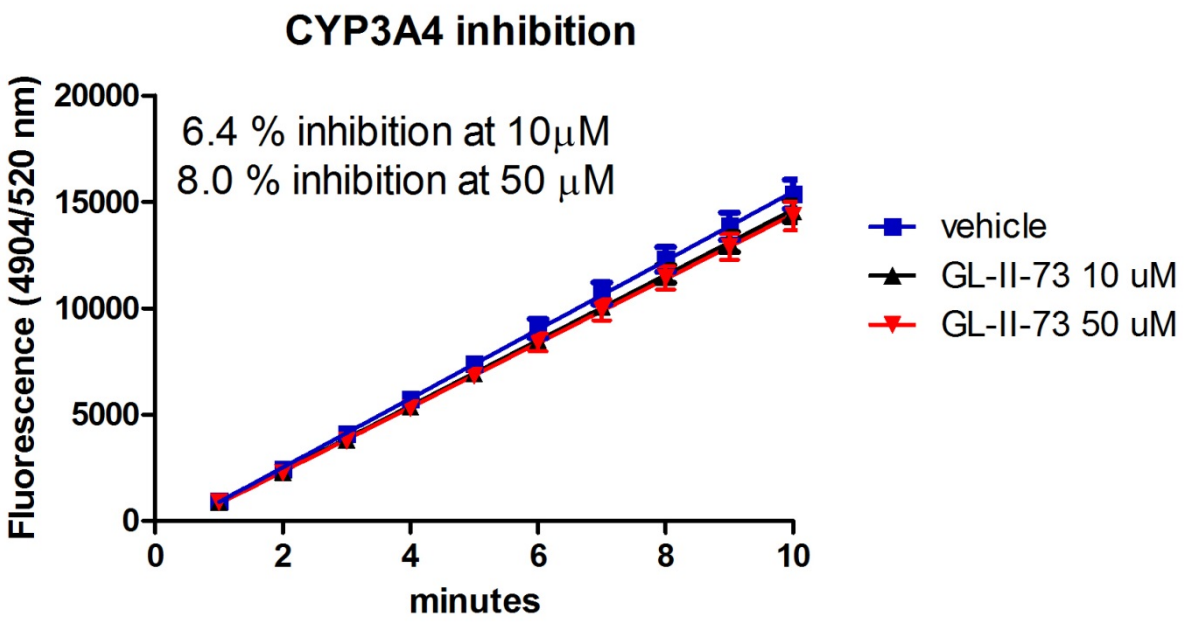

Conclusion: No effect of GL-II-73 on CYP3A4 noticed at 10µM or 50µM

3.2.3.5. Metabolic Stability Assays for GL-II-73 with Revathi Kodali

3.2.3.5.1. Metabolic Stability of GL-II-73 (Human and Mouse Liver Microsomal Assays)

As extracted from Prevot et al. (2019)[254], metabolism studies were performed in human and mouse liver microsomes, as described by Namjoshi et al. (2013).[269] The ligands were incubated at 10 μM with active or heat-inactivated human or mouse liver microsomes and appropriate cofactors. Aliquots were removed at different time points and assayed using liquid chromatography/tandem mass spectrometry (LC-MS/MS). To obtain pharmacokinetic profiles, mice were treated i.p. at 10 mg/kg and sacrificed at different time points (5 to 720 min post-injection) for brain and plasma quantification of ligands by ultraperformance LC-MS/MS. The analytical lower limit of quantification for the ligands examined ranged from 0.5 to 1.0 ng/mL in plasma, and from 0.2 to 1.0 ng/g in brain tissue.

Table 19: Metabolic Stability of GL-II-73 and GL-I-54 in Human or Mouse Liver Microsomes

Compound Name	Genus	Half-life (min) (HumanLM)	% left after 2 h. (HumanLM)	Half-life (min) (MouseLM)	% left after 2 h. (MouseLM)
GL-II-73	R-Isomer	280.56 ± 31	73.34 ± 0.6	472.69 ± 36	81 ± 0.3
GL-I-54	S-Isomer	112 ± 4	39 ± 1	52 ± 10	14.6 ± 4.7

(HLM and MLM respectively). The half-life is expressed in min and the remaining quantity of compounds after 1 h is expressed in %.

Summary of Data

In human liver microsomes, GL-II-73 was stable, wherein more than 73% remained after 2 h. The GL-II-73 (R-enantiomer) was much more stable than S-enantiomer GL-I-54 (39% remained after 2 h). In mouse liver microsomes, GL-II-73 was relatively stable with more than 81% remaining after 2 h. In regard to the stability of the enantiomers, GL-II-73 was much more stable than GL-I-54 in the mouse liver microsomes (81 % vs 14.6 %).

3.2.3.5.2. Metabolic Stability of GL-II-73 (Dog and Monkey Liver Microsomal Assay)

Table 20: Metabolic Stability of GL-II-73 in Dog and Monkey Liver Microsomes

Compound Name	Genus	Half-life (min) (DogLM)	% left after 2 h. (DogLM)	Half-life (min) (NHPLM)	% left after 2 h. (NHPLM)
GL-II-73	AMIDE	1312 min	93.1%	248 min	67%

3.2.3.6. Locomotion and Motor Coordination in Mice

3.2.3.6.1. Home Cage Locomotor Activity (with the Sibille/Banasr Group) – Distance Travelled

The mice (50% females) were placed in their home-cage, from which the lid was taken off to allow video recording from the top. The nesting material was also removed to ensure proper tracking of the animal at all times. Mice were administered with the drug 1 hour before being tested, and their activity was recorded for 30 min. The video tracking data was acquired using the software AnyMaze, and then analyzed using StatView.

Figure 65: Effect of GL-II-73 on Locomotor Activity

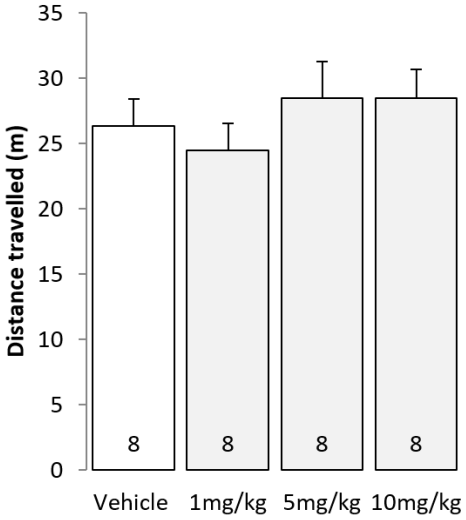

Data are expressed in meters of distance travelled (30 min session). ANOVA revealed statistical significance on the overall effect of treatment. Post hoc analysis showed GL-II-73 has no significant effect on locomotor activity. Differences between groups were tested using the post-hoc analysis of Scheffe (*p<0.05 compared to the "Vehicle" group).

	Veh	1 mg/kg	5 mg/kg	10 mg/kg
Number of Animals	8	8	8	8

Summary of Data

Analysis of the data demonstrated significant differences between groups (ANOVA: F (3,36)=3.8; p=0.016). Scheffe post hoc analysis revealed no significant effect of GL-II-73 at low doses (1 or 5 mg/kg) and a significant increase in locomotion at 10 mg/kg (p=0.02) as compared to the vehicle group.

3.2.3.6.2. Spontaneous Locomotor Activity (with the Savić Group)

Figure 66: Effect of Multiple Drugs on Locomotor Activity

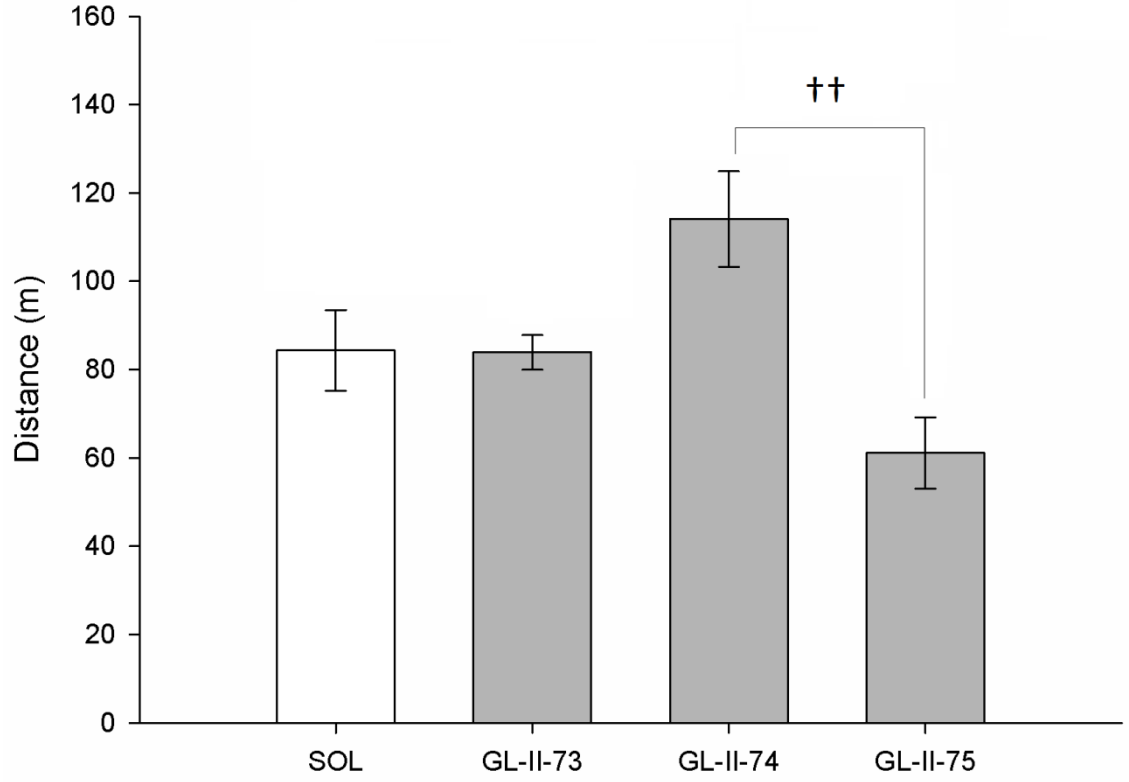

C57BL/6 mice were tested in an open field, for 1hr, their activity was recorded from a digital camera connected to the videotracking system AnyMaze. Mice were injected with 3 different drugs, depending on their group affiliation, and were immediately tested in the open field. The effect of GL-II-73, GL-II-74 and GL-II-75, all dosed i.p. at 10 mg/kg, was investigated on spontaneous locomotor activity during 60 min of recording in mice. All data are presented as the mean ± S.E.M. The number of animals per treatment group was 7, with exception of GL-II-73 (n=6). $^{++}P<0.01$ between GL-II-74 and GL-II-75 groups.

Figure 67: Effect of Multiple Drugs on Locomotor Activity, per Bin of 5 Minutes

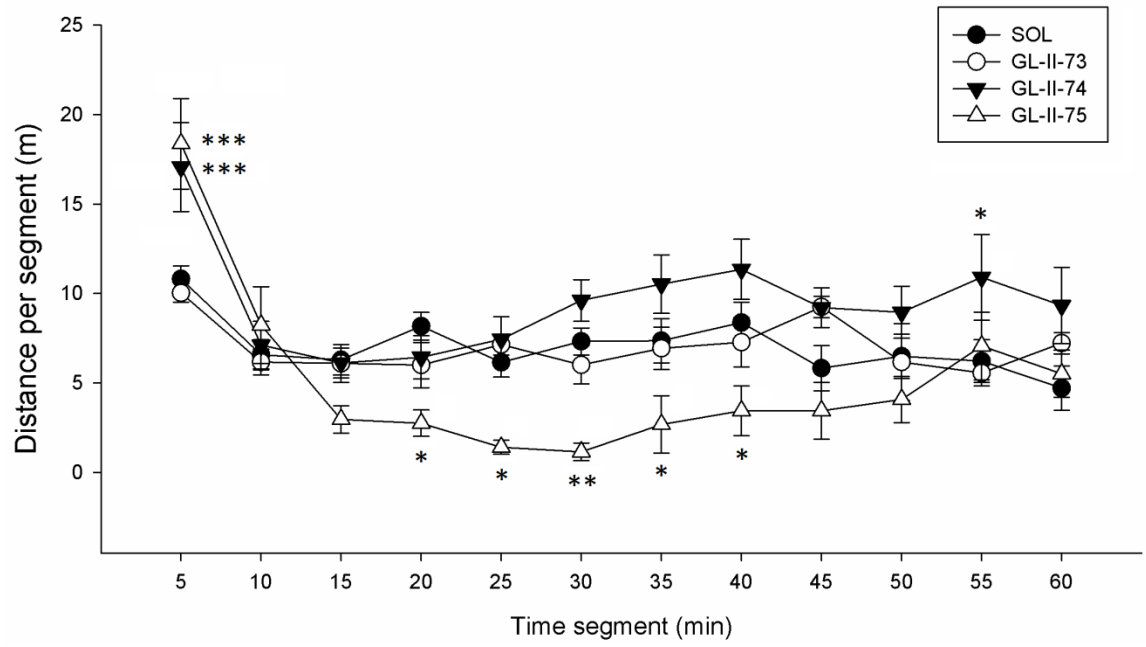

The effect of GL-II-73, GL-II-74 and GL-II-75, all dosed i.p. at 10 mg/kg, on distance traveled in 5-min bins during recording in the locomotor activity test in mice. All data are presented as the mean±S.E.M. $^{*}P<0.05$, $^{**}P<0.01$ and $^{***}P<0.001$ versus SOL group. Animals injected with GL-II-73 (white circle shapes) seem to behave similarly compared to animals receiving Vehicle (Black circle shapes).

Examination of the Summary of the Data

The overall distances traveled during 60 min of recording are presented in **Figure 66**, while illustrated in **Figure 67** is the distance traveled in 5-min bins. One-way ANOVA of the distance traveled during 60 min revealed an effect of treatment ($F(3,23)= 6,523$, $P=0.002$). However, GL-II-73 at 10 mg/kg did not elicit any significant effect on locomotor activity. A two-way repeated measures ANOVA of 5-min interval distances revealed a significant effect of all factors (Treatment: $F(3,253)=6.52$, $P=0.002$; Time: $F(11,253)=14.59$, $P<0.001$; Interaction: $F(33,253)=3.25$, $P<0.001$). The post hoc comparisons of 5-min bins, however, demonstrated that GL-II-73 did not have any significant effect on locomotion at any point of the 60 min recording.

3.2.3.6.3. Locomotor Coordination - Rotarod Experiments using GL-II-73

Figure 68: Effect of GL-II-73 on Locomotor Coordination

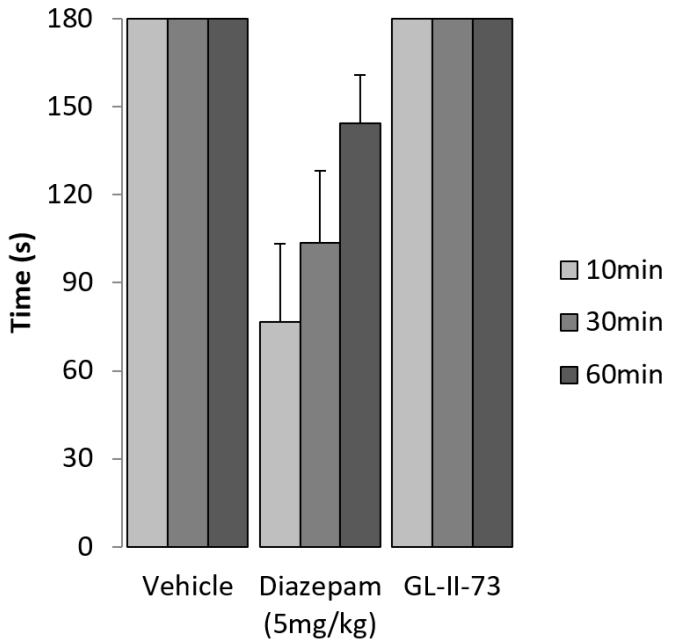

Female Swiss Webster mice were tested on a rotarod at 15 rpm for 3 min at 10, 30, and 60 min following compound exposure. Mice (N = 10) received a single oral injection via oral gavage of test compound (40 mg/kg), diazepam (5 mg/kg), or vehicle (2% polyethylene glycol, 2.5% hydroxypropylmethyl cellulose solution). The time of fall was recorded if it occurred prior to 3 min. **Effect of compounds on sensorimotor coordination.** Data are expressed as mean ± SEM (N = 10). ** ($p<.01$) or *** ($p<0.001$) significance compared to vehicle-treated mice. All compounds were able to be dissolved in the oral vehicle. GL-II-73 did not impair locomotor coordination at any timepoint tested, while diazepam significantly decreased the latency to fall from the rod, at all time points.

A Summary of Data is Represented Here.

The diazepam positive control (5 mg/kg) showed the greatest impairment of sensorimotor steadiness at 10 min, followed by 30 and 60 min. GL-II-73 was subsequently administered via oral gavage at 40 mg/kg in a vehicle of 2% polyethylene glycol and 2.5% hydroxypropylmethyl cellulose solution. GL-II-73 did not induce any sensorimotor impairment.

3.2.3.6.4. Rotarod Experiments – Replicated by the Savić Group

Figure 69: The Influence of the Increasing Doses of GL-II-73 on the Rotarod Performance

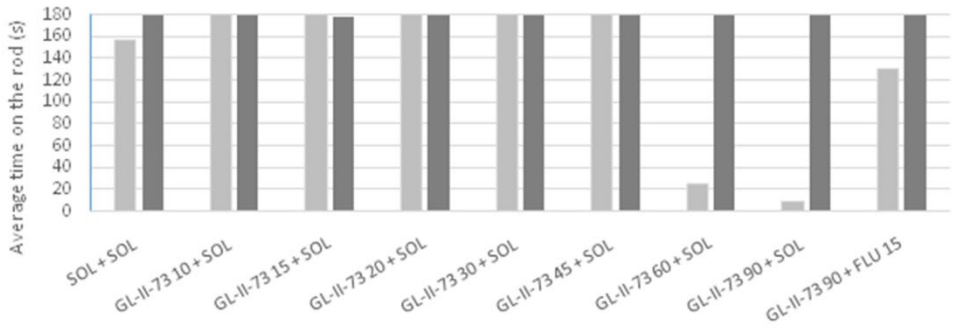

GL-II-73 does not incapacitate locomotor coordination with doses below 60mg/kg. When co-administered with flumazenil (benzodiazepine site blocker), the incapacitation effect of a high dose of GL-II-73 is abolished. C57BL/6 mice (n = 1–4 per treatment) received Solvent (SOL) or GL-II-73 at different doses and were tested on the rotarod, 15rpm for 5 minutes. The doses administered were 10, 15, 20, 30, 45, 60 and 90 mg/kg for GL-II-73. Additionally, the reliably incapacitating dose was co-administered with flumazenil at a dose of 15 mg/kg and their influence on rotarod performance was also observed.

A Summary of Data is Described Here.

Illustrated in **Figure 69** are the latencies to falling from the rotating rod recorded in mice injected i.p. with GL-II-73, on their own and in combination with flumazenil (15 mg/kg), the non-selective antagonist of the benzodiazepine binding site of $GABA_A$ receptors. It was observed that GL-II-73 displayed a much wider margin of safety, and the incapacitating effect of the 90 mg/kg dose was also preventable by flumazenil indicating, although a high dose, it was likely mediated by $GABA_A$ receptors.

Figure 70: Influence of Increasing Doses of GL-II-73 and Diazepam on Locomotor Coordination

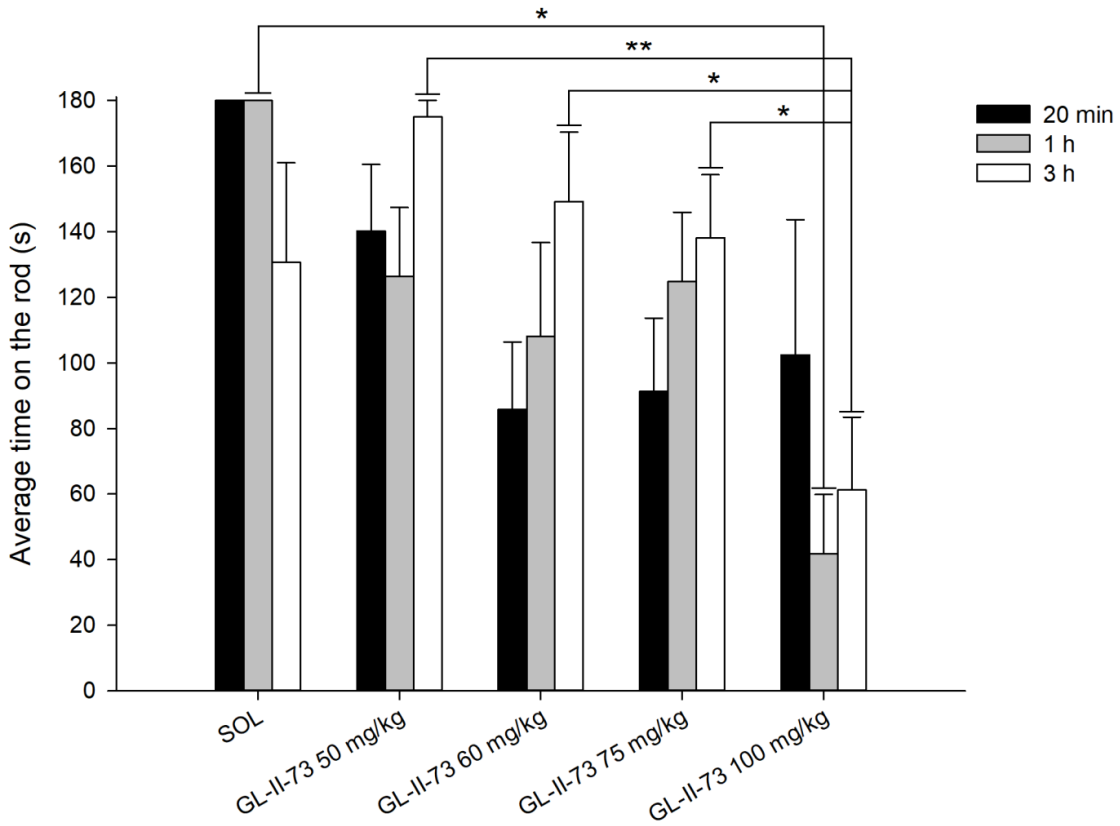

Rotarod Experiment: Replication with Oral Gavage. The influence of the increasing doses of GL-II-73 and diazepam (DZP) on the average time on the rod was assessed 20 minutes (20 min), 1 hour (1 h) and 3 hours (3 h) after oral gavage in male C57BL/6 mice (n = 1–5 per treatment). All data are presented as the mean ± S.E.M. One can see that the time on the rod is significantly decreased, 1hr after injection at the dose of 100mg/kg only.

3.2.3.6.5. Dose Escalation Study – Locomotor Assessment in Dogs

Figure 71: Heart Rate in Dogs after PO Administration of GL-II-73

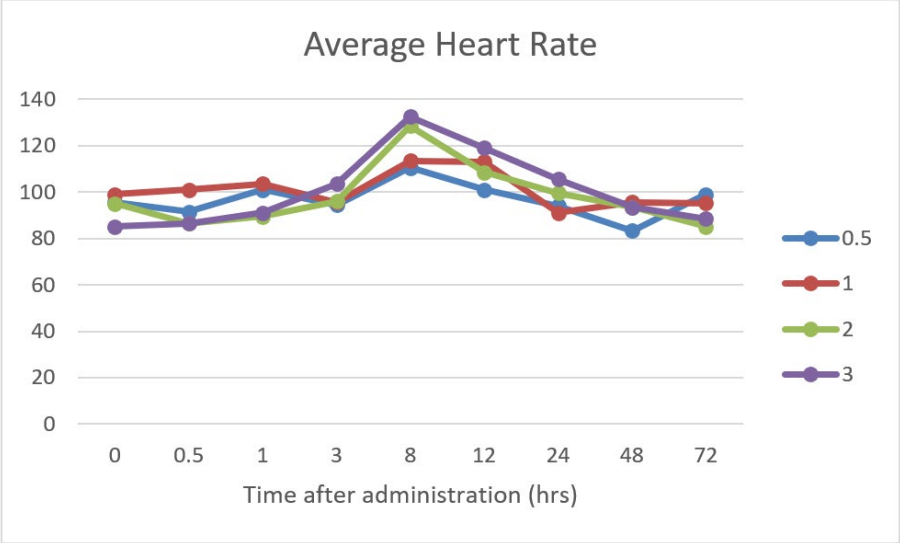

A dose escalation study was performed by a CRO – CanCog, Fergus ON (Canada). Doses were administered PO, at 0.5, 1, 2 or 3 mg/kg. Heart rate was measured. Dosing did not induce changes.

Figure 72: Respiration Rate in Dogs after PO administration of GL-II-73

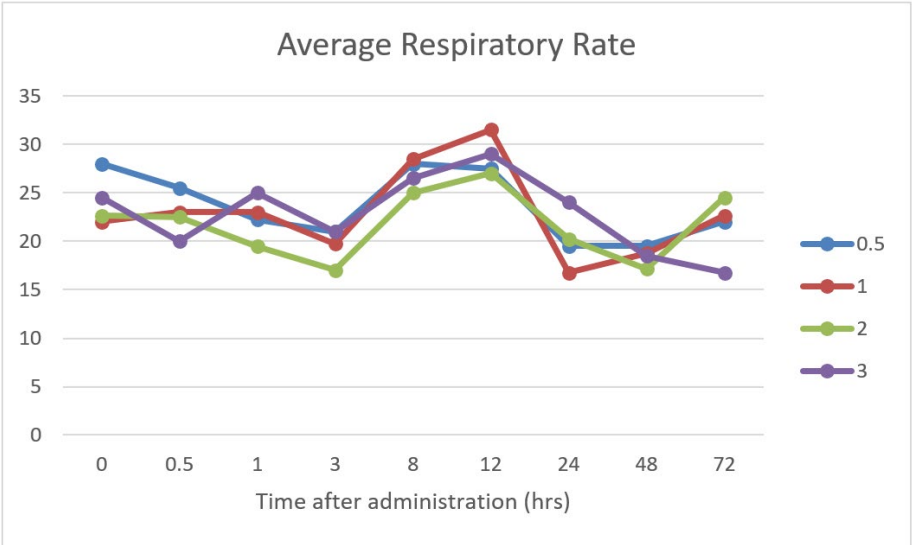

Respiration rate was measured. Dosing did not induce any change.

Figure 73: Body Temperature in Dogs after PO Administration

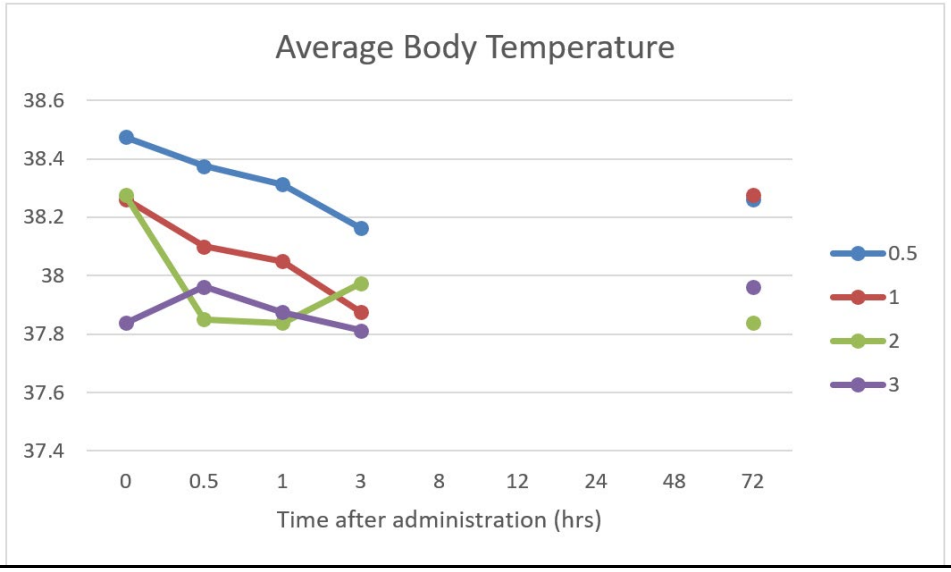

Body temperature was measured: increasing doses induced slight decrease in body temperature.

Figure 74: Average Activity in Dogs after PO Administration

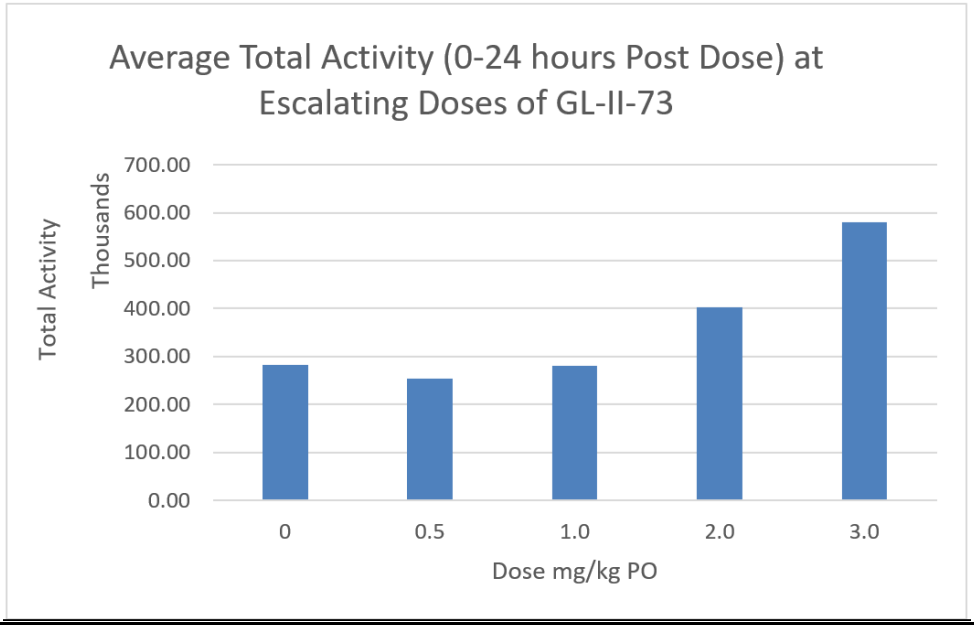

Average activity induced by the dosing was as follow: Increasing doses increased average activity over the first 24hrs post dosing. This is sometimes indicative of an anxiolytic effect.

Figure 75: Average Time at Each Activity Level per Dose

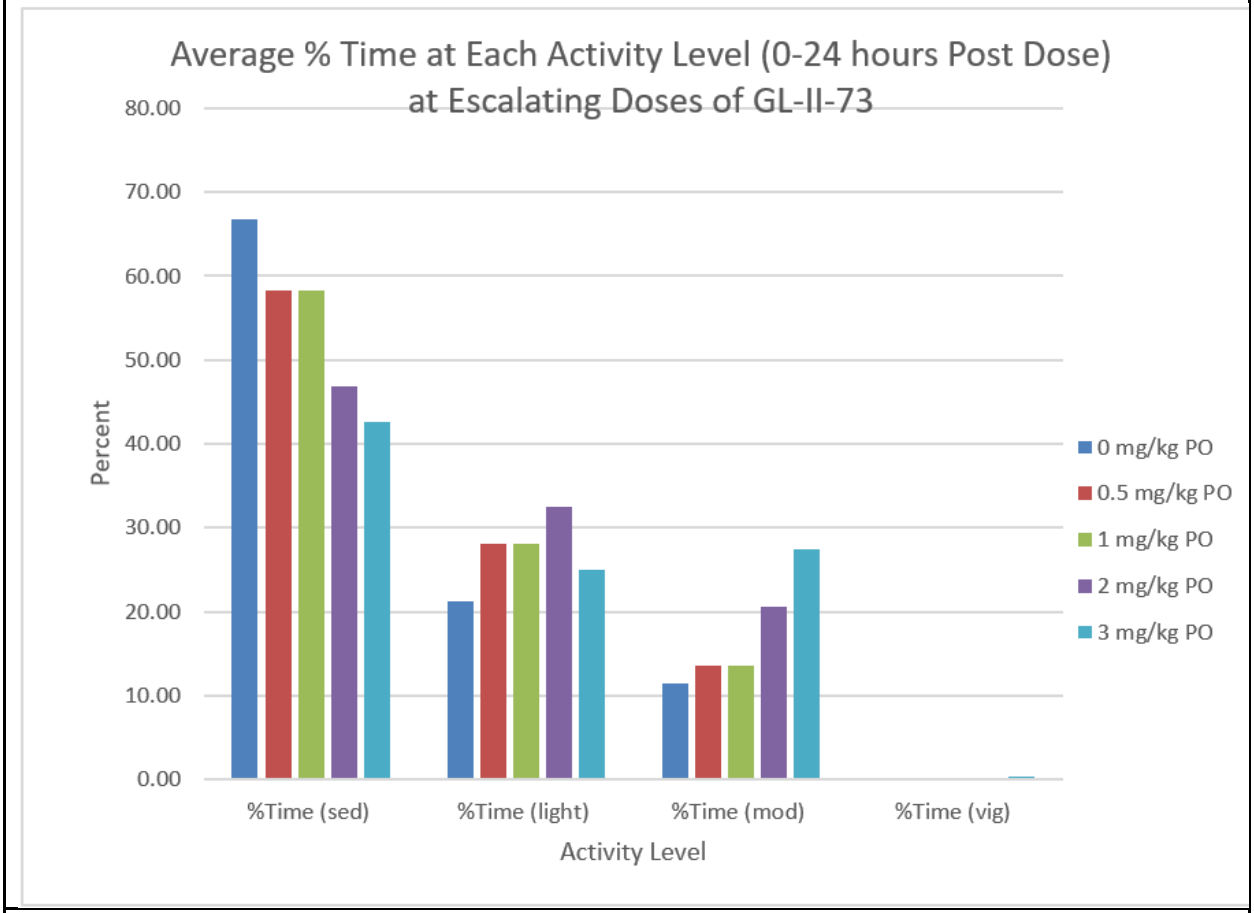

In more detail, increasing dosing decreased the time spent sedentary and increased the time spent mobile (suggesting no sedation effects at the tested doses). Again, increasing the dose of GL-II-73 appeared to increase the time spent active, suggesting no sedative effects at the proposed doses.

3.2.3.7. Cognition: The Influence of GL-II-73 on Working Memory in the Y Maze

Young male and female (50%) mice (Jackson Laboratories, Bar Harbor, USA) and old males (22 months-old) were single-housed. The young animals were subjected to a chronic stress protocol (CS) to induce a working memory deficit. They were placed in a 50mL Falcon® tube, twice a day, for 1hr during their diurnal cycle. CS was not applied on testing days. The cognition apparatus was a black plastic Y-maze with 3 arms, 26cm long, 8cm wide with sidewalls 13cm high and all separated by 120°; each arm having a sliding door. Mice were first habituated to the apparatus and to distal cues during 2 consecutive days over a 10 min free exploration session. The following day, animals performed a training session consisting of seven successive trials where they have to alternate between the 2 goal arms with an inter trial interval (ITI) of 30sec. The same general procedure used in the training session was implemented 24h later, except that the ITI was lengthened to 90s or 60s, for young or old animals respectively. The animals were acutely injected i.p. with vehicle, 1, 5 or 10 mg/kg dose of the test compounds or 1.5mg/kg DZP, 30min before the beginning of the test. To dissociate memory deficits from an eventual progressive loss of motivation, an 8th trial was added to the series which was separated from the 7th trial by a shorter ITI (5s). All animals failing to alternate at the 8th trial were excluded from the analysis. The alternation rate was calculated and was expressed in percentage: $Alternation\ rate = \frac{Alternation}{Maximum\ alternation\ possible}\ x\ 100$. The percentage of alternation during the entire task was considered as an index of working memory performance (50% of alternation corresponding to a random alternation rate). This test can be repeated weekly, with no requirement for habituating the animals again. This allows us to reduce the number of animals and test multiple doses or compounds in the same animals, with a week of

wash-out between experiments. We confirmed that the compounds were washed out of the organism of the mouse by conducting a pilot experiment that validated the design.

Figure 76: The Effect of GL-II-73 on Working Memory in Young Mice Exposed to Chronic Stress with Thomas Prevot and Etienne Sibille

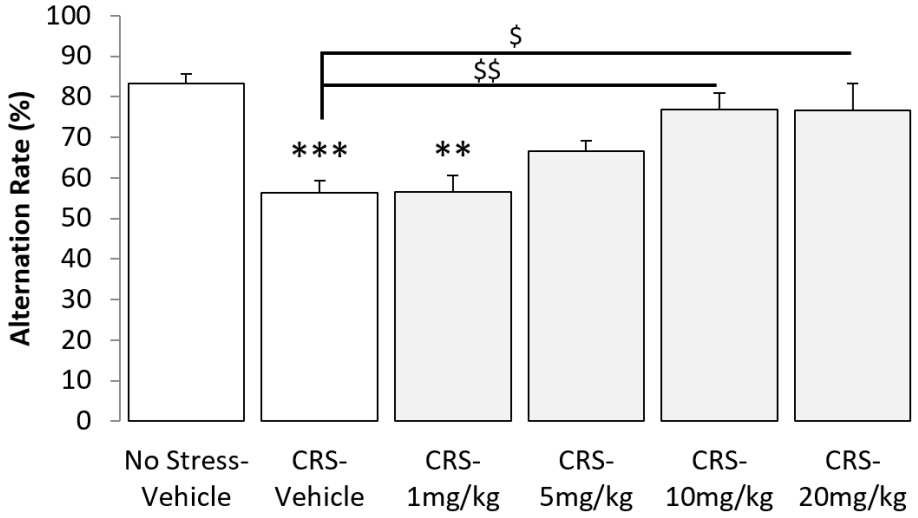

The chronic restraint stress (CRS) paradigm was used to induce a working memory deficit in young (2-3 months) animals. The animals were injected with GL-II-73 (0, 1, 5, 10 or 20 mg/kg) i.p. 30 min before testing. ANOVA revealed statistical significance on the overall effect of the treatment. Differences between groups were detected using post-hoc Scheffe analysis (**p<0.01 and ***p<0.001 compared to the "Control-Vehicle" group / $p<0.05 and $$$p<0.001 compared to the "CRS-Vehicle" group).

	Control Veh	CRS-Veh	CRS-1 mg/kg	CRS-5 mg/kg	CRS-10 mg/kg	CRS-20 mg/kg
Number of Animals	28	30	5	17	15	5

Figure 77: The Effects of GL-II-73 on Working Memory at 50mg/kg with Drs.Thomas Prevot and Etienne Sibille

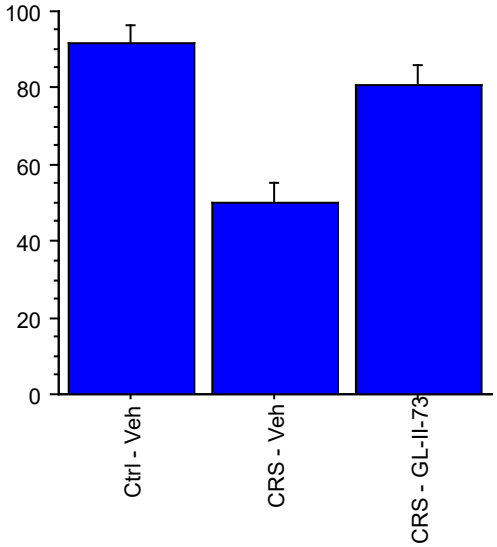

The alternation rate after GL-II-73 ip administration at 50mg/kg (N=4/5/6) was improved as compared to the vehicle. The chronic restraint stress (CRS) paradigm was used to induce a working memory deficit in young (2-3 months) animals. The animals were injected with GL-II-73 (50 mg/kg) i.p. 30 min before testing. ANOVA revealed statistical significance on the overall effect of the treatment. Differences between groups were detected using post-hoc Scheffe analysis $p<0.01$).

Figure 78: The Effect of the Racemic Mixture of GL-II-73 and GL-I-54 on Working Memory with Drs. Thomas Prevot and Etienne Sibille

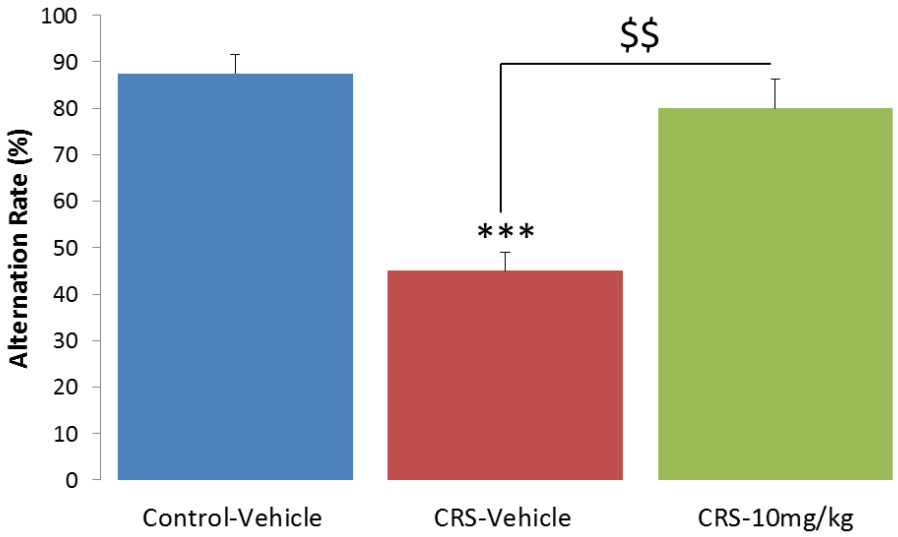

The effect of racemic mixture (GL-II-73/GL-I-54) on percent alternation rate in the Y-maze spatial alternation task assessing working memory in mice. Mice subjected to CRS were injected with the racemic mixture solution (10 mg/kg, ip., 5 mg/kg each enantiomer, 30 min before testing) or vehicle. ANOVA revealed statistical significance on the overall effect of manipulation. CRS animals showed a significant reduction in working memory and CRS mouse group injected with the racemic mix were statistically different from the CRS-vehicle group. Differences between groups were tested using the post-hoc analysis of Scheffe (***$p<0.001$ compared to the "Control-Vehicle" group / $$$p<0.01$ compared to the "CRS-Vehicle" group).

	Control Veh	CRS-Veh	CRS-10 mg/kg
Number of Animals	4	4	5

Figure 79: The Effect of GL-II-73 on Working Memory in Old Mice with Drs. Thomas Prevot and Etienne Sibille

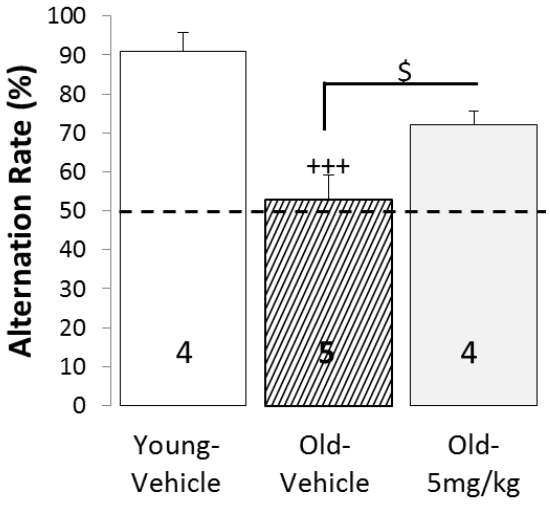

The effect of GL-II-73 on percent alternation rate in the Y-maze spatial alternation task assessing working memory in old mice. The 18 month-old mice studied were injected with GL-II-73 (5 mg/kg, i.p) or vehicle 30 min before testing. ANOVA revealed statistical significance on the overall effect of age and significant reversal of age-induced impairment in working memory in animals administered with GL-II-73 at 5 mg/kg. Differences between groups were tested using the post-hoc analysis of Scheffe (***$p<0.001$ compared to the "Young-Vehicle" group and $\$p<0.05$ compared to the "Old-Vehicle" group

A Summary of the Data is Described Below.

The effect on CRS-mice: Analysis of the data showed a significant difference between groups (ANOVA: $F(5,94)=17.5$; $p<0.0001$). Scheffe post hoc analysis showed that CRS induced significant reduction of working memory in this test ***$p<0.001$ when compared to control-vehicle group. This effect was reversed by administration of GL-II-73 (30 min before the test). Analysis of the results demonstrate that GL-II-73 has a procognitive effect at 10 mg/kg ($p=0.0002$) and 20 mg/kg ($p=0.049$) as compared to the CRS-Vehicle group.

The effect of racemic mixture on CRS-mice: Analysis of the data demonstrated significant differences between groups (ANOVA: $F(2,10)=16.82$; $p=0.0006$). Scheffe post hoc analysis

revealed a significant decreased performance in CRS-veh animals (p=0.001). The administration of the racemic mix (GL-II-73/GL-I-54) induced a reversal of the cognitive impairment induce by CRS (Scheffe post hoc analysis; p=0.003).

The effect on aged mice: Analysis of the data showed a significant difference between groups (ANOVA: F(2,12)=13.79; p=0.0008). Scheffe post hoc analysis revealed that administration of GL-II-73 has a significant pro-cognitive effect in aged animals at 5 mg/kg (p=0.04, as compared to the Young-Vehicle group).

Although it is not possible to tell with the data at hand, the rapid metabolism of the (S) isomer, GL-I-54, as compared to the longer lived (R) isomer, GL-II-73, in mice, it is entirely possible the major effect of the racemic mixture is from the activity in mice of the (R) isomer (GL-II-73). However, this does not explain the precognitive effect of the enantiomer GL-I-54. The time course of the precognitive effect might help in this vein.

3.2.3.8. Antidepressant Predictability (Forced Swim Test – FST)

Young male mice were tested in the forced swim test (FST), assessing for antidepressant efficacy. The mice (Jackson Laboratories) were sub-chronically injected via i.p. with vehicle or 1, 5 or 10 mg/kg of test compounds 24h, 20h and 1h before testing, as per standard methods in the field for testing potential antidepressant compounds.[270] Following standard protocol for DZP, animals were injected only once at the dose of 1.5mg/kg, 1h prior to testing. The protocol used was initially described by Porsolt et al.(1977)[270, 271], where mice were placed in an inescapable transparent tank filled with water (25cm, 26±1ºC). Animals were recorded for a period of 6min and a manual count of the immobile time in the tank was measured. Immobility is defined as the minimum amount of movement to stay afloat, between the second and the sixth minute of testing. The compounds that reduced immobility in the FST are considered to have potential antidepressant actions.

Figure 80: The Effect of GL-II-73 on Time Spent Immobile in the Forced Swim Test (FST)

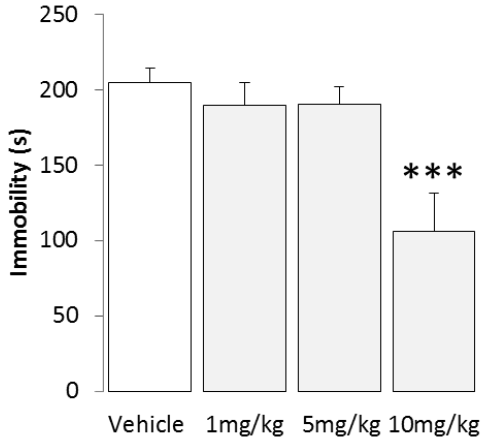

Dose response for GL-II-73 at 0, 1, 5 or 10 mg/kg administered i.p. (1 h before testing). ANOVA and post hoc analysis revealed a significant antidepressant-like efficacy at 10 mg/kg as compared to the vehicle group. *p<0.05 when compared to vehicle group.

	Vehicle	GL-II-73 1 mg/kg	GL-II-73 5 mg/kg	GL-II-73 10 mg/kg
Number of Animals	16	8	6	15

The Summary of the Data in the FST.

Examination of the data indicated a trend towards the difference between groups (ANOVA $F(3,34)=8.189;p=0.0614$). Furthermore, post hoc analysis indicated that GL-II-73 at 10 mg/kg significantly decreased the immobility as compared to vehicle group $*p<0.05$. Consequently, GL-II-73 is antidepressant in this assay.

3.2.3.9. Anxiolytic Predictability (Elevated Plus Maze – EPM)

The elevated plus maze (EPM) is designed to assess anxiety-like behaviors in rodents. The maze is made of four white Plexiglas arms, two open arms (29x7 cm), and two enclosed arms (29x7x17 cm) that formed a cross shape with the two open arms opposite to each other. The maze is 90 cm above the floor and illuminated at 100 lux. Young male and female (50%) mice (Jackson Laboratories) were injected i.p. with vehicle, 5 or 10mg/kg dose of test compound or 1.5mg/kg of DZP, 30 minutes prior to testing. They were placed individually on the central platform, facing an open arm, and allowed to explore the apparatus for 10 minutes. The behavior was recorded with a digital camera and analyzed using the ANY-maze Video Tracking System software (Stoelting Co, Wood Dale, IL, USA). The time in the open arms was used to calculate the percentage of time in the open arms presented in the results section using the following formula: $Percentage\ Time\ in\ open\ arm = \frac{Time\ in\ the\ open\ arm}{Total\ Time}\ x\ 100$.

Figure 81: The Effect of GL-II-73 on the Time Spent in the Open Arms of the Elevated Plus Maze

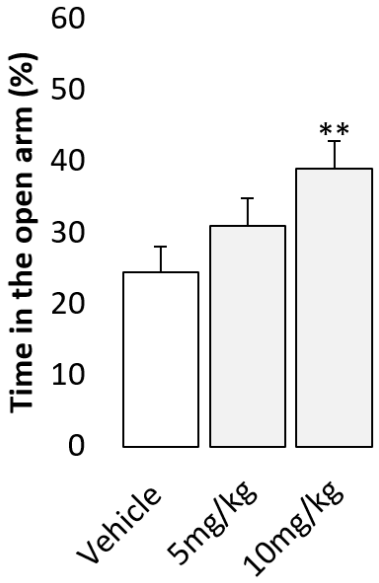

The dose response for GL-II-73 at 0, 5 or 10 mg/kg administered i.p. 30min before testing. ANOVA and post hoc analysis revealed a significant anxiolytic-like efficacy at 10 mg/kg as compared to the vehicle group. *p<0.05 when compared to vehicle group.

	Vehicle	GL-II-73 5 mg/kg	GL-II-73 10 mg/kg
Number of Animals	13	13	14

Summary of the Data

Data showed a trend between groups (ANOVA F(2,37)= 3.7 p=0.03). Furthermore, post hoc analysis identified that GL-II-73 at 10 mg/kg significantly increased the time spent in the open arms as compared to vehicle group **p<0.01, consequently in this assay GL-II-73 was anxiolytic.

Figure 82: Time Spent in the Shelter, Overnight, Before, During and after a Light Challenge

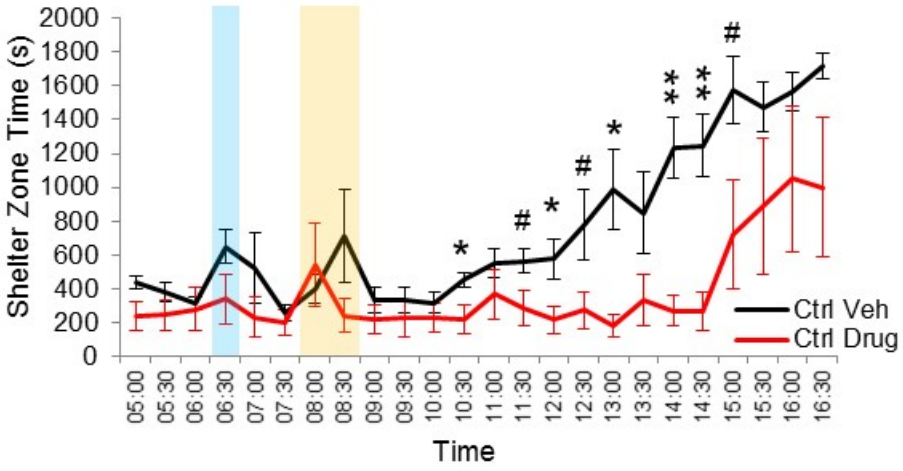

PhenoTyper Study: The anxiolytic properties of GL-II-73 were also assessed in a newly designed test. The test consists in placing the animals in the Phenotyper boxes (Noldus) set-up with normal bedding, water bottle, food tank and a shelter overnight. A camera placed in the ceiling of the box records the animal's movements which is analyzed using a video tracking software (Ethovision). After habitation to the apparatus and baseline behavior monitoring, a white spotlight can be applied over the food tank to induce anxiety (spotlight challenge). The animal's reaction to the challenge during (1hr) and after the application of the challenge is subsequently analyzed. The time spent in the shelter is used as a proxy of the anxiety-like phenotype of the animals. All animals were injected with either vehicle or GL-II-73 1.5h (blue) before the challenge (yellow).

Anxiolytic properties of GL-II-73 after acute injection at 10mg/kg: The time spent in the shelter over the night was recorded in non-stressed animals receiving either vehicle or GL-II-73. Data showed that both animal groups spent more time in the shelter during the spotlight challenge; however, the vehicle injected animals remained in the shelter zone over a longer period of time, while the GL-II-73 injected animals spent significantly less time hiding in the shelter.

The Summary of the Data

Examination of the data showed a promising anxiolytic property of GL-II-73. The confirmation of the anxiolytic properties of the compound are currently ongoing.

3.2.3.10. Cognition / Chronic Administration Studies (Young Mice) with Drs. Thomas Prevot and Etienne Sibille

The following sections are results of the data from studies of GL-II-73 on cognition, anxiety and depression.

Figure 83: The Effect of Chronic Administration of GL-II-73 on Working Memory

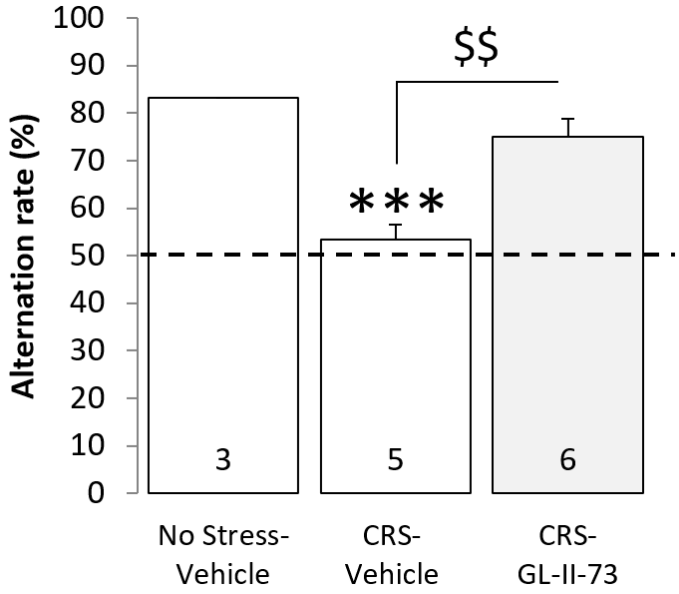

Male C57 mice were tested in the Y-Maze assessing working memory, as described in (G). The chronic restraint stress (CRS) paradigm was used to induce a working memory deficit in young (2-3 months) animals. The animals received GL-II-73 (30 mg/kg) in the drinking water for 10 days. Differences between groups were detected using post-hoc Scheffe analysis (*$p<0.05$ compared to the "Control-Vehicle" group / \$$p<0.05$ as compared to the "CRS-Vehicle" group). (n: "Ctrl-Veh"=3; CRS-Veh"=5; CRS+GL-II-73"=6).

3.2.3.11. Cognition –Anxiety / Chronic Studies in Old Animals.

Table 21: Brain and Plasma Concentrations After Chronic Administration of GL-II-73

	Brain		Plasma	
GL-II-73	**nmol/kg**	**ng/g**	**nM**	**ng/ml**
Young	87,5 ± 18	33,8 ± 7	1091,8 ± 444	421,9 ± 171
Old	36,06 ± 13,2	13,9 ± 5,1	505,75 ± 169	195,43 ± 65

The concentrations in the brain and in plasma after chronic administration were assessed after the 10 days of exposure. GL-II-73 was diluted in the drinking water at 30mg/kg and given to animals for 10 days.

Figure 84: Distance Travelled after Chronic Administration of GL-II-73 in Old Mice.

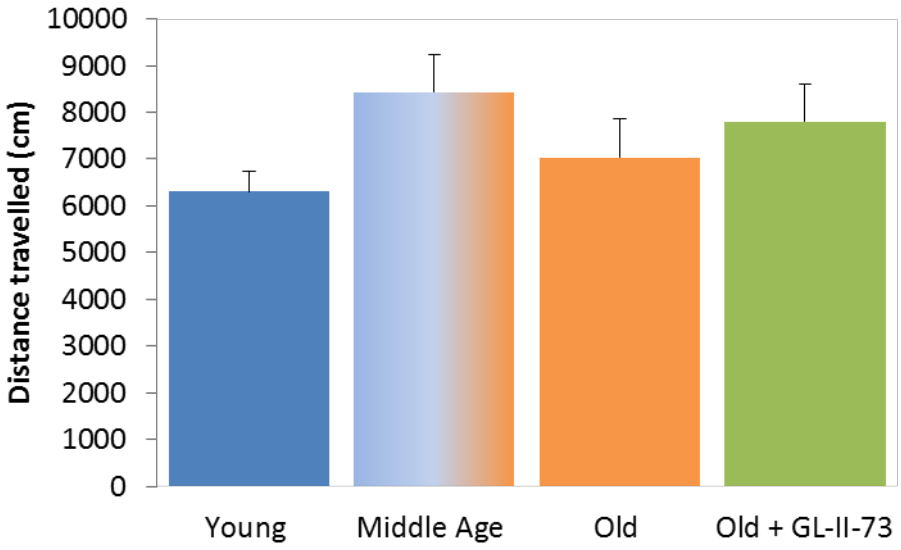

The chronic administration in the drinking water (OLD): Locomotor Activity. Male C57 mice (Charles River) were tested in the open field for locomotor activity for 1hr. The number of animals per treatment group was 10 young, 10 middle age, 9 old and 6 old treated. The effect of GL-II-73 administered at 30 mg/kg in the drinking water, on spontaneous locomotor activity during 60 min of recording in ageing mice. All data are presented as the mean distance travelled (cm) ± S.E.M.

Figure 85: Potential Anxiolytic Effect of GL-II-73 in Old Mice, When Given Chronically

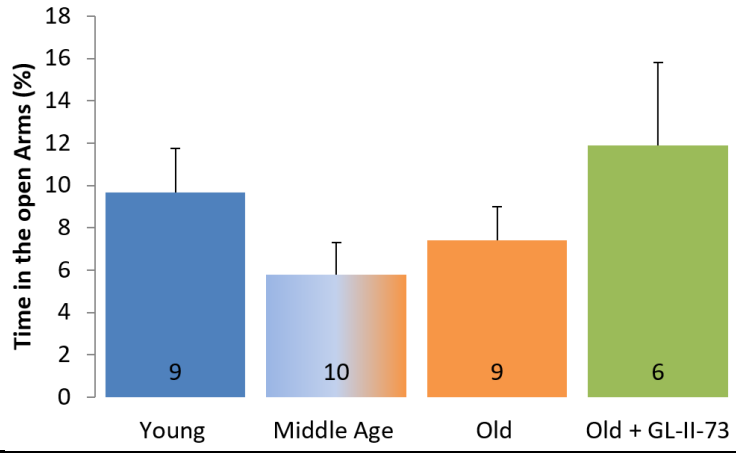

The chronic administration in the drinking water (OLD): Anxiolytic effects (EPM)
The male C57 mice were tested in the EPM as described before. Potential anxiolytic properties of GL-II-73, chronically administered at 30mg/kg (drinking Water). The anxiolytic properties of the compound were assessed in the elevated plus maze. The time spent in the open and closed arms were quantified and the percentage of time spent in the open arms was calculated. The results are expressed as a percentage.

Figure 86: Time Spent in the Shelter Before, During and After a Light Challenge

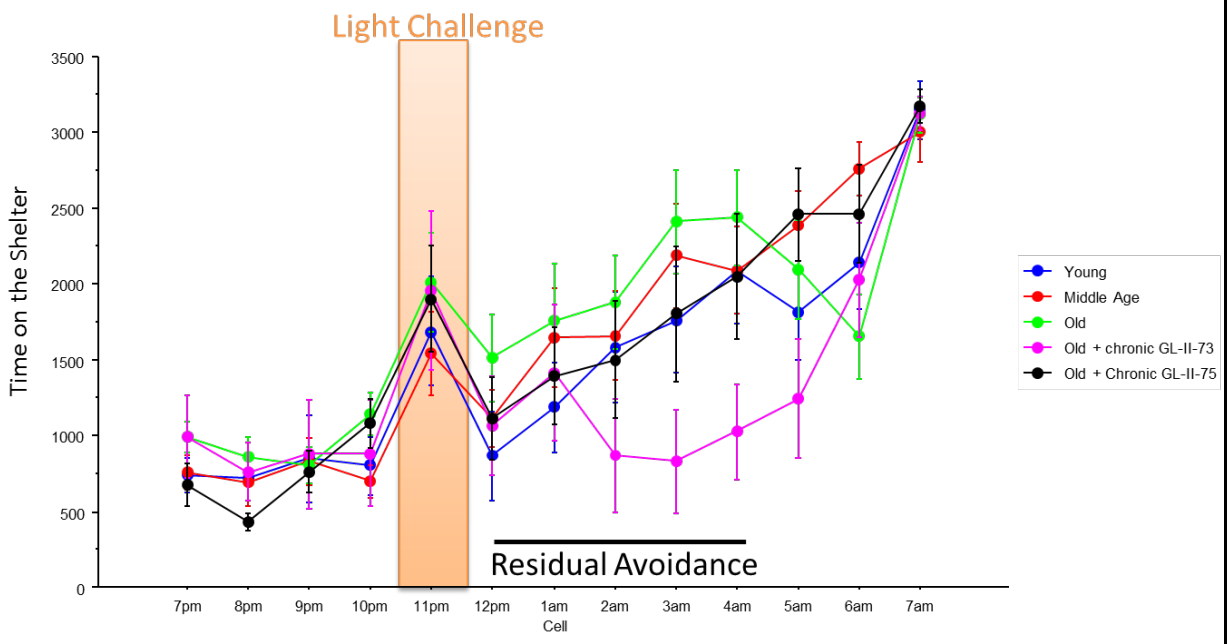

The chronic administration in the drinking water (OLD): Anxiolytic effects (Phenotyper Test) The phenotyper test has been developed by Prevot et al. (2019)[254] and assess conflict anxiety-like behavior in male C57 mice. The phenotyper is a home-cage like setting that allows the characterization of anxiety-like behavior of animals in response to a light challenge. Animals are placed in a box, with a top equipped with an IR camera and a light bulb in the corner of the food dispenser. At the opposite corner, an opaque shelter is placed to let the animal hide inside. The time spent in the shelter is analyzed as an index of residual anxiety after a light challenge occurring from 11pm to 12am. The number of animals per treatment group was 10 young, 10 middle age, 9 old and 6 old treated.

The Summary of the Data

The mice treated chronically with GL-II-73 exit the shelter after the light challenge and spend more time outside of the shelter, as compared to old mice, or even compared to young mice. The mice staying longer in the shelter exhibit a *residual avoidance* of the light, and hide longer. Here GL-II-73 reduces residual avoidance in old mice.

Figure 87: Residual Avoidance

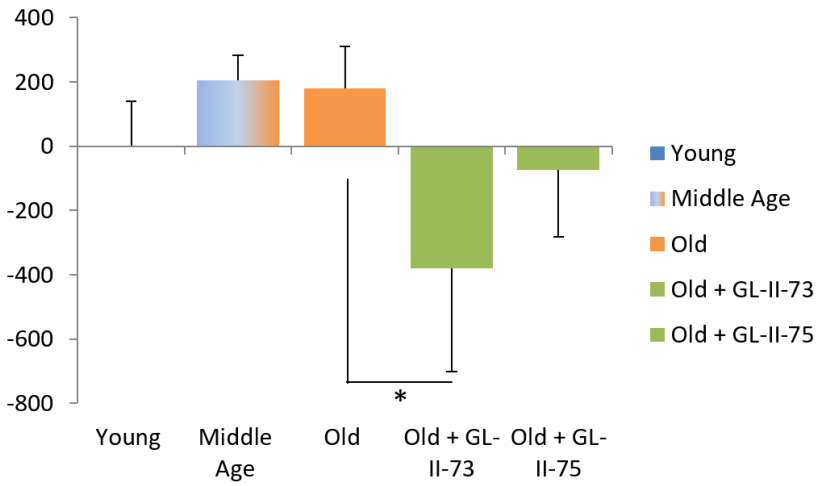

Residual avoidance can be calculated, using the raw data from the **Figure 86**. The formulae used to calculate the residual avoidance for each animal is: RA= [(Time in the shelter during the challenge – Average time after)$_{young}$ – (Time in the shelter during - Average time after)]/ [(Time in the shelter during the challenge – Average time after)$_{young}$ X 100. Although not significant, ageing slightly increases the residual avoidance. This residual avoidance is significantly reduced in animals receiving GL-II-73 in the drinking water, suggesting an anxiolytic effect of the compound administered chronically in old mice. Number of animals per treatment group was 10 young, 10 middle age, 9 old and 6 old treated.

Figure 88: The Effects of GLII-73 Administered Chronically, on Working Memory

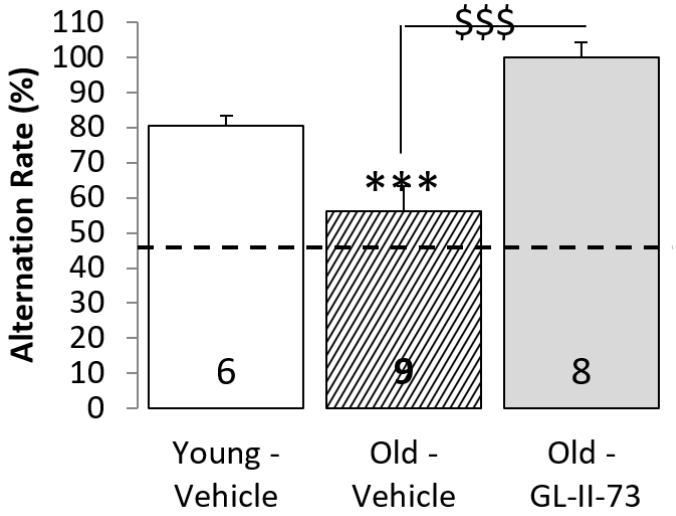

The chronic administration in the drinking water (OLD): Cognition;
The same Y-Maze assay was used to measure alternation rate in old mice for working memory. The 22-month-old mice studied were administered chronically with GL-II-73 (30 mg/kg, in the drinking water). The percent alternation rate in the Y-maze spatial alternation task was assessed as a proxy of working memory in old mice. ANOVA revealed statistical significance on the overall effect of age and significant reversal of age-induced impairment in working memory in animals administered with GL-II-73. Differences between groups were tested using the post-hoc analysis of Scheffe (*$p<0.05$ compared to the "Young-Vehicle" group and $\$\$\$p<0.001$ compared to the "Old-Vehicle" group.

The Summary of the Data:

The chronic administration of GL-II-73 at 30mg/kg in the drinking water had procognitive effects on the older animals.

Note: This experiment has been confirmed in another study.

3.2.3.12. Blockade Experiments Using the Bz Antagonist, Flumazenil

Figure 89: Flumazenil Blocks the Effects of GL-II-73 in the Y-Maze

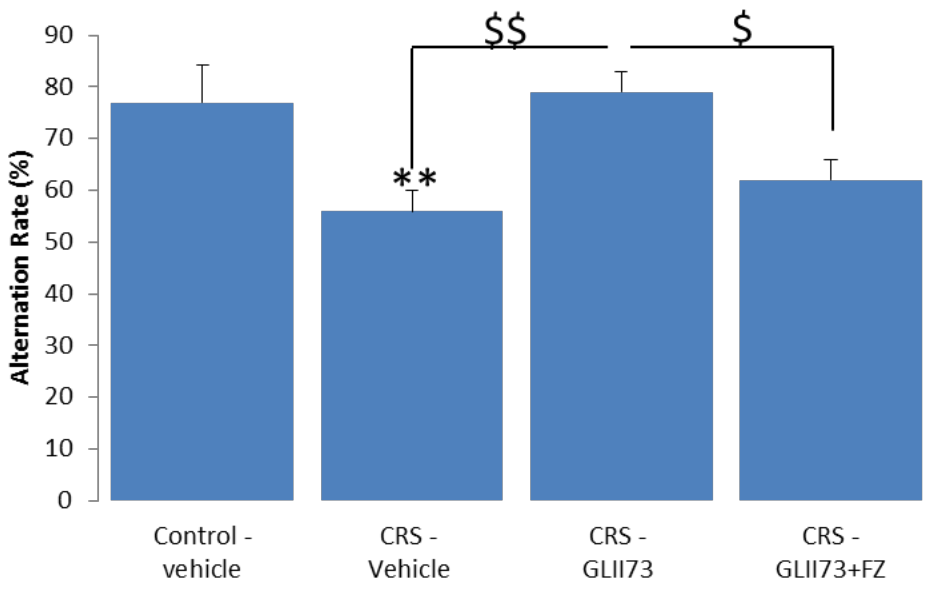

Blockade using Flumazenil

The mice were subjected to chronic restraint to induce a cognitive deficit in working memory. The chronic restraint stress (CRS) paradigm was used to induce a working memory deficit in young (2-3 months) animals. The animals were injected with vehicle, GL-II-73 (10mg/kg) or a combination of GL-II-73 (10mg/kg) and flumazenil (10mg/kg) i.p. 30 min before testing. Flumazenil blocks the effects of GL-II-73 on percent alternation rate in the Y-maze spatial alternation task assessing working memory in mice. ANOVA revealed statistical significance on the overall effect of the treatment. The differences between groups were detected using post-hoc Scheffe analysis (**p<0.01 and ***p<0.001 as compared to the "Control-Vehicle" group / $p<0.05 and $$p<0.01 as compared to the "CRS-Vehicle" group).

	Control Veh	CRS-Veh	CRS-GL-II-73	CRS-GLII73+FZ
Number of Animals	6	5	4	4

Figure 90: βCCt Blocks the Effects of GL-II-73 in the Y-Maze

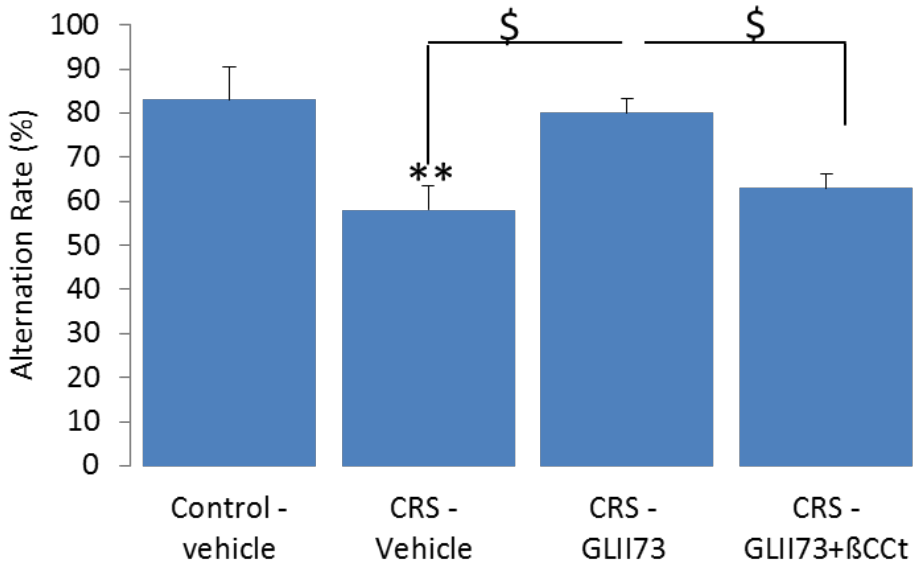

Blockade using βCCt – α1GABAARs antagonist

The chronic restraint stress (CRS) paradigm was used to induce a working memory deficit in young (2-3 months) animals. The animals were injected with vehicle, GL-II-73 (10mg/kg) or a combination of GL-II-73 (10mg/kg) and βCCt (10mg/kg) i.p. 30 min before testing. ANOVA revealed statistical significance on the overall effect of the treatment. βCCt blocks the effects of GL-II-73 on percent alternation rate in the Y-maze spatial alternation task assessing working memory in mice. The differences between groups were detected using post-hoc Scheffe analysis (**p<0.01 and ***p<0.001 as compared to the "Control-Vehicle" group / $p<0.05 and $$p<0.01 as compared to the "CRS-Vehicle" group).

	Control Veh	CRS-Veh	CRS-GL-II-73	CRS-GLII73+FZ
Number of Animals	6	6	5	5

Figure 91: XLI-093 Blocks the Effects of GL-II-73 in the Y-Maze

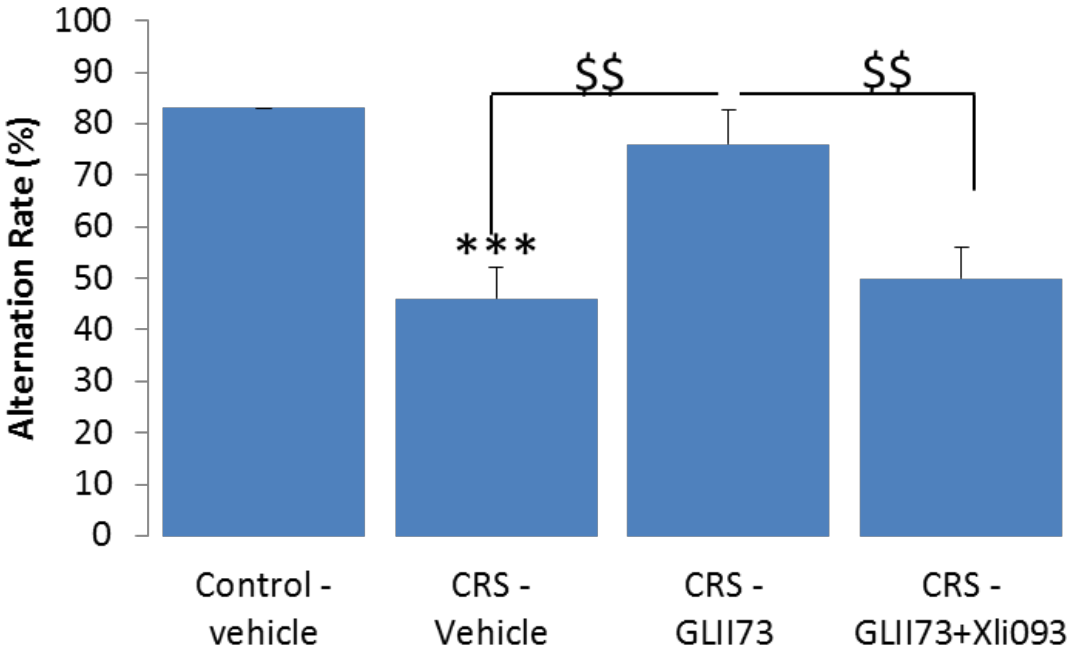

Blockade using Xli-093 – α5GABAARs antagonist

The chronic restraint stress (CRS) paradigm was used to induce a working memory deficit in young (2-3 months) animals. The animals were injected with vehicle, GL-II-73 (10mg/kg) or a combination of GL-II-73 (10mg/kg) and βCCt (10mg/kg) i.p. 30 min before testing. ANOVA revealed statistical significance on the overall effect of the treatment. Xli-093 blocks the effects of GL-II-73 on percent alternation rate in the Y-maze spatial alternation task assessing working memory in mice. The differences between groups were detected using post-hoc Scheffe analysis (**p<0.01 and ***p<0.001 as compared to the "Control-Vehicle" group / $p<0.05 and $$p<0.01 as compared to the "CRS-Vehicle" group).

	Control Veh	CRS-Veh	CRS-GL-II-73	CRS-GLII73+FZ
Number of Animals	5	5	5	6

Summary of Data:

The blockade of the benzodiazepine binding site of $GABA_A$ receptors prevents GL-II-73 from exerting its beneficial action on cognitive performances demonstrating, which demonstrates that

the efficacy of GL-II-73 was mediated by acting at the benzodiazepine site on the $GABA_A$ receptors. Blockade of the effects at the α1 or α5-$GABA_A$Rs had a similar effect, which was surprising, suggests that both receptor subtypes are required to exert an effect on cognitive functions in these assays.

3.2.3.13. The Acute and Chronic Treatment in Depression Models (Unpredictable Chronic Mild Stress)

Figure 92: The Effect of GL-II-73 on Cognition in a UCMS Model

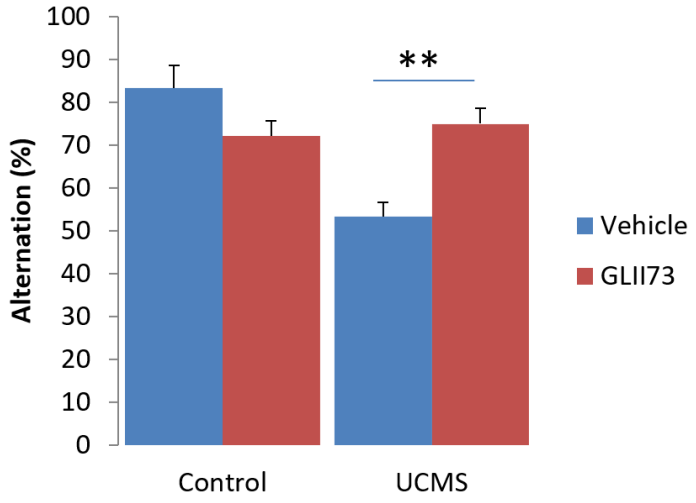

ACUTE STUDY-Cognition (Y maze):
(6 animals per group) The same Y-Maze assay was performed – see (G) for details.
Acute administration of GL-II-73 reversed UCMS induced cognitive deficits. The C57 mice (male and female) were subjected to UCMS for 6 weeks and tested in multiple assays. The UCMS consists in subjecting mice to two mild stressors per day, from a list of 10 stressors (tilt cage, wet bedding, no bedding, predator pee, restraint, bath etc.). In a first study, GL-II-73 was administered acutely (10mg/kg, IP) 30 minutes before each test.

Figure 93: The Effect of GL-II-73 on Anxiety-like Behavior in a UCMS Model

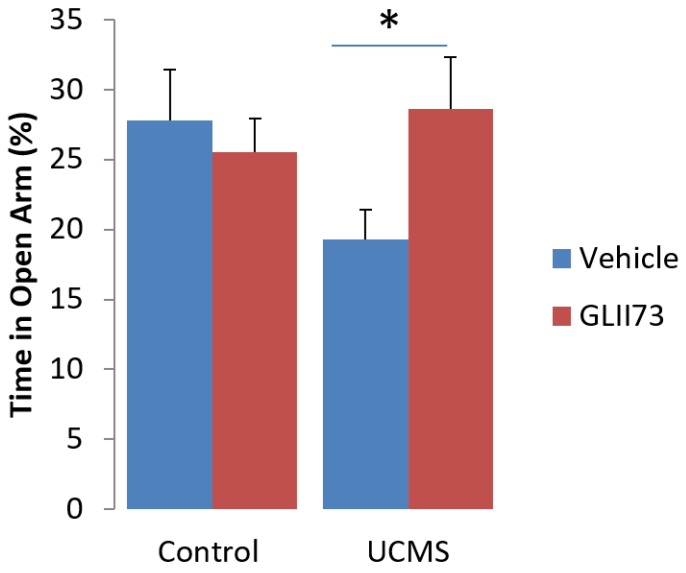

Anxiety (EPM): The acute administration of GL-II-73 reversed UCMS induced anxiety (12 animals per group).

Figure 94: The Effect of GL-II-73 on Immobility in the FST, in a UCMS Model

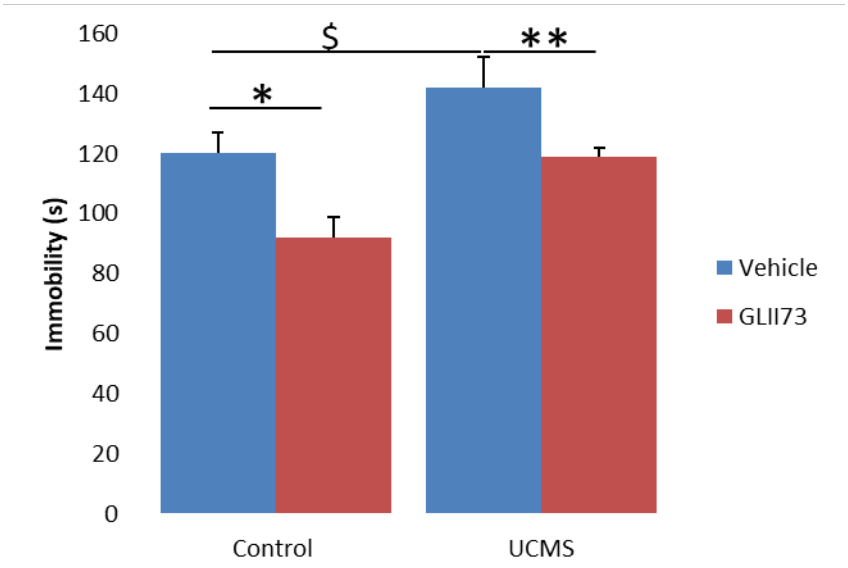

Depression/despair (forced swim test): The C57 Mice were tested in the FST, as previously described. The UCMS increased the time spent immobile, and acute administration of GL-II-73 decreased the time spent immobile, in control and UCMS conditions. The acute administration trended to reverse UCMS induced depressive-like behavior (12 animals per group).

Figure 95: The Effect of Chronic GL-II-73 on Alternation in the YMaze, After UCMS Exposure

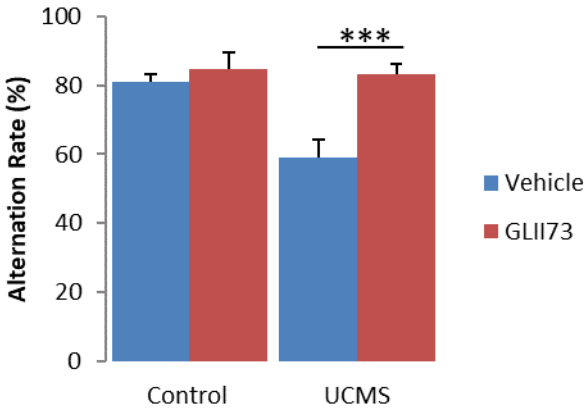

CHRONIC STUDY: In a second study, GL-II-73 was administered chronically, in the drinking water (30mg/kg) for 3 weeks. The same assays were used.
Cognition: Y-maze: the chronic treatment reversed UCMS induced cognitive deficits.

Figure 96: The Representative Images of CA1 Pyramidal Cells Between Groups (Control, UCMS, and UCMS+GL).

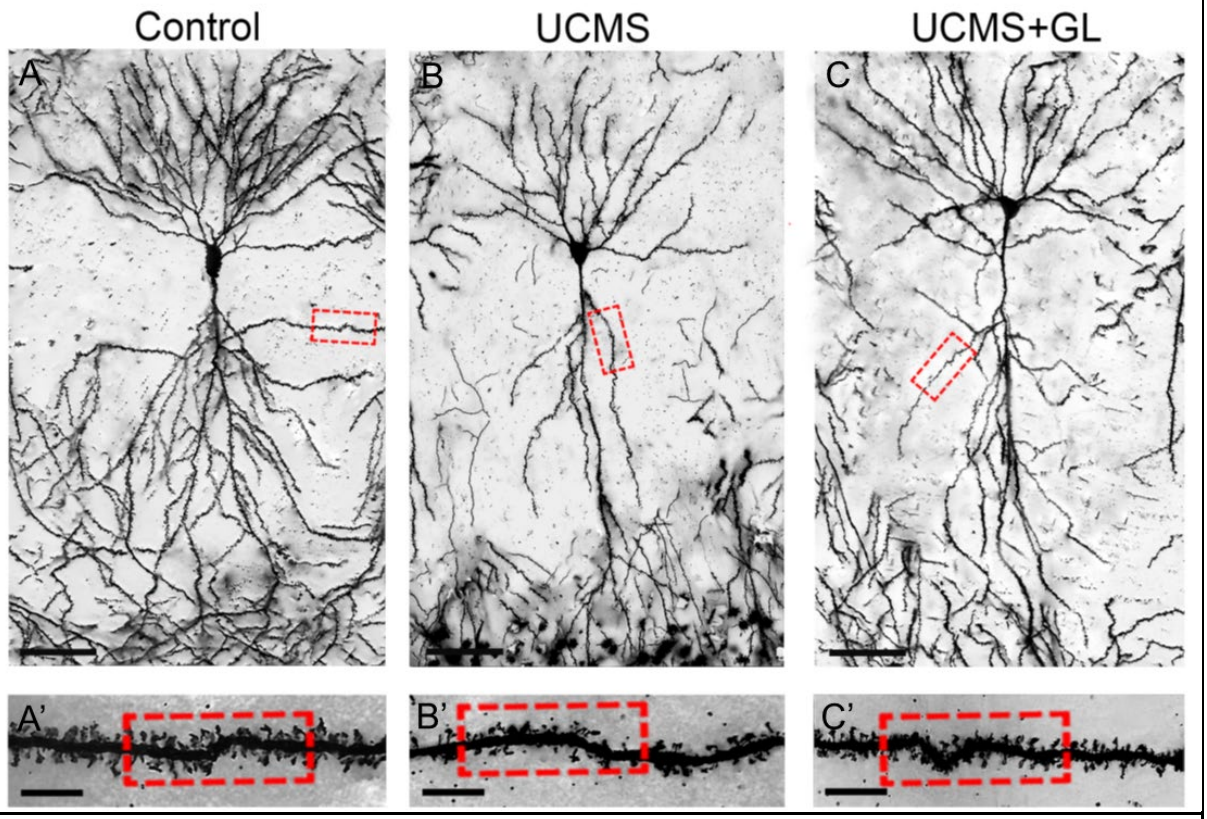

The effect of UCMS and chronic treatment with GL-II-73 on dendritic morphology in the CA1 and the PFC (Performed by NeuroDigiTech LLC).

The brains were harvested and soaked in Golgi staining solution (provided by the CRO) for 2 weeks. The brains were then rinsed and kept in 30% sucrose solution for shipment to the CRO. The brains were sectioned using a cryostat and coronal sections were mounted on slice. The slides included serial coronal sections that covered the anterior-to-posterior axis of the brain. The sampling of ROIs included the basal and apical dendrites of pyramidal cells in Layers II/III of PFC.

The sampling process was conducted as follows: The investigators first 1) previewed the entire rostro-caudal axis of ROIs, under low-mag Zeiss objectives (10x and 20x), 2), compared and located those with the least truncations of distal dendrites as possible under high-mag Zeiss objectives (40x and 63x), 3), and then 4) used a Zeiss 100x objective with immersion oil to perform 3D dendritic reconstruction and this was followed by counting of the spines throughout the entire dendritic trees. The criteria for selecting candidate neurons for analysis were based on i) visualization of a completely filled soma with no overlap of neighboring soma and completely filled dendrites, ii) the tapering of most distal dendrites; iii) the visualization of the complete 3-D profile of dendritic trees using the 3-D display of imaging software. The neurons with incomplete impregnation and/or neurons with truncations due to the plane of sectioning were not collected. Moreover, the cells with dendrites labeled retrogradely by impregnation in the surrounding neuropil were excluded (derived from Wu et al. (2004)[272]).

With the systematic registration and digital monitoring, the software was able to accurately record every step of the tracing/contouring and generate a 3D reconstructed dendritic morphology for subsequent spine counting. Automatic navigation of the digital probes with registered x-y-z coordinates of each 2D image stack was able to create a complete 3D digital profile for the dendrograms, spine density and Sholl analysis.

Figure 97: Comparison of Total Dendritic Lengths of Pyramidal Cells Between Groups.

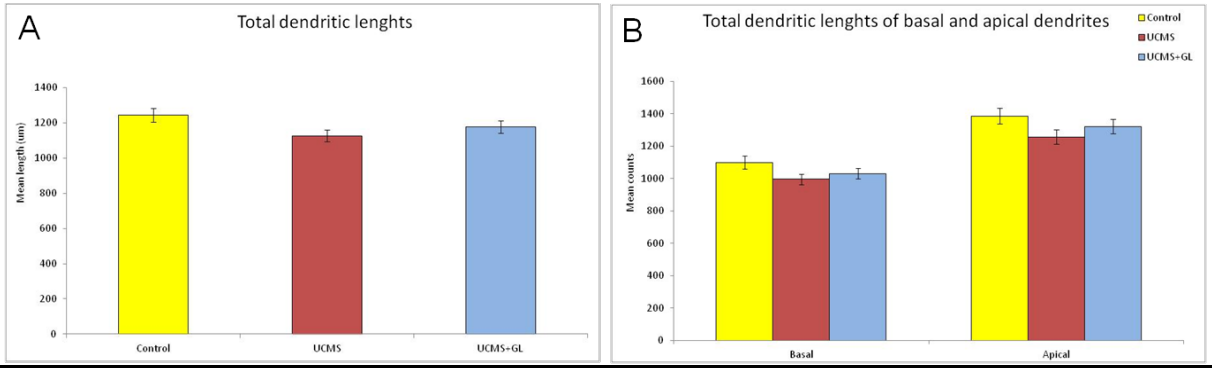

In total dendritic lengths (A), in comparison with control mice, there was no evidence of the significant reduction in total dendritic lengths of UCMS and UCMS+GL mice (A, $p>0.05$). In the break-down analysis, no difference was found in basal and apical dendrites between groups, respectively (B, $p>0.05$).

Figure 98: Comparison of Overall Spine Density of Pyramidal Cells Between Groups

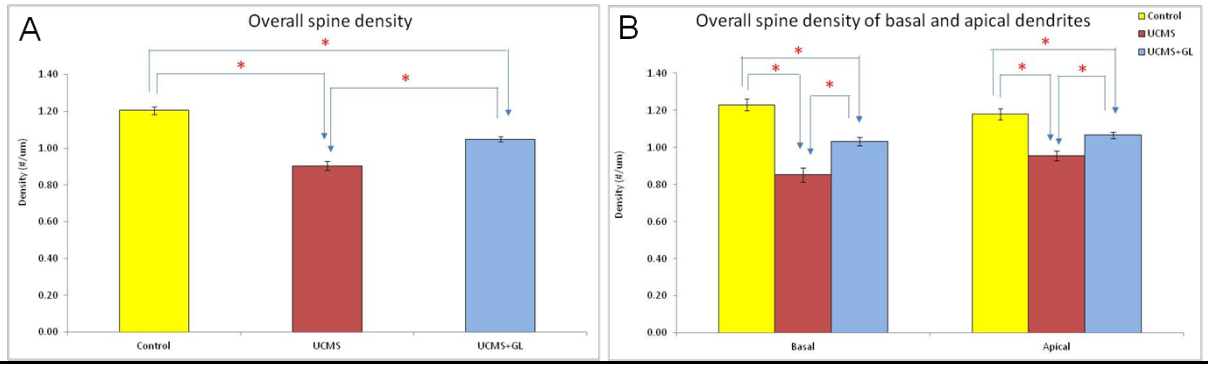

In the analysis of total spine counts, in comparison with with control mice, there was a significant reduction in total spine counts of UCMS mice as well as UCMS+GL mice, respectively ($p<0.05$). Also, UCMS+GL mice exhibited more spine counts than UCMS mice ($p<0.05$). In the break-down analysis, both control and UCMS+GL mice exhibited more spine counts of basal dendrites than UCMS mice, respectively (B-left, $p<0.05$). Also, control mice showed a higher level of spine counts than UCMS+GL mice ($p<0.05$). In the apical dendrite, control mice exhibited more spine counts than UCMS and UCMS+GL mice, respectively (B-right, $p<0.05$). Note that there was no difference in total spine counts of apical dendrites between UCMS and UCMS+GL mice ($p>0.05$).

Figure 99: Representative Images of PFC Pyramidal Cells Between Groups (Control, UCMS, and UCMS+GL).

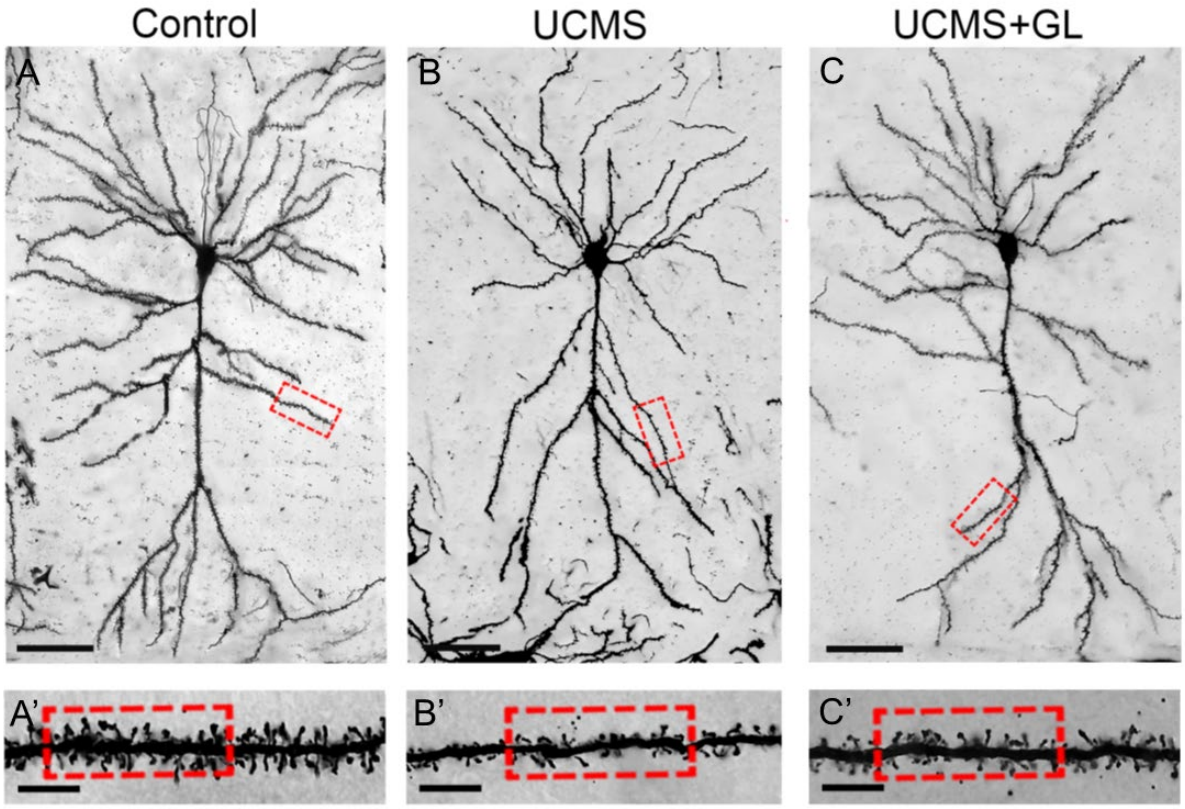

In the analysis of overall spine density, in comparison with control mice, both UCSM and UCSM+GL mice exhibited a reduction of the overall spine density, respectively (A, $p<0.05$). It was noted that UCMS+GL mice showed a higher level of overall spine density than UCMS mice ($p<0.05$). In the break-down analysis, UCMS mice showed a significant reduction in overall density of basal dendrites as compared to Control and UCMS+GL mice, respectively (B, $p<0.05$). It was also noted that UCMS+GL mice showed a lower level of overall spine density than control mice ($p<0.05$). Similarly, in the apical dendrites, UCMS mice exhibited a lower spine density than control and UCMS+GL mice, respectively (C, $p<0.05$). It is noted that UCMS+GL mice showed a lower spine density than control mice ($p<0.05$). This line of findings indicated that the GL treatment appeared to be effective in increasing both apical and basal dendrites of CA1 pyramidal cells of UCMS mice.

Figure 100: Comparison of Total Dendritic Lengths of Pyramidal Cells Between Groups.

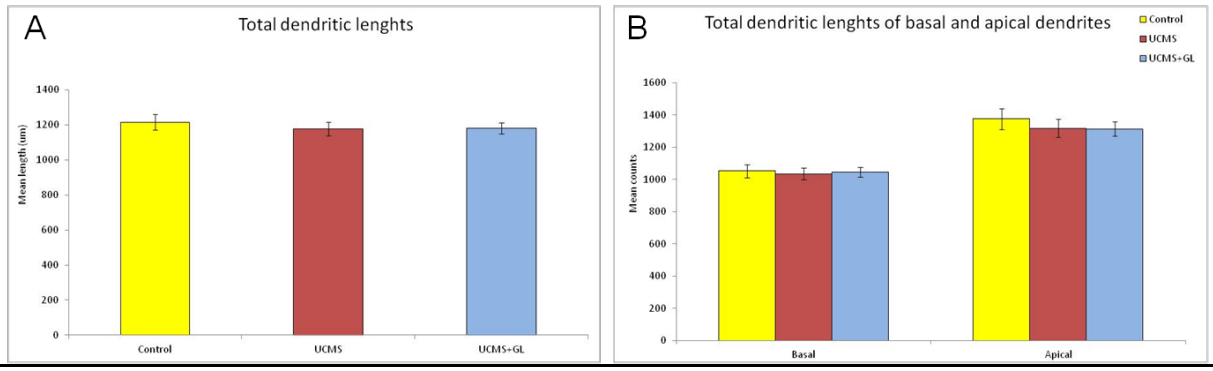

In total dendritic lengths (A), in comparison with control mice, there was no evidence of the significant reduction in total dendritic lengths of UCMS and UCMS+GL mice (A, $p>0.05$). In the break-down analysis, no difference was found in basal and apical dendrites between groups, respectively (B, $p>0.05$).

Figure 101: Comparison of Total Spine Counts of Pyramidal Cells Between Groups

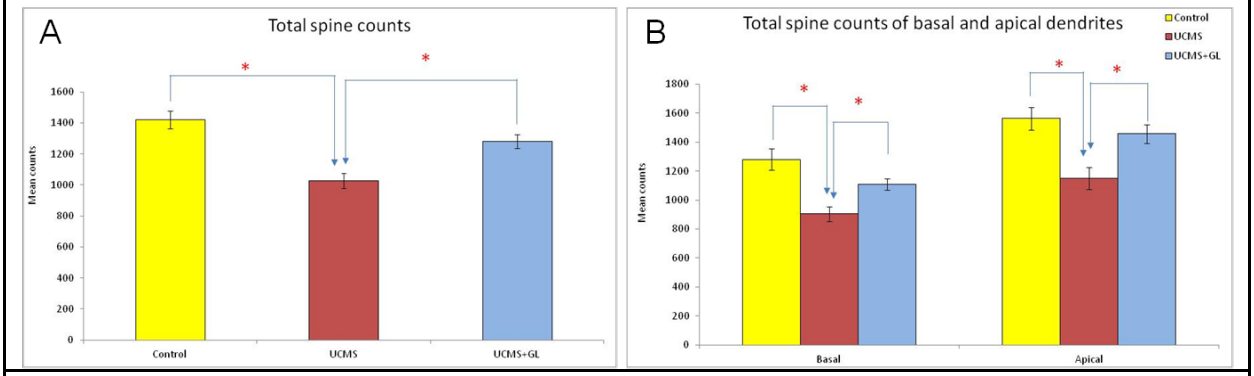

In the analysis of total spine counts, in comparison with control mice, there was a significant reduction in total spine counts of UCMS mice (A, $p<0.05$). Also, UCMS+GL mice exhibited more spine counts than UCMS mice ($p<0.05$). In the break-down analysis, both control and UCMS+GL mice exhibited more spine counts of basal dendrites than UCMS mice, respectively (B-left, $p<0.05$). Similarly, both control and UCMS+GL mice exhibited more spine counts of apical dendrites than UCMS mice, respectively (B-right, $p<0.05$). Note that there was no difference in total spine counts of both basal and apical dendrites between control and UCMS+GL mice, respectively ($p>0.05$).

Figure 102: Comparison of Overall Spine Density of Pyramidal Cells Between Groups.

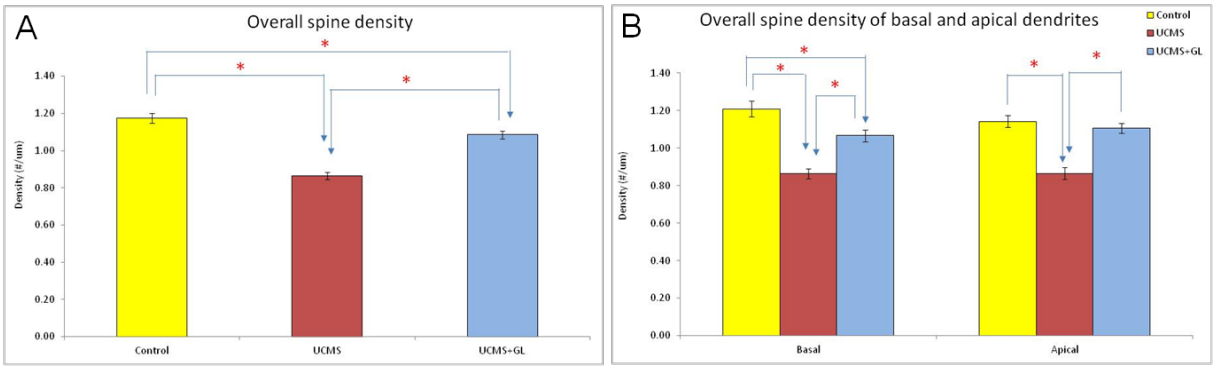

In the analysis of overall spine density, in comparison with control mice, UCSM and UCSM+GL mice exhibited a reduction of the overall spine density, respectively (A, $p<0.05$). It was noted that UCMS+GL mice showed a higher level of overall spine density than UCMS mice ($p<0.05$). In the break-down analysis, UCMS mice showed a significant reduction in overall density of basal dendrites as compared to control and UCMS+GL mice, respectively (B-left, $p<0.05$). It was also noted that UCMS+GL mice showed a lower level of overall spine density than Control mice ($p<0.05$). Moreover, in the apical dendrites, UCMS mice exhibited a lower spine density than control and UCMS+GL mice, respectively (B-right, $p<0.05$). It is noted that there was no difference in overall spine density in the apical dendrite between control and UCMS+GL mice ($p>0.05$). This line of findings indicated that the GL treatment appeared to be more effective in apical than basal dendrites of PFC pyramidal cells of UCMS mice.

3.2.3.14. The Effect of Chronic Administration in Old Mice: Behavior and Dendritic Morphology

Behavior

Figure 103: The Chronic Administration of GL-II-73 in the Drinking Water Reverses Age-related Cognitive Deficits

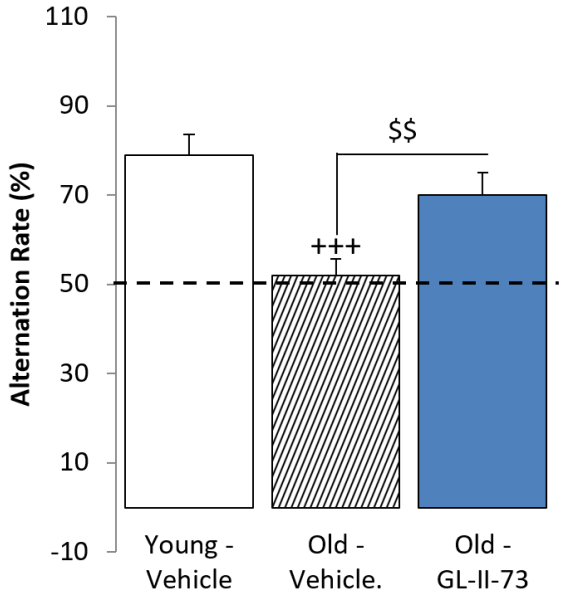

Behavior

Old (22months old) and young (2months) C57BL/6 male mice (Charles River) were used in this study. A subset of old mice received the compound GL-II-73 for 8 weeks in the drinking water at the concentration of 30mg/kg. Prior to administration of the compound to the animals, the average volume consumed was measured to obtain the daily consumption of 8mL per day. Based on this assessment, the compound was prepared in drinking water and provided fresh to the animals every other day. The group details are as follow: Young (N=9); Old (N=13) and Old+Treatment (N=6). Mice were tested in the Spontaneous Alternation Task as described in Prevot et al. (2019). ANOVA performed on the alternation rate revealed a significant difference between groups ($F(2;25)=11.34$; $p<0.001$). *Post hoc* analysis revealed a significant decrease in alternation rate induced by normal aging ($p<0.001$) and a significant effect of the compound at reversing the age-induced reduced alternation ($p<0.01$).

Analysis of Dendrite Morphology

Morphological analysis of pyramidal cells in Layer I/II of the PFC (Performed by NeuroDigiTech LLC)

The brains were harvested and soaked in Golgi staining solution (provided by the CRO) for 2 weeks. The brains were then rinsed and kept in 30% sucrose solution for shipment to the CRO. The brains were sectioned using a cryostat and coronal sections were mounted on slice. The slides included serial coronal sections that covered the anterior-to-posterior axis of the brain. The sampling of ROIs included the basal and apical dendrites of pyramidal cells in Layers II/III of the PFC.

The sampling process was conducted as follows: The investigators first 1) previewed the entire rostro-caudal axis of ROIs, under low-mag Zeiss objectives (10x and 20x), 2), compared and located those with the least truncations of distal dendrites as possible under high-mag Zeiss objectives (40x and 63x), 3), and then 4) used a Zeiss 100x objective with immersion oil to perform 3D dendritic reconstruction and this was followed by counting of the spines throughout the entire dendritic trees. The criteria for selecting candidate neurons for analysis were based on i) visualization of a completely filled soma with no overlap of neighboring soma and completely filled dendrites, ii) the tapering of most distal dendrites; iii) the visualization of the complete 3-D profile of dendritic trees using the 3-D display of imaging software. The neurons with incomplete impregnation and/or neurons with truncations due to the plane of sectioning were not collected. Moreover, cells with dendrites labeled retrogradely by impregnation in the surrounding neuropil were excluded (derived from Wu et al. (2004)[272]).

With the systematic registration and digital monitoring, the software was able to accurately record every step of the tracing/contouring and generate a 3D reconstructed dendritic morphology for subsequent spine counting. Automatic navigation of the digital probes with registered x-y-z coordinates of each 2D image stack was able to create a complete 3D digital profile for the dendrograms, spine density and Sholl analysis.

Illustrated in **Figure 104** are the representative images of a dendritic segment of pyramidal cells of three groups, respectively. In the following qualitative observations, Young mice exhibited more arborizations of the dendritic morphology than Old and Old+Treatment mices (see upper panel of **Figure 104**A-C). Moreover, Young mice showed higher spine counts than Old and Old+Treatment mice (Lower panel of **Figure 104**A-C). Note Old+Treatment mice appeared to have more spine counts than Old mice [(the box). See quantitative comparisons of spine counts between groups below].

Figure 104: Representative Images of PFC Pyramidal Cells Between Groups

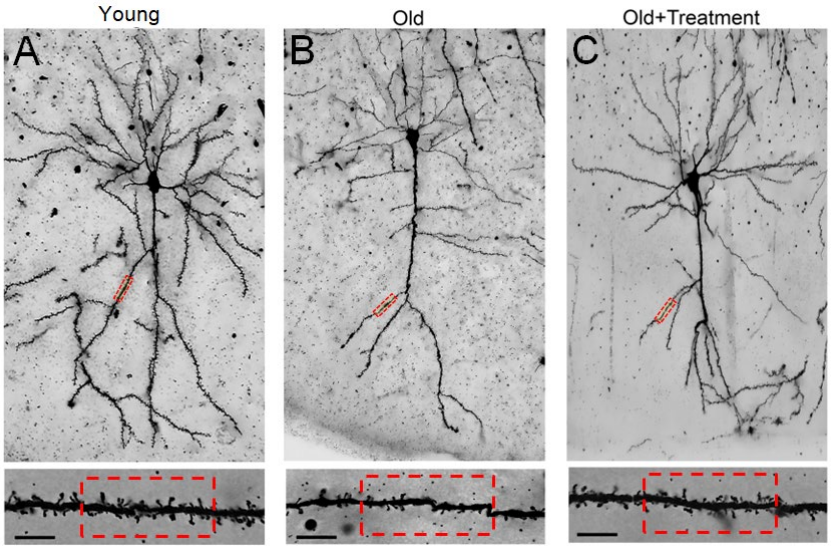

Compare tod Young mice (A), all aged mice showed reductions in spine counts of pyramidal cells (the box in lower panels of A-C). It was noted that Old+Treatment mice showed a higher spine count than Old mice [Scale bars: 5 µm]. Note: The quantitation of spine subtypes was not included in the current study.

Figure 105: Comparison of Total Dendritic Lengths of Pyramidal Cells Between Groups.

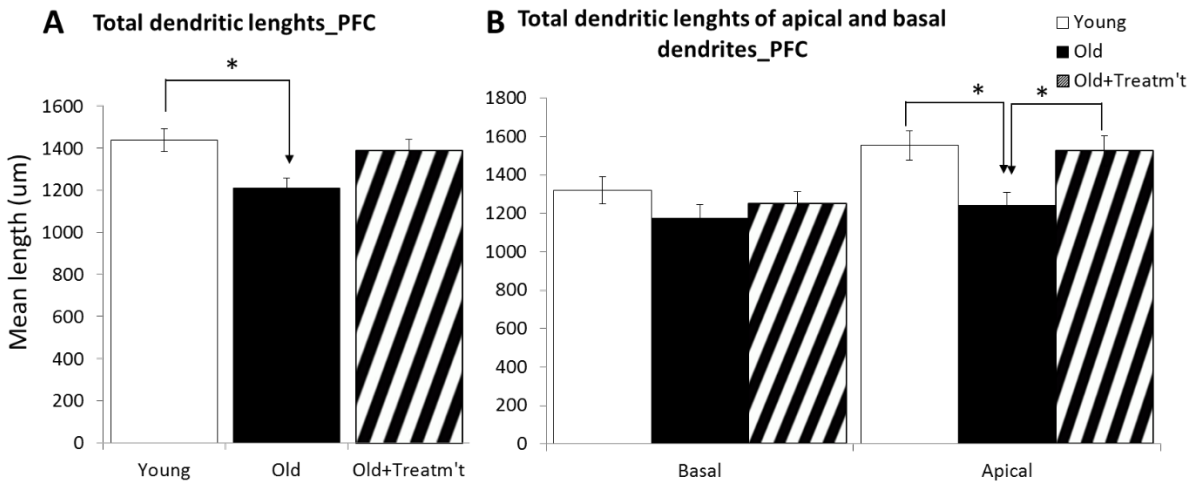

In total dendritic lengths (**Figure 105**), in comparison with Young mice, there was a significant reduction in total dendritic lengths of Old mice (**Figure 105**A, $p<0.05$), while no difference was found in Old+Treatment mice ($p>0.05$). In the break-down analysis, no difference was found in the basal dendrites between groups (**Figure 105**B, $p>0.05$). In the apical dendrites, both Young and Old+Treatment mice exhibited higher total dendritic lengths of apical dendrites than Old mice, respectively ($p<0.05$). Note that there was no difference between Young and Old+Treatment mice ($p>0.05$).

Figure 106: Comparison of Total Spine Counts of Pyramidal Cells Between Groups.

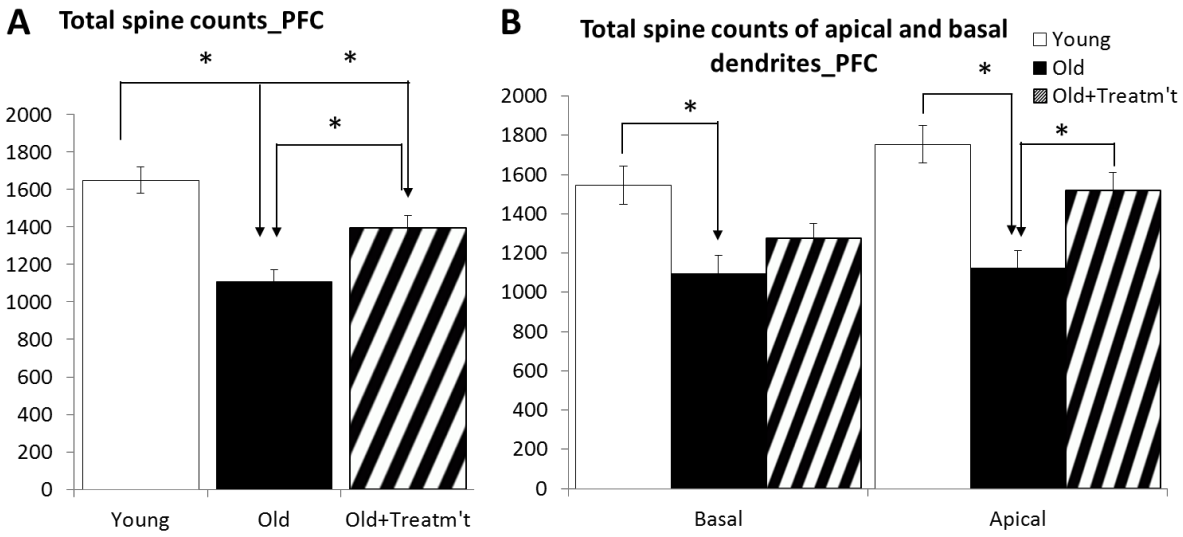

In the analysis of total spine counts, in comparison with Young mice, there was a significant reduction in total spine counts of Old and Old+Treatment mice, respectively (5A, $p<0.05$). Also, Old+Treatment mice showed higher spine counts than Old mice ($p<0.05$). In the break-down analysis, only Old mice showed a significant decrease in the basal dendrites as compared to Young mice (B, $p<0.05$). In the apical dendrites, both Young and Old+treatment mice exhibited a higher spine count than Old mice, respectively ($p<0.05$). Note that there was no difference in both basal and apical dendrites between Young and Old+Treatment mice ($p>0.05$).

Figure 107: Comparison of Overall Spine Density of Pyramidal Cells Between Groups.

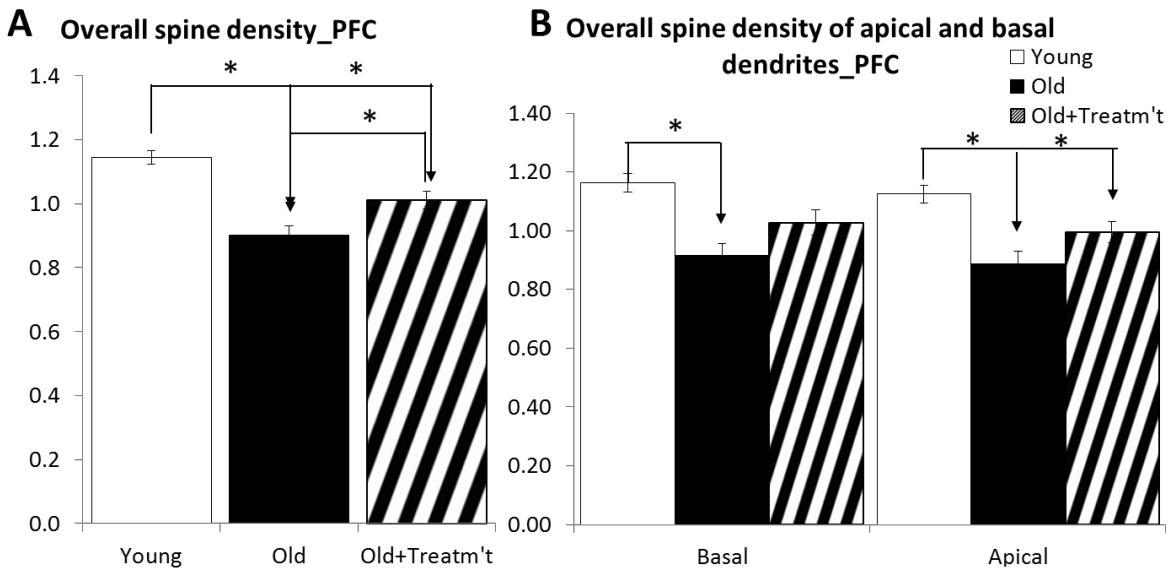

In the analysis of overall spine density, in comparison with Young mice, there was a significant reduction in spine density of Old and Old+Treatment mice, respectively (A, $p<0.05$). Also, Old+Treatment mice show a higher density than Old mice ($p<0.05$)*. In the break-down analysis, only Old mice showed a significant decrease in the basal dendrites as compared to Young mice (B, $p<0.05$). In the apical dendrites, Young mice exhibited a higher density than Old and Old+Treatment mice, respectively ($p<0.05$). Also, there was no difference between Old and Old+Treatment mice ($p>0.05$), which was likely due to the sample size being compromised by the break-down analysis. *It was noted that the p value was on the margin of statistical significance, given the sample size (n=4 per group) in the current study.

Figure 108: Representative Images of HPC Principle Cells Between Groups

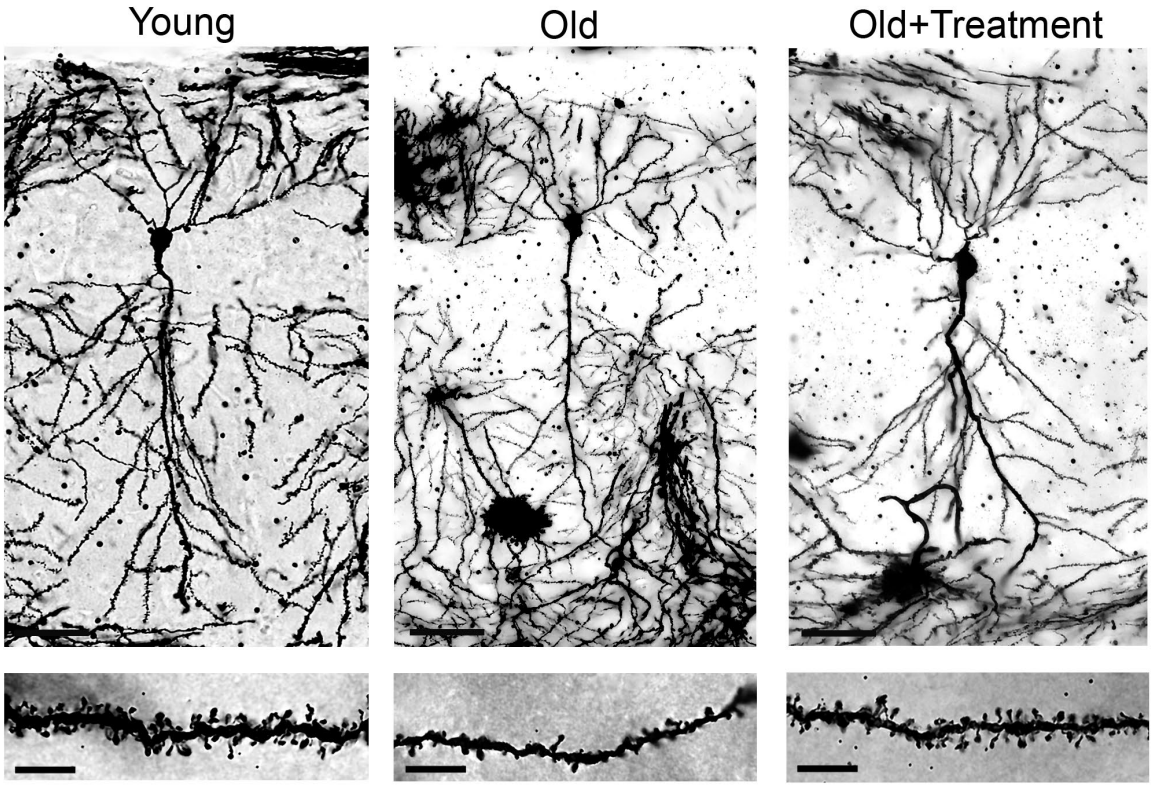

The morphological analysis of pyramidal cells in the CA1 of the hippocampus (Performed by NeuroDigiTech LLC). Similar techniques were used in the same sample to show efficacy at re-growing brain cells in the HPC. Compared to Young mice (A), all aged mice showed reductions in spine counts of pyramidal cells (the box in lower panels of A-C). It was noted that Old+Treatment mice showed a higher spine count than Old mice [Scale bars: 5 μm]. Note: The quantitation of spine subtypes was not included in the current study.

Figure 109: Comparison of Total Dendritic Lengths of Pyramidal Cells Between Groups.

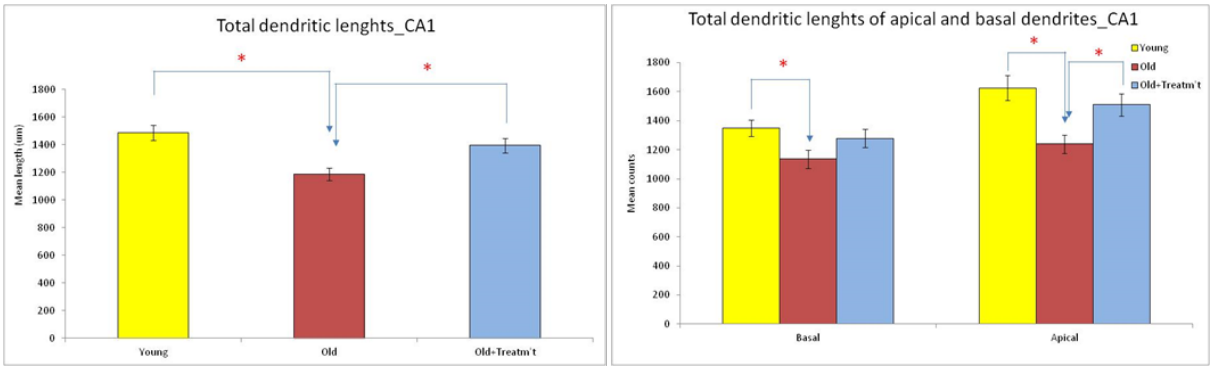

In total dendritic lengths, old mice exhibited a significant reduction as compared to Young and Old+Treatment mice, respectively ($p<0.05$). There was no difference between Young and Old+Treatment mice ($p>0.05$). In the break-down analysis, there was a reduction in total dendritic lengths of basal dendrites of Old mice as compared to that of Young mice ($p<0.05$). Also, Old+Treatment mice did not exhibit a significant difference from Young and from Old mice, respectively ($p>0.05$). In the apical dendrites, Old mice showed a reduction of total dendritic lengths than Young and Old+Treatment mice, respectively ($p<0.05$). Note that there was no difference between Young and Old+Treatment mice ($p>0.05$).

Figure 110: Comparison of Total Spine Counts of Pyramidal Cells Between Groups

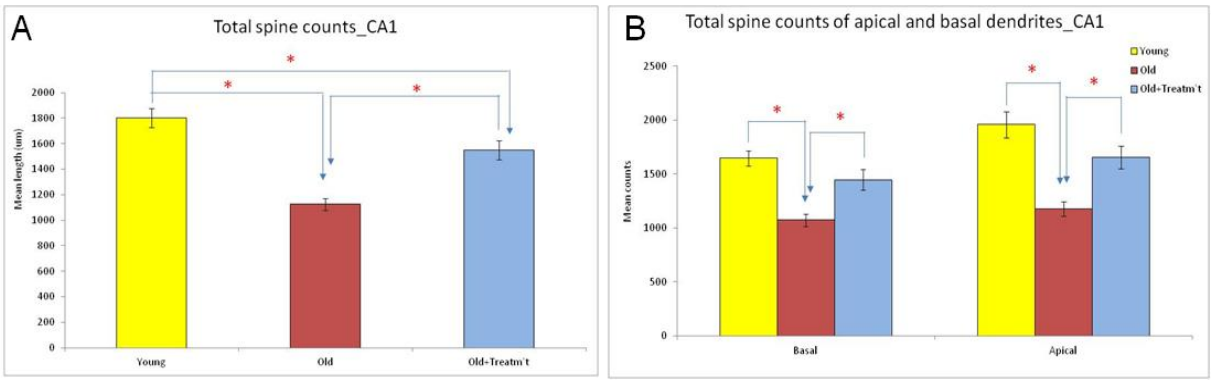

In the analysis of total spine counts, in comparison with Young mice, both Old and Old+Treatment mice exhbited a significant reduction in total spine counts of pyramidal cells, respectively ($p<0.05$). Also, Old+Treatment mice showed higher spine counts than Old mice ($p<0.05$). In the break-down analysis, Old mice showed a significant decrease in total spine counts of basal dendrites as compared to Young mice and Old+Treatment mice, respectively ($p<0.05$). In the apical dendrites, both Young and Old+treatment mice exhibited higher spine counts than Old mice, respectively ($p<0.05$). Note that there was no difference in both basal and apical dendrites between Young and Old+Treatment mice ($p>0.05$).

Figure 111: Comparison of Overall Spine Density of Pyramidal Cells Between Groups.

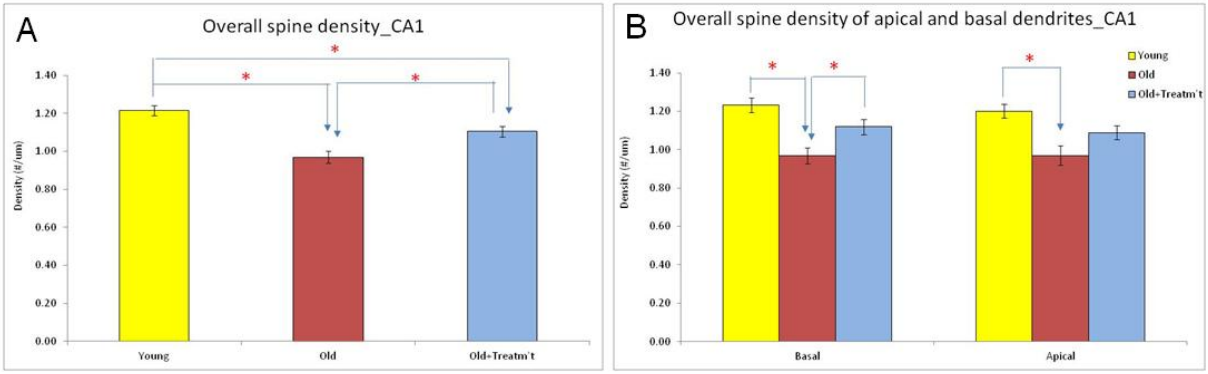

In the analysis of the overall spine density, in comparison with Young mice, both Old and Old+Treatment mice exhibited a significant reduction in the overall spine density of CA1 pyramidal cells, respectively ($p<0.05$). It was also noted that Old+Treatment mice show a higher spine density than Old mice ($p<0.05$). In the break-down analysis, Old mice showed a significant decrease in the basal dendrites as compared to Young and Old+Treatment mice, respectively ($p<0.05$). However, no difference was detected between Young and Old+Treatment mice ($p>0.05$). In the apical dendrites, Young mice exhibited a higher spine density than Old mice ($p<0.05$). Also, there was no difference between Old and Old+Treatment mice ($p>0.05$). Note that there was no difference in both basal and apical dendrites between Young and Old+Treatment mice ($p>0.05$).

Long lasting effect

Figure 112: Alternation Rate in Old Mice Receiving GL-II-73 Chronically, with or without a Washout Period

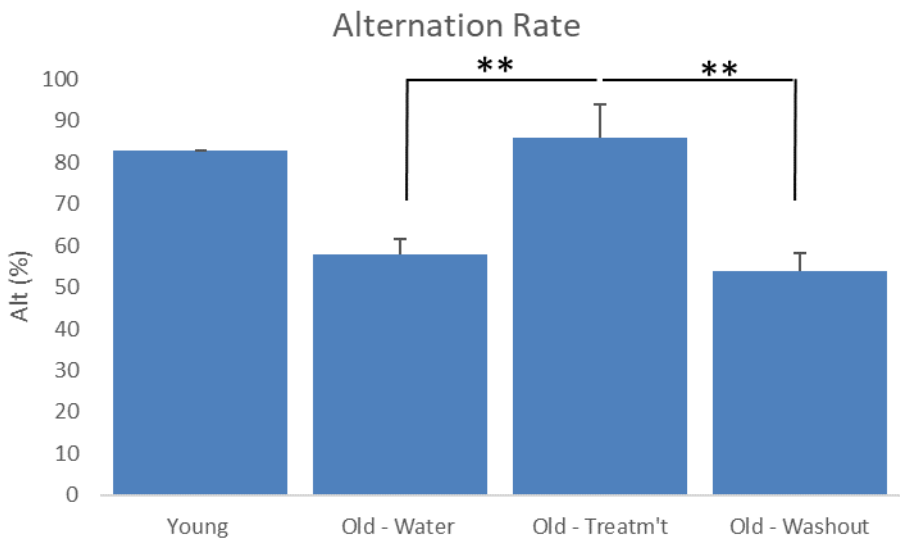

Behavior

The Old (22 months old) and Young (2 months) C57BL/6 male mice (Charles River) were used in this study. A subset of old mice received the compound GL-II-73 for 8 weeks in the drinking water at the concentration of 30mg/kg, another group received water, and another group received GL-II-73 for 8 weeks in the drinking water at the concentration of 30mg/kg and had a 1 week washout period before testing and brain collection. Prior to administration of the compound to the animals, the average volume consumed was measured to obtain the daily consumption of 8ml per day. Based on this assessment, the compound was prepared in drinking water and provided fresh to the animals every other day. The group details are as follow: Young (N=9); Old (N=13) and Old+Treatment (N=6). ANOVA on the alternation rate showed a main effect ($F(3;17)=9.4$; $p<0.001$). Chronic administration of GL-II-73 reversed decreased alternation rates in old mice, but not after a 1-week washout. The effect of the drug on cognition seems to require the compound to be on-board.

Figure 113: Comparison of Overall Spine Density of Pyramidal Cells Between Groups.

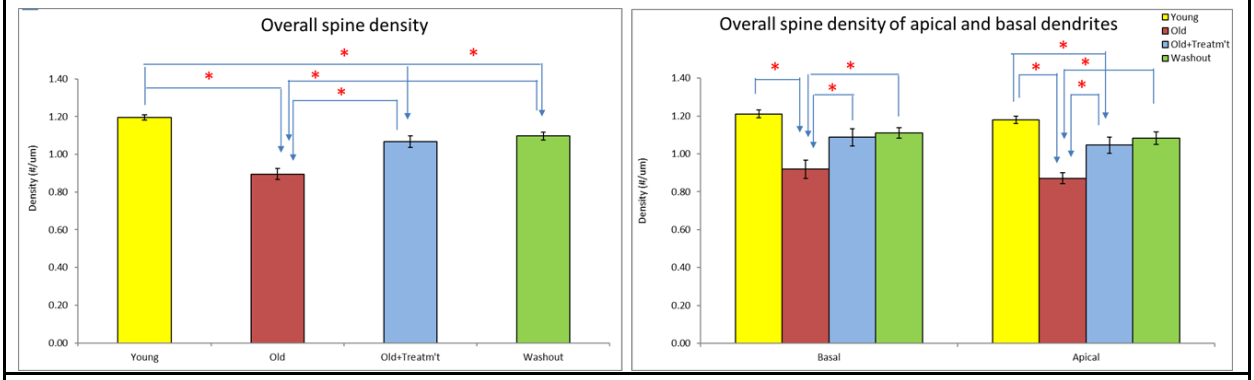

In comparison with Young mice, all aged mice (Old, Old+Treatment and Washout) exhibited a lower overall spine density, respectively (A, $p<0.05$). Also, both Old+Treatment and Washout mice exhibited a higher spine density than Old mice, respectively ($p<0.05$), whereas no difference was found between both treated groups (Old+Treatment and Washout) ($p>0.05$). Also, Young mice showed a higher spine density than Old+Treatment mice ($p<0.05$) but not Washout mice ($p>0.05$). In the break-down analysis, Old mice showed a significant decrease in the number of basal dendrites as compared to Young, Old+Treatment and Washout mice, respectively (B-left, $p<0.05$). Similarly, in the apical dendrites, Old mice exhibited a lower spine density than Young, Old+Treatment and Washout mice, respectively (B-right, $p<0.05$). Also, there was no difference between Young and Old+Treatment as well as Washout mice, respectively ($p>0.05$). Moreover, both treated (Old+Treatment and Washout) groups exhibited no significant difference in overall spine density ($p>0.05$).

A Summary of the Data:

When GL-II-73 is given chronically, GL-II-73 seems to reverse cognitive deficits and spine shrinkage while the compound was still on-board. If the compound was no longer on-board, cognitive deficits re-appear but morphology changes remain.

3.2.3.15. Growth of Dendrites and Spines in Neuronal Cell Culture

Figure 114: Images of Neuronal Culture with vehicle or GL-II-73, and Characterization of Spine Density (C) and Intersection in a Sholl Analysis (B)

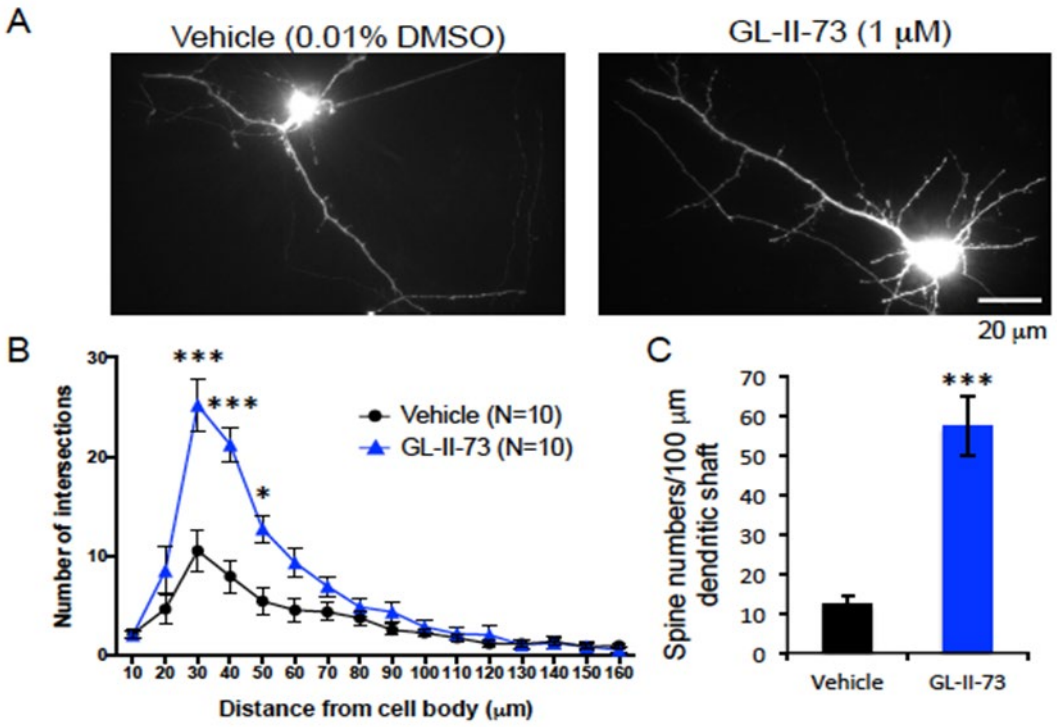

Mice expressing the recombinase CRE in pyramidal neurons (CamKII-Cre) were crossed with mice having a floxed expression of a green fluorescent protein (fGFP). Progeny of this breeding produced embryos expressing GFP in pyramidal neurons. Collection of embryos at E18 allowed us to collect the brains of the embryos and grow cells in a Petri Dish. After maturation and stabilization of the neurons (~2 weeks) the compound GL-II-73 was incubated in the Petri Dish at 1µM. Neurons were visualized after 24hrs.
Preliminary data suggest that incubation of GL-II-73 increases dendritic length and spine density in this assay.

Figure 115: Images of Neuronal Culture Incubated with Vehicle (Left Panels) or GL-II-73 (Right Panels)

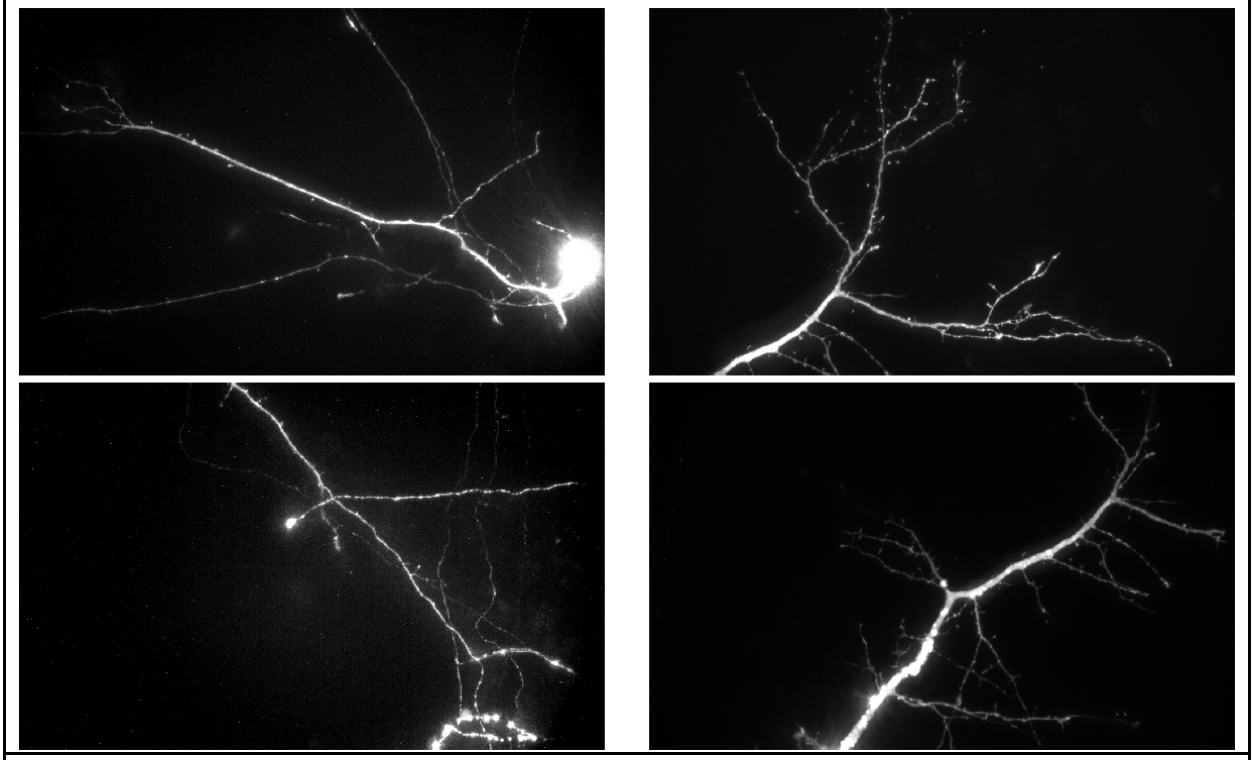

Images captured by Olympus DSU, 60x obj lens, 1500ms exposure/stk, Z-stack (12-15 steps, 0.76um)

3.2.3.16. Promoting the Generation of New Neurons in the Hippocampus

Mostly known during brain development, neurogenesis is also a phenomenon occurring in the adult brain. It was first recognized in the early 1960s, but was not fully accepted until the 1990s. Because stem cells can divide, and differentiate into many types of cells, their discovery in adult brains suggested that neurogenesis could hold the key to treating neurodegenerative conditions such as Alzheimer's disease. Since then, neurogenesis has also been found to occur in the hippocampi of adult humans, and more recently is has been confirmed to occur in the amygdala. Adult neurogenesis is known to occur in three regions in the mammalian brain:

- the subgranular zone (SGZ) of the **dentate gyrus in the hippocampus**, which is a region that is involved in regulating learning and memory
- the subventricular zone (SVZ), which is situated throughout the lateral walls of the brain's lateral ventricles.
- the amygdala

New neurons born in the SGZ migrate into the granule cell layer of the dentate gyrus and eventually become granule cells. These newborn neurons integrate into the existing circuitry and receive functional input.[273] Adult neurogenesis in the hippocampus is, therefore, defined as the progression from neural stem cells to mature dentate granule neurons. All stages of adult neurogenesis are regulated by physiological activity, including the proliferation, differentiation, fate determination of adult neural stem cells (NSCs) and progenitors, and the survival, maturation, and integration of newborn neurons[273]. Extracted from David et al. (2010)[274], the figure below shows the different steps of the hippocampal neurogenesis, from progenitors (green) to immature cells (orange, labelled with double-cortin DCX) to mature granule cell (blue,

labelled with NeuN). Neurogenesis can be evaluated at different stages by labeling different markers of the neurogenesis steps. Labeling KI67 can be used as a marker of proliferation, as it shows when the cells are maintaining chromosomes separated, i.e. splitting into 2 cells (proliferating). Using BrdU is used to show survival of newly proliferative cells. Bromodeoxyuridine (BrdU) can be incorporated into the newly synthesized DNA of replicating cells and is then maintained in the newly formed cells. Quantitative immunohistochemistry against BrdU is used as a proxy of survival. Finally, doublecortin can be used as a proxy of maturation.

Previous studies have shown that all steps of neurogenesis were down regulated in SV129 mice, and that chronic treatment with Fluoxetine (first line monoaminergic antidepressant) could increase the neurogenesis in this mouse line. In our case, we have decided to investigate the efficacy of our newly designed compound at increasing all steps of neurogenesis in this same model, as a first step towards exploring more in-depth efficacy linked to depression.

In this experiment, SV129 mice were treated with GL-II-73 for 4 weeks (30 mg/kg, PO). 2 weeks before euthanasia, they were injected with BrdU. Then brains were collected, sectioned and quantification of the different markers of the steps of neurogenesis was performed.

Figure 116: Experimental Design of the Administration of GL-II-73, Fluoxetine and Bromodeoxyuridine

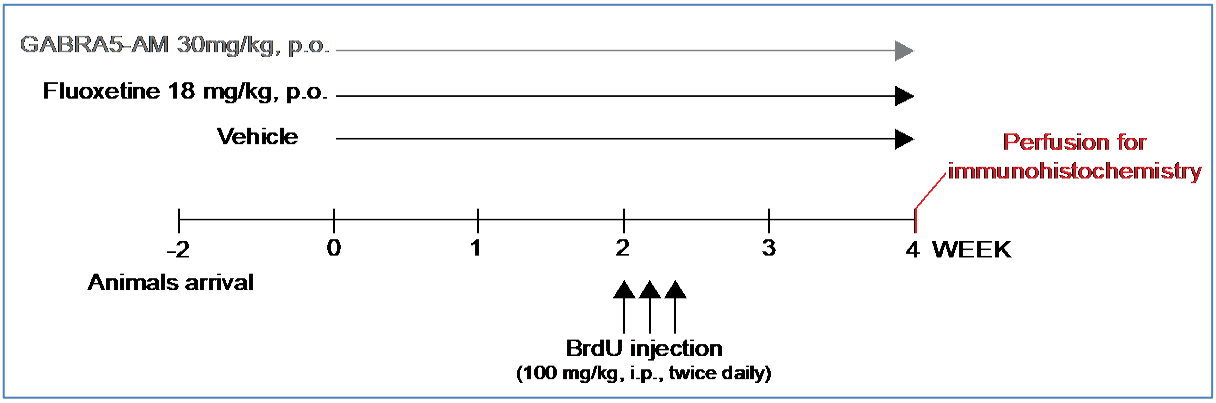

The results of the experiment in **Figure 116** are as follow:

The chronic GL-II-73 treatment (4 weeks) increased the **proliferation** of new cells, as shown by the increased in KI67 labeling in SV129 mice. Similar findings were reported with Fluoxetine (**Figure 117**). Chronic GLII73 treatment also increased **survival**, as shown by the increases in BrdU labeling in SV129 mice. Similar findings were reported with Fluoxetine (**Figure 117**). Chronic GL-II-73 treatment also increased **maturation**, as shown by the increased in DBX labeling in SV129 mice. Similar findings were reported with Fluoxetine (**Figure 118**).

Figure 117: Proliferation and Survival of New Neurons in the Hippocampus

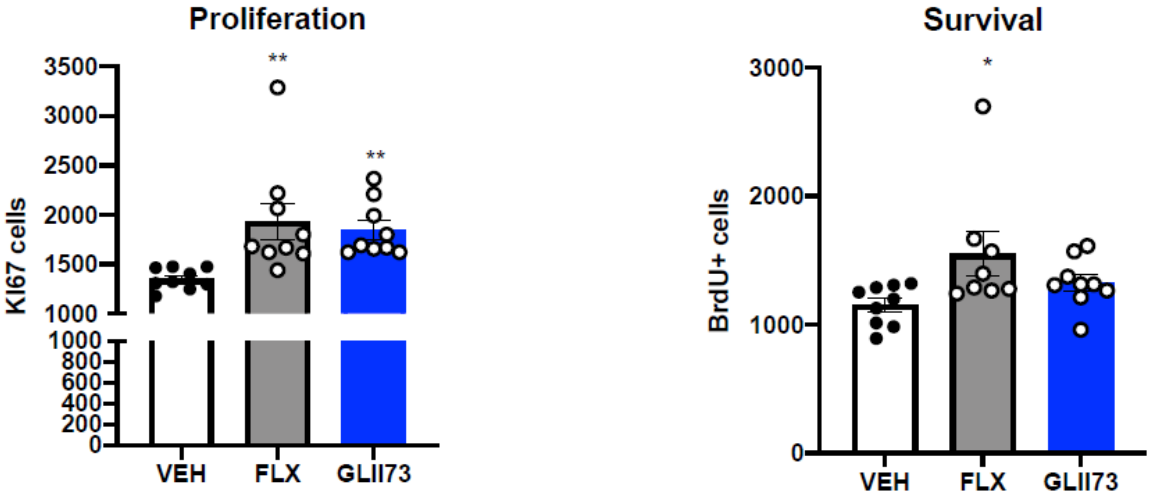

Figure 118: Maturation of New Neurons in the Hippocampus

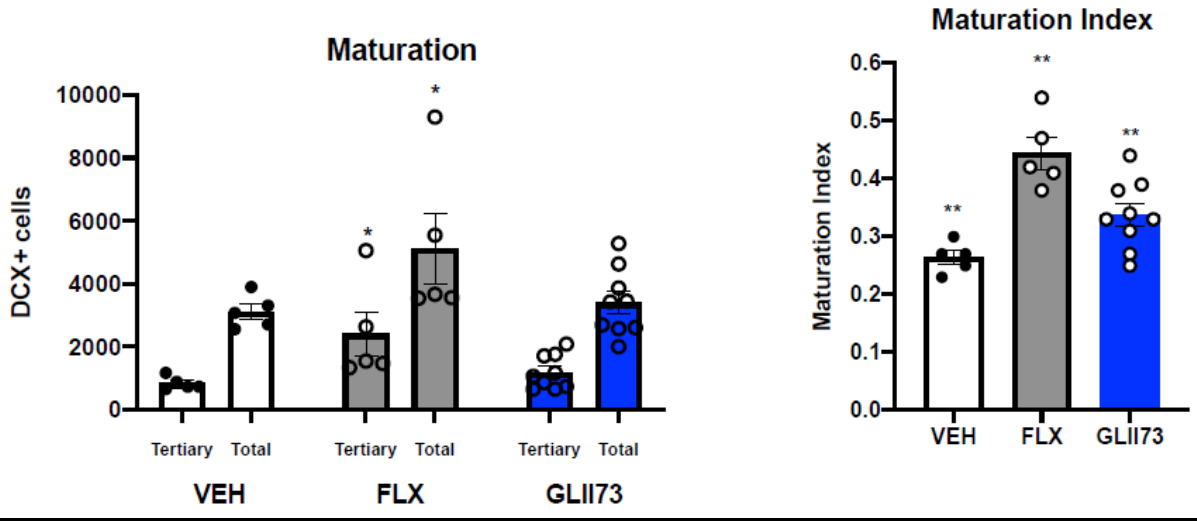

3.2.3.17. A Test of Abuse Liability

Figure 119: Water Versus GL-II-73 Consumption

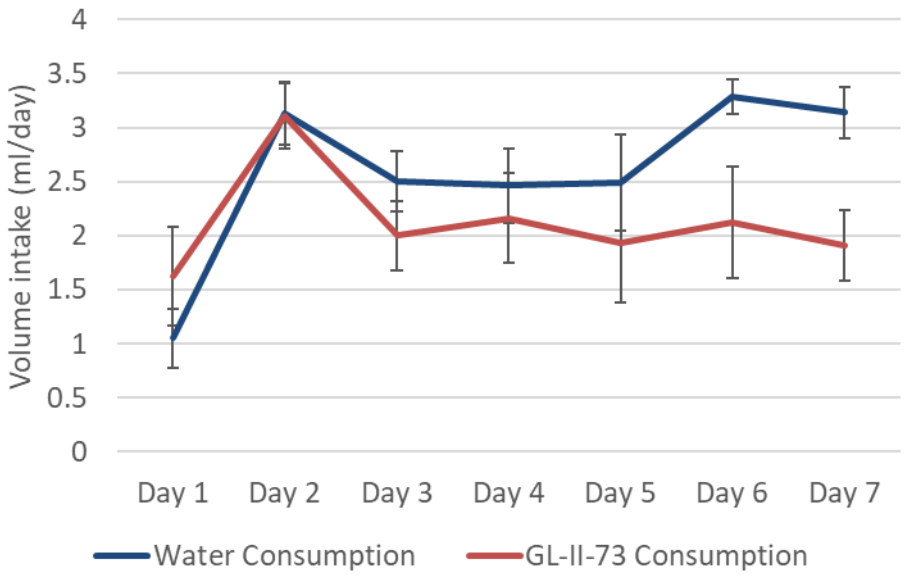

The C57 mice (N= 8; 50% females) were habituated to drink water through 2 bottles placed on the top of their cage lid. The water consumption was measured on 2 consecutive days to estimate the total volume intake per day. Then mice received GL-II-73, diluted in water at the dose of 30mg/kg, for 1 week, in both bottles. Finally, one bottle was filled with water, while the other was filed with GL-II-73 at 30mg/kg, and consumption was measured daily, for 7 days. Bottles were switched each day to prevent any side-preference bias. ANOVA, repeated measures, performed on the data shown did not identify a significant difference between water and GL-II-73 consumed over the 7 days. Mice consumed similar amounts of GL-II-73 and water when given the choice, even after 1 week of exclusive pre-exposure to GL-II-73. One can surmise that GL-II-73 is less consumed than water on day 6 and 7, further reinforcing the absence of preference for the drug.

3.2.3.18. First in Human – Electrophysiology on Human Pyramidal Neurons from the Hippocampus (*ex vivo*)

The ability to obtain whole cell and local field potential (LFP) recordings from *ex vivo* human cortical slices was previously demonstrated. Using whole cell *voltage* clamp recording, tonic GABAergic currents were induced using bath application of GABA, with subsequent application of GL-II-73. An all-points histogram for the baseline, GL-II-73 conditions and picrotoxin (PTX) epochs were fitted to Gaussian curves of the positive side of the histogram (red in **Figure 120**), with mean values defining tonic currents in epochs. It is shown that GL-II-73 increased tonic GABA currents in human, and potentially to a greater extent in mouse cortical slice preparations, with no effects on phasic GABA currents, likely reflecting the conservation of receptor structure and function across species. Next, whole-cell *current* clamp recordings were performed in mouse L2 neurons and show that GL-II-73 does not alter passive and active membrane properties (resting membrane potential, input resistance, membrane time constant, sag voltage, action potential threshold, rheobase and firing rates) (N=5, not shown), excluding non-specific effects.

Figure 120: GL-II-73 Contributes to Tonic Inhibition in Human and Mouse PyCs

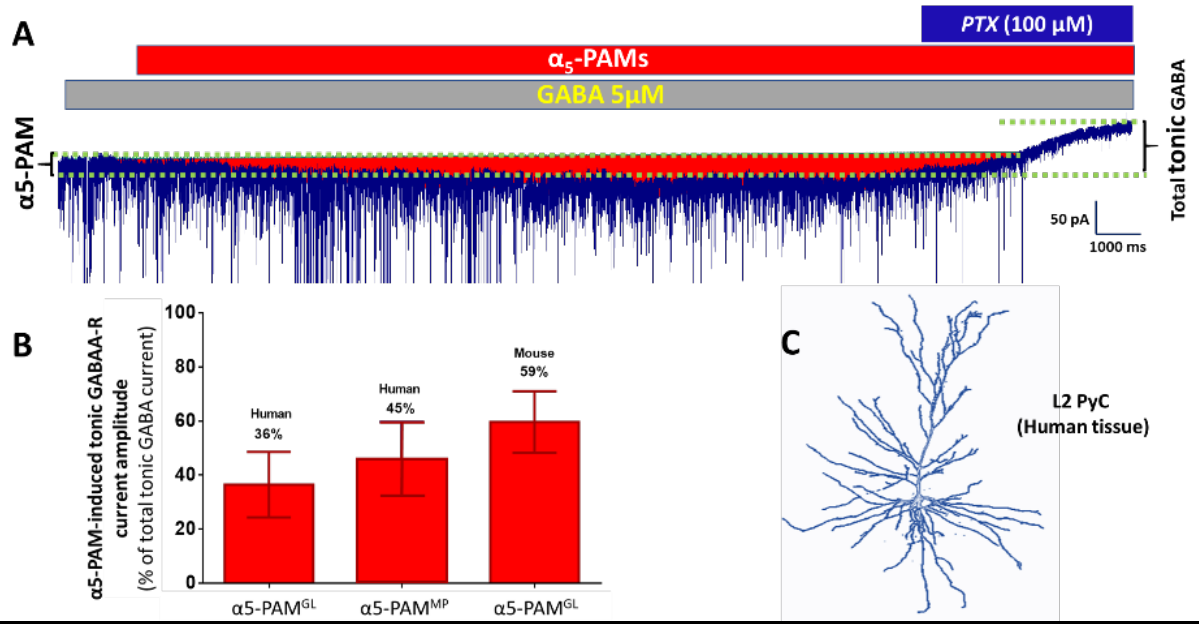

3.3. Discussion and Conclusions of GL-II-73

This study was based on the observation that normal aging induces neuronal loss contributing to cognitive decline. Here, we first confirmed that normal aging in mice induces cognitive deficits, with old mice exhibiting impaired working memory in the alternation task, consistent with previous finding.[250, 255, 256] Many compounds,[257] drugs,[258] natural extracts[256] or physical exercises[259] demonstrated potential at reversing cognitive decline in animal models, but with little-to-no success in human populations.[260, 261] This lack of efficacy can partially be explained by the focus of such approaches aiming at reversing the symptoms more than the underlying pathology. Indeed, it is unclear at the moment if treatment avenues that show pro-cognitive efficacy actually alleviate the underlying pathology, such as neuronal dysfunction or neuronal shrinkage. The companion tools, like radio-ligands for PET imaging can be developed to demonstrate such efficacy, but priority is still given at alleviating the symptoms.

In the context of aging, the "morphomolecular" senescence has a broad impact on different systems, including the GABAergic system. Reduced GABAergic functions are a hallmark of aging, and previous studies from our group demonstrated that targeting α5-$GABA_A$ receptors to bypass such deficits could reverse age-related cognitive decline.[250] In the present study, we investigated the potential combined efficacy of GL-II-73 on symptoms and underlying pathology, i.e. neuronal shrinkage. We demonstrated that chronic treatment with GL-II-73 not only reverses cognitive decline, but also reverses dendritic shrinkage and spine atrophy in the PFC and the CA1. Indeed, chronic treatment with GL-II-73 increased dendritic length, spine count and spine density in the both brain regions, in old mice. To our knowledge, it is the first time that a drug acting on the GABAergic system demonstrates neurotrophic effects, while commonly used benzodiazepines seem to decrease spine density in cortical pyramidal neurons.[262] Other drugs have shown neurotrophic effects,[263] such as ketamine for the treatment of depressive episodes.[264] Recent studies have shown that the antidepressant action of ketamine is mediated by its activity on NMDA receptor of GABA neurons.[265, 266] Further studies will be needed to identify what could be the mechanism of action of GL-II-73 permitting this neurotrophic effect, and if it has shared pathways with ketamine.

Interestingly, the neurotrophic effect of GL-II-73 was more pronounced in the apical segment of the pyramidal neuron dendrites as compared to the basal segment. It is known that the α5-$GABA_A$ receptors are located in the apical segment of the pyramidal neurons,[243] so these results suggest that the α5-$GABA_A$ receptors directly mediate this neurotrophic effect. However, a significant increase of spine counts and spine density in basal segment of pyramidal neurons of the CA1 from the treatment group was also observed. This effect can either suggest the

potential presence of the α5-$GABA_A$ receptors in the basal segment of pyramidal neurons of the CA1, or a generalized effect happening downstream of the apical effect. Such hypotheses would need to be validated but is consistent with previous findings showing that the α5-$GABA_A$ receptors are involved in the dendritic outgrowth and spine maturation of pyramidal neurons.[247]

When GL-II-73 is no longer given to the animals, the neurotrophic effect remains but the pro-cognitive effect diminishes. One could argue that the drug needs to be on board to improve cognitive performances continuously, even in the event of a strong neurotrophic effect. This would suggest that the neurotrophic effect alone is not sufficient to recover normal cognitive processes and suggests that the "rejuvenated" neurons are not as functional as neurons of younger animals. Here, we did not investigate if the "rejuvenated" neurons were similarly functional compared to neurons from younger animals, or if their functions were more similar to neurons from old animals. Using slice electrophysiology could answer this question and investigate if these neurons were truly rejuvenated or if the neurotrophic effect was limited to morphological features. In addition, the present study only tested 1 treatment duration (4 weeks) and 1 washout period (1 week). Investigating if longer treatment with GL-II-73 improves the stability of the cognitive functions when the treatment is stopped could be a solution to improve the functions of the rejuvenated neurons.

Despite promising results in mice suggesting a relief of the cognitive symptoms and a rejuvenation of neurons in brain regions involved in cognitive processes, it would be naïve to think that a single drug could reverse all the changes induced by normal aging. However, GL-II-73 is the first drug targeting an inhibitory system that shows neurotrophic, associated with

symptom relief. With its potential anxiolytic and antidepressant effects,[250] GL-II-73 could become a game changer for patients suffering from cognitive decline due to GABAergic downregulation. In the context of aging, and early stages of Alzheimer's disease, GL-II-73 could possibly be paired with Aducanumab,[226] a potent monoclonal antibody directed against β-amyloid oligomers, to further slowdown the progression of the disease and strengthen neuronal "health" and cognitive functions. Further testing in other cognitive domains, and other models (Alzheimer's disease, neurodegenerative disease etc.) will demonstrate the validity of this new drug for future therapeutic uses.

3.4. Improved Synthesis of α5-GABA$_A$R Subtype-selective Imidazodiazepines

The synthesis of 6-phenyl-4H-benzo[*f*]imidazo[1,5-*a*][1,4]diazepine-3-carboxylic acid derivatives was patented by Fryer in 1976[275] and two years later published by Walser and Fryer et al.[276] Three different benzodiazepines were used as staring materials with the following leaving groups in the 2 position: *N*-nitrosomethylamino,[277] dimorpholinylphosphinyloxy[278] and diethyl phosphate. However, the synthesis included 5-6 steps with an overall yield of 10-14%. A significant improvement was accomplished in the same year using a phenyl stabilized nitrone[279] under basic conditions that generated only 1-phenyl substituted ethyl 8-chloro-6-(2-fluorophenyl)-4*H*-benzo[*f*]imidazo[1,5-*a*][1,4]diazepine-3-carboxylates in one step with yields as high as 95%.[280] An alternative route was developed starting from quinazoline 3-oxides using carbanions that resulted in substituted 6-phenyl-4H-benzo[*f*]imidazo[1,5-*a*][1,4]diazepine-3-carboxylates in 45-55% yield over four steps.[281] The first general one-pot procedure to convert readily accessible 5-(2-fluorophenyl)-7-nitro-1,3-dihydro-2*H*-benzo[*e*][1,4]diazepin-2-one to ethyl 6-(2-fluorophenyl)-8-nitro-4*H*-benzo[*f*]imidazo[1,5-*a*][1,4]diazepine-3-carboxylate using diethyl chlorophosphate and ethyl isocyanoacetate was published in 1978 but no yields were reported.[282] The reaction was carried with the starting material in THF at 0 °C and the addition of potassium t-butoxide followed by sequential addition of diethyl chlorophosphate and a THF solution of ethyl isocyanate and potassium t-butoxide. More than a decade later Watjen et al.[283] used a similar method to react diazepines with sodium hydride in DMF and this was followed by the sequential addition of diethyl chlorophosphate at -20°C. Then a solution of lithium isopropyl amide and ethyl isocyanate at -78°C in THF was added. The only yield reported was 47% published for ethyl 7-chloro-5,6-dihydro-5-methyl-6-oxo-4*H*-benzo[*f*]imidazo[1,5-*a*][1,4]diazepine-3-carboxylate.[283]

A 44% yield was reported for ethyl 8-nitro-6-(4-chlorophenyl)-4*H*-benzo[*f*]imidazo[1,5-*a*][1,4]diazepine-3-carboxylate when the starting material and potassium *t*-butoxide was stirred in THF at 0 °C followed by the sequential addition of diethyl chlorophosphate, ethyl isocyanate and potassium *t*-butoxide.[284] Using ethyl (E)-2-(((dimethylamino)methylene)amino)acetate instead of ethyl isocyanoacetate did not improve the yield of this reaction.[285] An improvement yield of 58% for ethyl 8-bromo-6-(2-fluorophenyl)-4*H*-benzo[*f*]imidazo[1,5-*a*][1,4]diazepine-3-carboxylate was achieved when the starting material was treated with sodium hydride in THF and this was followed by the dropwise addition of diethyl chlorophosphate after which a slow addition of ethyl isocyanate and sodium hydride was carried out.[286] A systematic analysis of this reaction identified potassium *t*-butoxide as best base used at 1.1 equivalents for the reaction of the starting material and diethyl chlorophosphate (1.3 equivalents) at 0 °C. Then, this was followed by the slow sequential addition of ethyl isocyanate (1.1 equivalents) and sodium hydride (1.1 equivalents) at -35°C or below.[287] A combined yield of 87% was reported for ethyl 8-chloro-6-(2-phenyl)-4*H*-benzo[*f*]imidazo[1,5-*a*][1,4]diazepine-3-carboxylate when precipitated in diethyl ether and this was followed by column chromatography of the mother liquor. Several subsequent publications have used these conditions but the necessity for column chromatography to achieve moderate to good yields precluded large scale production.[147, 189, 190, 288, 289] Herein, we demonstrate the synthesis of (*R*)-8-bromo-6-(2-fluorophenyl)-4-methyl-4*H*-benzo[*f*]imidazo[1,5-*a*][1,4]diazepine-3-carboxylic acid using a 482 mmol scale.

3.4.1. Improvement of a Large-scale Process for MIDD0301

The biology and synthesis (**Scheme 27**) of **MIDD0301** has been reported before, but the discovery chemistry was not well-suited for scale up in a GMP manufacturing setting.[179, 180] Three steps of the synthesis required purification by column chromatography, while several steps exhibited typical scaleup issues such as efficient stirring, side product formation, optical purity issues, prolonged process times and yield loss upon scale up.[179, 180]

Scheme 27: Discovery Synthesis of **MIDD0301**

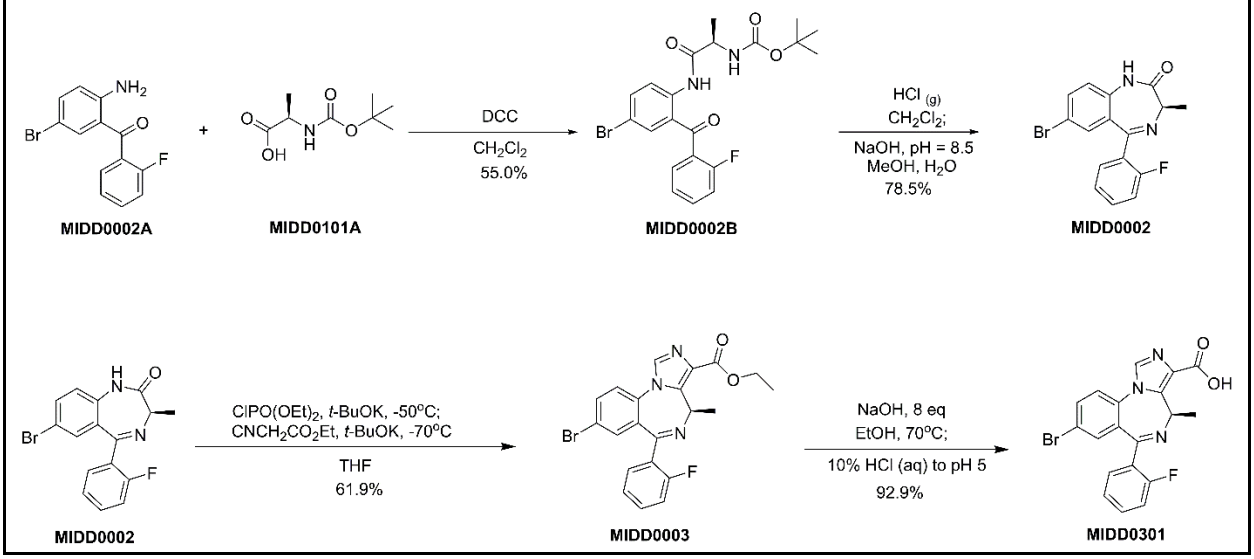

The amide coupling reaction proved to be problematic upon scale-up to achieve an efficient formation of the Boc-protected-β-amino amide intermediate (**MIDD0002B**) with complete consumption of aminobenzophenone, **MIDD0002A** in consistent yields. The original procedure (Table 1, entry 1) involved addition of the DCC coupling reagent to the reaction mixture, which contained **MIDD0002A** and the Boc-protected amino acid.[149] The extension of the reaction time

from 24 to 48 hours did not appreciably increase the yield (**Table 22, entry 2**), nor did elevating the reaction temperature to 35 - 40 ^{o}C (**Table 22, entry 3**). Neither did the addition of additional DCC and Boc-D-Ala-OH (**Table 22, entry 4**). Modification of the order of the addition of reagents was also attempted (**Table 22, entry 5-6**). First, Boc-D-Ala-OH (**MIDD0101A**) was added to a solution of **MIDD0002A** and DCC in dichloromethane (**entry 5**), which resulted in similar yields. Next, the aminobenzophenone **MIDD0002A** was added to a solution of Boc-D-Ala-OH (**MIDD0101A**) and DCC in dichloromethane (**entry 6**) which proved to be detrimental to the yield (5-10%), while providing evidence to support the multi-path reaction mechanism (**Scheme 28**) earlier proposed by Valuer and Bradlely.[290] The first step of the proposed mechanism involved formation of O-acylisourea **2**. Once formed, at least three plausible pathways are possible. The desired pathway to form amide **3** as well as the side-product, urea **4** involved the reaction of the O-acylisourea intermediate **2** with the amine. However, it was proposed the amine functional group on **MIDD0002A** was weakly basic because of the electron withdrawing nature of the 2'-fluorobenzoyl substituent, which hamperd the reactivity towards intermediate **2**. Consequently, the predominate pathways (**Scheme 28**) in the case of a weakly basic amine appeared to favor the inefficient pathway[291] wherein a second equivalent of Boc-D-Ala-OH (**MIDD0101A**) reacted with **2** to form anhydride **5** or the dead-end pathway.[290] The latter reaction was due to a 1,3-rearrangement of O-acylisourea **2**, which resulted, in the stable N-acylurea **6**. Additives such as DMAP were first reported by Neises and Wolfgang Steglich[292] in amide coupling reactions as an acyl transfer agent to circumvent the 1,3-rearrangement issue of the O-acylisourea intermediate by rapidly converting it to a more stable DMAP complex. However, the attempts in this work to utilize DMAP catalytically or stoichiometrically (**Table 22, entries 7 and 8**, respectively) did not improve the yield significantly and only complicated the purification. Unfortunately, switching

the solvent to acetonitrile (entry 9) or the coupling reagent to EDCI (**entries 10 and 11**) did not offer any advantage over the previous attempts to improve the amide coupling approach.

Scheme 28: Proposed Amide Coupling Mechanism

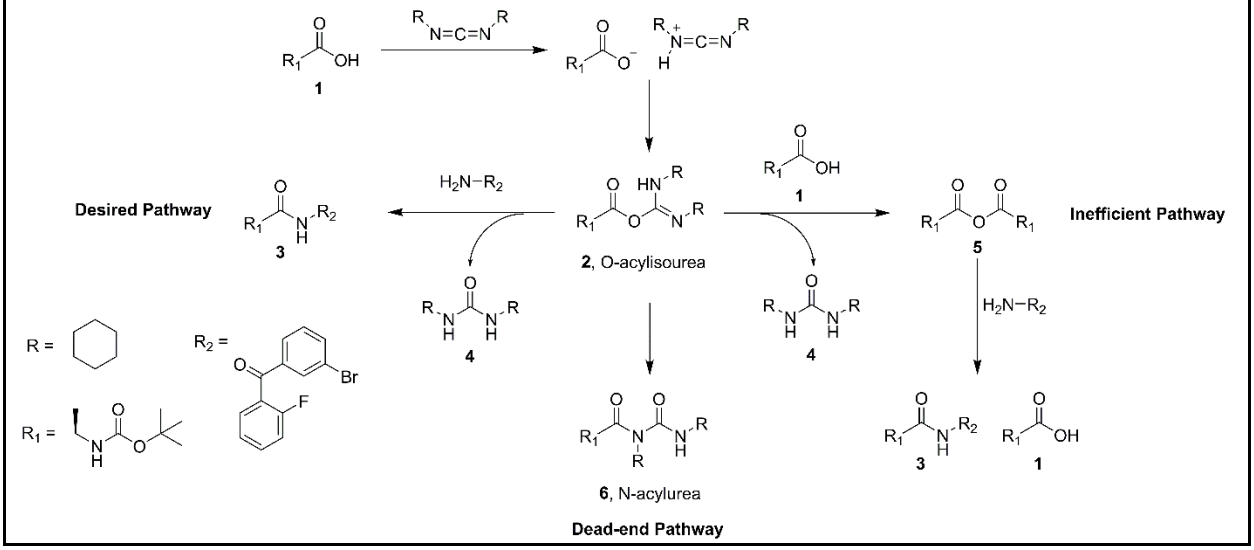

Next, the mixed carbonic anhydride approach was explored to forge the amide bond[293] using methyl-, ethyl-, and isobutylchloroformates (**Table 22, entries 12-14**). The conditions first reported by Anderson, et al.[294] and later used in the synthesis of similar benzodiazepine analogs by Reddy, et al.[295] were employed. The best yield observed of the Boc-protected-β-amino amide intermediate (**MIDD0002B**) was from the use of methyl chloroformate (52%).

Table 22: Amide Coupling Trials

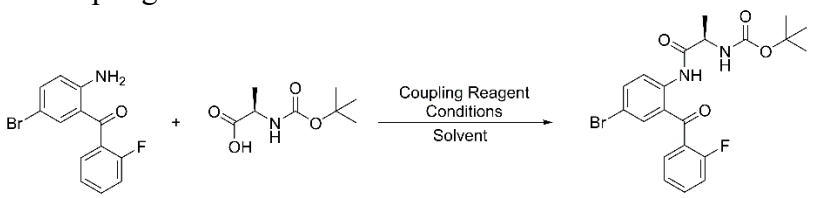

MIDD0002A MIDD0101A MIDD0002B

Entry	Coupling Reagent	Boc-Ala-OH	Additive	Conditions	Solvent	Yield
1	DCC, 1.2 eq	1.0 eq	None	24 h, rt	CH_2Cl_2	**58.6%**
2	DCC, 1.2 eq	1.0 eq	None	48 h, rt	CH_2Cl_2	**60.0%**
3	DCC, 1.2 eq	1.0 eq	None	24 h, 35-40°C	CH_2Cl_2	55.0%
4	DCC, 2.0 eq	2.0 eq	None	24 h, rt	CH_2Cl_2	**62.2%**
5	DCC, 1.2 eq	1.0 eq	None	Reverse Addition 24 h, rt	CH_2Cl_2	**57.2%**
6	DCC, 1.2 eq	1.0 eq	None	Reverse Addition 24 h, rt	CH_2Cl_2	9.6%
7	DCC, 1.2 eq	1.0 eq	DMAP, 0.1 eq	24 h, rt	CH_2Cl_2	53.4%
8	DCC, 1.2 eq	1.0 eq	DMAP, 1.0 eq	24 h, rt	CH_2Cl_2	50.2%
9	DCC, 1.2 eq	1.0 eq	None	24 h, rt	ACN	8.7%
10	EDC, 1.2 eq	1.0 eq	TEA, 1.2 eq	24 h, rt	CH_2Cl_2	10.2%
11	EDC, 1.2 eq	1.0 eq	DMAP, 1.2 eq	24 h, rt	CH_2Cl_2	38.8%
12	Methyl chloroformate	1.5 eq	N-Methyl morpholine, 3 eq	24 h, rt	THF	50%
13	Ethyl chloroformate	1.5 eq	N-Methyl morpholine, 3 eq	24 h, rt	THF	25%
14	Isobutyl chloroformate	1.5 eq	N-Methyl morpholine, 3 eq	24 h, rt	THF	22%

Because of the past work using acyl chlorides,[136] such as bromoacetyl bromide, to synthesize non-chiral benzodiazepines[136] and the work of Carpino, et al.[296] and Prabhu, et al.[297] to synthesize amino acid chlorides, we theorized that a combined approach could accomplish the goal of efficiently producing the β-amino amide intermediate with complete consumption of **MIDD0002A**. By following the reported procedure[296] FMOC-D-Ala-Cl (**MIDD0001**) was successfully synthesized from the corresponding FMOC-protected amino acid using thionyl chloride in high yield (**Scheme 29**). With the Fmoc-protected amino acid chloride, **MIDD0001** (1.2eq) in hand one was then able to successfully synthesize the Fmoc-protected-β-amino amide

intermediate (**MIDD0002C**) with complete consumption of aminobenzophenone **MIDD0002A** by simply stirring at room temperature in the presence of solid sodium bicarbonate. The cleavage of the protecting group with piperidine (6 eq) afforded the free β-amino amide intermediate (**MIDD0002D**), which was then condensed to form the benzodiazepine ring of **MIDD0002** in reasonable yields (68%).

Scheme 29: FMOC Route to **MIDD0002**

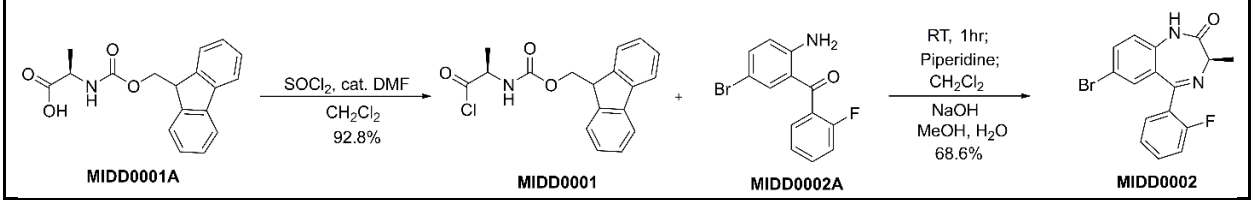

Despite the success of the FMOC-amino acid approach a critical optical purity issue during the scale-up trial employing the FMOC route was discovered (**Table 23, entry 5**). Presumably, epimerization of the chiral methyl group had occurred once the benzodiazepine ring had formed (**Scheme 30**), while under the basic condensation conditions. Upon this realization, a systematic analysis was conducted to investigate the root cause of the epimerization. During the discovery phase of the original synthetic route, the optical purity issue was not observed (**Table 23, entry 1**). However, on larger scale, longer reaction times (48 hrs) were required to obtain complete condensation of the β-amino amide intermediate, but with the unfortunate consequence of epimerization of the chiral methyl group which resulted in an optical purity of 53.9%EE (**Table 23, entry 2**). The condensation time could be shortened to 12 hr by increasing the amount hydroxide to 1 equivalent but this resulted in complete racemization of the chiral center in both the BOC and FMOC routes (**Table 23, entries 3 and 5**).

Scheme 30: Proposed Racemization Mechanism of **MIDD0002**

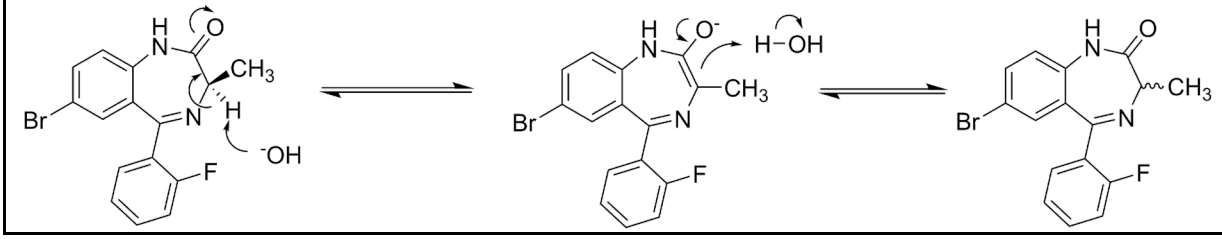

The conduction of the cyclization step under neutral conditions was then explored. First, the FMOC route was modified after removal of the protecting group using piperidine by washing the organic layer multiple times with water and aqueous bicarbonate to remove any traces of piperidine. Then, the reaction solvent was replaced by methanol and the subsequent cyclization was achieved in refluxing methanol (4 hours). One was encouraged that the cyclization could be achieved under neutral conditions (**Table 23, entry 6**), yet this method afforded only modest improvement in optical purity (76.9%EE). Presumably traces of piperidine were still present during the cyclization step or the epimerization occurred prior to that. Next, the BOC-route was revisited but instead of utilizing the original cyclization conditions, the mixture was heated in toluene at 60ºC for 4 hours. These conditions were employed to induce condensation but only after the organic reaction mixture had been washed several times with water and aqueous bicarbonate after cleavage of the protecting group using HCl gas. Gratifyingly, an optical purity of 99.2%EE was observed using neutral conditions and a non-polar solvent (**Table 23, entry 4**).

Table 23: Benzodiazepine Cyclization Trials

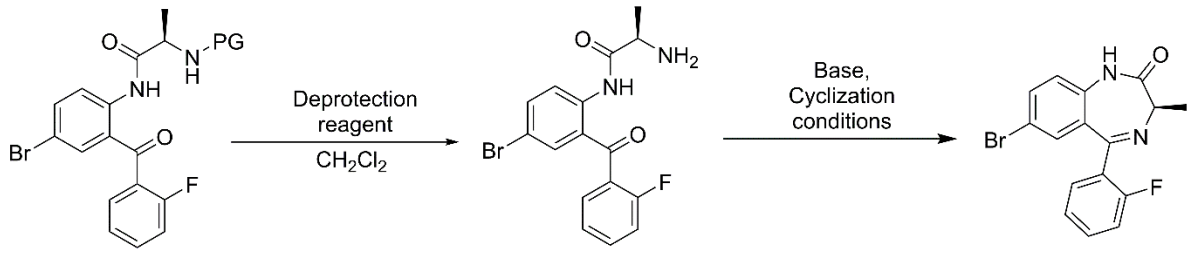

MIDD0002B, PG = Boc
MIDD0002C, PG = Fmoc

MIDD0002D

MIDD0002

Entry	Protecting Group (PG)	Deprotection Reagent	Base	Conditions	Solvent	%EE
1	BOC	HCl (g), sat.	NaOH, 0.1 eq	24 h, rt	MeOH / H_2O (9 : 1)	**99.9%**
2	BOC	HCl, 4.0 M in dioxane, 4.0 eq	NaOH, 0.1 eq	48 h, rt	MeOH / H_2O (9 : 1)	53.9%
3	BOC	HCl, 4.0 M in dioxane, 4.0 eq	NaOH, 1.0 eq	12 h, rt	MeOH / H_2O (9 : 1)	racemic
4	BOC	HCl, 4.0 M in dioxane, 4.0 eq	None	4 h, 60°C	Toluene	**99.2%**
5	FMOC	Piperidine, 6.0 eq	NaOH, 1.0 eq	12 h, rt	MeOH / H_2O (9 : 1)	racemic
6	FMOC	Piperidine, 6.0 eq	None	4 h, 60°C	MeOH	76.9%

Given the scale up challenges of the BOC-route mentioned earlier and the optical purity issues encountered in both approaches, we sought a new route and discovered the procedure developed by Fier and Whitakker[298] at Merck and Co where N-carboxyanhydrides (NCAs) were employed to synthesize optically pure amino acid derived benzodiazepines. Interestingly, similar neutral conditions and a non-polar solvent were used in their work for the condensation portion of the synthesis.

Since economical commercial sources of unnatural D-amino acid NCAs are limited we synthesized the N-carboxy-D-alanine anhydride (**MIDD0101**) internally. The typical procedures found in the literature involve using the free amino acid and phosgene gas[299, 300] or triphosgene.[301,

[302] Because of the hazardous nature of phosgene, the safer option of triphosgene was selected. Initial trials using the free amino acid (1.0 eq) and triphosgene (0.3eq) exhibited low yields (< 50%) and difficulty obtaining the product as a crystalline solid. One then turned to a procedure developed by Wilder and Mobashery[303] wherein Boc-protected amino acids (1 eq) were reacted with triphosgene in the presence of triethylamine (1 eq). This procedure exhibited consistent yields (55-60%) on small scale and delivered 35g (58% yield) of D-Alanine-NCA (**MIDD0101**) as a crystalline solid from a 5L flask on the large-scale campaign.

Scheme 31: NCA Route to **MIDD0002**

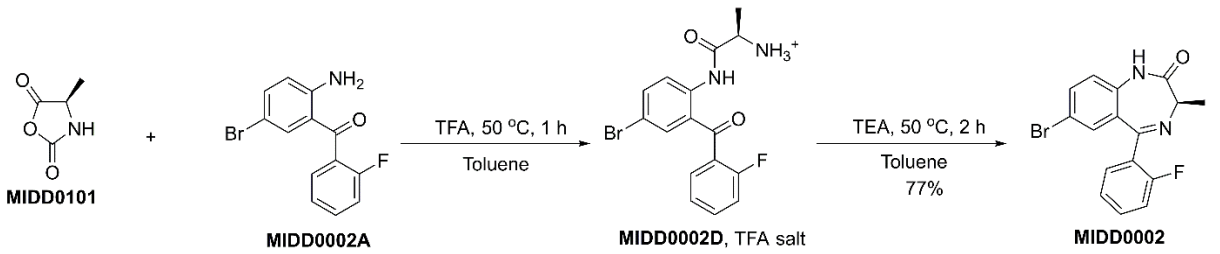

With the NCA (**MIDD0101**) in hand and to our delight, the aminobenzophenone (**MIDD0002A**) cleanly reacted with the Boc-D-Alanine NCA in toluene in the presence of trifluoroacetic acid (2 eq) to provide the β-amino amide intermediate **MIDD0002D** as the trifluoroacetate salt (**Scheme 31**). Addition of triethylamine (2 eq) induced condensation of the primary amine with the benzophenone carbonyl group to provide the optically pure (99.2%EE) benzodiazepine **MIDD0002** in good yields (77%). Upon reaction completion, an aqueous work-up removed the triethylammonium trifluoroacetate salt and the product was easily crystallized to remove traces of **MIDD0002A** and oligomeric impurities using an ethyl acetate / hexanes mixture to provide 127g with the process carried out in a 5 L flask. In summary, the new NCA route provided a more atom-economical and scalable approach to the synthesis of **MIDD0002** than the

FMOC route with improved yields and ensured optical purity over both the BOC and FMOC routes.

Scheme 32: Synthesis of Imidazodiazepine **MIDD0003**

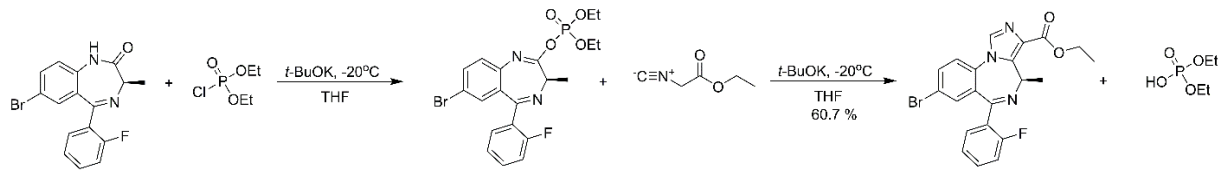

The third step of the synthesis of **MIDD0301** required installation of the imidazole ring C to produce imidazodiazepine **MIDD0003**. The established procedure[153] involved formation of the iminophosphate **MIDD0003A** (**Scheme 32**) by deprotonation of the starting amide using potassium *t*-butoxide and then addition of diethylchlorophosphate. The iminophosphate (**MIDD0003A**) was then subsequently reacted with the enolate of ethyl isocyanoacetate to furnish the desired imidazodiazepine **MIDD0003**. Several improvements to the original chemistry were required in order to provide a reliable and scalable procedure. Initially, the purification was conducted using column chromatography. Secondly, the reagents were added in an "all in one" fashion and specifically as a solid in the case of the potassium *t*-butoxide portions. Thirdly, each subsequent addition of reagents involved cooling of the reaction mixture to below -35°C, and then addition of the reagent and finally allowing the mixture to warm to 0°C for each portion of the procedure to react. With those challenges in mind one sought to develop a purification method by crystallization and to determine a reaction temperature in which the reagents could be added in a controlled fashion at a temperature in which they would react. By careful monitoring of the process by TLC it was determined that the iminophosphate **MIDD0003A** did not form until the

reaction temperature reached -20ºC. Similarly, it was determined that the reaction onset temperature of the iminophosphate with the enolate of ethyl isocyanoacetate was ~ -35 to -30ºC. Consequently, it was believed that by addition of the reagents in a controlled, dropwise fashion at -20 one could simply hold the reaction mixture at -20 to -15 ºC throughout the sequence of additions. The procedure, which resulted, involved first dissolving the **MIDD0002** in tetrahydrofuran and cooling the mixture to -20ºC. Then, a solution of potassium *t*-butoxide (1.3 eq) in THF at rt was added dropwise over 30 minutes to the reaction mixture. The reaction mixture was then held for 30 minutes at -20 to -15ºC to ensure complete deprotonation of the amide starting material. Next, diethylchlorophosphate (1.4 eq) at room temperature was added dropwise over 15 minutes. Within 2 hours after addition of the phosphate reagent, consumption of the amide was observed by TLC to generate iminophosphate intermediate **MIDD0003A**. Then, ethyl isocyanoacetate (1.3 eq) was added dropwise over 15 minutes and this was followed by a dropwise addition of a solution of potassium *t*-butoxide (1.3 eq) in THF at -20 to -15ºC. The isocyanoacetate / butoxide addition sequence was designed in this manner so that the enolate would react with the iminophosphate as soon as it formed. As predicted, the formation of imidazodiazepine **MIDD0003** was complete immediately after the *t*-butoxide addition with no detectable iminophosphate intermediate **MIDD0003A** observed. Upon completion of the reaction the **MIDD0003** product was partitioned into the organic layer using ethyl acetate and an aq bicarbonate work-up to remove the potassium salts and unreacted butoxide. The purification of the imidazodiazepine was achieved by crystallization using *t*-butyl methyl ether, which adequately removed traces of unreacted **MIDD0002** starting material and phosphate related byproducts. With the goal of eliminating the column chromatography and designing a more robust and scalable procedure, successful execution of the large-scale synthesis provided 96.6 g (60.7 % yield) of **MIDD0003**

carried out in a 5 L flask. Assessment of the optical purity (99.9%EE) confirmed that large-scale procedure to install the imidazole ring did not cause any observed epimerization of the chiral methyl group.

The final step of the **MIDD0301** synthesis to be refined for large-scale was saponification of the ethyl ester functionality at the C-3 position. For the early small-scale discovery procedure the saponification was carried out in ethanol, but this resulted in a thick reaction medium due to the formation of an insoluble and gel-like imidazocarboxylate salt. In addition, the acidification procedure employed hydrochloric acid to protonate the carboxylic acid function of the product and precipitate if from solution. As exhibited by Roni, et al.[253], **MIDD0301** exhibited a pH dependent equilibrium between a closed seven-membered ring and the open-ring acyclic benzophenone structure on hydrolysis where the open form was predominate at pH's at or below 3 in agreement with the literature. Therefore, careful control of the pH during the isolation phase of the procedure would be crucial to ensure efficient recovery of the product given the negligible aqueous solubility of MIDD0301 at pH 4 and increasing aqueous solubility as the open form of the compound when the pH was lower than 4. Finally, given the optically purity issues discovered during the **MIDD0002** step, confirmation of the optical purity during the saponification and isolation chemistry was paramount. Mechanistically, **MIDD0003** in theory would be susceptible to epimerization in the presence of strong base such as hydroxide anion (**Scheme 33**).

Scheme 33: Proposed Racemization Mechanism of **MIDD0003**

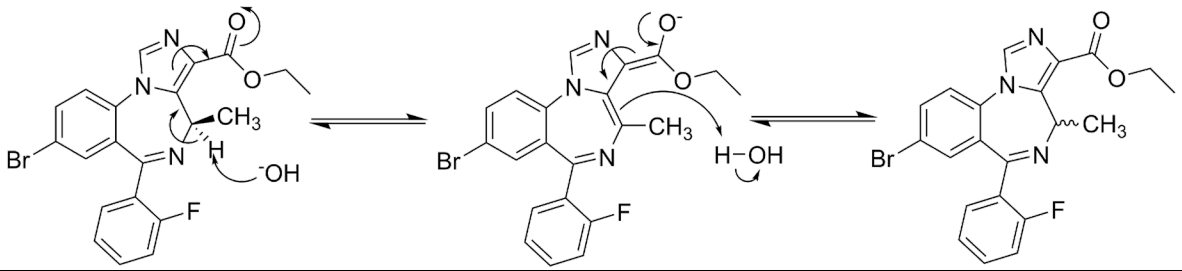

To address the difficulty in stirring the mixture originating from the insoluble sodium carboxylate salt observed in the discovery chemistry a simple solvent switch from ethanol to a 4 to 1 tetrahydrofuran / water mixture was employed. This change provided a mixture which remained an easily stirred biphasic mixture throughout the process. With the new reaction solvent in place, the hydroxide quantity was also reduced from 8 eq to 4 eq and the reaction temperature was lowered from 78ºC to 50ºC. Under these new reaction conditions, the saponification reaction was observed to be complete within 4 hours. The acidification was modified to utilize acetic acid rather than hydrochloric acid to alleviate the concern of overshooting the pH on large-scale and converting significant levels of **MIDD0301** into the open form. In fact, up to 6 equivalents of acetic acid could be used for the acidification to pH 4 with no appreciable open form observed. Once acidified, the reaction mixture was diluted with water and then the solvent was switched from tetrahydrofuran to methanol to precipitate out the product (**MIDD0301**) as a white solid in > 95% yield. Analysis of the optical purity revealed an excellent enantiomeric excess of the desired R-isomer (99.9%EE) hereby confirming the resistance of the imidazodiazepine to epimerize by reaction with hydroxide. With the newly developed saponification procedure in place, **MIDD0301** was the successfully synthesized on large-scale (5L flask) to provide 87.7 g of the target compound

in 97.5% yield for the last step. The HPLC purity and optical purity of the large-scale synthesis was found to be 97.2% with 99.9%EE, respectively. A recrystallization of the final product was also developed using ethanol to provide > 99% purity by HPLC when required.

In summary, a scalable and reproducible process has been developed (**Scheme 34**) to reliably synthesis the lead asthma ligand **MIDD0301** on multi-gram scale with excellent purity and enantiomeric excess.

Scheme 34: Improved Large-Scale Synthesis of **MIDD0301**

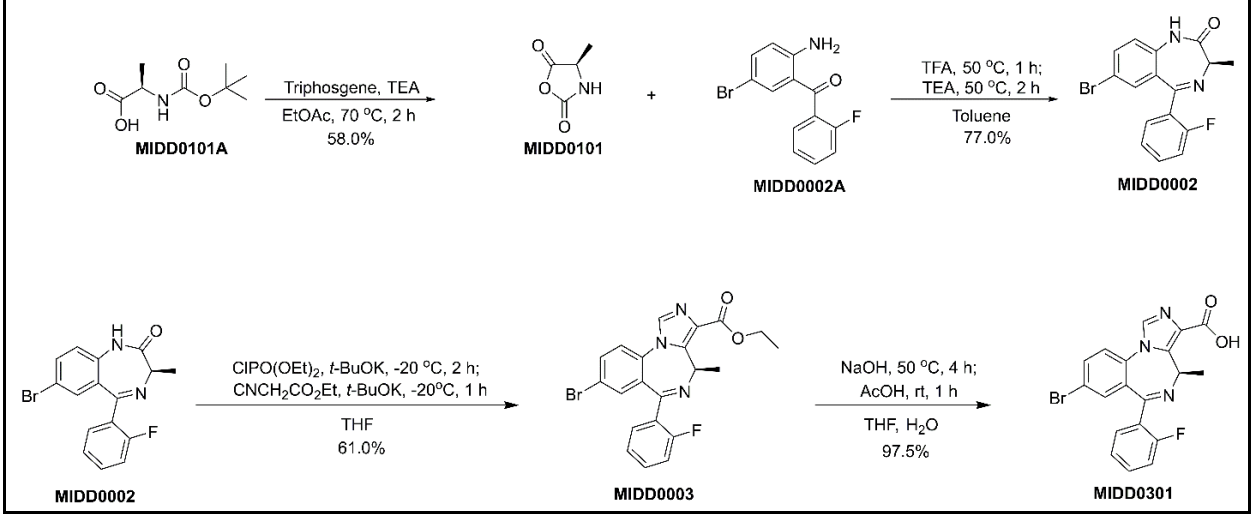

3.4.2. Experimental Section for MIDD0301

3.4.2.1. General Procedures for the Synthesis of MIDD0301

All reactions were performed in oven-dried round-bottom flasks with overhead mechanical stirrers under an argon atmosphere. The organic solvents were purified when necessary by standard methods or purchased from Sigma-Aldrich.™ Chemicals were purchased from either Sigma Aldrich™, Oakwood Chemical, Alfa Aesar, Matrix Scientific, or Acros Organic. The ^{1}H, ^{13}C and ^{19}F NMR spectral data were obtained on Bruker 300 MHz and 500 MHz instruments with the chemical shifts in δ (ppm) reported. The HRMS spectral data was obtained on a LCMS-IT-TOF spectrometer (Shimadzu Scientific).

3.4.2.1.1. N-Carboxy-D-Alanine Anhydride [MIDD0101]

To a solution of Boc-D-Alanine (100g, 528.5 mmol), triphosgene (62.7g, 211.4 mmol) and anhydrous ethyl acetate (4000mL), triethylamine (81.0mL, 581.4 mmol) was added dropwise over 60 min while keeping the temperature between 25 – 30ºC, and while monitoring the $CO_{2(g)}$ and $HCl_{(g)}$ evolution. The reaction mixture, which resulted was then allowed to stir 1 h at 25 – 30ºC and this was followed by 2 h at reflux (65 – 70ºC), at which point the reaction was deemed complete as gas evolution ceased. The reaction mixture (a white slurry) was then cooled to rt. The white solid (TEA-HCl and residual D-Alanine) was removed by filtration to yield a pale-yellow solution. The solid was washed with 2 portions of ethyl acetate (2 x 100 mL) and the filtrates were combined. The ethyl acetate was removed under reduced pressure to yield a semi-solid mass. The residue was then dissolved in dichloromethane (400 mL). The product was then precipitated by a

dropwise addition of hexanes (400mL) over 1 hr with vigorous stirring. The product slurry, which resulted, was then placed in a freezer at -20 °C for 12 hr to maximize product precipitation. The solid was filtered and washed with hexanes (250 mL x 2). The solid was dried under vacuum at rt to afford the product as an off-white solid (35.2 g, 58.0%): **^{1}H NMR** (500 MHz, DMSO-*d*$_6$) δ 9.01 (s, 1H), 4.48 (qd, *J* = 7.0, 1.1 Hz, 1H), 1.34 (d, *J* = 7.1 Hz, 3H); **^{13}C NMR** (126 MHz, DMSO-*d*$_6$) δ 172.88, 152.15, 53.28, 17.23; **HRMS** (ESI/IT-TOF): m/z [M + H]+ calcd for $C_4H_6NO_3$: 116.0348; found: 116.0350.

3.4.2.1.2. (*R*)-7-Bromo-5-(2-fluorophenyl)-3-methyl-1,3-dihydro-2*H*-benzo[*e*][1,4]diazepin-2-one [MIDD0002]

A mixture of 2-amino-5-bromo-2'-fluorobenzophenone (**MIDD0002A**, 140.7 g, 478.4 mmol), anhydrous trifluoroacetic acid (73.3 mL, 956.7 mmol) and anhydrous toluene (2200 mL) was allowed to stir at rt for 30 min to dissolve the starting material. Then solid N-carboxy-D-alanine anhydride (**MIDD0101**, 66.0g, 574.0 mmol) was then added to the reaction mixture. The reaction mixture was then heated at 50 – 55°C for 1 h, at which point the reaction was deemed complete (intermediate TFA salt formation, <5% 2-amino-5-bromo-2'-fluorobenzophenone remained) on analysis by TLC (silica gel and 50% ethyl acetate / hexanes). Upon completion of the reaction, anhydrous triethylamine (133.3 mL, 956.7 mmol) was added dropwise to the reaction mixture over a 30 min period, while maintaining the temperature at 50 – 55°C. The reaction mixture was then held at 50 – 55°C for 2 h, at which point the reaction was deemed complete (disappearance of intermediate TFA salt) on analysis by TLC (silica gel; 50% ethyl acetate / hexanes). Upon cooling the reaction mixture to rt, the solvents were removed under reduced pressure and the residue was dissolved in ethyl acetate (1500 mL) and water (1500 mL). The biphasic mixture, which resulted,

was allowed to stand for 15 min and the layers were separated. The organic layer was washed with 5% aq sodium bicarbonate solution (1500 mL) and then 10% aq sodium chloride solution (1500mL). The organic layer was dried (Na_2SO_4, 50 g). The ethyl acetate was removed under reduced pressure and the residue was solvent exchanged to 10% ethyl acetate / heptane (25 mL x 2). The residue was then slurried with 10% ethyl acetate / heptane (1700 mL) at 60 – 65ºC for 30 min to dissolve the starting material, MIDD0002A. Upon cooling to rt and after holding for 2 h, the solid product was collected by filtration and washed with 10% ethyl acetate / heptane (50 mL x 2) and then heptane (50 mL x 2). The solid was dried under vacuum at 35 – 40ºC to afford the product as an off-white solid (127.0 g, 77.0%): **^{1}H NMR** (500 MHz, $CDCl_3$) δ 9.69 (s, 1H), 7.63 – 7.59 (m, 1H), 7.59 (dd, *J* = 8.5, 2.3 Hz, 1H), 7.47 (dddd, *J* = 8.2, 7.0, 5.0, 1.8 Hz, 1H), 7.36 (d, *J* = 2.2 Hz, 1H), 7.26 (td, *J* = 7.5, 1.1 Hz, 1H), 7.12 (d, *J* = 8.6 Hz, 1H), 7.08 (ddd, *J* = 10.2, 8.3, 1.1 Hz, 1H), 3.79 (q, *J* = 6.5 Hz, 1H), 1.78 (d, *J* = 6.5 Hz, 3H); **^{13}C NMR** (126 MHz, $CDCl_3$) δ 172.39 (s), 164.53 (s), 160.45 (d, $^1J_{CF}$ = 251.9 Hz), 136.47 (s), 134.74 (s), 132.19 (d, $^3J_{CF}$ = 8.3 Hz), 132.03 (d, J_{CF} = 1.5 Hz, NOE coupling), 131.56 (d, $^3J_{CF}$ = 2.2 Hz), 130.15 (s), 127.13 (d, $^2J_{CF}$ = 12.4 Hz), 124.46 (d, $^4J_{CF}$ = 3.6 Hz), 122.98 (s), 116.54 (s), 116.29 (d, $^2J_{CF}$ = 21.5 Hz), 58.85 (s), 16.93 (s); **^{19}F NMR** (471 MHz, $CDCl_3$) δ -112.53; **HRMS** (ESI/IT-TOF): m/z [M + H]+ calcd for $C_{16}H_{13}BrFN_2O$: 347.0190; found: 347.0181; **[α] $^{25}_D$** = -195.5 (c 0.71, EtOAc); **HPLC Purity**: 99.2%; **Optical Purity**: 99.2%EE.

3.4.2.1.3. Ethyl (*R*)-8-bromo-6-(2-fluorophenyl)-4-methyl-4*H*-benzo[*f*]imidazo[1,5-*a*][1,4]diazepine-3-carboxylate [MIDD0003]

A mixture of (*R*)-7-bromo-5-(2-fluorophenyl)-3-methyl-1,3-dihydro-2*H*-benzo[*e*][1,4]diazepin-2-one (**MIDD0002**, 125.0 g, 360.0 mmol) and anhydrous tetrahydrofuran (2000 mL) was cooled to

-20 ºC using a dry ice / IPA bath. A solution of potassium t-butoxide (52.5 g, 468.0 mmol) in tetrahydrofuran (300 mL) was added dropwise to the reaction mixture over 30 min, while maintaining the temperature at -20 to -15 ºC. Upon completion of the addition, the reaction mixture was allowed to stir for an additional 60 min at -20 ºC. Diethyl chlorophosphate (72.8 mL, 504.1 mmol) was then added dropwise to the reaction mixture over 15 min while maintaining the temperature at -20 to -15 ºC. Upon completion of the addition, the reaction mixture was allowed to stir for an additional 2 h at -20 ºC at which point the reaction was deemed complete on analysis by TLC (silica gel; 100% ethyl acetate). Ethyl isocyanoacetate (51.2 mL, 468.0 mmol) was then added dropwise to the reaction mixture over 15 min while maintaining the temperature at -20 to -15 ºC. Then immediately, a solution of potassium t-butoxide (52.5 g, 468.0 mmol) in tetrahydrofuran (300 mL) was added dropwise to the reaction mixture over 30 min, while maintaining the temperature at -20 to -15 ºC. Upon completion of the addition, the reaction mixture was allowed to warm to rt and stir for an additional 1 h, at which point the reaction was deemed complete on analysis by TLC (silica gel; 100% ethyl acetate). The reaction mixture was then diluted with 5% aq sodium bicarbonate (2000 mL) and then ethyl acetate (2000 mL). The biphasic mixture, which resulted, was filtered to clear the emulsion, then allowed to stand for 30 min and the layers were separated. The aq layer was then extracted with ethyl acetate (2000 mL) and the combined organic layers were washed with 10% aq sodium bicarbonate solution (2000 mL) and then 20% aq sodium chloride solution (2000 mL). The organic layer was dried (Na_2SO_4, 250 g). The solvents were removed under reduced pressure. The solid residue, which resulted was solvent exchanged to *t*-butyl methyl ether (200mL x 2) and then the residue was slurried with *t*-butyl methyl ether (1000 mL) at 50 – 55ºC for 30 min. Upon cooling to rt and after holding for 12 h, the solid, which formed, was filtered and washed with *t*-butyl methyl ether (100 mL x 4).

The solid was dried under vacuum at 35 – 40ºC to afford the product as a white powder (96.6 g, 60.7%): **^{1}H NMR** (500 MHz, $CDCl_3$) δ 7.92 (s, 1H), 7.73 (dd, *J* = 8.5, 2.2 Hz, 1H), 7.60 (dt, *J* = 7.3, 3.9 Hz, 1H), 7.48 (d, *J* = 8.6 Hz, 1H), 7.50 – 7.42 (m, 1H), 7.42 (d, *J* = 2.2 Hz, 1H), 7.26 (td, *J* = 7.5, 1.1 Hz, 1H), 7.10 – 7.02 (m, 1H), 6.71 (q, *J* = 7.3 Hz, 1H), 4.54 – 4.28 (m, 2H), 1.42 (t, *J* = 7.1 Hz, 3H), 1.29 (d, *J* = 7.4 Hz, 3H); **^{13}C NMR** (126 MHz, $CDCl_3$) δ 162.93 (s), 162.67 (s), 160.10 (d, $^{1}J_{CF}$ = 250.7 Hz), 141.59 (s), 134.85 (s), 134.75 (s), 133.68 (s), 133.05 (s), 132.12 (d, $^{3}J_{CF}$ = 8.2 Hz), 131.17 (s), 129.59 (s), 128.42 (d, $^{2}J_{CF}$ = 12.3 Hz), 124.57 (d, $^{4}J_{CF}$ = 3.3 Hz), 123.65 (s), 120.96 (s), 116.25 (d, $^{2}J_{CF}$ = 21.4 Hz), 60.82 (s), 50.12 (s), 14.87 (s), 14.43 (s); **^{19}F NMR** (471 MHz, $CDCl_3$) δ -112.36; **HRMS** (ESI/IT-TOF): m/z [M + H]+ calcd for $C_{21}H_{18}BrFN_3O_2$: 442.0561; found: 442.0563; **[α] $^{25}_{D}$** = -42.1 (c 0.53, EtOAc); **HPLC Purity**: 97.5%; **Optical Purity**: 99.8%EE.

3.4.2.1.4. (*R*)-8-Bromo-6-(2-fluorophenyl)-4-methyl-4*H*-benzo[*f*]imidazo[1,5-*a*][1,4]diazepine-3-carboxylic acid [MIDD0301]

To a mixture of ethyl (*R*)-8-bromo-6-(2-fluorophenyl)-4-methyl-4*H*-benzo[*f*]imidazo[1,5-*a*][1,4]diazepine-3-carboxylate (**MIDD0003**, 96.0 g, 217.0 mmol) and tetrahydrofuran (1500 mL), a solution of sodium hydroxide (34.7 g, 868.2 mmol) in water (500 mL) was added dropwise over 15 min while keeping the temperature between 25 – 30 ºC. The reaction mixture, which resulted, was then heated to 50 – 55 ºC and held there for 4 h at which point the reaction was deemed complete on analysis by TLC analysis (silica gel and 100% ethyl acetate). Caution: Do no heat the reaction higher than 55 ºC or racemization may occur. The reaction mixture was then cooled to rt. The reaction mixture was then diluted with water (1000 mL). Glacial acetic acid (74.5 mL, 1302.3 mmol) was then added dropwise to the reaction mixture over 15 min while maintaining the

temperature at 20 to 25 ºC. The tetrahydrofuran was removed under reduced pressure. To the semisolid / slurry, which resulted, then methanol (750 mL) was added. The thin slurry which resulted was stirred at 55 – 60ºC for 30 min to homogenize the mixture. The slurry, which resulted was stirred at 20 – 25ºC for 12 h to maximize precipitation of the product. The solid was filtered off and washed with water (200 mL x 4). The solid was dried under vacuum at 35 – 40ºC to afford the product as an off-white powder (87.7 g, 97.5%): **^{1}H NMR** (500 MHz, DMSO-*d*$_6$) δ 12.83 (s, 1H), 8.42 (s, 1H), 8.09 – 7.92 (m, 1H), 7.89 (d, *J* = 8.7 Hz, 1H), 7.59 (t, *J* = 5.5 Hz, 1H), 7.55 (dtd, *J* = 7.5, 5.4, 2.5 Hz, 1H), 7.36 – 7.30 (m, 2H), 7.23 (dd, *J* = 10.7, 8.2 Hz, 1H), 6.52 (q, *J* = 7.3 Hz, 1H), 1.17 (d, *J* = 7.3 Hz, 3H); **^{13}C NMR** (126 MHz, DMSO-*d*$_6$) δ 164.68 (s), 162.37 (s), 159.85 (d, $^{1}J_{CF}$ = 248.3 Hz), 140.86 (s), 136.64 (s), 135.49 (s), 134.02 (s), 132.74 (d, $^{3}J_{CF}$ = 7.9 Hz), 132.38 (s), 131.93 (s), 130.89 (s), 129.58 (s), 128.70 (d, $^{2}J_{CF}$ = 11.7 Hz), 125.64 (s), 125.18 (d, $^{4}J_{CF}$ = 2.8 Hz), 120.26 (s), 116.43 (d, $^{2}J_{CF}$ = 21.1 Hz), 49.83 (s), 15.05 (s); **^{19}F NMR** (471 MHz, DMSO-*d*$_6$) δ -114.15; **HRMS** (ESI/IT-TOF): m/z [M + H]+ calcd for $C_{19}H_{14}BrFN_3O_2$: 414.0248; found: 414.0246; **[α] $^{25}_{D}$** = -107.9 (c 1.0, MeOH); **HPLC Purity**: 97.2%; **Optical Purity**: 99.9%.

3.4.2.1.5. (9*H*-Fluoren-9-yl)methyl (*R*)-(1-chloro-1-oxopropan-2-yl)carbamate [MIDD0001]

To a mixture of Fmoc-D-Alanine (**MIDD0001A**, 150 g, 481.8 mmol), N,N-dimethylformamide (3.7 mL, 48.2 mmol), and dichloromethane (3000 mL), thionyl chloride (351.4 mL, 4818.0 mmol) was added dropwise over 60 min while keeping the temperature between 25 – 30ºC and while monitoring the $SO_{2(g)}$ and $HCl_{(g)}$ evolution. The reaction mixture, which resulted, was then allowed to stir 1 h at 25 – 30ºC and this was followed by 2 h at 35 – 40ºC at which point the reaction was deemed complete by TLC using silica gel and 25% methanol / dichloromethane with 1%

triethylamine added. A 1 mL sample of the reaction mixture was quenched with 1 mL methanol containing a few drops of triethylamine prior to spotting on a TLC plate (silica gel). The reaction mixture was then cooled to rt. The solvents and excess thionyl chloride were removed under reduced pressure. The residual thionyl chloride was removed by drying the solid residue under reduced pressure at 40 – 45ºC. The solid residue was then dissolved in dichloromethane (350 mL). The product was then precipitated by a dropwise addition of heptane (3150mL) over 1 hr with vigorous stirring. The product slurry, which resulted, was then stirred at rt for 2 hr to maximize product precipitation. The solid was filtered and washed with 10 % dichloromethane / heptane (250 mL x 2). The solid was dried under vacuum at rt to afford the product as an off-white solid (147.5 g, 92.8%): **^{1}H NMR** (500 MHz, $CDCl_3$) δ 7.80 (d, *J* = 7.6 Hz, 2H), 7.65 – 7.53 (m, 2H), 7.48 – 7.40 (m, 2H), 7.35 (td, *J* = 7.4, 1.2 Hz, 2H), 5.37 – 5.22 (m, 1H), 4.64 (p, *J* = 7.4 Hz, 1H), 4.53 (dd, *J* = 10.6, 6.6 Hz, 1H), 4.45 (dd, *J* = 10.8, 6.9 Hz, 1H), 4.25 (t, *J* = 6.8 Hz, 1H), 1.57 (d, *J* = 7.3 Hz, 3H); **^{13}C NMR** (126 MHz, $CDCl_3$) δ 175.55, 155.48, 143.54, 141.36, 127.83, 127.15, 125.02, 124.95, 120.07, 67.34, 58.67, 47.09, 17.28; **HRMS** (ESI/IT-TOF): m/z [M + H]+ calcd for methyl ester $C_{19}H_{20}NO_4$: 326.3719; found: 326.3722.

3.4.2.1.6. (*R*)-7-Bromo-5-(2-fluorophenyl)-3-methyl-1,3-dihydro-2*H*-benzo[*e*][1,4]diazepin-2-one [MIDD0002]: FMOC route (Table 23, entry 5)

A mixture of 2-amino-5-bromo-2'-fluorobenzophenone (**MIDD0002A**, 120 g, 408.0 mmol) and dichloromethane (1200 mL) was stirred at rt for 30 min to dissolve the starting material. A solution of (9*H*-fluoren-9-yl)methyl (*R*)-(1-chloro-1-oxopropan-2-yl)carbamate (**MIDD0001**, 148 g, 448.8 mmol) in dichloromethane (1000 mL) was added dropwise to the reaction mixture at 25 – 30ºC over 60 min. The reaction mixture was then held at 25 – 30ºC for 1 h at which point the reaction

process was deemed complete on analysis by TLC (silica gel; 50% ethyl acetate / hexanes). Upon completion of the reaction, piperidine (241.8 mL, 2448 mmol) was added dropwise to the reaction mixture over 30 min while maintaining the temperature at 25 – 30°C. The reaction mixture was then held at 25 – 30°C for 12 h at which point the reaction was deemed complete by TLC analysis (silica gel; 50% ethyl acetate / hexanes). The reaction mixture was then diluted with 5% aq sodium bicarbonate (1200 mL). The biphasic mixture, which resulted, was allowed to stand for 15 min and the layers were separated. The aq layer was then extracted with dichloromethane (1200 mL) and the combined organic layers were washed with 5% aq sodium bicarbonate solution (1200 mL) and then twice with deionized water (1200 mL x 2). The solvents were removed under reduced pressure and the residue was dissolved in dichloromethane (1200 mL) and methanol (1200 mL). A solution of sodium hydroxide (16.3 g, 408.0 mmol) and deionized water (240 mL) was added dropwise to the reaction mixture over 15 min. The reaction mixture was then held at 25 – 30 °C for 12 h at which point the reaction was deemed complete on analysis by TLC (silica gel; 50% ethyl acetate / hexanes). Upon completion of the reaction the solvents were removed under reduced pressure. The semi-solid which resulted was dissolved in dichloromethane (1200 mL) and 10% aq sodium chloride (1200 mL). The biphasic mixture, which resulted, was allowed to stand for 15 min and the layers were separated. The aq layer was then extracted with dichloromethane (1200 mL) and the combined organic layers were then washed with a 10% aq sodium chloride (1200 mL). The organic layer was dried (Na_2SO_4, 200 g). The solvents were removed under reduced pressure and the residue was slurried with methanol (1600 mL) at 50 – 55 °C for 30 min. Upon cooling to rt and after holding for 3 h, the solid byproduct, 1-((9H-fluoren-9-yl)methyl)piperidine (**MIDD0002E**) was removed by filtration and washed with methanol (200 mL x 2). The methanol was removed under reduced pressure and the residue was solvent

exchanged to 10% ethyl acetate / heptane (200 mL x 2). The residue was then slurried with 10% ethyl acetate / heptane (1600 mL) at 60 – 65ºC for 30 min to dissolve the starting material, MIDD0002A. Upon cooling to rt and after holding for 2 h, the solid product was collected by filtration and washed with 10% ethyl acetate / heptane (50 mL x 2) and then heptane (50 mL x 2). The solid was dried under vacuum at 35 – 40ºC to afford the product as an off-white solid (97.3 g, 68.6%): **^{1}H NMR** (500 MHz, $CDCl_3$) δ 9.69 (s, 1H), 7.63 – 7.59 (m, 1H), 7.59 (dd, *J* = 8.5, 2.3 Hz, 1H), 7.47 (dddd, *J* = 8.2, 7.0, 5.0, 1.8 Hz, 1H), 7.36 (d, *J* = 2.2 Hz, 1H), 7.26 (td, *J* = 7.5, 1.1 Hz, 1H), 7.12 (d, *J* = 8.6 Hz, 1H), 7.08 (ddd, *J* = 10.2, 8.3, 1.1 Hz, 1H), 3.79 (q, *J* = 6.5 Hz, 1H), 1.78 (d, *J* = 6.5 Hz, 3H); **^{13}C NMR** (126 MHz, $CDCl_3$) δ 172.39 (s), 164.53 (s), 160.45 (d, $^{1}J_{CF}$ = 251.9 Hz), 136.47 (s), 134.74 (s), 132.19 (d, $^{3}J_{CF}$ = 8.3 Hz), 132.03 (d, J_{CF} = 1.5 Hz, NOE coupling), 131.56 (d, $^{3}J_{CF}$ = 2.2 Hz), 130.15 (s), 127.13 (d, $^{2}J_{CF}$ = 12.4 Hz), 124.46 (d, $^{4}J_{CF}$ = 3.6 Hz), 122.98 (s), 116.54 (s), 116.29 (d, $^{2}J_{CF}$ = 21.5 Hz), 58.85 (s), 16.93 (s); **HRMS** (ESI/IT-TOF): m/z [M + H]+ calcd for $C_{16}H_{13}BrFN_2O$: 347.0190; found: 347.0181; **HPLC Purity**: 99.9%; **Optical Purity**: racemic.

MIDD0002: FMOC route (Table 23, entry 6)

The same procedure as above (**entry 6**) was modified on 13.6 mmol scale to employ no sodium hydroxide and methanol at reflux (60 – 65ºC) for the benzodiazepine cyclization step to afford the product (**MIDD0002B**) as a white solid (2.8 g, 60.0%): **HPLC Purity**: 99.9%; **Optical Purity**: 76.9%. Caution: This epimerization was caused by residual piperidine still present in the reaction mixture.

3.4.2.1.7. *tert*-Butyl (*R*)-(1-((4-bromo-2-(2-fluorobenzoyl)phenyl)amino)-1-oxopropan-2-yl)carbamate [MIDD0002B]: DCC Route

MIDD0002B: DCC Route (Table 22, entry 1)

A mixture of 2-amino-5-bromo-2'-fluorobenzophenone (**MIDD0002A**, 60 g, 204.0 mmol), boc-D-alanine (**MIDD0101A**, 38.6 g, 204.0 mmol) and dichloromethane (300 mL) was stirred at rt for 30 min to dissolve the starting materials. The solution, which resulted, was cooled to 0-5°C. A solution of 1,3-dicyclohexylcarbodiimide (51.4 g, 248.9 mmol) in dichloromethane (200 mL) was then added dropwise to the reaction mixture over 30 min while keeping the temperature at 0-5°C. The white slurry, which resulted, was allowed to warm to rt with stirring over 24 hr, at which point analysis of the reaction progress by TLC indicated a 60/40 mixture of product to starting material (silica gel plate; 50% ethyl acetate / hexanes, ***Rf*** MIDD0002A: 0.5 / ***Rf*** MIDD0002B: 0.4). The dicyclohexyl urea byproduct was removed by filtration to afford a pale-yellow solution to which the solvents were removed under reduced pressure. The residue, which resulted, was triturated with hexanes (200 mL) to afford a pale-yellow solid. The solid was filtered and washed with hexanes (50 mL x 3). The solid was further purified (to remove residual starting material) by stirring with hexanes (200 mL) at reflux for 30 min. The slurry, which resulted, was allowed to cool to rt. The white solid, which resulted, was filtered and washed with hexanes (50mL x 3). The solid was dried under vacuum at 35 – 40°C to afford the product as a white solid (55.3 g, 58.6%): **^{1}H NMR** (300 MHz, $CDCl_3$) δ 11.68 (s, 1H), 8.71 (d, *J* = 9.0 Hz, 1H), 7.69 (dd, *J* = 9.0, 2.3 Hz, 1H), 7.64 – 7.53 (m, 2H), 7.51 – 7.42 (m, 1H), 7.35 – 7.27 (m, 1H), 7.21 (t, *J* = 9.1 Hz, 1H), 5.13 (s, 1H), 4.37 (s, 1H), 1.52 (d, *J* = 7.2 Hz, 3H), 1.45 (s, 9H); **^{13}C NMR** (75 MHz, $CDCl_3$) δ 195.47 (s), 172.42 (s), 159.56 (d, *J* = 253.2 Hz), 155.28 (s), 139.68 (s), 137.97 (s), 135.97 (d, *J* = 1.9 Hz),

133.62 (d, *J* = 8.4 Hz), 130.31 (d, *J* = 2.4 Hz), 126.77 (d, *J* = 14.5 Hz), 124.51 (s), 124.46 (s), 122.63 (s), 116.55 (d, *J* = 21.4 Hz), 114.95 (s), 80.26 (s), 51.86 (s), 28.26 (s), 18.58 (s); **HRMS** (ESI/IT-TOF) m/z: $[M + H]^+$ Calcd for $C_{21}H_{23}BrFN_2O_4$ 465.0820; found 465.0845.

MIDD0002B: DCC Route (Table 22, entry 2)

The same procedure as above (**entry 1**) was employed on 68 mmol scale using a 48 hr reaction time instead of 24 hr to afford the product (**MIDD0002B**) as a white solid (18.9 g, 60.0%).

MIDD0002B: DCC Route (Table 22, entry 3)

The same procedure as above (**entry 1**) was employed on 68 mmol scale using a 35-40ºC reaction temperature (instead of 20-25 ºC) for 24 hr to afford the product (**MIDD0002B**) as a white solid (17.4 g, 55.0%).

MIDD0002B: DCC Route (Table 22, entry 4)

The same procedure as above (**entry 1**) was modified (68 mmol scale) to employ 2 equivalents of Boc-D-alanine (136 mmol) and DCC (136 mmol), respectively to afford the product (**MIDD0002B**) as a white solid (19.6 g, 62.2%).

MIDD0002B: DCC Route (Table 22, entry 5)

The same procedure as above (**entry 1**) was modified (68 mmol scale) to switch the addition sequence of the reagents. To a mixture of 2-amino-5-bromo-2'-fluorobenzophenone, DCC and dichloromethane was added a solution of Boc-D-alanine in dichloromethane over 30 min, while

maintaining the temperature at 0-5ºC. The white slurry, which resulted, was allowed to warm to rt with stirring over 24 hr. After the same work-up procedure in **entry 1**, the product (**MIDD0002B**) was afforded as a white solid (18.1 g, 57.2%).

MIDD0002B: DCC Route (Table 22, entry 6)

The same procedure as above (**entry 1**) was modified (68 mmol scale) to switch the addition sequence of the reagents. To a mixture of Boc-D-alanine, DCC and dichloromethane was added a solution of 2-amino-5-bromo-2'-fluorobenzophenone in dichloromethane over 30 min while keeping the temperature at 0-5ºC. The white slurry, which resulted, was allowed to warm to rt with stirring over 24 hr. After the same work-up procedure in **entry 1**, the product (**MIDD0002B**) was afforded as a white solid (3.0 g, 9.6%).

MIDD0002B: DCC Route (Table 22, entry 7)

The same procedure as above (**entry 1**) was modified (68 mmol scale) to employ 0.1 equivalents of DMAP (6.8 mmol), which afforded the product (**MIDD0002B**) as a white solid (16.8 g, 53.4%).

MIDD0002B: DCC Route (Table 22, entry 8)

The same procedure as above (**entry 1**) was modified (68 mmol scale) to employ 1.0 equivalents of DMAP (68 mmol), which afforded the product (**MIDD0002B**) as a white solid (15.9 g, 50.2%).

MIDD0002B: DCC Route (Table 22, entry 9)

The same procedure as above (**entry 1**) was modified (68 mmol scale) to employ acetonitrile as the reaction solvent instead of dichloromethane, which afforded the product (**MIDD0002B**) as a white solid (2.7 g, 8.7%).

3.4.2.1.8. *tert*-Butyl (*R*)-(1-((4-bromo-2-(2-fluorobenzoyl)phenyl)amino)-1-oxopropan-2-yl)carbamate [MIDD0002B]: EDC Route (Table 22, entry 10)

A mixture of 2-amino-5-bromo-2'-fluorobenzophenone (**MIDD0002A**, 6.5 g, 22.1mmol), Boc-D-alanine (**MIDD0101A**, 4.6 g, 24.3 mmol), triethylamine (2.9g, 28.7 mmol) and dichloromethane (50 mL) was stirred at rt for 30 min to dissolve the starting materials. The solution, which resulted, was cooled to 0-5ºC and *N*-(3-dimethylaminopropyl)-*N′*-ethylcarbodimide hydrochloride (EDC, 5.5 g, 28.7 mmol) was added in one portion. The yellow solution, which resulted, was allowed to warm to rt with stirring over 24 hr, at which point analysis of the reaction progress by TLC indicated a 40/60 mixture of product to starting material (silica gel plate; 50% ethyl acetate /

hexanes, ***Rf*** MIDD0002A: 0.5 / ***Rf*** MIDD0002B: 0.4). The reaction mixture was diluted with water (50 mL). The biphasic mixture, which resulted, was allowed to stand for 15 min and the layers were separated. The organic layer was then washed with a solution of 25% aq potassium carbonate (50 mL) and then with 10% aq sodium chloride (50 mL). The organic layer was dried (Na_2SO_4, 200 g). The solvents were removed under reduced pressure and the residue was triturated with 10% ethyl acetate / hexanes (100 mL) to afford the product as a white solid. The solid, which resulted, was filtered and washed with hexanes (10mL x 2). The solid was dried under vacuum at 35 – 40ºC to afford the product as a white solid (1.0 g, 10.2%).

MIDD0002B: EDC Route (Table 22, entry 11)

The same procedure as above (**entry 10**) was employed using 4-(dimethylamino) pyridine (3.5g, 28.7 mmol) instead of TEA to afford the product (**MIDD0002B**) as a white solid (4.0 g, 38.8%).

3.4.2.1.9. *tert*-Butyl (*R*)-(1-((4-bromo-2-(2-fluorobenzoyl)phenyl)amino)-1-oxopropan-2-yl)carbamate [MIDD0002B]: Mixed Anhydride Route (Table 22, entry 12)

A mixture of Boc-D-alanine (MIDD0101A, 4.1g, 21.6 mmol) and *N*-methylmorpholine (2.7 mL, 32.3 mmol) in tetrahydrofuran (100 mL) was cooled to -20ºC using a dry ice / IPA bath. To the solution, which resulted, was added methyl chloroformate (1.7 mL, 32.3 mmol) dropwise over 20 min while keeping the temperature at -20 to -15ºC. To the white slurry, which resulted, was added a solution of 2-amino-5-bromo-2'-fluorobenzophenone (6.3 g, 21.6 mmol), *N*-methylmorpholine (2.7 mL, 32.3 mmol) and tetrahydrofuran (50 mL) dropwise to the reaction mixture over a 15 min period, while keeping the temperature at -20 to -15ºC. The white slurry, which resulted, was allowed to warm to rt with stirring over 24 hr, at which point analysis of the reaction progress by

TLC indicated a 50/50 mixture of product to starting material (silica gel; 50% ethyl acetate / hexanes, ***Rf*** MIDD0002A: 0.5 / ***Rf*** MIDD0002B: 0.4). The solvents were removed under reduced pressure. The residue, which resulted, was dissolved in dichloromethane (100 mL) and 25% aq sodium chloride (100 mL). The biphasic mixture, which resulted, was allowed to stand for 15 min and the layers were separated. The organic layer was then washed twice with 25% aq potassium carbonate (100 mL x 2). The organic layer was dried (Na_2SO_4). The solvents were removed under reduced pressure and the residue was triturated with 10% ethylacetate / hexanes (40 mL) to afford the product as a white solid. The solid, which resulted, was filtered and washed with hexanes (10mL x 2). The solid was dried under vacuum at 35 – 40°C to afford the product as a white solid (4.9 g, 50.0%).

MIDD0002B: Mixed Anhydride Route (Table 22, entry 13)

The same procedure as above (**entry 12**) was employed using ethyl chloroformate (3.1 mL, 32.3 mmol) instead to afford the product (**MIDD0002B**) as a white solid (2.2 g, 25%).

MIDD0002B: Mixed Anhydride Route (Table 22, entry 14)

The same procedure as above (**entry 12**) was employed using isobutyl chloroformate (4.2 mL, 32.3 mmol) instead to afford the product (**MIDD0002B**) as a white solid (2.7 g, 22%).

3.4.2.1.10. (*R*)-7-Bromo-5-(2-fluorophenyl)-3-methyl-1,3-dihydro-2*H*-benzo[*e*][1,4]diazepin-2-one [MIDD0002]: BOC route (Table 23, entry 2)

A mixture of *tert*-butyl-(*R*)-(1-((4-bromo-2-(2-fluorobenzoyl)phenyl)amino)-1-oxopropan-2-yl)carbamate (**MIDD0002B**, 55 g, 118.2 mmol) and dichloromethane (500 mL) was cooled to 0-

5 ºC. A solution of 4.0M hydrogen chloride in dioxane (118 mL, 472.8 mmol) was added dropwise to the reaction mixture at 0 – 5ºC over 60 min. The reaction mixture was then held at 0 – 5ºC for 4 h at which point the reaction was deemed complete by TLC analysis (silica gel and 50% ethyl acetate / hexanes). Upon completion of the reaction process, the reaction mixture was diluted with a solution of 10% aq sodium bicarbonate (500 mL). The biphasic mixture, which resulted, was allowed to stand for 15 min and the layers were separated. The aq layer was then extracted with dichloromethane (500 mL) and the combined organic layers were washed with 5% aq sodium bicarbonate solution (500 mL) and then twice with deionized water (500 mL x 2). The solvents were removed under reduced pressure and the residue was dissolved in methanol (500 mL). A solution of sodium hydroxide (0.5 g, 11.8 mmol) in deionized water (50 mL) was added dropwise to the reaction mixture over 15 min. The reaction mixture was then held at 20 – 25ºC for 48 h at which point the reaction was deemed complete on analysis by TLC (silica gel; 50% ethyl acetate / hexanes). Upon completion of the reaction the solvents were removed under reduced pressure. The semi-solid which resulted was dissolved in dichloromethane (500 mL) and 10% aq sodium chloride (500 mL). The biphasic mixture, which resulted, was allowed to stand for 15 min and the layers were separated. The aq layer was then extracted with dichloromethane (500 mL) and the combined organic layers were then washed with 10% aq sodium chloride (500 mL). The organic layer was dried (Na_2SO_4). The solvent was removed under reduced pressure and the residue was solvent exchanged to 10% ethyl acetate / heptane (200 mL x 2). The residue was then slurried with 10% ethyl acetate / heptane (500 mL) at 60 – 65ºC for 30 min to dissolve the starting material, **MIDD0002A**. Upon cooling to rt and after holding for 2 h, the solid product was collected by filtration and washed with 10% ethyl acetate / heptane (50 mL x 2) and then heptane (50 mL x 2). The solid was dried under vacuum at 35 – 40ºC to afford the product as an off-white solid (34.6 g,

84.2%): **^{1}H NMR** (500 MHz, $CDCl_3$) δ 9.69 (s, 1H), 7.63 – 7.59 (m, 1H), 7.59 (dd, *J* = 8.5, 2.3 Hz, 1H), 7.47 (dddd, *J* = 8.2, 7.0, 5.0, 1.8 Hz, 1H), 7.36 (d, *J* = 2.2 Hz, 1H), 7.26 (td, *J* = 7.5, 1.1 Hz, 1H), 7.12 (d, *J* = 8.6 Hz, 1H), 7.08 (ddd, *J* = 10.2, 8.3, 1.1 Hz, 1H), 3.79 (q, *J* = 6.5 Hz, 1H), 1.78 (d, *J* = 6.5 Hz, 3H); **^{13}C NMR** (126 MHz, $CDCl_3$) δ 172.39 (s), 164.53 (s), 160.45 (d, $^{1}J_{CF}$ = 251.9 Hz), 136.47 (s), 134.74 (s), 132.19 (d, $^{3}J_{CF}$ = 8.3 Hz), 132.03 (d, J_{CF} = 1.5 Hz, NOE coupling), 131.56 (d, $^{3}J_{CF}$ = 2.2 Hz), 130.15 (s), 127.13 (d, $^{2}J_{CF}$ = 12.4 Hz), 124.46 (d, $^{4}J_{CF}$ = 3.6 Hz), 122.98 (s), 116.54 (s), 116.29 (d, $^{2}J_{CF}$ = 21.5 Hz), 58.85 (s), 16.93 (s); **HRMS** (ESI/IT-TOF): m/z [M + H]+ calcd for $C_{16}H_{13}BrFN_2O$: 347.0190; found: 347.0181; **HPLC Purity**: 99.9%; **Optical Purity**: 53.9%.

MIDD0002: BOC route (Table 23, entry 3)

The same procedure as above (**entry 2**) was modified on 121.9 mmol scale to employ 1.0 eq sodium hydroxide (121.9 mmol) and a reaction time of 12 h at 20 – 25ºC for the benzodiazepine cyclization step to afford the product (**MIDD0002B**) as a white solid (21.0 g, 50.0%): **HPLC Purity**: 99.9%; **Optical Purity**: racemic.

MIDD0002: BOC route (Table 23, entry 4)

The same procedure as above (**entry 2**) was modified on 121.9 mmol scale to employ no sodium hydroxide and toluene at 60-65ºC for the benzodiazepine cyclization step to afford the product (**MIDD0002B**) as a white solid (21.0 g, 50.0%): **HPLC Purity**: 99.9%; **Optical Purity**: 99.9%. A mixture of *tert*-butyl-(*R*)-(1-((4-bromo-2-(2-fluorobenzoyl)phenyl)amino)-1-oxopropan-2-yl)carbamate (**MIDD0002B**, 56.7 g, 121.9 mmol) and dichloromethane (500 mL) was cooled to

0-5 ºC. A solution of 4.0M hydrogen chloride in dioxane (121 mL, 487.4 mmol) was added dropwise to the reaction mixture at 0 – 5ºC over 60 min. The reaction mixture was then held at 0 – 5ºC for 4 h at which point the reaction was deemed complete by TLC analysis (silica gel and 50% ethyl acetate / hexanes). Upon completion of the reaction process, the reaction mixture was diluted with a solution of 10% aq sodium bicarbonate (500 mL). The biphasic mixture, which resulted, was allowed to stand for 15 min and the layers were separated. The aq layer was then extracted with dichloromethane (500 mL) and the combined organic layers were washed with 5% aq sodium bicarbonate solution (500 mL) and then twice with deionized water (500 mL x 2). The solvents were removed under reduced pressure and the residue was dissolved in toluene (500 mL). The reaction mixture was then heated at 60 – 65ºC for 4 h at which point the reaction was deemed complete on analysis by TLC (silica gel; 50% ethyl acetate / hexanes). Upon completion of the reaction the solvents were removed under reduced pressure. The semi-solid which resulted was dissolved in dichloromethane (500 mL) and 10% aq sodium chloride (500 mL). The biphasic mixture, which resulted, was allowed to stand for 15 min and the layers were separated. The aq layer was then extracted with dichloromethane (500 mL) and the combined organic layers were then washed with 10% aq sodium chloride (500 mL). The organic layer was dried (Na_2SO_4). The solvent was removed under reduced pressure and the residue was solvent exchanged to 10% ethyl acetate / heptane (200 mL x 2). The residue was then slurried with 10% ethyl acetate / heptane (500 mL) at 60 – 65ºC for 30 min to dissolve the starting material, **MIDD0002A**. Upon cooling to rt and after holding for 2 h, the solid product was collected by filtration and washed with 10% ethyl acetate / heptane (50 mL x 2) and then heptane (50 mL x 2). The solid was dried under vacuum at 35 – 40ºC to afford the (**MIDD0002B**) as a white solid (21.0 g, 50.0%): **HPLC Purity**: 99.9%; **Optical Purity**: 99.9%.

3.4.2.2. General Analytical Procedures for the Synthesis of MIDD0301

3.4.2.2.1. Method 1: HPLC-PDA-MS Reverse Phase Method for Overall Purity Determination of MIDD0002 and MIDD0003

Purity was determined using absolute area %. 0.1% formic acid in methanol and 0.1% formic acid in water was used as mobile phase. High performance liquid chromatography (Shimadzu Nexara series) with a Photo Diode Array detector (PDA, Shimadzu SPD-M30A) and a single quadrupole mass analyzer (LCMS 2020, Shimadzu, Kyoto, Japan) was used. Analytes were separated by with a Restek Pinnacle-C18 (4.6 mm x 50 mm, 5 µm particle size) column with gradient elution at a flow rate of 0.8 mL/min. Time program of mobile phase elution included in Table 1. Data was acquired by PDA having a range of 190-700 nm but 254 nm was used for detection. Mass spectrometer was equipped with a DUIS ionization probe (having both electrospray and atmospheric pressure ionization). Mass range was set m/z 200-800 for both positive and negative mode. Scan speed was 5000 u/sec, Interface, desolvation line and heat block temperature was 350°C, 250°C and 400°C respectively. Nebulizing gas flow was 1.5 L/min and drying gas flow was 15 L/min.

Table 1. Time program for Method 1.

Time (min)	Mobile Phase B% (0.1% formic acid in Methanol)
0	40
3.5	55
5.5	55
10	70
11	100
12	100

3.4.2.2.2. Method 2: HPLC-PDA-MS Reverse Phase Method for Overall Purity Determination of MIDD0301

Purity was determined using absolute area %. 0.1% formic acid in methanol and 0.1% formic acid in water was used as mobile phase. High performance liquid chromatography (Shimadzu Nexara series) with a Photo Diode Array detector (PDA, Shimadzu SPD-M30A) and a single quadrupole mass analyzer (LCMS 2020, Shimadzu, Kyoto, Japan) was used. Analytes were separated by with a Restek Pinnacle-C18 (4.6 mm x 50 mm, 5 µm particle size) column with gradient elution at a flow rate of 0.8 mL/min. Time program of mobile phase elution included in Table 2. Data was acquired by PDA having a range of 190-700 nm but 254 nm was used for detection. Mass spectrometer was equipped with a DUIS ionization probe (having both electrospray and atmospheric pressure ionization). Mass range was set m/z 200-800 for both positive and negative mode. Scan speed was 5000 u/sec, Interface, desolvation line and heat block temperature was 350°C, 250°C and 400°C respectively. Nebulizing gas flow was 1.5 L/min and drying gas flow was 15 L/min.

Table 2. Time program for method 2

Time (min)	Mobile Phase B% (0.1% formic acid in Methanol)
0	40
2.7	80
3.7	100
4.2	100
5	40

3.4.2.2.3. Method 3: HPLC-DAD Normal Phase Method for the Determination of Optical Purity of *R*-MIDD0002

An isocratic mixture of 92% hexane and 8% ethanol was used as mobile phase to resolve R and S enantiomers of **MIDD0002**. An Agilent 1100 HPLC system consisting of a quaternary pump, autosampler and a DAD detector was used in combination with a Pirkle Whelk-01 column (4.6

mm x 25 cm, 5 μm particle size). A racemic mixture was used for the verification of the method. The S enantiomer eluted at 10.12 min and the R enantiomer at 11.89 min. The resolution between peaks was 2.8. Flow rate was 1 mL/min and DAD wavelength range was set 200-400 nm. A 254 nm wavelength was used for relative % area determination and the enantiomeric excess was calculated using % ee = (R-S)/(R+S) x 100.

3.4.2.2.4. Method 4: HPLC-DAD Normal Phase Method for the Determination of Optical Purity of *R*-MIDD0003

An isocratic mixture of 65% hexane and 35% ethanol was used as mobile phase to resolve R and S enantiomers of **MIDD0003**. An Agilent 1100 HPLC system consisting of a quaternary pump, autosampler and a DAD detector was used in combination with a Pirkle Whelk-01 column (4.6 mm x 25 cm, 5 μm particle size). A racemic mixture was used for the verification of the method. The R enantiomer eluted at 13.88 min and the S enantiomer at 23.69 min. The resolution between peaks was 5.6. Flow rate was 1 mL/min and DAD wavelength range was set 200-400 nm. A 254 nm wavelength was used for relative % area determination and the enantiomeric excess was calculated using % ee = (R-S)/(R+S) x 100.

3.4.2.2.5. Method 5: HPLC-DAD Normal Method for Determination of Optical Purity of R-MIDD0301

An isocratic mixture of 90% Hexane and 10% ethanol was used as mobile phase to resolve R and S enantiomers of **MIDD0301**. An Agilent 1100 HPLC system consisting of a quaternary pump, autosampler and a DAD detector was used in combination with a Chiralpak IB-N3 (4.6 mm x 15

cm, 3 μm). A racemic mixture was used for the verification of the method. The R enantiomer eluated at 9.60 min and the S enantiomer at 12.5 min. The resolution between peaks was 4.9. Flow rate was 1 mL/min and DAD wavelength range was set 200-400 nm. A 254 nm wavelength was used for relative % area determination and the enantiomeric excess was calculated using % ee = (R-S)/(R+S) x 100.

3.4.2.3. Chromatograms (HPLC Purity, Optical Purity and Mass Spectra) from the Synthesis of MIDD0301

3.4.2.3.1. HPLC Chromatogram (245 nm) for MIDD0002 (Method 1)

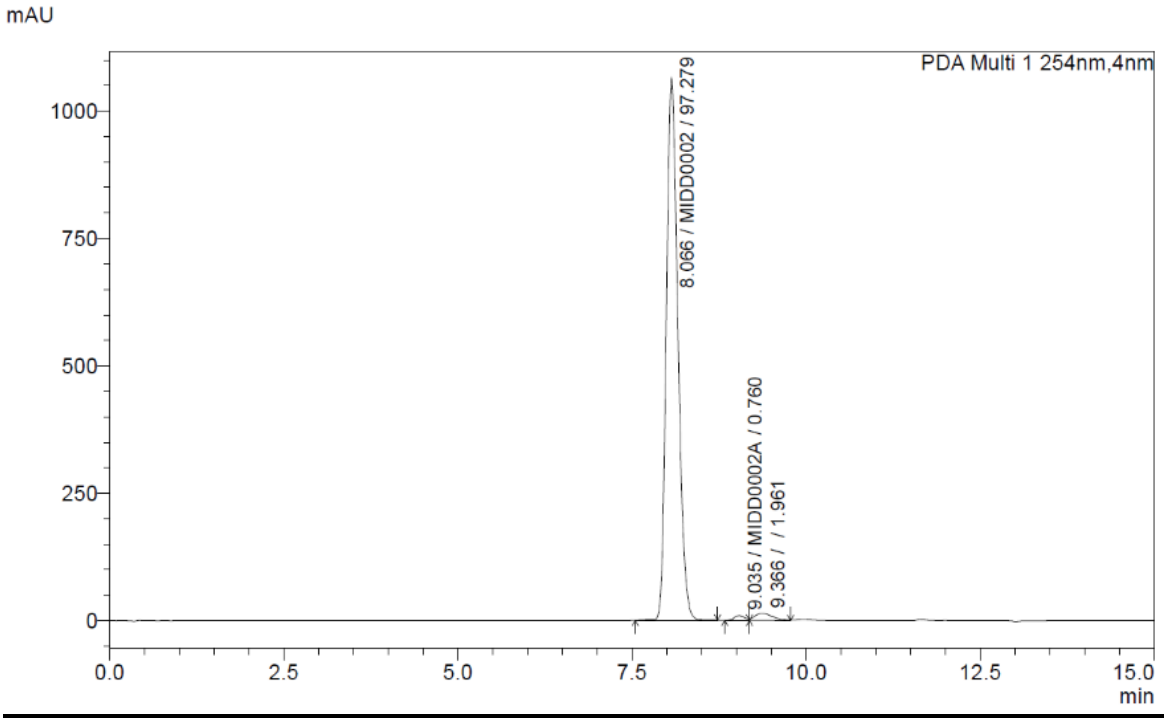

3.4.2.3.2. UV Spectrum of MIDD0002 and Impurities

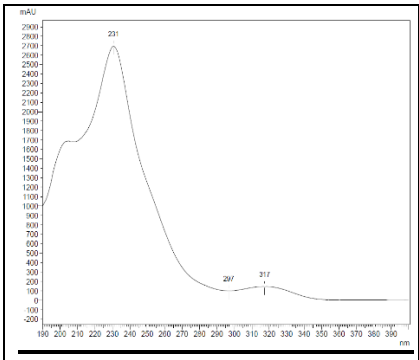	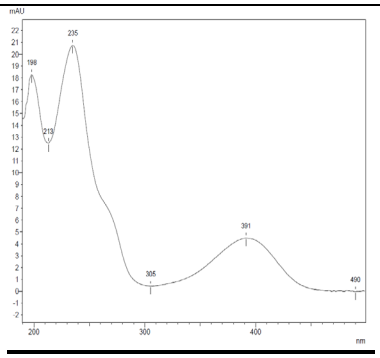	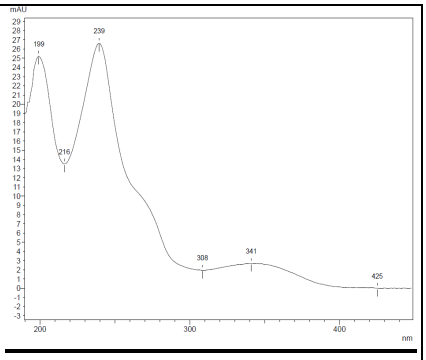
8.07 min (MIDD0002)	**9.04 min (MIDD0002a)**	**9.37 min (MIDD0002b)**

3.4.2.3.3. Mass Spectrum of MIDD0002 (RT 8.07 min, Method 1) (97.28 % absolute area)

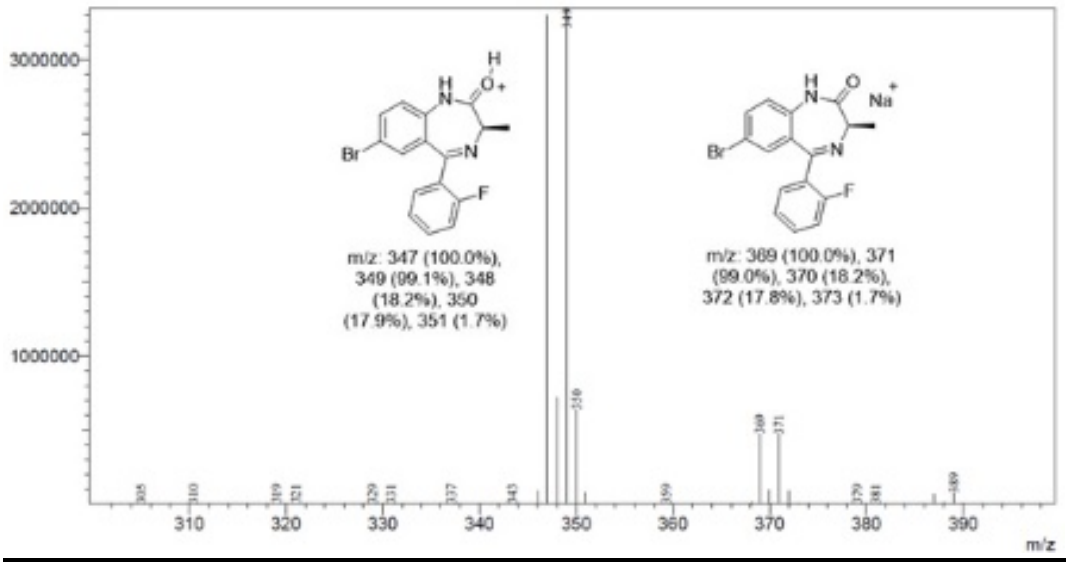

3.4.2.3.4. Mass Spectrum of Impurities (MIDD0002a) for Synthesis of MIDD0002: (RT 9.04, Method 1) (0.76 % absolute area)

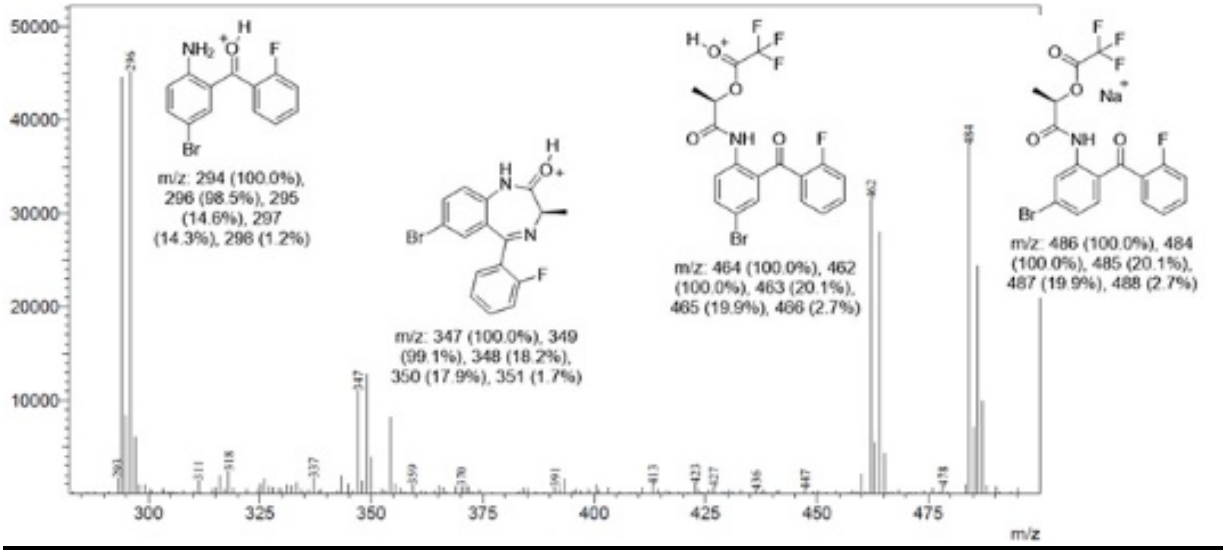

3.4.2.3.5. Mass Spectrum of MIDD0002b Impurity (RT 9.37 min, Method 1) (1.96 % absolute area)

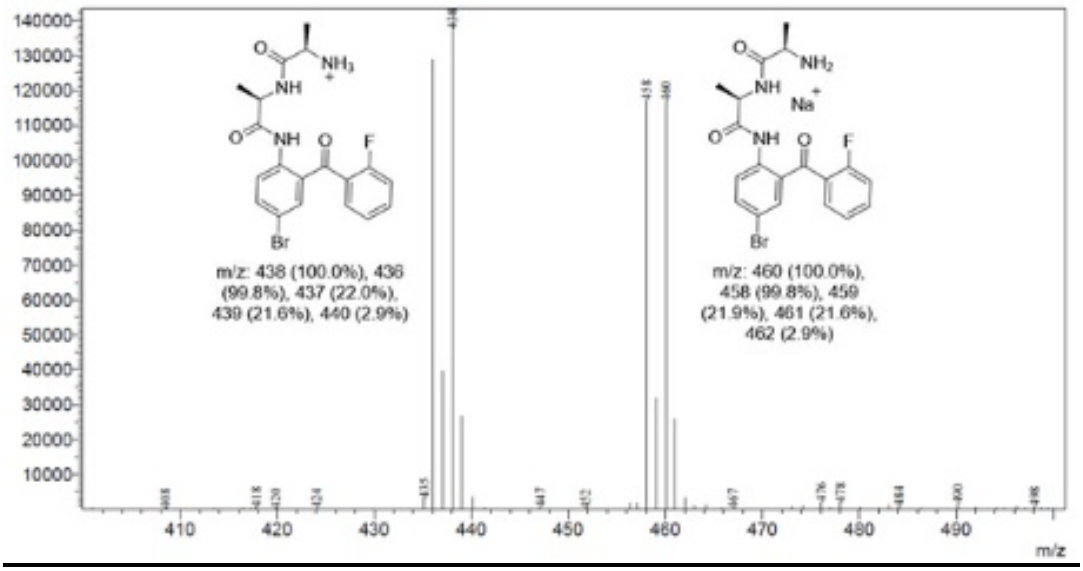

3.4.2.3.6. Optical Purity of MIDD0002 Determined by HPLC (Method 3)

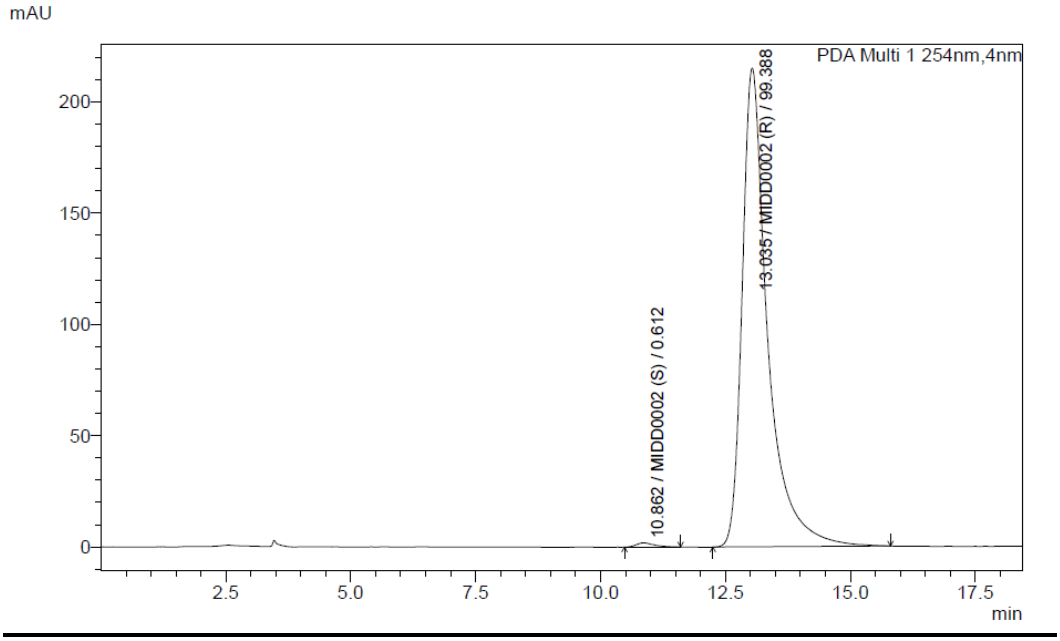

3.4.2.3.7. HPLC Chromatogram (245 nm) for MIDD0003 (Method 1)

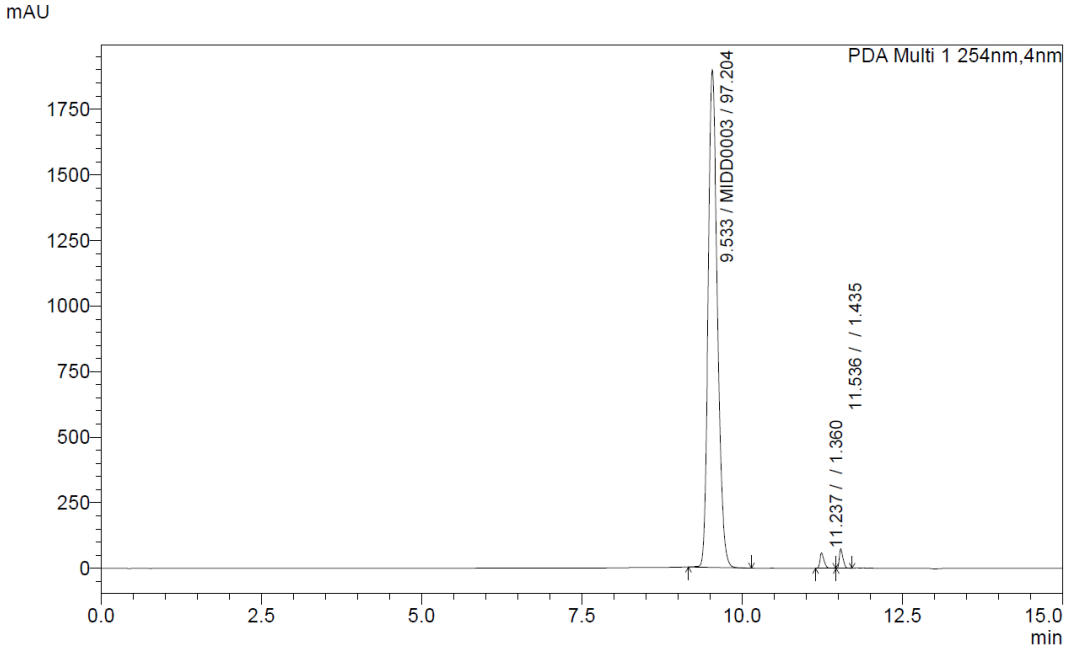

3.4.2.3.8. UV Spectrum of MIDD0003 and Impurities

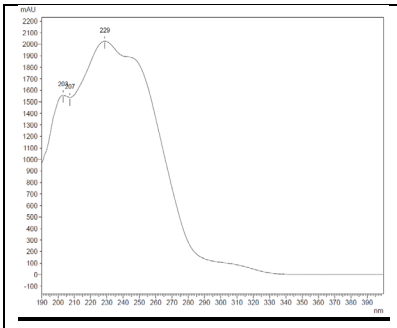	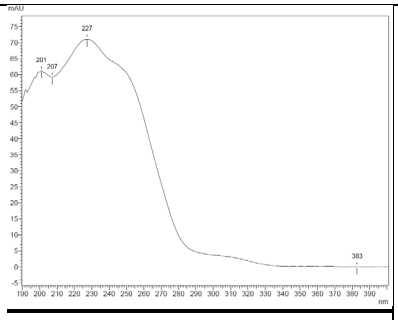	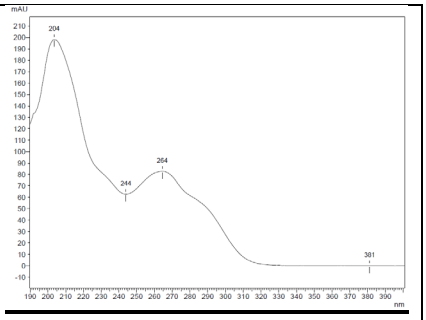
9.53 min (MIDD0003)	**11.23 min (MIDD0003a)**	**11.53 min (MIDD0003b)**

3.4.2.3.9. Mass spectrum of MIDD0003 (RT 9.55 min, Method 1) (97.20 % absolute area)

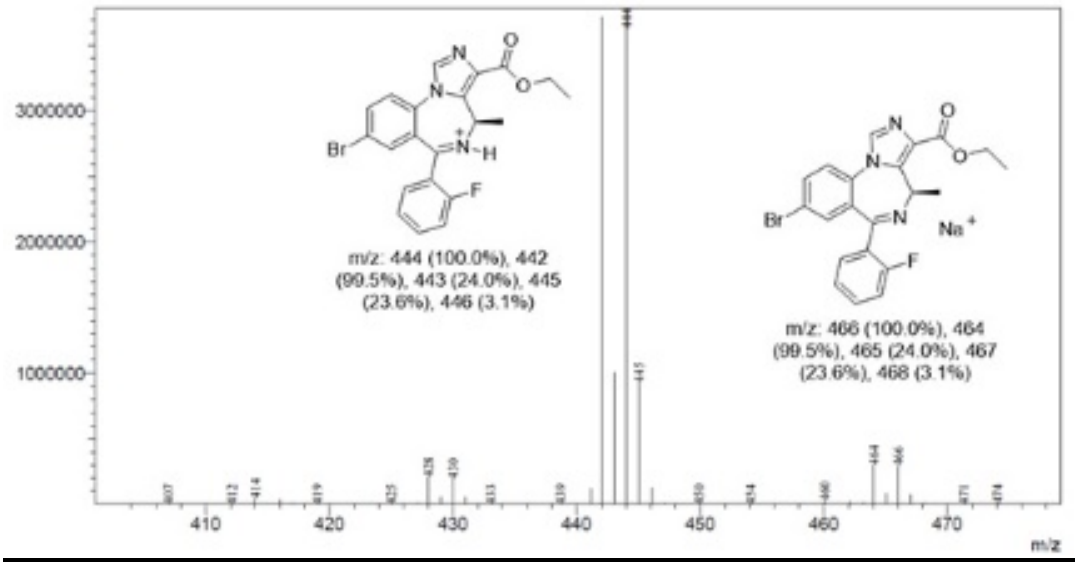

3.4.2.3.10. Mass Spectrum of MIDD0003a (RT 11.24 min, Method 1) (1.36 % absolute area)

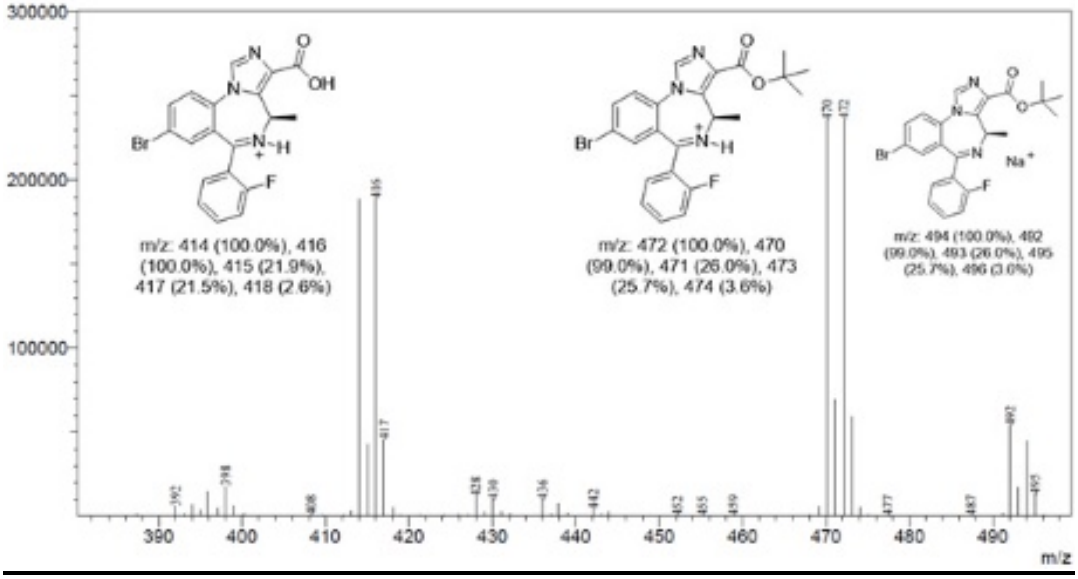

3.4.2.3.11. Mass spectrum of MIDD0003b (RT 11.54 min, method 1) (1.44 % absolute area)

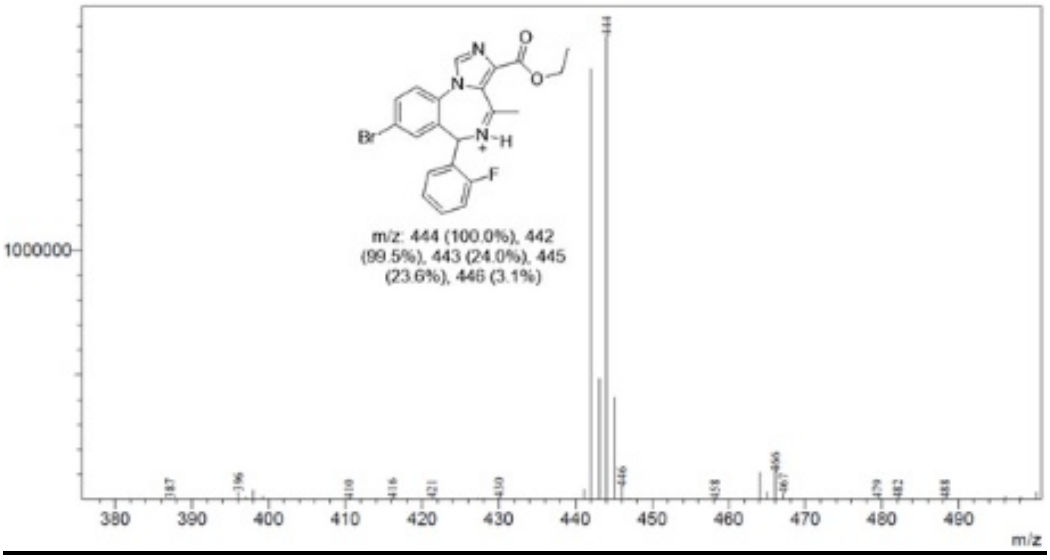

3.4.2.3.12. Optical Purity of MIDD0003 Determined by HPLC (Method 4) 99.0 % EE

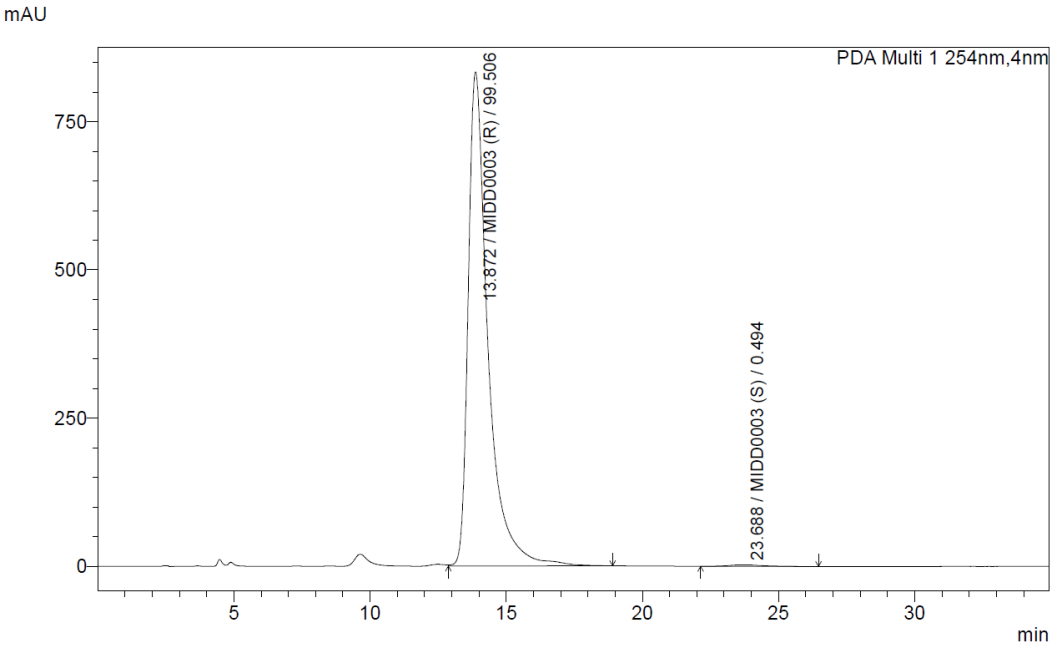

3.4.2.3.13. HPLC Chromatogram (245 nm) for MIDD0301 (Method 2)

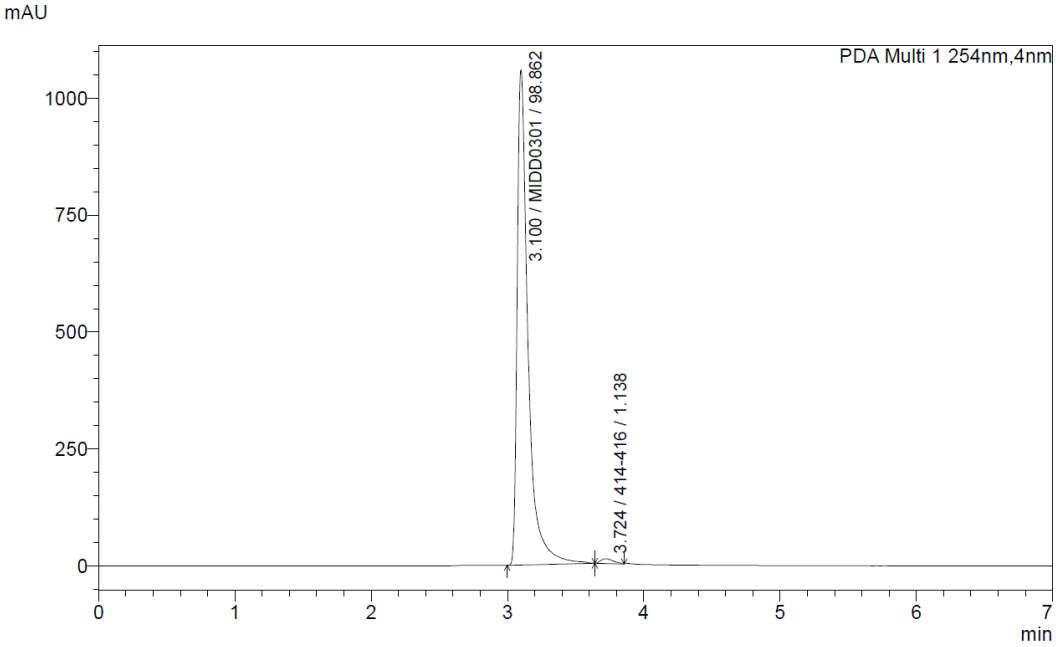

3.4.2.3.14. UV Spectrum of MIDD0301 and Impurities

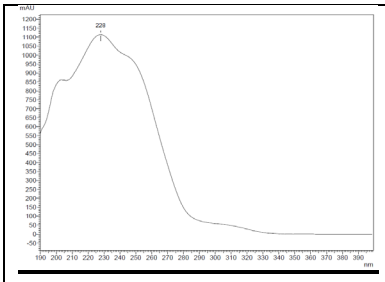	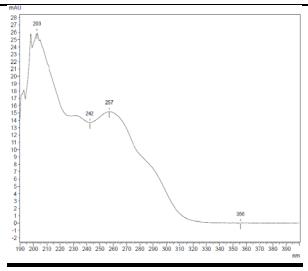
3.10 MIDD0301	**3.72 min MIDD0301a**

3.4.2.3.15. Mass Spectrum of MIDD0301 (RT 3.10 min, Method 2) (98.86 % absolute area)

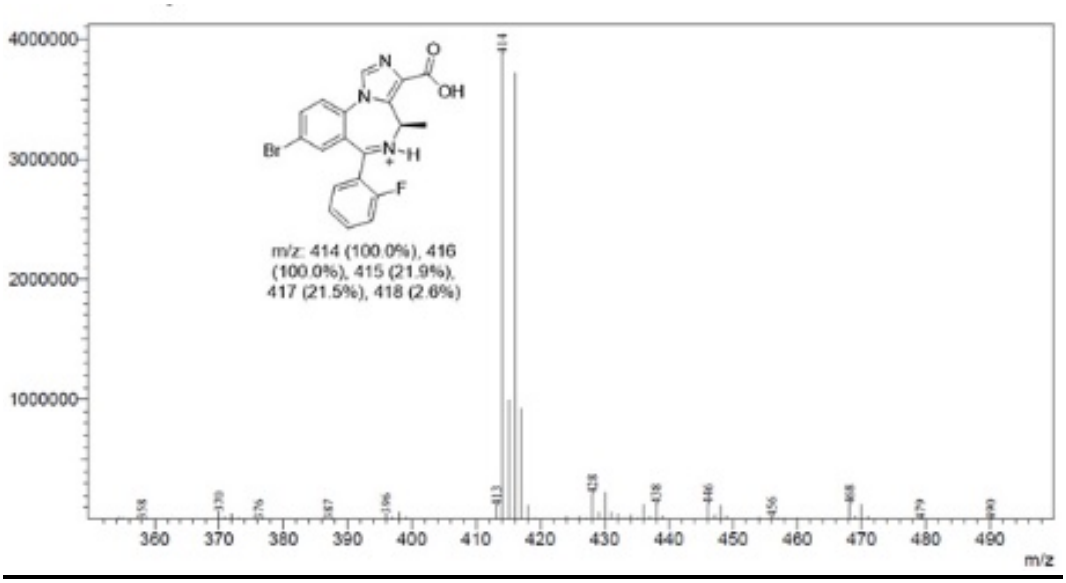

3.4.2.3.16. Mass Spectrum MIDD0301a (RT 3.72 min, Method 2) (1.14 % absolute area)

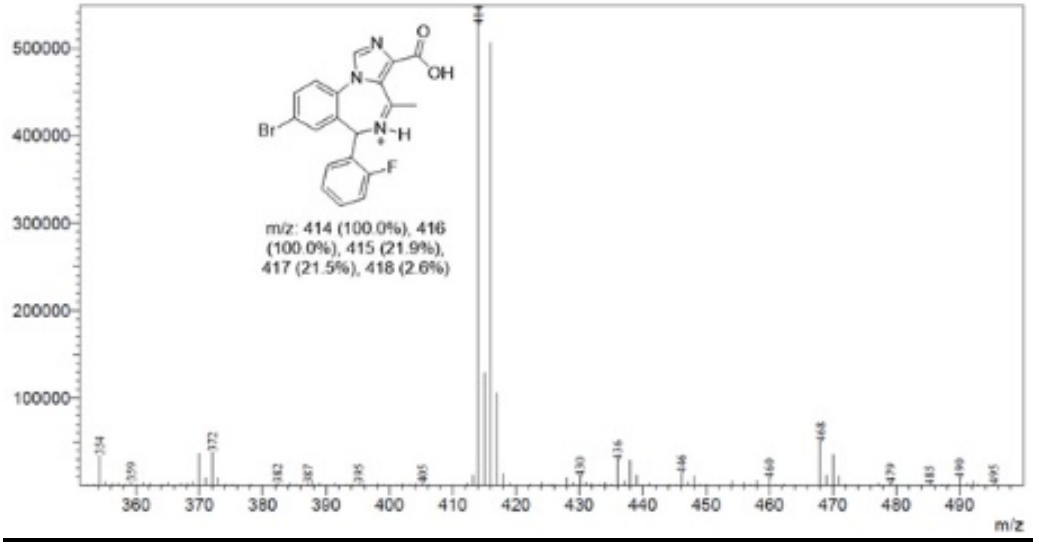

3.4.2.3.17. Optical purity of MIDD0301 determined by HPLC (Method 5) >99.2 % EE

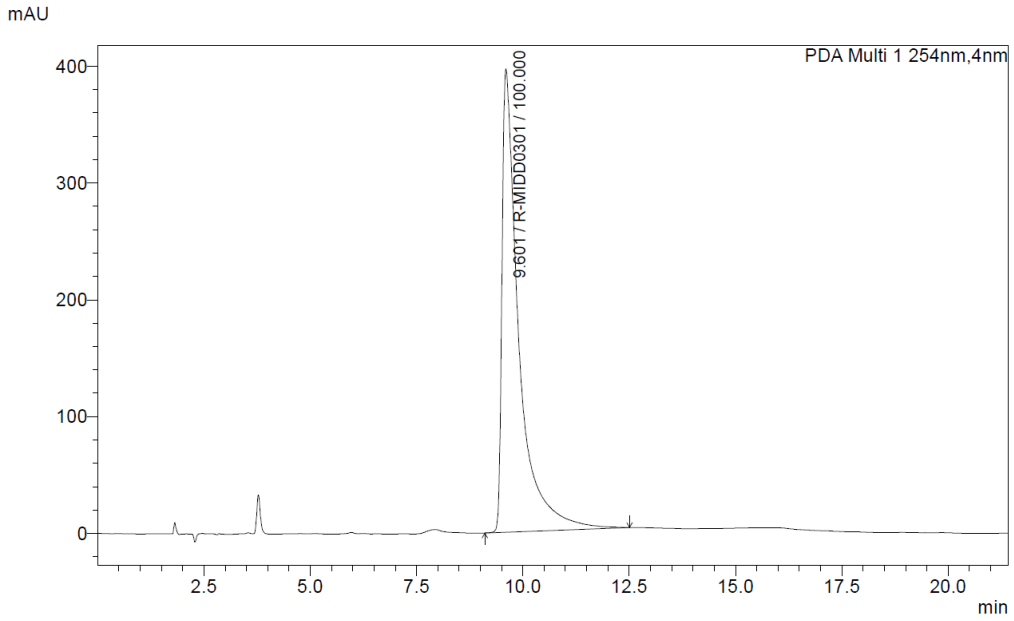

3.4.3. Large-scale Process Improvement of GL-II-73

The biology and synthesis (**Scheme 35**) of **GL-II-73** has been reported before,[254, 304] but the discovery chemistry was not well-suited for scale up in a GMP manufacturing setting and the overall yield was low (9.7%). Six steps of the seven synthetic steps required purification by column chromatography, while several steps exhibited typical scaleup issues such as efficient stirring, side product formation, optical purity issues, prolonged process times and yield loss upon scale up.

Scheme 35: Discovery Synthesis of **GL-II-73**

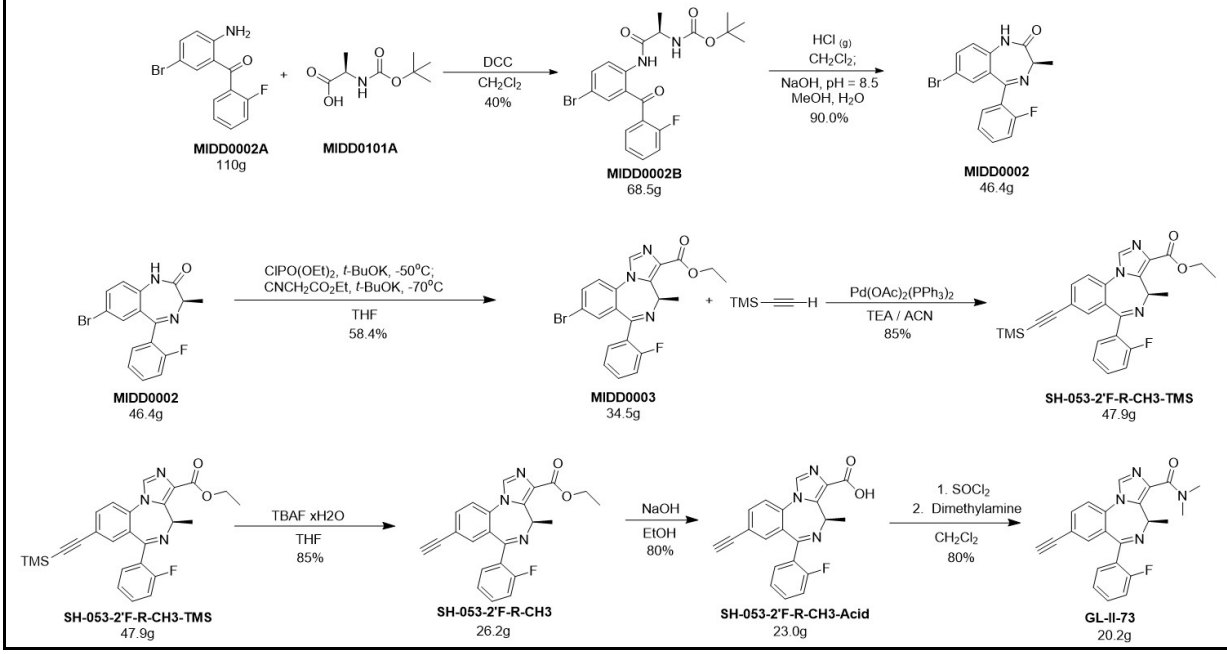

As with the MIDD0301, the same improvements were made in this process improvement endeavor towards a more efficient route to imidazodiazepine, **MIDD0003**. In addition, similar reaction conditions and purification steps were employed that were used with the **HZ-166** synthesis above in regard to the copper-free Sonogashira coupling (TIPs-acetylene with tri-ortho-

tolyl phosphine) reaction and the removal of the TIPS group to provide the aryl-acetylene **SH-053-2'F-R-CH$_3$**. The saponification reaction conditions required modification of the reaction solvent to avoid a thick reaction medium due to the formation of an insoluble and gel-like imidazocarboxylate salt. A switch of the reaction solvent to a THF/water mixture alleviated the stirring issue to afford **SH-053-2'F-R-CH$_3$-acid** in high yield (92%). The final step of the **GL-II-73** synthesis replaced the carboxylic acid function with a dimethyl amide group through an acyl chloride intermediate. The discovery route employed thionyl chloride in solvent quantities along with elevated temperature (60ºC) to afford the acyl chloride. The acyl chloride was then converted into the amide using dimethylamine (2.0 M in THF). Utilization of the catalytical Vilsmeier reagent allowed the reaction temperature to be lowered to 35-40ºC and stoichiometric quantities (10 eq) of thionyl chloride could then be employed to afford the acyl chloride. After conversion into the amide and an aqueous work-up, the product was purified by crystallization using *t*-butyl methyl ether.

In summary, the seven-step synthesis of **GL-II-73** was refined to provide a more reliable and robust procedure (**Scheme 36**) with an improved overall yield (17.0%). Chromatographic purification steps were replaced with large-scale crystallizations, while importantly, the overall reaction times were reduced. Most importantly, the optical purity of the R-methyl function was preserved throughout the synthesis with a final optical purity of 99.3%EE obtained. Additionally, the optical purity of the **MP-III-022** synthesis (**Scheme 37**) was confirmed to hold at 99.3%EE using the long-established methyl amine (33 wt% in ethanol) / sealed tube at 60ºC method.

Scheme 36: Improved **GL-II-73** Synthetic Scheme with 99%EE

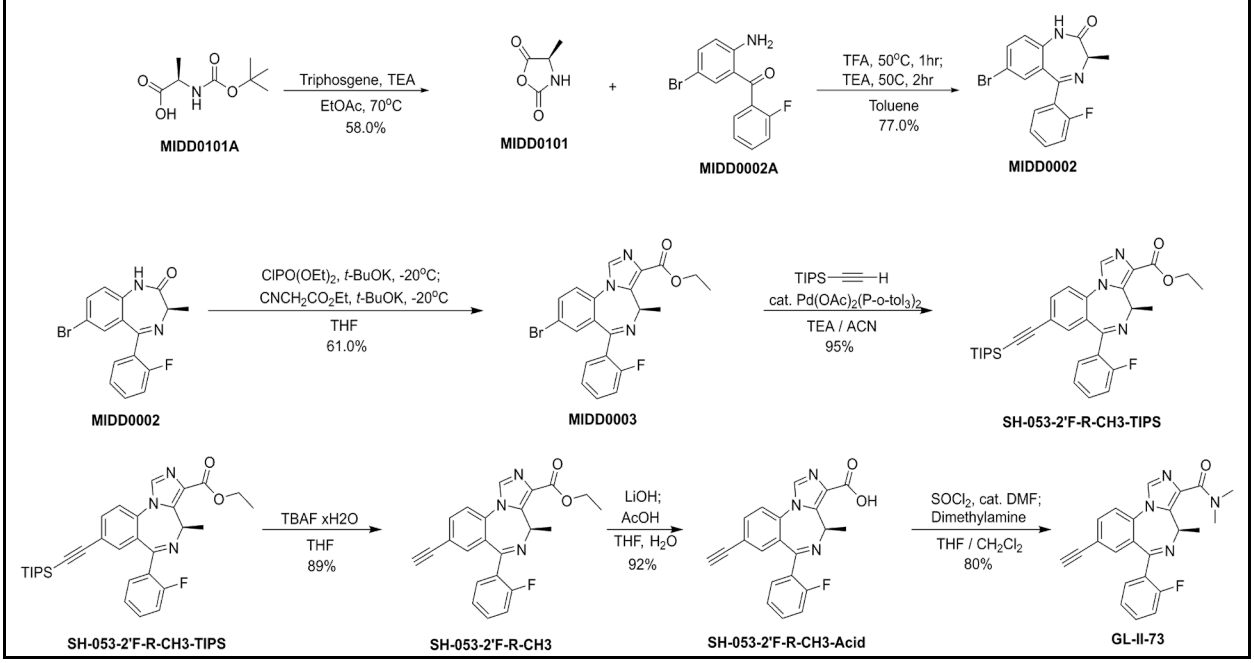

Scheme 37: Synthesis of Optically Pure **MP-III-022**

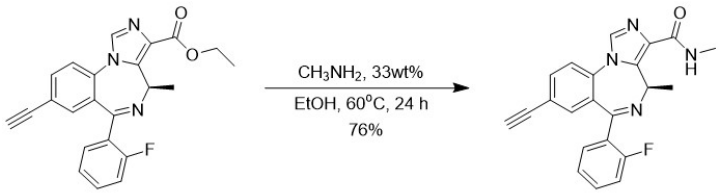

3.4.4. Experimental Section for GL-II-73 and MP-III-022

3.4.4.1. General Procedures for the Synthesis of GL-II-73 and MP-III-022

All reactions were performed in oven-dried round-bottom flasks with magnetic stir bars or overhead mechanical stirrers under an argon. Organic solvents were purified when necessary by standard methods (Vogel Preparative Organic Chemistry) or purchased from Sigma-Aldrich.™ Chemicals were purchased from either Sigma Aldrich™, Oakwood Chemical, Alfa Aesar, Matrix Scientific, or Acros Organic. The ^{1}H, ^{19}F, and ^{13}C NMR spectral data were obtained on Bruker 300 MHz and 500 MHz instruments with the chemical shifts in δ (ppm) reported. The HRMS spectral data were obtained on a LCMS-IT-TOF by Shimadzu Scientific.

3.4.4.1.1. N-Carboxy-D-Alanine Anhydride [MIDD0101]

To a solution of Boc-D-Alanine (100g, 528.5 mmol), triphosgene (62.7g, 211.4 mmol) and anhydrous ethyl acetate (4000mL), triethylamine (81.0mL, 581.4 mmol) was added dropwise over 60 min while keeping the temperature between 25 – 30 ºC and while monitoring the $CO_{2(g)}$ and $HCl_{(g)}$ evolution. The reaction mixture, which resulted, was then allowed to stir 1 h at 25 – 30 ºC and this was followed by 2 h at reflux (65 – 70 ºC) at which point the reaction was deemed complete as gas evolution had ceased. The reaction mixture (a white slurry) was then cooled to rt. The white solid (TEA-HCl and residual D-Alanine) was removed by filtration to yield a pale-yellow solution. The solid was washed with 2 portions of ethyl acetate (2 x 100 mL) and the filtrates were combined. The ethyl acetate was removed under reduced pressure to yield a semi-solid mass. The residue was then dissolved in dichloromethane (400 mL). The product was then

precipitated by a dropwise addition of hexanes (400mL) over 1 hr with vigorous stirring. The resulting product slurry was then placed in a freezer at -20 ºC for 12 hr to maximize product precipitation. The solid was filtered and washed with hexanes (250 mL x 2). The solid was dried under vacuum at rt to afford the product (**MIDD0101**) as an off-white solid (35.2 g, 58.0%): **^{1}H NMR** (500 MHz, DMSO-d_6) δ 9.01 (s, 1H), 4.48 (qd, J = 7.0, 1.1 Hz, 1H), 1.34 (d, J = 7.1 Hz, 3H); **^{13}C NMR** (126 MHz, DMSO-d_6) δ 172.88, 152.15, 53.28, 17.23; **HRMS** (ESI/IT-TOF): m/z [M + H]+ calcd for $C_4H_6NO_3$: 116.0348; found: 116.0350.

3.4.4.1.2. (*R*)-7-Bromo-5-(2-fluorophenyl)-3-methyl-1,3-dihydro-2H-benzo[*e*][1,4]diazepin-2-one [MIDD0002]

A mixture of 2-amino-5-bromo-2'-fluorobenzophenone (**MIDD0002A**, 140.7 g, 478.4 mmol), anhydrous trifluoroacetic acid (73.3 mL, 956.7 mmol) and anhydrous toluene (2200 mL) was stirred at rt for 30 min to dissolve the starting material. The solid N-carboxy-D-alanine anhydride (**MIDD0101**, 66.0g, 574.0 mmol) was then added to the reaction mixture. The reaction mixture was then heated at 50 – 55 ºC for 1 h at which point the reaction was deemed complete (intermediate TFA salt formation, <5% 2-amino-5-bromo-2'-fluorobenzophenone remained, ***Rf*** = 0.8 (100% EtOAc)) on analysis by TLC (silica gel; 50% ethyl acetate / hexanes). Upon completion of the reaction, anhydrous triethylamine (133.3 mL, 956.7 mmol) was added dropwise to the reaction mixture over 30 min while maintaining the temperature at 50 – 55 ºC. The reaction mixture was then held at 50 – 55 ºC for 2 h, at which point the reaction was deemed complete (disappearance of intermediate TFA salt, ***Rf*** = 0.1 (100% EtOAc)) by analysis by TLC (silica gel; 50% ethyl acetate / hexanes). Upon cooling the reaction mixture to rt, the solvents were removed under reduced pressure and the residue was dissolved in ethyl acetate (1500 mL) and water (1500

mL). The biphasic mixture, which resulted, was allowed to stand for 15 min and the layers were separated. The organic layer was washed with 5% aq sodium bicarbonate solution (1500 mL) and then 10% aq sodium chloride solution (1500mL). The organic layer was dried (Na_2SO_4, 50 g). The ethyl acetate was removed under reduced pressure and the residue was solvent exchanged to 10% ethyl acetate / heptane (25 mL x 2). The residue was then slurried with 10% ethyl acetate / heptane (1700 mL) at 60 – 65 ºC for 30 min to dissolve the starting material, **MIDD0002A**. Upon cooling to rt and after holding for 2 h, the solid product was collected by filtration and washed with 10% ethyl acetate / heptane (50 mL x 2) and then heptane (50 mL x 2). The solid was dried under vacuum at 35 – 40 ºC to afford the product as an off-white solid (127.0 g, 77.0%): ***Rf*** = 0.7 (100% EtOAc); **^{1}H NMR** (500 MHz, $CDCl_3$) δ 9.69 (s, 1H), 7.63 – 7.59 (m, 1H), 7.59 (dd, *J* = 8.5, 2.3 Hz, 1H), 7.47 (dddd, *J* = 8.2, 7.0, 5.0, 1.8 Hz, 1H), 7.36 (d, *J* = 2.2 Hz, 1H), 7.26 (td, *J* = 7.5, 1.1 Hz, 1H), 7.12 (d, *J* = 8.6 Hz, 1H), 7.08 (ddd, *J* = 10.2, 8.3, 1.1 Hz, 1H), 3.79 (q, *J* = 6.5 Hz, 1H), 1.78 (d, *J* = 6.5 Hz, 3H); **^{13}C NMR** (126 MHz, $CDCl_3$) δ 172.39 (s), 164.53 (s), 160.45 (d, $^1J_{CF}$ = 251.9 Hz), 136.47 (s), 134.74 (s), 132.19 (d, $^3J_{CF}$ = 8.3 Hz), 132.03 (d, J_{CF} = 1.5 Hz, NOE coupling), 131.56 (d, $^3J_{CF}$ = 2.2 Hz), 130.15 (s), 127.13 (d, $^2J_{CF}$ = 12.4 Hz), 124.46 (d, $^4J_{CF}$ = 3.6 Hz), 122.98 (s), 116.54 (s), 116.29 (d, $^2J_{CF}$ = 21.5 Hz), 58.85 (s), 16.93 (s); **^{19}F NMR** (471 MHz, $CDCl_3$) δ -112.53; **HRMS** (ESI/IT-TOF): m/z [M + H]+ calcd for $C_{16}H_{13}BrFN_2O$: 347.0190; found: 347.0181; **[α] ^{25}D** = -195.5 (c 0.71, EtOAc); **HPLC Purity**: 99.2%; **Optical Purity**: 99.2%EE.

3.4.4.1.3. Ethyl (*R*)-8-bromo-6-(2-fluorophenyl)-4-methyl-4*H*-benzo[f]imidazo[1,5-*a*][1,4]diazepine-3-carboxylate [MIDD0003]

A mixture of (*R*)-7-bromo-5-(2-fluorophenyl)-3-methyl-1,3-dihydro-2H-benzo[*e*][1,4]diazepin-2-one (**MIDD0002**, 125.0 g, 360.0 mmol) and anhydrous tetrahydrofuran (2000 mL) was cooled to -20 ºC using a dry ice / IPA bath. A solution of potassium *t*-butoxide (52.5 g, 468.0 mmol) in tetrahydrofuran (300 mL) was added dropwise to the reaction mixture over 30 min, while maintaining the temperature at -20 to -15 ºC. Upon completion of the addition, the reaction mixture was allowed to stir for an additional 60 min at -20 ºC. Diethyl chlorophosphate (72.8 mL, 504.1 mmol) was then added dropwise to the reaction mixture over 15 min while maintaining the temperature at -20 to -15 ºC. Upon completion of the addition, the reaction mixture was allowed to stir for an additional 2 h at -20 ºC, at which point the reaction was deemed complete on analysis by TLC (silica gel; 100% ethyl acetate; ***Rf: MIDD0002*** = 0.7, ***Rf: MIDD0002A*** = 0.5). Then, ethyl isocyanoacetate (51.2 mL, 468.0 mmol) was added dropwise to the reaction mixture over 15 min, while maintaining the temperature at -20 to -15 ºC. Immediately after which, a solution of potassium *t*-butoxide (52.5 g, 468.0 mmol) in tetrahydrofuran (300 mL) was added dropwise to the reaction mixture over 30 min, while maintaining the temperature at -20 to -15 ºC. Upon completion of the addition, the reaction mixture was allowed to warm to rt and stir for an additional 12 h, at which point the reaction was deemed complete on analysis by TLC (silica gel; 100% ethyl acetate; ***Rf: MIDD0002A*** = 0.5, ***Rf: MIDD0003*** = 0.4). The reaction mixture was then diluted with 5% aq sodium bicarbonate (2000 mL) and then ethyl acetate (2000 mL). The biphasic mixture, which resulted, was then allowed to stand for 30 min and the layers were separated. The aq layer was then extracted with ethyl acetate (2000 mL) and the combined organic layers were washed with 10% aq sodium bicarbonate solution (2000 mL) and then 20% aq sodium chloride

solution (2000 mL). The organic layer was dried (Na_2SO_4, 250 g). The solvents were removed under reduced pressure. The solid residue, which resulted was solvent exchanged to *t*-butyl methyl ether (200mL x 2) and then the residue was slurried with *t*-butyl methyl ether (1000 mL) at 50 – 55 °C for 30 min. Upon cooling to rt and after holding for 12 h, the solid was filtered and washed with *t*-butyl methyl ether (100 mL x 4). The solid was dried under vacuum at 35 – 40 °C to afford the product as a white powder (96.6 g, 60.7%); ***Rf*** = 0.4 (100% EtOAc); **^{1}H NMR** (500 MHz, $CDCl_3$) δ 7.92 (s, 1H), 7.73 (dd, *J* = 8.5, 2.2 Hz, 1H), 7.60 (dt, *J* = 7.3, 3.9 Hz, 1H), 7.48 (d, *J* = 8.6 Hz, 1H), 7.50 – 7.42 (m, 1H), 7.42 (d, *J* = 2.2 Hz, 1H), 7.26 (td, *J* = 7.5, 1.1 Hz, 1H), 7.10 – 7.02 (m, 1H), 6.71 (q, *J* = 7.3 Hz, 1H), 4.54 – 4.28 (m, 2H), 1.42 (t, *J* = 7.1 Hz, 3H), 1.29 (d, *J* = 7.4 Hz, 3H); **^{13}C NMR** (126 MHz, $CDCl_3$) δ 162.93 (s), 162.67 (s), 160.10 (d, $^1J_{CF}$ = 250.7 Hz), 141.59 (s), 134.85 (s), 134.75 (s), 133.68 (s), 133.05 (s), 132.12 (d, $^3J_{CF}$ = 8.2 Hz), 131.17 (s), 129.59 (s), 128.42 (d, $^2J_{CF}$ = 12.3 Hz), 124.57 (d, $^4J_{CF}$ = 3.3 Hz), 123.65 (s), 120.96 (s), 116.25 (d, $^2J_{CF}$ = 21.4 Hz), 60.82 (s), 50.12 (s), 14.87 (s), 14.43 (s); **^{19}F NMR** (471 MHz, $CDCl_3$) δ -112.36; **HRMS** (ESI/IT-TOF): m/z [M + H]+ calcd for $C_{21}H_{18}BrFN_3O_2$: 442.0561; found: 442.0563; **[α] $^{25}_D$** = -42.1 (c 0.53, EtOAc); **HPLC Purity**: 97.5%; **Optical Purity**: 99.8%EE.

3.4.4.1.4. Ethyl (*R*)-6-(2-fluorophenyl)-4-methyl-8-((triisopropylsilyl)ethynyl)-4*H*-benzo[*f*]imidazo [1,5-*a*][1,4]diazepine-3-carboxylate [SH-053-2'F-R-CH$_3$-TIPS]

A mixture of palladium acetate (1.25 g, 5.6 mmol), tri-o-tolylphosphine (3.39g, 11.1 mmol) and acetonitrile (300 mL) was stirred for 30 min at rt. To the reaction mixture was then added in sequence, ethyl (*R*)-8-bromo-6-(2-fluorophenyl)-4-methyl-4*H*-benzo[*f*]imidazo[1,5-*a*][1,4]diazepine-3-carboxylate (**MIDD0003**, 49.2 g, 111.2 mmol), triethylamine (31.1 mL, 222.5 mmol), (triisopropylsilyl)acetylene (29.9 mL, 133.5 mmol) and additional acetonitrile (400 mL).

The reaction mixture was then heated to reflux (75 °C) and held for 4 h at which point the reaction was deemed complete on analysis by TLC (silica gel; 100% ethyl acetate; ***Rf: MIDD0003*** = 0.4, ***Rf: SH-053-2'F-R-CH$_3$-TIPS*** = 0.6). Upon completion of the reaction, the mixture was cooled to rt and silica gel (25 g) was added. After stirring for 30 min, the spent catalyst on silica gel was removed by filtration and washed with acetonitrile (100 mL x 2). The solvents were removed under reduced pressure and the residue was dissolved in dichloromethane (700 mL) and 5% aq sodium bicarbonate (700 mL). The biphasic mixture, which resulted, was allowed to stand for 15 min and the layers were separated. The aq layer was then extracted with dichloromethane (700 mL) and the combined organic layers were washed with 5% aq sodium bicarbonate solution (700 mL) and then 10% aq sodium chloride solution (700 mL). The organic layer was dried (Na_2SO_4). The solvents were removed under reduced pressure and the residue was purified by flash chromatography using silica gel (600 g) and 50% ethyl acetate / hexanes. The pure fractions were pooled and the solvents were removed under reduced pressure. The oil, which resulted, was dried under reduced pressure at 40 °C for 2 h to afford the product as a clear, golden oil (64.2 g, 106%, HNMR analysis displayed 90wt% product, 10wt% solvents); ***Rf*** = 0.6 (100% EtOAc); **^{1}H NMR** (500 MHz, $CDCl_3$) δ 7.92 (s, 1H), 7.65 (d, *J* = 7.8 Hz, 1H), 7.58 (t, *J* = 7.1 Hz, 1H), 7.52 (d, *J* = 8.3 Hz, 1H), 7.46 – 7.38 (m, 1H), 7.31 (s, 1H), 7.23 (td, *J* = 7.6, 0.9 Hz, 1H), 7.02 (t, *J* = 9.2 Hz, 1H), 6.67 (q, *J* = 7.2 Hz, 1H), 4.38 (tdd, *J* = 10.8, 7.2, 3.8 Hz, 2H), 1.39 (t, *J* = 7.1 Hz, 3H), 1.12 – 1.02 (m, 24H); **^{13}C NMR** (126 MHz, $CDCl_3$) δ 163.35 (s), 162.94 (s), 160.13 (d, $^1J_{CF}$ = 250.8 Hz), 141.67 (s), 135.29 (s), 134.83 (s), 134.03 (s), 133.35 (s), 131.83 (d, $^3J_{CF}$ = 8.8 Hz), 131.18 (s), 129.58 (s), 129.45 (s), 128.72 (d, $^2J_{CF}$ = 12.4 Hz), 124.39 (d, $^4J_{CF}$ = 2.9 Hz), 122.99 (s), 122.07 (s), 116.11 (d, $^2J_{CF}$ = 21.5 Hz), 104.57 (s), 94.11 (s), 60.71 (s), 50.08 (s), 18.56 (s), 14.81 (s), 14.40 (s), 11.19 (s); **^{19}F NMR** (471 MHz, $CDCl_3$) δ -112.57; **HRMS** (ESI/IT-TOF): m/z [M + H]+ calcd

for $C_{32}H_{39}FN_3O_2Si$: 544.7663; found: 544.7667; **HPLC Purity**: 99.5%; **Optical Purity**: 99.9%EE.

3.4.4.1.5. Ethyl (*R*)-8-ethynyl-6-(2-fluorophenyl)-4-methyl-4*H*-benzo[*f*]imidazo[1,5-*a*][1,4]diazepine-3-carboxylate [SH-053-2'F-R-CH$_3$]

A mixture of ethyl (*R*)-6-(2-fluorophenyl)-4-methyl-8-((triisopropylsilyl)ethynyl)-4*H*-benzo[*f*]imidazo[1,5-*a*][1,4]diazepine-3-carboxylate (**SH-053-2'F-R-CH$_3$-TIPS**, 60.5 g, 111.3 mmol), water (6.0 mL) and tetrahydrofuran (600 mL) was cooled to -20 ºC using a dry ice / IPA bath. Tetrabutylammonium fluoride hydrate, 1M in THF (127.6 mL, 127.6 mmoL) was added dropwise to the reaction mixture over 30 min, while maintaining the temperature at -20 to -15 ºC. Upon completion of the addition, the reaction mixture was allowed to warm to rt and stir for an additional 60 min, at which point the reaction was deemed complete on analysis by TLC (silica gel; 100% ethyl acetate; ***Rf: SH-053-2'F-R-CH$_3$-TIPS*** = 0.6, ***Rf: SH-053-2'F-R-CH$_3$*** = 0.4). The reaction mixture was then diluted with ethyl acetate (600 mL) and 10% aq sodium chloride (600 mL). The biphasic mixture, which resulted, was allowed to stand for 15 min and the layers were separated. The aq layer was then extracted with ethyl acetate (600 mL) and the combined organic layers were washed with 10% aq sodium chloride solution (600 mL). The organic layer was dried (Na_2SO_4). The solvents were removed under reduced pressure and the residue was slurried with methanol (250 mL) at 50 – 55 ºC for 30 min. Water (250 mL) was then added to the product slurry and stirring was continued at 50 – 55 ºC for 30 min. Upon cooling to 20-25 ºC and after holding for 2 h, the solid was filtered and washed with 50% methanol/water (50 mL x 4) and then hexanes (50 mL x 3). The solid was dried under vacuum at 40 ºC to afford the product as a white crystalline solid (38.1 g, 88.6%): ***Rf*** = 0.4 (100% EtOAc); **^{1}H NMR** (500 MHz, $CDCl_3$) δ 7.94 (s, 1H), 7.70

(d, J = 7.5 Hz, 1H), 7.60 (t, J = 7.0 Hz, 1H), 7.57 (d, J = 8.3 Hz, 1H), 7.45 (dddd, J = 8.2, 7.1, 5.1, 1.8 Hz, 1H), 7.41 (s, 1H), 7.26 (td, J = 7.5, 1.1 Hz, 1H), 7.10 – 6.98 (m, 1H), 6.70 (q, J = 7.3 Hz, 1H), 4.54 – 4.25 (m, 2H), 3.16 (s, 1H), 1.42 (t, J = 7.1 Hz, 3H), 1.28 (d, J = 7.3 Hz, 3H); **^{13}C NMR** (126 MHz, $CDCl_3$) δ 163.22 (s), 162.94 (s), 160.12 (d, $^1J_{CF}$ = 250.4 Hz), 141.69 (s), 135.17 (s), 134.82 (s), 134.54 (s), 133.95 (s), 131.94 (d, $^3J_{CF}$ = 8.6 Hz), 131.18 (s), 129.66 (s), 129.57 (s), 128.68 (d, $^2J_{CF}$ = 12.1 Hz), 124.50 (d, $^4J_{CF}$ = 3.6 Hz), 122.19 (s), 121.64 (s), 116.21 (d, $^2J_{CF}$ = 21.4 Hz), 81.44 (s), 79.70 (s), 60.80 (s), 50.10 (s), 14.88 (s), 14.43 (s); **^{19}F NMR** (471 MHz, $CDCl_3$) δ -112.48; **HRMS** (ESI/IT-TOF) m/z: $[M + H]^+$ Calcd for $C_{21}H_{15}FN_3O_2$ 360.1143; found 360.1140; **[α] ^{25}D** = +13.8 (c 0.89, EtOAc); **HPLC Purity**: 99.8%; **Optical Purity**: 99.9%EE.

3.4.4.1.6. (*R*)-8-Bromo-6-(2-fluorophenyl)-4-methyl-4*H*-benzo[*f*]imidazo[1,5-*a*][1,4]diazepine-3-carboxylic acid [SH-053-2'F-R-CH$_3$-acid]

To a mixture of ethyl (*R*)-8-ethynyl-6-(2-fluorophenyl)-4-methyl-4*H*-benzo[*f*]imidazo[1,5-*a*][1,4]diazepine-3-carboxylate (**SH-053-2'F-R-CH$_3$**, 20.0 g, 51.6 mmol) and tetrahydrofuran (400 mL), a solution of lithium hydroxide (4.95 g, 206.5 mmol) and water (200 mL) was added dropwise over 15 min, while keeping the temperature between 25 – 30 ºC. The reaction mixture, which resulted, was then heated to 50 – 55 ºC and held for 4 h, at which point the reaction was deemed complete on analysis by TLC (silica gel; 100% ethyl acetate; ***Rf: SH-053-2'F-R-CH$_3$*** = 0.4, ***Rf: SH-053-2'F-R-CH$_3$-acid, Li salt*** = 0.0). Caution: The product may racemize if the reaction temperature is much higher than 55 ºC and the reaction time is much longer than 4 hr. The reaction mixture was then cooled to rt. The reaction mixture was then diluted with water (200 mL). Glacial acetic acid (17.7 mL, 309.7 mmol) was then added dropwise to the reaction mixture over 15 min, while maintaining the temperature at 20 to 25 ºC. The tetrahydrofuran was removed

under reduced pressure. To the semisolid / slurry, which resulted was added methanol (200 mL). The thin slurry, which resulted, was stirred at 40 – 45 ºC for 30 min to homogenize the mixture. The slurry, which resulted, was stirred at 20 – 25 ºC for 12 h to maximize product precipitation. The solid was filtered and washed with water (50 mL x 4). The solid was dried under vacuum at 35 – 40 ºC to afford the product as an off-white powder (17.0g, 91.6%); ***Rf*** = 0.3 (25% MeOH / CH_2Cl_2); **^{1}H NMR** (500 MHz, DMSO-*d*$_6$) δ 12.71 (s, 1H), 8.44 (s, 1H), 7.95 (d, *J* = 8.3 Hz, 1H), 7.82 (d, *J* = 8.2 Hz, 1H), 7.56 (dq, *J* = 13.4, 6.6, 6.1 Hz, 2H), 7.33 (t, *J* = 7.4 Hz, 1H), 7.23 (t, *J* = 9.2 Hz, 2H), 6.51 (d, *J* = 6.9 Hz, 1H), 4.37 (s, 1H), 1.16 (d, *J* = 7.1 Hz, 3H); **^{13}C NMR** (126 MHz, DMSO-*d*$_6$) δ 164.66, 162.88, 159.83 (d, $^1J_{CF}$ = 247.7 Hz), 140.97, 136.70, 135.57, 134.72, 133.20, 132.63 (d, $^3J_{CF}$ = 8.0 Hz), 131.90, 129.50, 129.37, 128.92 (d, $^2J_{CF}$ = 13.2 Hz), 125.17 (d, $^4J_{CF}$ = 3.2 Hz), 124.00, 121.14, 116.41 (d, $^2J_{CF}$ = 21.1 Hz), 83.46, 82.00, 49.80, 15.06; **^{19}F NMR** (471 MHz, DMSO-*d*$_6$) δ -113.78; **HRMS** (ESI/IT-TOF) m/z: $[M + H]^+$ Calcd for $C_{21}H_{15}FN_3O_2$ 360.1143; found 360.1140; **[α] ^{25}D** = -46.0 (c 1.0, MeOH); **HPLC Purity**: 99.8%; **Optical Purity**: 99.9%.

3.4.4.1.7. (*R*)-8-Ethynyl-6-(2-fluorophenyl)-*N,N*,4-trimethyl-4*H*-benzo[*f*]imidazo[1,5-*a*][1,4]diazepine-3-carboxamide [GL-II-73]

A mixture of (*R*)-8-bromo-6-(2-fluorophenyl)-4-methyl-4*H*-benzo[*f*]imidazo[1,5-*a*][1,4]diazepine-3-carboxylic acid (**SH-053-2'F-R-CH$_3$-acid**, 16.0 g, 44.5 mmol), *N,N*-dimethylformamide (0.3 g, 0.44 mmol) and dichloromethane (200 mL) was heated to 35 – 40 ºC at which point thionyl chloride (32.5 mL, 445.2 mmol) was added dropwise to the reaction mixture over 30 min and $SO_{2(g)}$ and $HCl_{(g)}$ evolution occurred. The reaction mixture, which resulted, was then held at 35 – 40 ºC for 2 h, at which point the reaction was deemed complete by TLC analysis (silica gel; 25% methanol / dichloromethane with 1% triethylamine added; ***Rf: SH-053-2'F-R-***

CH_3-acid = 0.3, ***Rf: SH-053-2'F-R-CH_3 Methyl ester*** = 0.7). A 1 mL sample of the reaction mixture was quenched with 1 mL of methanol containing a few drops of triethylamine prior to spotting it on the TLC plate. After analysis, by observing the methyl ester (TLC) vs. the acid, the reaction mixture was then cooled to rt. The solvents and excess thionyl chloride were removed under reduced pressure. The residual thionyl chloride was removed by adding and removing dichloromethane (100mL x 4) and then drying the solid residue under reduced pressure at 40 – 45 ^oC for 1 hr. The solid residue was then dissolved in dichloromethane (250 mL) and cooled to 0 – 5 ^oC. Dimethylamine, 2.0 M in THF (150mL, 293.9 mmol) was then added dropwise to the reaction mixture over 30 min, while maintaining the temperature at 0 to 5 ^oC. Upon completion of the addition, the reaction mixture was allowed to warm to rt and stir for an additional 60 min at which point the reaction was deemed complete on analysis by TLC (silica gel; 100% ethyl acetate). The reaction mixture was then diluted with 5% aq sodium bicarbonate (250 mL). The biphasic mixture, which resulted, was then allowed to stand for 30 min and the layers were separated. The aq layer was then extracted with dichloromethane (250 mL) and the combined organic layers were washed with 5% aq sodium bicarbonate solution (250 mL) and then 10% aq sodium chloride solution (250 mL). The organic layer was dried (Na_2SO_4, 25 g). The solvents were removed under reduced pressure. The solid residue, which resulted was triturated with *t*-butyl methyl ether (200 mL) at 40 – 45 ^oC for 30 min to homogenize the mixture. The slurry, which resulted, was held at 0 – 5 ^oC for 12 h to maximize product precipitation. The solid, which resulted, was filtered and washed with hexanes (25 mL x 2). The solid was dried under vacuum at 35 – 40 ^oC to afford the product as a pale yellow crystalline solid (13.7 g, 80.0%): ***Rf*** = 0.2 (100% EtOAc); **^{1}H NMR** (500 MHz, $CDCl_3$) δ 7.94 (s, 1H), 7.76 – 7.67 (m, 1H), 7.62 (td, *J* = 7.5, 1.8 Hz, 1H), 7.51 (d, *J* = 8.4 Hz, 1H), 7.45 (ddd, *J* = 7.6, 5.4, 2.0 Hz, 1H), 7.43 (s, 1H), 7.25 (td, *J* = 7.5, 1.1 Hz, 1H), 7.03 (dd,

J = 10.4, 8.2 Hz, 1H), 4.31 (q, *J* = 6.8 Hz, 1H), 3.15 (s, 1H), 3.12 (s, 3H), 3.00 (s, 3H), 1.92 (d, *J* = 7.1 Hz, 3H); **^{13}C NMR** (126 MHz, $CDCl_3$) δ 166.15, 162.63, 160.23 (d, $^1J_{CF}$ = 250.4 Hz), 135.33, 134.76, 134.65, 133.87, 133.73, 132.64, 132.09 (d, $^3J_{CF}$ = 8.2 Hz), 131.30 (d, $^3J_{CF}$ = 2.5 Hz), 129.24, 127.68 (d, $^2J_{CF}$ = 11.9 Hz), 124.53 (d, $^4J_{CF}$ = 3.6 Hz), 122.85, 121.52, 116.18 (d, $^2J_{CF}$ = 21.5 Hz), 81.57, 79.51, 52.21, 39.11, 35.04, 18.47; **^{19}F NMR** (471 MHz, $CDCl_3$) δ -112.55; **HRMS** (ESI/IT-TOF) m/z: [M + H] Calcd for $C_{23}H_{20}FN_4O$ 387.1616; found 387.1626; **[α] ^{25}D** = +31.4 (c 0.61, $CHCl_3$); **HPLC Purity**: 99.3%; **Optical Purity**: 99.5%.

3.4.4.1.8. (*R*)-8-Ethynyl-6-(2-fluorophenyl)-*N*,4-dimethyl-4*H*-benzo[*f*]imidazo[1,5-*a*][1,4]diazepine-3-carboxamide [MP-III-022]

A mixture of ethyl (*R*)-8-ethynyl-6-(2-fluorophenyl)-4-methyl-4*H*-benzo[*f*]imidazo[1,5-*a*][1,4]diazepine-3-carboxylate (**SH-053-2'F-R-CH$_3$**, 5.0 g, 12.9 mmol) and methyl amine (75 mL, 33wt% in EtOH) was placed in a sealed tube and heated to 45-50 °C for 24 h at which point the reaction was deemed complete on analysis by TLC (silica gel; 100% ethyl acetate; ***Rf: SH-053-2'F-R-CH$_3$*** = 0.4, ***Rf: MP-III-022*** = 0.2). The reaction mixture was cooled to rt. The solvents were removed under reduced pressure. The solid residue, which resulted was purified by flash chromatography using silica gel (150 g) and 100% ethyl acetate. The pure fractions were pooled and the solvents were removed under reduced pressure. The residue, which resulted, was triturated with hexanes (200 mL) at 20 – 25 °C. Upon holding for 2 h at rt, the solid was filtered and washed with hexanes (25 mL x 2). The solid was dried under vacuum at 35 – 40 °C to afford the product as a pale yellow crystalline solid (3.7 g, 76.0%): ***Rf*** = 0.2 (100% EtOAc); **^{1}H NMR** (500 MHz, $CDCl_3$) δ 7.83 (s, 1H), 7.68 (d, *J* = 8.4 Hz, 1H), 7.63 (t, *J* = 7.5 Hz, 1H), 7.53 (d, *J* = 8.3 Hz, 1H), 7.43 (ddd, *J* = 11.4, 6.6, 3.6 Hz, 1H), 7.41 (s, 1H), 7.24 (td,

J = 7.5, 1.1 Hz, 1H), 7.18 (s, 1H), 7.05 – 6.98 (m, 1H), 6.90 (q, *J* = 7.4 Hz, 1H), 3.15 (s, 1H), 2.96 (d, *J* = 5.0 Hz, 3H), 1.27 (d, *J* = 7.3 Hz, 3H); **^{13}C NMR** (126 MHz, $CDCl_3$) δ 163.31, 162.82, 160.12 (d, *J* = 250.2 Hz), 138.75, 134.97, 134.71, 133.93, 133.45, 131.80 (d, *J* = 9.1 Hz), 131.76, 131.36, 129.79, 128.86 (d, *J* = 12.7 Hz), 124.45 (d, *J* = 3.5 Hz), 122.04, 121.39, 116.07 (d, *J* = 21.6 Hz), 81.55, 79.52, 49.89, 25.61, 15.06; **^{19}F NMR** (471 MHz, $CDCl_3$) δ -112.40; **HRMS** (ESI/IT-TOF) m/z: $[M + H]^+$ Calcd for $C_{22}H_{18}FN_4O$ 373.1459, found: 373.1469; **[α] $^{25}_D$** = +11.1 (c 1.0, $CHCl_3$); **HPLC Purity**: 98.5%; **Optical Purity**: 99.3%.

3.4.4.2. General Analytical Procedures for of GL-II-73 and MP-III-022

The same analytical methods described above for the synthesis of MIDD0301 were used with GL-II-73 and MP-III-022 to determined overall HPLC purity (%) and optical purity (%EE).

3.5. Structural Analysis of α5-GABA$_A$R Subtype-selective Imidazodiazepines by NMR Spectroscopy

3.5.1. NMR Spectra of MIDD0101

3.5.1.1. ^{1}H NMR Spectrum of MIDD0101

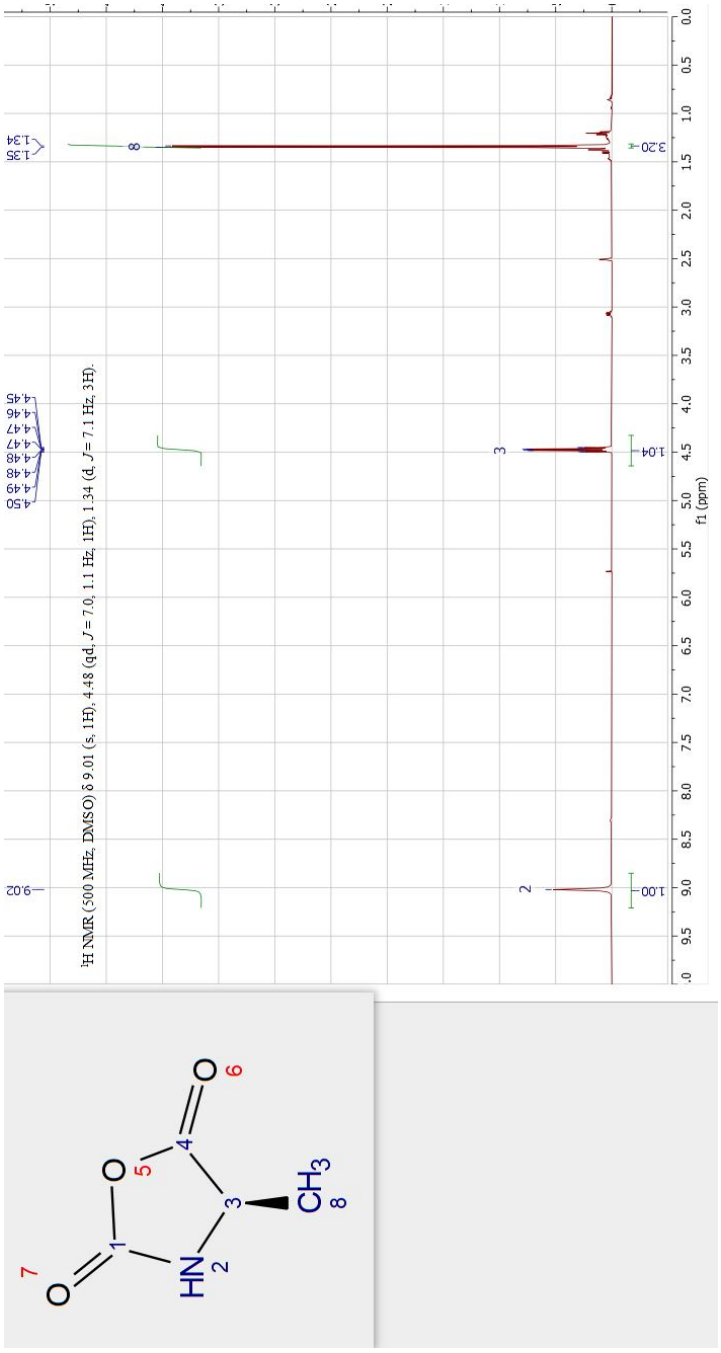

3.5.1.2. ^{13}C NMR Spectrum of MIDD0101

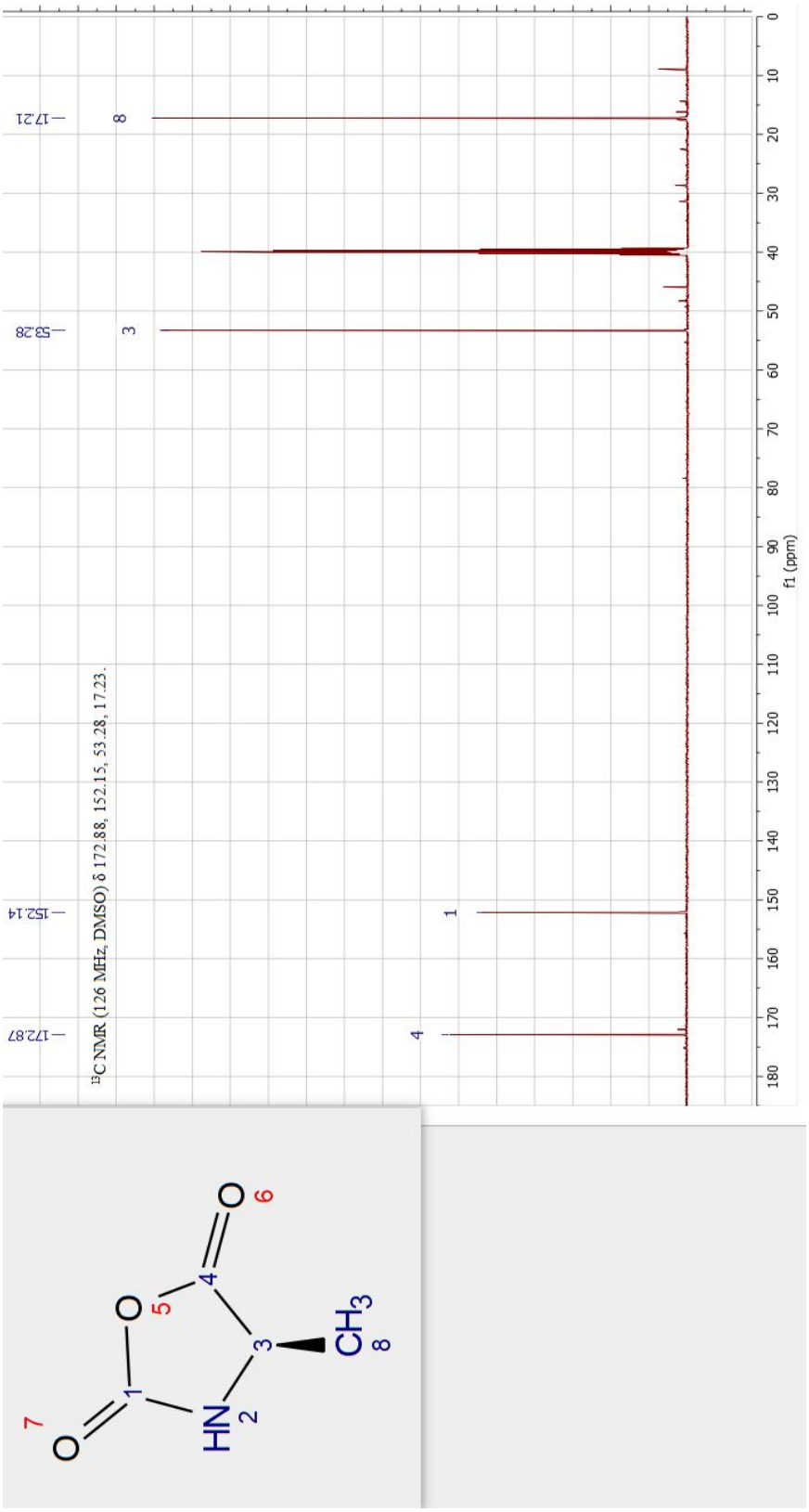

3.5.1.3. COSY Spectrum of MIDD0101

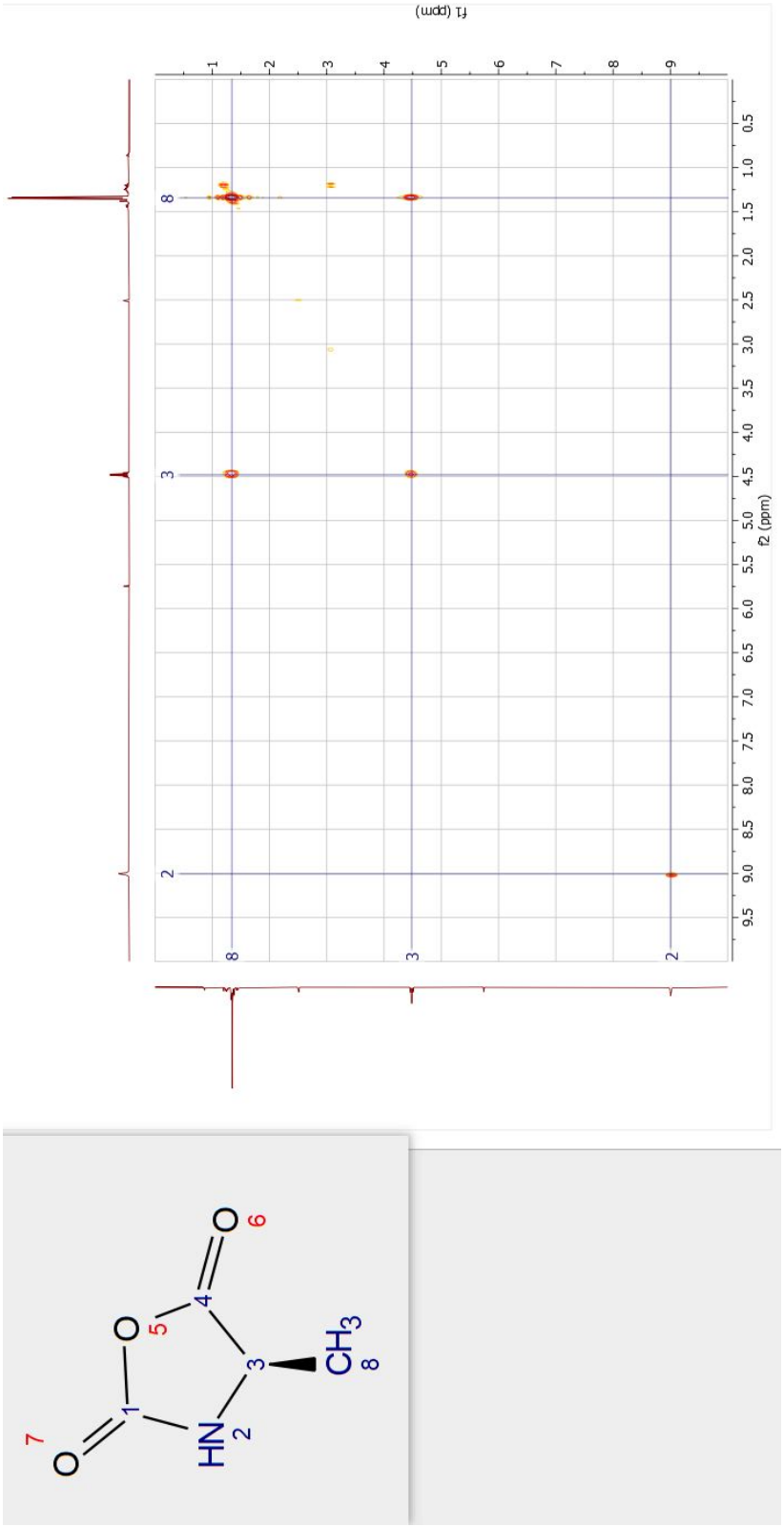

3.5.1.4. ^{1}H-^{13}C-HSQC Spectrum of MIDD0101

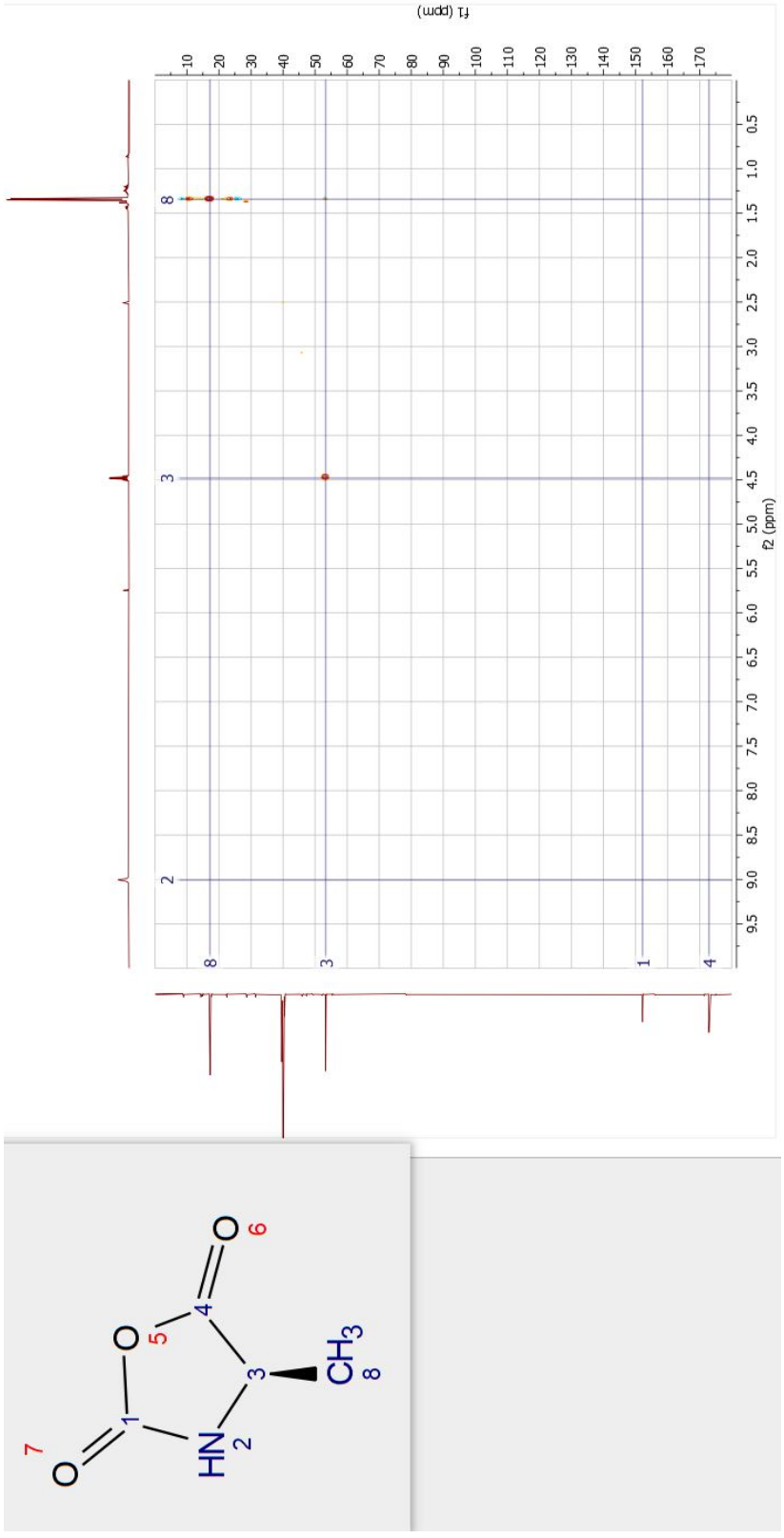

3.5.1.5. ^{1}H-^{13}C-HMBC Spectrum of MIDD0101

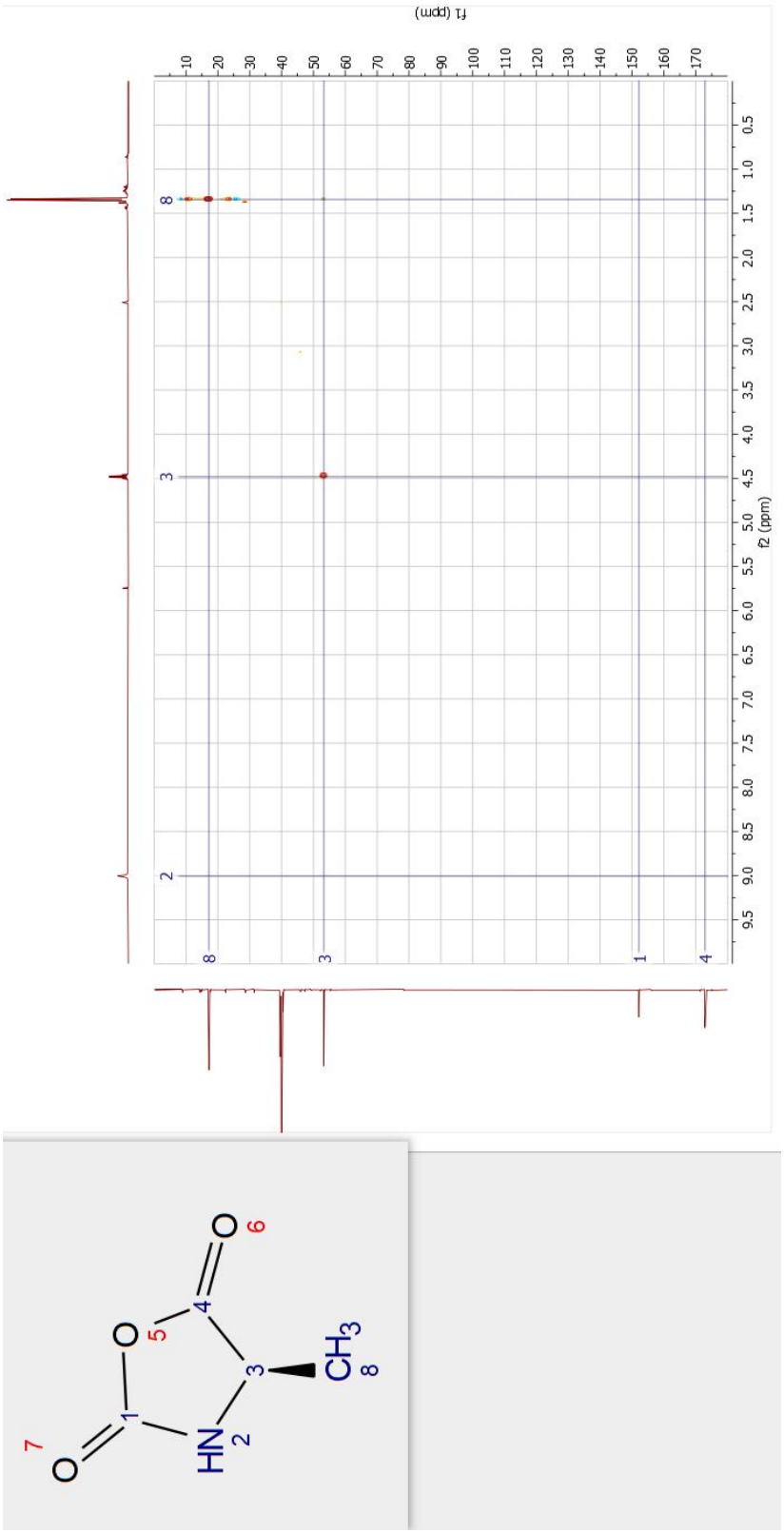

3.5.2. NMR Spectra of MIDD0002

3.5.2.1. ^{1}H NMR Spectrum of MIDD0002

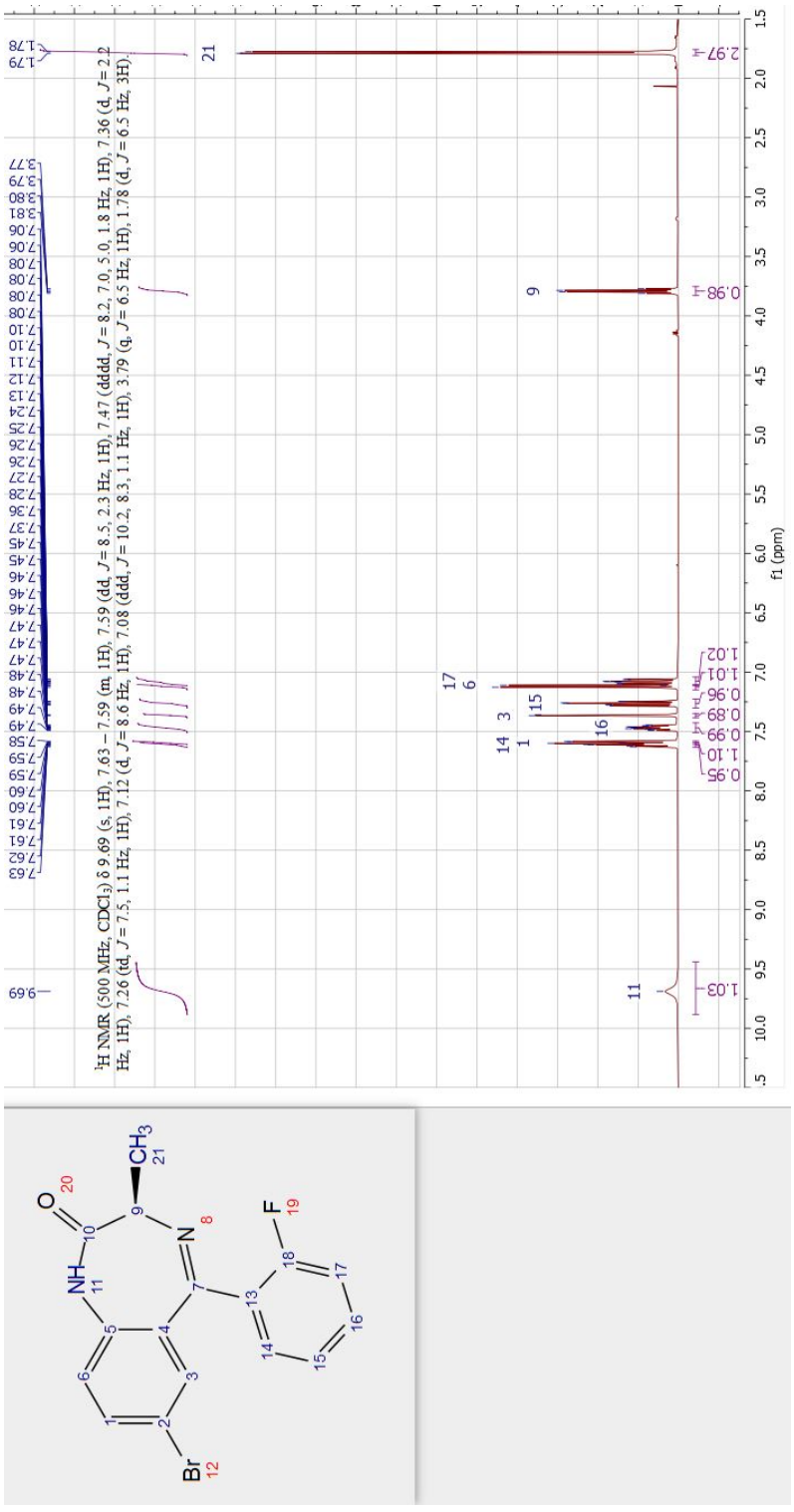

3.5.2.2. ^{13}C NMR Spectrum of MIDD0002

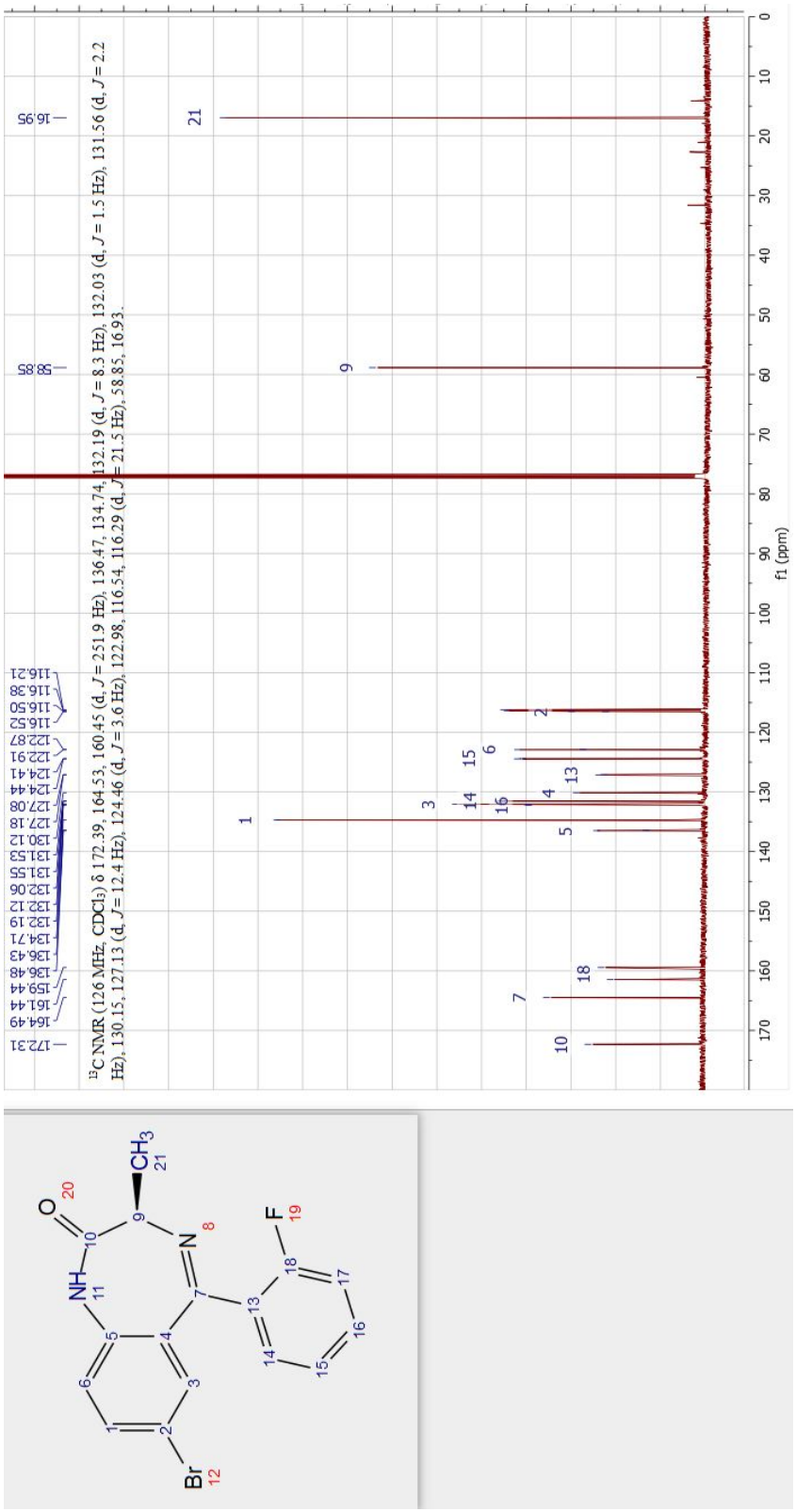

3.5.2.3. COSY Spectrum of MIDD0002

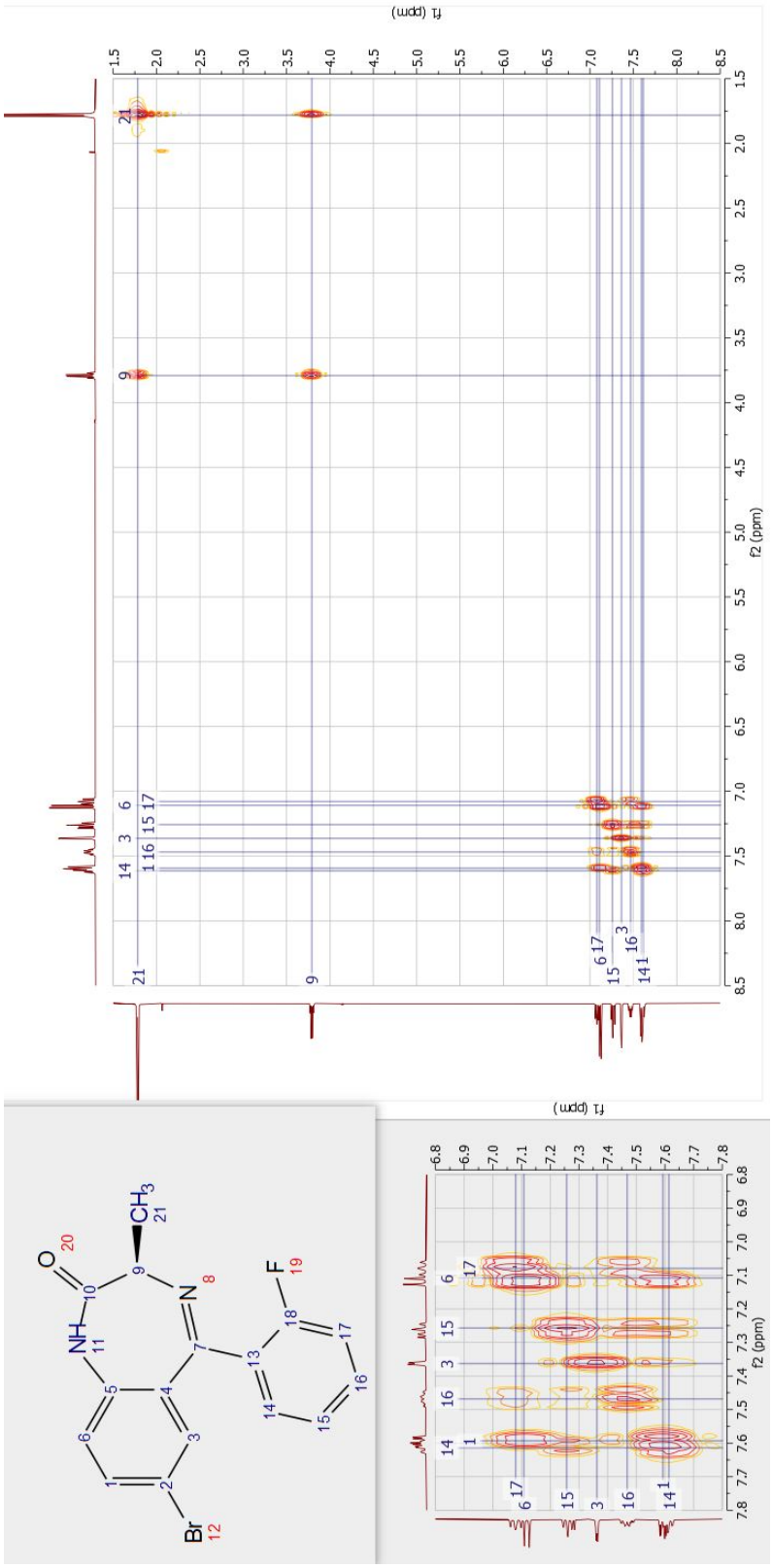

3.5.2.4. ^{1}H-^{13}C-HSQC Spectrum of MIDD0002

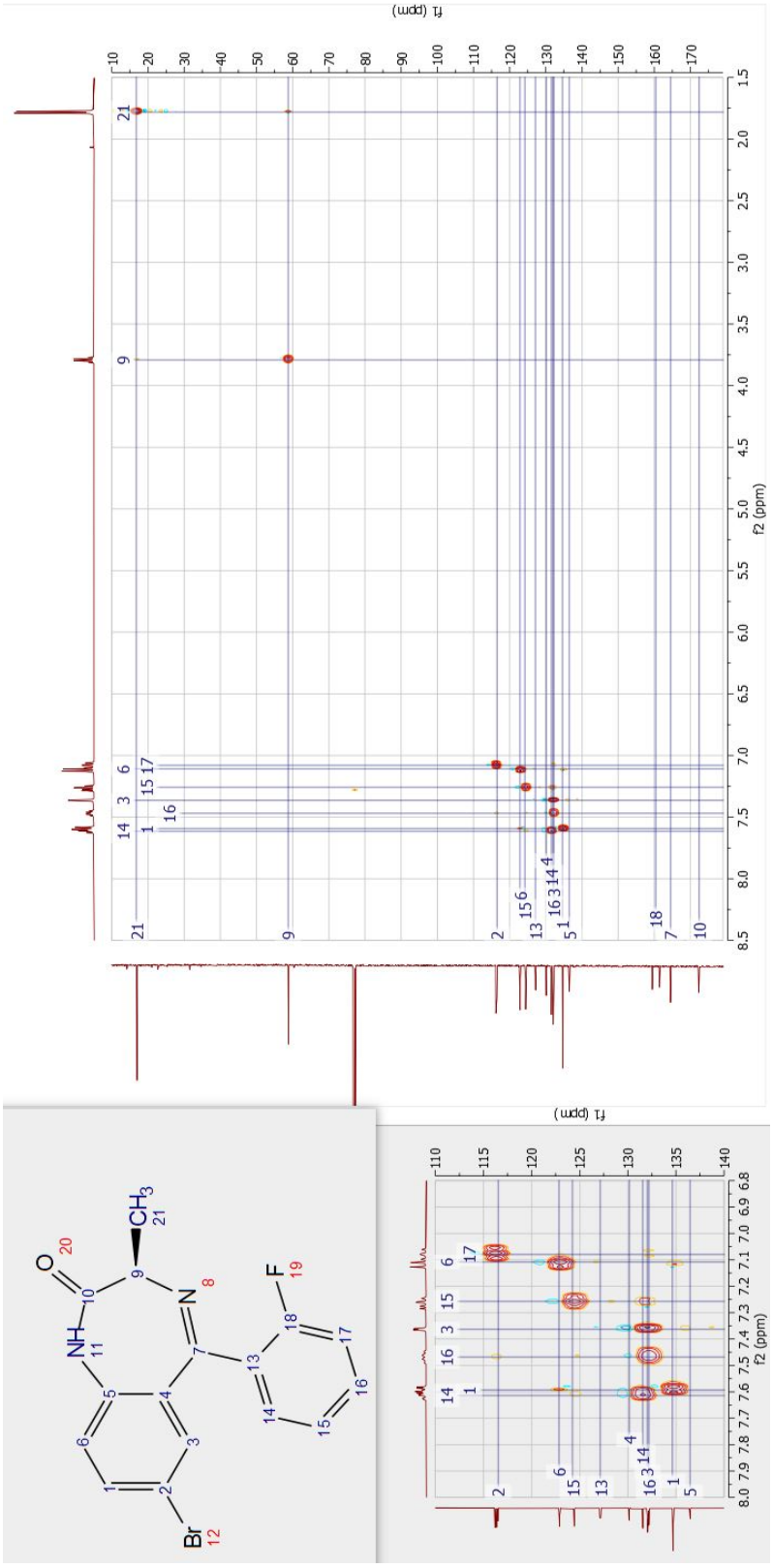

3.5.2.5. ^{1}H-^{13}C-HMBC Spectrum of MIDD0002

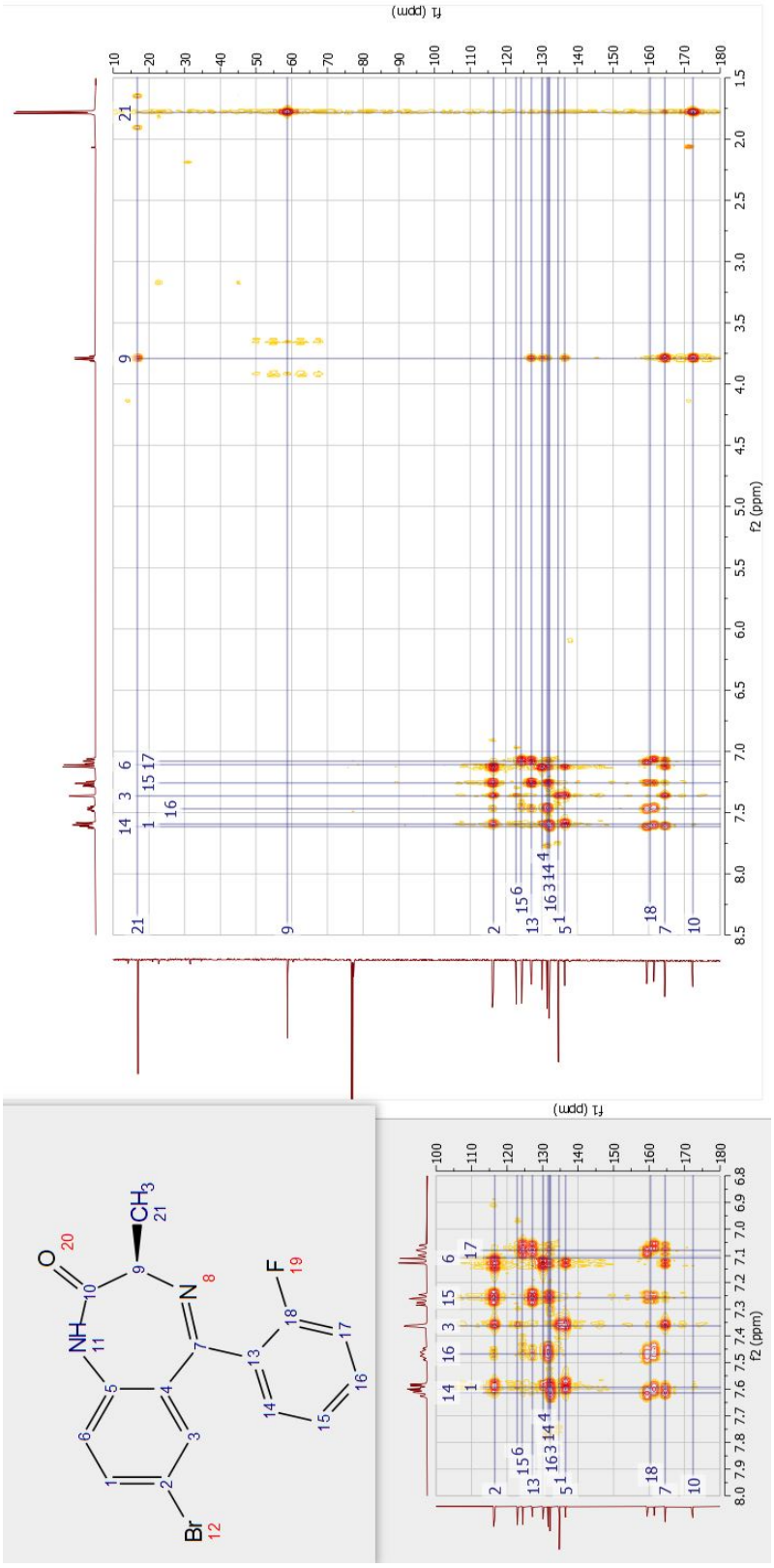

3.5.2.6. ROESY Spectrum of MIDD0002

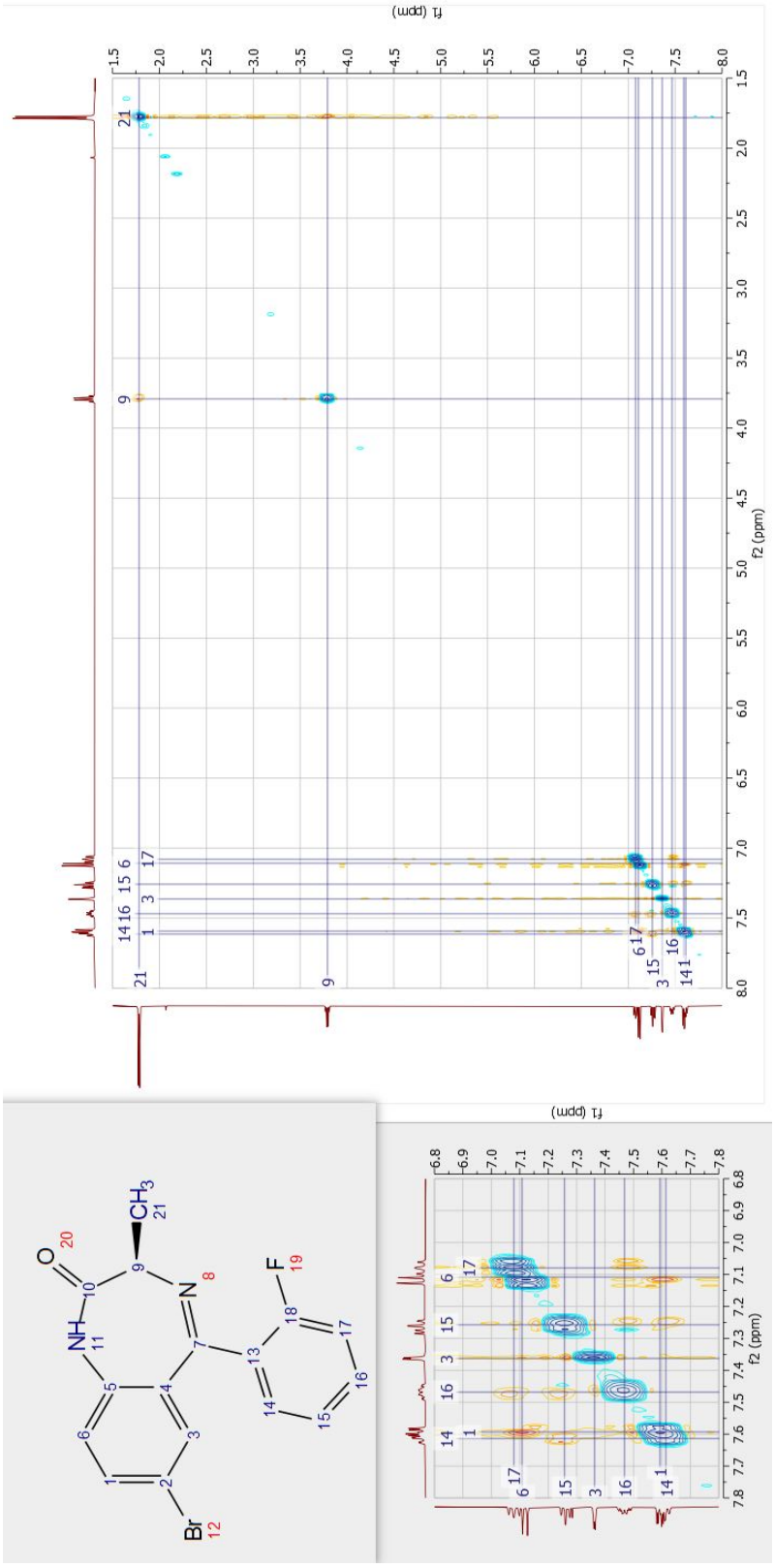

3.5.3. NMR Spectra of MIDD0003

3.5.3.1. ^{1}H NMR Spectrum of MIDD0003

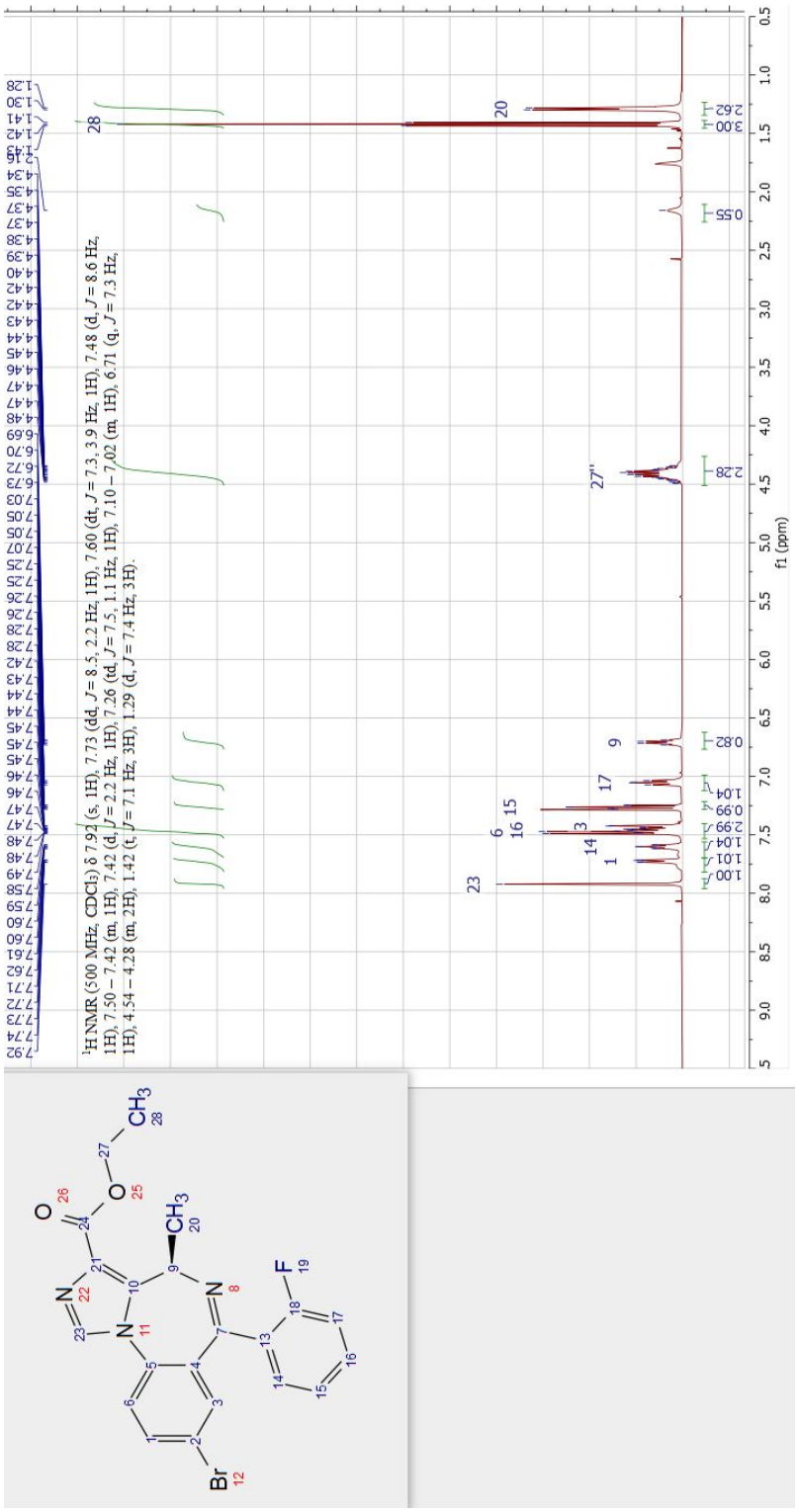

3.5.3.2. ^{13}C NMR Spectrum of MIDD0003

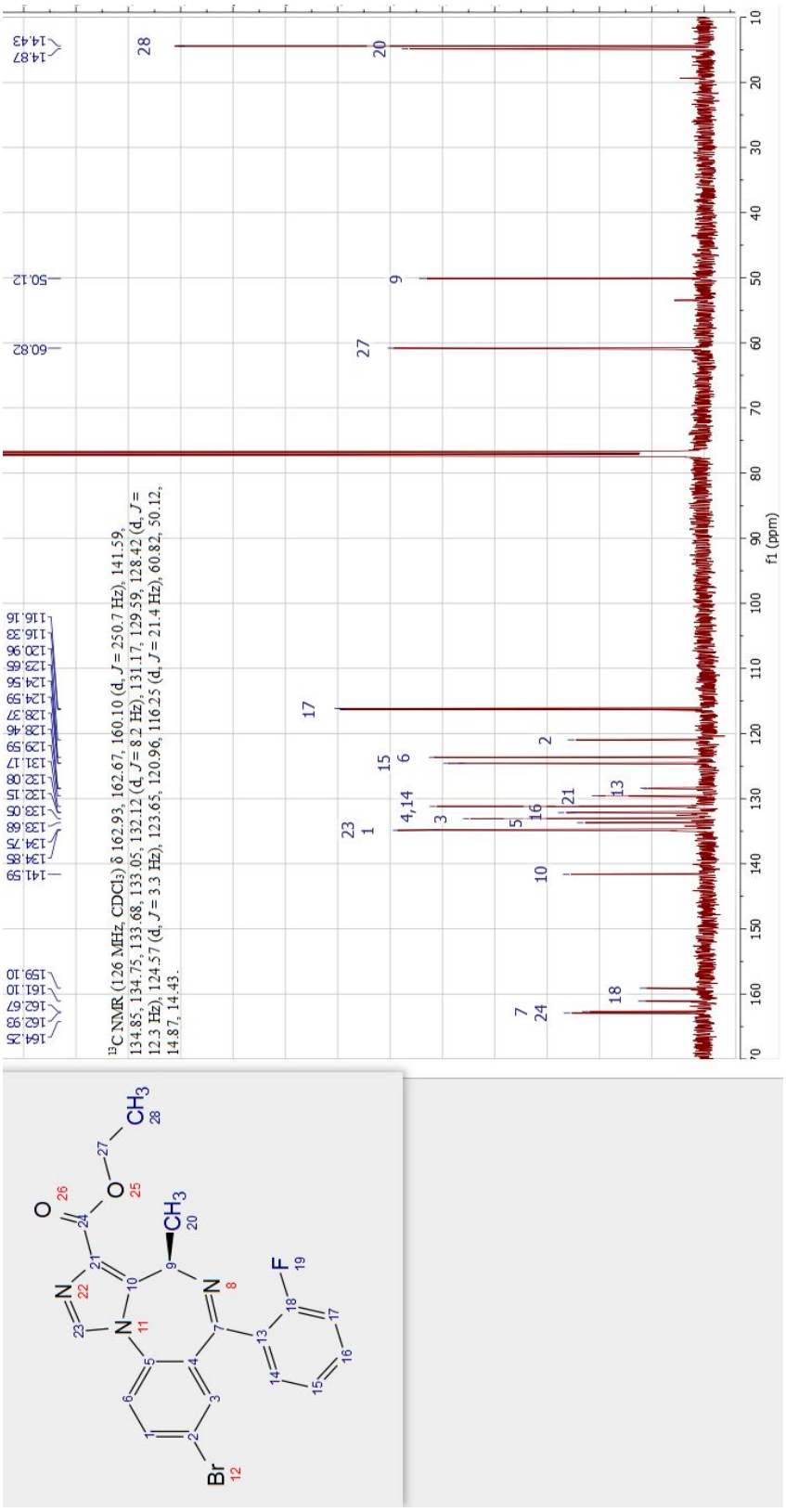

3.5.3.3. COSY Spectrum of MIDD0003

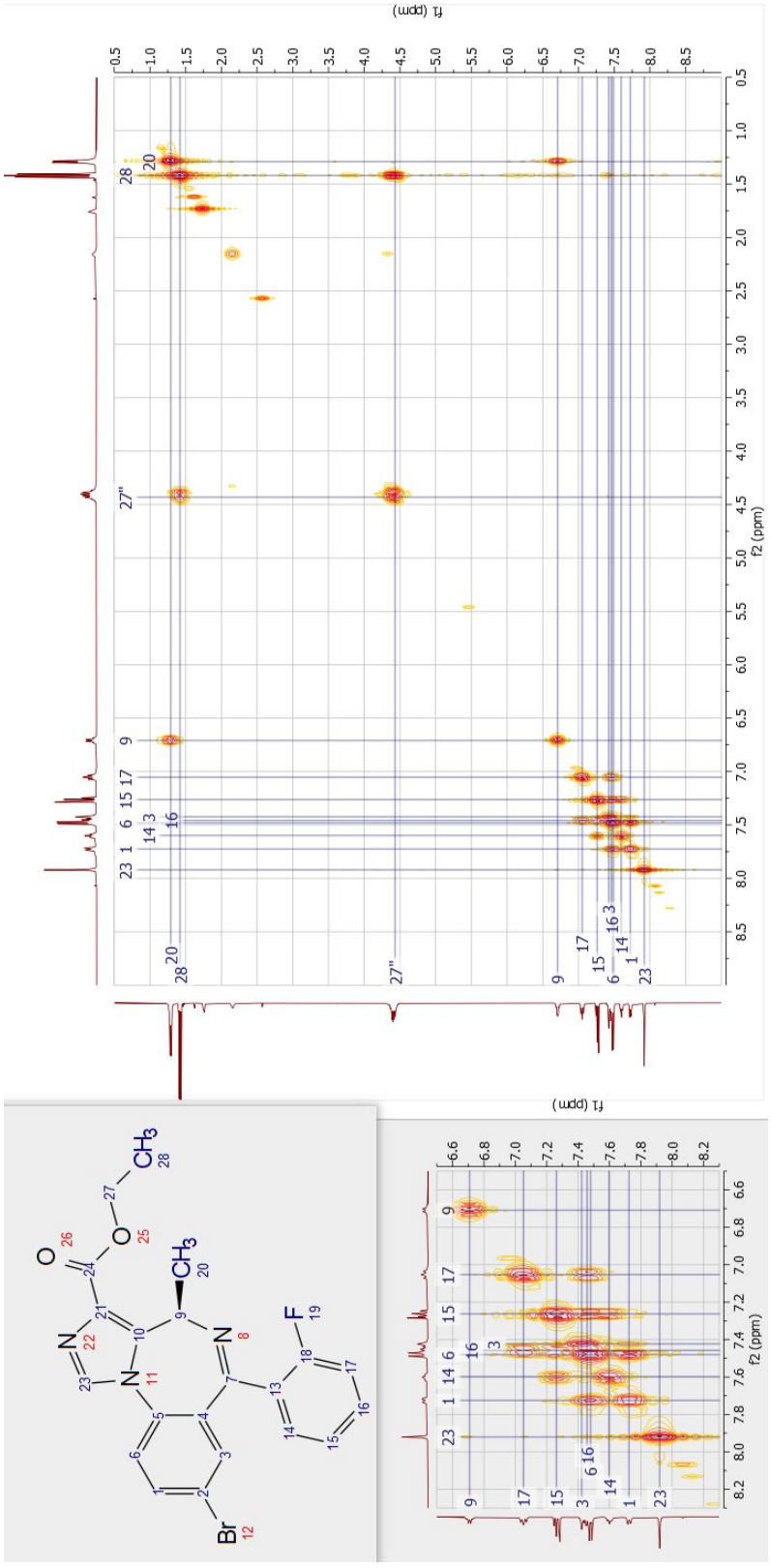

3.5.3.4. ^{1}H-^{13}C-HSQC Spectrum of MIDD0003

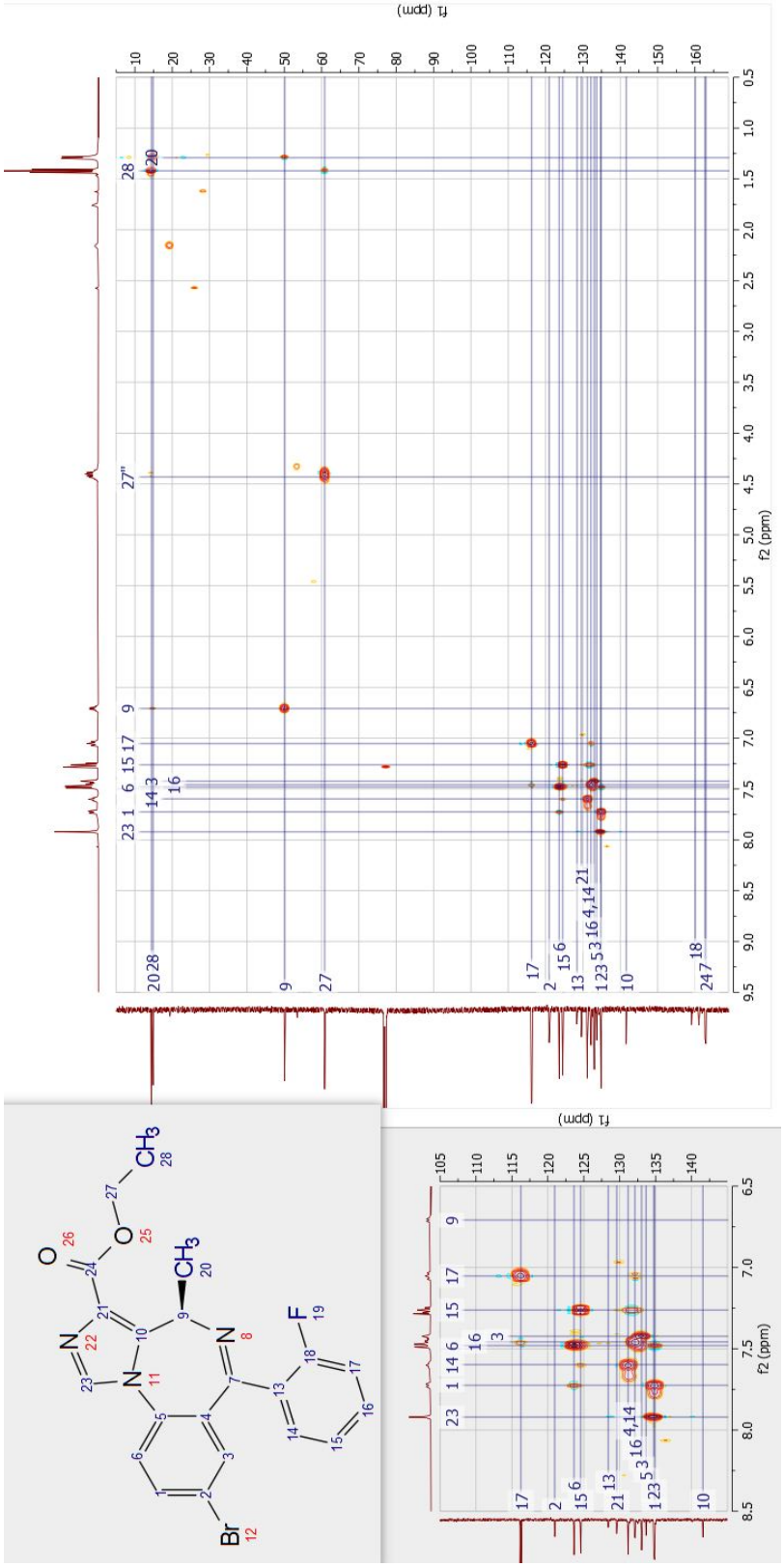

3.5.3.5. ^{1}H-^{13}C-HMBC Spectrum of MIDD0003

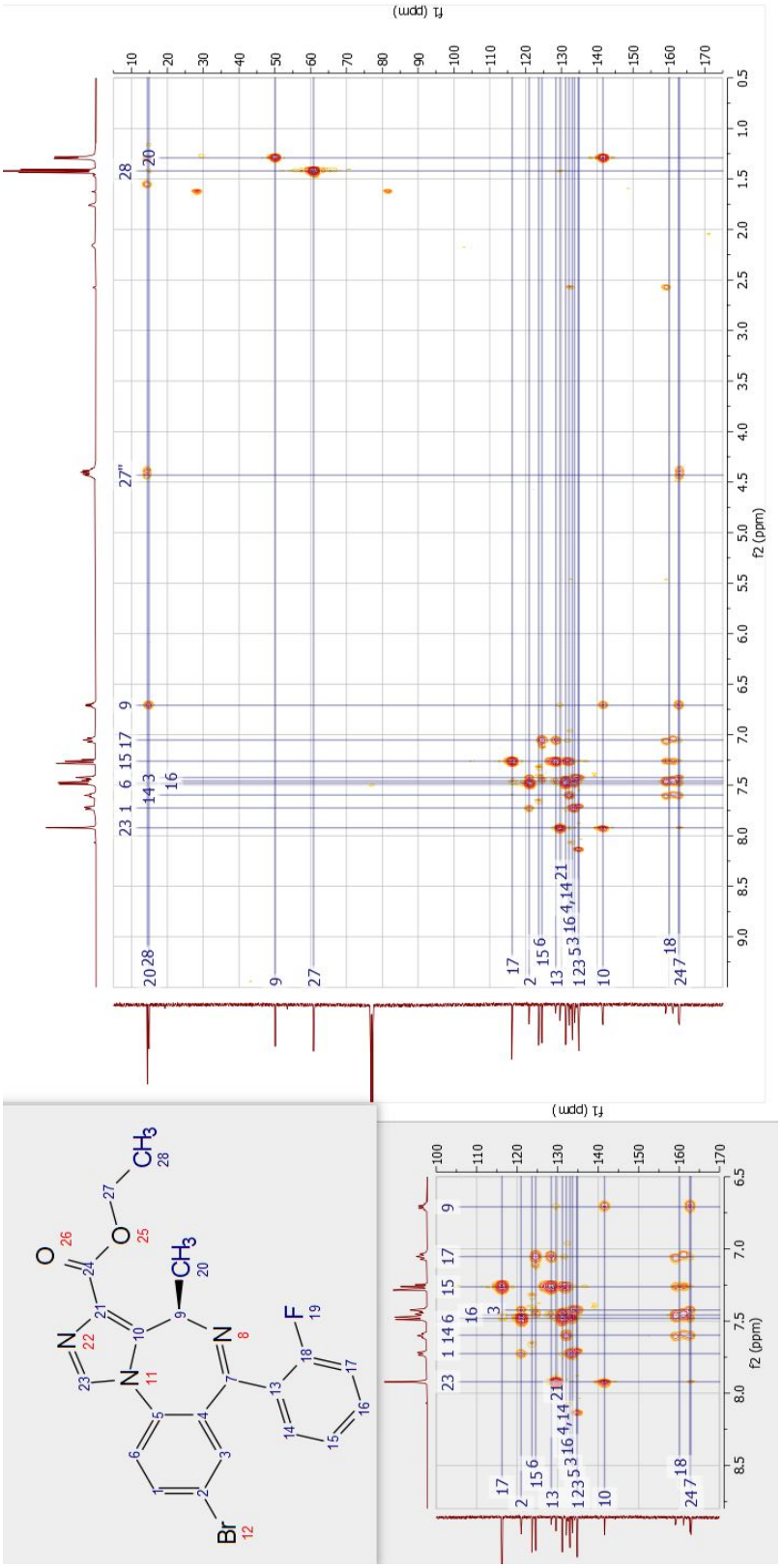

3.5.3.6. ROESY Spectrum of MIDD0003

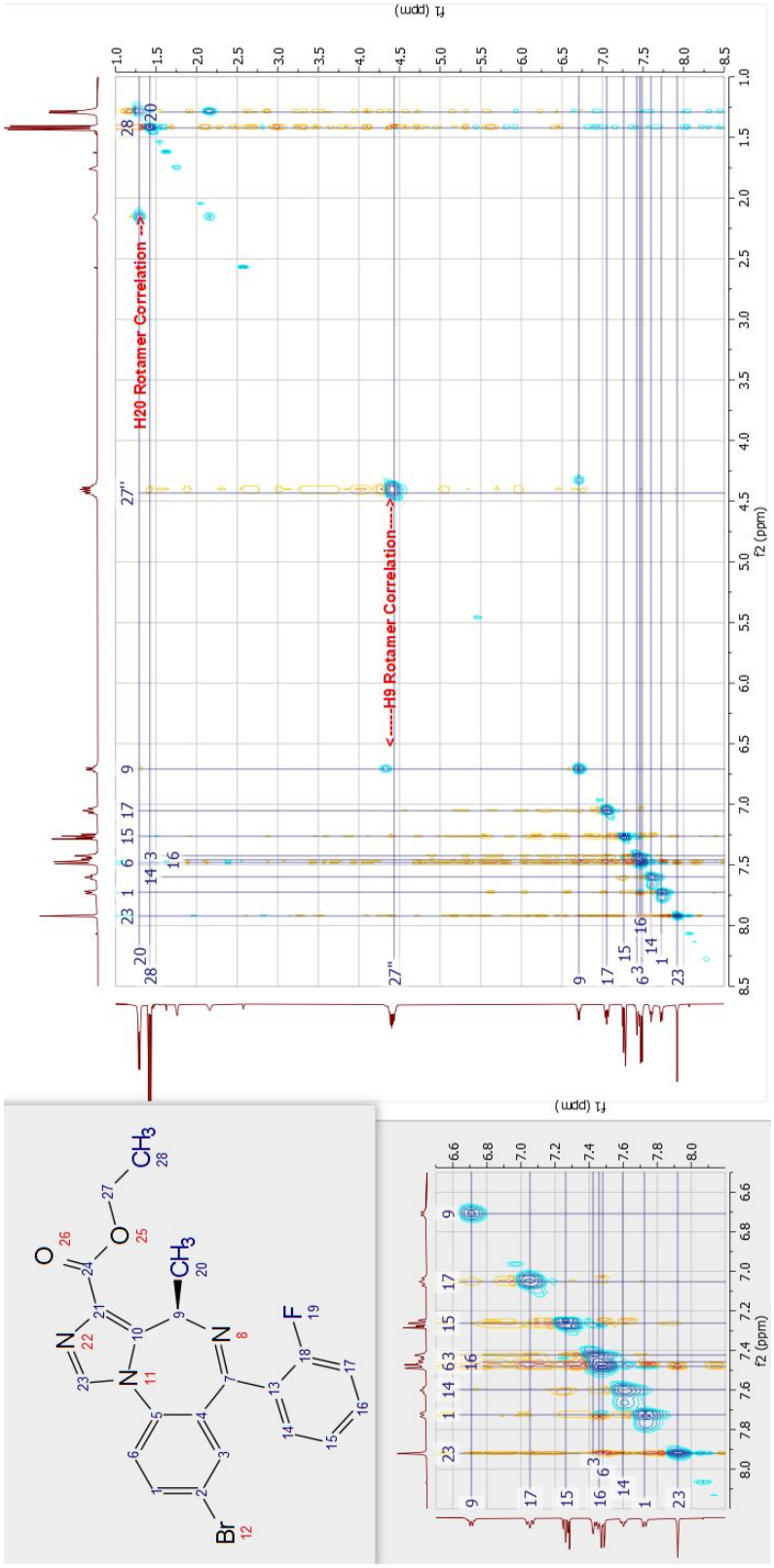

3.5.4. NMR Spectra of MIDD0301

3.5.4.1. ^{1}H NMR Spectrum of MIDD0301

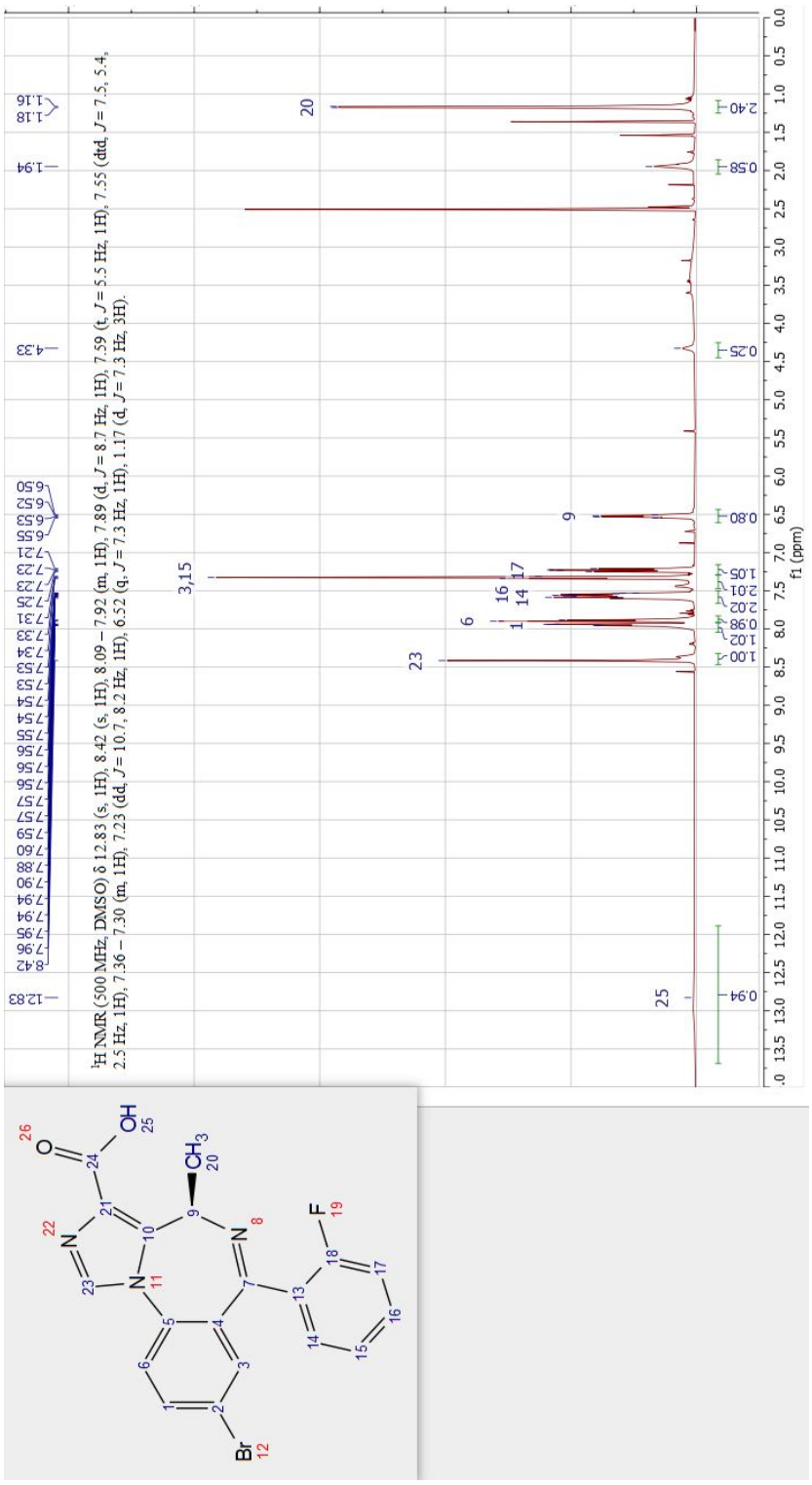

3.5.4.2. ^{13}C NMR Spectrum of MIDD0301

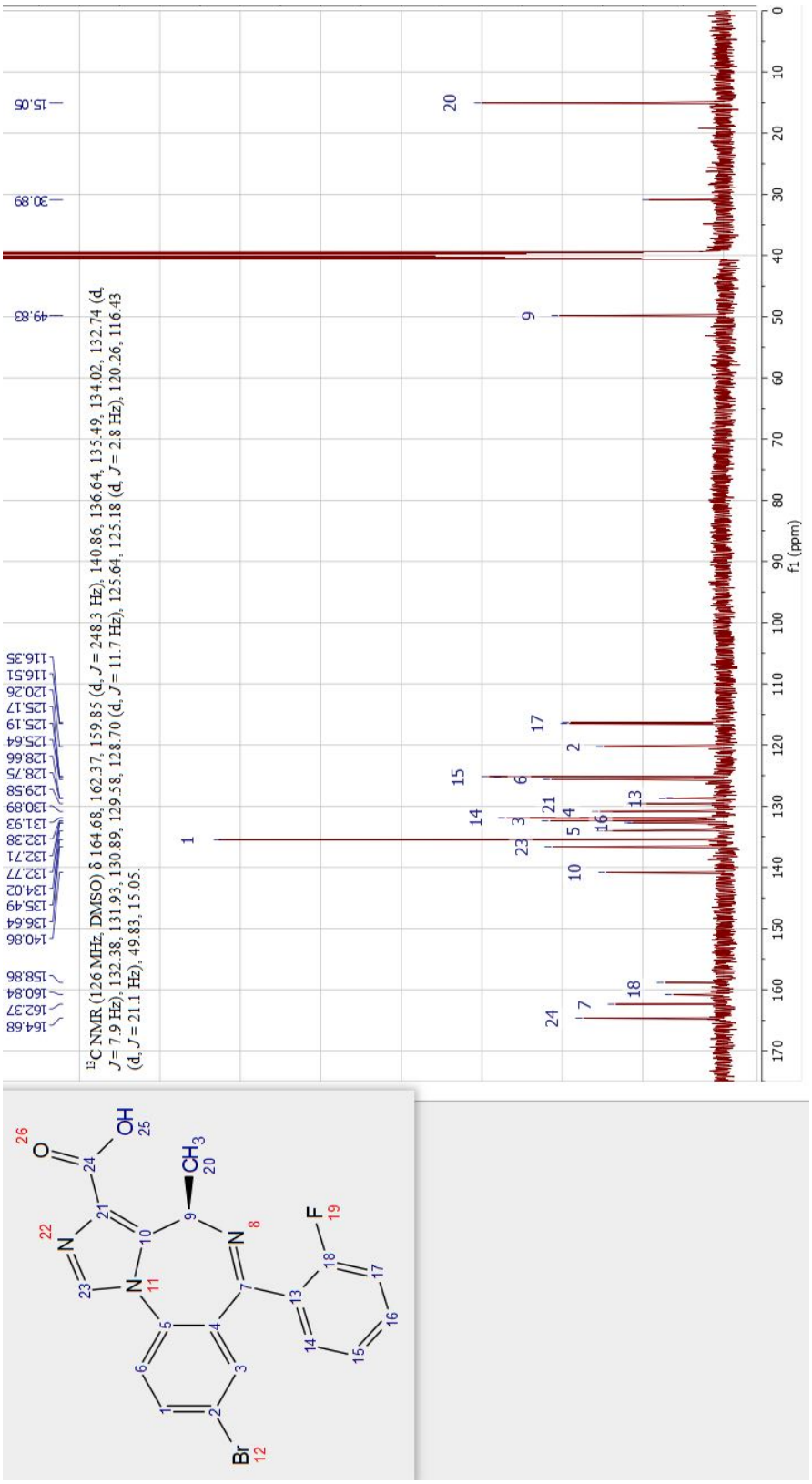

3.5.4.3. COSY Spectrum of MIDD0301

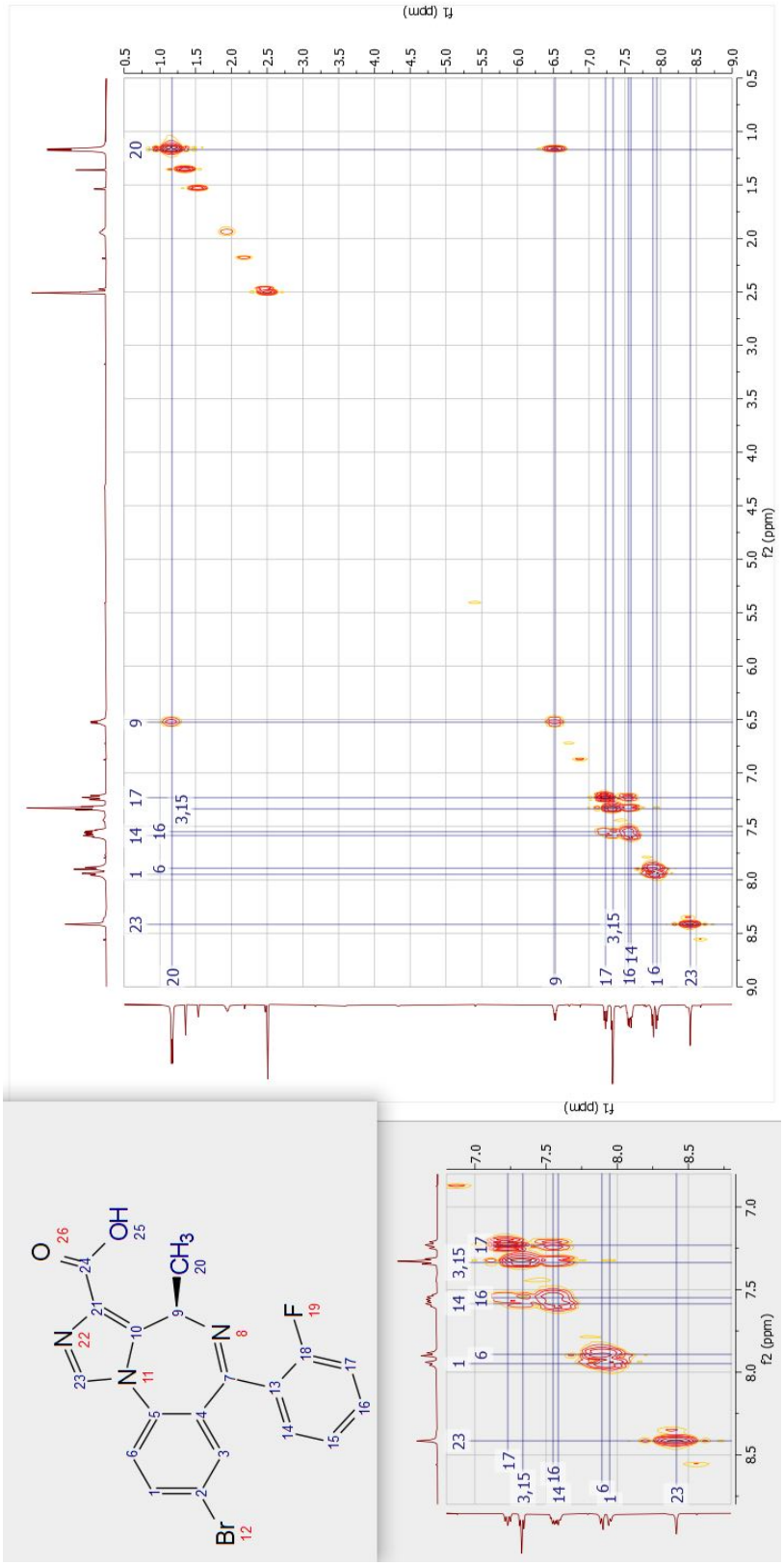

3.5.4.4. ^{1}H-^{13}C-HSQC Spectrum of MIDD0301

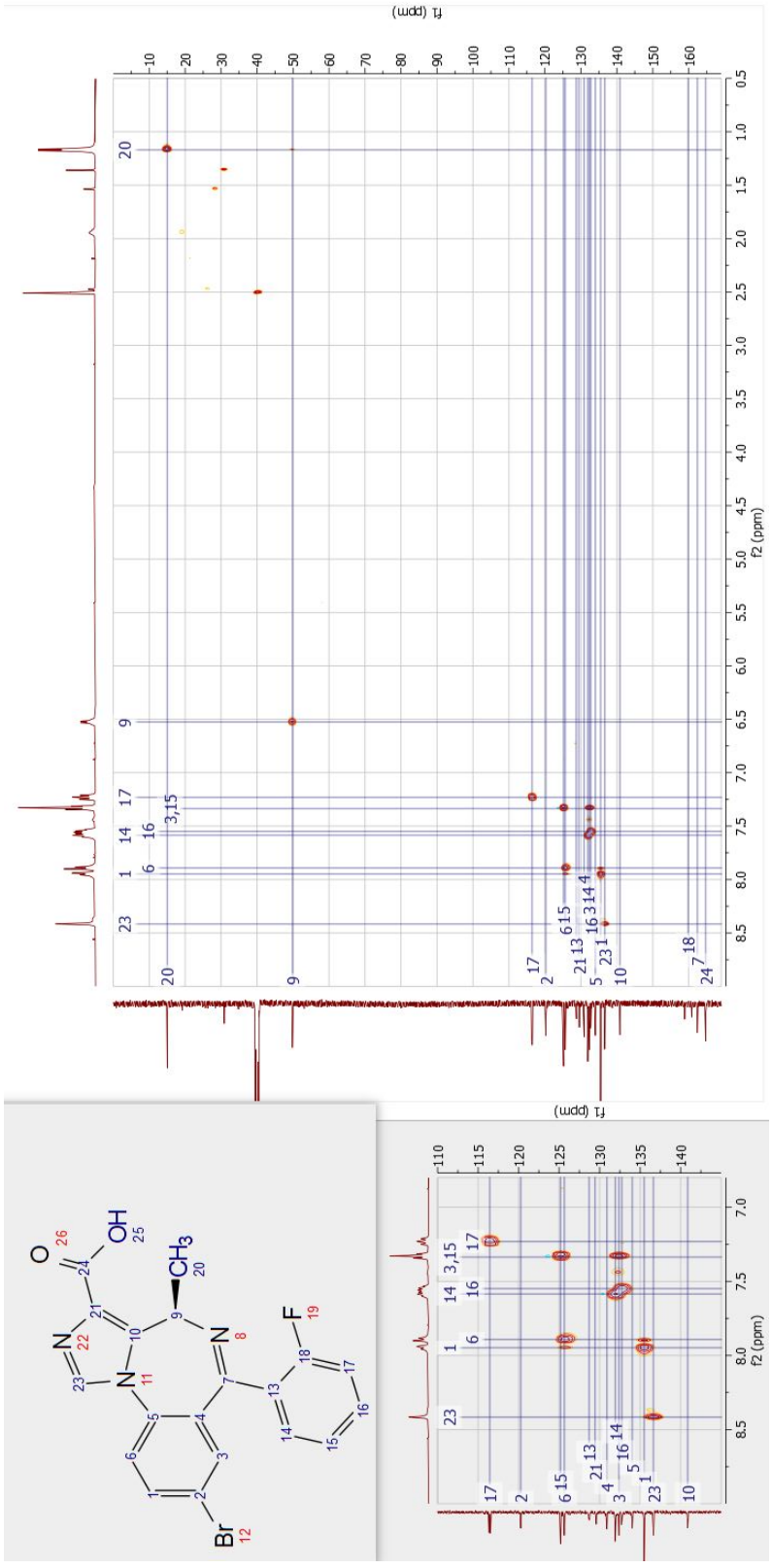

3.5.4.5. ^{1}H-^{13}C-HMBC Spectrum of MIDD0301

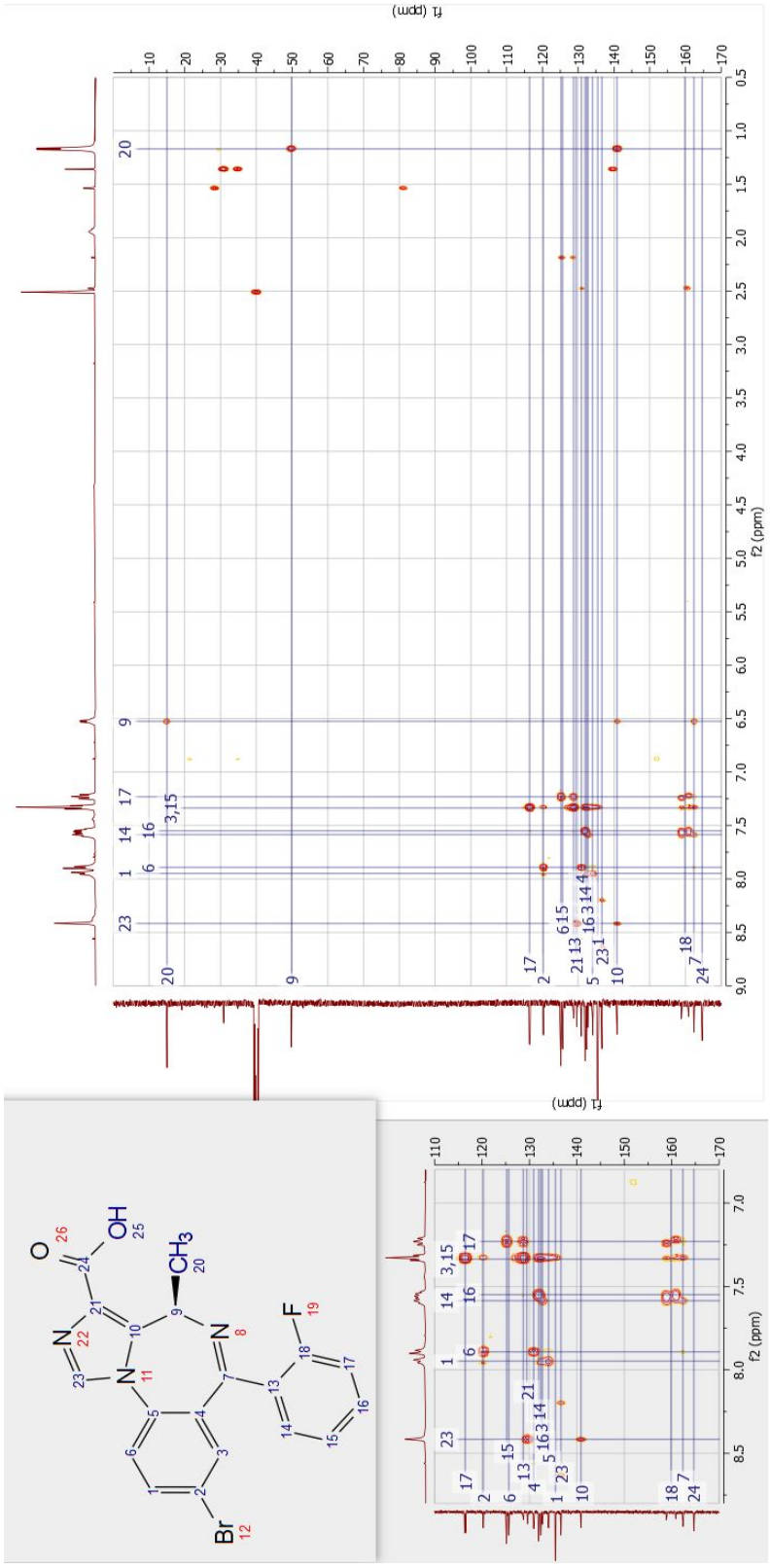

3.5.4.6. ROESY Spectrum of MIDD0301

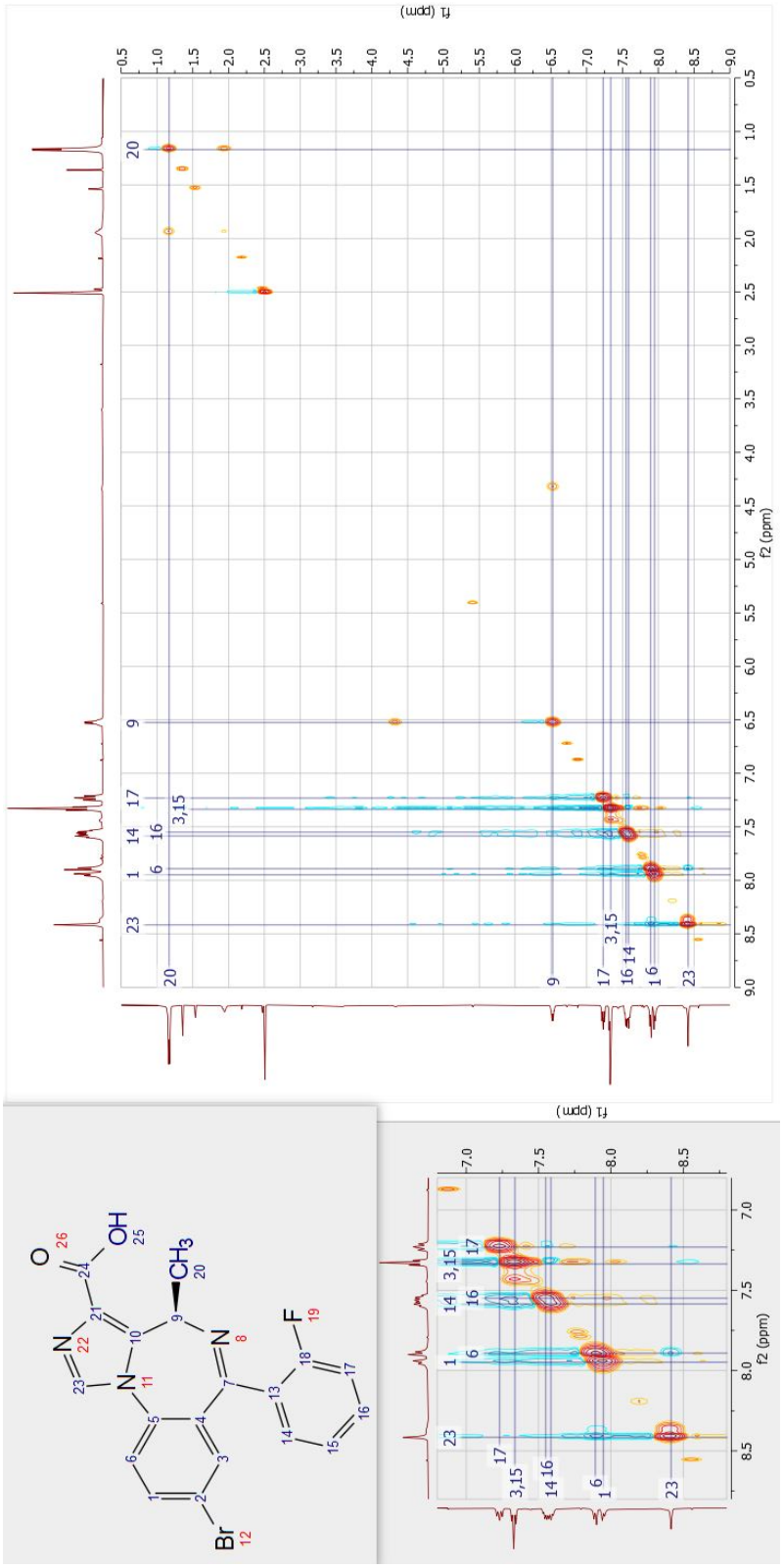

3.5.5. NMR Spectra of SH-053-2'F-R-CH3

3.5.5.1. ^{1}H NMR of SH-053-2'F-R-CH3

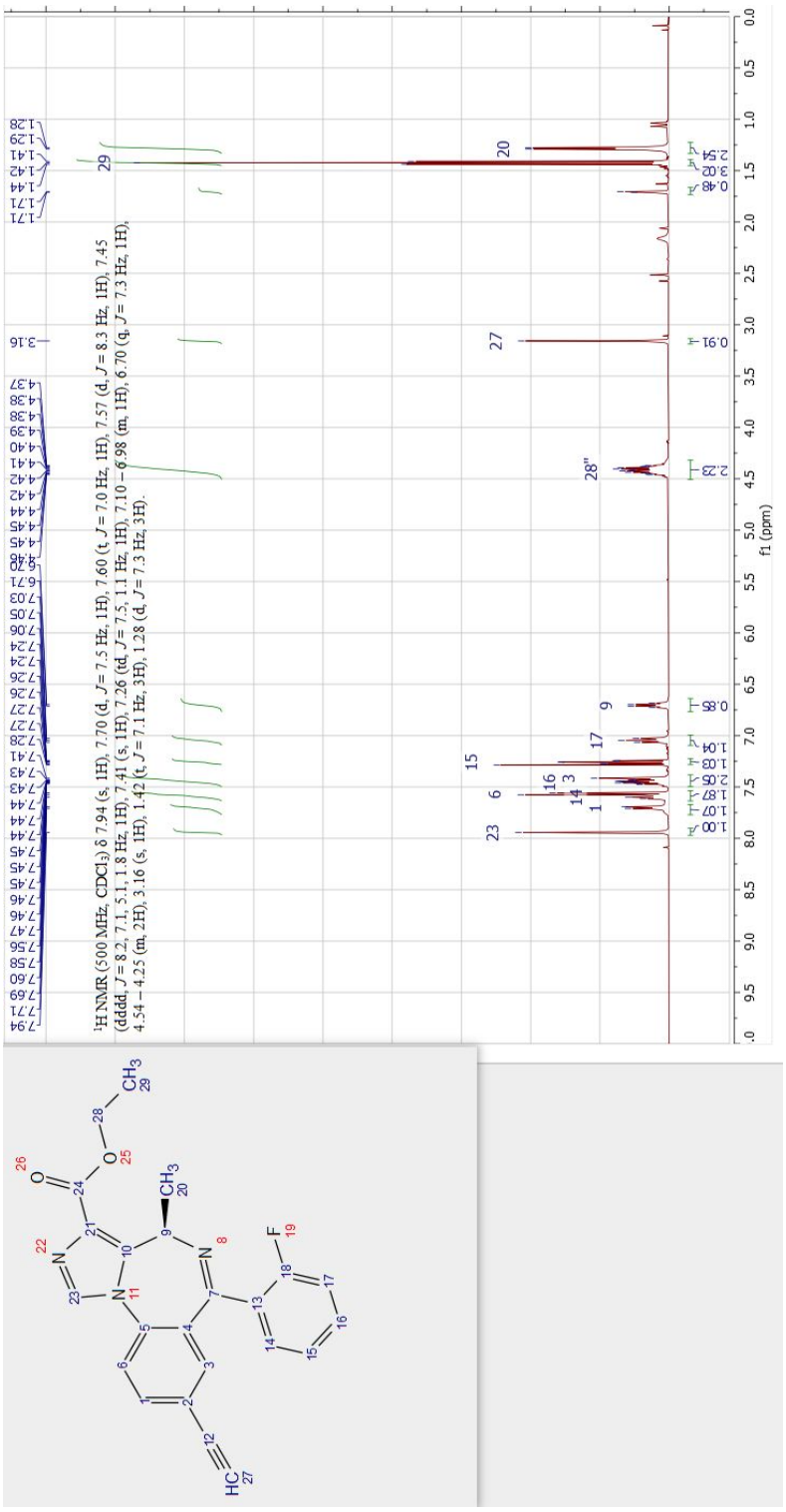

3.5.5.2. ^{13}C NMR of SH-053-2'F-R-CH3

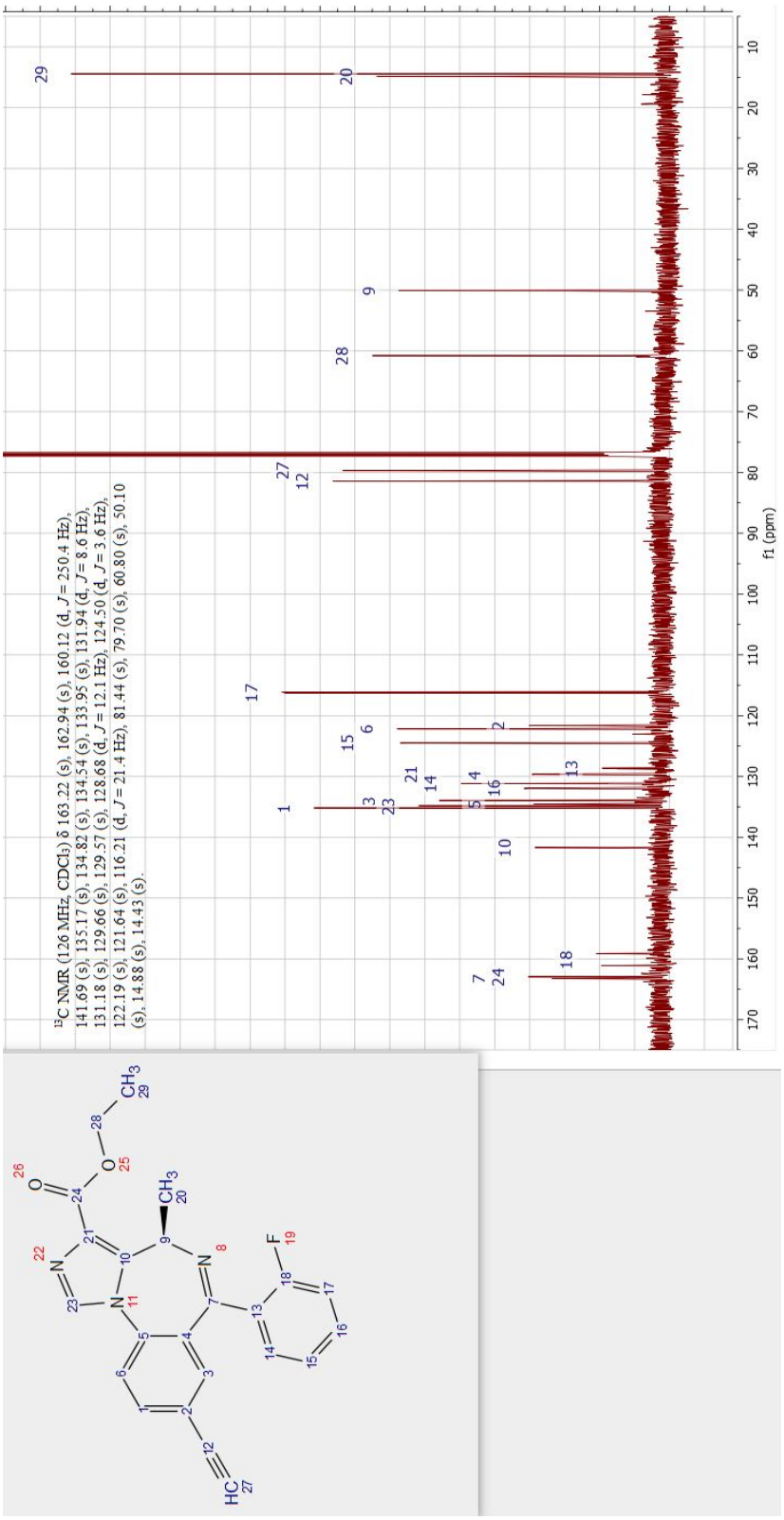

3.5.5.3. COSY Spectrum of SH-053-2'F-R-CH3

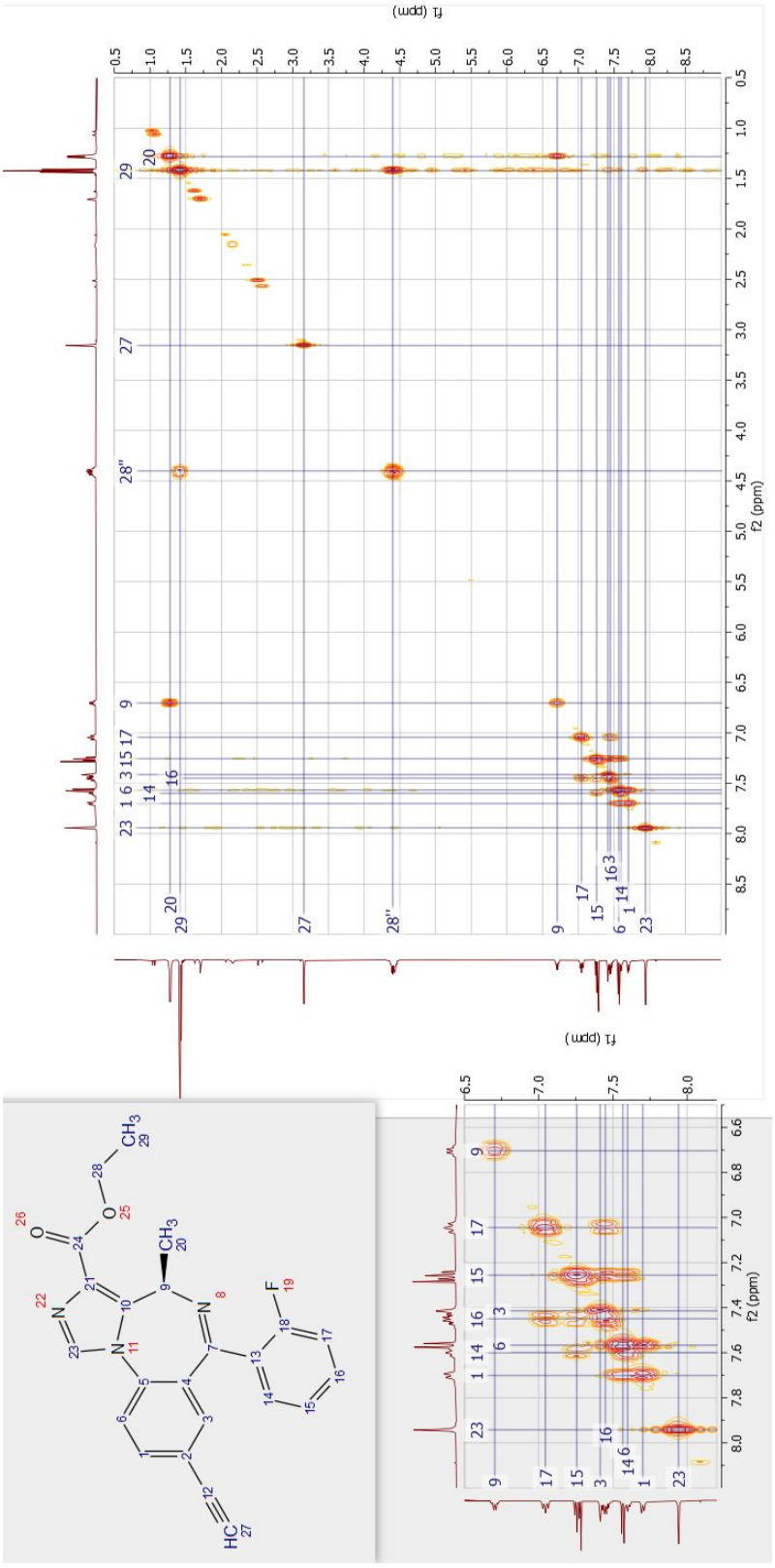

3.5.5.4. ^{1}H-^{13}C-HSQC Spectrum of SH-053-2'F-R-CH3

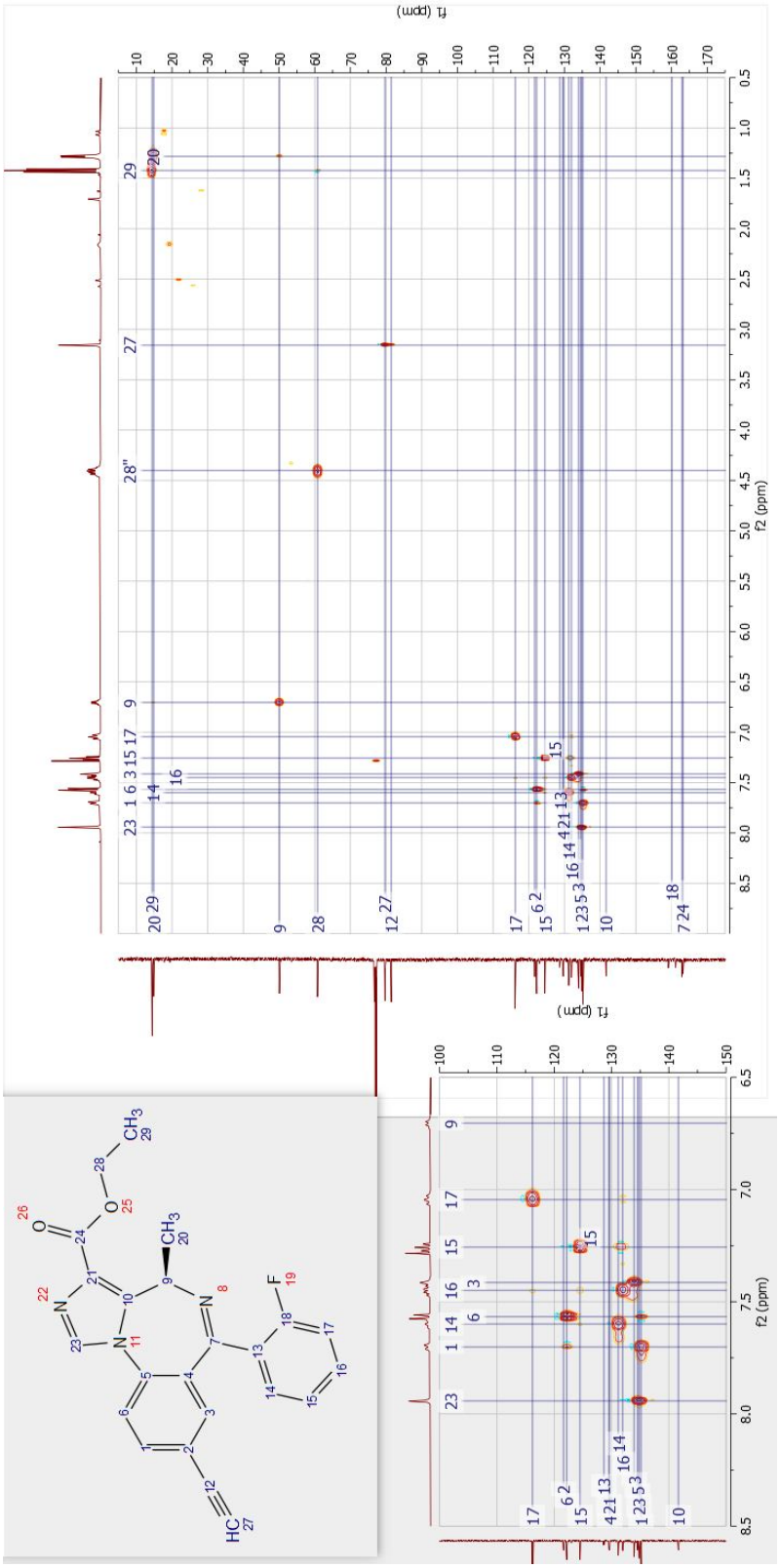

3.5.5.5. ^{1}H-^{13}C-HMBC Spectrum of SH-053-2'F-R-CH3

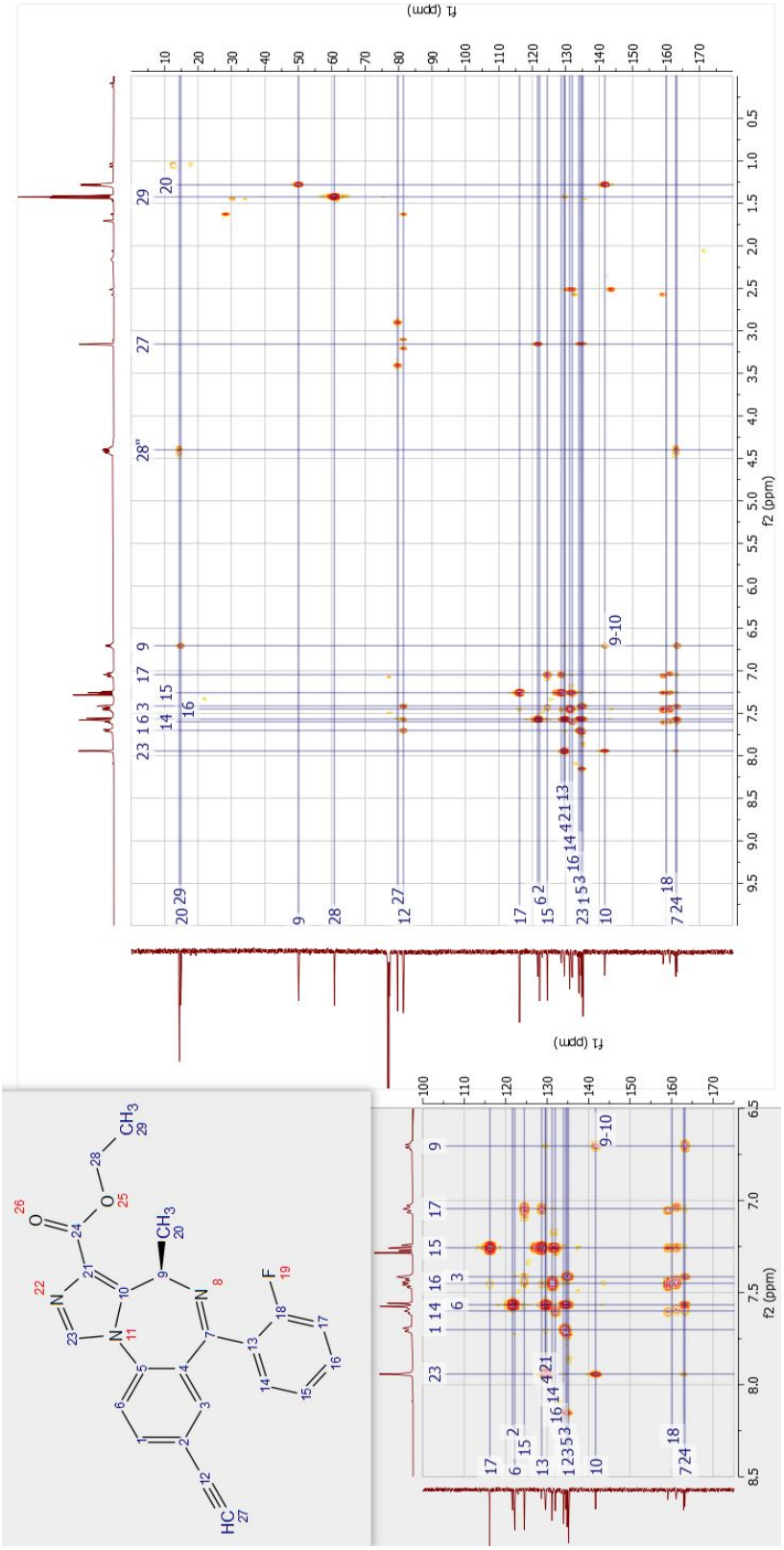

3.5.5.6. ROESY Spectrum of SH-053-2'F-R-CH3

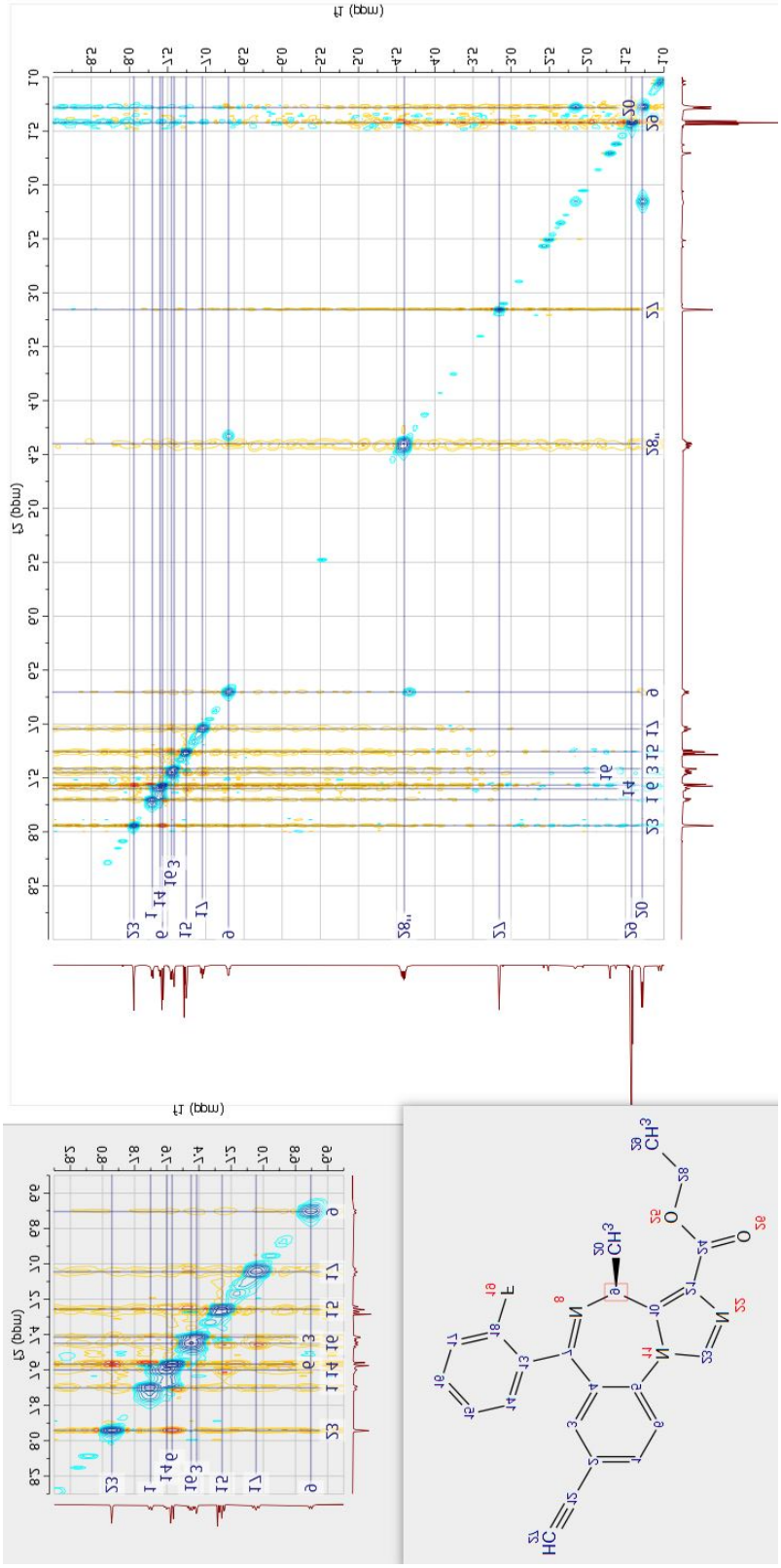

3.5.6. NMR Spectra of SH-053-2'F-R-CH3-acid

3.5.6.1. ^{1}H NMR of SH-053-2'F-R-CH3-acid

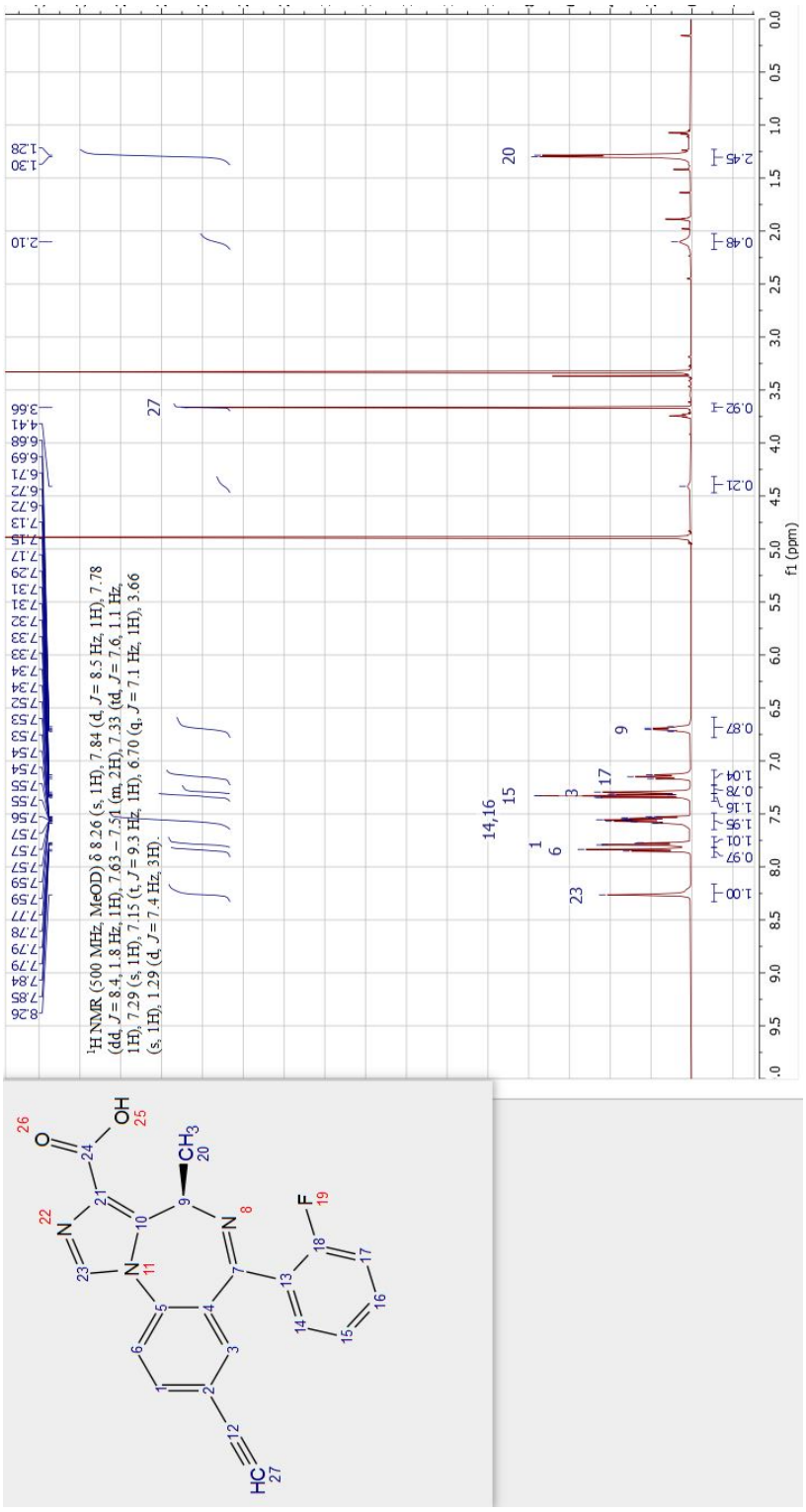

3.5.6.2. ^{13}C NMR of SH-053-2'F-R-CH3-acid

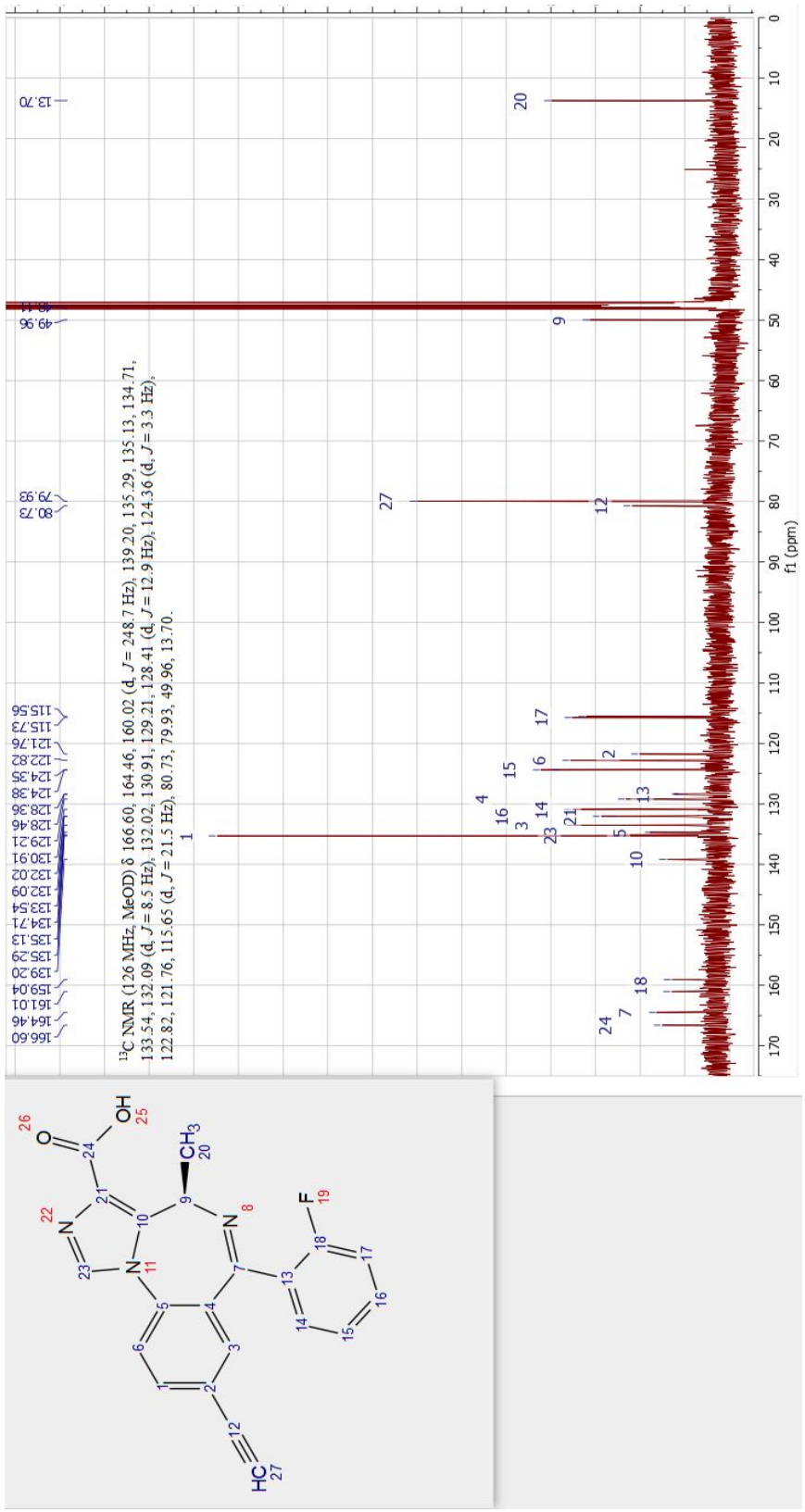

3.5.6.3. COSY Spectrum of SH-053-2'F-R-CH3-acid

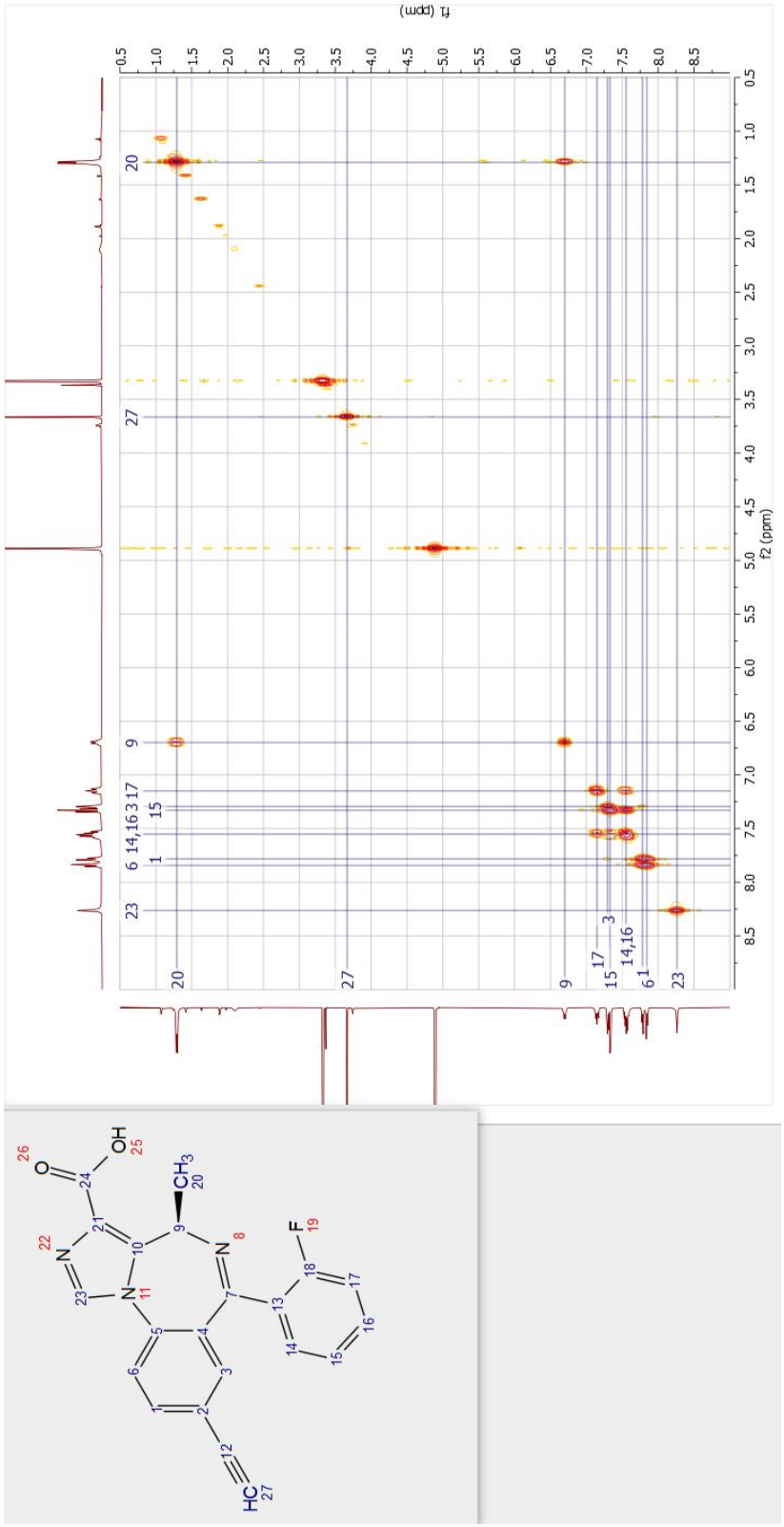

3.5.6.4. ^{1}H-^{13}C-HSQC Spectrum of SH-053-2'F-R-CH3-acid

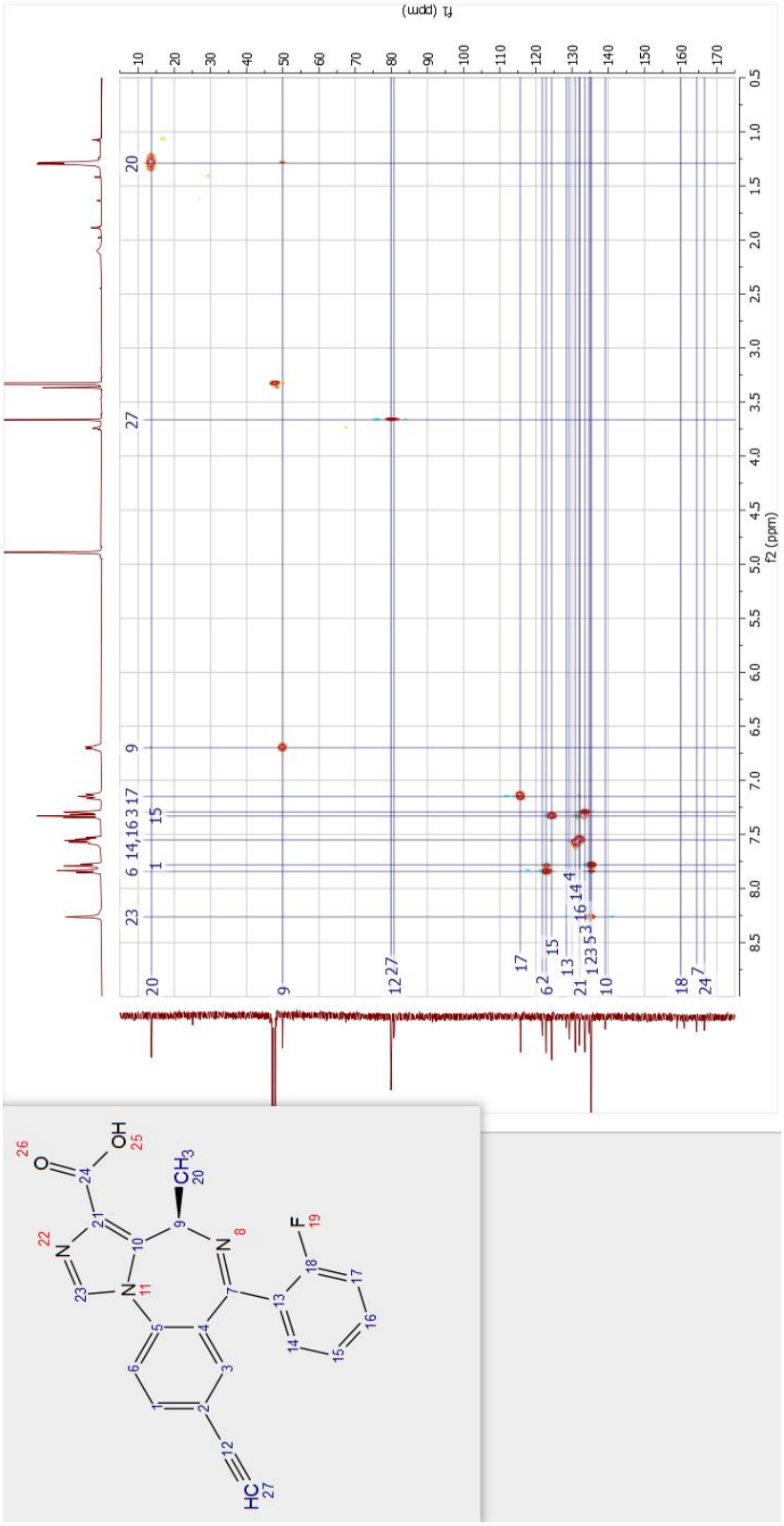

3.5.6.5. ^{1}H-^{13}C-HMBC Spectrum of SH-053-2'F-R-CH3-acid

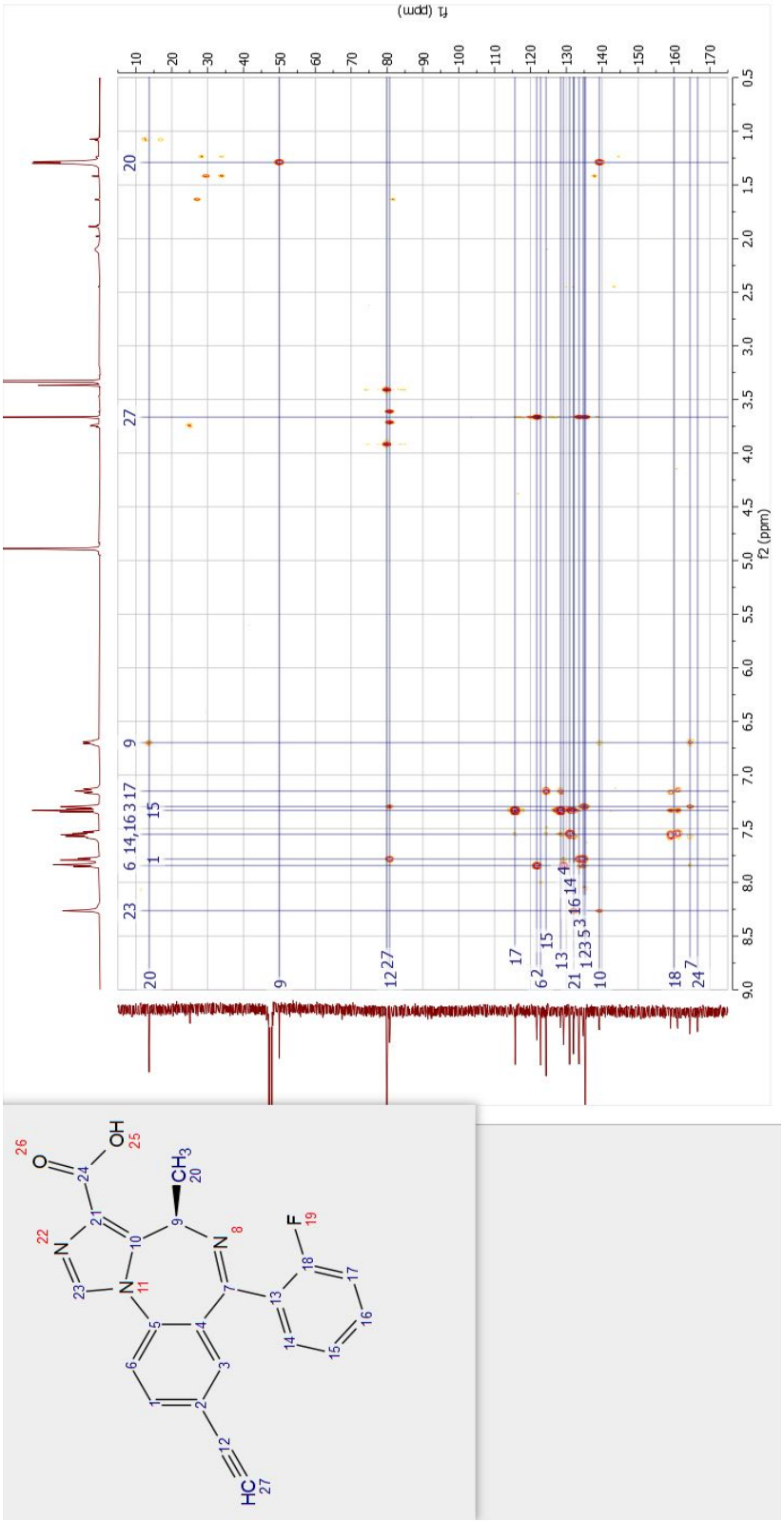

3.5.6.6. ROESY Spectrum of SH-053-2'F-R-CH3-acid

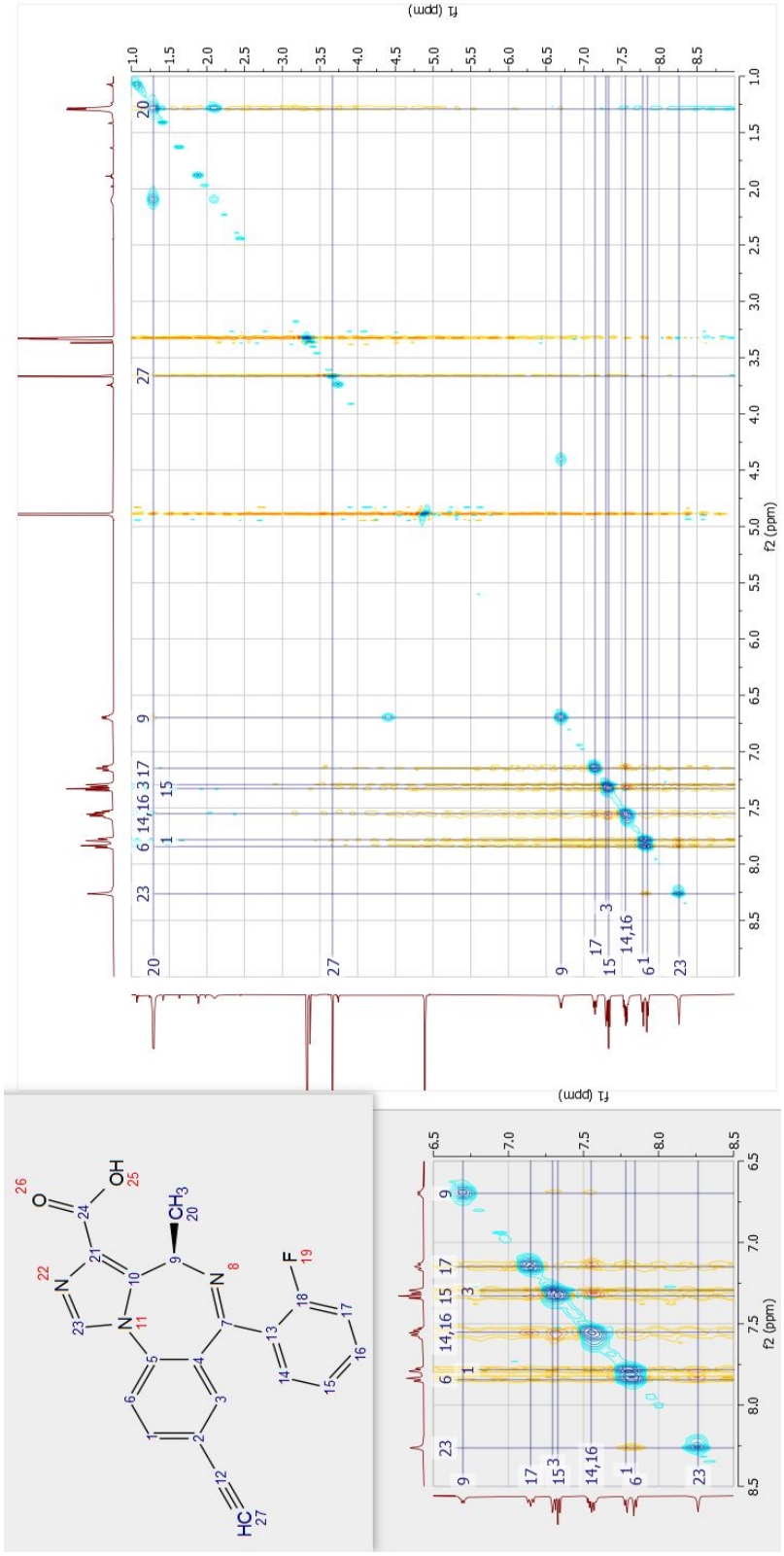

3.5.7. NMR Spectra of GL-II-73

3.5.7.1. ^{1}H NMR of GL-II-73

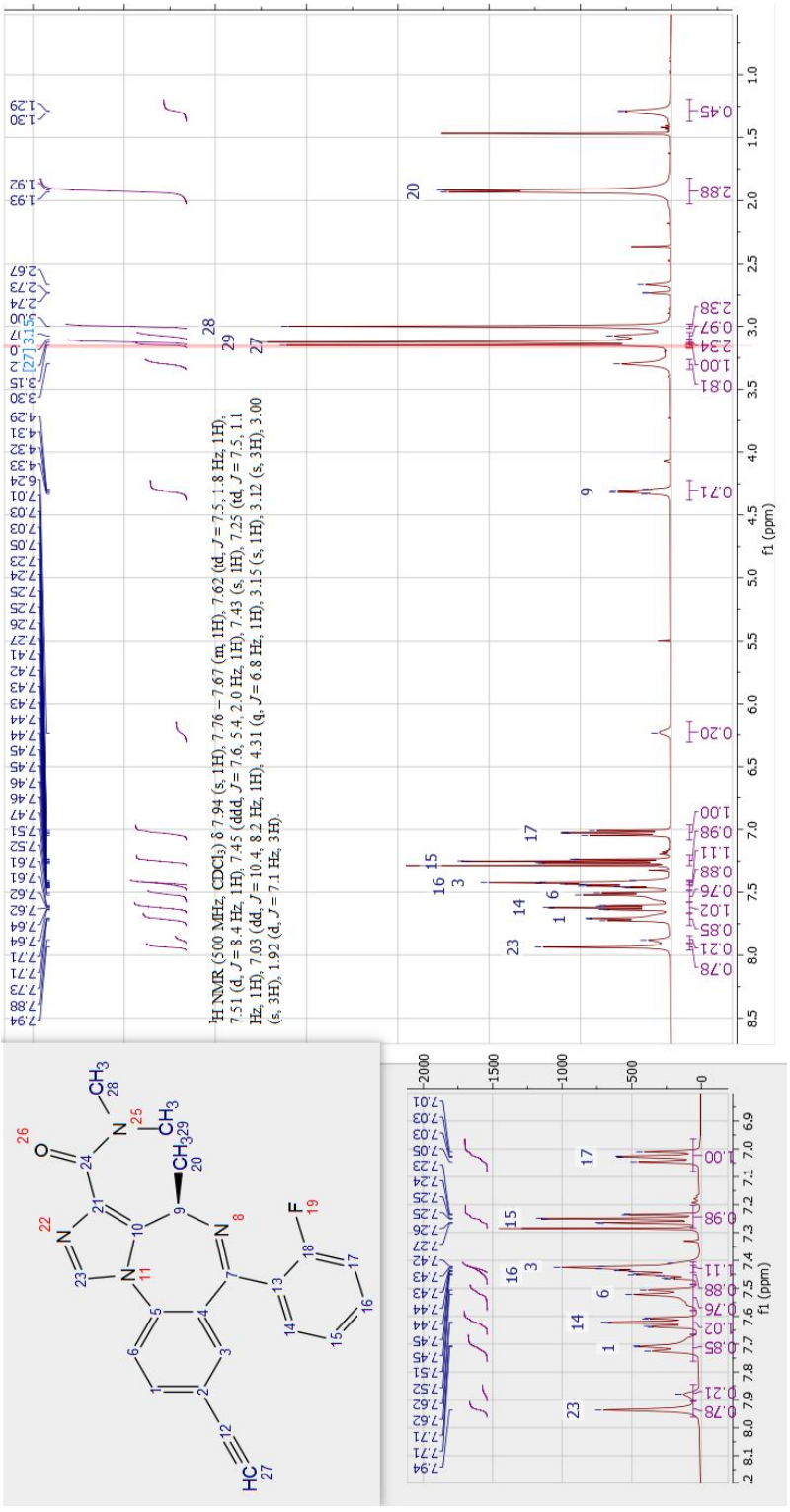

3.5.7.2. ^{13}C NMR of GL-II-73

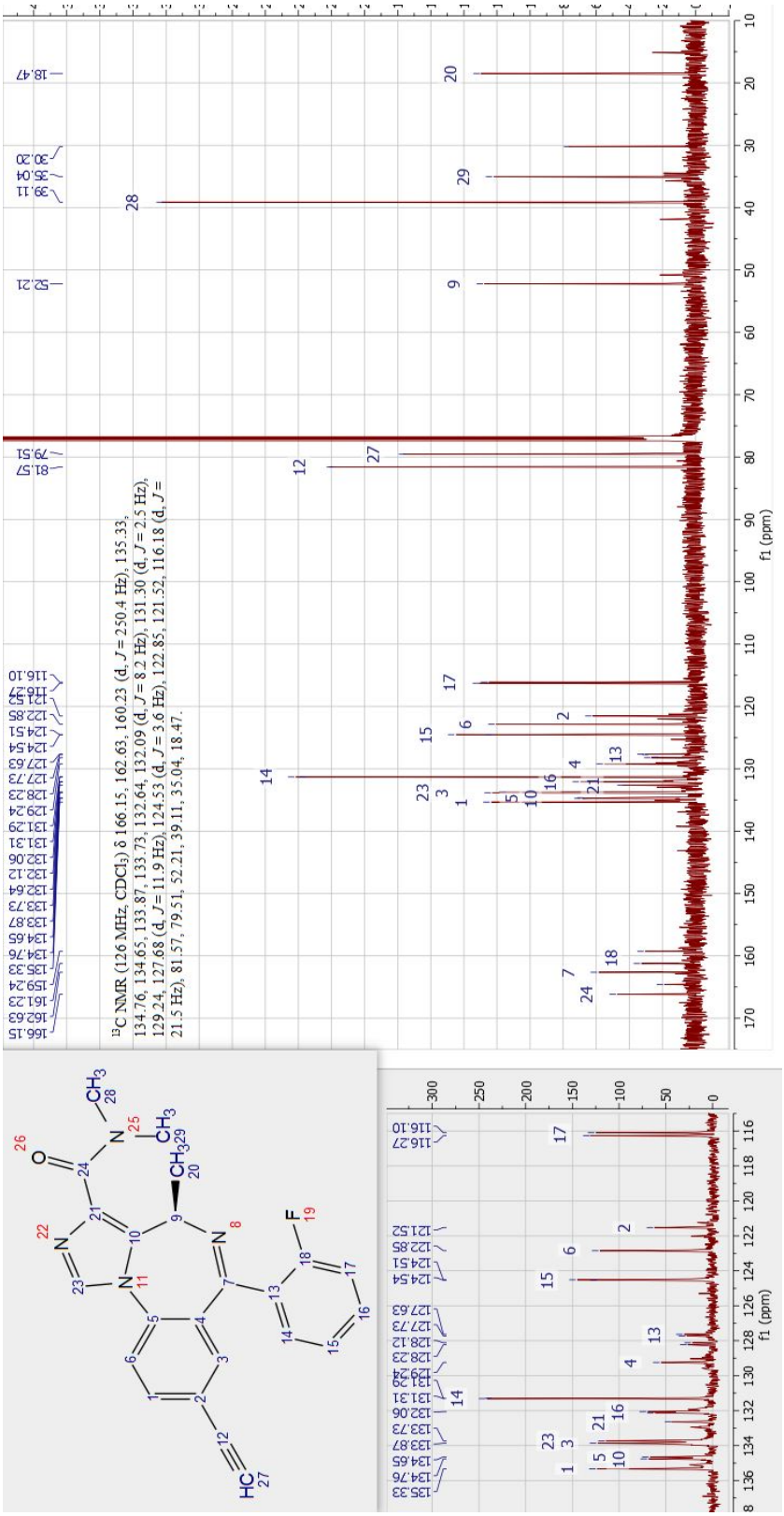

3.5.7.3. COSY Spectrum of GL-II-73

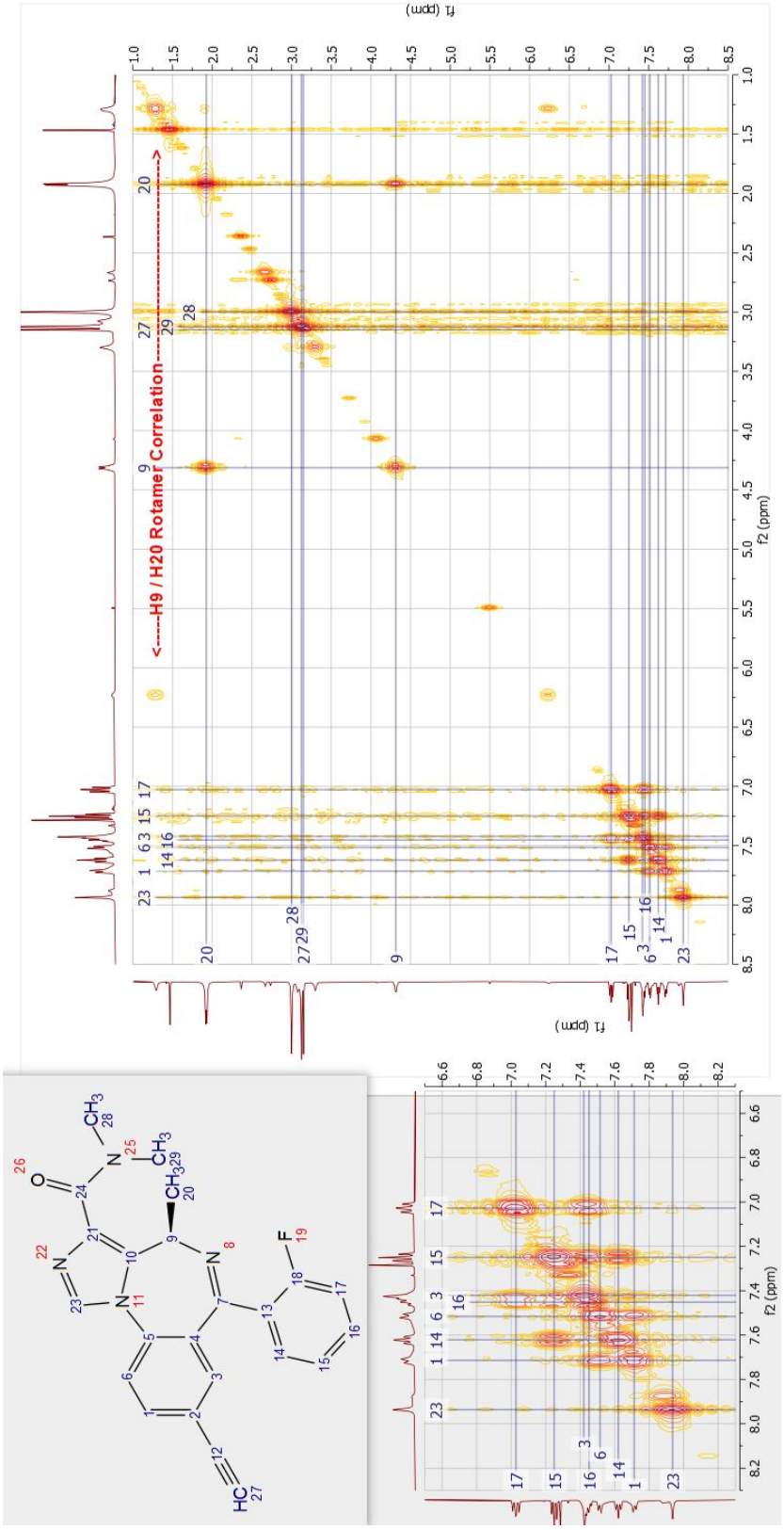

3.5.7.4. ^{1}H-^{13}C-HSQC Spectrum of GL-II-73

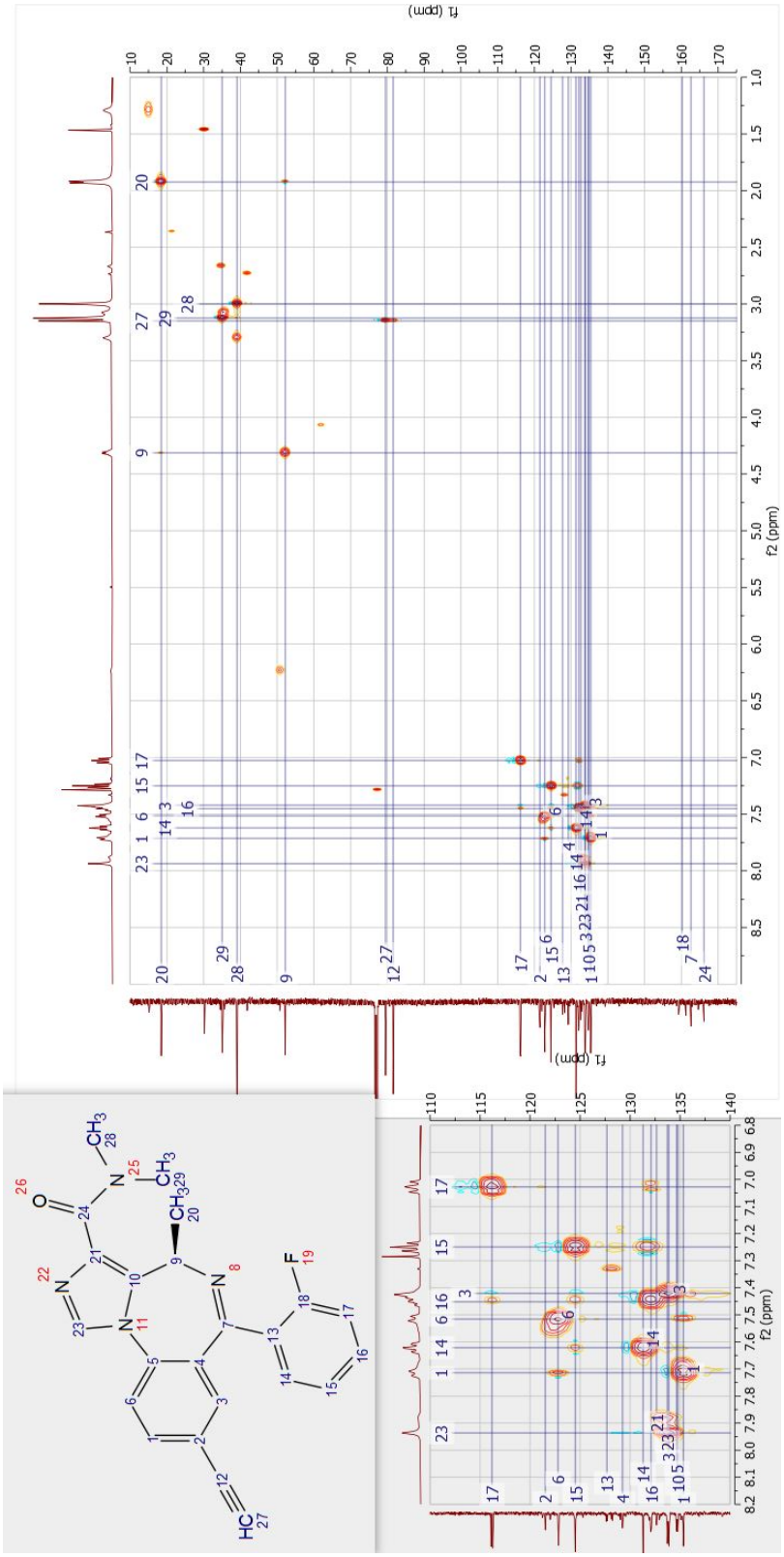

3.5.7.5. ^{1}H-^{13}C-HMBC Spectrum of GL-II-73

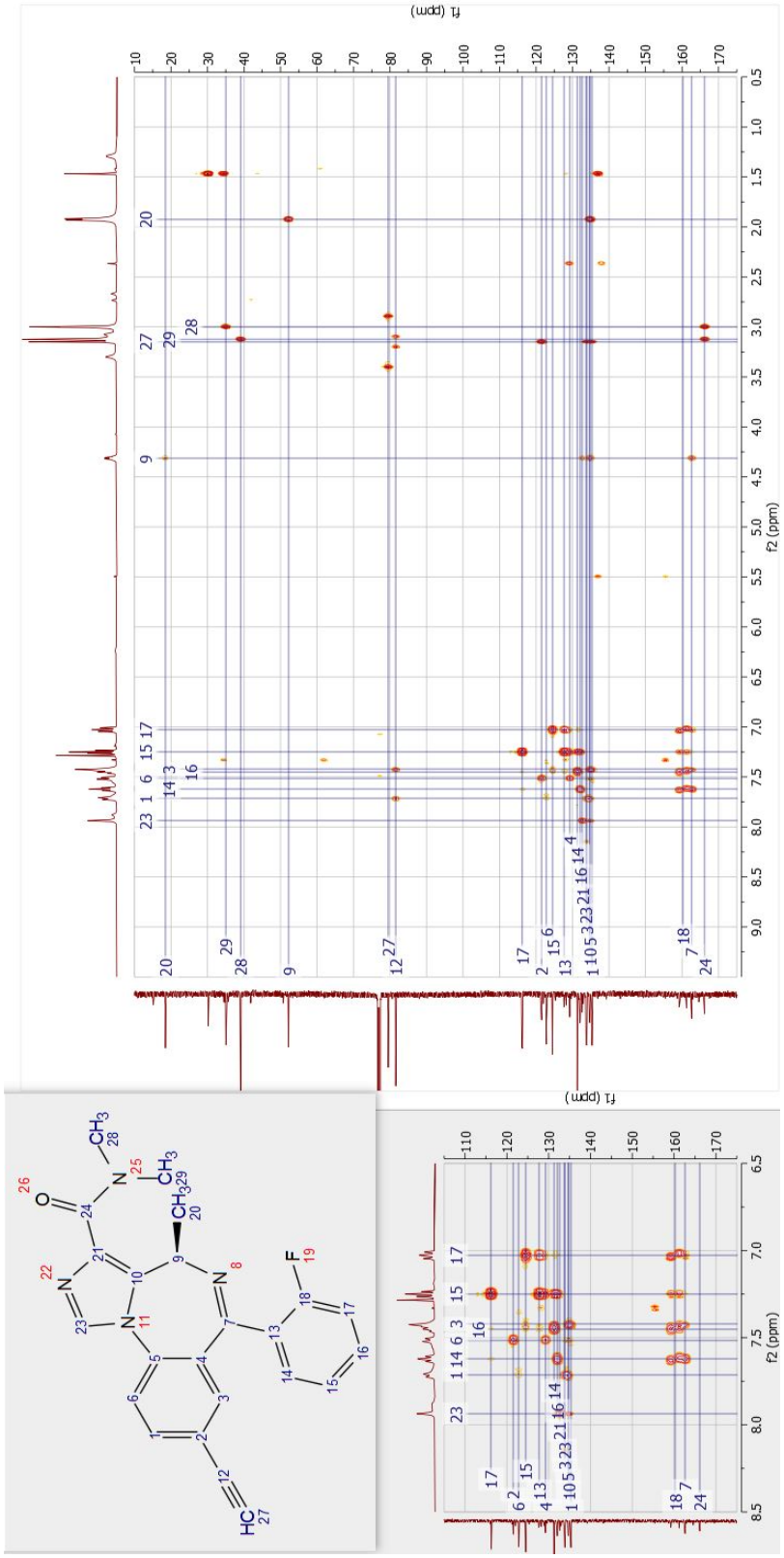

3.5.7.6. ROESY Spectrum of GL-II-73

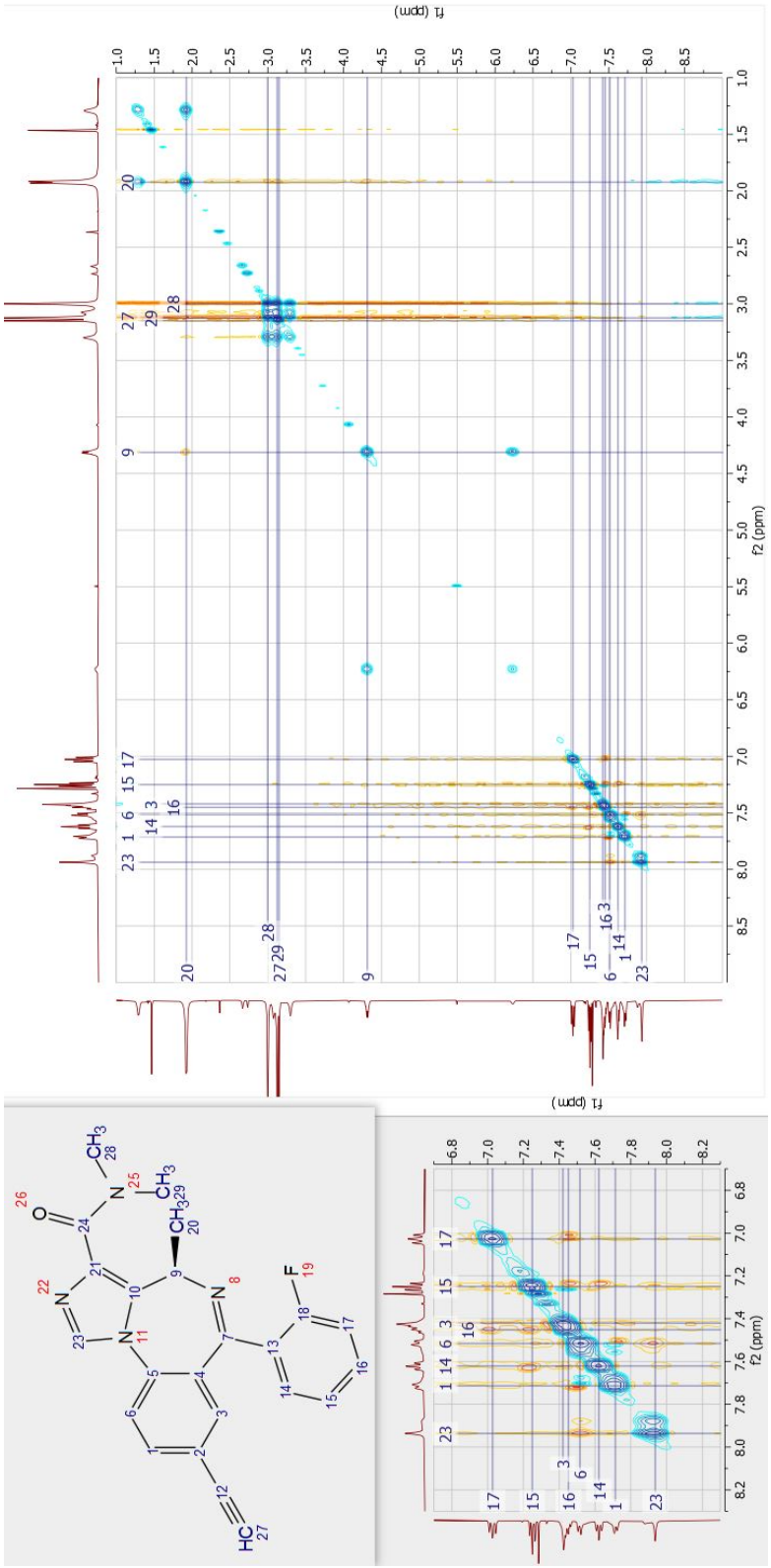

3.5.8. NMR Spectra of MP-III-022

3.5.8.1. ^{1}H NMR of MP-III-022

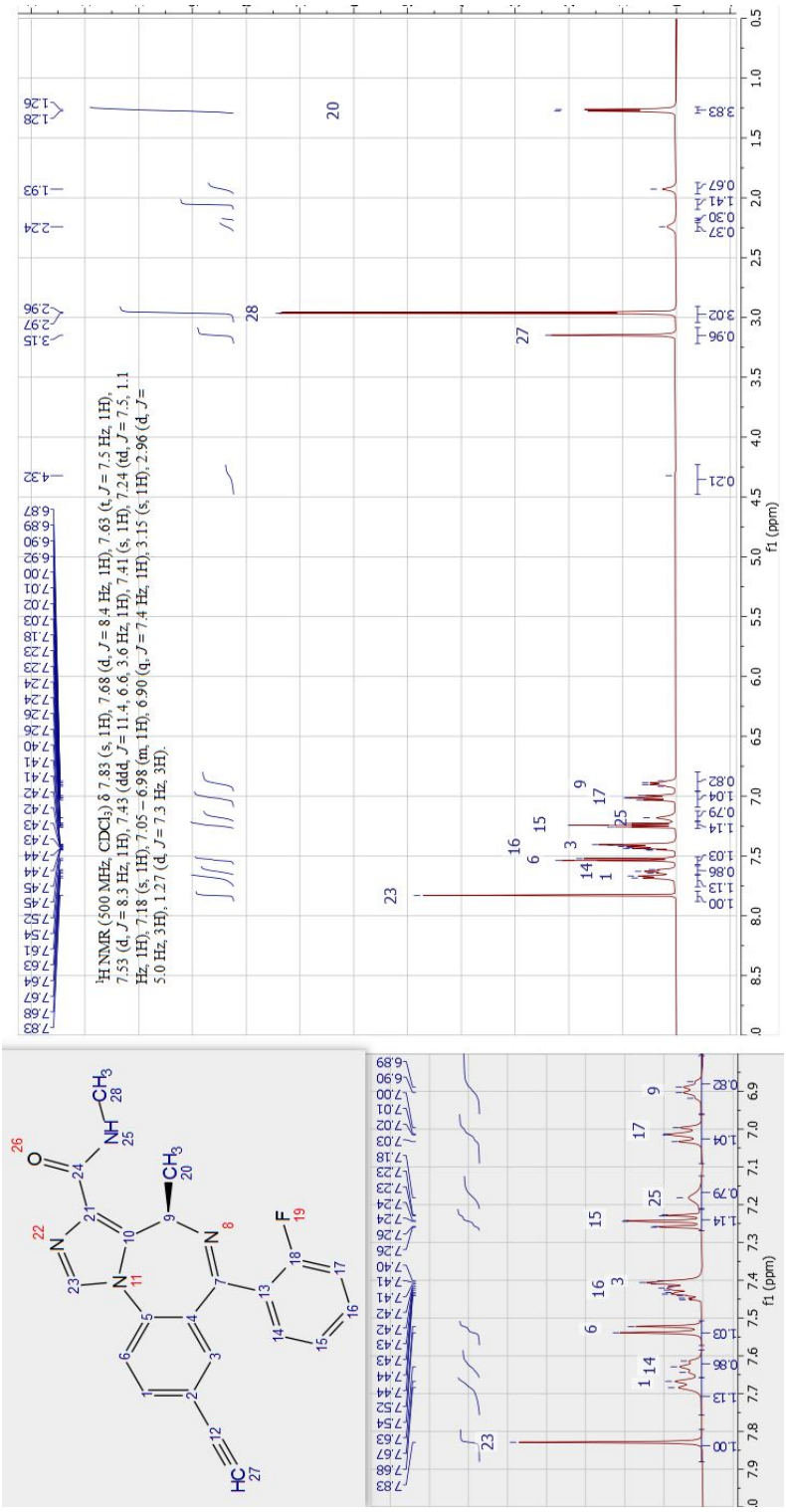

3.5.8.2. ^{13}C NMR of MP-III-022

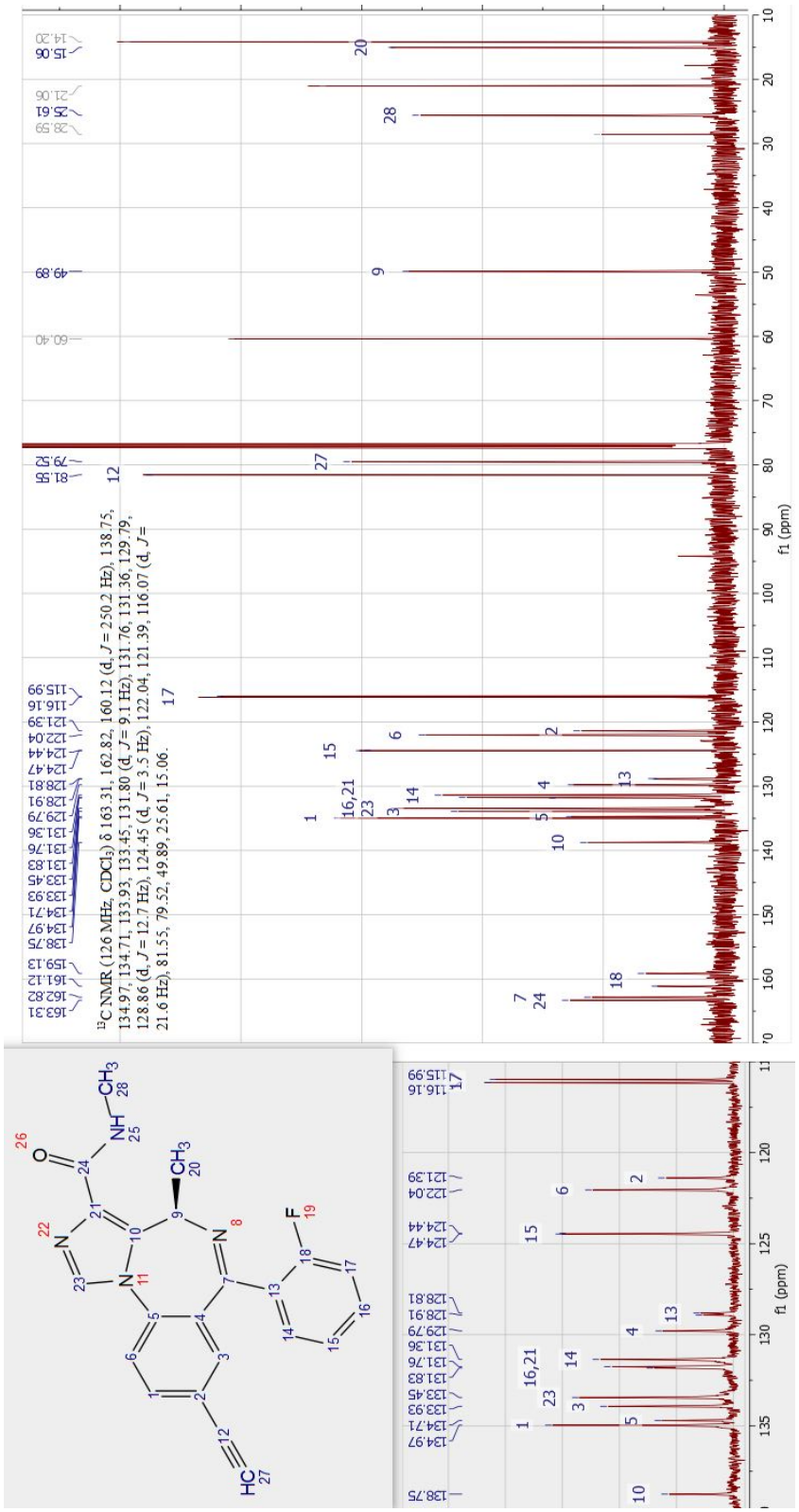

3.5.8.3. COSY Spectrum of MP-III-022

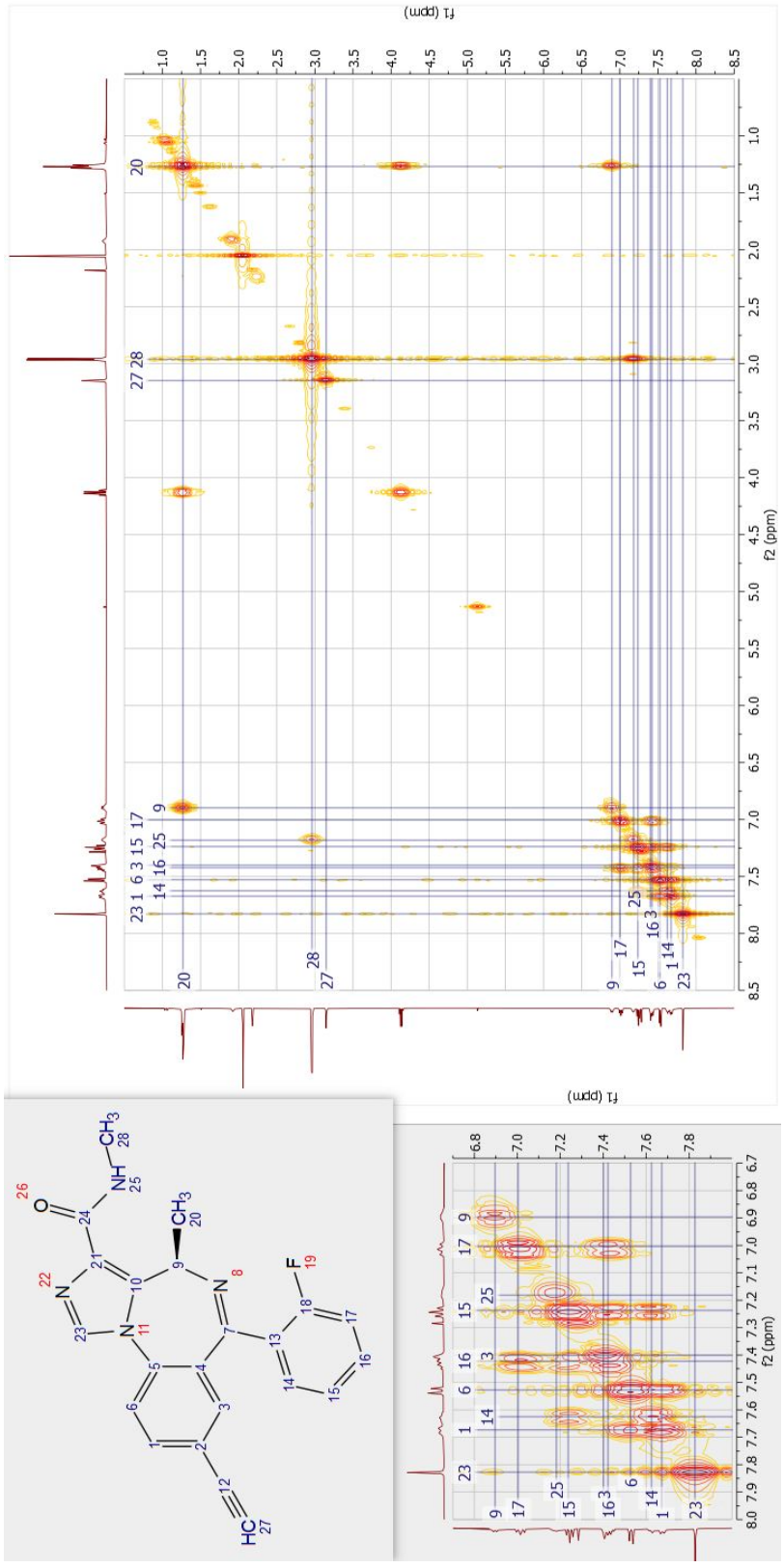

3.5.8.4. ^{1}H-^{13}C-HSQC Spectrum of MP-III-022

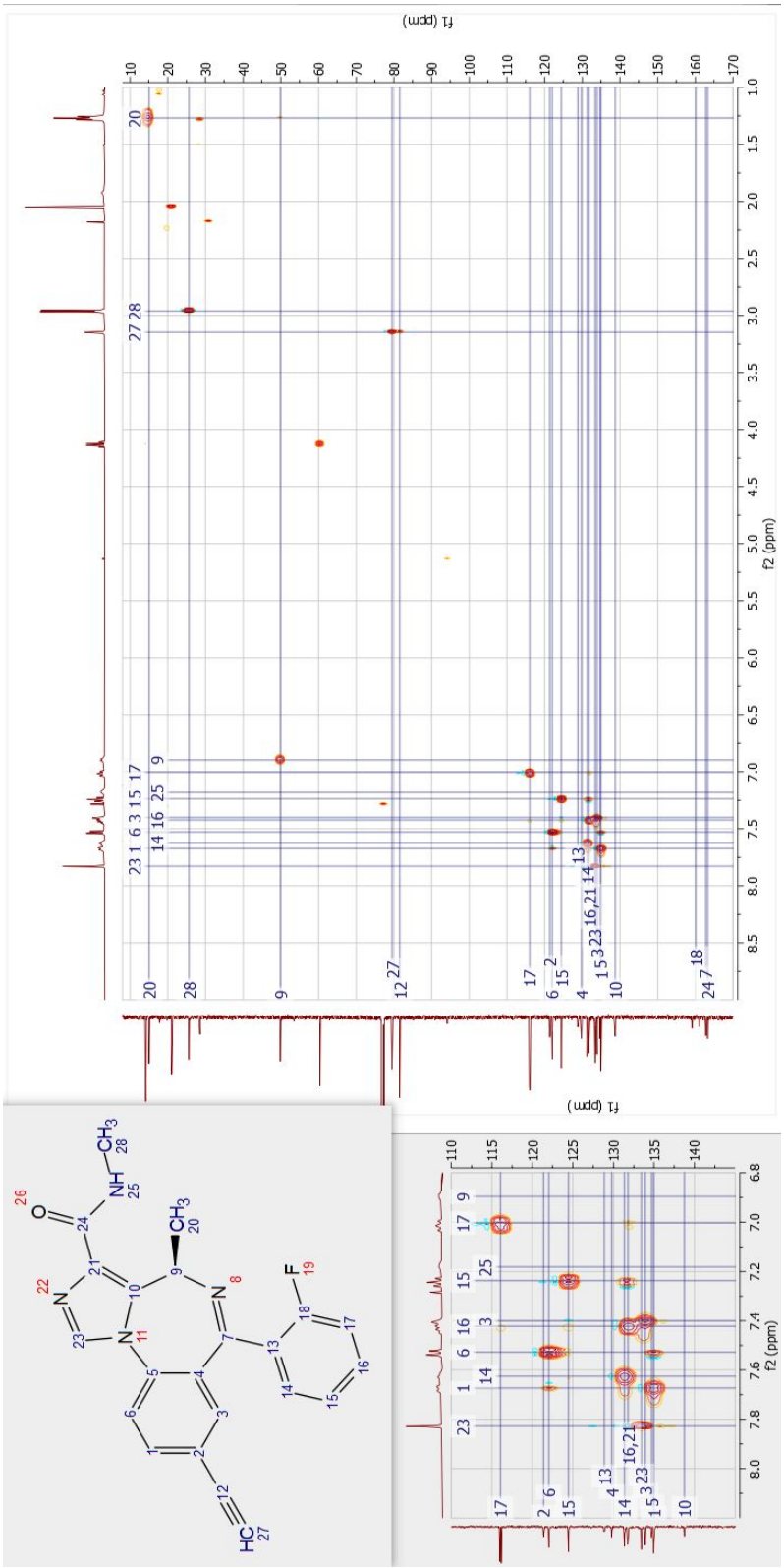

3.5.8.5. ^{1}H-^{13}C-HMBC Spectrum of MP-III-022

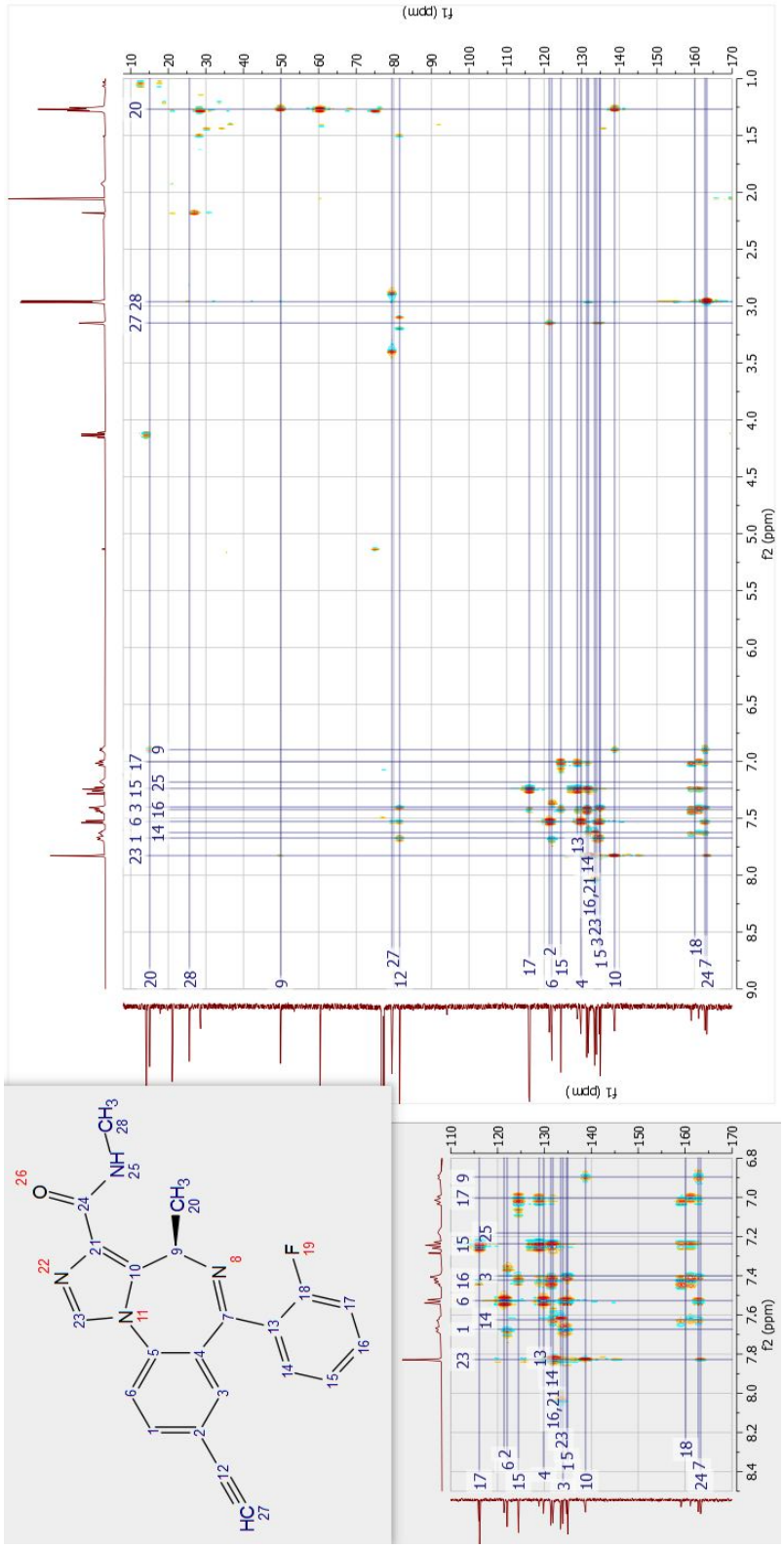

3.5.8.6. ROESY Spectrum of MP-III-022

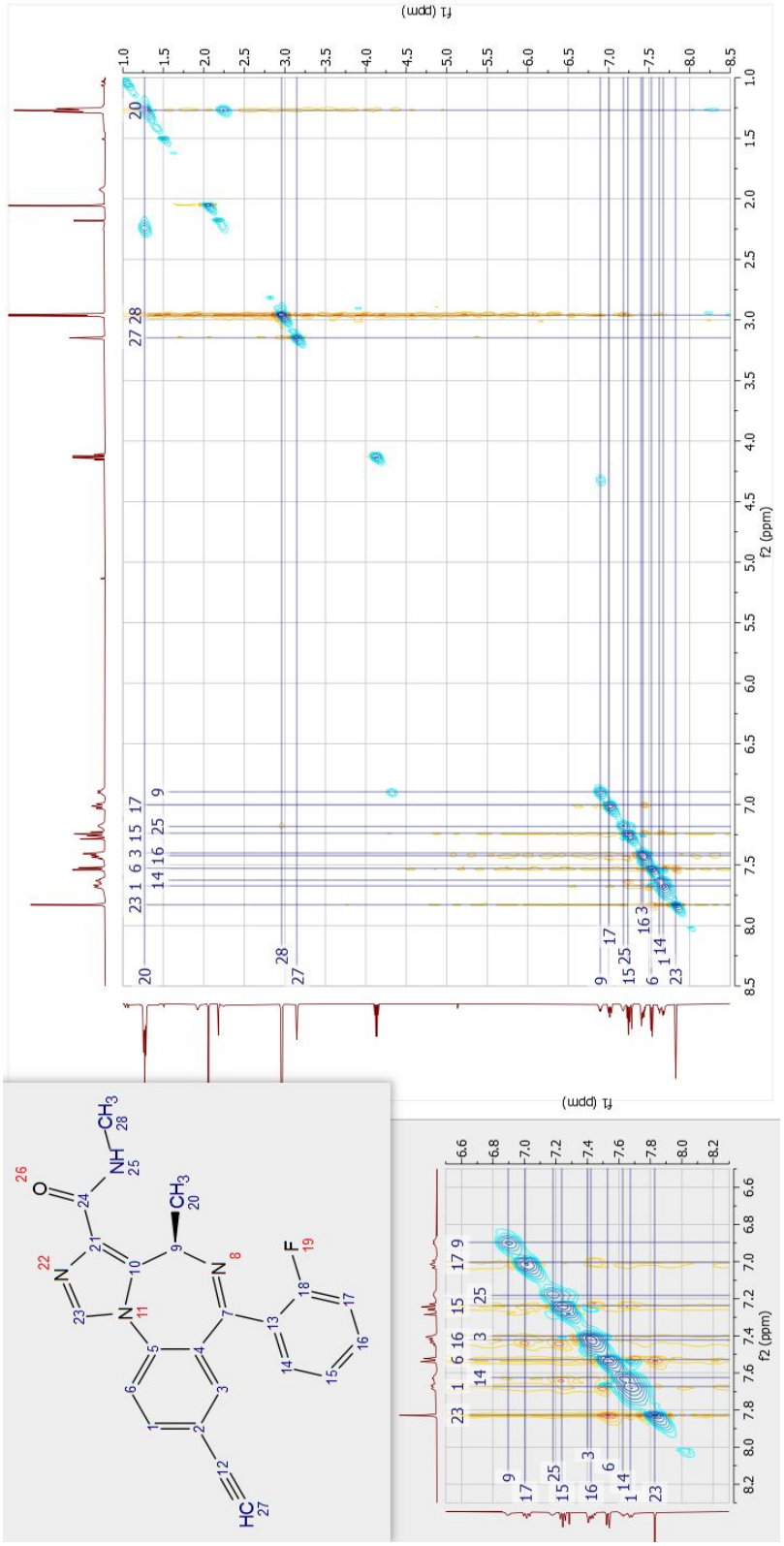

3.6. Determination of Conformational Isomers by NMR Spectroscopy of MIDD0002, MIDD0003, GL-II-73 and MP-III-022

Benzodiazepines contain a seven membered ring which confers interesting structural features observed in NMR spectroscopy experiments, especially in the case of the ligands synthesized in this work containing a chiral methyl group in the 3-position of the diazepine ring and a fluorine in the 2'-position of the pendant phenyl ring. Displayed in the ^{1}H NMR spectrum of MIDD0002 in **Figure 121** the methyl group protons (H21) appeared as a doublet (1.78 ppm) and the methine proton (H9) was a quartet (3.78 ppm). The energy minimization of the structure using Chimera X suggested the more stable conformation of the seven membered ring exists with the methyl group on the seven-membered ring in the pseudo axial position. Examination of the ^{13}C NMR spectra of MIDD0002 (**Figure 122**), interestingly, displayed C-F splitting of the carbon signals. All six carbons of the pendant phenyl ring exhibited the C-F splitting with the coupling constants noted below. Of note, carbon (C3) of the benzo ring exhibited splitting as a doublet ($^{NOE}J_{CF}$ = 1.5 Hz) via a NOE interaction (2.47Å minimum distance). The ^{13}C NMR spectra (**Figure 123**) of imidazodiazepine, MIDD0003, however, did not display this NOE interaction between C3 and the 2'F substituent of the pendant phenyl ring. Presumably, the imidazole ring impacts the conformation the diazepine ring in such a way that the rotation of the pendant phenyl ring does not result in the observation of the C-F NOE signal in the NMR spectrum.

Conformational isomers are observed in NMR experiments in this series of imidazodiazepine compounds, which contain a chiral methyl function by ring flipping of the

seven-membered ring. The methyl group can adopt a pseudo axial or pseudo equatorial conformation, which results from inversion of the seven-membered diazepine ring (**Figure 124**). When the methyl group was pseudo axial (H21), the methine proton (H9) was deshielded (6.71 ppm) by the carbonyl oxygen (2.36Å) of the ester function. In contrast, when the methyl group was pseudo equatorial, the methine proton (H9 Conformer) was observed at 4.35ppm. Analysis of the data in the ^{1}H NMR spectra suggested the pseudo axial-CH_3 conformation is a major isomer in a 3:1 ratio with the minor pseudo equatorial-CH_3 isomer. This conformational phenomenon can be observed additionally in the ^{19}F NMR spectrum wherein the two fluorine peaks integrated to a 3:1 ratio as well. As a method to verify the observed methyl and methine peaks are a result of two conformers, examination of the COSY spectrum (**Figure 125**) of MIDD0003 exhibited a correlation between the pseudo axial methyl (H21) and methine (H9) protons as well as the minor equatorial (H21 Conformer) and methine (H9 Conformer) protons. Finally, analysis of the ROESY spectrum (**Figure 126**) exhibited a NOE correlation between the conformeric methine protons (H9 and H9 Conformer), as well as the methyl protons (H21 and H21 Conformer), which suggests, the conformation flipping of the seven-membered diazepine ring occurs within the time frame of the ROESY NMR experiment.

Analysis of similar ^{1}H and ^{19}F NMR experiments for dimethylamide, GL-II-73, revealed the opposite of the ethyl ester, MIDD0003, wherein the observed major conformer contained a pseudo equatorial methyl (H21) function in a 3:1 pseudo equatorial to pseudo axial ratio. Herein, the fluorine peaks also integrated to a 3:1 ratio, but additionally in the case of GL-II-73, the imidazole proton (H23) and the dimethylamide protons (H28 and H29) exhibited unique and observable conformational peaks in the proton spectrum. The COSY spectrum (**Figure 128**) of

GL-II-73 confirmed the correlation of the methyl (H21 / H21 Conformer) and methine (H9 / H9 Conformer) signals. Examination of the ROESY spectrum (**Figure 129**) again exhibited a NOE correlation between the signals of methine protons (H9 and H9 Conformer), the methyl protons (H21 and H21 Conformer) as well as the dimethyl amide protons (H28 and H28 Conformer, H29 and H29 Conformers).

Finally, examination of the NMR experiments for monomethyl amide (MP-III-022) provided evidence that, as with ethyl ester (MIDD0003), the major conformational isomer contains chiral methyl group (H20) in the pseudo axial position. The ^{1}H and ^{19}F NMR experiments are shown in **Figure 130**, as well as the COSY in **Figure 131** and ROESY in **Figure 132** for the conformational analysis by NMR spectroscopy of MP-III-022.

An ^{1}H NMR coalescence experiment is another method to illustrate conformational isomers. In a coalescence experiment the temperature of the NMR probe is raised incrementally, and the spectrum retaken. Isomeric peaks due to conformers would broaden into the baseline at the coalescence temperature and then reemerge as a single peak at the average peak location. The coalescence spectra for MIDD0003 is displayed in **Figure 133** and the results exhibited that the conformational methyl protons (H20 and H20 Conformer) and methine protons (H9 and H9 Conformer) coalesced at ~368K, thereby confirming that these peaks were the result of a conformational flipping. Additionally, to confirm that the two fluorine peaks observed in the ^{19}F NMR experiment were the result of a similar effect, another coalescence experiment was conducted (**Figure 134**). In this case, the coalescence temperature was not observed, but the two fluorine peaks did indeed merge into one signal.

3.6.1. Analysis of Conformational Isomers of MIDD0002 Using NMR Spectroscopy

Figure 121: [1]HNMR and [19]FNMR of MIDD0002

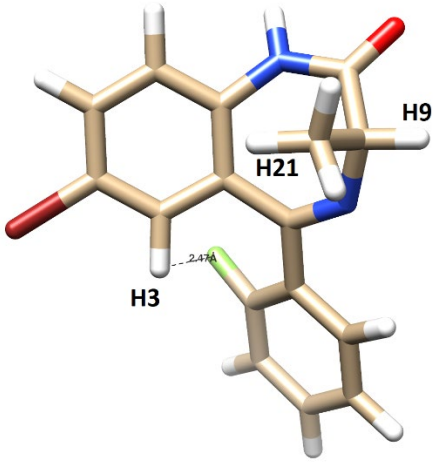

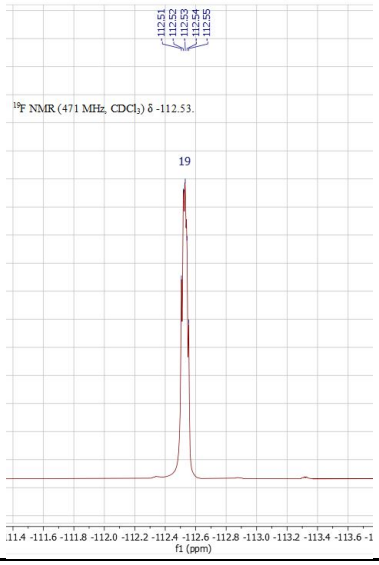

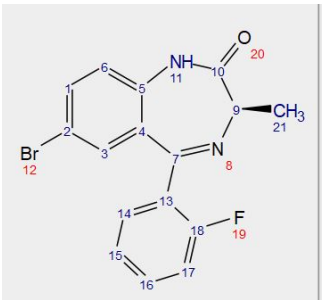

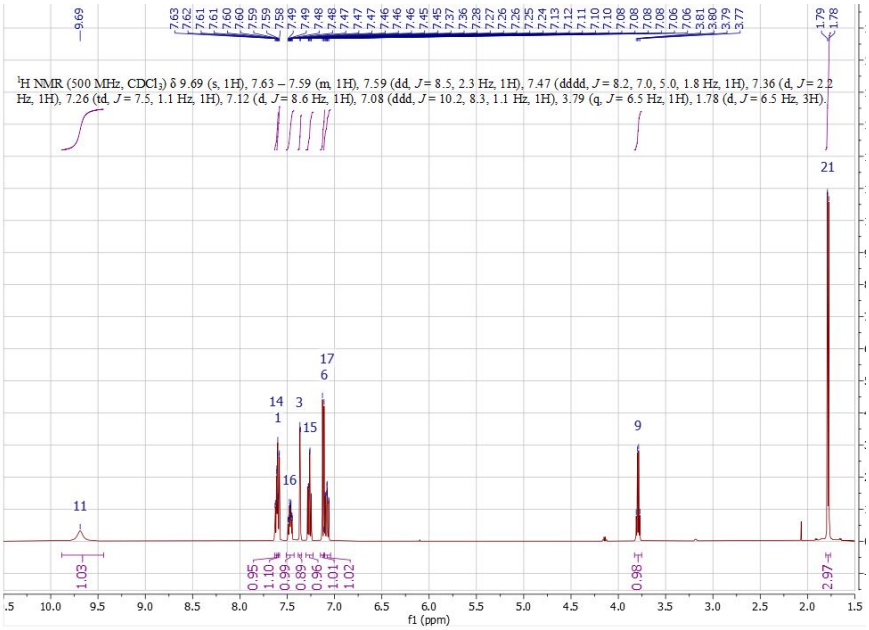

[1]HNMR: Note H9 (3.79ppm) and H21 (1.78ppm) positions.
[19]FNMR: Only one fluorine peak observed.

Figure 122: ^{13}CNMR Exhibiting C-F Coupling of MIDD0002

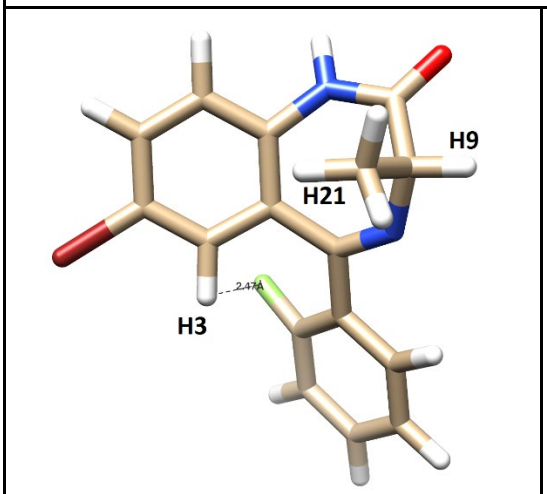

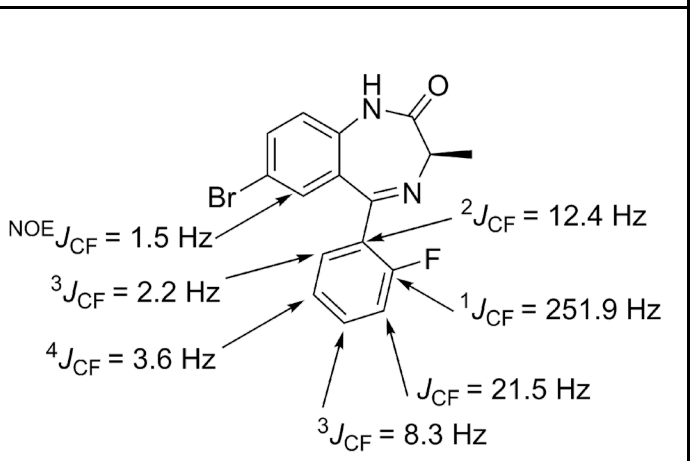

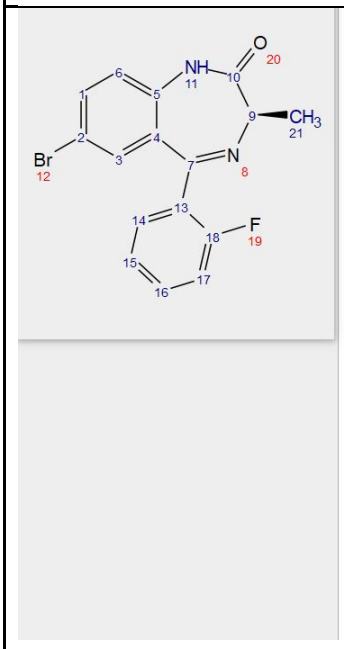

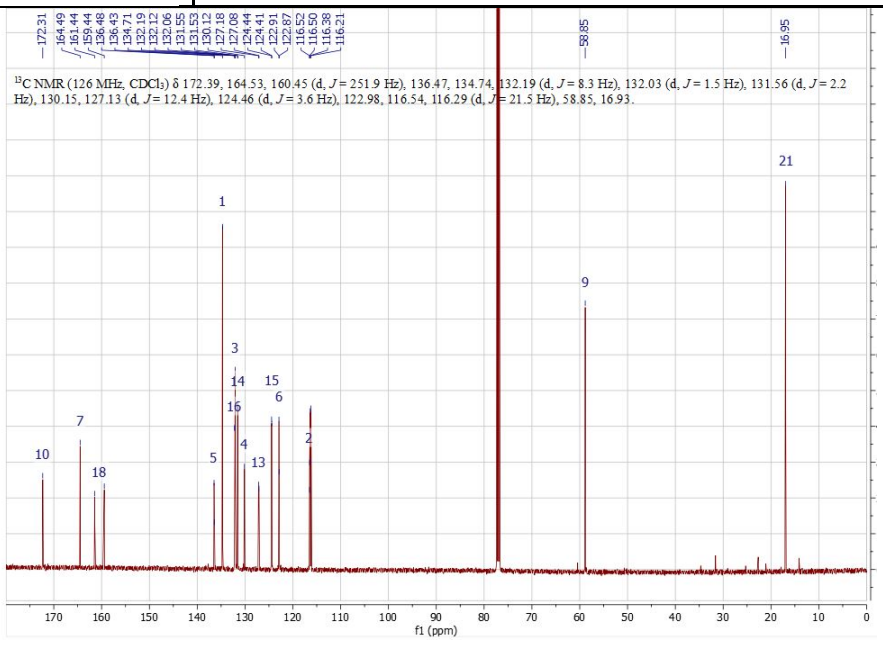

3.6.2. Analysis of Conformational Isomers of MIDD0003 Using NMR Spectroscopy

Figure 123: ^{13}CNMR Exhibiting C-F Coupling of MIDD0003

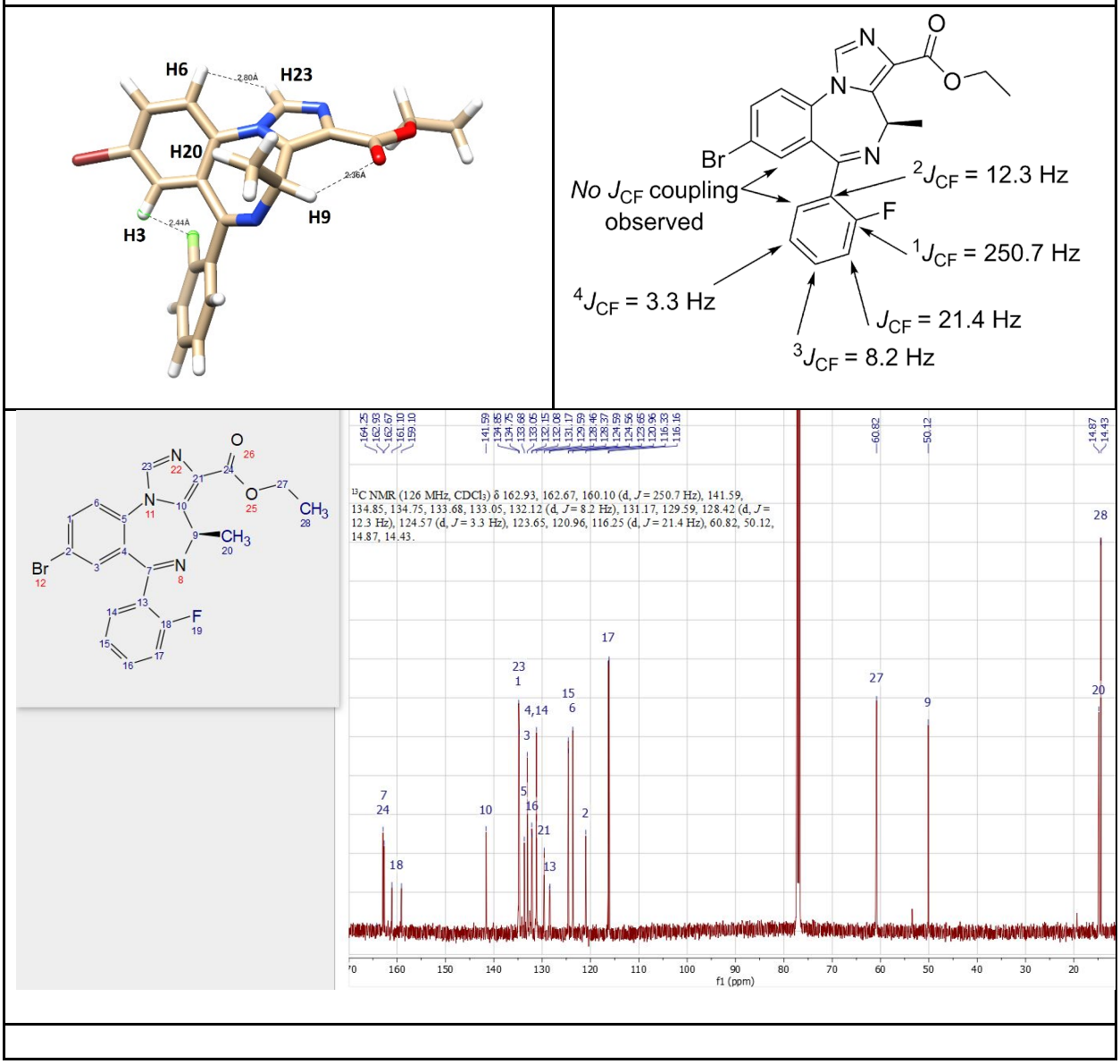

Figure 124: Comparison of MIDD0003 Conformers Using ^{1}HNMR & ^{19}FNMR.

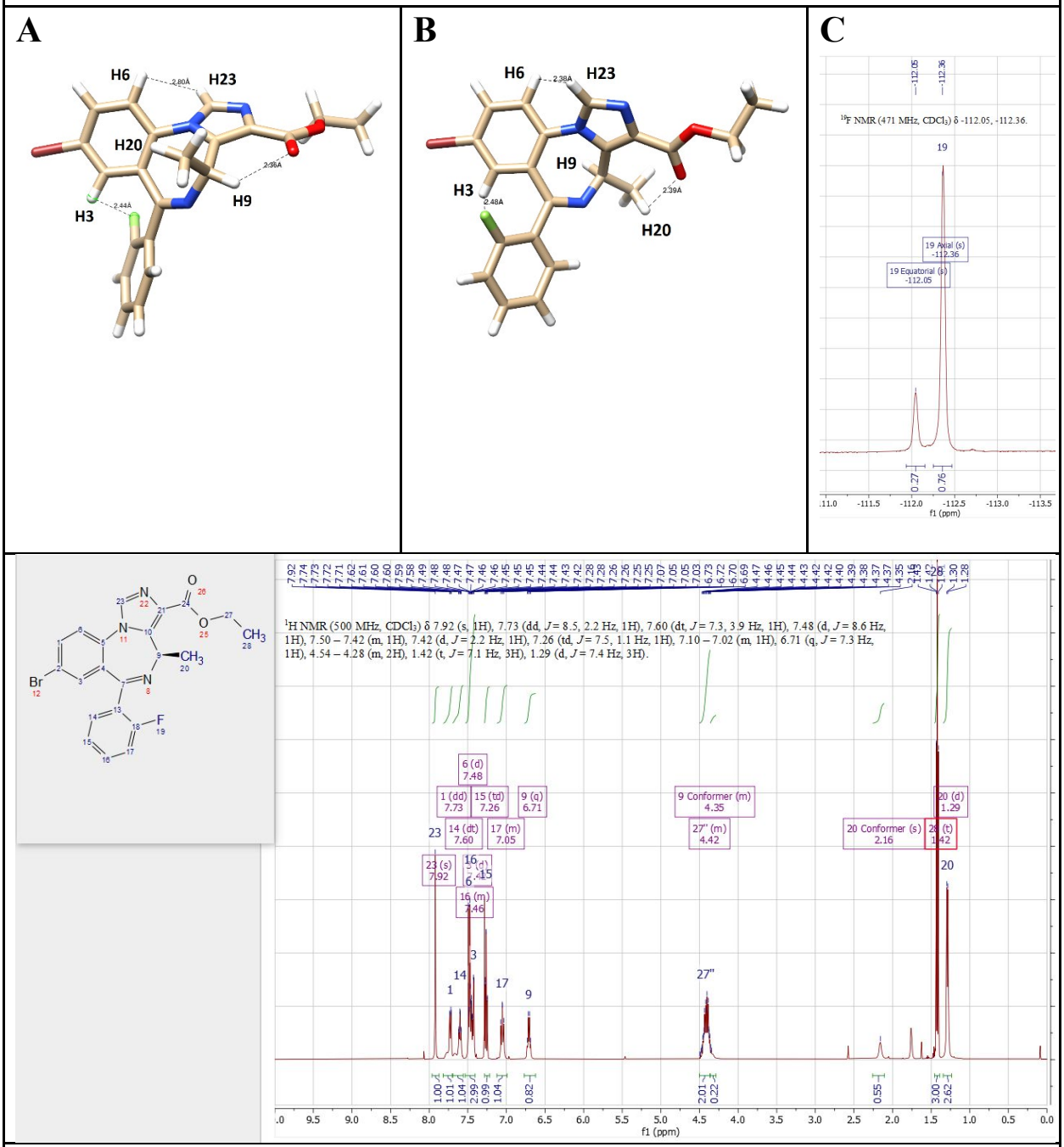

^{1}HNMR spectrum: Major Conformer (A): Pseudo Axial CH_3 Upfield (1.29 ppm) Pseudo Equatorial CH Deshielded (6.71 ppm). Minor Conformer (B): Pseudo Equatorial CH_3 Downfield (2.16 ppm) Pseudo Axial CH Shielded (4.35 ppm). Major / Minor isomeric ratio integrated to ~3:1 for all peaks listed. ^{19}FNMR spectra (C): Two fluorine peaks observed with ~3:1 ratio consistent with axial/equatorial ratio. Experiments Conducted on a Bruker 500 MHz NMR Spectrometer.

Figure 125: Comparison of MIDD0003 Conformers Using COSY

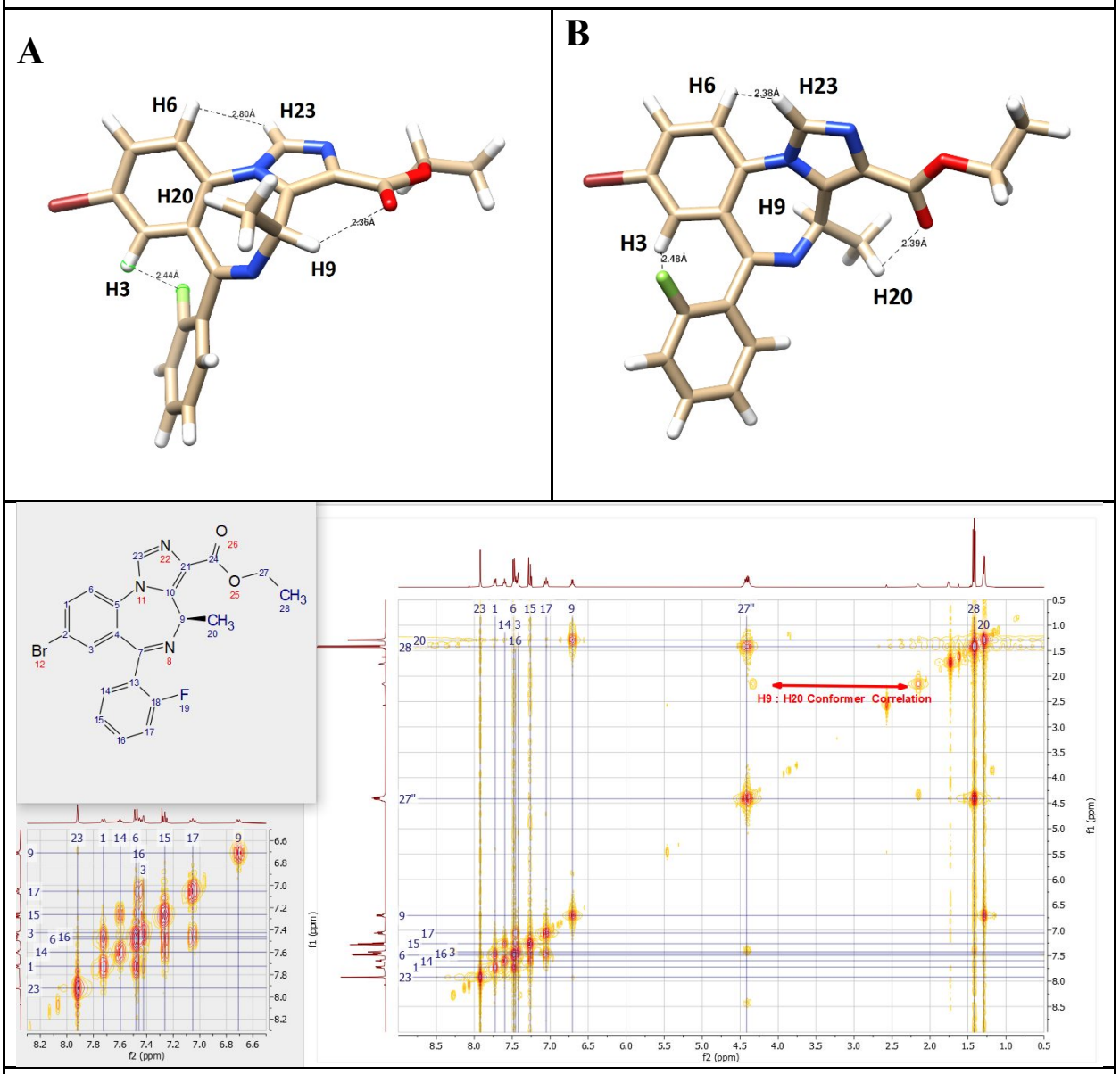

COSY Correlations: Major Conformer (A) H9 (6.71ppm) with H20 (1.29ppm). Minor Conformer (B) H9 (4.36ppm) with H20 (2.16 ppm). Experiments Conducted on a Bruker 500 MHz NMR Spectrometer.

Figure 126: Comparison of MIDD0003 Conformers Using ROESY

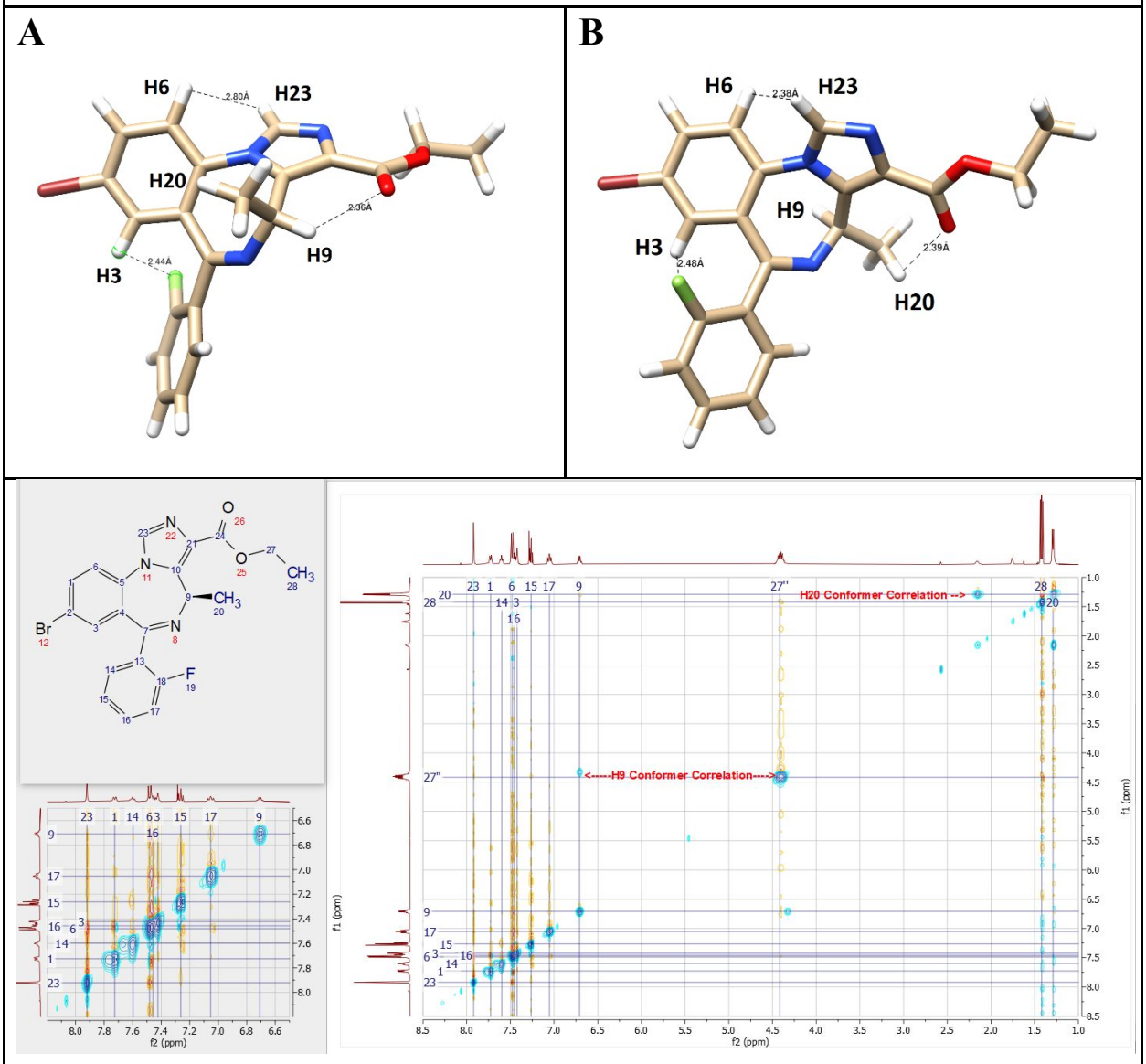

ROESY Correlations: H20: Major Conformer (A) Pseudo Axial CH_3 (1.29 ppm) with Minor Conformer (B) Pseudo Equatorial CH_3 (2.16 ppm). H9: Major Conformer (A) CH (6.71 ppm) with Minor Conformer (B) CH (4.36ppm). Experiments Conducted on a Bruker 500 MHz NMR Spectrometer.

3.6.3. Analysis of Conformational Isomers of GL-II-73 Using NMR Spectroscopy

Figure 127: Comparison of GL-II-73 Conformers Using ^{1}HNMR and ^{19}FNMR Evidence.

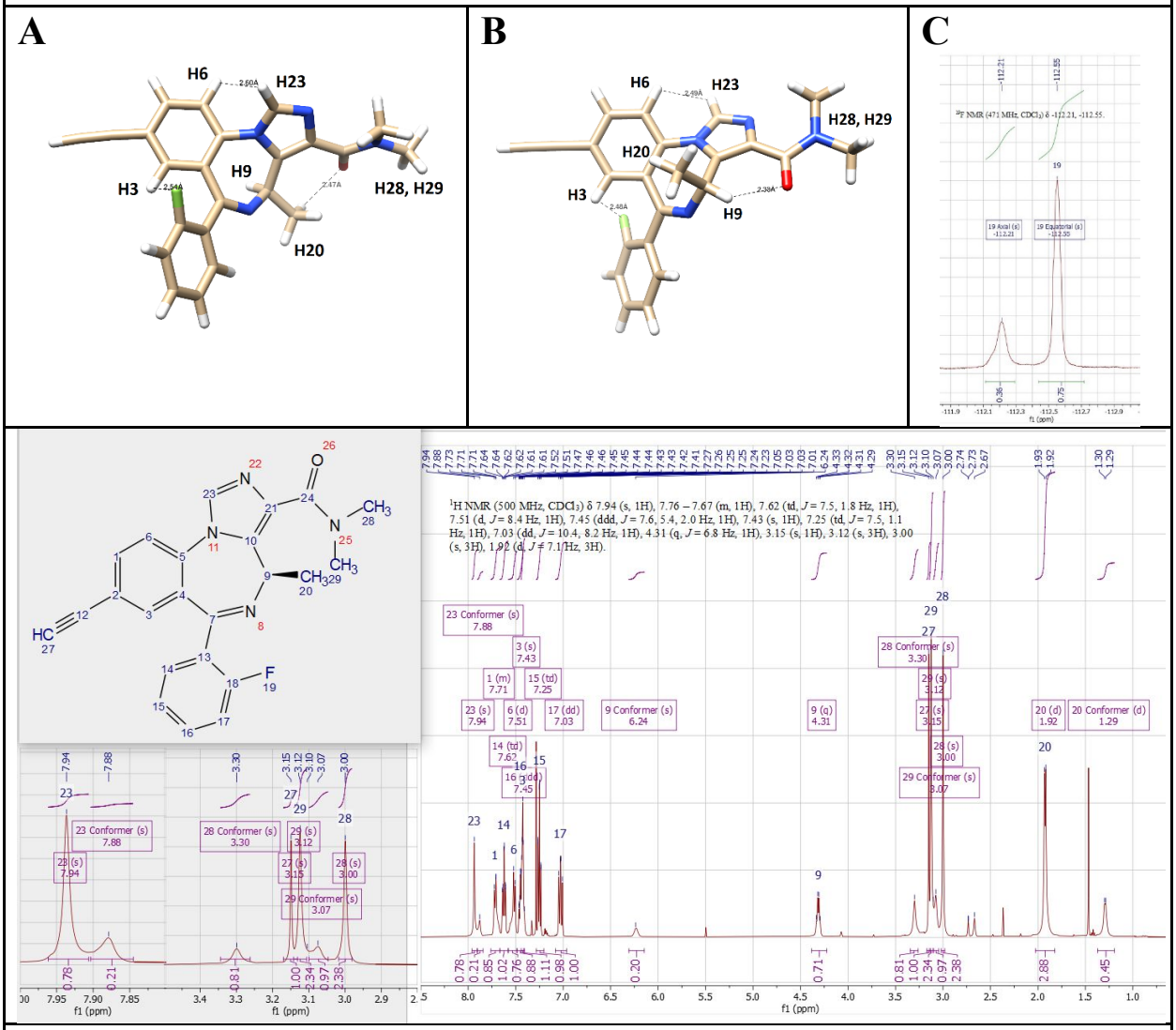

Major Conformer (A): pseudo equatorial CH_3 (H20, 1.92 ppm), pseudo axial CH shielded (H9, 4.31 ppm), imidazole proton (H23, 7.94ppm), amide CH_3's (H28 / H29, 3.00ppm / 3.12 ppm)
Minor Conformer (B): pseudo axial CH_3 (H20 Conformer, 1.29 ppm), pseudo equatorial CH deshielded (H9 Conformer, 6.24 ppm), imidazole proton (H23 Conformer, 7.88ppm), amide CH_3's (H28 Conformer / H29 Conformer, 3.30ppm / 3.07 ppm). Major / Minor isomeric ratio integrated to ~3:1 for all peaks listed. ^{19}FNMR spectra (C): Two fluorine peaks observed with ~3:1 ratio consistent with the axial/equatorial ratio. Experiments Conducted on a Bruker 500 MHz NMR Spectrometer.

Figure 128: Comparison of GL-II-73 Conformers Using COSY

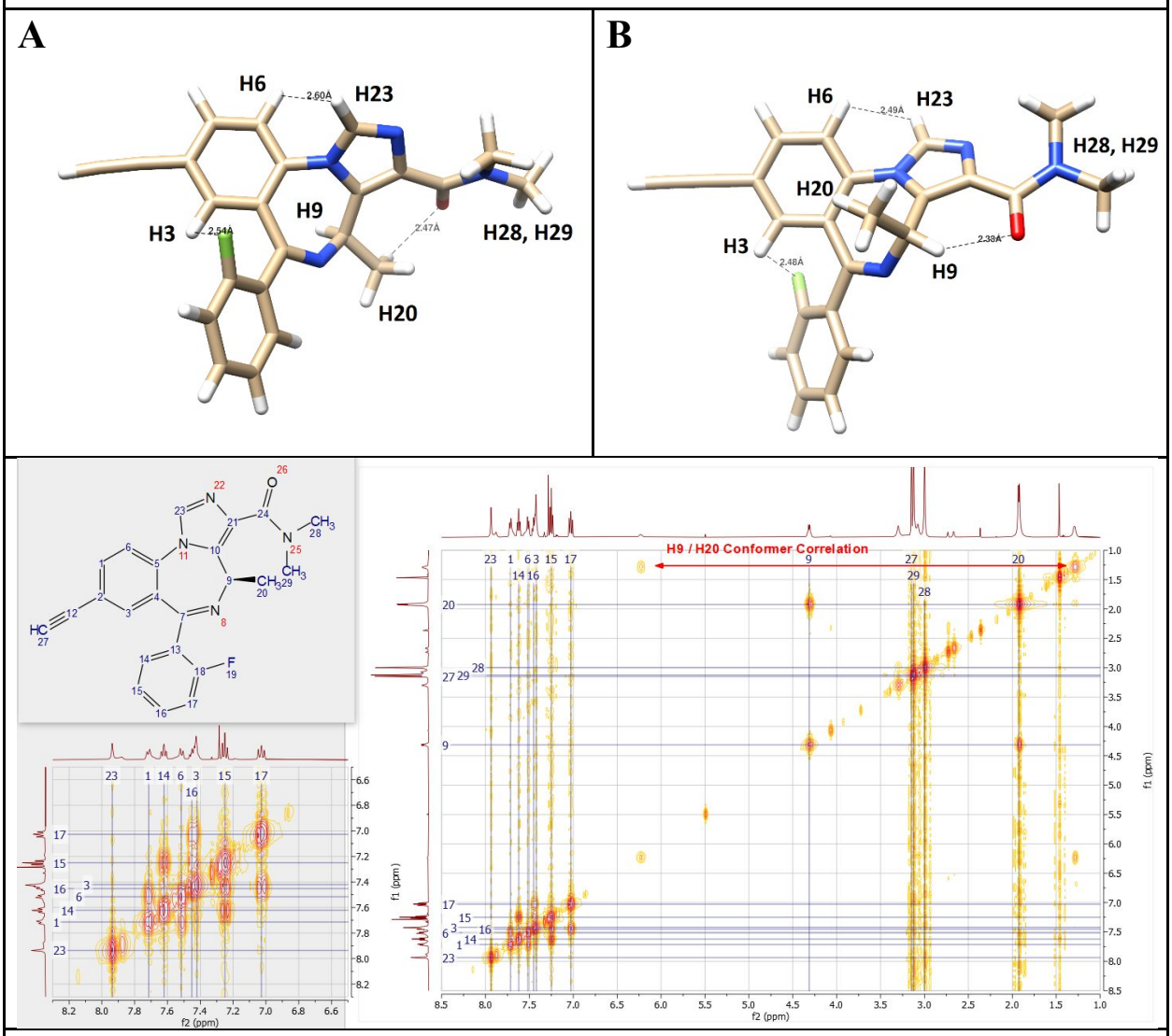

OSY Correlations: Major Conformer (A) H9 (4.31 ppm) with H20 (1.92 ppm). Minor Conformer (B) H9 (6.24 ppm) with H20 (1.29 ppm). Experiments Conducted on a Bruker 500 MHz NMR Spectrometer.

Figure 129: Comparison of GL-II-73 Conformers Using ROESY

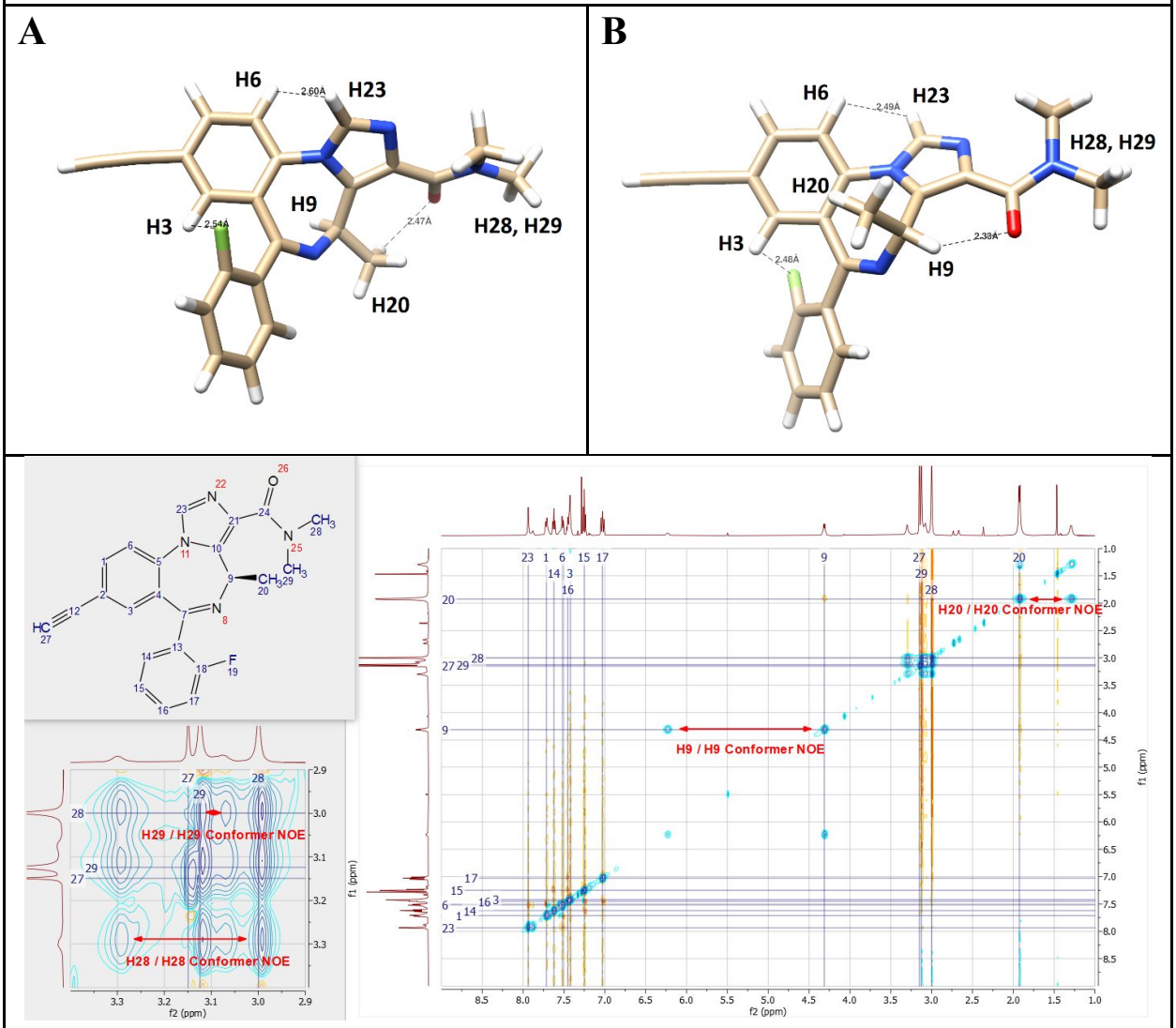

ROESY Correlations: H20: Major Conformer (A) pseudo equatorial CH_3 (1.92 ppm) with Minor Conformer (B) pseudo axial CH_3 (1.29 ppm). H9: Major Conformer (A) CH (4.31 ppm) with Minor Conformer (B) CH (6.24 ppm). H28: Major Conformer (A) amide CH_3 (3.00ppm) with minor conformer (B) amide CH_3 (3.30 ppm). H29: Major Conformer (A) amide CH_3 (3.12 ppm) with minor conformer (B) amide CH_3 (3.07 ppm). Experiments conducted on a Bruker 500 MHz NMR spectrometer.

3.6.4. Analysis of Conformational Isomers of MP-III-022 Using NMR Spectroscopy

Figure 130: Comparison of MP-III-022 Conformers Using ^{1}HNMR and ^{19}FNMR.

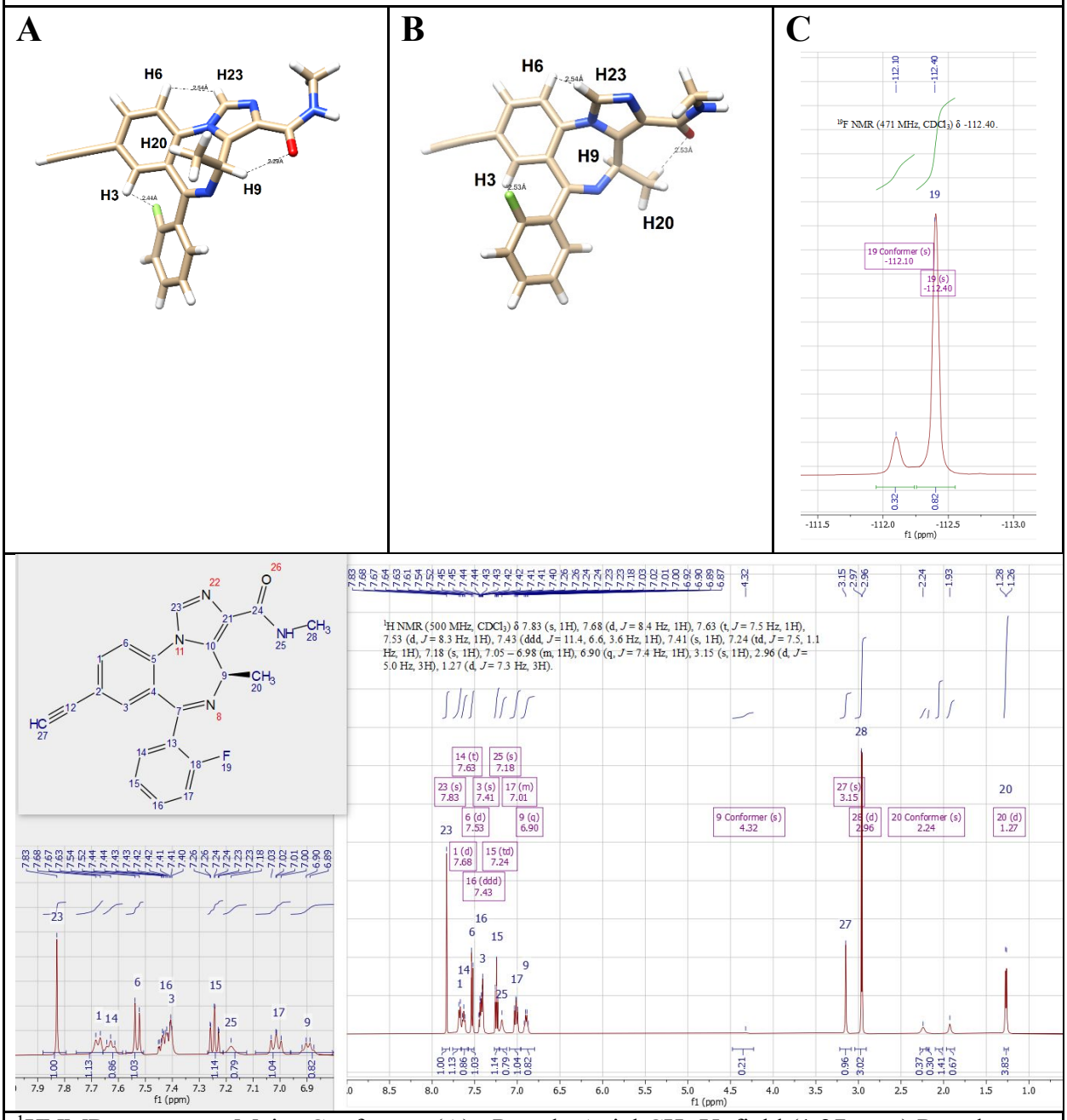

^{1}HNMR spectrum: Major Conformer (A): Pseudo Axial CH_3 Upfield (1.27 ppm) Pseudo Equatorial CH Deshielded (6.90 ppm). Minor Conformer (B): Equatorial CH_3 Downfield (2.24 ppm) Axial CH Shielded (4.32 ppm). Major / Minor isomeric ratio integrated to ~3:1 for all peaks listed. ^{19}FNMR spectra (C): Two fluorine peaks observed with ~3:1 ratio consistent with axial/equatorial ratio. Experiments Conducted on a Bruker 500 MHz NMR Spectrometer.

Figure 131: Comparison of MP-III-022 Conformers Using COSY

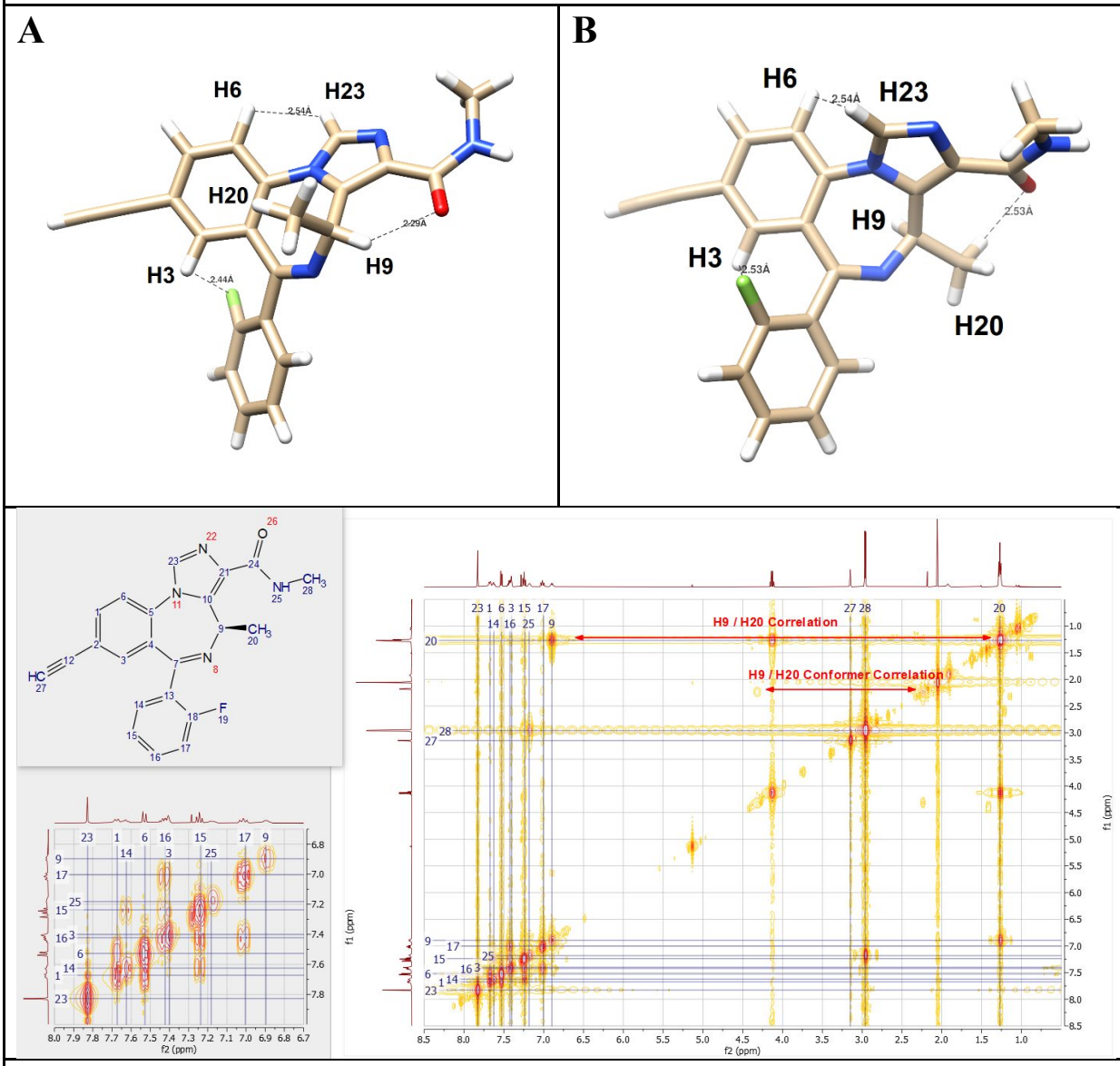

COSY Correlations: Major Conformer (A) H9 (6.90ppm) with H20 (1.27ppm). Minor Conformer (B) H9 (4.32ppm) with H20 (2.24 ppm). Experiments Conducted on a Bruker 500 MHz NMR Spectrometer.

Figure 132: Comparison of MP-III-022 Conformers Using NOESY

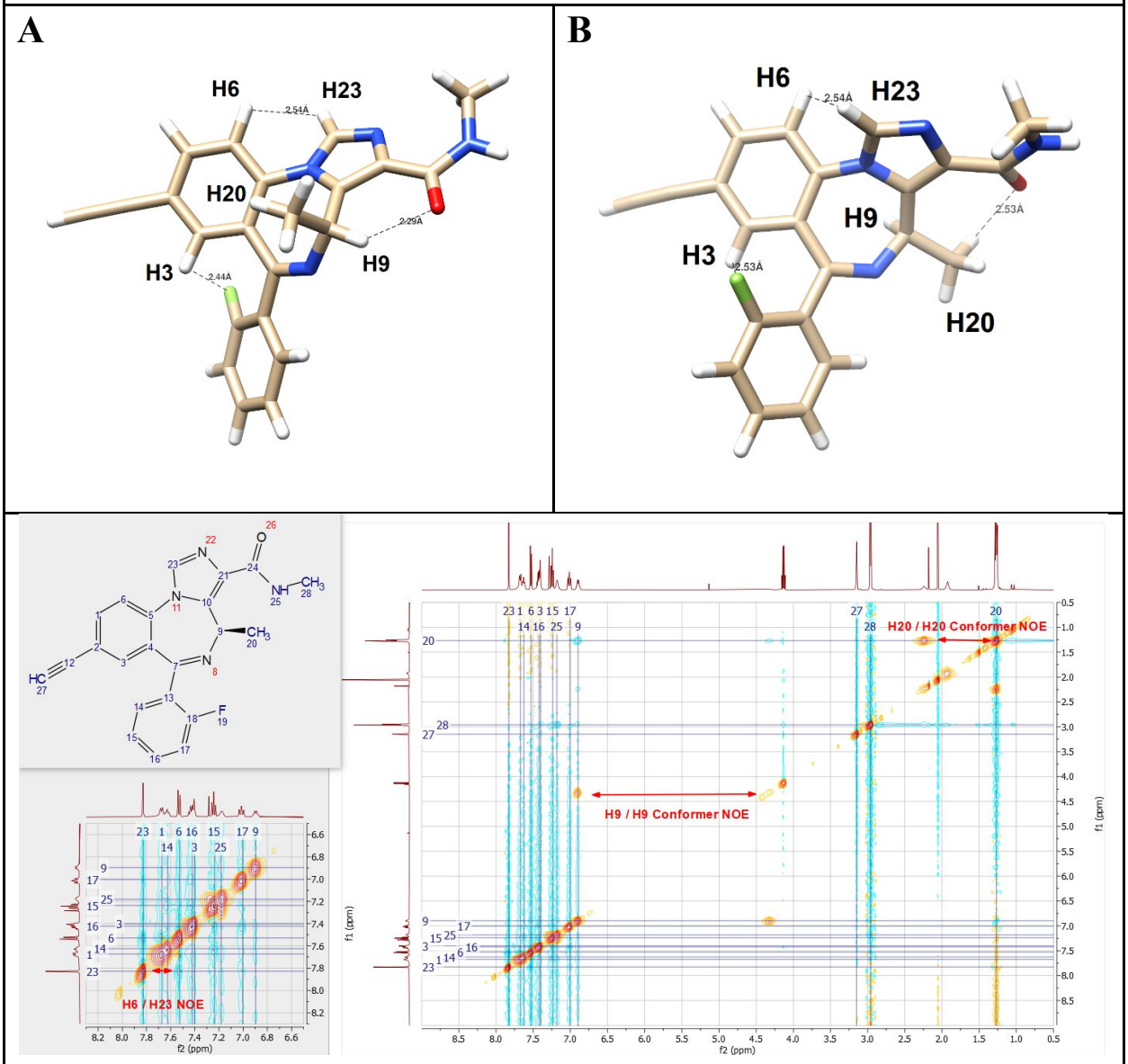

NOESY Correlations: H20: Major Conformer (A) Pseudo Axial CH_3 (1.27 ppm) with Minor Conformer (B) Pseudo Equatorial CH_3 (2.24 ppm). H9: Major Conformer (A) CH (6.90 ppm) with Minor Conformer (B) CH (4.32 ppm). Experiments Conducted on a Bruker 500 MHz NMR Spectrometer.

3.6.5. Coalescence Study of MIDD0003 Conformational Isomers Using NMR Spectroscopy

Figure 133: [1]HNMR Coalescence Study of MIDD0003 Conformers

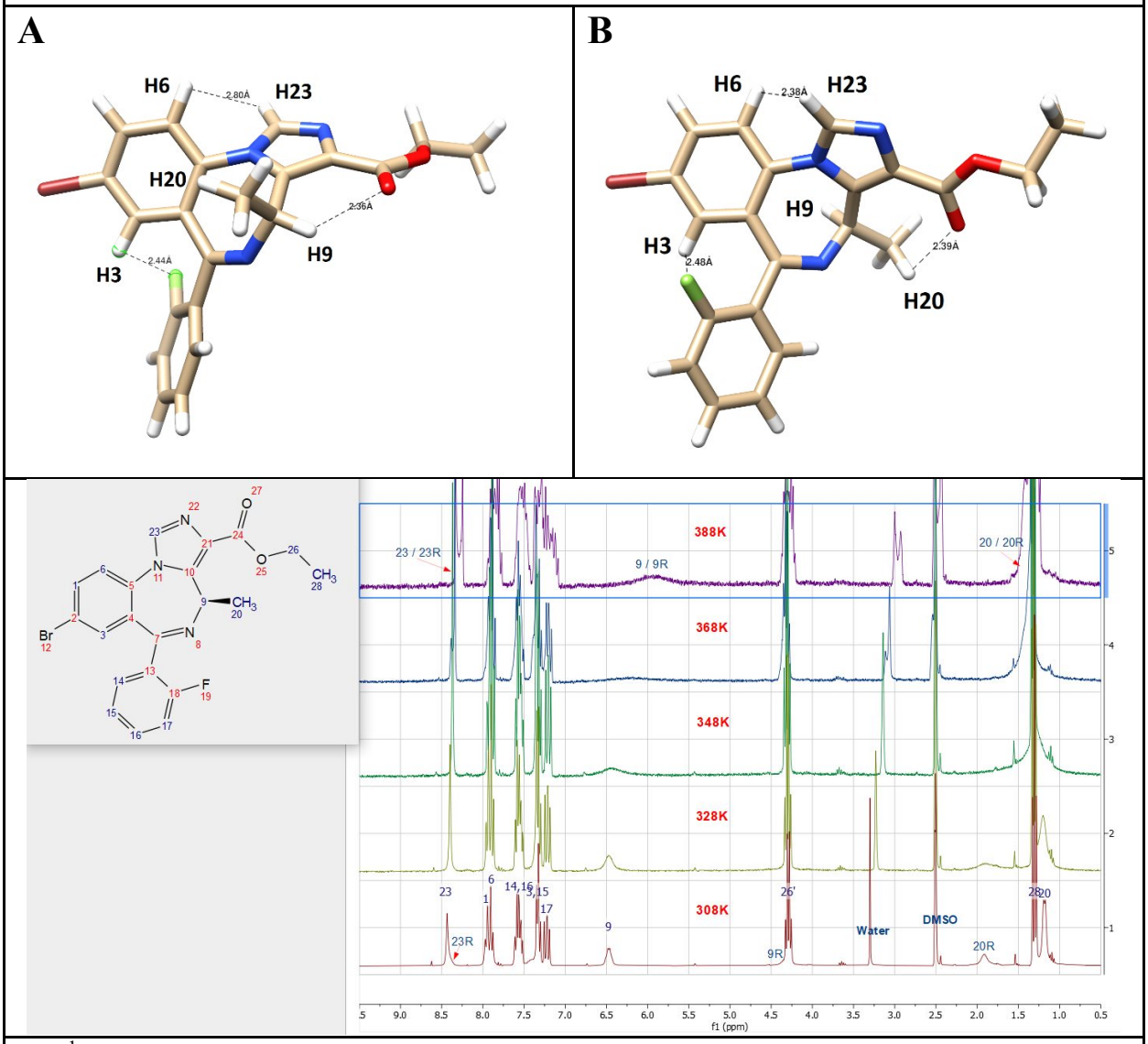

The [1]HNMR coalescence experiment exhibited how isomeric protons of major (A) and minor (B) conformers will broaden as T increases. Coalescence T was ~368K for H9. H9 reemerges at 388K at averaged peak location of H9 / H9R. Experiment Conducted on a Bruker 300 MHz NMR Spectrometer.

Figure 134: ^{19}FNMR Coalescence Study of MIDD0003 Conformers

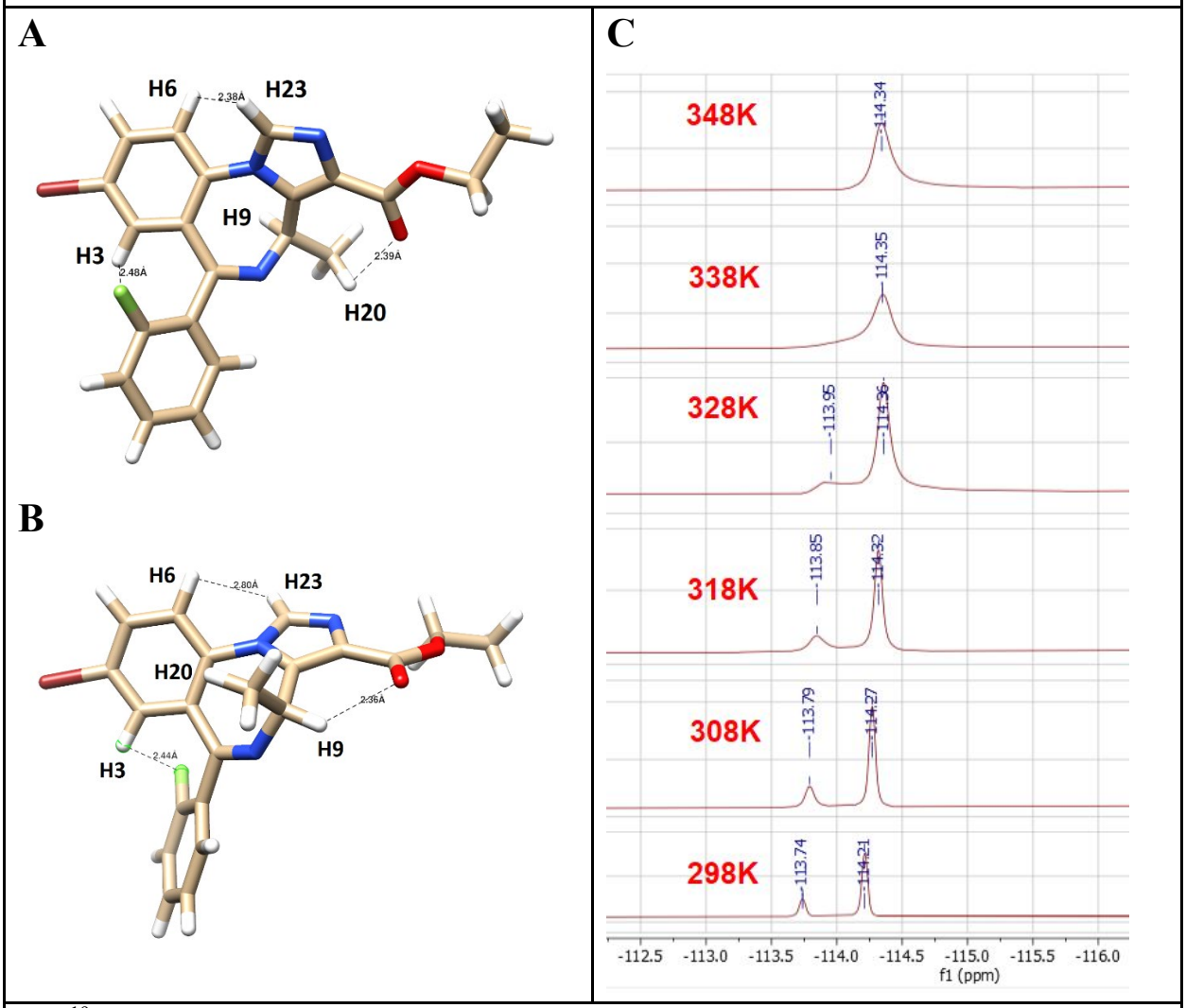

The ^{19}FNMR coalescence experiment exhibited how fluorine signals from major (A) and minor (B) conformers broaden together as the temperature of the probe was increased. Experiment conducted on a Brucker 500MHz NMR Spectrometer.

References

1. Masiulis, S.; Desai, R.; Uchanski, T.; Serna Martin, I.; Laverty, D.; Karia, D.; Malinauskas, T.; Zivanov, J.; Pardon, E.; Kotecha, A.; Steyaert, J.; Miller, K. W.; Aricescu, A. R., Gabaa Receptor Signalling Mechanisms Revealed by Structural Pharmacology. *Nature* **2019,** *565* (7740), 454-459.

2. Knutson, D. E.; Kodali, R.; Divovic, B.; Treven, M.; Stephen, M. R.; Zahn, N. M.; Dobricic, V.; Huber, A. T.; Meirelles, M. A.; Verma, R. S.; Wimmer, L.; Witzigmann, C.; Arnold, L. A.; Chiou, L. C.; Ernst, M.; Mihovilovic, M. D.; Savic, M. M.; Sieghart, W.; Cook, J. M., Design and Synthesis of Novel Deuterated Ligands Functionally Selective for the Gamma-Aminobutyric Acid Type a Receptor (Gabaar) Alpha6 Subtype with Improved Metabolic Stability and Enhanced Bioavailability. *J. Med. Chem.* **2018,** *61* (6), 2422-2446.

3. Olsen, R. W.; Sieghart, W., International Union of Pharmacology. Lxx. Subtypes of Gamma-Aminobutyric Acid(a) Receptors: Classification on the Basis of Subunit Composition, Pharmacology, and Function. Update. *Pharmacol. Rev.* **2008,** *60* (3), 243-260.

4. Olsen, R. W.; Sieghart, W., Gaba a Receptors: Subtypes Provide Diversity of Function and Pharmacology. *Neuropharmacol.* **2009,** *56* (1), 141-148.

5. Mortensen, M.; Patel, B.; Smart, T. G., Gaba Potency at Gaba(a) Receptors Found in Synaptic and Extrasynaptic Zones. *Front. Cell. Neurosci.* **2011,** *6*, 1-10.

6. Wisden, W.; Laurie, D. J.; Monyer, H.; Seeburg, P. H., The Distribution of 13 Gabaa Receptor Subunit Mrnas in the Rat Brain. I. Telencephalon, Diencephalon, Mesencephalon. *J. Neurosci.* **1992,** *12* (3), 1040-1062.

7. Pirker, S.; Schwarzer, C.; Wieselthaler, A.; Sieghart, W.; Sperk, G., Gabaa Receptors: Immunocytochemical Distribution of 13 Subunits in the Adult Rat Brain. *Neurosci.* **2000,** *101* (4), 815-850.

8. Sieghart, W., Structure and Pharmacology of Gamma-Aminobutyric Acida Receptor Subtypes. *Pharmacol. Rev.* **1995,** *47* (2), 181-234.

9. Sieghart, W.; Ernst, M., Heterogeneity of Gabaa Receptors: Revived Interest in the Development of Subtype-Selective Drugs. *Cur. Med. Chem.* **2005,** *5* (3), 217-242.

10. Ramerstorfer, J.; Furtmuller, R.; Sarto-Jackson, I.; Varagic, Z.; Sieghart, W.; Ernst, M., The Gabaa Receptor Alpha+Beta- Interface: A Novel Target for Subtype Selective Drugs. *J. Neurosci.* **2011,** *31* (3), 870-877.

11. Sieghart, W.; Ramerstorfer, J.; Sarto-Jackson, I.; Varagic, Z.; Ernst, M., A Novel Gaba(a) Receptor Pharmacology: Drugs Interacting with the Alpha(+) Beta(-) Interface. *Br. J. Pharmacol.* **2012,** *166* (2), 476-485.

12. Varagic, Z.; Ramerstorfer, J.; Huang, S.; Rallapalli, S.; Sarto-Jackson, I.; Cook, J.; Sieghart, W.; Ernst, M., Subtype Selectivity of Alpha+Beta- Site Ligands of Gabaa Receptors: Identification of the First Highly Specific Positive Modulators at Alpha6beta2/3gamma2 Receptors. *Br. J. Pharmacol.* **2013,** *169* (2), 384-399.

13. Varagic, Z.; Wimmer, L.; Schnurch, M.; Mihovilovic, M. D.; Huang, S.; Rallapalli, S.; Cook, J. M.; Mirheydari, P.; Ecker, G. F.; Sieghart, W.; Ernst, M., Identification of Novel Positive Allosteric Modulators and Null Modulators at the Gabaa Receptor Alpha+Beta- Interface. *Br. J. Pharmacol.* **2013,** *169* (2), 371-383.

14. Nusser, Z.; Sieghart, W.; Somogyi, P., Segregation of Different Gabaa Receptors to Synaptic and Extrasynaptic Membranes of Cerebellar Granule Cells. *J. Neurosci.* **1998,** *18* (5), 1693-1703.

15. Gutiérrez, A.; Khan, Z. U.; De Blas, A. L., Immunocytochemical Localization of the A6 Subunit of the Γ-Aminobutyric Acida Receptor in the Rat Nervous System. *J. Comp. Neuro.* **1996,** *365* (3), 504-510.

16. Yang, L.; Xu, T.; Zhang, K.; Wei, Z.; Li, X.; Huang, M.; Rose, G. M.; Cai, X., The Essential Role of Hippocampal Alpha6 Subunit-Containing Gabaa Receptors in Maternal Separation Stress-Induced Adolescent Depressive Behaviors. *Behav. Brain Res.* **2016,** *313*, 135-143.

17. Chiou, L. C.; Wu, C. Y.; Lee, H. J.; Du, J. C.; Hor, C. C.; Ernst, M.; Sieghart, W.; Cook, J., The Cerebellar Alpha6-Containing Gaba-a Receptor: A Novel Target for Neuropsychiatric Disorders. In *Neuroscience*, San Diego, CA, USA, 2016.

18. Liao, Y. H.; Lee, H. J.; Huang, W. J.; Fan, P. C.; Chiou, L. C., Hispidulin Alleviated Methamphetamine-Induced Hyperlocomotion by Acting at Alpha6 Subunit-Containing Gabaa Receptors in the Cerebellum. *Psychopharmacology.* **2016,** *233* (17), 3187-3199.

19. Fan, P. C.; Huang, M.; Sieghart, W.; Ernst, M.; Knutson, D. E.; Cook, J. M.; Chiou, L. C., The A6 Subunit-Containing Gabaa Receptors: A Novel Target for Migraine Therapy. In *The 18th Congress of International Headache Society (IHC2017)*, Vancouver, BC, Canada, 2017.

20. Kramer, P. R.; Bellinger, L. L., Reduced Gabaa Receptor Alpha6 Expression in the Trigeminal Ganglion Enhanced Myofascial Nociceptive Response. *Neurosci.* **2013,** *245*, 1-11.

21. Czernik, A. J.; Petrack, B.; Kalinsky, H. J.; Psychoyos, S.; Cash, W. D.; Tsai, C.; Rinehart, R. K.; Granat, F. R.; Lovell, R. A.; Brundish, D. E.; Wade, R., Cgs 8216: Receptor Binding Characteristics of a Potent Benzodiazepine Antagonist. *Life Sci.* **1982,** *30* (4), 363-372.

22. Boast, C. A.; Snowhill, E. W.; Simke, J. P., Cgs 8216 and Cgs 9896, Novel Pyrazoloquinoline Benzodiazepine Ligands with Benzodiazepine Agonist and Antagonist Properties. *Pharmacol. Biochem. Behav.* **1985,** *23* (4), 639-644.

23. Li, X.; Ma, C.; He, X.; Yu, J.; Han, D.; Zhang, C.; Atack, J. R.; Cook, J. M., Studies in Search of Diazepam-Insensitive Subtype Selective Agents for Gabaa/Bz Receptors. *Med. Chem. Res.* **2003,** *11* (9), 504-537.

24. Wong, G.; Gu, Z. Q.; Fryer, R. I.; Skolnick, P., Pyrazolo(4,3-C)Quinolines with High Affinities for "Diazepam- Insensitive" (Di)Gabaa/Benzodiazepine Receptors. *Med. Chem. Res.* **1992,** *2* (4), 217-224.

25. Clayton, T.; Chen, J.; Ernst, M.; Richter, L.; Cromer, B.; Morton, C.; Ng, H.; Kaczorowski, C.; Helmstetter, F.; Furtmuller, R.; Ecker, G.; Parker, M.; Sieghart, W.; Cook, J., An Updated Unified Pharmacophore Model of the Benzodiazepine Binding Site on Γ-Aminobutyric Acid Receptors: Correlation with Comparative Models. *Curr. Med. Chem.* **2007,** *14* (26), 2755-2775.

26. Clayton, T.; Poe, M. M.; Rallapalli, S.; Biawat, P.; Savic, M. M.; Rowlett, J. K.; Gallos, G.; Emala, C. W.; Kaczorowski, C. C.; Stafford, D. C.; Arnold, L. A.; Cook, J. M., A Review of the Updated Pharmacophore for the Alpha 5 Gaba(a) Benzodiazepine Receptor Model. *Int. J. Med. Chem.* **2015,** *2015*, 1-54.

27. Zhang, P.; Zhang, W.; Liu, R.; Harris, B.; Skolnick, P.; Cook, J. M., Synthesis of Novel Imidazobenzodiazepines as Probes of the Pharmacophore for "Diazepam-Insensitive" Gabaa Receptors. *J. Med. Chem.* **1995,** *38* (10), 1679-1688.

28. He, X.; Huang, Q.; Yu, S.; Ma, C.; McKernan, R.; Cook, J. M., Studies of Molecular Pharmacophore/Receptor Models for Gabaa/Bzr Subtypes: Binding Affinities of Symmetrically Substituted Pyrazolo[4,3-C]Quinolin-3-Ones at Recombinant Axβ3γ2 Subtypes and Quantitative Structure-Activity Relationship Studies Via a Comparative Molecular Field Analysis. *Drug. Des. Discov.* **1999,** *16* (1), 77-91.

29. Huang, Q.; He, X.; Ma, C.; Liu, R.; Yu, S.; Dayer, C. A.; Wenger, G. R.; McKernan, R.; Cook, J. M., Pharmacophore/Receptor Models for Gabaa/Bzr Subtypes (A1β3γ2, A5β3γ2, and A6β3γ2) Via a Comprehensive Ligand-Mapping Approach. *J. Med. Chem.* **2000,** *43* (1), 71-95.

30. Treven, M.; Siebert, D. C. B.; Holzinger, R.; Bampali, K.; Fabjan, J.; Varagic, Z.; Wimmer, L.; Steudle, F.; Scholze, P.; Schnurch, M.; Mihovilovic, M. D.; Ernst, M., Towards Functional Selectivity for Alpha6beta3gamma2 Gabaa Receptors: A Series of Novel Pyrazoloquinolinones. *Br. J. Pharmacol.* **2018,** *175* (3), 419-428.

31. Chiou, L.-C.; Cook, J.; Ernst, M.; Fan, P.-C.; Knutson, D.; Meirelles, M.; Mihovilovic, M.; Sieghart, W.; Varagic, Z.; Verma, R.; Wimmer, L.; Weizigmann, C.; Siebert, D. C. B.; Savic, M. M. Preparation of Ligands Selective to Alpha 6 Subunit-Ccontaining Gabaa Receptors and Their Methods of Use. WO2016196961, 2016.

32. Mirheydari, P.; Ramerstorfer, J.; Varagic, Z.; Scholze, P.; Wimmer, L.; Mihovilovic, M. M.; Sieghart, W.; Ernst, M., Unexpected Properties of Delta-Containing Gabaa Receptors in Response to Ligands Interacting with the Alpha+ Beta- Site. *Neurochem. Res.* **2014,** *39* (6), 1057-1067.

33. Jedrychowski, M.; Nilsson, E.; Bieck, P., Metabolic Fate of Cgs 8216, a Benzodiazepine Receptor Antagonist, in Rat and in Man. *Psychopharmacology.* **1986,** *88* (4), 529-530.

34. Harbeson, S. L.; Tung, R. D., Deuterium Medicinal Chemistry: A New Approach to Drug Discovery and Development. *Medchem News* **2014,** (2), 1-14.

35. Wiberg, K. B., The Deuterium Isotope Effect. *Chem. Rev.* **1955,** *55* (4), 713-743.

36. Meunier, B.; de Visser, S. P.; Shaik, S., Mechanism of Oxidation Reactions Catalyzed by Cytochrome P450 Enzymes. *Chem. Rev.* **2004,** *104* (9), 3947-3980.

37. Nelson, S. D.; Trager, W. F., The Use of Deuterium Isotope Effects to Probe the Active Site Properties, Mechanism of Cytochrome P450-Catalyzed Reactions, and Mechanisms of Metabolically Dependent Toxicity. *Drug. Metab. Dispos.* **2003,** *31* (12), 1481-1498.

38. Pajouhesh, H.; Lenz, G. R., Medicinal Chemical Properties of Successful Central Nervous System Drugs. *NeuroRx.* **2005,** *2* (4), 541-553.

39. Sangster, J., Octanol-Water Partition Coefficients of Simple Organic Compounds. *J. Phys. Chem. Ref. Data.* **1989,** *18* (3), 1111-1229.

40. Gillis, E. P.; Eastman, K. J.; Hill, M. D.; Donnelly, D. J.; Meanwell, N. A., Applications of Fluorine in Medicinal Chemistry. *J. Med. Chem.* **2015,** *58* (21), 8315-59.

41. O'Hagan, D., Understanding Organofluorine Chemistry. An Introduction to the C-F Bond. *Chem. Soc. Rev.* **2008,** *37* (2), 308-19.

42. Blanksby, S. J.; Ellison, G. B., Bond Dissociation Energies of Organic Molecules. *Acc. Chem. Res.* **2003,** *36* (4), 255-63.

43. Meanwell, N. A., Fluorine and Fluorinated Motifs in the Design and Application of Bioisosteres for Drug Design. *J. Med. Chem.* **2018,** *61* (14), 5822-5880.

44. Park, B. K.; Kitteringham, N. R.; O'Neill, P. M., Metabolism of Fluorine-Containing Drugs. *Annu Rev Pharmacol Toxicol* **2001,** *41*, 443-70.

45. Johnson, B. M.; Shu, Y. Z.; Zhuo, X.; Meanwell, N. A., Metabolic and Pharmaceutical Aspects of Fluorinated Compounds. *J. Med. Chem.* **2020**.

46. Fan, P. C.; Lai, T. H.; Hor, C. C.; Lee, M. T.; Huang, P.; Sieghart, W.; Ernst, M.; Knutson, D. E.; Cook, J.; Chiou, L. C., The Alpha6 Subunit-Containing Gabaa Receptor: A Novel Drug Target for Inhibition of Trigeminal Activation. *Neuropharmacology* **2018,** *140*, 1-13.

47. Tzeng, H. R.; Lee, M. T.; Knutson, D. E.; Fan, P. C.; Ernst, M.; Sieghart, W.; Cook, J. M.; Chiou, L. C., A6gabaa Receptor Positive Modulators Alleviate Migraine-Like Grimaces in Mice Via Compensating Gabaergic Deficit in Trigeminal Ganglia *Br. J. Pharmacol.* **2020,** *(Submitted for Publication)*.

48. Vasovic, D.; Divovic, B.; Treven, M.; Knutson, D. E.; Steudle, F.; Scholze, P.; Obradovic, A.; Fabjan, J.; Brkovic, B.; Sieghart, W.; Ernst, M.; Cook, J. M.; Savic, M. M., Trigeminal Neuropathic Pain Development and Maintenance in Rats Are Suppressed by a Positive Modulator of Alpha6 Gabaa Receptors. *Eur J Pain* **2019,** *23* (5), 973-984.

49. Knutson, D. E.; Vasovic, D.; Divovic, B.; Treven, M.; Steudle, F.; Scholze, P.; Brkovic, B.; Sieghart, W.; Ernst, M.; Cook, J. M.; Savic, M. M. In *Prevention of Trigeminal Neuropathic Pain Development in Rats Using Novel Deuterated Gabaar-A6 Subtype Selective Ligands*, 256th ACS National Meeting, Boston, MA, August 19-23, 2018; Boston, MA, 2018; pp MEDI-95.

50. Chiou, L. C.; Lee, H. J.; Ernst, M.; Huang, W. J.; Chou, J. F.; Chen, H. L.; Mouri, A.; Chen, L. C.; Treven, M.; Mamiya, T.; Fan, P. C.; Knutson, D. E.; Witzigmann, C.; Cook, J.; Sieghart, W.; Nabeshima, T., Cerebellar Alpha6 Subunit-Containing Gabaa Receptors: A Novel

Therapeutic Target for Disrupted Prepulse Inhibition in Neuropsychiatric Disorders. *Br. J. Pharmacol.* **2018,** *175*, 2414-2427.

51. Knutson, D. E.; Kodali, R.; Treven, M.; Divovic, B.; Lee, H.-J.; Chou, J.-F.; Chen, H.-L.; Chiou, L.-C.; Ernst, M.; Mihovilovic, M. D.; Savic, M. M.; Sieghart, W.; Cook, J. M. In *Treatment of Sensorimotor Gating Deficits in Neuropsychiatric Disorders Using Deuterated A6-Gabaar Subtype Selective Ligands*, 257th ACS National Meeting & Exposition, Orlando, FL, American Chemical Society: Orlando, FL, 2019; pp MEDI-0121.

52. Krise, J. P.; Zygmunt, J.; Georg, G. I.; Stella, V. J., Novel Prodrug Approach for Tertiary Amines: Synthesis and Preliminary Evaluation of N-Phosphonooxymethyl Prodrugs. *J. Med. Chem.* **1999,** *42* (16), 3094-100.

53. Ueda, Y.; Matiskella, J. D.; Golik, J.; Connolly, T. P.; Hudyma, T. W.; Venkatesh, S.; Dali, M.; Kang, S. H.; Barbour, N.; Tejwani, R.; Varia, S.; Knipe, J.; Zheng, M.; Mathew, M.; Mosure, K.; Clark, J.; Lamb, L.; Medin, I.; Gao, Q.; Huang, S.; Chen, C. P.; Bronson, J. J., Phosphonooxymethyl Prodrugs of the Broad Spectrum Antifungal Azole, Ravuconazole: Synthesis and Biological Properties. *Bioorg Med Chem Lett* **2003,** *13* (21), 3669-72.

54. Regueiro-Ren, A.; Naidu, B. N.; Zheng, X.; Hudyma, T. W.; Connolly, T. P.; Matiskella, J. D.; Zhang, Y.; Kim, O. K.; Sorenson, M. E.; Pucci, M.; Clark, J.; Bronson, J. J.; Ueda, Y., Novel Semi-Synthetic Nocathiacin Antibiotics: Synthesis and Antibacterial Activity of Bis- and Mono-O-Alkylated Derivatives. *Bioorg Med Chem Lett* **2004,** *14* (1), 171-5.

55. Mantyla, A.; Garnier, T.; Rautio, J.; Nevalainen, T.; Vepsalainen, J.; Koskinen, A.; Croft, S. L.; Jarvinen, T., Synthesis, in Vitro Evaluation, and Antileishmanial Activity of Water-Soluble Prodrugs of Buparvaquone. *J. Med. Chem.* **2004,** *47* (1), 188-95.

56. Wang, C.; Barluenga, S.; Koripelly, G. K.; Fontaine, J. G.; Chen, R.; Yu, J. C.; Shen, X.; Chabala, J. C.; Heck, J. V.; Rubenstein, A.; Winssinger, N., Synthesis of Pochoxime Prodrugs as Potent Hsp90 Inhibitors. *Bioorg Med Chem Lett* **2009,** *19* (14), 3836-40.

57. Mitchell, M. L.; Son, J. C.; Guo, H.; Im, Y. A.; Cho, E. J.; Wang, J.; Hayes, J.; Wang, M.; Paul, A.; Lansdon, E. B.; Chen, J. M.; Graupe, D.; Rhodes, G.; He, G. X.; Geleziunas, R.; Xu, L.; Kim, C. U., N1-Alkyl Pyrimidinediones as Non-Nucleoside Inhibitors of Hiv-1 Reverse Transcriptase. *Bioorg Med Chem Lett* **2010,** *20* (5), 1589-92.

58. Sams, A. G.; Mikkelsen, G. K.; Larsen, M.; Langgard, M.; Howells, M. E.; Schroder, T. J.; Brennum, L. T.; Torup, L.; Jorgensen, E. B.; Bundgaard, C.; Kreilgard, M.; Bang-Andersen, B., Discovery of Phosphoric Acid Mono-{2-[(E/Z)-4-(3,3-Dimethyl-Butyrylamino)-3,5-Difluoro-Benzoylimino]-Thiazol-3 -Ylmethyl} Ester (Lu Aa47070): A Phosphonooxymethylene Prodrug of a Potent and Selective Ha(2a) Receptor Antagonist. *J. Med. Chem.* **2011,** *54* (3), 751-64.

59. Kadow, J. F.; Ueda, Y.; Meanwell, N. A.; Connolly, T. P.; Wang, T.; Chen, C. P.; Yeung, K. S.; Zhu, J.; Bender, J. A.; Yang, Z.; Parker, D.; Lin, P. F.; Colonno, R. J.; Mathew, M.; Morgan, D.; Zheng, M.; Chien, C.; Grasela, D., Inhibitors of Human Immunodeficiency Virus Type 1 (Hiv-1) Attachment 6. Preclinical and Human Pharmacokinetic Profiling of Bms-663749, a Phosphonooxymethyl Prodrug of the Hiv-1 Attachment Inhibitor 2-(4-Benzoyl-1-Piperazinyl)-1-(4,7-Dimethoxy-1h-Pyrrolo[2,3-C]Pyridin-3-Yl)-2-Oxo Ethanone (Bms-488043). *J. Med. Chem.* **2012,** *55* (5), 2048-56.

60. Chen, K.; Risatti, C.; Bultman, M.; Soumeillant, M.; Simpson, J.; Zheng, B.; Fanfair, D.; Mahoney, M.; Mudryk, B.; Fox, R. J.; Hsaio, Y.; Murugesan, S.; Conlon, D. A.; Buono,

F. G.; Eastgate, M. D., Synthesis of the 6-Azaindole Containing Hiv-1 Attachment Inhibitor Pro-Drug, Bms-663068. *J. Org. Chem.* **2014,** *79* (18), 8757-67.

61. Flores-Ramos, M.; Ibarra-Velarde, F.; Hernandez-Campos, A.; Vera-Montenegro, Y.; Jung-Cook, H.; Canto-Alarcon, G. J.; Del Rivero, L. M.; Castillo, R., A Highly Water Soluble Benzimidazole Derivative Useful for the Treatment of Fasciolosis. *Bioorg Med Chem Lett* **2014,** *24* (24), 5814-5817.

62. Lu, H.; Rogowskyj, J.; Yu, W.; Venkatesh, A.; Khan, N.; Nakagawa, S.; Goossens, N.; Koh, A. P.; Higashi, T.; Gunasekaran, G.; Schwarz, M. E.; Hiotis, S. P.; Xu, X.; Kinney, W.; Hoshida, Y.; Block, T.; Cuconati, A.; Du, Y., Novel Substituted Aminothiazoles as Potent and Selective Anti-Hepatocellular Carcinoma Agents. *Bioorg Med Chem Lett* **2016,** *26* (23), 5819-5824.

63. Hartz, R. A.; Vrudhula, V. M.; Ahuja, V. T.; Grace, J. E.; Lodge, N. J.; Bronson, J. J.; Macor, J. E., Synthesis and Evaluation of Prodrugs of Corticotropin-Releasing Factor-1 (Crf1) Receptor Antagonist Bms-665053 Leading to Improved Oral Bioavailability. *Bioorg Med Chem Lett* **2017,** *27* (6), 1360-1363.

64. Van der Plas, S. E.; Kelgtermans, H.; De Munck, T.; Martina, S. L. X.; Dropsit, S.; Quinton, E.; De Blieck, A.; Joannesse, C.; Tomaskovic, L.; Jans, M.; Christophe, T.; van der Aar, E.; Borgonovi, M.; Nelles, L.; Gees, M.; Stouten, P.; Van Der Schueren, J.; Mammoliti, O.; Conrath, K.; Andrews, M., Discovery of N-(3-Carbamoyl-5,5,7,7-Tetramethyl-5,7-Dihydro-4h-Thieno[2,3-C]Pyran-2-Yl)-Lh-Pyr Azole-5-Carboxamide (Glpg1837), a Novel Potentiator Which Can Open Class Iii Mutant Cystic Fibrosis Transmembrane Conductance Regulator (Cftr) Channels to a High Extent. *J. Med. Chem.* **2018,** *61* (4), 1425-1435.

65. Zimmermann, S. C.; Tichy, T.; Vavra, J.; Dash, R. P.; Slusher, C. E.; Gadiano, A. J.; Wu, Y.; Jancarik, A.; Tenora, L.; Monincova, L.; Prchalova, E.; Riggins, G. J.; Majer, P.; Slusher, B. S.; Rais, R., N-Substituted Prodrugs of Mebendazole Provide Improved Aqueous Solubility and Oral Bioavailability in Mice and Dogs. *J. Med. Chem.* **2018,** *61* (9), 3918-3929.

66. Meanwell, N. A.; Krystal, M. R.; Nowicka-Sans, B.; Langley, D. R.; Conlon, D. A.; Eastgate, M. D.; Grasela, D. M.; Timmins, P.; Wang, T.; Kadow, J. F., Inhibitors of Hiv-1 Attachment: The Discovery and Development of Temsavir and Its Prodrug Fostemsavir. *J. Med. Chem.* **2018,** *61* (1), 62-80.

67. Wang, Z.; Yu, Z.; Kang, D.; Zhang, J.; Tian, Y.; Daelemans, D.; De Clercq, E.; Pannecouque, C.; Zhan, P.; Liu, X., Design, Synthesis and Biological Evaluation of Novel Acetamide-Substituted Doravirine and Its Prodrugs as Potent Hiv-1 Nnrtis. *Bioorg. Med. Chem.* **2019,** *27* (3), 447-456.

68. Mitrović, J. R.; Divović, B.; Knutson, D. E.; Đoković, J. B.; Vulić, P. J.; Ranđelović, D.; Čalija, B. R.; Cook, J. M.; Savić, M. M.; Savić, S. D., Nanocrystal Dispersion of Dk-I-56-1, a Poorly Soluble Pyrazoloquinolinone Positive Modulator of A6 Gabaa Receptors: Formulation Approach toward Improved Brain Delivery. *Int. J. Pharm.* **2020,** *(Submitted for Publication)*.

69. Trudell, M. L. I. The Synthesis and Study of the Pharmacologic Activity of 7,12-Dihydropyrido[3,2-B:5,4-B']Diindoles. A Novel Class of Rigid, Planar Benzodiaze-Pine Receptor Ligands. Ii. The Total Synthesis of the Indole Alkaloid, (±)Suaveoline [Ph.D. Thesis]. University of Wisconsin-Milwaukee, Milwaukee, WI, 1989.

70. Frahn, J. L.; Illman, R. J., Preparation of a 4-Methoxyphenylhydrazine and Some Other Arylhydrazines. *Aust. J. Chem.* **1974,** *27* (6), 1361-1365.

71. Fryer, R. I.; Zhang, P.; Rios, R.; Gu, Z. Q.; Basile, A. S.; Skolnick, P., Structure-Activity Relationship Studies at Benzodiazepine Receptor (Bzr): A Comparison of the Substituent Effects of Pyrazoloquinolinone Analogs. *J. Med. Chem.* **1993,** *36* (11), 1669-1673.

72. Goncalves, V.; Brannigan, J. A.; Whalley, D.; Ansell, K. H.; Saxty, B.; Holder, A. A.; Wilkinson, A. J.; Tate, E. W.; Leatherbarrow, R. J., Discovery of Plasmodium Vivax N-Myristoyltransferase Inhibitors: Screening, Synthesis, and Structural Characterization of Their Binding Mode. *J. Med. Chem.* **2012,** *55* (7), 3578-3582.

73. Gould, R. G.; Jacobs, W. A., The Synthesis of Certain Substituted Quinolines and 5,6-Benzoquinolines. *J. Am. Chem. Soc.* **1939,** *61* (10), 2890-2895.

74. Salmon, R., Oxalyl Chloride-Dimethylformamide. In *Encyclopedia of Regents for Organic Synthesis*, J. Wiley: Chichester, West Sussex, 2001.

75. Yokoyama, N.; Ritter, B.; Neubert, A. D., 2-Arylpyrazolo[4,3-C]Quinolin-3-Ones: A Novel Agonist, a Partial Agonist and an Antagonist of Benzodiazepines. *J. Med. Chem.* **1982,** *25* (4), 337-339.

76. Jeanty, M.; Blu, J.; Suzenet, F.; Guillaumet, G., Synthesis of 4- and 6-Azaindoles Via the Fischer Reaction. *Org. Lett.* **2009,** *11* (22), 5142-5145.

77. Malvacio, I.; Moyano, E. L.; Vera, D. M. A., Gas-Phase Synthesis of 3-Carboethoxy-Quinolin-4-Ones. A Comprehensive Computational Mechanistic Study to Uncover the Dark Side of the Gould–Jacobs Reaction. *RSC Advances* **2016,** *6* (87), 83973-83981.

78. Berka, K.; Hendrychova, T.; Anzenbacher, P.; Otyepka, M., Membrane Position of Ibuprofen Agrees with Suggested Access Path Entrance to Cytochrome P450 2c9 Active Site. *J. Phys. Chem. A.* **2011,** *115* (41), 11248-11255.

79. Knutson, D. E.; Divovic, B.; Kodali, R.; Kehoe, A. S.; Luecke, I. W.; Arnold, L.; Ernst, M.; Fisher, J.; Savic, M. M.; Sieghart, W.; Cook, J. M., Comparative Study of Deuteration Versus Fluorination of A6-Gabaar Subtype- Selective Ligands as Strategies to Enhance Bioavailability, and Their Impact on the Pharmacokinetic Profiles and A6-Gabaar Functional Selectivity. *Eur. J. Med. Chem.* **2020,** *(Manuscript in progress)*.

80. Knutson, D. E.; Divovic, B.; Kodali, R.; Kehoe, A. S.; Luecke, I. W.; Arnold, L.; Ernst, M.; Fisher, J.; Savic, M. M.; Sieghart, W.; Cook, J. M. In *Comparative Study of Deuteration Versus Fluorination of A6-Gabaar Subtype- Selective Ligands as Strategies to Enhance Bioavailability, and Their Impact on the Pharmacokinetic Profiles and A6-Gabaar Functional Selectivity*, 259th ACS National Meeting & Exposition, Philadelphia, PA, American Chemical Society: Philadelphia, PA, 2020; pp MEDI-0113.

81. Savic, M. M.; Majumder, S.; Huang, S.; Edwankar, R. V.; Furtmuller, R.; Joksimovic, S.; Clayton, T., Sr.; Ramerstorfer, J.; Milinkovic, M. M.; Roth, B. L.; Sieghart, W.; Cook, J. M., Novel Positive Allosteric Modulators of Gabaa Receptors: Do Subtle Differences in Activity at Alpha1 Plus Alpha5 Versus Alpha2 Plus Alpha3 Subunits Account for Dissimilarities in Behavioral Effects in Rats? *Prog. Neuropsychopharmacol. Biol. Psychiatry.* **2010,** *34* (2), 376-386.

82. Gelderblom, H.; Verweij, J.; Nooter, K.; Sparreboom, A., Cremophor El. *European Journal of Cancer* **2001,** *37* (13), 1590-1598.

83. Badary, O. A.; Al-Shabanah, O. A.; Al-Gharably, N. M.; Elmazar, M. M., Effect of Cremophor El on the Pharmacokinetics, Antitumor Activity and Toxicity of Doxorubicin in Mice. *Anticancer Drugs* **1998,** *9* (9), 809-15.

84. Sykes, E.; Woodburn, K.; Decker, D.; Kessel, D., Effects of Cremophor El on Distribution of Taxol to Serum Lipoproteins. *Br J Cancer* **1994,** *70* (3), 401-4.

85. Broadwell, R. D.; Salcman, M.; Kaplan, R. S., Morphologic Effect of Dimethyl Sulfoxide on the Blood-Brain Barrier. *Science* **1982,** *217* (4555), 164-6.

86. Jacob, S. W.; Herschler, R., Pharmacology of Dmso. *Cryobiology* **1986,** *23* (1), 14-27.

87. Pestel, S.; Martin, H. J.; Maier, G. M.; Guth, B., Effect of Commonly Used Vehicles on Gastrointestinal, Renal, and Liver Function in Rats. *J. Pharmacol. Toxicol. Methods* **2006,** *54* (2), 200-14.

88. Sigfridsson, K.; Nordmark, A.; Theilig, S.; Lindahl, A., A Formulation Comparison between Micro- and Nanosuspensions: The Importance of Particle Size for Absorption of a Model Compound, Following Repeated Oral Administration to Rats During Early Development. *Drug Dev. Ind. Pharm.* **2011,** *37* (2), 185-92.

89. Sigfridsson, K.; Lundqvist, A.; Strimfors, M., Evaluation of Exposure Properties after Injection of Nanosuspensions and Microsuspenions into the Intraperitoneal Space in Rats. *Drug Dev. Ind. Pharm.* **2013,** *39* (11), 1832-9.

90. Zuidema, J.; Kadir, F.; Titulaer, H. A. C.; Oussoren, C., Release and Absorption Rates of Intramuscularly and Subcutaneously Injected Pharmaceuticals (Ii). *Int. J. Pharm.* **1994,** *105* (3), 189-207.

91. Djordjevic, S. M.; Cekic, N. D.; Savic, M. M.; Isailovic, T. M.; Randelovic, D. V.; Markovic, B. D.; Savic, S. R.; Timic Stamenic, T.; Daniels, R.; Savic, S. D., Parenteral Nanoemulsions as Promising Carriers for Brain Delivery of Risperidone: Design, Characterization and in Vivo Pharmacokinetic Evaluation. *Int. J. Pharm.* **2015,** *493* (1-2), 40-54.

92. Jenks, W. P., *Catalysis in Chemistry and Enzymology*. Dover Publications Inc.: Mineola, NY, 1987.

93. Northrop, D. B., Steady-State Analysis of Kinetic Isotope Effects in Enzymic Reactions. *Biochem.* **1975,** *14* (12), 2644-2651.

94. Gomtsyan, A., Heterocycles in Drugs and Drug Discovery. *Chem. Heterocycl. Comp.* **2012,** *48* (1), 7-10.

95. Banks, W. A., Characteristics of Compounds That Cross the Blood-Brain Barrier. *BMC Neurol.* **2009,** *9 Suppl 1*, S3.

96. Waterhouse, R., Determination of Lipophilicity and Its Use as a Predictor of Blood–Brain Barrier Penetration of Molecular Imaging Agents. *Mol. Imaging Biol.* **2003,** *5* (6), 376-389.

97. Bewernick, B. H.; Urbach, A. S.; Broder, A.; Kayser, S.; Schlaepfer, T. E., Walking Away from Depression-Motor Activity Increases Ratings of Mood and Incentive Drive in Patients with Major Depression. *Psychiatry Res.* **2017,** *247*, 68-72.

98. Armarego, W. L. F.; Chai, C. L. L., *Purification of Laboratory Chemicals, 7th Edition*. Butterworth-Heinemann: New York, NY, 2012.

99. Pouchert, C. J.; Behnke, J., *The Aldrich Library of 13c and 1h Ft Nmr Spectra, 1st Edition*. Aldrich Chemical Co.: Milwaukee, WI, 1993; Vol. 2.

100. Lucero, B.; Gomes, C. R.; Frugulhetti, I. C.; Faro, L. V.; Alvarenga, L.; de Souza, M. C.; de Souza, T. M.; Ferreira, V. F., Synthesis and Anti-Hsv-1 Activity of Quinolonic Acyclovir Analogues. *Bioorg. Med. Chem. Lett.* **2006,** *16* (4), 1010-1013.

101. Forkuo, G. S.; Guthrie, M. L.; Yuan, N. Y.; Nieman, A. N.; Kodali, R.; Jahan, R.; Stephen, M. R.; Yocum, G. T.; Treven, M.; Poe, M. M.; Li, G.; Yu, O. B.; Hartzler, B. D.; Zahn, N. M.; Ernst, M.; Emala, C. W.; Stafford, D. C.; Cook, J. M.; Arnold, L. A., Development

of Gabaa Receptor Subtype-Selective Imidazobenzodiazepines as Novel Asthma Treatments. *Mol. Pharmacol.* **2016,** *13* (6), 2026-2038.

102. Forkuo, G. S.; Nieman, A. N.; Yuan, N. Y.; Kodali, R.; Yu, O. B.; Zahn, N. M.; Jahan, R.; Li, G.; Stephen, M. R.; Guthrie, M. L.; Poe, M. M.; Hartzler, B. D.; Harris, T. W.; Yocum, G. T.; Emala, C. W.; Steeber, D. A.; Stafford, D. C.; Cook, J. M.; Arnold, L. A., Alleviation of Multiple Asthmatic Pathologic Features with Orally Available and Subtype Selective Gabaa Receptor Modulators. *Mol. Pharmacol.* **2017,** *14* (6), 2088-2098.

103. Jahan, R.; Stephen, M. R.; Forkuo, G. S.; Kodali, R.; Guthrie, M. L.; Nieman, A. N.; Yuan, N. Y.; Zahn, N. M.; Poe, M. M.; Li, G.; Yu, O. B.; Yocum, G. T.; Emala, C. W.; Stafford, D. C.; Cook, J. M.; Arnold, L. A., Optimization of Substituted Imidazobenzodiazepines as Novel Asthma Treatments. *Eur. J. Med. Chem.* **2017,** *126*, 550-560.

104. Ramerstorfer, J.; Furtmuller, R.; Vogel, E.; Huck, S.; Sieghart, W., The Point Mutation Gamma 2f77i Changes the Potency and Efficacy of Benzodiazepine Site Ligands in Different Gabaa Receptor Subtypes. *Eur. J. Pharmacol.* **2010,** *636* (1-3), 18-27.

105. Picton, A. J.; Fisher, J. L., Effect of the Alpha Subunit Subtype on the Macroscopic Kinetic Properties of Recombinant Gaba(a) Receptors. *Brain Res* **2007,** *1165*, 40-9.

106. Khandelwal, A.; Bahadduri, P. M.; Chang, C.; Polli, J. E.; Swaan, P. W.; Ekins, S., Computational Models to Assign Biopharmaceutics Drug Disposition Classification from Molecular Structure. *Pharm. Res.* **2007,** *24* (12), 2249-2262.

107. Puthenkalam, R.; Hieckel, M.; Simeone, X.; Suwattanasophon, C.; Feldbauer, R. V.; Ecker, G. F.; Ernst, M., Structural Studies of Gabaa Receptor Binding Sites: Which Experimental Structure Tells Us What? *Front Mol Neurosci* **2016,** *9*, 44.

108. Maldifassi, M. C.; Baur, R.; Sigel, E., Molecular Mode of Action of Cgs 9895 at Alpha1 Beta2 Gamma2 Gabaa Receptors. *J. Neurochem.* **2016,** *138* (5), 722-30.

109. Zhu, S.; Noviello, C. M.; Teng, J.; Walsh, R. M., Jr.; Kim, J. J.; Hibbs, R. E., Structure of a Human Synaptic Gabaa Receptor. *Nature* **2018,** *559* (7712), 67-72.

110. Siebert, D. C. B.; Wieder, M.; Schlener, L.; Scholze, P.; Boresch, S.; Langer, T.; Schnurch, M.; Mihovilovic, M. D.; Richter, L.; Ernst, M.; Ecker, G. F., Sar-Guided Scoring Function and Mutational Validation Reveal the Binding Mode of Cgs-8216 at the Alpha1+/Gamma2- Benzodiazepine Site. *J Chem Inf Model* **2018,** *58* (8), 1682-1696.

111. Sadr, S. S.; Javanbakht, J.; Javidan, A. N.; Ghaffarpour, M.; Khamse, S.; Naghshband, Z., Descriptive Epidemiology: Prevalence, Incidence, Sociodemographic Factors, Socioeconomic Domains, and Quality of Life of Epilepsy: An Update and Systematic Review. *Arch Med Sci* **2018,** *14* (4), 717-724.

112. Gitto, R.; De Luca, L.; De Sarra, G., *Aniticonvulsants. In Burger's Medicinal Chemistry, Durg Discovery, and Development*. Seventh Edition ed.; John Wiley & Sons, Inc.: 2010.

113. Banerjee, J.; Chandra, S. P.; Kurwale, N.; Tripathi, M., Epileptogenic Networks and Drug-Resistant Epilepsy: Present and Future Perspectives of Epilepsy Research-Utility for the Epileptologist and the Epilepsy Surgeon. *Ann Indian Acad Neurol* **2014,** *17* (Suppl 1), S134-40.

114. Marson, A. G.; Al-Kharusi, A. M.; Alwaidh, M.; Appleton, R.; Baker, G. A.; Chadwick, D. W.; Cramp, C.; Cockerell, O. C.; Cooper, P. N.; Doughty, J.; Eaton, B.; Gamble, C.; Goulding, P. J.; Howell, S. J. L.; Hughes, A.; Jackson, M.; Jacoby, A.; Kellett, M.; Lawson, G. R.; Leach, J. P.; Nicolaides, P.; Roberts, R.; Shackley, P.; Shen, J.; Smith, D. F.; Smith, P. E. M.; Smith, C. T.; Vanoli, A.; Williamson, P. R., The Sanad Study of Effectiveness of

Valproate, Lamotrigine, or Topiramate for Generalised and Unclassifiable Epilepsy: An Unblinded Randomised Controlled Trial. *The Lancet* **2007,** *369* (9566), 1016-1026.

115. Sinha, S.; Siddiqui, K. A., Definition of Intractable Epilepsy. *Neurosciences (Riyadh)* **2011,** *16* (1), 3-9.

116. Avanzini, G.; Depaulis, A.; Tassinari, A.; de Curtis, M., Do Seizures and Epileptic Activity Worsen Epilepsy and Deteriorate Cognitive Function? *Epilepsia* **2013,** *54 Suppl 8*, 14-21.

117. Campbell Teskey, G.; Racine, R. J., Increased Spontaneous Unit Discharge Rates Following Electrical Kindling in the Rat. *Brain Research* **1993,** *624* (1-2), 11-18.

118. Racine, R. J., Modification of Seizure Activity by Electrical Stimulation: Ii. Motor Seizure. *Electroencephalography and Clinical Neurophysiology* **1972,** *32* (3), 281-294.

119. Witkin, J. M.; Tortella, F. C., Modulators of N-Methyl-D-Aspartate Protect against Diazepam- or Phenobarbital-Resistant Cocaine Convulsions. *Life Sci.* **1991,** *48* (11), PL51-PL56.

120. Holmes, G. L., The Long-Term Effects of Seizures on the Developing Brain: Clinical and Laboratory Issues. *Brain and Development* **1991,** *13* (6), 393-409.

121. Holmes, G. L., Epilepsy in the Developing Brain: Lessons from the Laboratory and Clinic. *Epilepsia* **1997,** *38* (1), 12-30.

122. DeGiorgio, C. M.; Curtis, A.; Hertling, D.; Moseley, B. D., Sudden Unexpected Death in Epilepsy: Risk Factors, Biomarkers, and Prevention. *Acta Neurol Scand* **2019,** *139* (3), 220-230.

123. Barker-Haliski, M. L.; Johnson, K.; Billingsley, P.; Huff, J.; Handy, L. J.; Khaleel, R.; Lu, Z.; Mau, M. J.; Pruess, T. H.; Rueda, C.; Saunders, G.; Underwood, T. K.; Vanegas, F.; Smith, M. D.; West, P. J.; Wilcox, K. S., Validation of a Preclinical Drug Screening Platform for Pharmacoresistant Epilepsy. *Neurochem. Res.* **2017,** *42* (7), 1904-1918.

124. Lewter, L. A.; Fisher, J. L.; Siemian, J. N.; Methuku, K. R.; Poe, M. M.; Cook, J. M.; Li, J. X., Antinociceptive Effects of a Novel Alpha2/Alpha3-Subtype Selective Gabaa Receptor Positive Allosteric Modulator. *ACS Chem Neurosci* **2017,** *8* (6), 1305-1312.

125. Poe, M. M.; Methuku, K. R.; Li, G.; Verma, A. R.; Teske, K. A.; Stafford, D. C.; Arnold, L. A.; Cramer, J. W.; Jones, T. M.; Cerne, R.; Krambis, M. J.; Witkin, J. M.; Jambrina, E.; Rehman, S.; Ernst, M.; Cook, J. M.; Schkeryantz, J. M., Synthesis and Characterization of a Novel Gamma-Aminobutyric Acid Type a (Gabaa) Receptor Ligand That Combines Outstanding Metabolic Stability, Pharmacokinetics, and Anxiolytic Efficacy. *J. Med. Chem.* **2016,** *59* (23), 10800-10806.

126. McKernan, R. M.; Rosahl, T. W.; Reynolds, D. S.; Sur, C.; Wafford, K. A.; Atack, J. R.; Farrar, S.; Myers, J.; Cook, G.; Ferris, P.; Garrett, L.; Bristow, L.; Marshall, G.; Macaulay, A.; Brown, N.; Howell, O.; Moore, K. W.; Carling, R. W.; Street, L. J.; Castro, J. L.; Ragan, C. I.; Dawson, G. R.; Whiting, P. J., Sedative but Not Anxiolytic Properties of Benzodiazepines Are Mediated by the Gaba(a) Receptor Alpha1 Subtype. *Nat Neurosci* **2000,** *3* (6), 587-92.

127. Witkin, J. M.; Li, G.; Golani, L. K.; Xiong, W.; Smith, J. L.; Ping, X.; Rashid, F.; Jahan, R.; Cerne, R.; Cook, J. M.; Jin, X., The Positive Allosteric Modulator of Alpha2/3-Containing Gabaa Receptors, Krm-Ii-81, Is Active in Pharmaco-Resistant Models of Epilepsy and Reduces Hyperexcitability after Traumatic Brain Injury. *J. Pharmacol. Exp. Ther.* **2020,** *372* (1), 83-94.

128. Witkin, J. M.; Smith, J. L.; Ping, X.; Gleason, S. D.; Poe, M. M.; Li, G.; Jin, X.; Hobbs, J.; Schkeryantz, J. M.; McDermott, J. S.; Alatorre, A. I.; Siemian, J. N.; Cramer, J. W.; Airey, D. C.; Methuku, K. R.; Tiruveedhula, V.; Jones, T. M.; Crawford, J.; Krambis, M. J.; Fisher, J. L.; Cook, J. M.; Cerne, R., Bioisosteres of Ethyl 8-Ethynyl-6-(Pyridin-2-Yl)-4h-

Benzo[F]Imidazo [1,5-a][1,4]Diazepine-3-Carboxylate (Hz-166) as Novel Alpha 2,3 Selective Potentiators of Gabaa Receptors: Improved Bioavailability Enhances Anticonvulsant Efficacy. *Neuropharmacology* **2018,** *137*, 332-343.

129. Witkin, J. M.; Cerne, R.; Davis, P. G.; Freeman, K. B.; do Carmo, J. M.; Rowlett, J. K.; Methuku, K. R.; Okun, A.; Gleason, S. D.; Li, X.; Krambis, M. J.; Poe, M.; Li, G.; Schkeryantz, J. M.; Jahan, R.; Yang, L.; Guo, W.; Golani, L. K.; Anderson, W. H.; Catlow, J. T.; Jones, T. M.; Porreca, F.; Smith, J. L.; Knopp, K. L.; Cook, J. M., The Alpha2,3-Selective Potentiator of Gabaa Receptors, Krm-Ii-81, Reduces Nociceptive-Associated Behaviors Induced by Formalin and Spinal Nerve Ligation in Rats. *Pharmacol Biochem Behav* **2019,** *180*, 22-31.

130. Knutson, D. E.; Smith, J. L.; Ping, X.; Jin, X.; Golani, L. K.; Li, G.; Tiruveedhula, V. V. N. P. B.; Rashid, F.; Mian, M. Y.; Jahan, R.; Sharmin, D.; Cerne, R.; Cook, J. M.; Witkin, J. M., The Imidazodiazepine Anticonvulsant, Krm-Ii-81, Produces Novel, Non-Diazepam-Like Antiepileptogentic Effects. *ACS Chemical Neuroscience* **2020,** *(submission in progress)*.

131. Löscher, W.; Schmidt, D., Which Animal Models Should Be Used in the Search for New Antiepileptic Drugs? A Proposal Based on Experimental and Clinical Considerations. *Epilepsy Research* **1988,** *2* (3), 145-181.

132. McNamara, J. O.; Bonhause, D. W.; Shin, C., The Kindling Model of Epilepsy. *P. A. Schwartzkroin, Ed., Epilepsy: Models, Mechanisms, and Concepts, Cambridge University Press, Cambridge* **1993**, 27-47.

133. White, H. S.; Woodhead, J. H.; Franklin, M. R.; Swinyard, E. A.; Wolf, H. H., *General Principles: Experimental Selection, Quantification, and Evaluation of Antiepileptic Drugs. In: Levy Rh, Mattson Rh, Meldrum Bs, Eds. Antiepileptic Drugs.* 4th edition ed.; New York: Raven Press, Ltd.: 1995.

134. Gasior, M.; Beekman, M.; Carter, R. B.; Goldberg, S. R.; Witkin, J. M., Antiepileptogenic Effects of the Novel Synthetic Neuroactive Steroid, Ganaxolone, against Pentylenetetrazol-Induced Kindled Seizures: Comparison with Diazepam and Valproate. *Drug Dev. Res.* **1998,** *44* (1), 21-33.

135. Gasior, M.; Ungard, J. T.; Beekman, M.; Carter, R. B.; Witkin, J. M., Acute and Chronic Effects of the Synthetic Neuroactive Steroid, Ganaxolone, against the Convulsive and Lethal Effects of Pentylenetetrazol in Seizure-Kindled Mice: Comparison with Diazepam and Valproate. *Neuropharmacology* **2000,** *39* (7), 1184-1196.

136. Cook, J.; Li, G.; Golani, L.; Jahan, R.; Rashid, F., Improved Synthesis of Anxiolytic, Anticonvulsant, and Antinociceptive A2/A3-Gaba(a)-Ergic Receptor Subtype Selective Ligands as Promising Agents to Treat Anxiety, Epilepsy, and Neuropathic Pain. *Synthesis* **2018,** *50* (20), 4124-4132.

137. Czuczwar, S. J.; Frey, H.-H.; Löscher, W., Antagonism of N-Methyl-D,L-Aspartic Acid-Induced Convulsions by Antiepileptic Drugs and Other Agents. *Eur. J. Pharmacol.* **1985,** *108* (3), 273-280.

138. Turski, W. A.; Cavalheiro, E. A.; Bortolotto, Z. A.; Mello, L. M.; Schwarz, M.; Turski, L., Seizures Produced by Pilocarpine in Mice: A Behavioral, Electroencephalographic and Morphological Analysis. *Brain Research* **1984,** *321* (2), 237-253.

139. Yamaguchi, S.-i.; Rogawski, M. A., Effects of Anticonvulsant Drugs on 4-Aminopyridine-Induced Seizures in Mice. *Epilepsy Research* **1992,** *11* (1), 9-16.

140. File, S. E.; Greenblatt, D. J.; Martin, I. L.; Brown, C., Long-Lasting Anticonvulsant Effects of Diazepam in Different Mouse Strains: Correlations with Brain Concentrations and Receptor Occupancy. *Psychopharmacology (Berl)* **1985,** *86* (1-2), 137-41.

141. Shenoy, A. K.; Miyahara, J. T.; Swinyard, E. A.; Kupferberg, H. J., Comparative Anticonvulsant Activity and Neurotoxicity of Clobazam, Diazepam, Phenobarbital, and Valproate in Mice and Rats. *Epilepsia* **1982,** *23* (4), 399-408.

142. Gasior, M.; Ungard, J. T.; Witkin, J. M., Chlormethiazole: Effectiveness against Toxic Effects of Cocaine in Mice. *J. Pharmacol. Exp. Ther.* **2000,** *295* (1), 153-61.

143. Kaminski, R. M.; Gasior, M.; Carter, R. B.; Witkin, J. M., Protective Efficacy of Neuroactive Steroids against Cocaine Kindled-Seizures in Mice. *Eur. J. Pharmacol.* **2003,** *474* (2-3), 217-222.

144. Cerne, R.; Fisher, J. F.; Siemian, J. N.; Smith, J. L.; Knutson, D. E.; Cook, J. M.; Witkin, J. M., Improvements in the Pharmacological Profile of Diazepam by Krm-Ii-81, an Imidizodiazepine Positive Allosteric Modulator of A2/3-Containing Gabaa Receptors: Preclinical Data Predict Enhanced Efficacy for Epilepsy, Chronic Pain, Anxiety, and Depression. *Pharmaceutical Sciences and Biomedical Analysis Journal* **2019,** *2* (117), 1-14.

145. Cook, J. M.; Huang, Q.; He, X.; Li, X.; Yu, J.; Han, D.; Lelas, S.; McElroy, J. Anxiolytic Agents with Reduced Sedative and Ataxic Effects. US007119196B2 2003.

146. Rivas, F. M.; Stables, J. P.; Murphree, L.; Edwankar, R. V.; Edwankar, C. R.; Huang, S.; Jain, H. D.; Zhou, H.; Majumder, S.; Sankar, S.; Roth, B. L.; Ramerstorfer, J.; Furtmuller, R.; Sieghart, W.; Cook, J. M., Antiseizure Activity of Novel Gamma-Aminobutyric Acid (a) Receptor Subtype-Selective Benzodiazepine Analogues in Mice and Rat Models. *J. Med. Chem.* **2009,** *52* (7), 1795-8.

147. Li, G. G.; Golani, L. K.; Jahan, R.; Rashid, F.; Cook, J. M., Improved Synthesis of Anxiolytic, Anticonvulsant, and Antinociceptive Alpha 2/Alpha 3-Gaba(a)-Ergic Receptor

Subtype Selective Ligands as Promising Agents to Treat Anxiety, Epilepsy, and Neuropathic. *Synthesis-Stuttgart* **2018,** *50* (20), 4124-4132.

148. Selnick, H. G.; Liverton, N. J.; Baldwin, J. J.; Butcher, J. W.; Claremon, D. A.; Elliott, J. M.; Freidinger, R. M.; King, S. A.; Libby, B. E.; McIntyre, C. J.; Pribush, D. A.; Remy, D. C.; Smith, G. R.; Tebben, A. J.; Jurkiewicz, N. K.; Lynch, J. J.; Salata, J. J.; Sanguinetti, M. C.; Siegl, P. K.; Slaughter, D. E.; Vyas, K., Class Iii Antiarrhythmic Activity in Vivo by Selective Blockade of the Slowly Activating Cardiac Delayed Rectifier Potassium Current Iks by (R)-2-(2,4-Trifluoromethyl)-N-[2-Oxo-5-Phenyl-1-(2,2,2-Trifluoroethyl)- 2, 3-Dihydro-1h-Benzo[E][1,4]Diazepin-3-Yl]Acetamide. *J. Med. Chem.* **1997,** *40* (24), 3865-8.

149. Cook, J. M.; Zhou, H.; Huang, S.; Srirama Sarma, P. V. V.; Zhang, C. Stereospecific Anxiolytic and Anticonvulsant Agents with Reduced Muscle-Relaxant, Sedative-Hypnotic and Ataxic Effects. US7618958B2, 2009.

150. Delépine, M., *Bull. Soc. Chim. Fr.* **1895,** *13*, 352-361.

151. Blažević, N.; Kajfež, F., A New Ring Closure Synthesis of 1,4-Benzodiazepines. Ii. *J. Heterocycl. Chem.* **1971,** *8* (5), 845-846.

152. Cepanec, I.; Litvić, M.; Pogorelić, I., Efficient Synthesis of 3-Hydroxy-1,4-Benzodiazepines Oxazepam and Lorazepam by New Acetoxylation Reaction of 3-Position of 1,4-Benzodiazepine Ring. *Organic Process Research & Development* **2006,** *10* (6), 1192-1198.

153. Yang, J.; Teng, Y.; Ara, S.; Rallapalli, S.; Cook, J. M., An Improved Process for the Synthesis of 4h-Imidazo[1,5-a][1,4]Benzodiazepines. *Synthesis (Stuttg)* **2009,** *40* (32), nihpa145687.

154. Cassar, L., Synthesis of Aryl- and Vinyl-Substituted Acetylene Derivatives by the Use of Nickel and Palladium Complexes. *J. Organomet. Chem.* **1975,** *93* (2), 253-257.

155. Dieck, H. A.; Heck, F. R., Palladium Catalyzed Synthesis of Aryl, Heterocyclic and Vinylic Acetylene Derivatives. *J. Organomet. Chem.* **1975,** *93* (2), 259-263.

156. Jover, J.; Cirera, J., Computational Assessment on the Tolman Cone Angles for P-Ligands. *Dalton Trans* **2019,** *48* (40), 15036-15048.

157. Tolman, C. A., Steric Effects of Phosphorus Ligands in Organometallic Chemistry and Homogeneous Catalysis. *Chem. Rev.* **1977,** *77* (3), 313-348.

158. Gazvoda, M.; Virant, M.; Pinter, B.; Kosmrlj, J., Mechanism of Copper-Free Sonogashira Reaction Operates through Palladium-Palladium Transmetallation. *Nat Commun* **2018,** *9* (1), 4814.

159. Collinson, N.; Kuenzi, F. M.; Jarolimek, W.; Maubach, K. A.; Cothliff, R.; Sur, C.; Smith, A.; Otu, F. M.; Howell, O.; Atack, J. R.; McKernan, R. M.; Seabrook, G. R.; Dawson, G. R.; Whiting, P. J.; Rosahl, T. W., Enhanced Learning and Memory and Altered Gabaergic Synaptic Transmission in Mice Lacking the Alpha 5 Subunit of the Gabaa Receptor. *J. Neurosci.* **2002,** *22* (13), 5572-80.

160. Korpi, E. R.; Mattila, M. J.; Wisden, W.; Luddens, H., Gaba(a)-Receptor Subtypes: Clinical Efficacy and Selectivity of Benzodiazepine Site Ligands. *Ann Med* **1997,** *29* (4), 275-82.

161. Crestani, F.; Keist, R.; Fritschy, J. M.; Benke, D.; Vogt, K.; Prut, L.; Bluthmann, H.; Mohler, H.; Rudolph, U., Trace Fear Conditioning Involves Hippocampal Alpha5 Gaba(a) Receptors. *Proc Natl Acad Sci U S A* **2002,** *99* (13), 8980-5.

162. Gill, K. M.; Grace, A. A., The Role of Alpha5 Gabaa Receptor Agonists in the Treatment of Cognitive Deficits in Schizophrenia. *Curr Pharm Des* **2014,** *20* (31), 5069-76.

163. Soh, M. S.; Lynch, J. W., Selective Modulators of Alpha5-Containing Gabaa Receptors and Their Therapeutic Significance. *Curr Drug Targets* **2015,** *16* (7), 735-46.

164. Martinez-Cue, C.; Martinez, P.; Rueda, N.; Vidal, R.; Garcia, S.; Vidal, V.; Corrales, A.; Montero, J. A.; Pazos, A.; Florez, J.; Gasser, R.; Thomas, A. W.; Honer, M.; Knoflach, F.; Trejo, J. L.; Wettstein, J. G.; Hernandez, M. C., Reducing Gabaa Alpha5 Receptor-Mediated Inhibition Rescues Functional and Neuromorphological Deficits in a Mouse Model of Down Syndrome. *J. Neurosci.* **2013,** *33* (9), 3953-66.

165. Benes, F. M.; Lim, B.; Matzilevich, D.; Walsh, J. P.; Subburaju, S.; Minns, M., Regulation of the Gaba Cell Phenotype in Hippocampus of Schizophrenics and Bipolars. *Proc Natl Acad Sci U S A* **2007,** *104* (24), 10164-9.

166. Lodge, D. J.; Grace, A. A., Hippocampal Dysfunction and Disruption of Dopamine System Regulation in an Animal Model of Schizophrenia. *Neurotox Res* **2008,** *14* (2-3), 97-104.

167. Gill, K. M.; Lodge, D. J.; Cook, J. M.; Aras, S.; Grace, A. A., A Novel Alpha5gaba(a)R-Positive Allosteric Modulator Reverses Hyperactivation of the Dopamine System in the Mam Model of Schizophrenia. *Neuropsychopharmacology* **2011,** *36* (9), 1903-11.

168. Gill, K. M.; Cook, J. M.; Poe, M. M.; Grace, A. A., Prior Antipsychotic Drug Treatment Prevents Response to Novel Antipsychotic Agent in the Methylazoxymethanol Acetate Model of Schizophrenia. *Schizophr Bull* **2014,** *40* (2), 341-50.

169. Benes, F. M., A New Paradigm for Understanding Gamma-Aminobutyric Acid Cell Pathology in Schizophrenia? *Biol Psychiatry* **2012,** *72* (9), 712-3.

170. Papadimitriou, G. N.; Dikeos, D. G.; Karadima, G.; Avramopoulos, D.; Daskalopoulou, E. G.; Vassilopoulos, D.; Stefanis, C. N., Association between the Gaba(a) Receptor Alpha5 Subunit Gene Locus (Gabra5) and Bipolar Affective Disorder. *Am J Med Genet* **1998,** *81* (1), 73-80.

171. Gallos, G.; Yim, P.; Chang, S.; Zhang, Y.; Xu, D.; Cook, J. M.; Gerthoffer, W. T.; Emala, C. W., Sr., Targeting the Restricted Alpha-Subunit Repertoire of Airway Smooth Muscle Gabaa Receptors Augments Airway Smooth Muscle Relaxation. *Am J Physiol Lung Cell Mol Physiol* **2012,** *302* (2), L248-56.

172. Fu, X. W.; Wood, K.; Spindel, E. R., Prenatal Nicotine Exposure Increases Gaba Signaling and Mucin Expression in Airway Epithelium. *Am. J. Respir. Cell Mol. Biol.* **2011,** *44* (2), 222-9.

173. Xiang, Y. Y.; Wang, S.; Liu, M.; Hirota, J. A.; Li, J.; Ju, W.; Fan, Y.; Kelly, M. M.; Ye, B.; Orser, B.; O'Byrne, P. M.; Inman, M. D.; Yang, X.; Lu, W. Y., A Gabaergic System in Airway Epithelium Is Essential for Mucus Overproduction in Asthma. *Nat Med* **2007,** *13* (7), 862-7.

174. Yocum, G. T.; Turner, D. L.; Danielsson, J.; Barajas, M. B.; Zhang, Y.; Xu, D.; Harrison, N. L.; Homanics, G. E.; Farber, D. L.; Emala, C. W., Gabaa Receptor Alpha4-Subunit Knockout Enhances Lung Inflammation and Airway Reactivity in a Murine Asthma Model. *Am J Physiol Lung Cell Mol Physiol* **2017,** *313* (2), L406-L415.

175. Sanders, R. D.; Grover, V.; Goulding, J.; Godlee, A.; Gurney, S.; Snelgrove, R.; Ma, D.; Singh, S.; Maze, M.; Hussell, T., Immune Cell Expression of Gabaa Receptors and the Effects of Diazepam on Influenza Infection. *J Neuroimmunol* **2015,** *282*, 97-103.

176. Gallos, G.; Gleason, N. R.; Zhang, Y.; Pak, S. W.; Sonett, J. R.; Yang, J.; Emala, C. W., Activation of Endogenous Gabaa Channels on Airway Smooth Muscle Potentiates Isoproterenol-Mediated Relaxation. *Am J Physiol Lung Cell Mol Physiol* **2008,** *295* (6), L1040-7.

177. Gallos, G.; Townsend, E.; Yim, P.; Virag, L.; Zhang, Y.; Xu, D.; Bacchetta, M.; Emala, C. W., Airway Epithelium Is a Predominant Source of Endogenous Airway Gaba and Contributes

to Relaxation of Airway Smooth Muscle Tone. *Am J Physiol Lung Cell Mol Physiol* **2013,** *304* (3), L191-7.

178. Mizuta, K.; Xu, D.; Pan, Y.; Comas, G.; Sonett, J. R.; Zhang, Y.; Panettieri, R. A., Jr.; Yang, J.; Emala, C. W., Sr., Gabaa Receptors Are Expressed and Facilitate Relaxation in Airway Smooth Muscle. *Am J Physiol Lung Cell Mol Physiol* **2008,** *294* (6), L1206-16.

179. Zahn, N. M.; Huber, A. T.; Mikulsky, B. N.; Stepanski, M. E.; Kehoe, A. S.; Li, G.; Schussman, M.; Rashid Roni, M. S.; Kodali, R.; Cook, J. M.; Stafford, D. C.; Steeber, D. A.; Arnold, L. A., Midd0301 - a First-in-Class Anti-Inflammatory Asthma Drug Targets Gabaa Receptors without Causing Systemic Immune Suppression. *Basic Clin Pharmacol Toxicol* **2019,** *125* (1), 75-84.

180. Forkuo, G. S.; Nieman, A. N.; Kodali, R.; Zahn, N. M.; Li, G.; Rashid Roni, M. S.; Stephen, M. R.; Harris, T. W.; Jahan, R.; Guthrie, M. L.; Yu, O. B.; Fisher, J. L.; Yocum, G. T.; Emala, C. W.; Steeber, D. A.; Stafford, D. C.; Cook, J. M.; Arnold, L. A., A Novel Orally Available Asthma Drug Candidate That Reduces Smooth Muscle Constriction and Inflammation by Targeting Gabaa Receptors in the Lung. *Mol Pharm* **2018,** *15* (5), 1766-1777.

181. Forkuo, G. S.; Guthrie, M. L.; Yuan, N. Y.; Nieman, A. N.; Kodali, R.; Jahan, R.; Stephen, M. R.; Yocum, G. T.; Treven, M.; Poe, M. M.; Li, G.; Yu, O. B.; Hartzler, B. D.; Zahn, N. M.; Ernst, M.; Emala, C. W.; Stafford, D. C.; Cook, J. M.; Arnold, L. A., Development of Gabaa Receptor Subtype-Selective Imidazobenzodiazepines as Novel Asthma Treatments. *Mol Pharm* **2016,** *13* (6), 2026-38.

182. Jahan, R.; Stephen, M. R.; Forkuo, G. S.; Kodali, R.; Guthrie, M. L.; Nieman, A. N.; Yuan, N. Y.; Zahn, N. M.; Poe, M. M.; Li, G.; Yu, O. B.; Yocum, G. T.; Emala, C. W.;

Stafford, D. C.; Cook, J. M.; Arnold, L. A., Optimization of Substituted Imidazobenzodiazepines as Novel Asthma Treatments. *Eur. J. Med. Chem.* **2017,** *126*, 550-560.

183. Yocum, G. T.; Perez-Zoghbi, J. F.; Danielsson, J.; Kuforiji, A. S.; Zhang, Y.; Li, G.; Rashid Roni, M. S.; Kodali, R.; Stafford, D. C.; Arnold, L. A.; Cook, J. M.; Emala, C. W., Sr., A Novel Gabaa Receptor Ligand Midd0301 with Limited Blood-Brain Barrier Penetration Relaxes Airway Smooth Muscle Ex Vivo and in Vivo. *Am J Physiol Lung Cell Mol Physiol* **2019,** *316* (2), L385-L390.

184. Forkuo, G. S.; Nieman, A. N.; Yuan, N. Y.; Kodali, R.; Yu, O. B.; Zahn, N. M.; Jahan, R.; Li, G.; Stephen, M. R.; Guthrie, M. L.; Poe, M. M.; Hartzler, B. D.; Harris, T. W.; Yocum, G. T.; Emala, C. W.; Steeber, D. A.; Stafford, D. C.; Cook, J. M.; Arnold, L. A., Alleviation of Multiple Asthmatic Pathologic Features with Orally Available and Subtype Selective Gabaa Receptor Modulators. *Mol Pharm* **2017,** *14* (6), 2088-2098.

185. *National Heat, Lung, and Blood Institute. Guidelines for the Diagnosis and Managment of Asthma, Full Report (August 2007)*.

186. Myers, T. R., Guidelines for Asthma Management: A Review and Comparison of 5 Current Guidelines. *Respir Care* **2008,** *53* (6), 767-9.

187. Raundhal, M.; Morse, C.; Khare, A.; Oriss, T. B.; Milosevic, J.; Trudeau, J.; Huff, R.; Pilewski, J.; Holguin, F.; Kolls, J.; Wenzel, S.; Ray, P.; Ray, A., High Ifn-Gamma and Low Slpi Mark Severe Asthma in Mice and Humans. *J Clin Invest* **2015,** *125* (8), 3037-50.

188. Schumann, C.; Kropf, C.; Wibmer, T.; Rudiger, S.; Stoiber, K. M.; Thielen, A.; Rottbauer, W.; Kroegel, C., Omalizumab in Patients with Severe Asthma: The Xclusive Study. *Clin Respir J* **2012,** *6* (4), 215-27.

189. Cook, J. M.; Edwankar, R. V.; Edwankar, C. R.; Huang, S.; Jain, H. D.; Yang, J.; Rivas, F. M.; Zhou, H. Preparation of Benzodiazepines, in Particular 1,4-Benzodiazepines, as Anxiolytic and Anticonvulsant Agents with Reduced Sedative and Ataxic Effects. 2010.

190. Cook, J. M.; Huang, S.; Edwankar, R.; Namjoshi, O. A.; Wang, Z.-J.; Huang, Q.; He, X.; Li, X.; Yu, J.; Han, D. Synthesis of Gabaa Receptor Subunit Selective Benzodiazepine Derivatives for Pain Suppression. 2010.

191. Prevot, T. D.; Sumitomo, A.; Tomoda, T.; Knutson, D. E.; Li, G.; Cook, J. M.; Sibille, E., Chronic Administration of a Positive Allosteric Modulator at the A5-Gabaa Receptor Reverses Age-Related Dendritic Shrinkage. **2020,** *Manuscript in Progress*.

192. *Nations U. World Population Report*; 2015.

193. *Nation U. World Population Prospects: The 2019 Revision*; 2019.

194. *Nations U. Global Issues: Ageing*; 2019.

195. Harada, C. N.; Natelson Love, M. C.; Triebel, K. L., Normal Cognitive Aging. *Clin Geriatr Med* **2013,** *29* (4), 737-52.

196. Moscoso Del Prado Martin, F., Vocabulary, Grammar, Sex, and Aging. *Cogn Sci* **2017,** *41* (4), 950-975.

197. Teubner-Rhodes, S.; Vaden, K. I., Jr.; Cute, S. L.; Yeatman, J. D.; Dougherty, R. F.; Eckert, M. A., Aging-Resilient Associations between the Arcuate Fasciculus and Vocabulary Knowledge: Microstructure or Morphology? *J Neurosci* **2016,** *36* (27), 7210-22.

198. Zahr, N. M.; Rohlfing, T.; Pfefferbaum, A.; Sullivan, E. V., Problem Solving, Working Memory, and Motor Correlates of Association and Commissural Fiber Bundles in Normal Aging: A Quantitative Fiber Tracking Study. *Neuroimage* **2009,** *44* (3), 1050-62.

199. Nyberg, L.; Lovden, M.; Riklund, K.; Lindenberger, U.; Backman, L., Memory Aging and Brain Maintenance. *Trends Cogn Sci* **2012,** *16* (5), 292-305.

200. Salthouse, T. A., Memory Aging from 18 to 80. *Alzheimer Dis Assoc Disord* **2003,** *17* (3), 162-7.

201. Salthouse, T. A., Aging and Measures of Processing Speed. *Biological Psychology* **2000,** *54* (1-3), 35-54.

202. Shanmugaratnam, S.; Kass, S. J.; Arruda, J. E., Age Differences in Cognitive and Psychomotor Abilities and Simulated Driving. *Accid Anal Prev* **2010,** *42* (3), 802-8.

203. Souchay, C.; Isingrini, M.; Espagnet, L., Aging, Episodic Memory Feeling-of-Knowing, and Frontal Functioning. *Neuropsychology* **2000,** *14* (2), 299-309.

204. Salthouse, T. A., The Aging of Working Memory. *Neuropsychology* **1994,** *8* (4), 535-543.

205. Hof, P. R.; Morrison, J. H., The Aging Brain: Morphomolecular Senescence of Cortical Circuits. *Trends Neurosci* **2004,** *27* (10), 607-13.

206. Terribilli, D.; Schaufelberger, M. S.; Duran, F. L.; Zanetti, M. V.; Curiati, P. K.; Menezes, P. R.; Scazufca, M.; Amaro, E., Jr.; Leite, C. C.; Busatto, G. F., Age-Related Gray Matter Volume Changes in the Brain During Non-Elderly Adulthood. *Neurobiol Aging* **2011,** *32* (2), 354-68.

207. Apostolova, L. G.; Green, A. E.; Babakchanian, S.; Hwang, K. S.; Chou, Y. Y.; Toga, A. W.; Thompson, P. M., Hippocampal Atrophy and Ventricular Enlargement in Normal Aging, Mild Cognitive Impairment (Mci), and Alzheimer Disease. *Alzheimer Dis Assoc Disord* **2012,** *26* (1), 17-27.

208. Terry, R. D.; DeTeresa, R.; Hansen, L. A., Neocortical Cell Counts in Normal Human Adult Aging. *Ann Neurol* **1987,** *21* (6), 530-9.

209. Cykowski, M. D.; Powell, S. Z.; Schulz, P. E.; Takei, H.; Rivera, A. L.; Jackson, R. E.; Roman, G.; Jicha, G. A.; Nelson, P. T., Hippocampal Sclerosis in Older Patients: Practical Examples and Guidance with a Focus on Cerebral Age-Related Tdp-43 with Sclerosis. *Arch Pathol Lab Med* **2017,** *141* (8), 1113-1126.

210. Luebke, J. I.; Medalla, M.; Amatrudo, J. M.; Weaver, C. M.; Crimins, J. L.; Hunt, B.; Hof, P. R.; Peters, A., Age-Related Changes to Layer 3 Pyramidal Cells in the Rhesus Monkey Visual Cortex. *Cereb Cortex* **2015,** *25* (6), 1454-68.

211. de Brabander, J. M.; Kramers, R. J.; Uylings, H. B., Layer-Specific Dendritic Regression of Pyramidal Cells with Ageing in the Human Prefrontal Cortex. *Eur J Neurosci* **1998,** *10* (4), 1261-9.

212. Shukla, R.; Prevot, T. D.; French, L.; Isserlin, R.; Rocco, B. R.; Banasr, M.; Bader, G. D.; Sibille, E., The Relative Contributions of Cell-Dependent Cortical Microcircuit Aging to Cognition and Anxiety. *Biol Psychiatry* **2019,** *85* (3), 257-267.

213. Jacobs, B.; Driscoll, L.; Schall, M., Life-Span Dendritic and Spine Changes in Areas 10 and 18 of Human Cortex: A Quantitative Golgi Study. *The Journal of Comparative Neurology* **1997,** *386* (4), 661-680.

214. Wallace, M.; Frankfurt, M.; Arellanos, A.; Inagaki, T.; Luine, V., Impaired Recognition Memory and Decreased Prefrontal Cortex Spine Density in Aged Female Rats. *Ann N Y Acad Sci* **2007,** *1097*, 54-7.

215. Dickstein, D. L.; Weaver, C. M.; Luebke, J. I.; Hof, P. R., Dendritic Spine Changes Associated with Normal Aging. *Neuroscience* **2013,** *251*, 21-32.

216. Ownby, R. L., Neuroinflammation and Cognitive Aging. *Curr Psychiatry Rep* **2010,** *12* (1), 39-45.

217. Nishimura, I.; Uetsuki, T.; Dani, S. U.; Ohsawa, Y.; Saito, I.; Okamura, H.; Uchiyama, Y.; Yoshikawa, K., Degenerationin Vivoof Rat Hippocampal Neurons by Wild-Type Alzheimer Amyloid Precursor Protein Overexpressed by Adenovirus-Mediated Gene Transfer. *The Journal of Neuroscience* **1998,** *18* (7), 2387-2398.

218. Ten Kate, M.; Barkhof, F.; Visser, P. J.; Teunissen, C. E.; Scheltens, P.; van der Flier, W. M.; Tijms, B. M., Amyloid-Independent Atrophy Patterns Predict Time to Progression to Dementia in Mild Cognitive Impairment. *Alzheimers Res Ther* **2017,** *9* (1), 73.

219. Rodrigue, K. M.; Kennedy, K. M.; Devous, M. D., Sr.; Rieck, J. R.; Hebrank, A. C.; Diaz-Arrastia, R.; Mathews, D.; Park, D. C., Beta-Amyloid Burden in Healthy Aging: Regional Distribution and Cognitive Consequences. *Neurology* **2012,** *78* (6), 387-95.

220. Rodrigue, K. M.; Kennedy, K. M.; Park, D. C., Beta-Amyloid Deposition and the Aging Brain. *Neuropsychol Rev* **2009,** *19* (4), 436-50.

221. Deng, X.; Li, M.; Ai, W.; He, L.; Lu, D.; Patrylo, P. R.; Cai, H.; Luo, X.; Li, Z.; Yan, X., Lipolysaccharide-Induced Neuroinflammation Is Associated with Alzheimer-Like Amyloidogenic Axonal Pathology and Dendritic Degeneration in Rats. *Adv Alzheimer Dis* **2014,** *3* (2), 78-93.

222. Fuhrmann, M.; Mitteregger, G.; Kretzschmar, H.; Herms, J., Dendritic Pathology in Prion Disease Starts at the Synaptic Spine. *J Neurosci* **2007,** *27* (23), 6224-33.

223. Heneka, M. T.; Carson, M. J.; Khoury, J. E.; Landreth, G. E.; Brosseron, F.; Feinstein, D. L.; Jacobs, A. H.; Wyss-Coray, T.; Vitorica, J.; Ransohoff, R. M.; Herrup, K.; Frautschy, S. A.; Finsen, B.; Brown, G. C.; Verkhratsky, A.; Yamanaka, K.; Koistinaho, J.; Latz, E.; Halle, A.; Petzold, G. C.; Town, T.; Morgan, D.; Shinohara, M. L.; Perry, V. H.; Holmes, C.; Bazan, N. G.; Brooks, D. J.; Hunot, S.; Joseph, B.; Deigendesch, N.; Garaschuk, O.; Boddeke,

E.; Dinarello, C. A.; Breitner, J. C.; Cole, G. M.; Golenbock, D. T.; Kummer, M. P., Neuroinflammation in Alzheimer's Disease. *The Lancet Neurology* **2015,** *14* (4), 388-405.

224. Jack, C. R., Jr.; Lowe, V. J.; Senjem, M. L.; Weigand, S. D.; Kemp, B. J.; Shiung, M. M.; Knopman, D. S.; Boeve, B. F.; Klunk, W. E.; Mathis, C. A.; Petersen, R. C., 11c Pib and Structural Mri Provide Complementary Information in Imaging of Alzheimer's Disease and Amnestic Mild Cognitive Impairment. *Brain* **2008,** *131* (Pt 3), 665-80.

225. Pike, K. E.; Savage, G.; Villemagne, V. L.; Ng, S.; Moss, S. A.; Maruff, P.; Mathis, C. A.; Klunk, W. E.; Masters, C. L.; Rowe, C. C., Beta-Amyloid Imaging and Memory in Non-Demented Individuals: Evidence for Preclinical Alzheimer's Disease. *Brain* **2007,** *130* (Pt 11), 2837-44.

226. Panza, F.; Lozupone, M.; Logroscino, G.; Imbimbo, B. P., A Critical Appraisal of Amyloid-Beta-Targeting Therapies for Alzheimer Disease. *Nat Rev Neurol* **2019,** *15* (2), 73-88.

227. Doig, A. J.; Del Castillo-Frias, M. P.; Berthoumieu, O.; Tarus, B.; Nasica-Labouze, J.; Sterpone, F.; Nguyen, P. H.; Hooper, N. M.; Faller, P.; Derreumaux, P., Why Is Research on Amyloid-Beta Failing to Give New Drugs for Alzheimer's Disease? *ACS Chem Neurosci* **2017,** *8* (7), 1435-1437.

228. Wong, T. P.; Marchese, G.; Casu, M. A.; Ribeiro-da-Silva, A.; Cuello, A. C.; De Koninck, Y., Imbalance Towards Inhibition as a Substrate of Aging-Associated Cognitive Impairment. *Neurosci Lett* **2006,** *397* (1-2), 64-8.

229. Legon, W.; Punzell, S.; Dowlati, E.; Adams, S. E.; Stiles, A. B.; Moran, R. J., Altered Prefrontal Excitation/Inhibition Balance and Prefrontal Output: Markers of Aging in Human Memory Networks. *Cereb Cortex* **2016,** *26* (11), 4315-4326.

230. Hua, T.; Kao, C.; Sun, Q.; Li, X.; Zhou, Y., Decreased Proportion of Gaba Neurons Accompanies Age-Related Degradation of Neuronal Function in Cat Striate Cortex. *Brain Res Bull* **2008,** *75* (1), 119-25.

231. Sibille, E., Molecular Aging of the Brain, Neuroplasticity, and Vulnerability to Depression and Other Brain-Related Disorders. *Dialogues Clin Neurosci* **2013,** *15* (1), 53-65.

232. Stanley, E. M.; Fadel, J. R.; Mott, D. D., Interneuron Loss Reduces Dendritic Inhibition and Gaba Release in Hippocampus of Aged Rats. *Neurobiol Aging* **2012,** *33* (2), 431 e1-13.

233. Cuypers, K.; Maes, C.; Swinnen, S. P., Aging and Gaba. *Aging (Albany NY)* **2018,** *10* (6), 1186-1187.

234. Bormann, J., The 'Abc' of Gaba Receptors. *Trends in Pharmacological Sciences* **2000,** *21* (1), 16-19.

235. Mohler, H., Gaba(a) Receptor Diversity and Pharmacology. *Cell Tissue Res* **2006,** *326* (2), 505-16.

236. Rozycka, A.; Liguz-Lecznar, M., The Space Where Aging Acts: Focus on the Gabaergic Synapse. *Aging Cell* **2017,** *16* (4), 634-643.

237. Caspary, D. M.; Hughes, L. F.; Ling, L. L., Age-Related Gabaa Receptor Changes in Rat Auditory Cortex. *Neurobiol Aging* **2013,** *34* (5), 1486-96.

238. Yu, Z. Y.; Wang, W.; Fritschy, J. M.; Witte, O. W.; Redecker, C., Changes in Neocortical and Hippocampal Gabaa Receptor Subunit Distribution During Brain Maturation and Aging. *Brain Res* **2006,** *1099* (1), 73-81.

239. Ruano, D.; Araujo, F.; Revilla, E.; Vela, J.; Bergis, O.; Vitorica, J., Gabaa and Alpha-Amino-3-Hydroxy-5-Methylsoxazole-4-Propionate Receptors Are Differentially Affected by Aging in the Rat Hippocampus. *J Biol Chem* **2000,** *275* (26), 19585-93.

240. Rissman, R. A.; De Blas, A. L.; Armstrong, D. M., Gaba(a) Receptors in Aging and Alzheimer's Disease. *J Neurochem* **2007,** *103* (4), 1285-92.

241. Luscher, B.; Fuchs, T.; Kilpatrick, C. L., Gabaa Receptor Trafficking-Mediated Plasticity of Inhibitory Synapses. *Neuron* **2011,** *70* (3), 385-409.

242. Rissman, R. A.; Mobley, W. C., Implications for Treatment: Gabaa Receptors in Aging, Down Syndrome and Alzheimer's Disease. *J Neurochem* **2011,** *117* (4), 613-22.

243. Hortnagl, H.; Tasan, R. O.; Wieselthaler, A.; Kirchmair, E.; Sieghart, W.; Sperk, G., Patterns of Mrna and Protein Expression for 12 Gabaa Receptor Subunits in the Mouse Brain. *Neuroscience* **2013,** *236*, 345-72.

244. Howell, O.; Atack, J. R.; Dewar, D.; McKernan, R. M.; Sur, C., Density and Pharmacology of A5 Subunit-Containing Gabaa Receptors Are Preserved in Hippocampus of Alzheimer's Disease Patients. *Neuroscience* **2000,** *98* (4), 669-675.

245. Rissman, R. A.; Mishizen-Eberz, A. J.; Carter, T. L.; Wolfe, B. B.; De Blas, A. L.; Miralles, C. P.; Ikonomovic, M. D.; Armstrong, D. M., Biochemical Analysis of Gabaa Receptor Subunits A1, A5, B1, B2 in the Hippocampus of Patients with Alzheimer's Disease Neuropathology. *Neuroscience* **2003,** *120* (3), 695-704.

246. Rissman, R. A.; Bennett, D. A.; Armstrong, D. M., Subregional Analysis of Gaba(a) Receptor Subunit Mrnas in the Hippocampus of Older Persons with and without Cognitive Impairment. *J Chem Neuroanat* **2004,** *28* (1-2), 17-25.

247. Brady, M. L.; Jacob, T. C., Synaptic Localization of Alpha5 Gaba (a) Receptors Via Gephyrin Interaction Regulates Dendritic Outgrowth and Spine Maturation. *Dev Neurobiol* **2015,** *75* (11), 1241-51.

248. Sigel, E.; Ernst, M., The Benzodiazepine Binding Sites of Gabaa Receptors. *Trends Pharmacol Sci* **2018,** *39* (7), 659-671.

249. Markota, M.; Rummans, T. A.; Bostwick, J. M.; Lapid, M. I., Benzodiazepine Use in Older Adults: Dangers, Management, and Alternative Therapies. *Mayo Clin Proc* **2016,** *91* (11), 1632-1639.

250. Prevot, T. D.; Li, G.; Vidojevic, A.; Misquitta, K. A.; Fee, C.; Santrac, A.; Knutson, D. E.; Stephen, M. R.; Kodali, R.; Zahn, N. M.; Arnold, L. A.; Scholze, P.; Fisher, J. L.; Markovic, B. D.; Banasr, M.; Cook, J. M.; Savic, M.; Sibille, E., Novel Benzodiazepine-Like Ligands with Various Anxiolytic, Antidepressant, or Pro-Cognitive Profiles. *Mol Neuropsychiatry* **2019,** *5* (2), 84-97.

251. Koh, M. T.; Rosenzweig-Lipson, S.; Gallagher, M., Selective Gaba(a) Alpha5 Positive Allosteric Modulators Improve Cognitive Function in Aged Rats with Memory Impairment. *Neuropharmacology* **2013,** *64*, 145-52.

252. Knutson, D. E.; Roni, M. S. R.; Mian, M. Y.; Cook, J. M.; Stafford, D. C.; Arnold, L. A., Improved Large Scale Synthesis of Clinical Asthma Candidate Midd0301. *Org. Process Res. Dev.* **2020**.

253. Roni, M. S. R.; Li, G.; Mikulsky, B. N.; Knutson, D. E.; Mian, M. Y.; Zahn, N. M.; Cook, J. M.; Stafford, D. C.; Arnold, L. A., The Effects of Ph on the Structure and Bioavailability of Imidazobenzodiazepine-3-Carboxylate Midd0301. *Mol Pharm* **2020**.

254. Prevot, Thomas D.; Li, G.; Vidojevic, A.; Misquitta, Keith A.; Fee, C.; Santrac, A.; Knutson, Daniel E.; Stephen, Michael R.; Kodali, R.; Zahn, Nicolas M.; Arnold, Leggy A.; Scholze, P.; Fisher, Janet L.; Marković, Bojan D.; Banasr, M.; Cook, James M.; Savic, M.;

Sibille, E., Novel Benzodiazepine-Like Ligands with Various Anxiolytic, Antidepressant, or Pro-Cognitive Profiles. *Molecular Neuropsychiatry* **2019,** *(accepted for publication)*, 1-14.

255. Magnusson, K. R.; Scruggs, B.; Zhao, X.; Hammersmark, R., Age-Related Declines in a Two-Day Reference Memory Task Are Associated with Changes in Nmda Receptor Subunits in Mice. *BMC Neurosci* **2007,** *8*, 43.

256. Beracochea, D.; Krazem, A.; Henkouss, N.; Haccard, G.; Roller, M.; Fromentin, E., Intake of Wild Blueberry Powder Improves Episodic-Like and Working Memory During Normal Aging in Mice. *Planta Med* **2016,** *82* (13), 1163-8.

257. Vandesquille, M.; Krazem, A.; Louis, C.; Lestage, P.; Beracochea, D., S 18986 Reverses Spatial Working Memory Impairments in Aged Mice: Comparison with Memantine. *Psychopharmacology (Berl)* **2011,** *215* (4), 709-20.

258. Van Dam, D.; Abramowski, D.; Staufenbiel, M.; De Deyn, P. P., Symptomatic Effect of Donepezil, Rivastigmine, Galantamine and Memantine on Cognitive Deficits in the App23 Model. *Psychopharmacology (Berl)* **2005,** *180* (1), 177-90.

259. Ma, C. L.; Ma, X. T.; Wang, J. J.; Liu, H.; Chen, Y. F.; Yang, Y., Physical Exercise Induces Hippocampal Neurogenesis and Prevents Cognitive Decline. *Behav Brain Res* **2017,** *317*, 332-339.

260. Garner, J. P., The Significance of Meaning: Why Do over 90% of Behavioral Neuroscience Results Fail to Translate to Humans, and What Can We Do to Fix It? *ILAR J* **2014,** *55* (3), 438-56.

261. Al Dahhan, N. Z.; De Felice, F. G.; Munoz, D. P., Potentials and Pitfalls of Cross-Translational Models of Cognitive Impairment. *Front Behav Neurosci* **2019,** *13*, 48.

262. Curto, Y.; Garcia-Mompo, C.; Bueno-Fernandez, C.; Nacher, J., Chronic Benzodiazepine Treatment Decreases Spine Density in Cortical Pyramidal Neurons. *Neurosci Lett* **2016,** *613*, 41-6.

263. Castren, E., Neurotrophic Effects of Antidepressant Drugs. *Curr Opin Pharmacol* **2004,** *4* (1), 58-64.

264. Duman, C. H.; Duman, R. S., Spine Synapse Remodeling in the Pathophysiology and Treatment of Depression. *Neurosci Lett* **2015,** *601*, 20-9.

265. Gerhard, D. M.; Pothula, S.; Liu, R. J.; Wu, M.; Li, X. Y.; Girgenti, M. J.; Taylor, S. R.; Duman, C. H.; Delpire, E.; Picciotto, M.; Wohleb, E. S.; Duman, R. S., Gaba Interneurons Are the Cellular Trigger for Ketamine's Rapid Antidepressant Actions. *J Clin Invest* **2020,** *130* (3), 1336-1349.

266. Ghosal, S.; Duman, C. H.; Liu, R. J.; Wu, M.; Terwilliger, R.; Girgenti, M. J.; Wohleb, E.; Fogaca, M. V.; Teichman, E. M.; Hare, B.; Duman, R. S., Ketamine Rapidly Reverses Stress-Induced Impairments in Gabaergic Transmission in the Prefrontal Cortex in Male Rodents. *Neurobiol Dis* **2020,** *134*, 104669.

267. Weaver, L. H.; Kwon, K.; Beckett, D.; Matthews, B. W., Corepressor-Induced Organization and Assembly of the Biotin Repressor: A Model for Allosteric Activation of a Transcriptional Regulator. *Proc Natl Acad Sci U S A* **2001,** *98* (11), 6045-50.

268. Alhambra, C.; Becker, C.; Blake, T.; Chang, A. H.; Damewood, J. R., Jr.; Daniels, T.; Dembofsky, B. T.; Gurley, D. A.; Hall, J. E.; Herzog, K. J.; Horchler, C. L.; Ohnmacht, C. J.; Schmiesing, R. J.; Dudley, A.; Ribadeneira, M. D.; Knappenberger, K. S.; Maciag, C.; Stein, M. M.; Chopra, M.; Liu, X. F.; Christian, E. P.; Arriza, J. L.; Chapdelaine, M. J., Development

and Sar of Functionally Selective Allosteric Modulators of Gabaa Receptors. *Bioorg. Med. Chem.* **2011,** *19* (9), 2927-38.

269. Namjoshi, O. A.; Wang, Z. J.; Rallapalli, S. K.; Johnson, E. M., Jr.; Johnson, Y. T.; Ng, H.; Ramerstorfer, J.; Varagic, Z.; Sieghart, W.; Majumder, S.; Roth, B. L.; Rowlett, J. K.; Cook, J. M., Search for Alpha3beta(2)/(3)Gamma2 Subtype Selective Ligands That Are Stable on Human Liver Microsomes. *Bioorg. Med. Chem.* **2013,** *21* (1), 93-101.

270. Porsolt, R. D.; Le Pichon, M.; Jalfre, M., Depression: A New Animal Model Sensitive to Antidepressant Treatments. *Nature* **1977,** *266* (5604), 730-2.

271. Porsolt, R. D., Animal Model of Depression. *Biomedicine / [publiee pour l'A.A.I.C.I.G.]* **1979,** *30* (3), 139-40.

272. Wu, H.; Wheeler, A.; Zare, R. N., Chemical Cytometry on a Picoliter-Scale Integrated Microfluidic Chip. *Proc Natl Acad Sci U S A* **2004,** *101* (35), 12809-13.

273. Zhao, C.; Deng, W.; Gage, F. H., Mechanisms and Functional Implications of Adult Neurogenesis. *Cell* **2008,** *132* (4), 645-60.

274. David, D. J.; Wang, J.; Samuels, B. A.; Rainer, Q.; David, I.; Gardier, A. M.; Hen, R., Implications of the Functional Integration of Adult-Born Hippocampal Neurons in Anxiety-Depression Disorders. *Neuroscientist* **2010,** *16* (5), 578-91.

275. Fryer, R. I.; Walser, A. Diazepine Derivatives. 1976.

276. Walser, A.; Flynn, T.; Fryer, R. I., Quinazolines and 1,4-Benzodiazepines. Lxxxv. Syntheses of 3-Substituted Imidazo[1,5-a][1,4]Benzodiazepines. *J. Heterocycl. Chem.* **1978,** *15* (4), 577-83.

277. Walser, A.; Fryer, R. I.; Sternbach, L. H.; Archer, M. C., Quinazolines and 1,4-Benzodiazepines. Lxv† Some Transformations of Chlordiazepoxide. *J. Heterocycl. Chem.* **1974,** *11* (4), 619-21.

278. Ning, R. Y.; Fryer, R. I.; Madan, P. B.; Sluboski, B. C., Quinazolines and 1,4-Benzodiazepines. 74. Phosphorylation of Ambident Anions. Preparation of Some Di-4-Morpholinylphosphinyloxy Imines Via -Phosphorylation of Anions of Lactams. *J. Org. Chem.* **1976,** *41* (16), 2720-24.

279. Buehler, E.; Brown, G. B., A General Synthesis of N-Hydroxyamino Acids. *J. Org. Chem.* **1967,** *32* (2), 265-67.

280. Walser, A.; Lauer, R. F.; Fryer, R. I., Quinazolines and 1,4-Benzodiazepines. Lxxxvii. Synthesis of 1- and 3-Phenylimidazo [1,5-a] [1,4] Benzodiazepines. *J. Heterocycl. Chem.* **1978,** *15* (5), 855-58.

281. Walser, A.; Flynn, T.; Mason, C.; Fryer, R. I., Quinazolines and 1,4-Benzodiazepines. Xcv. Synthesis of 1,4-Benzodiazepines by Ring Expansion of 2-Chloromethylquinazolines with Carbanions. *J. Heterocycl. Chem.* **1986,** *23* (5), 1303-14.

282. Walser, A. Synthesis of Imidazo[1,5-a]Diazepine-3-Carboxylates Us 4118386. 1978.

283. Watjen, F.; Baker, R.; Engelstoff, M.; Herbert, R.; MacLeod, A.; Knight, A.; Merchant, K.; Moseley, J.; Saunders, J.; Swain, C. J.; et al., Novel Benzodiazepine Receptor Partial Agonists: Oxadiazolylimidazobenzodiazepines. *J. Med. Chem.* **1989,** *32* (10), 2282-91.

284. Fryer, R. I.; Gu, Z. Q.; Wang, C. G., Synthesis of Novel, Substituted 4h-Imidazo[1,5-a][1,4]Benzodiazepines. *J. Heterocycl. Chem.* **1991,** *28* (7), 1661-1669.

285. Fryer, R. I.; Kudzma, L. V.; Gu, Z. Q.; Lin, K. Y.; Rafalko, P. W., Addition of Glycinate Enolate Equivalents to 1,4-Benzodiazepine Imino Phosphates - Preparation of Synthetically

Useful 2-(Ethyl Glycinat-Alpha-Ylidene)-1,4-Benzodiazepines and Related Derivatives. *J. Org. Chem.* **1991,** *56* (11), 3715-3719.

286. Cook, J. M.; Zhou, H.; Huang, S.; Sarma, P. V.; Zhang, C. Stereospecific Anxiolytic and Anticonvulsant Agents with Reduced Muscle Relaxant, Sedative-Hypnotic and Ataxic Effects, Us 7618958 2006.

287. Yang, J.; Teng, Y.; Ara, S.; Rallapalli, S.; Cook, J. M., An Improved Process for the Synthesis of 4h-Imidazo[1,5-a][1,4]Benzodiazepines. *Synthesis-Stuttgart* **2009,** (6), 1036-1040.

288. Taghizadeh, M. J.; Malakpouri, G. R.; Javidan, A., Improved and Scalable Methods for the Synthesis of Midazolam Drug and Its Analogues Using Isocyanide Reagents. *Journal of the Iranian Chemical Society* **2019,** *16* (4), 785-794.

289. Anzini, M.; Valenti, S.; Braile, C.; Cappelli, A.; Vomero, S.; Acaro, S.; Ortuso, F.; Marinelli, L.; Limongelli, V.; Novellino, E.; Betti, L.; Giannaccini, G.; Lucacchini, A.; Daniele, S.; Martini, C.; Ghelardini, C.; Mannelli, L. D.; Giorgi, G.; Mascia, M. P.; Biggio, G., New Insight into the Central Benzodiazepine Receptor-Ligand Interactions: Design, Synthesis, Biological Evaluation, and Molecular Modeling of 3-Substituted 6-Phenyl-4h-Imidazo[1,5-a][1,4]Benzodiazepines and Related Compounds. *J. Med. Chem.* **2011,** *54* (16), 5694-5711.

290. Valeur, E.; Bradley, M., Amide Bond Formation: Beyond the Myth of Coupling Reagents. *Chem. Soc. Rev.* **2009,** *38* (2), 606-31.

291. Montalbetti, C. A. G. N.; Falque, V., Amide Bond Formation and Peptide Coupling. *Tetrahedron* **2005,** *61* (46), 10827-10852.

292. Neises, B.; Steglich, W., Einfaches Verfahren Zur Veresterung Von Carbonsäuren. *Angew. Chem.* **1978,** *90* (7), 556-557.

293. Meienhofer, J., The Mixed Carbonic Anhydride Method of Peptide Synthesis. *Peptides* **1979,** *1*, 263-314.

294. Anderson, G. W.; Zimmerman, J. E.; Callahan, F. M., A Reinvestigation of the Mixed Carbonic Anhydride Method of Peptide Synthesis. *J. Am. Chem. Soc.* **1967,** *89* (19), 5012-7.

295. Reddy, D. R.; Ballante, F.; Zhou, N. J.; Marshall, G. R., Design and Synthesis of Benzodiazepine Analogs as Isoform-Selective Human Lysine Deacetylase Inhibitors. *Eur. J. Med. Chem.* **2017,** *127*, 531-553.

296. Carpino, L. A.; Cohen, B. J.; Stephens, K. E.; Sadat-Aalaee, S. Y.; Tien, J. H.; Langridge, D. C., (Fluoren-9-Ylmethoxy)Carbonyl (Fmoc) Amino Acid Chlorides. Synthesis, Characterization, and Application to the Rapid Synthesis of Short Peptide Segments. *J. Org. Chem.* **1986,** *51* (19), 3732-3734.

297. Prabhu, G.; Basavaprabhu; Narendra, N.; Vishwanatha, T. M.; Sureshbabu, V. V., Amino Acid Chlorides: A Journey from Instability and Racemization Toward broader Utility in Organic Synthesis Including Peptides and Their Mimetics. *Tetrahedron* **2015,** *71* (19), 2785-2832.

298. Fier, P. S.; Whittaker, A. M., An Atom-Economical Method to Prepare Enantiopure Benzodiazepines with N-Carboxyanhydrides. *Org. Lett.* **2017,** *19* (6), 1454-1457.

299. Bailey, J. L., 679. The Synthesis of Simple Peptides from Anhydro-N-Carboxyamino-Acids. *Journal of the Chemical Society (Resumed)* **1950**, 3461.

300. Brenner, M.; Photaki, I., Zur Herstellung Der Chlorid-Hydrochloride Der ?-AminosUren. *Helv. Chim. Acta* **1956,** *39* (6), 1525-1528.

301. Daly, W. H.; Poché, D., The Preparation of N-Carboxyanhydrides of A-Amino Acids Using Bis(Trichloromethyl)Carbonate. *Tetrahedron Lett.* **1988,** *29* (46), 5859-5862.

302. Van Dijk-Wolthuis, W. N. E.; van de Water, L.; van de Wetering, P.; Van Steenbergen, M. J.; Kettenes-van den Bosch, J. J.; Schuyl, W. J. W.; Hennink, W. E., Synthesis and Characterization of Poly-L-Lysine with Controlled Low Molecular Weight. *Macromol. Chem. Phys.* **1997,** *198* (12), 3893-3906.

303. Wilder, R.; Mobashery, S., The Use of Triphosgene in Preparation of N-Carboxy .Alpha.-Amino Acid Anhydrides. *J. Org. Chem.* **1992,** *57* (9), 2755-2756.

304. Li, G.; Stephen, M. R.; Kodali, R.; Zahn, N. M.; Poe, M. M.; Tiruveedhula, V. V. N. P. B.; Huber, A. T.; Schussman, M. K.; Qualmann, K.; Panhans, C. M.; Raddatz, N. J.; Baker, D. A.; Prevot, T. D.; Banasr, M.; Sibille, E.; Arnold, L. A.; Cook, J. M., Synthesis of Chiral Gabaa Receptor Subtype Selective Ligands as Potential Agents to Treat Schizophrenia as Well as Depression. *Arkivoc* **2018,** *2018* (4), 158-182.

305. Knutson, D. E.; Kodali, R.; Stephen, M. R.; Zahn, N. M.; Arnold, L. A.; Cook, J. M.; Dobricic, V.; Savic, M. M.; Mihovilovic, M. D.; Treven, M.; Ernst, M.; Sieghart, W., Novel Deuterated Gabaar-A6 Subtype Selective Ligands with Improved Metabolic Stability and Enhanced Bioavailability Targeting Trigeminal Orofacial Pain, Neuropsychiatric Disorders, and Depression. In *254th ACS National Meeting*, Washington, DC, 2017; pp MEDI-364.

306. Knutson, D. E.; Kodali, R.; Stephen, M. R.; Zahn, N. M.; Arnold, L. A.; Cook, J. M.; Dobricic, V.; Savic, M. M.; Mihovilovic, M. D.; Treven, M.; Ernst, M.; Sieghart, W. In *Novel Deuterated Gabaar-A6 Subtype Selective Ligands with Improved Metabolic Stability and Enhanced Bioavailability Targeting Trigeminal Orofacial Pain, Neuropsychiatric Disorders, and Depression*, 254th ACS National Meeting, Washington, DC, August 20-24, 2017; Washington, DC, 2017; pp MEDI-364.

307. Knutson, D. E.; Kodali, R.; Stephen, M. R.; Verma, R. S.; Witzigmann, C.; Meirelles, M. A.; Zahn, N. M.; Huber, A. T.; Arnold, L.; Savic, M. M.; Ernst, M.; Sieghart, W.; Cook, J. M. In *Design and Synthesis of Novel Deuterated Gabaar-A6 Subtype Selective Ligands with Improved Metabolic Stability and Enhanced Bioavailability*, 255th ACS National Meeting, New Orleans, LA, March 18-22, 2018; New Orleans, LA, 2018; pp MEDI-113.

308. Knutson, D. E.; Vasovic, D.; Divovic, B.; Treven, M.; Steudle, F.; Scholze, P.; Brkovic, B.; Sieghart, W.; Ernst, M.; Cook, J. M.; Savic, M. M., Prevention of Trigeminal Neuropathic Pain Development in Rats Using Novel Deuterated Gabaar-A6 Subtype Selective Ligands. In *256th ACS National Meeting*, Boston, MA, 2018; pp MEDI-95.

309. Knutson, D. E.; Li, G.; Prevot, T.; Arnold, L.; Chiou, L.-C.; Ernst, M.; Mihovilovic, M.; Savic, M.; Sieghart, W.; Sibille, E.; Cook, J. M. In *Combatting the Opioid and Benzodiazepine Epidemic by the Synthesis of Novel Safer Drugs Designed to Be Functionally Selective for A5- or A6-Containing Gabaa Receptors*, 258th ACS National Meeting & Exposition, San Diego, CA, American Chemical Society: San Diego, CA, 2019; pp MEDI-0157.

Appendix

4.1. X-ray Crystal Data for Selected Pyrazoloquinolinones (PQ's)

4.1.1. X-ray Crystal Data for DK-I-56-1 (8b)

Table 24: Crystal data and structure refinement for **DK-I-56-1 (8b)**.

Identification code	**cook190**	
Empirical formula	C_{18} H_{15} N_3 O3, 0.5 (H_2O)	
Formula weight	330.34	
Temperature	296(2) K	
Wavelength	1.54178 Å	
Crystal system	Triclinic	
Space group	P -1	
Unit cell dimensions	a = 8.3110(5) Å	α= 92.378(3)°.
	b = 14.1658(8) Å	β= 101.817(4)°.
	c = 14.2281(7) Å	γ = 102.562(3)°.
Volume	1593.86(16) $Å^3$	
Z	4	
Density (20ºC)	1.377 Mg/m^3	
Absorption coefficient	0.806 mm^{-1}	
F(000)	692	
Crystal size	0.123 x 0.086 x 0.020 mm^3	
Theta range for data collection	3.186 to 68.591°.	
Index ranges	-8<=h<=9, -17<=k<=16, -17<=l<=14	
Reflections collected	9055	
Independent reflections	4756 [R_{int}] = 0.0652]	
Completeness to theta = 67.679°	82.0 %	
Absorption correction	Semi-empirical from equivalents	
Max. and min. transmission	0.7530 and 0.5357	
Refinement method	Full-matrix least-squares on F^2	
Data / restraints / parameters	4756 / 44 / 488	
Goodness-of-fit on F^2	1.202	
Final R indices [I>2sigma(I)]	R_1 = 0.0956, wR_2 = 0.2029	
R indices (all data)	R_1 = 0.1484, wR_2 = 0.2167	
Largest diff. peak and hole	0.228 and -0.229 e.$Å^{-3}$	

Table 25: Atomic coordinates (x 10^4) and equivalent isotropic displacement parameters ($Å^2$x 10^3) for **DK-I-56-1 (8b)**. U(eq) is defined as one third of the trace of the orthogonalized U^{ij} tensor.

	x	y	z	U(eq)
C(1)	2160(10)	1303(5)	727(6)	101(3)
O(2)	3369(6)	1978(3)	1429(4)	83(2)
C(3)	4381(8)	2728(4)	1115(5)	58(2)
C(4)	5636(8)	3326(5)	1827(4)	60(2)
C(5)	6740(8)	4084(4)	1600(4)	52(2)
C(6)	6659(7)	4288(4)	627(3)	41(1)
C(7)	7775(7)	5064(4)	314(3)	38(1)
N(8)	9020(6)	5743(3)	832(3)	42(1)
N(9)	9700(6)	6326(3)	153(3)	42(1)
C(10)	8840(7)	6014(4)	-790(3)	44(2)
O(11)	9177(5)	6404(3)	-1522(2)	58(1)
C(12)	7580(7)	5185(4)	-697(3)	38(1)
C(13)	6294(8)	4576(4)	-1337(4)	46(2)
N(14)	5254(6)	3859(3)	-1048(3)	47(1)
C(15)	5384(7)	3685(4)	-75(4)	43(1)
C(16)	4241(8)	2908(4)	157(4)	52(2)
C(17)	11017(7)	7161(4)	507(4)	44(1)
C(18)	11514(9)	7435(4)	1479(4)	63(2)
C(19)	12742(9)	8276(5)	1826(5)	73(2)
C(20)	13493(9)	8846(5)	1208(5)	64(2)
O(21)	14677(6)	9704(3)	1485(4)	87(2)
C(22)	14855(11)	10125(5)	2432(5)	104(3)
C(23)	13052(8)	8549(4)	237(5)	62(2)
C(24)	11842(8)	7715(4)	-113(4)	55(2)
C(25)	5838(10)	8362(5)	5746(5)	92(2)
O(26)	5664(6)	7762(3)	4888(3)	76(1)
C(27)	6235(8)	6930(4)	4973(4)	54(2)
C(28)	6058(8)	6392(4)	4091(4)	59(2)
C(29)	6583(8)	5552(4)	4076(4)	54(2)
C(30)	7318(7)	5196(4)	4925(3)	44(1)
C(31)	7889(7)	4321(4)	4971(3)	43(1)
N(32)	7862(6)	3686(3)	4263(3)	49(1)
N(33)	8537(6)	2957(3)	4726(3)	48(1)
C(34)	9020(8)	3131(4)	5721(4)	49(2)
O(35)	9660(6)	2596(3)	6274(3)	64(1)
C(36)	8596(7)	4044(4)	5892(3)	46(2)
C(37)	8751(8)	4627(4)	6717(4)	53(2)
N(38)	8220(6)	5441(3)	6667(3)	51(1)
C(39)	7478(7)	5753(4)	5801(3)	45(1)
C(40)	6947(7)	6613(4)	5822(4)	51(2)
C(42)	8992(8)	2316(4)	3218(4)	53(2)

Table 25: (continued).

	x	y	z	U(eq)
C(41)	8771(7)	2183(4)	4147(4)	48(2)
C(43)	9246(9)	1580(5)	2659(4)	70(2)
C(44)	9291(9)	693(5)	3001(4)	69(2)
C(47)	9037(9)	547(5)	3918(4)	74(2)
C(48)	8781(8)	1291(4)	4493(4)	64(2)
O(45A)	9653(14)	66(4)	2346(5)	88(3)
C(46A)	9204(17)	-909(6)	2516(8)	112(5)
O(45B)	9150(60)	-239(11)	2635(18)	115(13)
C(46B)	9130(60)	-320(20)	1637(18)	121(16)
O(49A)	12208(7)	3260(5)	7791(3)	67(2)
O(49B)	12690(30)	2471(18)	7657(15)	80(10)

Table 26: Bond lengths [Å] and angles [°] for **DK-I-56-1 (8b)**.

C(1)-O(2)	1.419(8)	C(1)-H(1A)	0.9600
C(1)-H(1B)	0.9600	C(1)-H(1C)	0.9600
O(2)-C(3)	1.357(7)	C(3)-C(16)	1.383(8)
C(3)-C(4)	1.394(8)	C(4)-C(5)	1.349(8)
C(4)-H(4)	0.9300	C(5)-C(6)	1.417(7)
C(5)-H(5)	0.9300	C(6)-C(15)	1.397(7)
C(6)-C(7)	1.426(7)	C(7)-N(8)	1.317(6)
C(7)-C(12)	1.435(7)	N(8)-N(9)	1.422(6)
N(9)-C(10)	1.388(6)	N(9)-C(17)	1.418(6)
C(10)-O(11)	1.251(6)	C(10)-C(12)	1.424(7)
C(12)-C(13)	1.360(7)	C(13)-N(14)	1.321(7)
C(13)-H(13)	0.9300	N(14)-C(15)	1.402(6)
N(14)-H(14)	0.8600	C(15)-C(16)	1.388(8)
C(16)-H(16)	0.9300	C(17)-C(18)	1.374(7)
C(17)-C(24)	1.390(8)	C(18)-C(19)	1.386(8)
C(18)-H(18)	0.9300	C(19)-C(20)	1.370(9)
C(19)-H(19)	0.9300	C(20)-O(21)	1.371(7)
C(20)-C(23)	1.378(9)	O(21)-C(22)	1.417(8)
C(22)-H(22A)	0.9600	C(22)-H(22B)	0.9600
C(22)-H(22C)	0.9600	C(23)-C(24)	1.373(8)
C(23)-H(23)	0.9300	C(24)-H(24)	0.9300
C(25)-O(26)	1.423(7)	C(25)-H(25A)	0.9600
C(25)-H(25B)	0.9600	C(25)-H(25C)	0.9600
O(26)-C(27)	1.363(7)	C(27)-C(40)	1.371(7)
C(27)-C(28)	1.406(8)	C(28)-C(29)	1.354(8)
C(28)-H(28)	0.9300	C(29)-C(30)	1.403(7)
C(29)-H(29)	0.9300	C(30)-C(39)	1.413(7)
C(30)-C(31)	1.420(7)	C(31)-N(32)	1.316(6)
C(31)-C(36)	1.430(7)	N(32)-N(33)	1.405(6)
N(33)-C(34)	1.386(6)	N(33)-C(41)	1.415(6)
C(34)-O(35)	1.238(6)	C(34)-C(36)	1.435(8)
C(36)-C(37)	1.375(7)	C(37)-N(38)	1.320(7)
C(37)-H(37)	0.9300	N(38)-C(39)	1.395(6)
N(38)-H(38)	0.8600	C(39)-C(40)	1.384(7)
C(40)-H(40)	0.9300	C(42)-C(43)	1.363(8)
C(42)-C(41)	1.387(7)	C(42)-H(42)	0.9300
C(41)-C(48)	1.375(7)	C(43)-C(44)	1.371(8)
C(43)-H(43)	0.9300	C(44)-O(45B)	1.371(10)
C(44)-C(47)	1.381(9)	C(44)-O(45A)	1.382(7)
C(47)-C(48)	1.387(8)	C(47)-H(47)	0.9300
C(48)-H(48)	0.9300	O(45A)-C(46A)	1.395(8)
C(46A)-H(46A)	0.9600	C(46A)-H(46B)	0.9600
C(46A)-H(46C)	0.9600	O(45B)-C(46B)	1.415(10)
C(46B)-H(46D)	0.9600	C(46B)-H(46E)	0.9600

Table 26: (continued).

C(46B)-H(46F)	0.9600	O(49A)-H(49A)	0.821(11)
O(49A)-H(49B)	0.821(10)	O(49B)-H(49C)	0.820(11)
O(49B)-H(49D)	0.821(11)		
O(2)-C(1)-H(1A)	109.5	O(2)-C(1)-H(1B)	109.5
H(1A)-C(1)-H(1B)	109.5	O(2)-C(1)-H(1C)	109.5
H(1A)-C(1)-H(1C)	109.5	H(1B)-C(1)-H(1C)	109.5
C(3)-O(2)-C(1)	117.9(6)	O(2)-C(3)-C(16)	124.1(6)
O(2)-C(3)-C(4)	115.7(6)	C(16)-C(3)-C(4)	120.2(6)
C(5)-C(4)-C(3)	121.1(6)	C(5)-C(4)-H(4)	119.5
C(3)-C(4)-H(4)	119.5	C(4)-C(5)-C(6)	120.7(5)
C(4)-C(5)-H(5)	119.7	C(6)-C(5)-H(5)	119.7
C(15)-C(6)-C(5)	117.3(5)	C(15)-C(6)-C(7)	117.8(5)
C(5)-C(6)-C(7)	124.9(5)	N(8)-C(7)-C(6)	129.1(4)
N(8)-C(7)-C(12)	111.3(5)	C(6)-C(7)-C(12)	119.5(5)
C(7)-N(8)-N(9)	105.3(4)	C(10)-N(9)-C(17)	129.1(5)
C(10)-N(9)-N(8)	112.4(4)	C(17)-N(9)-N(8)	118.3(4)
O(11)-C(10)-N(9)	125.2(5)	O(11)-C(10)-C(12)	130.9(4)
N(9)-C(10)-C(12)	103.9(5)	C(13)-C(12)-C(10)	133.6(5)
C(13)-C(12)-C(7)	119.2(5)	C(10)-C(12)-C(7)	107.1(4)
N(14)-C(13)-C(12)	121.3(5)	N(14)-C(13)-H(13)	119.4
C(12)-C(13)-H(13)	119.4	C(13)-N(14)-C(15)	122.7(5)
C(13)-N(14)-H(14)	118.6	C(15)-N(14)-H(14)	118.6
C(16)-C(15)-C(6)	122.1(5)	C(16)-C(15)-N(14)	118.5(5)
C(6)-C(15)-N(14)	119.4(5)	C(3)-C(16)-C(15)	118.6(5)
C(3)-C(16)-H(16)	120.7	C(15)-C(16)-H(16)	120.7
C(18)-C(17)-C(24)	118.4(5)	C(18)-C(17)-N(9)	120.2(5)
C(24)-C(17)-N(9)	121.3(5)	C(17)-C(18)-C(19)	120.5(6)
C(17)-C(18)-H(18)	119.7	C(19)-C(18)-H(18)	119.7
C(20)-C(19)-C(18)	120.8(6)	C(20)-C(19)-H(19)	119.6
C(18)-C(19)-H(19)	119.6	C(19)-C(20)-O(21)	124.7(6)
C(19)-C(20)-C(23)	118.8(6)	O(21)-C(20)-C(23)	116.6(7)
C(20)-O(21)-C(22)	116.7(6)	O(21)-C(22)-H(22A)	109.5
O(21)-C(22)-H(22B)	109.5	H(22A)-C(22)-H(22B)	109.5
O(21)-C(22)-H(22C)	109.5	H(22A)-C(22)-H(22C)	109.5
H(22B)-C(22)-H(22C)	109.5	C(24)-C(23)-C(20)	120.8(6)
C(24)-C(23)-H(23)	119.6	C(20)-C(23)-H(23)	119.6
C(23)-C(24)-C(17)	120.5(5)	C(23)-C(24)-H(24)	119.7
C(17)-C(24)-H(24)	119.7	O(26)-C(25)-H(25A)	109.5
O(26)-C(25)-H(25B)	109.5	H(25A)-C(25)-H(25B)	109.5
O(26)-C(25)-H(25C)	109.5	H(25A)-C(25)-H(25C)	109.5
H(25B)-C(25)-H(25C)	109.5	C(27)-O(26)-C(25)	117.7(5)
O(26)-C(27)-C(40)	125.4(5)	O(26)-C(27)-C(28)	114.2(5)

Table 26: (continued).

C(40)-C(27)-C(28)	120.4(5)	C(29)-C(28)-C(27)	120.0(6)
C(29)-C(28)-H(28)	120.0	C(27)-C(28)-H(28)	120.0
C(28)-C(29)-C(30)	121.8(5)	C(28)-C(29)-H(29)	119.1
C(30)-C(29)-H(29)	119.1	C(29)-C(30)-C(39)	116.9(5)
C(29)-C(30)-C(31)	125.2(4)	C(39)-C(30)-C(31)	118.0(5)
N(32)-C(31)-C(30)	129.0(5)	N(32)-C(31)-C(36)	112.1(5)
C(30)-C(31)-C(36)	118.9(4)	C(31)-N(32)-N(33)	104.3(4)
C(34)-N(33)-N(32)	114.3(4)	C(34)-N(33)-C(41)	127.4(5)
N(32)-N(33)-C(41)	118.2(4)	O(35)-C(34)-N(33)	125.5(5)
O(35)-C(34)-C(36)	132.0(5)	N(33)-C(34)-C(36)	102.6(5)
C(37)-C(36)-C(31)	120.3(5)	C(37)-C(36)-C(34)	132.9(5)
C(31)-C(36)-C(34)	106.8(4)	N(38)-C(37)-C(36)	120.3(5)
N(38)-C(37)-H(37)	119.9	C(36)-C(37)-H(37)	119.9
C(37)-N(38)-C(39)	123.1(4)	C(37)-N(38)-H(38)	118.5
C(39)-N(38)-H(38)	118.5	C(40)-C(39)-N(38)	118.9(4)
C(40)-C(39)-C(30)	121.7(5)	N(38)-C(39)-C(30)	119.4(5)
C(27)-C(40)-C(39)	119.2(5)	C(27)-C(40)-H(40)	120.4
C(39)-C(40)-H(40)	120.4	C(43)-C(42)-C(41)	120.6(6)
C(43)-C(42)-H(42)	119.7	C(41)-C(42)-H(42)	119.7
C(48)-C(41)-C(42)	119.0(5)	C(48)-C(41)-N(33)	120.9(5)
C(42)-C(41)-N(33)	120.1(5)	C(42)-C(43)-C(44)	120.9(6)
C(42)-C(43)-H(43)	119.5	C(44)-C(43)-H(43)	119.5
O(45B)-C(44)-C(43)	137.9(12)	O(45B)-C(44)-C(47)	101.3(12)
C(43)-C(44)-C(47)	118.9(5)	C(43)-C(44)-O(45A)	112.0(6)
C(47)-C(44)-O(45A)	129.1(7)	C(44)-C(47)-C(48)	120.6(6)
C(44)-C(47)-H(47)	119.7	C(48)-C(47)-H(47)	119.7
C(41)-C(48)-C(47)	119.9(6)	C(41)-C(48)-H(48)	120.0
C(47)-C(48)-H(48)	120.0	C(44)-O(45A)-C(46A)	113.8(7)
O(45A)-C(46A)-H(46A)	109.5	O(45A)-C(46A)-H(46B)	109.5
H(46A)-C(46A)-H(46B)	109.5	O(45A)-C(46A)-H(46C)	109.5
H(46A)-C(46A)-H(46C)	109.5	H(46B)-C(46A)-H(46C)	109.5
C(44)-O(45B)-C(46B)	113(2)	O(45B)-C(46B)-H(46D)	109.5
O(45B)-C(46B)-H(46E)	109.5	H(46D)-C(46B)-H(46E)	109.5
O(45B)-C(46B)-H(46F)	109.5	H(46D)-C(46B)-H(46F)	109.5
H(46E)-C(46B)-H(46F)	109.5	H(49A)-O(49A)-H(49B)	105(5)
H(49C)-O(49B)-H(49D)	104(6)		

Table 27: Anisotropic displacement parameters ($Å^2 x\ 10^3$) for **DK-I-56-1 (8b)**. The anisotropic displacement factor exponent takes the form: $-2\pi^2[h^2 a^{*2} U^{11} + ... + 2\ h\ k\ a^*\ b^*\ U^{12}]$

	U^{11}	U^{22}	U^{33}	U^{23}	U^{13}	U^{12}
C(1)	73(6)	69(5)	147(8)	32(5)	9(6)	-5(5)
O(2)	73(4)	63(3)	106(4)	27(3)	13(3)	-1(3)
C(3)	55(5)	41(4)	81(5)	18(3)	17(4)	11(3)
C(4)	62(5)	62(4)	55(3)	10(3)	9(4)	16(4)
C(5)	56(4)	53(4)	44(3)	2(3)	5(3)	11(3)
C(6)	41(4)	37(3)	43(3)	-3(3)	8(3)	12(3)
C(7)	43(4)	37(3)	34(3)	-7(2)	3(3)	15(3)
N(8)	46(3)	40(3)	39(2)	0(2)	7(2)	10(2)
N(9)	48(3)	40(3)	38(2)	-2(2)	10(2)	10(2)
C(10)	48(4)	50(4)	32(3)	-14(3)	5(3)	17(3)
O(11)	77(3)	59(3)	35(2)	-4(2)	14(2)	8(2)
C(12)	41(4)	36(3)	33(3)	-10(2)	5(3)	8(3)
C(13)	55(4)	47(3)	36(3)	-8(3)	9(3)	17(3)
N(14)	43(3)	44(3)	45(3)	-15(2)	1(2)	3(2)
C(15)	49(4)	40(3)	44(3)	-3(3)	7(3)	20(3)
C(16)	47(4)	39(3)	63(4)	-3(3)	1(3)	8(3)
C(17)	43(4)	40(3)	47(3)	-6(3)	9(3)	12(3)
C(18)	77(5)	55(4)	45(3)	-7(3)	7(3)	3(4)
C(19)	80(6)	71(5)	54(4)	-16(4)	4(4)	1(4)
C(20)	56(5)	49(4)	81(4)	-14(4)	12(4)	8(4)
O(21)	75(4)	62(3)	107(4)	-24(3)	16(3)	-12(3)
C(22)	107(7)	72(5)	102(6)	-36(4)	-10(5)	-3(5)
C(23)	59(5)	50(4)	78(4)	-1(3)	24(4)	8(3)
C(24)	60(4)	54(4)	52(3)	-6(3)	17(3)	11(3)
C(25)	108(7)	69(5)	97(5)	-19(4)	17(5)	30(5)
O(26)	96(4)	67(3)	71(3)	-5(2)	16(3)	33(3)
C(27)	53(4)	48(4)	62(4)	-1(3)	19(3)	10(3)
C(28)	72(5)	62(4)	44(3)	2(3)	13(3)	19(4)
C(29)	63(4)	61(4)	37(3)	-5(3)	13(3)	16(3)
C(30)	47(4)	45(3)	35(3)	-2(2)	9(3)	3(3)
C(31)	48(4)	42(3)	35(3)	0(2)	9(3)	4(3)
N(32)	60(3)	49(3)	36(2)	-1(2)	6(2)	15(3)
N(33)	62(4)	44(3)	35(2)	0(2)	1(2)	15(3)
C(34)	56(4)	49(4)	37(3)	1(3)	3(3)	5(3)
O(35)	87(4)	56(3)	43(2)	5(2)	-5(2)	21(2)
C(36)	49(4)	48(3)	35(3)	-3(3)	5(3)	4(3)
C(37)	61(5)	52(4)	38(3)	0(3)	6(3)	4(3)
N(38)	66(4)	53(3)	31(2)	-8(2)	9(2)	9(3)
C(39)	49(4)	43(3)	37(3)	0(3)	11(3)	1(3)
C(40)	56(4)	50(4)	45(3)	-6(3)	16(3)	6(3)
C(42)	65(5)	49(4)	44(3)	1(3)	9(3)	13(3)

Table 27: (continued).

	U^{11}	U^{22}	U^{33}	U^{23}	U^{13}	U^{12}
C(41)	55(4)	40(3)	43(3)	-2(3)	3(3)	9(3)
C(43)	96(6)	70(5)	48(3)	1(3)	15(4)	31(4)
C(44)	89(5)	65(4)	55(3)	-10(3)	4(3)	33(4)
C(47)	102(6)	58(4)	61(3)	1(3)	4(3)	32(4)
C(48)	88(5)	56(4)	45(3)	4(3)	5(3)	17(4)
O(45A)	145(8)	63(4)	74(5)	5(3)	44(5)	44(5)
C(46A)	180(13)	60(6)	116(9)	6(5)	59(9)	43(6)
O(45B)	210(40)	67(10)	79(12)	-10(8)	36(14)	49(13)
C(46B)	220(50)	80(20)	79(12)	-10(11)	37(15)	70(20)
O(49A)	54(4)	94(6)	45(3)	-27(3)	2(3)	11(3)
O(49B)	83(19)	78(19)	61(13)	-9(12)	-7(12)	2(14)

Table 28: Hydrogen coordinates (x 10^4) and isotropic displacement parameters (Å^{2}x 10^3) for **DK-I-56-1 (8b)**.

	x	y	z	U(eq)
H(1A)	1373	1629	364	152
H(1B)	1565	797	1042	152
H(1C)	2725	1024	300	152
H(4)	5713	3201	2469	72
H(5)	7563	4475	2087	63
H(13)	6145	4666	-1990	55
H(14)	4465	3484	-1474	56
H(16)	3400	2517	-321	63
H(18)	11022	7054	1908	75
H(19)	13061	8456	2486	88
H(22A)	15623	10752	2523	156
H(22B)	15288	9714	2891	156
H(22C)	13774	10197	2525	156
H(23)	13582	8917	-187	74
H(24)	11571	7519	-769	66
H(25A)	5418	8928	5587	137
H(25B)	7008	8555	6067	137
H(25C)	5204	8007	6164	137
H(28)	5581	6612	3517	71
H(29)	6452	5201	3488	64
H(37)	9231	4449	7312	63
H(38)	8337	5795	7193	61
H(40)	7071	6971	6406	61
H(42)	8967	2912	2973	64
H(43)	9391	1681	2037	84
H(47)	9039	-56	4153	88
H(48)	8616	1188	5111	77
H(46A)	9958	-1027	3083	168
H(46B)	9279	-1310	1973	168
H(46C)	8068	-1061	2609	168
H(46D)	10052	158	1509	181
H(46E)	8080	-207	1280	181
H(46F)	9229	-955	1446	181
H(49A)	11530(90)	3070(70)	7280(30)	101
H(49B)	11680(90)	3500(60)	8130(50)	101
H(49C)	12600(300)	1900(90)	7500(200)	120
H(49D)	11800(300)	2600(160)	7330(150)	120

Table 29: Torsion angles [°] for **DK-I-56-1 (8b)**.

C(1)-O(2)-C(3)-C(16)	4.0(9)	C(1)-O(2)-C(3)-C(4)	-175.0(6)
O(2)-C(3)-C(4)-C(5)	178.6(6)	C(16)-C(3)-C(4)-C(5)	-0.5(9)
C(3)-C(4)-C(5)-C(6)	-0.3(9)	C(4)-C(5)-C(6)-C(15)	0.9(8)
C(4)-C(5)-C(6)-C(7)	-179.4(5)	C(15)-C(6)-C(7)-N(8)	177.3(5)
C(5)-C(6)-C(7)-N(8)	-2.4(9)	C(15)-C(6)-C(7)-C(12)	-1.4(7)
C(5)-C(6)-C(7)-C(12)	178.9(5)	C(6)-C(7)-N(8)-N(9)	-179.8(5)
C(12)-C(7)-N(8)-N(9)	-1.0(5)	C(7)-N(8)-N(9)-C(10)	1.3(5)
C(7)-N(8)-N(9)-C(17)	176.4(4)	C(17)-N(9)-C(10)-O(11)	5.0(8)
N(8)-N(9)-C(10)-O(11)	179.5(5)	C(17)-N(9)-C(10)-C(12)	-175.4(5)
N(8)-N(9)-C(10)-C(12)	-1.0(5)	O(11)-C(10)-C(12)-C(13)	-3.7(10)
N(9)-C(10)-C(12)-C(13)	176.9(5)	O(11)-C(10)-C(12)-C(7)	179.8(5)
N(9)-C(10)-C(12)-C(7)	0.3(5)	N(8)-C(7)-C(12)-C(13)	-176.7(5)
C(6)-C(7)-C(12)-C(13)	2.2(7)	N(8)-C(7)-C(12)-C(10)	0.4(6)
C(6)-C(7)-C(12)-C(10)	179.4(4)	C(10)-C(12)-C(13)-N(14)	-178.2(5)
C(7)-C(12)-C(13)-N(14)	-2.0(7)	C(12)-C(13)-N(14)-C(15)	0.9(8)
C(5)-C(6)-C(15)-C(16)	-0.6(7)	C(7)-C(6)-C(15)-C(16)	179.7(5)
C(5)-C(6)-C(15)-N(14)	-180.0(5)	C(7)-C(6)-C(15)-N(14)	0.3(7)
C(13)-N(14)-C(15)-C(16)	-179.4(5)	C(13)-N(14)-C(15)-C(6)	0.0(7)
O(2)-C(3)-C(16)-C(15)	-178.3(5)	C(4)-C(3)-C(16)-C(15)	0.7(9)
C(6)-C(15)-C(16)-C(3)	-0.2(8)	N(14)-C(15)-C(16)-C(3)	179.2(5)
C(10)-N(9)-C(17)-C(18)	168.9(5)	N(8)-N(9)-C(17)-C(18)	-5.3(7)
C(10)-N(9)-C(17)-C(24)	-11.6(8)	N(8)-N(9)-C(17)-C(24)	174.2(5)
C(24)-C(17)-C(18)-C(19)	3.6(9)	N(9)-C(17)-C(18)-C(19)	-176.8(6)
C(17)-C(18)-C(19)-C(20)	-0.4(10)	C(18)-C(19)-C(20)-O(21)	177.8(6)
C(18)-C(19)-C(20)-C(23)	-2.5(11)	C(19)-C(20)-O(21)-C(22)	-14.3(10)
C(23)-C(20)-O(21)-C(22)	166.0(6)	C(19)-C(20)-C(23)-C(24)	2.3(10)
O(21)-C(20)-C(23)-C(24)	-178.1(5)	C(20)-C(23)-C(24)-C(17)	1.0(9)
C(18)-C(17)-C(24)-C(23)	-3.9(9)	N(9)-C(17)-C(24)-C(23)	176.6(5)
C(25)-O(26)-C(27)-C(40)	1.0(10)	C(25)-O(26)-C(27)-C(28)	-178.4(6)
O(26)-C(27)-C(28)-C(29)	179.8(6)	C(40)-C(27)-C(28)-C(29)	0.4(10)
C(27)-C(28)-C(29)-C(30)	-0.4(10)	C(28)-C(29)-C(30)-C(39)	0.4(9)
C(28)-C(29)-C(30)-C(31)	179.6(6)	C(29)-C(30)-C(31)-N(32)	0.3(10)
C(39)-C(30)-C(31)-N(32)	179.5(6)	C(29)-C(30)-C(31)-C(36)	-179.2(6)
C(39)-C(30)-C(31)-C(36)	-0.1(8)	C(30)-C(31)-N(32)-N(33)	-178.4(6)
C(36)-C(31)-N(32)-N(33)	1.2(6)	C(31)-N(32)-N(33)-C(34)	-1.0(6)
C(31)-N(32)-N(33)-C(41)	-176.4(5)	N(32)-N(33)-C(34)-O(35)	-179.1(6)
C(41)-N(33)-C(34)-O(35)	-4.3(10)	N(32)-N(33)-C(34)-C(36)	0.5(7)
C(41)-N(33)-C(34)-C(36)	175.3(5)	N(32)-C(31)-C(36)-C(37)	179.0(6)
C(30)-C(31)-C(36)-C(37)	-1.3(9)	N(32)-C(31)-C(36)-C(34)	-1.0(7)
C(30)-C(31)-C(36)-C(34)	178.7(5)	O(35)-C(34)-C(36)-C(37)	-0.2(13)
N(33)-C(34)-C(36)-C(37)	-179.7(7)	O(35)-C(34)-C(36)-C(31)	179.8(6)
N(33)-C(34)-C(36)-C(31)	0.3(6)	C(31)-C(36)-C(37)-N(38)	1.2(9)
C(34)-C(36)-C(37)-N(38)	-178.8(6)	C(36)-C(37)-N(38)-C(39)	0.4(9)
C(37)-N(38)-C(39)-C(40)	179.4(6)	C(37)-N(38)-C(39)-C(30)	-1.9(9)
C(29)-C(30)-C(39)-C(40)	-0.5(9)	C(31)-C(30)-C(39)-C(40)	-179.7(5)
C(29)-C(30)-C(39)-N(38)	-179.2(5)	C(31)-C(30)-C(39)-N(38)	1.6(8)
O(26)-C(27)-C(40)-C(39)	-179.8(6)	C(28)-C(27)-C(40)-C(39)	-0.4(9)
N(38)-C(39)-C(40)-C(27)	179.2(5)	C(30)-C(39)-C(40)-C(27)	0.5(9)
C(43)-C(42)-C(41)-C(48)	-1.2(9)	C(43)-C(42)-C(41)-N(33)	178.9(6)
C(34)-N(33)-C(41)-C(48)	30.9(9)	N(32)-N(33)-C(41)-C(48)	-154.5(5)
C(34)-N(33)-C(41)-C(42)	-149.2(6)	N(32)-N(33)-C(41)-C(42)	25.4(8)
C(41)-C(42)-C(43)-C(44)	-0.1(10)	C(42)-C(43)-C(44)-O(45B)	162(3)
C(42)-C(43)-C(44)-C(47)	1.4(10)	C(42)-C(43)-C(44)-O(45A)	-176.7(8)
O(45B)-C(44)-C(47)-C(48)	-169(2)	C(43)-C(44)-C(47)-C(48)	-1.5(11)

O(45A)-C(44)-C(47)-C(48)	176.2(8)	C(42)-C(41)-C(48)-C(47)	1.1(9)
N(33)-C(41)-C(48)-C(47)	-179.0(6)	C(44)-C(47)-C(48)-C(41)	0.3(11)
C(43)-C(44)-O(45A)-C(46A)	-161.1(9)	C(47)-C(44)-O(45A)-C(46A)	21.1(15)
C(43)-C(44)-O(45B)-C(46B)	9(6)	C(47)-C(44)-O(45B)-C(46B)	172(3)

Table 30: Hydrogen bonds for **DK-I-56-1 (8b)** [Å and °].

D-H...A	d(D-H)	d(H...A)	d(D...A)	<(DHA)
N(14)-H(14)...O(49A)#1	0.86	1.90	2.664(7)	146.6
N(14)-H(14)...O(49B)#1	0.86	1.99	2.84(2)	172.1
C(24)-H(24)...O(11)	0.93	2.28	2.908(7)	123.9
C(28)-H(28)...O(49B)#2	0.93	2.62	3.24(3)	124.6
N(38)-H(38)...O(11)#3	0.86	1.91	2.745(5)	162.3
C(48)-H(48)...O(35)	0.93	2.42	2.940(6)	115.2
C(46A)-H(46A)...O(35)#4	0.96	2.50	3.197(11)	129.8
O(49A)-H(49A)...O(35)	0.821(11)	1.86(2)	2.668(6)	168(9)
O(49A)-H(49B)...N(8)#2	0.821(10)	2.04(2)	2.845(7)	165(8)
O(49B)-H(49D)...O(35)	0.821(11)	2.10(2)	2.90(2)	165(11)

Symmetry transformations used to generate equivalent atoms:
#1 x-1,y,z-1 #2 -x+2,-y+1,-z+1 #3 x,y,z+1
#4 -x+2,-y,-z+1

4.1.2. X-ray Crystal Data for MM-I-10 (14l)

Table 31: Crystal data and structure refinement for **MM-I-10 (14l)**.

Identification code	cook186	
Empirical formula	$C_{19}H_{13}F_6N_3O_3$	
Formula weight	445.32	
Temperature	100(2) K	
Wavelength	1.54178 Å	
Crystal system	Triclinic	
Space group	P-1	
Unit cell dimensions	a = 4.7627(3) Å	α= 67.735(2)°.
	b = 13.9518(7) Å	β= 84.014(2)°.
	c = 14.9299(8) Å	γ = 82.498(2)°.
Volume	908.62(9) $Å^3$	
Z	2	
Density (-173ºC)	1.628 Mg/m^3	
Absorption coefficient	1.351 mm^{-1}	
F(000)	452	
Crystal size	0.124 x 0.024 x 0.020 mm^3	
Theta range for data collection	3.204 to 74.576°.	
Index ranges	-4<=h<=5, -17<=k<=16, -17<=l<=18	
Reflections collected	8547	
Independent reflections	3468 [R_{int} = 0.0368]	
Completeness to theta = 67.679°	95.7 %	
Refinement method	Full-matrix least-squares on F^2	
Data / restraints / parameters	3468 / 0 / 287	
Goodness-of-fit on F^2	1.060	
Final R indices [I>2sigma(I)]	R_1 = 0.0427, wR_2 = 0.1136	
R indices (all data)	R_1 = 0.0458, wR_2 = 0.1163	
Largest diff. peak and hole	0.837 and -0.543 e.$Å^{-3}$	

Table 32: Atomic coordinates (x 10^4) and equivalent isotropic displacement parameters ($Å^2$x 10^3) for **MM-I-10 (14l)**. U(eq) is defined as one third of the trace of the orthogonalized U^{ij} tensor.

	x	y	z	U(eq)
F(1)	15101(2)	9366(1)	1004(1)	30(1)
F(2)	11082(2)	10265(1)	980(1)	35(1)
F(3)	13212(3)	9540(1)	2311(1)	38(1)
C(5)	11120(3)	8448(1)	1746(1)	22(1)
C(4)	12641(4)	9392(1)	1518(1)	25(1)
C(6)	9567(3)	8048(1)	2633(1)	23(1)
C(7)	7928(3)	7249(1)	2798(1)	22(1)
C(8)	7803(3)	6828(1)	2085(1)	21(1)
C(9)	6049(3)	6022(1)	2180(1)	20(1)
N(10)	4286(3)	5559(1)	2904(1)	21(1)
N(11)	3149(3)	4854(1)	2605(1)	20(1)
C(12)	4240(3)	4869(1)	1700(1)	21(1)
O(13)	3619(3)	4306(1)	1281(1)	26(1)
C(14)	6154(3)	5657(1)	1402(1)	21(1)
C(15)	7864(3)	6053(1)	575(1)	23(1)
N(16)	9442(3)	6808(1)	486(1)	22(1)
C(17)	9464(3)	7218(1)	1209(1)	21(1)
C(18)	11120(3)	8029(1)	1042(1)	22(1)
C(19)	1236(3)	4179(1)	3256(1)	21(1)
C(20)	607(4)	4200(1)	4183(1)	23(1)
C(21)	-1249(4)	3538(1)	4827(1)	24(1)
C(22)	-2449(3)	2854(1)	4544(1)	23(1)
O(23)	-4324(3)	2216(1)	5244(1)	29(1)
C(24)	-4480(4)	1256(1)	5271(1)	27(1)
F(25)	-6055(2)	757(1)	6050(1)	32(1)
F(26)	-5756(3)	1264(1)	4515(1)	55(1)
F(27)	-1996(3)	720(1)	5299(1)	60(1)
C(28)	-1886(4)	2840(2)	3623(1)	28(1)
C(29)	-45(4)	3501(1)	2979(1)	26(1)
O(30)	7126(3)	2666(1)	1192(1)	33(1)
C(31)	5626(5)	1779(2)	1684(2)	38(1)

Table 33: Bond lengths [Å] and angles [°] for **MM-I-10 (14l)**.

F(1)-C(4)	1.337(2)	F(2)-C(4)	1.352(2)
F(3)-C(4)	1.3360(19)	C(5)-C(18)	1.381(2)
C(5)-C(6)	1.399(2)	C(5)-C(4)	1.495(2)
C(6)-C(7)	1.375(2)	C(6)-H(6)	0.9500
C(7)-C(8)	1.406(2)	C(7)-H(7)	0.9500
C(8)-C(17)	1.411(2)	C(8)-C(9)	1.443(2)
C(9)-N(10)	1.310(2)	C(9)-C(14)	1.428(2)
N(10)-N(11)	1.4077(18)	N(11)-C(12)	1.390(2)
N(11)-C(19)	1.417(2)	C(12)-O(13)	1.252(2)
C(12)-C(14)	1.429(2)	C(14)-C(15)	1.373(2)
C(15)-N(16)	1.331(2)	C(15)-H(15)	0.9500
N(16)-C(17)	1.400(2)	N(16)-H(2)	0.90(2)
C(17)-C(18)	1.395(2)	C(18)-H(18)	0.9500
C(19)-C(29)	1.393(2)	C(19)-C(20)	1.395(2)
C(20)-C(21)	1.386(2)	C(20)-H(20)	0.9500
C(21)-C(22)	1.382(2)	C(21)-H(21)	0.9500
C(22)-C(28)	1.381(2)	C(22)-O(23)	1.411(2)
O(23)-C(24)	1.337(2)	C(24)-F(27)	1.310(2)
C(24)-F(25)	1.319(2)	C(24)-F(26)	1.331(2)
C(28)-C(29)	1.381(3)	C(28)-H(28)	0.9500
C(29)-H(29)	0.9500	O(30)-C(31)	1.419(2)
O(30)-H(30)	0.91(3)	C(31)-H(00A)	0.9800
C(31)-H(00B)	0.9800	C(31)-H(00C)	0.9800
C(18)-C(5)-C(6)	121.13(16)	C(18)-C(5)-C(4)	118.84(15)
C(6)-C(5)-C(4)	119.89(15)	F(3)-C(4)-F(1)	107.01(13)
F(3)-C(4)-F(2)	106.45(14)	F(1)-C(4)-F(2)	105.73(14)
F(3)-C(4)-C(5)	112.87(14)	F(1)-C(4)-C(5)	113.00(14)
F(2)-C(4)-C(5)	111.29(13)	C(7)-C(6)-C(5)	119.70(15)
C(7)-C(6)-H(6)	120.1	C(5)-C(6)-H(6)	120.1
C(6)-C(7)-C(8)	120.65(16)	C(6)-C(7)-H(7)	119.7
C(8)-C(7)-H(7)	119.7	C(7)-C(8)-C(17)	118.75(16)
C(7)-C(8)-C(9)	124.41(15)	C(17)-C(8)-C(9)	116.84(14)
N(10)-C(9)-C(14)	113.08(15)	N(10)-C(9)-C(8)	128.32(14)
C(9)-N(10)-N(11)	103.98(12)	C(12)-N(11)-N(10)	113.65(13)
C(12)-N(11)-C(19)	127.60(14)	N(10)-N(11)-C(19)	118.60(13)
O(13)-C(12)-N(11)	126.14(15)	O(13)-C(12)-C(14)	130.60(15)
N(11)-C(12)-C(14)	103.26(13)	C(15)-C(14)-C(9)	121.73(16)
C(15)-C(14)-C(12)	132.26(15)	C(9)-C(14)-C(12)	106.01(14)
N(16)-C(15)-C(14)	119.36(15)	N(16)-C(15)-H(15)	120.3
C(14)-C(15)-H(15)	120.3	C(15)-N(16)-C(17)	122.81(15)
C(15)-N(16)-H(2)	119.2(15)	C(17)-N(16)-H(2)	118.0(15)
C(18)-C(17)-N(16)	118.91(15)	C(18)-C(17)-C(8)	120.45(15)
N(16)-C(17)-C(8)	120.64(15)	C(5)-C(18)-C(17)	119.26(16)

Table 33: (continued).

C(5)-C(18)-H(18)	120.4	C(17)-C(18)-H(18)	120.4
C(29)-C(19)-C(20)	119.57(16)	C(29)-C(19)-N(11)	120.74(14)
C(20)-C(19)-N(11)	119.68(14)	C(21)-C(20)-C(19)	120.09(15)
C(21)-C(20)-H(20)	120.0	C(19)-C(20)-H(20)	120.0
C(22)-C(21)-C(20)	119.45(15)	C(22)-C(21)-H(21)	120.3
C(20)-C(21)-H(21)	120.3	C(28)-C(22)-C(21)	121.02(16)
C(28)-C(22)-O(23)	123.46(15)	C(21)-C(22)-O(23)	115.49(15)
C(24)-O(23)-C(22)	118.87(14)	F(27)-C(24)-F(25)	108.69(16)
F(27)-C(24)-F(26)	107.90(17)	F(25)-C(24)-F(26)	106.32(14)
F(27)-C(24)-O(23)	113.13(15)	F(25)-C(24)-O(23)	108.44(14)
F(26)-C(24)-O(23)	112.09(16)	C(22)-C(28)-C(29)	119.68(16)
C(22)-C(28)-H(28)	120.2	C(29)-C(28)-H(28)	120.2
C(28)-C(29)-C(19)	120.16(16)	C(28)-C(29)-H(29)	119.9
C(19)-C(29)-H(29)	119.9	C(31)-O(30)-H(30)	109.5
O(30)-C(31)-H(00A)	109.5	O(30)-C(31)-H(00B)	109.5
H(00A)-C(31)-H(00B)	109.5	O(30)-C(31)-H(00C)	109.5
H(00A)-C(31)-H(00C)	109.5	H(00B)-C(31)-H(00C)	109.5

Table 34: Anisotropic displacement parameters ($Å^2 x\ 10^3$) for **MM-I-10 (14l)**. The anisotropic displacement factor exponent takes the form: $-2\pi^2[h^2 a^{*2} U^{11} + ... + 2\ h\ k\ a^*\ b^*\ U^{12}]$

	U^{11}	U^{22}	U^{33}	U^{23}	U^{13}	U^{12}
F(1)	22(1)	34(1)	34(1)	-11(1)	2(1)	-8(1)
F(2)	29(1)	25(1)	46(1)	-9(1)	-9(1)	-1(1)
F(3)	50(1)	43(1)	28(1)	-17(1)	-2(1)	-23(1)
C(5)	19(1)	25(1)	23(1)	-9(1)	-5(1)	-1(1)
C(4)	22(1)	29(1)	24(1)	-11(1)	-5(1)	-2(1)
C(6)	23(1)	30(1)	21(1)	-14(1)	-4(1)	-1(1)
C(7)	22(1)	28(1)	19(1)	-11(1)	-2(1)	-2(1)
C(8)	19(1)	25(1)	19(1)	-9(1)	-5(1)	0(1)
C(9)	19(1)	25(1)	18(1)	-10(1)	-5(1)	1(1)
N(10)	21(1)	25(1)	20(1)	-11(1)	-4(1)	-4(1)
N(11)	21(1)	25(1)	18(1)	-10(1)	-2(1)	-5(1)
C(12)	21(1)	26(1)	18(1)	-10(1)	-3(1)	-2(1)
O(13)	30(1)	31(1)	22(1)	-15(1)	0(1)	-9(1)
C(14)	21(1)	26(1)	19(1)	-11(1)	-3(1)	-1(1)
C(15)	24(1)	28(1)	19(1)	-11(1)	-3(1)	-2(1)
N(16)	22(1)	29(1)	18(1)	-11(1)	0(1)	-5(1)
C(17)	19(1)	26(1)	19(1)	-10(1)	-4(1)	0(1)
C(18)	20(1)	27(1)	19(1)	-8(1)	-3(1)	-2(1)
C(19)	20(1)	24(1)	20(1)	-8(1)	-3(1)	-1(1)
C(20)	25(1)	27(1)	20(1)	-11(1)	-3(1)	-5(1)
C(21)	26(1)	29(1)	20(1)	-11(1)	-1(1)	-3(1)
C(22)	21(1)	26(1)	23(1)	-9(1)	1(1)	-3(1)
O(23)	33(1)	30(1)	28(1)	-14(1)	9(1)	-11(1)
C(24)	27(1)	30(1)	26(1)	-13(1)	3(1)	-8(1)
F(25)	36(1)	34(1)	27(1)	-11(1)	7(1)	-15(1)
F(26)	77(1)	70(1)	29(1)	-20(1)	3(1)	-49(1)
F(27)	33(1)	32(1)	96(1)	-9(1)	17(1)	1(1)
C(28)	29(1)	33(1)	28(1)	-17(1)	1(1)	-10(1)
C(29)	27(1)	33(1)	21(1)	-13(1)	1(1)	-8(1)
O(30)	37(1)	32(1)	32(1)	-16(1)	10(1)	-8(1)
C(31)	44(1)	33(1)	37(1)	-14(1)	9(1)	-12(1)

Table 35: Hydrogen coordinates (x 10^4) and isotropic displacement parameters (Å^{2}x 10^3) for **MM-I-10 (14l)**.

	x	y	z	U(eq)
H(2)	10560(50)	7066(18)	-55(17)	31(6)
H(6)	9645	8326	3119	28
H(7)	6869	6978	3400	27
H(15)	7920	5792	70	27
H(18)	12237	8291	452	26
H(20)	1451	4668	4373	28
H(21)	-1691	3553	5456	29
H(28)	-2762	2378	3434	34
H(29)	350	3492	2345	31
H(30)	6040(40)	3243(19)	1212(17)	49
H(00A)	4020	1807	1311	57
H(00B)	4923	1771	2327	57
H(00C)	6898	1147	1753	57

Table 36: Torsion angles [°] for **MM-I-10 (14l)**.

C(18)-C(5)-C(4)-F(3)	-161.41(15)	C(6)-C(5)-C(4)-F(3)	23.0(2)
C(18)-C(5)-C(4)-F(1)	-39.8(2)	C(6)-C(5)-C(4)-F(1)	144.58(15)
C(18)-C(5)-C(4)-F(2)	78.97(19)	C(6)-C(5)-C(4)-F(2)	-96.64(18)
C(18)-C(5)-C(6)-C(7)	-2.4(2)	C(4)-C(5)-C(6)-C(7)	173.10(15)
C(5)-C(6)-C(7)-C(8)	0.2(2)	C(6)-C(7)-C(8)-C(17)	2.0(2)
C(6)-C(7)-C(8)-C(9)	-177.19(15)	C(7)-C(8)-C(9)-N(10)	1.1(3)
C(17)-C(8)-C(9)-N(10)	-178.11(15)	C(7)-C(8)-C(9)-C(14)	-179.24(15)
C(17)-C(8)-C(9)-C(14)	1.5(2)	C(14)-C(9)-N(10)-N(11)	-0.07(17)
C(8)-C(9)-N(10)-N(11)	179.57(15)	C(9)-N(10)-N(11)-C(12)	0.85(17)
C(9)-N(10)-N(11)-C(19)	176.81(13)	N(10)-N(11)-C(12)-O(13)	178.62(15)
C(19)-N(11)-C(12)-O(13)	3.1(3)	N(10)-N(11)-C(12)-C(14)	-1.23(17)
C(19)-N(11)-C(12)-C(14)	-176.76(14)	N(10)-C(9)-C(14)-C(15)	179.49(15)
C(8)-C(9)-C(14)-C(15)	-0.2(2)	N(10)-C(9)-C(14)-C(12)	-0.67(19)
C(8)-C(9)-C(14)-C(12)	179.65(14)	O(13)-C(12)-C(14)-C(15)	1.1(3)
N(11)-C(12)-C(14)-C(15)	-179.09(17)	O(13)-C(12)-C(14)-C(9)	-178.75(17)
N(11)-C(12)-C(14)-C(9)	1.09(17)	C(9)-C(14)-C(15)-N(16)	-0.9(2)
C(12)-C(14)-C(15)-N(16)	179.34(17)	C(14)-C(15)-N(16)-C(17)	0.5(2)
C(15)-N(16)-C(17)-C(18)	-178.13(15)	C(15)-N(16)-C(17)-C(8)	0.9(2)
C(7)-C(8)-C(17)-C(18)	-2.2(2)	C(9)-C(8)-C(17)-C(18)	177.13(14)
C(7)-C(8)-C(17)-N(16)	178.85(14)	C(9)-C(8)-C(17)-N(16)	-1.9(2)
C(6)-C(5)-C(18)-C(17)	2.3(2)	C(4)-C(5)-C(18)-C(17)	-173.28(14)
N(16)-C(17)-C(18)-C(5)	179.04(14)	C(8)-C(17)-C(18)-C(5)	0.0(2)
C(12)-N(11)-C(19)-C(29)	-7.6(2)	N(10)-N(11)-C(19)-C(29)	177.07(14)
C(12)-N(11)-C(19)-C(20)	172.94(15)	N(10)-N(11)-C(19)-C(20)	-2.4(2)
C(29)-C(19)-C(20)-C(21)	0.9(2)	N(11)-C(19)-C(20)-C(21)	-179.59(15)
C(19)-C(20)-C(21)-C(22)	0.4(3)	C(20)-C(21)-C(22)-C(28)	-1.7(3)
C(20)-C(21)-C(22)-O(23)	-179.60(15)	C(28)-C(22)-O(23)-C(24)	34.9(2)
C(21)-C(22)-O(23)-C(24)	-147.27(16)	C(22)-O(23)-C(24)-F(27)	51.2(2)
C(22)-O(23)-C(24)-F(25)	171.84(13)	C(22)-O(23)-C(24)-F(26)	-71.1(2)
C(21)-C(22)-C(28)-C(29)	1.5(3)	O(23)-C(22)-C(28)-C(29)	179.26(16)
C(22)-C(28)-C(29)-C(19)	-0.1(3)	C(20)-C(19)-C(29)-C(28)	-1.1(3)
N(11)-C(19)-C(29)-C(28)	179.42(16)		

Table 37: Hydrogen bonds for **MM-I-10 (14l)** [Å and °].

D-H...A	d(D-H)	d(H...A)	d(D...A)	<(DHA)
N(16)-H(2)...O(30)#1	0.90(2)	1.86(2)	2.748(2)	168(2)
C(15)-H(15)...O(13)#2	0.95	2.27	3.1596(19)	154.8
C(28)-H(28)...F(26)	0.95	2.29	2.886(2)	120.0
C(29)-H(29)...O(13)	0.95	2.19	2.857(2)	125.9
O(30)-H(30)...O(13)	0.91	1.78	2.6889(19)	174.4
C(31)-H(00C)...F(2)#3	0.98	2.60	3.464(2)	146.8

Symmetry transformations used to generate equivalent atoms:
#1 -x+2,-y+1,-z #2 -x+1,-y+1,-z #3 x,y-1,z

4.1.3. X-ray Crystal Data for DK-IV-20-1 (14o)

Table 38: Crystal data and structure refinement for **DK-IV-20-1 (14o)**.

Identification code	cook188_isoprop	
Empirical formula	$C_{18}H_{12}F_3N_3O_3$, 0.5($C_4H_{10}O$)	
Formula weight	412.36	
Temperature	100(2) K	
Wavelength	1.54178 Å	
Crystal system	Triclinic	
Space group	P -1	
Unit cell dimensions	a = 8.038(3) Å	α= 98.146(9)°.
	b = 14.342(2) Å	β= 99.781(12)°.
	c = 17.107(5) Å	γ = 104.966(11)°.
Volume	1841.4(9) $Å^3$	
Z	4	
Density (-173ºC)	1.487 Mg/m^3	
Absorption coefficient	1.061 mm^{-1}	
F(000)	852	
Crystal size	0.204 x 0.020 x 0.020 mm^3	
Theta range for data collection	3.252 to 74.684°.	
Index ranges	-10<=h<=10, -17<=k<=15, -17<=l<=21	
Reflections collected	14650	
Independent reflections	6337 [R_{int} = 0.0321]	
Completeness to theta = 67.679°	88.6 %	
Absorption correction	Semi-empirical from equivalents	
Max. and min. transmission	0.7538 and 0.6042	
Refinement method	Full-matrix least-squares on F^2	
Data / restraints / parameters	6337 / 0 / 537	
Goodness-of-fit on F^2	1.041	
Final R indices [I>2sigma(I)]	R_1 = 0.0351, wR_2 = 0.0880	
R indices (all data)	R_1 = 0.0372, wR_2 = 0.0899	
Largest diff. peak and hole	0.254 and -0.227 e.$Å^{-3}$	

Table 39: Atomic coordinates (x 10^4) and equivalent isotropic displacement parameters ($Å^2$x 10^3) for **DK-IV-20-1 (14o)**. U(eq) is defined as one third of the trace of the orthogonalized U^{ij} tensor.

	x	y	z	U(eq)
C(1)	14427(2)	3742(1)	2242(1)	22(1)
O(2)	14623(1)	4691(1)	2709(1)	20(1)
C(3)	13939(2)	4717(1)	3382(1)	16(1)
C(4)	14066(2)	5670(1)	3788(1)	17(1)
C(5)	13443(2)	5791(1)	4481(1)	16(1)
C(6)	12665(2)	4978(1)	4803(1)	15(1)
C(7)	12017(2)	5034(1)	5540(1)	14(1)
N(8)	12024(2)	5825(1)	6038(1)	16(1)
N(9)	11301(2)	5447(1)	6668(1)	14(1)
C(10)	10831(2)	4430(1)	6559(1)	15(1)
O(11)	10167(1)	3931(1)	7027(1)	18(1)
C(12)	11304(2)	4145(1)	5805(1)	15(1)
C(13)	11180(2)	3244(1)	5363(1)	16(1)
N(14)	11773(2)	3196(1)	4678(1)	16(1)
C(15)	12533(2)	4032(1)	4385(1)	15(1)
C(16)	13167(2)	3900(1)	3676(1)	16(1)
C(17)	11089(2)	6121(1)	7304(1)	15(1)
C(18)	11033(2)	7052(1)	7176(1)	16(1)
C(19)	10790(2)	7716(1)	7787(1)	19(1)
C(20)	10615(2)	7444(1)	8517(1)	18(1)
O(21)	10232(1)	8109(1)	9107(1)	22(1)
C(22)	11573(2)	8655(1)	9707(1)	26(1)
F(23)	12952(2)	9127(1)	9440(1)	48(1)
F(24)	11017(1)	9315(1)	10124(1)	37(1)
F(25)	12161(2)	8135(1)	10213(1)	51(1)
C(26)	10677(2)	6528(1)	8659(1)	19(1)
C(27)	10921(2)	5860(1)	8048(1)	18(1)
C(28)	7674(2)	-486(1)	8150(1)	25(1)
O(29)	6598(1)	-1252(1)	7491(1)	22(1)
C(30)	5628(2)	-986(1)	6878(1)	17(1)
C(31)	4416(2)	-1780(1)	6303(1)	18(1)
C(32)	3324(2)	-1606(1)	5671(1)	16(1)
C(33)	3389(2)	-639(1)	5574(1)	14(1)
C(34)	2286(2)	-394(1)	4930(1)	14(1)
N(35)	1081(2)	-1004(1)	4329(1)	15(1)
N(36)	417(2)	-378(1)	3875(1)	14(1)
C(37)	1218(2)	616(1)	4188(1)	14(1)
O(38)	879(1)	1302(1)	3878(1)	18(1)
C(39)	2466(2)	616(1)	4901(1)	14(1)
C(40)	3702(2)	1347(1)	5476(1)	15(1)
N(41)	4739(2)	1116(1)	6071(1)	15(1)

Table 39: (continued).

	x	y	z	U(eq)
C(42)	4627(2)	144(1)	6143(1)	14(1)
C(43)	5754(2)	-24(1)	6795(1)	16(1)
C(44)	-794(2)	-821(1)	3132(1)	15(1)
C(45)	-1769(2)	-297(1)	2719(1)	17(1)
C(46)	-2888(2)	-744(1)	1972(1)	19(1)
C(47)	-3041(2)	-1712(1)	1653(1)	19(1)
O(48)	-4240(1)	-2178(1)	908(1)	24(1)
C(49)	-3568(2)	-2174(1)	242(1)	27(1)
F(50)	-4855(2)	-2673(1)	-386(1)	45(1)
F(51)	-2925(2)	-1278(1)	109(1)	44(1)
F(52)	-2280(2)	-2598(1)	268(1)	41(1)
C(53)	-2138(2)	-2253(1)	2068(1)	21(1)
C(54)	-1001(2)	-1807(1)	2807(1)	19(1)
O(55)	7246(1)	2594(1)	7149(1)	21(1)
C(56)	7593(2)	2839(1)	8015(1)	20(1)
C(57)	7114(2)	3762(1)	8312(1)	20(1)
C(58)	7733(2)	4110(1)	9226(1)	25(1)
C(59)	7018(2)	4941(1)	9543(1)	37(1)

Table 40: Bond lengths [Å] and angles [°] for **DK-IV-20-1 (14o)**.

C(1)-O(2)	1.4329(16)	C(1)-H(1A)	0.9800
C(1)-H(1B)	0.9800	C(1)-H(1C)	0.9800
O(2)-C(3)	1.3580(17)	C(3)-C(16)	1.3812(19)
C(3)-C(4)	1.4122(18)	C(4)-C(5)	1.368(2)
C(4)-H(4)	0.9500	C(5)-C(6)	1.4067(19)
C(5)-H(5)	0.9500	C(6)-C(15)	1.4111(18)
C(6)-C(7)	1.4430(19)	C(7)-N(8)	1.3170(17)
C(7)-C(12)	1.4263(18)	N(8)-N(9)	1.4179(15)
N(9)-C(10)	1.3862(17)	N(9)-C(17)	1.4123(17)
C(10)-O(11)	1.2444(17)	C(10)-C(12)	1.4401(19)
C(12)-C(13)	1.3715(18)	C(13)-N(14)	1.3362(18)
C(13)-H(13)	0.9500	N(14)-C(15)	1.3990(17)
N(14)-H(14)	0.8800	C(15)-C(16)	1.400(2)
C(16)-H(16)	0.9500	C(17)-C(18)	1.3936(18)
C(17)-C(27)	1.395(2)	C(18)-C(19)	1.3872(19)
C(18)-H(18)	0.9500	C(19)-C(20)	1.378(2)
C(19)-H(19)	0.9500	C(20)-C(26)	1.3813(19)
C(20)-O(21)	1.4180(16)	O(21)-C(22)	1.337(2)
C(22)-F(24)	1.3191(17)	C(22)-F(25)	1.3251(18)
C(22)-F(23)	1.329(2)	C(26)-C(27)	1.390(2)
C(26)-H(26)	0.9500	C(27)-H(27)	0.9500
C(28)-O(29)	1.4313(18)	C(28)-H(28A)	0.9800
C(28)-H(28B)	0.9800	C(28)-H(28C)	0.9800
O(29)-C(30)	1.3577(17)	C(30)-C(43)	1.3861(19)
C(30)-C(31)	1.413(2)	C(31)-C(32)	1.368(2)
C(31)-H(31)	0.9500	C(32)-C(33)	1.4087(18)
C(32)-H(32)	0.9500	C(33)-C(42)	1.408(2)
C(33)-C(34)	1.436(2)	C(34)-N(35)	1.3143(18)
C(34)-C(39)	1.4264(17)	N(35)-N(36)	1.4130(15)
N(36)-C(37)	1.3886(17)	N(36)-C(44)	1.4138(18)
C(37)-O(38)	1.2485(16)	C(37)-C(39)	1.441(2)
C(39)-C(40)	1.3758(19)	C(40)-N(41)	1.3377(18)
C(40)-H(40)	0.9500	N(41)-C(42)	1.3973(16)
N(41)-H(41)	0.8800	C(42)-C(43)	1.404(2)
C(43)-H(43)	0.9500	C(44)-C(45)	1.3962(19)
C(44)-C(54)	1.3991(18)	C(45)-C(46)	1.390(2)
C(45)-H(45)	0.9500	C(46)-C(47)	1.384(2)
C(46)-H(46)	0.9500	C(47)-C(53)	1.379(2)
C(47)-O(48)	1.4175(18)	O(48)-C(49)	1.3415(19)
C(49)-F(51)	1.3239(19)	C(49)-F(52)	1.3262(19)
C(49)-F(50)	1.3263(19)	C(53)-C(54)	1.385(2)
C(53)-H(53)	0.9500	C(54)-H(54)	0.9500
O(55)-C(56)	1.4337(18)	O(55)-H(55)	0.84(2)
C(56)-C(57)	1.5163(19)	C(56)-H(56A)	0.9900

Table 40: (continued).

C(56)-H(56B)	0.9900	C(57)-C(58)	1.526(2)
C(57)-H(57A)	0.9900	C(57)-H(57B)	0.9900
C(58)-C(59)	1.523(2)	C(58)-H(58A)	0.9900
C(58)-H(58B)	0.9900	C(59)-H(59A)	0.9800
C(59)-H(59B)	0.9800	C(59)-H(59C)	0.9800
O(2)-C(1)-H(1A)	109.5	O(2)-C(1)-H(1B)	109.5
H(1A)-C(1)-H(1B)	109.5	O(2)-C(1)-H(1C)	109.5
H(1A)-C(1)-H(1C)	109.5	H(1B)-C(1)-H(1C)	109.5
C(3)-O(2)-C(1)	117.28(11)	O(2)-C(3)-C(16)	124.89(12)
O(2)-C(3)-C(4)	114.82(12)	C(16)-C(3)-C(4)	120.29(12)
C(5)-C(4)-C(3)	120.27(12)	C(5)-C(4)-H(4)	119.9
C(3)-C(4)-H(4)	119.9	C(4)-C(5)-C(6)	121.14(12)
C(4)-C(5)-H(5)	119.4	C(6)-C(5)-H(5)	119.4
C(5)-C(6)-C(15)	117.76(12)	C(5)-C(6)-C(7)	125.16(12)
C(15)-C(6)-C(7)	117.07(12)	N(8)-C(7)-C(12)	112.94(12)
N(8)-C(7)-C(6)	128.19(12)	C(12)-C(7)-C(6)	118.84(12)
C(7)-N(8)-N(9)	103.80(10)	C(10)-N(9)-C(17)	127.95(11)
C(10)-N(9)-N(8)	113.91(10)	C(17)-N(9)-N(8)	118.10(10)
O(11)-C(10)-N(9)	125.67(12)	O(11)-C(10)-C(12)	131.32(12)
N(9)-C(10)-C(12)	103.01(11)	C(13)-C(12)-C(7)	121.36(12)
C(13)-C(12)-C(10)	132.32(12)	C(7)-C(12)-C(10)	106.33(11)
N(14)-C(13)-C(12)	119.53(12)	N(14)-C(13)-H(13)	120.2
C(12)-C(13)-H(13)	120.2	C(13)-N(14)-C(15)	122.96(11)
C(13)-N(14)-H(14)	118.5	C(15)-N(14)-H(14)	118.5
N(14)-C(15)-C(16)	118.27(11)	N(14)-C(15)-C(6)	120.22(12)
C(16)-C(15)-C(6)	121.51(12)	C(3)-C(16)-C(15)	119.01(12)
C(3)-C(16)-H(16)	120.5	C(15)-C(16)-H(16)	120.5
C(18)-C(17)-C(27)	120.19(12)	C(18)-C(17)-N(9)	119.06(12)
C(27)-C(17)-N(9)	120.75(12)	C(19)-C(18)-C(17)	119.88(13)
C(19)-C(18)-H(18)	120.1	C(17)-C(18)-H(18)	120.1
C(20)-C(19)-C(18)	119.14(12)	C(20)-C(19)-H(19)	120.4
C(18)-C(19)-H(19)	120.4	C(19)-C(20)-C(26)	122.02(12)
C(19)-C(20)-O(21)	117.77(12)	C(26)-C(20)-O(21)	120.04(12)
C(22)-O(21)-C(20)	117.19(11)	F(24)-C(22)-F(25)	107.72(13)
F(24)-C(22)-F(23)	108.32(13)	F(25)-C(22)-F(23)	106.61(15)
F(24)-C(22)-O(21)	108.14(13)	F(25)-C(22)-O(21)	113.18(13)
F(23)-C(22)-O(21)	112.68(13)	C(20)-C(26)-C(27)	119.01(13)
C(20)-C(26)-H(26)	120.5	C(27)-C(26)-H(26)	120.5
C(26)-C(27)-C(17)	119.75(12)	C(26)-C(27)-H(27)	120.1
C(17)-C(27)-H(27)	120.1	O(29)-C(28)-H(28A)	109.5
O(29)-C(28)-H(28B)	109.5	H(28A)-C(28)-H(28B)	109.5
O(29)-C(28)-H(28C)	109.5	H(28A)-C(28)-H(28C)	109.5

Table 40: (continued).

H(28B)-C(28)-H(28C)	109.5	C(30)-O(29)-C(28)	117.48(11)
O(29)-C(30)-C(43)	124.81(13)	O(29)-C(30)-C(31)	114.79(12)
C(43)-C(30)-C(31)	120.40(13)	C(32)-C(31)-C(30)	120.24(12)
C(32)-C(31)-H(31)	119.9	C(30)-C(31)-H(31)	119.9
C(31)-C(32)-C(33)	121.07(13)	C(31)-C(32)-H(32)	119.5
C(33)-C(32)-H(32)	119.5	C(42)-C(33)-C(32)	118.01(13)
C(42)-C(33)-C(34)	117.50(11)	C(32)-C(33)-C(34)	124.48(13)
N(35)-C(34)-C(39)	113.18(12)	N(35)-C(34)-C(33)	127.54(11)
C(39)-C(34)-C(33)	119.28(12)	C(34)-N(35)-N(36)	103.96(10)
C(37)-N(36)-N(35)	113.74(11)	C(37)-N(36)-C(44)	128.29(11)
N(35)-N(36)-C(44)	117.52(10)	O(38)-C(37)-N(36)	125.07(13)
O(38)-C(37)-C(39)	131.74(12)	N(36)-C(37)-C(39)	103.17(11)
C(40)-C(39)-C(34)	120.36(13)	C(40)-C(39)-C(37)	133.67(12)
C(34)-C(39)-C(37)	105.93(12)	N(41)-C(40)-C(39)	120.18(12)
N(41)-C(40)-H(40)	119.9	C(39)-C(40)-H(40)	119.9
C(40)-N(41)-C(42)	122.68(12)	C(40)-N(41)-H(41)	118.7
C(42)-N(41)-H(41)	118.7	N(41)-C(42)-C(43)	118.50(12)
N(41)-C(42)-C(33)	120.00(12)	C(43)-C(42)-C(33)	121.50(12)
C(30)-C(43)-C(42)	118.75(13)	C(30)-C(43)-H(43)	120.6
C(42)-C(43)-H(43)	120.6	C(45)-C(44)-C(54)	119.78(13)
C(45)-C(44)-N(36)	121.45(12)	C(54)-C(44)-N(36)	118.77(12)
C(46)-C(45)-C(44)	119.78(12)	C(46)-C(45)-H(45)	120.1
C(44)-C(45)-H(45)	120.1	C(47)-C(46)-C(45)	119.40(13)
C(47)-C(46)-H(46)	120.3	C(45)-C(46)-H(46)	120.3
C(53)-C(47)-C(46)	121.53(13)	C(53)-C(47)-O(48)	119.21(13)
C(46)-C(47)-O(48)	119.13(13)	C(49)-O(48)-C(47)	116.43(12)
F(51)-C(49)-F(52)	106.88(14)	F(51)-C(49)-F(50)	107.97(14)
F(52)-C(49)-F(50)	108.12(13)	F(51)-C(49)-O(48)	113.01(12)
F(52)-C(49)-O(48)	112.76(13)	F(50)-C(49)-O(48)	107.92(14)
C(47)-C(53)-C(54)	119.33(13)	C(47)-C(53)-H(53)	120.3
C(54)-C(53)-H(53)	120.3	C(53)-C(54)-C(44)	120.11(13)
C(53)-C(54)-H(54)	119.9	C(44)-C(54)-H(54)	119.9
C(56)-O(55)-H(55)	109.5	O(55)-C(56)-C(57)	112.14(12)
O(55)-C(56)-H(56A)	109.2	C(57)-C(56)-H(56A)	109.2
O(55)-C(56)-H(56B)	109.2	C(57)-C(56)-H(56B)	109.2
H(56A)-C(56)-H(56B)	107.9	C(56)-C(57)-C(58)	112.16(12)
C(56)-C(57)-H(57A)	109.2	C(58)-C(57)-H(57A)	109.2
C(56)-C(57)-H(57B)	109.2	C(58)-C(57)-H(57B)	109.2
H(57A)-C(57)-H(57B)	107.9	C(59)-C(58)-C(57)	112.33(14)
C(59)-C(58)-H(58A)	109.1	C(57)-C(58)-H(58A)	109.1
C(59)-C(58)-H(58B)	109.1	C(57)-C(58)-H(58B)	109.1
H(58A)-C(58)-H(58B)	107.9	C(58)-C(59)-H(59A)	109.5
C(58)-C(59)-H(59B)	109.5	H(59A)-C(59)-H(59B)	109.5

Table 40: (continued).

C(58)-C(59)-H(59C)	109.5	H(59A)-C(59)-H(59C)	109.5
H(59B)-C(59)-H(59C)	109.5		

Table 41: Anisotropic displacement parameters ($Å^2 x\ 10^3$)for **DK-IV-20-1 (14o)**. The anisotropic displacement factor exponent takes the form: $-2\pi^2[h^2 a^{*2} U^{11} + ... + 2\ h\ k\ a^*\ b^*\ U^{12}]$

	U^{11}	U^{22}	U^{33}	U^{23}	U^{13}	U^{12}
C(1)	24(1)	22(1)	19(1)	0(1)	5(1)	7(1)
O(2)	25(1)	19(1)	18(1)	4(1)	7(1)	7(1)
C(3)	13(1)	20(1)	15(1)	3(1)	0(1)	5(1)
C(4)	16(1)	16(1)	18(1)	6(1)	2(1)	3(1)
C(5)	16(1)	12(1)	19(1)	2(1)	1(1)	3(1)
C(6)	12(1)	14(1)	16(1)	3(1)	0(1)	4(1)
C(7)	10(1)	12(1)	17(1)	2(1)	-1(1)	2(1)
N(8)	16(1)	14(1)	16(1)	4(1)	5(1)	3(1)
N(9)	15(1)	12(1)	15(1)	3(1)	4(1)	2(1)
C(10)	12(1)	13(1)	18(1)	2(1)	0(1)	2(1)
O(11)	20(1)	14(1)	21(1)	5(1)	7(1)	2(1)
C(12)	12(1)	14(1)	17(1)	3(1)	1(1)	2(1)
C(13)	13(1)	13(1)	19(1)	4(1)	0(1)	1(1)
N(14)	16(1)	10(1)	18(1)	1(1)	2(1)	2(1)
C(15)	11(1)	14(1)	18(1)	3(1)	-1(1)	3(1)
C(16)	15(1)	14(1)	16(1)	1(1)	0(1)	5(1)
C(17)	11(1)	13(1)	18(1)	1(1)	1(1)	1(1)
C(18)	16(1)	16(1)	16(1)	4(1)	4(1)	2(1)
C(19)	19(1)	14(1)	22(1)	4(1)	3(1)	4(1)
C(20)	16(1)	17(1)	18(1)	-1(1)	3(1)	4(1)
O(21)	24(1)	23(1)	19(1)	-1(1)	5(1)	9(1)
C(22)	33(1)	22(1)	22(1)	-1(1)	2(1)	12(1)
F(23)	36(1)	37(1)	55(1)	-13(1)	11(1)	-6(1)
F(24)	50(1)	31(1)	29(1)	-9(1)	3(1)	20(1)
F(25)	80(1)	44(1)	27(1)	-2(1)	-15(1)	37(1)
C(26)	20(1)	20(1)	17(1)	5(1)	4(1)	3(1)
C(27)	20(1)	15(1)	20(1)	4(1)	3(1)	3(1)
C(28)	26(1)	28(1)	18(1)	3(1)	-2(1)	8(1)
O(29)	25(1)	22(1)	18(1)	6(1)	0(1)	8(1)
C(30)	17(1)	21(1)	15(1)	6(1)	6(1)	6(1)
C(31)	20(1)	14(1)	22(1)	6(1)	7(1)	5(1)
C(32)	16(1)	13(1)	19(1)	3(1)	5(1)	2(1)
C(33)	14(1)	14(1)	16(1)	3(1)	7(1)	3(1)
C(34)	13(1)	12(1)	16(1)	2(1)	7(1)	2(1)
N(35)	16(1)	12(1)	17(1)	5(1)	3(1)	4(1)
N(36)	15(1)	12(1)	15(1)	3(1)	3(1)	4(1)
C(37)	14(1)	12(1)	15(1)	1(1)	6(1)	2(1)
O(38)	22(1)	12(1)	19(1)	2(1)	2(1)	5(1)
C(39)	14(1)	13(1)	16(1)	2(1)	6(1)	3(1)
C(40)	17(1)	12(1)	16(1)	2(1)	6(1)	4(1)
N(41)	15(1)	11(1)	16(1)	0(1)	3(1)	1(1)

Table 41: (continued).

	U^{11}	U^{22}	U^{33}	U^{23}	U^{13}	U^{12}
C(42)	15(1)	14(1)	16(1)	3(1)	7(1)	3(1)
C(43)	14(1)	17(1)	14(1)	1(1)	4(1)	2(1)
C(44)	12(1)	15(1)	15(1)	2(1)	4(1)	1(1)
C(45)	17(1)	15(1)	18(1)	3(1)	6(1)	4(1)
C(46)	17(1)	22(1)	17(1)	5(1)	5(1)	6(1)
C(47)	14(1)	24(1)	14(1)	-1(1)	2(1)	1(1)
O(48)	18(1)	31(1)	16(1)	-3(1)	0(1)	1(1)
C(49)	30(1)	26(1)	20(1)	-2(1)	4(1)	4(1)
F(50)	44(1)	56(1)	19(1)	-10(1)	-1(1)	2(1)
F(51)	68(1)	32(1)	29(1)	9(1)	16(1)	5(1)
F(52)	46(1)	50(1)	34(1)	2(1)	17(1)	24(1)
C(53)	19(1)	16(1)	24(1)	-3(1)	4(1)	2(1)
C(54)	18(1)	16(1)	22(1)	1(1)	3(1)	5(1)
O(55)	20(1)	18(1)	18(1)	0(1)	4(1)	-4(1)
C(56)	22(1)	19(1)	18(1)	3(1)	4(1)	2(1)
C(57)	19(1)	20(1)	20(1)	4(1)	4(1)	3(1)
C(58)	24(1)	24(1)	21(1)	0(1)	4(1)	3(1)
C(59)	37(1)	36(1)	35(1)	-6(1)	11(1)	9(1)

Table 42: Hydrogen coordinates (x 10^4) and isotropic displacement parameters (Å^{2}x 10^3) for **DK-IV-20-1 (14o)**.

	x	y	z	U(eq)
H(1A)	13172	3379	2069	33
H(1B)	15039	3377	2573	33
H(1C)	14935	3822	1766	33
H(4)	14585	6228	3580	20
H(5)	13538	6436	4748	19
H(13)	10676	2658	5541	19
H(14)	11682	2614	4400	19
H(16)	13067	3257	3401	19
H(18)	11162	7231	6671	20
H(19)	10744	8351	7704	22
H(26)	10554	6357	9167	23
H(27)	10974	5228	8136	22
H(28A)	8603	-49	7957	37
H(28B)	8211	-778	8574	37
H(28C)	6944	-109	8369	37
H(31)	4359	-2437	6357	22
H(32)	2507	-2146	5291	19
H(40)	3819	2018	5451	18
H(41)	5523	1595	6431	18
H(43)	6588	511	7173	19
H(45)	-1668	364	2947	20
H(46)	-3543	-389	1683	22
H(53)	-2294	-2924	1849	25
H(54)	-362	-2171	3094	23
H(55)	8020(20)	2980(13)	6980(4)	32
H(56A)	8860	2937	8235	24
H(56B)	6908	2284	8220	24
H(57A)	5818	3631	8162	24
H(57B)	7656	4292	8040	24
H(58A)	7343	3549	9494	29
H(58B)	9038	4339	9366	29
H(59A)	7400	5498	9279	55
H(59B)	7468	5149	10129	55
H(59C)	5727	4709	9426	55

Table 43: Torsion angles [°] for **DK-IV-20-1 (14o)**.

C(1)-O(2)-C(3)-C(16)	4.1(2)	C(1)-O(2)-C(3)-C(4)	-175.97(12)
O(2)-C(3)-C(4)-C(5)	-179.16(12)	C(16)-C(3)-C(4)-C(5)	0.8(2)
C(3)-C(4)-C(5)-C(6)	-0.1(2)	C(4)-C(5)-C(6)-C(15)	-0.6(2)
C(4)-C(5)-C(6)-C(7)	178.21(13)	C(5)-C(6)-C(7)-N(8)	0.0(2)
C(15)-C(6)-C(7)-N(8)	178.77(13)	C(5)-C(6)-C(7)-C(12)	-178.21(13)
C(15)-C(6)-C(7)-C(12)	0.60(19)	C(12)-C(7)-N(8)-N(9)	0.65(15)
C(6)-C(7)-N(8)-N(9)	-177.60(13)	C(7)-N(8)-N(9)-C(10)	-0.67(15)
C(7)-N(8)-N(9)-C(17)	-178.63(12)	C(17)-N(9)-C(10)-O(11)	-2.0(2)
N(8)-N(9)-C(10)-O(11)	-179.71(12)	C(17)-N(9)-C(10)-C(12)	178.13(13)
N(8)-N(9)-C(10)-C(12)	0.41(15)	N(8)-C(7)-C(12)-C(13)	179.66(13)
C(6)-C(7)-C(12)-C(13)	-1.9(2)	N(8)-C(7)-C(12)-C(10)	-0.44(16)
C(6)-C(7)-C(12)-C(10)	178.00(12)	O(11)-C(10)-C(12)-C(13)	0.0(3)
N(9)-C(10)-C(12)-C(13)	179.89(15)	O(11)-C(10)-C(12)-C(7)	-179.87(14)
N(9)-C(10)-C(12)-C(7)	0.00(14)	C(7)-C(12)-C(13)-N(14)	1.5(2)
C(10)-C(12)-C(13)-N(14)	-178.35(14)	C(12)-C(13)-N(14)-C(15)	0.2(2)
C(13)-N(14)-C(15)-C(16)	177.83(13)	C(13)-N(14)-C(15)-C(6)	-1.5(2)
C(5)-C(6)-C(15)-N(14)	179.91(12)	C(7)-C(6)-C(15)-N(14)	1.00(19)
C(5)-C(6)-C(15)-C(16)	0.6(2)	C(7)-C(6)-C(15)-C(16)	-178.28(12)
O(2)-C(3)-C(16)-C(15)	179.19(13)	C(4)-C(3)-C(16)-C(15)	-0.7(2)
N(14)-C(15)-C(16)-C(3)	-179.27(12)	C(6)-C(15)-C(16)-C(3)	0.0(2)
C(10)-N(9)-C(17)-C(18)	-156.97(14)	N(8)-N(9)-C(17)-C(18)	20.67(18)
C(10)-N(9)-C(17)-C(27)	22.5(2)	N(8)-N(9)-C(17)-C(27)	-159.89(12)
	C(27)-C(17)-C(18)-C(19)	-0.8(2)	
N(9)-C(17)-C(18)-C(19)	178.68(13)	C(17)-C(18)-C(19)-C(20)	0.3(2)
C(18)-C(19)-C(20)-C(26)	0.1(2)	C(18)-C(19)-C(20)-O(21)	-175.24(12)
C(19)-C(20)-O(21)-C(22)	-101.22(16)	C(26)-C(20)-O(21)-C(22)	83.39(17)
C(20)-O(21)-C(22)-F(24)	171.43(12)	C(20)-O(21)-C(22)-F(25)	-69.32(17)
C(20)-O(21)-C(22)-F(23)	51.74(17)	C(19)-C(20)-C(26)-C(27)	-0.1(2)
O(21)-C(20)-C(26)-C(27)	175.14(13)	C(20)-C(26)-C(27)-C(17)	-0.4(2)
C(18)-C(17)-C(27)-C(26)	0.8(2)	N(9)-C(17)-C(27)-C(26)	-178.66(13)
C(28)-O(29)-C(30)-C(43)	7.83(19)	C(28)-O(29)-C(30)-C(31)	-171.67(12)
O(29)-C(30)-C(31)-C(32)	177.91(12)	C(43)-C(30)-C(31)-C(32)	-1.6(2)
C(30)-C(31)-C(32)-C(33)	0.5(2)	C(31)-C(32)-C(33)-C(42)	0.69(19)
C(31)-C(32)-C(33)-C(34)	-179.79(12)	C(42)-C(33)-C(34)-N(35)	178.38(12)
C(32)-C(33)-C(34)-N(35)	-1.1(2)	C(42)-C(33)-C(34)-C(39)	-1.05(17)
C(32)-C(33)-C(34)-C(39)	179.43(12)	C(39)-C(34)-N(35)-N(36)	-0.06(14)
C(33)-C(34)-N(35)-N(36)	-179.52(12)	C(34)-N(35)-N(36)-C(37)	0.59(14)
C(34)-N(35)-N(36)-C(44)	173.56(11)	N(35)-N(36)-C(37)-O(38)	178.09(11)
C(44)-N(36)-C(37)-O(38)	6.0(2)	N(35)-N(36)-C(37)-C(39)	-0.84(14)
C(44)-N(36)-C(37)-C(39)	-172.90(12)	N(35)-C(34)-C(39)-C(40)	-178.50(12)
C(33)-C(34)-C(39)-C(40)	1.01(18)	N(35)-C(34)-C(39)-C(37)	-0.44(15)
C(33)-C(34)-C(39)-C(37)	179.07(11)	O(38)-C(37)-C(39)-C(40)	-0.4(3)
N(36)-C(37)-C(39)-C(40)	178.42(14)	O(38)-C(37)-C(39)-C(34)	-178.09(13)
N(36)-C(37)-C(39)-C(34)	0.74(13)	C(34)-C(39)-C(40)-N(41)	-0.35(19)
C(37)-C(39)-C(40)-N(41)	-177.76(13)	C(39)-C(40)-N(41)-C(42)	-0.27(19)

Table 43: (continued).

C(40)-N(41)-C(42)-C(43)	-179.01(12)	C(40)-N(41)-C(42)-C(33)	0.20(18)
C(32)-C(33)-C(42)-N(41)	-179.98(11)	C(34)-C(33)-C(42)-N(41)	0.47(18)
C(32)-C(33)-C(42)-C(43)	-0.79(19)	C(34)-C(33)-C(42)-C(43)	179.66(12)
O(29)-C(30)-C(43)-C(42)	-177.97(12)	C(31)-C(30)-C(43)-C(42)	1.50(19)
N(41)-C(42)-C(43)-C(30)	178.90(11)	C(33)-C(42)-C(43)-C(30)	-0.30(19)
C(37)-N(36)-C(44)-C(45)	-20.5(2)	N(35)-N(36)-C(44)-C(45)	167.67(11)
C(37)-N(36)-C(44)-C(54)	159.18(13)	N(35)-N(36)-C(44)-C(54)	-12.62(17)
C(54)-C(44)-C(45)-C(46)	-2.5(2)	N(36)-C(44)-C(45)-C(46)	177.16(12)
C(44)-C(45)-C(46)-C(47)	1.0(2)	C(45)-C(46)-C(47)-C(53)	1.5(2)
C(45)-C(46)-C(47)-O(48)	177.34(12)	C(53)-C(47)-O(48)-C(49)	-88.45(17)
C(46)-C(47)-O(48)-C(49)	95.64(16)	C(47)-O(48)-C(49)-F(51)	-63.21(18)
C(47)-O(48)-C(49)-F(52)	58.13(17)	C(47)-O(48)-C(49)-F(50)	177.48(12)
C(46)-C(47)-C(53)-C(54)	-2.4(2)	O(48)-C(47)-C(53)-C(54)	-178.25(12)
C(47)-C(53)-C(54)-C(44)	0.8(2)	C(45)-C(44)-C(54)-C(53)	1.6(2)
N(36)-C(44)-C(54)-C(53)	-178.07(12)	O(55)-C(56)-C(57)-C(58)	-171.44(12)
C(56)-C(57)-C(58)-C(59)	-171.33(13)		

Table 44: Hydrogen bonds for **DK-IV-20-1 (14o)** [Å and °].

D-H...A	d(D-H)	d(H...A)	d(D...A)	<(DHA)
C(13)-H(13)...N(35)#1	0.95	2.49	3.4197(18)	166.2
N(14)-H(14)...O(38)#2	0.88	1.86	2.7157(15)	164.2
C(27)-H(27)...O(11)	0.95	2.33	2.9108(17)	118.7
C(31)-H(31)...N(8)#3	0.95	2.62	3.3982(18)	139.1
N(41)-H(41)...O(55)	0.88	1.84	2.7171(16)	177.0
C(45)-H(45)...O(38)	0.95	2.32	2.9118(19)	119.5
C(54)-H(54)...O(11)#1	0.95	2.55	3.3237(17)	138.6
O(55)-H(55)...O(11)	0.84	1.88	2.6806(15)	157.8

Symmetry transformations used to generate equivalent atoms:
#1 -x+1,-y,-z+1 #2 x+1,y,z #3 x-1,y-1,z

4.1.4. X-ray Crystal Data for DK-IV-22-1 (14p)

Table 45: Crystal data and structure refinement for **DK-IV-22-1 (14p)**.

Identification code	cook189	
Empirical formula	$C_{18}H_{13}BrF_3N_3O_3$	
Formula weight	456.22	
Temperature	100(2) K	
Wavelength	1.54178 Å	
Crystal system	Triclinic	
Space group	P-1	
Unit cell dimensions	a = 4.6782(5) Å	α= 112.627(8)°.
	b = 13.8511(15) Å	β= 95.564(8)°.
	c = 15.0471(19) Å	γ = 98.999(7)°.
Volume	875.60(18) $Å^3$	
Z	2	
Density (-173ºC)	1.730 Mg/m^3	
Absorption coefficient	3.735 mm^{-1}	
F(000)	456	
Crystal size	0.102 x 0.020 x 0.020 mm^3	
Theta range for data collection	3.230 to 74.646°.	
Index ranges	-5<=h<=4, -16<=k<=13, -14<=l<=15	
Reflections collected	3713	
Independent reflections	2131 [R_{int} = 0.0537]	
Completeness to theta = 67.679°	65.0 %	
Absorption correction	Semi-empirical from equivalents	
Max. and min. transmission	0.7538 and 0.3737	
Refinement method	Full-matrix least-squares on F^2	
Data / restraints / parameters	2131 / 2 / 257	
Goodness-of-fit on F^2	1.077	
Final R indices [I>2sigma(I)]	R_1 = 0.0797, wR_2 = 0.2076	
R indices (all data)	R_1 = 0.0844, wR_2 = 0.2133	
Largest diff. peak and hole	2.030 and -1.518 $e.Å^{-3}$	

Table 46: Atomic coordinates (x 10^4) and equivalent isotropic displacement parameters ($Å^2$x 10^3) for **DK-IV-22-1 (14p)**. U(eq) is defined as one third of the trace of the orthogonalized U^{ij} tensor.

	x	y	z	U(eq)
Br(1)	-7461(2)	331(1)	1257(1)	33(1)
C(2)	-4288(15)	1504(5)	1570(6)	24(2)
C(3)	-2500(15)	1915(6)	2474(6)	28(2)
C(4)	-77(16)	2728(6)	2678(6)	26(2)
C(5)	540(15)	3156(6)	2016(6)	25(2)
C(6)	3015(15)	3990(6)	2138(6)	25(2)
N(7)	5146(12)	4483(5)	2901(5)	24(2)
C(9)	5938(16)	5196(6)	1757(6)	24(2)
N(8)	6940(12)	5215(5)	2640(5)	23(2)
O(10)	7106(11)	5778(4)	1370(4)	29(1)
C(11)	3304(16)	4373(6)	1397(6)	24(2)
C(12)	1322(16)	3953(6)	548(6)	25(2)
N(13)	-944(13)	3170(5)	407(5)	28(2)
C(14)	-1420(16)	2758(6)	1106(6)	25(2)
C(15)	-3828(16)	1913(6)	885(6)	31(2)
C(16)	9481(15)	5900(6)	3341(6)	24(2)
C(17)	11306(16)	6643(6)	3138(7)	33(2)
C(18)	13729(17)	7320(7)	3839(7)	37(2)
C(19)	14261(15)	7253(6)	4722(6)	27(2)
O(20)	16677(12)	7893(4)	5469(4)	36(1)
C(21)	17656(17)	8899(7)	5595(7)	36(2)
F(22)	19664(10)	9371(4)	6399(4)	45(1)
F(23)	19015(13)	8931(5)	4870(4)	72(2)
F(24)	15645(13)	9459(5)	5644(5)	77(2)
C(25)	12476(16)	6504(6)	4922(6)	28(2)
C(26)	10030(17)	5836(6)	4240(6)	30(2)
O(27)	4931(12)	7440(4)	1292(4)	37(2)
C(28)	7100(20)	8366(7)	1875(8)	50(3)

Table 47: Bond lengths [Å] and angles [°] for **DK-IV-22-1 (14p)**.

Br(1)-C(2)	1.893(6)	C(2)-C(15)	1.373(12)
C(2)-C(3)	1.382(11)	C(3)-C(4)	1.384(10)
C(3)-H(3)	0.9500	C(4)-C(5)	1.373(12)
C(4)-H(4)	0.9500	C(5)-C(14)	1.427(11)
C(5)-C(6)	1.444(10)	C(6)-N(7)	1.319(9)
C(6)-C(11)	1.416(12)	N(7)-N(8)	1.411(8)
C(9)-O(10)	1.255(9)	C(9)-N(8)	1.354(11)
C(9)-C(11)	1.438(10)	N(8)-C(16)	1.435(9)
C(11)-C(12)	1.364(11)	C(12)-N(13)	1.329(9)
C(12)-H(12)	0.9500	N(13)-C(14)	1.395(11)
N(13)-H(13)	0.8800	C(14)-C(15)	1.402(10)
C(15)-H(15)	0.9500	C(16)-C(17)	1.378(11
C(16)-C(26)	1.392(12)	C(17)-C(18)	1.397(10)
C(17)-H(17)	0.9500	C(18)-C(19)	1.369(13)
C(18)-H(18)	0.9500	C(19)-C(25)	1.371(11)
C(19)-O(20)	1.414(8)	O(20)-C(21)	1.330(10)
C(21)-F(24)	1.300(10)	C(21)-F(22)	1.323(9)
C(21)-F(23)	1.327(11)	C(25)-C(26)	1.389(10)
C(25)-H(25)	0.9500	C(26)-H(26)	0.9500
O(27)-C(28)	1.413(9)	O(27)-H(27)	0.820(11)
C(28)-H(28A)	0.9800	C(28)-H(28B)	0.9800
C(28)-H(28C)	0.9800		
C(15)-C(2)-C(3)	122.1(6)	C(15)-C(2)-Br(1)	118.7(5)
C(3)-C(2)-Br(1)	119.2(6)	C(2)-C(3)-C(4)	119.0(7)
C(2)-C(3)-H(3)	120.5	C(4)-C(3)-H(3)	120.5
C(5)-C(4)-C(3)	121.7(8)	C(5)-C(4)-H(4)	119.2
C(3)-C(4)-H(4)	119.2	C(4)-C(5)-C(14)	118.4(7)
C(4)-C(5)-C(6)	126.7(7)	C(14)-C(5)-C(6)	114.9(7)
N(7)-C(6)-C(11)	113.0(6)	N(7)-C(6)-C(5)	127.0(7)
C(11)-C(6)-C(5)	120.0(7)	C(6)-N(7)-N(8)	103.4(6)
O(10)-C(9)-N(8)	126.4(6)	O(10)-C(9)-C(11)	129.7(7)
N(8)-C(9)-C(11)	103.9(6)	C(9)-N(8)-N(7)	114.2(6)
C(9)-N(8)-C(16)	128.6(6)	N(7)-N(8)-C(16)	117.1(6)
C(12)-C(11)-C(6)	121.5(7)	C(12)-C(11)-C(9)	132.9(8)
C(6)-C(11)-C(9)	105.6(7)	N(13)-C(12)-C(11)	119.7(7)
N(13)-C(12)-H(12)	120.1	C(11)-C(12)-H(12)	120.1
C(12)-N(13)-C(14)	122.5(7)	C(12)-N(13)-H(13)	118.8
C(14)-N(13)-H(13)	118.8	N(13)-C(14)-C(15)	118.6(7)
N(13)-C(14)-C(5)	121.3(7)	C(15)-C(14)-C(5)	120.1(7)
C(2)-C(15)-C(14)	118.6(7)	C(2)-C(15)-H(15)	120.7
C(14)-C(15)-H(15)	120.7	C(17)-C(16)-C(26)	120.2(7)
C(17)-C(16)-N(8)	120.1(7)	C(26)-C(16)-N(8)	119.6(6)
C(16)-C(17)-C(18)	119.3(8)	C(16)-C(17)-H(17)	120.4

Table 47: (continued).

C(18)-C(17)-H(17)	120.4	C(19)-C(18)-C(17)	120.3(7)
C(19)-C(18)-H(18)	119.9	C(17)-C(18)-H(18)	119.9
C(18)-C(19)-C(25)	120.7(7)	C(18)-C(19)-O(20)	124.2(7)
C(25)-C(19)-O(20)	115.1(7)	C(21)-O(20)-C(19)	119.3(6)
F(24)-C(21)-F(22)	109.8(8)	F(24)-C(21)-F(23)	106.7(8)
F(22)-C(21)-F(23)	106.1(6)	F(24)-C(21)-O(20)	115.0(7)
F(22)-C(21)-O(20)	108.3(7)	F(23)-C(21)-O(20)	110.7(8)
C(19)-C(25)-C(26)	119.9(8)	C(19)-C(25)-H(25)	120.1
C(26)-C(25)-H(25)	120.1	C(25)-C(26)-C(16)	119.7(7)
C(25)-C(26)-H(26)	120.2	C(16)-C(26)-H(26)	120.2
C(28)-O(27)-H(27)	113(2)	O(27)-C(28)-H(28A)	109.5
O(27)-C(28)-H(28B)	109.5	H(28A)-C(28)-H(28B)	109.5
O(27)-C(28)-H(28C)	109.5	H(28A)-C(28)-H(28C)	109.5
H(28B)-C(28)-H(28C)	109.5		

Table 48: Anisotropic displacement parameters ($Å^2 x\ 10^3$) for **DK-IV-22-1 (14p)**. The anisotropic displacement factor exponent takes the form: $-2\pi^2[h^2 a^{*2} U^{11} + ... + 2\ h\ k\ a^*\ b^*\ U^{12}]$

	U^{11}	U^{22}	U^{33}	U^{23}	U^{13}	U^{12}
Br(1)	35(1)	23(1)	34(1)	7(1)	1(1)	2(1)
C(2)	31(3)	16(3)	20(5)	7(4)	-1(3)	-3(3)
C(3)	31(3)	26(4)	30(5)	14(4)	9(3)	7(3)
C(4)	34(4)	21(4)	21(5)	6(4)	3(3)	9(3)
C(5)	32(3)	19(4)	17(5)	0(4)	6(3)	7(3)
C(6)	33(3)	21(4)	19(5)	4(4)	8(3)	11(3)
N(7)	31(3)	21(3)	20(4)	9(3)	2(3)	2(2)
C(9)	33(3)	20(4)	20(5)	7(4)	8(3)	7(3)
N(8)	31(3)	18(3)	20(4)	8(3)	6(3)	5(2)
O(10)	43(3)	25(3)	21(3)	10(3)	5(2)	7(2)
C(11)	38(4)	18(4)	17(5)	5(4)	3(3)	14(3)
C(12)	40(4)	22(4)	15(5)	7(4)	8(3)	10(3)
N(13)	36(3)	28(3)	20(4)	10(4)	0(3)	10(3)
C(14)	37(4)	25(4)	17(5)	7(4)	8(3)	17(3)
C(15)	30(3)	18(4)	30(5)	-4(4)	0(3)	7(3)
C(16)	29(3)	22(4)	22(5)	9(4)	6(3)	12(3)
C(17)	35(4)	30(4)	35(6)	16(4)	-2(4)	6(3)
C(18)	36(4)	29(4)	41(6)	13(5)	3(4)	-2(3)
C(19)	34(4)	23(4)	21(5)	9(4)	-3(3)	6(3)
O(20)	45(3)	26(3)	32(4)	13(3)	-10(2)	-2(2)
C(21)	39(4)	28(4)	42(6)	17(5)	-1(4)	5(4)
F(22)	49(3)	32(3)	41(3)	11(3)	-17(2)	-8(2)
F(23)	75(4)	77(4)	47(4)	32(4)	-12(3)	-38(3)
F(24)	60(3)	35(3)	99(5)	-4(3)	-26(3)	15(3)
C(25)	40(4)	26(4)	19(5)	9(4)	2(3)	10(3)
C(26)	39(4)	20(4)	25(5)	3(4)	9(3)	-1(3)
O(27)	48(3)	24(3)	30(4)	5(3)	-9(3)	4(2)
C(28)	59(5)	31(5)	53(7)	21(5)	-10(5)	-6(4)

Table 49: Hydrogen coordinates (x 10^4) and isotropic displacement parameters ($Å^2$x 10^3) for **DK-IV-22-1 (14p)**.

	x	y	z	U(eq)
H(3)	-2927	1643	2949	33
H(4)	1191	2996	3291	31
H(12)	1560	4221	59	30
H(13)	-2191	2900	-148	33
H(15)	-5113	1629	274	37
H(17)	10920	6694	2528	40
H(18)	15014	7828	3703	45
H(25)	12912	6443	5526	34
H(26)	8738	5339	4387	36
H(27)	5550(90)	6886(15)	1150(70)	56
H(28A)	8976	8292	1648	75
H(28B)	7308	8454	2558	75
H(28C)	6507	8994	1824	75

Table 50: Torsion angles [°] for **DK-IV-22-1 (14p)**.

C(15)-C(2)-C(3)-C(4)	-3.4(12)	Br(1)-C(2)-C(3)-C(4)	176.0(6)
C(2)-C(3)-C(4)-C(5)	2.0(12)	C(3)-C(4)-C(5)-C(14)	1.2(12)
C(3)-C(4)-C(5)-C(6)	-178.9(8)	C(4)-C(5)-C(6)-N(7)	0.7(13)
C(14)-C(5)-C(6)-N(7)	-179.4(7)	C(4)-C(5)-C(6)-C(11)	-178.0(7)
C(14)-C(5)-C(6)-C(11)	1.9(11)	C(11)-C(6)-N(7)-N(8)	-0.8(8)
C(5)-C(6)-N(7)-N(8)	-179.7(7)	O(10)-C(9)-N(8)-N(7)	178.8(7)
C(11)-C(9)-N(8)-N(7)	-1.1(9)	O(10)-C(9)-N(8)-C(16)	1.3(13)
C(11)-C(9)-N(8)-C(16)	-178.6(7)	C(6)-N(7)-N(8)-C(9)	1.2(8)
C(6)-N(7)-N(8)-C(16)	179.0(6)	N(7)-C(6)-C(11)-C(12)	179.4(7)
C(5)-C(6)-C(11)-C(12)	-1.6(12)	N(7)-C(6)-C(11)-C(9)	0.2(9)
C(5)-C(6)-C(11)-C(9)	179.1(7)	O(10)-C(9)-C(11)-C(12)	1.6(15)
N(8)-C(9)-C(11)-C(12)	-178.6(8)	O(10)-C(9)-C(11)-C(6)	-179.3(8)
N(8)-C(9)-C(11)-C(6)	0.6(8)	C(6)-C(11)-C(12)-N(13)	0.2(12)
C(9)-C(11)-C(12)-N(13)	179.2(8)	C(11)-C(12)-N(13)-C(14)	0.9(12)
C(12)-N(13)-C(14)-C(15)	-178.4(7)	C(12)-N(13)-C(14)-C(5)	-0.6(12)
C(4)-C(5)-C(14)-N(13)	179.1(7)	C(6)-C(5)-C(14)-N(13)	-0.8(11)
C(4)-C(5)-C(14)-C(15)	-3.1(11)	C(6)-C(5)-C(14)-C(15)	177.0(7)
C(3)-C(2)-C(15)-C(14)	1.5(12)	Br(1)-C(2)-C(15)-C(14)	-177.9(6)
N(13)-C(14)-C(15)-C(2)	179.7(7)	C(5)-C(14)-C(15)-C(2)	1.8(12)
C(9)-N(8)-C(16)-C(17)	-1.7(12)	N(7)-N(8)-C(16)-C(17)	-179.1(7)
C(9)-N(8)-C(16)-C(26)	175.9(8)	N(7)-N(8)-C(16)-C(26)	-1.5(10)
C(26)-C(16)-C(17)-C(18)	0.9(12)	N(8)-C(16)-C(17)-C(18)	178.5(7)
C(16)-C(17)-C(18)-C(19)	-0.8(13)	C(17)-C(18)-C(19)-C(25)	1.8(13)
C(17)-C(18)-C(19)-O(20)	179.1(8)	C(18)-C(19)-O(20)-C(21)	34.7(12)
C(25)-C(19)-O(20)-C(21)	-147.9(8)	C(19)-O(20)-C(21)-F(24)	49.4(12)
C(19)-O(20)-C(21)-F(22)	172.6(7)	C(19)-O(20)-C(21)-F(23)	-71.6(9)
C(18)-C(19)-C(25)-C(26)	-2.8(13)	O(20)-C(19)-C(25)-C(26)	179.7(7)
C(19)-C(25)-C(26)-C(16)	2.8(12)	C(17)-C(16)-C(26)-C(25)	-1.9(12)
N(8)-C(16)-C(26)-C(25)	-179.5(7)		

Table 51: Hydrogen bonds for **DK-IV-22-1 (14p)** [Å and °].

D-H...A	d(D-H)	d(H...A)	d(D...A)	<(DHA)
C(3)-H(3)...F(22)#1	0.95	2.59	3.230(10)	125.0
C(12)-H(12)...O(10)#2	0.95	2.30	3.187(10)	155.7
N(13)-H(13)...O(27)#3	0.88	1.89	2.766(9)	170.4
C(17)-H(17)...O(10)	0.95	2.20	2.859(10)	126.0
C(18)-H(18)...F(23)	0.95	2.31	2.893(9)	119.2
O(27)-H(27)...O(10)	0.820(11)	1.92(4)	2.694(8)	157(10)
C(28)-H(28C)...Br(1)#4	0.98	3.10	4.025(10)	158.5

Symmetry transformations used to generate equivalent atoms:
#1 -x+2,-y+1,-z+1 #2 -x+1,-y+1,-z #3 -x,-y+1,-z
#4 x+1,y+1,z

4.1.5. X-ray Crystal Data for DK-IV-19-1 (14r)

Table 52: Crystal data and structure refinement for **DK-IV-19-1 (14r)**.

Identification code	cook187	
Empirical formula	$C_{19}H_{16}F_3N_3O_3$	
Formula weight	391.35	
Temperature	293(2) K	
Wavelength	1.54178 Å	
Crystal system	Monoclinic	
Space group	$P2_1/n$	
Unit cell dimensions	a = 4.6892(2) Å	α= 90°.
	b = 25.1666(8) Å	β= 95.6743(13)°.
	c = 15.2602(5) Å	γ = 90°.
Volume	1792.05(11) $Å^3$	
Z	4	
Density (20ºC)	1.451 Mg/m^3	
Absorption coefficient	1.036 mm^{-1}	
F(000)	808	
Crystal size	0.604 x 0.103 x 0.084 mm^3	
Theta range for data collection	3.399 to 74.725°.	
Index ranges	-4<=h<=5, -31<=k<=31, -19<=l<=18	
Reflections collected	14451	
Independent reflections	3608 [R_{int} = 0.0422]	
Completeness to theta = 67.679°	99.4 %	
Absorption correction	Semi-empirical from equivalents	
Max. and min. transmission	0.7538 and 0.5722	
Refinement method	Full-matrix least-squares on F^2	
Data / restraints / parameters	3608 / 0 / 257	
Goodness-of-fit on F^2	1.041	
Final R indices [I>2sigma(I)]	R_1 = 0.0465, wR_2 = 0.1326	
R indices (all data)	R_1 = 0.0517, wR_2 = 0.1384	
Largest diff. peak and hole	0.235 and -0.199 $e.Å^{-3}$	

Table 53: Atomic coordinates (x 10^4) and equivalent isotropic displacement parameters ($Å^2$x 10^3) for **DK-IV-19-1 (14r)**. U(eq) is defined as one third of the trace of the orthogonalized U^{ij} tensor.

	x	y	z	U(eq)
C(1)	13656(4)	2815(1)	2208(1)	59(1)
F(2)	12082(3)	2382(1)	2277(1)	86(1)
F(3)	14817(3)	2763(1)	1453(1)	95(1)
F(4)	15805(3)	2780(1)	2841(1)	99(1)
C(5)	11921(3)	3309(1)	2258(1)	51(1)
C(6)	10377(4)	3506(1)	1498(1)	55(1)
C(7)	8511(3)	3922(1)	1555(1)	52(1)
C(8)	8150(3)	4155(1)	2368(1)	44(1)
C(9)	6174(3)	4580(1)	2496(1)	43(1)
N(10)	4362(3)	4809(1)	1907(1)	46(1)
N(11)	2969(3)	5191(1)	2382(1)	44(1)
C(12)	3916(3)	5201(1)	3270(1)	46(1)
O(13)	3021(3)	5504(1)	3835(1)	59(1)
C(14)	6043(3)	4790(1)	3357(1)	45(1)
C(15)	7746(3)	4594(1)	4062(1)	50(1)
N(16)	9552(3)	4198(1)	3946(1)	52(1)
C(17)	9806(3)	3966(1)	3125(1)	46(1)
C(18)	11683(3)	3541(1)	3064(1)	50(1)
C(19)	925(3)	5525(1)	1904(1)	44(1)
C(20)	333(4)	5446(1)	1002(1)	54(1)
C(21)	-1611(4)	5768(1)	520(1)	58(1)
C(22)	-2956(3)	6177(1)	918(1)	51(1)
O(23)	-4751(3)	6487(1)	365(1)	68(1)
C(24)	-6100(5)	6919(1)	739(1)	76(1)
C(25)	-2414(4)	6251(1)	1817(1)	59(1)
C(26)	-485(4)	5924(1)	2309(1)	58(1)
C(27)	6475(10)	6663(1)	4337(2)	141(2)
O(28)	6489(4)	6187(1)	4755(1)	82(1)

Table 54: Bond lengths [Å] and angles [°] for **DK-IV-19-1 (14r)**.

C(1)-F(2)	1.327(2)	C(1)-F(4)	1.328(2)
C(1)-F(3)	1.329(2)	C(1)-C(5)	1.492(2)
C(5)-C(18)	1.376(2)	C(5)-C(6)	1.396(2)
C(6)-C(7)	1.372(2)	C(6)-H(6)	0.9300
C(7)-C(8)	1.397(2)	C(7)-H(7)	0.9300
C(8)-C(17)	1.409(2)	C(8)-C(9)	1.441(2)
C(9)-N(10)	1.3078(19)	C(9)-C(14)	1.4243(18)
N(10)-N(11)	1.4045(17)	N(11)-C(12)	1.3832(17)
N(11)-C(19)	1.4209(19)	C(12)-O(13)	1.2539(18)
C(12)-C(14)	1.434(2)	C(14)-C(15)	1.367(2)
C(15)-N(16)	1.333(2)	C(15)-H(15)	0.9300
N(16)-C(17)	1.3973(19)	N(16)-H(16)	0.8600
C(17)-C(18)	1.394(2)	C(18)-H(18)	0.9300
C(19)-C(26)	1.381(2)	C(19)-C(20)	1.3918(19)
C(20)-C(21)	1.378(2)	C(20)-H(20)	0.9300
C(21)-C(22)	1.379(2)	C(21)-H(21)	0.9300
C(22)-O(23)	1.374(2)	C(22)-C(25)	1.383(2)
O(23)-C(24)	1.406(2)	C(24)-H(24A)	0.9600
C(24)-H(24B)	0.9600	C(24)-H(24C)	0.9600
C(25)-C(26)	1.387(2)	C(25)-H(25)	0.9300
C(26)-H(26)	0.9300	C(27)-O(28)	1.355(3)
C(27)-H(27A)	0.9600	C(27)-H(27B)	0.9600
C(27)-H(27C)	0.9600	O(28)-H(28)	0.89(3)
F(2)-C(1)-F(4)	106.03(16)	F(2)-C(1)-F(3)	105.40(16)
F(4)-C(1)-F(3)	106.11(15)	F(2)-C(1)-C(5)	111.77(14)
F(4)-C(1)-C(5)	113.37(15)	F(3)-C(1)-C(5)	113.51(15)
C(18)-C(5)-C(6)	120.69(15)	C(18)-C(5)-C(1)	119.50(15)
C(6)-C(5)-C(1)	119.62(15)	C(7)-C(6)-C(5)	119.97(14)
C(7)-C(6)-H(6)	120.0	C(5)-C(6)-H(6)	120.0
C(6)-C(7)-C(8)	120.69(14)	C(6)-C(7)-H(7)	119.7
C(8)-C(7)-H(7)	119.7	C(7)-C(8)-C(17)	118.76(14)
C(7)-C(8)-C(9)	124.60(13)	C(17)-C(8)-C(9)	116.64(13)
N(10)-C(9)-C(14)	112.68(13)	N(10)-C(9)-C(8)	128.08(12)
C(14)-C(9)-C(8)	119.23(13)	C(9)-N(10)-N(11)	104.55(11)
C(12)-N(11)-N(10)	113.42(12)	C(12)-N(11)-C(19)	128.78(12)
N(10)-N(11)-C(19)	117.73(11)	O(13)-C(12)-N(11)	126.02(14)
O(13)-C(12)-C(14)	130.63(13)	N(11)-C(12)-C(14)	103.35(12)
C(15)-C(14)-C(9)	121.13(15)	C(15)-C(14)-C(12)	132.87(13)
C(9)-C(14)-C(12)	106.00(12)	N(16)-C(15)-C(14)	119.67(13)
N(16)-C(15)-H(15)	120.2	C(14)-C(15)-H(15)	120.2
C(15)-N(16)-C(17)	122.91(13)	C(15)-N(16)-H(16)	118.5
C(17)-N(16)-H(16)	118.5	C(18)-C(17)-N(16)	119.33(13)
C(18)-C(17)-C(8)	120.26(13)	N(16)-C(17)-C(8)	120.40(14)

Table 54: (continued).

C(5)-C(18)-C(17)	119.55(14)	C(5)-C(18)-H(18)	120.2
C(17)-C(18)-H(18)	120.2	C(26)-C(19)-C(20)	119.29(14)
C(26)-C(19)-N(11)	121.96(13)	C(20)-C(19)-N(11)	118.75(13)
C(21)-C(20)-C(19)	120.02(15)	C(21)-C(20)-H(20)	120.0
C(19)-C(20)-H(20)	120.0	C(20)-C(21)-C(22)	120.78(14)
C(20)-C(21)-H(21)	119.6	C(22)-C(21)-H(21)	119.6
O(23)-C(22)-C(21)	115.60(14)	O(23)-C(22)-C(25)	125.05(15)
C(21)-C(22)-C(25)	119.35(15)	C(22)-O(23)-C(24)	117.53(14)
O(23)-C(24)-H(24A)	109.5	O(23)-C(24)-H(24B)	109.5
H(24A)-C(24)-H(24B)	109.5	O(23)-C(24)-H(24C)	109.5
H(24A)-C(24)-H(24C)	109.5	H(24B)-C(24)-H(24C)	109.5
C(22)-C(25)-C(26)	120.19(16)	C(22)-C(25)-H(25)	119.9
C(26)-C(25)-H(25)	119.9	C(19)-C(26)-C(25)	120.32(14)
C(19)-C(26)-H(26)	119.8	C(25)-C(26)-H(26)	119.8
O(28)-C(27)-H(27A)	109.5	O(28)-C(27)-H(27B)	109.5
H(27A)-C(27)-H(27B)	109.5	O(28)-C(27)-H(27C)	109.5
H(27A)-C(27)-H(27C)	109.5	H(27B)-C(27)-H(27C)	109.5
C(27)-O(28)-H(28)	109.5		

Table 55: Anisotropic displacement parameters ($Å^2 x\ 10^3$) for **DK-IV-19-1 (14r)**. The anisotropic displacement factor exponent takes the form: $-2\pi^2[h^2 a^{*2} U^{11} + ... + 2\ h\ k\ a^*\ b^*\ U^{12}]$

	U^{11}	U^{22}	U^{33}	U^{23}	U^{13}	U^{12}
C(1)	59(1)	57(1)	63(1)	-1(1)	8(1)	-3(1)
F(2)	92(1)	54(1)	115(1)	4(1)	19(1)	-9(1)
F(3)	115(1)	83(1)	94(1)	7(1)	50(1)	26(1)
F(4)	84(1)	92(1)	113(1)	-16(1)	-27(1)	29(1)
C(5)	49(1)	51(1)	52(1)	0(1)	7(1)	-7(1)
C(6)	60(1)	63(1)	42(1)	-7(1)	8(1)	-1(1)
C(7)	59(1)	61(1)	35(1)	0(1)	4(1)	0(1)
C(8)	47(1)	51(1)	35(1)	1(1)	4(1)	-8(1)
C(9)	47(1)	50(1)	32(1)	-1(1)	4(1)	-9(1)
N(10)	52(1)	52(1)	32(1)	-3(1)	5(1)	-2(1)
N(11)	53(1)	49(1)	30(1)	-4(1)	4(1)	-4(1)
C(12)	53(1)	53(1)	31(1)	-4(1)	4(1)	-9(1)
O(13)	72(1)	68(1)	35(1)	-13(1)	2(1)	4(1)
C(14)	51(1)	52(1)	32(1)	-3(1)	4(1)	-9(1)
C(15)	58(1)	59(1)	32(1)	-4(1)	2(1)	-6(1)
N(16)	60(1)	62(1)	33(1)	1(1)	-4(1)	-2(1)
C(17)	48(1)	53(1)	36(1)	0(1)	3(1)	-9(1)
C(18)	50(1)	56(1)	44(1)	4(1)	0(1)	-6(1)
C(19)	50(1)	49(1)	33(1)	-1(1)	5(1)	-6(1)
C(20)	74(1)	53(1)	35(1)	-5(1)	3(1)	6(1)
C(21)	78(1)	61(1)	33(1)	-3(1)	1(1)	6(1)
C(22)	58(1)	54(1)	41(1)	2(1)	2(1)	-1(1)
O(23)	87(1)	68(1)	47(1)	0(1)	-3(1)	21(1)
C(24)	86(1)	70(1)	70(1)	-7(1)	-6(1)	21(1)
C(25)	68(1)	65(1)	44(1)	-10(1)	4(1)	11(1)
C(26)	67(1)	69(1)	36(1)	-9(1)	3(1)	6(1)
C(27)	249(5)	74(2)	91(2)	10(1)	-21(2)	-3(2)
O(28)	106(1)	68(1)	64(1)	4(1)	-33(1)	-5(1)

Table 56: Hydrogen coordinates (x 10^4) and isotropic displacement parameters ($Å^2$x 10^3) for **DK-IV-19-1 (14r)**.

	x	y	z	U(eq)
H(6)	10613	3355	953	66
H(7)	7475	4050	1048	62
H(15)	7646	4738	4620	60
H(16)	10607	4078	4396	63
H(18)	12766	3416	3564	60
H(20)	1251	5175	724	65
H(21)	-2022	5709	-81	69
H(24A)	-4673	7155	1015	114
H(24B)	-7287	6790	1171	114
H(24C)	-7262	7106	286	114
H(25)	-3346	6521	2093	71
H(26)	-140	5974	2914	69
H(27A)	4902	6873	4499	211
H(27B)	6270	6607	3712	211
H(27C)	8243	6845	4504	211
H(28)	5280(70)	5968(9)	4454(15)	123

Table 57: Torsion angles [°] for **DK-IV-19-1 (14r)**.

F(2)-C(1)-C(5)-C(18)	90.07(19)	F(4)-C(1)-C(5)-C(18)	-29.7(2)
F(3)-C(1)-C(5)-C(18)	-150.87(16)	F(2)-C(1)-C(5)-C(6)	-84.8(2)
F(4)-C(1)-C(5)-C(6)	155.40(16)	F(3)-C(1)-C(5)-C(6)	34.2(2)
C(18)-C(5)-C(6)-C(7)	-2.7(2)	C(1)-C(5)-C(6)-C(7)	172.19(15)
C(5)-C(6)-C(7)-C(8)	0.5(3)	C(6)-C(7)-C(8)-C(17)	2.0(2)
C(6)-C(7)-C(8)-C(9)	-177.81(14)	C(7)-C(8)-C(9)-N(10)	2.0(2)
C(17)-C(8)-C(9)-N(10)	-177.77(14)	C(7)-C(8)-C(9)-C(14)	-178.88(14)
C(17)-C(8)-C(9)-C(14)	1.3(2)	C(14)-C(9)-N(10)-N(11)	0.51(16)
C(8)-C(9)-N(10)-N(11)	179.64(13)	C(9)-N(10)-N(11)-C(12)	0.08(16)
C(9)-N(10)-N(11)-C(19)	177.34(12)	N(10)-N(11)-C(12)-O(13)	-179.91(14)
C(19)-N(11)-C(12)-O(13)	3.2(2)	N(10)-N(11)-C(12)-C(14)	-0.60(16)
C(19)-N(11)-C(12)-C(14)	-177.49(13)	N(10)-C(9)-C(14)-C(15)	178.90(14)
C(8)-C(9)-C(14)-C(15)	-0.3(2)	N(10)-C(9)-C(14)-C(12)	-0.89(17)
C(8)-C(9)-C(14)-C(12)	179.90(12)	O(13)-C(12)-C(14)-C(15)	0.4(3)
N(11)-C(12)-C(14)-C(15)	-178.91(16)	O(13)-C(12)-C(14)-C(9)	-179.89(15)
N(11)-C(12)-C(14)-C(9)	0.84(15)	C(9)-C(14)-C(15)-N(16)	-0.4(2)
C(12)-C(14)-C(15)-N(16)	179.31(15)	C(14)-C(15)-N(16)-C(17)	0.1(2)
C(15)-N(16)-C(17)-C(18)	-178.01(14)	C(15)-N(16)-C(17)-C(8)	1.0(2)
C(7)-C(8)-C(17)-C(18)	-2.5(2)	C(9)-C(8)-C(17)-C(18)	177.36(13)
C(7)-C(8)-C(17)-N(16)	178.53(14)	C(9)-C(8)-C(17)-N(16)	-1.6(2)
C(6)-C(5)-C(18)-C(17)	2.2(2)	C(1)-C(5)-C(18)-C(17)	-172.68(14)
N(16)-C(17)-C(18)-C(5)	179.41(14)	C(8)-C(17)-C(18)-C(5)	0.4(2)
C(12)-N(11)-C(19)-C(26)	-1.1(2)	N(10)-N(11)-C(19)-C(26)	-177.83(14)
C(12)-N(11)-C(19)-C(20)	179.00(15)	N(10)-N(11)-C(19)-C(20)	2.2(2)
C(26)-C(19)-C(20)-C(21)	0.9(3)	N(11)-C(19)-C(20)-C(21)	-179.16(15)
C(19)-C(20)-C(21)-C(22)	1.1(3)	C(20)-C(21)-C(22)-O(23)	177.15(16)
C(20)-C(21)-C(22)-C(25)	-2.3(3)	C(21)-C(22)-O(23)-C(24)	-178.11(17)
C(25)-C(22)-O(23)-C(24)	1.3(3)	O(23)-C(22)-C(25)-C(26)	-177.90(17)
C(21)-C(22)-C(25)-C(26)	1.5(3)	C(20)-C(19)-C(26)-C(25)	-1.7(3)
N(11)-C(19)-C(26)-C(25)	178.36(16)	C(22)-C(25)-C(26)-C(19)	0.5(3)

Table 58: Hydrogen bonds for **DK-IV-19-1 (14r)** [Å and °].

D-H...A	d(D-H)	d(H...A)	d(D...A)	<(DHA)
C(15)-H(15)...O(13)#1	0.93	2.48	3.2739(17)	142.8
N(16)-H(16)...O(28)#2	0.86	1.91	2.7550(18)	169.0
C(26)-H(26)...O(13)	0.93	2.27	2.913(2)	125.7
O(28)-H(28)...O(13)	0.89	1.78	2.6686(18)	176.5

Symmetry transformations used to generate equivalent atoms:
#1 -x+1,-y+1,-z+1 #2 -x+2,-y+1,-z+1

4.2. Primary Radioligand Binding Assays for Synthesized Pyrazoloquinolinones (PQ's)

Table 59: Primary Radioligand Binding Assays. Compound-induced radioligand displacement assays for 46 receptors, transporters and channels conducted by the National Institute of Medical Health Psychoactive Drugs Screening Program (B. Roth et al., UNC, available at http://pdsp.med.unc.edu).[a]

Compound	Serotonin 5-HT$_{1A}$	Serotonin 5-HT$_{1B}$	Serotonin 5-HT$_{1D}$	Serotonin 5-HT$_{1E}$	Serotonin 5-HT$_{2A}$	Serotonin 5-HT$_{2B}$
Radioligand	[^{3}H]8-OH-DPAT	[^{3}H]GR127543	[^{3}H]GR127543	[^{3}H]5-HT	[^{3}H]Ketanserin	[^{3}H]LSD
8a[p]	9.7	12	27.5	1.3	12.8	28.6
8b[b,p]	-5.4	21.6	11.3	0	-2.8	46.3
8c[b,p]	11.1	22.8	28	-16.5	0.4	37.9
8d[b,p]	0.7	25.5	23.5	-18.9	1.2	47
8e[b,m]	-13.7	1.8	2.4	-4.2	-5.2	22.6
8f[b,o]	-6	-4.2	-10.2	-7.8	-13.7	21
8g[b,m]	-2.1	-8.2	-8.4	7.2	2.7	15.9
8h[b,o]	0.3	-8.6	-9.2	-0.8	-11.8	20.1
13a[b,e]	-2.6	-5	11.2	-1.5	3.5	25.6
13b[b,e]	-5.7	4.1	-1.4	1.8	-6.8	8
13c[b,e]	-0.7	-4.1	0.3	8.6	0.2	48.7
13i[b,e]	1.5	-4	-3.6	-5.1	5.9	27.3
8i[m]	-1.3	-14.8	5.6	1	12.2	8.3
8j[c,m]	-15.8	-8.5	-6.5	-5.4	-2.5	37.7
8l[c,p]	7.4	8	13.7	-11.3	-1.4	49.9
8m[c,o]	-8.2	-12.8	-10.2	9.1	-1.5	9.9
13e[c,e]	8.9	2.4	4.9	-1.3	9.4	37.1
13f[c,e]	-1.3	2.6	-8.3	-24.2	-11.1	3.9
8n[p]	-16.1	1.4	4.5	-1	5.7	15.3
8o[d,p]	1.8	9.7	6.5	-9.7	-2.6	**72.2**
8p[d,m]	-6.3	-9.5	-9.1	-3.5	-8.8	23.6
8q[d,o]	32.6	6.9	-11.7	-9.9	-15.5	45.5
13g[d,e]	2.7	-5.3	0.9	-25.2	-5.5	13.4
13h[d,e]	-10.7	-2.8	-5.9	-29.3	-6.4	23
8r[p]	33.8	13.1	5.9	1.4	-1.9	28.8
8s[m]	6.6	-0.1	3.1	-3.3	1.8	21
8t[o]	3.2	-8.6	-5.1	5.6	0.8	9

[a]Data are the percent inhibition induced by 10 μM of each respective compound on the specific binding at the screened target. The higher the number the more the radioligand was displaced. The number higher than 50% inhibition is considered meaningful and is shown in **bold** and highlighted. [b]**8a** related analogs in **red**. [c]**8i** related analogs in **blue**. [d]**8n** related analogs in **green**. [e]"A-ring" or "D-ring" N-hetero analogs. [f]BZP = benzodiazepine, DOR = δ-opioid receptor, KOR = κ-opioid receptor, MOR = μ-opioid receptor. [o]D-ring "*ortho*". [m]D-ring "*meta*". [p]D-ring "*para*".

Table 59: Primary Radioligand Binding Assays. Compound-induced radioligand displacement assays for 46 receptors, transporters and channels conducted by the National Institute of Medical Health Psychoactive Drugs Screening Program (B. Roth et al., UNC, available at http://pdsp.med.unc.edu).[a]

Compound	Serotonin 5-HT$_{2C}$	Serotonin 5-HT$_3$	Serotonin 5-HT$_{5a}$	Serotonin 5-HT$_6$	Serotonin 5-HT$_7$	Adrenergic α_{1A}
Radioligand	[^{3}H]Mesulergine	[^{3}H]LY278584	[^{3}H]LSD	[^{3}H]LSD	[^{3}H]LSD	[^{3}H]Prazosin
8a[p]	36.2	33.4	5.8	24.5	**78.6**	-14.2
8b[b,p]	7.8	14.6	3.9	2.4	**60.2**	-3.6
8c[b,p]	37.5	35.4	31.2	23.3	**69**	-1.9
8d[b,p]	7.1	21.3	20.2	1.4	**74.4**	-4.4
8e[b,m]	-3.6	14.4	-14.9	1.5	34.7	-20.1
8f[b,o]	-3.3	1.9	-4.1	-13.3	20.8	19.7
8g[b,m]	-14.6	8.1	-11.6	-9.3	-4.8	-17.9
8h[b,o]	-5.8	-8.4	-19.5	0.6	13.2	0
13a[b,e]	5.2	1.8	6.2	11.5	22.4	-18.9
13b[b,e]	-1.4	-6.3	-16.5	-3.8	15.6	-13.6
13c[b,e]	5	-7.4	-12.1	13	26.5	-7.9
13i[b,e]	5.6	10.4	-10.5	9.6	32.7	-9.2
8i[m]	10.3	24.2	-2.8	13.5	41.7	-9.6
8j[c,m]	-3.7	3.1	-9.1	1.9	20.7	-16.8
8l[c,p]	10.1	22.5	21.1	1.1	12.8	-6.8
8m[c,o]	-1.9	-6.4	-9.7	-7.1	0.4	-6.9
13e[c,e]	5.8	6.2	8.7	15.2	6.5	-6.9
13f[c,e]	-7.5	15.9	-7	-4.7	6.3	5.7
8n[p]	4.9	20.9	-0.4	10.4	**61.5**	-9.7
8o[d,p]	13.9	9.7	13.5	0.2	**54.6**	-6.9
8p[d,m]	-0.8	1.8	-10.2	-8.7	12.6	5.7
8q[d,o]	**73.8**	43.8	3	-16.4	15.9	2.5
13g[d,e]	**67.9**	-14.9	-14	-6.9	-13.7	-12.1
13h[d,e]	7.9	18.9	-1.5	-5.3	30.6	2.7
8r[p]	**76.4**	45.8	18.1	13.4	20.1	-20.1
8s[m]	0	-4.8	11.6	3.9	-4.3	-14.2
8t[o]	-0.3	5.7	11.2	6.9	1.1	-25.1

[a]Data are the percent inhibition induced by 10 μM of each respective compound on the specific binding at the screened target. The higher the number the more the radioligand was displaced. The number higher than 50% inhibition is considered meaningful and is shown in **bold** and highlighted. [b]**8a** related analogs in **red**. [c]**8i** related analogs in **blue**. [d]**8n** related analogs in **green**. [e]"A-ring" or "D-ring" N-hetero analogs. [f]BZP = benzodiazepine, DOR = δ-opioid receptor, KOR = κ-opioid receptor, MOR = μ-opioid receptor. [o]D-ring "*ortho*". [m]D-ring "*meta*". [p]D-ring "*para*".

Table 59: Primary Radioligand Binding Assays. Compound-induced radioligand displacement assays for 46 receptors, transporters and channels conducted by the National Institute of Medical Health Psychoactive Drugs Screening Program (B. Roth et al., UNC, available at http://pdsp.med.unc.edu).[a]

Compound	Adrenergic α_{2B}	Adrenergic α_{1D}	Adrenergic α_{2A}	Adrenergic α_{2B}	Adrenergic α_{2C}	Adrenergic β_1
Radioligand	**[^{3}H]Prazosin**	**[^{3}H]Clonidine**	**[^{3}H]Clonidine**	**[^{3}H]Clonidine**	**[^{3}H]Clonidine**	**[^{125}I]Iodopindolol**
8a[p]	11.9	-3.2	-8.7	6.4	2.6	-10.4
8b[b,p]	30.9	8.8	9.6	6.4	19.8	-7.8
8c[b,p]	20.8	16	18.7	18.9	26.4	-2.7
8d[b,p]	24.2	14.3	31.1	9.2	26.7	21.5
8e[b,m]	17.8	0.2	-4.8	6.8	0.5	-9.1
8f[b,o]	36.9	-3.3	16.3	3.3	17.5	-16.9
8g[b,m]	21.2	-1.6	-13.4	-30.3	-7.1	-15.8
8h[b,o]	31.6	-4.6	11	17.3	14.9	-4.7
13a[b,e]	37.8	3	-3.4	23.4	-7.5	2
13b[b,e]	14.7	-17	-102.5	-21.5	-48.2	-12.1
13c[b,e]	13.3	5.6	10.4	20	17	-16.2
13i[b,e]	8	9.2	14.6	33	10	-13.6
8i[m]	24.6	-3.9	-0.7	-5.7	5.5	7.7
8j[c,m]	23.6	-18.1	-7.9	-1.1	1.7	11.4
8l[c,p]	25	2.8	23.6	14.2	18.6	-3.4
8m[c,o]	26.5	-2.8	18.1	-2.3	20	1.6
13e[c,e]	22.7	11.7	6.4	37.1	13	44.1
13f[c,e]	39.4	-13.2	-6.3	19.5	-7.2	-13.6
8n[p]	25.1	-7.8	10.7	9.9	-7.1	-7.3
8o[d,p]	21.7	15.1	26.6	4.8	22.8	-6.6
8p[d,m]	39.4	-13.2	-6.3	19.5	-7.2	-13.6
8q[d,o]	25.9	1.8	18.9	11.7	17.5	-4.4
13g[d,e]	14.6	-14.1	-123.2	-37.9	14.3	7.3
13h[d,e]	12.6	9.6	-129.3	7.2	3.9	-16.7
8r[p]	5.4	0.4	-19.1	-1.4	-1.2	1
8s[m]	1	12.9	-17.6	-6.8	4.4	-10.2
8t[o]	11.4	4.9	-6.5	8.5	-0.1	1.7

[a]Data are the percent inhibition induced by 10 μM of each respective compound on the specific binding at the screened target. The higher the number the more the radioligand was displaced. The number higher than 50% inhibition is considered meaningful and is shown in **bold** and highlighted. [b]**8a** related analogs in **red**. [c]**8i** related analogs in **blue**. [d]**8n** related analogs in **green**. [e]"A-ring" or "D-ring" N-hetero analogs. [f]BZP = benzodiazepine, DOR = δ-opioid receptor, KOR = κ-opioid receptor, MOR = μ-opioid receptor. [o]D-ring "*ortho*". [m]D-ring "*meta*". [p]D-ring "*para*".

Table 59: Primary Radioligand Binding Assays. Compound-induced radioligand displacement assays for 46 receptors, transporters and channels conducted by the National Institute of Medical Health Psychoactive Drugs Screening Program (B. Roth et al., UNC, available at http://pdsp.med.unc.edu).[a]

Compound	Adrenergic β2	Adrenergic β3	BZP[f] Rat Brain Site	Dopamine D1	Dopamine D2	Dopamine D3
Radioligand	**[125I]Iodopindolol**	**[125I]Iodopindolol**	**[3H]Flunitrazepam**	**[3H]-SCH233930**	**[3H]-N-methyl-spiperone**	**[3H]-N-methyl-spiperone**
8a[p]	6.9	4	**92.4**	-0.1	-20.8	3.2
8b[b,p]	-19.7	-5.7	**96.2**	-17.8	-16.5	-7.4
8c[b,p]	-9.5	-19	**96.7**	13.5	-5	-5.8
8d[b,p]	8.6	-9.3	**94.5**	5.7	-18.3	-7.7
8e[b,m]	3.9	-11.6	**95**	10.1	-4.9	-1.3
8f[b,o]	-3.3	-7.3	**80.5**	-6.2	-3.9	13.8
8g[b,m]	7.4	-18.7	**99.3**	17.4	11.3	-10
8h[b,o]	1.4	-17.5	41.3	-2.4	-16	-5
13a[b,e]	-4.2	-6.3	**91.3**	6.1	-9	7.9
13b[b,e]	-6.3	-13.6	**93.7**	-15.2	9.5	5.5
13c[b,e]	3.4	-5.7	**98.2**	-3.9	-14.9	-3.6
13i[b,e]	7	-7.1	**96.9**	12.7	-3.1	0.6
8i[m]	12.6	-9.3	**94.1**	-12.1	-15.1	-5.1
8j[c,m]	-4.1	-3.6	**96.3**	4.2	-18.1	3.1
8l[c,p]	-8.7	5.2	**95**	-5.1	-11.2	-11.2
8m[c,o]	-8	-15.2	**88.7**	-16.2	-11.2	-3.3
13e[c,e]	-3.9	-2.7	**100.6**	-0.4	-2.6	7.2
13f[c,e]	5.3	-2.7	**95.6**	-1.8	15.1	16.6
8n[p]	1.7	-9.6	**93.2**	-1.8	-12.4	-0.8
8o[d,p]	-10.3	-19.7	**97.4**	-0.7	-14.4	-6.6
8p[d,m]	5.3	-2.7	**95.6**	-0.1	-13.8	6.3
8q[d,o]	-9.1	-23.3	42.2	11.9	-24.2	11.9
13g[d,e]	-17.8	9.8	**101.4**	2.2	19.1	-5.6
13h[d,e]	-5.1	-1.1	**93.3**	10.5	3.9	10.8
8r[p]	11.7	0.7	**91.5**	0	-19	8.6
8s[m]	4.5	1.9	**96.7**	-1.4	-2.9	-2.8
8t[o]	-9.9	5.9	**78**	-2.5	-11	7.6

[a]Data are the percent inhibition induced by 10 μM of each respective compound on the specific binding at the screened target. The higher the number the more the radioligand was displaced. The number higher than 50% inhibition is considered meaningful and is shown in **bold** and highlighted. [b]**8a** related analogs in **red**. [c]**8i** related analogs in **blue**. [d]**8n** related analogs in **green**. [e]"A-ring" or "D-ring" N-hetero analogs. [f]BZP = benzodiazepine, DOR = δ-opioid receptor, KOR = κ-opioid receptor, MOR = μ-opioid receptor. [o]D-ring "*ortho*". [m]D-ring "*meta*". [p]D-ring "*para*".

Table 59: Primary Radioligand Binding Assays. Compound-induced radioligand displacement assays for 46 receptors, transporters and channels conducted by the National Institute of Medical Health Psychoactive Drugs Screening Program (B. Roth et al., UNC, available at http://pdsp.med.unc.edu).[a]

Compound	Dopamine D_4	Dopamine D_5	Transporter Dopamine (DAT)	DOR[f]	$GABA_A$	Histamine H_1
Radioligand	[^{3}H]-N-methyl-spiperone	[^{3}H]-SCH233930	[^{3}H]WIN35428	[^{3}H]DADLE	[^{3}H]Muscimol	[^{3}H]Pyrilamine
8a[p]	-0.4	**57.9**	-7.8	10.8	13.1	52.4
8b[b,p]	-0.5	14.7	-6.7	6.3	6.8	48.7
8c[b,p]	5.4	8.5	-14	23.2	8.5	25.5
8d[b,p]	1.4	12.3	-7.7	5.9	2.6	28.9
8e[b,m]	-3	30.9	4.4	3.6	7.6	64.3
8f[b,o]	2.2	14.3	-5.2	28.6	1	14.8
8g[b,m]	-15	12.2	-32.4	9.5	-1.6	41.7
8h[b,o]	2	1.7	-1	-12.3	-5.2	49.8
13a[b,e]	-7.9	4	10.3	26	14.5	57.6
13b[b,e]	-9.5	7.5	12.4	-2.3	-9.2	48.7
13c[b,e]	-7.3	9	-10.4	-8.2	17.3	62.1
13i[b,e]	1.2	9.2	-9.5	-5.7	9.8	74.7
8i[m]	-6.7	44.9	5.3	-0.1	-0.5	64.7
8j[c,m]	-0.5	23.2	0.9	14.3	-2.9	56.2
8l[c,p]	-6.7	9	2	**50.8**	7.5	38.9
8m[c,o]	-4.1	-1.9	-7.1	0.2	-3.2	27.9
13e[c,e]	5.9	4.9	-1	**72.4**	18.5	51.9
13f[c,e]	5.4	-3.9	5.2	**58.6**	24.5	-12
8n[p]	3.7	40.8	2.8	-1	-9.9	71.8
8o[d,p]	1	17	-3.5	14.1	9.2	55.9
8p[d,m]	1.4	21.8	2.5	0.6	-4.8	31.4
8q[d,o]	-6.9	10	-9.2	-16.9	-3.1	37.8
13g[d,e]	2	0.1	-10.9	47.7	45.5	44.4
13h[d,e]	17.9	1.8	-12	20.1	**66.8**	-15
8r[p]	-0.3	**59.1**	5.2	31.4	-15.7	45.1
8s[m]	14.7	4.3	6.7	7.1	2.7	40.5
8t[o]	-0.8	5.7	15.4	-10	2.6	54.1

[a]Data are the percent inhibition induced by 10 μM of each respective compound on the specific binding at the screened target. The higher the number the more the radioligand was displaced. The number higher than 50% inhibition is considered meaningful and is shown in **bold** and highlighted. [b]**8a** related analogs in **red**. [c]**8i** related analogs in **blue**. [d]**8n** related analogs in **green**. [e]"A-ring" or "D-ring" N-hetero analogs. [f]BZP = benzodiazepine, DOR = δ-opioid receptor, KOR = κ-opioid receptor, MOR = μ-opioid receptor. [o]D-ring "*ortho*". [m]D-ring "*meta*". [p]D-ring "*para*".

Table 59: Primary Radioligand Binding Assays. Compound-induced radioligand displacement assays for 46 receptors, transporters and channels conducted by the National Institute of Medical Health Psychoactive Drugs Screening Program (B. Roth et al., UNC, available at http://pdsp.med.unc.edu).[a]

Compound	Histamine H_2	Histamine H_3	Histamine H_4	hERG binding	KOR[f]	Muscarinic M_1
Radioligand	[^{3}H]Tiotidine	[^{3}H]alpha-methylhistamine	[^{3}H]Histamine	N/A	[^{3}H]U69593	[^{3}H]QNB
8a[p]	-1.4	-1.5	-12.2	7.4	7.1	20.6
8b[b,p]	20.8	-1.3	-5.9	-0.1	11.9	8.5
8c[b,p]	-0.7	-3	0.6	6.9	22.8	16.9
8d[b,p]	-2.6	-6.3	13.2	8.7	10.1	17.6
8e[b,m]	23	-2	0.2	5.2	1.8	0
8f[b,o]	-5	2.4	1.3	-29.3	26.3	19.1
8g[b,m]	-1.5	-2.9	-9.7	-5.4	20.5	-7
8h[b,o]	-6.5	2.9	-9.9	-1	23.5	5.2
13a[b,e]	-1.8	10.9	-1.1	5.1	8.5	-19.5
13b[b,e]	1.5	11.7	-8.4	6.4	-4.7	-8
13c[b,e]	23.5	12	1.1	8.6	8.6	-0.8
13i[b,e]	24.1	32	-0.5	9.1	20.3	-1.2
8i[m]	7.5	3.9	-4.6	0.1	10.2	4.5
8j[c,m]	-0.5	2	0	-16.1	-3.8	-8.1
8l[c,p]	2.4	-9	-8.9	-2.5	15.9	-0.1
8m[c,o]	-12.1	-1.9	-7.8	-1.9	21.4	8
13e[c,e]	10.2	6.3	3.8	-1.2	21.2	9.3
13f[c,e]	7.7	-11	7.9	8.1	-2.1	-5.6
8n[p]	8.5	-4.6	-3.1	-2.7	14.5	3.9
8o[d,p]	13.8	2.6	13.8	8.8	26.5	5.6
8p[d,m]	-4.1	0.5	1.5	-15.1	1.2	18.2
8q[d,o]	-0.4	-4.7	-11.1	-4.1	30.9	-5.8
13g[d,e]	-7.4	-1.7	2.3	0.3	-3.8	-4.1
13h[d,e]	31.4	-10	-0.1	-10.3	-8.1	-9.3
8r[p]	-3.3	26.5	18.7	17.8	8.9	-4.5
8s[m]	-3.3	12.8	-5.3	4.6	4.7	-4.8
8t[o]	0.2	16.7	26.8	31.3	9.1	-1.7

[a]Data are the percent inhibition induced by 10 μM of each respective compound on the specific binding at the screened target. The higher the number the more the radioligand was displaced. The number higher than 50% inhibition is considered meaningful and is shown in **bold** and highlighted. [b]**8a** related analogs in **red**. [c]**8i** related analogs in **blue**. [d]**8n** related analogs in **green**. [e]"A-ring" or "D-ring" N-hetero analogs. [f]BZP = benzodiazepine, DOR = δ-opioid receptor, KOR = κ-opioid receptor, MOR = μ-opioid receptor. [o]D-ring "*ortho*". [m]D-ring "*meta*". [p]D-ring "*para*".

Table 59: Primary Radioligand Binding Assays. Compound-induced radioligand displacement assays for 46 receptors, transporters and channels conducted by the National Institute of Medical Health Psychoactive Drugs Screening Program (B. Roth et al., UNC, available at http://pdsp.med.unc.edu).[a]

Compound	Muscarinic M_2	Muscarinic M_3	Muscarinic M_4	Muscarinic M_5	MOR[f]
Radioligand	**[^{3}H]QNB**	**[^{3}H]QNB**	**[^{3}H]QNB**	**[^{3}H]QNB**	**[^{3}H]DAMGO**
8a[p]	-8.4	-4.5	10.9	-5.4	38.3
8b[b,p]	6	27	19.2	-4.8	**53.1**
8c[b,p]	6.9	13.6	-14	2.1	**50.8**
8d[b,p]	8.4	18.1	9.2	3.9	48.9
8e[b,m]	-2.6	5.2	-0.7	-6.6	3.2
8f[b,o]	15.4	7.3	-7.5	14.8	-11
8g[b,m]	-8.1	-15	-10	4.4	18.5
8h[b,o]	14.9	15.2	-37	-6	18.8
13a[b,e]	-16.6	-20	**53.2**	31.8	5.5
13b[b,e]	-24.1	-20	-12	-29.1	-4.5
13c[b,e]	10	-7.5	7	-13.6	4
13i[b,e]	17.8	-4	7.3	2.9	-1.6
8i[m]	-2.7	-0.3	-1.7	0.1	-0.6
8j[c,m]	2.6	15.2	-3.5	-5.2	-0.2
8l[c,p]	16.2	16.2	21.6	3.5	46.5
8m[c,o]	5.3	21.6	-26	9.4	-6
13e[c,e]	8.8	-16	15.6	48.7	21.4
13f[c,e]	-19.4	13.1	-2	4.3	10.8
8n[p]	-0.2	2.9	1.9	2.3	9.7
8o[d,p]	8	-3.2	31.5	0.1	**57.2**
8p[d,m]	4	6.9	-1.6	25.8	-1.7
8q[d,o]	14	-1.5	-22	-4.8	11.3
13g[d,e]	-17.8	-15	-8.1	-27.1	10.5
13h[d,e]	13.3	-1.1	-4.6	-2.4	24.3
8r[p]	-4.5	-21.3	-11	2.6	1.7
8s[m]	-4.8	-15.1	-13	23.9	5.8
8t[o]	-1.7	-29.7	-19	42.8	17.2

[a]Data are the percent inhibition induced by 10 μM of each respective compound on the specific binding at the screened target. The higher the number the more the radioligand was displaced. The number higher than 50% inhibition is considered meaningful and is shown in **bold** and highlighted. [b]**8a** related analogs in **red**. [c]**8i** related analogs in **blue**. [d]**8n** related analogs in **green**. [e]"A-ring" or "D-ring" N-hetero analogs. [f]BZP = benzodiazepine, DOR = δ-opioid receptor, KOR = κ-opioid receptor, MOR = μ-opioid receptor. [o]D-ring "*ortho*". [m]D-ring "*meta*". [p]D-ring "*para*".

Table 59: Primary Radioligand Binding Assays. Compound-induced radioligand displacement assays for 46 receptors, transporters and channels conducted by the National Institute of Medical Health Psychoactive Drugs Screening Program (B. Roth et al., UNC, available at http://pdsp.med.unc.edu).[a]

Compound	Transporter, Norepinephrine (NET)	Peripheral Benzodiazepine Receptor (PBR)	Transporter, Serotonin (SERT)	Sigma σ_1	Sigma σ_2
Radioligand	**[^{3}H]Nisoxetine**	**[^{3}H]PK11195**	**[^{3}H]Citalopram**	**[^{3}H]Pentazocine**	**[^{3}H]DTG**
8a[p]	18.1	8.1	1.3	-14.2	15.7
8b[b,p]	9.6	8	7.8	20	21.2
8c[b,p]	21.9	7.7	11.4	-5.3	20.7
8d[b,p]	18.8	9.2	16.4	-4.3	22.4
8e[b,m]	6.1	8.2	3.3	-5.1	1
8f[b,o]	25.2	-6.3	13.9	31.4	38.3
8g[b,m]	15	4.8	-12.7	10.6	6
8h[b,o]	39.9	8	27.7	17.5	29.3
13a[b,e]	2.1	-0.4	-6.1	-13.3	12.2
13b[b,e]	1.7	8.7	-20.7	-11.5	3.7
13c[b,e]	5.3	-7.1	6.3	15.6	16.5
13i[b,e]	5.6	9.9	-1.6	39	16.5
8i[m]	27.7	7.3	1.4	-2.7	10.8
8j[c,m]	0.5	12	-1.1	-3.4	-5.7
8l[c,p]	20.5	23	5.8	-5.4	8.8
8m[c,o]	36.6	-1.3	33.7	-7.4	42.2
13e[c,e]	8.6	10.7	-1.9	-1.5	15.1
13f[c,e]	-3.2	16.5	-7.5	-16.2	28.5
8n[p]	21.2	32.8	7.1	-5.3	6.8
8o[d,p]	3.7	42.5	11.2	-0.6	4.9
8p[d,m]	15.9	14	15.2	20	-5.5
8q[d,o]	29.7	8.7	18.6	-10.5	26.7
13g[d,e]	-8.3	2.4	-10	-13.5	15.1
13h[d,e]	-2.8	17.8	-18.5	-7.8	8.8
8r[p]	11.3	20	-6.6	-17.8	11.8
8s[m]	8.5	29.6	-10.9	-14.1	8.3
8t[o]	4.1	5	-6.1	-23.5	15.9

[a]Data are the percent inhibition induced by 10 μM of each respective compound on the specific binding at the screened target. The higher the number the more the radioligand was displaced. The number higher than 50% inhibition is considered meaningful and is shown in **bold** and highlighted. [b]**8a** related analogs in **red**. [c]**8i** related analogs in **blue**. [d]**8n** related analogs in **green**. [e]"A-ring" or "D-ring" N-hetero analogs. [f]BZP = benzodiazepine, DOR = δ-opioid receptor, KOR = κ-opioid receptor, MOR = μ-opioid receptor. [o]D-ring "*ortho*". [m]D-ring "*meta*". [p]D-ring "*para*".

4.3. Secondary Radioligand Binding Assays for Synthesized PQ's

Table 60: Secondary Radioligand Binding Assays. Binding affinity (Ki, nM) values obtained from non-linear regression of radioligand competition binding isotherms. Testing conducted by the National Institute of Medical Health Psychoactive Drugs Screening Program (B. Roth et al., UNC, available at http://pdsp.med.unc.edu).[a]

Compound	Serotonin 5-HT$_{2B}$	Serotonin 5-HT$_{2C}$	Serotonin 5-HT$_{7}$	BZP[f] Rat Brain Site	Dopamine D$_5$
8a[p]	NA	NA	**2599.0**	**2.7**	**10,000**
8b[b,p]	NA	NA	**2039.0**	**2.1**	NA
8c[b,p]	NA	NA	**2616.3**	**2.0**	NA
8d[b,p]	NA	NA	**2371.3**	**2.3**	NA
8e[b,m]	NA	NA	NA	**11.3**	NA
8f[b,o]	NA	NA	NA	**343.3**	NA
8g[b,m]	NA	NA	NA	**32.3**	NA
8h[b,o]	NA	NA	NA	NA	NA
13a[b,e]	NA	NA	NA	**28.3**	NA
13b[b,e]	NA	NA	NA	**21.7**	NA
13c[b,e]	NA	NA	NA	**8.16**	NA
13i[b,e]	NA	NA	NA	**2.6**	NA
8i[m]	NA	NA	NA	**1.4**	NA
8j[c,m]	NA	NA	NA	**1.2**	NA
8l[c,p]	NA	NA	NA	**0.4**	NA
8m[c,o]	NA	NA	NA	**98.0**	NA
13e[c,e]	NA	NA	NA	**2.0**	NA
13f[c,e]	NA	NA	NA	**2.2**	NA
8n[p]	NA	NA	**7603.7**	**12.2**	NA
8o[d,p]	**5193.0**	NA	**5836.3**	**5.5**	NA
8p[d,m]	NA	NA	NA	**50.4**	NA
8q[d,o]	NA	**10,000**	NA	NA	NA
13g[d,e]	NA	**10,000**	NA	**1.8**	NA
13h[d,e]	NA	NA	NA	**6.2**	NA
8r[p]	NA	**10,000**	NA	**0.4**	**10,000**
8s[m]	NA	NA	NA	**1.6**	NA
8t[o]	NA	NA	NA	**205.0**	NA

[a]Ki values are calculated from best fit IC_{50} values using the Cheng-Prusoff equation. Values are an average of n = 3. NA are for compounds/receptors not testing for Primary Screening results of < 50% inhibition (**Table S1**). [b]**8a** related analogs in **red**. [c]**8i** related analogs in **blue**. [d]**8n** related analogs in **green**. [e]"A-ring" or "D-ring" N-hetero analogs. [f]BZP = benzodiazepine, DOR = δ-opioid receptor, KOR = κ-opioid receptor, MOR = μ-opioid receptor. [o]D-ring "*ortho*". [m]D-ring "*meta*". [p]D-ring "*para*".

Table 60: Secondary Radioligand Binding Assays. Binding affinity (Ki, nM) values obtained from non-linear regression of radioligand competition binding isotherms. Testing conducted by the National Institute of Medical Health Psychoactive Drugs Screening Program (B. Roth et al., UNC, available at http://pdsp.med.unc.edu).[a]

Compound	DOR[f]	$GABA_A$	Muscarinic M_4	MOR[f]
8a[p]	NA	NA	NA	NA
8b[b,p]	NA	NA	NA	**3524.3**
8c[b,p]	NA	NA	NA	**4431.0**
8d[b,p]	NA	NA	NA	NA
8e[b,m]	NA	NA	NA	NA
8f[b,o]	NA	NA	NA	NA
8g[b,m]	NA	NA	NA	NA
8h[b,o]	NA	NA	NA	NA
13a[b,e]	NA	NA	**7852.0**	NA
13b[b,e]	NA	NA	NA	NA
13c[b,e]	NA	NA	NA	NA
13i[b,e]	NA	NA	NA	NA
8i[m]	NA	NA	NA	NA
8j[c,m]	NA	NA	NA	NA
8l[c,p]	**3640.7**	NA	NA	NA
8m[c,o]	NA	NA	NA	NA
13e[c,e]	**3820.7**	NA	NA	NA
13f[c,e]	**8499.3**	NA	NA	NA
8n[p]	NA	NA	NA	NA
8o[d,p]	NA	NA	NA	**6663.5**
8p[d,m]	NA	NA	NA	NA
8q[d,o]	NA	NA	NA	NA
13g[d,e]	NA	NA	NA	NA
13h[d,e]	NA	**1458.0**	NA	NA
8r[p]	NA	NA	NA	NA
8s[m]	NA	NA	NA	NA
8t[o]	NA	NA	NA	NA

[a]Ki values are calculated from best fit IC_{50} values using the Cheng-Prusoff equation. Values are an average of n = 3. NA are for compounds/receptors not testing for Primary Screening results of < 50% inhibition (**Table S1**). [b]**8a** related analogs in **red**. [c]**8i** related analogs in **blue**. [d]**8n** related analogs in **green**. [e]"A-ring" or "D-ring" N-hetero analogs. [f]BZP = benzodiazepine, DOR = δ-opioid receptor, KOR = κ-opioid receptor, MOR = μ-opioid receptor. [o]D-ring "*ortho*". [m]D-ring "*meta*". [p]D-ring "*para*".

4.4. Primary Radioligand Binding Assays for Additional PQ Analogs

Table 61: Primary Radioligand Binding Assays for additional PQ ligands. Compound-induced radioligand displacement assays for 46 receptors, transporters and channels conducted by the National Institute of Medical Health Psychoactive Drugs Screening Program (B. Roth et al., UNC, available at http://pdsp.med.unc.edu).[a]

Compound	Serotonin 5-HT$_{1A}$	Serotonin 5-HT$_{1B}$	Serotonin 5-HT$_{1D}$	Serotonin 5-HT$_{1E}$	Serotonin 5-HT$_{2A}$	Serotonin 5-HT$_{2B}$
Radioligand	[^{3}H]8-OH-DPAT	[^{3}H]GR127543	[^{3}H]GR127543	[^{3}H]5-HT	[^{3}H]Ketanserin	[^{3}H]LSD
PZ-II-029	9.7	12	27.5	1.3	12.8	28.6
DK-I-56-1	-5.4	21.6	11.3	0	-2.8	46.3
RV-I-37	22.3	-8.7	14.7	9.7	12.4	8.9
CW-02-073	13.4	10.9	20.7	12.3	16.3	16.5
CW-02-078	13.4	3	15.6	13.6	9.7	8.6
CW-02-079	17	23.9	24.1	17.2	14.2	17.9
CW-02-082	12.7	-0.3	30.3	11	11.8	9.4
MM-I-03	11.6	-16.6	18.5	3	13.8	18.3
MM-I-13	**64**	40.3	**74.5**	**70.1**	39.8	**56.8**
MM-I-18	4.1	14.3	12.7	-15.8	9.3	5.2
MM-I-09	2.4	-3.3	18.6	8.5	6.7	12.9
MM-I-06	10.2	-16.1	9.9	-21	10.5	20.5
MM-I-08	6.4	-11.1	11.2	7.9	12.8	23.6
MM-I-10	15.2	15.6	44.5	21.3	24.9	31.5
MM-I-11	18.1	8.2	31.5	2.7	14.7	18.8
MM-I-12	9.7	8.4	29.7	-3	20.8	**56.5**
DK-IV-19-1	-3.3	6.8	-4	-51.8	-6.1	**50**
DK-IV-20-1	12.4	17.2	17	-37.9	11.6	24.1
DK-IV-22-1	12.1	24.3	10.7	-49.3	4.3	25.8
DK-IV-23-1	19.1	13.9	19.4	-27.1	-7.6	42.9

[a]Data are the percent inhibition induced by 10 μM of each respective compound on the specific binding at the screened target. The higher the number the more the radioligand was displaced. The number higher than 50% inhibition is considered meaningful and is shown in **bold** and highlighted. [b]**6-methyl** related analogs in **red**. [c]**8-bromo-6-fluoro** related analogs in **blue**. [d]**7-trifluoromethyl** related analogs in **green**. [e]New Deutero/Fluoro analogs in **orange**. [f]BZP = benzodiazepine, DOR = δ-opioid receptor, KOR = κ-opioid receptor, MOR = μ-opioid receptor.

Table 61: Primary Radioligand Binding Assays for Additional PQ Ligands. Compound-induced radioligand displacement assays for 46 receptors, transporters and channels conducted by the National Institute of Medical Health Psychoactive Drugs Screening Program (B. Roth et al., UNC, available at http://pdsp.med.unc.edu).[a]

Compound	Serotonin 5-HT$_{2C}$	Serotonin 5-HT$_3$	Serotonin 5-HT$_{5a}$	Serotonin 5-HT$_6$	Serotonin 5-HT$_7$	Adrenergic α_{1A}
Radioligand	**[^{3}H]Mesulergine**	**[^{3}H]LY278584**	**[^{3}H]LSD**	**[^{3}H]LSD**	**[^{3}H]LSD**	**[^{3}H]Prazosin**
PZ-II-029	36.2	33.4	5.8	24.5	**78.6**	-14.2
DK-I-56-1	7.8	14.6	3.9	2.4	**60.2**	-3.6
RV-I-37	5.4	-3.2	15.5	5.1	6.9	-9.5
CW-02-073	11.5	4.5	17.9	11.9	**66.3**	3
CW-02-078	12.1	5.6	4.8	5.7	21.4	0.6
CW-02-079	15	6.3	14.7	1.8	**72.2**	4.4
CW-02-082	13.6	4.3	9.6	7	-8.6	9.3
MM-I-03	12.3	5.9	15.3	4.2	-17.6	1.2
MM-I-13	25.5	13.1	29.5	41	**59.8**	-5.6
MM-I-18	2.4	9.8	1.6	8.8	-14	-1.2
MM-I-09	5	-0.7	11.2	13.6	-4.4	0.7
MM-I-06	4.1	-2.2	6.3	12.6	38.6	9.9
MM-I-08	7.5	5.8	1.9	23.4	3.5	-4.7
MM-I-10	16.1	-3.4	13.2	-16.8	-6.7	15.1
MM-I-11	-1.8	0.4	0.3	-18.3	11.2	8.4
MM-I-12	16.5	4.5	3	-3.6	9.6	7.8
DK-IV-19-1	5.8	10.1	-4.2	3		-10.5
DK-IV-20-1	26.9	7.8	**63.6**	15.8	**66.1**	-7.2
DK-IV-22-1	**54.9**	-0.2	**66.9**	23.7	**66.1**	1.8
DK-IV-23-1	-5.1	3.6	33.5	11.5	11.4	-0.6

[a]Data are the percent inhibition induced by 10 μM of each respective compound on the specific binding at the screened target. The higher the number the more the radioligand was displaced. The number higher than 50% inhibition is considered meaningful and is shown in **bold** and highlighted. [b]**6-methyl** related analogs in **red**. [c]**8-bromo-6-fluoro** related analogs in **blue**. [d]**7-trifluoromethyl** related analogs in **green**. [e]New Deutero/Fluoro analogs in **orange**. [f]BZP = benzodiazepine, DOR = δ-opioid receptor, KOR = κ-opioid receptor, MOR = μ-opioid receptor.

Table 61: Primary Radioligand Binding Assays for Additional PQ Ligands. Compound-induced radioligand displacement assays for 46 receptors, transporters and channels conducted by the National Institute of Medical Health Psychoactive Drugs Screening Program (B. Roth et al., UNC, available at http://pdsp.med.unc.edu).[a]

Compound	Adrenergic α_{1B}	Adrenergic α_{1D}	Adrenergic α_{2A}	Adrenergic α_{2B}	Adrenergic α_{2C}	Adrenergic β_1
Radioligand	**[^{3}H]Prazosin**	**[^{3}H]Clonidine**	**[^{3}H]Clonidine**	**[^{3}H]Clonidine**	**[^{3}H]Clonidine**	**[^{125}I]Iodopindolol**
PZ-II-029	11.9	-3.2	-8.7	6.4	2.6	-10.4
DK-I-56-1	30.9	8.8	9.6	6.4	19.8	-7.8
RV-I-37	11.3	-1.6	15.1	15.3	-5.8	-11.3
CW-02-073	22.8	-2.1	5	7.4	8.5	-12
CW-02-078	23.2	-6.1	4.3	5.3	-6.8	-16.2
CW-02-079	31	-3.9	12.4	6.9	12.6	1.1
CW-02-082	18	-4	0.3	-8.2	-6.8	-16.2
MM-I-03	22.9	-0.6	3.7	-5.1	-6.2	-5.5
MM-I-13	41.9	-6.5	16.6	-0.2	5.7	31.2
MM-I-18	33.8	-19.1	28.9	-9.1	16.8	-14.5
MM-I-09	29.4	10	27.2	-3.4	30.5	-4
MM-I-06	30.4	0.8	14.6	6.5	-5.3	-13.6
MM-I-08	26.7	5.9	17.7	5.5	5.7	0.5
MM-I-10	19.1	15.7	-20.9	0.4	26.9	6.3
MM-I-11	35	-2.7	-7.3	-1.3	21.4	2.4
MM-I-12	41.7	0.7	-10.6	4.3	36.3	-9.7
DK-IV-19-1	21.3	3.2	28	6.5		2.9
DK-IV-20-1	20.9	25.5	35.4	40.2	-7.1	1.9
DK-IV-22-1	16.7	26.5	**56.1**	48.3	-19.6	3.9
DK-IV-23-1	25.6	4.1	**70.1**	35.3	18.8	-14.7

[a]Data are the percent inhibition induced by 10 μM of each respective compound on the specific binding at the screened target. The higher the number the more the radioligand was displaced. The number higher than 50% inhibition is considered meaningful and is shown in **bold** and highlighted. [b]**6-methyl** related analogs in **red**. [c]**8-bromo-6-fluoro** related analogs in **blue**. [d]**7-trifluoromethyl** related analogs in **green**. [e]New Deutero/Fluoro analogs in **orange**. [f]BZP = benzodiazepine, DOR = δ-opioid receptor, KOR = κ-opioid receptor, MOR = μ-opioid receptor.

Table 61: Primary Radioligand Binding Assays for Additional PQ Ligands. Compound-induced radioligand displacement assays for 46 receptors, transporters and channels conducted by the National Institute of Medical Health Psychoactive Drugs Screening Program (B. Roth et al., UNC, available at http://pdsp.med.unc.edu).[a]

Compound	Adrenergic β_2	Adrenergic β_3	BZP[f] Rat Brain Site	Dopamine D_1	Dopamine D_2	Dopamine D_3
Radioligand	**[^{125}I]Iodopindolol**	**[^{125}I]Iodopindolol**	**[^{3}H]Flunitrazepam**	**[^{3}H]-SCH233930**	**[^{3}H]-N-methyl-spiperone**	**[^{3}H]-N-methyl-spiperone**
PZ-II-029	6.9	4	**92.4**	-0.1	-20.8	3.2
DK-I-56-1	-19.7	-5.7	**96.2**	-17.8	-16.5	-7.4
RV-I-37	-6.5	6.3	**97.3**	17.1	-12.1	-1.9
CW-02-073	11	5.1	**88.3**	2.9	13.1	-5.7
CW-02-078	6.8	-4	**71.5**	28.6	8	17.8
CW-02-079	13.3	13	41.5	11.9	24.6	22.3
CW-02-082	10.4	-1.9	**91.7**	-14.4	13.8	10
MM-I-03	-4.7	-0.9	**94**	-23.8	20.5	19.2
MM-I-13	0.4	5.5	**90.3**	-3.2	29.8	31.4
MM-I-18	-6.6	1.8	**94.2**	-8.2	20.1	-13.8
MM-I-09	14.7	17.6	**68.9**	-13	21.2	-6.3
MM-I-06	5.8	19.1	**95.4**	20.7	-8.9	2.6
MM-I-08	2.6	-2.4	**97.2**	4.3	3.7	10.6
MM-I-10	16.8	32.2	**91**	15	5.3	16.5
MM-I-11	9	0.5	**97**	20.1	17.4	4.3
MM-I-12	14.4	7.2	**97.6**	11.5	19.8	26.8
DK-IV-19-1	-10.1	16.6	**96**	1.7	-2.9	-9.6
DK-IV-20-1	0.1	28.8	**90.1**	4.7	-10.1	0.2
DK-IV-22-1	5.1	27.8	**83.5**	-3.1	-7.6	-8
DK-IV-23-1	3.1	21.4	**95.5**	6.6	2.2	5.9

[a]Data are the percent inhibition induced by 10 μM of each respective compound on the specific binding at the screened target. The higher the number the more the radioligand was displaced. The number higher than 50% inhibition is considered meaningful and is shown in **bold** and highlighted. [b]**6-methyl** related analogs in **red**. [c]**8-bromo-6-fluoro** related analogs in **blue**. [d]**7-trifluoromethyl** related analogs in **green**. [e]New Deutero/Fluoro analogs in **orange**. [f]BZP = benzodiazepine, DOR = δ-opioid receptor, KOR = κ-opioid receptor, MOR = μ-opioid receptor.

Table 61: Primary Radioligand Binding Assays for Additional PQ Ligands. Compound-induced radioligand displacement assays for 46 receptors, transporters and channels conducted by the National Institute of Medical Health Psychoactive Drugs Screening Program (B. Roth et al., UNC, available at http://pdsp.med.unc.edu).[a]

Compound	Dopamine D_4	Dopamine D_5	Transporter Dopamine (DAT)	DOR[f]	$GABA_A$	Histamine H_1
Radioligand	**[^{3}H]-N-methyl-spiperone**	**[^{3}H]-SCH233930**	**[^{3}H]WIN35428**	**[^{3}H]DADLE**	**[^{3}H]Muscimol**	**[^{3}H]Pyrilamine**
PZ-II-029	-0.4	**57.9**	-7.8	10.8	13.1	52.4
DK-I-56-1	-0.5	14.7	-6.7	6.3	6.8	48.7
RV-I-37	-0.4	-14.2	45.1	2.6	15.3	-19.5
CW-02-073	14.7	25.4	**53.7**	17.2	-5.7	3.5
CW-02-078	-0.9	-4.5	**54.7**	11.1	-1.2	-4.6
CW-02-079	-1.6	3	**53.5**	16.2	25.3	7.3
CW-02-082	0	17.2	47.5	10.7	16.8	26.4
MM-I-03	-14.7	0.7	31.6	14.6	22	15.2
MM-I-13	6.3	7	35.8	12.9	16.7	26.6
MM-I-18	-6	12.9	19.2	-1.7	11	18.3
MM-I-09	-5	26.1	28.4	13.7	23.2	35.7
MM-I-06	1.8	25.8	17.9	-2.8	19	48
MM-I-08	4.5	6.4	**50.3**	18.9	-18.1	1.2
MM-I-10	9.5	31.9	**50**	31.3	-15.9	8.9
MM-I-11	2.2	13.6	**62.8**	3.9	5.6	-17.7
MM-I-12	-8.5	22.1	**66.8**	35.5	-10.8	-10.1
DK-IV-19-1	17	14.7	5.4	9.5	9.3	20
DK-IV-20-1	-6.3	7.2	2.1	15.7	13.1	**54.5**
DK-IV-22-1	-9.6	-4.8	20.4	8.6	9.6	**69.7**
DK-IV-23-1	6.3	8.8	5.7	18.7	29.9	**89.8**

[a]Data are the percent inhibition induced by 10 μM of each respective compound on the specific binding at the screened target. The higher the number the more the radioligand was displaced. The number higher than 50% inhibition is considered meaningful and is shown in **bold** and highlighted. [b]**6-methyl** related analogs in **red**. [c]**8-bromo-6-fluoro** related analogs in **blue**. [d]**7-trifluoromethyl** related analogs in **green**. [e]New Deutero/Fluoro analogs in **orange**. [f]BZP = benzodiazepine, DOR = δ-opioid receptor, KOR = κ-opioid receptor, MOR = μ-opioid receptor.

Table 61: Primary Radioligand Binding Assays for Additional PQ Ligands. Compound-induced radioligand displacement assays for 46 receptors, transporters and channels conducted by the National Institute of Medical Health Psychoactive Drugs Screening Program (B. Roth et al., UNC, available at http://pdsp.med.unc.edu).[a]

Compound	Histamine H_2	Histamine H_3	Histamine H_4	hERG binding	KOR[f]	Muscarinic M_1
Radioligand	**[^{3}H]Tiotidine**	**[^{3}H]alpha-methylhistamine**	**[^{3}H]Histamine**	**N/A**	**[^{3}H]U69593**	**[^{3}H]QNB**
PZ-II-029	-1.4	-1.5	-12.2	7.4	7.1	20.6
DK-I-56-1	20.8	-1.3	-5.9	-0.1	11.9	8.5
RV-I-37	34.4	-7.7	3.4	-14.1	1.8	-3.1
CW-02-073	43.9	-2.4	5.8	-10	-2.6	9.4
CW-02-078	43.5	-11.7	34.7	-0.7	-11.4	18.6
CW-02-079	**66.1**	7.4	18.5	-3.4	-8.1	8.8
CW-02-082	33.8	23.1	42	-5.6	7.2	16
MM-I-03	29.3	21.7	27.3	4.4	-2.7	5.8
MM-I-13	31	30.1	38.8	16.1	36.1	5.4
MM-I-18	32.9	47	33.9	19.9	16.5	15.9
MM-I-09	34.4	36.9	49.1	-1.5	3.3	31.6
MM-I-06	39.3	26.3	13.7	-16.3	21.2	6.7
MM-I-08	41.6	27.5	15.1	-9.6	13.5	27.6
MM-I-10	**51.2**	-12	22.6	0.9	**53.3**	12.7
MM-I-11	**55.4**	-10	1.7	9.2	-0.8	-11.4
MM-I-12	**74.9**	3	36.3	11.2	44.2	11
DK-IV-19-1	5.6	-7.7	-11	-4.5	16.8	13.8
DK-IV-20-1	8.5	9.1	-2.3	0.8	24.6	-8.3
DK-IV-22-1	7.4	22.5	-0.7	5.7	26.2	-0.4
DK-IV-23-1	3.7	16.8	3.6	1.3	16.4	-3.2

[a]Data are the percent inhibition induced by 10 μM of each respective compound on the specific binding at the screened target. The higher the number the more the radioligand was displaced. The number higher than 50% inhibition is considered meaningful and is shown in **bold** and highlighted. [b]**6-methyl** related analogs in **red**. [c]**8-bromo-6-fluoro** related analogs in **blue**. [d]**7-trifluoromethyl** related analogs in **green**. [e]New Deutero/Fluoro analogs in **orange**. [f]BZP = benzodiazepine, DOR = δ-opioid receptor, KOR = κ-opioid receptor, MOR = μ-opioid receptor.

Table 61: Primary Radioligand Binding Assays for Additional PQ Ligands. Compound-induced radioligand displacement assays for 46 receptors, transporters and channels conducted by the National Institute of Medical Health Psychoactive Drugs Screening Program (B. Roth et al., UNC, available at http://pdsp.med.unc.edu).[a]

Compound	Muscarinic M_2	Muscarinic M_3	Muscarinic M_4	Muscarinic M_5	MOR[f]
Radioligand	**[^{3}H]QNB**	**[^{3}H]QNB**	**[^{3}H]QNB**	**[^{3}H]QNB**	**[^{3}H]DAMGO**
PZ-II-029	-8.4	-4.5	10.9	-5.4	38.3
DK-I-56-1	6	27	19.2	-4.8	**53.1**
RV-I-37	-7.2	-5.8	-2.7	-12.3	-0.1
CW-02-073	-4.4	-6.8	-2.8	-7.3	35.4
CW-02-078	-5.9	2.1	-14.9	-7.7	-8.3
CW-02-079	4.5	9.9	-9.5	3.1	-3.2
CW-02-082	2.9	6.7	-12.7	15.2	-8.5
MM-I-03	0.3	16.6	-16.9	8.9	3.1
MM-I-13	7.6	12	-7.2	20.2	3.2
MM-I-18	8.6	-3.7	-3.6	25.6	1.1
MM-I-09	-3.2	6	18.9	27.8	1
MM-I-06	-7.8	13.9	12.6	20.9	22.7
MM-I-08	13	23.5	-3.8	23.7	13.5
MM-I-10	7.6	27	11.4	18.1	11.5
MM-I-11	17.3	21.6	2.7	20.4	12.9
MM-I-12	1.1	22.8	7.3	16	15.9
DK-IV-19-1	1.5	8.1	12.9	**53.2**	26.7
DK-IV-20-1	2.8	5.1	30.3	49.2	28.8
DK-IV-22-1	-1.3	25.6	27.2	36.1	28.7
DK-IV-23-1	-0.6	37	19.3	42.3	39.3

[a]Data are the percent inhibition induced by 10 μM of each respective compound on the specific binding at the screened target. The higher the number the more the radioligand was displaced. The number higher than 50% inhibition is considered meaningful and is shown in **bold** and highlighted. [b]**6-methyl** related analogs in **red**. [c]**8-bromo-6-fluoro** related analogs in **blue**. [d]**7-trifluoromethyl** related analogs in **green**. [e]New Deutero/Fluoro analogs in **orange**. [f]BZP = benzodiazepine, DOR = δ-opioid receptor, KOR = κ-opioid receptor, MOR = μ-opioid receptor.

Table 61: Primary Radioligand Binding Assays for Additional PQ Ligands. Compound-induced radioligand displacement assays for 46 receptors, transporters and channels conducted by the National Institute of Medical Health Psychoactive Drugs Screening Program (B. Roth et al., UNC, available at http://pdsp.med.unc.edu).[a]

Compound	Transporter, Norepinephrine (NET)	Peripheral Benzodiazepine Receptor (PBR)	Transporter, Serotonin (SERT)	Sigma σ_1	Sigma σ_2
Radioligand	**[^{3}H]Nisoxetine**	**[^{3}H]PK11195**	**[^{3}H]Citalopram**	**[^{3}H]Pentazocine**	**[^{3}H]DTG**
PZ-II-029	18.1	8.1	1.3	-14.2	15.7
DK-I-56-1	9.6	8	7.8	20	21.2
RV-I-37	46.4	9.6	-5.2	26.6	13.6
CW-02-073	34.1	2	8.8	2.1	**64.5**
CW-02-078	30.3	-3.5	-7.6	-3.9	**58.9**
CW-02-079	34	4.4	-2.2	2	**58.3**
CW-02-082	-8.7	4.7	0.3	-13.2	30.9
MM-I-03	-8	-5.3	-21.9	6	**54.8**
MM-I-13	6	8.1	-33.8	-15	22.7
MM-I-18	40.4	-5.7	-22.6	-16.5	12.5
MM-I-09	**50**	14	3.8	-4.2	2.3
MM-I-06	**50**	8	-15.4	1.6	**52.2**
MM-I-08	**50**	16.3	-15	-6	28.8
MM-I-10	41	30	-3.9	0.6	**62.7**
MM-I-11	38.3	-1.2	-10.2	0.5	1.8
MM-I-12	35.9	22.4	-6.7	16.5	**59.2**
DK-IV-19-1	**71.9**	32	-10.5	36.8	**63.8**
DK-IV-20-1	35.3	19.9	16.8	28.6	43.3
DK-IV-22-1	14.4	**68.7**	21.6	38.5	44.3
DK-IV-23-1	11	41.2	22.4	36.5	**81.9**

[a]Data are the percent inhibition induced by 10 μM of each respective compound on the specific binding at the screened target. The higher the number the more the radioligand was displaced. The number higher than 50% inhibition is considered meaningful and is shown in **bold** and highlighted. [b]**6-methyl** related analogs in **red**. [c]**8-bromo-6-fluoro** related analogs in **blue**. [d]**7-trifluoromethyl** related analogs in **green**. [e]New Deutero/Fluoro analogs in **orange**. [f]BZP = benzodiazepine, DOR = δ-opioid receptor, KOR = κ-opioid receptor, MOR = μ-opioid receptor.

4.5. Secondary Radioligand Binding Assays for Additional PQ Analogs

Table 62: Secondary Radioligand Binding Assays for Additional PQ Ligands. Binding affinity (Ki, nM) values obtained from non-linear regression of radioligand competition binding isotherms. Testing conducted by the National Institute of Medical Health Psychoactive Drugs Screening Program (B. Roth et al., UNC, available at http://pdsp.med.unc.edu).[a]

Compound	Serotonin 5-HT$_{1A}$	Serotonin 5-HT$_{1D}$	Serotonin 5-HT$_{1E}$	Serotonin 5-HT$_{2B}$	Serotonin 5-HT$_{2C}$
PZ-II-029 (8a)	NA	NA	NA	NA	**>10,000**
DK-I-56-1 (8b)	NA	NA	NA	NA	NA
RV-I-37 (14a)	NA	NA	NA	NA	NA
CW-02-073 (14b)	NA	NA	NA	NA	NA
CW-02-078 (14c)	NA	NA	NA	NA	NA
CW-02-079 (14d)	NA	NA	NA	NA	NA
CW-02-082 (14e)	NA	NA	NA	NA	NA
MM-I-03 (14f)	NA	NA	NA	NA	NA
MM-I-13 (14g)	**424**	**3297.3**	**1073.5**	**1743.0**	NA
MM-I-18 (14h)	NA	NA	NA	NA	NA
MM-I-09 (14k)	NA	NA	NA	NA	NA
MM-I-06 (14i)	NA	NA	NA	NA	NA
MM-I-08 (14j)	NA	NA	NA	NA	NA
MM-I-10 (14l)	NA	NA	NA	NA	NA
MM-I-11 (14m)	NA	NA	NA	NA	NA
MM-I-12 (14n)	NA	NA	NA	**1470.0**	NA
DK-IV-19-1 (14o)	NA	NA	**>10,000**	**3799.0**	NA
DK-IV-20-1 (14p)	NA	NA	**>10,000**	NA	NA
DK-IV-22-1 (14q)	NA	NA	**>10,000**	NA	**1138.0**
DK-IV-23-1 (14r)	NA	NA	**>10,000**	NA	NA

[a]Ki values are calculated from best fit IC_{50} values using the Cheng-Prusoff equation. Values are an average of n = 3. NA are for compounds/receptors not testing for Primary Screening results of < 50% inhibition (**Table S1**). [b]**6-methyl** related analogs in **red**. [c]**8-bromo-6-fluoro** related analogs in **blue**. [d]**7-trifluoromethyl** related analogs in **green**. [e]New Deutero/Fluoro analogs in **orange**. [f]BZP = benzodiazepine, DOR = δ-opioid receptor, KOR = κ-opioid receptor, MOR = μ-opioid receptor.

Table 62: Secondary Radioligand Binding Assays for Additional PQ Ligands. Binding affinity (Ki, nM) values obtained from non-linear regression of radioligand competition binding isotherms. Testing conducted by the National Institute of Medical Health Psychoactive Drugs Screening Program (B. Roth et al., UNC, available at http://pdsp.med.unc.edu).[a]

Compound	Serotonin 5-HT$_{5A}$	Serotonin 5-HT$_7$	Adrenergic α_{2A}	BZP[f] Rat Brain Site
PZ-II-029 (8a)	NA	**2599.0**	NA	**2.7**
DK-I-56-1 (8b)	NA	**2039.0**	NA	**2.1**
RV-I-37 (14a)	NA	NA	NA	**6.0**
CW-02-073 (14b)	NA	**488**	NA	**325.0**
CW-02-078 (14c)	NA	NA	NA	**733**
CW-02-079 (14d)	NA	**2353.0**	NA	**4655**
CW-02-082 (14e)	NA	NA	NA	**1095**
MM-I-03 (14f)	NA	NA	NA	**6.1**
MM-I-13 (14g)	NA	NA	NA	**164**
MM-I-18 (14h)	NA	NA	NA	**58**
MM-I-09 (14k)	NA	NA	NA	**2,200.00**
MM-I-06 (14i)	NA	NA	NA	**50**
MM-I-08 (14j)	NA	NA	NA	**122**
MM-I-10 (14l)	NA	NA	NA	**964**
MM-I-11 (14m)	NA	NA	NA	**134**
MM-I-12 (14n)	NA	NA	NA	**310**
DK-IV-19-1 (14o)	NA	NA	NA	**32**
DK-IV-20-1 (14p)	**792**	**1089.0**	NA	**444**
DK-IV-22-1 (14q)	**289**	**967**	**1844.0**	**686**
DK-IV-23-1 (14r)	NA	NA	**>10,000**	**28**

[a]Ki values are calculated from best fit IC_{50} values using the Cheng-Prusoff equation. Values are an average of n = 3. NA are for compounds/receptors not testing for Primary Screening results of < 50% inhibition (**Table S1**). [b]**6-methyl** related analogs in **red**. [c]**8-bromo-6-fluoro** related analogs in **blue**. [d]**7-trifluoromethyl** related analogs in **green**. [e]New Deutero/Fluoro analogs in **orange**. [f]BZP = benzodiazepine, DOR = δ-opioid receptor, KOR = κ-opioid receptor, MOR = μ-opioid receptor.

Table 62: Secondary Radioligand Binding Assays for Additional PQ Ligands. Binding affinity (Ki, nM) values obtained from non-linear regression of radioligand competition binding isotherms. Testing conducted by the National Institute of Medical Health Psychoactive Drugs Screening Program (B. Roth et al., UNC, available at http://pdsp.med.unc.edu).[a]

Compound	Dopamine D_1	Dopamine D_5	Transporter Dopamine (DAT)	Histamine H_1	Histamine H_2
PZ-II-029 (8a)	NA	**>10,000**	NA	NA	NA
DK-I-56-1 (8b)	NA	NA	NA	NA	NA
RV-I-37 (14a)	NA	NA	NA	NA	NA
CW-02-073 (14b)	NA	NA	**3301.0**	NA	NA
CW-02-078 (14c)	NA	NA	**5107.0**	NA	NA
CW-02-079 (14d)	NA	NA	**>10,000**	NA	**5,201.00**
CW-02-082 (14e)	NA	NA	NA	NA	NA
MM-I-03 (14f)	**10,000**	NA	NA	NA	NA
MM-I-13 (14g)	NA	NA	NA	NA	NA
MM-I-18 (14h)	NA	NA	NA	NA	NA
MM-I-09 (14k)	NA	NA	NA	NA	NA
MM-I-06 (14i)	NA	NA	NA	NA	NA
MM-I-08 (14j)	NA	NA	**5112.0**	NA	NA
MM-I-10 (14l)	NA	NA	**>10,000**	NA	**3,670.00**
MM-I-11 (14m)	NA	NA	**>10,000**	NA	**5,281.00**
MM-I-12 (14n)	NA	NA	**>10,000**	NA	**6,476.00**
DK-IV-19-1 (14o)	NA	NA	NA	NA	NA
DK-IV-20-1 (14p)	NA	NA	NA	**>10,000**	NA
DK-IV-22-1 (14q)	NA	NA	NA	**654**	NA
DK-IV-23-1 (14r)	NA	NA	NA	**>10,000**	NA

[a]Ki values are calculated from best fit IC_{50} values using the Cheng-Prusoff equation. Values are an average of n = 3. NA are for compounds/receptors not testing for Primary Screening results of < 50% inhibition (**Table S1**). [b]**6-methyl** related analogs in **red**. [c]**8-bromo-6-fluoro** related analogs in **blue**. [d]**7-trifluoromethyl** related analogs in **green**. [e]New Deutero/Fluoro analogs in **orange**. [f]BZP = benzodiazepine, DOR = δ-opioid receptor, KOR = κ-opioid receptor, MOR = μ-opioid receptor.

Table 62: Secondary Radioligand Binding Assays for Additional PQ Ligands. Binding affinity (Ki, nM) values obtained from non-linear regression of radioligand competition binding isotherms. Testing conducted by the National Institute of Medical Health Psychoactive Drugs Screening Program (B. Roth et al., UNC, available at http://pdsp.med.unc.edu).[a]

Compound	KOR[f]	Muscarinic M_5	MOR[f]	Transporter, Norepinephrine (NET)
PZ-II-029 (8a)	NA	NA	NA	NA
DK-I-56-1 (8b)	NA	NA	**3524.3**	NA
RV-I-37 (14a)	NA	NA	NA	NA
CW-02-073 (14b)	NA	NA	NA	NA
CW-02-078 (14c)	NA	NA	NA	NA
CW-02-079 (14d)	NA	NA	NA	NA
CW-02-082 (14e)	NA	NA	NA	NA
MM-I-03 (14f)	NA	NA	NA	NA
MM-I-13 (14g)	NA	NA	NA	NA
MM-I-18 (14h)	NA	NA	NA	NA
MM-I-09 (14k)	NA	NA	NA	**5814.0**
MM-I-06 (14i)	NA	NA	NA	**>10,000**
MM-I-08 (14j)	NA	NA	NA	**5937.0**
MM-I-10 (14l)	**>10,000**	NA	NA	NA
MM-I-11 (14m)	NA	NA	NA	NA
MM-I-12 (14n)	NA	NA	NA	NA
DK-IV-19-1 (14o)	NA	**>10,000**	NA	**>10,000**
DK-IV-20-1 (14p)	NA	NA	NA	NA
DK-IV-22-1 (14q)	NA	NA	NA	NA
DK-IV-23-1 (14r)	NA	NA	NA	NA

[a]Ki values are calculated from best fit IC_{50} values using the Cheng-Prusoff equation. Values are an average of n = 3. NA are for compounds/receptors not testing for Primary Screening results of < 50% inhibition (**Table S1**). [b]**6-methyl** related analogs in **red**. [c]**8-bromo-6-fluoro** related analogs in **blue**. [d]**7-trifluoromethyl** related analogs in **green**. [e]New Deutero/Fluoro analogs in **orange**. [f]BZP = benzodiazepine, DOR = δ-opioid receptor, KOR = κ-opioid receptor, MOR = μ-opioid receptor.

Table 62: Secondary Radioligand Binding Assays for Additional PQ Ligands. Binding affinity (Ki, nM) values obtained from non-linear regression of radioligand competition binding isotherms. Testing conducted by the National Institute of Medical Health Psychoactive Drugs Screening Program (B. Roth et al., UNC, available at http://pdsp.med.unc.edu).[a]

Compound	Peripheral Benzodiazepine Receptor (PBR)	Transporter, Serotonin (SERT)	Sigma σ_2
PZ-II-029 (8a)	NA	NA	NA
DK-I-56-1 (8b)	NA	NA	NA
RV-I-37 (14a)	NA	NA	NA
CW-02-073 (14b)	NA	NA	**213**
CW-02-078 (14c)	NA	NA	**218**
CW-02-079 (14d)	NA	NA	**112**
CW-02-082 (14e)	NA	NA	NA
MM-I-03 (14f)	NA	**>10,000**	**115**
MM-I-13 (14g)	NA	**>10,000**	NA
MM-I-18 (14h)	NA	**>10,000**	NA
MM-I-09 (14k)	NA	NA	NA
MM-I-06 (14i)	NA	NA	**179**
MM-I-08 (14j)	NA	NA	NA
MM-I-10 (14l)	NA	NA	**133**
MM-I-11 (14m)	NA	NA	NA
MM-I-12 (14n)	NA	NA	**151**
DK-IV-19-1 (14o)	NA	NA	**3,220.0**
DK-IV-20-1 (14p)	NA	NA	NA
DK-IV-22-1 (14q)	**8466.0**	NA	NA
DK-IV-23-1 (14r)	NA	NA	**2,132.0**

[a]Ki values are calculated from best fit IC_{50} values using the Cheng-Prusoff equation. Values are an average of n = 3. NA are for compounds/receptors not testing for Primary Screening results of < 50% inhibition (**Table S1**). [b]**6-methyl** related analogs in **red**. [c]**8-bromo-6-fluoro** related analogs in **blue**. [d]**7-trifluoromethyl** related analogs in **green**. [e]New Deutero/Fluoro analogs in **orange**. [f]BZP = benzodiazepine, DOR = δ-opioid receptor, KOR = κ-opioid receptor, MOR = μ-opioid receptor.

4.6. Cytotoxicity Studies for Selected Pyrazoloquinolinones

Table 63: Results of Cytotoxicity Studies on HEPG2 and HEK293 Cell Lines[a]

Compound	Toxicity in HEK293 (Kidney) LD_{50} (µM)	Toxicity in HEPG2 (Liver) LD_{50} (µM)
8b[b,p]	>400	>400
8c[b,p]	>400	>200
8d[b,p]	>400	>400
8e[b,m]	>200	>200
8f[b,o]	>400	>200
13c[b,e]	>400	>400
8j[c,m]	>400	>400
8l[c,p]	>400	>200
8m[c,o]	>400	>400
13e[c,e]	>400	>400
8o[d,p]	>400	>400
13g[d,e]	>400	>400

[a]Cellular viability studies confirmed that the ligands were not cytotoxic to HEPG2 or HEK293 Cell Lines. The compounds were incubated at different concentrations with specified cells for 48 h, followed by detection of viability using Cell-Titer Glo (Promega). The results were normalized using DMSO (negative) and 3-dibutylamino-1-(4-hexyl-phenyl)-propan-1-one (150 mM in DMSO final concentration, positive). Data were acquired by three independent experiments carried out in quadruplet. [b]**8a** related analogs in **red**. [c]**8i** related analogs in **blue**. [d]**8n** related analogs in **green**. [e]Select "D-ring" N-hetero analogs. [o]D-ring "*ortho*". [m]D-ring "*meta*". [p]D-ring "*para*".

Figure 135: Cytotoxicity of Deuterated and N-Hetero PQ's on HEK293 (Kidney) Cells (Left Panels: A,C,E) and HEPG2 (Liver) Cells (Right Panels: B,D,F)[a]

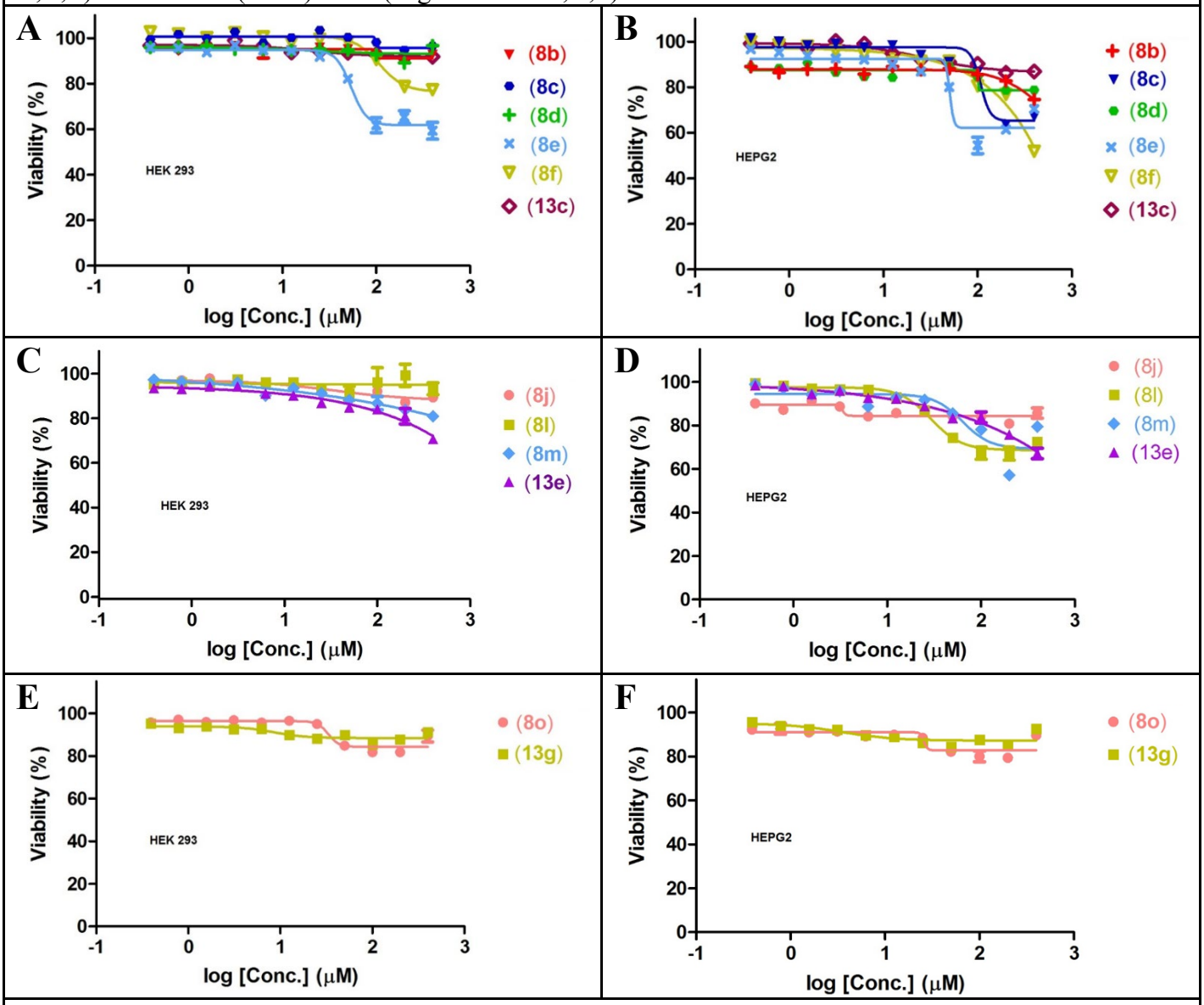

[a]**8a** related analogs (**A**, **B**). **8i** related analogs (**C**, **D**). **8n** related analogs (**E, F**). HEK 293 = kidney cells. (**A**, **C**, **E**). HEPG2 = liver cells (**B**, **D**, **F**). Cellular viability studies confirmed that the ligands were not cytotoxic to HEPG2 or HEK293 Cell Lines. The compounds were incubated at different concentrations with specified cells for 48 h, followed by detection of viability using Cell-Titer Glo (Promega). The results were normalized using DMSO (negative) and 3-dibutylamino-1-(4-hexyl-phenyl)-propan-1-one (150 mM in DMSO final concentration, positive). Data were acquired by three independent experiments carried out in quadruplet.

Figure 136: Cytotoxicity of Fluorinated PQ's on HEK293 (Kidney) Cells (Panel A) and HEPG2 (Liver) Cells (Panel B)[a]

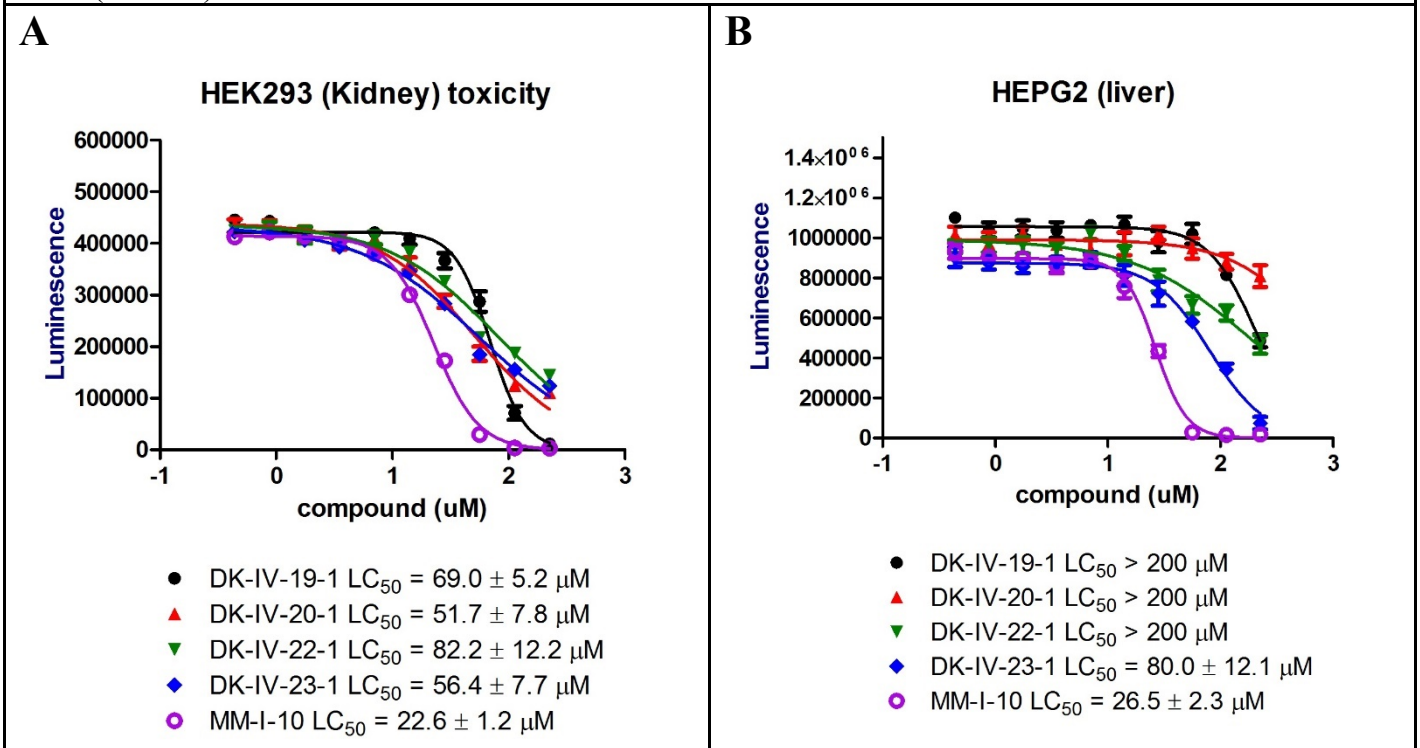

[a]Cellular viability studies exhibited that the fluorinated ligands were cytotoxic to HEPG2 or HEK293 Cell Lines. The compounds were incubated at different concentrations with specified cells for 48 h, followed by detection of viability using Cell-Titer Glo (Promega). The results were normalized using DMSO (negative) and 3-dibutylamino-1-(4-hexyl-phenyl)-propan-1-one (150 mM in DMSO final concentration, positive). Data were acquired by three independent experiments carried out in quadruplet.

4.7. Motor Coordination Studies of Selected Pyrazoloquinolinones on the Rotorod

Figure 137: Effect of Deuterated and N-Hetero PQ Ligands on Motor Coordination[a]

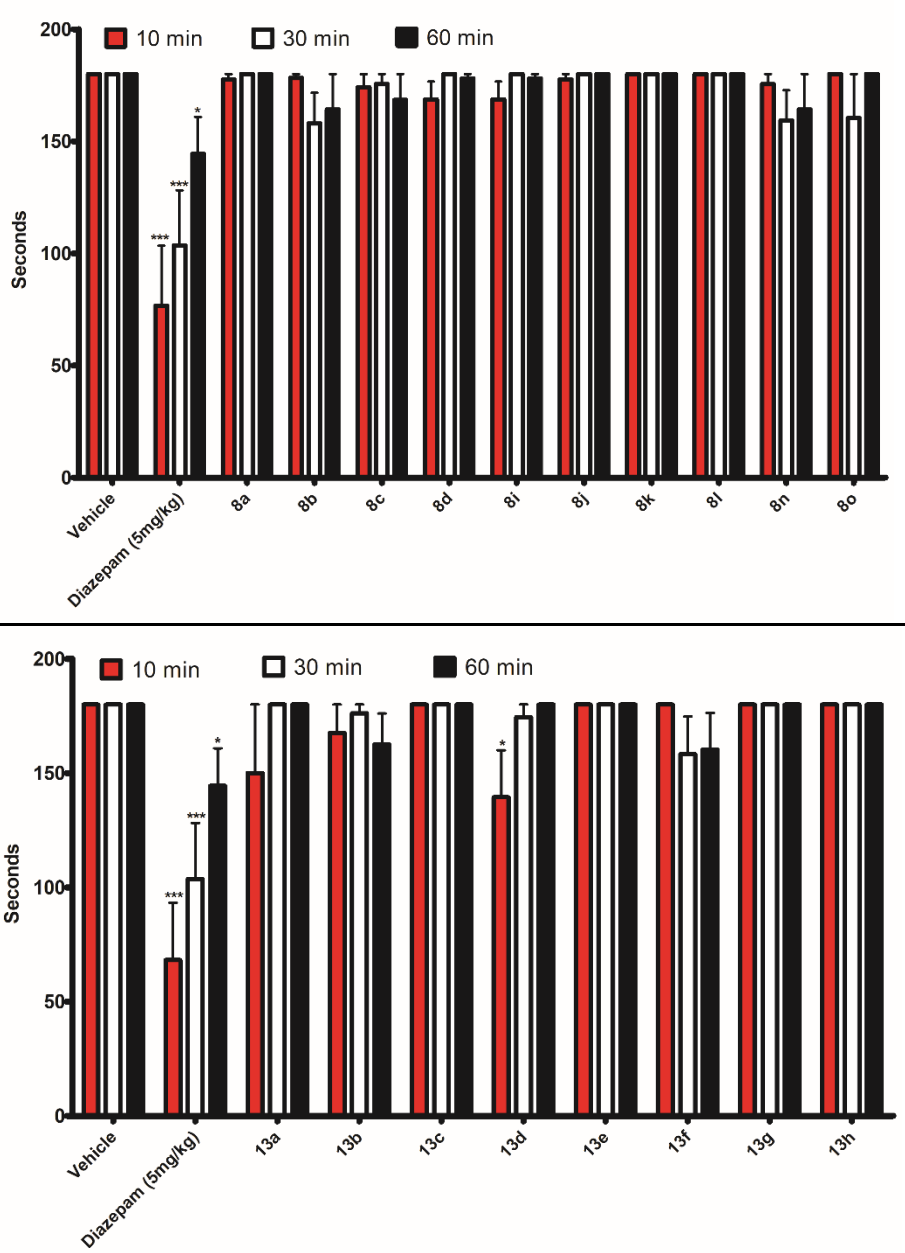

[a]Rotorod studies confirmed that deuteration of the methoxy groups (**A**) and N-hetero substitution and deuteration of the methoxy groups (**B**) of the parent ligands had no effect on motor coordination in contrast to the effects of diazepam at 5mg/kg. Female Swiss Webster mice were tested on a rotarod at 15 rpm for 3 min at 10, 30, and 60 min following compound exposure. Mice (N = 10) received a single injection via oral gavage (PO) of the test compounds (40 mg/kg), diazepam (5 mg/kg), or vehicle (2% polyethylene glycol, 2.5% hydroxypropylmethyl cellulose solution). The time of fall was recorded if it occurred prior to 3 min. Data are expressed as mean ± SEM (N = 10). ∗ ($p < 0.05$), ∗∗ ($p < 0.01$) or ∗∗∗ ($p < 0.001$) significance compared to vehicle-treated mice. All compounds dissolved in the oral vehicle.

Figure 138: Effect of Fluorinated PQ Ligands on Motor Coordination[a]

A

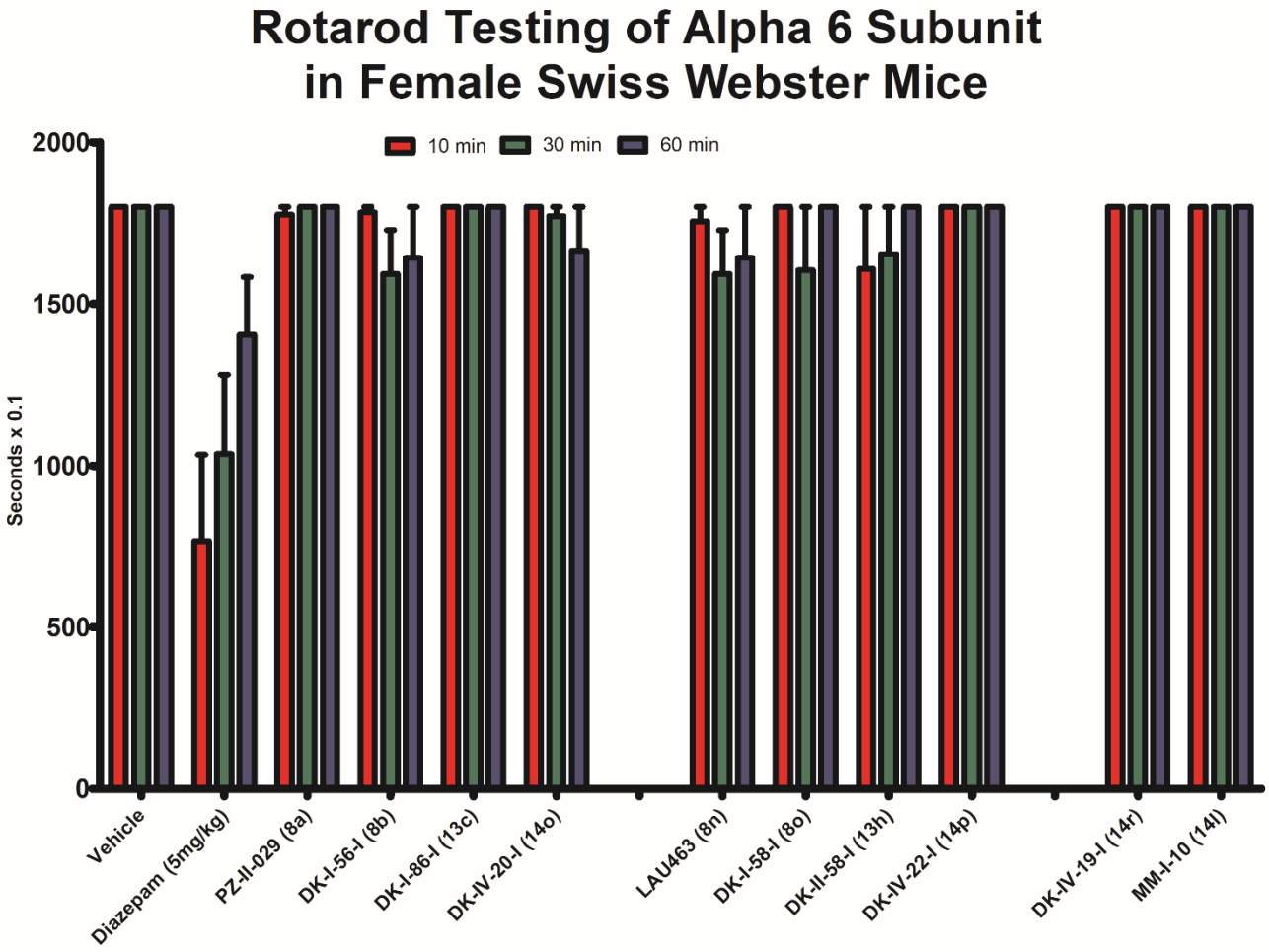

[a]Rotorod studies confirmed that the fluorinated analogs (14o, 14p, 14r and 14l) of the parent ligands had no effect on motor coordination in contrast to the effects of diazepam at 5mg/kg. Female Swiss Webster mice were tested on a rotarod at 15 rpm for 3 min at 10, 30, and 60 min following compound exposure. Mice (N = 10) received a single injection via oral gavage (PO) of the test compounds (40 mg/kg), diazepam (5 mg/kg), or vehicle (2% polyethylene glycol, 2.5% hydroxypropylmethyl cellulose solution). The time of fall was recorded if it occurred prior to 3 min. Data are expressed as mean ± SEM (N = 10). ∗ ($p < 0.05$), ∗∗ ($p < 0.01$) or ∗∗∗ ($p < 0.001$) significance compared to vehicle-treated mice. All compounds dissolved in the oral vehicle.

4.8. Human Liver (HLM) and Mouse Liver (MLM) Microsomal Assays for PQ's

Human Liver Microsomal Assay

Principal Investigator: Dr. Alexander Arnold
Operator: Revathi Kodali
Test Compound: **8a**
Concentration: 10 µM
Date: 02-16-2015
Facility: Milwaukee Institute for Drug Discovery

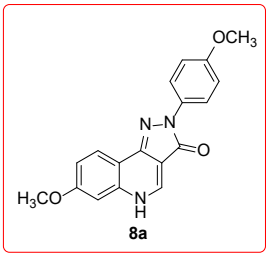

8a

Assay Protocol

Each evaluation included six independent assays carried out three at a time, on two different days

1. Preparation of solutions:
   a. 1 mM test compound in Acetonitrile.
   b. 0.5 µM Verapamil in Acetonitrile (ACN) as internal standard (store on ice).
2. For a total volume of Microsomal Assay Mixture (MAM) 390 µL, sufficient for seven time points, combine the following
   a. 282 µL of 18.2 mΩ of water.
   b. 80 µL of 0.5 M potassium phosphate buffer (p^H 7.4)
   c. 20 µL of NADPH A. (Corning life sciences, Cat # 451220)
   d. 4 µL of NADPH B. (Corning life sciences, Cat # 451200)
   e. 4 µL of test compound.
3. Sonicate MAM for 5 min and meanwhile thaw microsomes (20 mg/mL) (BD Gentest, Cat # 452156) on ice.
4. Aliquot 48.75 µL of MAM into separate Eppendorf 1.5 mL vials and label them the time points for 0, 10, 20, 30, 40, 50, and 60 min.
5. Arrange the timer. Microsomes should be added to all time points except the zero time point.
6. For each time point add 1.25 µL microsomes (Final concentration of 0.5 mg/mL) and place in the incubator (37 °C) and record the time.
7. At the end of each time interval add 100 µL of ice cold Verapamil solution in ACN and sonicate for 10 sec and spin down at 10,000 rpm for 5 minutes.
8. Take 100 µL of supernatant and transfer to Spin-X HPLC filter tubes (Corning Incorporated, Cat # 8169) and centrifuge at 13,000 rpm for 5 minutes and take 5 µL from this solution and dilute in 500 µL of LCMS grade methanol (Fischer scientific, CAS # 67-56-1) in an 2mL glass auto sampler vial (Microsolv, Cat # 95025-WCV)
9. The samples are analyzed by LCMS-8040. (Shimadzu)

Data:

Day 1:

Time (min)	Assay 1		Assay 2		Assay 3		% remaining		
	PZ-II-029 Peak area	Verapamil Peak area	PZ-II-029 Peak area	Verapamil Peak area	PZ-II-029 Peak area	Verapamil Peak area	Assay 1	Assay 2	Assay 3
0	33951	601221	32355	541076	43992	555548	100.83	99.66	100.23
10	42583	640770	15626	226765	42530	564189	118.67	114.84	95.42
20	38151	561437	41959	594788	46868	582371	121.34	117.57	101.87
30	40481	622191	28975	614244	42095	608270	116.18	78.62	87.60
40	37748	595368	36594	602489	41311	584370	113.21	101.23	89.48
50	33524	640546	38790	658705	36637	554181	93.45	98.14	83.68
60	25781	629252	38607	576764	39742	602548	73.16	99.66	83.48

Table 1: Peak areas and % remaining values

Day 2:

Time (min)	Assay 1		Assay 2		Assay 3		(% remaining)		
	PZ-II-029 Peak area	Verapamil Peak area	PZ-II-029 Peak area	Verapamil Peak area	PZ-II-029 Peak area	Verapamil Peak area	Assay 1	Assay 2	Assay 3
0	226304	837974	251250	676349	221151	719623	100.02	100.12	100.10
10	222165	845586	197063	750089	248601	823455	97.30	70.81	98.33
20	222847	820071	215134	732628	230949	796583	100.64	79.15	94.43
30	229722	686761	240649	736344	239432	735694	123.88	88.09	106.01
40	182530	767280	224208	775342	244256	778429	88.10	77.94	102.20
50	178928	748120	181502	692046	161580	705574	88.58	70.69	74.59
60	202738	761042	225933	676351	190088	732573	98.66	90.04	84.52

Table 2: Peak areas and % remaining values

Calculation:

From the peak area, Calculate the following

$$\text{Peak area ratio} = \frac{\text{Peak area of test compound (PZ-II-029)}}{\text{Peak area of internal standard (Verapamil)}}$$

$$\text{\% remaining at time T} = \frac{\text{Peak area ratio at particular time T}}{\text{Peak area ratio at zero time point}} * 100$$

(T = 0, 10, 20,30,40,50 and 60)

DATA ANALYSIS:

Day 1

Linear regression analysis:

Slope: -0.003961 ± 0.001458

At X= 60, Y = 4.465 ± 0.05385

R^2 = 0.2909

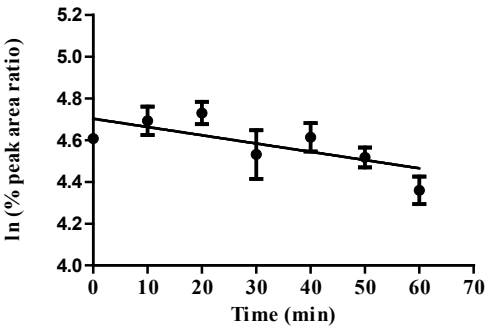

Metabolic Parameters:

Half-life: 175 min

V_d: 100 µL/mg

Intrinsic clearance: 0.4 µL/min/mg

Metabolic Rate: 8 nmol/min/mg

% remaining at 60 min: 87 ± 1.0 %

Day 2

Linear regression analysis:

Slope: -0.02768 ± 0.00138

At X = 60, Y = 4.446 ± 0.04892

R^2 = 0.1807

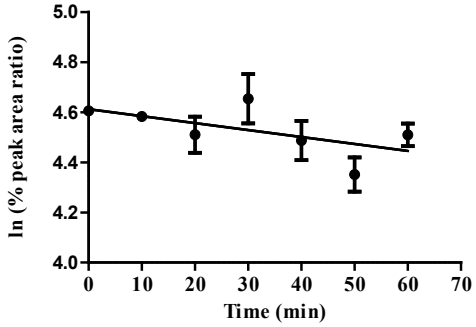

Metabolic Parameters:

Half-life: 250 min

V_d: 100 µL/mg

Intrinsic clearance: 0.277 µL/min/mg

Metabolic Rate: 5.6 nmol/min/mg

% remaining at 60 min: 85.2 ± 1.0 %

Note: The peak area ratios and natural log values are calculated using Microsoft excel 2010 and linear regression analysis is calculated using GraphPad prism.

Mouse Liver Microsomal Assay

Principal Investigator: Dr. Alexander Arnold
Operator: Revathi Kodali
Test Compound: **8a**
Concentration: 10 µM
Date: 04-08-2016
Facility: Milwaukee Institute for Drug Discovery

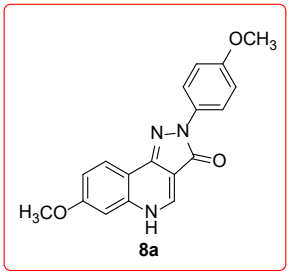

8a

Assay Protocol

Each evaluation included six independent assays carried out three at a time, on two different days

1. Preparation of solutions:
   a. 1 mM test compound in DMSO.
   b. 1 µM Verapamil in Acetonitrile (ACN) as internal standard (store on ice).
2. For a total volume of Microsomal Assay Mixture (MAM) 390 µL, sufficient for seven time points, combine the following
   a. 282 µL of 18.2 mΩ of water.
   b. 80 µL of 0.5 M potassium phosphate buffer (p^H 7.4)
   c. 20 µL of NADPH A. (Corning life sciences, Cat # 451220)
   d. 4 µL of NADPH B. (Corning life sciences, Cat # 451200)
   e. 4 µL of test compound.
3. Sonicate MAM for 5 min and meanwhile thaw microsomes (20 mg/mL) (Life technologies, Cat # MSMC-PL) on ice.
4. Aliquot 100 µL of ice cold ISTD into seven separate 1.5 mL conical vials and label them the time points for 0, 10, 20, 30, 40, 50, and 60 min.
5. Arrange the timer. Microsomes (Final concentration of 0.5 mg/mL) should be added to all time points except the zero time point.
6. Add 50 µL of the MAM solution to the conical vial labelled as zero time point. Place the remaining MAM solution in the incubator (37 ºC) for 5 min and initiate the reaction with addition of microsomes (8.8 µL) and record the time.
7. At the end of each time interval remove 50 µL and add to 100 µL ISTD in conical vial, sonicate for 10 sec and spin down at 10,000 rpm for 5 minutes.
8. Take 100 µL of supernatant and transfer to Spin-X HPLC filter tubes (Corning Incorporated, Cat # 8169) and centrifuge at 13,000 rpm for 5 minutes and take 5 µL from this solution and dilute in 495 µL of LCMS grade methanol (Fischer scientific, CAS # 67-56-1) in an 2mL glass auto sampler vial (Microsolv, Cat # 95025-WCV)
9. The samples are analyzed by LCMS-8040. (Shimadzu)

Data:

Day 1:

Time (min)	Assay 1		Assay 2		Assay 3		% remaining		
	PZ-II-029 Peak area	Verapamil Peak area	PZ-II-029 Peak area	Verapamil Peak area	PZ-II-029 Peak area	Verapamil Peak area	Assay 1	Assay 2	Assay 3
0	447665	859377	462433	863304	455184	863057	99.98	99.93	100.07
10	432708	843709	436278	848682	438533	859089	98.43	95.90	96.86
20	414199	856316	434993	857592	430385	861791	92.84	94.63	94.76
30	397811	862960	404695	858362	401549	865308	88.48	87.96	88.05
40	383712	861536	396789	858415	389825	856243	85.48	86.23	86.39
50	364496	848736	391027	856027	379552	864618	82.42	85.22	83.29
60	375359	853833	383683	870545	376641	877200	84.37	82.22	81.47

Table 1: Peak areas and % remaining values

Day 2:

Time (min)	Assay 1		Assay 2		Assay 3		(% remaining)		
	PZ-II-029 Peak area	Verapamil Peak area	PZ-II-029 Peak area	Verapamil Peak area	PZ-II-029 Peak area	Verapamil Peak area	Assay 1	Assay 2	Assay 3
0	505767	866531	461889	859715	473978	852607	99.94	100.04	99.98
10	485169	856481	449512	852390	461313	862061	96.99	98.20	96.24
20	455571	855136	424509	861092	444556	853068	91.22	91.80	93.72
30	434369	864280	404785	855574	412379	864451	86.05	88.10	85.79
40	423412	862610	394944	852059	407802	865784	84.05	86.31	84.71
50	394408	857542	382714	861341	396913	870869	78.75	82.74	81.97
60	403745	856301	375242	858103	397021	854640	80.73	81.43	83.55

Table 2: Peak areas and % remaining values

Calculation:

From the peak area, Calculate the following

$$\text{Peak area ratio} = \frac{\text{Peak area of test compound (PZ-II-029)}}{\text{Peak area of internal standard (Verapamil)}}$$

$$\text{\% remaining at time T (T = 0, 10, 20,30,40,50 and 60)} = \frac{\text{Peak area ratio at particular time T}}{\text{Peak area ratio at zero time point}} * 100$$

DATA ANALYSIS:

Day 1

Linear regression analysis:

Slope: -0.003424 ± 0.0001769

At X= 60, Y = 4.397 ± 0.006377

R^2 = 0.9517

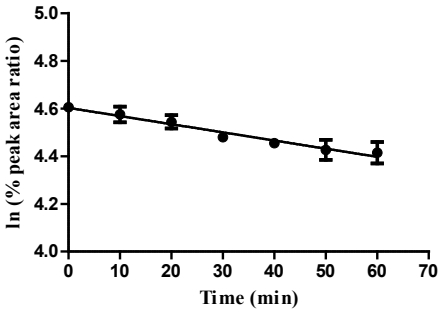

Metabolic Parameters:

Half-life: 202.39 ± 10.45 min

V_d: 100 µL/mg

Intrinsic clearance: 0.3424 µL/min/mg

Metabolic Rate: 6.848 nmol/min/mg

% remaining at 60 min: 81.20 ± 0.12 %

Day 2

Linear regression analysis:

Slope: -0.003723 ± 0.0002476

At X = 60, Y = 4.376 ± 0.008927

R^2 = 0.9225

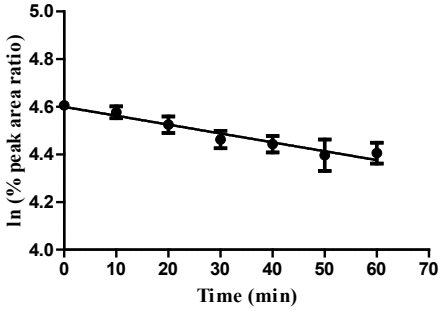

Metabolic Parameters:

Half-life: 186.14 ± 12.37 min

V_d: 100 µL/mg

Intrinsic clearance: 0.3723 µL/min/mg

Metabolic Rate: 7.446 nmol/min/mg

% remaining at 60 min: 79.51 ± 0.16 %

Note: The peak area ratios and natural log values are calculated using Microsoft excel 2010 and linear regression analysis is calculated using GraphPad prism.

Human Liver Microsomal Assay

Principal Investigator: Dr. Alexander Arnold
Operator: Revathi Kodali
Test Compound: **8b**
Concentration: 10 µM
Date: 05-04-2016
Facility: Milwaukee Institute for Drug Discovery

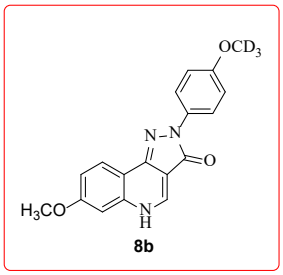

8b

Assay Protocol

Each evaluation included six independent assays carried out three at a time, on two different days

1. Preparation of solutions:
   a. 1 mM test compound in DMSO.
   b. 2 µM 4,5 Diphenyl Imidazole ice cold Acetonitrile (ISTD).
2. For a total volume of Microsomal Assay Mixture (MAM) 390 µL, sufficient for seven time points, combine the following
   a. 282 µL of 18.2 mΩ of water.
   b. 80 µL of 0.5 M potassium phosphate buffer (p^H 7.4)
   c. 20 µL of NADPH A. (Corning life sciences, Cat # 451220)
   d. 4 µL of NADPH B. (Corning life sciences, Cat # 451200)
   e. 4 µL of test compound.
3. Sonicate MAM for 5 min and meanwhile thaw microsomes (20 mg/mL) (BD Gentest, Cat # 452156) on ice.
4. Aliquot 100 µL of ice cold ISTD into seven separate 1.5 mL conical vials and label them the time points for 0, 10, 20, 30, 40, 50, and 60 min.
5. Arrange the timer. Microsomes (Final concentration of 0.5 mg/mL) should be added to all time points except the zero time point.
6. Add 50 µL of the MAM solution to the conical vial labelled as zero time point. Place the remaining MAM solution in the incubator (37 ºC) for 5 min and initiate the reaction with addition of microsomes (8.8 µL) and record the time.
7. At the end of each time interval remove 50 µL and add to 100 µL ISTD in conical vial, sonicate for 10 sec and spin down at 10,000 rpm for 5 minutes.
8. Take 100 µL of supernatant and transfer to Spin-X HPLC filter tubes (Corning Incorporated, Cat # 8169) and centrifuge at 13,000 rpm for 5 minutes and take 5 µL from this solution and dilute in 495 µL of LCMS grade methanol (Fischer scientific, CAS # 67-56-1) in an 2mL glass auto sampler vial (Microsolv, Cat # 95025-WCV)
9. The samples are analyzed by LCMS-8040. (Shimadzu)

Data:

Day 1:

Time (min)	Assay 1		Assay 2		Assay 3		% remaining		
	DK-I-56-1 Peak area	Verapamil Peak area	DK-I-56-1 Peak area	Verapamil Peak area	DK-I-56-1 Peak area	Verapamil Peak area	Assay 1	Assay 2	Assay 3
0	398212	2354869	384127	2302725	368877	2255486	100.06	99.88	99.72
10	361492	2153664	350612	2137443	364427	2307335	99.31	98.22	96.30
20	353751	2156111	351711	2207523	349893	2196606	97.08	95.40	97.12
30	353643	2216473	345716	2211492	331654	2156417	94.41	93.60	93.78
40	354234	2233525	343748	2144927	339505	2163298	93.84	95.96	95.69
50	336838	2133427	333079	2140599	328962	2168061	93.42	93.17	92.51
60	327874	2121028	353537	2272689	327292	2208601	91.46	93.14	90.36

Table 1: Peak areas and % remaining values

Day 2:

Time (min)	Assay 1		Assay 2		Assay 3		(% remaining)		
	DK-I-56-1 Peak area	Verapamil Peak area	DK-I-56-1 Peak area	Verapamil Peak area	DK-I-56-1 Peak area	Verapamil Peak area	Assay 1	Assay 2	Assay 3
0	387196	2270706	377106	2186412	386760	2248705	99.71	100.27	99.99
10	362459	2137087	356334	2114930	366413	2165630	99.18	97.95	98.36
20	364780	2211877	350046	2137002	370479	2212311	96.44	95.23	97.36
30	363646	2245148	349102	2151510	357194	2208806	94.71	94.33	94.02
40	340384	2162279	352923	2200550	350775	2182739	92.05	93.24	93.43
50	344590	2126528	347741	2190384	353240	2162260	94.76	92.30	94.98
60	349875	2221871	353066	2202566	336952	2140953	92.08	93.19	91.50

Table 2: Peak areas and % remaining values

Calculation:

From the peak area, Calculate the following

$$\text{Peak area ratio} = \frac{\text{Peak area of test compound (DK-I-56-1)}}{\text{Peak area of internal standard (ISTD)}}$$

$$\text{\% remaining at time T} = \frac{\text{Peak area ratio at particular time T}}{\text{Peak area ratio at zero time point}} * 100$$

(T = 0, 10, 20,30,40,50 and 60)

DATA ANALYSIS:

Day 1

Linear regression analysis:

Slope: -0.001342 ± 0.0001303

At X= 60, Y = 4.518 ± 0.004697

R^2 = 0.8481

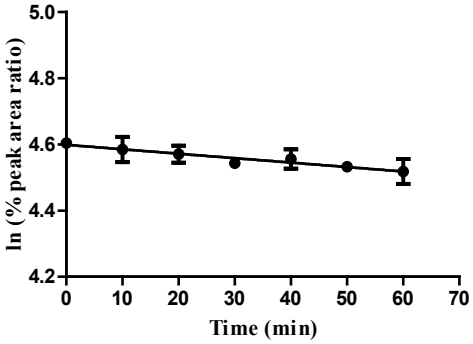

Metabolic Parameters:

Half-life: 516.39 ± 50.1 min

V_d: 100 µL/mg

Intrinsic clearance: 0.1342 µL/min/mg

Metabolic Rate: 2.684 nmol/min/mg

% remaining at 60 min: 91.65 ± 0.14 %

Day 2

Linear regression analysis:

Slope: -0.001326 ± 0.0001349

At X = 60, Y = 4.519 ± 0.004865

R^2 = 0.8357

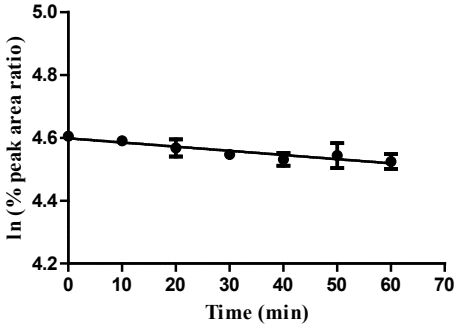

Metabolic Parameters:

Half-life: 522.62 ± 53.16 min

V_d: 100 µL/mg

Intrinsic clearance: 0.1326 µL/min/mg

Metabolic Rate: 2.652 nmol/min/mg

% remaining at 60 min: 91.74 ± 0.10 %

Note: The peak area ratios and natural log values are calculated using Microsoft excel 2010 and linear regression analysis is calculated using GraphPad prism.

Mouse Liver Microsomal Assay

Principal Investigator: Dr. Alexander Arnold
Operator: Revathi Kodali
Test Compound: **8b**
Concentration: 10 µM
Date: 05-04-2016
Facility: Milwaukee Institute for Drug Discovery

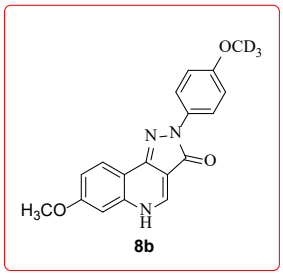

8b

Assay Protocol

Each evaluation included six independent assays carried out three at a time, on two different days

1. Preparation of solutions:
   a. 1 mM test compound in DMSO.
   b. 2 µM 4,5 Diphenyl Imidazole ice cold Acetonitrile (ISTD).
2. For a total volume of Microsomal Assay Mixture (MAM) 390 µL, sufficient for seven time points, combine the following
   a. 282 µL of 18.2 mΩ of water.
   b. 80 µL of 0.5 M potassium phosphate buffer (p^H 7.4)
   c. 20 µL of NADPH A. (Corning life sciences, Cat # 451220)
   d. 4 µL of NADPH B. (Corning life sciences, Cat # 451200)
   e. 4 µL of test compound.
3. Sonicate MAM for 5 min and meanwhile thaw microsomes (20 mg/mL) (Life technologies, Cat # MSMC-PL) on ice.
4. Aliquot 100 µL of ice cold ISTD into seven separate 1.5 mL conical vials and label them the time points for 0, 10, 20, 30, 40, 50, and 60 min.
5. Arrange the timer. Microsomes (Final concentration of 0.5 mg/mL) should be added to all time points except the zero time point.
6. Add 50 µL of the MAM solution to the conical vial labelled as zero time point. Place the remaining MAM solution in the incubator (37 ºC) for 5 min and initiate the reaction with addition of microsomes (8.8 µL) and record the time.
7. At the end of each time interval remove 50 µL and add to 100 µL ISTD in conical vial, sonicate for 10 sec and spin down at 10,000 rpm for 5 minutes.
8. Take 100 µL of supernatant and transfer to Spin-X HPLC filter tubes (Corning Incorporated, Cat # 8169) and centrifuge at 13,000 rpm for 5 minutes and take 5 µL from this solution and dilute in 495 µL of LCMS grade methanol (Fischer scientific, CAS # 67-56-1) in an 2mL glass auto sampler vial (Microsolv, Cat # 95025-WCV)
9. The samples are analyzed by LCMS-8040. (Shimadzu)

Data:

Day 1:

Time (min)	Assay 1		Assay 2		Assay 3		% remaining		
	DK-I-56-1 Peak area	Verapamil Peak area	DK-I-56-1 Peak area	Verapamil Peak area	DK-I-56-1 Peak area	Verapamil Peak area	Assay 1	Assay 2	Assay 3
0	388928	2307698	391664	2332218	402950	2417074	99.72	99.96	99.82
10	379319	2277526	364953	2238315	377640	2272011	98.55	97.05	99.52
20	371987	2305299	350938	2182276	355730	2231217	95.48	95.72	95.46
30	360570	2221865	344748	2175396	367885	2328394	96.02	94.33	94.61
40	355823	2247913	351540	2227323	352866	2210036	93.66	93.94	95.60
50	342826	2151478	363128	2309151	328306	2119895	94.28	93.60	92.73
60	351429	2183246	346906	2233889	348682	2236280	95.24	92.43	93.36

Table 1: Peak areas and % remaining values

Day 2:

Time (min)	Assay 1		Assay 2		Assay 3		(% remaining)		
	DK-I-56-1 Peak area	Verapamil Peak area	DK-I-56-1 Peak area	Verapamil Peak area	DK-I-56-1 Peak area	Verapamil Peak area	Assay 1	Assay 2	Assay 3
0	401832	2332034	399175	2395303	404444	2394973	100.18	99.79	99.92
10	398950	2326501	371579	2259018	381853	2286061	99.69	98.49	98.83
20	371128	2261581	372242	2319773	354429	2160499	95.40	96.08	97.07
30	365461	2192182	356359	2264013	354905	2197136	96.92	94.25	95.58
40	367394	2228779	341564	2141303	348008	2204773	95.83	95.51	93.39
50	355291	2187107	349208	2216275	354062	2198066	94.44	94.35	95.31
60	355799	2211839	350652	2298823	349085	2187612	93.52	91.33	94.42

Table 2: Peak areas and % remaining values

Calculation:

From the peak area, Calculate the following

$$\text{Peak area ratio} = \frac{\text{Peak area of test compound (DK-I-56-1)}}{\text{Peak area of internal standard (ISTD)}}$$

$$\text{\% remaining at time T} = \frac{\text{Peak area ratio at particular time T}}{\text{Peak area ratio at zero time point}} * 100$$

(T = 0, 10, 20,30,40,50 and 60)

DATA ANALYSIS:

Day 1

Linear regression analysis:

Slope: -0.001081 ± 0.0001303

At X= 60, Y = 4.529 ± 0.004696

R^2 = 0.7838

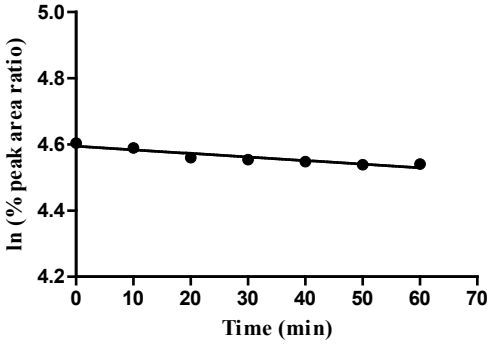

Metabolic Parameters:

Half-life: 641.07 ± 77 min

V_d: 100 µL/mg

Intrinsic clearance: 0.1081 µL/min/mg

Metabolic Rate: 2.162 nmol/min/mg

% remaining at 60 min: 92.66 ± 0.10 %

Day 2

Linear regression analysis:

Slope: -0.001124 ± 0.0001253

At X = 60, Y = 4.532 ± 0.004518

R^2 = 0.8089

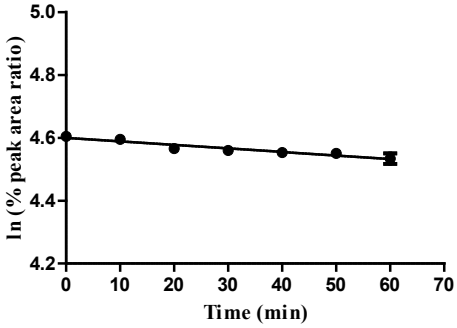

Metabolic Parameters:

Half-life: 616.54 ± 69 min

V_d: 100 µL/mg

Intrinsic clearance: 0.1124 µL/min/mg

Metabolic Rate: 2.248 nmol/min/mg

% remaining at 60 min: 92.94 ± 0.09 %

Note: The peak area ratios and natural log values are calculated using Microsoft excel 2010 and linear regression analysis is calculated using GraphPad prism.

Human Liver Microsomal Assay

Principal Investigator: Dr. Alexander Arnold
Operator: Revathi Kodali
Test Compound: **8c**
Concentration: 10 µM
Date: 06-17-2017
Facility: Milwaukee Institute for Drug Discovery

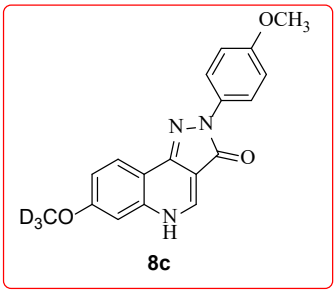

8c

Assay Protocol

Each evaluation included six independent assays carried out three at a time, on two different days

1. Preparation of solutions:
   a. 1 mM test compound in DMSO.
   b. 2 µM 4,5 Diphenyl Imidazole in Acetonitrile as internal standard (ISTD) (store on ice).
2. For a total volume of Microsomal Assay Mixture (MAM) 390 µL, sufficient for seven time points, combine the following
   a. 282 µL of 18.2 mΩ of water.
   b. 80 µL of 0.5 M potassium phosphate buffer (p^H 7.4)
   c. 20 µL of NADPH A. (Corning life sciences, Cat # 451220)
   d. 4 µL of NADPH B. (Corning life sciences, Cat # 451200)
   e. 4 µL of test compound.
3. Sonicate MAM for 5 min and meanwhile thaw microsomes (20 mg/mL) (BD Gentest, Cat # 452156) on ice.
4. Aliquot 100 µL of ice cold ISTD into seven separate 1.5 mL conical vials and label them the time points for 0, 10, 20, 30, 40, 50, and 60 min.
5. Arrange the timer. Microsomes (Final concentration of 0.5 mg/mL) should be added to all time points except the zero time point.
6. Add 50 µL of the MAM solution to the conical vial labelled as zero time point. Place the remaining MAM solution in the incubator (37 ºC) for 5 min and initiate the reaction with addition of microsomes (8.8 µL) and record the time.
7. At the end of each time interval remove 50 µL and add to 100 µL ISTD in conical vial, sonicate for 10 sec and spin down at 10,000 rpm for 5 minutes.
8. Take 100 µL of supernatant and transfer to Spin-X HPLC filter tubes (Corning Incorporated, Cat # 8169) and centrifuge at 13,000 rpm for 5 minutes and take 5 µL from this solution and dilute in 495 µL of LCMS grade methanol (Fischer scientific, CAS # 67-56-1) in an 2mL glass auto sampler vial (Microsolv, Cat # 95025-WCV)
9. The samples are analyzed by LCMS-8040. (Shimadzu)

Data:

Day 1:

Time (min)	Assay 1		Assay 2		Assay 3		% remaining		
	DK-II-3-1 Peak area	ISTD Peak area	DK-II-3-1 Peak area	ISTD Peak area	DK-II-3-1 Peak area	ISTD Peak area	Assay 1	Assay 2	Assay 3
0	236193	23908	240718	23550	242866	23587	100.00	99.99	99.99
10	232747	23689	228301	22980	236745	24005	99.45	97.19	95.77
20	220288	23974	235154	24176	220725	23502	93.01	95.15	91.20
30	229623	23893	230097	23822	231957	23406	97.28	94.49	96.24
40	226681	23894	228169	23790	232302	23693	96.03	93.82	95.21
50	226106	24008	224076	23499	222828	22836	95.33	93.28	94.76
60	209034	22893	224075	23243	222144	23009	92.42	94.31	93.76

Table 1: Peak areas and % remaining values

Day 2:

Time (min)	Assay 1		Assay 2		Assay 3		(% remaining)		
	DK-II-3-1 Peak area	ISTD Peak area	DK-II-3-1 Peak area	ISTD Peak area	DK-II-3-1 Peak area	ISTD Peak area	Assay 1	Assay 2	Assay 3
0	240293	23322	245499	23714	238099	23446	100.00	100.00	100.00
10	237690	23842	236607	23170	240575	24206	96.76	98.64	97.87
20	231496	23497	224523	23336	233912	23968	95.62	92.94	96.10
30	224366	22966	240144	24028	228386	23461	94.82	96.54	95.86
40	227905	24075	229073	23639	210756	22679	91.88	93.61	91.51
50	228544	23641	230508	23626	221648	23188	93.83	94.24	94.12
60	218997	23816	228654	24088	219423	22930	89.24	91.69	94.23

Table 2: Peak areas and % remaining values

Calculation:

From the peak area, Calculate the following

$$\text{Peak area ratio} = \frac{\text{Peak area of test compound (DK-II-3-1)}}{\text{Peak area of internal standard (ISTD)}}$$

$$\text{\% remaining at time T} = \frac{\text{Peak area ratio at particular time T}}{\text{Peak area ratio at zero time point}} * 100$$

(T = 0, 10, 20,30,40,50 and 60)

DATA ANALYSIS:

Day 1

Linear regression analysis:

Slope: -0.0008726 ± 0.0002206

At X= 60, Y = 4.534 ± 0.007955

$R^2 = 0.4515$

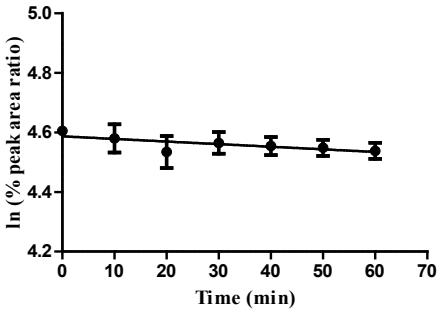

Metabolic Parameters:

Half-life: 794 ± 200 min

V_d: 100 µL/mg

Intrinsic clearance: 0.08726 µL/min/mg

Metabolic Rate: 1.7452 nmol/min/mg

% remaining at 60 min: 93 ± 0.16 %

Day 2

Linear regression analysis:

Slope: -0.001302± 0.0001877

At X = 60, Y = 4.517 ± 0.006767

$R^2 = 0.7171$

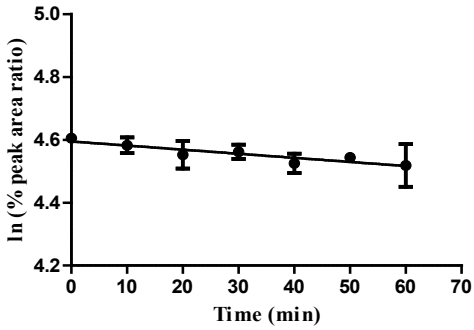

Metabolic Parameters:

Half-life: 532 ± 76 min

V_d: 100 µL/mg

Intrinsic clearance: 0.1302 µL/min/mg

Metabolic Rate: 2.604 nmol/min/mg

% remaining at 60 min: 91 ± 0.13 %

Note: The peak area ratios and natural log values are calculated using Microsoft excel 2010 and linear regression analysis is calculated using GraphPad prism.

Mouse Liver Microsomal Assay

Principal Investigator: Dr. Alexander Arnold
Operator: Revathi Kodali
Test Compound: **8c**
Concentration: 10 µM
Date: 04-08-2016
Facility: Milwaukee Institute for Drug Discovery

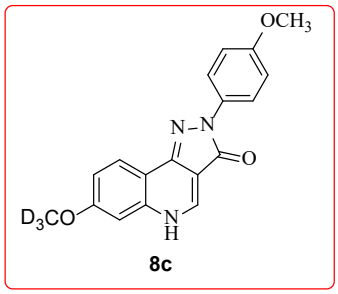

8c

Assay Protocol

Each evaluation included six independent assays carried out three at a time, on two different days

1. Preparation of solutions:
   a. 1 mM test compound in DMSO.
   b. 2 µM Verapamil in Acetonitrile (ACN) as internal standard (store on ice).
2. For a total volume of Microsomal Assay Mixture (MAM) 390 µL, sufficient for seven time points, combine the following
   a. 282 µL of 18.2 mΩ of water.
   b. 80 µL of 0.5 M potassium phosphate buffer (p^H 7.4)
   c. 20 µL of NADPH A. (Corning life sciences, Cat # 451220)
   d. 4 µL of NADPH B. (Corning life sciences, Cat # 451200)
   e. 4 µL of test compound.
3. Sonicate MAM for 5 min and meanwhile thaw microsomes (20 mg/mL) (Life technologies, Cat # MSMC-PL) on ice.
4. Aliquot 100 µL of ice cold ISTD into seven separate 1.5 mL conical vials and label them the time points for 0, 10, 20, 30, 40, 50, and 60 min.
5. Arrange the timer. Microsomes (Final concentration of 0.5 mg/mL) should be added to all time points except the zero time point.
6. Add 50 µL of the MAM solution to the conical vial labelled as zero time point. Place the remaining MAM solution in the incubator (37 ºC) for 5 min and initiate the reaction with addition of microsomes (8.8 µL) and record the time.
7. At the end of each time interval remove 50 µL and add to 100 µL ISTD in conical vial, sonicate for 10 sec and spin down at 10,000 rpm for 5 minutes.
8. Take 100 µL of supernatant and transfer to Spin-X HPLC filter tubes (Corning Incorporated, Cat # 8169) and centrifuge at 13,000 rpm for 5 minutes and take 5 µL from this solution and dilute in 495 µL of LCMS grade methanol (Fischer scientific, CAS # 67-56-1) in an 2mL glass auto sampler vial (Microsolv, Cat # 95025-WCV)
9. The samples are analyzed by LCMS-8040. (Shimadzu)

Data:

Day 1:

Time (min)	Assay 1		Assay 2		Assay 3		% remaining		
	DK-II-3-1 Peak area	Verapamil Peak area	DK-II-3-1 Peak area	Verapamil Peak area	DK-II-3-1 Peak area	Verapamil Peak area	Assay 1	Assay 2	Assay 3
0	111144	278595	98899	285987	104065	286966	99.98	99.94	99.90
10	107949	280252	95360	278895	99077	282663	96.53	98.82	96.56
20	106291	287540	92029	276919	96414	278874	92.64	96.05	95.24
30	104270	279360	91729	287346	97728	287461	93.54	92.26	93.65
40	101471	270388	93541	288645	96863	279779	94.05	93.66	95.37
50	105186	285058	92155	279402	94564	282182	92.48	95.32	92.31
60	106026	279377	95346	285213	97167	279799	95.11	96.61	95.66

Table 1: Peak areas and % remaining values

Day 2:

Time (min)	Assay 1		Assay 2		Assay 3		(% remaining)		
	DK-II-3-1 Peak area	Verapamil Peak area	DK-II-3-1 Peak area	Verapamil Peak area	DK-II-3-1 Peak area	Verapamil Peak area	Assay 1	Assay 2	Assay 3
0	92576	281935	98496	277116	100164	285161	100.11	100.12	100.07
10	92661	292879	95851	279035	96979	287881	96.45	96.76	95.97
20	89484	287644	97725	295691	83913	248471	94.84	93.09	96.21
30	91955	299743	96183	282336	95556	290799	93.53	95.96	93.61
40	90362	289887	94361	279974	97195	299641	95.03	94.93	92.41
50	87875	277434	92404	278043	93112	274697	96.56	93.61	96.57
60	88889	287296	92451	285458	92002	279777	94.32	91.23	93.68

Table 2: Peak areas and % remaining values

Calculation:

From the peak area, Calculate the following

$$\text{Peak area ratio} = \frac{\text{Peak area of test compound (DK-II-3-1)}}{\text{Peak area of internal standard (Verapamil)}}$$

$$\text{\% remaining at time T = (T = 0, 10, 20,30,40,50 and 60)} \quad \frac{\text{Peak area ratio at particular time T}}{\text{Peak area ratio at zero time point}} * 100$$

DATA ANALYSIS:

Day 1

Linear regression analysis:

Slope: -0.0007583 ± 0.0002330

At X= 60, Y = 4.536 ± 0.008400

R^2 = 0.3580

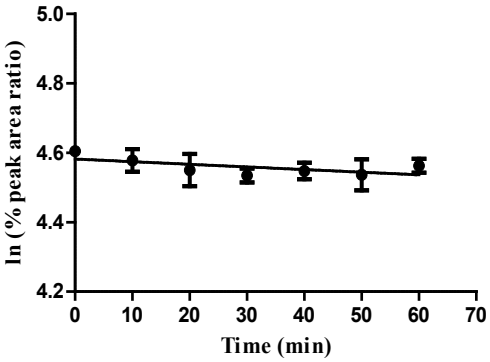

Metabolic Parameters:

Half-life: 913.88 ± 280.85 min

V_d: 100 µL/mg

Intrinsic clearance: 0.07583 µL/min/mg

Metabolic Rate: 1.5166 nmol/min/mg

% remaining at 60 min: 93.31 ± 0.17 %

Day 2

Linear regression analysis:

Slope: -0.0008643± 0.0002043

At X = 60, Y = 4.533 ± 0.007365

R^2 = 0.4852

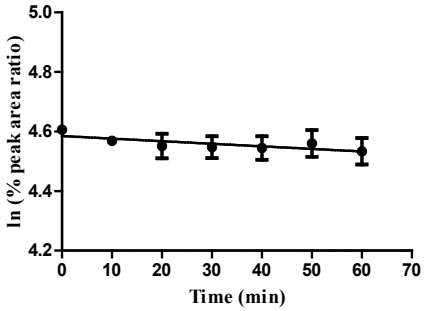

Metabolic Parameters:

Half-life: 801.80 ± 189.52 min

V_d: 100 µL/mg

Intrinsic clearance: 0.08643 µL/min/mg

Metabolic Rate: 1.7286 nmol/min/mg

% remaining at 60 min: 93.03 ± 0.15 %

Note: The peak area ratios and natural log values are calculated using Microsoft excel 2010 and linear regression analysis is calculated using GraphPad prism.

Human Liver Microsomal Assay

Principal Investigator: Dr. Alexander Arnold
Operator: Revathi Kodali
Test Compound: **8d**
Concentration: 10 µM
Date: 02-22-2016
Facility: Milwaukee Institute for Drug Discovery

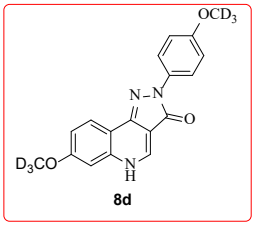

8d

Assay Protocol

Each evaluation included six independent assays carried out three at a time, on two different days

1. Preparation of solutions:
   a. 1 mM test compound in DMSO.
   b. 2 µM Verapamil in Acetonitrile (ACN) as internal standard (store on ice).
2. For a total volume of Microsomal Assay Mixture (MAM) 390 µL, sufficient for seven time points, combine the following
   a. 282 µL of 18.2 mΩ of water.
   b. 80 µL of 0.5 M potassium phosphate buffer (p^H 7.4)
   c. 20 µL of NADPH A. (Corning life sciences, Cat # 451220)
   d. 4 µL of NADPH B. (Corning life sciences, Cat # 451200)
   e. 4 µL of test compound.
3. Sonicate MAM for 5 min and meanwhile thaw microsomes (20 mg/mL) (BD Gentest, Cat # 452156) on ice.
4. Aliquot 100 µL of ice cold ISTD into seven separate 1.5 mL conical vials and label them the time points for 0, 10, 20, 30, 40, 50, and 60 min.
5. Arrange the timer. Microsomes (Final concentration of 0.5 mg/mL) should be added to all time points except the zero time point.
6. Add 50 µL of the MAM solution to the conical vial labelled as zero time point. Place the remaining MAM solution in the incubator (37 ºC) for 5 min and initiate the reaction with addition of microsomes (8.8 µL) and record the time.
7. At the end of each time interval remove 50 µL and add to 100 µL ISTD in conical vial, sonicate for 10 sec and spin down at 10,000 rpm for 5 minutes.
8. Take 100 µL of supernatant and transfer to Spin-X HPLC filter tubes (Corning Incorporated, Cat # 8169) and centrifuge at 13,000 rpm for 5 minutes and take 5 µL from this solution and dilute in 495 µL of LCMS grade methanol (Fischer scientific, CAS # 67-56-1) in an 2mL glass auto sampler vial (Microsolv, Cat # 95025-WCV)
9. The samples are analyzed by LCMS-8040. (Shimadzu)

Data:

Day 1:

Time (min)	Assay 1		Assay 2		Assay 3		% remaining		
	DK-I-60-3 Peak area	Verapamil Peak area	DK-I-60-3 Peak area	Verapamil Peak area	DK-I-60-3 Peak area	Verapamil Peak area	Assay 1	Assay 2	Assay 3
0	119623	751693	123300	762556	120046	764558	100.08	99.19	100.00
10	114114	768963	114322	764031	110461	740708	93.33	91.79	94.98
20	110327	769408	115777	753029	106689	743037	90.18	94.32	91.45
30	112935	756232	115004	757564	112745	750648	93.92	93.13	95.66
40	110428	744917	111041	740898	108647	736750	93.23	91.94	93.92
50	109616	758076	116028	753982	106766	745883	90.94	94.40	91.17
60	106932	741303	115257	745460	111099	754822	90.72	94.85	93.74

Table 1: Peak areas and % remaining values

Day 2:

Time (min)	Assay 1		Assay 2		Assay 3		(% remaining)		
	DK-I-60-3 Peak area	Verapamil Peak area	DK-I-60-3 Peak area	Verapamil Peak area	DK-I-60-3 Peak area	Verapamil Peak area	Assay 1	Assay 2	Assay 3
0	124924	767904	102412	749745	117099	759194	99.80	99.70	100.15
10	115805	748997	100631	765396	109568	740171	94.85	95.96	96.12
20	108862	713542	99251	769134	105247	741358	93.59	94.19	92.18
30	110702	750240	98189	771121	104484	736667	90.52	92.94	92.10
40	114315	765884	98401	763993	103824	742724	91.57	94.01	90.77
50	104617	699417	98970	776043	108827	751806	91.76	93.08	93.99
60	109088	730464	100918	777766	109146	763644	91.62	94.71	92.81

Table 2: Peak areas and % remaining values

Calculation:

From the peak area, Calculate the following

$$\text{Peak area ratio} = \frac{\text{Peak area of test compound (DK-I-60-3)}}{\text{Peak area of internal standard (Verapamil)}}$$

$$\text{\% remaining at time T = (T = 0, 10, 20,30,40,50 and 60)} \quad \frac{\text{Peak area ratio at particular time T}}{\text{Peak area ratio at zero time point}} * 100$$

DATA ANALYSIS:

Day 1

Linear regression analysis:

Slope: -0.0007917 ± 0.0002839

At X= 60, Y = 4.519 ± 0.01023

R^2 = 0.2905

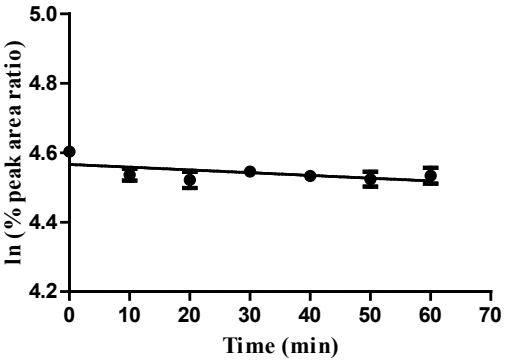

Metabolic Parameters:

Half-life: 875.33 ± 313 min

V_d: 100 µL/mg

Intrinsic clearance: 0.07917 µL/min/mg

Metabolic Rate: 1.5834 nmol/min/mg

% remaining at 60 min: 91.74 ± 0.20 %

Day 2

Linear regression analysis:

Slope: -0.001010 ± 0.0002414

At X = 60, Y = 4.514 ± 0.008704

R^2 = 0.4793

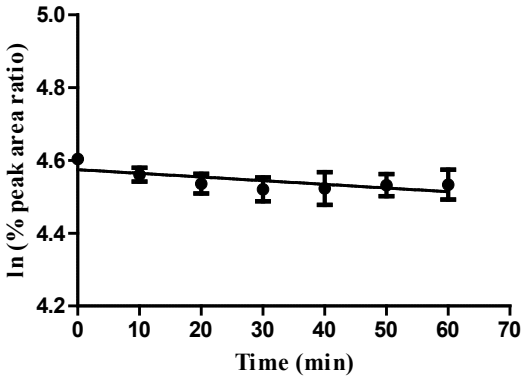

Metabolic Parameters:

Half-life: 686.13 ± 164 min

V_d: 100 µL/mg

Intrinsic clearance: 0.101 µL/min/mg

Metabolic Rate: 2.02 nmol/min/mg

% remaining at 60 min: 91.28 ± 0.17 %

Note: The peak area ratios and natural log values are calculated using Microsoft excel 2010 and linear regression analysis is calculated using GraphPad prism.

Mouse Liver Microsomal Assay

Principal Investigator: Dr. Alexander Arnold
Operator: Revathi Kodali
Test Compound: **8d**
Concentration: 10 µM
Date: 02-22-2016
Facility: Milwaukee Institute for Drug Discovery

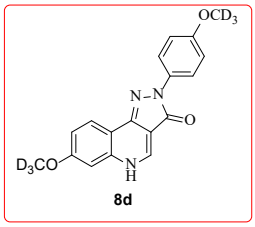

8d

Assay Protocol

Each evaluation included six independent assays carried out three at a time, on two different days

1. Preparation of solutions:
   a. 1 mM test compound in DMSO.
   b. 2 µM Verapamil in Acetonitrile (ACN) as internal standard (store on ice).
2. For a total volume of Microsomal Assay Mixture (MAM) 390 µL, sufficient for seven time points, combine the following
   a. 282 µL of 18.2 mΩ of water.
   b. 80 µL of 0.5 M potassium phosphate buffer (p^H 7.4)
   c. 20 µL of NADPH A. (Corning life sciences, Cat # 451220)
   d. 4 µL of NADPH B. (Corning life sciences, Cat # 451200)
   e. 4 µL of test compound.
3. Sonicate MAM for 5 min and meanwhile thaw microsomes (20 mg/mL) (Life technologies, Cat # MSMC-PL) on ice.
4. Aliquot 100 µL of ice cold ISTD into seven separate 1.5 mL conical vials and label them the time points for 0, 10, 20, 30, 40, 50, and 60 min.
5. Arrange the timer. Microsomes (Final concentration of 0.5 mg/mL) should be added to all time points except the zero time point.
6. Add 50 µL of the MAM solution to the conical vial labelled as zero time point. Place the remaining MAM solution in the incubator (37 ºC) for 5 min and initiate the reaction with addition of microsomes (8.8 µL) and record the time.
7. At the end of each time interval remove 50 µL and add to 100 µL ISTD in conical vial, sonicate for 10 sec and spin down at 10,000 rpm for 5 minutes.
8. Take 100 µL of supernatant and transfer to Spin-X HPLC filter tubes (Corning Incorporated, Cat # 8169) and centrifuge at 13,000 rpm for 5 minutes and take 5 µL from this solution and dilute in 495 µL of LCMS grade methanol (Fischer scientific, CAS # 67-56-1) in an 2mL glass auto sampler vial (Microsolv, Cat # 95025-WCV)
9. The samples are analyzed by LCMS-8040. (Shimadzu)

Data:

Day 1:

Time (min)	Assay 1		Assay 2		Assay 3		% remaining		
	DK-I-60-3 Peak area	Verapamil Peak area	DK-I-60-3 Peak area	Verapamil Peak area	DK-I-60-3 Peak area	Verapamil Peak area	Assay 1	Assay 2	Assay 3
0	106722	720638	112675	716355	108597	724437	100.06	100.18	99.93
10	104394	710505	111379	745295	109849	747161	99.27	95.18	98.01
20	98781	705588	108591	749281	107471	741115	94.59	92.31	96.67
30	103778	727932	109486	735798	99277	732657	96.32	94.77	90.33
40	102609	733376	105488	742147	109527	773078	94.53	90.53	94.45
50	101605	729328	112939	745040	106452	762456	94.13	96.55	93.07
60	102646	738921	107241	724588	109861	756321	93.86	94.26	96.83

Table 1: Peak areas and % remaining values

Day 2:

Time (min)	Assay 1		Assay 2		Assay 3		(% remaining)		
	DK-I-60-3 Peak area	Verapamil Peak area	DK-I-60-3 Peak area	Verapamil Peak area	DK-I-60-3 Peak area	Verapamil Peak area	Assay 1	Assay 2	Assay 3
0	104490	754231	102920	732920	108522	731478	99.66	100.30	100.24
10	100281	749451	105884	760165	110207	781689	96.26	99.49	95.261
20	95278	760108	102711	770740	103552	746542	90.17	95.18	93.72
30	100096	750328	100660	761342	103925	755479	95.97	94.43	92.94
40	94133	731526	97701	748691	105962	734495	92.57	93.21	97.47
50	101839	774789	103090	781126	104050	752296	94.56	94.26	93.45
60	99525	754772	98905	752921	103084	739907	94.86	93.83	94.13

Table 2: Peak areas and % remaining values

Calculation:

From the peak area, Calculate the following

$$\text{Peak area ratio} = \frac{\text{Peak area of test compound (DK-I-60-3)}}{\text{Peak area of internal standard (Verapamil)}}$$

$$\text{\% remaining at time T} = \frac{\text{Peak area ratio at particular time T}}{\text{Peak area ratio at zero time point}} * 100$$

(T = 0, 10, 20,30,40,50 and 60)

DATA ANALYSIS:

Day 1

Linear regression analysis:

Slope: -0.0008286 ± 0.0002774

At X= 60, Y = 4.534 ± 0.01000

R^2 = 0.3195

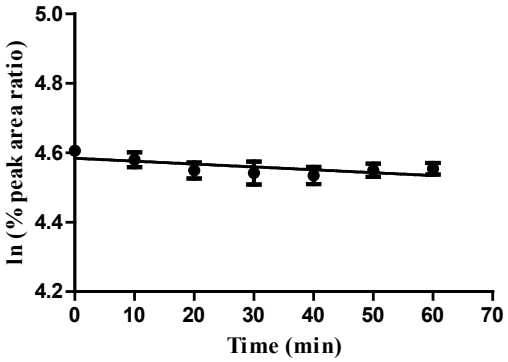

Metabolic Parameters:

Half-life: 836.35 ± 280 min

V_d: 100 µL/mg

Intrinsic clearance: 0.08286 µL/min/mg

Metabolic Rate: 1.6572 nmol/min/mg

% remaining at 60 min: 93.13 ± 0.20 %

Day 2

Linear regression analysis:

Slope: -0.0008083 ± 0.0002580

At X = 60, Y = 4.533 ± 0.009301

R^2 = 0.3407

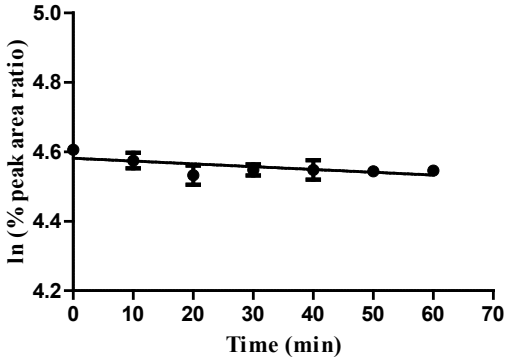

Metabolic Parameters:

Half-life: 857.35 ± 273 min

V_d: 100 µL/mg

Intrinsic clearance: 0.08083 µL/min/mg

Metabolic Rate: 1.6166 nmol/min/mg

% remaining at 60 min: 93.03 ± 0.19 %

Note: The peak area ratios and natural log values are calculated using Microsoft excel 2010 and linear regression analysis is calculated using GraphPad prism.

Human Liver Microsomal Assay

Principal Investigator: Dr. Alexander Arnold
Operator: Revathi Kodali
Test Compound: **8e**
Concentration: 10 µM
Date: 09-06-2017
Facility: Milwaukee Institute for Drug Discovery

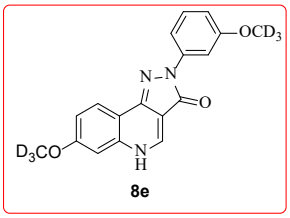

8e

Assay Protocol

Each evaluation included six independent assays carried out three at a time, on two different days

1. Preparation of solutions:
   a. 1 mM test compound in DMSO.
   b. 1 µM 4,5 Di Phenyl Imidazole in ice cold Acetonitrile (ISTD).
2. For a total volume of Microsomal Assay Mixture (MAM) 390 µL, sufficient for seven time points, combine the following
   a. 282 µL of 18.2 mΩ of water.
   b. 80 µL of 0.5 M potassium phosphate buffer (p^H 7.4)
   c. 20 µL of NADPH A. (Corning life sciences, Cat # 451220)
   d. 4 µL of NADPH B. (Corning life sciences, Cat # 451200)
   e. 4 µL of test compound.
3. Sonicate MAM for 5 min and meanwhile thaw microsomes (20 mg/mL) (BD Biosciences, Cat # 452156) on ice.
4. Aliquot 100 µL of ice cold ISTD into seven separate 1.5 mL conical vials and label them the time points for 0, 10, 20, 30, 40, 50, and 60 min.
5. Arrange the timer. Microsomes (Final concentration of 0.5 mg/mL) should be added to all time points except the zero time point.
6. Add 50 µL of the MAM solution to the conical vial labelled as zero time point. Place the remaining MAM solution in the incubator (37 ºC) for 5 min and initiate the reaction with addition of microsomes (8.8 µL) and record the time.
7. At the end of each time interval remove 50 µL and add to 100 µL ISTD in conical vial, sonicate for 10 sec and spin down at 10,000 rpm for 5 minutes.
8. Take 100 µL of supernatant and transfer to Spin-X HPLC filter tubes (Corning Incorporated, Cat # 8169) and centrifuge at 13,000 rpm for 5 minutes and take 5 µL from this solution and dilute in 495 µL of LCMS grade methanol (Fischer scientific, CAS # 67-56-1) in an 2mL glass auto sampler vial (Microsolv, Cat # 95025-WCV)
9. The samples are analyzed by LCMS-8040. (Shimadzu)

Data:

Day 1:

Time (min)	Assay 1		Assay 2		Assay 3		% remaining		
	DK-I-94-1 Peak area	ISTD Peak area	DK-I-94-1 Peak area	ISTD Peak area	DK-I-94-1 Peak area	ISTD Peak area	Assay 1	Assay 2	Assay 3
0	99306	99262	103648	98877	108203	95577	100.04	100.02	100.00
10	98286	99764	97179	99045	99005	90106	98.51	93.62	97.06
20	89132	92094	88632	88730	96921	89394	96.78	95.31	95.77
30	85234	90864	82687	83885	100259	92635	93.80	94.05	95.61
40	83864	93281	95998	100515	107622	105755	89.90	91.13	89.89
50	81572	89315	95124	97589	95099	90297	91.33	93.01	93.03
60	83372	93197	87647	90647	89690	92014	89.45	92.26	86.10

Table 1: Peak areas and % remaining values

Day 2:

Time (min)	Assay 1		Assay 2		Assay 3		(% remaining)		
	DK-I-94-1 Peak area	ISTD Peak area	DK-I-94-1 Peak area	ISTD Peak area	DK-I-94-1 Peak area	ISTD Peak area	Assay 1	Assay 2	Assay 3
0	106199	100912	107611	98271	105203	101265	100.03	100.00	99.98
10	97245	98407	106776	99495	99848	98640	93.93	98.00	97.42
20	97442	100104	94509	89958	97460	101350	92.52	95.94	92.55
30	79922	81324	90285	86895	95071	104982	93.41	94.88	87.16
40	95021	100662	101710	100862	89791	95078	89.73	92.09	90.89
50	98998	99580	88800	84984	98193	103362	94.50	95.42	91.43
60	98842	103127	100338	102233	89001	92949	91.10	89.63	92.15

Table 2: Peak areas and % remaining values

Calculation:

From the peak area, Calculate the following

$$\text{Peak area ratio} = \frac{\text{Peak area of test compound (DK-I-94-1)}}{\text{Peak area of internal standard (ISTD)}}$$

$$\text{\% remaining at time T} = \frac{\text{Peak area ratio at particular time T}}{\text{Peak area ratio at zero time point}} * 100$$

(T = 0, 10, 20,30,40,50 and 60)

DATA ANALYSIS:

Day 1

Linear regression analysis:

Slope: -0.001729 ± 0.0002190

At X= 60, Y = 4.492 ± 0.007895

R^2 = 0.7664

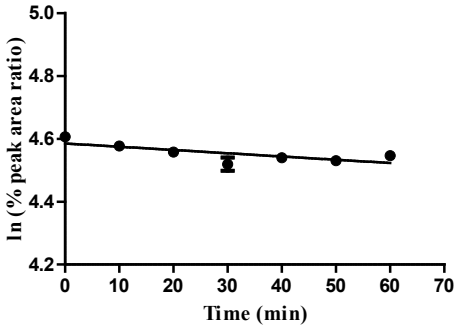

Metabolic Parameters:

Half-life: 400 ± 50 min

V_d: 2000 µL/mg

Intrinsic clearance: 0.1729 µL/min/mg

Metabolic Rate: 3.458 nmol/min/mg

% remaining at 60 min: 89 ± 0.15 %

Day 2

Linear regression analysis:

Slope: -0.001321 ± 0.0003047

At X = 60, Y = 4.503 ± 0.01098

R^2 = 0.4975

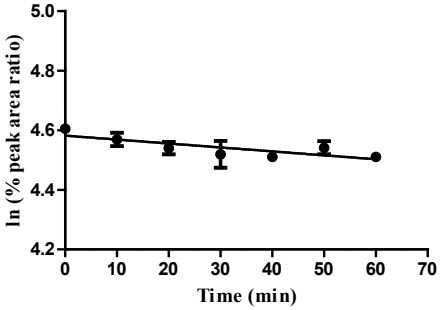

Metabolic Parameters:

Half-life: 524 ± 121 min

V_d: 2000 µL/mg

Intrinsic clearance: 0.1321 µL/min/mg

Metabolic Rate: 2.642 nmol/min/mg

% remaining at 60 min: 90 ± 0.22 %

Note: The peak area ratios and natural log values are calculated using Microsoft excel 2010 and linear regression analysis is calculated using GraphPad prism.

Mouse Liver Microsomal Assay

Principal Investigator: Dr. Alexander Arnold
Operator: Revathi Kodali
Test Compound: **8e**
Concentration: 10 µM
Date: 09-06-2017
Facility: Milwaukee Institute for Drug Discovery

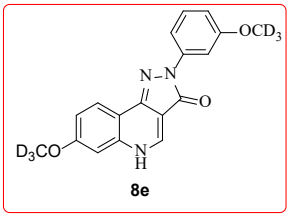

8e

Assay Protocol

Each evaluation included six independent assays carried out three at a time, on two different days

1. Preparation of solutions:
   a. 1 mM test compound in DMSO.
   b. 1 µM 4,5 Di Phenyl Imidazole in ice cold Acetonitrile (ISTD).
2. For a total volume of Microsomal Assay Mixture (MAM) 390 µL, sufficient for seven time points, combine the following
   a. 282 µL of 18.2 mΩ of water.
   b. 80 µL of 0.5 M potassium phosphate buffer (p^H 7.4)
   c. 20 µL of NADPH A. (Corning life sciences, Cat # 451220)
   d. 4 µL of NADPH B. (Corning life sciences, Cat # 451200)
   e. 4 µL of test compound.
3. Sonicate MAM for 5 min and meanwhile thaw microsomes (20 mg/mL) (Life technologies, Cat # MSMC-PL) on ice.
4. Aliquot 100 µL of ice cold ISTD into seven separate 1.5 mL conical vials and label them the time points for 0, 10, 20, 30, 40, 50, and 60 min.
5. Arrange the timer. Microsomes (Final concentration of 0.5 mg/mL) should be added to all time points except the zero time point.
6. Add 50 µL of the MAM solution to the conical vial labelled as zero time point. Place the remaining MAM solution in the incubator (37 ºC) for 5 min and initiate the reaction with addition of microsomes (8.8 µL) and record the time.
7. At the end of each time interval remove 50 µL and add to 100 µL ISTD in conical vial, sonicate for 10 sec and spin down at 10,000 rpm for 5 minutes.
8. Take 100 µL of supernatant and transfer to Spin-X HPLC filter tubes (Corning Incorporated, Cat # 8169) and centrifuge at 13,000 rpm for 5 minutes and take 5 µL from this solution and dilute in 495 µL of LCMS grade methanol (Fischer scientific, CAS # 67-56-1) in an 2mL glass auto sampler vial (Microsolv, Cat # 95025-WCV)
9. The samples are analyzed by LCMS-8040. (Shimadzu)

Data:

Day 1:

Time (min)	Assay 1		Assay 2		Assay 3		% remaining		
	DK-I-94-1 Peak area	ISTD Peak area	DK-I-94-1 Peak area	ISTD Peak area	DK-I-94-1 Peak area	ISTD Peak area	Assay 1	Assay 2	Assay 3
0	104572	99604	112024	110770	108778	96978	99.98	100.03	99.97
10	91738	90948	88211	90287	100246	92692	96.06	96.63	96.39
20	91764	95841	90046	92865	98441	94038	91.18	95.90	93.30
30	86135	89117	87391	93992	93748	92059	92.05	91.96	90.76
40	100441	100218	93070	99075	93657	90546	95.45	92.91	92.18
50	85762	89440	85410	89605	101654	94108	91.32	94.28	96.27
60	92817	99307	87745	100069	93007	91710	89.01	86.73	90.38

Table 1: Peak areas and % remaining values

Day 2:

Time (min)	Assay 1		Assay 2		Assay 3		(% remaining)		
	DK-I-94-1 Peak area	ISTD Peak area	DK-I-94-1 Peak area	ISTD Peak area	DK-I-94-1 Peak area	ISTD Peak area	Assay 1	Assay 2	Assay 3
0	104699	1018323	110764	98225	108659	96253	99.82	99.96	99.99
10	98572	996723	96734	93146	93783	86232	96.01	92.06	96.33
20	97486	965623	107264	100826	96862	90872	98.01	94.31	94.41
30	100088	1025797	110260	106074	94846	92762	94.72	92.15	90.56
40	97817	985235	97958	92817	91545	85352	96.39	93.56	95.00
50	89664	956232	98009	89823	89496	84533	91.03	96.73	93.77
60	91032	927232	91730	87674	99959	100318	95.31	92.75	88.25

Table 2: Peak areas and % remaining values

Calculation:

From the peak area, Calculate the following

$$\text{Peak area ratio} = \frac{\text{Peak area of test compound (DK-I-94-1)}}{\text{Peak area of internal standard (ISTD)}}$$

$$\text{\% remaining at time T} = \frac{\text{Peak area ratio at particular time T}}{\text{Peak area ratio at zero time point}} * 100$$

(T = 0, 10, 20,30,40,50 and 60)

DATA ANALYSIS:

Day 1

Linear regression analysis:

Slope: -0.001462 ± 0.0002736

At X= 60, Y = 4.498 ± 0.009865

R^2 = 0.6004

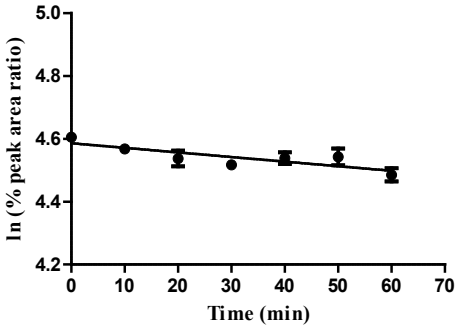

Metabolic Parameters:

Half-life: 474 ± 88 min

V_d: 2000 µL/mg

Intrinsic clearance: 0.1462 µL/min/mg

Metabolic Rate: 2.924 nmol/min/mg

% remaining at 60 min: 89 ± 0.2 %

Day 2

Linear regression analysis:

Slope: -0.0009774 ± 0.0002948

At X = 60, Y = 4.522 ± 0.01063

R^2 = 0.4687

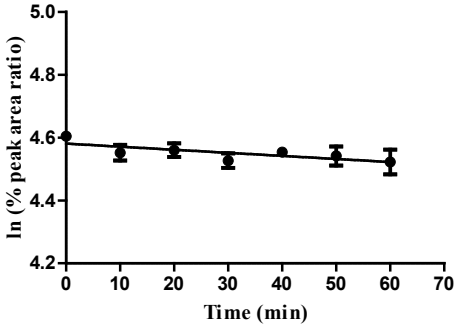

Metabolic Parameters:

Half-life: 709 ± 213 min

V_d: 2000 µL/mg

Intrinsic clearance: 0.09774 µL/min/mg

Metabolic Rate: 1.9548 nmol/min/mg

% remaining at 60 min: 92 ± 0.21 %

Note: The peak area ratios and natural log values are calculated using Microsoft excel 2010 and linear regression analysis is calculated using GraphPad prism.

Human Liver Microsomal Assay

Principal Investigator: Dr. Alexander Arnold
Operator: Revathi Kodali
Test Compound: **8f**
Concentration: 10 µM
Date: 09-06-2017
Facility: Milwaukee Institute for Drug Discovery

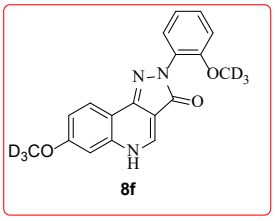

8f

Assay Protocol

Each evaluation included six independent assays carried out three at a time, on two different days

1. Preparation of solutions:
   a. 1 mM test compound in DMSO.
   b. 1 µM 4,5 Di Phenyl Imidazole in ice cold Acetonitrile (ISTD).
2. For a total volume of Microsomal Assay Mixture (MAM) 390 µL, sufficient for seven time points, combine the following
   a. 282 µL of 18.2 mΩ of water.
   b. 80 µL of 0.5 M potassium phosphate buffer (p^H 7.4)
   c. 20 µL of NADPH A. (Corning life sciences, Cat # 451220)
   d. 4 µL of NADPH B. (Corning life sciences, Cat # 451200)
   e. 4 µL of test compound.
3. Sonicate MAM for 5 min and meanwhile thaw microsomes (20 mg/mL) (BD Biosciences, Cat # 452156) on ice.
4. Aliquot 100 µL of ice cold ISTD into seven separate 1.5 mL conical vials and label them the time points for 0, 10, 20, 30, 40, 50, and 60 min.
5. Arrange the timer. Microsomes (Final concentration of 0.5 mg/mL) should be added to all time points except the zero time point.
6. Add 50 µL of the MAM solution to the conical vial labelled as zero time point. Place the remaining MAM solution in the incubator (37 ºC) for 5 min and initiate the reaction with addition of microsomes (8.8 µL) and record the time.
7. At the end of each time interval remove 50 µL and add to 100 µL ISTD in conical vial, sonicate for 10 sec and spin down at 10,000 rpm for 5 minutes.
8. Take 100 µL of supernatant and transfer to Spin-X HPLC filter tubes (Corning Incorporated, Cat # 8169) and centrifuge at 13,000 rpm for 5 minutes and take 5 µL from this solution and dilute in 495 µL of LCMS grade methanol (Fischer scientific, CAS # 67-56-1) in an 2mL glass auto sampler vial (Microsolv, Cat # 95025-WCV)
9. The samples are analyzed by LCMS-8040. (Shimadzu)

Data:

Day 1:

Time (min)	Assay 1		Assay 2		Assay 3		% remaining		
	DK-I-90-1 Peak area	ISTD Peak area	DK-I-90-1 Peak area	ISTD Peak area	DK-I-90-1 Peak area	ISTD Peak area	Assay 1	Assay 2	Assay 3
0	236608	97337	238736	98664	232713	100728	99.99	99.98	100.01
10	221427	95464	225705	100063	238008	110325	95.41	93.20	93.39
20	217811	98301	237758	101900	210143	100442	91.14	96.41	90.57
30	209423	93592	211271	94675	200168	93236	92.04	92.21	92.93
40	217846	93678	228590	100491	253235	117263	95.65	93.99	93.48
50	218429	98402	227561	105740	219220	100623	91.31	88.92	94.31
60	194463	87967	218960	98077	194235	94232	90.93	92.25	89.23

Table 1: Peak areas and % remaining values

Day 2:

Time (min)	Assay 1		Assay 2		Assay 3		(% remaining)		
	DK-I-90-1 Peak area	ISTD Peak area	DK-I-90-1 Peak area	ISTD Peak area	DK-I-90-1 Peak area	ISTD Peak area	Assay 1	Assay 2	Assay 3
0	238439	97456	225640	99282	232092	101664	99.98	99.98	99.99
10	221643	94344	214627	98997	219618	98274	96.00	95.38	97.88
20	213035	93895	201497	95083	213067	99571	92.72	93.23	93.73
30	199456	89662	198648	90822	231128	106927	90.90	96.22	94.68
40	226568	98362	199648	98765	210414	99083	94.13	88.93	93.01
50	197689	88901	227074	109028	245138	119022	90.87	91.62	90.21
60	244235	103839	190357	90631	233617	110390	96.12	92.40	92.69

Table 2: Peak areas and % remaining values

Calculation:

From the peak area, Calculate the following

$$\text{Peak area ratio} = \frac{\text{Peak area of test compound (DK-I-90-1)}}{\text{Peak area of internal standard (ISTD)}}$$

$$\text{\% remaining at time T (T = 0, 10, 20,30,40,50 and 60)} = \frac{\text{Peak area ratio at particular time T}}{\text{Peak area ratio at zero time point}} * 100$$

DATA ANALYSIS:

Day 1

Linear regression analysis:

Slope: -0.001160 ± 0.0002806

At X= 60, Y = 4.505 ± 0.01012

R^2 = 0.4734

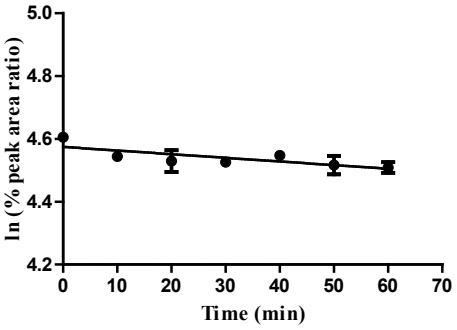

Metabolic Parameters:

Half-life: 597 ± 114 min

V_d: 2000 µL/mg

Intrinsic clearance: 0.116 µL/min/mg

Metabolic Rate: 2.32 nmol/min/mg

% remaining at 60 min: 90 ± 0.20 %

Day 2

Linear regression analysis:

Slope: -0.001161 ± 0.0002733

At X = 60, Y = 4.511 ± 0.009855

R^2 = 0.4869

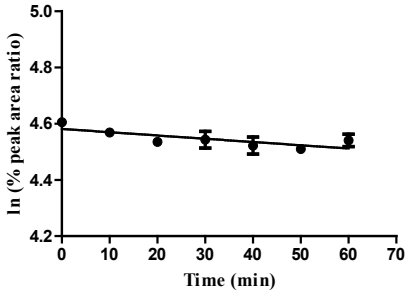

Metabolic Parameters:

Half-life: 596 ± 140 min

V_d: 2000 µL/mg

Intrinsic clearance: 0.1161 µL/min/mg

Metabolic Rate: 2.322 nmol/min/mg

% remaining at 60 min: 91 ± 0.19 %

Note: The peak area ratios and natural log values are calculated using Microsoft excel 2010 and linear regression analysis is calculated using GraphPad prism.

Mouse Liver Microsomal Assay

Principal Investigator: Dr. Alexander Arnold
Operator: Revathi Kodali
Test Compound: **8f**
Concentration: 10 µM
Date: 09-06-2017
Facility: Milwaukee Institute for Drug Discovery

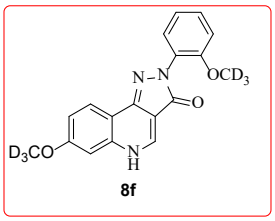

8f

Assay Protocol

Each evaluation included six independent assays carried out three at a time, on two different days

1. Preparation of solutions:
   a. 1 mM test compound in DMSO.
   b. 1 µM 4,5 Di Phenyl Imidazole in ice cold Acetonitrile (ISTD).
2. For a total volume of Microsomal Assay Mixture (MAM) 390 µL, sufficient for seven time points, combine the following
   a. 282 µL of 18.2 mΩ of water.
   b. 80 µL of 0.5 M potassium phosphate buffer (p^H 7.4)
   c. 20 µL of NADPH A. (Corning life sciences, Cat # 451220)
   d. 4 µL of NADPH B. (Corning life sciences, Cat # 451200)
   e. 4 µL of test compound.
3. Sonicate MAM for 5 min and meanwhile thaw microsomes (20 mg/mL) (Life technologies, Cat # MSMC-PL) on ice.
4. Aliquot 100 µL of ice cold ISTD into seven separate 1.5 mL conical vials and label them the time points for 0, 10, 20, 30, 40, 50, and 60 min.
5. Arrange the timer. Microsomes (Final concentration of 0.5 mg/mL) should be added to all time points except the zero time point.
6. Add 50 µL of the MAM solution to the conical vial labelled as zero time point. Place the remaining MAM solution in the incubator (37 ºC) for 5 min and initiate the reaction with addition of microsomes (8.8 µL) and record the time.
7. At the end of each time interval remove 50 µL and add to 100 µL ISTD in conical vial, sonicate for 10 sec and spin down at 10,000 rpm for 5 minutes.
8. Take 100 µL of supernatant and transfer to Spin-X HPLC filter tubes (Corning Incorporated, Cat # 8169) and centrifuge at 13,000 rpm for 5 minutes and take 5 µL from this solution and dilute in 495 µL of LCMS grade methanol (Fischer scientific, CAS # 67-56-1) in an 2mL glass auto sampler vial (Microsolv, Cat # 95025-WCV)
9. The samples are analyzed by LCMS-8040. (Shimadzu)

Data:

Day 1:

Time (min)	Assay 1		Assay 2		Assay 3		% remaining		
	DK-I-90-1 Peak area	ISTD Peak area	DK-I-90-1 Peak area	ISTD Peak area	DK-I-90-1 Peak area	ISTD Peak area	Assay 1	Assay 2	Assay 3
0	241015	101158	232121	96514	237717	97118	99.98	100.00	99.98
10	219368	99282	221359	100502	229086	99088	92.72	91.58	94.44
20	184449	86883	200265	93708	225289	98323	89.08	88.86	93.59
30	214468	96017	205879	93595	239342	110661	93.73	91.46	88.35
40	201613	87721	224035	100785	232965	102764	96.44	92.42	92.60
50	229599	104225	232073	100739	199529	90294	92.44	95.78	90.26
60	212634	98920	212532	99063	234749	102678	90.20	89.20	93.39

Table 1: Peak areas and % remaining values

Day 2:

Time (min)	Assay 1		Assay 2		Assay 3		(% remaining)		
	DK-I-90-1 Peak area	ISTD Peak area	DK-I-90-1 Peak area	ISTD Peak area	DK-I-90-1 Peak area	ISTD Peak area	Assay 1	Assay 2	Assay 3
0	225863	99888	232550	100642	240713	99946	100.00	99.98	100.01
10	209150	95201	197790	90137	229251	101497	97.16	94.95	93.80
20	210837	96633	235261	96779	218061	95274	96.49	105.19	95.04
30	207752	96722	218201	96298	210809	92709	94.99	98.08	94.43
40	221146	106906	226707	102711	219082	98772	91.49	95.50	92.11
50	219038	106179	220071	97924	245723	105505	91.23	97.26	96.72
60	215862	99176	242613	110405	223572	98877	96.26	95.08	93.90

Table 2: Peak areas and % remaining values

Calculation:

From the peak area, Calculate the following

$$\text{Peak area ratio} = \frac{\text{Peak area of test compound (DK-I-90-1)}}{\text{Peak area of internal standard (ISTD)}}$$

$$\text{\% remaining at time T (T = 0, 10, 20,30,40,50 and 60)} = \frac{\text{Peak area ratio at particular time T}}{\text{Peak area ratio at zero time point}} * 100$$

DATA ANALYSIS:

Day 1

Linear regression analysis:

Slope: -0.0008976 ± 0.0003729

At X= 60, Y = 4.507 ± 0.01345

R^2 = 0.2337

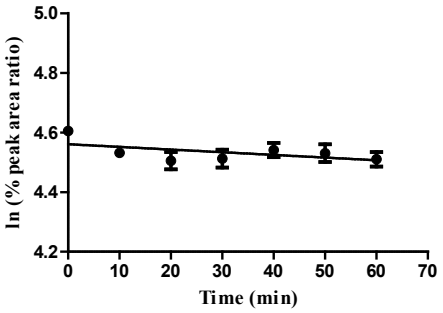

Metabolic Parameters:

Half-life: 772 ± 320 min

V_d: 2000 µL/mg

Intrinsic clearance: 0.08976 µL/min/mg

Metabolic Rate: 1.7952 nmol/min/mg

% remaining at 60 min: 90 ± 0.26 %

Day 2

Linear regression analysis:

Slope: -0.0007750 ± 0.0003317

At X = 60, Y = 4.542 ± 0.01196

R^2 = 0.2232

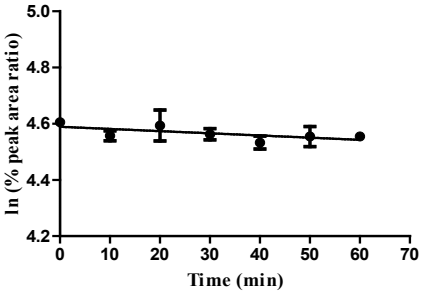

Metabolic Parameters:

Half-life: 894 ± 382 min

V_d: 2000 µL/mg

Intrinsic clearance: 0.0775 µL/min/mg

Metabolic Rate: 1.55 nmol/min/mg

% remaining at 60 min: 94 ± 0.25 %

Note: The peak area ratios and natural log values are calculated using Microsoft excel 2010 and linear regression analysis is calculated using GraphPad prism.

Human Liver Microsomal Assay

Principal Investigator: Dr. Alexander Arnold
Operator: Revathi Kodali
Test Compound: **8g**
Concentration: 10 µM
Date: 02-28-2017
Facility: Milwaukee Institute for Drug Discovery

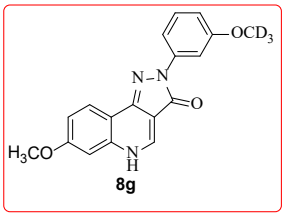

8g

Assay Protocol

Each evaluation included six independent assays carried out three at a time, on two different days

1. Preparation of solutions:
   a. 1 mM test compound in DMSO.
   b. 2 µM Verapamil in ice cold Acetonitrile (ISTD).
2. For a total volume of Microsomal Assay Mixture (MAM) 390 µL, sufficient for seven time points, combine the following
   a. 282 µL of 18.2 mΩ of water.
   b. 80 µL of 0.5 M potassium phosphate buffer (p^H 7.4)
   c. 20 µL of NADPH A. (Corning life sciences, Cat # 451220)
   d. 4 µL of NADPH B. (Corning life sciences, Cat # 451200)
   e. 4 µL of test compound.
3. Sonicate MAM for 5 min and meanwhile thaw microsomes (20 mg/mL) (BD Gentest, Cat # 452156) on ice.
4. Aliquot 100 µL of ice cold ISTD into seven separate 1.5 mL conical vials and label them the time points for 0, 10, 20, 30, 40, 50, and 60 min.
5. Arrange the timer. Microsomes (Final concentration of 0.5 mg/mL) should be added to all time points except the zero time point.
6. Add 50 µL of the MAM solution to the conical vial labelled as zero time point. Place the remaining MAM solution in the incubator (37 ºC) for 5 min and initiate the reaction with addition of microsomes (8.8 µL) and record the time.
7. At the end of each time interval remove 50 µL and add to 100 µL ISTD in conical vial, sonicate for 10 sec and spin down at 10,000 rpm for 5 minutes.
8. Take 100 µL of supernatant and transfer to Spin-X HPLC filter tubes (Corning Incorporated, Cat # 8169) and centrifuge at 13,000 rpm for 5 minutes and take 5 µL from this solution and dilute in 495 µL of LCMS grade methanol (Fischer scientific, CAS # 67-56-1) in an 2mL glass auto sampler vial (Microsolv, Cat # 95025-WCV)
9. The samples are analyzed by LCMS-8040. (Shimadzu)

Data:

Day 1:

Time (min)	Assay 1		Assay 2		Assay 3		% remaining		
	DK-II-69-1 Peak area	Verapamil Peak area	DK-II-69-1 Peak area	Verapamil Peak area	DK-II-69-1 Peak area	Verapamil Peak area	Assay 1	Assay 2	Assay 3
0	146343	225342	139505	220893	152522	221744	100.06	99.92	99.97
10	133193	223873	132626	221883	149931	227834	91.67	94.57	95.65
20	115456	200892	128584	220983	135453	223843	88.55	92.06	87.95
30	116606	211893	122428	224909	133485	230781	84.79	86.13	84.07
40	116438	218734	120510	222874	135799	227843	82.02	85.55	86.63
50	120161	220183	117807	212843	126294	223847	84.08	87.57	82.00
60	119406	212672	113426	213974	124042	211893	86.51	83.87	85.08

Table 1: Peak areas and % remaining values

Day 2:

Time (min)	Assay 1		Assay 2		Assay 3		(% remaining)		
	DK-II-69-1 Peak area	Verapamil Peak area	DK-II-69-1 Peak area	Verapamil Peak area	DK-II-69-1 Peak area	Verapamil Peak area	Assay 1	Assay 2	Assay 3
0	145576	233083	151061	221893	153983	219878	99.93	99.96	100.04
10	142272	241983	147544	226132	144817	220613	94.07	95.81	93.77
20	128656	220834	140312	220633	138088	219723	93.21	93.38	89.78
30	121095	221089	130976	219734	131811	220782	87.63	87.52	85.28
40	119820	220891	124223	216734	133859	221067	86.79	84.16	86.50
50	116786	221373	121034	220874	128083	221074	84.40	80.46	82.76
60	116967	224090	119293	212894	126552	223097	83.51	82.28	81.03

Table 2: Peak areas and % remaining values

Calculation:

From the peak area, Calculate the following

$$\text{Peak area ratio} = \frac{\text{Peak area of test compound (DK-II-69-1)}}{\text{Peak area of internal standard (Verapamil)}}$$

$$\text{\% remaining at time T = (T = 0, 10, 20,30,40,50 and 60)} \quad \frac{\text{Peak area ratio at particular time T}}{\text{Peak area ratio at zero time point}} * 100$$

DATA ANALYSIS:

Day 1

Linear regression analysis:

Slope: -0.002671 ± 0.0003856

At X= 60, Y = 4.406 ± 0.01390

R^2 = 0.7164

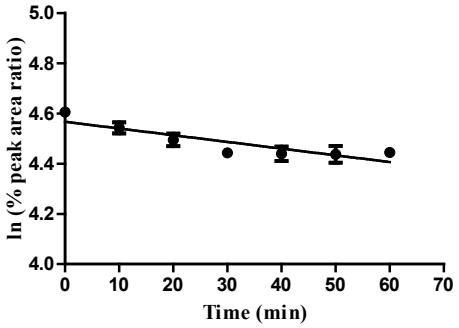

Metabolic Parameters:

Half-life: 259 ± 37.4 min

V_d: 2000 µL/mg

Intrinsic clearance: 0.2671 µL/min/mg

Metabolic Rate: 5.342 nmol/min/mg

% remaining at 60 min: 82 ± 0.26 %

Day 2

Linear regression analysis:

Slope: -0.003312 ± 0.0002282

At X = 60, Y = 4.389 ± 0.008229

R^2 = 0.9172

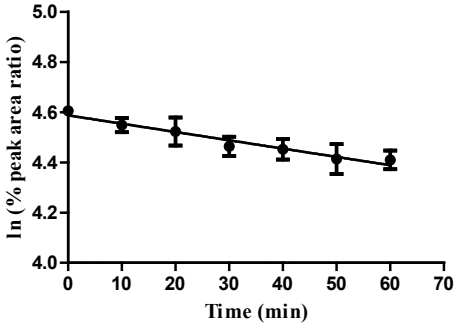

Metabolic Parameters:

Half-life: 209 ± 14 min

V_d: 2000 µL/mg

Intrinsic clearance: 0.3312 µL/min/mg

Metabolic Rate: 6.624 nmol/min/mg

% remaining at 60 min: 80.55 ± 0.15 %

Note: The peak area ratios and natural log values are calculated using Microsoft excel 2010 and linear regression analysis is calculated using GraphPad prism.

Mouse Liver Microsomal Assay

Principal Investigator: Dr. Alexander Arnold
Operator: Revathi Kodali
Test Compound: **8g**
Concentration: 10 µM
Date: 02-28-2017
Facility: Milwaukee Institute for Drug Discovery

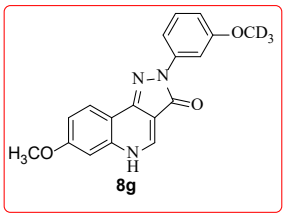

8g

Assay Protocol

Each evaluation included six independent assays carried out three at a time, on two different days

1. Preparation of solutions:
   a. 1 mM test compound in DMSO.
   b. 2 µM Verapamil in ice cold Acetonitrile (ISTD).
2. For a total volume of Microsomal Assay Mixture (MAM) 390 µL, sufficient for seven time points, combine the following
   a. 282 µL of 18.2 mΩ of water.
   b. 80 µL of 0.5 M potassium phosphate buffer (p^H 7.4)
   c. 20 µL of NADPH A. (Corning life sciences, Cat # 451220)
   d. 4 µL of NADPH B. (Corning life sciences, Cat # 451200)
   e. 4 µL of test compound.
3. Sonicate MAM for 5 min and meanwhile thaw microsomes (20 mg/mL) (Life technologies Cat # MSMC-PL) on ice.
4. Aliquot 100 µL of ice cold ISTD into seven separate 1.5 mL conical vials and label them the time points for 0, 10, 20, 30, 40, 50, and 60 min.
5. Arrange the timer. Microsomes (Final concentration of 0.5 mg/mL) should be added to all time points except the zero time point.
6. Add 50 µL of the MAM solution to the conical vial labelled as zero time point. Place the remaining MAM solution in the incubator (37 ºC) for 5 min and initiate the reaction with addition of microsomes (8.8 µL) and record the time.
7. At the end of each time interval remove 50 µL and add to 100 µL ISTD in conical vial, sonicate for 10 sec and spin down at 10,000 rpm for 5 minutes.
8. Take 100 µL of supernatant and transfer to Spin-X HPLC filter tubes (Corning Incorporated, Cat # 8169) and centrifuge at 13,000 rpm for 5 minutes and take 5 µL from this solution and dilute in 495 µL of LCMS grade methanol (Fischer scientific, CAS # 67-56-1) in an 2mL glass auto sampler vial (Microsolv, Cat # 95025-WCV)
9. The samples are analyzed by LCMS-8040. (Shimadzu)

Data:

Day 1:

Time (min)	Assay 1		Assay 2		Assay 3		% remaining		
	DK-II-69-1 Peak area	Verapamil Peak area	DK-II-69-1 Peak area	Verapamil Peak area	DK-II-69-1 Peak area	Verapamil Peak area	Assay 1	Assay 2	Assay 3
0	153307	220362	161694	223187	148441	225613	99.95	100.06	99.99
10	149050	221782	156208	231089	139993	226741	96.56	93.36	93.83
20	142585	217634	149017	218634	138699	221387	94.13	94.14	95.21
30	146408	219723	149645	226164	136482	230012	95.73	91.39	90.17
40	139114	220782	154545	226383	134468	221634	90.53	94.29	92.20
50	143809	220173	155963	224613	132242	212421	93.84	95.90	94.61
60	145754	221723	154323	231083	138278	230781	94.45	92.24	91.06

Table 1: Peak areas and % remaining values

Day 2:

Time (min)	Assay 1		Assay 2		Assay 3		(% remaining)		
	DK-II-69-1 Peak area	Verapamil Peak area	DK-II-69-1 Peak area	Verapamil Peak area	DK-II-69-1 Peak area	Verapamil Peak area	Assay 1	Assay 2	Assay 3
0	166184	221467	149474	221074	163260	220843	100.05	100.01	100.03
10	161409	230864	144162	222673	150466	221384	93.22	95.77	91.97
20	152157	221784	142196	221774	156739	220834	91.47	94.84	96.04
30	149888	221074	136979	220734	152815	221783	90.40	91.79	93.23
40	156102	223687	139293	230084	149011	224018	93.04	89.55	90.01
50	157420	217784	140291	221976	151630	223084	96.37	93.49	91.97
60	155484	218744	141615	220844	153046	220834	94.77	94.85	93.78

Table 2: Peak areas and % remaining values

Calculation:

From the peak area, Calculate the following

$$\text{Peak area ratio} = \frac{\text{Peak area of test compound (DK-II-69-1)}}{\text{Peak area of internal standard (Verapamil)}}$$

$$\text{\% remaining at time T (T = 0, 10, 20,30,40,50 and 60)} = \frac{\text{Peak area ratio at particular time T}}{\text{Peak area ratio at zero time point}} * 100$$

DATA ANALYSIS:

Day 1

Linear regression analysis:

Slope: -0.0008976 ± 0.0002707

At X= 60, Y = 4.521 ± 0.009762

R^2 = 0.3665

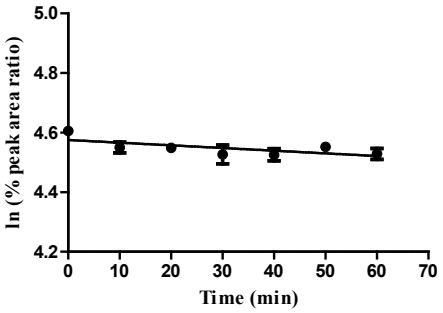

Metabolic Parameters:

Half-life: 772 ± 233 min

V_d: 2000 µL/mg

Intrinsic clearance: 0.08976 µL/min/mg

Metabolic Rate: 1.8 nmol/min/mg

% remaining at 60 min: 91 ± 0.20 %

Day 2

Linear regression analysis:

Slope: -0.0007190 ± 0.0003285

At X = 60, Y = 4.523 ± 0.01184

R^2 = 0.2014

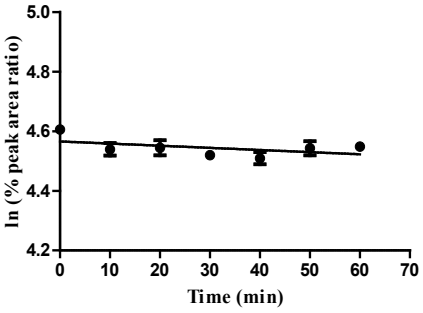

Metabolic Parameters:

Half-life: 963 ± 440 min

V_d: 2000 µL/mg

Intrinsic clearance: 0.0719 µL/min/mg

Metabolic Rate: 1.438 nmol/min/mg

% remaining at 60 min: 92.11 ± 0.42 %

Note: The peak area ratios and natural log values are calculated using Microsoft excel 2010 and linear regression analysis is calculated using GraphPad prism.

Human Liver Microsomal Assay

Principal Investigator: Dr. Alexander Arnold
Operator: Revathi Kodali
Test Compound: **8h**
Concentration: 10 µM
Date: 08-15-2016
Facility: Milwaukee Institute for Drug Discovery

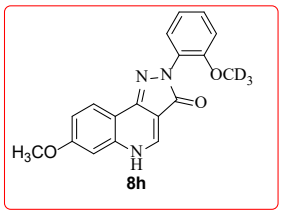

8h

Assay Protocol

Each evaluation included six independent assays carried out three at a time, on two different days

1. Preparation of solutions:
   a. 1 mM test compound in DMSO.
   b. 1 µM 4,5 Di Phenyl Imidazole in ice cold Acetonitrile (ISTD).
2. For a total volume of Microsomal Assay Mixture (MAM) 390 µL, sufficient for seven time points, combine the following
   a. 282 µL of 18.2 mΩ of water.
   b. 80 µL of 0.5 M potassium phosphate buffer (p^H 7.4)
   c. 20 µL of NADPH A. (Corning life sciences, Cat # 451220)
   d. 4 µL of NADPH B. (Corning life sciences, Cat # 451200)
   e. 4 µL of test compound.
3. Sonicate MAM for 5 min and meanwhile thaw microsomes (20 mg/mL) (BD Biosciences, Cat # 452156) on ice.
4. Aliquot 100 µL of ice cold ISTD into seven separate 1.5 mL conical vials and label them the time points for 0, 10, 20, 30, 40, 50, and 60 min.
5. Arrange the timer. Microsomes (Final concentration of 0.5 mg/mL) should be added to all time points except the zero time point.
6. Add 50 µL of the MAM solution to the conical vial labelled as zero time point. Place the remaining MAM solution in the incubator (37 ºC) for 5 min and initiate the reaction with addition of microsomes (8.8 µL) and record the time.
7. At the end of each time interval remove 50 µL and add to 100 µL ISTD in conical vial, sonicate for 10 sec and spin down at 10,000 rpm for 5 minutes.
8. Take 100 µL of supernatant and transfer to Spin-X HPLC filter tubes (Corning Incorporated, Cat # 8169) and centrifuge at 13,000 rpm for 5 minutes and take 5 µL from this solution and dilute in 495 µL of LCMS grade methanol (Fischer scientific, CAS # 67-56-1) in an 2mL glass auto sampler vial (Microsolv, Cat # 95025-WCV)
9. The samples are analyzed by LCMS-8040. (Shimadzu)

Data:

Day 1:

Time (min)	Assay 1		Assay 2		Assay 3		% remaining		
	DK-I-88-1 Peak area	ISTD Peak area	DK-I-88-1 Peak area	ISTD Peak area	DK-I-88-1 Peak area	ISTD Peak area	Assay 1	Assay 2	Assay 3
0	6000289	1978232	5748309	1978368	5972862	1976526	100.00	99.98	99.99
10	5901413	1976237	5536714	1962372	5691768	1967236	98.45	97.09	95.74
20	5359689	1986821	5121505	1956326	5328681	1972367	88.94	90.08	89.40
30	4963413	1896723	5038993	2089872	5116871	1962373	86.27	82.97	86.28
40	5041133	2004384	4914971	2000832	4926787	2000838	82.92	84.53	81.48
50	5063056	1978278	4897310	1977634	5029505	1962727	84.38	85.21	84.79
60	4821518	1976267	4696893	1967623	4942498	1978367	80.43	82.14	82.66

Table 1: Peak areas and % remaining values

Day 2:

Time (min)	Assay 1		Assay 2		Assay 3		(% remaining)		
	DK-I-88-1 Peak area	ISTD Peak area	DK-I-88-1 Peak area	ISTD Peak area	DK-I-88-1 Peak area	ISTD Peak area	Assay 1	Assay 2	Assay 3
0	5779507	1987367	5999039	1987362	5972450	2000712	100.00	99.98	100.00
10	5360319	1978234	5686090	1978872	5660860	1997326	93.17	95.17	94.94
20	5169958	1936478	5426852	1978382	5350046	1972366	91.80	90.86	90.87
30	4896189	1965272	5125434	1923438	5107424	1978723	85.67	88.26	86.47
40	4817341	1976362	5036722	1942562	4940485	1982356	83.82	85.88	83.49
50	4729919	1976326	4850232	1897823	4826268	1972367	82.30	84.65	81.97
60	4835545	1956347	4921510	1987231	4795722	1956237	84.99	82.03	82.12

Table 2: Peak areas and % remaining values

Calculation:

From the peak area, Calculate the following

$$\text{Peak area ratio} = \frac{\text{Peak area of test compound (DK-I-88-1)}}{\text{Peak area of internal standard (ISTD)}}$$

$$\text{\% remaining at time T = (T = 0, 10, 20,30,40,50 and 60)} \quad \frac{\text{Peak area ratio at particular time T}}{\text{Peak area ratio at zero time point}} * 100$$

DATA ANALYSIS:

Day 1

Linear regression analysis:

Slope: -0.003402 ± 0.0003355

At X= 60, Y = 4.381 ± 0.01210

R^2 = 0.8440

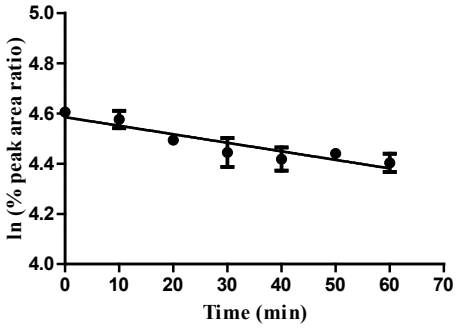

Metabolic Parameters:

Half-life: 203.70 ± 20.88 min

V_d: 2000 µL/mg

Intrinsic clearance: 0.3402 µL/min/mg

Metabolic Rate: 6.804 nmol/min/mg

% remaining at 60 min: 79.19 ± 0.22 %

Day 2

Linear regression analysis:

Slope: -0.003190 ± 0.0002445

At X = 60, Y = 4.390 ± 0.008814

R^2 = 0.8997

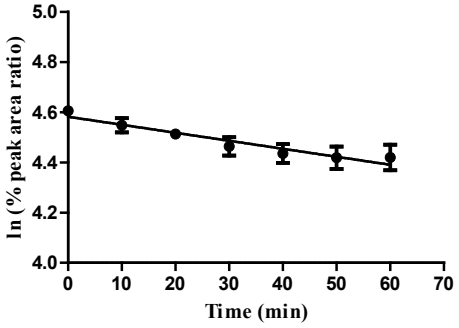

Metabolic Parameters:

Half-life: 217.24 ± 16.65 min

V_d: 2000 µL/mg

Intrinsic clearance: 0.319 µL/min/mg

Metabolic Rate: 6.38 nmol/min/mg

% remaining at 60 min: 80.64 ± 0.16 %

Note: The peak area ratios and natural log values are calculated using Microsoft excel 2010 and linear regression analysis is calculated using GraphPad prism.

Mouse Liver Microsomal Assay

Principal Investigator: Dr. Alexander Arnold
Operator: Revathi Kodali
Test Compound: **8h**
Concentration: 10 µM
Date: 08-15-2016
Facility: Milwaukee Institute for Drug Discovery

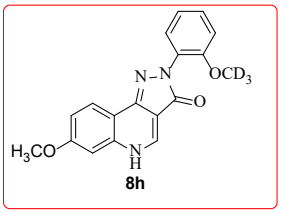

8h

Assay Protocol

Each evaluation included six independent assays carried out three at a time, on two different days

1. Preparation of solutions:
   a. 1 mM test compound in DMSO.
   b. 1 µM 4,5 Di Phenyl Imidazole in ice cold Acetonitrile (ISTD).
2. For a total volume of Microsomal Assay Mixture (MAM) 390 µL, sufficient for seven time points, combine the following
   a. 282 µL of 18.2 mΩ of water.
   b. 80 µL of 0.5 M potassium phosphate buffer (p^H 7.4)
   c. 20 µL of NADPH A. (Corning life sciences, Cat # 451220)
   d. 4 µL of NADPH B. (Corning life sciences, Cat # 451200)
   e. 4 µL of test compound.
3. Sonicate MAM for 5 min and meanwhile thaw microsomes (20 mg/mL) (Life technologies, Cat # MSMC-PL) on ice.
4. Aliquot 100 µL of ice cold ISTD into seven separate 1.5 mL conical vials and label them the time points for 0, 10, 20, 30, 40, 50, and 60 min.
5. Arrange the timer. Microsomes (Final concentration of 0.5 mg/mL) should be added to all time points except the zero time point.
6. Add 50 µL of the MAM solution to the conical vial labelled as zero time point. Place the remaining MAM solution in the incubator (37 ºC) for 5 min and initiate the reaction with addition of microsomes (8.8 µL) and record the time.
7. At the end of each time interval remove 50 µL and add to 100 µL ISTD in conical vial, sonicate for 10 sec and spin down at 10,000 rpm for 5 minutes.
8. Take 100 µL of supernatant and transfer to Spin-X HPLC filter tubes (Corning Incorporated, Cat # 8169) and centrifuge at 13,000 rpm for 5 minutes and take 5 µL from this solution and dilute in 495 µL of LCMS grade methanol (Fischer scientific, CAS # 67-56-1) in an 2mL glass auto sampler vial (Microsolv, Cat # 95025-WCV)
9. The samples are analyzed by LCMS-8040. (Shimadzu)

Data:

Day 1:

Time (min)	Assay 1		Assay 2		Assay 3		% remaining		
	DK-I-88-1 Peak area	ISTD Peak area	DK-I-88-1 Peak area	ISTD Peak area	DK-I-88-1 Peak area	ISTD Peak area	Assay 1	Assay 2	Assay 3
0	5864208	1923424	5986197	1923456	6104405	1986723	99.99	100.00	99.98
10	5842143	2001663	5946613	2000102	5915367	1945623	95.72	95.53	98.93
20	5901471	1946432	5800697	1986746	5952081	2000103	99.44	93.82	96.84
30	5730111	1923513	5881350	1959021	5742564	1976326	97.70	96.47	94.55
40	5654542	1968542	5896694	1943252	5652491	1928635	94.21	97.50	95.37
50	5524788	1951543	5744072	1956723	5542147	1962538	92.85	94.33	91.89
60	5612563	1954739	5686981	1921344	5698561	1964251	94.17	95.11	94.40

Table 1: Peak areas and % remaining values

Day 2:

Time (min)	Assay 1		Assay 2		Assay 3		(% remaining)		
	DK-I-88-1 Peak area	ISTD Peak area	DK-I-88-1 Peak area	ISTD Peak area	DK-I-88-1 Peak area	ISTD Peak area	Assay 1	Assay 2	Assay 3
0	5984998	2034364	5968027	1998737	6002413	2098478	99.99	99.99	100.01
10	5824131	1987474	5806107	1962761	5701055	1998834	99.60	99.06	99.72
20	5507668	1923454	5702257	1978383	5563421	2001543	97.32	96.52	97.18
30	5502585	1978848	5750415	1957672	5417161	1976832	94.51	98.37	95.81
40	5287891	1923646	5658083	1998922	5306658	2008383	93.43	94.79	92.38
50	5558948	1996765	5642027	1956732	5300999	1988734	94.62	96.56	93.20
60	5652513	2087247	5532053	1981238	5234824	1978724	92.05	93.51	92.50

Table 2: Peak areas and % remaining values

Calculation:

From the peak area, Calculate the following

$$\text{Peak area ratio} = \frac{\text{Peak area of test compound (DK-I-88-1)}}{\text{Peak area of internal standard (ISTD)}}$$

$$\text{\% remaining at time T} = \frac{\text{Peak area ratio at particular time T}}{\text{Peak area ratio at zero time point}} * 100$$

(T = 0, 10, 20,30,40,50 and 60)

DATA ANALYSIS:

Day 1

Linear regression analysis:

Slope: -0.0009083 ± 0.0001941

At X= 60, Y = 4.538 ± 0.006998

R^2 = 0.5355

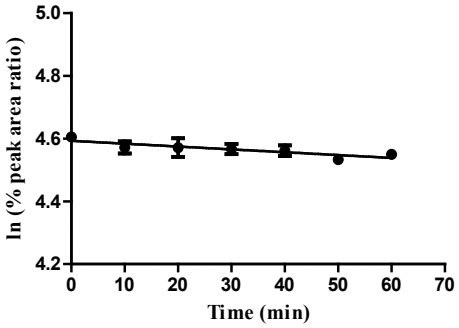

Metabolic Parameters:

Half-life: 762.96 ± 163.04 min

V_d: 2000 µL/mg

Intrinsic clearance: 0.09083µL/min/mg

Metabolic Rate: 1.8166 nmol/min/mg

% remaining at 60 min: 93.50 ± 0.14 %

Day 2

Linear regression analysis:

Slope: -0.001288 ± 0.0001431

At X = 60, Y = 4.528 ± 0.005159

R^2 = 0.8101

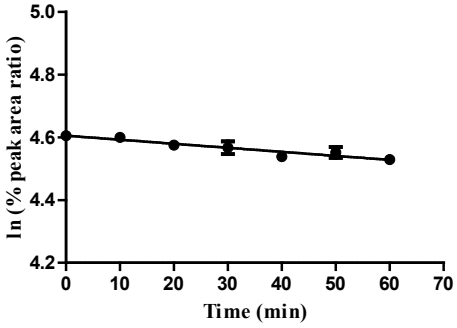

Metabolic Parameters:

Half-life: 538.04 ± 59.97 min

V_d: 2000 µL/mg

Intrinsic clearance: 0.1288 µL/min/mg

Metabolic Rate: 2.576 nmol/min/mg

% remaining at 60 min: 92.57 ± 0.10 %

Note: The peak area ratios and natural log values are calculated using Microsoft excel 2010 and linear regression analysis is calculated using GraphPad prism.

Human Liver Microsomal Assay

Principal Investigator: Dr. Alexander Arnold
Operator: Revathi Kodali
Test Compound: **8i**
Concentration: 10 µM
Date: 04-06-2016
Facility: Milwaukee Institute for Drug Discovery

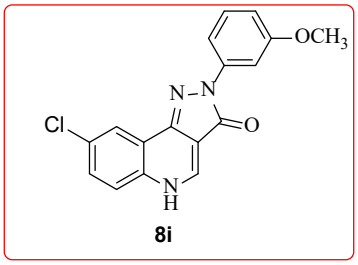

8i

Assay Protocol

Each evaluation included six independent assays carried out three at a time, on two different days

1. Preparation of solutions:
   a. 1 mM test compound in DMSO.
   b. 1 µM Verapamil in ice cold Acetonitrile (ISTD).
2. For a total volume of Microsomal Assay Mixture (MAM) 390 µL, sufficient for seven time points, combine the following
   a. 282 µL of 18.2 mΩ of water.
   b. 80 µL of 0.5 M potassium phosphate buffer (p^H 7.4)
   c. 20 µL of NADPH A. (Corning life sciences, Cat # 451220)
   d. 4 µL of NADPH B. (Corning life sciences, Cat # 451200)
   e. 4 µL of test compound.
3. Sonicate MAM for 5 min and meanwhile thaw microsomes (20 mg/mL) (BD Gentest, Cat # 452156) on ice.
4. Aliquot 100 µL of ice cold ISTD into seven separate 1.5 mL conical vials and label them the time points for 0, 10, 20, 30, 40, 50, and 60 min.
5. Arrange the timer. Microsomes (Final concentration of 0.5 mg/mL) should be added to all time points except the zero time point.
6. Add 50 µL of the MAM solution to the conical vial labelled as zero time point. Place the remaining MAM solution in the incubator (37 ºC) for 5 min and initiate the reaction with addition of microsomes (8.8 µL) and record the time.
7. At the end of each time interval remove 50 µL and add to 100 µL ISTD in conical vial, sonicate for 10 sec and spin down at 10,000 rpm for 5 minutes.
8. Take 100 µL of supernatant and transfer to Spin-X HPLC filter tubes (Corning Incorporated, Cat # 8169) and centrifuge at 13,000 rpm for 5 minutes and take 5 µL from this solution and dilute in 495 µL of LCMS grade methanol (Fischer scientific, CAS # 67-56-1) in an 2mL glass auto sampler vial (Microsolv, Cat # 95025-WCV)
9. The samples are analyzed by LCMS-8040. (Shimadzu)

Data:

Day 1:

Time (min)	Assay 1		Assay 2		Assay 3		% remaining		
	LAU 159 Peak area	Verapamil Peak area	LAU 159 Peak area	Verapamil Peak area	LAU 159 Peak area	Verapamil Peak area	Assay 1	Assay 2	Assay 3
0	80398	770706	79247	781412	81322	768705	100.30	100.41	99.80
10	78100	757087	75533	774930	79581	765630	99.19	96.50	98.05
20	76832	781877	73032	767002	76372	772311	94.48	94.27	93.29
30	71132	765148	68999	781510	73574	768806	89.38	87.41	90.28
40	68442	762279	65432	770550	67089	772739	86.33	84.07	81.90
50	68744	780528	68583	780384	68078	762260	84.68	87.01	84.25
60	65384	761871	66839	782566	66854	769953	82.52	84.56	81.91

Table 1: Peak areas and % remaining values

Day 2:

Time (min)	Assay 1		Assay 2		Assay 3		(% remaining)		
	LAU 159 Peak area	Verapamil Peak area	LAU 159 Peak area	Verapamil Peak area	LAU 159 Peak area	Verapamil Peak area	Assay 1	Assay 2	Assay 3
0	83578	764869	81348	762725	82729	765486	100.24	99.67	100.06
10	81869	773664	79781	777443	80586	777335	97.08	95.90	95.99
20	77477	756111	76199	767523	78620	780606	94.00	92.78	93.25
30	76977	787473	73745	781492	76424	776417	89.68	88.19	91.14
40	70419	763525	68213	764927	71372	768298	84.61	83.34	86.01
50	69693	773427	66577	770599	70639	768061	82.66	80.74	85.15
60	71664	761028	68158	772689	69696	778601	86.39	82.43	82.88

Table 2: Peak areas and % remaining values

Calculation:

From the peak area, Calculate the following

$$\text{Peak area ratio} = \frac{\text{Peak area of test compound (LAU 159)}}{\text{Peak area of internal standard (Verapamil)}}$$

$$\text{\% remaining at time T} = \frac{\text{Peak area ratio at particular time T}}{\text{Peak area ratio at zero time point}} * 100$$

(T = 0, 10, 20,30,40,50 and 60)

DATA ANALYSIS:

Day 1

Linear regression analysis:

Slope: -0.003394 ± 0.0002532

At X= 60, Y = 4.401 ± 0.009130

R^2 = 0.9044

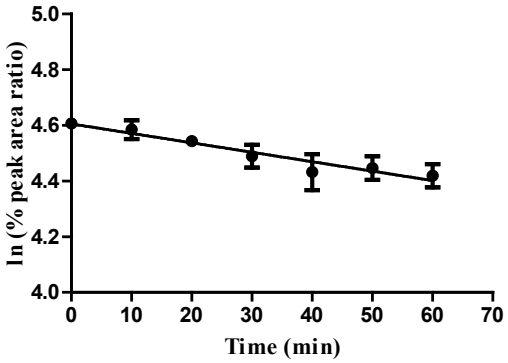

Metabolic Parameters:

Half-life: 204.18 ± 15.23 min

V_d: 100 µL/mg

Intrinsic clearance: 0.3394 µL/min/mg

Metabolic Rate: 6.788 nmol/min/mg

% remaining at 60 min: 81.53 ± 0.16 %

Day 2

Linear regression analysis:

Slope: -0.003310 ± 0.0002487

At X = 60, Y = 4.399 ± 0.008968

R^2 = 0.9031

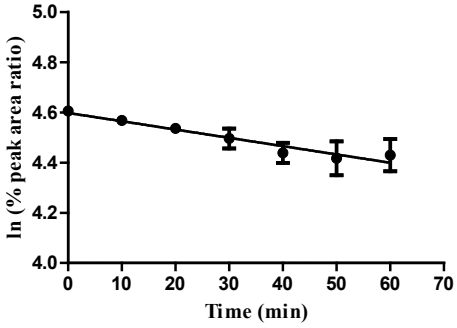

Metabolic Parameters:

Half-life: 209.36 ± 15.73 min

V_d: 100 µL/mg

Intrinsic clearance: 0.331 µL/min/mg

Metabolic Rate: 6.62 nmol/min/mg

% remaining at 60 min: 81.36 ± 0.16 %

Note: The peak area ratios and natural log values are calculated using Microsoft excel 2010 and linear regression analysis is calculated using GraphPad prism.

Mouse Liver Microsomal Assay

Principal Investigator: Dr. Alexander Arnold
Operator: Revathi Kodali
Test Compound: **8i**
Concentration: 10 µM
Date: 04-06-2016
Facility: Milwaukee Institute for Drug Discovery

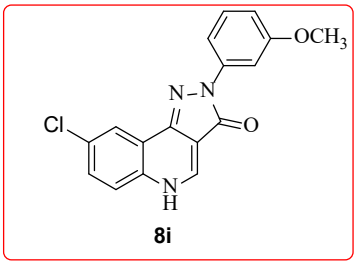

8i

Assay Protocol

Each evaluation included six independent assays carried out three at a time, on two different days

1. Preparation of solutions:
   a. 1 mM test compound in DMSO.
   b. 1 µM Verapamil in ice cold Acetonitrile (ISTD).
2. For a total volume of Microsomal Assay Mixture (MAM) 390 µL, sufficient for seven time points, combine the following
   a. 282 µL of 18.2 mΩ of water.
   b. 80 µL of 0.5 M potassium phosphate buffer (p^H 7.4)
   c. 20 µL of NADPH A. (Corning life sciences, Cat # 451220)
   d. 4 µL of NADPH B. (Corning life sciences, Cat # 451200)
   e. 4 µL of test compound.
3. Sonicate MAM for 5 min and meanwhile thaw microsomes (20 mg/mL) (Life technologies, Cat # MSMC-PL) on ice.
4. Aliquot 100 µL of ice cold ISTD into seven separate 1.5 mL conical vials and label them the time points for 0, 10, 20, 30, 40, 50, and 60 min.
5. Arrange the timer. Microsomes (Final concentration of 0.5 mg/mL) should be added to all time points except the zero time point.
6. Add 50 µL of the MAM solution to the conical vial labelled as zero time point. Place the remaining MAM solution in the incubator (37 ºC) for 5 min and initiate the reaction with addition of microsomes (8.8 µL) and record the time.
7. At the end of each time interval remove 50 µL and add to 100 µL ISTD in conical vial, sonicate for 10 sec and spin down at 10,000 rpm for 5 minutes.
8. Take 100 µL of supernatant and transfer to Spin-X HPLC filter tubes (Corning Incorporated, Cat # 8169) and centrifuge at 13,000 rpm for 5 minutes and take 5 µL from this solution and dilute in 495 µL of LCMS grade methanol (Fischer scientific, CAS # 67-56-1) in an 2mL glass auto sampler vial (Microsolv, Cat # 95025-WCV)
9. The samples are analyzed by LCMS-8040. (Shimadzu)

Data:

Day 1:

Time (min)	Assay 1		Assay 2		Assay 3		% remaining		
	LAU 159 Peak area	Verapamil Peak area	LAU 159 Peak area	Verapamil Peak area	LAU 159 Peak area	Verapamil Peak area	Assay 1	Assay 2	Assay 3
0	86708	777698	85735	782218	85879	767074	100.44	99.64	99.96
10	76231	777526	74721	778315	78865	772011	88.32	87.27	91.21
20	66139	765299	68247	762276	70083	761217	77.85	81.39	82.20
30	59435	769865	60822	775396	66560	780394	69.55	71.30	76.15
40	57074	767913	58779	767323	62645	779036	66.95	69.63	71.79
50	55032	771478	57997	779151	55850	769895	64.26	67.66	64.77
60	53264	763246	54568	780889	53737	780280	62.87	63.52	61.49

Table 1: Peak areas and % remaining values

Day 2:

Time (min)	Assay 1		Assay 2		Assay 3		(% remaining)		
	LAU 159 Peak area	Verapamil Peak area	LAU 159 Peak area	Verapamil Peak area	LAU 159 Peak area	Verapamil Peak area	Assay 1	Assay 2	Assay 3
0	86093	772034	86606	765303	84547	764973	99.56	100.14	99.57
10	75885	766501	74432	759018	77931	776061	88.39	86.78	90.46
20	67311	761581	67630	769773	67513	766499	78.91	77.75	79.35
30	61790	776182	61097	764013	63949	787136	71.07	70.76	73.19
40	58705	768779	57288	768303	58017	774773	68.18	65.98	67.46
50	56741	777107	55177	776275	53768	768066	65.19	62.90	63.06
60	55772	768839	54383	778823	53547	771612	64.76	61.79	62.51

Table 2: Peak areas and % remaining values

Calculation:

From the peak area, Calculate the following

$$\text{Peak area ratio} = \frac{\text{Peak area of test compound (LAU 159)}}{\text{Peak area of internal standard (Verapamil)}}$$

$$\text{\% remaining at time T} = \frac{\text{Peak area ratio at particular time T}}{\text{Peak area ratio at zero time point}} * 100$$

(T = 0, 10, 20,30,40,50 and 60)

DATA ANALYSIS:

Day 1

Linear regression analysis:

Slope: -0.007724 ± 0.0004410

At X= 60, Y = 4.100 ± 0.01590

R^2 = 0.9417

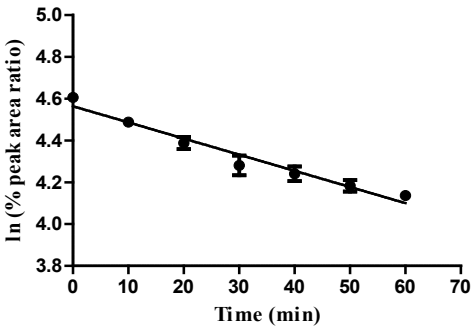

Metabolic Parameters:

Half-life: 89.72 ± 5.12 min

V_d: 100 µL/mg

Intrinsic clearance: 0.7724 µL/min/mg

Metabolic Rate: 15.448 nmol/min/mg

% remaining at 60 min: 60.34 ± 0.23 %

Day 2

Linear regression analysis:

Slope: -0.007837 ± 0.0004718

At X = 60, Y = 4.083 ± 0.01701

R^2 = 0.9356

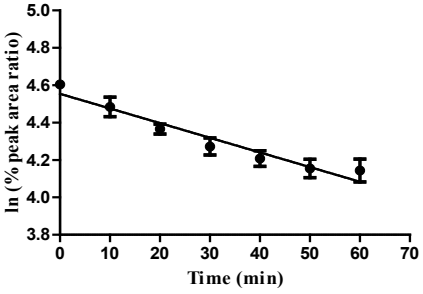

Metabolic Parameters:

Half-life: 88.42 ± 5.32 min

V_d: 100 µL/mg

Intrinsic clearance: 0.7837 µL/min/mg

Metabolic Rate: 15.674 nmol/min/mg

% remaining at 60 min: 59.32 ± 0.24 %

Note: The peak area ratios and natural log values are calculated using Microsoft excel 2010 and linear regression analysis is calculated using GraphPad prism.

Human Liver Microsomal Assay

Principal Investigator: Dr. Alexander Arnold
Operator: Revathi Kodali
Test Compound: **8j**
Concentration: 10 µM
Date: 05-06-2016
Facility: Milwaukee Institute for Drug Discovery

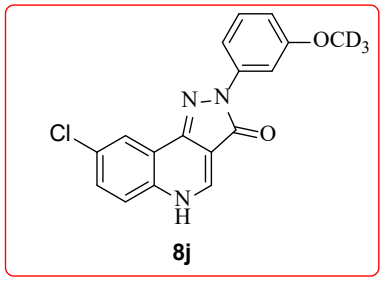

8j

Assay Protocol

Each evaluation included six independent assays carried out three at a time, on two different days

1. Preparation of solutions:
   a. 1 mM test compound in DMSO.
   b. 2 µM 4,5 Diphenyl Imidazole in ice cold Acetonitrile (ISTD).
2. For a total volume of Microsomal Assay Mixture (MAM) 390 µL, sufficient for seven time points, combine the following
   a. 282 µL of 18.2 mΩ of water.
   b. 80 µL of 0.5 M potassium phosphate buffer (p^H 7.4)
   c. 20 µL of NADPH A. (Corning life sciences, Cat # 451220)
   d. 4 µL of NADPH B. (Corning life sciences, Cat # 451200)
   e. 4 µL of test compound.
3. Sonicate MAM for 5 min and meanwhile thaw microsomes (20 mg/mL) (BD Gentest, Cat # 452156) on ice.
4. Aliquot 100 µL of ice cold ISTD into seven separate 1.5 mL conical vials and label them the time points for 0, 10, 20, 30, 40, 50, and 60 min.
5. Arrange the timer. Microsomes (Final concentration of 0.5 mg/mL) should be added to all time points except the zero time point.
6. Add 50 µL of the MAM solution to the conical vial labelled as zero time point. Place the remaining MAM solution in the incubator (37 ºC) for 5 min and initiate the reaction with addition of microsomes (8.8 µL) and record the time.
7. At the end of each time interval remove 50 µL and add to 100 µL ISTD in conical vial, sonicate for 10 sec and spin down at 10,000 rpm for 5 minutes.
8. Take 100 µL of supernatant and transfer to Spin-X HPLC filter tubes (Corning Incorporated, Cat # 8169) and centrifuge at 13,000 rpm for 5 minutes and take 5 µL from this solution and dilute in 495 µL of LCMS grade methanol (Fischer scientific, CAS # 67-56-1) in an 2mL glass auto sampler vial (Microsolv, Cat # 95025-WCV)
9. The samples are analyzed by LCMS-8040. (Shimadzu)

Data:

Day 1:

Time (min)	Assay 1		Assay 2		Assay 3		% remaining		
	DK-I-59-1 Peak area	ISTD Peak area	DK-I-59-1 Peak area	ISTD Peak area	DK-I-59-1 Peak area	ISTD Peak area	Assay 1	Assay 2	Assay 3
0	332661	2109886	331693	2088212	324161	2109905	99.79	99.90	99.76
10	321980	2089987	316452	2009030	317270	2100090	97.50	99.06	98.10
20	319442	2109877	321330	2087202	311732	2082911	95.82	96.82	97.18
30	300905	2009948	302080	1989310	299219	2008386	94.75	95.50	96.74
40	310592	2100979	313763	2099050	292364	2002890	93.56	94.01	94.78
50	319432	2193028	301923	2009884	288651	1968260	92.18	94.47	95.22
60	310961	2099871	295863	2008786	303022	2089233	93.72	92.63	94.18

Table 1: Peak areas and % remaining values

Day 2:

Time (min)	Assay 1		Assay 2		Assay 3		(% remaining)		
	DK-I-59-1 Peak area	ISTD Peak area	DK-I-59-1 Peak area	ISTD Peak area	DK-I-59-1 Peak area	ISTD Peak area	Assay 1	Assay 2	Assay 3
0	331986	2092889	334435	2102273	318009	2083826	99.76	100.05	99.74
10	333335	2089284	320734	2028733	323313	2198835	100.34	99.43	96.10
20	321611	2109091	308978	2000783	305776	2089206	95.90	97.12	95.66
30	316422	2109273	326793	2163622	313245	2183287	94.34	94.99	93.77
40	313007	2098285	315920	2089327	303331	2078788	93.81	95.09	95.37
50	309075	2012827	316116	2109029	315823	2183281	96.57	94.26	94.54
60	311918	2091878	306049	2089289	300968	2082891	93.77	92.12	94.44

Table 2: Peak areas and % remaining values

Calculation:

From the peak area, Calculate the following

$$\text{Peak area ratio} = \frac{\text{Peak area of test compound (DK-I-59-1)}}{\text{Peak area of internal standard (Verapamil)}}$$

$$\text{\% remaining at time T} = \frac{\text{Peak area ratio at particular time T}}{\text{Peak area ratio at zero time point}} * 100$$

(T = 0, 10, 20,30,40,50 and 60)

DATA ANALYSIS:

Day 1

Linear regression analysis:

Slope: -0.001113 ± 0.0001062

At X= 60, Y = 4.531 ± 0.003829

R^2 = 0.8526

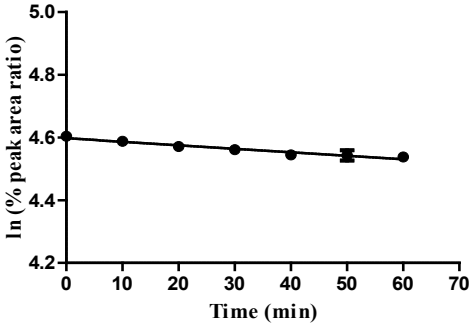

Metabolic Parameters:

Half-life: 622.64 ± 60 min

V_d: 100 µL/mg

Intrinsic clearance: 0.1113 µL/min/mg

Metabolic Rate: 2.226 nmol/min/mg

% remaining at 60 min: 92.85 ± 0.07 %

Day 2

Linear regression analysis:

Slope: -0.001026 ± 0.0001577

At X = 60, Y = 4.534 ± 0.005687

R^2 = 0.6902

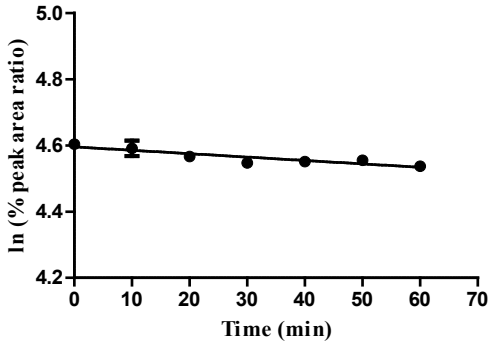

Metabolic Parameters:

Half-life: 675.43 ± 103 min

V_d: 100 µL/mg

Intrinsic clearance: 0.1026 µL/min/mg

Metabolic Rate: 2.052 nmol/min/mg

% remaining at 60 min: 93.13 ± 0.11 %

Note: The peak area ratios and natural log values are calculated using Microsoft excel 2010 and linear regression analysis is calculated using GraphPad prism.

Mouse Liver Microsomal Assay

Principal Investigator: Dr. Alexander Arnold
Operator: Revathi Kodali
Test Compound: **8j**
Concentration: 10 µM
Date: 05-06-2016
Facility: Milwaukee Institute for Drug Discovery

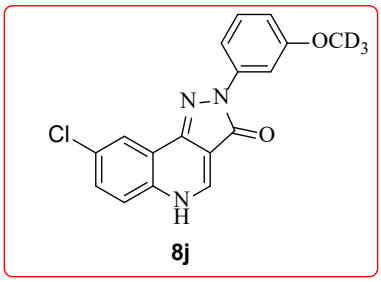

8j

Assay Protocol

Each evaluation included six independent assays carried out three at a time, on two different days

1. Preparation of solutions:
   a. 1 mM test compound in DMSO.
   b. 2 µM 4,5 Diphenyl Imidazole in ice cold Acetonitrile (ISTD).
2. For a total volume of Microsomal Assay Mixture (MAM) 390 µL, sufficient for seven time points, combine the following
   a. 282 µL of 18.2 mΩ of water.
   b. 80 µL of 0.5 M potassium phosphate buffer (p^H 7.4)
   c. 20 µL of NADPH A. (Corning life sciences, Cat # 451220)
   d. 4 µL of NADPH B. (Corning life sciences, Cat # 451200)
   e. 4 µL of test compound.
3. Sonicate MAM for 5 min and meanwhile thaw microsomes (20 mg/mL) (BD Gentest, Cat # 452156) on ice.
4. Aliquot 100 µL of ice cold ISTD into seven separate 1.5 mL conical vials and label them the time points for 0, 10, 20, 30, 40, 50, and 60 min.
5. Arrange the timer. Microsomes (Final concentration of 0.5 mg/mL) should be added to all time points except the zero time point.
6. Add 50 µL of the MAM solution to the conical vial labelled as zero time point. Place the remaining MAM solution in the incubator (37 ºC) for 5 min and initiate the reaction with addition of microsomes (8.8 µL) and record the time.
7. At the end of each time interval remove 50 µL and add to 100 µL ISTD in conical vial, sonicate for 10 sec and spin down at 10,000 rpm for 5 minutes.
8. Take 100 µL of supernatant and transfer to Spin-X HPLC filter tubes (Corning Incorporated, Cat # 8169) and centrifuge at 13,000 rpm for 5 minutes and take 5 µL from this solution and dilute in 495 µL of LCMS grade methanol (Fischer scientific, CAS # 67-56-1) in an 2mL glass auto sampler vial (Microsolv, Cat # 95025-WCV)
9. The samples are analyzed by LCMS-8040. (Shimadzu)

Data:

Day 1:

Time (min)	Assay 1		Assay 2		Assay 3		% remaining		
	DK-I-59-1 Peak area	ISTD Peak area	DK-I-59-1 Peak area	ISTD Peak area	DK-I-59-1 Peak area	ISTD Peak area	Assay 1	Assay 2	Assay 3
0	364668	2067368	384616	2097328	382943	2018928	100.22	100.21	99.83
10	334364	2087386	358462	2023892	372601	2100921	91.01	96.78	93.34
20	339956	2193899	337084	2083872	359689	2082817	88.04	88.39	90.89
30	313196	2027898	324275	2089289	353631	2120902	87.75	84.81	87.75
40	301354	2087323	319986	2172783	320297	2010256	82.03	80.47	83.85
50	285346	2000988	290054	2008751	320503	2178237	81.02	78.90	77.44
60	285294	2183826	301279	2153539	302164	2073280	74.22	76.44	76.70

Table 1: Peak areas and % remaining values

Day 2:

Time (min)	Assay 1		Assay 2		Assay 3		(% remaining)		
	DK-I-59-1 Peak area	ISTD Peak area	DK-I-59-1 Peak area	ISTD Peak area	DK-I-59-1 Peak area	ISTD Peak area	Assay 1	Assay 2	Assay 3
0	344482	1997834	344482	2009283	367481	1982372	100.24	100.26	100.20
10	335911	2082382	335911	2058389	360082	2072061	93.78	95.43	93.93
20	320196	2100381	320196	2089389	343194	2089499	88.63	89.61	88.78
30	307994	2081282	307994	2044013	317081	1997383	86.03	88.11	85.81
40	306138	2082919	286138	1968703	313906	2004773	85.45	84.99	84.63
50	306151	2182981	286151	2072378	300644	1998990	81.53	80.74	81.29
60	289745	2188239	279745	2109823	301367	2047582	76.98	77.53	79.55

Table 2: Peak areas and % remaining values

Calculation:

From the peak area, Calculate the following

$$\text{Peak area ratio} = \frac{\text{Peak area of test compound (DK-I-59-1)}}{\text{Peak area of internal standard (Verapamil)}}$$

$$\text{\% remaining at time T} = \frac{\text{Peak area ratio at particular time T}}{\text{Peak area ratio at zero time point}} * 100$$

(T = 0, 10, 20,30,40,50 and 60)

DATA ANALYSIS:

Day 1

Linear regression analysis:

Slope: -0.004473 ± 0.0002139

At X= 60, Y = 4.324 ± 0.007712

R^2 = 0.9584

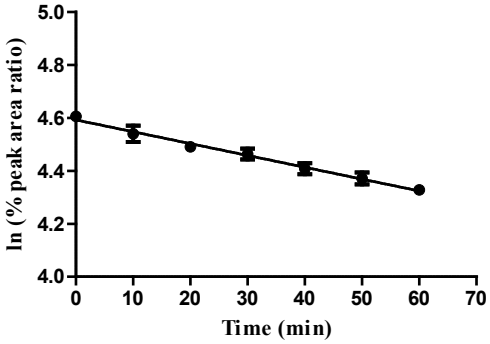

Metabolic Parameters:

Half-life: 154.92 ± 7.4 min

V_d: 100 µL/mg

Intrinsic clearance: 0.4473 µL/min/mg

Metabolic Rate: 8.946 nmol/min/mg

% remaining at 60 min: 75.48 ± 0.13 %

Day 2

Linear regression analysis:

Slope: -0.003925 ± 0.0001689

At X = 60, Y = 4.354 ± 0.006089

R^2 = 0.9660

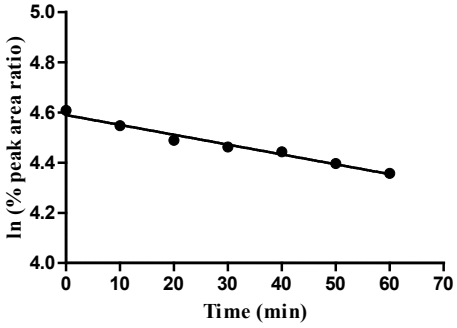

Metabolic Parameters:

Half-life: 176.56 ± 8 min

V_d: 100 µL/mg

Intrinsic clearance: 0.3925 µL/min/mg

Metabolic Rate: 7.85 nmol/min/mg

% remaining at 60 min: 77.7 ± 0.10 %

Note: The peak area ratios and natural log values are calculated using Microsoft excel 2010 and linear regression analysis is calculated using GraphPad prism.

Human Liver Microsomal Assay

Principal Investigator: Dr. Alexander Arnold
Operator: Revathi Kodali
Test Compound: **8k**
Concentration: 10 µM
Date: 05-11-2016
Facility: Milwaukee Institute for Drug Discovery

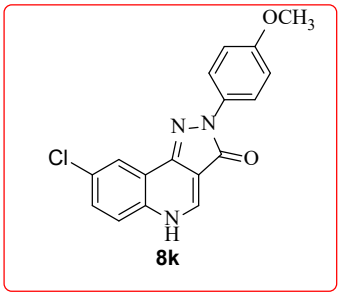

8k

Assay Protocol

Each evaluation included six independent assays carried out three at a time, on two different days

1. Preparation of solutions:
   a. 1 mM test compound in DMSO.
   b. 1 µM 4,5 Di Phenyl Imidazole in ice cold Acetonitrile (ISTD).
2. For a total volume of Microsomal Assay Mixture (MAM) 390 µL, sufficient for seven time points, combine the following
   a. 282 µL of 18.2 mΩ of water.
   b. 80 µL of 0.5 M potassium phosphate buffer (p^H 7.4)
   c. 20 µL of NADPH A. (Corning life sciences, Cat # 451220)
   d. 4 µL of NADPH B. (Corning life sciences, Cat # 451200)
   e. 4 µL of test compound.
3. Sonicate MAM for 5 min and meanwhile thaw microsomes (20 mg/mL) (BD Gentest, Cat # 452156) on ice.
4. Aliquot 100 µL of ice cold ISTD into seven separate 1.5 mL conical vials and label them the time points for 0, 10, 20, 30, 40, 50, and 60 min.
5. Arrange the timer. Microsomes (Final concentration of 0.5 mg/mL) should be added to all time points except the zero time point.
6. Add 50 µL of the MAM solution to the conical vial labelled as zero time point. Place the remaining MAM solution in the incubator (37 ºC) for 5 min and initiate the reaction with addition of microsomes (8.8 µL) and record the time.
7. At the end of each time interval remove 50 µL and add to 100 µL ISTD in conical vial, sonicate for 10 sec and spin down at 10,000 rpm for 5 minutes.
8. Take 100 µL of supernatant and transfer to Spin-X HPLC filter tubes (Corning Incorporated, Cat # 8169) and centrifuge at 13,000 rpm for 5 minutes and take 5 µL from this solution and dilute in 495 µL of LCMS grade methanol (Fischer scientific, CAS # 67-56-1) in an 2mL glass auto sampler vial (Microsolv, Cat # 95025-WCV)
9. The samples are analyzed by LCMS-8040. (Shimadzu)

Data:

Day 1:

Time (min)	Assay 1		Assay 2		Assay 3		% remaining		
	PZ-II-028 Peak area	ISTD Peak area	PZ-II-028 Peak area	ISTD Peak area	PZ-II-028 Peak area	ISTD Peak area	Assay 1	Assay 2	Assay 3
0	324755	191542	346172	193172	339347	194350	100.02	100.00	100.00
10	303291	193874	334280	205037	314958	188485	92.29	90.97	95.70
20	279364	189575	312886	197462	294465	185685	86.94	88.42	90.82
30	262109	190556	281620	190809	269697	189934	81.15	82.36	81.32
40	261473	193926	266162	185650	252097	179750	79.54	80.00	80.32
50	236291	183965	260227	190263	263532	199428	75.77	76.32	75.68
60	224000	184270	238445	182098	249488	202810	71.71	73.07	70.45

Table 1: Peak areas and % remaining values

Day 2:

Time (min)	Assay 1		Assay 2		Assay 3		(% remaining)		
	PZ-II-028 Peak area	ISTD Peak area	PZ-II-028 Peak area	ISTD Peak area	PZ-II-028 Peak area	ISTD Peak area	Assay 1	Assay 2	Assay 3
0	340040	192439	331759	189954	345868	200640	100.00	99.97	99.99
10	318242	195404	324573	197827	312513	192301	92.17	93.91	94.26
20	305569	192981	299895	188781	299459	194073	89.61	90.93	89.50
30	298265	197605	286592	196819	274487	192160	85.42	83.35	82.85
40	285918	201639	280896	200397	262591	191811	80.24	80.23	79.40
50	261825	192246	264588	191591	253613	189168	77.07	79.05	77.76
60	247898	189899	259822	195517	241724	191307	73.87	76.06	73.29

Table 2: Peak areas and % remaining values

Calculation:

From the peak area, Calculate the following

$$\text{Peak area ratio} = \frac{\text{Peak area of test compound (PZ-II-028)}}{\text{Peak area of internal standard (ISTD)}}$$

$$\text{\% remaining at time T} = \frac{\text{Peak area ratio at particular time T}}{\text{Peak area ratio at zero time point}} * 100$$

(T = 0, 10, 20,30,40,50 and 60)

DATA ANALYSIS:

Day 1

Linear regression analysis:

Slope: -0.005374 ± 0.0002025

At X= 60, Y = 4.269 ± 0.007303

R^2 = 0.9737

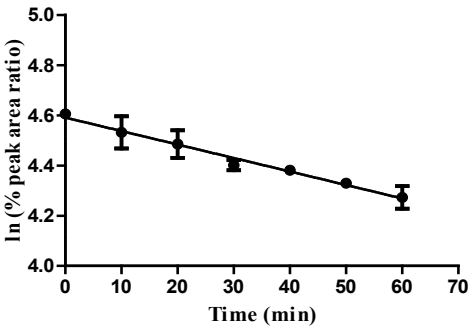

Metabolic Parameters:

Half-life: 129 ± 4.85 min

V_d: 100 µL/mg

Intrinsic clearance: 0.5374 µL/min/mg

Metabolic Rate: 10.748 nmol/min/mg

% remaining at 60 min: 71.45 ± 0.12 %

Day 2

Linear regression analysis:

Slope: -0.004882 ± 0.0001744

At X = 60, Y = 4.299 ± 0.006290

R^2 = 0.9763

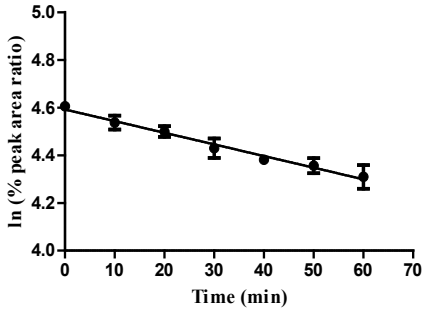

Metabolic Parameters:

Half-life: 142 ± 5 min

V_d: 100 µL/mg

Intrinsic clearance: 0.4882 µL/min/mg

Metabolic Rate: 9.764 nmol/min/mg

% remaining at 60 min: 73.6 ± 0.10 %

Note: The peak area ratios and natural log values are calculated using Microsoft excel 2010 and linear regression analysis is calculated using GraphPad prism.

Mouse Liver Microsomal Assay

Principal Investigator: Dr. Alexander Arnold
Operator: Revathi Kodali
Test Compound: **8k**
Concentration: 10 µM
Date: 05-11-2016
Facility: Milwaukee Institute for Drug Discovery

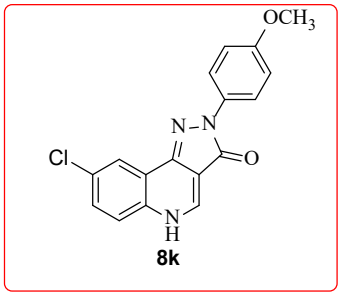

8k

Assay Protocol

Each evaluation included six independent assays carried out three at a time, on two different days

1. Preparation of solutions:
   a. 1 mM test compound in DMSO.
   b. 1 µM 4,5 Di Phenyl Imidazole in ice cold Acetonitrile (ISTD).
2. For a total volume of Microsomal Assay Mixture (MAM) 390 µL, sufficient for seven time points, combine the following
   a. 282 µL of 18.2 mΩ of water.
   b. 80 µL of 0.5 M potassium phosphate buffer (p^H 7.4)
   c. 20 µL of NADPH A. (Corning life sciences, Cat # 451220)
   d. 4 µL of NADPH B. (Corning life sciences, Cat # 451200)
   e. 4 µL of test compound.
3. Sonicate MAM for 5 min and meanwhile thaw microsomes (20 mg/mL) (Life technologies, Cat # 452156) on ice.
4. Aliquot 100 µL of ice cold ISTD into seven separate 1.5 mL conical vials and label them the time points for 0, 10, 20, 30, 40, 50, and 60 min.
5. Arrange the timer. Microsomes (Final concentration of 0.5 mg/mL) should be added to all time points except the zero time point.
6. Add 50 µL of the MAM solution to the conical vial labelled as zero time point. Place the remaining MAM solution in the incubator (37 ºC) for 5 min and initiate the reaction with addition of microsomes (8.8 µL) and record the time.
7. At the end of each time interval remove 50 µL and add to 100 µL ISTD in conical vial, sonicate for 10 sec and spin down at 10,000 rpm for 5 minutes.
8. Take 100 µL of supernatant and transfer to Spin-X HPLC filter tubes (Corning Incorporated, Cat # 8169) and centrifuge at 13,000 rpm for 5 minutes and take 5 µL from this solution and dilute in 495 µL of LCMS grade methanol (Fischer scientific, CAS # 67-56-1) in an 2mL glass auto sampler vial (Microsolv, Cat # 95025-WCV)
9. The samples are analyzed by LCMS-8040. (Shimadzu)

Data:

Day 1:

Time (min)	Assay 1		Assay 2		Assay 3		% remaining		
	PZ-II-028 Peak area	ISTD Peak area	PZ-II-028 Peak area	ISTD Peak area	PZ-II-028 Peak area	ISTD Peak area	Assay 1	Assay 2	Assay 3
0	366061	199827	336466	199039	337673	194171	99.99	100.02	100.00
10	354142	209737	307305	201713	319153	196427	92.16	90.14	93.43
20	304089	196538	280904	200559	304912	203823	84.45	82.87	86.02
30	289982	197643	269131	194897	289487	198575	80.08	81.70	83.83
40	272301	194366	254952	193436	270560	199235	76.47	77.98	78.09
50	261248	192467	244954	194893	259999	196266	74.09	74.37	76.17
60	243264	198621	224892	194818	226288	196987	66.85	68.30	66.05

Table 1: Peak areas and % remaining values

Day 2:

Time (min)	Assay 1		Assay 2		Assay 3		(% remaining)		
	PZ-II-028 Peak area	ISTD Peak area	PZ-II-028 Peak area	ISTD Peak area	PZ-II-028 Peak area	ISTD Peak area	Assay 1	Assay 2	Assay 3
0	343831	194879	339147	198969	346744	205015	100.01	99.97	100.01
10	323549	200214	312795	193433	313614	199614	91.61	94.84	92.91
20	308786	196656	297763	196507	289897	192823	89.01	88.87	88.90
30	294808	196426	288071	200701	288541	202020	85.08	84.18	84.46
40	281641	198577	271681	201071	264187	195683	80.40	79.24	79.83
50	270456	199404	264391	197514	257406	198739	76.88	78.51	76.59
60	237481	198225	230209	198359	220656	197443	67.91	68.06	66.08

Table 2: Peak areas and % remaining values

Calculation:

From the peak area, Calculate the following

$$\text{Peak area ratio} = \frac{\text{Peak area of test compound (PZ-II-028)}}{\text{Peak area of internal standard (ISTD)}}$$

$$\text{\% remaining at time T} = \frac{\text{Peak area ratio at particular time T}}{\text{Peak area ratio at zero time point}} * 100$$

(T = 0, 10, 20,30,40,50 and 60)

DATA ANALYSIS:

Day 1

Linear regression analysis:

Slope: -0.006044 ± 0.0002685

At X= 60, Y = 4.224 ± 0.009680

R^2 = 0.9639

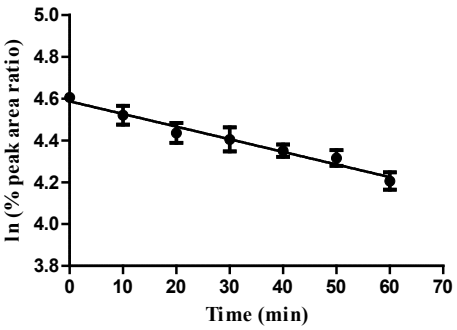

Metabolic Parameters:

Half-life: 114.65 ± 5 min

V_d: 100 µL/mg

Intrinsic clearance: 0.6044 µL/min/mg

Metabolic Rate: 12.088 nmol/min/mg

% remaining at 60 min: 68.30 ± 0.15 %

Day 2

Linear regression analysis:

Slope: -0.005946 ± 0.0002748

At X = 60, Y = 4.251 ± 0.009908

R^2 = 0.9610

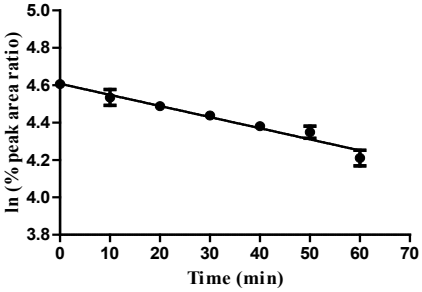

Metabolic Parameters:

Half-life: 116.54 ± 5 min

V_d: 100 µL/mg

Intrinsic clearance: 0.5946 µL/min/mg

Metabolic Rate: 11.892 nmol/min/mg

% remaining at 60 min: 70.17 ± 0.16 %

Note: The peak area ratios and natural log values are calculated using Microsoft excel 2010 and linear regression analysis is calculated using GraphPad prism.

Human Liver Microsomal Assay

Principal Investigator: Dr. Alexander Arnold
Operator: Revathi Kodali
Test Compound: **8l**
Concentration: 10 µM
Date: 05-11-2016
Facility: Milwaukee Institute for Drug Discovery

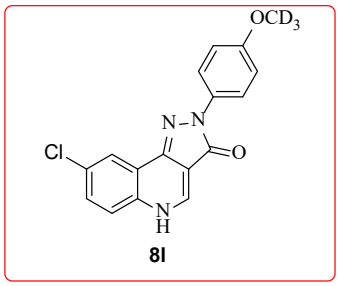

8l

Assay Protocol

Each evaluation included six independent assays carried out three at a time, on two different days

1. Preparation of solutions:
   a. 1 mM test compound in DMSO.
   b. 1 µM 4,5 Di Phenyl Imidazole in ice cold Acetonitrile (ISTD).
2. For a total volume of Microsomal Assay Mixture (MAM) 390 µL, sufficient for seven time points, combine the following
   a. 282 µL of 18.2 mΩ of water.
   b. 80 µL of 0.5 M potassium phosphate buffer (p^H 7.4)
   c. 20 µL of NADPH A. (Corning life sciences, Cat # 451220)
   d. 4 µL of NADPH B. (Corning life sciences, Cat # 451200)
   e. 4 µL of test compound.
3. Sonicate MAM for 5 min and meanwhile thaw microsomes (20 mg/mL) (BD Gentest, Cat # 452156) on ice.
4. Aliquot 100 µL of ice cold ISTD into seven separate 1.5 mL conical vials and label them the time points for 0, 10, 20, 30, 40, 50, and 60 min.
5. Arrange the timer. Microsomes (Final concentration of 0.5 mg/mL) should be added to all time points except the zero time point.
6. Add 50 µL of the MAM solution to the conical vial labelled as zero time point. Place the remaining MAM solution in the incubator (37 ºC) for 5 min and initiate the reaction with addition of microsomes (8.8 µL) and record the time.
7. At the end of each time interval remove 50 µL and add to 100 µL ISTD in conical vial, sonicate for 10 sec and spin down at 10,000 rpm for 5 minutes.
8. Take 100 µL of supernatant and transfer to Spin-X HPLC filter tubes (Corning Incorporated, Cat # 8169) and centrifuge at 13,000 rpm for 5 minutes and take 5 µL from this solution and dilute in 495 µL of LCMS grade methanol (Fischer scientific, CAS # 67-56-1) in an 2mL glass auto sampler vial (Microsolv, Cat # 95025-WCV)
9. The samples are analyzed by LCMS-8040. (Shimadzu)

Data:

Day 1:

Time (min)	Assay 1		Assay 2		Assay 3		% remaining		
	DK-I-93-1 Peak area	ISTD Peak area	DK-I-93-1 Peak area	ISTD Peak area	DK-I-93-1 Peak area	ISTD Peak area	Assay 1	Assay 2	Assay 3
0	250625	192387	237170	198327	234647	199878	99.97	99.98	99.99
10	242335	189302	224245	189872	225979	200083	98.24	98.74	96.20
20	238422	192987	232415	201838	222414	198723	94.81	96.27	95.33
30	238094	194382	225682	200982	220003	197823	94.00	93.88	94.72
40	223222	189899	217775	197267	216509	198727	90.21	92.30	92.80
50	227512	190923	213875	189283	206397	189982	91.45	94.47	92.53
60	243612	200837	217353	189231	213670	189238	93.09	96.03	96.17

Table 1: Peak areas and % remaining values

Day 2:

Time (min)	Assay 1		Assay 2		Assay 3		(% remaining)		
	DK-I-93-1 Peak area	ISTD Peak area	DK-I-93-1 Peak area	ISTD Peak area	DK-I-93-1 Peak area	ISTD Peak area	Assay 1	Assay 2	Assay 3
0	232555	181934	254844	198536	235043	183806	100.01	99.97	99.98
10	231871	188134	242801	189616	239432	190946	96.43	99.72	98.03
20	230713	189672	241871	199585	235141	194722	95.17	94.38	94.41
30	229991	194398	231837	187871	217874	183237	92.57	96.10	92.96
40	217135	179986	229810	188630	229989	192164	94.39	94.88	93.57
50	214187	180515	236366	193786	230808	196736	92.84	94.99	91.72
60	239230	196288	209997	177296	220264	186986	95.36	92.24	92.10

Table 2: Peak areas and % remaining values

Calculation:

From the peak area, Calculate the following

$$\text{Peak area ratio} = \frac{\text{Peak area of test compound (DK-I-93-1)}}{\text{Peak area of internal standard (ISTD)}}$$

$$\text{\% remaining at time T} = \frac{\text{Peak area ratio at particular time T}}{\text{Peak area ratio at zero time point}} * 100$$

(T = 0, 10, 20,30,40,50 and 60)

DATA ANALYSIS:

Day 1

Linear regression analysis:

Slope: -0.001044 ± 0.0002330

At X= 60, Y = 4.525 ± 0.008401

R^2 = 0.5138

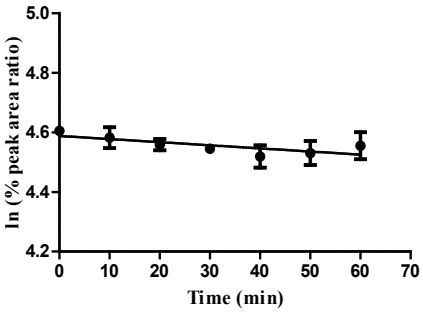

Metabolic Parameters:

Half-life: 663.8 ± 148 min

V_d: 100 µL/mg

Intrinsic clearance: 0.1044 µL/min/mg

Metabolic Rate: 2.088 nmol/min/mg

% remaining at 60 min: 92.29 ± 0.17 %

Day 2

Linear regression analysis:

Slope: -0.001125 ± 0.0001897

At X = 60, Y = 4.523 ± 0.006839

R^2 = 0.6493

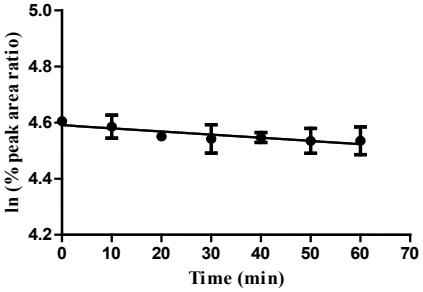

Metabolic Parameters:

Half-life: 616 ± 103.87 min

V_d: 100 µL/mg

Intrinsic clearance: 0.1125 µL/min/mg

Metabolic Rate: 2.25 nmol/min/mg

% remaining at 60 min: 92.11 ± 0.13 %

Note: The peak area ratios and natural log values are calculated using Microsoft excel 2010 and linear regression analysis is calculated using GraphPad prism.

Mouse Liver Microsomal Assay

Principal Investigator: Dr. Alexander Arnold
Operator: Revathi Kodali
Test Compound: **8l**
Concentration: 10 µM
Date: 05-11-2016
Facility: Milwaukee Institute for Drug Discovery

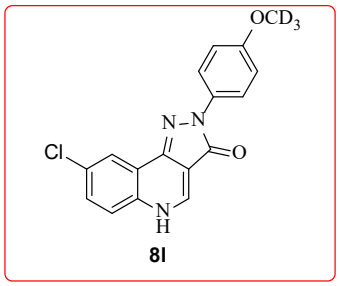

8l

Assay Protocol

Each evaluation included six independent assays carried out three at a time, on two different days

1. Preparation of solutions:
   a. 1 mM test compound in DMSO.
   b. 1 µM 4,5 Di Phenyl Imidazole in ice cold Acetonitrile (ISTD).
2. For a total volume of Microsomal Assay Mixture (MAM) 390 µL, sufficient for seven time points, combine the following
   a. 282 µL of 18.2 mΩ of water.
   b. 80 µL of 0.5 M potassium phosphate buffer (p^H 7.4)
   c. 20 µL of NADPH A. (Corning life sciences, Cat # 451220)
   d. 4 µL of NADPH B. (Corning life sciences, Cat # 451200)
   e. 4 µL of test compound.
3. Sonicate MAM for 5 min and meanwhile thaw microsomes (20 mg/mL) (Life technologies, Cat # MSMC-PL) on ice.
4. Aliquot 100 µL of ice cold ISTD into seven separate 1.5 mL conical vials and label them the time points for 0, 10, 20, 30, 40, 50, and 60 min.
5. Arrange the timer. Microsomes (Final concentration of 0.5 mg/mL) should be added to all time points except the zero time point.
6. Add 50 µL of the MAM solution to the conical vial labelled as zero time point. Place the remaining MAM solution in the incubator (37 ºC) for 5 min and initiate the reaction with addition of microsomes (8.8 µL) and record the time.
7. At the end of each time interval remove 50 µL and add to 100 µL ISTD in conical vial, sonicate for 10 sec and spin down at 10,000 rpm for 5 minutes.
8. Take 100 µL of supernatant and transfer to Spin-X HPLC filter tubes (Corning Incorporated, Cat # 8169) and centrifuge at 13,000 rpm for 5 minutes and take 5 µL from this solution and dilute in 495 µL of LCMS grade methanol (Fischer scientific, CAS # 67-56-1) in an 2mL glass auto sampler vial (Microsolv, Cat # 95025-WCV)
9. The samples are analyzed by LCMS-8040. (Shimadzu)

Data:

Day 1:

Time (min)	Assay 1		Assay 2		Assay 3		% remaining		
	DK-I-93-1 Peak area	ISTD Peak area	DK-I-93-1 Peak area	ISTD Peak area	DK-I-93-1 Peak area	ISTD Peak area	Assay 1	Assay 2	Assay 3
0	247869	200832	242560	198728	240012	200383	100.01	99.96	99.98
10	241961	198938	229981	189972	228890	192038	98.56	99.14	99.49
20	219944	189239	219837	190398	227377	198723	94.18	94.56	95.50
30	219892	192783	223091	198289	222356	199873	92.43	92.14	92.86
40	215733	190283	223609	199089	202388	187327	91.87	91.98	90.18
50	217308	200038	210655	198289	201168	193989	88.03	87.00	86.56
60	210081	198238	199705	190098	197997	199723	85.87	86.03	82.75

Table 1: Peak areas and % remaining values

Day 2:

Time (min)	Assay 1		Assay 2		Assay 3		(% remaining)		
	DK-I-93-1 Peak area	ISTD Peak area	DK-I-93-1 Peak area	ISTD Peak area	DK-II-93-1 Peak area	ISTD Peak area	Assay 1	Assay 2	Assay 3
0	223619	198287	256949	198289	230099	200812	99.97	99.98	99.98
10	216310	198732	253937	200198	222023	199128	96.49	97.87	97.29
20	214081	201832	243196	200928	208449	192983	94.03	93.39	94.25
30	211543	200783	238604	199289	210719	198997	93.40	92.38	92.40
40	207923	201838	235187	198181	198300	189877	91.32	91.56	91.13
50	197590	198328	224951	199823	201107	199887	88.32	86.86	87.79
60	203382	208278	213838	192566	203202	208787	86.56	85.68	84.926

Table 2: Peak areas and % remaining values

Calculation:

From the peak area, Calculate the following

$$\text{Peak area ratio} = \frac{\text{Peak area of test compound (DK-I-93-1)}}{\text{Peak area of internal standard (ISTD)}}$$

$$\text{\% remaining at time T} = \frac{\text{Peak area ratio at particular time T}}{\text{Peak area ratio at zero time point}} * 100$$

(T = 0, 10, 20,30,40,50 and 60)

DATA ANALYSIS:

Day 1

Linear regression analysis:

Slope: -0.002795 ± 0.0001334

At X= 60, Y = 4.445 ± 0.004847

R^2 = 0.9579

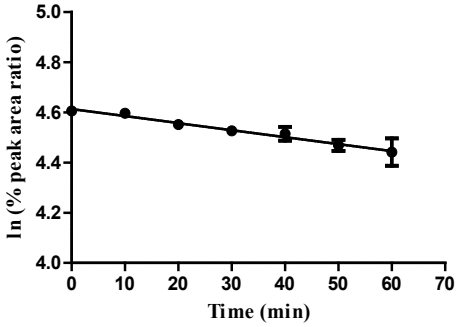

Metabolic Parameters:

Half-life: 247.94 ± 11.92 min

V_d: 100 µL/mg

Intrinsic clearance: 0.2795 µL/min/mg

Metabolic Rate: 5.59 nmol/min/mg

% remaining at 60 min: 85.19 ± 0.09 %

Day 2

Linear regression analysis:

Slope: -0.002487 ± 9.365e^{-}005

At X = 60, Y = 4.453 ± 0.003377

R^2 = 0.9738

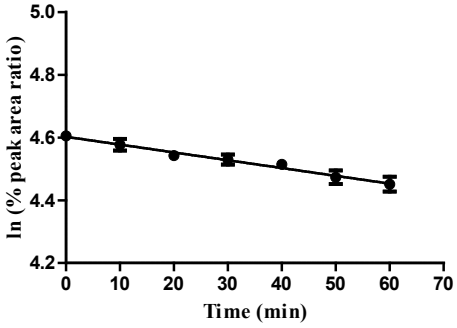

Metabolic Parameters:

Half-life: 277.86 min

V_d: 100 µL/mg

Intrinsic clearance: 0.2494 µL/min/mg

Metabolic Rate: 4.988 nmol/min/mg

% remaining at 60 min: 85.88 ± 0.06 %

Note: The peak area ratios and natural log values are calculated using Microsoft excel 2010 and linear regression analysis is calculated using GraphPad prism.

Human Liver Microsomal Assay

Principal Investigator: Dr. Alexander Arnold
Operator: Revathi Kodali
Test Compound: **8m**
Concentration: 10 µM
Date: 05-31-2016
Facility: Milwaukee Institute for Drug Discovery

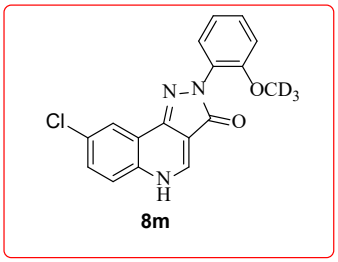

8m

Assay Protocol

Each evaluation included six independent assays carried out three at a time, on two different days

1. Preparation of solutions:
   a. 1 mM test compound in DMSO.
   b. 1 µM 4,5 Di Phenyl Imidazole in ice cold Acetonitrile (ISTD).
2. For a total volume of Microsomal Assay Mixture (MAM) 390 µL, sufficient for seven time points, combine the following
   a. 282 µL of 18.2 mΩ of water.
   b. 80 µL of 0.5 M potassium phosphate buffer (p^H 7.4)
   c. 20 µL of NADPH A. (Corning life sciences, Cat # 451220)
   d. 4 µL of NADPH B. (Corning life sciences, Cat # 451200)
   e. 4 µL of test compound.
3. Sonicate MAM for 5 min and meanwhile thaw microsomes (20 mg/mL) (BD Gentest, Cat # 452156) on ice.
4. Aliquot 100 µL of ice cold ISTD into seven separate 1.5 mL conical vials and label them the time points for 0, 10, 20, 30, 40, 50, and 60 min.
5. Arrange the timer. Microsomes (Final concentration of 0.5 mg/mL) should be added to all time points except the zero time point.
6. Add 50 µL of the MAM solution to the conical vial labelled as zero time point. Place the remaining MAM solution in the incubator (37 ºC) for 5 min and initiate the reaction with addition of microsomes (8.8 µL) and record the time.
7. At the end of each time interval remove 50 µL and add to 100 µL ISTD in conical vial, sonicate for 10 sec and spin down at 10,000 rpm for 5 minutes.
8. Take 100 µL of supernatant and transfer to Spin-X HPLC filter tubes (Corning Incorporated, Cat # 8169) and centrifuge at 13,000 rpm for 5 minutes and take 5 µL from this solution and dilute in 495 µL of LCMS grade methanol (Fischer scientific, CAS # 67-56-1) in an 2mL glass auto sampler vial (Microsolv, Cat # 95025-WCV)
9. The samples are analyzed by LCMS-8040. (Shimadzu)

Data:

Day 1:

Time (min)	Assay 1		Assay 2		Assay 3		% remaining		
	DK-I-87-1 Peak area	ISTD Peak area	DK-I-87-1 Peak area	ISTD Peak area	DK-I-87-1 Peak area	ISTD Peak area	Assay 1	Assay 2	Assay 3
0	3152581	2574057	3090759	2547745	3041212	2506826	99.98	100.01	100.01
10	2808908	2335235	2912951	2501008	3038858	2554152	98.19	96.01	98.08
20	2866087	2400484	2847348	2427550	3040589	2629818	97.46	96.69	95.31
30	2972032	2516908	2927928	2523366	2843286	2411572	96.39	95.65	97.19
40	2710230	2301818	2876918	2476615	2874748	2490507	96.11	95.76	95.15
50	2957325	2548271	2899982	2513844	2742462	2389247	94.73	95.10	94.62
60	2886265	2480002	2892799	2482830	2789089	2399249	95.00	96.05	95.83

Table 1: Peak areas and % remaining values

Day 2:

Time (min)	Assay 1		Assay 2		Assay 3		(% remaining)		
	DK-I-87-1 Peak area	ISTD Peak area	DK-I-87-1 Peak area	ISTD Peak area	DK-I-87-1 Peak area	ISTD Peak area	Assay 1	Assay 2	Assay 3
0	3064533	2514855	3043938	2506906	3099337	2509389	99.96	100.01	100.00
10	3025303	2515223	2932365	2477887	3077022	2522920	98.67	97.48	98.75
20	2918654	2479369	2875835	2458655	3122423	2592134	96.56	96.34	97.53
30	2959314	2499725	2920979	2521593	2905454	2453499	97.11	95.41	95.88
40	2905799	2468160	2862172	2445543	3022306	2568476	96.58	96.40	95.27
50	2993719	2551914	2886596	2500423	2911271	2452557	96.23	95.09	96.11
60	2858457	2445646	2914618	2493893	2867156	2457617	95.88	96.26	94.46

Table 2: Peak areas and % remaining values

Calculation:

From the peak area, Calculate the following

$$\text{Peak area ratio} = \frac{\text{Peak area of test compound (DK-I-87-1)}}{\text{Peak area of internal standard (ISTD)}}$$

$$\text{\% remaining at time T} = \frac{\text{Peak area ratio at particular time T}}{\text{Peak area ratio at zero time point}} * 100$$

(T = 0, 10, 20,30,40,50 and 60)

DATA ANALYSIS:

Day 1

Linear regression analysis:

Slope: -0.0007000 ± 0.0001150

At X= 60, Y = 4.550 ± 0.004145

R^2 = 0.6612

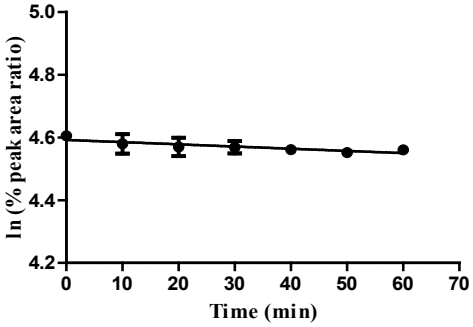

Metabolic Parameters:

Half-life: 990 ± 162.64 min

V_d: 100 µL/mg

Intrinsic clearance: 0.07 µL/min/mg

Metabolic Rate: 1.4 nmol/min/mg

% remaining at 60 min: 94.63 ± 0.08 %

Day 2

Linear regression analysis:

Slope: -0.0006988 ± 0.0001008

At X = 60, Y = 4.553 ± 0.003633

R^2 = 0.7168

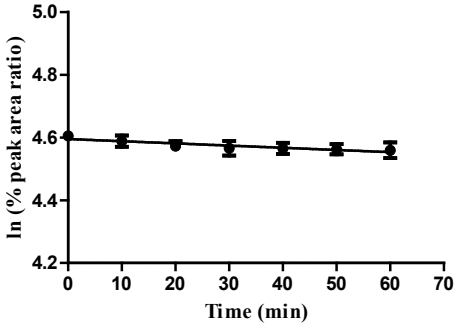

Metabolic Parameters:

Half-life: 991.70 ± 143.05 min

V_d: 100 µL/mg

Intrinsic clearance: 0.06988 µL/min/mg

Metabolic Rate: 1.3976 nmol/min/mg

% remaining at 60 min: 94.91 ± 0.07 %

Note: The peak area ratios and natural log values are calculated using Microsoft excel 2010 and linear regression analysis is calculated using GraphPad prism.

Mouse Liver Microsomal Assay

Principal Investigator: Dr. Alexander Arnold
Operator: Revathi Kodali
Test Compound: **8m**
Concentration: 10 µM
Date: 05-31-2016
Facility: Milwaukee Institute for Drug Discovery

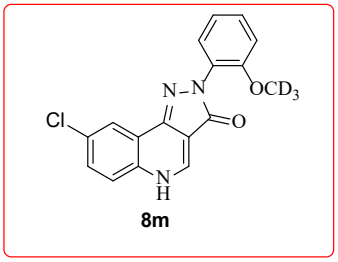

8m

Assay Protocol

Each evaluation included six independent assays carried out three at a time, on two different days

1. Preparation of solutions:
   a. 1 mM test compound in DMSO.
   b. 1 µM 4,5 Di Phenyl Imidazole in ice cold Acetonitrile (ISTD).
2. For a total volume of Microsomal Assay Mixture (MAM) 390 µL, sufficient for seven time points, combine the following
   a. 282 µL of 18.2 mΩ of water.
   b. 80 µL of 0.5 M potassium phosphate buffer (p^H 7.4)
   c. 20 µL of NADPH A. (Corning life sciences, Cat # 451220)
   d. 4 µL of NADPH B. (Corning life sciences, Cat # 451200)
   e. 4 µL of test compound.
3. Sonicate MAM for 5 min and meanwhile thaw microsomes (20 mg/mL) (Life technologies, Cat # MSMC-PL) on ice.
4. Aliquot 100 µL of ice cold ISTD into seven separate 1.5 mL conical vials and label them the time points for 0, 10, 20, 30, 40, 50, and 60 min.
5. Arrange the timer. Microsomes (Final concentration of 0.5 mg/mL) should be added to all time points except the zero time point.
6. Add 50 µL of the MAM solution to the conical vial labelled as zero time point. Place the remaining MAM solution in the incubator (37 ºC) for 5 min and initiate the reaction with addition of microsomes (8.8 µL) and record the time.
7. At the end of each time interval remove 50 µL and add to 100 µL ISTD in conical vial, sonicate for 10 sec and spin down at 10,000 rpm for 5 minutes.
8. Take 100 µL of supernatant and transfer to Spin-X HPLC filter tubes (Corning Incorporated, Cat # 8169) and centrifuge at 13,000 rpm for 5 minutes and take 5 µL from this solution and dilute in 495 µL of LCMS grade methanol (Fischer scientific, CAS # 67-56-1) in an 2mL glass auto sampler vial (Microsolv, Cat # 95025-WCV)
9. The samples are analyzed by LCMS-8040. (Shimadzu)

Data:

Day 1:

Time (min)	Assay 1		Assay 2		Assay 3		% remaining		
	DK-I-87-1 Peak area	ISTD Peak area	DK-I-87-1 Peak area	ISTD Peak area	DK-I-87-1 Peak area	ISTD Peak area	Assay 1	Assay 2	Assay 3
0	3010880	2496127	3000020	2474890	3119712	2577903	100.01	100.01	100.01
10	2919613	2469905	3060634	2584737	2940036	2414532	98.01	97.70	100.63
20	2877808	2467796	2948704	2550083	2891272	2464767	96.69	95.40	96.94
30	2949345	2509812	2864981	2476848	2814761	2424509	97.44	95.43	95.94
40	2874816	2447825	2859953	2478746	2787443	2412483	97.38	95.19	95.49
50	2823464	2438940	2907401	2505846	2929879	2500532	95.99	95.73	96.83
60	2868479	2500485	2916626	2545748	2888867	2478648	95.12	94.52	96.32

Table 1: Peak areas and % remaining values

Day 2:

Time (min)	Assay 1		Assay 2		Assay 3		(% remaining)		
	DK-I-87-1 Peak area	ISTD Peak area	DK-I-87-1 Peak area	ISTD Peak area	DK-I-87-1 Peak area	ISTD Peak area	Assay 1	Assay 2	Assay 3
0	3063855	2554326	3017647	2477860	3122426	2581928	100.04	99.98	100.02
10	3073622	2574381	3128942	2598728	2931678	2492897	99.57	98.85	97.27
20	2896000	2493902	3052088	2606005	2961703	2533688	96.85	96.15	96.68
30	2857230	2502888	2998628	2583360	3062090	2603003	95.21	95.29	97.30
40	2887437	2489385	2914665	2515120	2981544	2573374	96.73	95.14	95.83
50	2896283	2494688	2913298	2498493	2828265	2495987	96.82	95.73	93.72
60	2883458	2492776	2987679	2537837	2861939	2487628	96.47	96.65	95.15

Table 2: Peak areas and % remaining values

Calculation:

From the peak area, Calculate the following

$$\text{Peak area ratio} = \frac{\text{Peak area of test compound (DK-I-87-1)}}{\text{Peak area of internal standard (ISTD)}}$$

$$\text{\% remaining at time T} = \frac{\text{Peak area ratio at particular time T}}{\text{Peak area ratio at zero time point}} * 100$$

(T = 0, 10, 20,30,40,50 and 60)

DATA ANALYSIS:

Day 1

Linear regression analysis:

Slope: -0.0007107 ± 0.0001294

At X= 60, Y = 4.553 ± 0.004665

R^2 = 0.6136

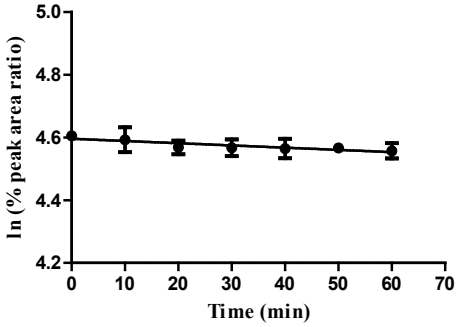

Metabolic Parameters:

Half-life: 975.09 ± 177.5 min

V_d: 100 µL/mg

Intrinsic clearance: 0.07107 µL/min/mg

Metabolic Rate: 1.4214 nmol/min/mg

% remaining at 60 min: 94.91± 0.10 %

Day 2

Linear regression analysis:

Slope: -0.0006857 ± 0.0001368

At X = 60, Y = 4.553 ± 0.004934

R^2 = 0.5692

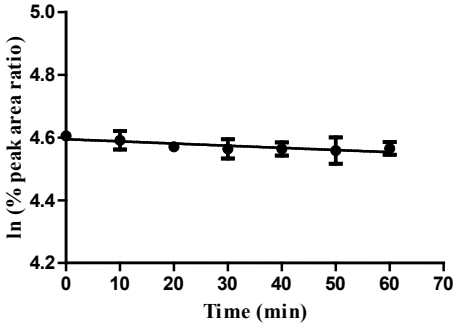

Metabolic Parameters:

Half-life: 1010.64 ± 201.62 min

V_d: 100 µL/mg

Intrinsic clearance: 0.06857 µL/min/mg

Metabolic Rate: 1.3714 nmol/min/mg

% remaining at 60 min: 94.91 ± 0.10 %

Note: The peak area ratios and natural log values are calculated using Microsoft excel 2010 and linear regression analysis is calculated using GraphPad prism.

Human Liver Microsomal Assay

Principal Investigator: Dr. Alexander Arnold
Operator: Revathi Kodali
Test Compound: **8n**
Concentration: 10 µM
Date: 04-13-2016
Facility: Milwaukee Institute for Drug Discovery

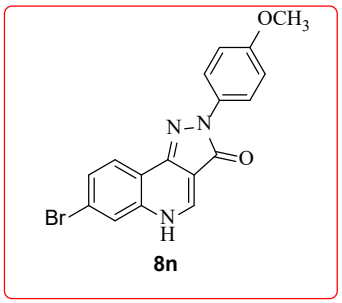

8n

Assay Protocol

Each evaluation included six independent assays carried out three at a time, on two different days

1. Preparation of solutions:
   a. 1 mM test compound in DMSO.
   b. 0.5 µM 4,5 Diphenyl Imidazole in ice cold Acetonitrile (ISTD).
2. For a total volume of Microsomal Assay Mixture (MAM) 390 µL, sufficient for seven time points, combine the following
   a. 282 µL of 18.2 mΩ of water.
   b. 80 µL of 0.5 M potassium phosphate buffer (p^H 7.4)
   c. 20 µL of NADPH A. (Corning life sciences, Cat # 451220)
   d. 4 µL of NADPH B. (Corning life sciences, Cat # 451200)
   e. 4 µL of test compound.
3. Sonicate MAM for 5 min and meanwhile thaw microsomes (20 mg/mL) (BD Gentest, Cat # 452156) on ice.
4. Aliquot 100 µL of ice cold ISTD into seven separate 1.5 mL conical vials and label them the time points for 0, 10, 20, 30, 40, 50, and 60 min.
5. Arrange the timer. Microsomes (Final concentration of 0.5 mg/mL) should be added to all time points except the zero time point.
6. Add 50 µL of the MAM solution to the conical vial labelled as zero time point. Place the remaining MAM solution in the incubator (37 ºC) for 5 min and initiate the reaction with addition of microsomes (8.8 µL) and record the time.
7. At the end of each time interval remove 50 µL and add to 100 µL ISTD in conical vial, sonicate for 10 sec and spin down at 10,000 rpm for 5 minutes.
8. Take 100 µL of supernatant and transfer to Spin-X HPLC filter tubes (Corning Incorporated, Cat # 8169) and centrifuge at 13,000 rpm for 5 minutes and take 5 µL from this solution and dilute in 495 µL of LCMS grade methanol (Fischer scientific, CAS # 67-56-1) in an 2mL glass auto sampler vial (Microsolv, Cat # 95025-WCV)
9. The samples are analyzed by LCMS-8040. (Shimadzu)

Data:

Day 1:

Time (min)	Assay 1		Assay 2		Assay 3		% remaining		
	LAU 463 Peak area	ISTD Peak area	LAU 463 Peak area	ISTD Peak area	LAU 463 Peak area	ISTD Peak area	Assay 1	Assay 2	Assay 3
0	40017	110382	41858	119807	38420	110467	99.87	100.10	99.94
10	36405	108314	36156	110853	34332	107107	92.59	93.45	92.10
20	35068	111286	33804	108649	33885	114225	86.80	89.14	85.24
30	31839	109123	30803	108326	29669	103425	80.37	81.47	82.43
40	29562	109819	29855	110849	28562	110188	74.15	77.17	74.48
50	24886	99310	25961	103663	27453	109407	69.03	71.75	72.10
60	23335	100114	25309	115500	26763	116484	64.21	62.78	66.02

Table 1: Peak areas and % remaining values

Day 2:

Time (min)	Assay 1		Assay 2		Assay 3		(% remaining)		
	LAU 463 Peak area	ISTD Peak area	LAU 463 Peak area	ISTD Peak area	LAU 463 Peak area	ISTD Peak area	Assay 1	Assay 2	Assay 3
0	49475	117867	49987	119544	48124	110902	99.94	100.03	99.98
10	45683	118348	44098	114025	47589	117783	91.90	92.52	93.09
20	39116	104050	37792	102482	38666	103094	89.50	88.22	86.41
30	42354	116764	36851	107165	37992	110412	86.36	82.26	79.28
40	34884	102256	38809	117335	33961	102324	81.22	79.12	76.47
50	39590	126003	34528	108682	35448	110883	74.80	76.00	73.66
60	33816	121431	32387	118994	38044	127573	66.30	65.11	68.71

Table 2: Peak areas and % remaining values

Calculation:

From the peak area, Calculate the following

$$\text{Peak area ratio} = \frac{\text{Peak area of test compound (LAU 463)}}{\text{Peak area of internal standard (Verapamil)}}$$

$$\text{\% remaining at time T (T = 0, 10, 20,30,40,50 and 60)} = \frac{\text{Peak area ratio at particular time T}}{\text{Peak area ratio at zero time point}} * 100$$

DATA ANALYSIS:

Day 1

Linear regression analysis:

Slope: -0.007155 ± 0.0001949

At X= 60, Y = 4.178 ± 0.007028

R^2 = 0.9861

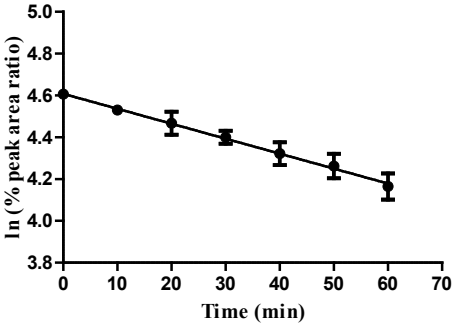

Metabolic Parameters:

Half-life: 96.85 ± 2.63 min

V_d: 100 µL/mg

Intrinsic clearance: 0.7155 µL/min/mg

Metabolic Rate: 14.31 nmol/min/mg

% remaining at 60 min: 65.23 ± 0.10 %

Day 2

Linear regression analysis:

Slope: -0.006250 ± 0.0002926

At X = 60, Y = 4.228 ± 0.01055

R^2 = 0.9600

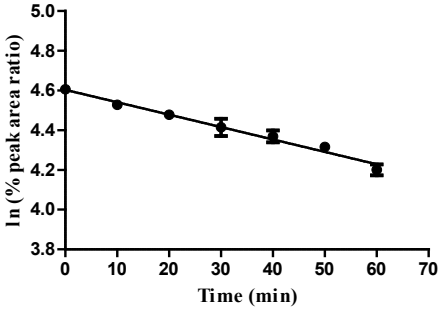

Metabolic Parameters:

Half-life: 110.88 ± 5.19 min

V_d: 100 µL/mg

Intrinsic clearance: 0.625 µL/min/mg

Metabolic Rate: 12.5 nmol/min/mg

% remaining at 60 min: 68.5 ± 0.17 %

Note: The peak area ratios and natural log values are calculated using Microsoft excel 2010 and linear regression analysis is calculated using GraphPad prism.

Mouse Liver Microsomal Assay

Principal Investigator: Dr. Alexander Arnold
Operator: Revathi Kodali
Test Compound: **8n**
Concentration: 10 µM
Date: 04-13-2016
Facility: Milwaukee Institute for Drug Discovery

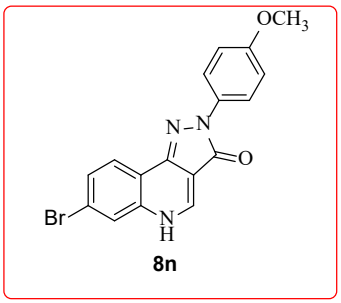

8n

Assay Protocol

Each evaluation included six independent assays carried out three at a time, on two different days

1. Preparation of solutions:
   a. 1 mM test compound in DMSO.
   b. 0.5 µM 4,5 Diphenyl Imidazole in ice cold Acetonitrile (ISTD).
2. For a total volume of Microsomal Assay Mixture (MAM) 390 µL, sufficient for seven time points, combine the following
   a. 282 µL of 18.2 mΩ of water.
   b. 80 µL of 0.5 M potassium phosphate buffer (p^H 7.4)
   c. 20 µL of NADPH A. (Corning life sciences, Cat # 451220)
   d. 4 µL of NADPH B. (Corning life sciences, Cat # 451200)
   e. 4 µL of test compound.
3. Sonicate MAM for 5 min and meanwhile thaw microsomes (20 mg/mL) (Life technologies, Cat # MSMC-PL) on ice.
4. Aliquot 100 µL of ice cold ISTD into seven separate 1.5 mL conical vials and label them the time points for 0, 10, 20, 30, 40, 50, and 60 min.
5. Arrange the timer. Microsomes (Final concentration of 0.5 mg/mL) should be added to all time points except the zero time point.
6. Add 50 µL of the MAM solution to the conical vial labelled as zero time point. Place the remaining MAM solution in the incubator (37 ºC) for 5 min and initiate the reaction with addition of microsomes (8.8 µL) and record the time.
7. At the end of each time interval remove 50 µL and add to 100 µL ISTD in conical vial, sonicate for 10 sec and spin down at 10,000 rpm for 5 minutes.
8. Take 100 µL of supernatant and transfer to Spin-X HPLC filter tubes (Corning Incorporated, Cat # 8169) and centrifuge at 13,000 rpm for 5 minutes and take 5 µL from this solution and dilute in 495 µL of LCMS grade methanol (Fischer scientific, CAS # 67-56-1) in an 2mL glass auto sampler vial (Microsolv, Cat # 95025-WCV)
9. The samples are analyzed by LCMS-8040. (Shimadzu)

Data:

Day 1:

Time (min)	Assay 1		Assay 2		Assay 3		% remaining		
	LAU 463 Peak area	ISTD Peak area	LAU 463 Peak area	ISTD Peak area	LAU 463 Peak area	ISTD Peak area	Assay 1	Assay 2	Assay 3
0	48890	112924	49279	113143	49215	113661	99.98	99.89	100.00
10	45153	112247	43675	107282	47056	117053	92.90	93.37	92.84
20	38035	103753	42468	116346	40403	109584	84.66	83.71	85.14
30	39080	108516	39403	111577	40013	113332	83.17	80.99	81.53
40	34991	101201	34999	104471	35979	112089	79.85	76.83	74.13
50	33923	105799	32017	103609	34231	110384	74.05	70.87	71.61
60	30997	104638	31893	109310	32070	112609	68.41	66.91	65.77

Table 1: Peak areas and % remaining values

Day 2:

Time (min)	Assay 1		Assay 2		Assay 3		(% remaining)		
	LAU 463 Peak area	ISTD Peak area	LAU 463 Peak area	ISTD Peak area	LAU 463 Peak area	ISTD Peak area	Assay 1	Assay 2	Assay 3
0	49868	114209	48673	113475	50609	115332	99.91	99.98	99.95
10	45918	111248	43511	106649	45190	108674	94.45	95.10	94.72
20	40638	108555	41931	111724	43760	113925	85.66	87.48	87.49
30	39591	107243	41207	112646	40629	107987	84.47	85.27	85.70
40	42615	117892	38437	108907	39788	108268	82.71	82.26	83.71
50	37730	112216	35424	110108	39287	115905	76.94	74.99	77.21
60	34666	113551	30020	105567	32646	109583	69.86	66.28	67.86

Table 2: Peak areas and % remaining values

Calculation:

From the peak area, Calculate the following

$$\text{Peak area ratio} = \frac{\text{Peak area of test compound (LAU 463)}}{\text{Peak area of internal standard (Verapamil)}}$$

$$\text{\% remaining at time T} = \frac{\text{Peak area ratio at particular time T}}{\text{Peak area ratio at zero time point}} * 100$$

(T = 0, 10, 20,30,40,50 and 60)

DATA ANALYSIS:

Day 1

Linear regression analysis:

Slope: -0.006435 ± 0.0002287

At X= 60, Y = 4.208 ± 0.008246

R^2 = 0.9766

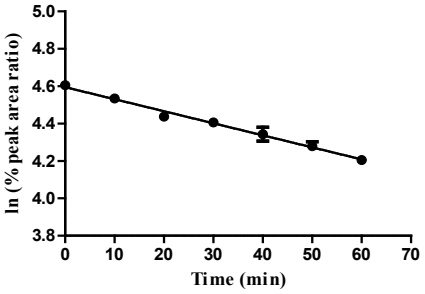

Metabolic Parameters:

Half-life: 107.69 ± 3.82 min

V_d: 100 µL/mg

Intrinsic clearance: 0.6435 µL/min/mg

Metabolic Rate: 12.87 nmol/min/mg

% remaining at 60 min: 67.22 ± 0.13 %

Day 2

Linear regression analysis:

Slope: -0.005840 ± 0.0003190

At X = 60, Y = 4.259 ± 0.01150

R^2 = 0.9464

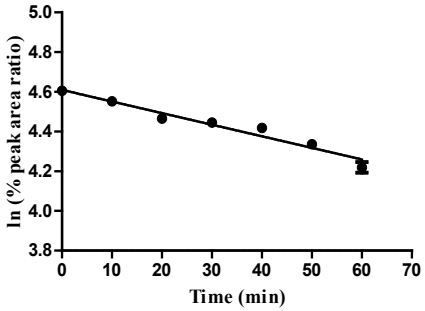

Metabolic Parameters:

Half-life: 118.66 ± 6.48 min

V_d: 100 µL/mg

Intrinsic clearance: 0.584 µL/min/mg

Metabolic Rate: 11.68 nmol/min/mg

% remaining at 60 min: 70.7 ± 0.19 %

Note: The peak area ratios and natural log values are calculated using Microsoft excel 2010 and linear regression analysis is calculated using GraphPad prism.

Human Liver Microsomal Assay

Principal Investigator: Dr. Alexander Arnold
Operator: Revathi Kodali
Test Compound: **8o**
Concentration: 10 µM
Date: 05-05-2016
Facility: Milwaukee Institute for Drug Discovery

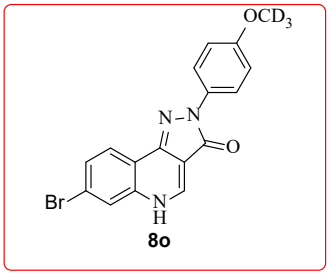

8o

Assay Protocol

Each evaluation included six independent assays carried out three at a time, on two different days

1. Preparation of solutions:
   a. 1 mM test compound in DMSO.
   b. 0.5 µM 4,5 Diphenyl Imidazole in ice cold Acetonitrile (ISTD).
2. For a total volume of Microsomal Assay Mixture (MAM) 390 µL, sufficient for seven time points, combine the following
   a. 282 µL of 18.2 mΩ of water.
   b. 80 µL of 0.5 M potassium phosphate buffer (p^H 7.4)
   c. 20 µL of NADPH A. (Corning life sciences, Cat # 451220)
   d. 4 µL of NADPH B. (Corning life sciences, Cat # 451200)
   e. 4 µL of test compound.
3. Sonicate MAM for 5 min and meanwhile thaw microsomes (20 mg/mL) (BD Gentest, Cat # 452156) on ice.
4. Aliquot 100 µL of ice cold ISTD into seven separate 1.5 mL conical vials and label them the time points for 0, 10, 20, 30, 40, 50, and 60 min.
5. Arrange the timer. Microsomes (Final concentration of 0.5 mg/mL) should be added to all time points except the zero time point.
6. Add 50 µL of the MAM solution to the conical vial labelled as zero time point. Place the remaining MAM solution in the incubator (37 ºC) for 5 min and initiate the reaction with addition of microsomes (8.8 µL) and record the time.
7. At the end of each time interval remove 50 µL and add to 100 µL ISTD in conical vial, sonicate for 10 sec and spin down at 10,000 rpm for 5 minutes.
8. Take 100 µL of supernatant and transfer to Spin-X HPLC filter tubes (Corning Incorporated, Cat # 8169) and centrifuge at 13,000 rpm for 5 minutes and take 5 µL from this solution and dilute in 495 µL of LCMS grade methanol (Fischer scientific, CAS # 67-56-1) in an 2mL glass auto sampler vial (Microsolv, Cat # 95025-WCV)
9. The samples are analyzed by LCMS-8040. (Shimadzu)

Data:

Day 1:

Time (min)	Assay 1		Assay 2		Assay 3		% remaining		
	DK-I-58-1 Peak area	ISTD Peak area	DK-I-58-1 Peak area	ISTD Peak area	DK-I-58-1 Peak area	ISTD Peak area	Assay 1	Assay 2	Assay 3
0	52579	105204	49506	99051	48659	98086	99.95	99.96	100.01
10	45825	93541	44451	93116	48471	98801	97.97	95.47	98.91
20	43583	94565	43623	95700	46503	99016	92.17	91.16	94.68
30	42546	96285	40594	92790	42711	96764	88.37	87.49	88.99
40	40999	96785	41454	96231	41457	96490	84.72	86.15	86.62
50	37334	91894	39270	94259	40259	95854	81.25	83.32	84.67
60	39122	95274	39560	97477	37942	93234	82.12	81.16	82.04

Table 1: Peak areas and % remaining values

Day 2:

Time (min)	Assay 1		Assay 2		Assay 3		(% remaining)		
	DK-I-58-1 Peak area	ISTD Peak area	DK-I-58-1 Peak area	ISTD Peak area	DK-I-58-1 Peak area	ISTD Peak area	Assay 1	Assay 2	Assay 3
0	49813	99775	51634	107495	53015	106527	100.05	100.07	99.93
10	48894	100371	46330	100245	51318	103178	97.62	96.28	99.87
20	46014	97980	45490	99937	46137	100422	94.11	94.83	92.25
30	45730	101697	42043	99140	44245	99348	90.11	88.34	89.42
40	42831	97947	40003	95150	41764	97359	87.63	87.58	86.13
50	41858	98511	44806	109872	42381	101831	85.15	84.95	83.57
60	43517	106102	40987	101673	42905	101517	82.19	83.98	84.86

Table 2: Peak areas and % remaining values

Calculation:

From the peak area, Calculate the following

$$\text{Peak area ratio} = \frac{\text{Peak area of test compound (DK-I-58-1)}}{\text{Peak area of internal standard (Verapamil)}}$$

$$\text{\% remaining at time T} = \frac{\text{Peak area ratio at particular time T}}{\text{Peak area ratio at zero time point}} * 100$$

(T = 0, 10, 20,30,40,50 and 60)

DATA ANALYSIS:

Day 1

Linear regression analysis:

Slope: -0.003567 ± 0.0001743

At X= 60, Y = 4.389 ± 0.006286

R^2 = 0.9566

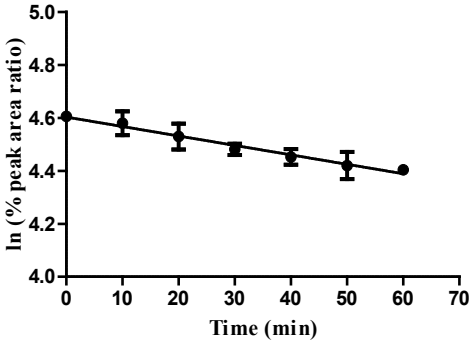

Metabolic Parameters:

Half-life: 194.28 ± 9.48 min

V_d: 100 µL/mg

Intrinsic clearance: 0.3567 µL/min/mg

Metabolic Rate: 7.134 nmol/min/mg

% remaining at 60 min: 80.55 ± 0.11 %

Day 2

Linear regression analysis:

Slope: -0.003224 ± 0.0001677

At X = 60, Y = 4.411 ± 0.006045

R^2 = 0.9511

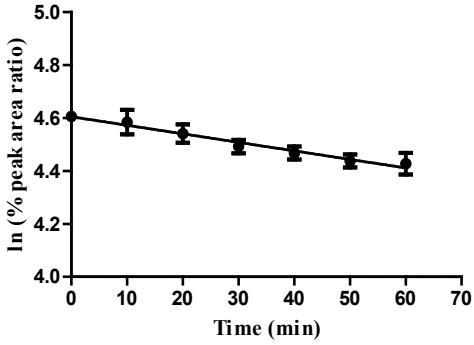

Metabolic Parameters:

Half-life: 214.95 ± 11.18 min

V_d: 100 µL/mg

Intrinsic clearance: 0.3224 µL/min/mg

Metabolic Rate: 6.448 nmol/min/mg

% remaining at 60 min: 82.35 ± 0.11 %

Note: The peak area ratios and natural log values are calculated using Microsoft excel 2010 and linear regression analysis is calculated using GraphPad prism.

Mouse Liver Microsomal Assay

Principal Investigator: Dr. Alexander Arnold
Operator: Revathi Kodali
Test Compound: **8o**
Concentration: 10 µM
Date: 05-05-2016
Facility: Milwaukee Institute for Drug Discovery

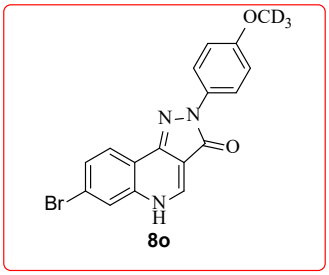

8o

Assay Protocol

Each evaluation included six independent assays carried out three at a time, on two different days

1. Preparation of solutions:
   a. 1 mM test compound in DMSO.
   b. 0.5 µM 4,5 Diphenyl Imidazole in ice cold Acetonitrile (ISTD).
2. For a total volume of Microsomal Assay Mixture (MAM) 390 µL, sufficient for seven time points, combine the following
   a. 282 µL of 18.2 mΩ of water.
   b. 80 µL of 0.5 M potassium phosphate buffer (p^H 7.4)
   c. 20 µL of NADPH A. (Corning life sciences, Cat # 451220)
   d. 4 µL of NADPH B. (Corning life sciences, Cat # 451200)
   e. 4 µL of test compound.
3. Sonicate MAM for 5 min and meanwhile thaw microsomes (20 mg/mL) (BD Gentest, Cat # 452156) on ice.
4. Aliquot 100 µL of ice cold ISTD into seven separate 1.5 mL conical vials and label them the time points for 0, 10, 20, 30, 40, 50, and 60 min.
5. Arrange the timer. Microsomes (Final concentration of 0.5 mg/mL) should be added to all time points except the zero time point.
6. Add 50 µL of the MAM solution to the conical vial labelled as zero time point. Place the remaining MAM solution in the incubator (37 ºC) for 5 min and initiate the reaction with addition of microsomes (8.8 µL) and record the time.
7. At the end of each time interval remove 50 µL and add to 100 µL ISTD in conical vial, sonicate for 10 sec and spin down at 10,000 rpm for 5 minutes.
8. Take 100 µL of supernatant and transfer to Spin-X HPLC filter tubes (Corning Incorporated, Cat # 8169) and centrifuge at 13,000 rpm for 5 minutes and take 5 µL from this solution and dilute in 495 µL of LCMS grade methanol (Fischer scientific, CAS # 67-56-1) in an 2mL glass auto sampler vial (Microsolv, Cat # 95025-WCV)
9. The samples are analyzed by LCMS-8040. (Shimadzu)

Data:

Day 1:

Time (min)	Assay 1		Assay 2		Assay 3		% remaining		
	DK-I-58-1 Peak area	ISTD Peak area	DK-I-58-1 Peak area	ISTD Peak area	DK-I-58-1 Peak area	ISTD Peak area	Assay 1	Assay 2	Assay 3
0	45407	99025	45778	109217	48351	111002	99.90	100.03	99.90
10	39689	88172	39750	98111	47817	112502	98.06	96.69	97.48
20	38346	95002	36676	101161	40927	111059	87.93	86.5	84.52
30	36091	94410	37944	107423	36126	98426	83.28	84.30	84.18
40	38332	101105	37964	110739	40143	115678	82.59	81.82	79.59
50	37879	103619	29626	91731	30557	93383	79.64	77.08	75.05
60	35899	101755	28546	92601	31989	100220	76.86	73.57	73.20

Table 1: Peak areas and % remaining values

Day 2:

Time (min)	Assay 1		Assay 2		Assay 3		(% remaining)		
	DK-I-58-1 Peak area	ISTD Peak area	DK-I-58-1 Peak area	ISTD Peak area	DK-I-58-1 Peak area	ISTD Peak area	Assay 1	Assay 2	Assay 3
0	47531	108669	49814	114293	53117	126614	100.09	99.96	99.88
10	41907	100372	46729	109931	47056	115838	95.54	97.49	96.72
20	39682	102754	44889	113608	43666	116211	88.37	90.62	89.46
30	36906	100187	42827	112938	41706	120148	84.29	86.97	82.64
40	32951	94121	40182	112083	36083	105504	80.11	82.22	81.43
50	32511	95049	36769	103352	35590	109154	78.27	81.59	77.63
60	31896	99642	34866	105232	34822	111570	73.25	75.99	74.31

Table 2: Peak areas and % remaining values

Calculation:

From the peak area, Calculate the following

$$\text{Peak area ratio} = \frac{\text{Peak area of test compound (DK-I-58-1)}}{\text{Peak area of internal standard (Verapamil)}}$$

$$\text{\% remaining at time T} = \frac{\text{Peak area ratio at particular time T}}{\text{Peak area ratio at zero time point}} * 100$$

(T = 0, 10, 20,30,40,50 and 60)

DATA ANALYSIS:

Day 1

Linear regression analysis:

Slope: -0.005018 ± 0.0003001

At X= 60, Y = 4.296 ± 0.01082

R^2 = 0.9364

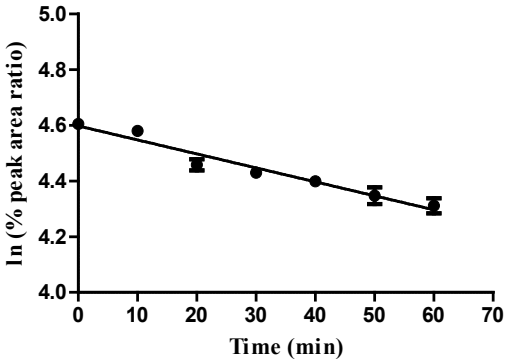

Day 2

Linear regression analysis:

Slope: -0.004920 ± 0.0002135

At X = 60, Y = 4.308 ± 0.007697

R^2 = 0.9511

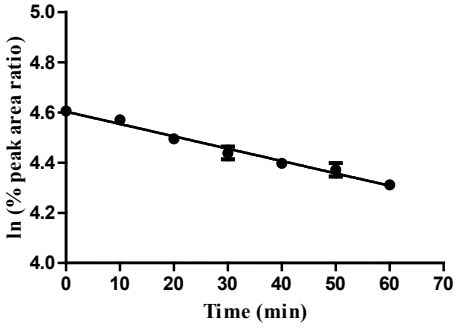

Metabolic Parameters:

Half-life: 138.10 ± 8.25 min

V_d: 100 µL/mg

Intrinsic clearance: 0.5018 µL/min/mg

Metabolic Rate: 10.036 nmol/min/mg

% remaining at 60 min: 73.40 ± 0.18 %

Metabolic Parameters:

Half-life: 140.85 ± 6.11 min

V_d: 100 µL/mg

Intrinsic clearance: 0.492 µL/min/mg

Metabolic Rate: 9.84 nmol/min/mg

% remaining at 60 min: 74.29 ± 0.13 %

Note: The peak area ratios and natural log values are calculated using Microsoft excel 2010 and linear regression analysis is calculated using GraphPad prism.

Human Liver Microsomal Assay

Principal Investigator: Dr. Alexander Arnold
Operator: Revathi Kodali
Test Compound: **8p**
Concentration: 10 µM
Date: 02-28-2017
Facility: Milwaukee Institute for Drug Discovery

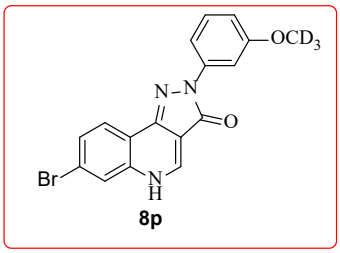

8p

Assay Protocol

Each evaluation included six independent assays carried out three at a time, on two different days

1. Preparation of solutions:
   a. 1 mM test compound in DMSO.
   b. 3 µM Verapamil in ice cold Acetonitrile (ISTD).
2. For a total volume of Microsomal Assay Mixture (MAM) 390 µL, sufficient for seven time points, combine the following
   a. 282 µL of 18.2 mΩ of water.
   b. 80 µL of 0.5 M potassium phosphate buffer (p^H 7.4)
   c. 20 µL of NADPH A. (Corning life sciences, Cat # 451220)
   d. 4 µL of NADPH B. (Corning life sciences, Cat # 451200)
   e. 4 µL of test compound.
3. Sonicate MAM for 5 min and meanwhile thaw microsomes (20 mg/mL) (BD Gentest, Cat # 452156) on ice.
4. Aliquot 100 µL of ice cold ISTD into seven separate 1.5 mL conical vials and label them the time points for 0, 10, 20, 30, 40, 50, and 60 min.
5. Arrange the timer. Microsomes (Final concentration of 0.5 mg/mL) should be added to all time points except the zero time point.
6. Add 50 µL of the MAM solution to the conical vial labelled as zero time point. Place the remaining MAM solution in the incubator (37 ºC) for 5 min and initiate the reaction with addition of microsomes (8.8 µL) and record the time.
7. At the end of each time interval remove 50 µL and add to 100 µL ISTD in conical vial, sonicate for 10 sec and spin down at 10,000 rpm for 5 minutes.
8. Take 100 µL of supernatant and transfer to Spin-X HPLC filter tubes (Corning Incorporated, Cat # 8169) and centrifuge at 13,000 rpm for 5 minutes and take 5 µL from this solution and dilute in 495 µL of LCMS grade methanol (Fischer scientific, CAS # 67-56-1) in an 2mL glass auto sampler vial (Microsolv, Cat # 95025-WCV)
9. The samples are analyzed by LCMS-8040. (Shimadzu)

Data:

Day 1:

Time (min)	Assay 1		Assay 2		Assay 3		% remaining		
	DK-I-92-1 Peak area	Verapamil Peak area	DK-I-92-1 Peak area	Verapamil Peak area	DK-I-92-1 Peak area	Verapamil Peak area	Assay 1	Assay 2	Assay 3
0	59983	321908	58272	320874	62965	326832	100.18	99.78	99.82
10	50570	320891	51796	331636	59165	330127	84.72	85.81	92.86
20	48532	331288	48615	332097	50049	327548	78.76	80.43	79.17
30	45866	320891	42178	326711	45910	327644	76.84	70.93	72.60
40	42711	331008	40045	323974	41991	330194	69.37	67.91	65.89
50	39783	322898	43199	326744	43192	327634	66.24	72.64	68.30
60	40250	321356	41123	330100	45947	331073	67.33	68.44	71.90

Table 1: Peak areas and % remaining values

Day 2:

Time (min)	Assay 1		Assay 2		Assay 3		(% remaining)		
	DK-I-92-1 Peak area	Verapamil Peak area	DK-I-92-1 Peak area	Verapamil Peak area	DK-I-92-1 Peak area	Verapamil Peak area	Assay 1	Assay 2	Assay 3
0	58466	325834	57839	331063	61445	328646	100.24	99.83	99.98
10	52258	327543	50774	327534	52235	327167	89.13	88.58	85.37
20	43637	300183	44263	327846	46981	326348	81.21	77.14	76.98
30	44482	328643	41357	324543	43352	320087	75.61	72.81	72.42
40	41402	325673	39919	329634	40509	326849	71.02	69.20	66.27
50	39693	328964	40765	331208	41609	326183	67.40	70.33	68.21
60	39214	330132	39549	330974	42418	323491	66.35	68.28	70.12

Table 2: Peak areas and % remaining values

Calculation:

From the peak area, Calculate the following

$$\text{Peak area ratio} = \frac{\text{Peak area of test compound (DK-I-92-1)}}{\text{Peak area of internal standard (Verapamil)}}$$

$$\text{\% remaining at time T} = \frac{\text{Peak area ratio at particular time T}}{\text{Peak area ratio at zero time point}} * 100$$

(T = 0, 10, 20,30,40,50 and 60)

DATA ANALYSIS:

Day 1

Linear regression analysis:

Slope: -0.006219 ± 0.0006880

At X= 60, Y = 4.161 ± 0.02481

R^2 = 0.8114

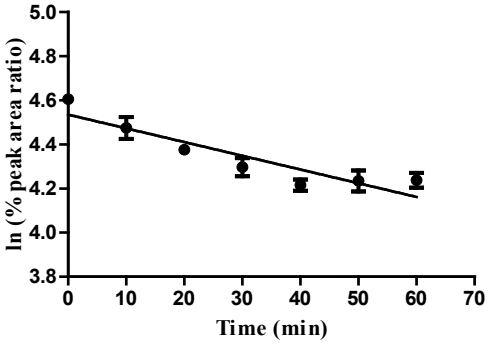

Metabolic Parameters:

Half-life: 111 ± 12 min

V_d: 100 µL/mg

Intrinsic clearance: 0.6219 µL/min/mg

Metabolic Rate: 12.43 nmol/min/mg

% remaining at 60 min: 64 ± 0.32 %

Day 2

Linear regression analysis:

Slope: -0.006312 ± 0.0006039

At X = 60, Y = 4.157 ± 0.02178

R^2 = 0.8518

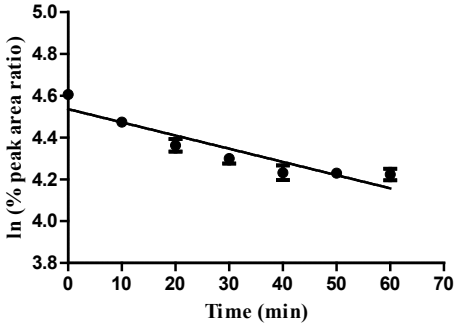

Metabolic Parameters:

Half-life: 109 ± 10 min

V_d: 100 µL/mg

Intrinsic clearance: 0.6312 µL/min/mg

Metabolic Rate: 12.624 nmol/min/mg

% remaining at 60 min: 63 ± 0.33 %

Note: The peak area ratios and natural log values are calculated using Microsoft excel 2010 and linear regression analysis is calculated using GraphPad prism.

Mouse Liver Microsomal Assay

Principal Investigator: Dr. Alexander Arnold
Operator: Revathi Kodali
Test Compound: **8p**
Concentration: 10 µM
Date: 02-28-2017
Facility: Milwaukee Institute for Drug Discovery

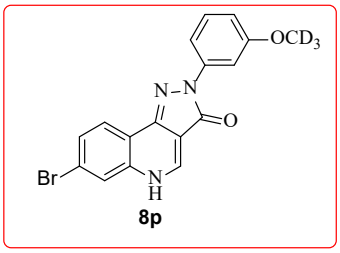

8p

Assay Protocol

Each evaluation included six independent assays carried out three at a time, on two different days

1. Preparation of solutions:
   a. 1 mM test compound in DMSO.
   b. 3 µM Verapamil in ice cold Acetonitrile (ISTD).
2. For a total volume of Microsomal Assay Mixture (MAM) 390 µL, sufficient for seven time points, combine the following
   a. 282 µL of 18.2 mΩ of water.
   b. 80 µL of 0.5 M potassium phosphate buffer (p^H 7.4)
   c. 20 µL of NADPH A. (Corning life sciences, Cat # 451220)
   d. 4 µL of NADPH B. (Corning life sciences, Cat # 451200)
   e. 4 µL of test compound.
3. Sonicate MAM for 5 min and meanwhile thaw microsomes (20 mg/mL) (Life technologies, Cat # MSMC-PL) on ice.
4. Aliquot 100 µL of ice cold ISTD into seven separate 1.5 mL conical vials and label them the time points for 0, 10, 20, 30, 40, 50, and 60 min.
5. Arrange the timer. Microsomes (Final concentration of 0.5 mg/mL) should be added to all time points except the zero time point.
6. Add 50 µL of the MAM solution to the conical vial labelled as zero time point. Place the remaining MAM solution in the incubator (37 ºC) for 5 min and initiate the reaction with addition of microsomes (8.8 µL) and record the time.
7. At the end of each time interval remove 50 µL and add to 100 µL ISTD in conical vial, sonicate for 10 sec and spin down at 10,000 rpm for 5 minutes.
8. Take 100 µL of supernatant and transfer to Spin-X HPLC filter tubes (Corning Incorporated, Cat # 8169) and centrifuge at 13,000 rpm for 5 minutes and take 5 µL from this solution and dilute in 495 µL of LCMS grade methanol (Fischer scientific, CAS # 67-56-1) in an 2mL glass auto sampler vial (Microsolv, Cat # 95025-WCV)
9. The samples are analyzed by LCMS-8040. (Shimadzu)

Data:

Day 1:

Time (min)	Assay 1		Assay 2		Assay 3		% remaining		
	DK-I-92-1 Peak area	Verapamil Peak area	DK-I-92-1 Peak area	Verapamil Peak area	DK-I-92-1 Peak area	Verapamil Peak area	Assay 1	Assay 2	Assay 3
0	56473	328643	54532	330183	56831	328124	99.90	100.09	100.11
10	52879	326447	52410	328634	53076	320843	94.17	96.65	95.62
20	49695	325843	49012	327634	49066	327843	88.67	90.66	86.51
30	49248	328643	47078	328634	46463	327563	87.12	86.82	81.99
40	47758	325766	44351	324451	44309	325684	85.23	82.84	78.64
50	46538	329766	42829	319874	46234	330198	82.04	81.14	80.93
60	43351	300784	44611	320073	46103	321843	83.79	84.47	82.80

Table 1: Peak areas and % remaining values

Day 2:

Time (min)	Assay 1		Assay 2		Assay 3		(% remaining)		
	DK-I-92-1 Peak area	Verapamil Peak area	DK-I-92-1 Peak area	Verapamil Peak area	DK-I-92-1 Peak area	Verapamil Peak area	Assay 1	Assay 2	Assay 3
0	64419	324783	61391	326673	62173	327893	100.17	99.96	99.79
10	63199	327912	58288	327684	58681	326874	97.33	94.61	94.48
20	58267	331287	52796	326943	54301	328743	88.82	85.89	86.93
30	55696	327564	50682	331084	52864	325873	85.87	81.42	85.38
40	52483	328634	51361	327439	51100	328964	80.65	83.43	81.75
50	53109	320734	52568	323289	52717	330023	83.62	86.49	84.07
60	54167	331674	51031	334087	52001	326484	82.48	81.24	83.82

Table 2: Peak areas and % remaining values

Calculation:

From the peak area, Calculate the following

$$\text{Peak area ratio} = \frac{\text{Peak area of test compound (DK-I-92-1)}}{\text{Peak area of internal standard (Verapamil)}}$$

$$\text{\% remaining at time T} = \frac{\text{Peak area ratio at particular time T}}{\text{Peak area ratio at zero time point}} * 100$$

(T = 0, 10, 20,30,40,50 and 60)

DATA ANALYSIS:

Day 1

Linear regression analysis:

Slope: -0.003323 ± 0.0004092

At X= 60, Y = 4.376 ± 0.01475

R^2 = 0.7763

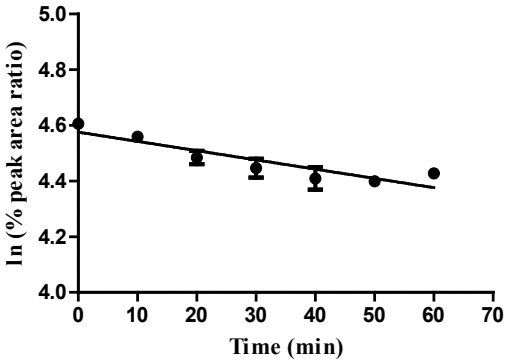

Metabolic Parameters:

Half-life: 208 ± 25 min

V_d: 100 µL/mg

Intrinsic clearance: 0.3323 µL/min/mg

Metabolic Rate: 6.646 nmol/min/mg

% remaining at 60 min: 79 ± 0.26 %

Day 2

Linear regression analysis:

Slope: -0.003129 ± 0.0004255

At X = 60, Y = 4.381 ± 0.01534

R^2 = 0.7399

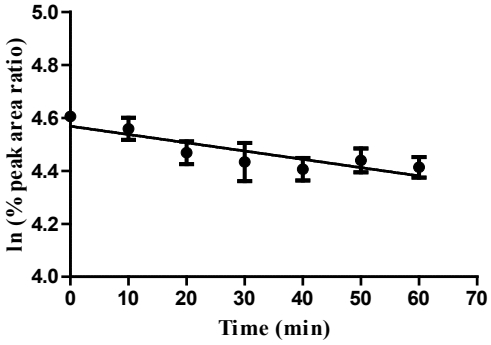

Metabolic Parameters:

Half-life: 221 ± 30 min

V_d: 100 µL/mg

Intrinsic clearance: 0.3129 µL/min/mg

Metabolic Rate: 6.258 nmol/min/mg

% remaining at 60 min: 80 ± 0.30 %

Note: The peak area ratios and natural log values are calculated using Microsoft excel 2010 and linear regression analysis is calculated using GraphPad prism.

Human Liver Microsomal Assay

Principal Investigator: Dr. Alexander Arnold
Operator: Revathi Kodali
Test Compound: **8q**
Concentration: 10 µM
Date: 08-15-2016
Facility: Milwaukee Institute for Drug Discovery

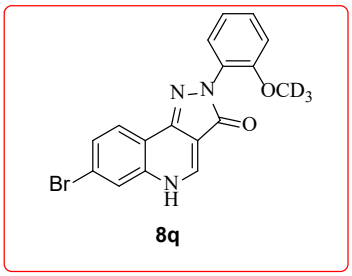

8q

Assay Protocol

Each evaluation included six independent assays carried out three at a time, on two different days

1. Preparation of solutions:
   a. 1 mM test compound in DMSO.
   b. 1 µM 4,5 Di Phenyl Imidazole in ice cold Acetonitrile (ISTD).
2. For a total volume of Microsomal Assay Mixture (MAM) 390 µL, sufficient for seven time points, combine the following
   a. 282 µL of 18.2 mΩ of water.
   b. 80 µL of 0.5 M potassium phosphate buffer (p^H 7.4)
   c. 20 µL of NADPH A. (Corning life sciences, Cat # 451220)
   d. 4 µL of NADPH B. (Corning life sciences, Cat # 451200)
   e. 4 µL of test compound.
3. Sonicate MAM for 5 min and meanwhile thaw microsomes (20 mg/mL) (BD Biosciences, Cat # 452156) on ice.
4. Aliquot 100 µL of ice cold ISTD into seven separate 1.5 mL conical vials and label them the time points for 0, 10, 20, 30, 40, 50, and 60 min.
5. Arrange the timer. Microsomes (Final concentration of 0.5 mg/mL) should be added to all time points except the zero time point.
6. Add 50 µL of the MAM solution to the conical vial labelled as zero time point. Place the remaining MAM solution in the incubator (37 ºC) for 5 min and initiate the reaction with addition of microsomes (8.8 µL) and record the time.
7. At the end of each time interval remove 50 µL and add to 100 µL ISTD in conical vial, sonicate for 10 sec and spin down at 10,000 rpm for 5 minutes.
8. Take 100 µL of supernatant and transfer to Spin-X HPLC filter tubes (Corning Incorporated, Cat # 8169) and centrifuge at 13,000 rpm for 5 minutes and take 5 µL from this solution and dilute in 495 µL of LCMS grade methanol (Fischer scientific, CAS # 67-56-1) in an 2mL glass auto sampler vial (Microsolv, Cat # 95025-WCV)
9. The samples are analyzed by LCMS-8040. (Shimadzu)

Data:

Day 1:

Time (min)	Assay 1		Assay 2		Assay 3		% remaining		
	DK-I-89-1 Peak area	ISTD Peak area	DK-I-89-1 Peak area	ISTD Peak area	DK-I-89-1 Peak area	ISTD Peak area	Assay 1	Assay 2	Assay 3
0	565063	1986723	588540	1967352	555706	1976123	100.14	100.05	100.07
10	543616	1967237	563545	1967235	547671	1976236	97.30	95.80	98.62
20	526501	1967236	539026	1896235	516591	1897823	94.23	95.07	96.86
30	504039	1967236	545481	2000823	500945	1897236	90.21	91.18	93.96
40	522804	1963562	562762	1987328	511914	1967263	93.75	94.70	92.60
50	525487	2000732	541596	1966237	524543	1987623	92.48	92.12	93.91
60	529045	1967235	542507	1956253	527483	1965232	94.69	92.74	95.51

Table 1: Peak areas and % remaining values

Day 2:

Time (min)	Assay 1		Assay 2		Assay 3		(% remaining)		
	DK-I-89-1 Peak area	ISTD Peak area	DK-I-89-1 Peak area	ISTD Peak area	DK-I-89-1 Peak area	ISTD Peak area	Assay 1	Assay 2	Assay 3
0	542091	2008782	528526	1962632	563729	1989123	99.94	100.10	100.14
10	497942	1899972	498199	1967236	535488	2000126	97.06	94.14	94.60
20	508446	1972628	496390	1978236	528768	1988367	95.46	93.28	93.96
30	507591	1988316	500842	1956625	538342	1976213	94.55	95.15	96.25
40	511063	1987236	509942	1972637	515849	1963256	95.24	96.10	92.84
50	497689	1967262	497074	1976236	545138	2008362	93.69	93.50	95.91
60	506687	1972367	508595	1978236	516138	1967235	95.14	95.57	92.70

Table 2: Peak areas and % remaining values

Calculation:

From the peak area, Calculate the following

$$\text{Peak area ratio} = \frac{\text{Peak area of test compound (DK-I-89-1)}}{\text{Peak area of internal standard (ISTD)}}$$

$$\text{\% remaining at time T} = \frac{\text{Peak area ratio at particular time T}}{\text{Peak area ratio at zero time point}} * 100$$

(T = 0, 10, 20,30,40,50 and 60)

DATA ANALYSIS:

Day 1

Linear regression analysis:

Slope: -0.001035 ± 0.0002435

At X= 60, Y = 4.523 ± 0.0008781

R^2 = 0.4871

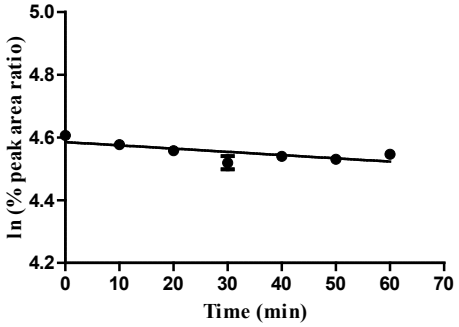

Metabolic Parameters:

Half-life: 669.5652 ± 157.52 min

V_d: 100 µL/mg

Intrinsic clearance: 0.1035 µL/min/mg

Metabolic Rate: 2.07 nmol/min/mg

% remaining at 60 min: 92.11 ± 0.17 %

Day 2

Linear regression analysis:

Slope: -0.0006738 ± 0.0002075

At X = 60, Y = 4.539 ± 0.007480

R^2 = 0.3570

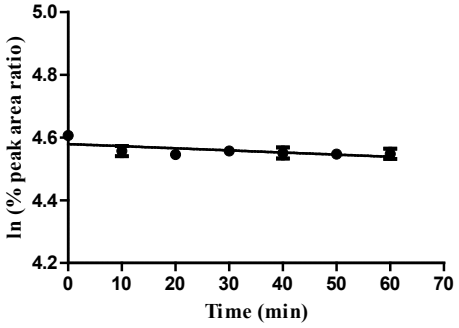

Metabolic Parameters:

Half-life: 1028.95 ± 316.72 min

V_d: 100 µL/mg

Intrinsic clearance: 0.06738 µL/min/mg

Metabolic Rate: 1.3476 nmol/min/mg

% remaining at 60 min: 93.59 ± 0.15 %

Note: The peak area ratios and natural log values are calculated using Microsoft excel 2010 and linear regression analysis is calculated using GraphPad prism.

Mouse Liver Microsomal Assay

Principal Investigator: Dr. Alexander Arnold
Operator: Revathi Kodali
Test Compound: **8q**
Concentration: 10 µM
Date: 08-15-2016
Facility: Milwaukee Institute for Drug Discovery

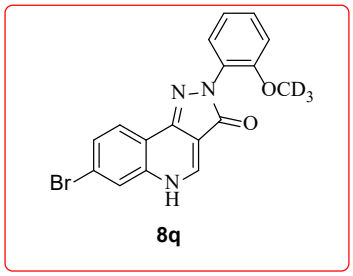

8q

Assay Protocol

Each evaluation included six independent assays carried out three at a time, on two different days

1. Preparation of solutions:
   a. 1 mM test compound in DMSO.
   b. 1 µM 4,5 Di Phenyl Imidazole in ice cold Acetonitrile (ISTD).
2. For a total volume of Microsomal Assay Mixture (MAM) 390 µL, sufficient for seven time points, combine the following
   a. 282 µL of 18.2 mΩ of water.
   b. 80 µL of 0.5 M potassium phosphate buffer (p^H 7.4)
   c. 20 µL of NADPH A. (Corning life sciences, Cat # 451220)
   d. 4 µL of NADPH B. (Corning life sciences, Cat # 451200)
   e. 4 µL of test compound.
3. Sonicate MAM for 5 min and meanwhile thaw microsomes (20 mg/mL) (Life technologies, Cat # MSMC-PL) on ice.
4. Aliquot 100 µL of ice cold ISTD into seven separate 1.5 mL conical vials and label them the time points for 0, 10, 20, 30, 40, 50, and 60 min.
5. Arrange the timer. Microsomes (Final concentration of 0.5 mg/mL) should be added to all time points except the zero time point.
6. Add 50 µL of the MAM solution to the conical vial labelled as zero time point. Place the remaining MAM solution in the incubator (37 ºC) for 5 min and initiate the reaction with addition of microsomes (8.8 µL) and record the time.
7. At the end of each time interval remove 50 µL and add to 100 µL ISTD in conical vial, sonicate for 10 sec and spin down at 10,000 rpm for 5 minutes.
8. Take 100 µL of supernatant and transfer to Spin-X HPLC filter tubes (Corning Incorporated, Cat # 8169) and centrifuge at 13,000 rpm for 5 minutes and take 5 µL from this solution and dilute in 495 µL of LCMS grade methanol (Fischer scientific, CAS # 67-56-1) in an 2mL glass auto sampler vial (Microsolv, Cat # 95025-WCV)
9. The samples are analyzed by LCMS-8040. (Shimadzu)

Data:

Day 1:

Time (min)	Assay 1		Assay 2		Assay 3		% remaining		
	DK-I-89-1 Peak area	ISTD Peak area	DK-I-89-1 Peak area	ISTD Peak area	DK-I-89-1 Peak area	ISTD Peak area	Assay 1	Assay 2	Assay 3
0	576315	1967238	541302	1967322	566955	1967623	99.98	100.05	100.04
10	512948	1967625	464987	2007882	498225	1976723	88.97	84.21	87.51
20	451074	1956523	459273	1976235	481299	1897262	78.68	84.50	88.08
30	440035	2008287	424206	1965232	425241	1976232	74.78	78.49	74.71
40	413011	1942356	407167	1962362	401432	1987233	72.57	75.45	70.14
50	395228	1976233	356213	1976232	384691	1999733	68.25	65.54	66.79
60	366164	1972362	333006	1965253	347012	1978273	63.36	61.61	60.90

Table 1: Peak areas and % remaining values

Day 2:

Time (min)	Assay 1		Assay 2		Assay 3		(% remaining)		
	DK-I-89-1 Peak area	ISTD Peak area	DK-I-89-1 Peak area	ISTD Peak area	DK-I-89-1 Peak area	ISTD Peak area	Assay 1	Assay 2	Assay 3
0	549917	1976232	529475	1967253	575556	1976253	100.09	100.05	100.08
10	496314	1967232	459274	1956232	489236	1976232	90.75	87.27	85.07
20	458183	1972632	407367	1923762	459517	2000872	83.55	78.71	78.92
30	432253	1977623	391427	1952352	414530	1998762	78.62	74.53	71.26
40	395301	1955235	363066	2008273	416702	1962352	72.72	67.20	72.97
50	350019	1956232	359469	2000072	369384	1962533	64.36	66.81	64.68
60	338001	1997232	334995	1976232	363915	1976318	60.87	63.01	63.27

Table 2: Peak areas and % remaining values

Calculation:

From the peak area, Calculate the following

$$\text{Peak area ratio} = \frac{\text{Peak area of test compound (DK-I-89-1)}}{\text{Peak area of internal standard (ISTD)}}$$

$$\text{\% remaining at time T} = \frac{\text{Peak area ratio at particular time T}}{\text{Peak area ratio at zero time point}} * 100$$

(T = 0, 10, 20,30,40,50 and 60)

DATA ANALYSIS:

Day 1

Linear regression analysis:

Slope: -0.007506 ± 0.0003722

At X= 60, Y = 4.124 ± 0.01342

R^2 = 0.9554

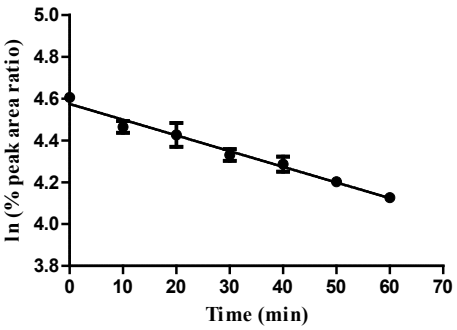

Metabolic Parameters:

Half-life: 93.32 ± 4.577 min

V_d: 100 µL/mg

Intrinsic clearance: 0.7506 µL/min/mg

Metabolic Rate: 15.012 nmol/min/mg

% remaining at 60 min: 61.80 ± 0.2%

Day 2

Linear regression analysis:

Slope: -0.000738 ± 0.0002075

At X = 60, Y = 4.539 ± 0.007480

R^2 = 0.9480

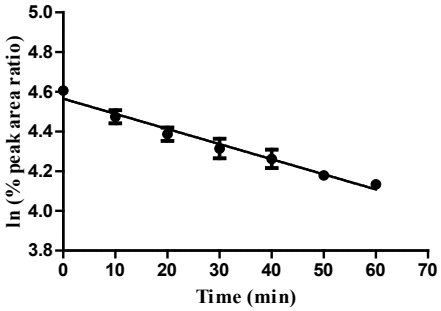

Metabolic Parameters:

Half-life: 91.01 ± 4.89 min

V_d: 100 µL/mg

Intrinsic clearance: 0.7614 µL/min/mg

Metabolic Rate: 15.228 nmol/min/mg

% remaining at 60 min: 60.82 ± 0.21 %

Note: The peak area ratios and natural log values are calculated using Microsoft excel 2010 and linear regression analysis is calculated using GraphPad prism.

Human Liver Microsomal Assay

Principal Investigator: Dr. Alexander Arnold
Operator: Revathi Kodali
Test Compound: **13a**
Concentration: 10 µM
Date: 04-04-2016
Facility: Milwaukee Institute for Drug Discovery

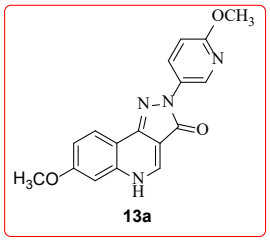

13a

Assay Protocol

Each evaluation included six independent assays carried out three at a time, on two different days

1. Preparation of solutions:
   a. 1 mM test compound in DMSO.
   b. 2 µM Verapamil in ice cold Acetonitrile (ISTD).
2. For a total volume of Microsomal Assay Mixture (MAM) 390 µL, sufficient for seven time points, combine the following
   a. 282 µL of 18.2 mΩ of water.
   b. 80 µL of 0.5 M potassium phosphate buffer (p^H 7.4)
   c. 20 µL of NADPH A. (Corning life sciences, Cat # 451220)
   d. 4 µL of NADPH B. (Corning life sciences, Cat # 451200)
   e. 4 µL of test compound.
3. Sonicate MAM for 5 min and meanwhile thaw microsomes (20 mg/mL) (BD Gentest, Cat # 452156) on ice.
4. Aliquot 100 µL of ice cold ISTD into seven separate 1.5 mL conical vials and label them the time points for 0, 10, 20, 30, 40, 50, and 60 min.
5. Arrange the timer. Microsomes (Final concentration of 0.5 mg/mL) should be added to all time points except the zero time point.
6. Add 50 µL of the MAM solution to the conical vial labelled as zero time point. Place the remaining MAM solution in the incubator (37 ºC) for 5 min and initiate the reaction with addition of microsomes (8.8 µL) and record the time.
7. At the end of each time interval remove 50 µL and add to 100 µL ISTD in conical vial, sonicate for 10 sec and spin down at 10,000 rpm for 5 minutes.
8. Take 100 µL of supernatant and transfer to Spin-X HPLC filter tubes (Corning Incorporated, Cat # 8169) and centrifuge at 13,000 rpm for 5 minutes and take 5 µL from this solution and dilute in 495 µL of LCMS grade methanol (Fischer scientific, CAS # 67-56-1) in an 2mL glass auto sampler vial (Microsolv, Cat # 95025-WCV)
9. The samples are analyzed by LCMS-8040. (Shimadzu)

Data:

Day 1:

Time (min)	Assay 1		Assay 2		Assay 3		% remaining		
	DK-II-13-1 Peak area	Verapamil Peak area	DK-II-13-1 Peak area	Verapamil Peak area	DK-II-13-1 Peak area	Verapamil Peak area	Assay 1	Assay 2	Assay 3
0	1481304	2370706	1498648	2486412	1501602	2348705	99.97	99.95	100.05
10	1456174	2437087	1350839	2314930	1463439	2365630	95.60	96.77	96.81
20	1404302	2411877	1255093	2237002	1456023	2412311	93.15	93.04	94.45
30	1389377	2345148	1412423	2551510	1491949	2508806	94.79	91.80	93.06
40	1388276	2362279	1458393	2570550	1464132	2402739	94.03	94.08	95.36
50	1340079	2326528	1421667	2590384	1449469	2462260	92.16	91.01	92.12
60	1379227	2321871	1490076	2602566	1523329	2540953	95.04	94.94	93.82

Table 1: Peak areas and % remaining values

Day 2:

Time (min)	Assay 1		Assay 2		Assay 3		(% remaining)		
	DK-II-13-1 Peak area	Verapamil Peak area	DK-II-13-1 Peak area	Verapamil Peak area	DK-II-13-1 Peak area	Verapamil Peak area	Assay 1	Assay 2	Assay 3
0	1399330	2454869	1450558	2502725	1427070	2455486	100.00	99.93	100.03
10	1429964	2553664	1368760	2437443	1484773	2607335	98.24	96.82	98.01
20	1446883	2656111	1351638	2507523	1397386	2496606	95.56	92.93	96.33
30	1342793	2516473	1374490	2511492	1343836	2456417	93.61	94.35	94.16
40	1310764	2433525	1364299	2444927	1362123	2463298	94.49	96.20	95.17
50	1364772	2533427	1327910	2440599	1341635	2468061	94.51	93.80	93.56
60	1329779	2421028	1303521	2372689	1356927	2508601	96.36	94.72	93.10

Table 2: Peak areas and % remaining values

Calculation:

From the peak area, Calculate the following

$$\text{Peak area ratio} = \frac{\text{Peak area of test compound (RJ-02-71)}}{\text{Peak area of internal standard (Verapamil)}}$$

$$\text{\% remaining at time T} = \frac{\text{Peak area ratio at particular time T}}{\text{Peak area ratio at zero time point}} * 100$$

(T = 0, 10, 20,30,40,50 and 60)

DATA ANALYSIS:

Day 1

Linear regression analysis:

Slope: -0.0009131 ± 0.0002255

At X= 60, Y = 4.525 ± 0.008131

R^2 = 0.4632

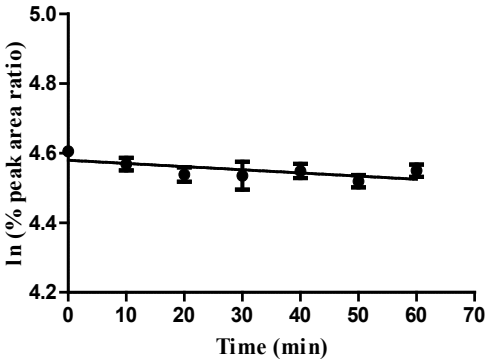

Metabolic Parameters:

Half-life: 759 ± 187.4 min

V_d: 100 µL/mg

Intrinsic clearance: 0.09131 µL/min/mg

Metabolic Rate: 1.8262 nmol/min/mg

% remaining at 60 min: 92.29 ± 0.16 %

Day 2

Linear regression analysis:

Slope: -0.0008369 ± 0.0001796

At X = 60, Y = 4.537 ± 0.006474

R^2 = 0.5334

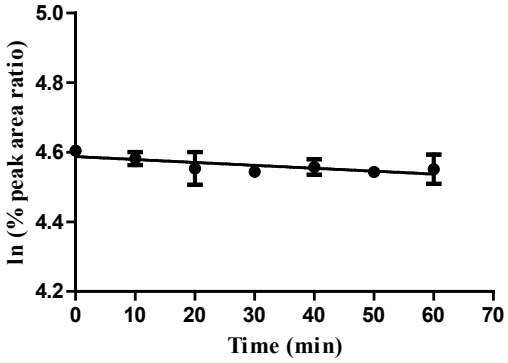

Metabolic Parameters:

Half-life: 828.05 ± 177.7 min

V_d: 100 µL/mg

Intrinsic clearance: 0.08369 µL/min/mg

Metabolic Rate: 1.6738 nmol/min/mg

% remaining at 60 min: 93.41 ± 0.13 %

Note: The peak area ratios and natural log values are calculated using Microsoft excel 2010 and linear regression analysis is calculated using GraphPad prism.

Mouse Liver Microsomal Assay

Principal Investigator: Dr. Alexander Arnold
Operator: Revathi Kodali
Test Compound: **13a**
Concentration: 10 µM
Date: 04-04-2016
Facility: Milwaukee Institute for Drug Discovery

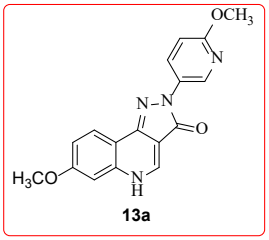

13a

Assay Protocol

Each evaluation included six independent assays carried out three at a time, on two different days

1. Preparation of solutions:
   a. 1 mM test compound in DMSO.
   b. 2 µM Verapamil in ice cold Acetonitrile (ISTD).
2. For a total volume of Microsomal Assay Mixture (MAM) 390 µL, sufficient for seven time points, combine the following
   a. 282 µL of 18.2 mΩ of water.
   b. 80 µL of 0.5 M potassium phosphate buffer (p^H 7.4)
   c. 20 µL of NADPH A. (Corning life sciences, Cat # 451220)
   d. 4 µL of NADPH B. (Corning life sciences, Cat # 451200)
   e. 4 µL of test compound.
3. Sonicate MAM for 5 min and meanwhile thaw microsomes (20 mg/mL) (Life technologies, Cat # MSMC-PL) on ice.
4. Aliquot 100 µL of ice cold ISTD into seven separate 1.5 mL conical vials and label them the time points for 0, 10, 20, 30, 40, 50, and 60 min.
5. Arrange the timer. Microsomes (Final concentration of 0.5 mg/mL) should be added to all time points except the zero time point.
6. Add 50 µL of the MAM solution to the conical vial labelled as zero time point. Place the remaining MAM solution in the incubator (37 ºC) for 5 min and initiate the reaction with addition of microsomes (8.8 µL) and record the time.
7. At the end of each time interval remove 50 µL and add to 100 µL ISTD in conical vial, sonicate for 10 sec and spin down at 10,000 rpm for 5 minutes.
8. Take 100 µL of supernatant and transfer to Spin-X HPLC filter tubes (Corning Incorporated, Cat # 8169) and centrifuge at 13,000 rpm for 5 minutes and take 5 µL from this solution and dilute in 495 µL of LCMS grade methanol (Fischer scientific, CAS # 67-56-1) in an 2mL glass auto sampler vial (Microsolv, Cat # 95025-WCV)
9. The samples are analyzed by LCMS-8040. (Shimadzu)

Data:

Day 1:

Time (min)	Assay 1		Assay 2		Assay 3		% remaining		
	DK-II-13-1 Peak area	Verapamil Peak area	DK-II-13-1 Peak area	Verapamil Peak area	DK-II-13-1 Peak area	Verapamil Peak area	Assay 1	Assay 2	Assay 3
0	1304666	2507698	1412769	2632218	1438349	2617074	100.05	99.94	99.92
10	1342708	2677526	1390974	2638315	1388751	2572011	96.43	98.17	98.17
20	1273565	2705299	1352636	2882276	1344844	2631217	90.53	87.39	92.92
30	1164418	2621865	1218984	2675396	1302788	2728394	85.40	84.84	86.81
40	1152356	2747913	1225500	2827323	1155798	2510036	80.64	80.71	83.72
50	1097786	2651478	1185584	2809151	1084204	2519895	79.62	78.59	78.22
60	1059723	2683246	1109773	2833889	1065161	2636280	75.95	72.92	73.46

Table 1: Peak areas and % remaining values

Day 2:

Time (min)	Assay 1		Assay 2		Assay 3		(% remaining)		
	DK-II-13-1 Peak area	Verapamil Peak area	DK-II-13-1 Peak area	Verapamil Peak area	DK-II-13-1 Peak area	Verapamil Peak area	Assay 1	Assay 2	Assay 3
0	1482791	2532034	1435822	2495303	1398346	2494973	99.934	100.07	100.08
10	1373230	2426501	1400615	2559018	1403527	2586061	96.575	95.18	96.91
20	1381544	2561581	1262111	2419773	1308674	2460499	92.036	90.71	94.97
30	1298371	2492182	1240184	2564013	1240839	2497136	88.904	84.12	88.73
40	1211580	2528779	1264080	2641303	1194202	2504773	81.761	83.23	85.13
50	1148195	2487107	1206014	2716275	1145296	2498066	78.781	77.21	81.87
60	1107205	2511839	1146511	2698823	1051518	2487612	75.221	73.88	75.48

Table 2: Peak areas and % remaining values

Calculation:

From the peak area, Calculate the following

$$\text{Peak area ratio} = \frac{\text{Peak area of test compound (DK-II-13-1)}}{\text{Peak area of internal standard (Verapamil)}}$$

$$\text{\% remaining at time T} = \frac{\text{Peak area ratio at particular time T}}{\text{Peak area ratio at zero time point}} * 100$$

(T = 0, 10, 20,30,40,50 and 60)

DATA ANALYSIS:

Day 1

Linear regression analysis:

Slope: -0.005095 ± 0.0002029

At X= 60, Y = 4.306 ± 0.007317

R^2 = 0.9707

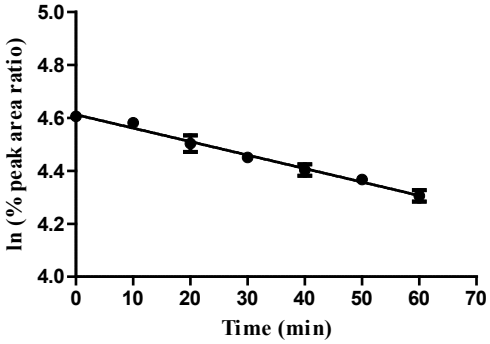

Metabolic Parameters:

Half-life: 136.05 ± 5.41 min

V_d: 100 µL/mg

Intrinsic clearance: 0.5095 µL/min/mg

Metabolic Rate: 10.19 nmol/min/mg

% remaining at 60 min: 74.14 ± 0.12 %

Day 2

Linear regression analysis:

Slope: -0.004868 ± 0.0002081

At X = 60, Y = 4.323 ± 0.007503

R^2 = 0.9664

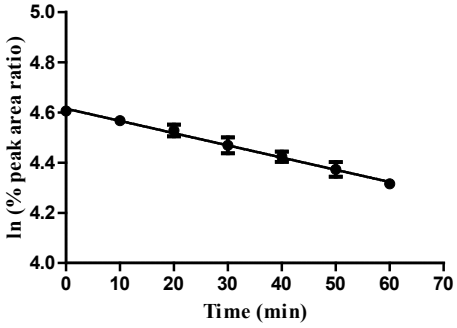

Metabolic Parameters:

Half-life: 142.35 ± 6.08 min

V_d: 100 µL/mg

Intrinsic clearance: 0.4868 µL/min/mg

Metabolic Rate: 9.736 nmol/min/mg

% remaining at 60 min: 75.4 ± 0.13 %

Note: The peak area ratios and natural log values are calculated using Microsoft excel 2010 and linear regression analysis is calculated using GraphPad prism.

Human Liver Microsomal Assay

Principal Investigator: Dr. Alexander Arnold
Operator: Revathi Kodali
Test Compound: **13b**
Concentration: 10 µM
Date: 05-26-2016
Facility: Milwaukee Institute for Drug Discovery

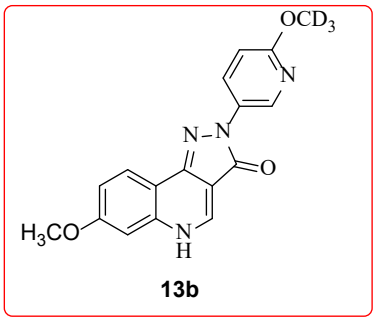

13b

Assay Protocol

Each evaluation included six independent assays carried out three at a time, on two different days

1. Preparation of solutions:
   a. 1 mM test compound in DMSO.
   b. 1 µM 4,5 Di Phenyl Imidazole in ice cold Acetonitrile (ISTD).
2. For a total volume of Microsomal Assay Mixture (MAM) 390 µL, sufficient for seven time points, combine the following
   a. 282 µL of 18.2 mΩ of water.
   b. 80 µL of 0.5 M potassium phosphate buffer (p^H 7.4)
   c. 20 µL of NADPH A. (Corning life sciences, Cat # 451220)
   d. 4 µL of NADPH B. (Corning life sciences, Cat # 451200)
   e. 4 µL of test compound.
3. Sonicate MAM for 5 min and meanwhile thaw microsomes (20 mg/mL) (BD Gentest, Cat # 452156) on ice.
4. Aliquot 100 µL of ice cold ISTD into seven separate 1.5 mL conical vials and label them the time points for 0, 10, 20, 30, 40, 50, and 60 min.
5. Arrange the timer. Microsomes (Final concentration of 0.5 mg/mL) should be added to all time points except the zero time point.
6. Add 50 µL of the MAM solution to the conical vial labelled as zero time point. Place the remaining MAM solution in the incubator (37 ºC) for 5 min and initiate the reaction with addition of microsomes (8.8 µL) and record the time.
7. At the end of each time interval remove 50 µL and add to 100 µL ISTD in conical vial, sonicate for 10 sec and spin down at 10,000 rpm for 5 minutes.
8. Take 100 µL of supernatant and transfer to Spin-X HPLC filter tubes (Corning Incorporated, Cat # 8169) and centrifuge at 13,000 rpm for 5 minutes and take 5 µL from this solution and dilute in 495 µL of LCMS grade methanol (Fischer scientific, CAS # 67-56-1) in an 2mL glass auto sampler vial (Microsolv, Cat # 95025-WCV)
9. The samples are analyzed by LCMS-8040. (Shimadzu)

Data:

Day 1:

Time (min)	Assay 1		Assay 2		Assay 3		% remaining		
	DK-II-60-1 Peak area	ISTD Peak area	DK-II-60-1 Peak area	ISTD Peak area	DK-II-60-1 Peak area	ISTD Peak area	Assay 1	Assay 2	Assay 3
0	1756284	244343	1782966	254410	1795237	251121	99.99	98.87	99.99
10	1711624	243619	1744921	249823	1715529	246573	97.74	98.54	97.32
20	1649870	242568	1670054	246155	1650907	240772	94.62	95.71	95.91
30	1808744	268236	1658112	243636	1501247	221933	93.81	96.01	94.62
40	1774043	267372	1604211	236708	1582982	236575	92.30	95.61	93.59
50	1825221	271861	1605309	243519	1551608	232314	93.40	93.00	93.42
60	1875923	276783	1655851	247573	1565995	231980	94.29	94.36	94.42

Table 1: Peak areas and % remaining values

Day 2:

Time (min)	Assay 1		Assay 2		Assay 3		(% remaining)		
	DK-II-60-1 Peak area	ISTD Peak area	DK-II-60-1 Peak area	ISTD Peak area	DK-II-60-1 Peak area	ISTD Peak area	Assay 1	Assay 2	Assay 3
0	1739396	244473	1856188	260736	1851128	259070	99.99	100.00	100.00
10	1652649	235465	1752613	246751	1827173	261334	98.64	99.77	97.85
20	1607764	234543	1687805	248930	1731129	253844	96.34	95.24	95.44
30	1587724	240500	1630521	245489	1674483	247539	92.78	93.29	94.67
40	1588819	236967	1704883	257676	1624422	244069	94.23	92.94	93.15
50	1510170	221788	1619423	242663	1630685	248648	95.70	93.74	91.78
60	1487839	224359	1686917	247210	1562091	233734	93.20	95.85	93.53

Table 2: Peak areas and % remaining values

Calculation:

From the peak area, Calculate the following

$$\text{Peak area ratio} = \frac{\text{Peak area of test compound (DK-II-60-1)}}{\text{Peak area of internal standard (ISTD)}}$$

$$\text{\% remaining at time T} = \frac{\text{Peak area ratio at particular time T}}{\text{Peak area ratio at zero time point}} * 100$$

(T = 0, 10, 20,30,40,50 and 60)

DATA ANALYSIS:

Day 1

Linear regression analysis:

Slope: -0.0009821 ± 0.0001453

At X= 60, Y = 4.530 ± 0.005238

R^2 = 0.7063

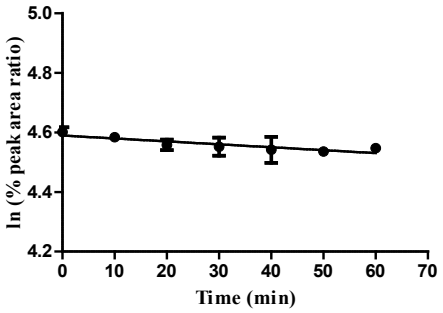

Metabolic Parameters:

Half-life: 554 ± 81.9 min

V_d: 100 µL/mg

Intrinsic clearance: 0.1251 µL/min/mg

Metabolic Rate: 2.502 nmol/min/mg

% remaining at 60 min: 92.75 ± 0.10 %

Day 2

Linear regression analysis:

Slope: -0.0001098 ± 0.0001911

At X = 60, Y = 4.527 ± 0.006892

R^2 = 0.6344

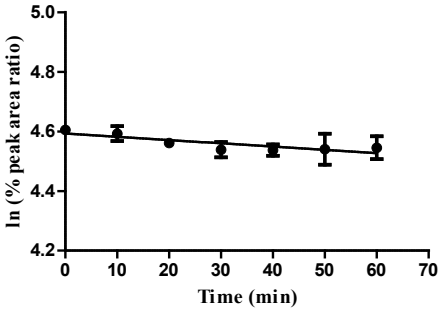

Metabolic Parameters:

Half-life: 631.14 ± 110 min

V_d: 100 µL/mg

Intrinsic clearance: 0.1098 µL/min/mg

Metabolic Rate: 2.196 nmol/min/mg

% remaining at 60 min: 92.4 ± 0.14 %

Note: The peak area ratios and natural log values are calculated using Microsoft excel 2010 and linear regression analysis is calculated using GraphPad prism.

Mouse Liver Microsomal Assay

Principal Investigator: Dr. Alexander Arnold
Operator: Revathi Kodali
Test Compound: **13b**
Concentration: 10 µM
Date: 05-26-2016
Facility: Milwaukee Institute for Drug Discovery

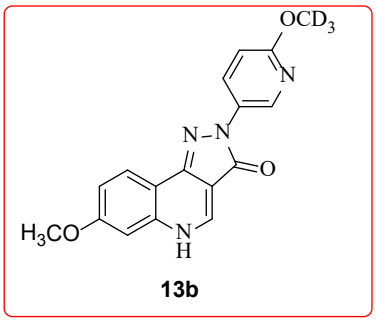

13b

Assay Protocol

Each evaluation included six independent assays carried out three at a time, on two different days

1. Preparation of solutions:
   a. 1 mM test compound in DMSO.
   b. 1 µM 4, 5 Di Phenyl Imidazole in ice cold Acetonitrile (ISTD).
2. For a total volume of Microsomal Assay Mixture (MAM) 390 µL, sufficient for seven time points, combine the following
   a. 282 µL of 18.2 mΩ of water.
   b. 80 µL of 0.5 M potassium phosphate buffer (p^H 7.4)
   c. 20 µL of NADPH A. (Corning life sciences, Cat # 451220)
   d. 4 µL of NADPH B. (Corning life sciences, Cat # 451200)
   e. 4 µL of test compound.
3. Sonicate MAM for 5 min and meanwhile thaw microsomes (20 mg/mL) (Life technologies, Cat # MSMC-PL) on ice.
4. Aliquot 100 µL of ice cold ISTD into seven separate 1.5 mL conical vials and label them the time points for 0, 10, 20, 30, 40, 50, and 60 min.
5. Arrange the timer. Microsomes (Final concentration of 0.5 mg/mL) should be added to all time points except the zero time point.
6. Add 50 µL of the MAM solution to the conical vial labelled as zero time point. Place the remaining MAM solution in the incubator (37 ºC) for 5 min and initiate the reaction with addition of microsomes (8.8 µL) and record the time.
7. At the end of each time interval remove 50 µL and add to 100 µL ISTD in conical vial, sonicate for 10 sec and spin down at 10,000 rpm for 5 minutes.
8. Take 100 µL of supernatant and transfer to Spin-X HPLC filter tubes (Corning Incorporated, Cat # 8169) and centrifuge at 13,000 rpm for 5 minutes and take 5 µL from this solution and dilute in 495 µL of LCMS grade methanol (Fischer scientific, CAS # 67-56-1) in an 2mL glass auto sampler vial (Microsolv, Cat # 95025-WCV)
9. The samples are analyzed by LCMS-8040. (Shimadzu)

Data:

Day 1:

Time (min)	Assay 1		Assay 2		Assay 3		% remaining		
	DK-II-60-1 Peak area	ISTD Peak area	DK-II-60-1 Peak area	ISTD Peak area	DK-II-60-1 Peak area	ISTD Peak area	Assay 1	Assay 2	Assay 3
0	1980897	286787	1989357	292666	2031686	294323	100.00	100.00	99.99
10	1928833	281364	1980914	301476	1981596	297128	99.25	96.67	96.61
20	1702400	252372	1803535	270907	2053633	308914	97.66	97.94	96.30
30	1593574	248948	1653173	256710	1946765	302009	92.67	94.74	93.38
40	1696744	257276	1647899	254711	1890234	290171	95.48	95.18	94.36
50	1666664	254754	1607831	256199	1846752	285585	94.71	92.33	93.67
60	1649310	253220	1848227	291005	1873190	292113	94.30	93.44	92.89

Table 1: Peak areas and % remaining values

Day 2:

Time (min)	Assay 1		Assay 2		Assay 3		(% remaining)		
	DK-II-60-1 Peak area	ISTD Peak area	DK-II-60-1 Peak area	ISTD Peak area	DK-II-60-1 Peak area	ISTD Peak area	Assay 1	Assay 2	Assay 3
0	2058936	337209	1947564	316544	2038726	335006	99.99	99.99	99.99
10	2096283	349902	1911365	323345	2002739	338162	98.11	96.07	97.31
20	2000575	343357	1982961	342398	1980098	347159	95.42	94.12	93.71
30	2047619	351527	1916376	339357	2019605	348138	95.39	91.77	95.32
40	1898193	330966	1938881	340193	1954188	344708	93.92	92.62	93.15
50	1784526	304689	1915426	337783	2096104	373344	95.92	92.16	92.25
60	1791485	318892	1994882	341903	2007358	355040	92.00	94.82	92.90

Table 2: Peak areas and % remaining values

Calculation:

From the peak area, Calculate the following

$$\text{Peak area ratio} = \frac{\text{Peak area of test compound (DK-II-60-1)}}{\text{Peak area of internal standard (ISTD)}}$$

$$\text{\% remaining at time T} = \frac{\text{Peak area ratio at particular time T}}{\text{Peak area ratio at zero time point}} * 100$$

(T = 0, 10, 20,30,40,50 and 60)

DATA ANALYSIS:

Day 1

Linear regression analysis:

Slope: -0.001099 ± 0.0001523

At X= 60, Y = 4.529 ± 0.005492

R^2 = 0.7325

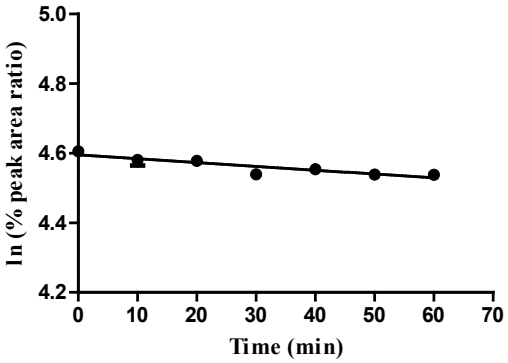

Metabolic Parameters:

Half-life: 630.57 ± 87.38 min

V_d: 100 µL/mg

Intrinsic clearance: 0.1099 µL/min/mg

Metabolic Rate: 2.198 nmol/min/mg

% remaining at 60 min: 92.66 ± 0.11 %

Day 2

Linear regression analysis:

Slope: -0.0001067 ± 0.0001939

At X = 60, Y = 4.523 ± 0.006992

R^2 = 0.6143

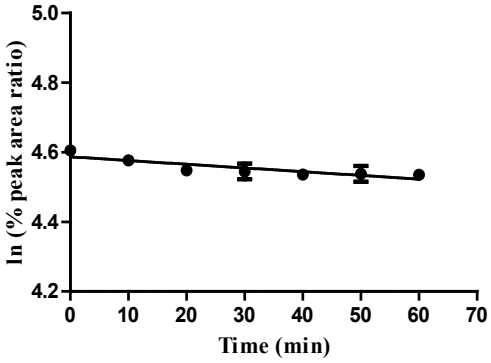

Metabolic Parameters:

Half-life: 649.48 ± 118 min

V_d: 100 µL/mg

Intrinsic clearance: 0.1067 µL/min/mg

Metabolic Rate: 2.134 nmol/min/mg

% remaining at 60 min: 92.11 ± 0.14 %

Note: The peak area ratios and natural log values are calculated using Microsoft excel 2010 and linear regression analysis is calculated using GraphPad prism.

Human Liver Microsomal Assay

Principal Investigator: Dr. Alexander Arnold
Operator: Revathi Kodali
Test Compound: **13c**
Concentration: 10 µM
Date: 02-24-2016
Facility: Milwaukee Institute for Drug Discovery

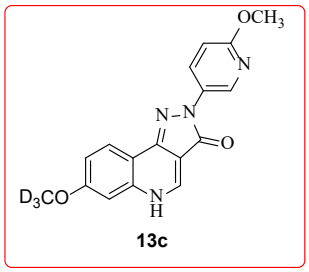

13c

Assay Protocol

Each evaluation included six independent assays carried out three at a time, on two different days

1. Preparation of solutions:
   a. 1 mM test compound in DMSO.
   b. 1 µM Verapamil in Acetonitrile (ACN) as internal standard (store on ice).
2. For a total volume of Microsomal Assay Mixture (MAM) 390 µL, sufficient for seven time points, combine the following
   a. 282 µL of 18.2 mΩ of water.
   b. 80 µL of 0.5 M potassium phosphate buffer (p^H 7.4)
   c. 20 µL of NADPH A. (Corning life sciences, Cat # 451220)
   d. 4 µL of NADPH B. (Corning life sciences, Cat # 451200)
   e. 4 µL of test compound.
3. Sonicate MAM for 5 min and meanwhile thaw microsomes (20 mg/mL) (BD Gentest, Cat # 452156) on ice.
4. Aliquot 100 µL of ice cold ISTD into seven separate 1.5 mL conical vials and label them the time points for 0, 10, 20, 30, 40, 50, and 60 min.
5. Arrange the timer. Microsomes (Final concentration of 0.5 mg/mL) should be added to all time points except the zero time point.
6. Add 50 µL of the MAM solution to the conical vial labelled as zero time point. Place the remaining MAM solution in the incubator (37 ºC) for 5 min and initiate the reaction with addition of microsomes (8.8 µL) and record the time.
7. At the end of each time interval remove 50 µL and add to 100 µL ISTD in conical vial, sonicate for 10 sec and spin down at 10,000 rpm for 5 minutes.
8. Take 100 µL of supernatant and transfer to Spin-X HPLC filter tubes (Corning Incorporated, Cat # 8169) and centrifuge at 13,000 rpm for 5 minutes and take 5 µL from this solution and dilute in 495 µL of LCMS grade methanol (Fischer scientific, CAS # 67-56-1) in an 2mL glass auto sampler vial (Microsolv, Cat # 95025-WCV)
9. The samples are analyzed by LCMS-8040. (Shimadzu)

Data:

Day 1:

Time (min)	Assay 1		Assay 2		Assay 3		% remaining		
	DK-I-86-1 Peak area	Verapamil Peak area	DK-I-86-1 Peak area	Verapamil Peak area	DK-I-86-1 Peak area	Verapamil Peak area	Assay 1	Assay 2	Assay 3
0	792373	761693	787587	762552	759063	767398	100.02	99.98	100.01
10	775249	778963	759323	778215	722382	763900	95.69	94.45	95.61
20	747907	769408	720325	751835	705108	755157	93.46	92.74	94.41
30	752648	766232	732194	737114	704567	740283	94.44	96.15	96.23
40	745127	774917	729292	745328	715307	764064	92.45	94.72	94.66
50	748105	768076	736837	751091	714739	751444	93.65	94.96	96.17
60	742196	751303	716214	761424	695197	750039	94.98	91.05	93.71

Table 1: Peak areas and % remaining values

Day 2:

Time (min)	Assay 1		Assay 2		Assay 3		(% remaining)		
	DK-I-86-1 Peak area	Verapamil Peak area	DK-I-86-1 Peak area	Verapamil Peak area	DK-I-86-1 Peak area	Verapamil Peak area	Assay 1	Assay 2	Assay 3
0	792080	771654	755622	767152	750685	764993	100.04	99.99	100.03
10	763307	762869	718899	751779	725054	769289	97.52	97.08	96.07
20	739985	759373	712962	769369	684187	740762	94.97	94.08	94.15
30	732020	765124	701439	754561	700784	761722	93.24	94.37	93.78
40	731777	774078	696706	768514	704575	751634	92.14	92.03	95.55
50	713226	743504	690888	750265	694976	761536	93.49	93.48	93.02
60	713143	761196	697143	765448	701108	768530	91.31	92.46	92.99

Table 2: Peak areas and % remaining values

Calculation:

From the peak area, Calculate the following

$$\text{Peak area ratio} = \frac{\text{Peak area of test compound (DK-I-86-1)}}{\text{Peak area of internal standard (Verapamil)}}$$

$$\text{\% remaining at time T} = \frac{\text{Peak area ratio at particular time T}}{\text{Peak area ratio at zero time point}} * 100$$

(T = 0, 10, 20,30,40,50 and 60)

DATA ANALYSIS:

Day 1

Linear regression analysis:

Slope: -0.0007571 ± 0.0002152

At X= 60, Y = 4.533 ± 0.007758

R^2 = 0.3946

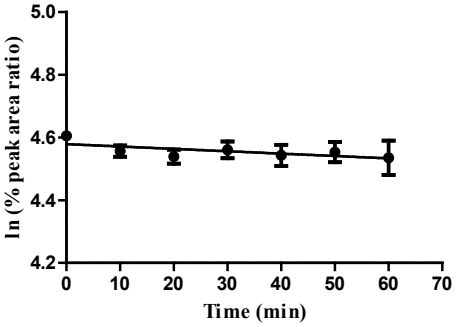

Metabolic Parameters:

Half-life: 915.33 ± 260 min

V_d: 100 µL/mg

Intrinsic clearance: 0.07571 µL/min/mg

Metabolic Rate: 1.5142 nmol/min/mg

% remaining at 60 min: 93.03 ± 0.16 %

Day 2

Linear regression analysis:

Slope: -0.001176 ± 0.0001580

At X = 60, Y = 4.517 ± 0.005695

R^2 = 0.7448

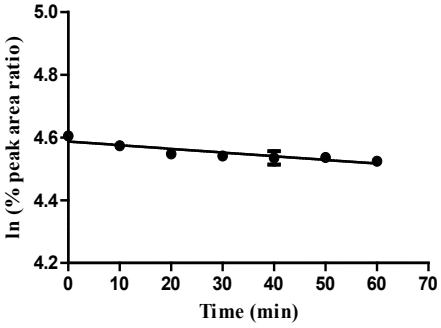

Metabolic Parameters:

Half-life: 589.28 ± 261.93 min

V_d: 100 µL/mg

Intrinsic clearance: 0.1176 µL/min/mg

Metabolic Rate: 2.352 nmol/min/mg

% remaining at 60 min: 91.56 ± 0.11 %

Note: The peak area ratios and natural log values are calculated using Microsoft excel 2010 and linear regression analysis is calculated using GraphPad prism.

Mouse Liver Microsomal Assay

Principal Investigator: Dr. Alexander Arnold
Operator: Revathi Kodali
Test Compound: **13c**
Concentration: 10 µM
Date: 02-24-2016
Facility: Milwaukee Institute for Drug Discovery

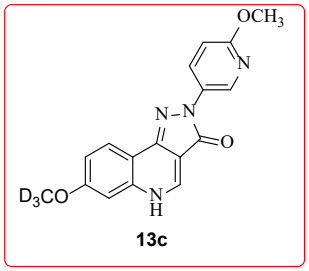

13c

Assay Protocol

Each evaluation included six independent assays carried out three at a time, on two different days

1. Preparation of solutions:
   a. 1 mM test compound in DMSO.
   b. 1 µM Verapamil in Acetonitrile (ACN) as internal standard (store on ice).
2. For a total volume of Microsomal Assay Mixture (MAM) 390 µL, sufficient for seven time points, combine the following
   a. 282 µL of 18.2 mΩ of water.
   b. 80 µL of 0.5 M potassium phosphate buffer (p^H 7.4)
   c. 20 µL of NADPH A. (Corning life sciences, Cat # 451220)
   d. 4 µL of NADPH B. (Corning life sciences, Cat # 451200)
   e. 4 µL of test compound.
3. Sonicate MAM for 5 min and meanwhile thaw microsomes (20 mg/mL) (Life technologies, Cat # 452156) on ice.
4. Aliquot 100 µL of ice cold ISTD into seven separate 1.5 mL conical vials and label them the time points for 0, 10, 20, 30, 40, 50, and 60 min.
5. Arrange the timer. Microsomes (Final concentration of 0.5 mg/mL) should be added to all time points except the zero time point.
6. Add 50 µL of the MAM solution to the conical vial labelled as zero time point. Place the remaining MAM solution in the incubator (37 ºC) for 5 min and initiate the reaction with addition of microsomes (8.8 µL) and record the time.
7. At the end of each time interval remove 50 µL and add to 100 µL ISTD in conical vial, sonicate for 10 sec and spin down at 10,000 rpm for 5 minutes.
8. Take 100 µL of supernatant and transfer to Spin-X HPLC filter tubes (Corning Incorporated, Cat # 8169) and centrifuge at 13,000 rpm for 5 minutes and take 5 µL from this solution and dilute in 495 µL of LCMS grade methanol (Fischer scientific, CAS # 67-56-1) in an 2mL glass auto sampler vial (Microsolv, Cat # 95025-WCV)
9. The samples are analyzed by LCMS-8040. (Shimadzu)

Data:

Day 1:

Time (min)	Assay 1		Assay 2		Assay 3		% remaining		
	DK-I-86-1 Peak area	Verapamil Peak area	DK-I-86-1 Peak area	Verapamil Peak area	DK-I-86-1 Peak area	Verapamil Peak area	Assay 1	Assay 2	Assay 3
0	748286	763242	722465	767929	769758	742901	100.04	99.97	100.01
10	713998	749342	706222	755366	756894	758618	97.22	99.35	96.30
20	690434	750832	686823	767153	764830	773294	93.83	95.14	95.46
30	702462	771060	663671	745862	736979	755844	92.96	94.55	94.11
40	694160	769174	670892	771278	738418	765370	92.08	92.43	93.12
50	688116	768297	669515	747483	701337	740371	91.39	95.18	91.43
60	699208	755159	658858	761861	731836	752534	94.48	91.90	93.87

Table 1: Peak areas and % remaining values

Day 2:

Time (min)	Assay 1		Assay 2		Assay 3		(% remaining)		
	DK-I-86-1 Peak area	Verapamil Peak area	DK-I-86-1 Peak area	Verapamil Peak area	DK-I-86-1 Peak area	Verapamil Peak area	Assay 1	Assay 2	Assay 3
0	703150	745961	719185	771365	719185	771365	99.95	100.03	100.04
10	685315	755803	699396	769657	699396	769657	96.15	97.50	97.81
20	668828	748912	653994	753512	653994	753512	94.70	93.12	95.01
30	672903	766432	670496	743115	670496	743115	93.10	96.81	93.92
40	675455	755264	664193	756441	664193	756441	94.83	94.21	92.71
50	671149	779998	656754	750123	656754	750123	91.24	93.94	92.52
60	652813	760945	643312	766695	643312	766695	90.97	90.02	93.06

Table 2: Peak areas and % remaining values

Calculation:

From the peak area, Calculate the following

$$\text{Peak area ratio} = \frac{\text{Peak area of test compound (DK-I-86-1)}}{\text{Peak area of internal standard (Verapamil)}}$$

$$\text{\% remaining at time T = (T = 0, 10, 20,30,40,50 and 60)} \quad \frac{\text{Peak area ratio at particular time T}}{\text{Peak area ratio at zero time point}} * 100$$

DATA ANALYSIS:

Day 1

Linear regression analysis:

Slope: -0.001192 ± 0.0001908

At X= 60, Y = 4.518 ± 0.006880

R^2 = 0.6724

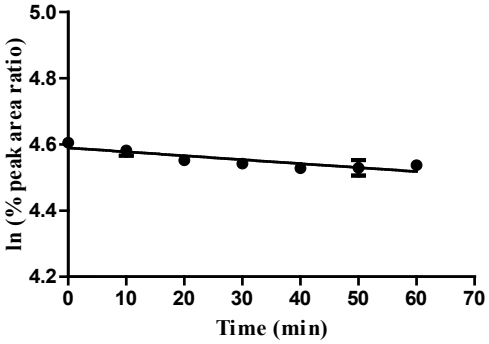

Metabolic Parameters:

Half-life: 581.37 ± 93 min

V_d: 100 µL/mg

Intrinsic clearance: 0.1192 µL/min/mg

Metabolic Rate: 2.384 nmol/min/mg

% remaining at 60 min: 91.65 ± 0.14 %

Day 2

Linear regression analysis:

Slope: -0.001333 ± 0.0001630

At X = 60, Y = 4.512 ± 0.005877

R^2 = 0.7789

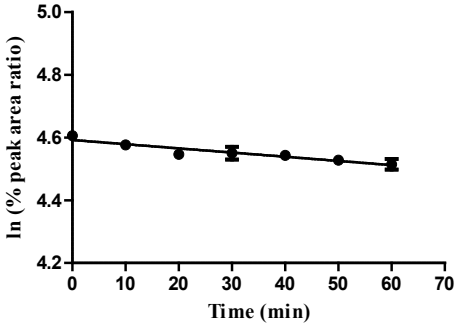

Metabolic Parameters:

Half-life: 519.88 ± 63.57 min

V_d: 100 µL/mg

Intrinsic clearance: 0.1333 µL/min/mg

Metabolic Rate: 2.666 nmol/min/mg

% remaining at 60 min: 91.10 ± 0.11 %

Note: The peak area ratios and natural log values are calculated using Microsoft excel 2010 and linear regression analysis is calculated using GraphPad prism.

Human Liver Microsomal Assay

Principal Investigator: Dr. Alexander Arnold
Operator: Revathi Kodali
Test Compound: **13d**
Concentration: 10 µM
Date: 02-28-2017
Facility: Milwaukee Institute for Drug Discovery

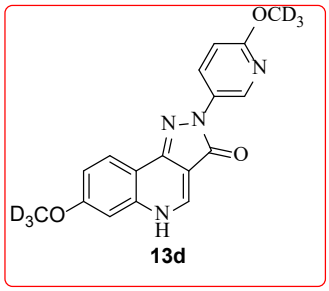

13d

Assay Protocol

Each evaluation included six independent assays carried out three at a time, on two different days

1. Preparation of solutions:
   a. 1 mM test compound in DMSO.
   b. 3 µM Verapamil in ice cold Acetonitrile (ISTD).
2. For a total volume of Microsomal Assay Mixture (MAM) 390 µL, sufficient for seven time points, combine the following
   a. 282 µL of 18.2 mΩ of water.
   b. 80 µL of 0.5 M potassium phosphate buffer (p^H 7.4)
   c. 20 µL of NADPH A. (Corning life sciences, Cat # 451220)
   d. 4 µL of NADPH B. (Corning life sciences, Cat # 451200)
   e. 4 µL of test compound.
3. Sonicate MAM for 5 min and meanwhile thaw microsomes (20 mg/mL) (BD Gentest, Cat # 452156) on ice.
4. Aliquot 100 µL of ice cold ISTD into seven separate 1.5 mL conical vials and label them the time points for 0, 10, 20, 30, 40, 50, and 60 min.
5. Arrange the timer. Microsomes (Final concentration of 0.5 mg/mL) should be added to all time points except the zero time point.
6. Add 50 µL of the MAM solution to the conical vial labelled as zero time point. Place the remaining MAM solution in the incubator (37 ºC) for 5 min and initiate the reaction with addition of microsomes (8.8 µL) and record the time.
7. At the end of each time interval remove 50 µL and add to 100 µL ISTD in conical vial, sonicate for 10 sec and spin down at 10,000 rpm for 5 minutes.
8. Take 100 µL of supernatant and transfer to Spin-X HPLC filter tubes (Corning Incorporated, Cat # 8169) and centrifuge at 13,000 rpm for 5 minutes and take 5 µL from this solution and dilute in 495 µL of LCMS grade methanol (Fischer scientific, CAS # 67-56-1) in an 2mL glass auto sampler vial (Microsolv, Cat # 95025-WCV)
9. The samples are analyzed by LCMS-8040. (Shimadzu)

Data:

Day 1:

Time (min)	Assay 1		Assay 2		Assay 3		% remaining		
	DK-III-6-1 Peak area	Verapamil Peak area	DK-III-6-1 Peak area	Verapamil Peak area	DK-III-6-1 Peak area	Verapamil Peak area	Assay 1	Assay 2	Assay 3
0	153644	364063	140809	360823	147344	361083	100.00	100.06	100.01
10	144930	355973	134322	361783	140461	358982	96.47	95.19	95.90
20	145649	357844	131921	362018	135460	349781	96.45	93.43	94.91
30	136721	362984	135283	358972	133692	361193	89.25	96.63	90.72
40	141558	359723	126286	359981	131160	357892	93.25	89.95	89.82
50	133488	348756	128461	363874	136171	359671	90.70	90.52	92.79
60	134498	358623	128686	361211	136437	362084	88.87	91.34	92.35

Table 1: Peak areas and % remaining values

Day 2:

Time (min)	Assay 1		Assay 2		Assay 3		(% remaining)		
	DK-III-6-1 Peak area	Verapamil Peak area	DK-III-6-1 Peak area	Verapamil Peak area	DK-III-6-1 Peak area	Verapamil Peak area	Assay 1	Assay 2	Assay 3
0	148525	357823	147750	359789	151645	358973	100.01	99.91	100.10
10	143805	357791	140631	361882	146568	360078	96.84	94.55	96.45
20	141879	359721	133414	362874	143690	358612	95.04	89.45	94.94
30	140050	362073	138462	362991	143387	362543	93.20	92.81	93.72
40	134914	362734	133414	359834	140961	361834	89.62	90.21	92.31
50	140699	361764	140398	358976	141144	362893	93.71	95.16	92.16
60	140461	359722	136812	360823	146875	361383	94.08	92.25	96.30

Table 2: Peak areas and % remaining values

Calculation:

From the peak area, Calculate the following

$$\text{Peak area ratio} = \frac{\text{Peak area of test compound (DK-III-6-1)}}{\text{Peak area of internal standard (Verapamil)}}$$

$$\text{\% remaining at time T} = \frac{\text{Peak area ratio at particular time T}}{\text{Peak area ratio at zero time point}} * 100$$

(T = 0, 10, 20,30,40,50 and 60)

DATA ANALYSIS:

Day 1

Linear regression analysis:

Slope: -0.001523 ± 0.0002458

At X= 60, Y = 4.494 ± 0.008864

R^2 = 0.6688

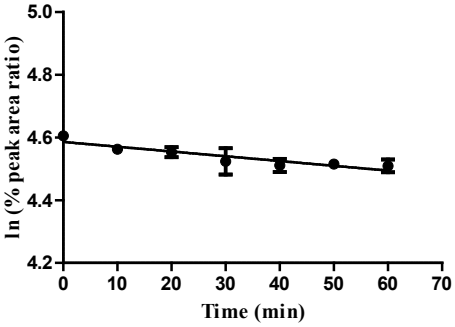

Metabolic Parameters:

Half-life: 455 ± 73 min

V_d: 100 µL/mg

Intrinsic clearance: 0.1523 µL/min/mg

Metabolic Rate: 3.046 nmol/min/mg

% remaining at 60 min: 89 ± 0.20 %

Day 2

Linear regression analysis:

Slope: -0.0008976 ± 0.0003018

At X = 60, Y = 4.520 ± 0.01088

R^2 = 0.3177

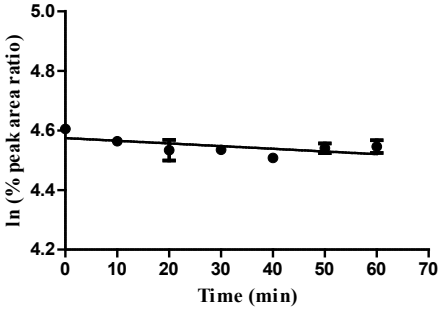

Metabolic Parameters:

Half-life: 772 ± 260 min

V_d: 100 µL/mg

Intrinsic clearance: 0.08976 µL/min/mg

Metabolic Rate: 1.7952 nmol/min/mg

% remaining at 60 min: 91 ± 0.6 %

Note: The peak area ratios and natural log values are calculated using Microsoft excel 2010 and linear regression analysis is calculated using GraphPad prism.

Mouse Liver Microsomal Assay

Principal Investigator: Dr. Alexander Arnold
Operator: Revathi Kodali
Test Compound: **13d**
Concentration: 10 µM
Date: 02-28-2017
Facility: Milwaukee Institute for Drug Discovery

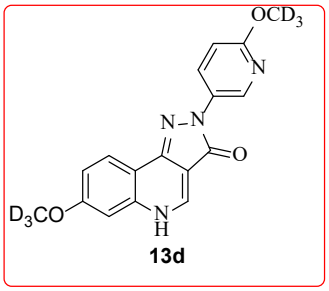

13d

Assay Protocol

Each evaluation included six independent assays carried out three at a time, on two different days

1. Preparation of solutions:
   a. 1 mM test compound in DMSO.
   b. 3 µM Verapamil in ice cold Acetonitrile (ISTD).
2. For a total volume of Microsomal Assay Mixture (MAM) 390 µL, sufficient for seven time points, combine the following
   a. 282 µL of 18.2 mΩ of water.
   b. 80 µL of 0.5 M potassium phosphate buffer (p^H 7.4)
   c. 20 µL of NADPH A. (Corning life sciences, Cat # 451220)
   d. 4 µL of NADPH B. (Corning life sciences, Cat # 451200)
   e. 4 µL of test compound.
3. Sonicate MAM for 5 min and meanwhile thaw microsomes (20 mg/mL) (Life technologies, Cat # MSMC-PL) on ice.
4. Aliquot 100 µL of ice cold ISTD into seven separate 1.5 mL conical vials and label them the time points for 0, 10, 20, 30, 40, 50, and 60 min.
5. Arrange the timer. Microsomes (Final concentration of 0.5 mg/mL) should be added to all time points except the zero time point.
6. Add 50 µL of the MAM solution to the conical vial labelled as zero time point. Place the remaining MAM solution in the incubator (37 ºC) for 5 min and initiate the reaction with addition of microsomes (8.8 µL) and record the time.
7. At the end of each time interval remove 50 µL and add to 100 µL ISTD in conical vial, sonicate for 10 sec and spin down at 10,000 rpm for 5 minutes.
8. Take 100 µL of supernatant and transfer to Spin-X HPLC filter tubes (Corning Incorporated, Cat # 8169) and centrifuge at 13,000 rpm for 5 minutes and take 5 µL from this solution and dilute in 495 µL of LCMS grade methanol (Fischer scientific, CAS # 67-56-1) in an 2mL glass auto sampler vial (Microsolv, Cat # 95025-WCV)
9. The samples are analyzed by LCMS-8040. (Shimadzu)

Data:

Day 1:

Time (min)	Assay 1		Assay 2		Assay 3		% remaining		
	DK-III-6-1 Peak area	Verapamil Peak area	DK-III-6-1 Peak area	Verapamil Peak area	DK-III-6-1 Peak area	Verapamil Peak area	Assay 1	Assay 2	Assay 3
0	148490	360183	152920	361083	148522	359971	100.06	99.88	99.90
10	140281	359723	145884	358916	140207	358672	94.65	95.86	94.65
20	135278	354189	143711	358778	136552	356153	92.70	94.47	92.83
30	134096	339989	140660	356891	143925	371083	95.73	92.95	93.91
40	134133	360821	137701	360073	140962	360123	90.22	90.19	94.77
50	139839	358872	145090	361792	144050	359723	94.57	94.58	96.96
60	134525	357821	139905	360513	140084	356278	91.25	91.52	95.20

Table 1: Peak areas and % remaining values

Day 2:

Time (min)	Assay 1		Assay 2		Assay 3		(% remaining)		
	DK-III-6-1 Peak area	Verapamil Peak area	DK-III-6-1 Peak area	Verapamil Peak area	DK-III-6-1 Peak area	Verapamil Peak area	Assay 1	Assay 2	Assay 3
0	150286	358974	145675	361284	148487	360083	99.91	100.05	100.09
10	143342	360173	141379	360083	142375	357982	94.98	97.42	96.53
20	140747	362894	138591	358673	138487	358901	92.56	95.88	93.65
30	136267	358513	140387	361008	141195	361008	90.71	96.49	94.93
40	143712	358971	133847	358900	142345	358978	95.54	92.54	96.24
50	140353	358921	137409	361287	139865	354793	93.32	94.37	95.68
60	139598	365723	139295	360078	140622	356872	91.09	95.99	95.64

Table 2: Peak areas and % remaining values

Calculation:

From the peak area, Calculate the following

$$\text{Peak area ratio} = \frac{\text{Peak area of test compound (DK-III-6-1)}}{\text{Peak area of internal standard (Verapamil)}}$$

$$\text{\% remaining at time T (T = 0, 10, 20,30,40,50 and 60)} = \frac{\text{Peak area ratio at particular time T}}{\text{Peak area ratio at zero time point}} * 100$$

DATA ANALYSIS:

Day 1

Linear regression analysis:

Slope: -0.0008512 ± 0.0002741

At X= 60, Y = 4.524 ± 0.009883

R^2 = 0.3367

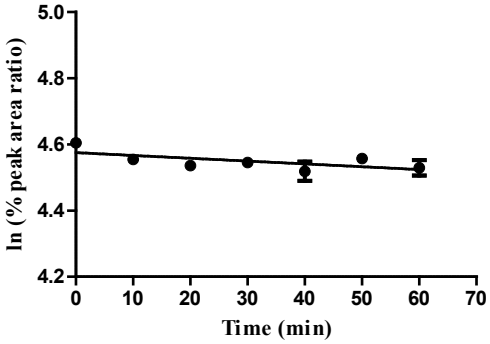

Metabolic Parameters:

Half-life: 814 ± 262 min

V_d: 100 µL/mg

Intrinsic clearance: 0.08512 µL/min/mg

Metabolic Rate: 1.7024 nmol/min/mg

% remaining at 60 min: 92 ± 0.42 %

Day 2

Linear regression analysis:

Slope: -0.0007512 ± 0.0002533

At X = 60, Y = 4.535 ± 0.009133

R^2 = 0.3164

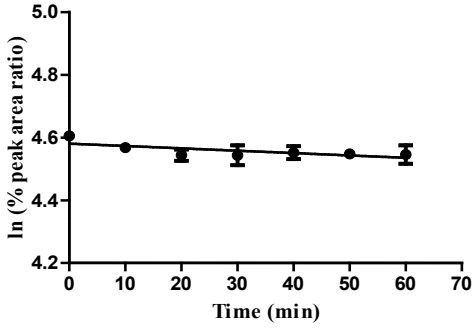

Metabolic Parameters:

Half-life: 922 ± 311 min

V_d: 100 µL/mg

Intrinsic clearance: 0.07512 µL/min/mg

Metabolic Rate: 1.5024 nmol/min/mg

% remaining at 60 min: 93 ± 0.18 %

Note: The peak area ratios and natural log values are calculated using Microsoft excel 2010 and linear regression analysis is calculated using GraphPad prism.

Human Liver Microsomal Assay

Principal Investigator: Dr. Alexander Arnold
Operator: Revathi Kodali
Test Compound: **13e**
Concentration: 10 µM
Date: 05-26-2016
Facility: Milwaukee Institute for Drug Discovery

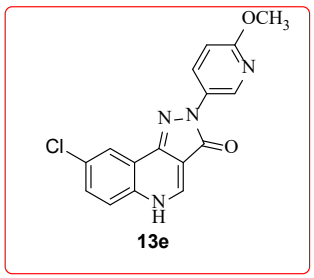

13e

Assay Protocol

Each evaluation included six independent assays carried out three at a time, on two different days

1. Preparation of solutions:
   a. 1 mM test compound in DMSO.
   b. 1 µM 4,5 Di Phenyl Imidazole in ice cold Acetonitrile (ISTD).
2. For a total volume of Microsomal Assay Mixture (MAM) 390 µL, sufficient for seven time points, combine the following
   a. 282 µL of 18.2 mΩ of water.
   b. 80 µL of 0.5 M potassium phosphate buffer (p^H 7.4)
   c. 20 µL of NADPH A. (Corning life sciences, Cat # 451220)
   d. 4 µL of NADPH B. (Corning life sciences, Cat # 451200)
   e. 4 µL of test compound.
3. Sonicate MAM for 5 min and meanwhile thaw microsomes (20 mg/mL) (BD Gentest, Cat # 452156) on ice.
4. Aliquot 100 µL of ice cold ISTD into seven separate 1.5 mL conical vials and label them the time points for 0, 10, 20, 30, 40, 50, and 60 min.
5. Arrange the timer. Microsomes (Final concentration of 0.5 mg/mL) should be added to all time points except the zero time point.
6. Add 50 µL of the MAM solution to the conical vial labelled as zero time point. Place the remaining MAM solution in the incubator (37 ºC) for 5 min and initiate the reaction with addition of microsomes (8.8 µL) and record the time.
7. At the end of each time interval remove 50 µL and add to 100 µL ISTD in conical vial, sonicate for 10 sec and spin down at 10,000 rpm for 5 minutes.
8. Take 100 µL of supernatant and transfer to Spin-X HPLC filter tubes (Corning Incorporated, Cat # 8169) and centrifuge at 13,000 rpm for 5 minutes and take 5 µL from this solution and dilute in 495 µL of LCMS grade methanol (Fischer scientific, CAS # 67-56-1) in an 2mL glass auto sampler vial (Microsolv, Cat # 95025-WCV)
9. The samples are analyzed by LCMS-8040. (Shimadzu)

Data:

Day 1:

Time (min)	Assay 1		Assay 2		Assay 3		% remaining		
	DK-II-18-1 Peak area	ISTD Peak area	DK-II-18-1 Peak area	ISTD Peak area	DK-II-18-1 Peak area	ISTD Peak area	Assay 1	Assay 2	Assay 3
0	5644208	1919825	5875547	1981129	5841039	1934689	99.99	99.99	100.00
10	5456553	1899842	5706009	1973504	5797339	1962833	97.69	97.48	97.83
20	5328278	1918500	5552056	1938966	5512970	1884596	94.46	96.54	96.89
30	5168256	1864504	5636298	2016714	5444451	1881687	94.28	94.22	95.83
40	5385979	1966025	5540361	2025809	5515331	1975225	93.18	92.20	92.48
50	5440986	2009443	5449974	1939177	5358680	1895764	92.09	94.75	93.62
60	5504710	2003905	5206503	1888636	5485574	1981129	93.43	92.94	91.71

Table 1: Peak areas and % remaining values

Day 2:

Time (min)	Assay 1		Assay 2		Assay 3		(% remaining)		
	DK-II-18-1 Peak area	ISTD Peak area	DK-II-18-1 Peak area	ISTD Peak area	DK-II-18-1 Peak area	ISTD Peak area	Assay 1	Assay 2	Assay 3
0	5710121	2003409	5613818	1965608	5604288	1995291	100.00	100.00	99.99
10	5452301	1929979	5571224	1958058	5522406	2000126	99.12	99.62	98.29
20	5400422	1918141	5301727	1920970	5297920	1926830	98.78	96.63	97.88
30	5182982	1899424	5302594	1936282	5227006	1955810	95.74	95.88	95.14
40	5159406	1912916	5164528	1949451	5194723	1988147	94.63	92.76	93.01
50	4880937	1855401	5027967	1935829	5150225	2000688	92.30	90.94	91.64
60	5141039	1926599	4959117	1880283	5016219	1915448	93.63	92.34	93.23

Table 2: Peak areas and % remaining values

Calculation:

From the peak area, Calculate the following

$$\text{Peak area ratio} = \frac{\text{Peak area of test compound (DK-II-18-1)}}{\text{Peak area of internal standard (ISTD)}}$$

$$\text{\% remaining at time T} = \frac{\text{Peak area ratio at particular time T}}{\text{Peak area ratio at zero time point}} * 100$$

(T = 0, 10, 20,30,40,50 and 60)

DATA ANALYSIS:

Day 1

Linear regression analysis:

Slope: -0.001251 ± 0.0001340

At X= 60, Y = 4.519 ± 0.004832

R^2 = 0.8210

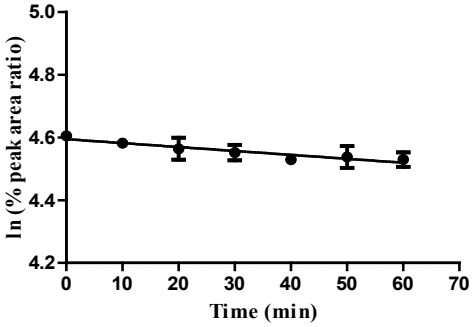

Metabolic Parameters:

Half-life: 554 ± 48 min

V_d: 100 µL/mg

Intrinsic clearance: 0.1251 µL/min/mg

Metabolic Rate: 2.502 nmol/min/mg

% remaining at 60 min: 91.74 ± 0.10%

Day 2

Linear regression analysis:

Slope: -0.001481 ± 0.0001282

At X = 60, Y = 4.517 ± 0.004621

R^2 = 0.8754

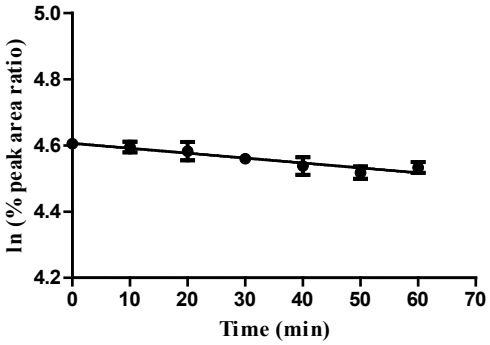

Metabolic Parameters:

Half-life: 468 ± 40 min

V_d: 100 µL/mg

Intrinsic clearance: 0.1481 µL/min/mg

Metabolic Rate: 2.962 nmol/min/mg

% remaining at 60 min: 91.56 ± 0.10 %

Note: The peak area ratios and natural log values are calculated using Microsoft excel 2010 and linear regression analysis is calculated using GraphPad prism.

Mouse Liver Microsomal Assay

Principal Investigator: Dr. Alexander Arnold
Operator: Revathi Kodali
Test Compound: **13e**
Concentration: 10 µM
Date: 05-26-2016
Facility: Milwaukee Institute for Drug Discovery

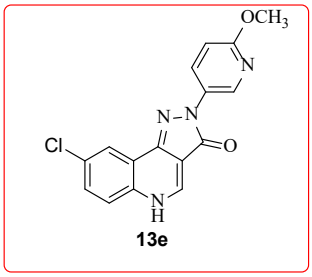

13e

Assay Protocol

Each evaluation included six independent assays carried out three at a time, on two different days

1. Preparation of solutions:
   a. 1 mM test compound in DMSO.
   b. 1 µM 4,5 Di Phenyl Imidazole in ice cold Acetonitrile (ISTD).
2. For a total volume of Microsomal Assay Mixture (MAM) 390 µL, sufficient for seven time points, combine the following
   a. 282 µL of 18.2 mΩ of water.
   b. 80 µL of 0.5 M potassium phosphate buffer (p^H 7.4)
   c. 20 µL of NADPH A. (Corning life sciences, Cat # 451220)
   d. 4 µL of NADPH B. (Corning life sciences, Cat # 451200)
   e. 4 µL of test compound.
3. Sonicate MAM for 5 min and meanwhile thaw microsomes (20 mg/mL) (Life technologies, Cat # MSMC-PL) on ice.
4. Aliquot 100 µL of ice cold ISTD into seven separate 1.5 mL conical vials and label them the time points for 0, 10, 20, 30, 40, 50, and 60 min.
5. Arrange the timer. Microsomes (Final concentration of 0.5 mg/mL) should be added to all time points except the zero time point.
6. Add 50 µL of the MAM solution to the conical vial labelled as zero time point. Place the remaining MAM solution in the incubator (37 ºC) for 5 min and initiate the reaction with addition of microsomes (8.8 µL) and record the time.
7. At the end of each time interval remove 50 µL and add to 100 µL ISTD in conical vial, sonicate for 10 sec and spin down at 10,000 rpm for 5 minutes.
8. Take 100 µL of supernatant and transfer to Spin-X HPLC filter tubes (Corning Incorporated, Cat # 8169) and centrifuge at 13,000 rpm for 5 minutes and take 5 µL from this solution and dilute in 495 µL of LCMS grade methanol (Fischer scientific, CAS # 67-56-1) in an 2mL glass auto sampler vial (Microsolv, Cat # 95025-WCV)
9. The samples are analyzed by LCMS-8040. (Shimadzu)

Data:

Day 1:

Time (min)	Assay 1		Assay 2		Assay 3		% remaining		
	DK-II-18-1 Peak area	ISTD Peak area	DK-II-18-1 Peak area	ISTD Peak area	DK-II-18-1 Peak area	ISTD Peak area	Assay 1	Assay 2	Assay 3
0	4937563	1972562	5251403	1995612	5086726	1981323	100.00	100.01	100.01
10	4743029	2003783	5151998	2000212	5005602	1988213	94.56	97.89	98.07
20	4568830	1954232	5062891	2003111	4934856	2000123	93.40	96.06	96.11
30	4439613	1968634	4805231	1941987	4731044	1961422	90.09	94.04	93.96
40	4389231	1987724	4773953	1973222	4667774	1985162	88.22	91.95	91.59
50	4226640	1963123	4573238	1968173	4496211	1961134	86.01	88.31	89.31
60	4119508	1948631	4436071	1982333	4386336	1971123	84.46	85.05	86.68

Table 1: Peak areas and % remaining values

Day 2:

Time (min)	Assay 1		Assay 2		Assay 3		(% remaining)		
	DK-II-18-1 Peak area	ISTD Peak area	DK-II-18-1 Peak area	ISTD Peak area	DK-II-18-1 Peak area	ISTD Peak area	Assay 1	Assay 2	Assay 3
0	5010208	1974234	5302584	1989204	5058876	2000125	99.99	99.98	100.01
10	4862143	2001223	5170493	1956723	4837587	1939444	95.72	99.11	98.62
20	4641383	1962434	4986012	1922437	4623018	1914324	93.18	97.28	95.49
30	4706895	1962123	4947326	2004601	4676723	2000220	94.51	92.57	92.45
40	4539738	1981983	4819685	2000281	4537177	1921683	90.24	90.37	93.35
50	4412058	2002404	4444467	1945434	4381492	1963739	86.81	85.69	88.22
60	4214014	1934115	4422823	1981423	4265317	1944343	85.84	83.72	86.74

Table 2: Peak areas and % remaining values

Calculation:

From the peak area, Calculate the following

$$\text{Peak area ratio} = \frac{\text{Peak area of test compound (DK-II-18-1)}}{\text{Peak area of internal standard (ISTD)}}$$

$$\text{\% remaining at time T} = \frac{\text{Peak area ratio at particular time T}}{\text{Peak area ratio at zero time point}} * 100$$

(T = 0, 10, 20,30,40,50 and 60)

DATA ANALYSIS:

Day 1

Linear regression analysis:

Slope: -0.002564 ± 0.0001760

At X= 60, Y = 4.451 ± 0.006346

R^2 = 0.9178

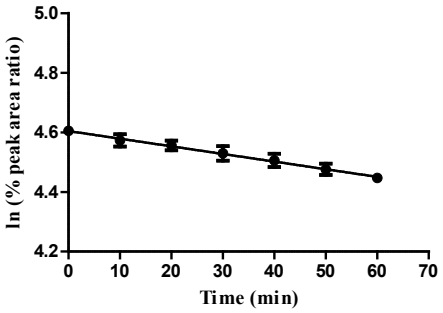

Metabolic Parameters:

Half-life: 270.28 ± 18.55 min

V_d: 100 µL/mg

Intrinsic clearance: 0.2564 µL/min/mg

Metabolic Rate: 5.128 nmol/min/mg

% remaining at 60 min: 85.7 ± 0.12%

Day 2

Linear regression analysis:

Slope: -0.002679 ± 0.0001699

At X = 60, Y = 4.449 ± 0.006127

R^2 = 0.9290

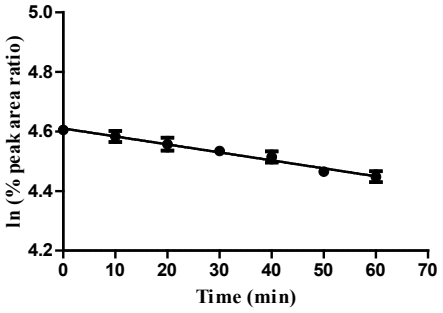

Metabolic Parameters:

Half-life: 258.67 ± 16.4 min

V_d: 100 µL/mg

Intrinsic clearance: 0.2679 µL/min/mg

Metabolic Rate: 5.358 nmol/min/mg

% remaining at 60 min: 85.54 ± 0.11%

Note: The peak area ratios and natural log values are calculated using Microsoft excel 2010 and linear regression analysis is calculated using GraphPad prism.

Human Liver Microsomal Assay

Principal Investigator: Dr. Alexander Arnold
Operator: Revathi Kodali
Test Compound: **13f**
Concentration: 10 µM
Date: 05-11-2016
Facility: Milwaukee Institute for Drug Discovery

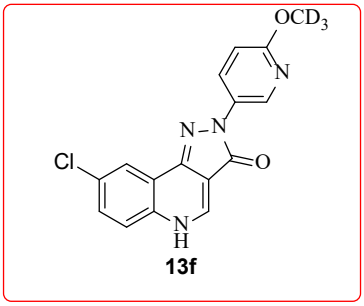

13f

Assay Protocol

Each evaluation included six independent assays carried out three at a time, on two different days

1. Preparation of solutions:
   a. 1 mM test compound in DMSO.
   b. 1 µM 4,5 Di Phenyl Imidazole in ice cold Acetonitrile (ISTD).
2. For a total volume of Microsomal Assay Mixture (MAM) 390 µL, sufficient for seven time points, combine the following
   a. 282 µL of 18.2 mΩ of water.
   b. 80 µL of 0.5 M potassium phosphate buffer (p^H 7.4)
   c. 20 µL of NADPH A. (Corning life sciences, Cat # 451220)
   d. 4 µL of NADPH B. (Corning life sciences, Cat # 451200)
   e. 4 µL of test compound.
3. Sonicate MAM for 5 min and meanwhile thaw microsomes (20 mg/mL) (BD Gentest, Cat # 452156) on ice.
4. Aliquot 100 µL of ice cold ISTD into seven separate 1.5 mL conical vials and label them the time points for 0, 10, 20, 30, 40, 50, and 60 min.
5. Arrange the timer. Microsomes (Final concentration of 0.5 mg/mL) should be added to all time points except the zero time point.
6. Add 50 µL of the MAM solution to the conical vial labelled as zero time point. Place the remaining MAM solution in the incubator (37 ºC) for 5 min and initiate the reaction with addition of microsomes (8.8 µL) and record the time.
7. At the end of each time interval remove 50 µL and add to 100 µL ISTD in conical vial, sonicate for 10 sec and spin down at 10,000 rpm for 5 minutes.
8. Take 100 µL of supernatant and transfer to Spin-X HPLC filter tubes (Corning Incorporated, Cat # 8169) and centrifuge at 13,000 rpm for 5 minutes and take 5 µL from this solution and dilute in 495 µL of LCMS grade methanol (Fischer scientific, CAS # 67-56-1) in an 2mL glass auto sampler vial (Microsolv, Cat # 95025-WCV)
9. The samples are analyzed by LCMS-8040. (Shimadzu)

Data:

Day 1:

Time (min)	Assay 1		Assay 2		Assay 3		% remaining		
	DK-II-59-1 Peak area	ISTD Peak area	DK-II-59-1 Peak area	ISTD Peak area	DK-II-59-1 Peak area	ISTD Peak area	Assay 1	Assay 2	Assay 3
0	3214207	196202	3239494	197689	3238583	200205	100.00	99.99	100.00
10	3173922	195337	3033035	189883	3108369	194321	99.18	97.47	98.88
20	3191550	200098	3261666	208782	3003935	190879	97.36	95.33	97.28
30	3099038	197935	3121234	200528	2905054	192940	95.57	94.98	93.08
40	2898276	189598	3008858	196575	2893897	189441	93.31	93.40	94.43
50	2855181	189062	3105323	199671	2992260	197581	92.18	94.90	93.62
60	3053840	200759	3071294	200786	2996742	194351	92.85	93.34	95.32

Table 1: Peak areas and % remaining values

Day 2:

Time (min)	Assay 1		Assay 2		Assay 3		(% remaining)		
	DK-II-59-1 Peak area	ISTD Peak area	DK-II-59-1 Peak area	ISTD Peak area	DK-II-59-1 Peak area	ISTD Peak area	Assay 1	Assay 2	Assay 3
0	3395328	205696	3206463	199836	3202311	199243	99.99	100.00	100.00
10	3197486	196263	3107429	195452	2971772	189697	98.69	99.08	97.47
20	2980275	190238	2969809	189676	3060284	199223	94.90	97.58	95.57
30	2995384	192622	3081130	201603	2942815	196349	94.20	95.25	93.25
40	2963889	191551	2906813	196822	3090401	201279	93.73	92.04	95.53
50	3237009	207483	2995395	199070	3007720	198190	94.51	93.78	94.42
60	3179593	200002	3092217	199044	2949833	192390	96.30	96.82	95.39

Table 2: Peak areas and % remaining values

Calculation:

From the peak area, Calculate the following

$$\text{Peak area ratio} = \frac{\text{Peak area of test compound (DK-II-59-1)}}{\text{Peak area of internal standard (ISTD)}}$$

$$\text{\% remaining at time T} = \frac{\text{Peak area ratio at particular time T}}{\text{Peak area ratio at zero time point}} * 100$$

(T = 0, 10, 20,30,40,50 and 60)

DATA ANALYSIS:

Day 1

Linear regression analysis:

Slope: -0.0001161 ± 0.0001473

At X= 60, Y = 4.527 ± 0.005309

R^2 = 0.7658

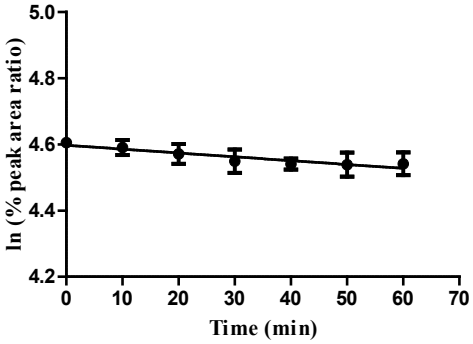

Metabolic Parameters:

Half-life: 596.89 ± 75.73 min

V_d: 100 µL/mg

Intrinsic clearance: 0.1161 µL/min/mg

Metabolic Rate: 2.322 nmol/min/mg

% remaining at 60 min: 92.4 ± 0.10 %

Day 2

Linear regression analysis:

Slope: -0.0008107 ± 0.0002054

At X = 60, Y = 4.541 ± 0.007406

R^2 = 0.4505

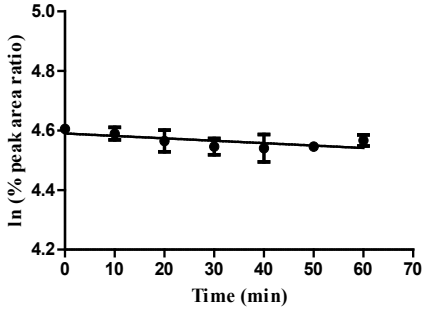

Metabolic Parameters:

Half-life: 854.81 ± 216.57 min

V_d: 100 µL/mg

Intrinsic clearance: 0.08107 µL/min/mg

Metabolic Rate: 1.6214 nmol/min/mg

% remaining at 60 min: 93.78 ± 0.15 %

Note: The peak area ratios and natural log values are calculated using Microsoft excel 2010 and linear regression analysis is calculated using GraphPad prism.

Mouse Liver Microsomal Assay

Principal Investigator: Dr. Alexander Arnold
Operator: Revathi Kodali
Test Compound: **13f**
Concentration: 10 µM
Date: 05-11-2016
Facility: Milwaukee Institute for Drug Discovery

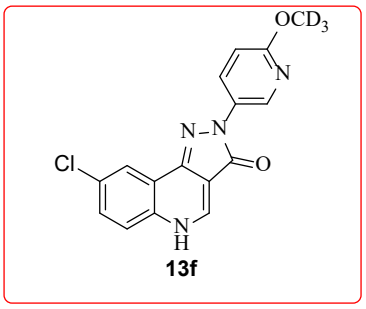

13f

Assay Protocol

Each evaluation included six independent assays carried out three at a time, on two different days

1. Preparation of solutions:
   a. 1 mM test compound in DMSO.
   b. 1 µM 4,5 Di Phenyl Imidazole in ice cold Acetonitrile (ISTD).
2. For a total volume of Microsomal Assay Mixture (MAM) 390 µL, sufficient for seven time points, combine the following
   a. 282 µL of 18.2 mΩ of water.
   b. 80 µL of 0.5 M potassium phosphate buffer (p^H 7.4)
   c. 20 µL of NADPH A. (Corning life sciences, Cat # 451220)
   d. 4 µL of NADPH B. (Corning life sciences, Cat # 451200)
   e. 4 µL of test compound.
3. Sonicate MAM for 5 min and meanwhile thaw microsomes (20 mg/mL) (Life technologies, Cat # MSMC-PL) on ice.
4. Aliquot 100 µL of ice cold ISTD into seven separate 1.5 mL conical vials and label them the time points for 0, 10, 20, 30, 40, 50, and 60 min.
5. Arrange the timer. Microsomes (Final concentration of 0.5 mg/mL) should be added to all time points except the zero time point.
6. Add 50 µL of the MAM solution to the conical vial labelled as zero time point. Place the remaining MAM solution in the incubator (37 ºC) for 5 min and initiate the reaction with addition of microsomes (8.8 µL) and record the time.
7. At the end of each time interval remove 50 µL and add to 100 µL ISTD in conical vial, sonicate for 10 sec and spin down at 10,000 rpm for 5 minutes.
8. Take 100 µL of supernatant and transfer to Spin-X HPLC filter tubes (Corning Incorporated, Cat # 8169) and centrifuge at 13,000 rpm for 5 minutes and take 5 µL from this solution and dilute in 495 µL of LCMS grade methanol (Fischer scientific, CAS # 67-56-1) in an 2mL glass auto sampler vial (Microsolv, Cat # 95025-WCV)
9. The samples are analyzed by LCMS-8040. (Shimadzu)

Data:

Day 1:

Time (min)	Assay 1		Assay 2		Assay 3		% remaining		
	DK-II-59-1 Peak area	ISTD Peak area	DK-II-59-1 Peak area	ISTD Peak area	DK-II-59-1 Peak area	ISTD Peak area	Assay 1	Assay 2	Assay 3
0	3434185	199292	3403798	199962	3467119	198537	100.00	100.00	100.00
10	3261135	192712	3308124	200914	3316748	193077	98.20	96.73	98.37
20	3277305	198836	3252309	201825	3294910	194431	95.65	94.66	97.04
30	3195052	200928	3204258	202859	3226537	202460	92.27	92.79	91.26
40	3116114	198399	3109879	202925	3283568	207620	91.14	90.03	90.56
50	3075182	199859	2943205	199172	3189757	206428	89.29	86.81	88.48
60	2962666	201067	2891865	203629	2942467	196355	85.50	83.43	85.81

Table 1: Peak areas and % remaining values

Day 2:

Time (min)	Assay 1		Assay 2		Assay 3		(% remaining)		
	DK-II-59-1 Peak area	ISTD Peak area	DK-II-59-1 Peak area	ISTD Peak area	DK-II-59-1 Peak area	ISTD Peak area	Assay 1	Assay 2	Assay 3
0	3272456	203581	3398083	203758	3394417	199950	100.00	100.00	100.00
10	3194621	200636	3224902	198751	3152045	190949	99.05	97.29	97.23
20	3118089	199275	3116033	200838	3175198	198429	97.34	93.03	94.26
30	3030724	196565	3012793	200320	3136068	198920	95.92	90.18	92.86
40	2867077	195909	2931859	199978	3054711	193801	91.04	87.91	92.84
50	2812061	200539	2890102	197907	2933773	200393	87.23	87.56	86.24
60	2718349	203636	2806729	199949	2908503	200605	83.04	84.17	85.40

Table 2: Peak areas and % remaining values

Calculation:

From the peak area, Calculate the following

$$\text{Peak area ratio} = \frac{\text{Peak area of test compound (DK-II-59-1)}}{\text{Peak area of internal standard (ISTD)}}$$

$$\text{\% remaining at time T} = \frac{\text{Peak area ratio at particular time T}}{\text{Peak area ratio at zero time point}} * 100$$

(T = 0, 10, 20,30,40,50 and 60)

DATA ANALYSIS:

Day 1

Linear regression analysis:

Slope: -0.002686 ± 0.0001145

At X= 60, Y = 4.448 ± 0.004129

R^2 = 0.9666

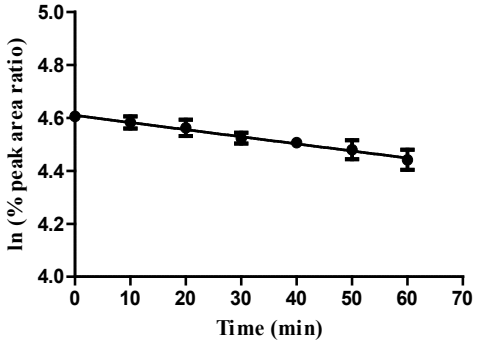

Metabolic Parameters:

Half-life: 258.004 ± 10.99 min

V_d: 100 µL/mg

Intrinsic clearance: 0.2686 µL/min/mg

Metabolic Rate: 5.372 nmol/min/mg

% remaining at 60 min: 85.45 ± 0.07 %

Day 2

Linear regression analysis:

Slope: -0.002849 ± 0.0001933

At X = 60, Y = 4.440 ± 0.006969

R^2 = 0.9196

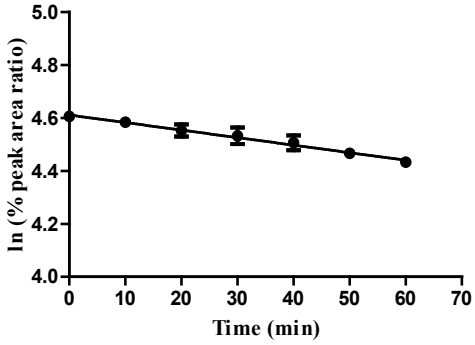

Metabolic Parameters:

Half-life: 243.24 ± 16.5 min

V_d: 100 µL/mg

Intrinsic clearance: 0.2849 µL/min/mg

Metabolic Rate: 5.698 nmol/min/mg

% remaining at 60 min: 84.77 ± 0.13 %

Note: The peak area ratios and natural log values are calculated using Microsoft excel 2010 and linear regression analysis is calculated using GraphPad prism.

Human Liver Microsomal Assay

Principal Investigator: Dr. Alexander Arnold
Operator: Revathi Kodali
Test Compound: **13g**
Concentration: 10 µM
Date: 05-26-2016
Facility: Milwaukee Institute for Drug Discovery

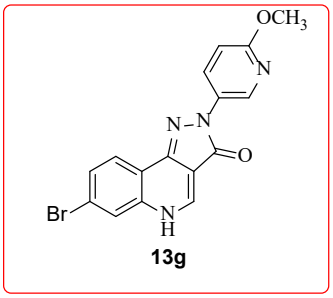

13g

Assay Protocol

Each evaluation included six independent assays carried out three at a time, on two different days

1. Preparation of solutions:
   a. 1 mM test compound in DMSO.
   b. 2 µM 4,5 Di Phenyl Imidazole in ice cold Acetonitrile (ISTD).
2. For a total volume of Microsomal Assay Mixture (MAM) 390 µL, sufficient for seven time points, combine the following
   a. 282 µL of 18.2 mΩ of water.
   b. 80 µL of 0.5 M potassium phosphate buffer (p^H 7.4)
   c. 20 µL of NADPH A. (Corning life sciences, Cat # 451220)
   d. 4 µL of NADPH B. (Corning life sciences, Cat # 451200)
   e. 4 µL of test compound.
3. Sonicate MAM for 5 min and meanwhile thaw microsomes (20 mg/mL) (BD Gentest, Cat # 452156) on ice.
4. Aliquot 100 µL of ice cold ISTD into seven separate 1.5 mL conical vials and label them the time points for 0, 10, 20, 30, 40, 50, and 60 min.
5. Arrange the timer. Microsomes (Final concentration of 0.5 mg/mL) should be added to all time points except the zero time point.
6. Add 50 µL of the MAM solution to the conical vial labelled as zero time point. Place the remaining MAM solution in the incubator (37 ºC) for 5 min and initiate the reaction with addition of microsomes (8.8 µL) and record the time.
7. At the end of each time interval remove 50 µL and add to 100 µL ISTD in conical vial, sonicate for 10 sec and spin down at 10,000 rpm for 5 minutes.
8. Take 100 µL of supernatant and transfer to Spin-X HPLC filter tubes (Corning Incorporated, Cat # 8169) and centrifuge at 13,000 rpm for 5 minutes and take 5 µL from this solution and dilute in 495 µL of LCMS grade methanol (Fischer scientific, CAS # 67-56-1) in an 2mL glass auto sampler vial (Microsolv, Cat # 95025-WCV)
9. The samples are analyzed by LCMS-8040. (Shimadzu)

Data:

Day 1:

Time (min)	Assay 1		Assay 2		Assay 3		% remaining		
	DK-II-48-1 Peak area	ISTD Peak area	DK-II-48-1 Peak area	ISTD Peak area	DK-II-48-1 Peak area	ISTD Peak area	Assay 1	Assay 2	Assay 3
0	1239575	409876	1282331	408077	1272732	424404	100.00	100.01	99.99
10	1272583	421502	1278046	415028	1275562	432495	99.84	98.00	98.34
20	1254337	431729	1305269	428021	1229879	422496	96.07	97.05	97.06
30	1221632	426097	1270878	425579	1208114	431322	94.80	95.04	93.39
40	1213285	426869	1251740	426921	1237850	438598	93.99	93.31	94.10
50	1206569	425741	1245491	420860	1245919	441826	93.71	94.18	94.02
60	1193565	413673	1243063	414198	1229125	429212	95.41	95.51	95.48

Table 1: Peak areas and % remaining values

Day 2:

Time (min)	Assay 1		Assay 2		Assay 3		(% remaining)		
	DK-II-48-1 Peak area	ISTD Peak area	DK-II-48-1 Peak area	ISTD Peak area	DK-II-48-1 Peak area	ISTD Peak area	Assay 1	Assay 2	Assay 3
0	1370833	444955	1198733	408906	1220048	417681	99.99	99.98	100.00
10	1328181	436723	1164859	407987	1222948	422920	98.71	97.37	98.99
20	1336173	447939	1160980	415555	1180805	419134	96.81	95.28	96.44
30	1288471	435125	1118801	402193	1145140	415499	96.11	94.87	94.35
40	1303844	448160	1129419	413993	1175925	416876	94.42	93.04	96.57
50	1310818	441914	1141621	409483	1163535	424257	96.27	95.08	93.89
60	1272477	436169	1153092	414963	1182693	435717	94.69	94.77	92.92

Table 2: Peak areas and % remaining values

Calculation:

From the peak area, Calculate the following

$$\text{Peak area ratio} = \frac{\text{Peak area of test compound (DK-II-48-1)}}{\text{Peak area of internal standard (ISTD)}}$$

$$\text{\% remaining at time T} = \frac{\text{Peak area ratio at particular time T}}{\text{Peak area ratio at zero time point}} * 100$$

(T = 0, 10, 20,30,40,50 and 60)

DATA ANALYSIS:

Day 1

Linear regression analysis:

Slope: -0.0009583 ± 0.0001613

At X= 60, Y = 4.537 ± 0.005817

R^2 = 0.6500

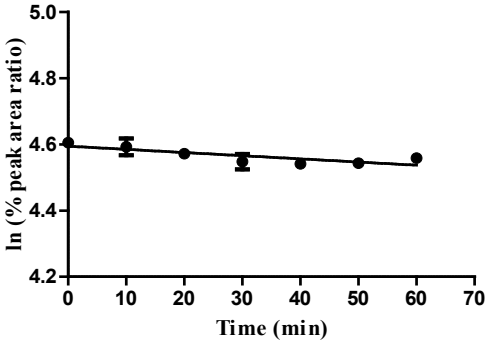

Metabolic Parameters:

Half-life: 723.15 ± 121 min

V_d: 100 µL/mg

Intrinsic clearance: 0.09583 µL/min/mg

Metabolic Rate: 1.9166 nmol/min/mg

% remaining at 60 min: 93.41 ± 0.12%

Day 2

Linear regression analysis:

Slope: -0.0009464 ± 0.0001399

At X = 60, Y = 4.538 ± 0.005045

R^2 = 0.7066

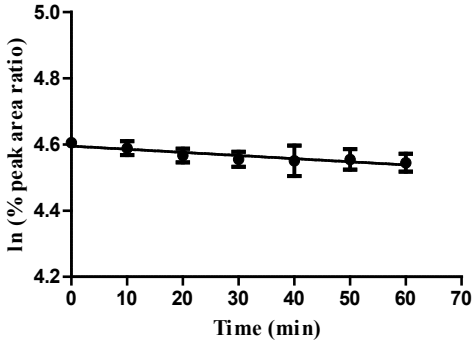

Metabolic Parameters:

Half-life: 732.24 ± 108.2 min

V_d: 100 µL/mg

Intrinsic clearance: 0.09464 µL/min/mg

Metabolic Rate: 1.8928 nmol/min/mg

% remaining at 60 min: 93.5 ± 0.10 %

Note: The peak area ratios and natural log values are calculated using Microsoft excel 2010 and linear regression analysis is calculated using GraphPad prism.

Mouse Liver Microsomal Assay

Principal Investigator: Dr. Alexander Arnold
Operator: Revathi Kodali
Test Compound: **13g**
Concentration: 10 µM
Date: 05-26-2016
Facility: Milwaukee Institute for Drug Discovery

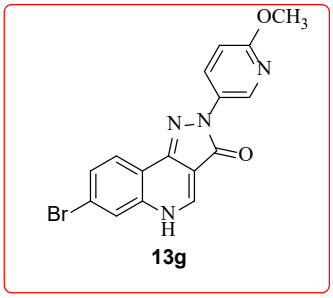

13g

Assay Protocol

Each evaluation included six independent assays carried out three at a time, on two different days

1. Preparation of solutions:
   a. 1 mM test compound in DMSO.
   b. 2 µM 4,5 Di Phenyl Imidazole in ice cold Acetonitrile (ISTD).
2. For a total volume of Microsomal Assay Mixture (MAM) 390 µL, sufficient for seven time points, combine the following
   a. 282 µL of 18.2 mΩ of water.
   b. 80 µL of 0.5 M potassium phosphate buffer (p^H 7.4)
   c. 20 µL of NADPH A. (Corning life sciences, Cat # 451220)
   d. 4 µL of NADPH B. (Corning life sciences, Cat # 451200)
   e. 4 µL of test compound.
3. Sonicate MAM for 5 min and meanwhile thaw microsomes (20 mg/mL) (Life technologies, Cat # MSMC-PL) on ice.
4. Aliquot 100 µL of ice cold ISTD into seven separate 1.5 mL conical vials and label them the time points for 0, 10, 20, 30, 40, 50, and 60 min.
5. Arrange the timer. Microsomes (Final concentration of 0.5 mg/mL) should be added to all time points except the zero time point.
6. Add 50 µL of the MAM solution to the conical vial labelled as zero time point. Place the remaining MAM solution in the incubator (37 ºC) for 5 min and initiate the reaction with addition of microsomes (8.8 µL) and record the time.
7. At the end of each time interval remove 50 µL and add to 100 µL ISTD in conical vial, sonicate for 10 sec and spin down at 10,000 rpm for 5 minutes.
8. Take 100 µL of supernatant and transfer to Spin-X HPLC filter tubes (Corning Incorporated, Cat # 8169) and centrifuge at 13,000 rpm for 5 minutes and take 5 µL from this solution and dilute in 495 µL of LCMS grade methanol (Fischer scientific, CAS # 67-56-1) in an 2mL glass auto sampler vial (Microsolv, Cat # 95025-WCV)
9. The samples are analyzed by LCMS-8040. (Shimadzu)

Data:

Day 1:

Time (min)	Assay 1		Assay 2		Assay 3		% remaining		
	DK-II-48-1 Peak area	ISTD Peak area	DK-II-48-1 Peak area	ISTD Peak area	DK-II-48-1 Peak area	ISTD Peak area	Assay 1	Assay 2	Assay 3
0	1285705	419827	1242554	422780	1356651	447903	100.01	100.00	99.99
10	1284540	435905	1313352	447517	1327774	441532	96.23	99.85	99.28
20	1292275	437096	1264515	444110	1274051	435877	96.55	96.88	96.49
30	1287912	429522	1236947	446158	1274901	437129	97.92	94.33	96.28
40	1254958	444035	1226739	439257	1271572	442179	92.30	95.02	94.93
50	1237554	436140	1245217	450546	1280902	443536	92.66	94.03	95.34
60	1254241	438615	1282355	457098	1250474	439668	93.38	95.45	93.89

Table 1: Peak areas and % remaining values

Day 2:

Time (min)	Assay 1		Assay 2		Assay 3		(% remaining)		
	DK-II-48-1 Peak area	ISTD Peak area	DK-II-48-1 Peak area	ISTD Peak area	DK-II-48-1 Peak area	ISTD Peak area	Assay 1	Assay 2	Assay 3
0	1307622	464746	1292157	462060	1295383	483598	99.98	99.98	99.98
10	1286526	464981	1272404	460828	1283952	495797	98.32	98.71	96.66
20	1243863	463202	1260023	460005	1173740	463148	95.42	97.93	94.59
30	1227268	468808	1222300	454360	1178574	460559	93.02	96.18	95.52
40	1232887	472905	1269061	482260	1113808	448574	92.64	94.08	92.68
50	1293819	482688	1280879	488503	1177897	471287	95.25	93.74	93.29
60	1236291	469676	1283362	474787	1150736	458568	93.54	96.64	93.67

Table 2: Peak areas and % remaining values

Calculation:

From the peak area, Calculate the following

$$\text{Peak area ratio} = \frac{\text{Peak area of test compound (DK-II-48-1)}}{\text{Peak area of internal standard (ISTD)}}$$

$$\text{\% remaining at time T} = \frac{\text{Peak area ratio at particular time T}}{\text{Peak area ratio at zero time point}} * 100$$

(T = 0, 10, 20,30,40,50 and 60)

DATA ANALYSIS:

Day 1

Linear regression analysis:

Slope: -0.001060 ± 0.0001535

At X= 60, Y = 4.535 ± 0.005534

R^2 = 0.7150

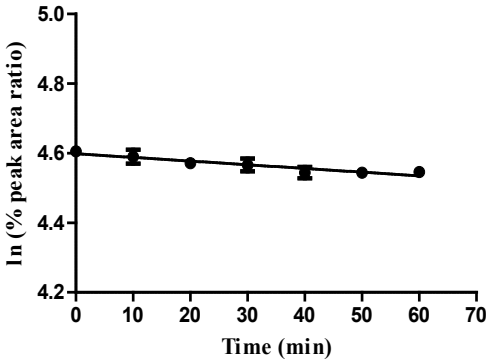

Metabolic Parameters:

Half-life: 653.15 ± 94.58 min

V_d: 100 µL/mg

Intrinsic clearance: 0.1061 µL/min/mg

Metabolic Rate: 2.122 nmol/min/mg

% remaining at 60 min: 93.22 ± 0.11%

Day 2

Linear regression analysis:

Slope: -0.0009786 ± 0.0001849

At X = 60, Y = 4.533 ± 0.006666

R^2 = 0.5959

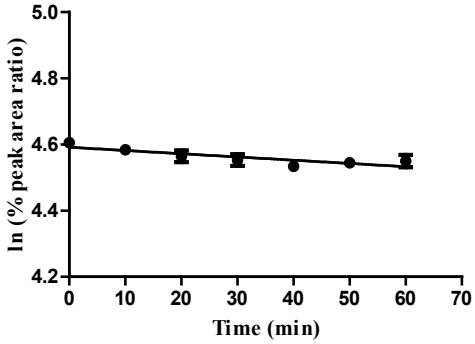

Metabolic Parameters:

Half-life: 708.15 ± 133.8 min

V_d: 100 µL/mg

Intrinsic clearance: 0.09786 µL/min/mg

Metabolic Rate: 1.9572 nmol/min/mg

% remaining at 60 min: 93.03 ± 0.13 %

Note: The peak area ratios and natural log values are calculated using Microsoft excel 2010 and linear regression analysis is calculated using GraphPad prism.

Human Liver Microsomal Assay

Principal Investigator: Dr. Alexander Arnold
Operator: Revathi Kodali
Test Compound: **13h**
Concentration: 10 µM
Date: 05-26-2016
Facility: Milwaukee Institute for Drug Discovery

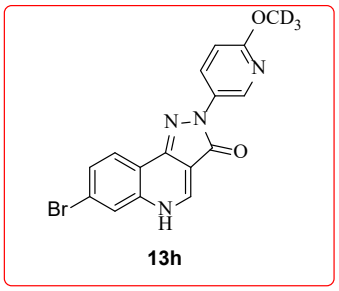

13h

Assay Protocol

Each evaluation included six independent assays carried out three at a time, on two different days

1. Preparation of solutions:
   a. 1 mM test compound in DMSO.
   b. 1 µM 4,5 Di Phenyl Imidazole in ice cold Acetonitrile (ISTD).
2. For a total volume of Microsomal Assay Mixture (MAM) 390 µL, sufficient for seven time points, combine the following
   a. 282 µL of 18.2 mΩ of water.
   b. 80 µL of 0.5 M potassium phosphate buffer (p^H 7.4)
   c. 20 µL of NADPH A. (Corning life sciences, Cat # 451220)
   d. 4 µL of NADPH B. (Corning life sciences, Cat # 451200)
   e. 4 µL of test compound.
3. Sonicate MAM for 5 min and meanwhile thaw microsomes (20 mg/mL) (BD Gentest, Cat # 452156) on ice.
4. Aliquot 100 µL of ice cold ISTD into seven separate 1.5 mL conical vials and label them the time points for 0, 10, 20, 30, 40, 50, and 60 min.
5. Arrange the timer. Microsomes (Final concentration of 0.5 mg/mL) should be added to all time points except the zero time point.
6. Add 50 µL of the MAM solution to the conical vial labelled as zero time point. Place the remaining MAM solution in the incubator (37 ºC) for 5 min and initiate the reaction with addition of microsomes (8.8 µL) and record the time.
7. At the end of each time interval remove 50 µL and add to 100 µL ISTD in conical vial, sonicate for 10 sec and spin down at 10,000 rpm for 5 minutes.
8. Take 100 µL of supernatant and transfer to Spin-X HPLC filter tubes (Corning Incorporated, Cat # 8169) and centrifuge at 13,000 rpm for 5 minutes and take 5 µL from this solution and dilute in 495 µL of LCMS grade methanol (Fischer scientific, CAS # 67-56-1) in an 2mL glass auto sampler vial (Microsolv, Cat # 95025-WCV)
9. The samples are analyzed by LCMS-8040. (Shimadzu)

Data:

Day 1:

Time (min)	Assay 1		Assay 2		Assay 3		% remaining		
	DK-II-58-1 Peak area	ISTD Peak area	DK-II-58-1 Peak area	ISTD Peak area	DK-II-58-1 Peak area	ISTD Peak area	Assay 1	Assay 2	Assay 3
0	1421837	1942342	1419848	1962134	1417715	1912342	100.00	99.94	100.04
10	1380499	1892342	1403676	1955231	1459331	1961234	99.66	99.15	100.41
20	1378668	1912344	1392460	1942316	1386585	1891234	98.48	99.02	98.94
30	1368091	1923804	1423956	2000134	1363567	1886236	97.15	98.33	97.55
40	1380251	1923424	1423495	2012342	1449749	1978234	98.03	97.70	98.90
50	1411529	1979443	1414892	1965474	1408869	1933454	97.41	99.43	98.33
60	1423608	1983905	1398364	1962344	1456496	1991273	98.03	98.42	98.71

Table 1: Peak areas and % remaining values

Day 2:

Time (min)	Assay 1		Assay 2		Assay 3		(% remaining)		
	DK-II-58-1 Peak area	ISTD Peak area	DK-II-58-1 Peak area	ISTD Peak area	DK-II-58-1 Peak area	ISTD Peak area	Assay 1	Assay 2	Assay 3
0	1508498	2008329	1480681	1967456	1471597	1992344	100.01	99.94	99.94
10	1441371	1924324	1470155	1963452	1457755	2000126	99.73	99.43	98.62
20	1435215	1934535	1458718	1949042	1405631	1922344	98.78	99.39	98.94
30	1424084	1899991	1437127	1943214	1402880	1931234	99.80	98.21	98.29
40	1421610	1923434	1440579	1949987	1412381	1943244	98.41	98.10	98.35
50	1418164	1889474	1423051	1934324	1427904	2000688	99.94	97.70	96.57
60	1410739	1934543	1429296	1923444	1416949	1934324	97.10	98.68	99.12

Table 2: Peak areas and % remaining values

Calculation:

From the peak area, Calculate the following

$$\text{Peak area ratio} = \frac{\text{Peak area of test compound (DK-II-58-1)}}{\text{Peak area of internal standard (ISTD)}}$$

$$\text{\% remaining at time T} = \frac{\text{Peak area ratio at particular time T}}{\text{Peak area ratio at zero time point}} * 100$$

(T = 0, 10, 20,30,40,50 and 60)

DATA ANALYSIS:

Day 1

Linear regression analysis:

Slope: -0.0003012 ± 8.169e^{-005}

At X= 60, Y = 4.583 ± 0.002945

R^2 = 0.4171

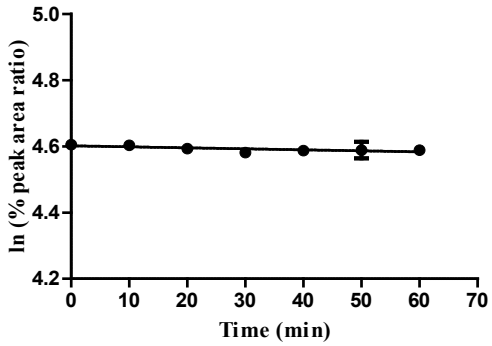

Metabolic Parameters:

Half-life: 2300.8 min

V_d: 100 µL/mg

Intrinsic clearance: 0.03012 µL/min/mg

Metabolic Rate: 0.6024 nmol/min/mg

% remaining at 60 min: 97.80 ± 0.06 %

Day 2

Linear regression analysis:

Slope: -0.0002976 ± 8.722e^{-005}

At X = 60, Y = 4.584 ± 0.003145

R^2 = 0.3799

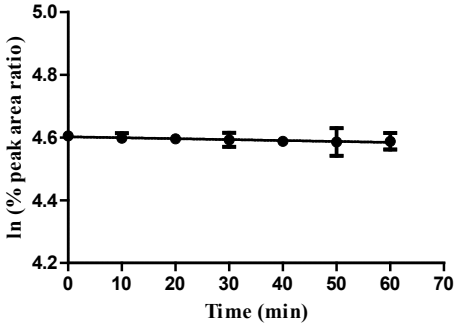

Metabolic Parameters:

Half-life: 2328.6 min

V_d: 100 µL/mg

Intrinsic clearance: 0.02976 µL/min/mg

Metabolic Rate: 0.5952 nmol/min/mg

% remaining at 60 min: 97.90 ± 0.06 %

Note: The peak area ratios and natural log values are calculated using Microsoft excel 2010 and linear regression analysis is calculated using GraphPad prism.

Mouse Liver Microsomal Assay

Principal Investigator: Dr. Alexander Arnold
Operator: Revathi Kodali
Test Compound: **13h**
Concentration: 10 µM
Date: 05-26-2016
Facility: Milwaukee Institute for Drug Discovery

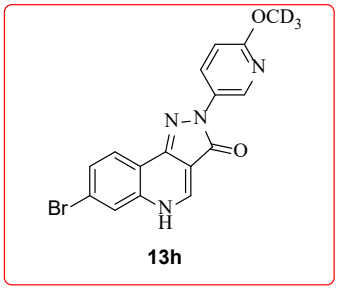

13h

Assay Protocol

Each evaluation included six independent assays carried out three at a time, on two different days

1. Preparation of solutions:
   a. 1 mM test compound in DMSO.
   b. 1 µM 4,5 Di Phenyl Imidazole in ice cold Acetonitrile (ISTD).
2. For a total volume of Microsomal Assay Mixture (MAM) 390 µL, sufficient for seven time points, combine the following
   a. 282 µL of 18.2 mΩ of water.
   b. 80 µL of 0.5 M potassium phosphate buffer (p^H 7.4)
   c. 20 µL of NADPH A. (Corning life sciences, Cat # 451220)
   d. 4 µL of NADPH B. (Corning life sciences, Cat # 451200)
   e. 4 µL of test compound.
3. Sonicate MAM for 5 min and meanwhile thaw microsomes (20 mg/mL) (Life technologies, Cat # 452156) on ice.
4. Aliquot 100 µL of ice cold ISTD into seven separate 1.5 mL conical vials and label them the time points for 0, 10, 20, 30, 40, 50, and 60 min.
5. Arrange the timer. Microsomes (Final concentration of 0.5 mg/mL) should be added to all time points except the zero time point.
6. Add 50 µL of the MAM solution to the conical vial labelled as zero time point. Place the remaining MAM solution in the incubator (37 ºC) for 5 min and initiate the reaction with addition of microsomes (8.8 µL) and record the time.
7. At the end of each time interval remove 50 µL and add to 100 µL ISTD in conical vial, sonicate for 10 sec and spin down at 10,000 rpm for 5 minutes.
8. Take 100 µL of supernatant and transfer to Spin-X HPLC filter tubes (Corning Incorporated, Cat # 8169) and centrifuge at 13,000 rpm for 5 minutes and take 5 µL from this solution and dilute in 495 µL of LCMS grade methanol (Fischer scientific, CAS # 67-56-1) in an 2mL glass auto sampler vial (Microsolv, Cat # 95025-WCV)
9. The samples are analyzed by LCMS-8040. (Shimadzu)

Data:

Day 1:

Time (min)	Assay 1		Assay 2		Assay 3		% remaining		
	DK-II-58-1 Peak area	ISTD Peak area	DK-II-58-1 Peak area	ISTD Peak area	DK-II-58-1 Peak area	ISTD Peak area	Assay 1	Assay 2	Assay 3
0	1435197	1954234	1423673	1973613	1424627	1943243	100.05	100.04	100.01
10	1443000	2001324	1412024	2000234	1404550	1928213	98.23	97.91	99.37
20	1409619	1932414	1417757	2003412	1435097	2000123	99.38	98.15	97.88
30	1386905	1910094	1380284	1956728	1427626	1971422	98.92	97.83	98.79
40	1388622	1952344	1392320	1931324	1413076	1935162	96.90	99.98	99.61
50	1415644	1952344	1365942	1924234	1407763	1942342	98.78	98.45	98.87
60	1400478	1928631	1362173	1934144	1405660	1962361	98.93	97.68	97.72

Table 1: Peak areas and % remaining values

Day 2:

Time (min)	Assay 1		Assay 2		Assay 3		(% remaining)		
	DK-II-58-1 Peak area	ISTD Peak area	DK-II-58-1 Peak area	ISTD Peak area	DK-II-58-1 Peak area	ISTD Peak area	Assay 1	Assay 2	Assay 3
0	1415534	1978364	1437757	2000783	1431126	1978362	99.93	99.94	100.05
10	1406743	1997364	1404661	1958912	1415235	1967532	98.36	99.73	99.48
20	1412266	1989874	1401648	1989783	1416480	2000732	99.12	97.97	97.92
30	1352676	1897634	1408788	1967562	1400171	1967623	99.55	99.58	98.42
40	1407009	1974777	1391135	1940782	1423223	1996723	99.51	99.69	98.58
50	1378771	1962365	1390888	1963265	1395581	1965356	98.12	98.53	98.21
60	1421844	2000837	1403716	1987673	1412645	1967236	99.24	98.22	99.32

Table 2: Peak areas and % remaining values

Calculation:

From the peak area, Calculate the following

$$\text{Peak area ratio} = \frac{\text{Peak area of test compound (DK-II-58-1)}}{\text{Peak area of internal standard (ISTD)}}$$

$$\text{\% remaining at time T} = \frac{\text{Peak area ratio at particular time T}}{\text{Peak area ratio at zero time point}} * 100$$

(T = 0, 10, 20,30,40,50 and 60)

DATA ANALYSIS:

Day 1

Linear regression analysis:

Slope: -0.0001821 ± 9.454e^{-005}

At X= 60, Y = 4.587 ± 0.003409

R^2 = 0.1634

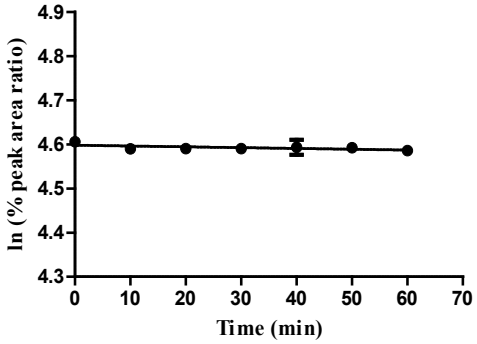

Metabolic Parameters:

Half-life: 3805.6 min

V_d: 100 µL/mg

Intrinsic clearance: 0.01821 µL/min/mg

Metabolic Rate: 0.3642 nmol/min/mg

% remaining at 60 min: 98.19 ± 0.07 %

Day 2

Linear regression analysis:

Slope: -0.0001476 ± 7.506e^{-005}

At X = 60, Y = 4.591 ± 0.002706

R^2 = 0.1691

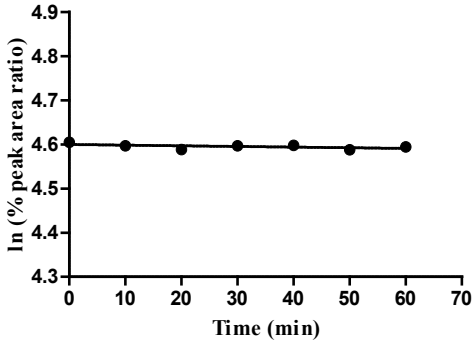

Metabolic Parameters:

Half-life: 4695.12 min

V_d: 100 µL/mg

Intrinsic clearance: 0.01476 µL/min/mg

Metabolic Rate: 0.2952 nmol/min/mg

% remaining at 60 min: 98.59 ± 0.05 %

Note: The peak area ratios and natural log values are calculated using Microsoft excel 2010 and linear regression analysis is calculated using GraphPad prism.

Human Liver Microsomal Assay

Principal Investigator: Dr. Alexander Arnold
Operator: Revathi Kodali
Test Compound: **13i**
Concentration: 10 µM
Date: 12-18-2017
Facility: Milwaukee Institute for Drug Discovery

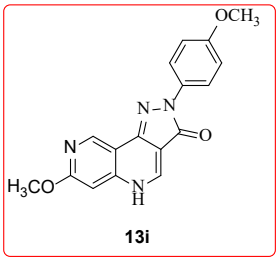

13i

Assay Protocol

Each evaluation included six independent assays carried out three at a time, on two different days

10. Preparation of solutions:
    c. 1 mM test compound in DMSO.
    d. 1 µM 4,5 Di Phenyl Imidazole in ice cold Acetonitrile (ISTD).
11. For a total volume of Microsomal Assay Mixture (MAM) 390 µL, sufficient for seven time points, combine the following
    f. 282 µL of 18.2 mΩ of water.
    g. 80 µL of 0.5 M potassium phosphate buffer (p^H 7.4)
    h. 20 µL of NADPH A. (Corning life sciences, Cat # 451220)
    i. 4 µL of NADPH B. (Corning life sciences, Cat # 451200)
    j. 4 µL of test compound.
12. Sonicate MAM for 5 min and meanwhile thaw microsomes (20 mg/mL) (BD Biosciences, Cat # 452156) on ice.
13. Aliquot 100 µL of ice cold ISTD into seven separate 1.5 mL conical vials and label them the time points for 0, 10, 20, 30, 40, 50, and 60 min.
14. Arrange the timer. Microsomes (Final concentration of 0.5 mg/mL) should be added to all time points except the zero time point.
15. Add 50 µL of the MAM solution to the conical vial labelled as zero time point. Place the remaining MAM solution in the incubator (37 ºC) for 5 min and initiate the reaction with addition of microsomes (8.8 µL) and record the time.
16. At the end of each time interval remove 50 µL and add to 100 µL ISTD in conical vial, sonicate for 10 sec and spin down at 10,000 rpm for 5 minutes.
17. Take 100 µL of supernatant and transfer to Spin-X HPLC filter tubes (Corning Incorporated, Cat # 8169) and centrifuge at 13,000 rpm for 5 minutes and take 5 µL from this solution and dilute in 495 µL of LCMS grade methanol (Fischer scientific, CAS # 67-56-1) in an 2mL glass auto sampler vial (Microsolv, Cat # 95025-WCV)
18. The samples are analyzed by LCMS-8040. (Shimadzu)

Data:

Day 1:

Time (min)	Assay 1		Assay 2		Assay 3		% remaining		
	CW03-030 Peak area	ISTD Peak area	CW03-030 Peak area	ISTD Peak area	CW03-030 Peak area	ISTD Peak area	Assay 1	Assay 2	Assay 3
0	54463	122039	59964	120743	51713	120553	100.06	99.92	99.99
10	53675	119669	57444	119934	49323	119380	100.57	96.37	96.30
20	49025	118364	54634	120220	48219	119071	92.87	91.43	94.39
30	50811	120347	54972	119244	50374	122775	94.66	92.75	95.64
40	50209	117947	55783	118776	47867	119489	95.44	94.49	93.37
50	51373	119429	54310	120015	48485	120371	96.44	91.05	93.89
60	50053	121245	54343	117623	50031	119252	92.56	92.96	97.79

Table 1: Peak areas and % remaining values

Day 2:

Time (min)	Assay 1		Assay 2		Assay 3		(% remaining)		
	CW03-030 Peak area	ISTD Peak area	CW03-030 Peak area	ISTD Peak area	CW03-030 Peak area	ISTD Peak area	Assay 1	Assay 2	Assay 3
0	52360	118118	57747	120217	50843	121863	100.06	100.07	100.05
10	52744	120519	54744	118523	49417	118623	98.79	96.22	99.90
20	50870	122550	54007	118470	48444	120175	93.70	94.97	96.67
30	51424	121231	52223	120610	47045	123076	95.75	90.20	91.66
40	50503	124126	53668	119522	46736	120907	91.84	93.54	92.69
50	49277	118289	52233	117465	46091	121033	94.03	92.63	91.32
60	47525	116313	52483	119375	44808	119405	92.23	91.59	89.99

Table 2: Peak areas and % remaining values

Calculation:

From the peak area, Calculate the following

$$\text{Peak area ratio} = \frac{\text{Peak area of test compound (CW-03-030)}}{\text{Peak area of internal standard (ISTD)}}$$

$$\text{\% remaining at time T} = \frac{\text{Peak area ratio at particular time T}}{\text{Peak area ratio at zero time point}} * 100$$

(T = 0, 10, 20,30,40,50 and 60)

DATA ANALYSIS:

Day 1

Linear regression analysis:

Slope: -0.0008524 ± 0.0002775

At X= 60, Y = 4.532 ± 0.01001

R^2 = 0.3318

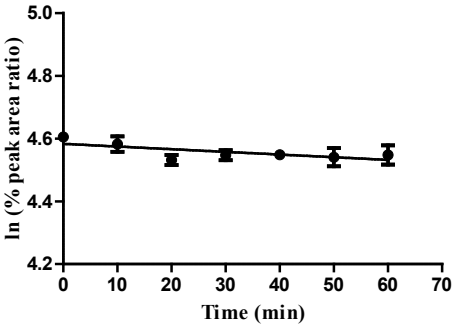

Metabolic Parameters:

Half-life: 813 ± 265 min

V_d: 100 µL/mg

Intrinsic clearance: 0.08524 µL/min/mg

Metabolic Rate: 1.7048 nmol/min/mg

% remaining at 60 min: 93 ± 0.2 %

Day 2

Linear regression analysis:

Slope: -0.001504 ± 0.0002098

At X = 60, Y = 4.505 ± 0.007563

R^2 = 0.7300

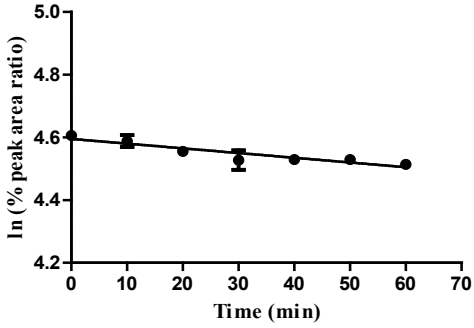

Metabolic Parameters:

Half-life:460 ± 64 min

V_d: 100 µL/mg

Intrinsic clearance: 0.1504 µL/min/mg

Metabolic Rate: 3.008 nmol/min/mg

% remaining at 60 min: 90 ± 0.15 %

Note: The peak area ratios and natural log values are calculated using Microsoft excel 2010 and linear regression analysis is calculated using GraphPad prism.

Mouse Liver Microsomal Assay

Principal Investigator: Dr. Alexander Arnold
Operator: Revathi Kodali
Test Compound: **13i**
Concentration: 10 µM
Date: 12-18-2017
Facility: Milwaukee Institute for Drug Discovery

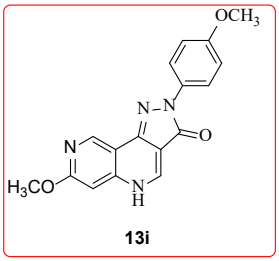

13i

Assay Protocol

Each evaluation included six independent assays carried out three at a time, on two different days

19. Preparation of solutions:
    e. 1 mM test compound in DMSO.
    f. 1 µM 4,5 Di Phenyl Imidazole in ice cold Acetonitrile (ISTD).
20. For a total volume of Microsomal Assay Mixture (MAM) 390 µL, sufficient for seven time points, combine the following
    k. 282 µL of 18.2 mΩ of water.
    l. 80 µL of 0.5 M potassium phosphate buffer (p^H 7.4)
    m. 20 µL of NADPH A. (Corning life sciences, Cat # 451220)
    n. 4 µL of NADPH B. (Corning life sciences, Cat # 451200)
    o. 4 µL of test compound.
21. Sonicate MAM for 5 min and meanwhile thaw microsomes (20 mg/mL) (Life technologies, Cat # MSMC-PL) on ice.
22. Aliquot 100 µL of ice cold ISTD into seven separate 1.5 mL conical vials and label them the time points for 0, 10, 20, 30, 40, 50, and 60 min.
23. Arrange the timer. Microsomes (Final concentration of 0.5 mg/mL) should be added to all time points except the zero time point.
24. Add 50 µL of the MAM solution to the conical vial labelled as zero time point. Place the remaining MAM solution in the incubator (37 ºC) for 5 min and initiate the reaction with addition of microsomes (8.8 µL) and record the time.
25. At the end of each time interval remove 50 µL and add to 100 µL ISTD in conical vial, sonicate for 10 sec and spin down at 10,000 rpm for 5 minutes.
26. Take 100 µL of supernatant and transfer to Spin-X HPLC filter tubes (Corning Incorporated, Cat # 8169) and centrifuge at 13,000 rpm for 5 minutes and take 5 µL from this solution and dilute in 495 µL of LCMS grade methanol (Fischer scientific, CAS # 67-56-1) in an 2mL glass auto sampler vial (Microsolv, Cat # 95025-WCV)
27. The samples are analyzed by LCMS-8040. (Shimadzu)

Data:

Day 1:

Time (min)	Assay 1		Assay 2		Assay 3		% remaining		
	CW03-030 Peak area	ISTD Peak area	CW03-030 Peak area	ISTD Peak area	CW03-030 Peak area	ISTD Peak area	Assay 1	Assay 2	Assay 3
0	54849	123424	56485	120211	55454	121817	100.08	99.97	100.04
10	54555	123689	54728	119879	54672	121646	99.33	97.13	98.77
20	51623	120410	52185	121097	53823	119279	96.56	91.68	99.17
30	50768	119304	53305	121049	50484	120090	95.84	93.69	92.39
40	51926	118435	51176	118460	53462	118334	98.74	91.91	99.29
50	53303	120736	51554	120332	51049	117545	99.43	91.15	95.44
60	50830	121128	50523	119293	50781	120366	94.51	90.11	92.72

Table 1: Peak areas and % remaining values

Day 2:

Time (min)	Assay 1		Assay 2		Assay 3		(% remaining)		
	CW03-030 Peak area	ISTD Peak area	CW03-030 Peak area	ISTD Peak area	CW03-030 Peak area	ISTD Peak area	Assay 1	Assay 2	Assay 3
0	53258	119305	56261	121550	57983	118109	100.09	99.97	99.98
10	52592	121231	53815	120470	53196	119751	97.26	96.48	90.47
20	51090	118281	52692	118234	54834	120263	96.84	96.25	92.86
30	51137	123924	51407	120551	52352	117266	92.52	92.10	90.92
40	52069	118562	51496	117290	55905	120825	98.46	94.82	94.23
50	50529	120743	52890	119520	53056	113142	93.83	95.57	95.50
60	47670	119553	51690	121416	54464	118362	89.40	91.95	93.71

Table 2: Peak areas and % remaining values

Calculation:

From the peak area, Calculate the following

$$\text{Peak area ratio} = \frac{\text{Peak area of test compound (CW-03-030)}}{\text{Peak area of internal standard (ISTD)}}$$

$$\text{\% remaining at time T} = \frac{\text{Peak area ratio at particular time T}}{\text{Peak area ratio at zero time point}} * 100$$

(T = 0, 10, 20,30,40,50 and 60)

DATA ANALYSIS:

Day 1

Linear regression analysis:

Slope: -0.001045 ± 0.0003219

At X= 60, Y = 4.534 ± 0.01161

R^2 = 0.3569

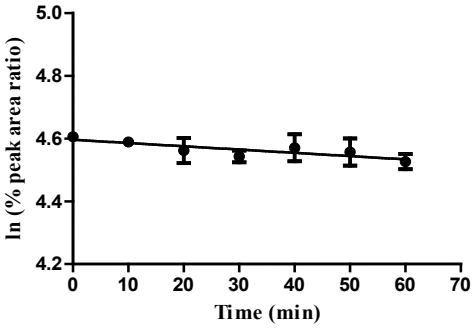

Metabolic Parameters:

Half-life: 663 ± 204 min

V_d: 100 µL/mg

Intrinsic clearance: 0.1045 µL/min/mg

Metabolic Rate: 2.09 nmol/min/mg

% remaining at 60 min: 93 ± 0.25 %

Day 2

Linear regression analysis:

Slope: -0.0008940 ± 0.0003124

At X = 60, Y = 4.526 ± 0.001126

R^2 = 0.3012

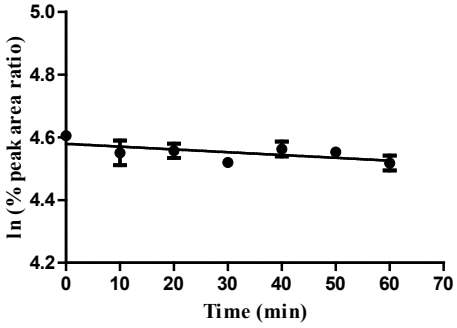

Metabolic Parameters:

Half-life:775 ± 270 min

V_d: 100 µL/mg

Intrinsic clearance: 0.0894 µL/min/mg

Metabolic Rate: 1.788 nmol/min/mg

% remaining at 60 min: 92 ± 0.3 %

Note: The peak area ratios and natural log values are calculated using Microsoft excel 2010 and linear regression analysis is calculated using GraphPad prism.

Human Liver Microsomal Assay

Principal Investigator: Dr. Alexander Arnold
Operator: Revathi Kodali
Test Compound: CW-02-82
Concentration: 10 µM
Date: 11-28-2018
Facility: Milwaukee Institute for Drug Discovery

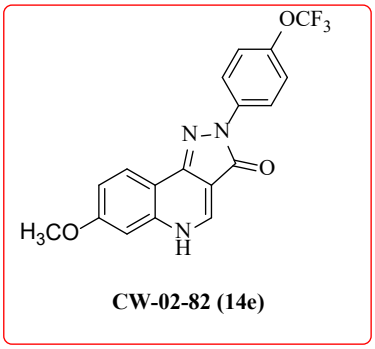

CW-02-82 (14e)

Assay Protocol

Each evaluation included six independent assays carried out three at a time, on two different days

1. Preparation of solutions:
   a. 1 mM test compound in DMSO.
   b. 1 µM 4,5 Di Phenyl Imidazole in ice cold Acetonitrile (ISTD).
2. For a total volume of Microsomal Assay Mixture (MAM) 390 µL, sufficient for seven time points, combine the following
   a. 282 µL of 18.2 mΩ of water.
   b. 80 µL of 0.5 M potassium phosphate buffer (p^H 7.4)
   c. 20 µL of NADPH A. (Corning life sciences, Cat # 451220)
   d. 4 µL of NADPH B. (Corning life sciences, Cat # 451200)
   e. 4 µL of test compound.
3. Sonicate MAM for 5 min and meanwhile thaw microsomes (20 mg/mL) (BD Gentest, Cat # 452156) on ice.
4. Aliquot 100 µL of ice cold ISTD into seven separate 1.5 mL conical vials and label them the time points for 0, 10, 20, 30, 40, 50, and 60 min.
5. Arrange the timer. Microsomes (Final concentration of 0.5 mg/mL) should be added to all time points except the zero time point.
6. Add 50 µL of the MAM solution to the conical vial labelled as zero time point. Place the remaining MAM solution in the incubator (37 ºC) for 5 min and initiate the reaction with addition of microsomes (8.8 µL) and record the time.
7. At the end of each time interval remove 50 µL and add to 100 µL ISTD in conical vial, sonicate for 10 sec and spin down at 10,000 rpm for 5 minutes.
8. Take 100 µL of supernatant and transfer to Spin-X HPLC filter tubes (Corning Incorporated, Cat # 8169) and centrifuge at 13,000 rpm for 5 minutes and take 5 µL from this solution and dilute in 495 µL of LCMS grade methanol (Fischer scientific, CAS # 67-56-1) in an 2mL glass auto sampler vial (Microsolv, Cat # 95025-WCV)
9. The samples are analyzed by LCMS-8040. (Shimadzu)

Data:

Day 1:

Time (min)	Assay 1		Assay 2		Assay 3		% remaining		
	CW-02-82 Peak area	ISTD Peak area	CW-02-82 Peak area	ISTD Peak area	CW-02-82 Peak area	ISTD Peak area	Assay 1	Assay 2	Assay 3
0	286942	1312434	277302	1213625	281715	1321242	99.833	100.21	100.10
10	279988	1404355	265729	1238294	239331	1201234	91.037	94.12	93.53
20	267136	1349110	308876	1410732	206585	1101234	90.415	96.03	88.07
30	224857	1200691	279787	1359329	223735	1240209	85.513	90.275	84.69
40	239756	1321131	226797	1118415	236833	1326156	82.867	88.94	83.84
50	203333	1123914	201981	1043788	221223	1295040	82.610	84.87	80.19
60	190757	1111989	271951	1478221	263168	1478296	78.331	80.68	83.57

Table 1: Peak areas and % remaining values

Day 2:

Time (min)	Assay 1		Assay 2		Assay 3		(% remaining)		
	CW-02-82 Peak area	ISTD Peak area	CW-02-82 Peak area	ISTD Peak area	CW-02-82 Peak area	ISTD Peak area	Assay 1	Assay 2	Assay 3
0	308228	1228392	297384	1328394	301983	1278339	99.968	99.941	100.098
10	327834	1398834	280034	1294385	278347	1298284	93.371	96.583	90.846
20	277464	1230974	264673	1389344	266343	1274343	89.802	85.046	88.561
30	288238	1348902	234333	1249304	268346	1338343	85.133	83.737	84.960
40	276347	1279834	241938	1238848	262644	1364364	86.026	87.184	81.569
50	264748	1266464	227348	1283453	272647	1467347	83.285	79.079	78.733
60	287543	1443782	224373	1332894	252478	1334792	79.346	75.150	80.149

Table 2: Peak areas and % remaining values

Calculation:

From the peak area, Calculate the following

$$\text{Peak area ratio} = \frac{\text{Peak area of test compound (CW-02-82)}}{\text{Peak area of internal standard (ISTD)}}$$

$$\text{\% remaining at time T = (T = 0, 10, 20,30,40,50 and 60)} \quad \frac{\text{Peak area ratio at particular time T}}{\text{Peak area ratio at zero time point}} * 100$$

DATA ANALYSIS:

Day 1

Linear regression analysis:

Slope: -0.003375 ± 0.0003311

At X= 60, Y = 4.380 ± 0.01944

R^2 = 0.8454

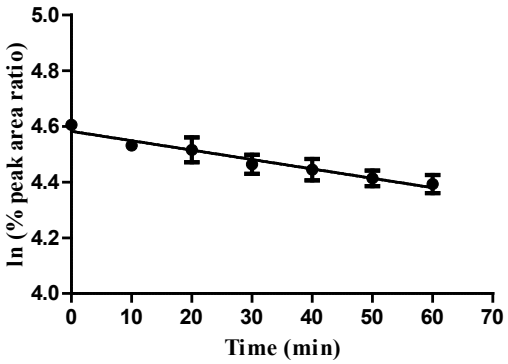

Metabolic Parameters:

Half-life: 205 ± 20 min

V_d: 2000 µL/mg

Intrinsic clearance: 0.3375 µL/min/mg

Metabolic Rate: 6.75 nmol/min/mg

% remaining at 60 min: 80 ± 0.4 %

Day 2

Linear regression analysis:

Slope: -0.0003850 ± 0.0003355

At X = 60, Y = 4.348 ± 0.01210

R^2 = 0.8739

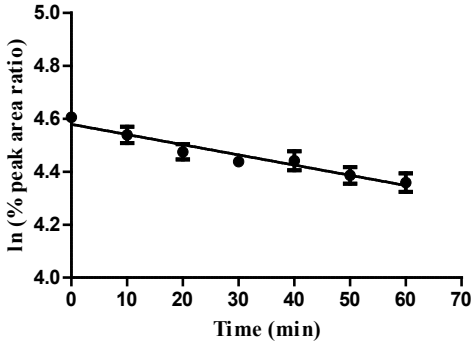

Metabolic Parameters:

Half-life: 180 ± 15 min

V_d: 2000 µL/mg

Intrinsic clearance: 0.385 µL/min/mg

Metabolic Rate: 7.7 nmol/min/mg

% remaining at 60 min: 77 ± 0.5 %

Note: The peak area ratios and natural log values are calculated using Microsoft excel 2010 and linear regression analysis is calculated using GraphPad prism.

Mouse Liver Microsomal Assay

Principal Investigator: Dr. Alexander Arnold
Operator: Revathi Kodali
Test Compound: CW-02-82
Concentration: 10 µM
Date: 11-28-2018
Facility: Milwaukee Institute for Drug Discovery

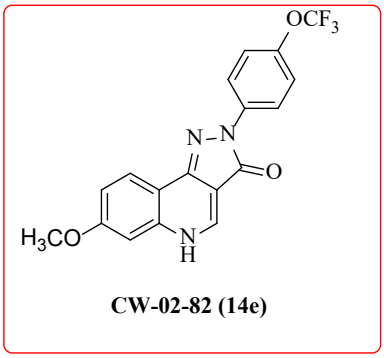

CW-02-82 (14e)

Assay Protocol

Each evaluation included six independent assays carried out three at a time, on two different days

1. Preparation of solutions:
   a. 1 mM test compound in DMSO.
   b. 1 µM 4,5 Di Phenyl Imidazole in ice cold Acetonitrile (ISTD).
2. For a total volume of Microsomal Assay Mixture (MAM) 390 µL, sufficient for seven time points, combine the following
   a. 282 µL of 18.2 mΩ of water.
   b. 80 µL of 0.5 M potassium phosphate buffer (p^H 7.4)
   c. 20 µL of NADPH A. (Corning life sciences, Cat # 451220)
   d. 4 µL of NADPH B. (Corning life sciences, Cat # 451200)
   e. 4 µL of test compound.
3. Sonicate MAM for 5 min and meanwhile thaw microsomes (20 mg/mL) (Life technologies, Cat # MSMC-PL) on ice.
4. Aliquot 100 µL of ice cold ISTD into seven separate 1.5 mL conical vials and label them the time points for 0, 10, 20, 30, 40, 50, and 60 min.
5. Arrange the timer. Microsomes (Final concentration of 0.5 mg/mL) should be added to all time points except the zero time point.
6. Add 50 µL of the MAM solution to the conical vial labelled as zero time point. Place the remaining MAM solution in the incubator (37 ºC) for 5 min and initiate the reaction with addition of microsomes (8.8 µL) and record the time.
7. At the end of each time interval remove 50 µL and add to 100 µL ISTD in conical vial, sonicate for 10 sec and spin down at 10,000 rpm for 5 minutes.
8. Take 100 µL of supernatant and transfer to Spin-X HPLC filter tubes (Corning Incorporated, Cat # 8169) and centrifuge at 13,000 rpm for 5 minutes and take 5 µL from this solution and dilute in 495 µL of LCMS grade methanol (Fischer scientific, CAS # 67-56-1) in an 2mL glass auto sampler vial (Microsolv, Cat # 95025-WCV)
9. The samples are analyzed by LCMS-8040. (Shimadzu)

Data:

Day 1:

Time (min)	Assay 1		Assay 2		Assay 3		% remaining		
	CW-02-82 Peak area	ISTD Peak area	CW-02-82 Peak area	ISTD Peak area	CW-02-82 Peak area	ISTD Peak area	Assay 1	Assay 2	Assay 3
0	320103	1410083	276473	1342893	297834	1286743	100.00	99.94	100.20
10	300843	1327484	240274	1224849	289466	1321834	99.83	95.22	94.80
20	257024	1227483	263050	1428734	266343	1401844	92.24	89.37	82.24
30	259930	1318344	280371	1529438	262305	1348945	86.85	88.98	84.17
40	241132	1287343	221132	1287634	250464	1328734	82.51	83.36	81.60
50	220823	1287673	233124	1323467	233893	1228934	75.54	85.50	82.39
60	222959	1136264	246488	1489344	221922	1180348	86.44	80.34	81.39

Table 1: Peak areas and % remaining values

Day 2:

Time (min)	Assay 1		Assay 2		Assay 3		(% remaining)		
	CW-02-82 Peak area	ISTD Peak area	CW-02-82 Peak area	ISTD Peak area	CW-02-82 Peak area	ISTD Peak area	Assay 1	Assay 2	Assay 3
0	281517	1410892	301823	1267349	277834	1374729	99.76	100.06	100.05
10	258373	1373483	297433	1362729	267450	1338934	94.05	91.70	98.88
20	242893	1422893	286343	1389489	246485	1324950	85.35	86.58	92.09
30	202037	1227294	276433	1372944	248349	1409292	82.31	84.59	87.23
40	211788	1219127	280043	1500284	226944	1308349	86.86	78.42	85.87
50	228439	1428934	286436	1428935	239343	1398240	79.93	84.22	84.74
60	216488	1326734	248343	1338549	210349	1324393	81.58	77.95	78.62

Table 2: Peak areas and % remaining values

Calculation:

From the peak area, Calculate the following

$$\text{Peak area ratio} = \frac{\text{Peak area of test compound (CW-02-82)}}{\text{Peak area of internal standard (ISTD)}}$$

$$\text{\% remaining at time T (T = 0, 10, 20,30,40,50 and 60)} = \frac{\text{Peak area ratio at particular time T}}{\text{Peak area ratio at zero time point}} * 100$$

DATA ANALYSIS:

Day 1

Linear regression analysis:

Slope: -0.003526 ± 0.0004879

At X= 60, Y = 4.371 ± 0.01759

R^2 = 0.7333

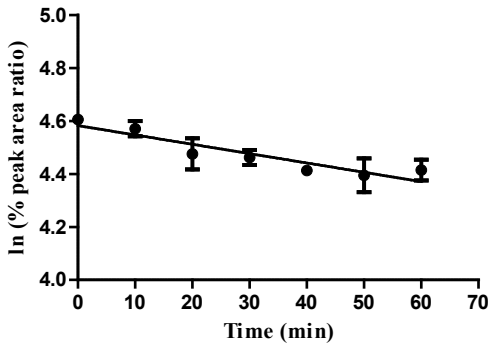

Metabolic Parameters:

Half-life: 196 ± 27 min

V_d: 2000 µL/mg

Intrinsic clearance: 0.3526 µL/min/mg

Metabolic Rate: 7.052 nmol/min/mg

% remaining at 60 min: 79 ± 0.3 %

Day 2

Linear regression analysis:

Slope: -0.0003612 ± 0.0004129

At X = 60, Y = 4.362 ± 0.01489

R^2 = 0.8011

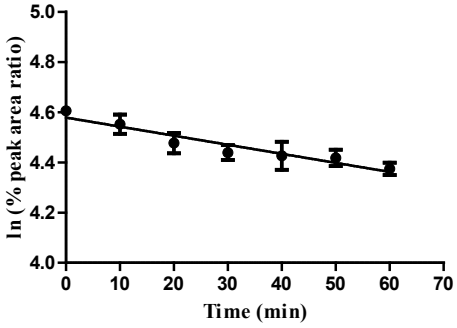

Metabolic Parameters:

Half-life: 191 ± 2 min

V_d: 2000 µL/mg

Intrinsic clearance: 0.3612 µL/min/mg

Metabolic Rate: 7.2 nmol/min/mg

% remaining at 60 min: 78 ± 0.5 %

Note: The peak area ratios and natural log values are calculated using Microsoft excel 2010 and linear regression analysis is calculated using GraphPad prism.

Human Liver Microsomal Assay

Principal Investigator: Dr. Alexander Arnold
Operator: Revathi Kodali
Test Compound: MM-I-06
Concentration: 10 µM
Date: 11-25-2018
Facility: Milwaukee Institute for Drug Discovery

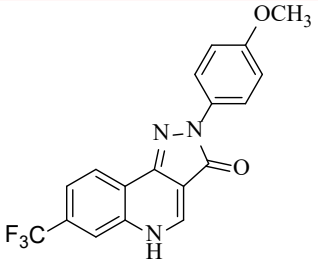

MM-I-06 (14i)

Assay Protocol

Each evaluation included six independent assays carried out three at a time, on two different days

1. Preparation of solutions:
   a. 1 mM test compound in DMSO.
   b. 0.5 µM 4,5 Di Phenyl Imidazole in ice cold Acetonitrile (ISTD).
2. For a total volume of Microsomal Assay Mixture (MAM) 390 µL, sufficient for seven time points, combine the following
   a. 282 µL of 18.2 mΩ of water.
   b. 80 µL of 0.5 M potassium phosphate buffer (p^H 7.4)
   c. 20 µL of NADPH A. (Corning life sciences, Cat # 451220)
   d. 4 µL of NADPH B. (Corning life sciences, Cat # 451200)
   e. 4 µL of test compound.
3. Sonicate MAM for 5 min and meanwhile thaw microsomes (20 mg/mL) (BD Gentest, Cat # 452156) on ice.
4. Aliquot 100 µL of ice cold ISTD into seven separate 1.5 mL conical vials and label them the time points for 0, 10, 20, 30, 40, 50, and 60 min.
5. Arrange the timer. Microsomes (Final concentration of 0.5 mg/mL) should be added to all time points except the zero time point.
6. Add 50 µL of the MAM solution to the conical vial labelled as zero time point. Place the remaining MAM solution in the incubator (37 ºC) for 5 min and initiate the reaction with addition of microsomes (8.8 µL) and record the time.
7. At the end of each time interval remove 50 µL and add to 100 µL ISTD in conical vial, sonicate for 10 sec and spin down at 10,000 rpm for 5 minutes.
8. Take 100 µL of supernatant and transfer to Spin-X HPLC filter tubes (Corning Incorporated, Cat # 8169) and centrifuge at 13,000 rpm for 5 minutes and take 5 µL from this solution and dilute in 495 µL of LCMS grade methanol (Fischer scientific, CAS # 67-56-1) in an 2mL glass auto sampler vial (Microsolv, Cat # 95025-WCV)
9. The samples are analyzed by LCMS-8040. (Shimadzu)

Data:

Day 1:

Time (min)	Assay 1		Assay 2		Assay 3		% remaining		
	MM-I-06 Peak area	ISTD Peak area	MM-I-06 Peak area	ISTD Peak area	MM-I-06 Peak area	ISTD Peak area	Assay 1	Assay 2	Assay 3
0	2522048	873195	2315304	915303	2446416	862532	100.01	99.98	100.01
10	2018558	762849	2106114	893221	2367328	911408	91.62	93.19	91.58
20	1857412	737178	2263011	936968	2089323	794499	87.24	95.46	92.72
30	1902204	780823	2032161	879487	2400486	897121	84.35	91.32	94.35
40	2058065	797912	1907359	829331	2079364	816167	89.31	90.90	89.83
50	2147699	805487	1983981	845474	2150400	833913	92.32	92.75	90.92
60	2237197	856321	1801951	762344	2014742	768822	90.46	93.42	92.40

Table 1: Peak areas and % remaining values

Day 2:

Time (min)	Assay 1		Assay 2		Assay 3		(% remaining)		
	MM-I-06 Peak area	ISTD Peak area	MM-I-06 Peak area	ISTD Peak area	MM-I-06 Peak area	ISTD Peak area	Assay 1	Assay 2	Assay 3
0	2447557	885036	2217174	845418	2343233	908132	100.01	99.98	100.01
10	2279028	855768	1871184	767896	1834450	815010	96.31	92.90	87.24
20	1994490	800037	1858480	766238	1735453	742940	90.16	92.46	90.54
30	1871842	763562	1752258	800083	1905460	828880	88.66	83.49	89.10
40	1926036	765905	1894463	816518	1901239	858325	90.94	88.45	85.85
50	2002232	804935	1819667	765775	1747950	740458	89.96	90.59	91.49
60	1891027	781179	1812404	811416	1763450	809036	87.54	85.15	84.48

Table 2: Peak areas and % remaining values

Calculation:

From the peak area, Calculate the following

$$\text{Peak area ratio} = \frac{\text{Peak area of test compound (MM-I-06)}}{\text{Peak area of internal standard (ISTD)}}$$

$$\text{\% remaining at time T} = \frac{\text{Peak area ratio at particular time T}}{\text{Peak area ratio at zero time point}} * 100$$

(T = 0, 10, 20,30,40,50 and 60)

DATA ANALYSIS:

Day 1

Linear regression analysis:

Slope: -0.0009631 ± 0.0004142

At X= 60, Y = 4.498 ± 0.01493

R^2 = 0.2215

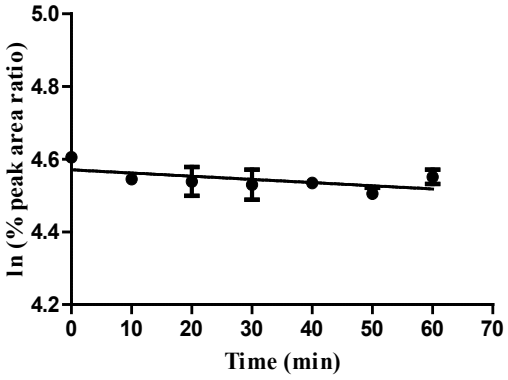

Metabolic Parameters:

Half-life: 719 ± 309 min

V_d: 2000 µL/mg

Intrinsic clearance: 0.0096 µL/min/mg

Metabolic Rate: 1.923 nmol/min/mg

% remaining at 60 min: 89 ± 0.3 %

Day 2

Linear regression analysis:

Slope: -0.0001871 ± 0.0004105

At X = 60, Y = 4.450 ± 0.01480

R^2 = 0.5224

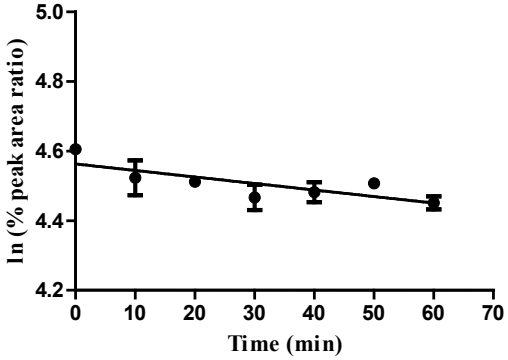

Metabolic Parameters:

Half-life: 370 ± 81 min

V_d: 2000 µL/mg

Intrinsic clearance: 0.1871 µL/min/mg

Metabolic Rate: 3.742 nmol/min/mg

% remaining at 60 min: 85 ± 0.2 %

Note: The peak area ratios and natural log values are calculated using Microsoft excel 2010 and linear regression analysis is calculated using GraphPad prism.

Mouse Liver Microsomal Assay

Principal Investigator: Dr. Alexander Arnold
Operator: Revathi Kodali
Test Compound: MM-I-06
Concentration: 10 µM
Date: 11-25-2018
Facility: Milwaukee Institute for Drug Discovery

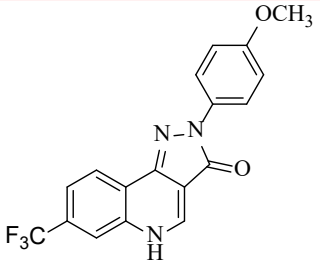

MM-I-06 (14i)

Assay Protocol

Each evaluation included six independent assays carried out three at a time, on two different days

1. Preparation of solutions:
   a. 1 mM test compound in DMSO.
   b. 0.5 µM 4,5 Di Phenyl Imidazole in ice cold Acetonitrile (ISTD).
2. For a total volume of Microsomal Assay Mixture (MAM) 390 µL, sufficient for seven time points, combine the following
   a. 282 µL of 18.2 mΩ of water.
   b. 80 µL of 0.5 M potassium phosphate buffer (p^H 7.4)
   c. 20 µL of NADPH A. (Corning life sciences, Cat # 451220)
   d. 4 µL of NADPH B. (Corning life sciences, Cat # 451200)
   e. 4 µL of test compound.
3. Sonicate MAM for 5 min and meanwhile thaw microsomes (20 mg/mL) (BD Gentest, Cat # 452156) on ice.
4. Aliquot 100 µL of ice cold ISTD into seven separate 1.5 mL conical vials and label them the time points for 0, 10, 20, 30, 40, 50, and 60 min.
5. Arrange the timer. Microsomes (Final concentration of 0.5 mg/mL) should be added to all time points except the zero time point.
6. Add 50 µL of the MAM solution to the conical vial labelled as zero time point. Place the remaining MAM solution in the incubator (37 ºC) for 5 min and initiate the reaction with addition of microsomes (8.8 µL) and record the time.
7. At the end of each time interval remove 50 µL and add to 100 µL ISTD in conical vial, sonicate for 10 sec and spin down at 10,000 rpm for 5 minutes.
8. Take 100 µL of supernatant and transfer to Spin-X HPLC filter tubes (Corning Incorporated, Cat # 8169) and centrifuge at 13,000 rpm for 5 minutes and take 5 µL from this solution and dilute in 495 µL of LCMS grade methanol (Fischer scientific, CAS # 67-56-1) in an 2mL glass auto sampler vial (Microsolv, Cat # 95025-WCV)
9. The samples are analyzed by LCMS-8040. (Shimadzu)

Data:

Day 1:

Time (min)	Assay 1		Assay 2		Assay 3		% remaining		
	MM-I-06 Peak area	ISTD Peak area	MM-I-06 Peak area	ISTD Peak area	MM-I-06 Peak area	ISTD Peak area	Assay 1	Assay 2	Assay 3
0	2440123	852526	2260236	827962	2101976	897438	100.00	99.99	100.00
10	2649565	960089	1809248	729767	1812342	798703	96.42	90.84	96.88
20	2040170	811062	2128614	841990	1859151	829583	87.81	92.63	95.60
30	2089505	783981	1856714	763170	1701270	815888	93.15	89.11	89.04
40	2129579	791099	2274218	886301	2032199	929573	94.07	93.91	93.34
50	2250682	854198	1979189	790781	1826610	892484	92.32	91.69	87.38
60	2414833	878748	2172444	874711	1849033	849644	96.08	90.95	92.92

Table 1: Peak areas and % remaining values

Day 2:

Time (min)	Assay 1		Assay 2		Assay 3		(% remaining)		
	MM-I-06 Peak area	ISTD Peak area	MM-I-06 Peak area	ISTD Peak area	MM-I-06 Peak area	ISTD Peak area	Assay 1	Assay 2	Assay 3
0	2584543	890473	2237849	866592	2088247	896256	100.01	100.01	99.99
10	2315117	844733	1896894	799081	1844855	854451	94.44	91.93	92.66
20	2396000	900906	1927236	842342	1967433	871118	91.65	88.62	96.92
30	1881855	700177	1916460	800964	1759943	821491	92.65	92.68	91.97
40	2103232	801646	2296969	948703	1895287	882079	90.40	93.77	92.27
50	1879069	721023	1651280	724451	1868195	838339	89.80	88.27	95.62
60	2045625	768775	1887303	804555	1881003	908585	91.69	90.85	88.82

Table 2: Peak areas and % remaining values

Calculation:

From the peak area, Calculate the following

$$\text{Peak area ratio} = \frac{\text{Peak area of test compound (MM-I-06)}}{\text{Peak area of internal standard (ISTD)}}$$

$$\text{\% remaining at time T} = \frac{\text{Peak area ratio at particular time T}}{\text{Peak area ratio at zero time point}} * 100$$

(T = 0, 10, 20,30,40,50 and 60)

DATA ANALYSIS:

Day 1

Linear regression analysis:

Slope: -0.001008 ± 0.0003882

At X= 60, Y = 4.507 ± 0.01400

R^2 = 0.2621

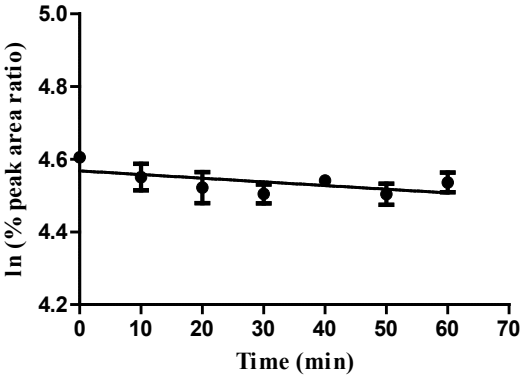

Metabolic Parameters:

Half-life: 687 ± 264 min

V_d: 2000 µL/mg

Intrinsic clearance: 0.1008 µL/min/mg

Metabolic Rate: 2.016 nmol/min/mg

% remaining at 60 min: 91 ± 0.4 %

Day 2

Linear regression analysis:

Slope: -0.001224 ± 0.0003222

At X = 60, Y = 4.496 ± 0.01162

R^2 = 04316

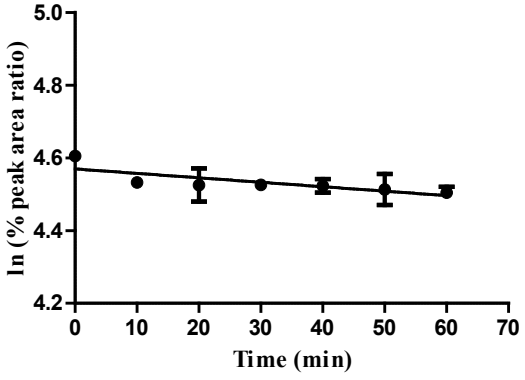

Metabolic Parameters:

Half-life: 566 ± 148 min

V_d: 2000 µL/mg

Intrinsic clearance: 0.1224 µL/min/mg

Metabolic Rate: 2.448 nmol/min/mg

% remaining at 60 min: 90 ± 0.2 %

Note: The peak area ratios and natural log values are calculated using Microsoft excel 2010 and linear regression analysis is calculated using GraphPad prism.

Human Liver Microsomal Assay

Principal Investigator: Dr. Alexander Arnold
Operator: Revathi Kodali
Test Compound: MM-I-10
Concentration: 10 µM
Date: 11-26-2018
Facility: Milwaukee Institute for Drug Discovery

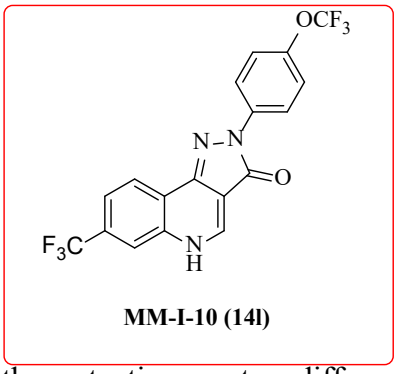

MM-I-10 (14l)

Assay Protocol

Each evaluation included six independent assays carried out three at a time, on two different days

1. Preparation of solutions:
   a. 1 mM test compound in DMSO.
   b. 1.5 µM 4,5 Di Phenyl Imidazole in ice cold Acetonitrile (ISTD).
2. For a total volume of Microsomal Assay Mixture (MAM) 390 µL, sufficient for seven time points, combine the following
   a. 282 µL of 18.2 mΩ of water.
   b. 80 µL of 0.5 M potassium phosphate buffer (p^H 7.4)
   c. 20 µL of NADPH A. (Corning life sciences, Cat # 451220)
   d. 4 µL of NADPH B. (Corning life sciences, Cat # 451200)
   e. 4 µL of test compound.
3. Sonicate MAM for 5 min and meanwhile thaw microsomes (20 mg/mL) (BD Gentest, Cat # 452156) on ice.
4. Aliquot 100 µL of ice cold ISTD into seven separate 1.5 mL conical vials and label them the time points for 0, 10, 20, 30, 40, 50, and 60 min.
5. Arrange the timer. Microsomes (Final concentration of 0.5 mg/mL) should be added to all time points except the zero time point.
6. Add 50 µL of the MAM solution to the conical vial labelled as zero time point. Place the remaining MAM solution in the incubator (37 ºC) for 5 min and initiate the reaction with addition of microsomes (8.8 µL) and record the time.
7. At the end of each time interval remove 50 µL and add to 100 µL ISTD in conical vial, sonicate for 10 sec and spin down at 10,000 rpm for 5 minutes.
8. Take 100 µL of supernatant and transfer to Spin-X HPLC filter tubes (Corning Incorporated, Cat # 8169) and centrifuge at 13,000 rpm for 5 minutes and take 5 µL from this solution and dilute in 495 µL of LCMS grade methanol (Fischer scientific, CAS # 67-56-1) in an 2mL glass auto sampler vial (Microsolv, Cat # 95025-WCV)
9. The samples are analyzed by LCMS-8040. (Shimadzu)

Data:

Day 1:

Time (min)	Assay 1		Assay 2		Assay 3		% remaining		
	MM-I-10 Peak area	ISTD Peak area	MM-I-10 Peak area	ISTD Peak area	MM-I-10 Peak area	ISTD Peak area	Assay 1	Assay 2	Assay 3
0	1721837	1542342	2019848	1662134	2117715	1712342	100.03	99.98	99.97
10	1880499	1792342	1803676	1555231	1959331	1701234	94.01	95.42	93.10
20	1778668	1712344	1592460	1342316	1886585	1691234	93.07	97.61	90.17
30	1868091	1723804	1823956	1642234	1763567	1586236	97.10	91.38	89.87
40	1980251	1923424	1923495	1712342	2049749	1748234	92.25	92.42	94.78
50	1711529	1679443	2014892	1865474	1808869	1600454	91.31	88.86	91.36
60	1923608	1783905	1798364	1562344	1956496	1701273	96.62	94.70	92.96

Table 1: Peak areas and % remaining values

Day 2:

Time (min)	Assay 1		Assay 2		Assay 3		(% remaining)		
	MM-I-10 Peak area	ISTD Peak area	MM-I-10 Peak area	ISTD Peak area	MM-I-10 Peak area	ISTD Peak area	Assay 1	Assay 2	Assay 3
0	2122268	1595074	2114373	1631265	2339888	1656232	99.96	100.01	99.98
10	2103689	1666258	2219693	1721170	2538868	1883292	94.85	99.50	95.40
20	2365182	1807673	2101813	1664564	2284676	1711652	98.30	97.42	94.46
30	2085108	1636312	1892304	1574978	2421506	1863733	95.73	92.70	91.95
40	1944883	1566161	1727539	1488336	2204732	1639635	93.29	89.56	95.16
50	1852600	1445156	1590455	1305084	2293448	1687189	96.31	94.03	96.20
60	1551673	1261307	1625708	1343792	2496754	1834792	92.42	93.34	96.30

Table 2: Peak areas and % remaining values

Calculation:

From the peak area, Calculate the following

$$\text{Peak area ratio} = \frac{\text{Peak area of test compound (MM-I-10)}}{\text{Peak area of internal standard (ISTD)}}$$

$$\text{\% remaining at time T (T = 0, 10, 20,30,40,50 and 60)} = \frac{\text{Peak area ratio at particular time T}}{\text{Peak area ratio at zero time point}} * 100$$

DATA ANALYSIS:

Day 1

Linear regression analysis:

Slope: -0.0008774 ± 0.0003451

At X= 60, Y = 4.518 ± 0.01244

R^2 = 0.2538

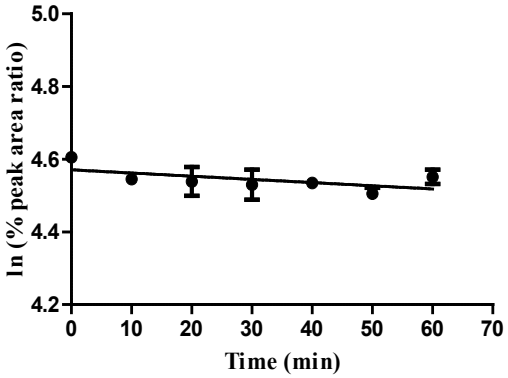

Metabolic Parameters:

Half-life: 789 ± 36 min

V_d: 2000 µL/mg

Intrinsic clearance: 0.08774 µL/min/mg

Metabolic Rate: 1.7548 nmol/min/mg

% remaining at 60 min: 91.65 ± 0.25 %

Day 2

Linear regression analysis:

Slope: -0.0008893 ± 0.0002723

At X = 60, Y = 4.533 ± 0.009819

R^2 = 0.3595

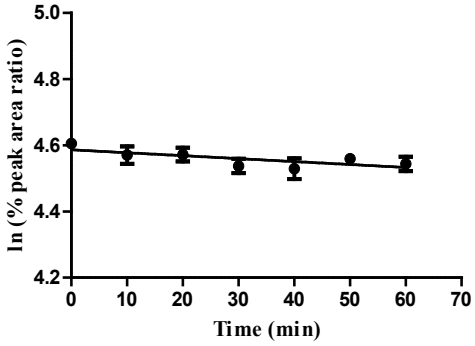

Metabolic Parameters:

Half-life: 779 ± 24 min

V_d: 2000 µL/mg

Intrinsic clearance: 0.08893 µL/min/mg

Metabolic Rate: 1.7786 nmol/min/mg

% remaining at 60 min: 93 ± 0.2 %

Note: The peak area ratios and natural log values are calculated using Microsoft excel 2010 and linear regression analysis is calculated using GraphPad prism.

Mouse Liver Microsomal Assay

Principal Investigator: Dr. Alexander Arnold
Operator: Revathi Kodali
Test Compound: MM-I-10
Concentration: 10 µM
Date: 11-11-2018
Facility: Milwaukee Institute for Drug Discovery

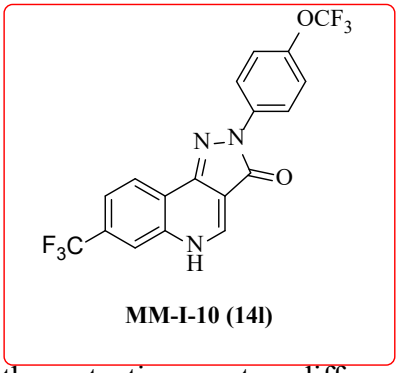

MM-I-10 (14l)

Assay Protocol

Each evaluation included six independent assays carried out three at a time, on two different days

1. Preparation of solutions:
   a. 1 mM test compound in DMSO.
   b. 1.5 µM 4,5 Di Phenyl Imidazole in ice cold Acetonitrile (ISTD).
2. For a total volume of Microsomal Assay Mixture (MAM) 390 µL, sufficient for seven time points, combine the following
   a. 282 µL of 18.2 mΩ of water.
   b. 80 µL of 0.5 M potassium phosphate buffer (p^H 7.4)
   c. 20 µL of NADPH A. (Corning life sciences, Cat # 451220)
   d. 4 µL of NADPH B. (Corning life sciences, Cat # 451200)
   e. 4 µL of test compound.
3. Sonicate MAM for 5 min and meanwhile thaw microsomes (20 mg/mL) (Life technologies Cat # MSMC-PL) on ice.
4. Aliquot 100 µL of ice cold ISTD into seven separate 1.5 mL conical vials and label them the time points for 0, 10, 20, 30, 40, 50, and 60 min.
5. Arrange the timer. Microsomes (Final concentration of 0.5 mg/mL) should be added to all time points except the zero time point.
6. Add 50 µL of the MAM solution to the conical vial labelled as zero time point. Place the remaining MAM solution in the incubator (37 ºC) for 5 min and initiate the reaction with addition of microsomes (8.8 µL) and record the time.
7. At the end of each time interval remove 50 µL and add to 100 µL ISTD in conical vial, sonicate for 10 sec and spin down at 10,000 rpm for 5 minutes.
8. Take 100 µL of supernatant and transfer to Spin-X HPLC filter tubes (Corning Incorporated, Cat # 8169) and centrifuge at 13,000 rpm for 5 minutes and take 5 µL from this solution and dilute in 495 µL of LCMS grade methanol (Fischer scientific, CAS # 67-56-1) in an 2mL glass auto sampler vial (Microsolv, Cat # 95025-WCV)
9. The samples are analyzed by LCMS-8040. (Shimadzu)

Data:

Day 1:

Time (min)	Assay 1		Assay 2		Assay 3		% remaining		
	MM-I-10 Peak area	ISTD Peak area	MM-I-10 Peak area	ISTD Peak area	MM-I-10 Peak area	ISTD Peak area	Assay 1	Assay 2	Assay 3
0	1742756	1634054	1654372	1573613	1673498	1443243	99.95	100.03	99.96
10	1603248	1588299	1513377	1538334	1587843	1528213	94.60	93.60	89.57
20	1291208	1309545	1452509	1603412	1663602	1530123	92.40	86.19	93.72
30	1516740	1496780	1587568	1556728	1567438	1471422	94.97	97.03	91.83
40	1423607	1547765	1498165	1561324	1755660	1535162	86.20	91.29	98.58
50	1808802	1780212	1483124	1524234	1561987	1442342	95.22	92.58	93.35
60	1501377	1528880	1595812	1604144	1652854	1562361	92.03	94.65	91.20

Table 1: Peak areas and % remaining values

Day 2:

Time (min)	Assay 1		Assay 2		Assay 3		(% remaining)		
	MM-I-10 Peak area	ISTD Peak area	MM-I-10 Peak area	ISTD Peak area	MM-I-10 Peak area	ISTD Peak area	Assay 1	Assay 2	Assay 3
0	1733982	1538546	1615387	1607699	1645233	1452987	100.00	99.97	100.02
10	1670375	1638354	1574328	1595536	1674843	1536291	90.45	98.18	96.30
20	1609332	1430406	1552092	1682872	1545556	1545334	99.83	91.77	88.35
30	1605044	1590310	1450639	1545228	1651031	1550770	89.55	93.41	94.05
40	1561885	1473496	1538832	1637823	1805007	1658837	94.05	93.48	96.12
50	1397737	1433227	1502467	1609820	1674520	1605750	86.53	92.86	92.12
60	1629484	1573361	1435391	1583401	1569790	1455678	91.89	90.2	95.26

Table 2: Peak areas and % remaining values

Calculation:

From the peak area, Calculate the following

$$\text{Peak area ratio} = \frac{\text{Peak area of test compound (MM-I-10)}}{\text{Peak area of internal standard (ISTD)}}$$

$$\text{\% remaining at time T} = \frac{\text{Peak area ratio at particular time T}}{\text{Peak area ratio at zero time point}} * 100$$

(T = 0, 10, 20,30,40,50 and 60)

DATA ANALYSIS:

Day 1

Linear regression analysis:

Slope: -0.0006893 ± 0.0004439

At X= 60, Y = 4.519 ± 0.01601

R^2 = 0.1126

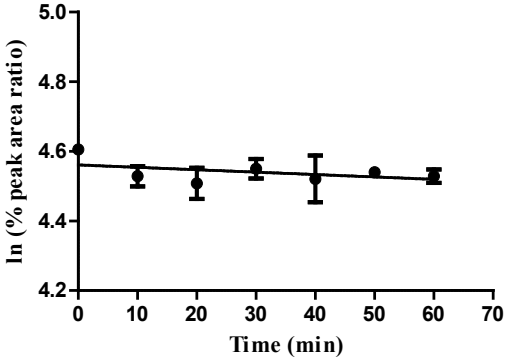

Metabolic Parameters:

Half-life: 1005 ± 647 min

V_d: 2000 µL/mg

Intrinsic clearance: 0.0689 µL/min/mg

Metabolic Rate: 1.3786 nmol/min/mg

% remaining at 60 min: 91.7 ± 0.4 %

Day 2

Linear regression analysis:

Slope: -0.0001131 ± 0.0003984

At X = 60, Y = 4.509 ± 0.01437

R^2 = 0.2978

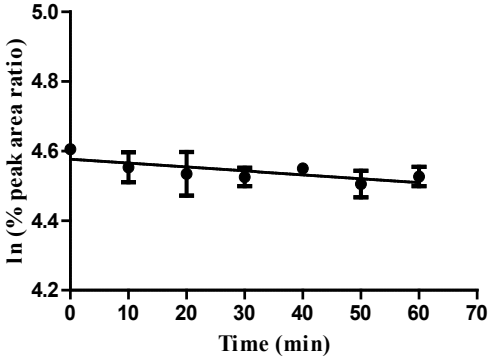

Metabolic Parameters:

Half-life: 612 ± 20 min

V_d: 2000 µL/mg

Intrinsic clearance: 0.1131 µL/min/mg

Metabolic Rate: 2.262 nmol/min/mg

% remaining at 60 min: 90 ± 2 %

Note: The peak area ratios and natural log values are calculated using Microsoft excel 2010 and linear regression analysis is calculated using GraphPad prism.

Human Liver Microsomal Assay

Principal Investigator: Dr. Alexander Arnold
Operator: Revathi Kodali
Test Compound: DK-IV-20-1
Concentration: 10 µM
Date: 12-25-2018
Facility: Milwaukee Institute for Drug Discovery

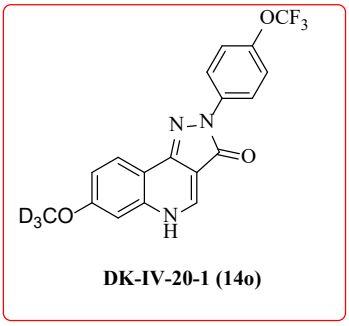

DK-IV-20-1 (14o)

Assay Protocol

Each evaluation included six independent assays carried out three at a time, on two different days

1. Preparation of solutions:
   a. 1 mM test compound in DMSO.
   b. 5 µM 4,5 Di Phenyl Imidazole in ice cold Acetonitrile (ISTD).
2. For a total volume of Microsomal Assay Mixture (MAM) 390 µL, sufficient for seven time points, combine the following
   a. 282 µL of 18.2 mΩ of water.
   b. 80 µL of 0.5 M potassium phosphate buffer (p^H 7.4)
   c. 20 µL of NADPH A. (Corning life sciences, Cat # 451220)
   d. 4 µL of NADPH B. (Corning life sciences, Cat # 451200)
   e. 4 µL of test compound.
3. Sonicate MAM for 5 min and meanwhile thaw microsomes (20 mg/mL) (BD Gentest, Cat # 452156) on ice.
4. Aliquot 100 µL of ice cold ISTD into seven separate 1.5 mL conical vials and label them the time points for 0, 10, 20, 30, 40, 50, and 60 min.
5. Arrange the timer. Microsomes (Final concentration of 0.5 mg/mL) should be added to all time points except the zero time point.
6. Add 50 µL of the MAM solution to the conical vial labelled as zero time point. Place the remaining MAM solution in the incubator (37 ºC) for 5 min and initiate the reaction with addition of microsomes (8.8 µL) and record the time.
7. At the end of each time interval remove 50 µL and add to 100 µL ISTD in conical vial, sonicate for 10 sec and spin down at 10,000 rpm for 5 minutes.
8. Take 100 µL of supernatant and transfer to Spin-X HPLC filter tubes (Corning Incorporated, Cat # 8169) and centrifuge at 13,000 rpm for 5 minutes and take 5 µL from this solution and dilute in 495 µL of LCMS grade methanol (Fischer scientific, CAS # 67-56-1) in an 2mL glass auto sampler vial (Microsolv, Cat # 95025-WCV)
9. The samples are analyzed by LCMS-8040. (Shimadzu)

Data:

Day 1:

Time (min)	Assay 1		Assay 2		Assay 3		% remaining		
	DKIV23-1 Peak area	ISTD Peak area	DKIV23-1 Peak area	ISTD Peak area	DKIV23-1 Peak area	ISTD Peak area	Assay 1	Assay 2	Assay 3
0	3647212	48672362	3544559	48626237	3644635	47896343	99.91	99.85	100.12
10	3431611	46782392	3395927	47515632	3308414	46994408	97.80	97.90	92.63
20	3230928	46729223	3206914	46312526	3284633	47838945	92.18	94.85	90.34
30	3293593	47561212	3306928	50027328	3517295	48850499	92.33	90.55	94.73
40	3213006	47125462	3265818	49101739	3484703	49768060	90.90	91.11	92.13
50	3310903	46412541	3491989	51083284	3395305	47947191	95.11	93.64	93.17
60	3218327	48273464	3121094	46812811	3294107	48928291	88.89	91.33	88.58

Table 1: Peak areas and % remaining values

Day 2:

Time (min)	Assay 1		Assay 2		Assay 3		(% remaining)		
	DK-IV23-1 Peak area	ISTD Peak area	DKIV23-1 Peak area	ISTD Peak area	DK-IV23-1 Peak area	ISTD Peak area	Assay 1	Assay 2	Assay 3
0	3585552	48331088	3623919	48160859	3544313	46000777	100.25	100.32	100.06
10	3467371	46964695	3412058	46264755	3401871	47545694	99.76	98.33	92.92
20	3157757	43448751	3302730	48673240	3317345	46336512	98.23	90.44	92.97
30	3268110	46282276	3225179	46623521	3431657	47902544	95.42	92.33	93.37
40	3355494	48521454	3372970	48116373	3326534	47313337	93.45	93.67	91.30
50	3245416	47526181	3291241	46414243	3479217	48478644	92.20	94.47	93.25
60	3135049	46414165	3118919	47032622	3231291	46568890	91.27	88.19	90.13

Table 2: Peak areas and % remaining values

Calculation:

From the peak area, Calculate the following

$$\text{Peak area ratio} = \frac{\text{Peak area of test compound (DK-IV-20-1)}}{\text{Peak area of internal standard (ISTD)}}$$

$$\text{\% remaining at time T (T = 0, 10, 20,30,40,50 and 60)} = \frac{\text{Peak area ratio at particular time T}}{\text{Peak area ratio at zero time point}} * 100$$

DATA ANALYSIS:

Day 1

Linear regression analysis:

Slope: -0.001379 ± 0.0002803

At X= 60, Y = 4.498 ± 0.01011

R^2 = 0.5601

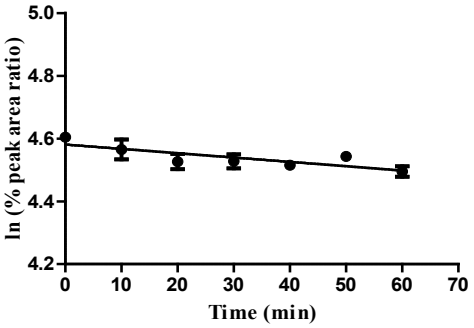

Metabolic Parameters:

Half-life: 502 ± 102 min

V_d: 2000 µL/mg

Intrinsic clearance: 0.1379 µL/min/mg

Metabolic Rate: 2.758 nmol/min/mg

% remaining at 60 min: 89 ± 0.3 %

Day 2

Linear regression analysis:

Slope: -0.001474 ± 0.0002682

At X = 60, Y = 4.502 ± 0.09671

R^2 = 0.6137

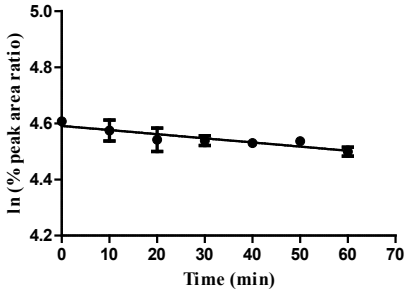

Metabolic Parameters:

Half-life: 470 ± 86 min

V_d: 2000 µL/mg

Intrinsic clearance: 0.1474 µL/min/mg

Metabolic Rate: 2.948 nmol/min/mg

% remaining at 60 min: 90 ± 0.3 %

Note: The peak area ratios and natural log values are calculated using Microsoft excel 2010 and linear regression analysis is calculated using GraphPad prism.

Mouse Liver Microsomal Assay

Principal Investigator: Dr. Alexander Arnold
Operator: Revathi Kodali
Test Compound: DK-IV-20-1
Concentration: 10 µM
Date: 12-25-2018
Facility: Milwaukee Institute for Drug Discovery

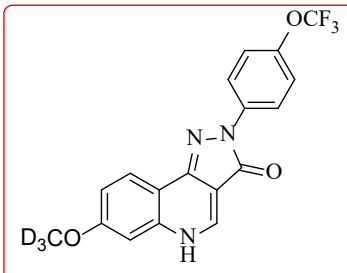

DK-IV-20-1 (14o)

Assay Protocol

Each evaluation included six independent assays carried out three at a time, on two different days

1. Preparation of solutions:
   a. 1 mM test compound in DMSO.
   b. 5 µM 4,5 Di Phenyl Imidazole in ice cold Acetonitrile (ISTD).
2. For a total volume of Microsomal Assay Mixture (MAM) 390 µL, sufficient for seven time points, combine the following
   a. 282 µL of 18.2 mΩ of water.
   b. 80 µL of 0.5 M potassium phosphate buffer (p^H 7.4)
   c. 20 µL of NADPH A. (Corning life sciences, Cat # 451220)
   d. 4 µL of NADPH B. (Corning life sciences, Cat # 451200)
   e. 4 µL of test compound.
3. Sonicate MAM for 5 min and meanwhile thaw microsomes (20 mg/mL) (BD Gentest, Cat # 452156) on ice.
4. Aliquot 100 µL of ice cold ISTD into seven separate 1.5 mL conical vials and label them the time points for 0, 10, 20, 30, 40, 50, and 60 min.
5. Arrange the timer. Microsomes (Final concentration of 0.5 mg/mL) should be added to all time points except the zero time point.
6. Add 50 µL of the MAM solution to the conical vial labelled as zero time point. Place the remaining MAM solution in the incubator (37 ºC) for 5 min and initiate the reaction with addition of microsomes (8.8 µL) and record the time.
7. At the end of each time interval remove 50 µL and add to 100 µL ISTD in conical vial, sonicate for 10 sec and spin down at 10,000 rpm for 5 minutes.
8. Take 100 µL of supernatant and transfer to Spin-X HPLC filter tubes (Corning Incorporated, Cat # 8169) and centrifuge at 13,000 rpm for 5 minutes and take 5 µL from this solution and dilute in 495 µL of LCMS grade methanol (Fischer scientific, CAS # 67-56-1) in an 2mL glass auto sampler vial (Microsolv, Cat # 95025-WCV)
9. The samples are analyzed by LCMS-8040. (Shimadzu)

Data:

Day 1:

Time (min)	Assay 1		Assay 2		Assay 3		% remaining		
	DKIV20-1 Peak area	ISTD Peak area	DKIV20-1 Peak area	ISTD Peak area	DKIV20-1 Peak area	ISTD Peak area	Assay 1	Assay 2	Assay 3
0	3564665	48110738	3425751	46435352	3483276	47050299	100.12	99.69	100.04
10	3467006	47376549	3296980	47114674	3347252	45461140	98.89	94.56	99.49
20	3385197	47871157	3285703	47826371	3244921	46799062	95.50	92.83	93.69
30	3255981	47183146	2960080	44622084	2987960	45892541	93.23	89.64	87.98
40	3083604	46665383	2962851	46533793	3002551	46090410	89.29	86.04	88.03
50	3026809	46523265	2965964	47137657	2686556	45483588	87.91	85.02	79.82
60	2884161	46403937	2721257	46023263	2897226	47554566	83.99	79.90	82.33

Table 1: Peak areas and % remaining values

Day 2:

Time (min)	Assay 1		Assay 2		Assay 3		(% remaining)		
	DK-IV23-1 Peak area	ISTD Peak area	DKIV23-1 Peak area	ISTD Peak area	DK-IV23-1 Peak area	ISTD Peak area	Assay 1	Assay 2	Assay 3
0	3654015	49955868	3525266	48502857	3412837	46041901	100.19	99.56	100.16
10	3456918	49659463	3281905	48560859	3329825	46914325	95.36	92.58	95.91
20	3325986	47222278	3216567	46595670	3246180	45278166	96.48	94.56	96.88
30	3335008	48929781	2952838	46171019	3111878	47399013	93.36	87.60	88.72
40	3167666	48903941	2995625	48001880	3006577	46973540	88.73	85.48	86.49
50	3094970	49479414	2988011	48438505	2880397	46968082	85.68	84.50	82.87
60	3026729	49302011	2726569	47380894	2892228	48698995	84.09	78.83	80.25

Table 2: Peak areas and % remaining values

Calculation:

From the peak area, Calculate the following

$$\text{Peak area ratio} = \frac{\text{Peak area of test compound (DK-IV-20-1)}}{\text{Peak area of internal standard (ISTD)}}$$

$$\text{\% remaining at time T (T = 0, 10, 20,30,40,50 and 60)} = \frac{\text{Peak area ratio at particular time T}}{\text{Peak area ratio at zero time point}} * 100$$

DATA ANALYSIS:

Day 1

Linear regression analysis:

Slope: -0.003413 ± 0.0002608

At X= 60, Y = 4.404 ± 0.009404

R^2 = 0.9001

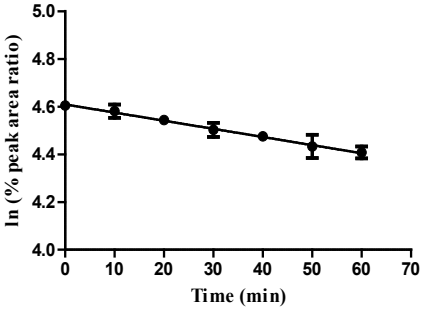

Metabolic Parameters:

Half-life: 203 ± 16 min

V_d: 2000 µL/mg

Intrinsic clearance: 0.3413 µL/min/mg

Metabolic Rate: 6.826 nmol/min/mg

% remaining at 60 min: 82 ± 0.25 %

Day 2

Linear regression analysis:

Slope: -0.003427 ± 0.0002595

At X = 60, Y = 4.399 ± 0.09355

R^2 = 0.9018

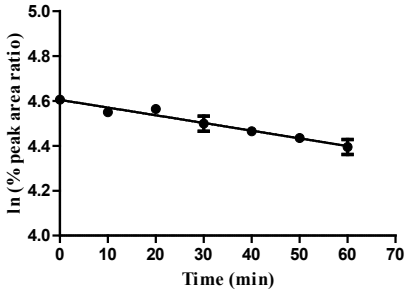

Metabolic Parameters:

Half-life: 202 ± 15 min

V_d: 2000 µL/mg

Intrinsic clearance: 0.3427 µL/min/mg

Metabolic Rate: 6.854 nmol/min/mg

% remaining at 60 min: 81 ± 0.3 %

Note: The peak area ratios and natural log values are calculated using Microsoft excel 2010 and linear regression analysis is calculated using GraphPad prism.

Human Liver Microsomal Assay

Principal Investigator: Dr. Alexander Arnold
Operator: Revathi Kodali
Test Compound: DK-IV-22-1
Concentration: 10 µM
Date: 12-21-2018
Facility: Milwaukee Institute for Drug Discovery

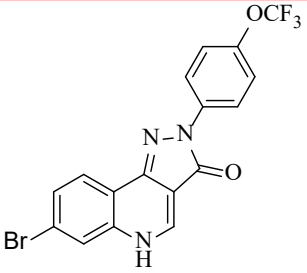

DK-IV-22-1 (14p)

Assay Protocol

Each evaluation included six independent assays carried out three at a time, on two different days

1. Preparation of solutions:
   a. 1 mM test compound in DMSO.
   b. 5 µM 4,5 Di Phenyl Imidazole in ice cold Acetonitrile (ISTD).
2. For a total volume of Microsomal Assay Mixture (MAM) 390 µL, sufficient for seven time points, combine the following
   a. 282 µL of 18.2 mΩ of water.
   b. 80 µL of 0.5 M potassium phosphate buffer (p^H 7.4)
   c. 20 µL of NADPH A. (Corning life sciences, Cat # 451220)
   d. 4 µL of NADPH B. (Corning life sciences, Cat # 451200)
   e. 4 µL of test compound.
3. Sonicate MAM for 5 min and meanwhile thaw microsomes (20 mg/mL) (BD Gentest, Cat # 452156) on ice.
4. Aliquot 100 µL of ice cold ISTD into seven separate 1.5 mL conical vials and label them the time points for 0, 10, 20, 30, 40, 50, and 60 min.
5. Arrange the timer. Microsomes (Final concentration of 0.5 mg/mL) should be added to all time points except the zero time point.
6. Add 50 µL of the MAM solution to the conical vial labelled as zero time point. Place the remaining MAM solution in the incubator (37 ºC) for 5 min and initiate the reaction with addition of microsomes (8.8 µL) and record the time.
7. At the end of each time interval remove 50 µL and add to 100 µL ISTD in conical vial, sonicate for 10 sec and spin down at 10,000 rpm for 5 minutes.
8. Take 100 µL of supernatant and transfer to Spin-X HPLC filter tubes (Corning Incorporated, Cat # 8169) and centrifuge at 13,000 rpm for 5 minutes and take 5 µL from this solution and dilute in 495 µL of LCMS grade methanol (Fischer scientific, CAS # 67-56-1) in an 2mL glass auto sampler vial (Microsolv, Cat # 95025-WCV)
9. The samples are analyzed by LCMS-8040. (Shimadzu)

Data:

Day 1:

Time (min)	Assay 1		Assay 2		Assay 3		% remaining		
	DKIV22-1 Peak area	ISTD Peak area	DKIV22-1 Peak area	ISTD Peak area	DKIV22-1 Peak area	ISTD Peak area	Assay 1	Assay 2	Assay 3
0	386727	54618506	361062	51292232	368766	53212546	101.15	100.56	99.00
10	364436	52214685	397112	53037025	363007	51449929	99.70	106.94	100.73
20	338323	51172153	379957	53909725	358434	52302407	94.45	100.86	97.92
30	331833	50683502	386865	55908779	362201	51625451	93.53	98.51	100.28
40	320950	49363916	381262	56075057	359526	52111925	92.88	97.31	98.59
50	348356	50399938	355513	52734491	358026	55099802	98.74	96.08	92.25
60	354157	48783905	356188	52155995	378943	54638137	103.70	97.61	99.79

Table 1: Peak areas and % remaining values

Day 2:

Time (min)	Assay 1		Assay 2		Assay 3		(% remaining)		
	DK-IV22-1 Peak area	ISTD Peak area	DKIV22-1 Peak area	ISTD Peak area	DK-IV22-1 Peak area	ISTD Peak area	Assay 1	Assay 2	Assay 3
0	341203	48536436	374373	46231834	369888	53051091	100.42	101.22	99.60
10	335266	50349422	366482	49812988	362957	50844434	95.12	91.96	101.90
20	370362	53530970	383355	51036040	364351	52784361	98.83	93.89	98.69
30	362077	50234726	369590	48009081	332716	48879794	102.97	96.22	97.20
40	351251	50264014	393961	50968242	353659	49881032	99.80	96.61	101.86
50	342247	49813108	386599	51039634	368297	54641318	98.12	94.68	96.90
60	350429	50350387	387586	49840995	351224	51835924	99.46	97.20	96.96

Table 2: Peak areas and % remaining values

Calculation:

From the peak area, Calculate the following

$$\text{Peak area ratio} = \frac{\text{Peak area of test compound (DK-IV-22-1)}}{\text{Peak area of internal standard (ISTD)}}$$

$$\text{\% remaining at time T = (T = 0, 10, 20,30,40,50 and 60)} \quad \frac{\text{Peak area ratio at particular time T}}{\text{Peak area ratio at zero time point}} * 100$$

DATA ANALYSIS:

Day 1

Linear regression analysis:

Slope: -0.0005393 ± 0.0003706

At X= 60, Y = 4.574 ± 0.01336

R^2 = 0.1003

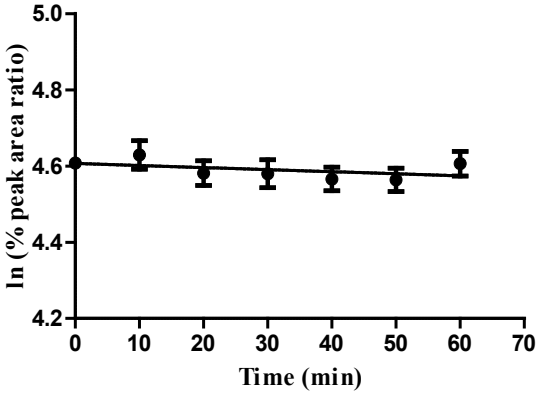

Metabolic Parameters:

Half-life: 1285 ± 882 min

V_d: 2000 µL/mg

Intrinsic clearance: 0.05393 µL/min/mg

Metabolic Rate: 1.0786 nmol/min/mg

% remaining at 60 min: 96 ± 0.3 %

Day 2

Linear regression analysis:

Slope: -0.0001905 ± 0.0003204

At X = 60, Y = 4.579 ± 0.001155

R^2 = 0.01827

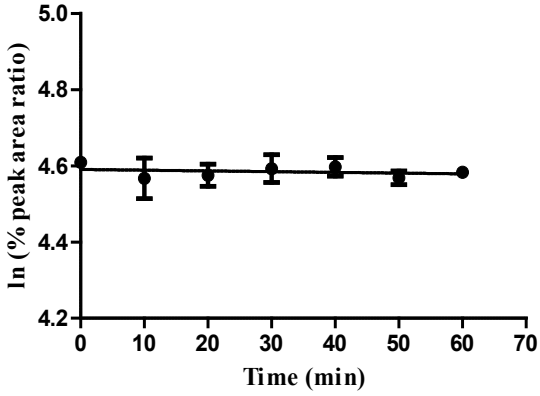

Metabolic Parameters:

Half-life: 3637 ± 612 min

V_d: 2000 µL/mg

Intrinsic clearance: 0.01905 µL/min/mg

Metabolic Rate: 0.381 nmol/min/mg

% remaining at 60 min: 97 ± 0.25 %

Note: The peak area ratios and natural log values are calculated using Microsoft excel 2010 and linear regression analysis is calculated using GraphPad prism.

Mouse Liver Microsomal Assay

Principal Investigator: Dr. Alexander Arnold
Operator: Revathi Kodali
Test Compound: DK-IV-22-1
Concentration: 10 µM
Date: 12-21-2018
Facility: Milwaukee Institute for Drug Discovery

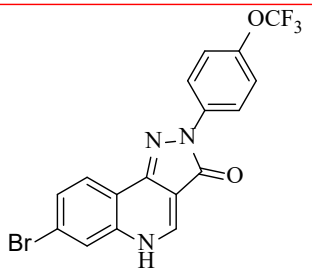

DK-IV-22-1 (14p)

Assay Protocol

Each evaluation included six independent assays carried out three at a time, on two different days

1. Preparation of solutions:
   a. 1 mM test compound in DMSO.
   b. 5 µM 4,5 Di Phenyl Imidazole in ice cold Acetonitrile (ISTD).
2. For a total volume of Microsomal Assay Mixture (MAM) 390 µL, sufficient for seven time points, combine the following
   a. 282 µL of 18.2 mΩ of water.
   b. 80 µL of 0.5 M potassium phosphate buffer (p^H 7.4)
   c. 20 µL of NADPH A. (Corning life sciences, Cat # 451220)
   d. 4 µL of NADPH B. (Corning life sciences, Cat # 451200)
   e. 4 µL of test compound.
3. Sonicate MAM for 5 min and meanwhile thaw microsomes (20 mg/mL) (Life technologies, Cat # MSMC-PL) on ice.
4. Aliquot 100 µL of ice cold ISTD into seven separate 1.5 mL conical vials and label them the time points for 0, 10, 20, 30, 40, 50, and 60 min.
5. Arrange the timer. Microsomes (Final concentration of 0.5 mg/mL) should be added to all time points except the zero time point.
6. Add 50 µL of the MAM solution to the conical vial labelled as zero time point. Place the remaining MAM solution in the incubator (37 ºC) for 5 min and initiate the reaction with addition of microsomes (8.8 µL) and record the time.
7. At the end of each time interval remove 50 µL and add to 100 µL ISTD in conical vial, sonicate for 10 sec and spin down at 10,000 rpm for 5 minutes.
8. Take 100 µL of supernatant and transfer to Spin-X HPLC filter tubes (Corning Incorporated, Cat # 8169) and centrifuge at 13,000 rpm for 5 minutes and take 5 µL from this solution and dilute in 495 µL of LCMS grade methanol (Fischer scientific, CAS # 67-56-1) in an 2mL glass auto sampler vial (Microsolv, Cat # 95025-WCV)
9. The samples are analyzed by LCMS-8040. (Shimadzu)

Data:

Day 1:

Time (min)	Assay 1		Assay 2		Assay 3		% remaining		
	DKIV22-1 Peak area	ISTD Peak area	DKIV22-1 Peak area	ISTD Peak area	DKIV22-1 Peak area	ISTD Peak area	Assay 1	Assay 2	Assay 3
0	356622	51241647	358839	51456348	349708	49973655	99.42	99.62	99.96
10	362385	52204808	365818	49407255	311077	45853463	99.16	105.77	96.91
20	344764	49680901	341434	49606483	348591	48971564	99.17	98.32	101.69
30	343648	50183750	350806	50514854	344856	50165335	97.86	99.29	98.20
40	369660	52047405	367345	52269517	362292	50616098	101.62	100.39	102.22
50	363653	51948113	346350	52450223	360367	51753216	100	94.33	99.47
60	345313	51225030	339236	51482895	344469	50839481	96.01	94.13	96.79

Table 1: Peak areas and % remaining values

Day 2:

Time (min)	Assay 1		Assay 2		Assay 3		(% remaining)		
	DK-IV22-1 Peak area	ISTD Peak area	DKIV22-1 Peak area	ISTD Peak area	DK-IV22-1 Peak area	ISTD Peak area	Assay 1	Assay 2	Assay 3
0	357282	51041378	354065	50327744	369898	45956809	99.99	100.50	100.61
10	334566	47465110	352281	48463597	372807	48514461	100.65	103.84	96.05
20	348967	49645996	355275	50174904	386414	50389728	100.16	101.15	95.85
30	344940	50388017	338374	49551672	405501	50832470	97.95	97.55	99.715
40	375031	52586237	369276	56201768	395083	51805325	10.882	93.86	95.329
50	357294	52034689	343035	51091449	423859	57777394	9.092	95.91	91.70
60	349396	52088455	330828	47706212	407358	50769770	95.85	99.06	100.25

Table 2: Peak areas and % remaining values

Calculation:

From the peak area, Calculate the following

$$\text{Peak area ratio} = \frac{\text{Peak area of test compound (DK-IV-22-1)}}{\text{Peak area of internal standard (ISTD)}}$$

$$\text{\% remaining at time T (T = 0, 10, 20,30,40,50 and 60)} = \frac{\text{Peak area ratio at particular time T}}{\text{Peak area ratio at zero time point}} * 100$$

DATA ANALYSIS:

Day 1

Linear regression analysis:

Slope: -0.0005595 ± 0.0002667

At X= 60, Y = 4.579 ± 0.09616

R^2 = 0.1881

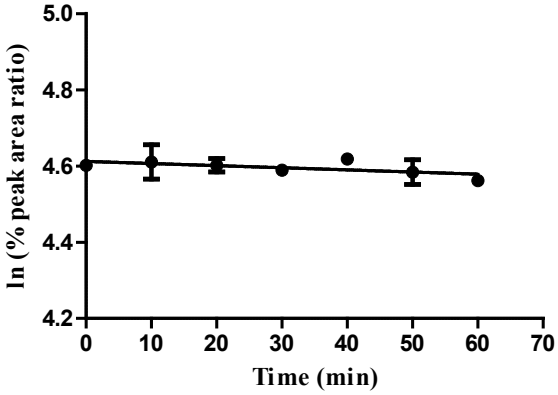

Metabolic Parameters:

Half-life: 1238 ± 590 min

V_d: 2000 µL/mg

Intrinsic clearance: 0.05595 µL/min/mg

Metabolic Rate: 1.119 nmol/min/mg

% remaining at 60 min: 97.4 ± 0.25 %

Day 2

Linear regression analysis:

Slope: -0.0006512 ± 0.0003056

At X = 60, Y = 4.569 ± 0.001102

R^2 = 0.011928

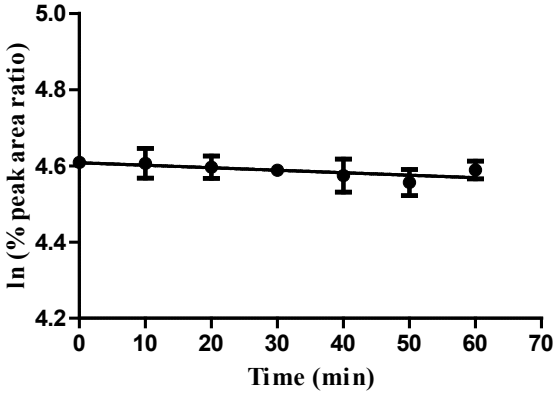

Metabolic Parameters:

Half-life: 1064 ± 499 min

V_d: 2000 µL/mg

Intrinsic clearance: 0.06512 µL/min/mg

Metabolic Rate: 1.3024 nmol/min/mg

% remaining at 60 min: 96.4 ± 0.3 %

Note: The peak area ratios and natural log values are calculated using Microsoft excel 2010 and linear regression analysis is calculated using GraphPad prism.

Human Liver Microsomal Assay

Principal Investigator: Dr. Alexander Arnold
Operator: Revathi Kodali
Test Compound: DK-IV-23-1
Concentration: 10 µM
Date: 12-25-2018
Facility: Milwaukee Institute for Drug Discovery

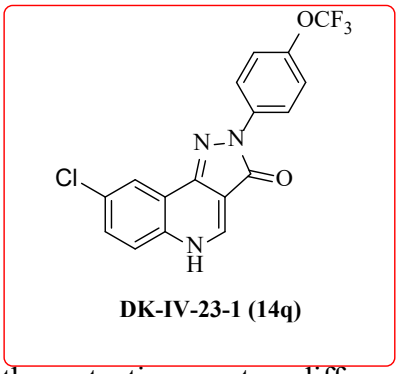

DK-IV-23-1 (14q)

Assay Protocol

Each evaluation included six independent assays carried out three at a time, on two different days

1. Preparation of solutions:
   a. 1 mM test compound in DMSO.
   b. 5 µM 4,5 Di Phenyl Imidazole in ice cold Acetonitrile (ISTD).
2. For a total volume of Microsomal Assay Mixture (MAM) 390 µL, sufficient for seven time points, combine the following
   a. 282 µL of 18.2 mΩ of water.
   b. 80 µL of 0.5 M potassium phosphate buffer (p^H 7.4)
   c. 20 µL of NADPH A. (Corning life sciences, Cat # 451220)
   d. 4 µL of NADPH B. (Corning life sciences, Cat # 451200)
   e. 4 µL of test compound.
3. Sonicate MAM for 5 min and meanwhile thaw microsomes (20 mg/mL) (BD Gentest, Cat # 452156) on ice.
4. Aliquot 100 µL of ice cold ISTD into seven separate 1.5 mL conical vials and label them the time points for 0, 10, 20, 30, 40, 50, and 60 min.
5. Arrange the timer. Microsomes (Final concentration of 0.5 mg/mL) should be added to all time points except the zero time point.
6. Add 50 µL of the MAM solution to the conical vial labelled as zero time point. Place the remaining MAM solution in the incubator (37 ºC) for 5 min and initiate the reaction with addition of microsomes (8.8 µL) and record the time.
7. At the end of each time interval remove 50 µL and add to 100 µL ISTD in conical vial, sonicate for 10 sec and spin down at 10,000 rpm for 5 minutes.
8. Take 100 µL of supernatant and transfer to Spin-X HPLC filter tubes (Corning Incorporated, Cat # 8169) and centrifuge at 13,000 rpm for 5 minutes and take 5 µL from this solution and dilute in 495 µL of LCMS grade methanol (Fischer scientific, CAS # 67-56-1) in an 2mL glass auto sampler vial (Microsolv, Cat # 95025-WCV)
9. The samples are analyzed by LCMS-8040. (Shimadzu)

Data:

Day 1:

Time (min)	Assay 1		Assay 2		Assay 3		% remaining		
	DKIV23-1 Peak area	ISTD Peak area	DKIV23-1 Peak area	ISTD Peak area	DKIV23-1 Peak area	ISTD Peak area	Assay 1	Assay 2	Assay 3
0	397963	56611955	368885	52125358	361274	51254549	100.42	101.09	100.69
10	388782	54723194	372606	52164132	355015	50186411	101.49	102.04	101.05
20	380721	54701573	379233	53380590	362789	51876673	99.42	101.49	99.90
30	369481	55241996	358850	53493948	351345	51717475	95.54	95.83	97.05
40	372657	55269780	362987	53319999	362810	52384243	96.32	97.25	98.94
50	365725	56348764	357825	53195640	360612	53107420	92.72	96.09	97.00
60	376855	57444817	369854	55578015	352228	52161108	93.71	95.06	96.46

Table 1: Peak areas and % remaining values

Day 2:

Time (min)	Assay 1		Assay 2		Assay 3		(% remaining)		
	DK-IV23-1 Peak area	ISTD Peak area	DKIV23-1 Peak area	ISTD Peak area	DK-IV23-1 Peak area	ISTD Peak area	Assay 1	Assay 2	Assay 3
0	351092	48879360	350753	50577100	346651	49121502	102.61	99.07	100.81
10	349247	49477174	340133	50185611	339590	50582041	100.83	96.82	95.90
20	356684	50551325	336437	49850755	318569	50160848	100.79	96.41	90.72
30	335212	50797085	325470	50922639	323113	50163181	94.27	91.30	92.01
40	345002	52003609	336870	51464523	319210	48852960	94.77	93.51	93.34
50	356812	52525598	345619	54188960	344935	53589290	97.04	91.11	91.95
60	368841	52321168	350501	53533499	332885	51164447	100.78	93.53	92.94

Table 2: Peak areas and % remaining values

Calculation:

From the peak area, Calculate the following

$$\text{Peak area ratio} = \frac{\text{Peak area of test compound (DK-IV-23-1)}}{\text{Peak area of internal standard (ISTD)}}$$

$$\text{\% remaining at time T = (T = 0, 10, 20,30,40,50 and 60)} \quad \frac{\text{Peak area ratio at particular time T}}{\text{Peak area ratio at zero time point}} * 100$$

DATA ANALYSIS:

Day 1

Linear regression analysis:

Slope: -0.001171 ± 0.0001171

At X= 60, Y = 4.550 ± 0.006169

R^2 = 0.7116

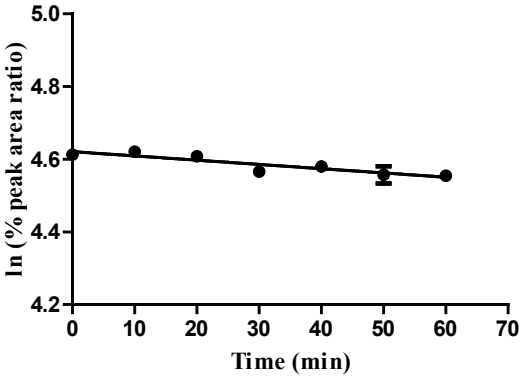

Metabolic Parameters:

Half-life: 591 ± 86 min

V_d: 2000 µL/mg

Intrinsic clearance: 0.1171 µL/min/mg

Metabolic Rate: 2.342 nmol/min/mg

% remaining at 60 min: 94.6 ± 0.3 %

Day 2

Linear regression analysis:

Slope: -0.0009798 ± 0.0003769

At X = 60, Y = 4.531 ± 0.01359

R^2 = 0.2623

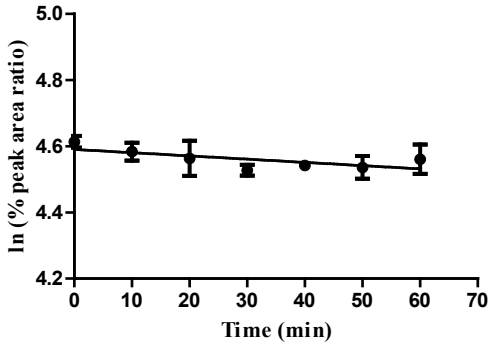

Metabolic Parameters:

Half-life: 707 ± 272 min

V_d: 2000 µL/mg

Intrinsic clearance: 0.09798 µL/min/mg

Metabolic Rate: 1.9595 nmol/min/mg

% remaining at 60 min: 92.8± 0.27 %

Note: The peak area ratios and natural log values are calculated using Microsoft excel 2010 and linear regression analysis is calculated using GraphPad prism.

Mouse Liver Microsomal Assay

Principal Investigator: Dr. Alexander Arnold
Operator: Revathi Kodali
Test Compound: DK-IV-23-1
Concentration: 10 µM
Date: 12-25-2018
Facility: Milwaukee Institute for Drug Discovery

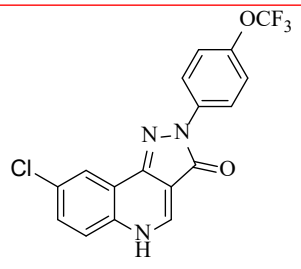

DK-IV-23-1 (14q)

Assay Protocol

Each evaluation included six independent assays carried out three at a time, on two different days

1. Preparation of solutions:
   a. 1 mM test compound in DMSO.
   b. 5 µM 4,5 Di Phenyl Imidazole in ice cold Acetonitrile (ISTD).
2. For a total volume of Microsomal Assay Mixture (MAM) 390 µL, sufficient for seven time points, combine the following
   a. 282 µL of 18.2 mΩ of water.
   b. 80 µL of 0.5 M potassium phosphate buffer (p^H 7.4)
   c. 20 µL of NADPH A. (Corning life sciences, Cat # 451220)
   d. 4 µL of NADPH B. (Corning life sciences, Cat # 451200)
   e. 4 µL of test compound.
3. Sonicate MAM for 5 min and meanwhile thaw microsomes (20 mg/mL) (Life technologies, Cat # MSMC-PL) on ice.
4. Aliquot 100 µL of ice cold ISTD into seven separate 1.5 mL conical vials and label them the time points for 0, 10, 20, 30, 40, 50, and 60 min.
5. Arrange the timer. Microsomes (Final concentration of 0.5 mg/mL) should be added to all time points except the zero time point.
6. Add 50 µL of the MAM solution to the conical vial labelled as zero time point. Place the remaining MAM solution in the incubator (37 ºC) for 5 min and initiate the reaction with addition of microsomes (8.8 µL) and record the time.
7. At the end of each time interval remove 50 µL and add to 100 µL ISTD in conical vial, sonicate for 10 sec and spin down at 10,000 rpm for 5 minutes.
8. Take 100 µL of supernatant and transfer to Spin-X HPLC filter tubes (Corning Incorporated, Cat # 8169) and centrifuge at 13,000 rpm for 5 minutes and take 5 µL from this solution and dilute in 495 µL of LCMS grade methanol (Fischer scientific, CAS # 67-56-1) in an 2mL glass auto sampler vial (Microsolv, Cat # 95025-WCV)
9. The samples are analyzed by LCMS-8040. (Shimadzu)

Data:

Day 1:

Time (min)	Assay 1		Assay 2		Assay 3		% remaining		
	DKIV23-1 Peak area	ISTD Peak area	DKIV23-1 Peak area	ISTD Peak area	DKIV23-1 Peak area	ISTD Peak area	Assay 1	Assay 2	Assay 3
0	339798	48602805	341061	48176329	324680	46476137	99.87	101.13	99.79
10	297529	49652797	324068	50521260	301747	49326646	85.60	91.63	87.39
20	318772	52465696	307358	51083172	309960	50440264	86.79	85.95	87.78
30	323896	54479671	322244	51477168	313515	50512036	84.93	89.48	88.66
40	319697	55818024	319023	51357849	310713	50925016	81.82	88.74	87.16
50	317220	53597832	312620	52744964	317837	52058314	84.55	84.67	87.22
60	305425	52563495	300194	52682918	326103	52925562	83	81.40	88.02

Table 1: Peak areas and % remaining values

Day 2:

Time (min)	Assay 1		Assay 2		Assay 3		(% remaining)		
	DK-IV23-1 Peak area	ISTD Peak area	DKIV23-1 Peak area	ISTD Peak area	DK-IV23-1 Peak area	ISTD Peak area	Assay 1	Assay 2	Assay 3
0	341137	48273282	314515	45093775	331589	46880368	100.95	99.63	101.04
10	312913	53059249	305715	50326291	325498	52065740	84.24	86.71	89.31
20	307241	50355815	300969	50986113	306625	52288142	87.13	84.28	83.73
30	309665	52453421	306617	51270231	310639	52268148	84.37	85.34	84.03
40	319470	52839719	311413	51130480	364165	65699421	86.37	87.08	79.18
50	316613	53027835	297570	51047043	304018	52211465	85.29	83.76	83.83
60	340115	55111762	288918	51201935	298226	53040044	88.16	80.10	80.324

Table 2: Peak areas and % remaining values

Calculation:

From the peak area, Calculate the following

$$\text{Peak area ratio} = \frac{\text{Peak area of test compound (DK-IV-23-1)}}{\text{Peak area of internal standard (ISTD)}}$$

$$\text{\% remaining at time T (T = 0, 10, 20,30,40,50 and 60)} = \frac{\text{Peak area ratio at particular time T}}{\text{Peak area ratio at zero time point}} * 100$$

DATA ANALYSIS:

Day 1

Linear regression analysis:

Slope: -0.002146 ± 0.0004690

At X= 60, Y = 4.415 ± 0.01691

R^2 = 0.5244

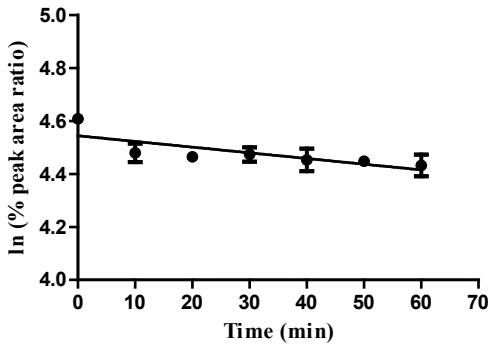

Metabolic Parameters:

Half-life: 322 ± 70 min

V_d: 2000 µL/mg

Intrinsic clearance: 0.2146 µL/min/mg

Metabolic Rate: 4.292 nmol/min/mg

% remaining at 60 min: 82.6 ± 0.3 %

Day 2

Linear regression analysis:

Slope: -0.002343 ± 0.0005509

At X = 60, Y = 4.393 ± 0.01986

R^2 = 0.4876

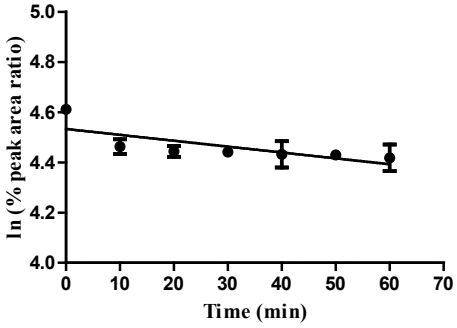

Metabolic Parameters:

Half-life: 295 ± 69 min

V_d: 2000 µL/mg

Intrinsic clearance: 0.02343 µL/min/mg

Metabolic Rate: 4.686 nmol/min/mg

% remaining at 60 min: 80.8 ± 0.36 %

Note: The peak area ratios and natural log values are calculated using Microsoft excel 2010 and linear regression analysis is calculated using GraphPad prism.

Human Liver Microsomal Assay

Principal Investigator: Dr. Alexander Arnold
Operator: Revathi Kodali
Test Compound: DK-IV-19-1
Concentration: 10 µM
Date: 12-25-2018
Facility: Milwaukee Institute for Drug Discovery

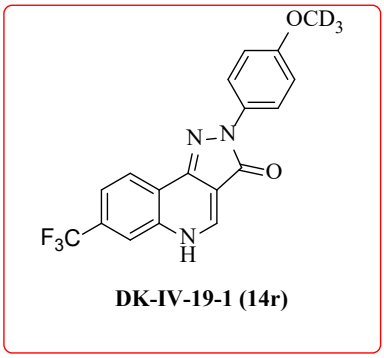

DK-IV-19-1 (14r)

Assay Protocol

Each evaluation included six independent assays carried out three at a time, on two different days

1. Preparation of solutions:
   a. 1 mM test compound in DMSO.
   b. 5 µM 4,5 Di Phenyl Imidazole in ice cold Acetonitrile (ISTD).
2. For a total volume of Microsomal Assay Mixture (MAM) 390 µL, sufficient for seven time points, combine the following
   a. 282 µL of 18.2 mΩ of water.
   b. 80 µL of 0.5 M potassium phosphate buffer (p^H 7.4)
   c. 20 µL of NADPH A. (Corning life sciences, Cat # 451220)
   d. 4 µL of NADPH B. (Corning life sciences, Cat # 451200)
   e. 4 µL of test compound.
3. Sonicate MAM for 5 min and meanwhile thaw microsomes (20 mg/mL) (BD Gentest, Cat # 452156) on ice.
4. Aliquot 100 µL of ice cold ISTD into seven separate 1.5 mL conical vials and label them the time points for 0, 10, 20, 30, 40, 50, and 60 min.
5. Arrange the timer. Microsomes (Final concentration of 0.5 mg/mL) should be added to all time points except the zero time point.
6. Add 50 µL of the MAM solution to the conical vial labelled as zero time point. Place the remaining MAM solution in the incubator (37 ºC) for 5 min and initiate the reaction with addition of microsomes (8.8 µL) and record the time.
7. At the end of each time interval remove 50 µL and add to 100 µL ISTD in conical vial, sonicate for 10 sec and spin down at 10,000 rpm for 5 minutes.
8. Take 100 µL of supernatant and transfer to Spin-X HPLC filter tubes (Corning Incorporated, Cat # 8169) and centrifuge at 13,000 rpm for 5 minutes and take 5 µL from this solution and dilute in 495 µL of LCMS grade methanol (Fischer scientific, CAS # 67-56-1) in an 2mL glass auto sampler vial (Microsolv, Cat # 95025-WCV)
9. The samples are analyzed by LCMS-8040. (Shimadzu)

Data:

Day 1:

Time (min)	Assay 1		Assay 2		Assay 3		% remaining		
	DKIV23-1 Peak area	ISTD Peak area	DKIV23-1 Peak area	ISTD Peak area	DKIV23-1 Peak area	ISTD Peak area	Assay 1	Assay 2	Assay 3
0	1456704	71880342	1417327	73957165	1509187	71744353	101.32	100.86	100.17
10	1325657	71049872	1357906	73319985	1519946	71146707	93.29	97.47	101.73
20	1325903	69360719	1291713	70757756	1515156	72662220	95.58	96.08	99.29
30	1472140	73258868	1330986	70651044	1493197	73104888	100.47	99.15	97.26
40	1468450	71606625	1279540	71767376	1273390	64726364	102.53	93.83	93.68
50	1344527	74029867	1393570	74839396	1115903	55435062	90.81	98.00	95.85
60	1376401	74160802	1236609	70343146	1462643	72132749	92.79	92.52	96.55

Table 1: Peak areas and % remaining values

Day 2:

Time (min)	Assay 1		Assay 2		Assay 3		(% remaining)		
	DK-IV23-1 Peak area	ISTD Peak area	DKIV23-1 Peak area	ISTD Peak area	DK-IV23-1 Peak area	ISTD Peak area	Assay 1	Assay 2	Assay 3
0	1535699	80410665	1418018	74867343	1520870	80080389	100.51	99.68	99.95
10	1383795	74266235	1310809	71832237	1452383	78656481	98.06	96.04	97.18
20	1365763	74888240	1299288	72647840	1434742	79337154	95.98	94.13	95.18
30	1338966	73987423	1321119	73645748	1576910	82398638	95.24	94.41	100.72
40	1433349	76113985	1256412	70723766	1435821	76994089	99.11	93.50	98.15
50	1365100	78135548	1280660	71463758	1445835	81744367	91.95	94.31	93.09
60	1395391	78135087	1343599	72643875	1451849	78813609	93.99	97.34	96.95

Table 2: Peak areas and % remaining values

Calculation:

From the peak area, Calculate the following

$$\text{Peak area ratio} = \frac{\text{Peak area of test compound (DK-IV-19-1)}}{\text{Peak area of internal standard (ISTD)}}$$

$$\text{\% remaining at time T (T = 0, 10, 20,30,40,50 and 60)} = \frac{\text{Peak area ratio at particular time T}}{\text{Peak area ratio at zero time point}} * 100$$

DATA ANALYSIS:

Day 1

Linear regression analysis:

Slope: -0.0009631 ± 0.0003284

At X= 60, Y = 4.546 ± 0.001184

R^2 = 0.3116

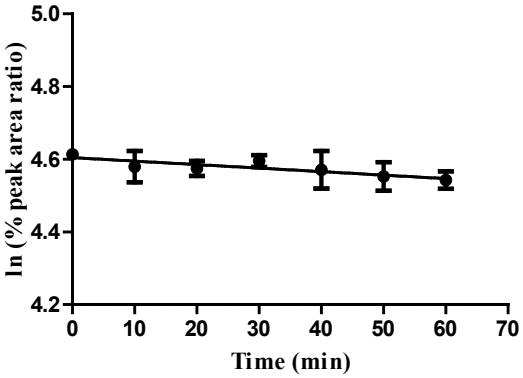

Metabolic Parameters:

Half-life: 719 ± 245 min

V_d: 2000 µL/mg

Intrinsic clearance: 0.09631 µL/min/mg

Metabolic Rate: 1.9262 nmol/min/mg

% remaining at 60 min: 94.6 ± 0.3 %

Day 2

Linear regression analysis:

Slope: -0.0006702 ± 0.0002585

At X = 60, Y = 4.549 ± 0.09319

R^2 = 0.2614

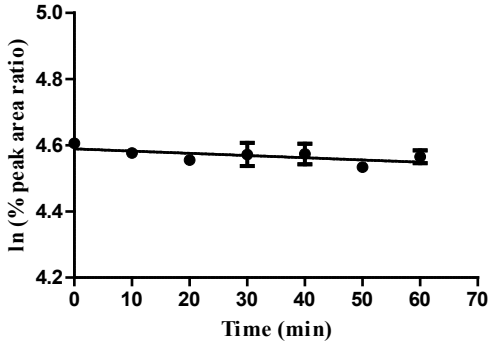

Metabolic Parameters:

Half-life: 1034 ± 398 min

V_d: 2000 µL/mg

Intrinsic clearance: 0.06702 µL/min/mg

Metabolic Rate: 1.3404 nmol/min/mg

% remaining at 60 min: 92.8± 0.27 %

Note: The peak area ratios and natural log values are calculated using Microsoft excel 2010 and linear regression analysis is calculated using GraphPad prism.

Mouse Liver Microsomal Assay

Principal Investigator: Dr. Alexander Arnold
Operator: Revathi Kodali
Test Compound: DK-IV-19-1
Concentration: 10 µM
Date: 12-25-2018
Facility: Milwaukee Institute for Drug Discovery

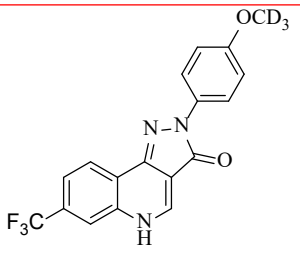

DK-IV-19-1 (14r)

Assay Protocol

Each evaluation included six independent assays carried out three at a time, on two different days

1. Preparation of solutions:
   a. 1 mM test compound in DMSO.
   b. 5 µM 4,5 Di Phenyl Imidazole in ice cold Acetonitrile (ISTD).
2. For a total volume of Microsomal Assay Mixture (MAM) 390 µL, sufficient for seven time points, combine the following
   a. 282 µL of 18.2 mΩ of water.
   b. 80 µL of 0.5 M potassium phosphate buffer (p^H 7.4)
   c. 20 µL of NADPH A. (Corning life sciences, Cat # 451220)
   d. 4 µL of NADPH B. (Corning life sciences, Cat # 451200)
   e. 4 µL of test compound.
3. Sonicate MAM for 5 min and meanwhile thaw microsomes (20 mg/mL) (BD Gentest, Cat # 452156) on ice.
4. Aliquot 100 µL of ice cold ISTD into seven separate 1.5 mL conical vials and label them the time points for 0, 10, 20, 30, 40, 50, and 60 min.
5. Arrange the timer. Microsomes (Final concentration of 0.5 mg/mL) should be added to all time points except the zero time point.
6. Add 50 µL of the MAM solution to the conical vial labelled as zero time point. Place the remaining MAM solution in the incubator (37 ºC) for 5 min and initiate the reaction with addition of microsomes (8.8 µL) and record the time.
7. At the end of each time interval remove 50 µL and add to 100 µL ISTD in conical vial, sonicate for 10 sec and spin down at 10,000 rpm for 5 minutes.
8. Take 100 µL of supernatant and transfer to Spin-X HPLC filter tubes (Corning Incorporated, Cat # 8169) and centrifuge at 13,000 rpm for 5 minutes and take 5 µL from this solution and dilute in 495 µL of LCMS grade methanol (Fischer scientific, CAS # 67-56-1) in an 2mL glass auto sampler vial (Microsolv, Cat # 95025-WCV)
9. The samples are analyzed by LCMS-8040. (Shimadzu)

Data:

Day 1:

Time (min)	Assay 1		Assay 2		Assay 3		% remaining		
	DKIV23-1 Peak area	ISTD Peak area	DKIV23-1 Peak area	ISTD Peak area	DKIV23-1 Peak area	ISTD Peak area	Assay 1	Assay 2	Assay 3
0	1532299	76327196	1555050	78321871	1531041	80846373	100.37	99.27	99.67
10	1458928	74906082	1494997	77180323	1533236	80214450	97.38	96.85	100.60
20	1468755	73522346	1659556	82430222	1472784	78061099	99.88	100.66	99.30
30	1376463	72429047	1577451	81495259	1481552	80378219	95.02	96.78	97.01
40	1409701	74786376	1633513	84230317	1622316	85733411	94.24	96.96	99.59
50	1448406	76375311	1640454	85814196	1589484	85855930	94.82	95.58	97.43
60	1431946	74195544	1593726	84451182	1503784	84238915	96.49	94.35	93.95

Table 1: Peak areas and % remaining values

Day 2:

Time (min)	Assay 1		Assay 2		Assay 3		(% remaining)		
	DK-IV23-1 Peak area	ISTD Peak area	DKIV23-1 Peak area	ISTD Peak area	DK-IV23-1 Peak area	ISTD Peak area	Assay 1	Assay 2	Assay 3
0	1613982	77082382	1587374	7864374	1711312	8136743	99.70	99.92	100.15
10	1570375	76638354	1425331	7682623	1625231	7836291	97.57	91.84	98.76
20	1529776	79945064	1478266	7623572	1690359	8045334	91.12	95.99	100.05
30	1644678	83949348	1437809	7535228	1478886	7650770	93.29	94.46	92.04
40	1615399	81303818	1509123	7767823	1592938	7667837	94.61	96.17	98.92
50	1590635	83569908	1494059	7608820	1416051	7361750	90.63	97.20	91.59
60	1625413	82043570	1397181	7563401	1446366	7232378	94.34	91.45	95.23

Table 2: Peak areas and % remaining values

Calculation:

From the peak area, Calculate the following

$$\text{Peak area ratio} = \frac{\text{Peak area of test compound (DK-IV-19-1)}}{\text{Peak area of internal standard (ISTD)}}$$

$$\text{\% remaining at time T (T = 0, 10, 20,30,40,50 and 60)} = \frac{\text{Peak area ratio at particular time T}}{\text{Peak area ratio at zero time point}} * 100$$

DATA ANALYSIS:

Day 1

Linear regression analysis:

Slope: -0.0008143 ± 0.0001794

At X= 60, Y = 4.555 ± 0.006467

R^2 = 0.5203

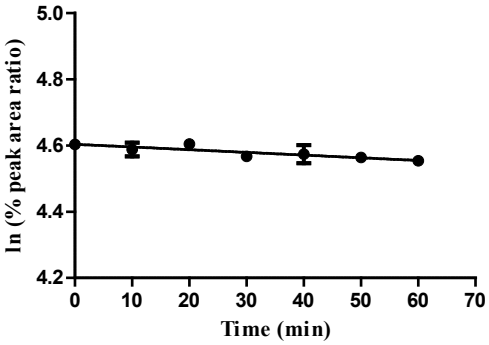

Metabolic Parameters:

Half-life: 851 ± 187 min

V_d: 2000 µL/mg

Intrinsic clearance: 0.08143 µL/min/mg

Metabolic Rate: 1.6286 nmol/min/mg

% remaining at 60 min: 95 ± 0.4 %

Day 2

Linear regression analysis:

Slope: -0.0008810 ± 0.0003304

At X = 60, Y = 4.532 ± 0.01191

R^2 = 0.2723

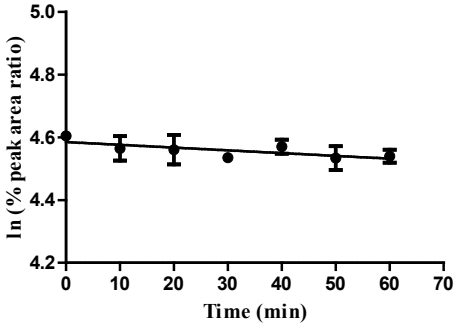

Metabolic Parameters:

Half-life: 786 ± 295 min

V_d: 2000 µL/mg

Intrinsic clearance: 0.08801 µL/min/mg

Metabolic Rate: 1.762 nmol/min/mg

% remaining at 60 min: 93± 3 %

Note: The peak area ratios and natural log values are calculated using Microsoft excel 2010 and linear regression analysis is calculated using GraphPad prism.

4.9. Poster Presentations

4.9.1. Novel Deuterated GABAAR-α6 Subtype Selective Ligands with Improved Metabolic Stability. Targeting Trigeminal Orofacial Pain, Neuropsychiatric Disorders, & Depression[305]

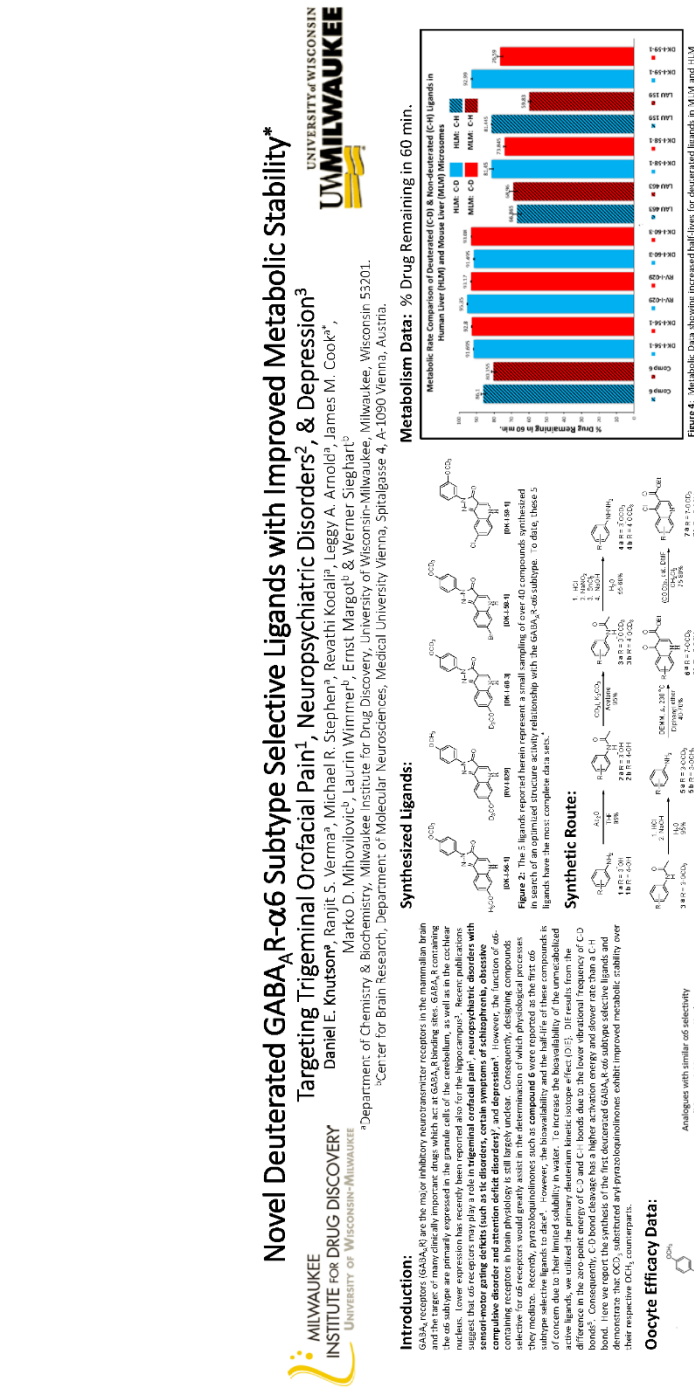

4.9.2. Novel Deuterated GABAAR-α6 Subtype Selective Ligands with Improved Metabolic Stability and Enhanced Bioavailability Targeting Trigeminal Orofacial Pain, Neuropsychiatric Disorders, and Depression[306]

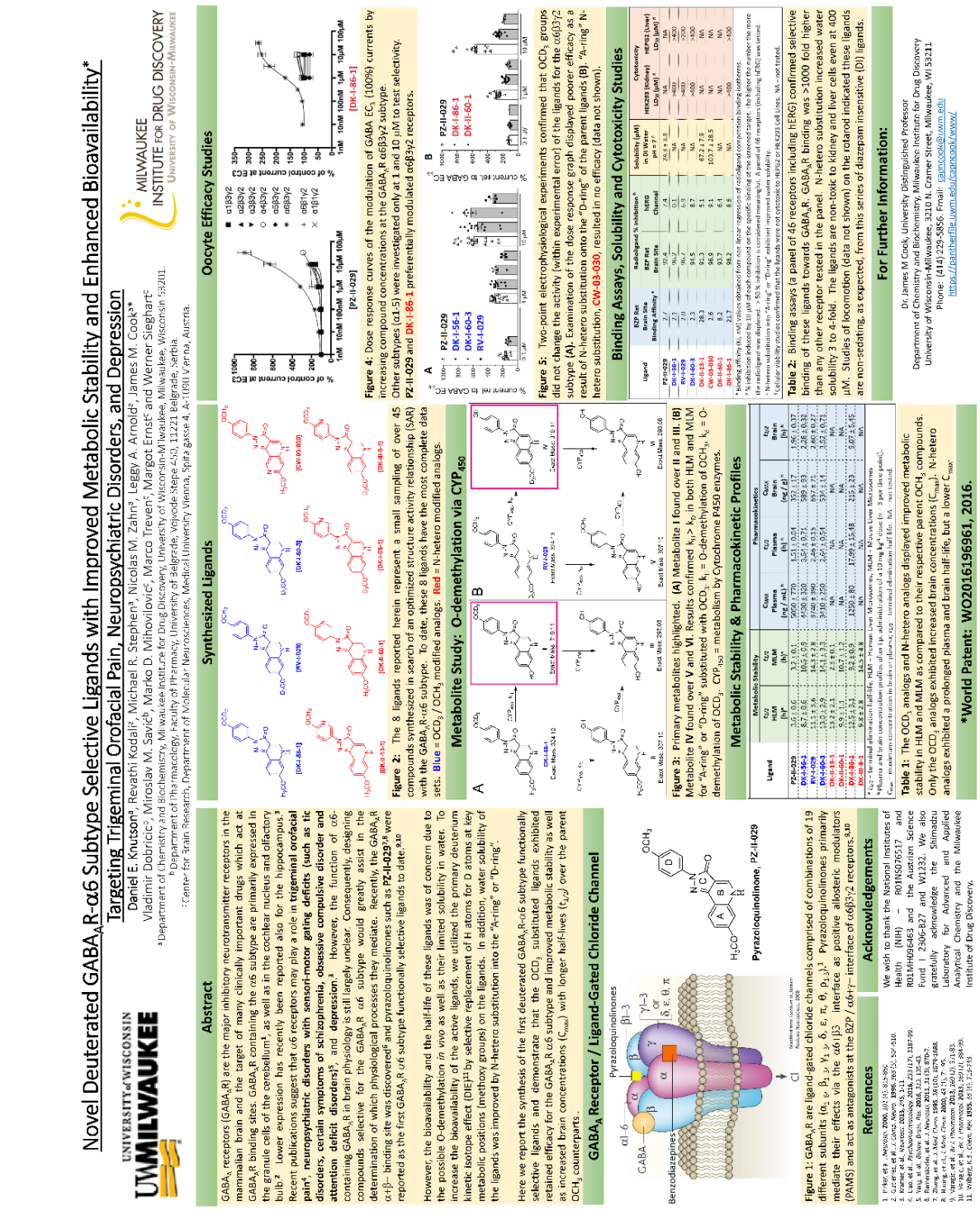

4.9.3. Design and Synthesis of Novel Deuterated GABAAR-a6 Subtype Selective Ligands with Improved Metabolic Stability and Enhanced Bioavailability[307]

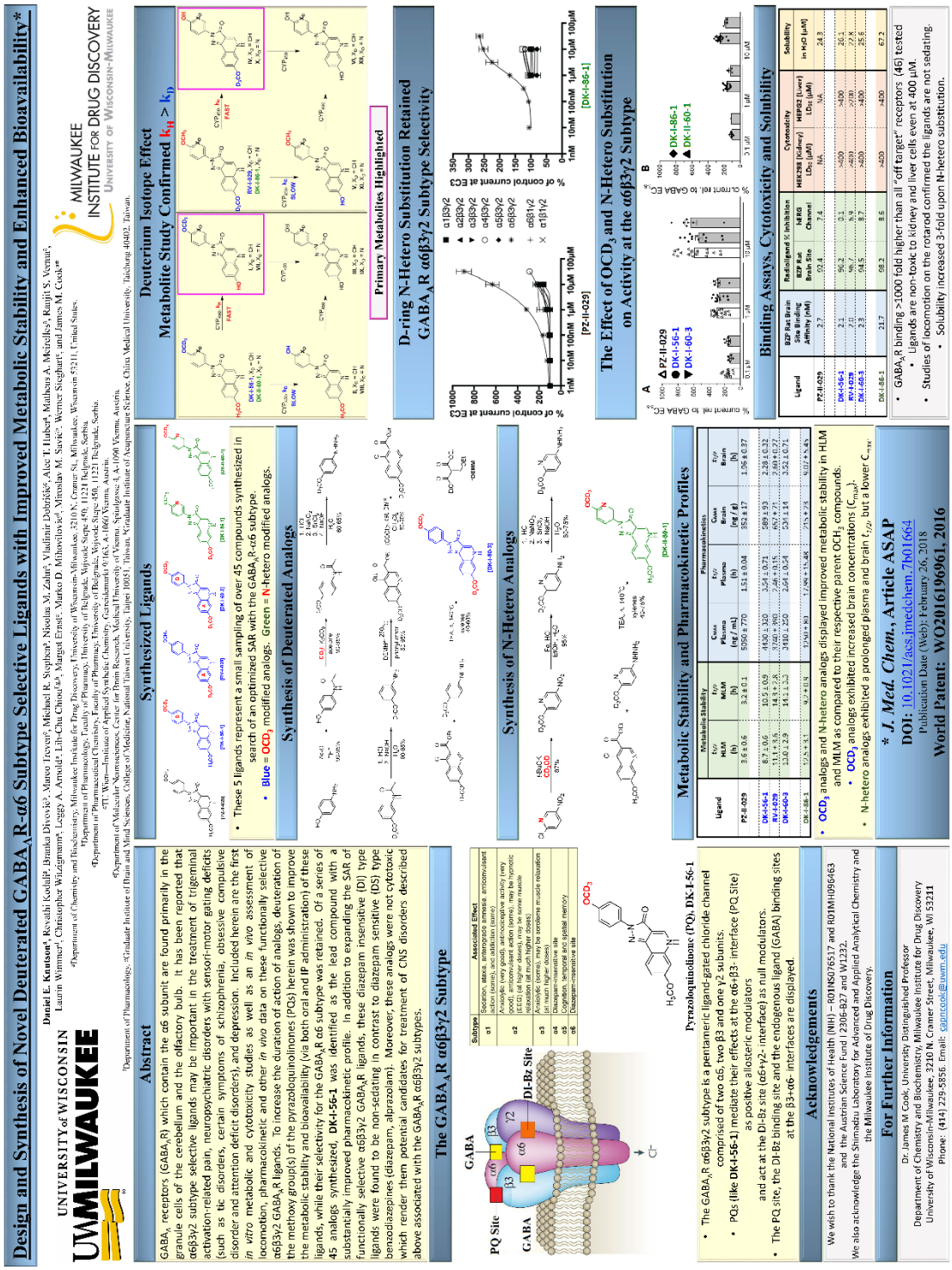

4.9.4. Prevention of Trigeminal Neuropathic Pain Development in Rats Using Novel Deuterated GABAAR-α6 Subtype Selective Ligands[308]

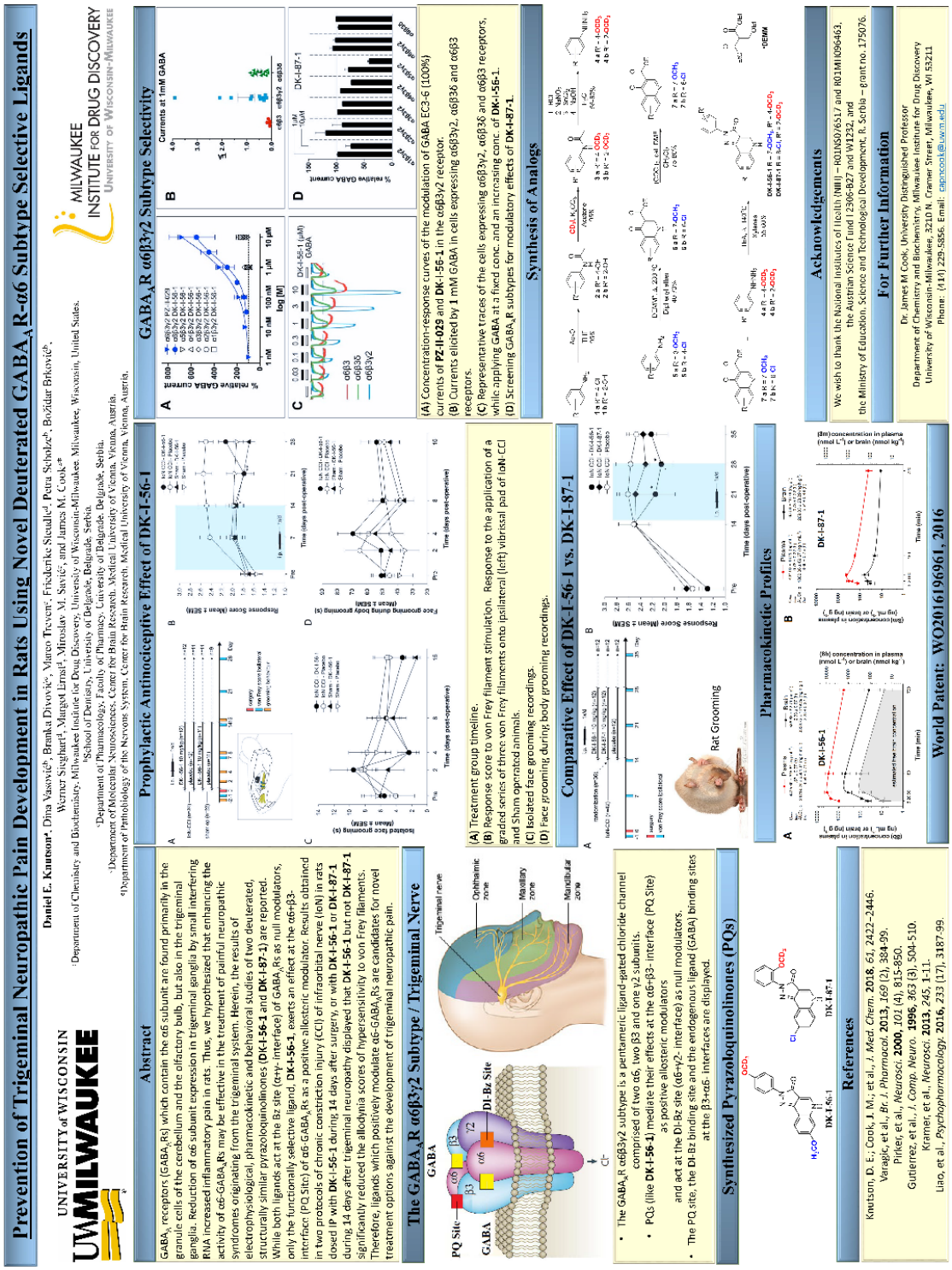

4.9.5. Treatment of Sensorimotor Gating Deficits in Neuropsychiatric Disorders Using Deuterated α6-GABA$_A$R Subtype Selective Ligands[51]

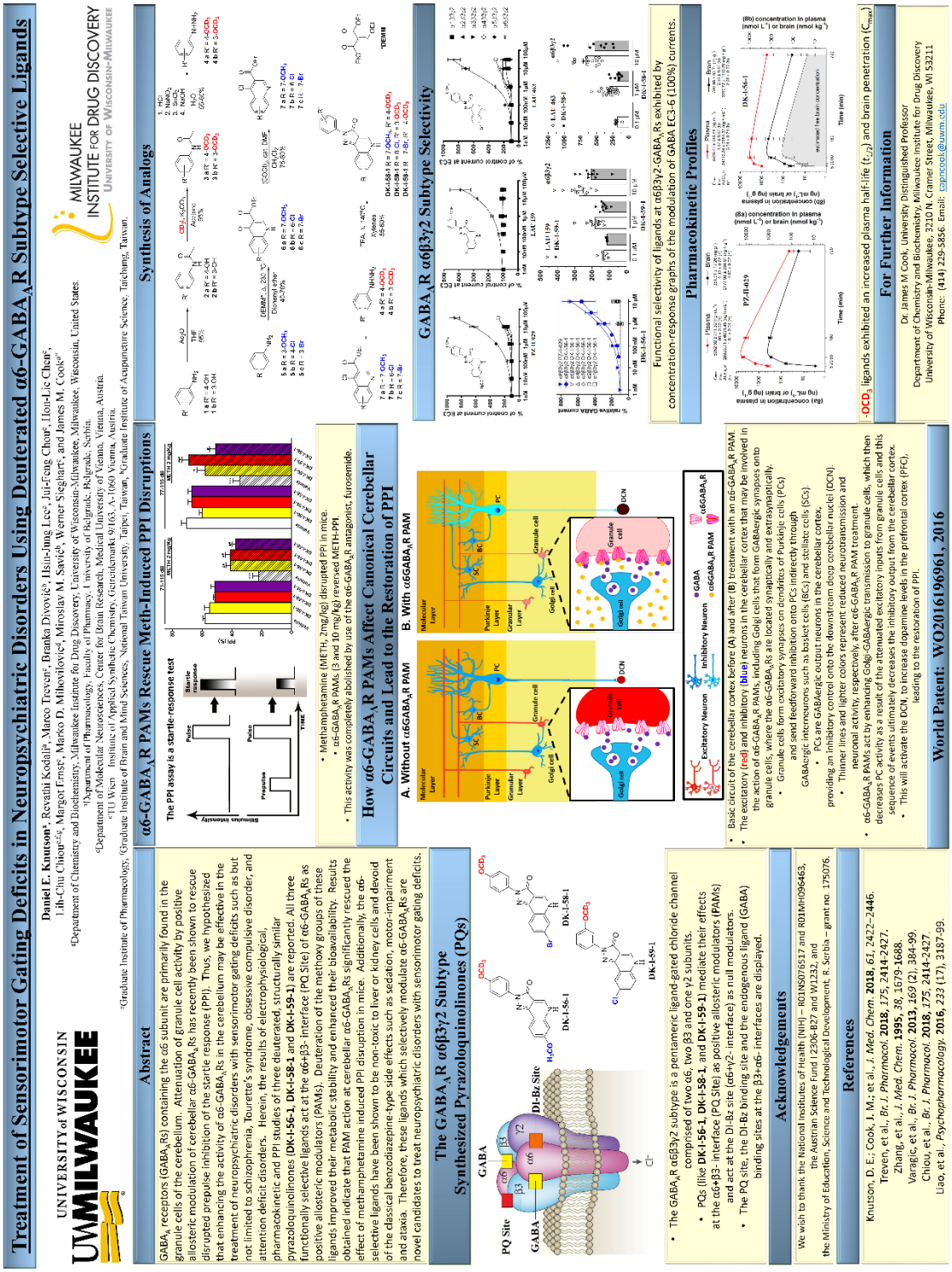

4.9.6. Combatting the Opioid and Benzodiazepine Epidemic by the Synthesis of Novel Safer Drugs Designed to be Functionally Selective for α5- or α6-containing $GABA_A$ Receptors[309]

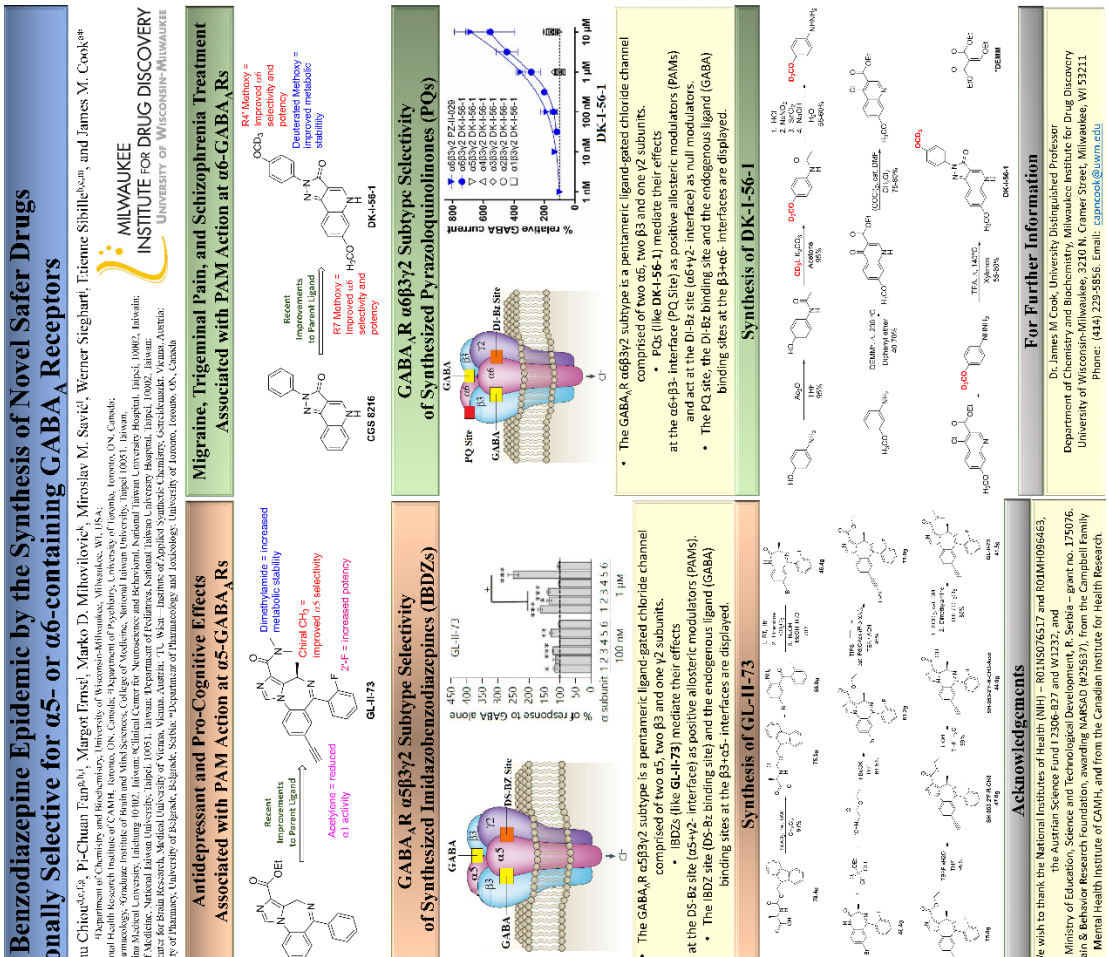

4.9.7. A Comparative Study of Deuteration Versus Fluorination of α6-GABA$_A$R Subtype-Selective Ligands as Strategies to Enhance Bioavailability, and their Impact on the Pharmacokinetic Profiles and α6-GABA$_A$R Functional Selectivity[80]

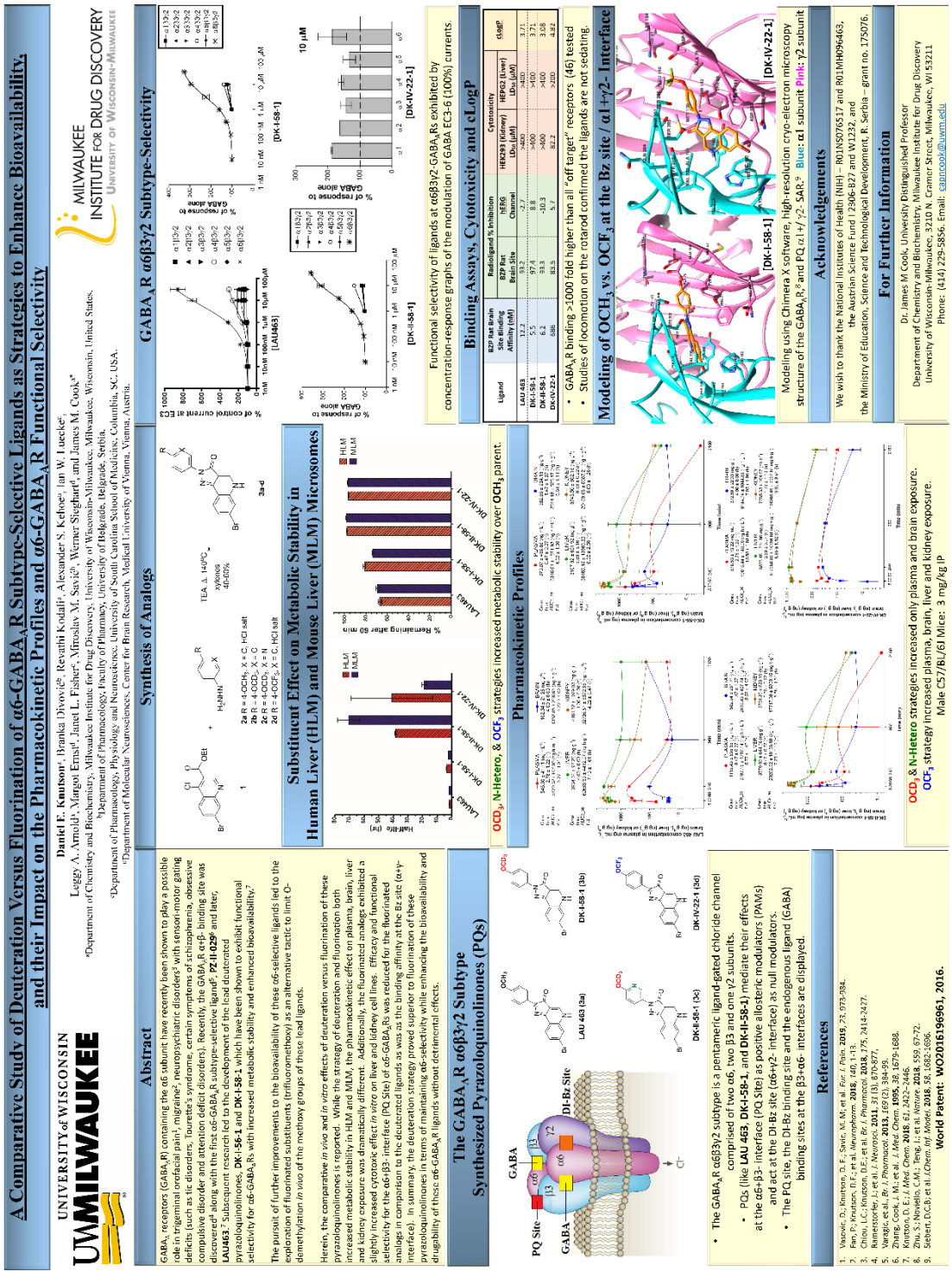

4.10. Poster Presentations by Collaborators with Our Group

4.10.1. The Search for Water Soluble α6 Bz/GABA$_A$ Receptor Subtype Selective Ligands in Order to Determine Their *in vivo* Activity

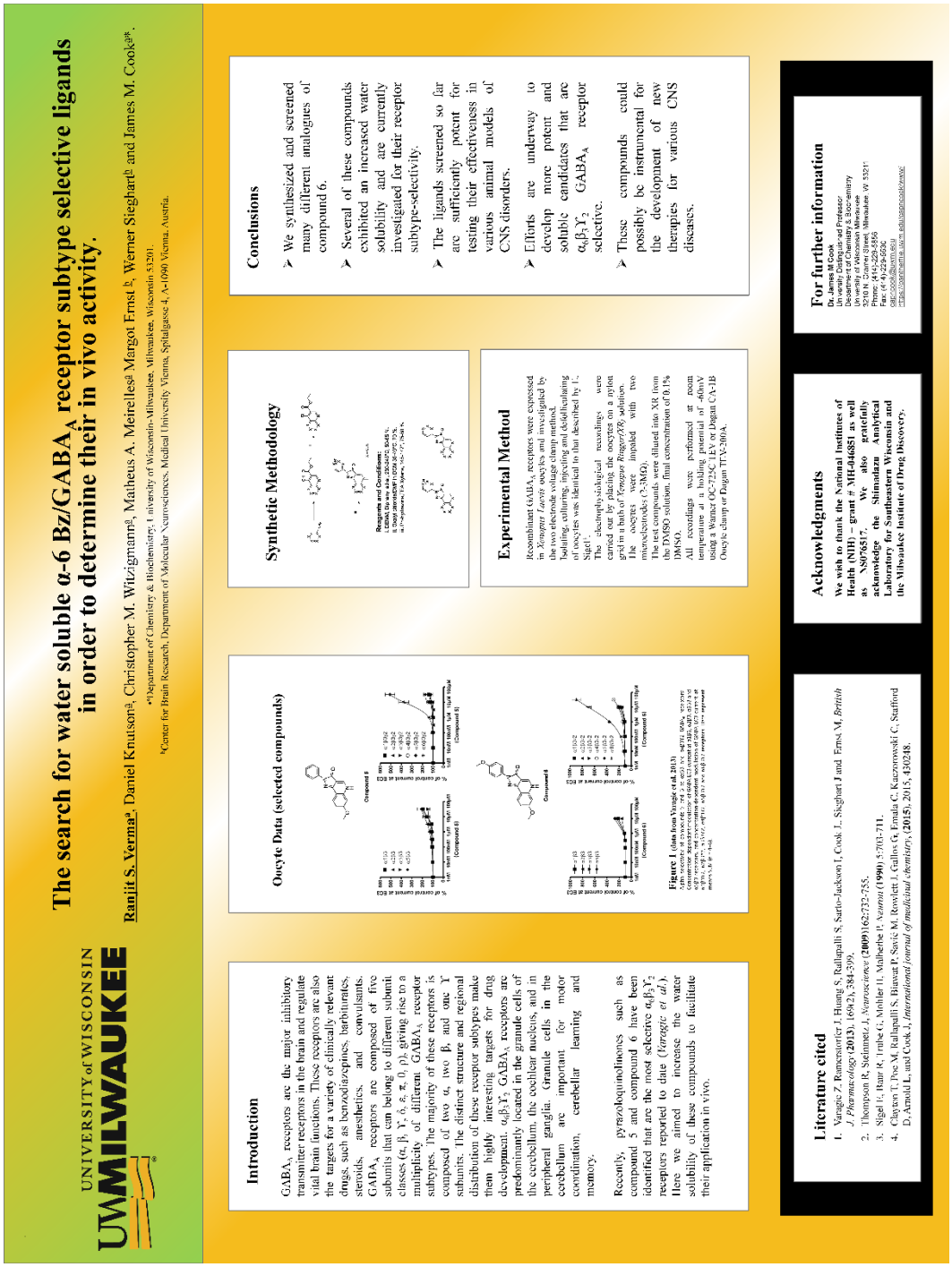

4.10.2. Nanonization of New Patent Protected Substances—Carrier Selection of Preclinical Research: Physiochemical and *in vivo* Behavioral Characterization

NANONIZATION OF NEW PATENT PROTECTED SUBSTANCES – CARRIER SELECTION FOR PRECLINICAL RESEARCH: PHYSICOCHEMICAL AND *IN VIVO* BEHAVIORAL CHARACTERIZATION

J. Mitrović,[1] B. Divović,[2] VD. Dobričić,[3] BR. Čalija,[1] PJ. Vulić,[4] DE. Knutson,[5] JM. Cook,[5] MM. Savić,[2] SD. Savić[1*]

[1] University of Belgrade-Faculty of Pharmacy, Department of Pharmaceutical Technology and Cosmetology, Belgrade, Serbia
[2] University of Belgrade-Faculty of Pharmacy, Department of Pharmacology, Belgrade, Serbia
[3] University of Belgrade-Faculty of Pharmacy, Department of Pharmaceutical Chemistry, Belgrade, Serbia
[4] University of Belgrade–Faculty of Mining and Geology, Chair of Mineralogy, Belgrade, Serbia
[5] University of Wisconsin-Milwaukee, Department of Chemistry and Biochemistry, Milwaukee Institute for Drug Discovery, Milwaukee, Wisconsin, United States
* snezana.savic@pharmacy.bg.ac.rs

INTRODUCTION

Deuterated pyrazoloquinolinones, $GABA_A$ receptor ligands, are being investigated for neuropsychiatric disorders treatment. Among others, DK-I-56-1 (7-Methoxy-2-(4-methoxy-d3-phenyl)-2,5-dihydro-3H-pyrazolo-[4,3-c]quinolin-3-one) was chosen as the lead component [1]. Because of its low solubility in water (6.27 ± 0.74 μg/ml) **nanosuspension** formulation for prospective parenteral administration was carried out [2]. Moreover, the potential of this carrier to deliver DK-I-56-1 to the brain without possible sedation which followed nanoemulsion administration as vehicle, was analyzed by *in vivo* behavioral tests.

MATERIAL AND METHODS

Nanocrystal dispersions were prepared by **wet ball milling**. DK-I-56-1 (0.2%) was dispersed in aqueous stabilizer solution (polysorbate 80 (0.1%) (*P80*); polysorbate 80 (0.05%) and poloxamer 407 (0.05%)(*P80+P407*); polysorbate 80 (0.05%) and d-α-Tocopheryl polyethylene glycol 1000 succinate (0.05%)(*P80+TPGS*) or polysorbate 80 (0.05%) and poloxamer 188 (0.05%)(*P80+P188*)) and homogenized on rotor stator homogenizer. The dispersion was then separated to 2 ml Eppendorf tubes containing 60% *v/v* 0.1-0.2 mm yttrium stabilized zirconium beads and shook for 1h using a beads-milling cell disruptor equipment [3] (*Figure 1*). For spontaneous locomotor activity (SLA) test, tonicity of nanosuspension of DK-I-56-1 was adjusted by 2.5% glycerol.

Figure 1: Nanosuspension preparation

Obtained formulations were characterized in terms of particle size (z-ave), polydispersity index (PdI) and zeta potential after one, 7, 14 and 21 days. For complete physicochemical characterization differential scanning calorimetry (DCS) and X-ray powder diffraction (XRPD) analysis were conducted. Dissolution studies were performed by reverse dialysis bag method with 6 time points sampling (5, 15, 30, 60, 120, 180 min.) which were analyzed by UPHLC-MS/MS. For statistical analysis one way ANOVA with SNK as post hoc test was used with $p<0.05$ as statistically significant.

RESULTS

Particle size of nanosuspensions one day after preparation was in range 208.7–250.6 nm and PdI was <0.250 in all formulations (*Figure 2*). Zeta potential was above -20 mV (*Figure 3*). After 3 weeks of storage, although z-ave and PdI slightly increased, no agglomeration was observed. During this time sedimentation occurred, but after easy redispersion by shaking formulations remained stable for hours.

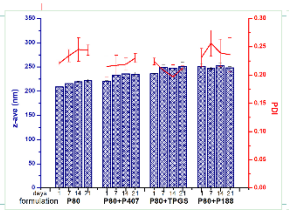

Figure 2: Nanosuspension particle size (z-ave) and PDI

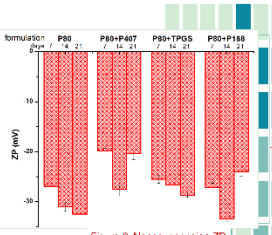

Figure 3: Nanosuspension ZP

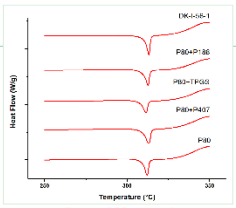

Figure 4: DSC curves of nanosuspensions and DK-I-56-1.

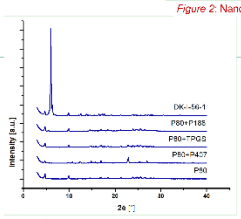

Figure 5: X-ray powder patterns of nanosuspensions and DK-I-56-1.

DSC analysis indicated that DK-I-56-1 remained in crystalline state (*Figure 4*), which was confirmed by **XRPD** (*Figure 5*).

Dissolution studies showed significant increase of dissolution rate of nanosuspension stabilized by polysorbate 80 when compared to suspension with same composition (*Figure 6*). Observed dissolution rate increase could be undoubtedly associated with smaller particle size.

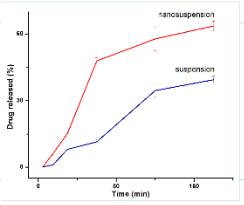

Figure 6: Dissolution profiles of DK-I-56-1 nanosuspension and suspension.

SLA test proved that intraperitoneally administered nanosuspension could deliver DK-I-56-1 to the brain. Hyperlocomotion (expressed as longer total distance travelled) was observed in mice treated with nanosuspension compared to mice treated with placebo or saline ($F(2,31)=7.126$, $p<0.01$), while corresponding placebo was not behaviorally active when compared to saline ($p=0.289$).

CONCLUSION

Nanosuspension formulation could improve DK-I-56-1 physicochemical properties and should be further investigated as promising carriers for brain drug delivery.

REFERENCES

[1] Knutson DE. et al. J Med Chem 61 (2018) 2422-2446.
[2] Sharma P. et al. Int J Pharm 408 (2011) 138-151.
[3] Corrias F. et al. Int J Pharm 524 (2017) 1-8.

ACKNOWLEDGMENT

This work was financially supported by the Ministry of Education, Science and Technological Development, Republic of Serbia, within the framework of Projects TR34031 and OI175076.

4.10.3. Nanosuspensions of Novel Deuterated Pyrazoloquinolinones Ligand (DK-I-56-1): Lyophilization Procedure Development Through Cryoprotectant Selection and Stability Study

NANOSUSPENSIONS OF NOVEL DEUTERATED PYRAZOLOQUINOLINONES LIGAND (DK-I-56-1): LYOPHILIZATION PROCEDURE DEVELOPMENT THROUGH CRYOPROTECTANT SELECTION AND STABILITY STUDY

Jelena Mitrović, Maja Bjelošević, Jelena Đoković, Pegi Ahlin Grabnar, Odon Planinšek, Daniel Knutson, James Cook, Miroslav Savić, Snežana Savić
e-mail: snezana.savic@pharmacy.bg.ac.rs

ABSTRACT

Despite of good pharmacodynamics of DK-I-56-1, novel deuterated pyrazoloquinolinones ligand, low solubility limits its administration. Nanosuspensions can help to overcome this problem, but its small particle size usually leads to particle agglomeration in short period of time. This phenomenon can be prevented by performing lyophilization. In this study cryoprotectants selection as well as characterization (particle size measurements after redispersion, scanning electron microscopy, differential scanning calorimetry and thermogravimetric measurements) of obtained freeze dried preparations was carried out. It was observed that sucrose/mannitol ratio 1:1 and 3:2 in total concentration of 10% can preserve particle size during lyophilization. However, after stability study conducted during one month storage at 25 °C and 40 °C, particle size remained in submicron range only in one sample. Changes in particle size were also followed by changes in polymorphic form of mannitol. It can be concluded that changes of crystal forms in freeze dried preparations during storage could jeopardize their stability, and therefore should be carefully examined.

Keywords: nanosuspension, particle size, lyophilization, sucrose, mannitol.

INTRODUCTION

DK-I-56-1 (7-Methoxy-2-(4-methoxy-d3-phenyl)-2,5-dihydro-3H-pyrazolo[4,3-c]quinolin-3-one), has a potential therapeutic use in the treatment of depression, migraine and some neuropsychiatric disorders. Despite its good efficacy, low solubility hinder its administration. Nanosuspension formulation could be a promising tool to overcome these limitations. However, due to small particle size, nanocrystals tend to agglomerate during storage, which then compromises their application. By converting them to solid products it is possible to prevent agglomeration and increase stability. For this purpose, lyophilization is commonly used method. For formulation stabilization during lyophilization it is necessary to add cryoprotectants, and usually also bulking agent. The aim of this research was to investigate different ratios of sucrose and mannitol in lyophilization of nanosuspensions with respect to particle size preservation and acceptable cake appearance.

RESEARCH CONCEPT

Nanocrystal dispersions stabilized by polysorbate 80 (NS1) or combination of polysorbate 80 and poloxamer 407 (NS2) were prepared by wet ball milling. After addition of mannitol, sucrose or sucrose and mannitol in different ratios, samples were frozen and then freeze dried for 24h. Samples were characterized after lyophilization and after one month storage at 25 °C or 40 °C. Particle size was measured using Zetasizer Nano ZS (Malvern Instruments, UK) and Mastersizer (Malvern Mastersizer 2000 equipped with a small volume dispersion cell, Malvern, UK). The morphology of samples was investigated using field emission scanning electron microscopy (SEM: Zeiss Ultra Plus, Carl Zeis GmbH, Germany). Differential scanning calorimetry (DSC) (DSC1; Mettler Toledo, Switzerland) measurements were conducted in order to determine Tg' and Tg values. To determine residual water content, thermogravimetric measurements (TGA) (TGA/DSC 1 Mettler Toledo, Switzerland) were performed.

RESULTS AND DISCUSSION

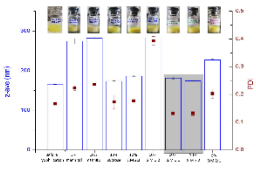

Figure 1 – Particle size (z-ave) and polydispersity index (PDI) of freeze-dried samples after reconstitution (5-sucrose, M-mannitol)

In the first phase of experiments optimal cryoprotectants and their concentration was selected. Small size increase after redispersion was observed in samples with 10% sucrose, and sucrose/ mannitol ratio 2:1, 1:1 and 3:2, compared to other samples in which agglomeration was evident (Figure 1). Because of poor cake appearance of samples with 10% sucrose and sucrose:mannitol ratio 2:1, samples with sucrose:mannitol 1:1 and 3:2 were chosen for further analysis.

Particle size of chosen samples after lyophilization and subsequent redispersion increased for 50 nm (NS1) or 10 nm (NS2), and did not change significantly after 24h (Figure 2). After one month storage at 25 °C and 40 °C one sample (freeze dried NS1 with sucrose/mannitol 1:1, kept at 25 °C) remained stable regarding particle size, while agglomeration occurred in all other samples. This fenomenon was characterized by around fourfold particle size increase and additional peak > 1 μm in Mastersizer results.

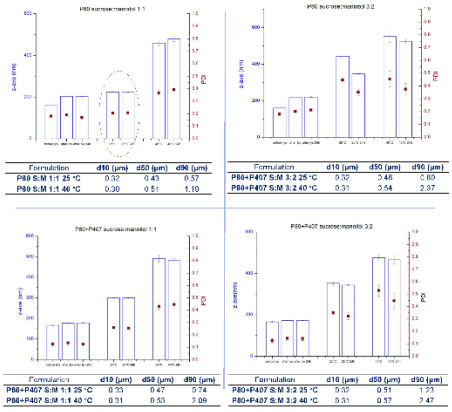

Formulation	d10 (μm)	d50 (μm)	d90 (μm)
P80 S:M 1:1 25 °C	0.32	0.43	0.57
P80 S:M 1:1 40 °C	0.30	0.51	1.10

Formulation	d10 (μm)	d50 (μm)	d90 (μm)
P80+P407 S:M 3:2 25 °C	0.32	0.46	0.60
P80+P407 S:M 3:2 40 °C	0.31	0.54	2.37

Formulation	d10 (μm)	d50 (μm)	d90 (μm)
P80+P407 S:M 1:1 25 °C	0.33	0.47	0.74
P80+P407 S:M 1:1 40 °C	0.51	0.53	1.09

Formulation	d10 (μm)	d50 (μm)	d90 (μm)
P80+P407 S:M 3:2 25 °C	0.32	0.51	1.23
P80+P407 S:M 3:2 40 °C	0.51	0.57	2.47

Figure 2 – Particle size (z-ave), polydispersity index (PDI) and distribution results (d10, d50 and d90) of freeze dried samples before lyophilization and after reconstitution and storage at 25 °C and 40 °C

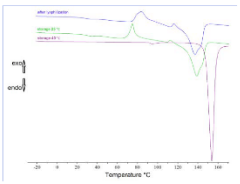

Figure 3 – DSC thermogram of freeze dried samples of NS1 with sucrose/mannitol 1:1 after lyophilization and after one month storage at 25 °C and 40 °C

DSC curves analysis showed that Tg' (glass transition temperature of the maximally freeze-concentrated solution) of all samples (including placebo) was around -39 °C, while on DSC curves of solid samples exotermic peak at around 80 °C and endotermic peak at 134-139 °C were visible. On DSC curves of samples stored at 25 °C and 40 °C, no exotermic peak was present, and endotermic peak was shifted to higher temperatures (152 °C). DSC profile of one sample (NS1 with sucrose/mannitol ratio 1:1 kept at 25 °C), did not change during observed period (Figure 3). Change in DSC curve could be explained by polymorphic change of mannitol during storage, probably to δ form.

TGA measurements indicated low moisture content, from 0.1-0.3%, in all samples.

Because of small amount of active substance in samples, it was difficult to visualize nanocrystals on SEM images. However, it was noticed that particles form aggregates, which were not homogenously spread in excipients (Figure 4).

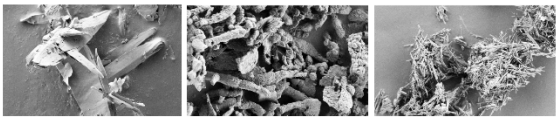

Figure 4 – SEM images of unprocessed DK-I-56-1 (left), freeze dried sample of NS2 with cryoprotectants (middle) and freeze dried sample of NS2 with sucrose/mannitol 1:1 after one month storage at 25 °C (right)

CONCLUSION

Lyophilization could be a promising method for improvement of DK-I-56-1 nanosuspensions stability. By selecting proper cryoprotectant and bulking agent ratios and concentrations, freeze dried products with satisfying properties could be obtained. However, mannitol polymorphic changes might jeopardize particle size preservation over time. For this reason, despite of good results after lyophilization, changes that might occur during storage must be taken into account and examined carefully. Different freeze drying conditions, cryoprotectant choice and storage conditions may help to overcome particle growth and agglomeration.

ACKNOWLEDGMENT

This work was realized within the framework of the projects TR34031 and OI175076, supported by the Ministry of Education, Science and Technological Development of the Republic of Serbia and CEEPUS project CIII-RS-1113-02-1819-M-118533 - Central European Knowledge Alliance for Teaching, Learning & Research in Pharmaceutical Technology (CEKA PharmTech).

REFERENCES

Anko M. et al., 2019, Int. J. Pharm., Vol. 564, pp. 106–116
Knutson D. E. et al., 2018, J. Med. Chem., Vol. 61(6), pp. 2422-2446.
Liao X., Krishnamurthy R. and Suryanarayanan R., 2007, Pharm. Res., Vol. 24(2), pp. 370-376.
Müller R. H., Gohla S., and Keck C. M., 2011, Eur. J. Pharm. Biopharm., Vol. 78(1), pp.1-9.
Van Eerdenbrugh B., Van den Mooter G., and Augustijns P., 2008, Int. J. Pharm., Vol. 364(1), pp. 64-75.
Wang L. et al., 2018, J. Microencapsul., Vol. 35(3), pp. 241-248.
Yue P. F. et al., 2014, Int. J. Pharm., Vol. 475(1-2), pp. 35-48.

4.10.4. A Novel Drug Target for Migraine: the GABA$_A$ Receptor α6 Subtype in Trigeminal Ganglia

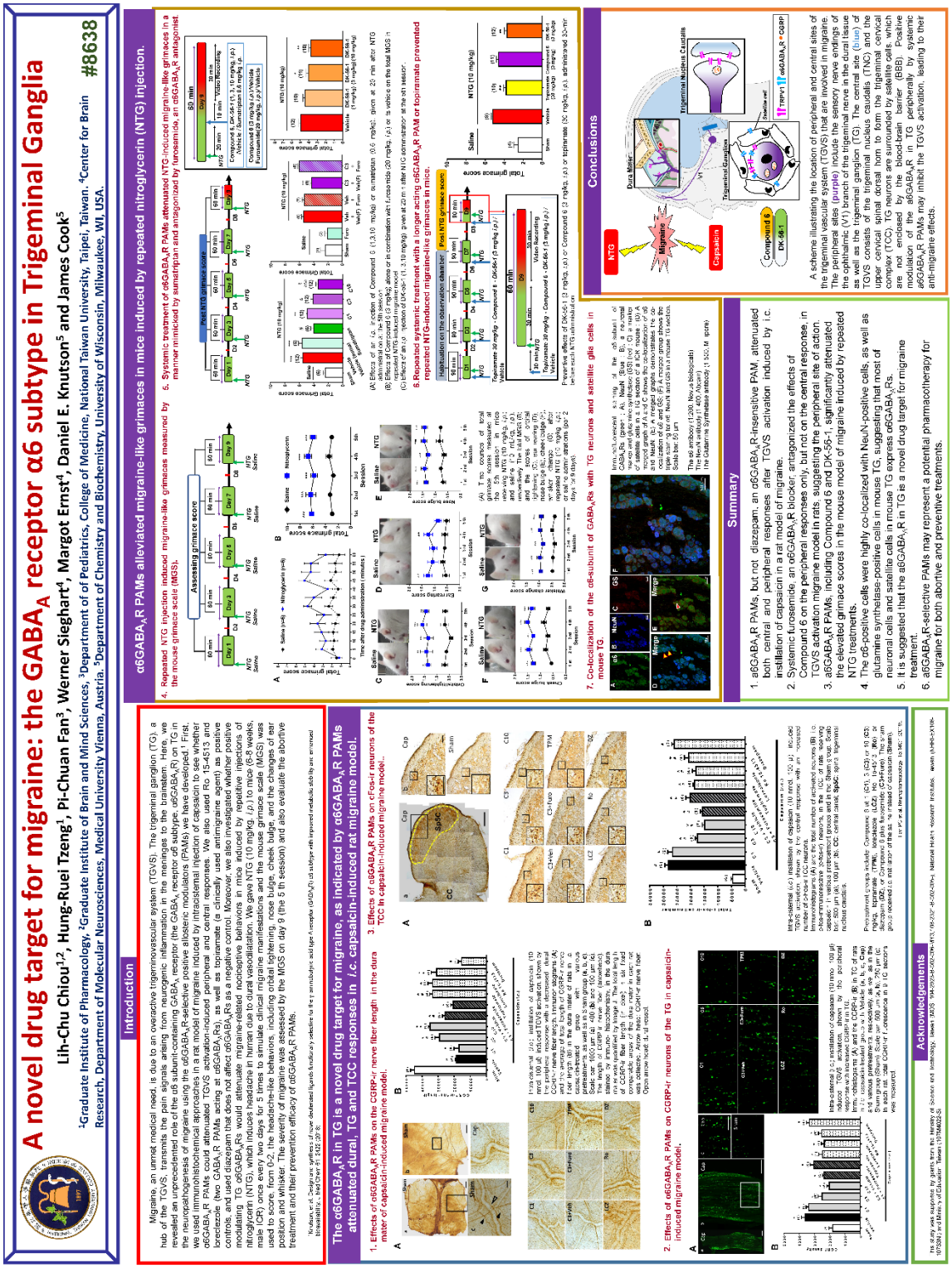

4.10.5. Studies Using von Frey Testing and Hot Plate Technique to Evaluate the Effects of Opioids, Novel Benzodiazepine-like Drugs, and Their Combinations

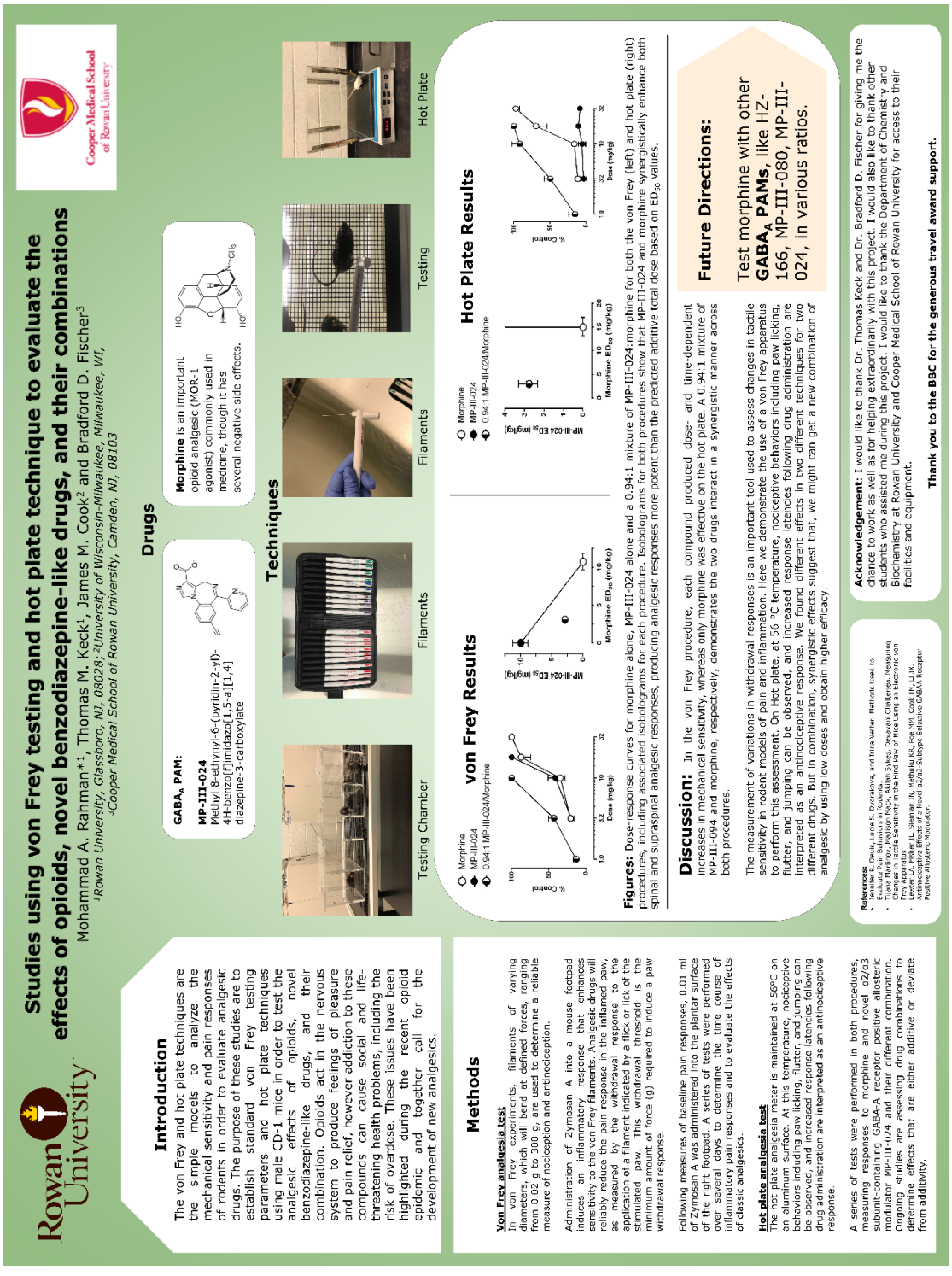

4.10.6. Role of GABA-A Receptor Subtypes in Respiratory Depression Induced by Benzodiazepines Alone and Combined With Fentanyl

Role of GABA-A Receptor Subtypes in Respiratory Depression Induced by Benzodiazepines Alone and Combined With Fentanyl

G. G. Haddad[1]; D. C. Majure[1]; J. E. Cook[2]; D. Ruedi-Bettschen[2]; D. K. Knutson[3]; G. Li[3]; J. M. Cook[3]; K. B. Freeman[2] and D. M. Platt[2]
[1]Medical Student Research Program, University of Mississippi Medical Center (UMMC), Jackson, MS USA; [2]Department of Psychiatry & Human Behavior, UMMC, Jackson, MS USA; [3]Department of Chemistry & Biochemistry, University of Wisconsin, Milwaukee WI USA

INTRODUCTION

- Benzodiazepines (BZs) are prescribed as anxiolytics, sleep aids, muscle relaxants, and seizure abortives.
- BZs are safe, but their lethality is increased greatly when combined with opioids.
- BZs modulate GABA-A receptors, which are Cl- ion channels comprised of 5 subunits (2 alpha, 2 beta, 1 gamma). Each subunit has several isoforms and the alpha isoform appears to dictate the pharmacology of the receptor.
- Understanding the role of different alpha subunit-containing GABA-A receptors in the respiratory depressant effects of benzodiazepines may allow for the development of compounds with improved safety profiles when combined with opioids.
- We evaluated the respiratory depressant effects of alprazolam (nonselective BZ), zolpidem (alpha1-preferring BZ), YT-III-31 (alpha3-selective BZ), and MP-III-022 (alpha5-selective BZ), alone or in combination with the opioid fentanyl, using whole body plethysmography.

- Supported by AA016179.

METHODS
Respiratory Measurement & Drug Administration

Figure 1. Whole body plethysmograph – ventilation data collection system.

Subjects:
- 8 adult male Sprague-Dawley rats, dosed in counter balanced fashion

Drugs:

Compound	Mechanism of action	Pretreatment Time	Route of admin
Alprazolam	Nonselective PAM*	30 min	i.p.
Zolpidem	Alpha1 preferring GABA-A PAM*	20 min	i.p.
YT-III-31	Alpha3 selective GABA-A PAM*	20 min	i.p.
MP-III-022	Alpha5 selective GABA-A PAM*	20 min	i.p.
Fentanyl	μ-opioid receptor agonist	15 min	s.c.
Propylene glycol/saline	Vehicle	20 min	s.c.

*Positive allosteric modulator

Respiration parameters:
- Minute volume (mL/min): volume of air inhaled or exhaled from lung each minute
- Frequency (BPM): number of breaths per minute
- Tidal volume (mL): amount of air inhaled during normal breathing, signifies depth of respiration.
- All parameters measured for 10 minutes

Statistics:
- Data for each parameter were analyzed with one-way repeated measures ANOVAs followed by Bonfermoi t-test comparing drug doses to vehicle or drug combinations to fentanyl alone.

RESULTS

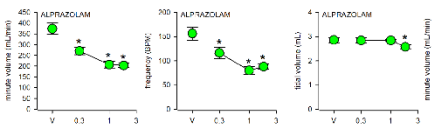

Figure 2. Dose-response functions for alprazolam on respiration parameters show decreases in minute volume driven by decreases in frequency and tidal volume. "V"=vehicle. *=P<0.05 compared to V.

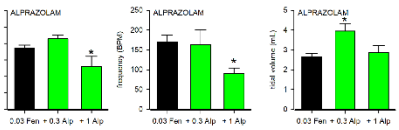

Figure 5. Combinations of fentanyl with alprazolam show significant decreases in minute volume driven by decreases in frequency compared to fentanyl alone. "Fen"=fentanyl, "Alp"=alprazolam. *=P<0.05 compared to 0.03 fentanyl.

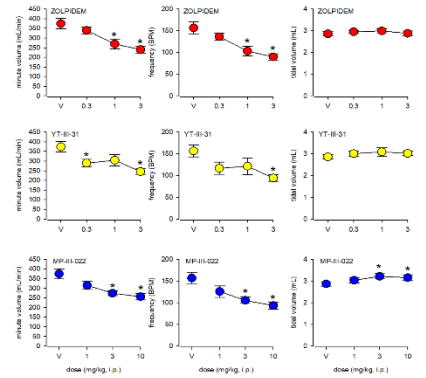

Figure 3. Dose-response functions for selective GABA-A receptor PAMs on respiration parameters show decreases in minute volume at high doses driven by decreases in frequency with preserved tidal volume. "V"=Vehicle. *=P<0.05 compared to V.

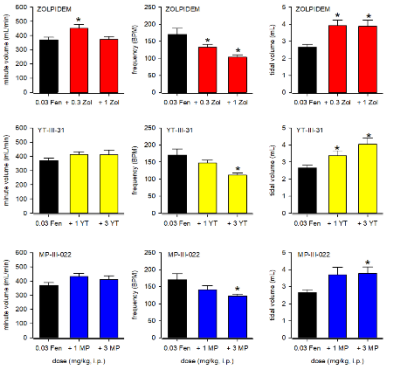

Figure 6. Combinations of fentanyl with selective GABA-A receptor PAMs show preserved minute volume, despite decreases in frequency, due to compensatory increases in tidal volumes. "Fen"= Fentanyl, "Zol"=zolpidem, "YT"=YT-III-31, "MP"=MP-III-022. *=P<0.05 compared to 0.03 fen.

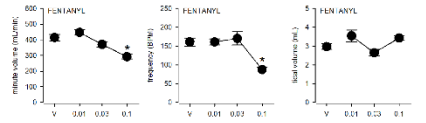

Figure 4. Dose-response function for fentanyl on respiration parameters show a decrease in minute volume driven by a significant decrease in frequency but not tidal volume. "V"=Vehicle. *=P<0.05 compared to V.

CONCLUSIONS

- According to the CDC, opioid deaths totaled over 32,000 in 2015 with roughly 7,500 overdose deaths involving a BZ. Understanding the GABAergic mechanisms that contribute to the increased risk for overdose when the drug classes are combined may allow for the development of safer anxiolytics, sleep aids, etc.
- Although all GABA-A PAMs produced decreases in minute volume and frequency, only the nonselective PAM alprazolam also suppressed tidal volume.
- Combined with fentanyl, the highest dose of alprazolam decreased both minute volume and frequency. In contrast, although all of the GABA-A selective PAMs decreased breath frequency when combined with fentanyl, no changes in minute volume were evident due to compensatory increases in tidal volume.
- Together, these results suggest that selectivity for alpha1, 3, or 5 subtypes may provide some protection from respiratory depression (alone or combined with opioids).
- Alprazolam's less favorable profile may be due to its affinity for multiple GABA-A subtypes and/or its positive modulation of alpha2 GABA-A subtypes. Future studies will investigate compounds with selectivity for alpha2/3 GABA-A subtypes and compare their respiratory effects to our data with YT-III-31.

4.10.7. Imbalanced Tonic Inhibition Between the Cortex and Thalamus Causes Epileptiform Activity in Mice Model of Angelman Syndrome

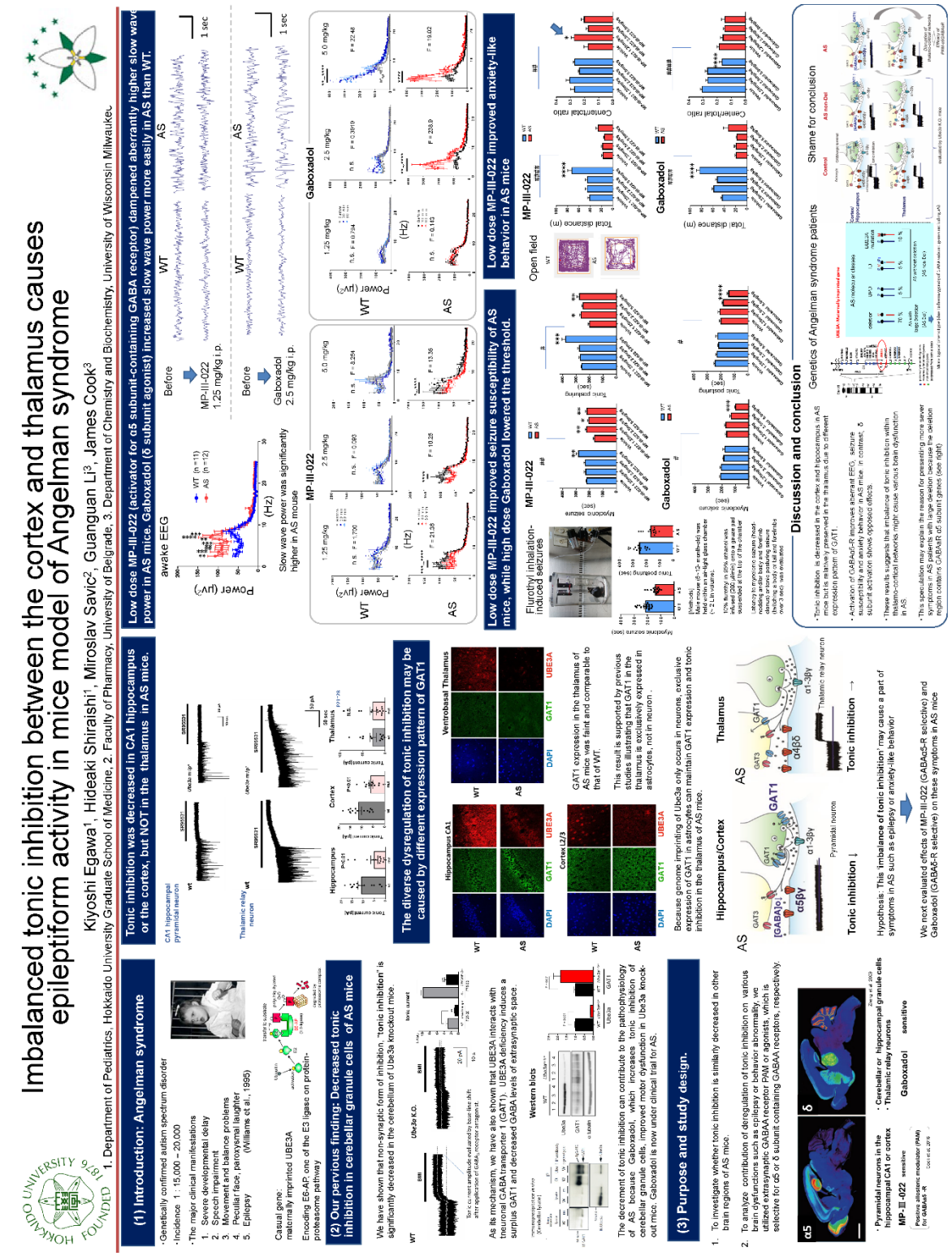

4.10.8. The Effect of a GABAA α5 Agonist on Mechanical Allodynia Following Nerve Injury

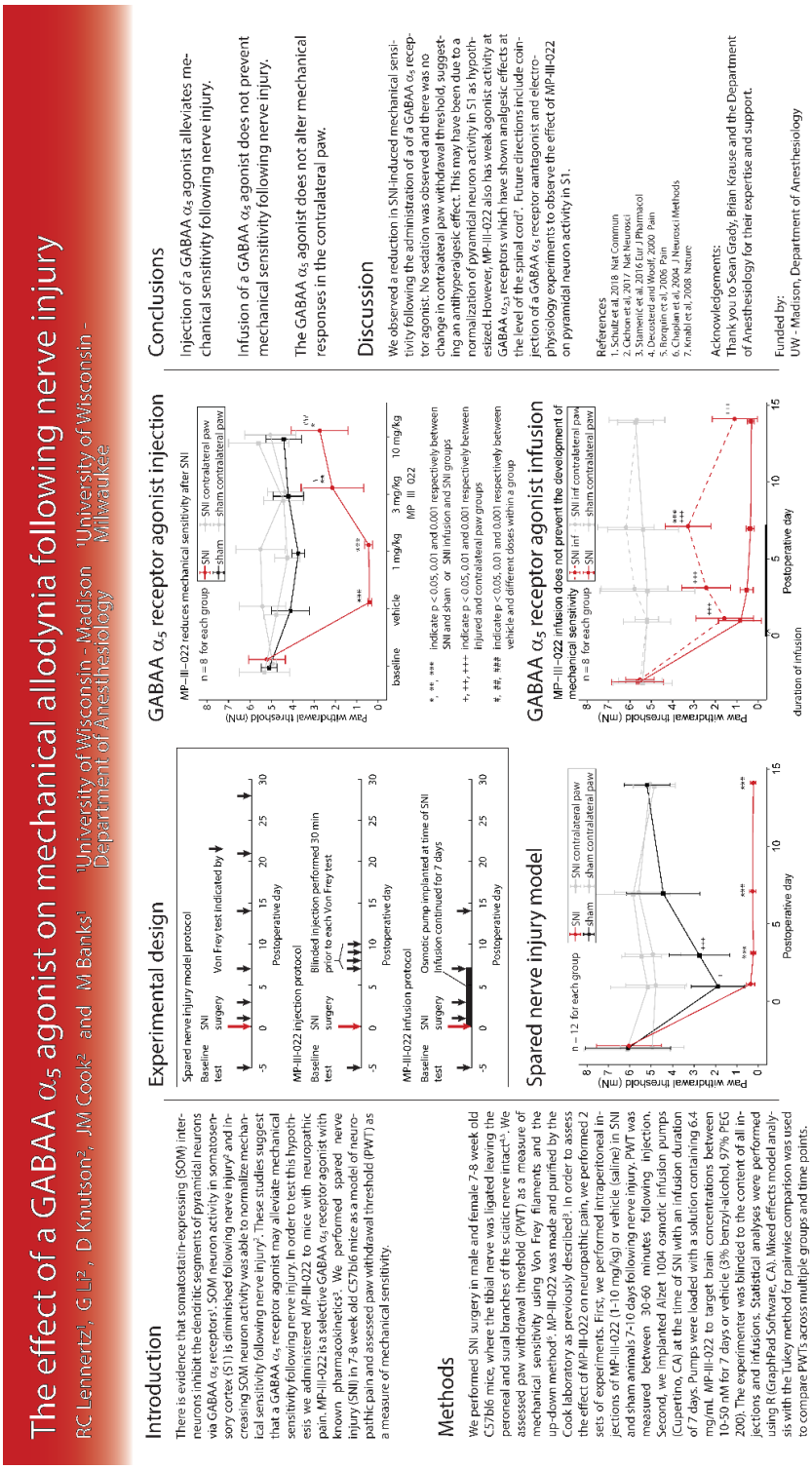

Pro-cognitive and neurotrophic effects of a novel molecule enhancing α5-GABA-A receptor function in adult or aged mice

Sibille E.[1,2,3], Cook J.[4], Li G[4], Knutson D.E.[4], Mian Y.[4], Mondal P.[4], David D.J.[5], Mendez-David I.[5], Guilloux J-P.[5] and Prevot T.D.[1,2]

[1]Campbell Family Mental Health Research Institute of CAMH, Toronto; [2]Dept of Psychiatry, University of Toronto; [3] Dept of Pharmacology and Toxicology, University of Toronto; [4]Dept of Chemistry and Biochemistry, University of Wisconsin, Milwaukee; [5] CESP/UMRS 1178, Univ Paris-Sud, Fac Pharmacie, INSERM, Université Paris-Saclay, Châtenay-Malabry, France.

Background and Aims

Altered GABA function is frequently reported in depression[1] during aging[2] or Alzheimer's disease[3], and is associated with low mood and altered cognitive functions[4]. In brain regions involved in regulating mood and cognition (i.e. prefrontal cortex and hippocampus), GABA neurons expressing somatostatin (SST) inhibit excitatory neurons by targeting their dendrites, and signaling in part through α5-containing GABA-A receptors (GABAA-R)[5].

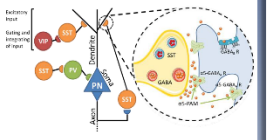

Simplified scheme of the prefrontal microcircuit (adapted from Fee et al., 2017)

Our group developed a new compound, GL-II-73 acting as a positive allosteric modulator (PAM) at the α5-GABAA-Rs. It displays anxiolytic, antidepressant and pro-cognitive effects in mouse model of depression and aging[6]. The proposed mechanism is through regulating defective excitation-inhibition balance.

Here, we hypothesized that **enhancing α5-GABAA-R activity would restore cellular morphology, participating in the pro-cognitive effects, by reversing dendritic shrinkage due to aging and/or fostering neurogenesis.**

Results: GL-II-73, given chronically…

… reverses cognitive deficits and dendritic shrinkage in distal dendrites of the PFC and the CA1 in old mice.

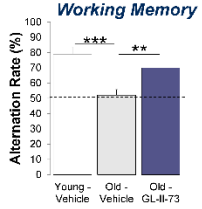

In the drinking water at 30mg/kg, GL-II-73 significantly reversed age-related decrease in alternation rate. *** $p<0.001$ compared to Old-Vehicle. Dash-line = chance

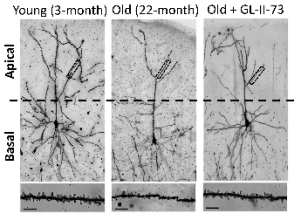

Pyramidal neurons from the PFC of young, old and old-treated mice, stained with Golgi/Cox. Bottom section represents a close-up on marked dendritic tree.

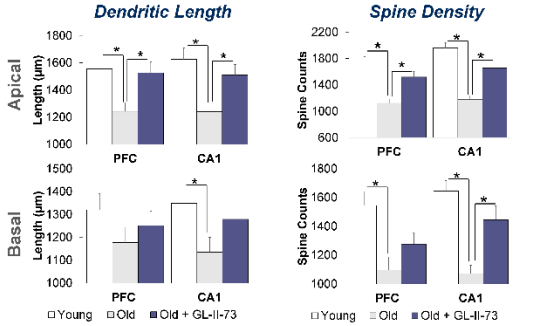

Aging reduces dendritic length and spine density in the PFC and CA1 of the hippocampus. Given chronically at 30mg/kg in the drinking water, GL-II-73 significantly reversed age-related decrease dendritic length and spine density. *$p<0.05$ compared to Old-Vehicle

… increases adult hippocampal neurogenesis in the CA1 of young 129S6/SvEvTac mice.

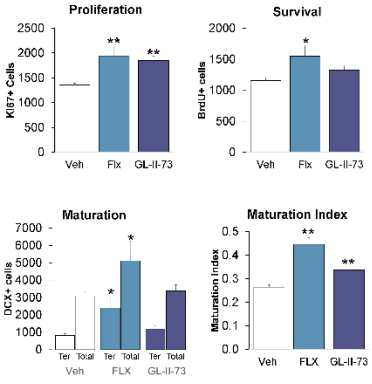

Chronic treatment with fluoxetine (Flx) or GL-II-73 increased the number of KI67+ cells in the CA1 of the HPC (left panel). Flx also significantly increased the number of BrdU+ cells, while the effect of GL-II-73 was not significant. *$p<0.05$ **$p<0.01$ compared to Veh group

Chronic treatment with Flx increases the number of DCX+ cells in the CA1 of the HPC, considering tertiary branches or total number of branches of the dendritic tree. GL-II-73 seemed to have a more discret effect, however revealed by the index calculation. *$p<0.05$, **$p<0.01$ compared to Veh group.

Conclusions

Chronic administration of GL-II-73:

- **reverses neuronal atrophy** in old mice. This effect is particularly marked in the **apical segment** of the dendritic tree, where α5-containing GABAA receptors are localized, **in both the PFC and the HPC.** Studies are on-going in chronically-stressed mice.
- increases **proliferation** of progenitor cells, increased survival of newborn cells (non significant), and accelerated **maturation** of newborn cells in the hippocampus of 129S6 mice.

GL-II-73 displays **symptomatic** and **"disease-modifying"** therapeutic efficacies for the treatment of **mood** and **cognitive** symptoms in disorders characterized by low GABA function, such as psychiatric disorders, normal aging and Alzheimer's disease.

Methods.

Male C57Bl/6 mice (Charles River) were obtained as retired breeders at the age of 10 months and kept until they reached 22 months. Young counterpart were purchased separately at 2 months of age (N=8 per group). The drug GL-II-73 was administered chronically in the drinking water at the concentration of 30mg/kg for 2 months. Cognition was assessed in the Ymaze for working memory: mice had to spontaneously alternate between the 2 goal arms of a Y-Maze, each trials being separated by a 60sec intertrial interval. After behavioral testing, brains (N=4 per group) were collected and soaked in Golgi/Cox staining solution. The CRO NeuroDigiTech performed the quantification for dendritic length and spine numbers with the software NeuroLucida (N=40 cells per groups, 8+ cell/mouse). For the neurogenesis study, 129S6/SvEvTac mice were used (8weeks old, N=10 per group). Mice were given GL-II-73 (30mg/kg, p.o.) or Fluoxetine (Flx, 18mg/kg, p.o.) for 42 days and its effects on all adult hippocampal neurogenesis steps (proliferation of newborn cells, survival and maturation of newborn neurons) were assessed using standard immuno assays against BrdU, KI-67 and DCX, respectively.

References. 1. Lin and Sibille, 2015 Mol Psychiatry 2.Gavilan et al, 2007 J NeuroChemistry 3.Fuhrer et al, 2017 Neuroscience 4.Fee et al, 2017 Biol Psyciatry 5.Schulz et al, 2018, Nature Comm 6.Prevot et al, 2019 Mol Neuropsy

Etienne.Sibille@camh.ca or thomas.prevot@camh.ca

CURRICULUM VITAE

Daniel E. Knutson

Place of Birth: Belvidere, IL, USA

Education

PhD in Chemistry, University of Wisconsin-Milwaukee, 2015-2020.

Expected Graduation, May 2020.

Research Advisor: Dr. James M. Cook.

BS in Chemistry with High Honors, Rockford College, 1995-1997.

Positions Held

1996-1997	Chemical Operator, Pierce Chemical Company, Rockford, IL.
1997-2005	Process Development Chemist, Sigma-Aldrich (SAFC), Milwaukee, WI.
2005-2013	Production Supervisor, Sigma-Aldrich (SAFC), Sheboygan, WI.
2013-2014	Manufacturing Supervisor, Sigma-Aldrich (SAFC), Madison, WI.
2015-Present	Graduate Research and Teaching Assistant, University of Wisconsin-Milwaukee, Milwaukee, WI.

Scholarly Awards

1. **R1 Distinguished Dissertator Fellowship (R1DDF),** Academic Year 2019-2020, University of Wisconsin-Milwaukee, Graduate School.
2. **Outstanding Teaching Assistant Award,** May 2018, University of Wisconsin-Milwaukee, Department of Chemistry and Biochemistry
3. **ACS Milwaukee Travel Grant,** Mar 2018, American Chemical Society-Milwaukee Section
4. **ACS MEDI Travel Grant,** Feb 2018, American Chemical Society-Division of Medicinal Chemistry
5. **Three Minute Thesis (3MT) Finalist,** April 10, 2019
6. **Three Minute Thesis (3MT) Finalist,** April 4, 2018
7. **Chancellor's Graduate Student Award** (received every semester appointed as a TA from **2015-2018**)

Research Profiles

https://orcid.org/0000-0002-8043-767X

https://www.researchgate.net/profile/Daniel_Knutson2

https://www.mendeley.com/profiles/daniel-knutson/

RESEARCH

Scholarly Publications

1. **Knutson, D. E.**; Kodali, R.; Divovic, B.; Treven, M.; Stephen, M. R.; Zahn, N. M.; Dobricic, V.; Huber, A. T.; Meirelles, M. A.; Verma, R. S.; Wimmer, L.; Witzigmann, C.; Arnold, L. A.; Chiou, L. C.; Ernst, M.; Mihovilovic, M. D.; Savic, M. M.; Sieghart, W.; Cook, J. M., Design and Synthesis of Novel Deuterated Ligands Functionally Selective for the gamma-Aminobutyric Acid Type A Receptor (GABAAR) alpha6 Subtype with Improved Metabolic Stability and Enhanced Bioavailability. *J. Med. Chem.* **2018,** *61* (6), 2422-2446. DOI: 10.1021/acs.jmedchem.7b01664.

2. Chiou, L. C.; Lee, H. J.; Ernst, M.; Huang, W. J.; Chou, J. F.; Chen, H. L.; Mouri, A.; Chen, L. C.; Treven, M.; Mamiya, T.; Fan, P. C.; **Knutson, D. E**.; Witzigmann, C.; Cook, J.; Sieghart, W.; Nabeshima, T., Cerebellar alpha6 Subunit-Containing GABAA Receptors: A Novel Therapeutic Target for Disrupted Prepulse Inhibition in Neuropsychiatric Disorders. *Br. J. Pharmacol.* **2018,** *175*, 2414-2427. DOI: 10.1111/bph.14198.

3. Fan, P. C.; Lai, T. H.; Hor, C. C.; Lee, M. T.; Huang, P.; Sieghart, W.; Ernst, M.; **Knutson, D. E.**; Cook, J. M.; Chiou, L. C., The α6 Subunit-Containing GABAA Receptor: A Novel Drug Target for Inhibition of Trigeminal Activation. *Neuropharmacol.* **2018,** *140*, 1-13. DOI: 10.1016/j.neuropharm.2018.07.017.

4. Neumann, E.; Rudolf, U.; **Knutson, D. E**.; Li, G.; Cook, J. M.; Hentschke, H.; Antkowiak, B.; Drexler, B., Zolpidem Activation of alpha 1-Containing GABAA Receptors Selectively Inhibits High Frequency Action Potential Firing of Cortical Neurons. *Front. Pharmacol.* **2019,** *9*. DOI: 10.3389/fphar.2018.01523.

5. Witkin, J. M.; **Knutson, D. E.**; Rodriguez, G. J.; Shi, S., Rapid-Acting Antidepressants. *Curr. Pharm. Des.* **2018,** *24* (22), 2556-2563. DOI: 10.2174/1381612824666180730104707.

6. Vasovic, D.; Divovic, B.; Treven, M.; Knutson, D. E.; Steudle, F.; Scholze, P.; Obradovic, A.; Fabjan, J.; Brkovic, B.; Sieghart, W.; Ernst, M.; Cook, J. M.; Savic, M. M. Trigeminal neuropathic pain development and maintenance in rats are suppressed by a positive modulator of alpha6GABAA receptors. *Eur. J. Pain.* **2019**, (published online). DOI: 10.1002/ejp.1365.

7. Prevot, T. D.; Li, G.; Vidojevic, A.; Misquitta, K. A.; Fee, C.; Santrac, A.; **Knutson, D. E**.; Stephen, M. R.; Kodali, R.; Zahn, N. M.; Arnold, L.; Scholze, P.; Fisher, J. L.; Markovic, B.

D.; Banasr, M.; Cook, J. M.; Savic, M. M.; Stibille, E. Novel benzodiazepine-like ligands with various anxiolytic, antidepressant or pro-cognitive profiles. *Mol. Neuropsychiatry.* **2019**, (published online). DOI: 10.1159/000496086.

8. Cerne, R.; Fisher, J.F.; Siemian, J.N.; Smith, J.L.; **Knutson, D.E.**; Cook, J.M.; Witkin, J.M. Improvements in the pharmacological profile of diazepam by KRM-II-81, an imidizodiazepine positive allosteric modulator of a2/3-containing $GABA_A$ receptors: Preclinical data predict enhanced efficacy for epilepsy, chronic pain, anxiety, and depression, *Pharmaceutical Sciences and Biomedical Analysis Journal*, 2(1):117, **2019**.

9. Roni, M. S. R.; Li, G.; Mikulsky, B. N.; **Knutson, D.E.**; Mian, Y.; Zahn, N.M.; Cook, J.M.; Stafford, D.C.; Arnold, L.A. The effect of pH on the structure and bio-availability of asthma drug candidate MIDD0301. *Molecular Pharmaceutics*, (published online), **2020**. DOI: 10.1021/acs.molpharmaceut.9b01210.

10. Prevot, T.D.; Sumitomo, A.; Tomoda, T.; **Knutson, D.E.**; Li, G.; Cook, J.M.; Sibille, E. Chroni administration of a positive allosteric modulator at the alpha 5-GABAA receptor reverses age-related dendritic shrinkage. *Preprint*, **2020**. DOI: 10.1101/2020.02.28.964742.

11. Tzeng, H.R.; Lee, M.T.; Fan, P.C.; **Knutson, D.E.**; Sieghart, W.; Cook, J.M.; Chiou, L. C. α6GABBA receptor positive modulators alleviate migraine-like grimaces in mice via compensating GABAergic deficit in trigeminal ganglia. *Br. J. Pharmacol,* (under review). **2020**.

12. Mitrović, J.R.; Divović, B.; **Knutson, D.E.**; Đoković, J.B., Vulić, P.J.; Ranđelović, D.; Dobričić, V.D.; Calija, B.R.; Cook, J.M.; Savić, M.M.; Savić, S.D. Nanocrystal dispersion of DK-I-56-1, a poorly soluble pyrazoloquinolinone positive modulator of α6 GABAA receptors: formulation approach toward improved brain delivery. *International Journal of Pharmaceutics,* (under review), **2020.**

13. Knutson, D.E.; Divovic, B.; Kodali, R.; Kehoe, A.S.; Luecke, I.W.; Arnold, L.A.; Ernst, M.; Fisher, J.L.; Savic, M.M.; Sieghart, W.; Cook, J.M. A Comparative Study of Deuteration Versus Fluorination of α6-$GABA_AR$ Subtype- Selective Ligands as Strategies to Enhance Bioavailability, and their Impact on the Pharmacokinetic Profiles and α6-$GABA_AR$ Functional Selectivity. *Eur. J. Med. Chem,* (manuscript in progress), **2020**.

14. Knutson, D.E.; Roni, M.S.R.; Mian, M.Y.; Li, G.; Cook, J.M.; Stafford, D.C.; Arnold, L.A. Improved Large Scale Synthesis of Clinical Asthma Candidate MIDD0301. *Organic Process Research & Development*, (submission in progress), **2020**.

15. Knutson, D.E.; Smith, J.L.; Ping, X.; Jin, X.; Golani, L.K.; Li, G.; Tiruveedhula, V.V.N.P.B.; Rashid, F.; Mian, M. Y.; Jahan, R.; Sharmin, D.; Cerne, R.; Cook, J. M.; Witkin,

J. M. The imidazodiazepine anticonvulsant, KRM-II-81, produces novel, non-diazepam-like antiepileptogentic effects. *ACS Chemical Neuroscience*, (submission in progress), **2020**.

16. Biggerstaff, A.; Kivell, B.; Cerne, R.; Smith, J. L.; Mian, M. D.; Golani, L. K.; Rashid, F.; Sharmin, D.; **Knutson, D.E.**; Cook, J. M.; Witkin, J. M. The α2,3-selective potentiators of $GABA_A$ receptors, KRM-II-81 and MP-III-80, are antinociceptive against chemotherapy-induced pain with anxiolytic-like effects in mice. *Pharmacology, Biochemistry and Behavior*, (under review), **2020**.

Other Publications

1. **Knutson, D. E.**; Smith M. "Chemistry 344: Organic Chemistry Laboratory Course Manual". Department of Chemistry and Biochemistry, UW-Milwaukee, **2018**.

Conference Presentations

1. **Knutson, D. E.**; Verma, R. S.; Stephen, M. R.; Kodali, R.; Arnold, L. A.; Cook, J. M.; Mihovilovic, M. D.; Wimmer, L.; Ernst, M.; Sieghart, W., Novel Deuterated GABAAR-α6 Subtype Selective Ligands with Improved Metabolic Stability. Targeting Trigeminal Orofacial Pain, Neuropsychiatric Disorders, & Depression. In *5th Annual ICBS Conference*, Madison, WI, 2016.

2. **Knutson, D. E.**; Kodali, R.; Stephen, M. R.; Zahn, N. M.; Arnold, L. A.; Cook, J. M.; Dobricic, V.; Savic, M. M.; Mihovilovic, M. D.; Treven, M.; Ernst, M.; Sieghart, W., Novel Deuterated GABAAR-α6 Subtype Selective Ligands with Improved Metabolic Stability and Enhanced Bioavailability Targeting Trigeminal Orofacial Pain, Neuropsychiatric Disorders, and Depression. In *254th ACS National Meeting*, Washington, DC, August, 2017. **Sci-Mix** and **General Poster Session**. DOI: 10.13140/RG.2.2.15698.40643

3. **Knutson, D. E.**; Kodali, R.; Stephen, M. R.; Verma, R. S.; Witzigmann, C.; Meirelles, M. A.; Zahn, N. M.; Huber, A. T.; Arnold, L.; Savic, M. M.; Ernst, M.; Sieghart, W.; Cook, J. M., Design and Synthesis of Novel Deuterated GABAAR-a6 Subtype Selective Ligands with Improved Metabolic Stability and Enhanced Bioavailability. In *35th Herbert C. Brown Lectures in Organic Chemistry*, Purdue University, 2018.

4. **Knutson, D. E.**; Kodali, R.; Stephen, M. R.; Verma, R. S.; Witzigmann, C.; Meirelles, M. A.; Zahn, N. M.; Huber, A. T.; Arnold, L.; Savic, M. M.; Ernst, M.; Sieghart, W.; Cook, J. M., Design and Synthesis of Novel Deuterated GABAAR-a6 Subtype Selective Ligands with Improved Metabolic Stability and Enhanced Bioavailability. In *255th ACS National Meeting*, New Orleans, LA, March, 2018. **General Poster Session**. DOI: 10.13140/RG.2.2.32475.62241

5. **Knutson, D. E.**; Vasovic, D.; Divovic, B.; Treven, M.; Steudle, F.; Scholze, P.; Brkovic, B.; Sieghart, W.; Ernst, M.; Cook, J. M.; Savic, M. M., Prevention of Trigeminal Neuropathic Pain Development in Rats Using Novel Deuterated GABAAR-α6 Subtype Selective Ligands. In *256th ACS National Meeting*, Boston, MA, August 2018. **Sci-Mix** and **General Poster Session**. DOI: 10.13140/RG.2.2.36250.49601

6. **Knutson, D.E.**; Kodali, R.; Treven, M.; Divović, B.; Lee, H. J.; Chou, J. F.; Chen, H. L.; Chiou, L. C.; Ernst, M.; Mihovilovic, M. D.; Savić, M. M.; Sieghart, W.; and Cook, J. M. Treatment of Sensorimotor Gating Deficits in Neuropsychiatric Disorders Using Deuterated α6-$GABA_AR$ Subtype Selective Ligands. In *257th ACS National Meeting*, Orlando, FL, March, 2019.

7. **Knutson, D.E**.; Kodali, R.; Treven, M.; Divović, B.; Lee, H. J.; Chou, J. F.; Chen, H. L.; Chiou, L. C.; Ernst, M.; Mihovilovic, M. D.; Savić, M. M.; Sieghart, W.; and Cook, J. M. Treatment of Sensorimotor Gating Deficits in Neuropsychiatric Disorders Using Deuterated α6-$GABA_AR$ Subtype Selective Ligands. In *35th Herbert C. Brown Lectures in Organic*

Chemistry, Purdue University, 2019.

8. **Knutson, D.E**.; Li, G.; Prevot, T.; Arnold, L.A.; Chiou, L.C.; Fan, P.C.; Ernst, M.; Mihovilovic, M.D.; Savić, M.M.; Sieghart, W.; Sibille, E.; Cook, J.M. Combatting the Opioid and Benzodiazepine Epidemic by the Synthesis of Novel Safer Drugs Designed to be Functionally Selective for α5- or α6-containing $GABA_A$ Receptors. In *258th ACS National Meeting*, San Diego, CA, August 2019. **General Poster Session.**

9. **Knutson, D.E.**; Divovic, B.; Kodali, R.; Kehoe, A.S.; Luecke, I.W.; Arnold, L.A.; Ernst, M.; Fisher, J.L.; Savic, M.M.; Sieghart, W.; Cook, J.M. A Comparative Study of Deuteration Versus Fluorination of α6-$GABA_AR$ Subtype- Selective Ligands as Strategies to Enhance Bioavailability, and their Impact on the Pharmacokinetic Profiles and α6-$GABA_AR$ Functional Selectivity. In *259th ACS National Meeting*, Philadelphia, PA, March 2020. **Sci-Mix** and **General Poster Session.**

Patents

1. Chiou, L.-C.; Cook, J.; Ernst, M.; Fan, P.-C.; **Knutson, D.**; Meirelles, M.; Mihovilovic, M.; Sieghart, W.; Varagic, Z.; Verma, R.; Wimmer, L.; Weizigmann, C.; Siebert, D. C. B.; Savic, M. M. Preparation of Ligands Selective to Alpha 6 Subunit-Containing Gabbai Receptors and their Methods of Use. WO2016196961, 2016.

Oral Presentations

1. Three Minute Thesis Competition, UW-Milwaukee, "Combatting the Opioid and Benzodiazepine Epidemic by the Design and Synthesis of Novel Safer Drugs", April 10, 2019. https://www.youtube.com/watch?v=hVaxOPiJsGU&feature=youtu.be

2. First Look Forum, Milwaukee, WI, "Novel Compounds for Neuropsychiatric Disorders and Trigeminal Pain", April 26, 2018.

3. Three Minute Thesis Competition, UW-Milwaukee, "Design and Synthesis of Compounds Selective for Brain Receptors Associated with Depression", April 4, 2018. https://www.youtube.com/watch?v=VZiZYU54e40&feature=youtu.be

4. Dr. Feringa Visit, UW-Milwaukee, "Novel Deuterated $GABA_AR$-a6 Subtype Selective Ligands with Improved Metabolic Stability and Enhanced Bioavailability", September 29, 2017.

News Article Links

1. WUWM 89.7 Radio Interview, February 27, 2020. UWM Researches Have Developed Chemical Compounds That Could Provide Non-Addictive Pain Relief. https://www.wuwm.com/post/uwm-researchers-have-developed-chemical-compounds-could-provide-non-addictive-pain-relief?fbclid=IwAR1yM_9BuN7aLFaZmtU2uNyG_K2ezQe1kfbqopG6vHoS57q4jheFDIbrkZI#stream/0

2. UWM Research Magazine Article, February 21, 2019. A promising search for relief without addiction. https://uwm.edu/news/a-promising-search-for-relief-without-addiction/?fbclid=IwAR13qklfXDHauPUzFfeVFNNdA_mTB85STZT5UY3ScIlnv_cR8-S9KzksrfM

3. Center for Addition and Mental Health News Release, February 14, 2019. New molecules reverse memory loss linked to depression, aging. https://www.camh.ca/en/camh-news-and-stories/new-molecules-reverse-memory-loss-linked-to-depression-aging?fbclid=IwAR3JQA-ezl6xxFbayYigrd1imPnJ6JntDAxsuSeYQrJ6qf0ogbnGkFmy05g

4. Bioforward Wisconsin, April 4, 2018. https://www.bioforward.org/first-look-forum-showcases-marketable-academic-research/